INTERNATIONAL CONFERENCE OF YOUNG SCIENTISTS ON ENERGY ISSUES

The 9th annual conference of Young Scientists on Energy Issues

ISSN 1822-7554

Conference proceedings

www.cyseni.com

24-25 May, 2012
Kaunas, Lithuania

Dear Reader of the Conference proceedings,

The International Conference of Young Scientists on Energy Issues 2012 has been organized for nine times since 2004.The initiative for such a event came from young, enthusiastic researchers in Lithuanian Energy Institute (LEI). They realised that there are a lot of young, smart and science-oriented young people doing research in the energy area and they do need a place and time to meet each other to share their views, generate ideas, present various stories of successful results and failures which definitely occur in the science. The first conference was organized by young researchers with the supervision of experienced scientists from LEI only in 2004.

In 2005 it became a national conference with participants from Kaunas University of Technology, Vilnius Gediminas Technical University, Vilnius University, Vytautas Magnus University – in fact from all science and education institutions of Lithuania involved in energy-related topics. The next year (2006) was devoted to strengthen status of the conference among young researchers and their experienced supervisors and bring the message that in a small country we can reach our targets with joint efforts only.

In 2007 the organising committee decided to put emphasis on regional and international dimension. The participants from neighbouring countries – Belarus and Poland participated in the conference for the first time. We realised that facing challenges in energy research young researchers need to be brought together as many as possible to create a critical mass to be competent and competitive for the future research. Thus, the conference is not only intended for the increase of the participants competence by involvement of best experienced scientists as peer reviewers, involvement of the participants in the review process of their colleagues (educational exercise), it is intended to expand geographically.

In 2008 we welcome the participants from Belarus, Estonia, India, Latvia, Lithuania and Russia. In 2009 the outcome of the conference (in terms of scientific papers) was contributed by the young scientists from Belarus, Estonia, Italy, Latvia, Lithuania, Nigeria and Ukraine.

With a growing attention to this annual event the conference proceedings included the papers with scientific results of researchers from various Lithuanian science and research institutions and foreign institutions (Belarus, Estonia, Germany, Italy, Latvia, Nigeria, Norway and Ukraine) in 2010.

In total 69 papers of young scientists' from various Lithuanian science and research institutions and foreign institutions in Belarus, Estonia, Germany, Latvia, Nigeria, Poland, Taiwan and Ukraine were reviewed and accepted for the publication in 2011.

This year even 82 young scientists took part in the conference (CYSENI 2012) and presented the results of their research. The participants were from various Lithuanian science and research institutions (Lithuanian Energy Institute, Kaunas University of Technology, Vilnius Gediminas Technical University, Vytautas Magnus University, Vilnius University, Center for Physical Sciences and Technology and Lithuanian Research Centre for Agriculture and Forestry) and foreign institutions Latvia (University of Latvia, Institute of Physical Energetics, Riga Technical University, Latvia University of Agriculture and Institute of Technical Physics), Estonia (Tallinn University of Technology), Poland (Institute of Nuclear Chemistry and Technology), Belarus (A.V. Luikov Heat and Mass Transfer Institute), Ukraine (A. N. Podgorny Institute for Mechanical Engineering Problems of the National Academy of Sciences of Ukraine), Russia (Ufa State Aircraft Engineering University), Sweden (Umeå University), Germany (Technical University of Braunschweig), Portugal (Institute for Systems Engineering and Computers at Coimbra, University of Aveiro), Brazil (University of Sao Paulo), Indonesia (Gadjah Mada University), Taiwan (Feng Chia University)

This event in our institute is usually full of pleasant atmosphere, interesting and valuable discussions, cheerful social program. The greetings and acknowledgments of the participants encourage us to keep these moments in mind and improve the future CYSENI conferences. Regarding the next year we already now invite you to the tenth International Conference of Young Scientists on Energy Issues 2013, which will be held in 29-31 May, 2013 in Kaunas, Lithuania.

Organisers

Conference organising committee

Board of Young scientists association of Lithuanian Energy Institute
Prof. dr. habil. Eugenijus Uspuras, Director of Lithuanian Energy Institute
dr. Rolandas Urbonas, Head of Information department of Lithuanian Energy Institute
Jolanta Kazakevičienė, Studies administrator of Lithuanian Energy Institute

Conference management

dr. Diana Meilutytė-Barauskienė

Conference secretariat

dr. Diana Meilutytė-Barauskienė
Darius Justinavičius
Jolanta Kazakevičienė

Technical support

Tadas Kaliatka
Liudvikas Žiemys (photograph)

Programming (website, conference proceedings)

Darius Jakimavičius
Mantas Valantinavičius (www.cyseni.com)

Layout

Zita Cvilikienė
Laima Vasiliauskienė
dr. Asta Narkūnienė
Alina Varnaitė

SCIENTIFIC COMMITTEE

1. **Hydrogen and fuel cells**

Dr. Darius Milčius
(Lietuvos energetikos institutas, Lietuva) (Lithuanian Energy Institute, Lithuania)
http://www.hydrogen.lt/index.php?mn=research&id=milciuscv&ln=lt

Prof. Bjørn C. Hauback
(Fizikos departamentas, Energetinių technologijų institutas, Norvegija)
(Physics Department, Institute for Energy Technology, Norway)
http://www.mn.uio.no/fysikk/english/people/aca/bjorh/index.html

2 **Renewable energy sources and their use**

Dr. Mantas Marčiukaitis
(Lietuvos energetikos institutas, Lietuva) (Lithuanian Energy Institute, Lithuania)
http://en.scientificcommons.org/mantas_marciukaitis

3. **Smart energy networks**

Prof. Dr. Panos M. Pardalos
(Floridos Universitetas, JAV) (University of Florida, USA)
http://www.ise.ufl.edu/pardalos/index.html

Dr. Virginijus Radziukynas
(Lietuvos energetikos institutas, Lietuva) (Lithuanian Energy Institute, Lithuania)
http://www.lei.lt/main.php?m=158&k=1

4. **Energy efficiency and savings**

Prof. Dr. Namejs Zeltins
(Fizikinės energetikos institutas, Latvija) (Institute of Physical energetics, Latvia)
http://www.lza.lv/scientists/zeltinshn.htm

Prof. Habil. Dr. Vytautas Martinaitis
(Vilniaus Gedimino technikos universitetas, Lietuva) (Vilnius Gediminas Technical University, Lithuania)
http://www.pek.ap.vgtu.lt/en/51129/CV/8869

Prof. Dr. Andres Siirde
(Talino technologijos universitetas, Estija) (Tallinn University of Technology, Estonia)
http://www.etis.ee/portaal/isikuCV.aspx?LastNameFirstLetter=S&PersonVID=38322&FromUrl0=isikud.aspx&lang=en

5. **Knowledges for energy policy making**

Prof. Dr. Andris Kreslins
(Rygos technikos universitetas, Latvija) (Riga Technical University, Latvia)
http://www.lza.lv/scientists/KreslinsA.htm

Habil. Dr. Vaclovas Miškinis
(Lietuvos energetikos institutas, Lietuva) (Lithuanian Energy Institute, Lithuania)
http://www.lei.lt/main.php?m=159&k=1

6. **Investigations in the fields of thermal physics, fluid mechanics and metrology**

Academician prof. Habil. Dr. Sergej Zhdanok
(A. V. Lykovo Šilumos ir masės mainų institutas, Baltarusija)
(A. V. Luikov Heat & Mass Transfer Institute, Belarus)
http://nasb.gov.by/eng/members/academicians/zhdanok.php

Prof. Dr. Myriam Lazard
Institut Prime, ENSIP
Ecole Nationale Supérieure des Ingénieurs de Poitiers, FRANCE
http://www.wseas.us/conferences/2011/florence/hte/Plenary8.htm

7. **Nanosciences and Nanotechnologies, investigations on multifunction materials**

Prof. Dr. Enn Mellikov
(Mokslo akademijos narys, Estija) (Member of the Estonian Academy of Sciences, Estonia)
(http://www.akadeemia.ee/en/membership/_members/mellikov/)

8. **Investigations of combustion and plasma processes**

Dr. Victor A. Zhovyansky
(Nacionalinė mokslų akademija, Ukraina) (National Academy of Sciences of Ukraine, Ukraine)
http://www.ingas.org.ua/index.files/Page5004.htm

Dr. Bernhard Peters
(Luksemburgo universitetas, Liuksemburgas) (University of Luxembourg, Luxemburg)
http://wwwen.uni.lu/recherche/fstc/research_unit_in_engineering_science_rues/members/bernhard_peters

9. **Global change and ecosystems**

Prof. Habil. Dr. Ralf Ebinghaus
(Luneburg‘o universitetas, Vokietija) (Lüneburg University, Germany)
http://coast.gkss.de/aos/staff/ebinghaus/index.html

Prof. Dr. Sten Bergström
(Švedijos meteorologijos ir hidrologijos institutas, Švedija)
(Swedish Meteorological and Hydrological Institute, Sweden)
http://www.bioone.org/doi/abs/10.1579/0044-7447-33.4.176

10. **Fusion energy**

Dr. Sigitas Rimkevičius
(Lietuvos energetikos institutas, Lietuva) (Lithuanian Energy Institute, Lithuania)
http://www.lei.lt/main.php?m=263&k=9

Prof. Dr. Finn Ravndal
(Oslo universitetas, Norvegija) (University of Oslo, Norway)
http://folk.uio.no/finnr/, http://en.scientificcommons.org/finn_ravndal

Dr. Luis E. Herranz
(UPSO universitetas, Ispanija) (UPCO University, Spain)
http://www.ciemat.es/portal.do?IDR=754&TR=C

11. **Nuclear fission and radiation protection**

Prof. Habil. Dr. Eugenijus Ušpuras
(Lietuvos energetikos institutas, Lietuva) (Lithuanian Energy Institute, Lithuania)
http://www.eurosafe-forum.org/eugenijus-uspuras

Prof. Dr. Pierre-Etienne Labeau
(Briuselio universitetas, Belgija) (Briussels University, Belgium)
http://mntek3.ulb.ac.be/pub/pel/perso.html

Dr. Alessandro Petruzzi
(Pizos universitetas, Italija) (University of Pisa, Italy)
http://www.unipi.it/english/index.htm

By countries:

- Lithuania – 7 members;
- Latvia – 2 members;
- Estonia – 2 member;
- Belgium –1 member;
- USA – 1 member;
- Germany – 1 member;
- Sweden – 1 member;
- Norway – 2 members;
- Belarus – 1 member;
- France – 1member
- Ukraine – 1 member
- Luxembourg – 1 member
- Spain – 1 member
- Italy – 1 member

Total: 23 members.

CONTENT

I. HYDROGEN AND FUEL CELLS (4)

II. RENEWABLE ENERGY SOURCES AND THEIR USE (11)

III. SMART ENERGY NETWORKS (4)

IV. ENERGY EFFICIENCY AND SAVINGS (14)

V. KNOWLEDGES FOR ENERGY POLICY MAKING (14)

VI. INVESTIGATIONS IN THE FIELDS OF THERMAL PHYSICS, FLUID MECHANICS AND METROLOGY (8)

VII. NANOSCIENCES AND NANOTECHNOLOGIES, INVESTIGATIONS ON MULTIFUNCTION MATERIALS (6)

VIII. INVESTIGATIONS OF COMBUSTION AND PLASMA PROCESSES (9)

IX. GLOBAL CHANGE AND ECOSYSTEMS (5)

XI. NUCLEAR FISSION AND RADIATION PROTECTION (4)

CYSENI 2012, May 24–25, Kaunas, Lithuania
ISSN 1822-7554, www.cyseni.com

BIO-HYDROGEN PRODUCTION ASSESSMENT USING FERMENTATIVE BACTERIA AND CRUDE GLYCEROL AS SUBSTRATE

I. Dimanta, V. Nikolajeva, A. Gruduls, I. Muižnieks
Faculty of Biology, University of Latvia
Kronvalda bulv. 4, Riga, LV-1010 – Latvia
Phone 00 371 29776085
Email: ilze.dimanta@lu.lv

J. Kleperis
Institute of Solid State Physics, University of Latvia
Kengaraga iela. 8, Riga, LV-1063 - Latvia
Email: kleperis@latnet.lv

ABSTRACT

Hydrogen production via biological processes is perspective and advantageous way for alternative energy production. Microorganisms are capable to produce hydrogen during fermentation of organic substrates. Industrial and agricultural waste can be used as feedstock for hydrogen producing bacteria. One of the substrates that can be effectively used for microbial hydrogen production is glycerol, which is a by-product from the process of biodiesel production. Different bacterial isolates were tested for hydrogen gas production rates from glycerol substrate with test-systems constructed in our laboratory. Test-systems were optimised to allow adequate substrate and bacterial strain hydrogen productivity estimation in liquid and gaseous phase. It was concluded that several of the isolated bacterial strains are suitable for bio-hydrogen production using crude glycerol as substrate. Assessment was developed to establish whether microbial conversion of crude glycerol is economically and environmentally viable possibility for bio-hydrogen production. Raw material cost noticeably decreases because of large quantities of available crude glycerol after biodiesel production and the highly reduced nature of carbon in glycerol *per se*.

1. INTRODUCTION

Biological production of hydrogen, using bacteria, is a promising and advantageous area, especially when hydrogen is gained from a variety of renewable resources [1,2]. Industrial and agricultural organic waste used as feedstock for hydrogen producing bacteria is a perspective way for alternative energy production and it noticeably decreases the raw material cost. During the conversion of organic wastes, in anaerobic environment, hydrogen gas is produced as a by-product. Substantial factors like availability and cost are highly important in the selection of waste materials to be used in hydrogen production with fermentative bacteria [3]. One of the substrates that can be effectively used for microbial hydrogen production is glycerol, which is a by-product from the process of biodiesel production. Because of large quantities available of crude glycerol and the highly reduced nature of carbon in glycerol per se, microbial conversion of it seems to be economically and environmentally viable possibility, especially because, over the last several years, the demand and production of biodiesel has remarkably increased [4,5]. Numerous anaerobic and facultatively anaerobic bacteria, e.g. belonging to family *Clostridiaceae, Enterobacteriaceae* and others, can produce hydrogen from carbohydrate containing organic wastes. Glycerol like glucose can be fermented by *E. coli* to produce hydrogen at acid pH [6]. Environmental conditions like medium pH and temperature are the major parameters to be controlled in the hydrogen production, because they affect bacterial produced gas qualitative and quantitative content and hydrogen yield and rate. Hydrogen production using glycerol is 1.5-fold higher at pH 5.5 than at pH 6.5 [7]. Anaerobic conditions have to be maintained during the hydrogen production process, which are ensured by bubbling media with reducing agents such as argon or nitrogen [3]. Parameters of hydrogen gas are measured by classic volumetric, mass-spectrometric and chromatography methods or using chemical gas sensors. To measure hydrogen gas concentration in liquid a hydrogen electrode is used (Pt or other noble metal – gold, rhodium, palladium, etc.), for example, Clark electrodes, where the cathode is polarized versus internal Ag/AgCl anode which is placed behind an electrically insulating silicone rubber membrane [8-10].

2. MATERIALS AND METHODS

1. Strains

Aneurinibacillus aneurinilyticus Microbial Strain Collection of Latvia (MSCL) 1018, *Clostridium sporogenes* MSCL 764,*Eubacterium limosum* MSCL 840, *Kluyvera ascorbata* MSCL 732, *Paenibacillus pabuli* MSCL 1006, isolated in Latvia, *Escherichia coli BW25113 hyaB hybC hycA fdoG frdC ldhA aceE::kan* (from prof. T.K. Wood, USA).

2. Media and experimental set up

Bacterial cultures were inoculated in 200 ml flasks containing Luria-Bertani (LB) [5 g/L yeast extract, 10 g/L tryptone, 10 g/L sodium chloride, 15 g/L Bacto agar] [11]. The flasks were aerobically shaken at 37°C for 12 hours at 150 rpm using a multi-shaker PSU-20 (BioSan, Latvia) with the exception of *Clostridium sporogenes* (cultivated in the Thioglycollate resazurin broth (Bio-Rad, France) for two days without shaking). Optical density (OD) calibration curve was used to find out number of cells in 1mL of culture [12]. The bacteria concentration in the fresh culture was 10^7 CFU/mL. The overnight culture in LB liquid medium was mixed (1:1) with phosphate buffered saline (PBS) pH 7.3 (0.8 g/l NaCl, 0.2 g/l KCl, 1.43 g/L Na_2HPO_4, 0.2 g/L KH_2PO_4) [13] in a vessel sterilized for measurements. The PBS contained a complex trace element medium pH 5.5 [0.039g/L $Fe(NH_4)_2{\cdot}SO_4{\cdot}6H_2O$, 0.172 mg/L Na_2SeO_3, 0.02 mg/L $NiCl_2$, 0.4 mg/L $(NH_4)_6Mo_7O_{24}$] [14]. Crude glycerol (98% wt/wt, determined with HPLC analysis) from biodisel fuel production was used as substrate, final concentration of glycerol used was 240 mM. Glycerol was sterilized through 0.2 µm membrane filters. Substrate was added at the start of experiment. Argon gas bubbling through the media was used to sustain anaerobic environment.

3. Analytical methods

3.1. Liquid phase analysis

Experimental test-system with separate glass chambers for simultaneous measurements and hydrogen and oxygen Clark-type microsensors (Unisense, Denmark) were used to determine hydrogen production rate in the liquid phase. Both hydrogen and oxygen microsensors were connected with the signal amplifier − a pico-ammeter and an A/D current converter connected to PC using USB port. Microsensors were calibrated in liquid culture medium for zero concentrations. Sensors were calibrated in LB medium using 99.999% pure hydrogen and 99.99% pure argon. Microsensor tip was sterilized using 96% ethanol, 0.1 M NaOH and distilled water every time when it is taken out from the sample [15].

3.2. Gas analysis

For hydrogen analysis in the gas phase the RGAPro-100 mass-spectrometer connected to the experimental test-system was used. Evolved gases were collected with the syringe from the tests system with graduated gas holder and tested qualitatively in the mass-spectrometer. Influence of partial pressure of hydrogen (pH_2) was investigated by cultivating the strains in experimental bottles with various liquid to gas ratios.

3. RESULTS AND DISCUSSION

Three facultative anaerobic bacteria strains (*Aneurinibacillus aneurinilyticus* MSCL 1018, *Kluyvera ascorbata* MSCL 732, *Paenibacillus pabuli* MSCL 1006*)*, one strictly anaerobic bacterium strain (*Clostridium sporogenes* MSCL 764*)* and one modified strain (*E. coli* BW25113 *hyaB hybC hycA fdoG frdC ldhA aceE::kan*) capability to produce hydrogen during fermentation of glycerol as substrate was investigated in different experimental systems. Bacterial strain hydrogen production rates using different substrate fermentation are shown in Table 1.

Table 1. H_2 production maximum rates with all strains and substrates

Bacterial strain	H_2 production rate in liquid phase, mmol/L/h	H_2 production rate in gaseous phase, mmol/L/h
A. aneurinilyticus MSCL 1018	0.06	0
E. coli BW25113	0.125	0.04
K. ascorbata MSCL 732	0.09	0.04
C. sporogenes MSCL 764	1.5	1.42
E. limosum MSCL 840	0.07	0.18
P. pabuli MSCL 1006	0.08	0

Hydrogen production measurements in liquid phase on the sample with different bacterial strains using glycerol as substrate are shown in Fig.1. H_2 production rate with *C.sporogenes* in liquid phase reached 1,5 mmol H_2/L/h, in gaseous phase - 1,42 mmol H_2/L/h. Hydrogen production rate is time dependent – higher rate of hydrogen production is at the fermentation process beginning when concentration increases, but after three hours of fermentation, it decreases. Measurements with *A. aneurinilyticus*, *E. limosum*, *K. ascorbata*, *P. Pabuli and E.coli* showed that these strains weren't producing substantial amount of hydrogen using crude glycerol as substrate, for example, *E.coli* BW25113 produced 0,125 mmol/L/h and *E.limosum* produced 0,07 mmol H_2/L/h. However, using 1M crude glycerol, *E.coli* BW25113 produced maximally 0,8 mmol H_2/L/h in gaseous phase (measurements were made in prototype bioreactor).

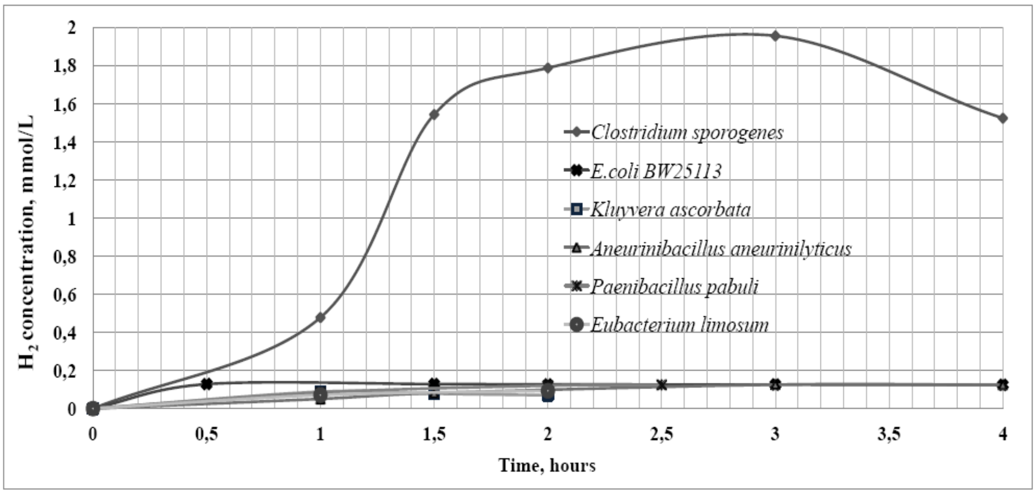

Fig. 1. Hydrogen production measurements in liquid phase on the sample with different bacterial strains using glycerol as substrate

Mass-spectrometric analysis was used to estimate hydrogen production generation results in gaseous phase as well as constancy of anaerobic conditions in the bioreactor test-system. The constancy of oxygen, nitrogen (not above 2% of total gas volume) gas concentrations evidences that the system had reliable anaerobic conditions (Fig. 2.).

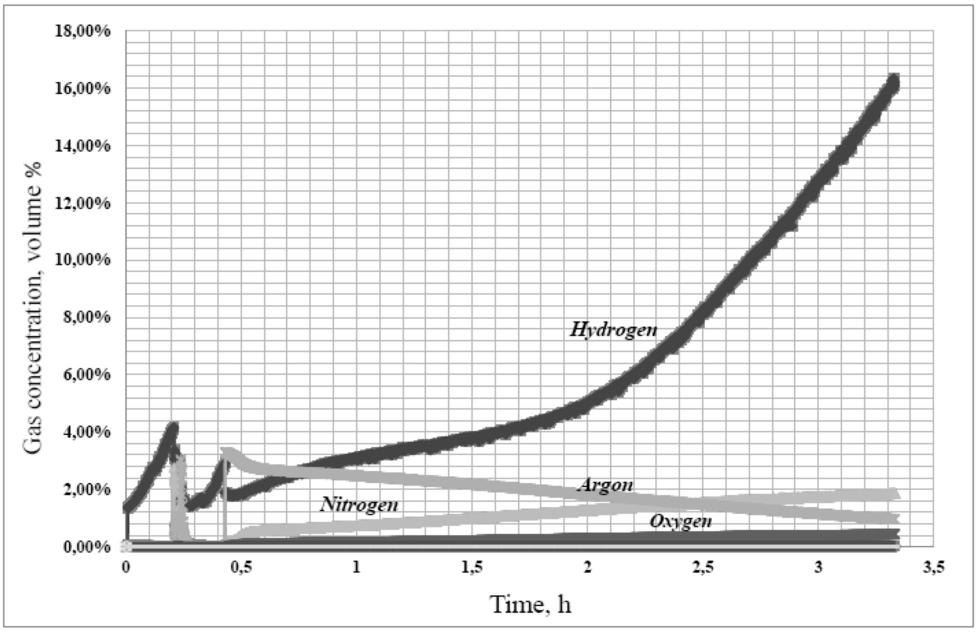

Fig. 2. Mass-spectometric analysis of the sample with bacteria *E.coli* BW25113 *hyaB hybC hycA fdoG frdC ldhA aceE*

Results with the prototype bioreactor showed that medium stirring and gas sparging has a significant impact on hydrogen production efficiency. There was an experiment carried out with discontinuous stirring, as well as discontinuous gas sparging to explore their influence on hydrogen production. Constant stirring do increase the overall hydrogen concentration and when it is turned off, the hydrogen concentration slowly decrases in overall fermentation process. In gaseous phase concentration alterations are not very obvious until the saturation is reached. However, substantial increase in hydrogen concentration in gaseous phase is achieved when inert gas sparging is maintained periodically.

4. CONCLUSIONS

Developed methods and lab-scale test systems allow adequate substrate and bacterial strain hydrogen productivity estimation. Various bacterial strains were analyzed for hydrogen generation productivity parameters using glycerol as substrate. Two of the studied bacterial strains (*Clostridium sporogenes* MSCL 764 and *Escherichia coli BW25113*, respectively) showed comparatively high results and are good candidates for further investigations of bio-hydrogen production from crude glycerol, which is a perspective substrate to be used in fermentation process: rapidly convertible, large quantities of crude glycerol available. The maximum of hydrogen production with glycerol as substrate was reached by *C. sporogenes* (1.5 H_2mmol/L/h). Test-systems were optimised to allow on-line estimation of substrate utilization and hydrogen production in liquid and gaseous phase and the factors, influencing the bacterial capability to produce hydrogen at fermentation of glycerol, as well as the possibilities to optimize the measuring process were investigated. Higher hydrogen concentration in gaseous state was achieved by using constant liquid mixing and argon gas bubbling through the cultivation medium.

5. ACKNOWLEDGEMENTS

We acknowledge the support of Latvian National Research Programme Research Program in Energetics, prof. T.K. Wood (USA) for *E. coli* BW25113, the University of Latvia for supporting this research, and the European Social Fund for the scholarship to Ilze Dimanta.

REFERENCES

1. HOLLADAY, J.D., HU, J., KING, D.L., WANG, Y. 2009. An overview of hydrogen production Technologies, *Catalysis Today*, 139, p. 244–260.
2. LEVIN, D.B., PITT, L., LOVE, M. 2004. Biohydrogen production: prospects and limitations to practical application. *International Journal of Hydrogen Energy*, 29, p. 173–185.
3. KAPDAN, I.K., KARGI, F. 2006. Bio-hydrogen production from waste materials. *Enzyme and Microbial Technology*, 38, p. 569–582.
4. ADHIKARi, S., FERNANDO, S.D., HARYANTO, A. 2009. Hydrogen production from glycerol: An update. *Energy Conversion and Management*, 50, p. 2600–2604.
5. ITO, T., NAKASHIMADA, Y., SENBA, K., MATSUI, T., NISHIO, N. 2005. Hydrogen and ethanol production from glycerol-containing wastes discharged after biodiesel manufacturing process. *Journal of Bioscience and Bioengineering*, 3, p. 260–265.
6. DHARMADI, Y., MURARKA, A., GONSALEZ, R. 2006. Anaerobic fermentation of glycerol by *Escherichia coli*: a new platform for metabolic Engineering. *Biotechnol Bioeng*., 94, 8219.
7. TRCHOUNIAN, K., SANCHEZ-TORRES, V., WOOD, T.K., TRCHOUNIAN, A. 2011. *Escherichia coli* hydrogenase activity and H_2 production under glycerol fermentation at a low pH. *International Journal of Hydrogen Energy*, 36, p. 4323-433.
8. PAUSS, A., ANDRE, G., PERRIER, M., GUIOT, R. 1990. Liquid-to-gas transfer in anaerobic processes: Inevitable transfer limitations of methane and hydrogen in the biomethanation process. *Appl. Environ. Microbiol., 56,* p. 1636–1644.
9. REVSBECH, N. P., JØRGENSEN, B.B. (1986). Microelectrodes: Their Use in Microbial Ecology. *Advances in Microbial Ecology, 9*. New York: Plenum, p. 293−352.
10. KLEPERE, I., MUIZNIEKS, I., KLEPERIS, J. 2010. A bacterial hydrogen production test system for measuring H_2 concentrations in liquids and gases. *Latvian Journal of Physics and Technical Sciences,* 2, p. 60–68.
11. ATLAS M. R. 2004. *Handbook of microbiological media*, Luria Bertani media: Handbook of microbiological media (3rd ed-n). CRC Press, p. 942.

12. WIDDEL. F. 2007. *Theory and measurement of Bacterial growth*, Grundpraktikum Mikrobiologie, 4. Sem. (B.Sc.). Bremen: Universität Bremen.
13. PENFOLD, D.W., FORSTER, C.F., MACASKIE, L.E. 2003. Increased hydrogen production by *Escherichia coli* strain HD 701 in comparison with wild-type strain MC4100. *Enzyme and Microbial Technology,* 33, p. 185–189.
14. MAEDA, T., SANCHEZ-TORRES, V., WOOD, T.K. 2008. Metabolic engineering to enhance bacterial hydrogen production. *Microbial Biotechnol*., 1, 30–39.
15. UNISENSE A/S 2007**.** Hydrogen sensor manual**,** Micro-Respiration System manual,. Denmark:, 19 p.

CYSENI 2012, May 24–25, Kaunas, Lithuania
ISSN 1822-7554, www.cyseni.com

STUDY OF SURFACE TOPOGRAPHY EFFECTS INITIATED BY TREATMENT OF THIN TI FILMS IN WATER PLASMA

K. Gedvilas, L. Pranevičius
Vytautas Magnus University
Vileikos st. 8, LT-44404, Kaunas, Lithuania
Email: k.gedvilas@gmf.vdu.lt

ABSTRACT

The changes of surface topography of thin Ti films induced by interaction of ions extracted from low-pressure water vapour plasma are studied. Titanium 0.2 - 0.7 µm thickness films were deposited on silicon wafer substrates using magnetron sputter deposition technique and immersed in water vapour plasma at pressure of about 10 Pa. It is shown experimentally that surface roughness increases and depends on the intensity of radiation. The root mean square roughness increased from the 5 nm for as-deposited Ti film up to 464 nm after its plasma treatment at 300 W for 20 min. The roughening mechanisms and dominant processes are discussed. The presented results are explained on the basis of the formation of oxide phases synthesized in the near-surface region of Ti film

Keywords: Titanium; Water vapour; Plasma; Surface roughness

1. INTRODUCTION

Due to the enormous variety of applications, from photocatalysis to medicine, the studies of titanium and its alloys is a continuously growing field of research [1–4]. For instance, metallic Ti is a key material in aircraft construction [5] and its malleability and chemical activity promotes its use as a better material [6]. On the other hand, its large biocompatibility comes from the formation of a surface oxide layer and the catalyst capability is also related to the properties of the metallic Ti films grown on it [7, 8]. Thus, the interest goes from metallic Ti to its different oxides, including the chemical behaviour of the different metal–metal and metal–oxide interfaces. It is well known that oxidation of titanium is modified by water vapor present in oxidant environment. Such changes might consist of microstructural changes in the scale, enhancement or decrease in the oxidation rate and changes in transport processes through the oxide. Thin oxidized films exhibit physical properties differing with those from related nanopowder and bulk materials. These particular physical properties mainly originate from: the presence of mixed crystalline and/or amorphous oxide and metal phases, film residual stresses due to some degree of disparities in film-substrate thermal properties, crystallite grain size, crystallite orientation and non-stoichiometry [9,10]. It results from both the oxidation method and the concomitant two-dimensional nature of the films. The lateral expansion of TiO_2 induces surface roughening.

The fundamental difference with respect to nanopowder materials is the presence of a substrate which might alter kinetics and thermodynamics of the processes. Thin film is clamped to the substrate and therefore cannot expand freely in the in-plane direction as oxidation proceeds in it. Adhesion forces at the film–substrate interface act in opposite direction to prevent the expansion of the film, creating considerable in-plane stresses of the order of several GPa. Consequently, oxidation of thin metallic films induces higher stresses than oxidation of bulk metals. It generates large compressive in-plane stresses, microstructural defects and ultimately large plastic deformations.

Usually nucleation rates of new oxide phases depends on free energies which are extraordinary sensitive to the conditions under which the experiment is run: pressure, impurity concentrations as well as temperature. According the nucleation model, when the concentration of oxygen reaches a critical value, the rearrangement of the lattice with the eventual formation of small grains of oxide occures. The small grains of oxide grows by inward diffusion of the oxygen ions and/or inward diffusion of metal ions. Eventually, these grains grow to the extent that their boundaries overlap, resulting in a particle oxide core. Reproducibility of experimental data is difficult to achieve and the theoretical prediction of oxidation rate is subject to large uncertainties. It is therefore of primary importance to understand effects of the intrinsic properties related to film thickness.

Oxidation of thin Ti surfaces in water vapour results in the formation of a nanostructured hydrated titanium oxide layer. The neutral water molecules arriving to the surface from the water vapor oxidize Ti atoms ($Ti_xO_y + (2x\text{-}y)H_2O = xTiO_2 + (2x\text{-}y)\ H_2$). These possible oxidation reactions are highly thermodynamically favourable. The oxidation reactions in water vapor form molecular H_2 (not atomic H)) [11]. In this way, the oxidized surface layer is enriched by H atoms arriving from plasma and H_2 molecules as reaction by-products. The H_2 molecules tend to diffuse out of the oxidized layer. The atomic H moves in the oxide layer, until it either reacts with an oxide, or encounters another atomic H to recombine into H_2 and diffuses out of the oxide. The lateral expansion of TiO_2 induces surface roughening [11,12]. The mechanism by which the oxide influences hydrogen permeation into Ti is still not well established.

In this work we study the changes of surface topography of Ti films initiated by plasma treatment under low and high-flux irradiation by ions extracted from water vapor plasma.

2. EPERIMENTAL TECHNIQUE

Titanium 0.2–0.7 µm thickness films were deposited on silicon (111) substrates using magnetron sputter-deposition technique in PVD-75 vacuum system. After deposition thin film Ti samples were taken away from the sample holder and placed on the top of the magnetron at the titanium cathode. The titanium magnetron was water cooled. After evacuating the chamber down to 10^{-2} Pa, the vapor of distilled water was injected and the plasma generator was activated at a power in the range of 50–300 W. The electron temperature for this water vapor plasma source is between 1.5 and 4 eV.

All samples were divided into two main groups by the thickness of Ti film: (i) thin (200–300 nm thickness) and (ii) thick (600–700 nm thickness). The samples of these main groups were additionaly divided into two subgroups according to the intensity of their irradiation: (i) low-flux (the ion current density to the sample of about $1\mu A/cm^2$), and (ii) high-flux (the ion current density about $10 mA/cm^2$). The samples affected by low-flux ion irradiation are denoted by the letter L, and the samples affected by the high-flux ion irradiation - by the letter H.

The thickness and surface topography of Ti films were measured using the nanoprofilometer (AMBIOS XP 200). The mean surface roughness depth (Rz) was evaluated as the average height of the peak-to-valley values calculated over the all scanned length. It corresponds to Rz ISO standard called “Ten Point Average Roughness”. The average height value is calculated using values of 5 highest peaks (Y_p), and 5 deepest valleys (Y_v), as expressed by Eq. 1 and shown in Fig. 1.

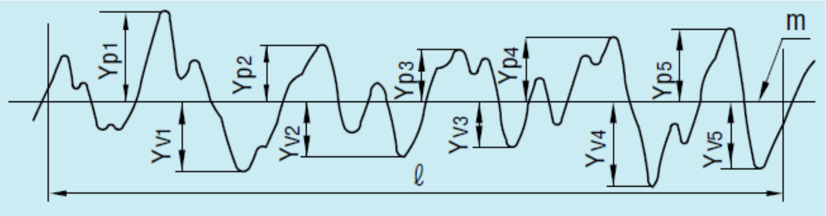

Fig. 1. Ten-point mean roughness (Rz)

$$Rz = \frac{|Y_{p1}+Y_{p2}+Y_{p3}+Y_{p4}+Y_{p5}| + |Y_{v1}+Y_{v2}+Y_{v3}+Y_{v4}+Y_{v5}|}{5} \qquad (1)$$

In this study, Rz has been calculated over the entire scanned length as

$$Rz = \frac{|\sum Y_{pi}| + |\sum Y_{vi}|}{n}, \qquad (i = 1..n) \tag{2}$$

Another widely used surface roughness parameter – Rq (root mean square) was calculated as

$$R_q = \sqrt{\frac{1}{n}\sum_{i=1}^{n} y_i^2} \tag{3}$$

The mean surface roughness of the sample was calculated over the fixed lenght of profile which was equal to 1 mm.

The surface views before and after plasma treatment were investigated by the scanning electron (SEM, JEOL JSM – 5600) and optical microscopes. The elemental composition of plasma treated films was analyzed by energy dispersive X–ray spectroscopy (EDX, Bruker Quad 5040).

3. RESULTS

Figs. 2–5 illustrate typical profiles of surface topography and SEM surface views for different samples: Fig. 2 – as-deposited titanium film, Figs. 3 and 4 respectively for thin and thick Ti films after plasma treatment for 20 min at 300W (a - low, and b – high-flux radiation), and Fig. 5 – thick Ti film after plasma treatment for 60 min at 50W (high ion flux radiation), respectively.

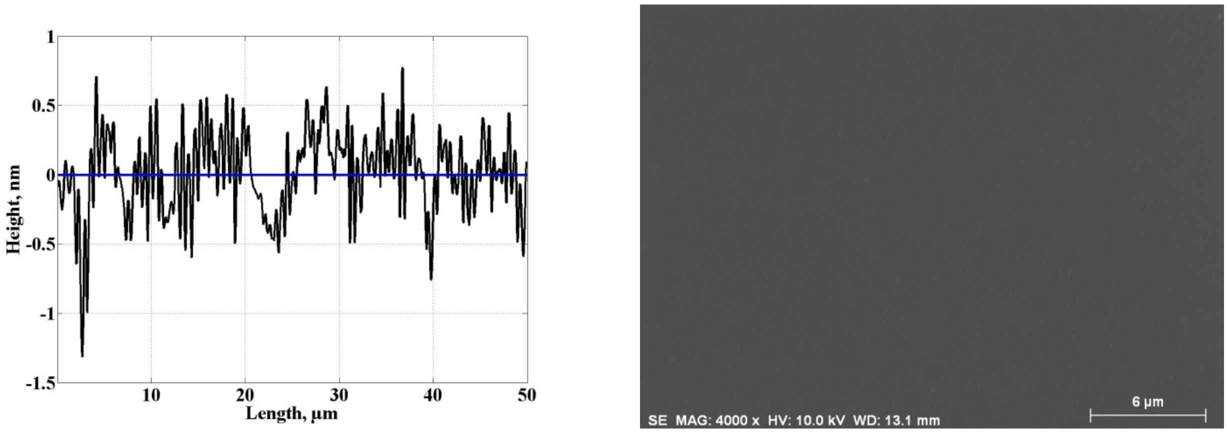

Fig. 2. Surface topography and SEM surface view of as-deposited titanium film

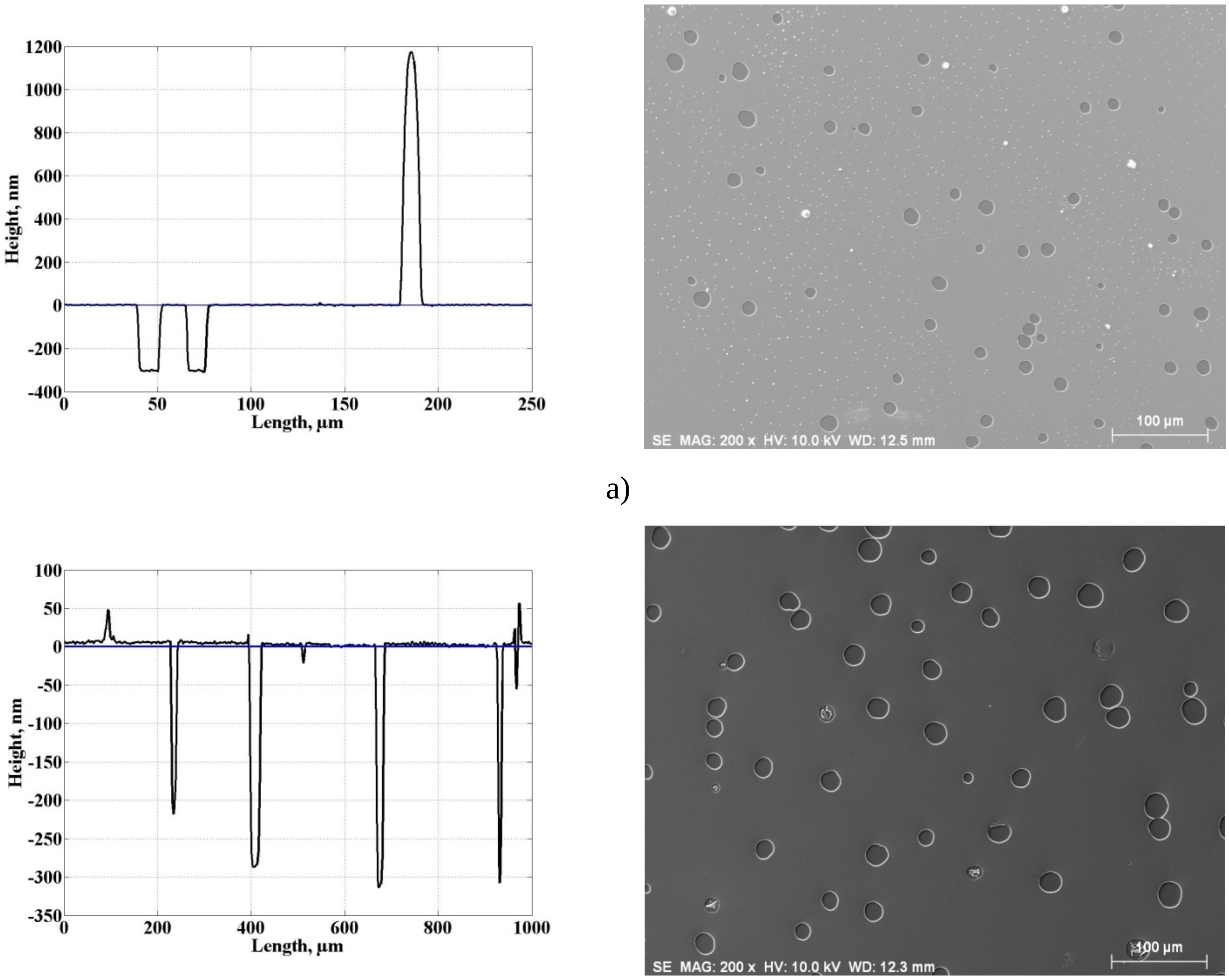

a)

b)

Fig. 3. Surface topography and SEM surface view of plasma treated thin Ti film for 20 min at 300W under a) high and b) low-flux ion irradiation

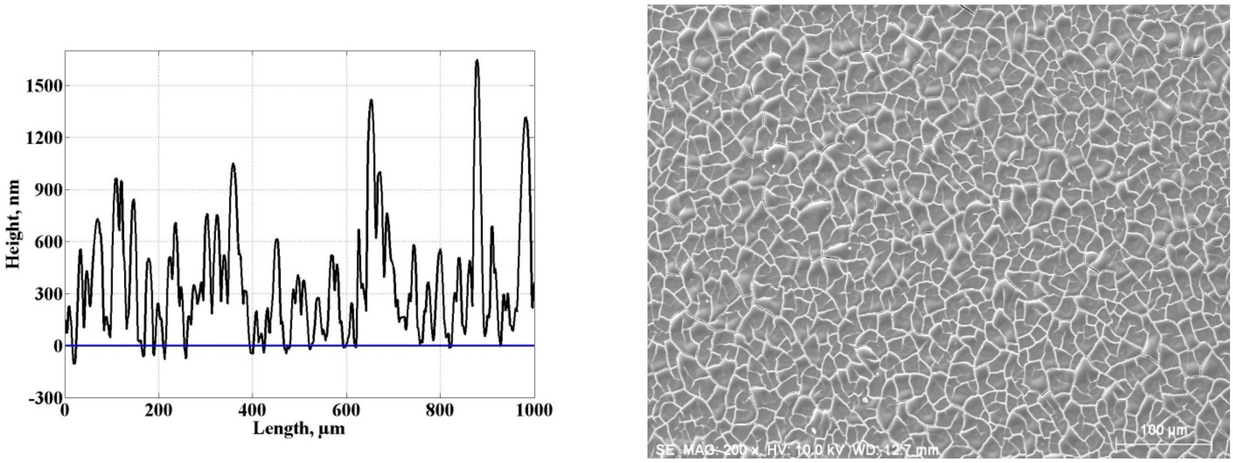

a)

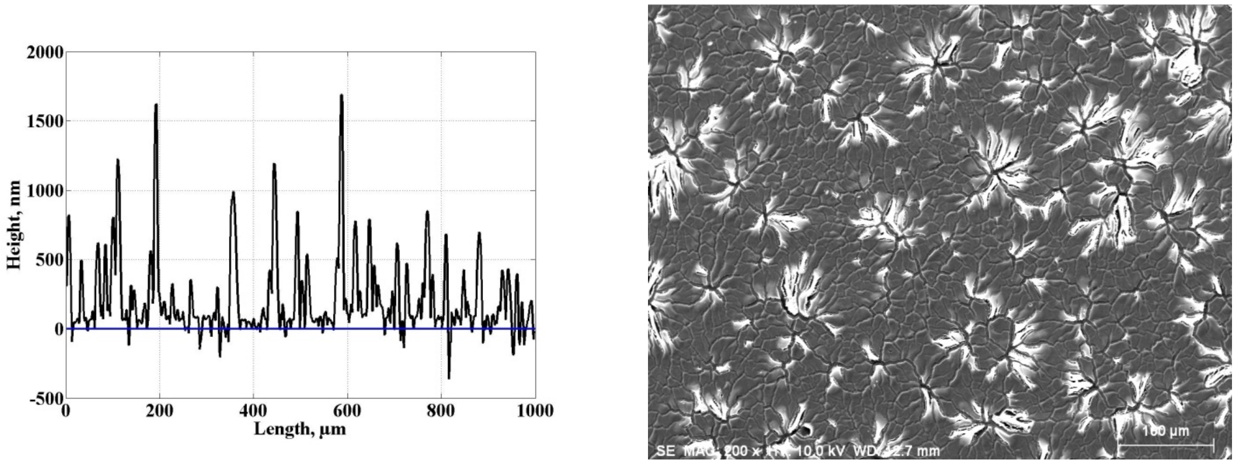

b)

Fig. 4. Surface topography and SEM surface view of plasma treated thick Ti film for 20 min at 300 W affected by a) high and b) low flux ion-radiation

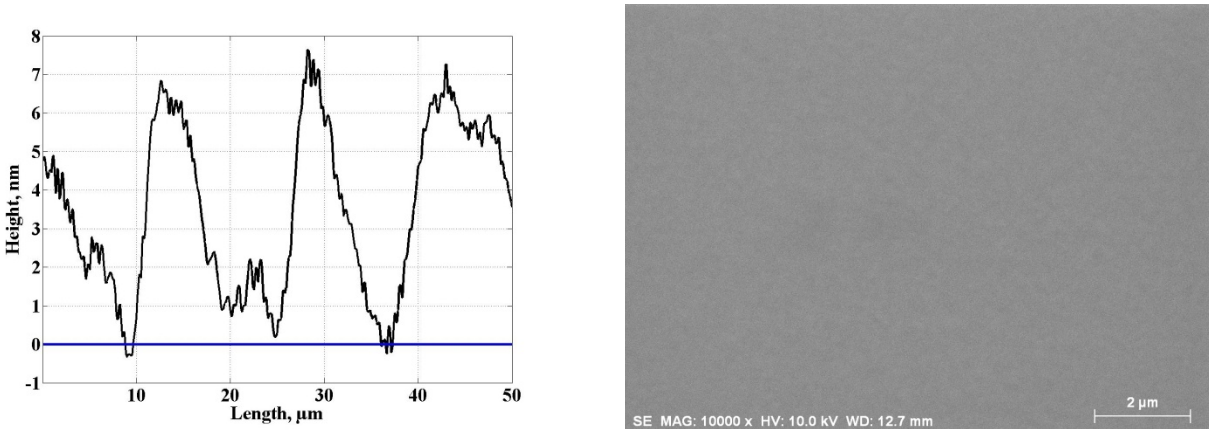

Fig. 5. Surface topography and SEM surface view of plasma treated thick Ti film for 60 min at 50 W under high-flux ion irradiation

Tables 1 and 2 summarize surface roughness measurement results for thin and thick Ti films, respectively.

Table 1. Results of surface roughness of thin Ti films

Thin Titanium films			Roughness difference before and after treatment (R_after - R_before), nm			
Plasma power, W	Time, min	Sample No.	H, Rz	L, Rz	H, Rq	L, Rq
200	5	1	4.4	2.7	5.7	-0.3
	20	2	24.3	-0.1	57.2	2.3
300	5	3	180.9	47.3	147.3	49.9
	20	4	74.8	38.8	136.5	57.9

Table 2. Results of surface roughness of thick Ti films

Thick Titanium films			Roughness difference before and after treatment (R_after - R_before), nm			
Plasma Power, W	Time, min	Sample No.	H, Rz	L, Rz	H, Rq	L, Rq
20	60	5	3.1	3.6	2.8	2.6
50	60	6	-0.3	5.8	-3.8	-0.4
300	20	7	564.7	885.7	223	464

Plasma treatment parameters, such as duration and power dissipated in plasma, are included in the tables. Letters L and H indicate low and high-flux treatment modes, respectively. For all as-deposited Ti films, the average surface roughness is equal to about 4.5 nm for Rz and about 4 nm for Rq. It is seen that almost for all cases the surface roughness increases after plasma treatment. It was registered that the mean surface roughness increases significantly after exposition in high-density water vapour plasma at 300 W: to 181 nm(Rz) for thin and to 886 nm (Rz) for thick Ti film. However, we observed that changes of surface roughness are different for samples treated by low and high-flux ion irradiation: for thin films, roughness is higher for Ti film areas treated by high-flux than for areas treated by low-flux irradiation (Table 1, samples 3 and 4), and for thick films – conversely, roughness is higer for areas treated by low-flux than for areas treated by high-flux irradiation (Table 2, sample 7). The same trend is registered and for other plasma processing power parameters (Tables 1 and 2, samples 1, 2, 5 and 6). This fact is considered as the manifestation of the formation of new oxide phases in the near surface region of Ti film. It was observed that after the exposition in low density water vapour plasma at 50 W for 60 min the Ti film surface becomes periodically bumpy (Fig.5) with height amplitude equal to 8 nm and period equal to around 15-18 µm. After the exposition of Ti fim in highly ionized water vapour at 300 W for 20 min, thin film becomes holey (Fig.3). The mean diameter of holes corresponds to the size of water island layers and theirs height is equal to the film thickness of 300 nm. When the film is thick, the observed buckle-and-crack network (Fig.4) can be attributed to TiO_2 phase precipitation within the Ti film. Presumably, the atomic oxygen interacts at the sites formed during film bulk cracking process and produces M-O links which, in turn, activates formation of new cracks. Therefore, spontaneous film cracking may be maintained by the oxidation process. The generation rate of new sites for oxygen rather than the strain may be the major factor for oxidation kinetics. These observations can be analyzed on the basis of recent understanding about the dynamic properties of adsorbate and the transport of adsorbed particles along grain boundaries of nanometer size materials [10, 11]. As rapid uptake of oxygen and hydrogen through the grain boundaries in open contact with the hydrogen occurs, plastic deformation and grain fragmentation take place with lateral slow inward diffusion of reactive atoms through the grain boundaries. The high compressive stresses lead to film detachment in a form of buckling. The structure eventually fails by adhesive film debonding from the surface of the substrate.

Surface views show that oxidation is favored on surfaces containing defects. There is a suggestion that the water adsorption on the surface of growing oxide islands acts to form a more permeable scale and thus allow gas access and thereby enhances the H and O permeation rate. An important observation is that whisker formation is encouraged. It is possible that the tip of the whisker is catalytically active in promoting dissociation of the oxidant. The protrusions evolve even under very mild plasma conditions. The surface protrusions dictate the nucleation and subsequent oxidation of a Ti film by promoting the development of a three-dimensional granular morphology in the coating.

The oxidation rate of surface areas uncovered by water island layers is significantly less. A wide range of interference colours appear on the surface, showing that maximum oxide thickness is of the order of hundred of nanometres. Analysis of these samples by SEM-EDS and optical microscope show that some colouration indicates reduced oxygen content. The sunset-yellow colour has an O/Ti ratio of 1.3. The rose layer has an O/Ti ratio of 1.5. The dull grey colouration have samples of ratio 1.6-1.7. The light beige with a grey tinge underneath has an O/Ti ratio of about 1.8-1.9, and stoichiometrically oxidized Ti films have the white colouration.

4. DISCUSSIONS

For incident ions extracted from water vapor plasma, the altered chemical composition of the surface layers leads to changes in surface topography. At high fluences, a saturation concentration of trapped ions is reached, which is determined by a balance among the incident ion flux, the diffusion of the implanted ions into the bulk, the flux of backscattered and removed due to sputtering atomsIt is necessary to divide the surface topography changes on the microscopic (atomic) and macroscopic level. The development of surface structures is closely related to the range and trapping mechanism of implanted gas ions and to the properties of the gas-solid system. It means that the development of surface geometry depends on the type and energy of incident ions. In the range of low ion energies and heavy ions, penetration process is negligible and sputtering process prevails in the formation of surface geometry. It will produce the rearrangement of the first atomic layer and the appearance of micro non-homogeneities.

It is known that titania coating exposed to ultraviolet light have the extraordinary property of complete wettability for water. The plasma radiation removes some of the oxygen atoms from the surface of the titania, resulting in a patchwork of nanoscale domains where hydroxyl groups became adsorbed, which produces the superhydrophilicity. The outermost layer becomes highly defected and new pathways for the transport of water molecules and hydrogen atoms become possible. Impinged water clusters adsorb on the bare surface and spread laterally across the surface driven by superwettability effects. Water molecules and clusters are not reflected on the water islands and in the presence of plasma radiation due to water supper-hydrophilic properties converge to thin film rapidly. Irradiation of wetted surface areas leads to the split of hydroxyl radicals, resulting from dissociation of water molecules and oxidation of Ti, into their atomic components hydrogen and oxygen [11,12]. The mobile H atoms in TiO_2 are trapped at radiation defects while the H atoms detrapped from trapping centers diffuse through the oxide layer into the bulk and, taking into account titanium's high affinity for hydrogen, are absorbed by the titanium, and consequently are stored in the bulk. One of the reasons why atomic hydrogen is limited in its ability to reduce titanium oxides is that H atoms may use the oxide surface as a catalyst for recombination to molecular hydrogen rather than reacting with oxide. The trapping process dominates in the defected shallow implant zone.

Water vapor plasma treated titanium has been shown to cleave. Cutting in the form of "popping off" discrete blisters was observed. The location of the cut correlates well with the wetted areas and can be explained by damage induced in-plane stress and the corresponding elastic out-of-plane strain. One of the main issues concerning their mechanical performance is the type and magnitude of residual stresses around the crystalline precipitates. These stresses arise due to the thermal and elastic mismatch between the crystalline precipitates and the matrix. Residual stresses may or may not generate microcracks around the precipitates depending on their magnitude and crystal size.

In view of both fundamental physical interest and substantial technological interest the problem of surface topography after ion irradiation is still not resolved. Important role of surface topography for the mechanism of heterogeneous processes in plasma environment requires deeper understanding of the physics of generation of surface defects and the development of surface topography.

5. CONCLUSIONS

It is shown experimentally that surface roughness of Ti films increases after treatment in water vapor plasma. The initial stages of the development of surface structures on the initially smooth surface (on the atomic scale) are determined by the stochastic nature of the sputtering process. The evolution of surface roughness depends on the intensity of irradiation. The roughening mechanisms and dominant processes are discussed. The comparative analysis of surfaces affected by high and low-flux ion irradiation have been conducted. In all cases, initially smooth surfaces become rough after plasma irradiation, especially when Ti films are affected by highly ionized water vapour at 300 W. The root mean square rougness increased from the 5 nm for as-deposited Ti film up to 464 nm after its plasma treatment at 300 W for 20 min.

ACKNOWLEDGEMENT

This research was funded by a grant (Nr. ATE-02/2010) from the Research Council of Lithuania. The authors are grateful for the support of the Lithuanian Energy Institute and Vytautas Magnus University administration.

REFERENCES

1. U. DIEBOLD and T. MADEY Surf. Sci. Spectra 4 (1996), p. 227.
2. J. POUILLEAU, D. DEVILLIERS, F. GARRIDO, S. Durand-Vidal and E. MAHE Material Science. Eng. B 47 (1997), p. 235.
3. G. LASSALETTA, A. FERNANDEZ and A. GONZALEZ-ELIPE J. Electron Spectr. Rel. Phen. 87 (1997), p. 61,
4. Q. GUO, W. OH and D. GOODMAN Surface science. 437 (1999), p. 49.
5. S. SHEVELL, *Fundamental of Flight*, 2nd Edition, Prentice-Hall, Englewood, Cliffs, NJ, 1989.
6. J. HANRA J. VACUUM Sci. Technol. 13 (1976), p. 471.
7. U. MULLER and R. HAUERT *Thin Solid Films* 290–292 (1996), p. 323.
8. J. BIENER, M. BAUMER, J. WANG and R. MADIX Surf. Sci. 450 (2000), p. 12.
9. M. DORNHEIM, S. DOPPIU, G. BARKHORDARIAN, U. BOESENBERG, T. KLASSEN, O. GUTEISCH and R. BORMANN Hydrogen storage in magnesium-based hydrides and hydride composites. Scr. Mater.: 56 (2007), Nr. 10, p. 841-846
10. A.I. LIVSHITS, F. SUBE, M.N. SOLOVYEV, M.E. NOTKIN, and M. BACAL *Plasma driven super permeation of hydrogen through group via metals*. Journal of Applied Physics: Vol. 84 (1998), p. 2558
11. P. PEREZ, On the influence of water vapour on the oxidation behaviour of pure Ti, Corrosion Science 49 (2007) p. 1172-1185.
12. J. A. CHAPMAN, E. F. KIRKNESS, O. SIMAKOV, Chemistry: water splitting, Nature, 464 (2010) p. 468.

CYSENI 2012, May 24–25, Kaunas, Lithuania
ISSN 1822-7554, www.cyseni.com

ON OXIDATION MECHANISM OF Ti FILMS IN WATER VAPOUR PLASMA

M. Urbonavicius, D. Girdzevicius, T. Rajackas, S. Tuckute, L.L. Pranevicius
Vytautas Magnus University
Vileikos str. 8, 44404 – Lithuania
Phone+370 643 63871
Email: marius.urbonavcius@fc.vdu.lt, dalius
girdzevicius@fc.vdu.lt,
tomas.rajackas@fc.vdu.lt

ABSTRACT

Titanium oxide is widely used in industry for its good mechanical, electrical and optical properties. Physical vapour deposition is a method that enables us to obtain the layers with desirable properties. The aim of this research is to oxidize titanium using water vapour plasma immersion ion implantation (PIII) technology and to develop the understanding about the mechanism of oxygen transport in Ti film. Samples were characterized after treatment at different dissipated power in plasma levels and durations. All of them have been analyzed by nanoprofilometer, SEM (scanning electron microscopy), EDS (energy dispersive X – ray spectroscopy), AES (Auger electron spectroscopy), GDOES (glow discharge optical emission spectroscopy), XRD (X – ray diffraction).

A deep penetration of oxygen was observed in plasma treated titanium films after theirs exposition during 5–60 min using AES analysis. XRD analysis reveals the formation of new phases: TiO_2 and non – stoichiometric TiO_x peaks were identified. Different O/Ti ratio values in the film areas affected by different intensities of plasma radiation have been registered by EDS. EDS results are in agreement with results of film resistivity analysis performed using four – point probe resistivity method.

It is shown that the titanium oxidation rate strongly depends on the surface coverage by adsorbed water layers and RF power dissipated in plasma. Plasma radiation activates surface of titania, promotes its superwettability properties and drastically increases the rate of oxidation whereas hydroxyl (OH) radicals are the main oxidant. Furthermore, there are other processes which determine oxygen permeation and transportation mechanism during PIII of water vapour. Such processes are oxygen adsorption, trapping, type and structure of Ti film, presence of Ti^{n+}/oxygen vacancies, and etc.

Keywords: *Ion implantation, water vapour plasma, oxygen transport, electrical resistivity, oxidation*

1. INTRODUCTION

There is a considerable interest in titanium dioxide (TiO_2), because of its availability, nontoxicity, physical and chemical stability, relatively low price and astonishing properties [1]. Recently, a lot of attention is paid to titanium dioxide thin films due to their potential in several applications. Today TiO_2 is used as an important environmental material in the field of air and water purification, fabrication of self-cleaning and antibacterial surfaces.

This material is widely discussed in the area of environmental photocatalysis and area of photoinduced hydrophilicity, which can lead not only to self-cleaning surfaces, but also antifogging ones [2]. It's photocatalytic features is used in degradation of organic macromolecules and pollutants, eliminating odours, bacteria, moulds [4]. The capacity of TiO_2 surface to decompose water can be used in hydrogen production, which is ideal clean energy and raw material for industry. Today hydrogen is basically produced by steam reforming of methane. Photocatalytic water molecule splitting into hydrogen and oxygen is a challenging reaction, but it could be breakthrough in energy and environmental fields [3].

The photoactive and photocatalytic characteristics of titanium dioxide may be modified by changing its physical properties such as particle size, crystallinity, crystal structure [5]. They also depend on bulk defect density, impurities, surface area and film thickness. The surface reactions and mechanisms have been broadly studied since the photocatalytic effect was discovered [6-8]. So it is important to understand the mechanism of titanium oxidation, the rate of oxide growth and structure.

We used water vapor-plasma immersion ion implantation (PIII) as a method to oxidize titanium. It is known that the main oxidants are hydroxyl radicals in water vapour plasma [9-10]. The treatment of Ti surface in water vapour plasma results the formation of adsorbed inhomogenous OH layer on the surface and oxidation of Ti [11]. During the plasma treatment titanium coatings are irradiated by ultraviolet radiation (UV) and ionic bombardment [12]. Titania exposed to UV has great wettability for water because of removal of some oxygen atoms from the surface [2]. Also, oxygen atoms are preferentially sputtered due to ballistic processes induced by energetic incident ions. Water molecules are adsorbed dissociatively on the surface of plasma activated titania. Oxygen atoms are used to oxidize near-surface layers of Ti film, while mobile H atoms leave TiO_2 layer and are accommodated in the bulk of Ti film or at the film- substrate interface.

In this paper, the effects of titanium surface coverage with adsorbed water molecules and power dissipated by energy source in plasma on the titanium oxidation is studied and the Ti oxidation mechanism is discussed.

2. EXPERIMENTAL

2.1. Oxidation technique

A direct current (DC) magnetron sputtering deposition (MSD) was used to form titanium films on monocrystalline silicon substrates. This method was used, because of high adhesive strength and homogeneous film thickness distribution. Fabricated Ti films were 300–550 nm thickness approximately. Kurt J. Lesker company‘s PVD – 75 vacuum system was used. We chose plasma ion immersion implantation (PIII) as a method for titanium film oxidation. Samples were located on the surface of Ti magnetron cathode (Fig. 1).

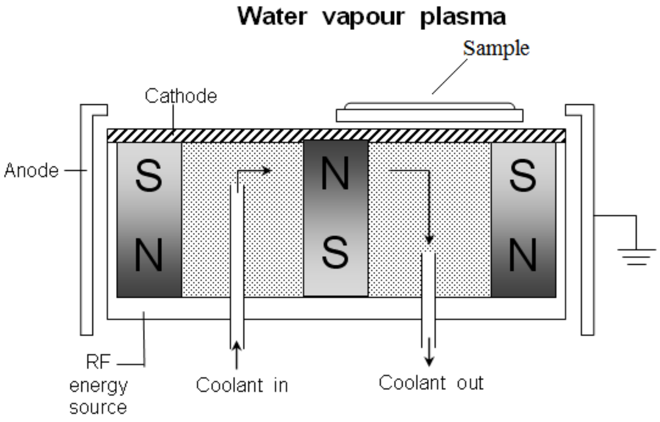

Fig. 1. The location of sample on the magnetron cathode

The vacuum chamber was evacuated to a base pressure of about $2{\cdot}10^{-4}$ Pa. Pure water (ph=7) vapour was injected into the vacuum chamber using mass flow controller, which maintained a constant vapor flow rate. Water vapour PIII treatment was carried out at a working pressure of 10 Pa. RF energy source sustained plasma at 20-300 W power.

2.2. Analysis methods

Surface height topography of Ti films was measured using the nanoprofilometer (AMBIOS XP 200). The microstructure of the samples was characterized by X - ray diffraction (XRD) method using Bruker diffractometer (Bruker D8). The measurements were performed using 2θ angle in the range 20° – 70° using Cu Kα radiation in steps of 0.01°. The identification of peaks has been done using EVA *Search – Match* software. The surface views before and after water vapour plasma treatments were investigated by the scanning electron (SEM, JEOL JSM – 5600) and microscopy. The elemental composition of plasma treated films was analyzed by energy dispersive X–ray spectroscopy (EDS, Bruker Quad 5040). The distribution profiles of O in Ti films were measured by Auger Electron Spectroscopy (AES, PHI 700XI AUGER NANOPROBE) and by glow discharge optical emission spectroscopy (GDOES, Spectruma Analytic GMBH). Electrical conductivity of plasma treated Ti films was measured using four – point probe method (Jandel universal probe).

3. RESULTS

Fig. 2 shows the XRD patterns of as-deposited and plasma treated samples (about 450 nm thickness). Samples were treated in water vapour plasma at 200 W (Fig. 2a) and 300 W (Fig. 2b) RF power for 5 min. Spectrum of as-deposited titanium film did not show any peaks except silicon substrate peak. It is typical for amorphous titanium. XRD patterns of samples treated at 20 W and 50 W seem almost the same like as-deposited titanium. Peaks of TiO, $TiO_{0.48}$ and TiO_2 were registered plasma treated samples at at 200 W. TiO_2, Ti_3O_5 and $(H_2O)Ti_4O_7(OH)_2$ peaks were identified at 300 W withTiO_2 phase as predominant. The changes of microstructure were observed even after plasma exposition during 5 min.

The oxidation rate of titanium in water vapour plasma mainly depends on the RF power dissipated in plasma. With the increase of dissipated power the oxidation rate increases. More oxygen diffuse into the bulk and TiO phase gradually changes to the most chemical stable phase – TiO_2 (rutile) Superwettability effect depends on plasma radiation intensity [2]. The UV radiation and ionic bombardment intensity is increasing with power, which means higher rate of surface activation and better superwettability. Therefore oxidation rate increases accordingly.

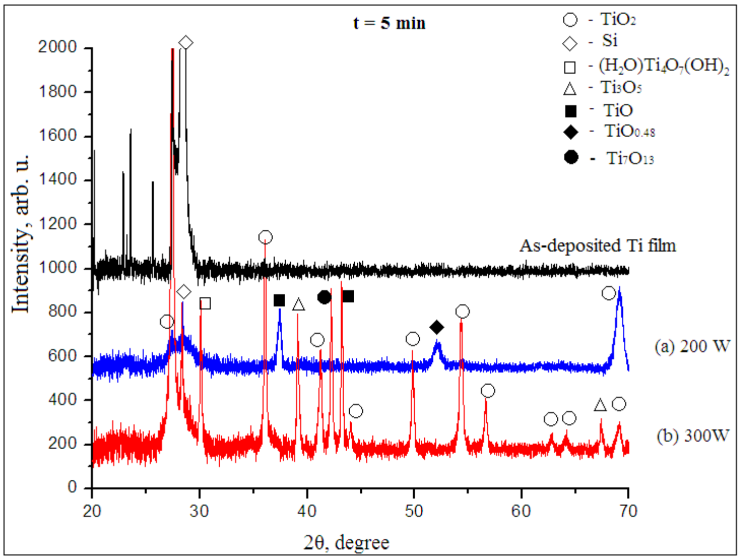

Fig. 2. XRD paterns of amorphous as-deposited Ti film and after water vapour plasma treatment a) at 200 W and b) at 300 W. Plasma treatment time is 5 min.

Fig. 3 shows SEM views of as-deposited (Fig. 3a) and plasma treated samples (Fig. 3 b-f). The surface views seem unchanged for samples treated at 50 W for 60 min. With the increase of the

RF power dissipated in plasma, more holes crossing entire film thickness (Fig. 3 c-e) and blisters (Fig. 3f) was observed. They are result of water island layers formed by adsorbed water molecules and water clusters which are injected through a nozzle into a vacuum chamber. The inhomogenous surface coverage with water island layers forms different boundary conditions for oxidation of areas covered and uncovered by water layers. Preliminary results show that hydrogen during oxidation diffuses through TiO_2 layer and is accommodated at the boundary of substrate-film tending to form gas blisters. Stored hydrogen generates high stresses which lead to film detachment from the substrate. It was observed that after treatment at 300 W (Fig. 3e) some islands coalescence and the size of holes increases.

A wide range of interference colors appear on the surface of treated samples, showing different hues and saturations. Various colors indicate to the different oxygen concentration in the coating. EDS analysis showed that values of O/Ti ratio varies from 1.3 to 2.1 in dependence of RF dissipated power and treatment duration (Table 1).

Table 1. Plasma treatment conditions and EDS results

Sample	A	B	C	D	E
P, W	50	200	200	300	300
t, min	60	5	20	5	20
Thickness, nm	510	410	440	350	400
EDS, O/Ti ratio	1.3	1.7	1.7	2.1	1.9

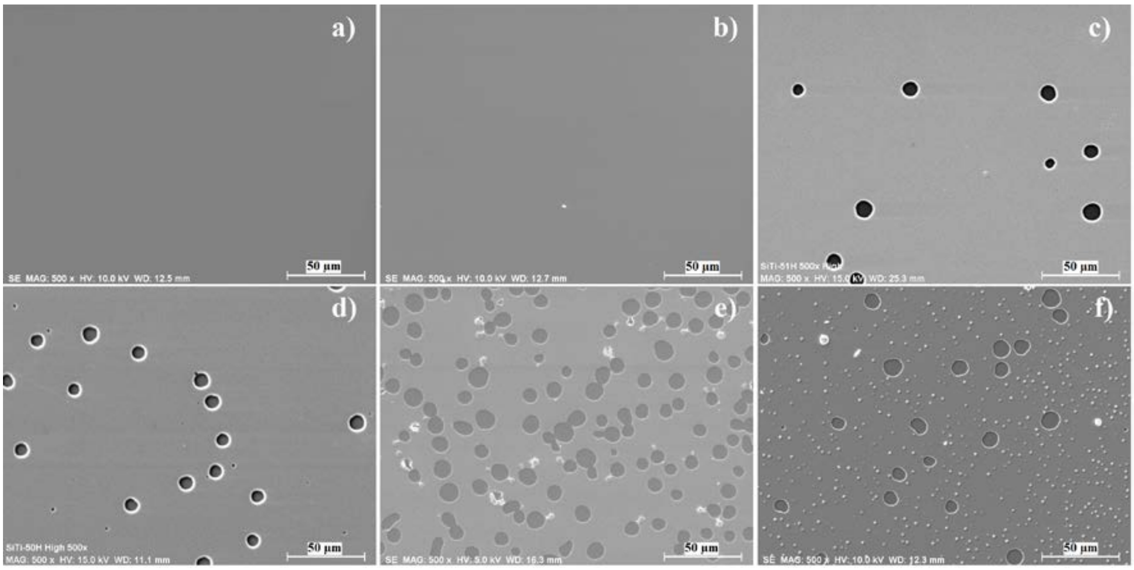

Fig. 3. SEM views of Ti surface: a) as-deposited Ti; and treated b) 50 W, 60 min; c) 200 W, 5 min; d) 200 W, 20 min; e) 300 W, 5 min; f) 300 W, 20 min.

Fig. 4 includes Ti film surface topography height profiles measured by nanoprofilometer: a) as-deposited, and treated b) 50 W, 60 min, c) 200 W, 5 min, d) 200 W, 20 min, e) 300 W, 5 min and f) 300 W, 20 min. Holey and bumpy surface was registered after plasma treatment at 200 and 300 W. Surface topography did not change after treatment at 50 W (Fig. 4b). Height of holes is equal to the entire thickness of Ti film (about 450 nm) (Fig. 4 c-e). Height amplitude of bumpy surface is equal to about 21 nm (Fig. 4d).

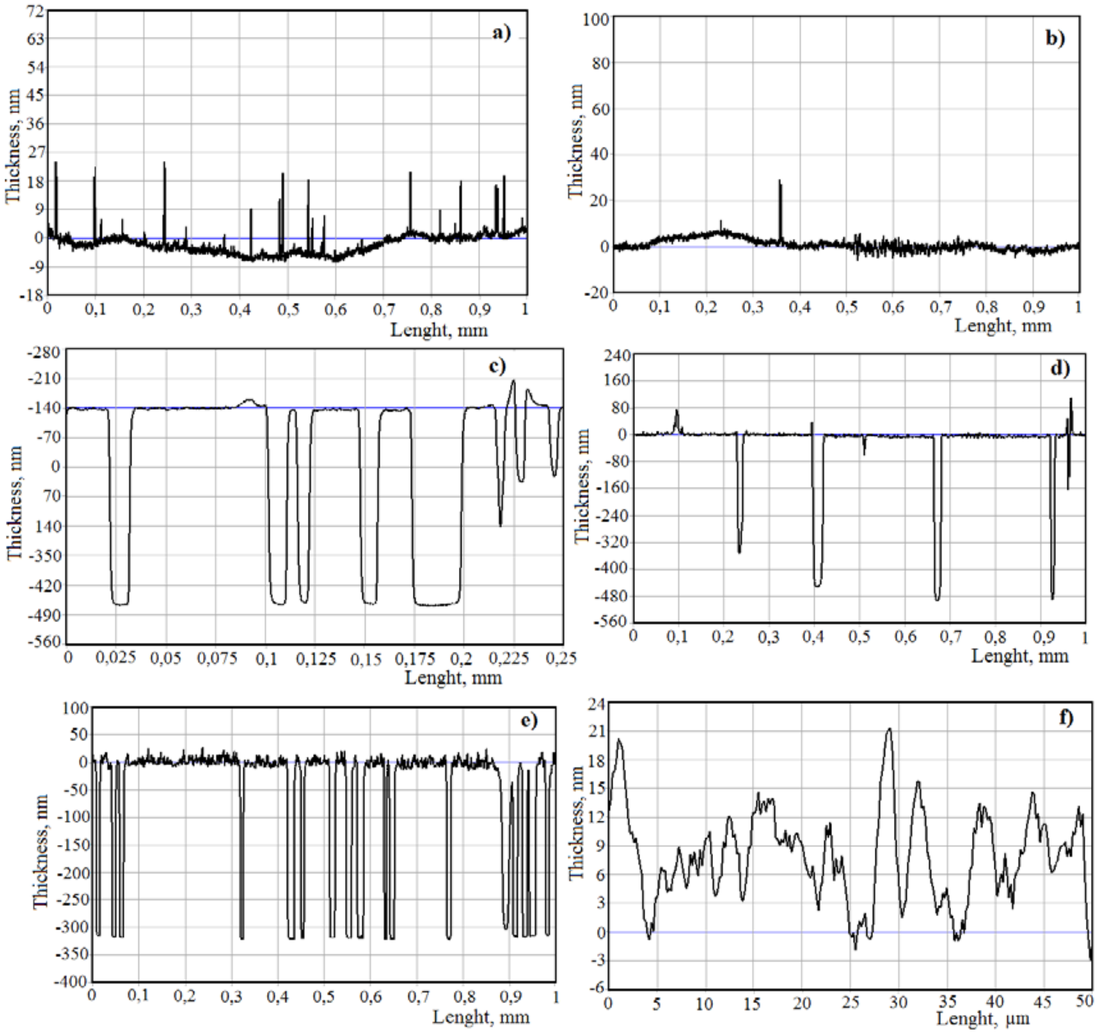

Fig. 4. The profiles of Ti film surface topography: a) as-deposited; and treated b) 50 W, 60 min; c) 200 W, 5 min; d) 200 W, 20min; e) 300 W, 5 min; f) 300 W, 20 min.

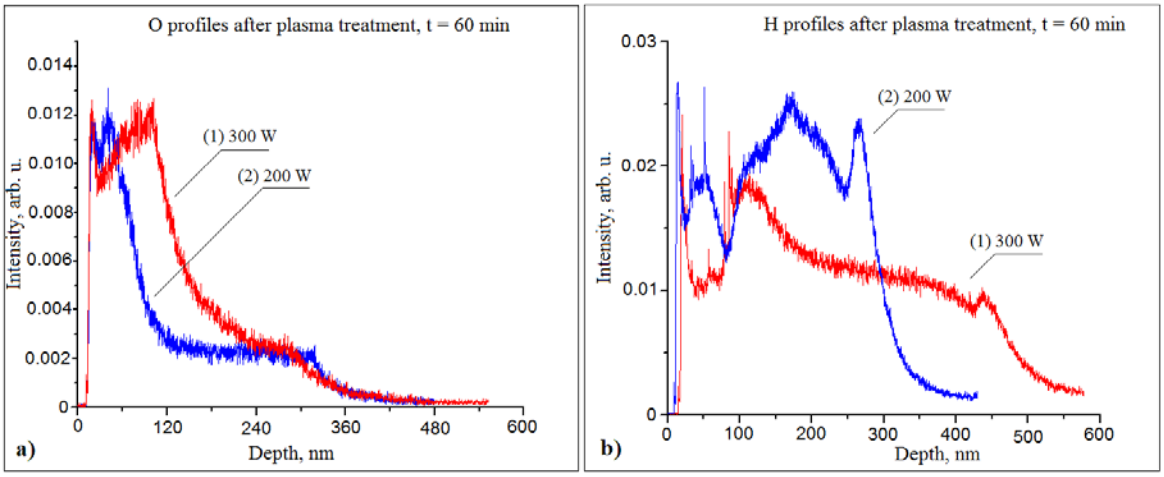

Fig. 5. GDOES distribution profiles of O (a) and H (b) atoms across the Ti film treated at 300 W (1) and 200 W (2)

Hydroxyl radicals located on the surface due to plasma radiation split into hydrogen and oxygen. Oxidation and hydrogenation of Ti layer occures simultaneously where hydrogen diffuse into the bulk along the grain boundaries of oxidised titanium. Fig. 5 shows the distribution profiles of oxygen (Fig. 5a) and hydrogen (Fig. 5b) across the thickness of Ti film after plasma irradiation at different energy source RF power. Before 200 W plasma treatment the thickness of sample was about 500 nm and before 300 W treatment thickness of sample was approximately 550 nm. Oxygen profile has a tendency to decrease exponentially across the thickness of Ti film. It‘s worth mentioning, that O concentration decreases faster for the sample treated at lower power (Fig. 5a, curve 2), particularly at outer layers of surface. This fact correlates with the decrease of energy of incident ions. Hydrogen distribution profile has a wide peak at about 200 nm and considerable decline starting from 270 nm at 200 W (Fig. 5b, curve 2), while at 300 W hydrogen distribution is more homogeneous and H atoms penetrate deeper into the bulk (Fig. 5b, curve 1).

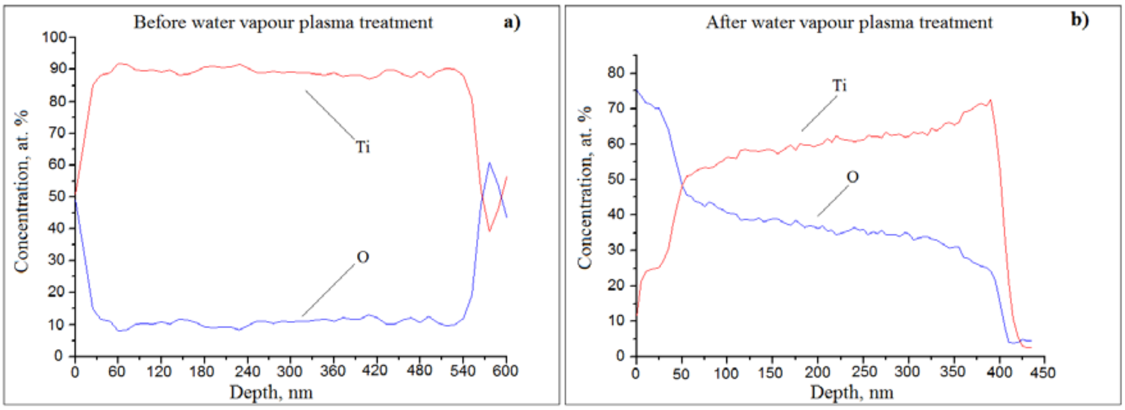

Fig. 6. The Auger distribution profiles of O and Ti atoms in Ti film: a) untreated, and b) plasma treated

Fig. 6 includes the AES distribution profiles of Ti and O atoms in untreated (Fig. 6a) and plasma treated (Fig. 6b) Ti film. It is seen that oxygen atoms are distributed over the estimated film thickness of 400 nm. The Auger oxygen depth profile shows a sharp decrease of oxygen concentration from 75 at. % to 45 at. % at the surface followed by a gradual decrease through the entire film thickness in the bulk to the values around the maximum solubility of oxygen in titanium (35 at.%) (Fig. 6b). The segregated TiO_2 (rutile) was observed in the near surface region of treated samples. EDS results before treatment showed 80 at. % of titanium and 20 at. % of oxygen and after treatment 53 at. % of O, 47 at. % of Ti.

It is well known that hydrogen tends to occupy tetrahedral interstitial sites in the group of transition metals [13]. The solubility of hydrogen depends on the phase of Ti. The H solubility is higher for β-phase (12 tetrahedral and 6 octahedral interstices) than for α-phase (4 tetrahedral and 2 octahedral interstitial sites). The presence of hydrogen in the sample results lattice expansions [14].

Moreover, the amount of hydrogen in Ti modifies such parameter as surface resistivity of thin film. Small amounts of hydrogen in α-Ti lattice form disordered interstial solution and act like scattering centers for conduction electrons. Observations show that resistivity increases for such conditions. On the other hand, β-Ti absorbs more hydrogen. These atoms occupy tetrahedral voids and the contribution of scattering centers in the lattice diminishes. Consequently, the resistivity decreases [15].

Surface resistivity (Ω/□ or Ω/square) of Ti thin film was measured using 4 – point probe method and resistivity calculations were made using the equation:

$$R_s = k\frac{V}{I}, \tag{1}$$

where *V* is the measured voltage, *I* is the applied current and $k = \frac{\pi}{ln2} = 4.53$.

Measurements were made for as-deposited Ti/Si sample and for titanium thin films treated in water vapor plasma. As it is shown in Fig. 7, the resistivity of measured samples remains constant when *I* increases.

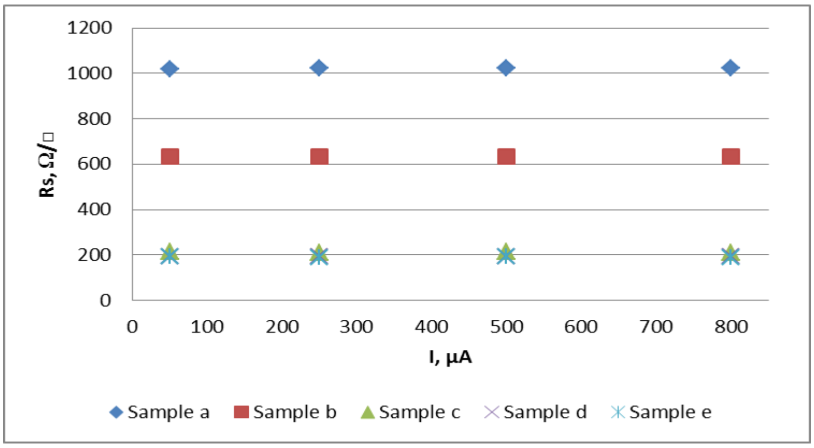

Fig. 7. Resistivity dependence of applied current

Furthermore, as it was claimed above, the resistivity of Ti top layer has to increace when smaller amount of hydrogen atoms gets in the sample. The measured resistivity for each sample is in good agreement with the literature predicted. Fig. 8. shows how the film resistivity changes for different power dissipated in plasma and exposure time.

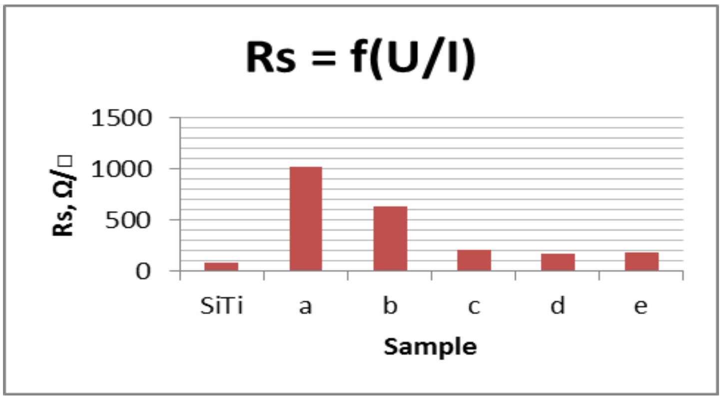

Sample a	Sample b	Sample c	Sample d	Sample e
20W, 60 min.	50W, 60 min.	200W, 5 min.	200W, 20 min.	300W, 20 min.

Fig. 8. Resistivity of the samples obtained for different treatment parameters

As it seen in Fig. 8, the film resistivity decreases when applied power increases. Consequently, assumptions about hydrogen influence on resistivity are in good agreement with experimental results. Also, surface resistivity could be influenced by different oxygen content.

4. DISCUSSION

Wetted Ti thin films in the presence of plasma radiation are oxidized [16]. Simultaneous oxidation and hydrogenation take place in the formation of titanium oxides and storing hydrogen in the bulk of oxidized nanocrystalline Ti. It is supported with XRD, GDOES and electrical resistivity results. Titania films exposed to UV light have excellent water wettability properties (superwettability). The scheme of the oxidation of Ti film in water vapor plasma is shown in Fig. 9. Under plasma radiation some of oxygen atoms are removed from the titania surface (Fig. 9a). Surface becomes activated. Bombardment with heavy energetic ions arriving from water vapour plasma removes preferentially oxygen atoms and titania surface becomes even more activated (Fig. 9b). These two, ionic and UV, radiation components result into formation of many nanoscale domains where hydroxyl groups OH are adsorbed. The surface energy increases and surface becomes wettable. Water molecules or clusters cover the activated surface area and form water island layers in contact with activated surface, which leads to the formation of hydroxyl radicals on the surface (Fig. 9c).

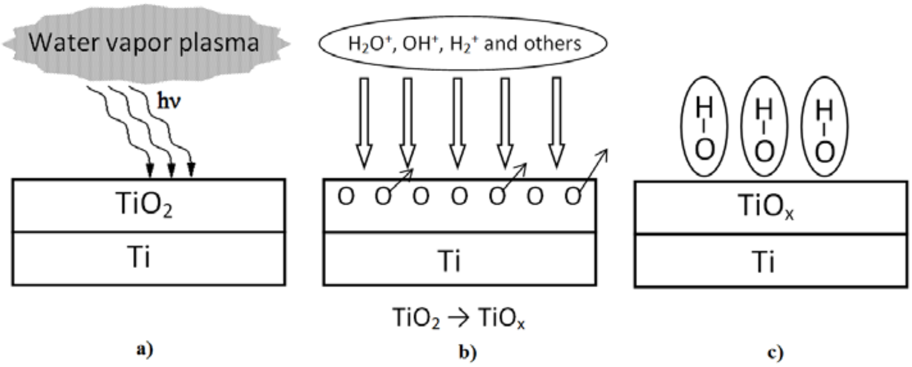

Fig. 9. Plasma enhanced process on the surface of Ti film

Plasma irradiation splits OH radicals into their atomic components hydrogen and oxygen. During treatment in plasma the surface becomes defected and mobile H^+ ions are trapped at radiation defects. When the H^+ ions are detrapped from trapping centers they diffuse through the oxide layer into the bulk and, taking into account titanium's high affinity for hydrogen, are absorbed by the titanium, and consequently are stored in the bulk. Eventually they reach silicon substrate, which is not permeable to hydrogen. H^+ ions attach electrons and form molecular H_2, which accumulates and causes huge residual bulk stresses (Fig. 10). Blisters and holes are formed as showed in SEM surface views. Samples are located on the magnetron cathode therefore electrons can easily reach back side of the substrate-film boundary. Dissociated O atoms migrate on the surface partly forming O_2 molecules, which is desorbed, partly moving into the bulk.

Oxidation kinetics depends on many properties, such as adsorption, the presence of Ti^{n+}/oxygen vacancies, type and microstructure of titanium, impurities. Titanium oxide properties determine hydrogen diffusion into the bulk [17].

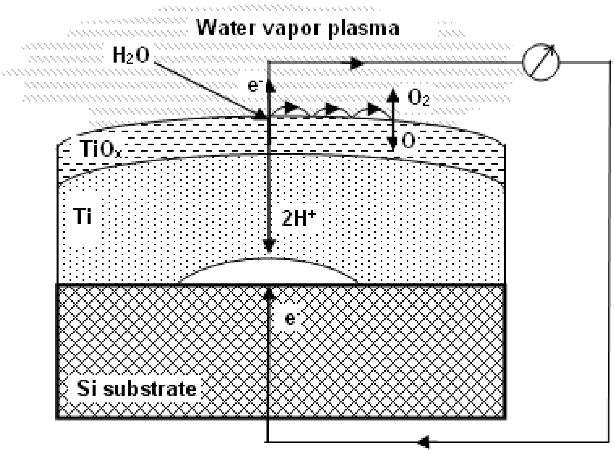

$$H_2O \rightarrow \frac{1}{2}O_2 + 2H^+ + 2e^-$$

Fig. 10. The mechanism of split of water molecules

5. CONCLUSIONS

It is shown, the water vapour plasma treatment of thin titanium films leads to theirs simultaneous oxidation and hydrogenation. The oxidation rate mainly depends on the energy source dissipated power in plasma. Even after 5 minutes treatment in water vapour plasma XRD results show the formation of titanium oxides, therefore time is not the main factor in this oxidation process. Major oxidants are hydroxyl radicals which create a superwettability effect on the activated surface area. Ionic bombardment and plasma radiation remove oxygen atoms from the surface and leads to the creation of highly reactive surface with high concentration of hydroxyls. Water-splitting process occurs on the plasma activated surface. Oxygen atoms transform Ti into TiO_2 while hydrogen atoms diffuse into the bulk and accumulate at the boundary of substrate-film resulting in the formation of blisters and holes across the entire film thickness. Probably, hydrogen at interstitial and different oxygen content determines various electrical resistivities of the films.

REFERENCES

1. NOWOTNY J., BAK T., NOWOTNY M. K., SHEPPARD L.R. Titanium dioxide for solar-hydrogen I. Functional properties. *International Journal of Hydrogen Energy*, 2007, Vol. 32, p. 2609–2629.
2. FUJISHIMA A., RAO T. N., TRYK D. A. Titanium dioxide photocatalysis. *Journal of Photochemistry and Photobiology C: Photochemistry Reviews*, 2000, Vol. 1, p. 1–21.
3. ABEA R. Recent progress on photocatalytic and photoelectrochemical water splitting under visible light irradiation. *Journal of Photochemistry and Photobiology C: Photochemistry Reviews*, 2010, Vol. 11, p. 179–209.
4. JÕKS S., KLAUSON D., KRICHEVSKAYA M., PREIS S., QI F., WEBER A., MOISEEV A., DEUBENER J. Gas-phase photocatalytic activity of nanostructured titanium dioxide from flame aerosol synthesis. *Applied Catalysis B: Environmental*, 2012, Vol. 111–112, p. 1–9.
5. MOGYOROSI K., BALAZS N., SRANKO D. F., TOMBACZ E., DEKANY I., OSZKO A., SIPOS P., DOMBI A. The effect of particle shape on the activity of nanocrystalline TiO2 photocatalysts in phenol decomposition. Part 3: The importance of surface quality. *Applied Catalysis B: Environmental*, 2010, Vol. 96, p. 577–585.
6. CHEN X., LIU L., YU Y. P., MAO S. S. Increasing solar absorption for photocatalysis with black hydrogenated titanium dioxide nanocrystals. *Science*, 2011, Vol. 331, p. 746–749.
7. PADMANABHAN P.V., SREEKUMAR K.P., THIYAGARAJAN T K., SATPUTE R.U., BHANUMURTHY K., SENGUPTA P. Nano-crystalline titanium dioxide formed by reactive plasma synthesis. *Vacuum*, 2006, Vol. 80, p. 1252–1255.
8. MOHAMEDA R.M., MCKINNEY D.L., SIGMUND W.M. Enhanced nanocatalysts. *Materials Science and Engineering*, 2012, Vol. 73, p. 1–13.
9. XIE Y., LIU X., LIU X., HUANG A., DING C., CHU PAUL K. Improvement of surface bioactivity on titanium by water and hydrogen plasma immersion ion implantation. *Biomaterials*, 2005, Vol. 26, p. 6129–6135.
10. SUZUKI T., SABURI T., TOKUNAMI R., MURATA H., FUJII Y. Dominant species for oxidation of stainless steel surface in water vapor plasma. *Thin Solid Films*, 2006, Vol. 506–507, p. 342–345.
11. PEREZ P. On the influence of water vapor on the oxidation behavior of pure Ti. *Corrosion Science*, 2007, Vol. 49, p. 1172–1185.
12. NGUYEN S., FOSTER J., GALLIMORE A. Operating a radio-frequency plasma source on water vapour. *Review of scientific instruments*, 2009, Vol. 80, p. 1–8.
13. WIPF, H., KAPPESSER, B., WERNER, R. Hydrogen diffusion in titanium and zirconium hydrides. *Alloys and Compounds*, 2000, Vol. 310, p. 190–195.
14. ELIEZER, D., TAL-GUTELMACHER, E., BOELLINGHAUS, TH. Hydrogen embrittlement in hydride – and non hydride – forming systems – microstructural/phase changes and cracking

mechanisms, [referred on the 19th of February in 2012 y.]. Link to the internet <http://www.icf11.com/proceeding/EXTENDED/5766.pdf>

15. DROGOWSKA K., FLEGE, S., SCHMITT, C. & COMP. Hydrogen Charging effects in Pd/Ti/TiO_2/Ti thin films deposited on Si(111) studied by ion beam analysis methods. *Advances in Materials Science and Engineering*, 2011, Vol. 2012, p. 1–8.
16. OH J.S., KAWAMURA K., PRAMANIK B.K., HATTA A. Investigation of water-vapor plasma excited by microwaves as ultraviolet light source. *Plasma Science*, 2009, Vol. 37, p. 107–112.
17. ZENG Y., NOEL J. J., NORTON P. R., SHOESMITH D. W. Hydrogen transport through thin titanium oxides. *Journal of Electroanalytical Chemistry*, 2010, Vol. 649, p. 277–285.

ACKNOWLEDGEMENT

This research was funded by a grant (Nr. ATE-02/2010) from the Research Council of Lithuania.

CYSENI 2012, May 24–25, Kaunas, Lithuania
ISSN 1822-7554, www.cyseni.com

SEPARATION OF SYNTHESIS GAS COMPONENTS USING POLYMER AND METALLIC MEMBRANES

A.G. Chmielewski, K. Wawryniuk
Institute of Nuclear Chemistry and Technology
Dorodna str.16, 03-195 – Poland
Phone (+48) 22 504 11 64
Email: k.wawryniuk@ichtj.waw.pl

A.G. Chmielewski, J. Antczak
Warsaw University of Technology
1 Waryńskiego str., 00-645 – Poland

ABSTRACT

The increase of demand for "clean" and efficient energy results in use of hydrogen for energy purposes as a potential, long-term solution of the growing energy crisis. Currently, on an industrial scale in hydrogen production technologies by coal gasification, two-stage system is used to synthesis gas (main components: CO, H_2, CO_2, CH_4) purification. The first stage includes use of one or two water gas shift (WGS) reactors to increase the concentration of hydrogen in the gas mixture. In the second stage can be used: pressure swing adsorption (PSA) unit, cryogenic distillation or membrane technology. Many types of membranes can potentially be used in hydrogen purification process. Membrane systems have many advantages such as small size, reliable and effective performance, low energy consumption, and simplicity of operation and maintenance. This paper discusses the advantages and disadvantages of different hydrogen separation membranes: polymer and metallic such as palladium alloys. The polymer materials used in hydrogen separation from synthesis gas are for example polyimides, which are characterized by low manufacturing costs, high thermal, chemical and mechanical resistance (high glass transition temperature), the possibility of working at high pressure and selectivity for hydrogen transport as compared to the other components of synthesis gas. However, they are sensitive to certain chemicals such as hydrochloric acid, sulphur oxides and carbon dioxide, which diminish their operation parameters. High purity of hydrogen (up to 99.99%) can be obtained by use of pure palladium or palladium alloys membranes. Metallic membranes used for separation of hydrogen can be: pure metals, binary alloys, Pd alloys with 3–5 other metals, amorphous alloys, metals (Pd) coated by Ta, V or other metals.

Keywords: synthesis gas, hydrogen separation, membrane separation, polymer membrane, metallic membrane

1. INTRODUCTION

Hydrogen in the free state is in the upper atmosphere and volcanic gases. On the Earth, almost exclusively, hydrogen occurs in compounds: water, hydrocarbons (petroleum, natural gas) and all organic compounds (in living organisms). Nearly 2% (about 6 Exajoules[1]) of the world's primary energy is stored in the 41 million tons of H_2 which is produced industrially on yearly basis. [1]. Hydrogen is abundantly available in the universe and possesses the highest energy content per unit of weight compared to any of the known fuel. For example hydrogen is characterized by 2.5 times higher energy density value (120 MJ /kg) than gasoline. At the same time for its ignition 15-fold lower amount of heat is required [2]. Hydrogen as an energy carrier is characterized by environmental (no CO_2 emissions during combustion and the only side effects are heat and water that returns to the natural circulation in nature) and economic benefits. Industrial production

---

[1] 1 EJ = 10^{18} joules

of hydrogen includes the reaction of hydrocarbons with steam, gasification of coal, coke or biomass, plasma technology, and electrolysis of water.

This paper includes review of hydrogen membrane separation methods using polymeric and metallic materials.

2. MEMBRANE SEPARATION OF GASES – REVIEW

Membranes used for hydrogen separation from its mixture with other gases like methane, carbon monoxide, carbon dioxide can be divided to porous and dense types. When pore size is small compared to the mean-free-path of the gas molecules, gas of lower molecular weight permeates through membrane much faster. In microporous membranes the flux is directly proportional to the pressure, whereas in palladium membranes, it is proportional to the square root of the pressure.

Membrane separation of gas can be attributed to four mechanisms: a. Knudsen diffusion (occurs when the pore diameter in the effective layer is smaller than the mean free path for the permeating gas), b. molecular sieving (operates on a size-exclusion principle), c. solution-diffusion (based on both solubility and diffusivity of gas molecules in an effective barrier), and d. surface diffusion (can occur in parallel with Knudsen diffusion).

Permeability is a basic property of the membrane material and is independent of the membrane thickness. Permeability can be expressed as the product of the diffusion coefficient and the solubility constant and is temperature dependent. The permeability can be expressed by the Arrhenius equation [2]:

$$\rho_{H2} = K \exp\left(\frac{-E}{RT}\right). \tag{1}$$

where K is the preexpotential factor constant, E is the activation energy, R is the gas constant, and T is the absolute temperature.

Similarly, the ability of a membrane to separate gases is characterized by the selectivity of the membrane. Ideal selectivity (or separation factor) is defined as the ratio of the permeability of the penetrants. The selectivity of hydrogen over carbon monoxide can be expressed as [2]:

$$\alpha_{H2/CO} = \frac{P_{H2}}{P_{CO}} \tag{2}$$

where $\alpha_{H2/CO}$ is an ideal selectivity of the hydrogen to the carbon monoxide gas and P_{CO} is the carbon monoxide permeability.

Several methods are available for the formation of metallic membranes such as phase inversion, rolling, electroless-plating, chemical vapor deposition (CVD), sputtering, spray pyrolysis, coatings, metal deposition, sol-gel, and others [4]. Polymer membranes are selective skin layer on flat sheets or asymmetric hollow fibres. The important polymer material properties defining the separation performance are molecular structure, glass transition temperature (Tg), crystallinity, degree of crosslinking, and as a function of these variables, durability with respect to possible degradation or loss of performance [5].

In other classification, hydrogen membranes (based on the materials used) can be categorized into two types: a. organic (polymer) and b. inorganic (metallic, carbon and ceramic) [2]. In the table 1 different properties of main groups of membranes are shown. Commercial-scale membrane for hydrogen separation are supplied by the following companies: Grace MS (Aker-Kvaerner), Medal (Du Pont/Air Liquid), Permea (Air Products), Ube Industries, Union Carbide (Dow), UOP (Separex) [2].

Table 1. Properties of the relevant hydrogen selective membranes [3]

	Dense polymer	Micro porous ceramic	Dense metallic	Porous carbon	Dense ceramic
Temperature range	<100 °C	200-600 °C	300-600 °C	500-900 °C	600-900 °C
H_2 selectivity	low	5-139	>1000	4-20	>1000
H_2 flux (10^{-3} mol/m^2 s) at dP=1 bar	low	60-300	60-300	10-200	6-80
Stability issues	Swelling, compaction, mechanical strength	Stability in H_2O	Phase transition	Brittle, oxidising	Stability in CO_2
Poisoning issues	HCl, SO_x, (CO_2)		H_2S, HCl, CO	Strong adsorbing, vapours, organics	H_2S
Materials	Polymers	Silica, alumina, zirconia, titania, zeolites	Palladium alloy	Carbon	Proton conducting ceramics (mainly $SrCeO_{3-\delta}$ $BaCeO_{3-\delta}$
Transport mechanism	Solution/diffusion	Molecular sieving	Solution/diffusion	Surface diffusion; molecular sieving	Solution/diffusion (proton conduction)
Development status	Commercial by Air Products, Linde, BOC, Air Liquide	Prototype tubular silica membranes available up to 90 cm. Other materials only small samples (cm^2)	Commercial by Johnson Matthey; prototype membrane tubes available up to 60 cm	Small membrane modules commercial, mostly small samples (cm^2) available for testing	Small samples available for testing

In membrane separation raw gas flows through the module and is separated on two streams – permeate (enriched in hydrogen) and retentate (depleted in hydrogen). The scheme of the process is shown on the Fig. 1.

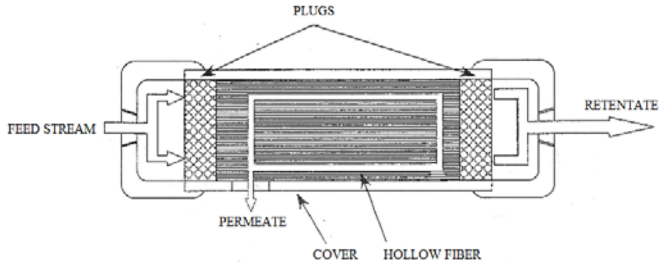

Fig. 1. The scheme membrane module with hollow fibres

2.1. Polymer membranes for hydrogen separation

Hydrogen has a relatively small molecular size compared to other gases and exhibits high selectivity ratio in glassy polymers. The ideal membrane possesses a high flux as well as a high selectivity. However, ussually there is a compromise between selectivity and flux rate. The degree of separation is highly depends on both membrane selectivity and permeability [8].

Polymer membranes are the dense type and can be further divided into glassy and rubbery polymeric membranes [2]. The gas transport through the dense polymeric membranes is based on a solution-diffusion mechanism, which occurs in three steps. First, on the high pressure side (in the upstream) the gas molecules dissolve on the membrane face. Next, the penetrated molecules diffuse across the membrane until it is desorbed at the downstream face of the membrane. The relationship between diffusivity and solubility can be described by the equation:

$$P = D \cdot S, \tag{3}$$

where P is the permeability coefficient, in the Barrer (10^{-10} cm^3 (STP) cm^{-2} s^{-1} cm Hg^{-1}), D is the diffusivity coefficient (cm^2 s^{-1}) representing the mobility of molecules across the membrane and S – the solubility coefficient (cm^3 (STP) cm Hg^{-1}), which indicates the solubility of the gas molecules within the membrane.

The transport of gases through nonporous polymer membranes can be described by the solution-diffusion mechanism. This transport is a concentration gradient driven process, which is generally well described by Fick's first law:

$$J_i = -D \frac{dc_i}{dx}, \tag{4}$$

where J is the flux of species i through the membrane, D is the diffusion coefficient of species i in the membrane and dc_i/dx is the local concentration gradient of species i at a given position in membrane [8].

The operating temperatures for polymer membranes are about 373 K [3]. Good ability to cope with high pressure drops and low cost are key advantages of polymer membranes. However, limited mechanical strength, relatively high sensitivity to swelling and compaction, susceptibility to certain chemicals such as hydrochloric acid, sulphur oxides, and CO_2 make polymer membranes less attractive.

Polyimide is a glassy polymer which is known as a suitable material for gas separation. This polymer has high glass transition temperature, lower density and extremely large free volume (up to 20%). Increase of temperature enhances the hydrogen permeance in polyimide composite membranes. The carbon monoxide plasticizes the polymer and thus its permeance increases with increase of pressure. However, in mixed gas experiments, competitive sorption and concentration polarization effects reduce hydrogen permeance at elevated pressures [4].

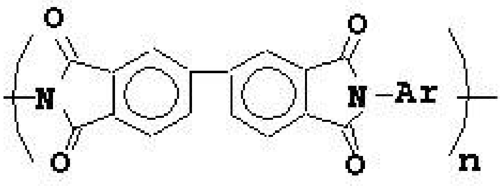

Fig. 2. Molecular structure of polyimide [4]

Table 2. Hydrogen separation membrane [8]

Membrane Type	Selectivity		Hydrogen permeance (GPU)[2]
	H_2/CO	H_2/CH_4	
Polyimide A	100	250	100
Polyimide B-H	56	125	500
Polysulfone	1,7	33	100

Phase inversion is the most frequently used method for commercially available polymer membrane preparation [2].

2.2. Metallic membranes for hydrogen recovery

Hydrogen transport through Pd includes the following: a. dissociatively adsorbing H_2 onto the metal surface, b. diffusing atomic H through bulk metal, and c. associatively desorbing H_2 from metal surface [2].

Hydrogen flux can be straightforwardly derived into an expression known as Sievert's law [2]:

$$N_{H2} = \frac{\rho_{H2}(P^n{}_{H,feed} - P^n{}_{H,perm})}{l},$$

where N_{H2} is the hydrogen flux; ρ_{H2} is the hydrogen permeability; l is the membrane thickness; $P^n{}_{H,feed}$ and $P^n{}_{H,perm}$ are the hydrogen partial pressures in the retentate and permeate sides, respectively, exponent "n" sometimes deviates from the ideal value of 0.5. It is noted that the Sievert's law strictly pertains to metallic membranes. The flux is inversely proportional to the thickness of the membrane, however, reduction of the thickness would reduce mechanical stability of the membrane.

Electroless-plating became the most popular technique for the preparation of supported Pd based membranes, because Pd has sufficient autocatalytic activity. Sputtering is especially useful when ternary or quaternary alloys are desired [6].

High-purity hydrogen (up to 99,9999%) could be available through dense metallic membranes and especially through Pd and its alloys [2]. Metallic membranes for hydrogen separation could be of many types, such as a. pure metals: Pd, V, Ta, Nb, and Ti; b. binary alloys of Pd: Pd-Cu, Pd-Ag, Pd-Y, and also Pd alloyed with N, Au, Ce, and Fe; c. complex alloys: Pd alloyed with 3–5 other metals; d. amorphous alloys: typically Group IV and Group V metals; e. coated metals: Pd over Ta, V, etc. Although Nb, Ta, and V have approximately 10–15 x greater permeability than that of Pd, these metals form oxide layers and are difficult to use as hydrogen separation membranes. This problem could be overcome by coating a thin layer of Pd on the surface of the aforementioned metals. Moreover, Nb, Ta, and V metals are cheaper than Pd, and they could meet the cost target of the system. Because of the presence of a two-phase region below the critical temperature, Pd membranes are not suitable for use at low temperatures (<573 K). Use of Pd membranes at low temperature causes hydrogen embrittlement. To combat this problem, Pd is alloyed with other materials such as Cu, Ag, Ru, Y, Ni, Au, Ce, and Ta. Thermal and chemical stability of Pd, the higher diffusivity of atomic hydrogen, and reduction of poisoning effect on the hydrogen transport mechanism in Pd caused by hydrogen sulfide and other feedstock can also be improved by alloying. Thin membranes would reduce the cost of materials as well as increase the hydrogen flux. The thin membranes are prepared on supports. In the case of metallic membranes, a challenge is that the *n*th order term in Sievert's law varies between 0,5 and 1 as membrane thickness decreases [2, 6].

---

[2] 1 GPU = 10^{-6} (cm^3 (STP)/(cm^2 · s · cm Hg)) = 7,501· 10^{-12} (m^3 (STP)/(m^2· s · Pa))

Palladium and platinum metals or their alloys have been used in fuel cells as membranes for the separation and purification of hydrogen from other gases for more than 50 years. Fuel cells are the cleanest and most efficient technology for producing electricity. They operate using hydrogen and oxygen as reactants, producing electric current and water as products [6].

Transport mechanism in these membranes requires the presence of a special catalytic surface on which, the hydrogen gas dissociates. Subsequently, free electrons and protons are conducted through the membrane layer and then the molecules hydrogen reasociates at the product side. The selectivity of hydrogen is usually very large, because the solid metal layer effectively stops large atoms and molecules such as CO, CO_2, O_2, N_2, etc.

3. CONCLUSIONS

On the basis of the membrane's operating temperature, polymer membranes are mainly suitable for temperature below 373 K, whereas porous carbon and dense ceramic membranes are suitable for a higher temperature range (773-1173 K). Metallic membranes would be suitable around 573-873 K. It is reported that the selectivity of Pd for H_2 separation was lost at >823 K because of the tin present at the interface of Pd and the support. The dense-metallic and ceramic membranes are highly selective for H_2 permeation [5, 2].

4. REFERENCES

1. OCKWIG, N., NENOFF, T., Membranes for Hydrogen Separation. *Chem. Rev.* 2007, 107, p. 4078-4110.
2. ADHIKARI, S., FERNANDO, S., Hydrogen Membrane Separation Techniques, *Ind. Eng. Chem. Res.* 2006, 45, p. 875–881.
3. KLUITERS, S. C., Status review on membrane systems for hydrogen separation. *Energy Center of The Netherlands*, Petten, The Netherlands, 2004.
4. PEER, M., MAHDEYARFAR, M., MOHAMMADI, T., Investigation of syngas ratio adjustment using a polyimide membrane, *Chemical Engineering and Processing* 48 (2009), p. 755–761.
5. PABBY, A.K., RIZVI, S., SASTRE, A. M., Handbook of Membrane Separations, Chemical, Pharmaceutical, Food and Biotechnological Applications, *Taylor & Francis Group, LLC*, 2009.
6. FROST, C., ROBINSON, M., The Application of Ultra-Thin Palladium Alloy Metal Foils in Gas-Phase Hydrogen Separation or Purification, *Hydrogen Economy*, 2007.
7. AL-RABIAH, A., Membrane Technology for Hydrogen Separation in Ethylene Plants, Department of Chemical Engineering, King Saud University.

CYSENI 2012, May 24–25, Kaunas, Lithuania
ISSN 1822-7554, www.cyseni.com

METHANOL SYNTHESIS FROM BIO-HYDROGEN

Kuo-Hsin Lin, Alex C.C. Chang[*]
Department of Chemical Engineering, Feng Chia University
100 Wenhua Road, 40724 Taichung, Taiwan
Phone +886-4-2451-7250 Ext 3664
Email:P9945950@fcu.edu.tw; acchang@fcu.edu.tw

Chen-Yeon Chu, Chiu-Yue Lin
Green Energy Development Center, Feng Chia University
100 Wenhua Road, 40724 Taichung, Taiwan
Phone +886-4-2451-7250 Ext.6210
Email:cychu@fcu.edu.tw; cylin@fcu.edu.tw
[*]*corresponding author*

ABSTRACT

The aim of this study is using bio-hydrogen to produce methanol through the methanol synthesis. The bio-hydrogen is obtained from the effluent gas of anaerobic fermentation process, where the effluent gas is composed of H_2 (25-75%) and CO_2. The fair purity of hydrogen always limited its applications; therefore, the aim of this study is to deal with this problem. Furthermore, the process is an exothermic reaction and it proceeds under volume contraction so that the higher methanol yield must be obtained at low temperature and high pressure.

The commercial catalyst MDC-3 ($Cu/Zn/Al_2O_3$) is employed in the preliminary experiments at 250 ^oC, 30 bar, 2400 ml/g-hr and with a fixed H_2/CO_2 ratio of 3. The results show the reaction is reaching stability in the first 30 minutes with an average CO_2 conversion of 8.8% and methanol yield of 19.2%. It also found a trace of dimethyl ether (less than 0.1%) and CO (2.5%) produced during the course of reaction, where the later one is generated through the reverse water gas shift reaction. Consequently, the overall reaction at least involved three reactions as following: (1) CO_2 hydrogenation reaction; (2) CO hydrogenation reaction; (3) reverse water gas shift reaction. The thermodynamic equilibrium is also evaluated by the MATLAB software from 10–30 bar and 200–300 ^oC.

Keywords Bio-hydrogen, Methanol synthesis

1. INTRODUCTION

Green house gas emission has caught much more attentions around the world and leading to the global warming effects. In the past decades, fossil fuel was the major energy resource and released considerable amount of carbon dioxide during its usage. Therefore, seeking for the alternatively energy resource is the most promising issue for the present time. Bio-energy is considered as one of the most potential energy resource among all renewable energies. Conventionally, bio-energy can be produced from the thermal-chemical or the biological processes. In the recent years, our group devoted in integrating both of the processes and developed a new one which could not only effectively produce bio-energy (hydrogen, methane, enthanol, butanol, etc.) but also make full use of biomass as well as argricultural waste. Unfortuntely, the fair purity of hydrogen (25-75 %) [1] always limits its application and the purification of hydrogen is not widely developed yet. Therefore, in this study the methanol synthesis using bio-hydrogen is considered as an alternative chance.

Methanol sythesis ($CO_2 + 3H_2 \rightarrow CH_3O_H + H_2O$) was proposed by BASF in 1923 [2], which firstly introduced the zinc/chromite catalyst for the industral application. The catalyst showed a low activity and consequently the process had to be carried out at high temperatures and pressures in order to reach a profitable yield of methanol (573–633K, 25 MPa). Although it showed low activity for methanol synthesis, it was used and improved for a long period until the 1950s. For the present time, the most favourable catalyst is copper/zinc oxide/alumina catalyst. The copper/zinc system was characterized by a particularly high activity [3-5] and the addition of alumina was found to be able to stablize the thermal resistance of the catalyst [5].

In this work, methanol synthesis was carried out at 250 ^{o}C with employing commercial catalyst, MDC-3, as the promoter. The feedstock was composed of H_2 and CO_2, where its composition was referred to the effluent gas of anaerobic process. The thermodynamic equilibrium is also evaluated by MATLAB software in pressure range of 10-30 bars and temperature range of 200–300 ^{o}C.

2. EXPERIMENTAL

The schematic diagram of the experimental appratus is shown in Fig. 1. The reaction was carried out in a fixed-bed tubular stainless steel reactor (O.D. = 1/2”), with 1 g of the catalysts (MDC-3) being placed at the center of the reactor between two quartz wool and fixed at temperature of 250 ^{o}C by a tubular furnace. The pressure was controlled (10, 20 and 30 bars) by a back pressure regulator, which was installed at the end of reactor. Before the reaction, the catalyst was reduced in situ with 10% H_2/Ar stream for 2 hours. The Space velocity of feedstock was fixed at 3600 ml/g-hr and the composition was varied from H_2/CO_2 ratio of 1, 2 and 3. Every test was proceed for 15 hours and the effluent gas was also heated at 150 ^{o}C to prevent condensation. Gas chromatograph (SRI 8610C) was equipped with a thermal conductivity detector (TCD) and a flame ionization detector to analyze the gas products. The definition of conversion, selectivity and concentration was described by equations as shown below,

$$X_i = \frac{n_i - n_i^0}{n_i^0} \times 100\% \quad , i = CO_2, H_2, \tag{1}$$

$$S_{MeOH} = \frac{n_{MeOH}}{n_{CO_2}^0 - n_{CO_2}} \times 100\%, \tag{2}$$

$$C_i = \frac{n_i}{N_T} \times 100\%, \tag{3}$$

where X_i stands the conversion of i species, n_i stands moles of i species at time t, S stands the selectivity, C_i stands the concentration of i species, and N_T representes total moles of all species.

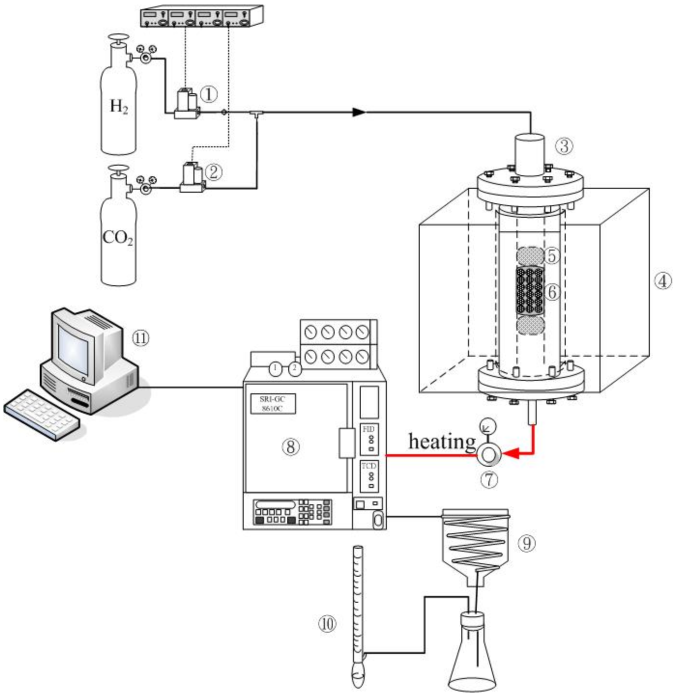

Fig. 1. Schematic diagram of this study: (1) H_2 mass flowmeter, (2) CO_2 mass flowmeter, (3) reactor, (4) furnace, (5) glass wool, (6) catalyst, (7) back pressure regulator, (8) gas chromatograph, (9) cooling device, (10) soap-bubble flowmeter, (11) personal computer

3. RESULTS AND DISCUSSION

In this study, the thermodynamic equilibrium for methanol synthesis was computed by the MATLAB software in the temperature range of 200-300 ^{o}C, pressure range of 10-30 bar and H_2/CO_2 ratio of 3 and 1. The computation results were shown in Fig. 2. The computation showed that the selectivity of methanol decreased with increasing temperature in all cases. For the cases of H_2/CO_2 ratio of 1, the equilibrium conversion of CO_2 showed opposite trend with selectivity, which was suggested by the competition of side reactions. Furthermore, the computation showed the reaction indeed depended on the pressure, temperature and feedstock ratio. Incresing the feedstock ratio from H_2/CO_2 ratio of 1 to 3, the conversion of carbon dioxide and hydrogen increased obviously as well as methanol selectivity. It also seemed that the reaction was depending much more on the feedstock ratio than pressure. Table 1 shows the results of experimental runs. Generally, CO_2 conversion was increased with increasing pressure as well as incresing H_2/CO_2 ratio. However, the conversion of hydrogen and methanol selectivity did not follow this trend. The experimental runs showed the best methanol selectivity was 40.50 % at the condition of 20 bar and H_2/CO_2 ratio of 2. It had to mention that for the case of 10 bar (H_2/CO_2 = 1, 2 and 3) it did not detected any methanol from FID detector due to its concentration was out of detection.

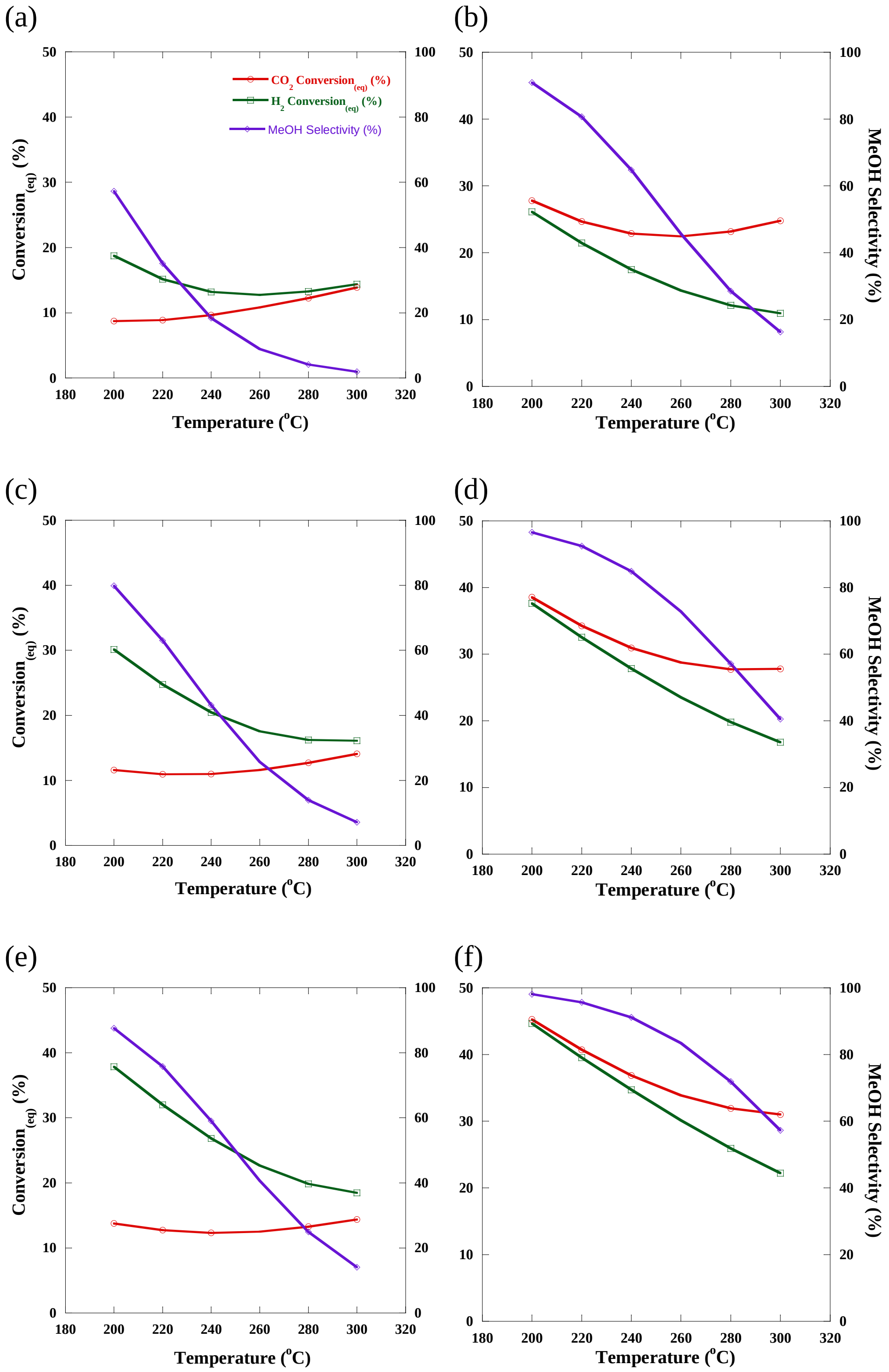

Fig. 2. Computation results of equilibrium conversion of CO_2 and H_2, and selectivity of methanol: (a)10 bar, $H_2/CO_2 = 1$, (b) 10 bar, $H_2/CO_2 = 3$,(c) 20 bar, $H_2/CO_2 = 1$, (d) 20 bar, $H_2/CO_2 = 3$, (e) 30 bar, $H_2/CO_2 = 1$, (f) 30 bar, $H_2/CO_2 = 3$.

Table 1. Results of experimental runs

H_2/CO_2	Pressure (bar)	X_{CO2} (%)	X_{H2} (%)	S_{MeOH} (%)
1	10	13.97	11.89	N/D
1	20	13.25	15.20	9.71
1	30	7.24	14.10	22.21
2	10	15.22	5.38	N/D
2	20	7.66	8.94	40.50
2	30	15.89	8.15	18.67
3	10	19.84	2.78	N/D
3	20	29.39	7.91	12.43
3	30	23.17	7.26	20.34

Reaction condition, 250 ^{o}C, space velocity of 3600 ml/g-cat.-hr.
N/D, not detected.

Fig. 3 shows the computation of equilibrium concentration of each species. Methanol concentration was decreased with increasing temperature in all cases since the reaction was exothermic. The computation showed again that methanol synthesis was depending much more on H_2/CO_2 ratio than pressure. CO concentration was highly depending on temperature due to the reverse waster gas shift reaction, which was also the main side reaction. Table 2 shows the species concentration of experimental runs. For the case of same H_2/CO_2 ratio, CO concentration was decreased with increasing pressure indicating that reverse water gas shift reaction was apparently restricted by pressure. However, it also could be explained by the weakness competition comparing with CO_2 hydrogenation reaction. H_2O concentration showed an opposite trend with CO, which was suggested that the reaction accompanied with CO hydrogenation reaction so that CO was futher reacted with hydrogen to produce methanol. Methanol concentration was increased slightly with both increasing H_2/CO_2 ratio and pressure.

Table 2. Species concentration of the experimental runs

H_2/CO_2	Pressure (bar)	Concentration (%)				
		CO_2	H_2	CO	MeOH	H_2O
1	10	45.83	45.93	4.20	N/D	4.03
1	20	47.66	43.37	4.08	0.70	4.18
1	30	49.29	42.93	3.00	0.78	3.70
2	10	28.09	63.84	4.12	N/D	3.94
2	20	30.01	60.93	3.89	0.87	4.30
2	30	32.35	59.03	3.35	1.11	4.13
3	10	17.39	74.73	3.97	N/D	3.90
3	20	19.13	71.78	3.69	0.98	4.40
3	30	21.20	69.97	3.28	1.28	4.25

Reaction condition, 250 ^{o}C, space velocity of 3600 ml/g-cat.-hr.
N/D, not detected.

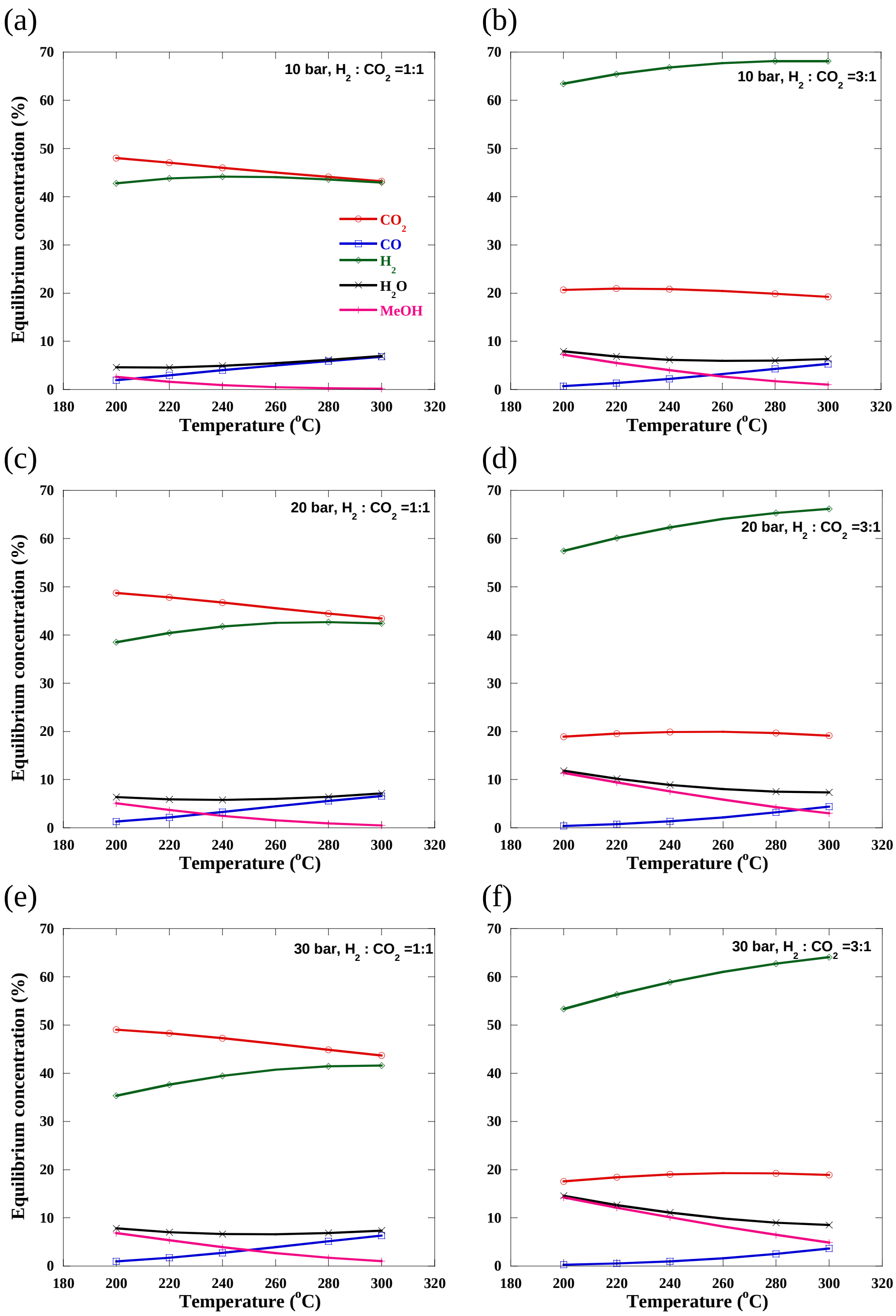

Fig 3. Computation results of equilibrium concentration: (a)10 bar, H_2/CO_2 = 1, (b) 10 bar, H_2/CO_2 = 3,(c) 20 bar, H_2/CO_2 = 1, (d) 20 bar, H_2/CO_2 = 3, (e) 30 bar, H_2/CO_2 = 1, (f) 30 bar, H_2/CO_2 = 3

4. CONCLUSION

In this study, the methanol synthesis was carried out and computed under mild conditions (10–30 bar). The feedstock was modulated according to anaerobic fermentation process. The experimental results showed the whole reaction took place under kinetic control regime. Futhermore, the reaction was much more depending on feedstock ratio than reaction pressure. The competition intensity of side reaction also affected the product distribution. Computation results show the reaction was favored under high pressure condition, which was also consistent with the experimental ones. Furthermore, it was diffcult to determine the optimal condition both from computations and experiments. In general, the optimization was always evaluated and determined by the degree of yield. However, the computation was based on the feedstock ratio, temperature and pressure, and irrelevant to the feedstock rate and production rate so the yield could not be determined. In the present work, we proposed a posibility of utilizing bio-hydrogen which also benefit to climate and environment.

REFERENCE

1. Chang A.C.C., Tu Y.H., Huang M.H., Lay C.H., Lin C.Y. Hydrogen production by the anaerobic fermentation from acid hydrolyzed rice straw hydrolysate. International Journal of Hydrogen Energy 2011:36:14280-14288.
2. Asinger F. Methanol-Chemie-und Energierohstoff. Springer Verlag 1986.
3. Macnaughton N.J., Pinto A., Rogerson P.L. Development of methanol technology for future fuel and chemical markets. Energy progress 1984:4:232-241.
4. Dybkjaer I. Design of ammonia and methanol synthesis reactors, in ASI-NATO Conference: Chemical Reactor Design and Technology 1985:London (Ontario):795-819.
5. Dry R.J. Possibilities for the development of large-capacity methanol synthesis reactors for synfuel production. Industrial & Engineering Chemistry Research 1988:**27**:616-624.

FORMATION OF COPPER ZINC TIN SULFIDE IN CADMIUM IODIDE FOR MONOGRAIN MEMBRANE SOLAR CELLS

G. Nkwusi, I. Leinemann, M. Grossberg, M. Altosaar, D. Meissner
Institute of Materials Science, Tallinn University of Technology
Ehitajate tee 5, 19086 Tallinn – Estonia
Phone +3726203362
Email: godswillnkwusi@yahoo.com

R. Traksmaa
Centre for Materials Research, Tallinn University of Technology
Ehitajate tee 5, 19086 Tallinn – Estonia

T. Kaljuvee
Laboratory of Inorganic Materials, Tallinn University of Technology
Ehitajate tee 5, 19086 Tallinn – Estonia

ABSTRACT

The formation process of the quaternary Cu_2ZnSnS_4 compound in CdI_2 is studied. Focus is on chemical reactions between the binary precursor compounds involved in the formation process of CZTS and reactions of the precursor compounds with molten CdI_2 as a flux material. The aim was to describe conditions for the synthesis of CZTS as an absorber material and to determine the presence of cadmium and secondary phases in the final product. Differential thermal analysis (DTA) was used to show the thermal effects, including the melting points, the various phase transitions and possible reactions in the samples. Closed quartz vacuum ampoules were used for the heating/cooling process of the mixtures. An empty ampoule was used as a reference. Various mixtures of the individual precursors with CdI_2 as well as the mixtures used for CZTS synthesis in CdI_2 were annealed and quenched from different temperatures. The phase composition of the mixtures was determined by X-Ray diffraction (XRD), Energy Dispersive X-ray (EDX), and Raman Spectroscopy. A possible chemical route of the CZTS formation is discussed. It was found that CZTS forms from Cu_2SnS_3 and ZnS if sufficient elemental S is added into the precursor mixtures.

Keywords : Cu_2ZnSnS_4, XRD, EDX, Raman, DTA

1. INTRODUCTION

Resulting from the world's fast population growth rate, the increasing energy demand in the near future forces us to seek environmentally clean and economically viable alternative energy resources that could replace those we have currently without any fear of further significant environmental impact. Among the various options available to alternative sources of energy, solar energy has been proven a viable alternative to meet our energy demands. But despite being clean and inexhaustible, the energy produced from solar radiation has only contributed a very minimal percentage of the total energy demand. During the past decades, considerable work has been done in order to achieve the aim of taking solar derived energy to a significant level in the energy sector and substantial progress has been made. Followed from proper considerations, it is expedient to develop a solar panel from environmentally friendly and readily available materials at low cost. So far the most efficient semiconductor compounds used as solar absorber materials in large scale production are $CuInGaSe_2$ (CIGS) and CdTe (company First Solar) with record conversion efficiencies of 20.2 and 17.3%, respectively [1–5]. The market for thin-film PV grew at a 60% annual rate from 2002 to 2007 and is still growing rapidly. Cu_2ZnSnS_4 (CZTS) with an absorption coefficient $> 10^{-4}$ cm^{-1} as an absorber material has received increasing attention in the past few years due to the enormous advantages embedded in it in terms of material availability, product efficiency relative to the cost of production and ease of handling. It may become a perfect replacement for CIGS, CdTe and other absorber materials that have been developed. Currently CZTS has had quite an enormous improvement in terms of performance proven already to yield solar efficiencies of more than 10%, as reached by the IBM company using hydrazine solutions [4]. In the monograin technology a solvent material is used for absorber material synthesis, a so-called flux material (CdI_2). A molten phase between the solid precursor particles acts as a contracting or repelling agent depending on its amount. An isothermal recrystallization of semiconductor polycrystalline powders in the presence of a liquid phase of a suitable solvent material in an amount sufficient for repelling the initial crystallites leads to the formation and growth of semiconductor powder materials with single-crystalline grain structure and narrow-disperse granularity, a so-called monograin powders. In thin film technologies, flux materials are also often used in the form of some low melting precursor that is consumed in the film growth process – molten phase between particles enables sintering and crystal growth (for example, CuSe in thin film deposition of CIGS). The role of flux material makes the main difference between monograin growth and thin film synthesis methods, such as physical vapour deposition, chemical vapour deposition (CVD) or chemical baths deposition (CBD), widely used for thin film synthesis. The driving force in the isothermal crystalline growth process of monograin materials is in the differences in the surface energies of crystals of different sizes. The growth of single-crystalline powder grains takes place at temperatures higher than the melting point of the used flux material – much lower than the melting point of the semiconductor compound. An optimal amount of the used flux material is observed if the volume of the liquid phase is around 0.7 of the volume of the solid phase. The advantage of using a flux is that it allows powder materials to be produced where every grain is single-crystalline and has uniform composition [6, 7]. In monograin layer (MGL) solar cells each single crystal is working as an individual solar cell.

A production process of MGL solar cells has been developed in our spin-off company Crystalsol for the first production line for flexible CZTS solar cell modules. A roll-to-roll process was designed for the large scale device preparation. Cu_2ZnSnS_4 (CZTS) monograin powders synthesized in KI have been used as absorber materials in monograin membrane solar cells with efficiencies around 8 %.

The monograin powder growth of semiconductor compounds in molten salts started in the Philips Company. Ties Siebold te Velde from the Philips Company filed the first patent in 1964 on LED based ZnS or CdS films, using already a p/n junction and during the next year he filed the first patent on monograin membrane devices [8].

The monograin powder granulometry is characterized by sieving analysis. Due to the large grain size, the XRD measurements are not used to measure the grain size and the Touc plots cannot be used to characterize the crystalline material. Narrow granulometric fractions (in between 32–100 µm) of the grown monograin powder grains of CZTS are separated by sieving and are used as an absorber material in MGL solar cell structures: graphite/CZTSe/CdS/ZnO. Powder crystals are covered with CdS thin layer by chemical bath deposition. A monolayer of nearly unitize grains is embedded into a thin layer of epoxy resin, so that the contamination of upper surfaces of crystals with epoxy is avoided. The polymer film thickness was adjusted to half of the grain size. Since the grains sink into the polymer and reach the underneath rubber glue layer, after washing completely off the rubber glue, the lower part of each grain sticks out of the polymer film. After polymerization of epoxy, ZnO window layer is deposited onto the front side of the monograin layer by RF-sputtering. Solar cell structure is completed by the vacuum evaporation of 1–2 µm thick In grid contacts onto the ZnO window layer. After gluing the structures on glass, the back contact area of crystals is opened by etching epoxy with H_2SO_4, followed by an additional abrasive treatment. The back contact is made using graphite paste [9].

One of the peculiarities of the materials synthesized and recrystallized in molten salts is the high level of contamination of the semiconductor compound with constituent elements of the used salt. Therefore, the replacement of KI with some other salt not containing K as a foreign element for the CZTS compound, for example, with CdI_2 is of great importance. In our previous report [10] we studied the formation process of $Cu_2ZnSnSe_4$ in CdI_2. It is known that Cd from CdI_2 incorporates to the crystals of CZTSe forming a solid solution of $Cu_2Zn_xCd_{1-x}SnSe_4$. In $Cu_2Zn_xCd_{1-x}SnSe_4$ solid solutions the direct band gap of material is shifting to the lower energy side, as shown in [11]. The band gap value of Cu_2CdSnS_4 is 1.39 eV by Matsushita et al. [12]. However, the formation of Cu_2ZnSnS_4 in CdI_2 has not yet been studied. The incorporation of Cd to the crystal lattice of Cu_2ZnSnS_4 could shift the band gap energy of the solar absorber material from 1.43 eV (CZTS) [11, 13] to the lower energy side, enabling better fitting with solar spectrum. CdI_2 as a flux was chosen due to the low melting temperature in comparison with KI and NaI, which have also been used as flux materials for the synthesis of $Cu_2ZnSnSe_4$. Our previous research showed that the formation of single-crystalline powder grains takes place at temperatures just above the melting point of the flux material, but much lower than the melting point of the semiconductor compound itself (990 °C) [12].

In the present work various mixtures of the individual precursors with CdI_2 as well as the mixtures used for CZTS synthesis in CdI_2 were annealed and quenched at different temperatures and the phase compositions of the mixtures were analysed by X-Ray diffraction (XRD), Energy Dispersive X-ray (EDX) and Raman Spectroscopy. The possible chemical route of the CZTS formation is discussed.

2. METHODOLOGY

The synthesis of quaternary Cu_2ZnSnS_4 powders from the binary precursors Cu_2S, SnS, and ZnS with additional S were carried out in molten CdI_2 using sealed quatz vacuum ampoules. The precursors and the flux material were mixed by grinding in an agate mortar in a mass ratio of 1:1, and sealed in a degassed quartz vacuum ampoule. The precursors for CZTS synthesis were used in their stoichiometric ratio. A DTA set up was used to determine the temperatures of phase changes and chemical interactions between the initial binaries and the flux material. As a reference point, an empty degassed and sealed quartz ampoule of equal mass was used. The heating rate was 5 °C/min and two heating cycles were recorded starting from room temperatures up to 800 °C. The temperatures of the peak positions in the DTA curves are determined. To identify thermal effects found in the DTA curves, probe mixtures with identical proportions as in the DTA samples (using larger amounts than for DTA samples) were prepared and heated separate individual probes for every heating and every cooling. The samples were either heated up or cooled down and then quenched at the specified temperatures. The phases formed in these samples were determined by Raman and XRD analysis after opening the ampoules. The number of samples prepared for Raman and XRD measurements corresponds to the number of peaks in the DTA curves. The Raman spectra were recorded using a Horiba LabRam HR high resolution spectrometer equipped with a multichannel CCD detection system in backscattering configuration. Incident laser light of 532 nm was focused on different 1 μm^2 spots of the studied sample and an average of five readings were taken for every sample to obtain an average result of the sample. The XRD measurements were performed using a Bruker D5005 diffractometer. For the analysis, the ICDD-4 + 2009 data base was used. EDX was used to determine the elemental composition of the precursors and the formed compounds.

3. RESULTS AND DISCUSSION

3.1. Interactions of individual precursor compounds with CdI_2 as a flux material

Our previous report showed that pure CdI_2 has an endothermic effect in the DTA heating curve at 385 °C attributed to its melting process [10]. When elemental S was added to CdI_2 in the present study, there was no chemical reaction observed, but a decrease of the melting point from 385 to 370 °C was noticeable in the DTA heating curve and to 382 °C in the cooling curve. Also, DTA curves of ZnS mixture with CdI_2 show melting/solidification of the mixture at 379/351 °C, no chemical reaction was observed by XRD.

CdI_2 mixed with SnS melted at 347 °C. CdS and different iodides (SnI_4, Sn_2SI_2) formed at the same time. SnS+CdI_2 freezed at 300 °C.

The Cu_2S+CdI_2 mixture melted at 353 °C. CuI, $Cu_2Cd_3I_4S_2$ formed and Cu_2S transformed to $Cu_{1.96}S$ in the same temperature range of melting. $Cu_{1.96}S$ retransformed to Cu_2S by cooling down in accordance with the report in [14]. An endothermic peak around 400 °C in the DTA heating curve (Fig. 1, 1a) of the Cu_2S+CdI_2 mixture corresponds to the formation of CdS and Cu_4Cd_3 intermetallic compound. The mixture of Cu_2S+CdI_2 freezed at 333 °C. The phases formed during heating and cooling are given in Table 1.

3.2. Interactions between mixtures of precursors and CdI_2 as a flux material

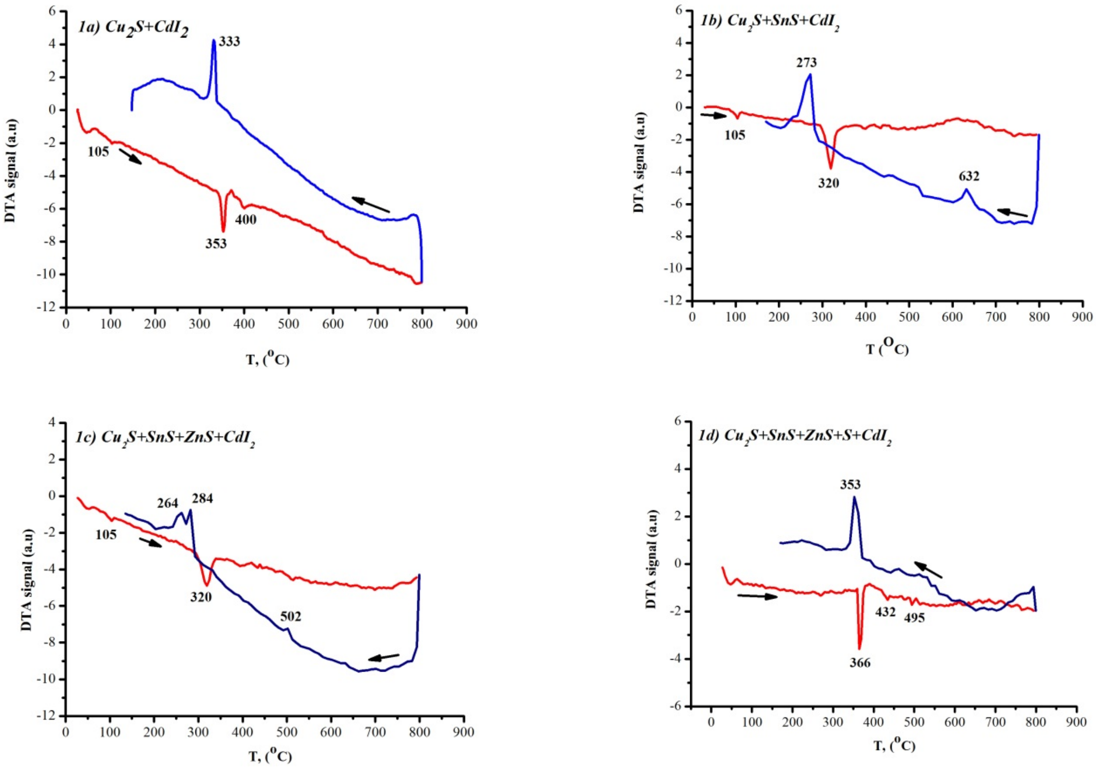

Fig. 1. DTA heating (red) and cooling (blue) curves of the quasi-binary system (1a), ternary systems (1b, 1c), and the sample of the mixture used for the quaternary CZTS synthesis (1d)

The peak of low intensity at 105 °C in the Fig. 1 (1a, 1b, 1c) DTA heating curves can be attributed to the phase transformation of monoclinic to low-chalcocite (αCh) Cu_2S , which is stable up to 103.5 ± 0.5 °C for a stoichiometric composition of Cu_2S, and up to 90 ± 2 °C for 33.41 at. % S [15].

The S-deficient (considering the possible formation of the stable compounds Cu_2SnS_3 and Cu_2ZnSnS_4) mixtures of $Cu_2S+SnS+CdI_2$ and $Cu_2S+SnS+ZnS+CdI_2$ (see fig. 1b and 1c) melt at 320 °C and did not form any new compounds even if heated up to 800 °C, in the cooling cycle both effects – at 632 and 502 °C – correspond to the formation of CdS, CuI and Sn_2SI_2 [16] as detected by XRD presented, see in Table 1. The existance of $Cu_{1.96}S$ was found between 250-320 °C. In other regions of temperatures Cu_2S existed. The mixtures solidified at 273 and 284 °C. The peak at 264 °C involves not just the solidification process of the $Cu_2S+SnS+ZnS+CdI_2$ mixture, but it also involves the incorporation of Cd into the ZnS structure, the formation of $(Zn_{1-x}Cd_x)S$ and ZnI_2, while the released S reacts with Cu_2S and SnS forming the ternary compounds $Cu_2Sn_3S_7$ [17] and Cu_4SnS_6 [18]. In the second heating cycle the ternary compounds decompose forming $Cu_{81}Sn_{22}$ and CuS phases (Table 1).

Table 1. Overview of the phases detected by Raman and XRD. EDX elemental composition data were used for an additional confirmation of the formed phases. The samples were prepared und quenched at slightly higher temperatures than the observed effects in the DTA heating curves, and at slightly lower temperatures than the effects in the cooling curves

Studied mixture	Annealing temperature ^{O}C	Phases by XRD	Phases by Raman	
			Compound	Raman shift, cm^{-1}
$ZnS+CdI_2$	Heated up to 800 °C	ZnS, CdI_2	-	-
$SnS+CdI_2$	Heated up to 800 °C	CdI_2, CdS, Sn_2SI_2, SnI_4, SnS	CdS	301 [5]
	Heated up to 800 °C and cooled down to 250 °C	CdI_2, CdS, Sn_2SI_2, SnI_4, SnS	-	-
Cu_2S+CdI_2	Heated up to 370 °C	$Cu_{1.96}S$, CuI, $Cu_2Cd_3I_4S_2$	CdI_2 CuI CdS	110 [10] 148 [6, 7] 294 [5]
	Heated up to 400 °C	CdI_2, CdS, CuI, Cu_4Cd_3	CdI_2	111 [10]
	Heat up to 800 °C and cooled down to 330 °C	CdI_2, CdS, Cu_2S, $Cu_2Cd_3I_4S_2$	CdI_2 CuI CdS	111 [10] 150 [6, 7] 298 [5]
$Cu_2S+SnS+CdI_2$ Sulphur deficient composition for Cu_2S+SnS_3 formation	Heated up to 800 °C and cooled down to 270 °C	CdI_2, CdS, Cu_2S, $Cu_{1.96}S$, CuI Sn_2SI_2	Raman spectra are very difficult to analyze due to the overlapping of peaks of multi-component systems.	
	Heated up to 800 °C and cooled down to 150 °C, then heated up to 290 °C	CdI_2, CdS, Cu_2S, CuI, SnS, Sn_2SI_2		
$Cu_2S+ZnS+$ SnS $+CdI_2$ Sulphur deficient composition for CZTS	Heated up to 760 °C	CdI_2, Cu_2S, SnS, ZnS	Raman spectra are very difficult to analyze due to the overlapping of peaks of multi-component systems.	
	Heated up to 800 °C and cooled down to 270 °C	CdI_2, CdS, Cu_2S, SnS, Sn_2SI_2, ZnS, CuI,		
	Heated up to 800 °C and cooled down to 250 °C	CdI_2, CdS, Cu_2S, $Cu_{1.96}S$, CuI, $Cu_2Sn_3S_7$, Cu_4SnS_6, Sn_2SI_2, ZnS, ZnI_2, $(Zn_{1-x}Cd_x)S$		

	Heated up to 800 °C and cooled down to 150 °C, then heated up to 290 °C	CdI_2, CdS, Cu_2S, CuI, SnS, Sn_2SI_2		
	Heated up to 800 °C and cooled down to 150 °C, then heated up to 320 °C	CdI_2, CdS, Cu_2S, $Cu_{1.96}S$, CuS, CuI, $Cu_{81}Sn_{22}$, Sn_2SI_2, ZnI_2,		
Cu_2S+ZnS+ SnS+S+CdI_2	Heated up to 500 °C	CdI_2, Cu_2SnS_3, Cu_2ZnSnS_4**, ZnI_2	CdI_2 CuI $Cu_2Zn_xCd_{1-x}SnS_4$	110 [10] 145 [6, 7] 336*
	Heated up to 800 °C	CdI_2, CuI, Cu_2SnS_3, Cu_2ZnSnS_4**	CdI_2 CuI $Cu_2Zn_xCd_{1-x}SnS_4$	110 [10] 145 [6, 7] 336*
	Heated up to 800 °C and cooled down to 600 °C	CdI_2, Cu_8S_5, Cu_2SnS_3, SnI_4, Cu_2ZnSnS_4**	CdI2 CuI $Cu_2Zn_xCd_{1-x}SnS_4$	110 [10] 146 [6, 7] 335*
	Heated up to 800 °C and cooled down to 350 °C	CdI_2, CuI, SnI_4, Cu_2ZnSnS_4**	CdI_2 CuI CZTS $Cu_2Zn_xCd_{1-x}SnS_4$	110 [10] 145 [6, 7] 166, 250, 286, 336*, 374 [19]

* Raman peak position of Cu_2ZnSnS_4 is shifted from 338 cm^{-1} to 336 cm^{-1} due to the Cd incorporation into Cu_2ZnSnS_4 and formation of solid solution of $Cu_2Zn_xCd_{1-x}SnS_4$ [11].

** Close lattice parameters do not allow to identify $Cu_2Zn_xCd_{1-x}SnS_4$ phase from Cu_2ZnSnS_4 phase by XRD patterns [12], EDX analyses show about 3 at% of Cd in CZTS monograins synthesized in CdI_2.

3.3. Synthesis of CZTS

The mixture of the binary precursors corresponding to the required stoichiometric compositon for the formation of pure Cu_2ZnSnS_4 in CdI_2 (Cu_2S+SnS+ZnS+S+CdI_2) melts and solidificates at 366 and 353 °C, showing endo/exo-thermic peaks in DTA curves. Besides the formation of CZTS, a Cu_2SnS_3 ternary compound [17, 18] and ZnI_2 were found in the sample, when heated and quenched at 500 °C.

The endothermic effects at 432 °C and 495 °C correspond to the border crossing of the equilibrium between stoichiometrical Cu_2S (Cu-rich) and Cu-deficient areas to form the defect compound $Cu_{2-x}S$ [15].

Samples quenched at 800 °C show that the ternary compound reacts with ZnS to form CZTS as a final product. The secondary phases CuI, $Cu_{2-x}S$, and SnI_4 remain in the cooling process. The detected phases are presented with their characteristic peaks in the Raman spectra (Fig. 1) and in the XRD pattern (Fig. 2), taken from the sample that were heated up to 800 °C and cooled down to 350 °C. CZTS is the prevailing phase with its characterestic Raman peaks at 166, 250, 286, 336, 374 cm^{-1}. CdI_2 at 110 cm^{-1} and CuI at 145 cm^{-1} was detected. CuI is dissolvable in KI or NaI solutions, as also reported in our previous report, allowing to separate single phase CZTS [6].

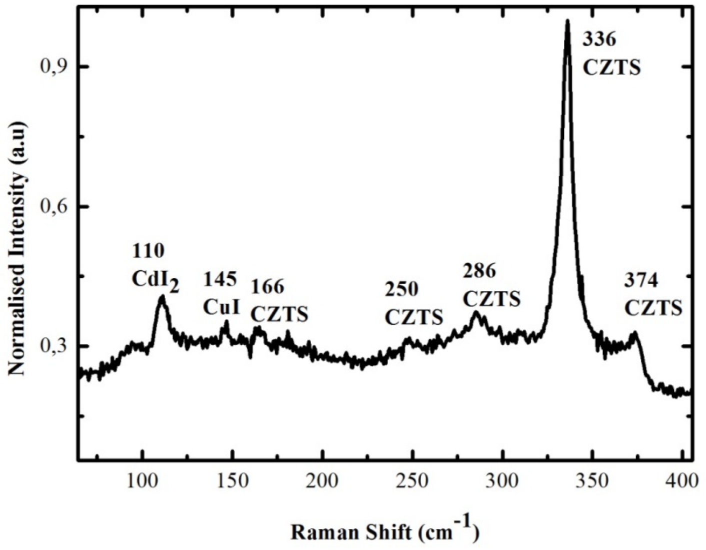

Fig. 1. Raman spectrum of the mixture of Cu_2S+SnS+ZnS+S+CdI_2 heated up to 800 °C, cooled to 350 °C and quenched. Raman peak position of CZTS is shifted from 338 cm^{-1} to 336 cm^{-1} due to the Cd incorporation into CZTS and formation of solid solution of $Cu_2Zn_xCd_{1-x}SnS_4$ [11]

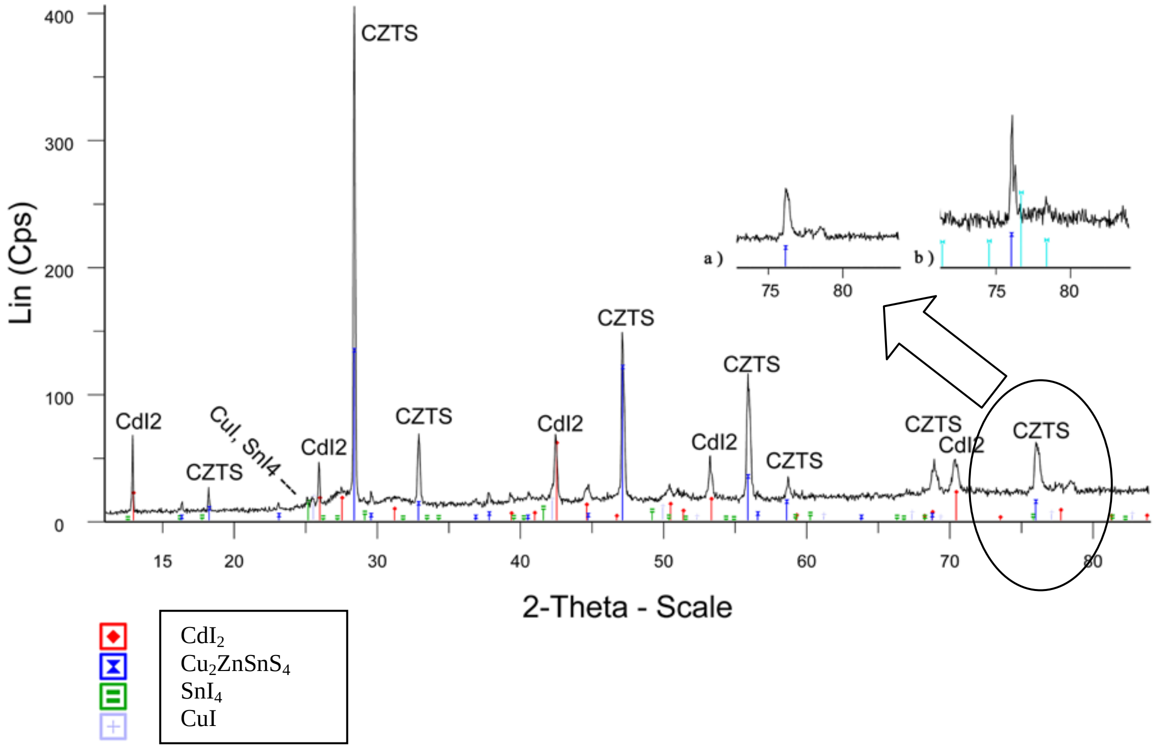

Fig. 2. XRD pattern of the mixture of Cu_2S+SnS+ZnS+S+CdI_2 heated up to 800 °C, cooled to 350 °C and quenched. The marked pattern area was used for determination of CZTS (dark blue in Figure a) and CZTS co-existing with Cu_2SnS_3 (light blue in b) phases

It is seen from Table 1, that ZnS reacts with CdI_2 only if other binaries are present, forming ZnI_2 and Cd-containing ternary sulphides $Zn_{1-x}Cd_xS$, detectable by XRD and EDS. In CdI_2 forms solid solution of $Cu_2Zn_xCd_{1-x}SnS_4$ at T≥500 °C. The chemical pathway of CZTS synthesis in CdI_2 can be described as follows:

$$SnS + S \rightarrow SnS_2 \quad [17, 18], \tag{1}$$

$$Cu_2S + SnS_2 \rightarrow Cu_2SnS_3 \quad [17, 18], \tag{2}$$

$$ZnS + x\ CdI_2 \rightarrow Zn_{1-x}Cd_xS + x\ ZnI_2 \text{ (only in the presence of other binaries)} \tag{3}$$

$$Cu_2SnS_3 + Zn_{1-x}Cd_xS \rightarrow Cu_2Zn_{1-x}Cd_xSnS_4, \tag{4}$$

$$\text{or } Cu_2S + SnS + Zn_{1-x}Cd_xS + S \rightarrow Cu_2Zn_{1-x}Cd_xSnS_4, \tag{5}$$

CZTS formation can be described as two stage process: first Cu_2SnS_3 forms from Cu_2S, SnS and S (1, 2); secondly Cu_2SnS_3 reacts with $Zn_{1-x}Cd_xS$ forming $Cu_2Zn_{1-x}Cd_xSnS_4$ (3, 4). However, $Cu_2Zn_{1-x}Cd_xSnS_4$ can be directly formed from the binaries Cu_2S, SnS, $Zn_{1-x}Cd_xS$ in the presence of sufficient amount of elemental sulphur (5).

4. CONCLUSIONS

CdI_2 mixed with ZnS, Cu_2S or SnS melts at temperatures much lower than pure CdI_2 due to the freezing-point depression effect. CdS and different iodine-containing compounds (SnI_4, Sn_2SI_2, CuI, and $Cu_2Cd_3I_4S_2$) form in CdI_2+Cu_2S and CdI_2+SnS. ZnS reacts with CdI_2 only if other binaries are present forming ZnI_2 and Cd-containing ternary sulphides $Zn_{1-x}Cd_xS$.

In the S-deficient mixtures (considering the stoichiometry of Cu_2SnS_3 and Cu_2ZnSnS_4), the ternary compound Cu_2SnS_3 and quaternary CZTS do not form.

In CdI_2 the mixture of precursors with stoichiometric composition results in solid solution of $Cu_2Zn_xCd_{1-x}SnS_4$ at T≥500°C. Additional sulphur leads to successful CZTS synthesis.

CZTS formation can be discribed as two stage process: first forms Cu_2SnS_3; secondly Cu_2SnS_3 reacts with $Zn_{1-x}Cd_xS$, forming $Cu_2Zn_xCd_{1-x}SnS_4$. Also, $Cu_2Zn_xCd_{1-x}SnS_4$ can be directly formed from the binaries in the presence of sufficient amounts of elemental sulphur. A single phase $Cu_2Zn_xCd_{1-x}SnS_4$ can be separated by washing away the flux and removing secondary phases by etching.

5. ACKNOWLEDGEMENTS

This research was supported by the Doctoral Studies and Internationalization Program DoRa of the European Social Funds, the Estonian Ministry of Education and Research Contracts No. SF0140099s08, TK117, AR10128 and by grants (No 8964, ETF 9425).

REFERENCES

1. FANG, Z., WANG, X., WU, H., ZHAO, C. Achievements and Challenges of CdS/CdTe Solar Cells. *International Journal of Photoenergy*, 2011, Vol. 2011, p. 1–8.
2. ROSE, D., HASOON, F., DHERE, R., ALBIN, D., RIBELIN, R., LI, X., MAHATHONGDY, Y., GESSERT, T., SHELDON, P. Fabrication Procedures and Process Sensitivities for CdS/CdTe Solar Cells. *Prog. Photovolt: Res. Appl.*, 1999, Vol. 7, p. 331–340.
3. ROMEO, N., BOSIO, A., TEDESCHI, R., CANEVARI, V. Growth of polycrystalline CdS and CdTe thin layers for high efficiency thin film solar cells. *Materials Chemistry and Physics*, 2000, Vol. 66, p. 201–206.

4. REPINS, I., BEALL, C., VORA, N., DEHART, C., KUCIAUSKAS, D., DIPPO, P., TO, B., MANN, J., HSU, W., GOODRICH, A., NOUFI, R. Co-evaporated $Cu_2ZnSnSe_4$ films and devices. *Solar Energy Materials & Solar Cells*, 2012, doi: 10.1016/j.solmat.2012.01.008
5. OLADEJI, I., CHOW, L., LIU, J., CHU, W., BUSTAMANTE, A., FREDRICKSEN, C., SCHULTE, A. Comparative study of CdS thin films deposited by single, continuous, and multiple dip chemical processes. *Thin Solid Films*, 2000, Vol. 359, p. 154–159.
6. LEINEMANN, I. Comparison of copper zinc tin selenide formation in molten potassium iodide and sodium iodide as flux materials. CYSENI 2011. Proceeding of annual conference of young scientists on energy issues. [CD]. Kaunas: Lithuanian Energy Institute. 2011 May 26–27.
7. KLAVINA, I., KALJUVEE, T., TIMMO, K., RAUDOJA, J., TRAKSMAA, R., ALTOSAAR, M., MEISSNER, D. Study of $Cu_2ZnSnSe_4$ monograin formation in molten KI starting from binary chalcogenides. *Thin Solid Films*, 2011, Vol. 519, p. 7399–7402.
8. TE VELDE, T. Electrical monograin layers having a radiation permeable electrode. US3480818, 1969, November 25.
9. MELLIKOV, E., HIIE, J., ALTOSAAR, M. Powder materials and technologies for solar cells. *International Journal of Materials & Product Technology*, 2007, Vol. 28, p. 91–311.
10. KLAVINA, I. CZTS ($Cu_2ZnSnSe_4$) crystal growth and use in monograin membrane solar cells. CYSENI 2010. Proceeding of annual conference of young scientists on energy issues. [CD]. Kaunas: Lithuanian Energy Institute. 2010 May 27–28.
11. ALTOSAAR. M, RAUDOJA, J., TIMMO, K., DANILSON, M., GROSSBERG, M., KRUSTOK, J., MELLIKOV, E. $Cu_2Zn_{1-x}Cd_xSn(Se_{1-y}S_y)_4$ solid solutions as absorber materials for solar cells. *Phys. stat. sol.*, 2008, Vol. 205a, No. 1, p. 167–170.
12. MATSUSHITA, H., ICHIKAWA, T., KATSUI, A. Structural, thermodynamical and optical properties of Cu_2-II-IV-VI_4 quaternary compound. *Journal of Materials Science*, 2005, Vol. 40, p. 2003–2005.
13. KASK, E., RAADIK, T., GROSSBERG, M., JOSEPSON, R., KRUSTOK, J. Deep defects in Cu_2ZnSnS_4 monograin solar cells. *Energy Procedia*, 2011, Vol. 10, p. 261–265.
14. DUMON A., LICHANOT A., GROMB S. Study of Cu-S phase diagram in compositional area $Cu_{2.000}S$-$Cu_{1.960}S$. *Chim. Phys.*, 1974, Vol. 71, No. 3, p. 407–414.
15. CHAKRABATI, D. J.; LAUGHLIN, D. E.: *Bull. Alloy Phase Diagrams 4*, 1983.
16. EMELEUS, H., SHARPE, A. *Advances in Inorganic Chemistry and Radiochemistry:* New York: Academic Press, Inc., 1980. 255 p. ISBN 0 -12-023623.
17. OLEKSEYUK, I., DUDCHAK, I., PISKACH, L. Phase equilibria in the Cu_2-Zn-SnS_2 system. *Journal of Alloys and Compounds*, 2004, Vol. 368, p. 135–143.
18. SCHURR, R., HÖLZING, A., JOST, S., HOCK, R., VOSS, T., SCHULZE, J., KIRBS, A., ENNAOUI, A., LUX-STEINER, M., WEBER, A., KÖTSCHAU, I., SCHOCK, H. The crystallisation of Cu_2ZnSnS_4 thin film solar cell absorbers from co-electroplated Cu-Zn-Sn precursors. *Thin Solid Films*, 2009, Vol. 517, p. 2465–2468.
19. FERNANDES, P., SALOME, P., CUNHA, A. Sudy of polycrystalline Cu_2ZnSnS_4 films by Raman scattering. *Journal of Alloys and Compounds*, 2011, Vol. 509, p. 7600–7606.

CYSENI 2012, May 24–25, Kaunas, Lithuania
ISSN 1822-7554, www.cyseni.com

BIOMASS POTENTIAL OF PERENNIAL ENERGY GRASSES

V. Tilvikienė, L. Šarūnaitė, L. Pocienė, Ž. Kadžiulienė
Institute of Agriculture,
Lithuanian Research Centre for Agriculture and Forestry
Instituto al. 1, LT-58344 – Lithuania
Phone +37034737752
Email: vita@lzi.lt

ABSTRACT

Rising energy prices, environmental problems, and Lithuania's energy dependence make us to look for alternative renewable energy sources. Consideration of our country's climatic condition, one of the most promising sources of renewable energy could be biomass. Perennial grasses can be used for the production of biofuel, bioplastics or other biomaterials. One of the most important factors in selecting perennial grasses for bioenergy is to get as high biomass yield as possible. There are a lot of energy grasses in Europe, which are grown for biogas production or burning. The biomass potential depend on growing conditions, this is why the selection of energy grasses should be done in all climate zones. The selection of perennial energy crops in Lithuanian institute of Agriculture was started in 2007. During this period the adaptability and productivity of traditional and introduced perennial grasses were analyzed. Studies include traditional grasses as - cocksfoot (*Dactylis glomerata* L.), tall fescue (*Festuca arundinacea* Schreb), reed canary grass (*Phalaris arundinacea* L.), and other herbaceous plants – *Miscanthus x gigantheus*, cup plant (*Silphium perfoliatum* L.), Virginia mallow (*Sida hermafrodita* R.) and others crops. Few of them showed high biomass yield and have potential to be promising energy crops. The biomass yield of traditional perennial grasses and others herbaceous plants in average of three year of use ranged between 8 and 14 t ha^{-1}.

Keywords: perennial grasses, biomass yield, bioenergy potential

1. INTRODUCTION

In past few years the very high attention in Europe is given to bioenergy. Till now the most popular bioenergy source in Lithuania was wood, but increasing interest in bioenergy sector and new processing technologies suggest looking for alternative energy sources in all sectors. At the moment sludge from waste water treatment, residues from food and fodder industry are used for biogas production [1], but the very high potential of raw materials for bioenergy could also be in agriculture [2; 17; 18]. It is known, that the surplus of straw is used as solid fuel for heating, but the demand of biomass for bioenergy is much higher, than it can be covered by using straw.

The one of most suitable source for bioenergy in agriculture are perennial grasses [3; 4]. Perennials can be grown in one place without reseeding more than 10 years; they do not require a lot of fertilizer and their quality can be managed by the cutting frequency, fertilization or by choosing the most suitable variety of grasses [5; 6; 7; 8]. Different requirements of biomass quality are for biogas production and for solid fuels, but there is one, which is the same for all bioenergy sources – it is biomass yield [9]. In different weather conditions the biomass yield of the same crops is different. Lewandowski et al. (2000) [10] reported, that in warm regions *Miscanthus giganteus* can produce more than 25 t ha^{-1} of dry biomass yield, but in a northern climate it's productivity is only about 10 t ha^{-1} or less.

The aim of this study was to evaluate the biomass potential of traditional and introduced perennial grasses, used for biogas production and for solid fuel.

2. METHODOLOGY

Field experiments were carried out in Lithuanian Institute of Agriculture, the first was established in 2008, the second one – in 2009. In this paper the average results of these experiments were analysed. Tall fescue (*Festuca arundinacea* Schreb), cocksfoot (*Dactylis glomerata* L.) and reed canary grass (*Phalaris arundinacea* L.) were grown on the *Endocalcari-Endohypogleyic Cambisol* (*CMg-n-w-can*) soil. Swards, fertilized with 90 and 180 kg ha^{-1} of mineral nitrogen fertilizer were cut three (first cut at heading stage) and four (firs cut at flowering stage) times per season. Traditional perennial grasses were grown for biogas production.

The experiment of growing introduced energy crops was established in 2007. *Miscanthus x giganteus*, cup plant (*Silphium perfoliatum* L.), Virginia mallow (*Sida hermafrodita* R.) were grown on the *Eutri-Cambic Arenosol* (*Arb-eu*) soil. Introduced perennial grasses were grown for solid fuel. They were cut once a year in late autumn after first frosts. The biomass yield of not fertilized swards was compared to those, which were fertilized with 60 and 120 kg ha^{-1} of mineral nitrogen fertilizer.

3. RESULTS AND DISCUSSION

3.1. Traditional perennial grasses for bioenergy

The selection of energy crops should be started from the traditional crops, because it is already known about their growing for other purposes and overwintering abilities. The main question for the researchers is how to get the highest biomass yield with the appropriate biomass quality for bioenergy. One of the ways to get bioenergy is biogas production.

In our research the average results of two year of sward use suggested, that growing technology had great importance on the productivity of tall fescue, cocksfoot and reed canary grass biomass for biogas. Tall fescue and reed canary grass produced the highest dry matter (DM) yield, when they have been cut twice per season (first cut at flowering) (Fig. 1). The average DM yield of tall fescue fertilized with 90 kg ha^{-1} of mineral nitrogen fertilizer was 9.399 t ha^{-1}, fertilized with 180 kg ha^{-1} – 9.878 t ha^{-1}. Reed canary grass yielded respectively 8.201 t ha^{-1} and 9.209 t ha^{-1}. In previous research Ruzgas and Kadžiulis (1989) [11] recommended to cut cocksfoot swards, fertilized with 240–360 kg ha^{-1} of mineral nitrogen fertilizer, three times per season. Our research suggested that cocksfoot, fertilized with lower nitrogen rates 90 and 180 kg ha^{-1} also tolerant frequent harvest. Cocksfoot produced the higher DM yield when swards were cut three times per season, compared to those which were harvested twice per season.

Reed canary grass significant effected to the fertilization with higher rate of nitrogen fertilizer. This confirmed the results of research, made in Estonia, where DM yield of reed canary grass increased continuously with the increase in nitrogen fertilizer input [12]. In our research the additional rate of 90 kg ha^{-1} of nitrogen fertilizer gave 1.200 tons of DM. The influence of higher rate of fertilizer was not very high for cocksfoot, but the results of our experiment confirmed those of Vasiliauskienė et al. (1989) [13] where it was noticed, that fertilization with higher rate of nitrogen fertilizer significantly increase biomass yield of early grasses. The lowest effect of nitrogen fertilizer was found on tall fescue.

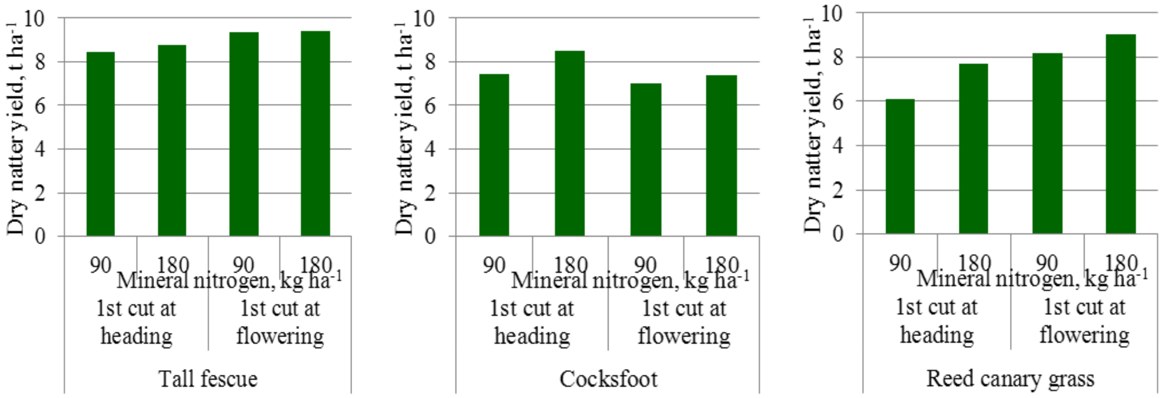

Fig. 1. The average biomass yield in the first and the second year of tall fescue, cocksfoot and reed canary grass growth

When we grow perennials, it is very important to get high DM yield every year, but the characteristics of grasses and also weather conditions greatly affect the productivity. In our two year experiment the very high reduction in DM yield of tall fescue and cocksfoot was measured in the second year of sward use (2010 in the first experiment and 2011 in the second experiment), compared to the yield of the first year (2009 in the first experiment and 2010 in the second experiment) of sward use (Fig. 2). Reed canary grass yield usually is lower in the first growing years [12]. In our research DM yield of this grass in the second year of sward use was similar to the DM yield of first year of swards use.

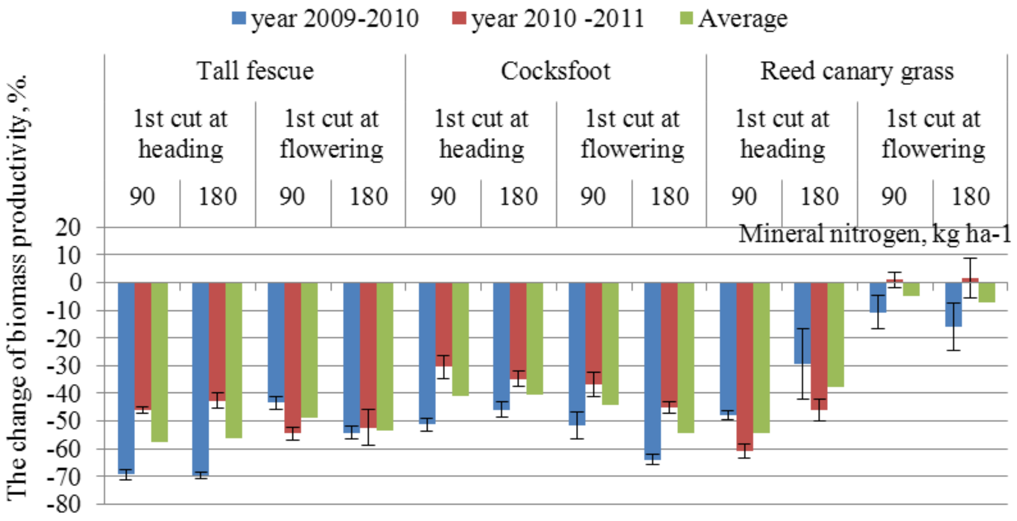

Fig. 2. The change of tall fescue, cocksfoot and reed canary grass biomass yield from the first to the second year of use

The biomass yield of traditional grasses was influenced by the cutting frequency and rate of nitrogen fertilizer. In two year of the experiment the most productive were tall fescue and reed canary grass.

3.2. Introduced perennial grasses for bioenergy

The need of high yielding energy crops give us to look for alternative – introduced crops. In Northern European countries there are few promising energy crops such as Virginia mallow and *Miscanthus* [14], which possibly could be grown in Lithuania [15; 16]. In our research the DM yield of not fertilized Virginia mallow was 6.997 t ha^{-1} in the first year of sward use, 11.626 t ha^{-1} in the second year and 10.504 t ha^{-1} in the third year of sward use (table 1). The fertilization with higher rate of nitrogen fertilizer increased the biomass yield.

The DM yield of *Miscanthus giganteus* vary significant in different weather conditions. In the first year of sward use not fertilized swards of *Miscanthus giganteus* produced 4.621 t ha^{-1} dry matter yield, in the second – 11.224 t ha^{-1} [15]. In the third year of sward use the biomass yield of this grass significantly decreased and was only 4.883 t ha^{-1}. The reduction of biomass yield could be influenced by weather conditions, because part of plants were damaged by the frost in spring, but more research are needed to prove the tendency. The fertilization with higher rate of nitrogen fertilizer had significant higher effect on DM only in the third year of sward use *Miscanthus giganteus.*

And the last, but not least energy crop, which was analysed in our research, was cup plant. In the first year of sward use the dry matter biomass yield of cup plant was 3.389 t ha^{-1}. In the second year of sward use the biomass yield of cup plant was more than three times higher, compared to the first year, but it decreased again in the third year of sward use. The fertilization with higher rate of nitrogen fertilizer had significant higher effect on biomass yield only in the third year of sward use.

Table 1. Biomass yield of introduced perennial grasses.

Grasses	Fertilization	Dry matter yield, t DM ha^{-1}		
		Year		
		2008	2009	2010
Virginia mallow	N_0	6.997	11.626	10.504
	N_{60}	9.548	12.372	14.003
	N_{120}	7.324	14.291	8.948
R_{05}		2.835	2.847	2.005
Cup plant	N_0	3.389	11.850	4.541
	N_{60}	4.327	18.125	9.833
	N_{120}	3.801	18.202	6.757
R_{05}		1.965	1.810	2.019
Miscanthus giganteus	N_0	4.621	11.224	4.883
	N_{60}	6.549	11.015	7.219
	N_{120}	6.824	12.236	7.797
R_{05}		1.981	2.209	2.374

The selected introduced energy crops showed the promising results of their productivity in the second year of sward use, but the reduction of biomass yield in the third year suggest to proceed the research and to look if this was effected by the influence of weather conditions or by other factors.

CONSLUSIONS

The biomass yield of traditional grasses was influenced by the cutting frequency and rate of nitrogen fertilizer. In two year of the experiment the most productive were tall fescue and reed canary grass. The average dry matter biomass yield of tall fescue fertilized with 90 kg ha^{-1} of mineral nitrogen fertilizer was 9.399 t ha^{-1}, fertilized with 180 kg ha^{-1} – 9.878 t ha^{-1}. Reed canary grass yielded respectively 8.201 t ha^{-1} and 9.209 t ha^{-1}.

The selected introduced energy crops showed the promising results of their productivity in the second year of sward use, but the reduction of biomass yield in the third year of sward use suggest to prolong the research with introduced herbaceous crops.

REFERENCES

1. HE P. J. Anaerobic digestion: An intriguing long history in China. *Waste Management*, 2010, Vol. 30, No. 4, p. 549–550.
2. AMON, T., AMON, B., KRYVORUCHKO, V., ZOLLITSCH, W., MAYER, K., GRUBER, L. Biogas production from maize and dairy cattle manure – influence of biomass composition on the methane yield. *Agricultural Ecosystems and Environment*, 2007, vol. 118, p. 173–182.
3. CEOTTO, E. Grasslands for bioenergy production. A review. *Agronomy for Sustainable Development*, 2008, Vol. 28(1), p. 47–55.
4. GUNASEELAN, V. N. Anaerobic digestion of biomass for methane production: a review. *Biomass and Bioenergy*, 1997, Vol. 13, p. 83–114.
5. HEJDUK, S., HRABĚ, F. Influence of different systems of grazing, type of swards and fertilizing on underground phytomass of pastures. *Plant, Soil and Environment*, 2003, Vol. 49, p. 18–23.
6. KANAPECKAS J., LEMEŽIENĖ N., TARAKANOVAS P., NEKROŠAS S., PAPLAUSKIENĖ V. Dependince of the productivity and quality of perennial grasses on time of heading. *Agricultural Sciences* 1999, Nr. 1, p. 10-16.
7. KANAPECKAS J., LEMEŽIENĖ N., BUTKUTĖ B., STUKONIS V. Evaluation of tall fescue (*Festuca arundinace* Scherb.) varieties and wild ecotypes as feedstock for biogas production. *Žemdirbystė=Agriculture*, 2011, Vol. 98, No. 2, p. 149–156.
8. LEMEŽIENĖ, N., KANAPECKAS, J., BUTKUTE, B. Varieties, breeding lines and ecotypes of cocksfoot (*Dactylis glomerata* L.) that are the most suitable for biogas production. *Žemdirbystė=Agriculture*, 2009, Vol. 96, p. 36–46.
9. PROCHNOW, A., HEIERMANN, M., PLÖCHL, M., LINKE, B., IDLER, C., AMON, T., HOBBS, P. Bioenergy from Permanent Grassland – A Review: 1. Biogas. *Bioresource Technology*, 2009, Vol. 100, p. 4931–4944.
10. LEWANDOWSKI I., CLIFTON-BROWN J.C., SCURLOCK J.M.O., HUISMAN W. Miscanthus: European experience with a novel energy crop. *Biomass and bioenergy*, 2000, Vol. 19, p. 209–227.
11. SANDERSON M.A., ADLER P.R. Perennial Forages as Second Generation Bioenergy Crops. *International Journal of Molecular Sciences*, 2008, Vol. 9, p. 768–788.
12. KUKK L., ASTOVER A., ROOSTALU H., ROSSNER H., TAMM I. The Dependence of Reed Canary Grass (*Phalaris arundinacea* L.) Energy efficiency and profitability on nitrogen fertilization and transportation distance http://www.eau.ee/~agronomy/vol08Spec1/p08s115.pdf [04 03 2012].
13. VASILIAUSKIENE, V., DAPKUS, R., MASAUSKIENE, A., SVIRSKIENE, A. Rates of nitrogen and its distribution on early pasturable herbages. *Žemdirbystė=Agriculture*, 1989, Vol. 37, p. 69–81.
14. WRÓBLEWSKA H., KOMOROWICZ M., PAWŁOWSKI J., CICHY W. Chemical and energetical properties of selected lignocellulose raw materials. *Foloa Forestalia polonica,* 2009, – Issue 40, p. 67–78.
15. KRYŽEVIČIENĖ A., KADŽIULIENĖ Ž., ŠARŪNAITĖ L., DABKEVIČIUS Z., TILVIKIENĖ V., ŠLEPETYS J. Cultivation of *Miscanthus* × *giganteus* for biofuel and its

tolerance of Lithuania's climate. *Žemdirbystė-Agriculture*, 2011, Vol. 98 (3). p. 267–274.

16. KRYŽEVIČIENĖ A., ŠARŪNAITĖ L., STUKONIS V. Miscanthus (Miscanthus giganteus), Virginia mallow (Sida Hermaphrodita) Cup plant (Silphium perfoliatum) and mugwort (Artemisia), biofuels production in Lithuania. *Soil stability in ecologically and socially sensitive areas: scientific articles.* Akademija, 2009, p. 195–199.
17. NAVICKAS K., VENSLAUSKAS K., ZUPERKA V., NEKROSIUS A., KULIKAUSKAS T. Energy balance of biogas production from perennial grasses. *Engineering for rural development*, 2011, p. 382–387.
18. NAVICKAS K. Biogas for farming, energy conversion and environment protection, *International symposium, Biogas, technology and environment, University of Maribor, Faculty of Agriculture*, 2007, p. 25–29.

CYSENI 2012, May 24–25, Kaunas, Lithuania
ISSN 1822-7554, www.cyseni.com

STUDY ON TECHNOLOGY IMPLEMENTATION CONCEPT OF ALGAE CULTIVATION AS AN ALTERNATIVE ENERGY FOR COMMUNITY

S.N.A.F. Rahma
Bachelor of Science, Faculty of Biology, Gadjah Mada University
Teknika Selatan Street, Sekip Utara, Yogyakarta 55281 – Indonesia
Phone +62 82136104534
Email: snazizah87@gmail.com

A. Saputra
Master of Mechanical Engineering, University of Aveiro
Campo Universitario de Santiago 3810-193 Aveiro – Portugal
Phone +351 966773020
Email: artupasida_13@yahoo.co.id

ABSTRACT

Depleting of fossil fuel supplies as unrenewable energy source have been forced peoples to find some alternative energy sources. Alternative energy source become a contentious issue in resolving this problem. Algae cultivation is one of the solutions which can be used to reduce our dependence to fossil fuels. The objective of this study is to describe a prospect of microalgae cultivation technology and its positive benefits for a community in Indonesia as an alternative energy sources. As we know that, algae are the one solution which has being developed to cover energy crisis problem and for produce an alternative energy nowadays. In addition, algae also could reduce CO_2 gas which can cause greenhouse effect.

Microalgae can be growth faster than other terrestrial plants. The yield of microalgae oil could produce approximately 58.700-136.900 litre/ha. This biofuel contain no sulphur, no toxic and highly biodegradable. There are many of method can be used for cultivating microalgae to get oil from microalgae. Bioreactor is the advanced technology method to cultivate algae for getting higher yield oil.

An oil of microalgae could be used as biodiesel or fuel for jet machine. Not only for biofuel, biomass from algae also can produce methane gas for providing the electricity. The green waste from residue of oil extract could produce butane. Many benefits of microalgae which cause this plant are very interesting to learn. Therefore, a technology implementation concept of algae cultivation for a community is needed before dropping to the field. So the success of this concept will be a positive impact on the lives of local people.

Keywords: algae cultivation, community, alternative energy, technology implementation concept

1. INTRODUCTION

Oil and gas are the most of consumption energy source used in the world. Every year, increasing of demand oil and gas always become interesting main topic, because it makes depleting of oil and gas in earth. World energy consumption is estimated will increase 40% for 20 years later. Increasing of industry and transportation in every year have been effect on increasing energy consumption especially oil and gas consumption. In 2006, oil and gas consumption especially in transportation have reached 51.66% in Indonesia. It makes depleting fossil fuel reserves in Indonesia. Therefore, this unrenewable energy source has forced Indonesian people to find some alternative energy. Algae is the one of renewable alternative energy source which has benefit for the community. Algae could become biofuel as substitution for oil and gas. Recently, Surakarta has been becoming pioneer of car industry in Indonesia. Cars that made by groups of student in vocational senior high school at Surakarta are still in processing of examination. These cars that called “kiat ESEMKA” still using oil as their fuel. Not only oil, but also they will improve it car with gas as fuel. Both of energy source are unrenewable energy source, therefore algae biofuel could be propose to replace both fuel. Until now, there are many car that begin to build in Indonesia. It has been known that algae could produce more oil than other terrestrial plant. Microalgae is type of algae that used for biodiesel production. Microalgae can be treated into an advanced biofuel such as green diesel, jet fuel, ethanol, methane and butanol. Not only as biofuel, microalgae has been developed in cosmetic, fish food, human supplement, and other product. In addition, culture of microalgae is easy because algae could exist in saline, brackish, wastewater, and marine. Therefore, the objective of this study is to know about the prospect of culture algae and their benefits for Indonesia. [2, 6, 1]

2. MICROALGAE UTILIZATION AS AN ALTERNATIVE ENERGY SOURCE

2.1. Microalgae as An Alternative Energy Source

Algae use sunlight and carbon dioxide to create biomass. It has many benefits in life. Algae often use as protein or nutritional source, cosmetics, and as biofuel substituting oil and gas. It also could be treated become biodiesel for vehicle fuel. This plant could grow in unbenefit environment such as wastewater. Not only wastewater, algae could exist in brackish, saline, bogs, swamps, marshes and marine. Algae has two classification comprise of macroalgae and microalgae. Macroalgae is multicellular organism and has large size, while microalgae is unicellular organism and has tiny size (1-100µm). Microalgae is distincted from macroalgae and seaweed. It has potentially for producing until 200 times more oil than soybean or other terrestrial plant, as described in table 1.

Table 1. Oil production from varies of plant

Plant	Oil production (l/ha)
Corn	172
Soybean	446
Sunflower	1190
Castor	1892
Coconut	2689
Palm	5950
Microalgae (lipid content 70%)	136.900
Microalgae (lipid content 30%)	58.700

In addition, some microalgae strains are also could double their mass several times per day. They live as single or cluster in marine or freshwater. Approximately 40–50% of oxygen in the atmosphere is produced by microalgae. There are a hundred species of algae that exist in Indonesia because Indonesia has a large of marine, many river, swamps or marshes. Sunlight in all year also provides the existence of algae in this country. It should have easily to find some microalgae for cultivate in order to produce oil and other nutrient product. Lipid content in microalgae is very influence whether microalgae has potential source for biodiesel production. It should has high lipid in biomass and higher in productivity, such as *Chlorella vulgaris*, *Nannochloropsis*, *Botrycoccus braunii* and *Diatomae* species as described in Table 2.

Table 2. Lipid contents in varieties of microalgae (Mata et al. 2010)

Marine And Freshwater Microalgae Species	Lipid content (% dry weight biomass)
Ankistrodesmus sp.	24.0-31.0
Botryococcus braunii	25.0-75.0
Chaetoceros muelleri	33.6
Chaetoceros calcitrans	14.6-16.4/39.8
Chlorella emersonii	25.0-63.0
Chlorella protothecoides	14.6-57.8
Chlorella sorokiniana	19.0-22.0
Chlorella vulgaris	5.0-58.0
Chorella sp.	10.0-48.0
Chlorella pyrenoidosa	2.0
Chlorella	18.0-57.0
Chlorococcum sp.	19.3
Crypthecodinium cohnii	20.0-51.1
Dunaliella salina	6.0-25.0
Dunaliella primolecta	23.1
Dunaliella tertiolecta	16.7-71.0
Dunaliella sp.	17.5-67.0
Ellipsoidion sp.	27.4
Euglena gracilis	14.0-20.0
Haematococcus pluvialis	25.0
Isochrysis galbana	7.0-40.0
Isochrysis sp.	7.1-33
Monodus subterraneus	16.0
Monallanthus salina	20.00-22.0
Nannochloris sp.	20.0-56.0
Nannochloropsis oculata	22.7-29.7
Nannochloropsis sp.	12.0-53.0
Neochloris oleoabundans	29.0-65.0
Nitzschia sp.	16.0-47.0
Oocystis pusilla	10.5
Pavlova salina	30.9
Pavlova lutheri	35.5
Phaeodactylum tricornutum	18.0-57.0
Porphyridium cruentum	9.0-18.8/60.7
Scenesdemus obliquus	11.0-55.0
Scenesdesmus quadricauda	1.9-18.4
Scenedesmus sp.	19.6-21.1
Skeletonema sp.	13.3-31.8
Skeletonema costatum	13.5-51.3
Spirulina platensis	4.0-16.6
Spirulina maxima	4.0-9.0
Thalassiosira pseudonana	20.6
Tetraselmis suecica	8.5-23.0
Tetraselmis sp.	12.6-14.7

[3, 18, 4, 8, 10]

2.2. Microalgae Growing Methods

Like plant, microalgae need three requirements to grow which comprises of sunlight, carbondioxide, and water. Based on research, it has known that microalgae has specific term to growth. Microalgae need appropriate place (open ponds) or equipment (closed photo-bioreactor) that supports their growth. Microalgae has growth temperature adaptation in range 25–30°C. The salinity of water is 17.6 with conductivity value as range 457-488 and pH in range 6.5-8. Microalgae also has ability to convert solar energy to chemical energy. Algae use solar energy to fix carbon dioxide into biomass during photosynthesis process. Therefore, the water must be enrichment with carbon dioxide during cultivation of Algae. Eventhough algae could live in all habitat water, algae can be so picky. Algae can be cultivated in large ponds or in closed photo-bioreactors placed on non-arable land in variety of climate (including of desert). After harvesting from ponds or photo-bioreactor, algae could be treated to be different product including biofuel or some nutreutical.

Eventhough microalgae is easier to live in all habitat water, we still need growing methods in order to have biofuel product output. There are two ways for cultivating microalgae consist of open pond and closed photo-bioreactor:

2.2.1 Open Ponds

Open ponds are common way for microalgae cultivation. Lake, fish pond, pool include of artificial pool. Artificial pool could be made use PVC, cement and clayey. Open ponds have advantages and disadvantages. Open pond easily to made and cheap because it just need sun light for photosynthesis system, eventhough sun light couldn`t reach in deepness of big volume scale open pond. The other challenges in cultivation of algae are including of algae could die because of too much sunlight, temperature must be steady, overcrowding could inhibit their growth and biomass productivity can be contaminated with unwanted other algae. Rain and evaporation could make salinity and pH imbalances. If we want to cultivate in ponds, we must be maintain temperature, pH, sunlight and salinity steady. Open ponds need continuous addition of water because of evaporation. In addition, open system (ponds) need to improve control or light penetration and improve with inexpensive removable covers for decrease possibility of rain or sunlight penetration. The artificial open ponds need certain estimation and requirement to build as Fig. 1.

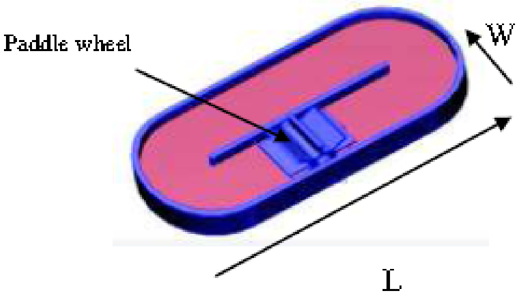

Fig. 1. Geometry algae open Ponds (L: length of open pond, W: channel wide)

According to research analysis of open ponds, it has known that increasing of fluid speed could be decrease dead zone in open ponds. Dead zone is zone whereas microalgae couldn`t grow. Fluid speed also influence on microalgae growth rate. The bigger L/w can equalize distribution speed. Equalization of distribution speed could improve microalgae growthness. [17, 4, 15, 5]

2.2.2. Photo-Bioreactor

Photo-bioreactor is the best equipment for cultivate and harvest microalgae. It is a reactor that helps microalgae for better cultivating. It is made from transparent glass and commonly placed in outdoors for illuminating by sunlight. Either it is could be placed indoors illuminating with UV light. Photo-bioreactor must be set up to maintain sunlight directly to algae, keep temperature, salinity and pH steady. It should has scalability, especially in mixing and gas exchange (both oxygen and carbon dioxide). The culture in photo-bioreactor must be returned to degassing zone-an area where microalgae broth is bubbled with air to remove oxygen. Also, Carbon dioxide fed up in this photo-bioreactor. Temperature of Photo-bioreactor must be maintained efficiently. It must be cooling during daylight hours and also regulated well in night hours.

The advantages of this photo-bioreactor are this closed system lose less water because it doesn't get evaporating like open system. Photo-bioreactor also can provide better light that produce high volumetric cell density. It also could prevent contamination from unwanted microalgae. Nevertheless, it is more expensive than open ponds. This disadvantage could be improved with engineering design or inexpensive material such as using plastic bag instead of heavy tubes. Photo-bioreactor for microalgae cultivation in Indonesia is still in developing process. For instead, photo-bioreactor that already built in Environmental Technology Center BPPT (Badan Pengkajian dan Penerapan Teknologi), Jakarta. Cost of photo-bioreactor prototype reach until 50 million rupiahs. This multitubular airlift photo-bioreactor has function for mitigating CO_2 using *Chlorella* sp. for reducing or absorbing carbondioxide from industry. It has known that this photo-bioreactor design were succeed for absorbing carbon dioxide approximately 4.8–6% per day with absorbing power reach to 0.8-1 gram/litre medium/day.

Fig. 2. Multitubular Airlift Photo-Bioreactor Design for Cultivating Microalgae That Developed In BPPT

This photo-bioreactor has already used by Emision of Indolacto Milk Factory, Ciracas. Emission of factory is absorb by compressor into container, then flows to acrylic pipe whereas microalgae had cultured. [18, 13, 15]

3. ECONOMICAL AND ENVIRONMENTAL BENEFIT OF MICROALGAE CULTIVATION FOR INDONESIA

Microalgae cultivation has many advantages for Indonesia include of economical and environmental benefits:

3.1. Economical Benefits

Cultivation of microalgae doesn`t need arable land. Algae could grow in waste water or place which has poor nutrition. Microalgae could developing in surface of water, they have simple structure and reproductive structure than other terrestrial plant (don`t have true roots, leaves, stems or vascular tissue). Nevertheless, they have photosynthesis mechanism like other plant. They could assimilate their own nutrition in water such as nitrogen, fosfor so that it can produce 100 more oil crop per area than other plant. Microalgae could be extracted and treated become microalgae biofuel. Not only biofuel, but residu from extraction of microalgae oil could be produce include of methane, bioethanol, fertilizer etc. [11, 1]

3.2. Environmental Benefits

Microalgae can absorb carbon dioxide and release oxygen. This advantage could provide for reducing carbon dioxide emission from Industry in Indonesia. It can provide to prevent air pollution and greenhouse effect in Indonesia. It has been usually growing and developing near factory for absorbing carbon dioxide. For instead, *Chlorella* sp. could cultured for mitigating CO_2. Microalgae cultivation also could be used for wastewater or sewage treatment. They could treat both municipal and industrial sewage as water recycling. Government has been doing research as remedial for water pollutan from industry. For instead, based on research, it has known that microalgae such as *Spirulina* sp., *Oscillatoria* sp., *Microcystis* sp., they could absorb chromium metal. In addition, it could increase production of microalgae biomass. [9,14]

4. CHALLENGES OF MICROALGAE CULTIVATION AND THEIR DEVELOPMENT PRODUCT ON INDONESIA

4.1. Challenges of Microalgae Cultivation

Cultivation of microalgae also has little problem in Indonesia. It because of Indonesia has rain and evaporation. Cultivation in open ponds need some regulation and control about sunlight penetration and continuous addition water. The cheaper opened pond is to cultivate microalgae in swimming pool. The best way for microalgae cultivating is photo-bioreactor. It because unwanted microalgae could be eliminated. Unfortunately, cultivation on photo-bioreactor is still cost intensive and also expensive. Nevertheless, it could be solved using plastic bag instead of heavy tube. According to Bayu (2010), an advanced genetic engineering must be implemented in microalgae in order to enhance their quality [1, 4].

4.2. Challenges of Their Development Product

4.2.1. Development of Microalgae Biodiesel

Microalgae biofuel has already been observed in Indonesia. The main problem development of microalgae biofuel in Indonesia is the production cost could reach 2.8 dollar/litre. It is much higher than production cost of palm or castor oil which reach 0.52 dollar/litre. There is company that already developing microalgae biofuel in Jakarta, Indonesia. Indonesia government also has already developing this product for biofuel vehicle. Nevertheless, there are still not much people know and use algae biofuel. Oil from fossil fuel is still used by Indonesian people, because just little vehicle in Indonesia that use biofuel, and Indonesia still depend on oil from fossil fuel. Algae biofuel has more advantages than oil from fossil fuel including of contain no sulfur, no toxic and highly biodegradable, but Indonesia market is still lack of consumer [1, 3, 11].

4.2.2. Development of Other Product

Microalgae can be used as many benefit product. Not only biodiesel, but microalgae could be treated become human food, fish food, fertilizer, cosmetic materials. In Indonesia, Microalgae has been developed as fish food in order to fish production, such as *Spirulina* sp. has been developed for feeding fish in BBAP Jepara. *Chlorella pyrenoidosa* that produce Lutein also treated for cosmetic material.[7]

5. CONCLUSION

Indonesia has potential source for having cultivation of microalgae in order to produce algae biofuel. There are two ways for microalgae cultivation consist of open system (ponds) and closed photo-bioreactor. Open ponds need precise estimation in length of ponds and channel wide for produce the best cultivation for improve yield of microalgae. Photo-bioreactor need precise temperature, steady pH, and in exchange of carbon dioxide and oxygen. Both of open system and closed system have advantages and disadvantages. Microalgae cultivation has many benefit for Indonesia include of wastewater treatment, mitigation of CO_2 (reducing carbon dioxide and prevent green house effect), producing biofuel that have possibility to replace fossil fuel for provide advanced of car industry in Indonesia, etc. Nevertheless, there are still some challenges for microalgae cultivating in Indonesia. Therefore, if microalgae cultivation could be developing, it will be have good impact in Indonesia.

REFERENCES

1. BAYU, A. Biodiesel Dari Mikroalga Laut : Potensi dan Tantangan. *Oseana*, 2010, Vol. XXXV, No. 1, p. 15–24. ISSN 0216.
2. CHADIE. *Mobil ESEMKA Terlalu Canggih untuk Ukuran Buatan Lokal*, 2012 – [referred on the 4th march 2012]. Link to the internet < http://www.mediaindonesia.com>
3. CHRISTI,Y. Biodiesel from Microalgae. *Biotechnology advanced*, 2007, Vol. 25, p. 294-306.
4. CHENG, Kuan C.; OGDEN, Kimberly L. *Alga Biofuels : The Research*, 2011, American Institute of Chemical Engineering, p. 42–47.
5. HADIYANTO; SAMIDJAN, I; KUMORO, Andri C., SILVIANA. Produksi Mikroalga Berbiomassa Tinggi dalam Bioreaktor Open Pond. Prosiding Seminar Nasional Teknik Kimia “Kejuangan”. Pengembangan Teknologi Kimia Untuk Pengolahan Sumber Daya Alam Indonesia 2010. hal : 46-51. ISSN 1693-4393.
6. *Kementerian Koordinator Bidang Perekonomian Republik Indonesia*. Resume Minyak Bumi, 2011 – [referred on the 29th February in 2012]. Link to the internet < http://www.ekon.go.id >
7. KUSMIATI. Peningkatan Produksi Lutein Dari Mikroalga Chlorella pyrenoidosa untuk Penyediaan Bahan Baku Kosmetika dan Uji Efektivitas Sebagai Antioksidan (In Vivo). Pusat Penelitian Bioteknologi Lembaga Ilmu Pengetahuan Indonesia (LIPI) 2010.
8. MATA, Teresa M; MARTINS, Antonio A.; CAETANO, Nidia S. Microalgae for Biodiesel Production and Other Application : A review. *Renewable and Sustainable Energy Reviews*, 2010, Vol. 14, p.217–232.
9. MULYANTO, A. Microalga (*Chlorella* sp.) Sebagai Agensia Penambat Gas Karbon dioksida. *J.Hidrosfir Indonesia*, 2010, Vol. 5, No. 2, p. 13–23. ISSN 1907-1043.
10. NUGROHO, Kus A.; PARAMITA, Vidia, Potensi Ganggang Mikro Sebagai Sumber Energi Terbarukan, 2011- [referred on the 4th march in 2012]. Link to the internet < http://konversi.wordpress.com>

11. Oilgae. About Algae, 2012 – [referred on 4th march in 2012]. Link to the internet <http://www.oilgae.com/algae/algae.html>
12. PANGGABEAN, M.G.L; SOETOMO ; NOERDJITO, Diah R; AFDAL. Mikroalga Laut Sebagai Produsen Biodiesel. Pusat Penelitian Oseanografi Lembaga Ilmu Pengetahuan Indonesia 2010.
13. PRASETYA, W. BPPT : Fotobioreaktor mampu Serap 90% CO_2, 2010 – [reffered on 21th april in 2012]. Link to the internet <http://www.sigapbencana-bansos.info/berita/4802-bppt-fotobioreaktor-mikroalgae-mampu-serap-90-co2.html>
14. SHOLIHAT, R.; NILAWATI, Tina S., 2008. Potensi Mikroalga Mati pada Kolam Stabilisasi Pengolahan Air Kotor Sebagai Biosorbent Logam Berat Krom. Data Penelitian Universitas Pendidikan Indonesia.
15. UGWU, C.U; AOYAGI, H.; UCHIYAMA, H. 2007. Photobioreactors for Mass Cultivation of Algae. Bioresource Technology. In press.
16. WAGNER, L. *Biodiesel from Algae Oil*. Mora Associates Ltd, 2007, p. 1–3
17. WULANDARI, Asri P.; NADERIA F.; PATTALIA, Annisa E.; PERMATA, Dilaekha R. Identifikasi Mikroalgae di Sekitar Pantai Pangandaran dan Potensi Pertumbuhannya pada Formulasi Medium Ekstrak Tauge (MET). Prosiding Seminar Nasional Limnologi V tahun 2010, p. 1–8.
18. WEN, Z.; JOHNSON, Michael B. Microalgae As Feedstock for Biofuel production. Virginia Cooperative Extension 2009. Publication 442-886. p. 1–7.

CYSENI 2012, May 24–25, Kaunas, Lithuania
ISSN 1822-7554, www.cyseni.com

HEAT LOSSES INFLUENCE ON SOLAR THERMAL SYSTEMS

P.Shipkovs[1,2], **A.Snegirjovs**[1,2], **L.Migla**[1,2]
1 Institute of Physical Energetics
Aizkraukles 21, LV-1006 Riga – Latvia
Email: shipkovs@edi.lv

2 Riga Technical University
Azenes 16/20, LV-1048 Riga – Latvia
Email: andrejs.snegirjovs@rtu.lv

ABSTRACT

Heat losses are more than 30% from the collector field yield gain in typical solar thermal systems in Baltic countries region. Heat losses increase arises mainly from reduced outdoor air temperature. Outdoor air temperature is lower in Baltic countries region in comparison with other European countries where solar collectors are more widespread. This creates the need for solar thermal system optimization in Baltic region.

A dynamic modelling program with real meteorological data was used, consider of many factors dynamic changes for heat losses determination in separate components of a solar thermal system.

Meteorological data was collected at the “Solar energy testing polygon” at the Institute of Physical Energetics in Latvia. Meteorological data of several years were collected and entered into the modelling program. The results of modelling program have been compared with the results of solar collectors testing in the real conditions in solar energy polygon. A lot of the results were compared and several regularities were obtained.

Solar collectors productivity dependence from the system heat losses was determined. Efficiency of some systems elements increases with reduction of heat carrier temperature as a result of heat losses. Therefore, the overall efficiency of solar thermal system decreases nonlinearly at heat losses increase.

Dependence of heat losses quantity from conductivity coefficient of the separate components of the solar thermal system was included in the studies for deeper and wider research. These dependencies were determined for conductivity coefficient of solar collector, pipeline and tank insulation.

Obtained regularities allow to figure out yields and energy saving more precisely and get more accurate cost analysis in solar thermal systems. It will help further for this system optimization.

Keywords: Renewable Energy; Solar thermal systems; efficiency increasing

1. INTRODUCTION

The average efficiency of the solar thermal systems (STS) for well- designed thermal systems with glazed flat- plate collectors is about 30–35% in Baltic countries region. Global solar radiation is about 1100–1190 kW/m^2 per annum, each square meter of thermal energy. If evacuated tube collectors are used, the efficiency increased to about 35–40%, because of the collectors the lower heat losses.

A significant part of solar collectors absorbed energy is consumed as heat losses in solar collectors, in solar collector circuit and in accumulation tank. The heat losses in solar collector circuit and accumulation tank are more than 30% from the collector field yield gain in typical solar thermal systems in Baltic countries region.

Heat losses are dependent mostly from temperature difference between outdoor air and absorber or heat carrier temperature.

Annual global solar radiation is lower in Baltic countries region in comparison with other European countries where solar collectors are more widespread. And outdoor air temperature range is below average values in Europe. This creates the need for solar thermal system optimization in Baltic countries region. Determination of regularity of the main factors which could influence STS productivity is necessary for STS optimization [2].

The same typical STS were tested in different Europe regions using dynamic simulating program. Results were equated to 1 square meter of solar collector absorber.

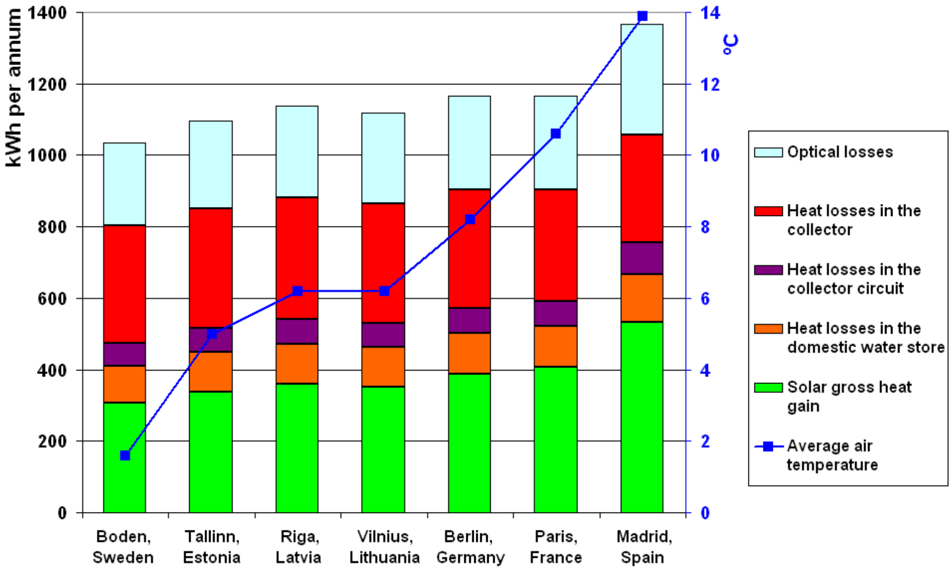

Fig. 1. STS productivity and energy losses in different part of solar thermal systems in different counties

As shown in fig.1 the solar collector heat losses are larger in Baltic country region than in Berlin by 3%, Paris by 9% and Madrid by 13%. It is larger notwithstanding the fact that STS work hours is more in warmer regions. If consider the numerical values, pipeline heat losses is higher in warmer regions. But if consider proportionally to global solar radiation that falls on solar collectors, heat losses is lower in collector circuit in warmer regions. Therefore regularities of heat losses and coefficient of thermal conductivity of the single components of the STS differ in Baltic country regions than in warmer regions.

The results of studies about of heat losses dependence from conductivity coefficient of the single components of the solar thermal system are described in this report. This dependence was determined for conductivity coefficient of: solar collector, pipeline and tank insulation.

2. METHODS

Heat losses in different parts of STS change with weather condition. The cooling of heat carrier exists in pipeline in time when heat carrier circulation stops.

For quantification of these effects, computer simulations are necessary. POLYSUN was used for determination of annual productivity of solar collectors and quantity of heat losses from thermal conductivity coefficients of the single component of the STS. POLYSUN is dynamic simulation program specified for the STS.

The weather condition data from “solar energy testing polygon” was integrated into the program with an hourly resolution. Solar energy testing polygon is located at the Institute of Physical Energetic in Latvia. High accuracy measuring equipment was used for weather data collecting. Global solar radiation was detected with CMP3 and CMP21 pyranometers. Outdoor air temperature was measured with PT100 resistance thermometer. Period of data collection is 4 years, from 2008 to 2011.

The STS productivity (Q_{STS}) is equal to solar collector produced energy (Q_c) minus heat losses in the single components of the STS:

$$Q_{STS} = Q_c - H_p - H_a \text{ [kWh]}^{[4]}. \quad (1)$$

Where: H_p – heat losses in pipes (kWh), H_a – heat losses in accumulation tank (kWh).

Heat losses depend from the thermal conductivity coefficient and the temperature difference between heat carrier and surrounding air or between absorber and outdoor air temperature. Thermal conductivity coefficient is constant for single component of STS, but temperature difference change over time.

The (q_c) solar collector instant productivity is calculated from the available irradiance at the absorber, converted into the heat, minus the thermal losses through convection and radiation:

$$q_c = G_a - h_c \text{ [W/m}^2\text{]}^{[1]} \quad (2)$$

Where G_a is available irradiance (W/m^2), and h_c represents the thermal losses (W/m^2).

The available irradiance is obtained mathematically from product of: the irradiance hitting the glass pane, G; the degree of transmission of the glass, τ; and the degree of absorption of the absorber, α:

$$G_a = G \cdot \tau \cdot \alpha \text{ [W/m}^2\text{]}^{[1]} \quad (3)$$

The thermal losses of solar collector are dependent on the temperature difference between the absorber and the air, $\Delta\theta$. To a first approximation (for low absorber temperatures) this relationship is linear, and can be described by the heat loss coefficient, K_C (W/m^2):

$$h_c = K_c \cdot \Delta\theta \text{ [W/m}^2\text{]} \quad (4)$$

At higher absorber temperatures the thermal losses no longer increase linearly with the temperature difference but instead increase more strongly as a result of increasing thermal radiation. The characteristic line therefore has some curvature and the equation in a second order approximation is:

$$h_c = c1 \cdot \Delta\theta + c2 \cdot \Delta\theta^2 \text{ [W/m}^2\text{]}^{[1]} \quad (5)$$

Where *c1* is linear heat losses coefficient of solar collector (W/(m^2*K)) and *c2* is the quadratic heat losses coefficient (W/(m^2*K^2)).

Coefficient of thermal conductivity in pipeline (K_P) was calculated taking into account: λ the thermal conductivity of the insulating material (W/(m^2*K)); *l* pipes length (m); *ln* is natural logarithm; *D* is the outside dimension of the insulated pipe (mm); *d* is the outside diameter of pipe:

$$K_P = \frac{\lambda \cdot l}{\ln\left(\frac{D}{d}\right)} \text{ [W/(m*K)]}^{[1]} \quad (6)$$

Accumulation tank is cylinder form in most cases. Therefore calculation of coefficient of thermal conductivity of accumulation tank (K_A) was similar as pipe calculation plus thermal conductivity from area in top and bottom of accumulation tank:

$$K_A = \frac{\lambda \cdot l}{\ln\left(\frac{D}{d}\right)} + \lambda \cdot \pi \cdot \left(\frac{d}{2}\right)^2 \text{ [W/(m*K)].} \tag{7}$$

Where π is a mathematical constant (≈3.14).

Average parameters of typical STS are entered into the program. Average parameters of 40 evacuated tube and 85 flat plate collectors have been used in simulation program. The nominal parameters of STS simulations: tilt angle of solar collectors 60º and 45º; η0, optical efficiency of solar collectors 0.77; c1, linear heat losses coefficient of solar collector 3.5 and 1.25 (W/(m^2*K)); c2, the quadratic heat losses coefficient 0.015 (W/(m^2*K^2)); volume of accumulation tank 0.1m^3 per square meter of solar collector; K$_p$, thermal conductivity of pipeline 0.28 W/K per square meter of solar collector; K$_a$, thermal conductivity of accumulation tank 0.47 W/K per square meter of solar collector, hot water consumption 30 -50 liters per day per square meter of solar collector. Some of those values were changed to obtain it influence on STS productivity and heat losses.

A lot of results data from dynamic simulation program were analysed with the table calculation programs.

3. RESULTS AND DISCUSSION

3.1. Collector’s heat losses

The biggest heat losses of STS are from solar collectors. It is necessary to determinate regularities between solar collector field yields and η0, c1and c2 solar collector coefficients in each particular region. It is necessary to determinate this regularities according operation of the solar collectors in the whole STS for determination of accurate solar gross heat gain. Then the characteristics number of η0, c1 and c2 will be the criteria for comparing the qualities of different collectors.

Value of c1 was changed in simulation models for determination of regularities between linear heat loss coefficient of solar collector and solar collectors field yield. η0 was changed for determination of the same regularities for solar collectors with different optical losses.

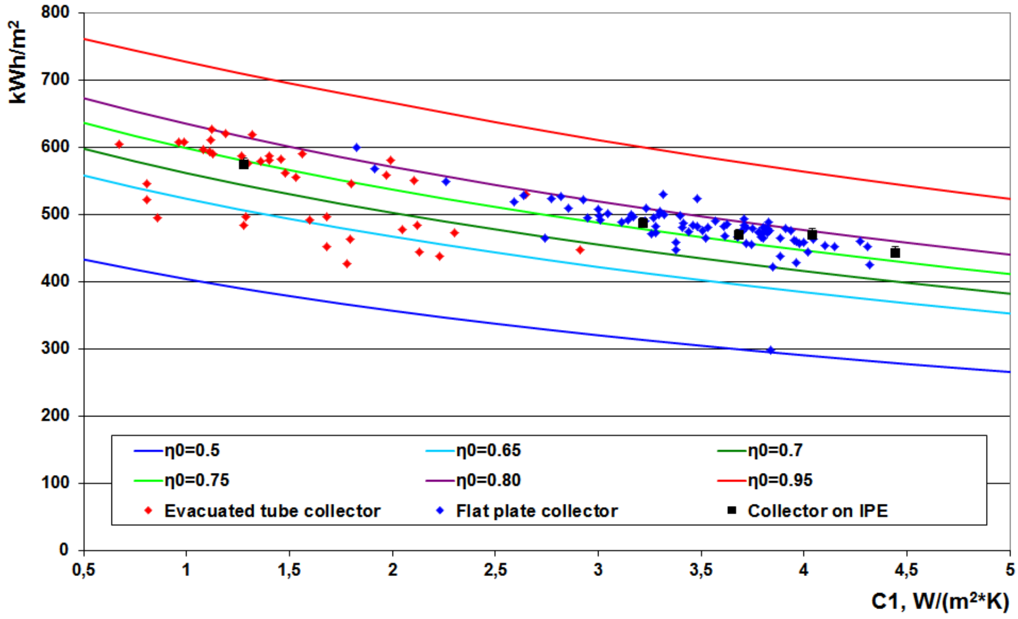

Fig. 2. Regularities of c1 and solar collector annual field yield, taking into account η0

The Fig. 2 shows results of STS simulations with different η0 and c1 solar collector coefficients. The results with different type of solar collectors were also displayed at Fig. 2. There are popular flat plate and evacuated tube solar collectors with Solar Keymark testing certifications. Results show that field yield is from 420 to 530 kWh/m^2 per annum for flat plate, and from 450 to 610 kWh/m^2 per annum for evacuated tube solar collectors. c1 is about from 0.8 to 2.4 W/(m^2*K) for evacuated tube solar collectors, and about from 2.6 to 4.3 W/(m^2*K) for flat plate solar collectors.

Dispersion of η0 for evacuated tube collectors is more than for flat plate solar collectors. This is probably because of evacuated tube solar collector manufacturers pay more attention on solar collectors thermal conductivity than optical transmittance. The results show that booth parameters have relatively big effects at solar collector field yield.

The results of solar collectors testing on solar energy testing polygon are displayed at Fig.1 with black points. These solar collectors were tested in real weather condition. The some nominal parameters of STS on solar energy polygon are different from nominal parameters of STS in simulating program. Therefore quantity of solar collector produced energy lower by 1.8% at solar energy polygon than in simulation program.

The efficiency of the same solar collectors is lower in Baltic country region in comparison with other European countries where solar collectors are more common. Mostly it is lower because of higher thermal losses of solar collectors.

The efficiency, η of a solar collector is defined as ratio of solar collectors produced energy (Qc) to the global solar radiation (R) per annum:

$$\eta = Qc/R$$

Global radiation is about 1140kWh per annum in inclined surface at 60 degree from horizontal in Latvia.

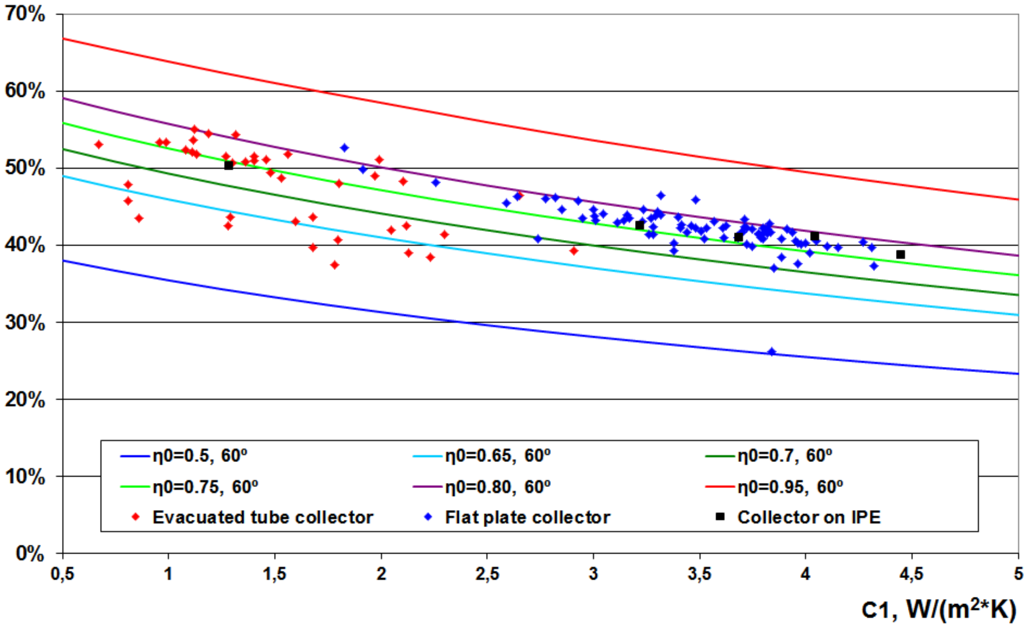

Fig. 3. Regularities of c1 and solar collector annual efficiency, taking into account η0

Fig. 3 show that efficiency of flat plate solar collectors is about 37–46% in Baltic country region. Efficiency of evacuated tube solar collectors is about 39–53%.

The less is the optical losses in solar collectors, the more is absorbed energy and consequently average absorber temperature increase. And as mentioned in methodology the thermal losses are dependent on the temperature difference between the absorber and outside air, on the insulation, and on the construction of the collectors. Therefore if c1 increases, solar collectors annual efficiency decreases more rapidly with higher η0.

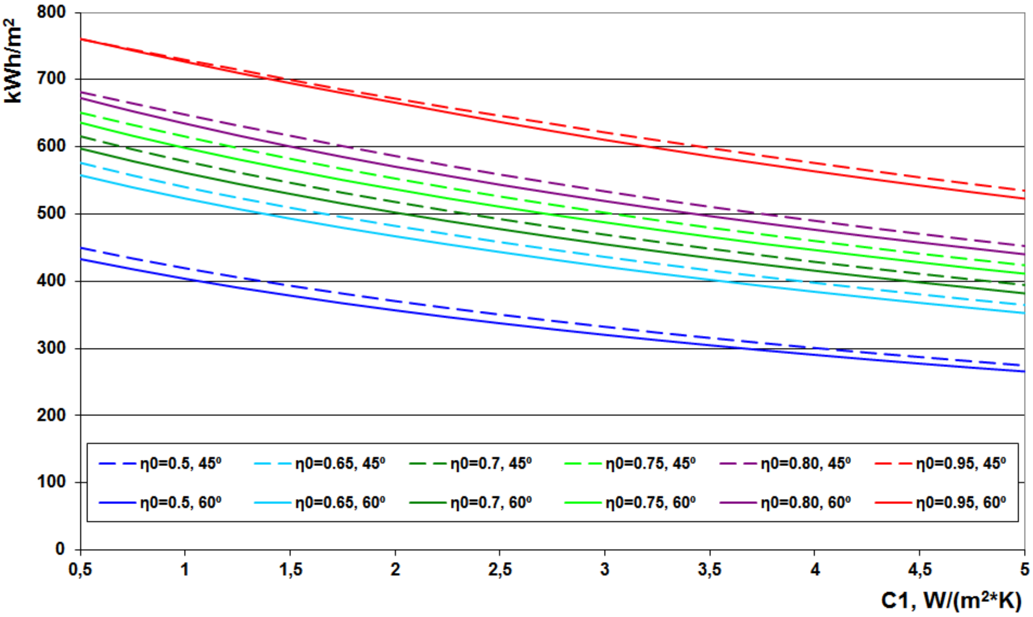

Fig. 4. Comparison of solar collector annual field yield on 60 and 45 degree of tilt angle of solar collector

The highest annual solar radiation is on slope surface at about 40–44 degree tilt angle in Baltic countries region. The less is title angle of surface, the less is amount of solar radiation on cold months and it is more on warmer months. It is because of sun is closer to zenith in summer. Total solar radiation increase at 45 degree tilt angle with comparison 60 degree tilt angle and the fig.4 shows that solar collector annual productivity increases average on 13 kWh per square meter of absorber. But uneven annual distribution decreases the possibility of solar collectors using.

If observe solar collector efficiency, it is lower for most common type of solar collector mounted at 45 degree with comparison at 60 degree. It is because of annual solar radiation increasing is much more than solar collectors productivity increasing in comparing the two angles. Decreasing of solar collectors efficiency is about 0.5 – 0.7% for flat plate collectors and 0.4–1.2 for evacuated tube solar collector.

The results from solar energy testing polygon show that the temperature increasing over 100°C happens rarely in typical flat plate solar collector in Baltic country region. Therefore quadratic heat losses coefficient has less impact than linear heat losses coefficient for flat plate collectors.

The most of collectors have c2 in range from 0.0025 to 0.02 W/(m^2*K^2).

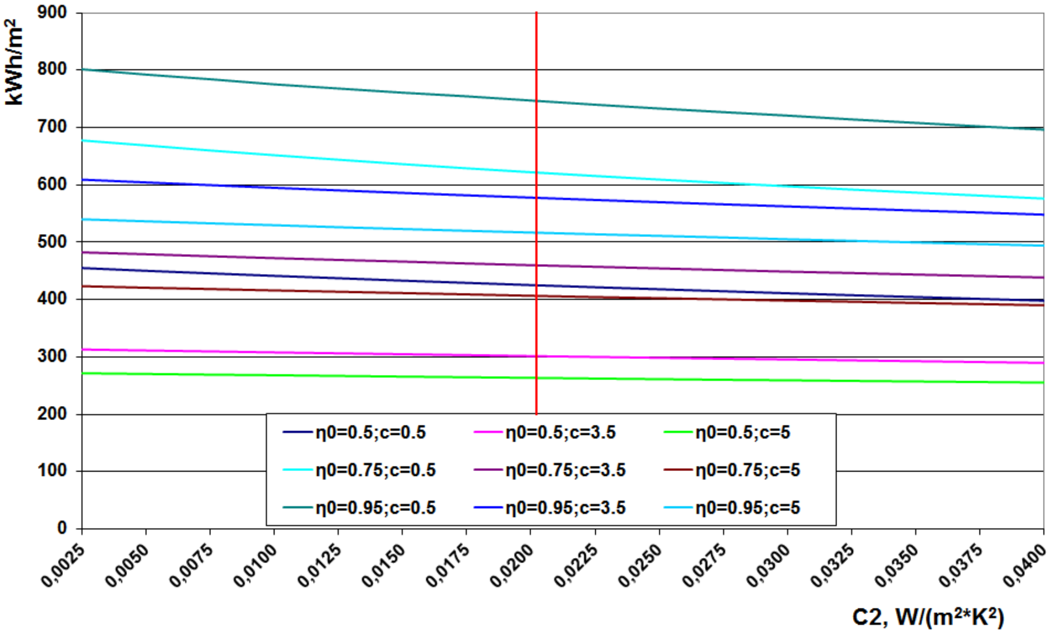

Fig. 5. Regularities of c2 and solar collector field yield, with different η0 and c1 combinations.

The Fig. 5 shows that c2 can decrease solar collector field yield at about 1.4–4.9 % for popular type of solar collectors in c2 range from 0.0025 to 0.02 W/(m^2*K^2). The highest c2 influence is for collector with lower c1 such as evacuated tube collectors. It is because of temperature of collector elevate due to lower heat losses from low c1.

3.2. Pipeline heat losses

Pipeline heat losses are equal to coefficient of thermal conductivity and temperature difference between heat carrier and outdoor or indoor. Pipeline length, pipes diameter, thickness of insulation, and the thermal conductivity of the insulating material impact at coefficient of thermal conductivity of pipeline.

Length, diameter and insulation of pipeline of solar collector circuit are diverse in different STS. It depended from distance between collector and accumulation tank, from building type and form, from the amount of collectors etc. In simulation the length, diameter and insulation of pipeline was same for indoor and outdoor piece. Therefore the results are average values of simulation for outdoor and indoor pipelines. The pipeline heat losses increase with increasing of thermal energy carried through them. The amount of carried thermal energy depends from solar collector produced thermal energy. Therefore it is necessary to consider solar collector produced thermal energy in STS for detection of heat losses from pipeline coefficient of thermal conductivity.

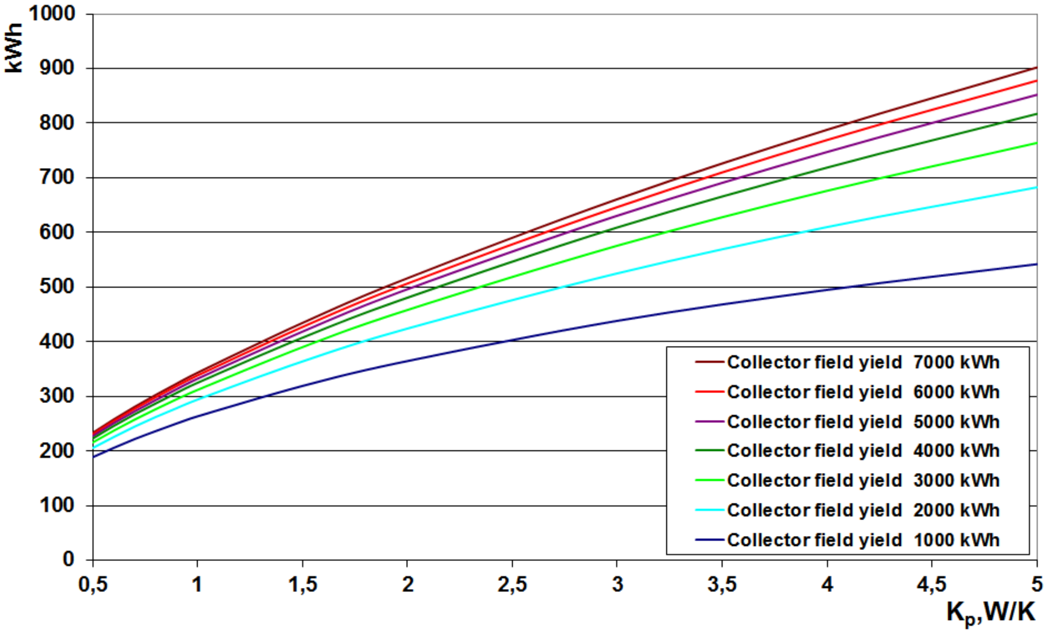

Fig. 6. Regularities of heat losses and coefficient of thermal conductivity in pipeline, taking into account collector produced thermal energy

Pipeline heat losses is about 30–75 kWh per square meter of absorber. It can impact solar gross heat gain up to 9%.

Average length of flow and return pipeline is about 40 m in typical STS. The coefficient of thermal conductivity of insulated pipeline is 0.06 W/K per pipeline meter for poorly insulated, 0.032 (W/K)/m for good insulated, and 0.025 (W/K)/m for very good insulated pipeline.[3]

3.3. Accumulation tank heat losses

Accumulation tank heat losses depend from solar collector produced energy, auxiliary heating produced energy, area of accumulation tank, tank insulation and hot water consumption.

An auxiliary heater heats only the top of accumulation tank. This stratification of the temperature reduces the tank heat losses. Heat losses in lower levels of the tank arise from work of solar collectors. Simulation program consider existence of temperature stratification on 12 different altitudes of accumulation tank.

The additional heat losses are from the total tank heating over 55°C temperature of hot water. The increasing volume of the tank reduces overheating chance. Also it increases solar collector efficiency with reducing heat carrier temperature from accumulation tank. But the reducing volume of the tank reduces tank surface area, which also impact heat losses. Therefore it is necessary to obtain balance between solar collectors generated thermal energy and volume of the accumulation tank.

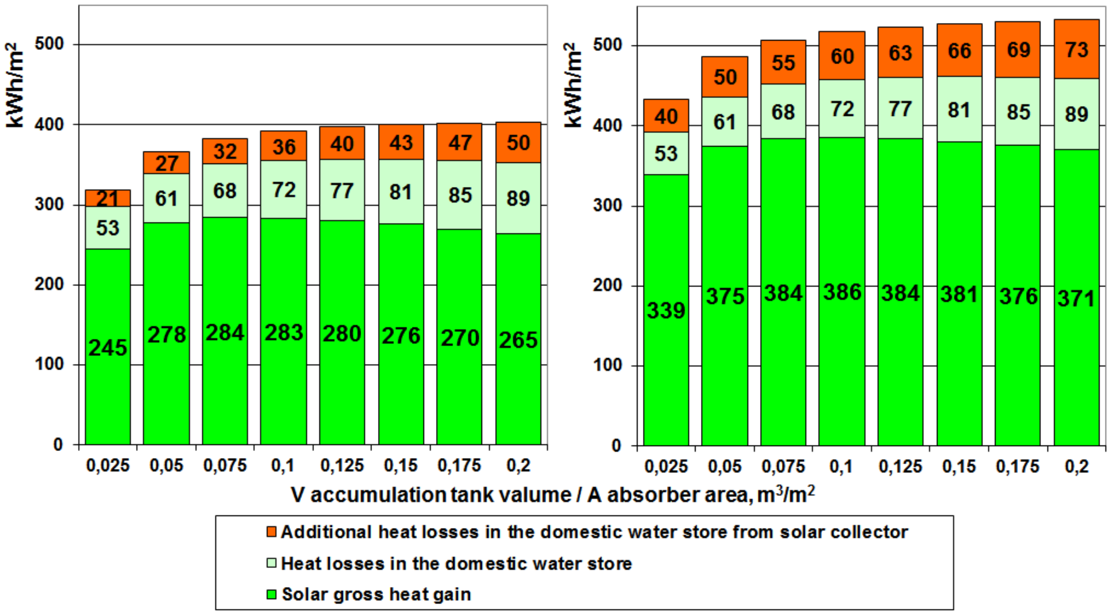

Fig. 7. Regularities of amount of heat losses per square meter of absorber and ratio of accumulation tank volume to absorber area

The results of simulation show that optimal ratio is 0.1 m^3 volume of accumulation tank per square metre of absorber. Fig.7. show that the solar collectors productivity are significantly less at ratio under $0.1 m^3/m^2$. The quantity of heat losses from accumulation tank increase more rapidly than increasing of solar collector thermal energy production at ratio increasing over $0.1\ m^3/m^2$.

The most popular types of accumulation tank were simulated to obtain regularities of coefficient of thermal conductivity and heat losses from accumulation tank.

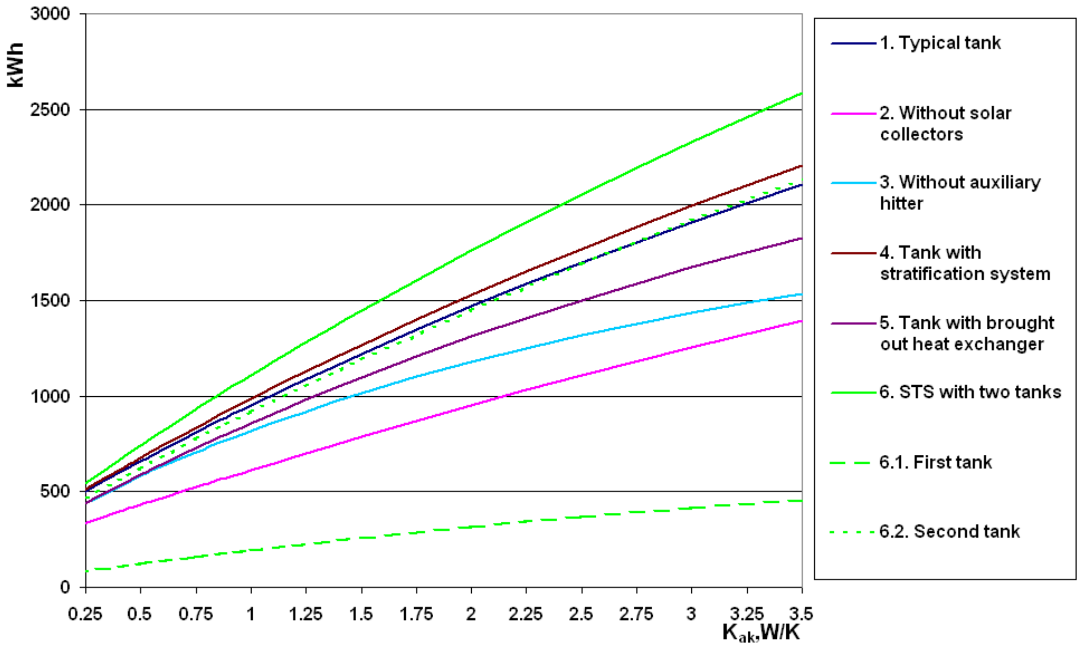

Fig.8. Regularities of coefficient of thermal conductivity and heat losses from accumulation tank for different tank type

Comparing first system with system “without solar collectors” it is possible to determinate quantity of heat losses from tank without solar collectors influence. The fig.8 show that heat losses from tank without solar collectors influence is about 64–67% from quantity of heat losses in common used accumulation tank in typical STS. The heat exchanger imposition from accumulation tank reduces heat losses from accumulation tank. But in this case additional heat losses arise from heat exchanger direct to air. The stratification system using gives same results as in typical tank. The highest heat losses are in STS type with two accumulation tank. It is due to higher total surface area of tanks with the same insulation. Difference between heat losses from different type of accumulation tank is up to 26 % from the solar gross heat gain.

4. CONCLUSIONS

Heat losses are higher in Baltic countries region in comparison with other European countries where solar collectors are more widespread.

Solar collectors productivity dependence from the η0 solar collectors optical efficiency, c1 linear and c2 quadratic heat loss coefficient of solar collector was determined for Baltic countries region. This gives the possibility of comparing the quality of different collectors in according to weather condition in Baltic countries region by using characteristics of η0, c1 and c2.

Annual solar collector field yield is from 420 to 530 kWh/m^2 for flat plate, and from 450 to 610 kWh/m^2 for evacuated tube solar collectors.

Solar collector efficiency dependence from the η0, c1 and c2 was determined for Baltic countries region. Efficiency of flat plate solar collectors is about 37–46%, and 39–53% for evacuated tube solar collectors.

Heat losses dependence from the coefficient of thermal conductivity in pipeline was determined, taking into account collector produced thermal energy in Baltic countries region. Coefficient of thermal conductivity in pipeline can impact solar gross heat gain up to 9%.

The results of simulation show that optimal ratio is 0.1 m^3 volume of accumulation tank per square metre of absorber.

Heat losses dependence from coefficient of thermal conductivity was determined for different type of accumulation tank. Difference between heat losses from different type of accumulation tank is up to 26 % from the solar gross heat gain.

REFERENCES

1. *Planning and Installing Solar Thermal Systems*, United Kingdom: James & James, 2005. 300 p.
2. SHIPKOVS P., KASHKAROVA G., LEBEDEVA K. Solar Collectors Operation Methods Effect on System Efficiency. *ISESCO Science and Technology Vision*, May 2011, Vol. 7, No. 11, p. 38–42
3. SHIPKOVS P., SNEGIRJOVS A., VANAGS M., MIGLA L. Determination of cost-effective pipelines insulation of solar thermal system. CYSENI 2011. Proceedings of annual conference of young scientists on energy issues. [CD].Kaunas: Lithuanian Energy Institute.2011May 26-27.
4. WEISS W. *Solar heating system for houses*, A design handbook for solar combisystems. – James & James, 2003. 310 p.

This work has been supported by the European Social Fund within the project «Support for the implementation of doctoral studies at Riga Technical University»

CYSENI 2012, May 24–25, Kaunas, Lithuania
ISSN 1822-7554, www.cyseni.com

USING STRAW FOR HIGH EFFIENCY HEATING IN FARMING

Klāvs Vagoliņš, Guntars Frīdenbergs, Pēteris Šipkovs
Institute of Heat, Gas and Water technology,
Riga Technical University
Azenes 16, LV- Riga, Latvia
Phone +371 26143214
Email: klavs@inos.lv

ABSTRACT

The publication „Using straw for high efficiency heating in farming” contains of theoretical and research parts. In the theoretical part of the publication straw is viewed as a fuel for producing heating energy, types of straw boilers and ways for using straw as fuel for heating is collected.

At the beginning the objectives are determinated, the vitality of the theme is researched and positive and negative aspects for using straw as fuel for energy production are being gathered.

In the research part of the thesis main parameters of real package-type straw boiler are collected and analyzed when two different types of straw are burned. After research author of the thesis concludes that no matter which kind of straw is being burned, the classical assembly connection of straw boiler isn't energy effective and a new assembly connection is given.

All package type straw boilers contain of a huge accumulation tank to equate temperature fluctuations. All the water circulation is being organized through the tank which has great heat yield area so great amount of heat is given away.

Author has given solution for this problem. All package type boilers have water cooled firebox door. When a new bale of straw is put into the firebox, the circulation is organized through the heat exchanger, at the same time flue-gas economizer and door cooling water is heating up a small accumulation tank. When the temperature falls under given boarder, 3-way valves changes circulation from heat exchanger-consumer to accumulation tank-consumer. After putting a new bale, temperature rises and system work usual way. So there's no need for as huge amount of water to be heated and kept on high temperature all the time.

1. INTRODUCTION

Use of straw for farm heating system purposes is growing, as it reduces farmers' dependence on fossil fuels and associated costs, instead of creating a practical and environmentally friendly alternative fuels. In addition, they always have access to cheap fuel. Much of the farmers annually produce enough straw to ensure their heating systems with fuel. However, if they would have to buy straw, it usually pays off, as part of the agricultural straw waste is to be somewhere is to be exercised or converted into compost. Also huge amount of CO_2 is emitted in atmosphere from different industrial plants, technological processes and urban high-power boiler plants that continues to contribute to global warming; the so-called "Greenhouse effect" in the past decade has drastically changed the climate of the Earth. Carbon dioxide absorbs infrared radiation and prevents its proper reflection in space. Similarly, fossil energy resources are non-renewable natural resource and the volume rapidly diminishes.

2. MODEL

Object that my researches are based on is classical round bale straw boiler. The nominal power of exact boiler is 0,6 MW. Boiler is made in Latvia by company “AGB serviss”. This boiler is used

for producing heat energy to provide temperature regime in greenhouse. Greenhouse is used for growing vegetables here in Latvia that are being sold in Latvian market. The dimensions of the greenhouse are: W=20 m;
L= 40 m;
H=5.5 m.


Fig. 1. Straw boiler

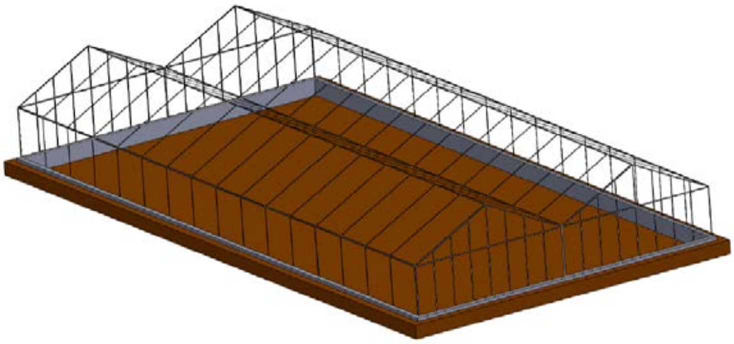
Fig. 2. Model of greenhouse

Aim of the research is to make this straw boiler more effective as well as to reduce amount of fuel used for producing same amount of energy.

The research object has a classical assembly installation where all system water is circulating through the accumulation tank to reduce temperature differences, so the heat exchanger is heating up all the amount of water in the accumulation tank. The accumulation tank has a huge heating surface of 45 m^3 so it’s not so energy effective. But this assembly still has a drastic temperature differences which are not acceptable.

Water circulation in heating circuit is provided with the help of forced circulation. The circulation pump is triggered automatically by firing the boiler.

The research was lasting for 4 weeks. In research were collected data about: inside and outside temperature, power and heat values used in greenhouse and produced by the boiler as well as temperature regime of the system water. As shows the following chart, temperature differences are too high. And it’s not acceptable for providing constant regime of temperature in the greenhouse.

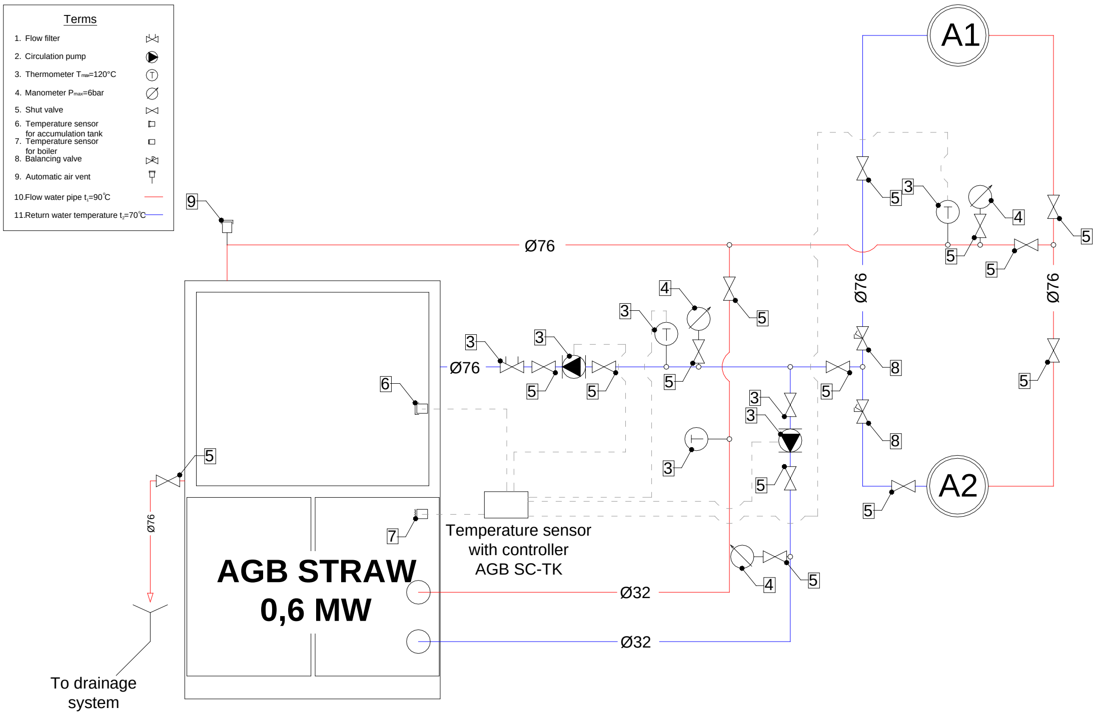

Fig. 3. Classical assembly installation scheme

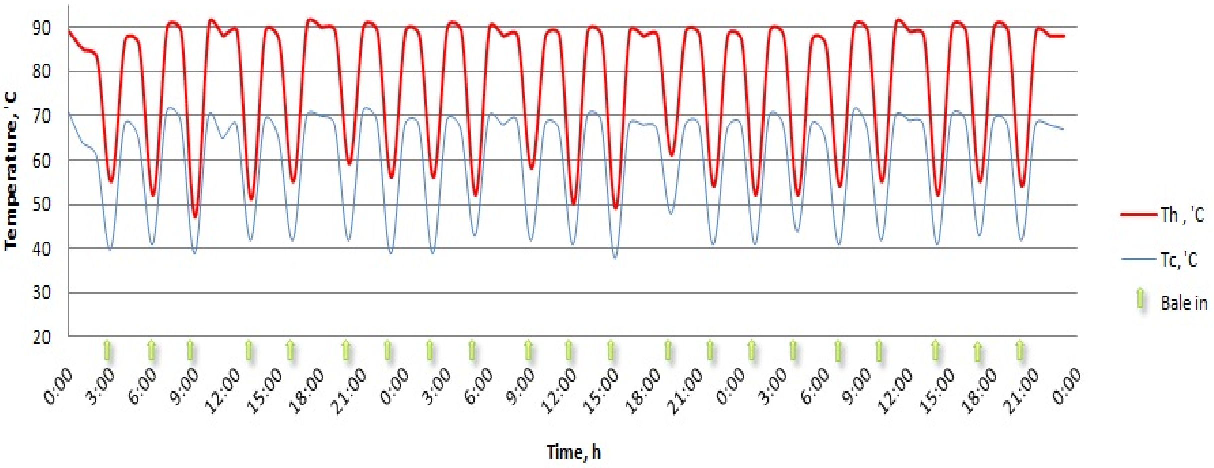

Th, °C – temperature of flow water;

Tc, °C – temperature of return water;

Bale in – time when fresh 2 bales are inserted.

Fig. 4. System temperature regime

According to the problem of temperature differences it’s necessary to improve the classical assembly installation system to reduce fluctuations of temperature. As shown in the diagram, boiler installation is able to operate for long periods at a steady mode. Critical are moments of time when a "portion" of straw is burnt out, and while the other is inserted into the furnace and until the furnace starts working at a nominal capacity. These time instants, lasts up to 20 minutes, which means that the accumulation tank has to ensure temperature uniformity of heating circuit for only 20 minutes.

The solution is following; during the time when the boiler is being burnt, the circuit is heated up directly from the boiler’s heat exchanger. At the same time, separate accumulation tank with a relatively small volume is heated up through the flue-gas economizer and the door of boiler's furnace. The volume of this accumulation tank (20 m^3) is smaller than the one that's used in classical assembly installation and has small heat transfer surface. The boiler is not usually used with a nominal capacity, which results in excess heat energy, thereby economizer with the help of this energy is returns the heat to accumulation tank.

At a time when the furnace filled up with the next "portion" of fresh straw, temperature in the heat exchanger begins to reduce and the sensor gives an impulse to the boiler's control system to switch direction of 3-way valves and to start using the heat accumulated in the tank. When the furnace is burning again and the temperature of the heat exchanger reach the required operating temperature, sensor dives an impulse again to boiler's control system and 3-way valves are switched to the standard mode.

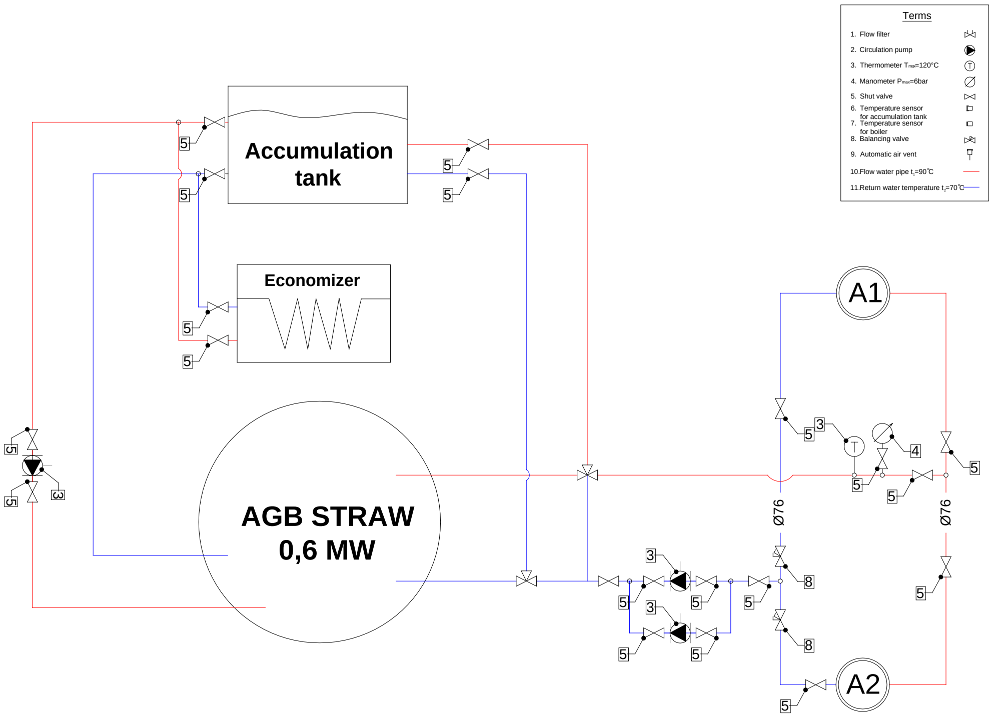

Fig. 5. Improved assembly installation scheme

Using improved assembly installation scheme was obtained that fluctuations of the system water temperatures between supply and return flows have been reduced as well as the amount of fuel consumption.

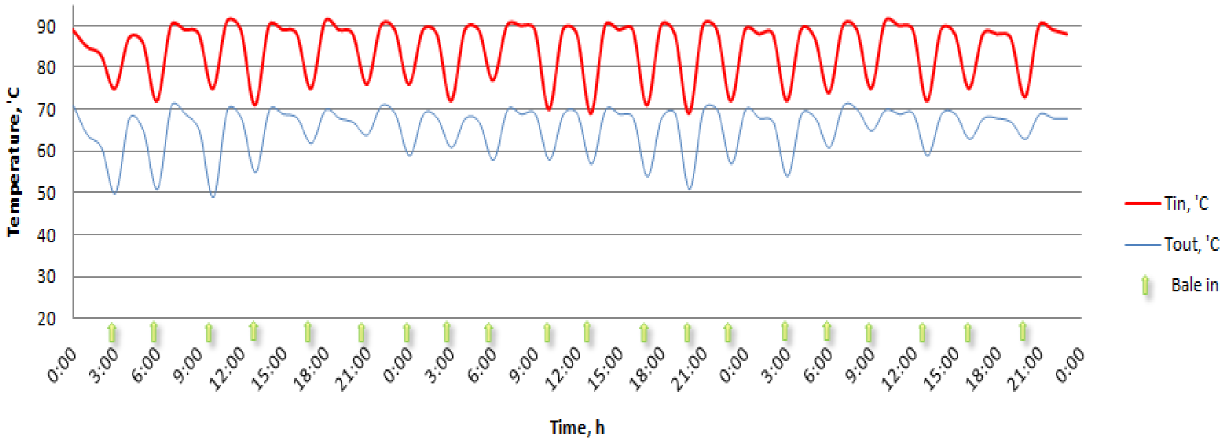

Tin, °C – temperature of flow water;

Tout, °C – temperature of return water;

Bale in – time when fresh 2 bales are inserted.

Fig. 6. System temperature regime using improved assembly installation scheme

Comparing the data obtained using classical assembly installation scheme with data obtained using improved assembly installation scheme; it is shown in the Fig. 6. That the efficiency of the boiler has improved for average about 4%. The data were compared in a 3-day period using about the same weather conditions and fuel humidity.

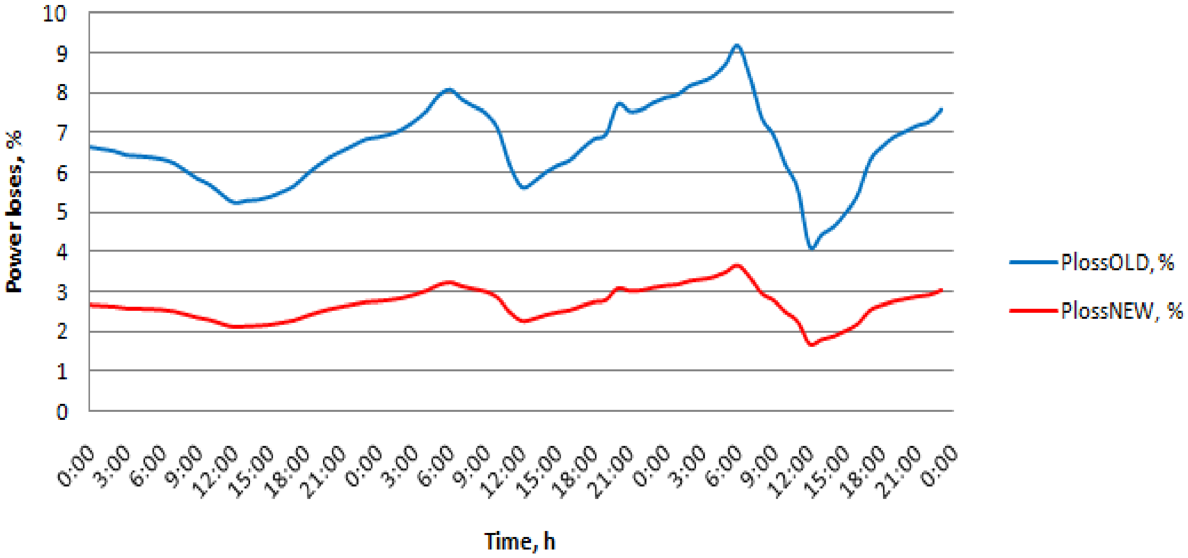

P_{loss}OLD – power loses using old assembly scheme;

P_{loss}NEW – power loses using new assembly scheme.

Fig. 7. Comparison of heat loses

3. CONCLUSION

This study is significant that the conversion of the classic straw boiler pump group scheme gives a reduction of temperature fluctuations, as well as lower fuel consumption based on the fact that a large volume accumulation tank is being replaced by smaller, as well as ongoing boiler circulation does not happen through the accumulation tank which has a large heat transfer area. fuel consumption reduction is obtained on the basis of efficiency, or loss of reduction, which means that the fuel directly from the resulting heat is used effectively. Loss comparison between the classic pump group scheme and the improved assembly connection scheme shown in the Fig. 7.

REFERENCES

1. KRĒSLIŅŠ A., ĶIGURS J. Ēku apkures sistēmas - Avots. 1983 – 120 p.
2. NIBERG B.E., NORDSTREM K.. TA ieteikumi apkures sistēmu modernizēšanai. Tour & Andersson, Zviedrijā. Tulk. Uģis Osis un Lilita Zadeika - AS LAFIPA 1995 – 74 p.
3. Būvniecības, enerģētikas un mājokļu valsts aģentūra. Atjaunojamo energoresursu potenciāls Latvijā - SIA „Gandrs“ – 60 p.
4. REAY D., KEW P. HEAT PIPES. Theory, design and applications – Butterworth – Heinemann. Fifth edition, 2006 – 130 p.
5. Ecoenergy, Wood fuelled boiler biomass energy services district heating. Ecoenergy Limited – British Gas – 4l p.
6. Energy 2000. Haulingplan., 1998 – 107 p.
7. AISTARA G. Kā panākt siltuma taupīšanu ar maziem ieguldījumiem? – Rīga. SIA „Vides Projekti’’ – 42 p.
8. NIKOLAISEN L. Straw for Energy production – Copenhagen, 1998 – 53l p.
9. RUBĪNA M. SILTUMAPGĀDE. Problēmas un risinājumi pašvaldību administratīvās teritorijās – Rīga, LZA FEI, 2002 – 171 p.
10. AKMENS P., KRĒSLIŅŠ A. Ēku apkure un ventilācija. I daļa – Zvaigzne ABC. 1995 – 166 p.
11. AKMENS P., KRĒSLIŅŠ A.. Ēku apkure un ventilācija. II daļa. – Zvaigzne ABC. 1995 – 167 p.
12. ŠIPKOVS P., RUBĪNA M., KAŠKAROVA G. Siltumapgādē izmantosim vietējo kurināmo – koksnes un citu biomasu – Rīga, 2003 – 50 p.
13. Plumbing and Mechanical magazine 1994, July 12, 2000.
14. SEĻEGOVSKIS R. Apsildes sistēmu elementu aprēķina metodika un piemēri – Jelgava, 2008 – 59 p.
15. Status for Stirlingmotor – Institut foe Energytechnic – 1997.
16. ROAD W. The Brilliance of Bioenergy.

LONG TERM VARIATIONS OF SOLAR RADIATION

P. Vilkinis, A. Kanapickas
Department of Physics, Vytautas Magnus University
Vileikos 8, LT-44404 Kaunas – Lithuania
Phone +37037327922
Email: p.vilkinis@fc.vdu.lt

ABSTRACT

The variability of solar irradiance is the most important issue that determines the reliability of solar power generation in short-term time scales. For long time scales the energy produced by solar irradiation has to be predicted with high certainty. However, environmental parameters such as global temperature, precipitations, cloud cover have changed drastically during last century. Therefore, the overall performance of photovoltaic (PV) solar panels would have been affected by these changes. In present work the effect of cloudiness on the availability of solar energy is analyzed for 18 sites. For the analysis measured daily sunshine duration data was used (Lithuanian Hydrometeorological Service, European climate assessment dataset). For the statistical analysis Pearson correlation and Mann-Kendall trend test was applied. It was established that for most examined sites the amount of solar irradiation is increasing. It was shown that the increase for some sites is significant and reaches 8-11 % over 30 year. Obtained results have shown that it is important to account solar insolation changes for the future solar applications such as photovoltaic electricity generation.

Keywords: renewable energy; extra-terrestrial radiation; cloudiness; solar irradiance; sunshine duration

1. INTRODUCTION

The contribution of power production by photovoltaic (PV) systems to the electricity supply is constantly increasing over the past 20 years [1]. However, solar photovoltaic designers are seeking solution for optimal performance from an input of solar energy because of great intrinsic variability of this natural energy resource. The benefit of installed solar panels depends highly on fluctuating solar power at all time scales. The forecast information of solar irradiance at short time scale is necessary for the management of the electricity grids and for solar energy trading. On the other hand, the strategy of solar electricity development in a particular region depends on long term solar irradiation forecast.

In the last decades, global warming has been studied with special attention focused on the role of changes in solar irradiance (and the solar wind) on a variety of timescales and the relevance of cloud cover [2]. Most climate models assume that as an increasing amount of greenhause gases induces slightly increasing atmospheric temperatures. As a consequence, the overall evaporation from the planet surface also increases. Recent studies [3] have shown that decadal warming is accompanied by increases in tropospheric specific humidity.

Therefore, on a global scale there should be an increased amount of water vapour in the atmosphere. Three basic sky conditions can be identified: clear skies, partially clouded skies and overcast skies. The typical patterns of cloud cover vary according to geographic locations. In high latitude maritime climates, overcast skies may persist day after day in winter with only rare breaks of sunshine. Statistics of cloud cover and daily sunshine, which are widely available, yield qualitative information that can help in design of photovoltaic systems [4].

The importance of cloudiness variability to solar electricity generation are widely studied, many models are used to predict direct and diffuse radiation from the sky [4, 5]. However, long term changes in cloudiness which may cause decrease in surface irradiation are poorly studied.

Therefore, the task of the paper is to investigate climate change induced long time patterns of solar radiation energy fluxes that can be deduced from available meteorological data.

2. METHOTODOLOGY

2.1 Definitions

The solar radiation on a horizontal surface from sun is known as the global short-wave radiation. The global short-wave radiation flux**,** i.e. radiant energy flow per unit time, is known as the irradiance, we will refer as G, W m^{-2}. The integral of irradiance flux over any period is called the irradiation. Typical integration periods are the hour, which yields the hourly global irradiation, G_h, [MJ m^{-2} h^{-1} or Wh m^{-2} h^{-1}], the day G_d [MJ m^{-2} d^{-1} or Wh m^{-2} d^{-1}] and the month G_t, [MJ m^{-2} per month or Wh m^{-2} per month].

Solar radiation data are often presented in a dimensionless form called the Clearness Index [4]. The Clearness Index, often called the *KT* value, is obtained by dividing the global irradiation at the surface on the horizontal plane, G_t, by the corresponding extraterrestrial irradiation on a horizontal plane, G_0, for the same time period. Three integration time periods are in common use: hourly, daily and monthly. In this paper hourly sunshine duration data will be used to calculate monthly and annual averages. The monthly mean clearness index *KT,* is G_t/G_0, where G_t is monthly average of global irradiation at the surface.

Monthly average number of instrument-recorded bright daily sunshine hours S_t in hours where obtained from [6]. Average day length in hours S_0 was calculated as shown below.

The solar constant I_{sol}, is the extraterrestrial irradiance of the solar beam at mean solar distance. The accepted value is 1367 W m^{-2}. The distance of the Earth from the Sun varies slightly according to the time of the year because of the eccentricity of the Earth's orbit. The dimensionless eccentricity correction factor of the mean solar distance is ε. The extraterrestrial irradiance normal to beam is therefore εI_{sol} , W m^{-2}.

2.2 Model

Theoretical determinations of the direct, diffuse and directional intensities of diffuse irradiance would require data on the type and optical properties of clouds, cloud amount, thickness, position and the number of layers. These data are rarely collected on a routine basis. However, sunshine hours and total cloud-cover data (i.e. the fraction of sky covered by clouds) are widely and easily available [6]. The monthly average daily global radiation on a horizontal surface can be estimated through the number of bright sunshine hours. The widely used model suggests that the ratio of the average daily global radiation G_t and cloudless radiation G_t/G_0 is related to the monthly mean daily fraction of possible sunshine S_t [5] by

$$\frac{G_t}{G_0} = a_1 + b_1 \frac{S_t}{S_0}, \tag{1}$$

where S_t is the monthly average number of instrument-recorded bright daily sunshine hours, S_0 is the average day length in hours; a_1 and b_1 are constants for different locations. There are different models to estimate these constants, overview of these models can be found elsewhere [6]. In this work following expressions that accounts for most corrections important for these values are used:

$$a_1 = -0.309 + 0.539\cos\Phi - 0.0693h + 0.29\frac{S_t}{S_0}, \tag{2}$$

$$b_1 = 1.527 - 1.027\cos\Phi + 0.0936h + 0.359\frac{S_t}{S_0}, \tag{3}$$

where Φ (degrees) is the latitude, and *h* (km) is the elevation of the location above sea level. The hourly extraterrestrial radiation on a horizontal surface G_0 can be determined by:

$$G_0 = \frac{24}{\pi} I_{\mathrm{sol}}\varepsilon\cos\Phi\cos\delta\left(\sin w_s - \frac{\pi}{180} w_s \cos w_s\right). \tag{4}$$

ε – the dimensionless eccentricity correction factor of the Earth’s orbit and is given by:

$$\varepsilon = 1.00011 + 0.034221\cos\Gamma + 0.00128\sin\Gamma + 0.000719\cos 2\Gamma + 0.000077\sin 2\Gamma, \tag{5}$$

where the day angle Γ (radians) is given by:

$$\Gamma = 2\pi\left(\frac{N-1}{365}\right). \tag{6}$$

In the latter expression *N* is the day number of the year, ranging from 1 to 365. w_s (radians) is the sunset-hour angle for a horizontal surface, δ (radians) is declination - one of the two coordinates of the equatorial coordinate system in astronomy. Declination is comparable to geographic latitude, but projected onto the celestial sphere and is measured in degrees north and south of the celestial equator.

The sunset-hour angle w_s can be calculated by following equation:

$$w_s = \frac{\pi}{180\sin(-\tan\delta\cdot\tan\Phi)} \tag{7}$$

Length of a day was calculated the following expression:

$$S_0 = \frac{2}{15} w_s \tag{8}$$

2.3 Data

In order to evaluate the variation of the solar radiation energy fluxes over large time scales 18 sites were examined. Daily sunshine data were obtained from European Climate Assessment & Dataset project website (ECA) [6]. Data details are presented in Table 1. Sites chosen for the examination have continuous daily data while the data of other sites are truncated.

Table 1. General information about meteorological data used in the investigation

	Site	**Latitude**	**Longitude**	**Station elevation, m**	**Data availability, years**	**Data span, years**
1.	Kaunas, LT	54:52 N	23:49 E	30	1924 - 2004	81
2.	Seville, ES	37:25 N	5:52 W	12	1951 - 2010	60
3.	Pamplona, ES	41:49 N	1:39 W	431	1954 - 2010	57
4.	Castellon, ES	39:59 N	0:2 W	27	1954 - 2010	57
5.	Cuenca, ES	40:4 N	2:9 W	946	1951 – 2010	60
6.	Melilla, ES	35:18 N	2:57 W	29	1971 - 2010	40
7.	Valkenburg, NL	52:10 N	4:25 E	82	1952 - 2011	60
8.	Innsbruck, AT	47:16 N	11:23 E	578	1952 - 2011	60
9.	Vienna, AT	48:12 N	16:22 E	166	1908 - 2010	103
10.	Hurbanovo, SK	47:52 N	8:11 E	109	1951 - 2009	59
11.	Zurich, CH	47:22 N	8:11 E	411	1901 - 2009	109

12.	Frankfurt, DE	50:6 N	8:41 E	112	1951 - 2010	60
13.	Gorlitz, DE	51:9 N	59:14 E	209	1951 - 2011	61
14.	Potsdam, DE	52:24 N	13:4 E	32	1893 - 2010	118
15.	Nuremberg, DE	49:27 N	11:5 E	305	1956 - 2010	55
16.	Oslo, NO	59:56 N	10:45 E	4	1953 - 2010	58
17.	Nimes, FR	43:50 N	4:21 E	68	1943 - 2004	62
18	Orleans, FR	47:54 N	1:54 E	96	1950 - 2004	55

2.4 Calculations

All downloaded data were prepared in a simple text format. Then a fortran program was written to manage all amount of data. All information (year, month, day, sunshine duration) was read from text files and stored into appropriate data arrays. The calculations of required values (averages of particular month or year) were simplified by writing appropriate functions. The program allowed to chose the form of output, suitable for the further analysis. All parameters described in previous section were calculated using (1–8) equations.

For the evaluation of correlation between data series linear regression was applied and the coefficient of determination R^2 (the square of the Pearson correlation coefficient) was used for the description of the correlation. However, the time series used in this study exhibit a trend such that there is a barely distinguishable change over time. In order to find out if there is a trend, the Mann-Kendall test was used. The Mann-Kendall test does not require any assumptions to the statistical distribution of the data (e.g. normal, lognormal, etc.) and can be used with data sets which include irregular sampling intervals and missing data [7]. The determination of trend in Mann-Kendall test is based on calculation of probability. If the computed probability is greater than the level of significance (usually 95 %), there is a trend. If the computed probability is less than the level of significance, there is no trend. The no-trend result simply means that the Mann-Kendall trend test could not discern either an up or a down trend for the given set of data. The Mann-Kendall test was carried out using MS excel with installed xlstat2012 package [8].

3. RESULTS

3.1 Global radiation

Calculation of the monthly average daily global radiation on a horizontal surface (1) includes constants a_1 and b_1 that are location dependent. The relevance of a_1 and b_1 can be checked through the evaluation of correlation between calculated and measured values. Measured values of the global irradiation on a horizontal surface were obtained from *Surface meteorology and Solar Energy* center [9]. This center provides the solar irradiation and meteorological data derived from satellite measurements over 22 year time period (July 1983 – December 2004). The solar data are then determined taking into account visible and infrared radiances, and cloud and surface properties inferred from International Satellite Cloud Climatology Project. The results of correlation between satellite measurement based data, G_{tsat} [kWh m^{-2} d^{-1}], and calculated values, G_{tcalc}, for two sites (Kaunas, LT, and Seville, ES) are shown in Fig. 1. Table 2 presents values of correlation coefficient between G_{tsat} and G_{tcalc} for all 18 sites included into present investigation (mean daily values, July 1983 – December 2004).

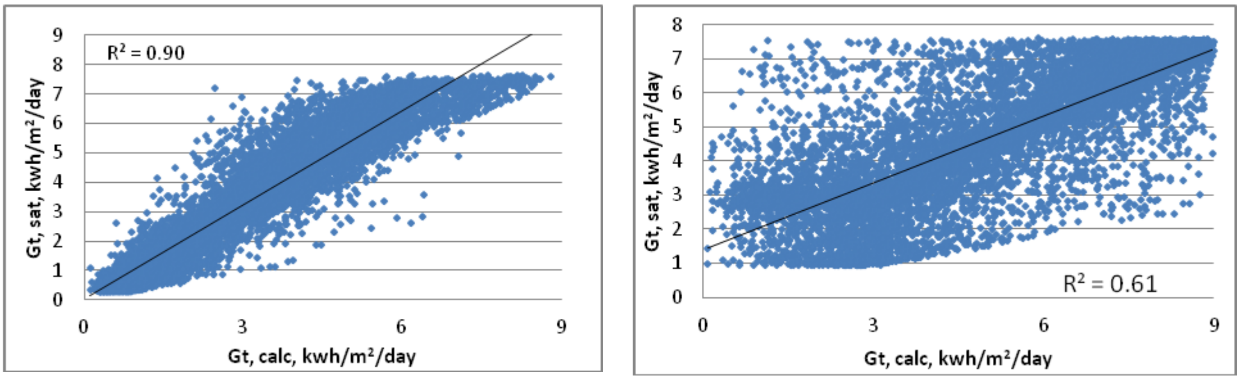

a) Kaunas, LT

b) Seville, ES

Fig. 1. Graphical representation of correlation between satellite measurement based data of the insolation incident on a horizontal surface, G_{tsat}, and calculated values, G_{tcalc}, for a) Kaunas and b) Seville (mean daily values, July 1983 – December 2004)

It is seen that the coefficient of linear correlation between daily values of G_{tsat} and G_{tcalc} exceed 0.9 for the most cases. World Climate Research Program estimated that most routine-operation solar-radiation ground sites have "end-to-end" uncertainties from 6 to 12% [10]. From the other hand, the solar radiation data are derived from an improved inversion algorithm (SRB Release 3.0) which provides an overall improvement in the estimation of the surface solar radiation of about 2.8 % [10]. Therefore, obtained correlation between G_{tsat} and G_{tcalc} shows that calculated values of the global irradiation G_t are in good agreement with satellite derived values. This means, that the values of coefficients a_1 and b_1 (2, 3) are suitable for the evaluation of global radiation.

Table 2. Correlation between satellite measurements based data of the insolation incident on a horizontal surface, G_{tsat}, and calculated values, G_{tcalc}, for 18 sites included into present investigation

	Site	G_{tsat} - G_{tcalc} correlation, R^2		Site	G_{tsat} - G_{tcalc} correlation, R^2
1.	Kaunas, LT	0.944	10.	Hurbanovo, SK	0.947
2.	Seville, ES	0.693	11.	Zurich, CH	0.881
3.	Pamplona, ES	0.936	12.	Frankfurt, DE	0.945
4.	Castellon, ES	0.928	13.	Gorlitz, DE	0.949
5.	Cuenca, ES	0.920	14.	Potsdam, DE	0.791
6.	Melilla, ES	0.856	15.	Nuremberg, DE	0.952
7.	Valkenburg, NL	0.936	16.	Oslo, NO	0.943
8.	Innsbruck, AT	0.595	17.	Nimes, FR	0.951
9.	Vienna, AT	0.946	18	Orleans, FR	0.933

In is seen that for some sites the correlation between G_{tsat} and G_{tcalc} is less significant. Possible reasons of the mismatch can be: the size of grid cell (1 degree latitude × longitude), particularly, the average elevation of the earth's surface enclosed by the dimensions of the grid cell; local meteorological conditions at the baseline measurement sites (fog, clouds), particularly, at the sites located near mountains; local air pollution [10]. For these cases, a_1 and b_1 should be evaluated using additional data or a different model has to be used for the determination of the average daily global radiation G_t.

3.2 Sunshine duration

Main parameter under consideration in present work is the daily sunshine duration. Annual average values of daily sunshine duration for cities Kaunas (a) and Seville (b) are presented in

Fig. 2. Data are plotted for the whole period of the sunshine duration data available. First, in order to analyze the data the linear regression was applied for these data (solid line). As was mentioned above, it is difficult to distinguish a trend in the time series such as used in this study. In order to find out if there is a trend, the Mann-Kendall test was used. The results of this test applied for the solar irradiation data is presented in the next subsection (Table 3).

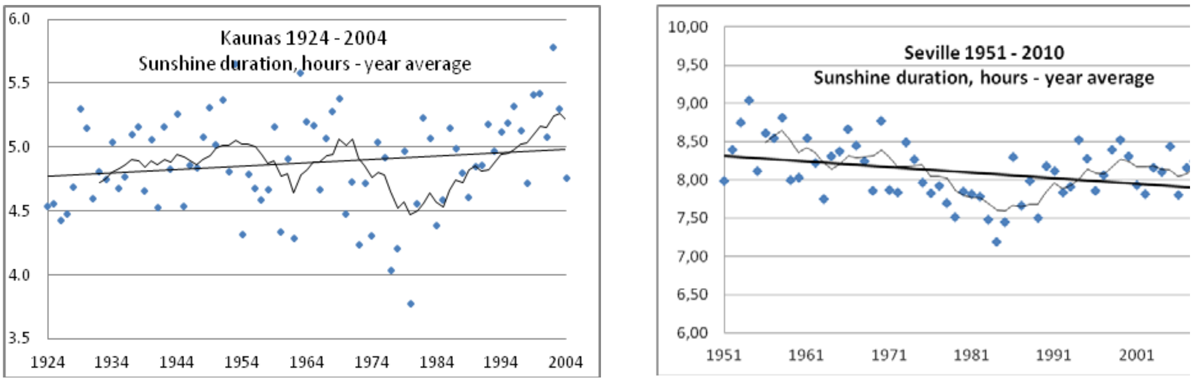

a) Kaunas, LT b) Seville, ES

Fig. 2. Daily sunshine duration in a) Kaunas (period 1924 – 2004) and in b) Seville (period 1951 – 2010), mean annual values, hours in decimal format).

The average sunshine duration through the year is presented in Fig. 3 (Kaunas and Seville sites). The averaging period is chosen 30 years because this is standart time interval used commonly to define climate – the weather averaged over a long period. There is a clear evidence that sunshine duration depends on the season of the year or month.

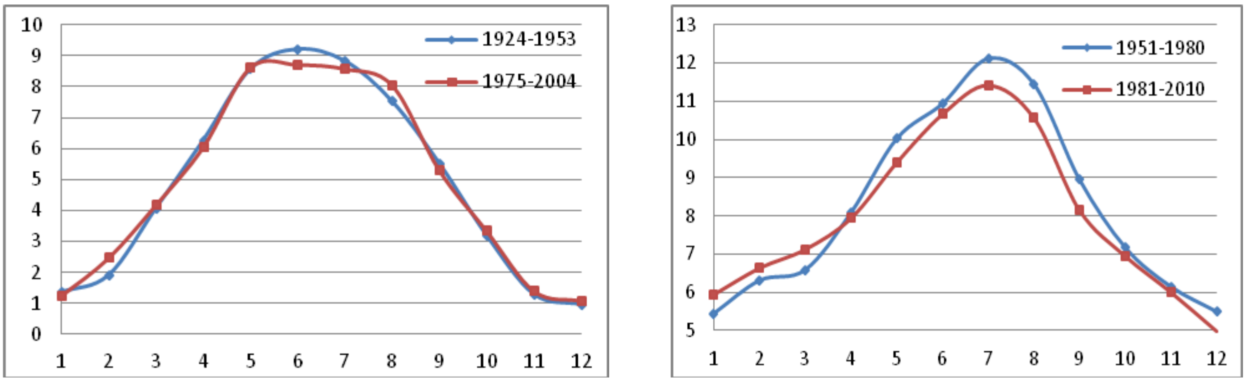

a) Kaunas, LT b) Seville, ES

Fig.3. Average sunshine duration dependence on month in a) Kaunas and in b) Seville, mean monthly values averaged on time intervals shown in graphs

The average daily solar irradiation G_t (MJ m^{-2} day^{-1}) was calculated for each month using model described in previous section. The results of calculations for selected months (January, April, July and October) are shown in Fig. 4 (for Kaunas a), (for Seville b). For the reference a trend line is drawn for each month using simple linear regression model. It can be seen that the daily irradiation at Kaunas location slightly increases with time during all months. For this location the increase statistically is not significant. However, solar irradiation at Seville region is decreasing with time on a global scale with stronger tendency. This decrease is particularly evident during summer time. In order to elucidate the significance of the observed changes in solar irradiation the Mann-Kendall test was applied.

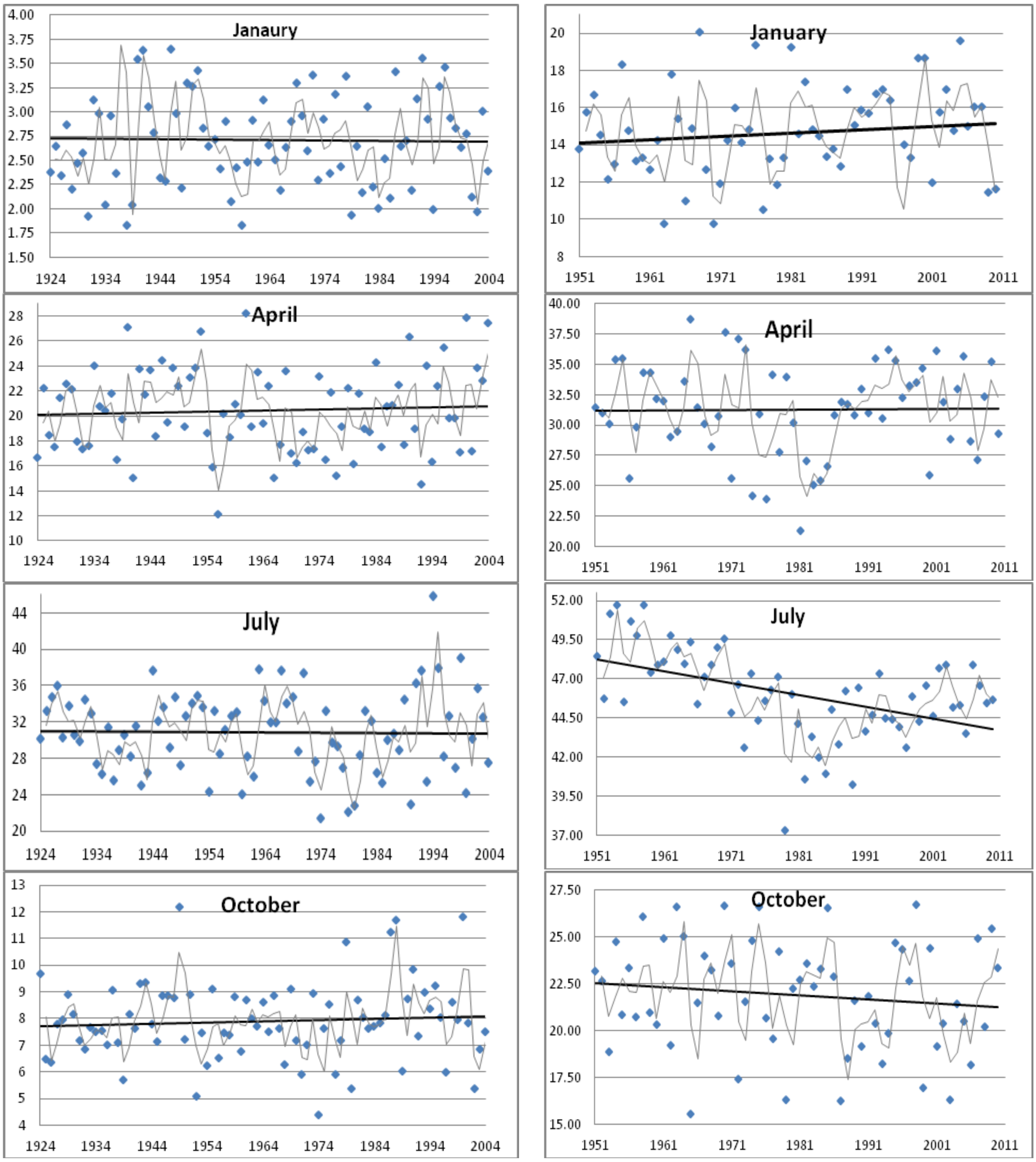

Fig. 4. Variation of daily average solar irradiation (MJ m^{-2} day^{-1}) in Kaunas, period 1924–2004 (left) and in Seville, period 1951–2004 (right) for selected months

3.3 Solar insolation variation trends

The changes of sunshine duration and solar insolation over long time period are shown in Table 3. All parameters was calculated for the same time period equal to 30 years. Notation of parameters used in the table are as follows: Δt_{30} denotes the change of a daily sunshine duration over 30 time period; ΔE_{30} is the change of a daily solar insolation over the same time period; $(\Delta t/t)_{30}$ and $(\Delta E/E)_{30}$ are relative values, where t is mean total daily sunshine duration and E is mean total daily solar insolation. Data span represents the amount of the data in years used for the analysis and p is propability, obtained from Mann-Kendall trend test.

As an example let’s take $(\Delta E/E)_{30}$ = +0.100 (Pamplona, ES). This simple means that over 30 year time period the solar insolation increased 10 % at this site, whereas the sunshine duration increased 14.7%.

The propability p is obtained from Mann-Kendall trend test. If propability p is greater than α = 1-0.95, there is no trend. If propability is less than α ($p < \alpha$), then there is a trend. The level of significance usually is taken equal to 95 % (0.95). The cases with a trend detected are marked bold in Table 3.

Table 3. Variations of solar insolation over 30 year time period

Site	Δt_{30}, min d^{-1}	ΔE_{30}, MJ m^{-2} d^{-1}	$(\Delta t/t)_{30}$	$(\Delta E/E)_{30}$	Data span, years	p, Mann – Kendall trend test
Kaunas, LT	**+4.70**	**+0.063**	**0.015**	**0.004**	**81**	**0.016**
Seville, ES	-12.90	-2.00	-0.025	-0.045	60	0.134
Pamplona, ES	**+44.20**	**+1.97**	**0.147**	**0.100**	**57**	**<0.0001**
Castellon, ES	-2.00	-0.09	-0.005	-0.007	57	0.808
Cuenca, ES	+3.90	+0.13	0.009	0.008	60	0.528
Melilla, ES	**+47.30**	**+2.62**	**0.120**	**0.110**	**40**	**0.002**
Valkenburg, NL	**+30.00**	**+1.30**	**0.135**	**0.080**	**60**	**<0.0001**
Innsbruck, AT	**+30.00**	**+1.15**	**0.125**	**0.080**	**60**	**<0.0001**
Vienna, AT	+6.70	+0.24	0.023	0.015	103	0.097
Hurbanovo, SK	+8.14	+0.43	0.025	0.020	59	0.695
Zurich, CH	-2.48	-0.17	-0.011	-0.011	109	0.181
Frankfurt, DE	+7.80	+0.34	0.030	0.025	60	0.583
Gorlitz, DE	+1.92	+0.11	0.005	0.005	61	0.936
Potsdam, DE	**+5.34**	**+0.28**	**0.020**	**0.015**	**118**	**0.012**
Nuremberg, DE	-3.76	-0.14	-0.013	-0.010	55	0.611
Oslo, NO	+5.74	+0.41	0.021	0.026	58	0.697
Nimes, FR	-3.34	-0.16	-0.010	-0.005	62	0.117
Orleans, FR	-3.93	-0.14	-0.011	-0.005	55	0.120

Obtained results show that solar irradiation changes over long time periods. It is seen that for most examined sites, the amount of solar energy available for electricity generation is increasing. For some sites the rise of 8-11 % over 30 year is significant.

The reasons of these variations of solar insolation can be related to the climate changes [11], particularly, temperature as the main parameter describing climate. The increase in atmospheric temperatures enhances overall evaporation from the surface and therefore tropospheric specific humidity also increases. This leads to the augmentation of the cloudiness. Indeed, it is shown, that there are positive linear relationships between the global radiation and temperature [12].

The explanation of the variations of daily solar irradiation is difficult because it includes complex climate models for the meteorological data analysis. Also it can be noted, that there is still no model that could explain the mechanisms of the intensity of cloud cover. For example, changes in global cloudiness can be caused by variations in the intensity of galactic cosmic rays in the atmosphere [13]. The effect of variation in cloudiness on the climate can be considered in following ways: a relation between the radiation balance of the earth-atmosphere system and variations in the amount of cloud cover or effective cloud top height; the effect on the surface temperature of variations in cloudiness; and the “feedback” effects relating changes in surface temperature to the formation of clouds [14].

Observed long term changes in solar irradiation affect the amount of the solar energy: for some regions the availability of solar energy increases as for some regions – decreases. To evaluate the consequences of sunshine variations on energy produced by photovoltaic panels or heating more work should done. Particularly, one should account the diffuse radiation which highly depends on type of cloud cover, on orientation of solar panels, on air pollution [15].

4. CONCLUSIONS

The analysis of sunshine duration for time periods that are sufficiently long to account the impacts of climate change has shown the evidence that solar irradiation varies with a trend that is characteristic for particular geographical site. It is shown that for most examined sites the amount of solar irradiation is increasing. The increase for some sites is significant and equal to 8–11 % over 30 year. Obtained results show that it is important to account solar insolation changes for the future solar applications such as photovoltaic electricity generation. To analyze the consequences of the long term sunshine variations on the amount of the solar energy use additional investigations should be done.

5. REFERENCES

1. DICNER F. The analysis on photovoltaic electricity generation status, potential and policies of the leading countries in solar energy. *Renewable and Sustainable Energy Reviews*, 2011, Vol. 15, p. 713–720.
2. ERLYKIN A.D, SLOAN T., WOLFENDALE A. W. Clouds, solar irradiance and mean surface temperature over the last century. *Journal of Atmospheric and Solar – Terrestrial Physics*, 2006, Vol. 72, p. 425–434.
3. DESSLER A.E., DAVIS S.M. Trends in tropospheric humidity from reanalysis systems. *Journal of geophysical research*, 2010, Vol. 115, 5 p.
4. PAGE J. The role of solar radiation climatology in the design of photovoltaic systems, in: MARKVART T., CASTANER L. *Practical Handbook of Photovoltaics: Fundamentals and Applications*. Elsevier, Oxford, 2003, p. 5–66.
5. WONG L.T., CHOW W.K. Solar radiation model. *Applied Energy*, 2001, Vol. 69, p. 191–224.
6. European Climate Assessment and Dataset. Link to the internet <http://eca.knmi.nl/dailydata/index.php>.
7. GILBERT O.R., Statistical Methods for Environmental Pollution Monitoring, Van Nostrand Reinhold, New York, NY, ISBN 0-442-23050-8.

a. XLSTAT. Link to the internet <http://www.xlstat.com/en/download.html>

8. Atmospheric Science Data Center. Link to the internet <http://eosweb.larc.nasa.gov/cgi-bin/sse/daily.cgi?email=>
9. Surface Meteorology and Solar Energy. A renewable energy resource web site. Link to the internet <http://eosweb.larc.nasa.gov/sse/documents/SSE6Methodology.pdf>
10. CROOK A.J.,JONES A.L.,FORSTER P.M.,CROOK R. Climate change impacts on future photovoltaic and concentrated solar power energy output. *Energy AND Environmental Science*, 2011, Vol. 4, p. 3101–109.
11. TAHAS S.V., RISTOU D., COSMA C. Trends of the global solar radiation and air temperature in Cluj-Napoca, Romania (1984–2008). *Romanian Joural of Physics*, 2011, Vol. 56, p. 784–789.
12. PERRY C.A. Evidence for a physical linkage between galactic cosmic rays and regional climate time series. *Advances in space research*, 2007, Vol. 40, p. 353–364.
13. PARK S., DESER C., ALEXANDER A.M. Estimation of the surface heat flux response to sea surface temperature anomalies over the Global Oceans. *Journal of climate***,** 2005, Vol. 18, p. 4582–4599.
14. KELLY N.A., GIBSON T.L. Increasing the solar photovoltaic energy capture on sunny and cloudy days. *Solar Energy*, 2011, Vol. 85, p. 111–125.

CYSENI 2012, May 24–25, Kaunas, Lithuania
ISSN 1822-7554, www.cyseni.com

HUMAN KINETIC ENERGY HARVESTING LINEAR GENERATOR

Chueh-Cheng Wu, Hong-Tai Chen, Sy-Ruen Huang, Gung-Ching Li, Chen-Yeon Chu
Feng Chia University
No. 100, Wenhwa Rd., Taichung, 407 – Taiwan
Phone +886-4-24517250 ext.3818
Email: *jazzwu@hotmail.com*, *srhuang@fcu.edu.tw*, *acchang@fcu.edu.tw*, *cychu@fcu.edu.tw*

ABSTRACT

This study presents a research about a multivariable linear generator that converts human kinetic energy directly into electrical energy. Based on the varying induction segment length over time, this study established an operational simulation of the multivariable linear generator while simultaneously constructing a multivariable generator device that considers the relationship between the number of vertical movements, the change in induction coils, the magnetic flux density, and other coefficients. Using finite element analysis, this study then analyzed the magnetic flux distribution for a single-stem linear generator and optimized the wiring. This method can be used to determine the wiring direction and coil thickness. The attraction between the magnet and the iron core is used to overcome the alternating magnetic fields, and linear motion with less stress is used to generate power. The generator developed in this study which can generate 21.21W power in 0.36 square meters area.

Keywords: Wave energy, multivariable linear generator, finite element analysis, magnetic flux density, relative coefficient

1. INTRODUCTION

Since the oil crisis, countries around the world have focused on the shortage of fossil fuels. Pure, recyclable, pollution-free, developable, and sustainable new resources are set to be the primary future energy developments. Wave energy is an area where the research has not yet converged towards industrial solutions [1]. Wave energy on the other hand has an estimated potential of around 1000–10,000 GW, which is in the same order of magnitude as world electrical energy consumption [2]. Kinetic energy is typically converted into electrical energy using electromagnetic, piezoelectric or electrostatic transduction mechanisms [3]. The linear generator proposed in this study can directly convert wave kinetic energy into electricity. With magnetic flux flowing in two opposite directions over its coils, and with the magnetic fields alternating over time, this structure produces alternating current sources. Furthermore, this study considers the wear and tear on the equipment, such as hysteresis loss, eddy current loss, and copper loss, to analyze the overall efficiency. Finally, finite element analysis is used to analyze the two-dimension spatial flux distribution and the loss of electricity. Linear generators that use changes in magnetic flux to generate electricity have been proposed previously, but with drastically different wiring methods and flux directions and using concaved and convexed iron bars to produce straight movement [4]. However, for magnetic flux circuits, iron bars that move with time create varying levels of permeability between the air gaps and the iron bars, directly affecting the amount of magnetic flux produced. The pole shoes order the channels for the line of magnetic flux, adjust the injected direction of the magnetic force, and decrease flux leakage [5]. Eight vertical and independent induction coil magnets can be used inside the generator to create an octagonal cylindrical linear generator. This generator constructed in a nearly circular shape propels magnetic flux and increases the area for induction. Experiments regarding the ratio between pole spacing and wire spacing, which analyzed simulations for magnetic poles using different numbers of grooves per unit, indicated that when the grooves per unit are 1 ($q=1$), high-order harmonics increase substantially [6]. Linear generators also can be combined with shock absorbers of vehicles to convert shock energy to electrical power. A four-phase linear generator is better solution this application considering generator operation balance and the shock absorbers operation smooth [7]. The generator converted DC to AC and primarily used pulse width modulation to obtain the appropriate alternating current to start the hybrid car motor which has a linear generator [8]. For wave energy applications, the direct-drive linear generator control used in and eliminated the induction voltage equation. Additionally, using Simulink for the simulations enabled analysis of the frequency of response, the one-way induction voltage, the one-way induction current, and the average power [9]. The finite element analysis is used to simulate a small linear wave energy converter, and used the salient polar flux injection method to construct a low-speed linear generator with a rated power of 10 kW and an operating frequency of 13.4 HZ, but at a high manufacturing cost [10]. At least four stators are required when designing stators to maintain the balanced force of linear motion. The wear and tear caused by operations, however, can be reduced [11][12].

This study constructs an electricity generation system using a linear generator and low-stress linear motion. By improving current linear generator structures, this system can maintain a constant level of electricity under low stress. The structure is then optimized using finite element analysis software to form a complete power supply system. The popsoased human kinetic energy harvesting linear generator can be modified to a wave power generator.

2. MAGNETIC FIELD ANALYSIS

The magnetic circuit analysis for generators primarily analyzes the distribution of structural material and their magnetic properties. The following section describes the magnetic field distribution and the magnetostatics in the overall structure of the linear generator. First, to determine the magnetic flux density, magnetic vectors are identified and solved using a partial differential equation (Eq. (1)).

$$\nabla \times \mathbf{H} = \mathbf{0} \tag{1}$$

Next, the scalar magnetic potential function φ_{mp} is entered directly into the equation. The inverse gradient for this function is defined as the magnetic field strength, and the curl free vector field can be expressed as the scalar field gradient (Eq. (2)).

$$\mathbf{H} = -\nabla \varphi_{mp} \tag{2}$$

Because of the primarily non-linear properties of the magnetic material, a variable **M** must be introduced to describe the extent of magnetization of the material. From the linear relationship between the magnetization vector **M** and magnetic field strength, the relationship between the magnetic flux density and magnetic field strength can be determined.

$$\mathbf{M} = x_m \mathbf{H} \tag{3}$$

$$\mathbf{B} = \mu_0(\mathbf{H} + \mathbf{M}) = \mu_0(1 + x_m)\mathbf{H} = \mu_0 \mu_r \mathbf{H} = \mu \mathbf{H} \tag{4}$$

where the divergence and curl of the set magnetic flux density in free space is

$$\nabla \cdot \mathbf{B} = \oint\!\!\oint_S \mathbf{B} \cdot ds = 0 \tag{5}$$

$$\nabla \times \mathbf{B} = \mu_0 \mathbf{J} \tag{6}$$

Equation (5) shows that the relationship of the magnetic field strength divergence is Eq. (7) and the magnetic charge density is Eq. (8).

$$\nabla \cdot [\mu_0(\mathbf{H} + \mathbf{M})] = 0 \tag{7}$$

$$-\nabla \cdot \mathbf{M} = \rho_m \tag{8}$$

If the magnetization vector M is constant, the divergence is zero. Using Eqs. (2) and (8), Poisson's equation (9) of the scalar magnetic potential can be determined.

$$\nabla \cdot \mathbf{H} = \nabla \cdot (-\nabla \varphi_{mp}) = \nabla^2 \varphi_{mp} = -\rho_m \tag{9}$$

Under uniform magnetization, the defined magnetic charge density is zero and the potential function satisfies Laplace's equation, as shown in Eq. (10).

$$\nabla^2 \varphi_{mp} = 0 \tag{10}$$

3. GENERATOR MODEL DESIGN

The structural variables in generators are relatively complex. The bipolarity and spatial limitations of the generator's magnet must be applied to the commuted DC generator. The changing coil flux cutting caused by the displacement of the magnetic pole can be determined using the wave movement equation. Additionally, analyzing the change in the number of coils because of displacement reveals the induction voltage value. The following sections introduce the design for single variable and multivariable linear generators.

3.1 Single variable linear generator

First, assuming an ideal wave with an ideal sine wave motion equation, the diagram is shown in Fig. 1. The amplitude was set to *d*; thus, the maximum value of this wave is d/2. Conducting periodic sinusoidal motion, the motion equation is Eq. (11) and the time-varying relationship between the wave length and magnetic flux is shown in Eq. (12).

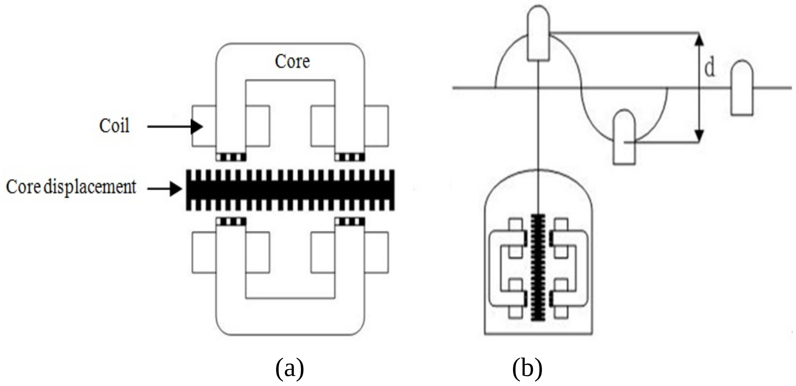

Fig. 1. Single variable linear generator design (a) generator (b) wave motion

$$S(t) = \frac{d}{2}\sin(\omega t) \tag{11}$$

$$\varphi(t) = \varphi_{\max} \sin(2\pi \cdot \frac{S(t)}{\tau}) \tag{12}$$

By directly integrating the time from Eq. (2), the induced electromotive force can be determined, as shown in Eq. (13).

$$v = -\frac{d\varphi(t)}{dt} = -n\varphi_{\max}\omega\pi\frac{d}{\tau}\cos(\omega t)\cos(\frac{\pi d}{\tau}\sin(\omega t)) \tag{13}$$

where d is the wave amplitude, τ is the period of magnetic variance, ω is the angular velocity ($\omega=\frac{2\pi}{\tau}$), and $\varphi_{\max}$ is the maximum magnetic flux value.

3.2 Multivariable linear generator

Considering the relationship between the multiple vertical movements, the changed induction coils, the magnetic flux density, and relative coefficients, a multivariable electrical generation device was constructed. The internal structure of this multivariable generator is shown in Fig. 2.

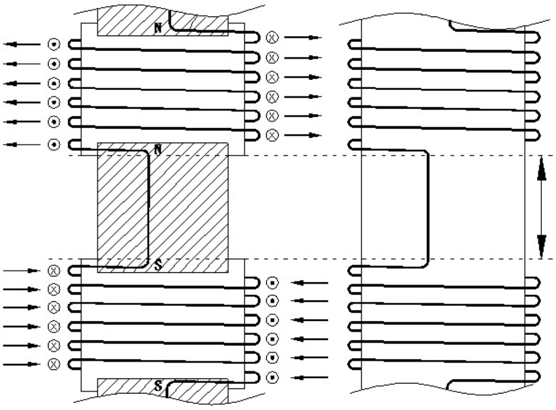

Fig. 2. Salient pole magnetic column coil wiring

The voltage produced is denoted by υ and the integration path length is denoted by ℓ. The speed and direction of moving objects has an outer product with the B direction of the magnetic field density, and the constant direction of the magnetic field density is perpendicular to the direction of motion (see Eq. (14)).

$$v=U\cdot B\cdot l \tag{14}$$

where υ is the induced voltage, U is the relative velocity of the induction coils and flux density, B is the magnetic flux density, and ℓ is the length of the induction line.

However, vertical motion linear generators are affected by the aggregate impact force with the wave motion. This force directly affects the velocity and acceleration of the magnetic pole displacement and the vertical displacement speed within one unit of time (15). The time-varying induction coils are shown in Eq. (16), and the magnetic flux change is shown in Eq. (17).

$$U=U_0+(a\cdot t) \tag{15}$$

$$l=\left[\frac{S(t)-(d\cdot(k-1))}{d}\right]L\cdot h=(\frac{S'}{d})\cdot L\cdot h\ ,S>d \tag{16}$$

$$B(t)=B_{\max}\cdot\sin(2\pi\cdot\frac{S(t)}{D}) \tag{17}$$

where $B_{\max}$ is the flux density on the surface of the magnetic pole, S is the amount of displacement, and D is the wave length for one period.

In the vertical salient pole magnetic cylinder, magnetic flux is ejected outward near the N pole and drawn inward near the S pole. Magnetic flux density is then formed perpendicular to the induction coils, achieving electromotive force. The following section explains the actual structural design and experiment results for the multivariable linear generator.

Table 1 showed that differences of single variable and multivariate linear generator. Based on this reason that magnet movment force of multivariate linear generator than single variable linear generator, this study designed a multivariable generator for harvesting kinetic energy.

Table 1 Differences of single variable and multivariate linear generator

	Multivariate linear generator	Single variable linear generator
Magnet movment force	low	high
Energy desity	low	high
Variable analysis	difficult	easy
Displacement demand	high	Magnet number can be increased to reduce the displacement demand with adjustment flexibility
cost	low	high
Three-phase power	no	yes

4. EXPERIMENT RESULTS

4.1 Single stem linear generator energy conversion efficiency

As discussed in the previous section, a multivariable linear generator was constructed using multiple single-stem linear generators. To maintain the output power, this study limited the overall displacement of the generator floor to within 5 cm.

When a single-stem linear generation system does not consider internal resistance, the alternating current is input in the full-wave rectifier and converted into direct current. The following series of equations can calculate the power provided by a pedal generator (18).

$$P = \frac{V_{rms}^2}{R_{Load}} \tag{18}$$

We did free fall cylinder experimentation (only gravity without spring force) to estimate energy conversion efficiency of generator. The average power was 0.4570 W and the load was 200 ohms. The potential energy conversion efficiency P_p is calculated as follows:

$$P_P = \frac{W_P}{t} = \frac{mgh}{t} = \frac{0.56 \times 0.198 \times 9.8}{0.37} = 2.9368(W) \tag{19}$$

The single-stem linear generator experiencing load had an average power of 0.457 (*W*) and a total efficiency of 0.1556 shown in Eq. (20)

$$E_{ejj} = \frac{0.457}{2.9368} = 0.1556 \tag{20}$$

4.2 ANSYS magnetic circuit analysis

After discovering the conversion efficiency, this experiment used ANSYS to analyze the magnetic circuit distribution of the single-stem linear generator. First, a single groove was formed in the structure to establish the projected magnet area and increase the magnetic flux scattered. This study found that in the red vector section one magnetic pole was fired directly at the other magnetic pole and did not intersect with the induction coil. Properties perpendicular to the surface when the magnetic flux is ejected were used to increase the intersection between the induction coils and the magnetic flux. The magnetic flux density value graph is displayed in Fig. 3. Magnetic saturation occurred around the polar shoes. When the stator wall thickness was set at 1.5 mm, sufficient magnetic flux density was maintained.

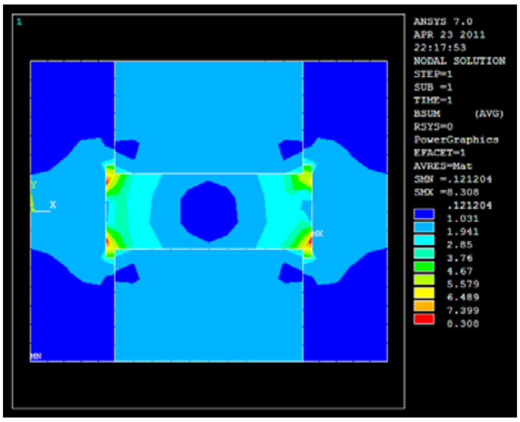

Fig. 3. Magnetic flux density value

4.3 Multivariable linear generator model

Next, the experiment integrated the single-stem linear generator into a generator board with multiple generators. We found that in this multiple set structure, magnetic poles interfere with each other. Therefore, the spacing between magnetic cylinders must be lengthened to prevent this problem from occurring. The multiple set generator board schematic is shown in Fig. 4.

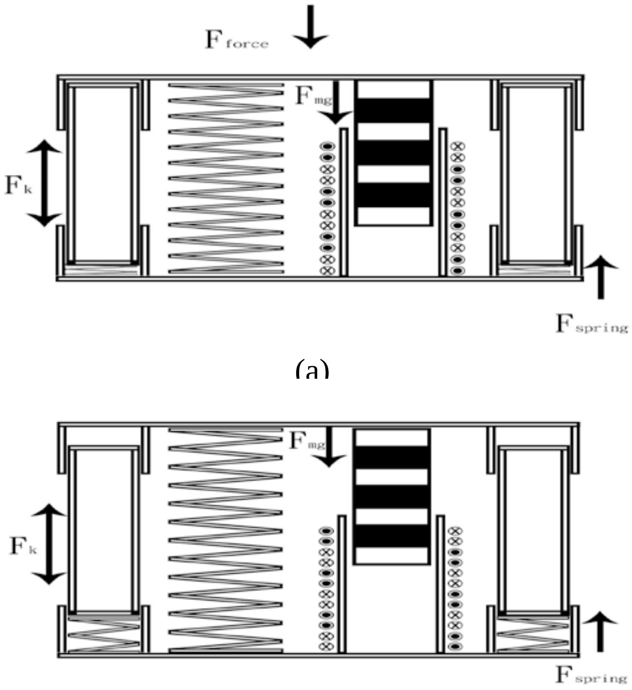

(a)

(b)

Fig. 4. Magnet movement in a linear generator: (a) Under pressure (b) Risen

When under pressure, the entire force is expressed mathematically in Eq. (21)-(22). Then, the spring rising is expressed in Eq. (23)-(24) [13].

$$F_{total} = ma = F_{mg} + F_{force} - F_{spring} - F_k - F_{stop} \tag{21}$$

$$F_{mg} + F_{force} > F_{spring} \tag{22}$$

$$F_{total} = -ma = -F_{spring} + F_k + F_{stop} \tag{23}$$

$$F_{spring} > F_{mg} \tag{24}$$

where F_{total} is the aggregate force, F_{mg} is the gravitational force on the moving section, F_{force} is the external force of the wave buoyancy, F_{spring} is the elasticity of the spring or the opposite magnetic force of the magnetic pole installed on the bottom, F_k is the friction along the pipe walls, F_{stop} is the force of the plastic tube on the device when the device is stopped, *a* is the gravitational acceleration, and *m* is the total mass of the system's moving section.

4.4 Multivariable generator actual electric measurements

The internal structure of the multivariable generator is shown in Fig. 5. We installed 21 single-stem linear generators which have 9 layers 0.17 mm diameter wires on a metal board. The actual measurement and simulation value comparison for open circuit of the generator is shown in Fig. 6; the simulated waveform is very similar to measured waveform.

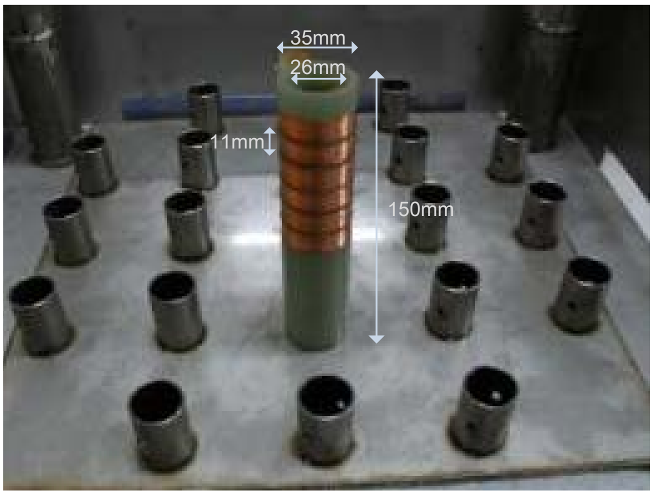

Fig. 5. Internal structure of the liner-direct generator; just only one column coil installed in this figure

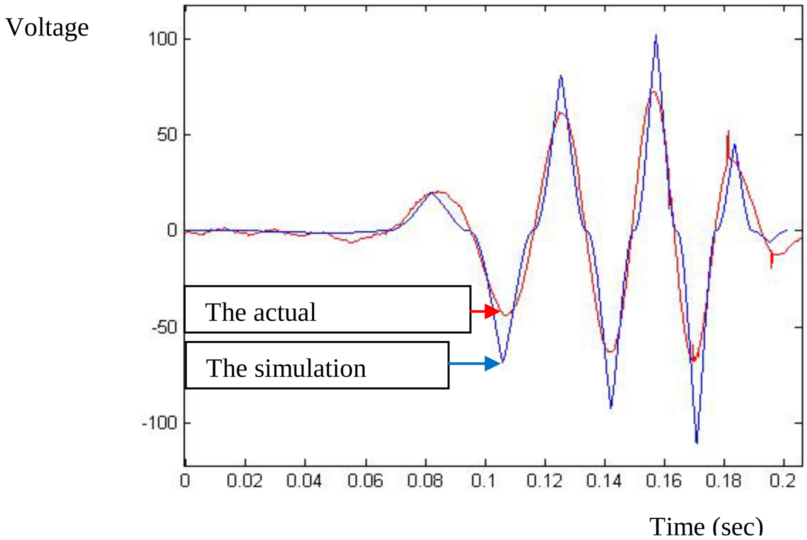

Fig. 6. The actual measurement and simulation value comparison for open circuit

For this example in this study, the total area of the system which is 0.36 square meters are installed 21 magnet linear generator columns. Each linear generator column can output power of 1.01 W. Therefore, the output power is 21.21 W totally, i.e. 58.91 W per square meter in this prototype design. Fig. 7 presents the linear generator which can generate eletric power by transforming human kinetic energy. The LED (light-emitting diode) emits light by elerctric power generated while vertical movements happening.

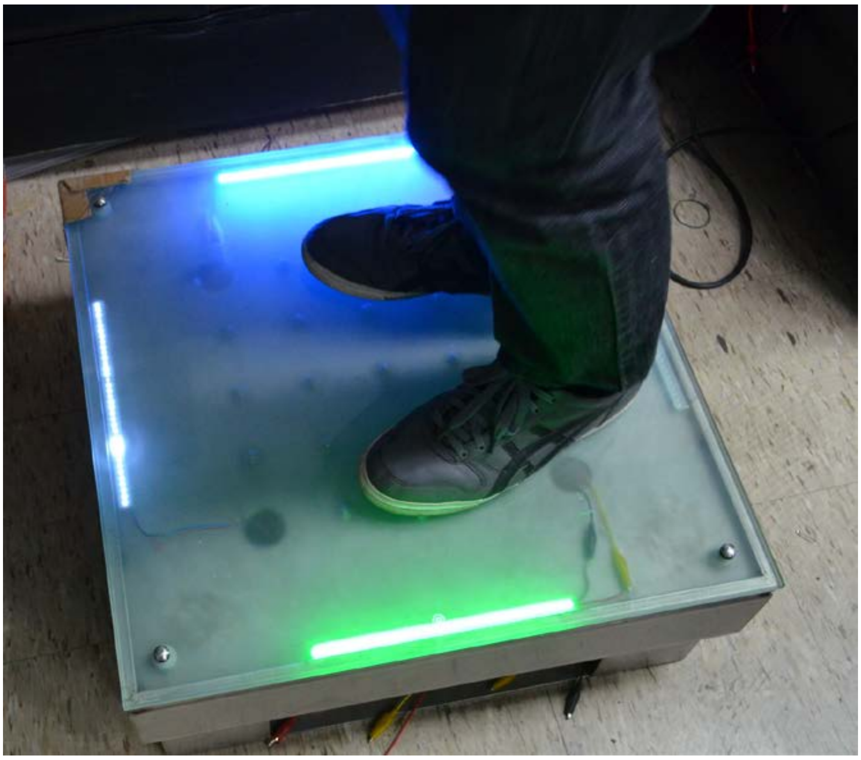

Fig. 7. The LED provides light when an objective has vertical motions at the human kinetic energy generator

5. CONCLUSION

This study designed established a low cost, simple structure human kinetic energy linear generator prototype which output 21.21W power totally and will finish a wave generator prototype in the future. After adjusting the form of the magnetic poles by using finite element analysis software, the number of intersections between the induction coils and the magnetic flux was successfully increased. The simulated vertical motion properties of the wave provided the impetus for a permanent magnet. By ensuring the magnet and the coils moved in opposite directions and cutting the lines of magnetic flux to produce induction voltage. This study presented the process of designing a linear generator that can be used in the future, under varying force environments, to develop the ideal generator for a given environmental force, thereby improving the power generation efficiency. Further research is needed to determine appropriate wire coil, magnet, rotor movement distance, fluid dynamics design, and structure strength design.

ACKNOWLEDGEMENTS

The authors thank the National Science Council of Taiwan for supporting the research under the grants of NSC 100-2221-E-035-006-, NSC 100-2627-E-035-001-, NSC 99-3113-P-194-001-, NSC 99-2632-E-035-001-MY3.

REFERENCES

1. I. Glendenning. Ocean wave power. Applied Energy, Volume 3, Issue 3, July 1977, p.197–222.
2. Miguel Estebana, David Learyb, Current developments and future prospects of offshore wind and ocean energy, Applied Energy, Vol. 90, Issue 1, February 2012, p. 128–136.
3. Beeby S.P, Tudor M.J. and White N.M. 2006 Energy harvesting vibration sources for microsystems applications Meas. Sci. Technol. 17 R175–R195.
4. Ma Muiller and NJ Baker, “A Low Speed Reciprocating Permanent Magnet Generator for Direct Drive Wave Energy Converter”. International Conference on Power Electronics Machines and Drives (CP487), Bath, UK, 16-18 April 2002.
5. Lorand Szabo, Claudiu Oprea, Joan-Adrian Viorel, Kairoly Agoston Biro “Novel Permanent Magnet Tubular Linear Generator for Wave Energy Converter”, Electric Machines & Drives Conference, 2007. IEMDC '07. IEEE International.
6. Irina A. Ivanova, Olov Ågren, Hans Bernhoff, and Mats Leijon, “Simulation of Wave energy Converter with Octagonal linear Generator”, 2005 IEEE.
7. Lei Zuo, Brian Scully, Jurgen Shestani and Yu Zhou,”Design and characterization of an electromagnetic energy harvester for vehicle suspensions”, 2010 Smart Materials and Structure.
8. Ahmad M. Eid, S. K. Kwon, Hyun Woo Lee, and Mutsuo Nakaoka, “Linear Engine Couple Linear Generator Starting for Hybrid Electric Vehicle Application”, 2006 ICEE.
9. J.K.H. Shek, D.E. Macpherson, M.A. Mueller and J. Xiang,”Reaction Force Control of Linear Electric Generator for Direct Drive Wave energy Conversion”, 2007 IEEE.
10. Mueller, M.A. et al., "Dynamic Modelling of a Linear Vernier Hybrid Permanent Magnet Machine Coupled to a Wave Energy Emulator Test Rig," Conference Record of the International Conference on Electrical Machines （ICEM '2004）, Cracow （Poland）, on CD： 495.pdf, 2004.
11. Mats Leijon, Hans BernhoffI, Olov Ågren, Jan Isberg, Jan Sundberg, Marcus Berg,Karl Erik Karlsson, and Arne Wolfbrandt, ”Multiphysics Simulation of Wave Energy to Electric Energy Conversion by Permanent Magnet Linear Generator”, 2004 IEEE.

12. Neil Hodgins, Ozan Keysan, Alasdair McDonald & Markus Mueller, “Linear Generator for Direct Drive Wave Energy Applications”, XIX International Conference on Electrical Machines – ICEM 2010, Rome.
13. Karin Thorburn, Karl-Erik Karlsson, Arne Wolfbrandt, Mikael Eriksson, Mats Leijon. Time stepping finite element analysis of a variable speed synchronous generator with rectifier. Applied Energy, Volume 83, Issue 4, April 2006, p. 371–386.

CYSENI 2012, May 24–25, Kaunas, Lithuania
ISSN 1822-7554, www.cyseni.com

INVESTIGATION OF THERMAL CRACKING OF SYNGAS TAR FROM BIOMASS GASIFICATION BY CATALYTIC STEAM REFORMING

K. Zakarauskas, N. Striugas, G. Stravinskas
Lithuanian Energy Institute
Laboratory of CombustionProcesses
Breslaujos str. 3, LT-44403 Kaunas – Lithuania
Phone (+370 37) 401830
Email: zakarauskas@mail.lei.lt

ABSTRACT

Gasification of biomass and other biological waste is one of the alternative ways of energy production in order to reduce environmental pollution and wider use of renewable energy sources. One of obstacles of implementing gasification technology into industry is presence of tars in resulting synthetic gas. The tars reduce operation time of technological equipment by condensing, adhering and baking on the surfaces. At present time syngas is being cleaned by condensing on scrubbers. This method is effective enough, but not economically profitable – part of calorific compounds is being removed, also polluted water remains. In order to optimize gasification processes, research of new ways of tar removal from syngas is being carried out in the world [1]. One of the new ways is catalytic reforming. During the process tar hydrocarbons are additionally gasified down to final reaction products, which results in increase of resulting gas yield and calorific value.

Results of thermal cracking with catalytic reforming of tars present in syngas from biomass gasification using two types of catalysts – dolomite and activated carbon obtained from used tyres – are presented in this article. Composition of tar hydrocarbons in syngas from biomass gasification was investigated and performance of thermal cracking was evaluated by comparing remaining tar hydrocarbon composition and quantities at different temperatures and residence times on catalyst. Also, analysis of the experimental results and comparison with results from other authors is presented, which will allow to define optimal parameters for most efficient tar cleaning from synthetic gas.

Keywords: Biomass gasification, tars, steam reforming, dolomite, char

1. INTRODUCTION

Gasification is thermo-chemical process, when solid carbonaceous materials are converted into a gas. The obtained synthesis gas must be cleaned from tar in order to use them in large or micro turbines, internal combustion engines for electricity generation, chemical reactors for production of fuel, chemical substances. Currently, gas is cleaned from tar by condensing it in scrubbers. It is uneconomical cleaning method, since cleaning waste forms. Therefore, it is seeking for more effective methods and one of them is catalytic thermal decomposition of tar [1].

During catalytic thermal decomposition of tar it is additionally gasified to synthesis gas. This reduces the quantity of tar and increases the gas output. The studies using the model of aromatic compounds and the main materials of tar, i.e., benzene and naphtalene, as well as two catalysts: activated tyre char and calcined dolomite [2], have already been carried out earlier. The studies showed [2] that tyre char catalyst is more effective than dolomite, when decomposing heavier hydrocarbons. Although the quantity of benzene in real tar is the highest, it is not the most problematic compound, and it would impede technological application of gasified gas. This process is impeded by compounds of heavier molecular mass, the condensation point of which occures at high temperature (100–250°C). Therefore, it was decided to carry out the studies with real tar, present in wood gas, seeking to determine the activity of these catalysts in regard of thermal decomposition of tar compounds, depending on temperature and catalyst quantity.

2. METHODOLOGY

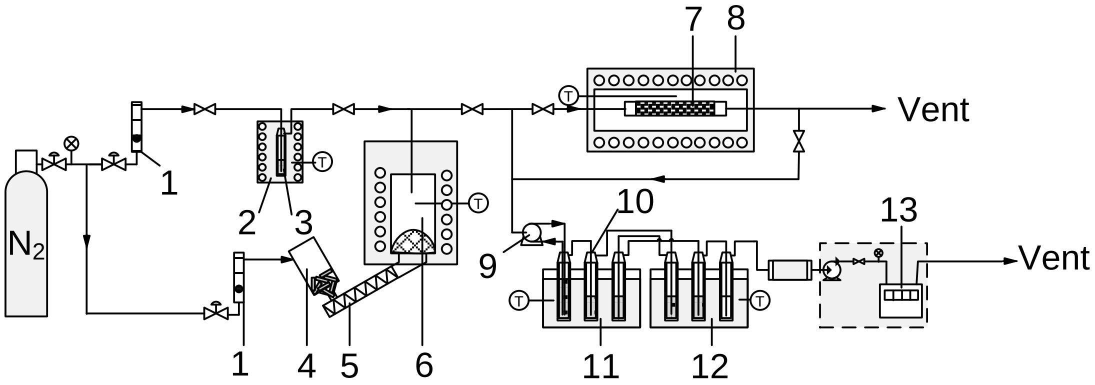

Fig. 1. Scheme of the experimental rig

1 – rotameter; 2 – heater; 3 – water evaporator; 4 – biomass pellet container; 5 – screw conveyer; 6 – biomass pyrolysis reactor; 7 – catalytic bed; 8 – steam reforming reactor; 9 – peristaltic pump; 10 – gas washing bottles; 11 – heated bath; 12 – cooled bath; 13 - gas flowmeter.

The experimental set-up consists of three main parts: the system of making a gas mixture with tar, the catalytic reactor and tar condensers. Biomass tar decomposition experiments are carried out in the following way: nitrogen is supplied to evaporator (3) by the flow of 0.9 l/min. Water is evaporated at constant temperature (90.5°C) in evaporator (0,5g/min). Nitrogen flow, flowing through evaporator (3), saturates with certain water quantity. Vapour concentration is regulated by changing the temperature of evaporated H_2O. Other measured nitrogen flow (1.8 l/min) for pyrolysis gas transportation is supplied to container (4) with fuel pellets. Coniferous (spruce and pine) wood pellets are used in experimental studies (humidity – 5.2%, calorific value – 19 MJ/kg, ash content – 0.35 %. Screw conveyor (5) supplies a constant quantity of fuel pellets, i.e., 5 g/min, to reactor of pyrolysis (6). Constant temperature of 850 °C is maintained in pyrolysis reactor(6). The obtained pyrolysis gas with tar are mixed with nitrogen and water vapour before going to catalytic reactor(8). The obtained gas mixture goes to tar steam reforming reactor(8).

Catalyst bed (7) is mounted inside the reactor (8). Thermocouple (K-type) is installed in the reactor, according to which the constant required temperature (700, 800 and 900 °C) is maintained. The standard methodology was followed, when determining the tar concentration in gas flow before and after catalytic reactor, which is based on cold trapping [3].

The quantity of gas flow, flowed during experiment, is summated by gas meter 13. The obtained samples are weighted and analyzed by gas chromatography. Sample analysis is carried out by Varian GC-3800 gas chromatograph, the methodology of analytical analysis is used for compound detection [4].

While analyzing tar catalytic – thermal decomposition, experimental tests of two types were carried out, using dolomite and tyre char catalysts. The activity of each catalyst was examined at different temperatures (700, 800 and 900°C) and quantities of catalysts, at constant initial tar concentration in gas.

3. RESULTS AND DISCUSSION

The results (Table 1), show that tar consists of benzene, toluene, naphthalene, acenaphthylene mainly, and total concentration of calibrated tar in initial gas is equal to 21.1 g/m^3.

Table 1. Tar composition in synthesis gas

Compound	Concentration g/m^3	Dolomite catalyst (v=0.04 s^{-1})			Tyre tar (v=0.04 s^{-1})		
		700°C	800°C	900°C	700°C	800°C	900°C
Benzene	8.7	3.3	2.5	0.7	2.6	0.5	0
Toluene	1.7	0.5	0.5	0.1	0.5	0	0
Naphthalene	4.8	0.8	0.8	0	0.7	0.1	0
Acenaphthylene	1.7	0.1	0.1	0	0.1	0	0
Fluorene	0.5	0.1	0.1	0	0	0	0
Phenanthrene	1.1	0	0	0	0.1	0	0
Antracene	0.6	0	0	0	0	0	0
Fluoranthene	0.8	0	0	0	0	0	0
Pyrene	0.6	0	0	0	0	0	0
Benz[a]anthracene	0.3	0	0	0	0	0	0
Other tar	0.3	0	0	0	0	0	0
Total tar	**21.1**	**4.9**	**4.0**	**0.8**	**4.0**	**0.6**	**0**

3.1. Dolomite Catalyst

First of all the experiments were carried out, using different quantities of calcined dolomite at constant temperature (900°C) and steam/carbon ratio ($H_2O/C=1$). Calcined dolomite was used, since due to larger surface area it is more active for tar decomposition [5]. In order to depict the obtained results, the concept of space velocity was introduced. It defines the relation between space velocity and catalyst volume:

$$v = Q/V \,, \tag{1}$$

where Q – flow of producer gas through the catalyst bed, m^3/s; V – volume of catalyst in the bed, m^3.

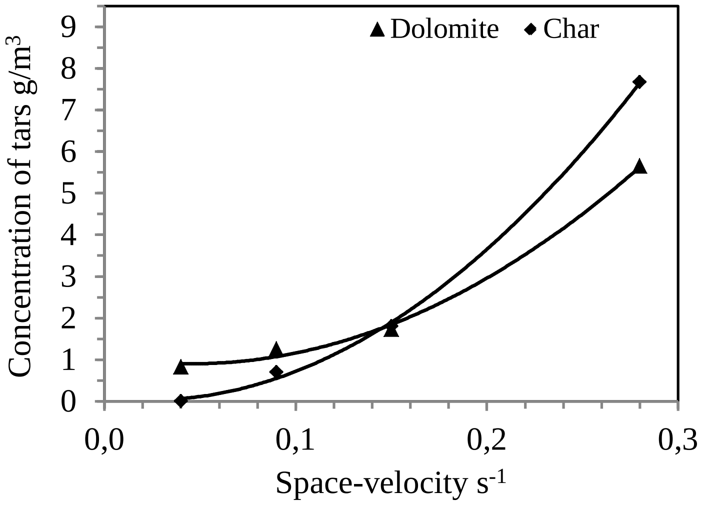

Fig. 2. Tar concentration in gas after catalyst at different space velocities at constant temperature of 900°C

Total concentration of tar decreases to 5.7g/m^3 at space velocity of v=0.28 s^{-1}. To simulate as full conversion to tar as possible, the quantity of catalyst was increased under the same gas flow. After reducing space velocity to v=0.15 s^{-1} total tar concentration decreased to 1.7g/m^3. At lowest studied space velocity (v=0.04 s^{-1}) total tar concentration in gas decreases to 0.8 g/m^3. At this point only two residual compounds were detected, i.e., benzene and toluene. Due to low condensation temperature the presence of benzene and toluene would not cause any serious problems, since the temperature of gas dew point is below -20°C.

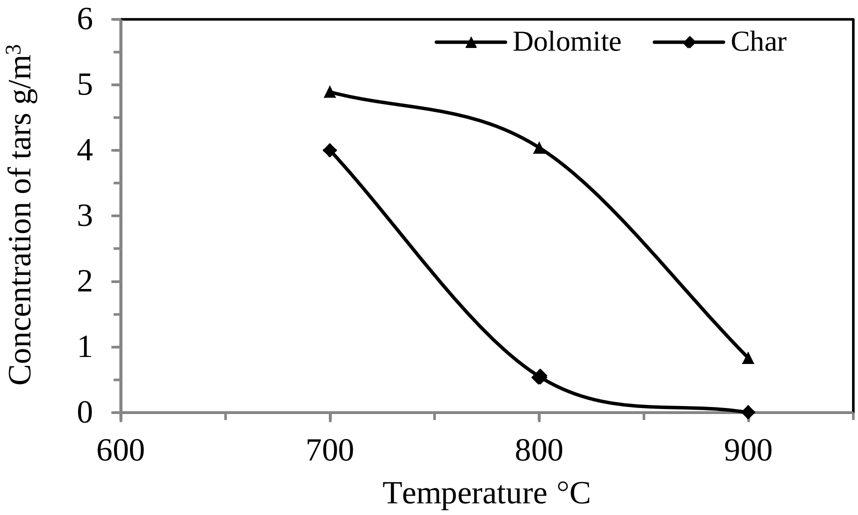

Fig. 3. Tar concentration after catalyst at different temperatures at constant space velocities of v=0.04 s^{-1}

The change of tar concentration, depending on temperature, is presented in figure 3 at constant space velocity of v=0.04 s^{-1}. The influence of temperature is obvious: tar concentration in gas decreases from initial 21.1 g/m^3 up to 4.9 g/m^3 , 4.0 g/m^3 and 0.8 g/m^3 at 700°C , 800°C and 900°C respectively.

3.2. Char Catalyst

As in case of dolomite, effectiveness studies of activated char catalyst were performed at different space velocities at constant temperature (900°C) and quantity of water vapour (H_2O/C=1). At highest space velocity v=0.28^{-1}, tar concentration decreases to 7.7g/m^3 (Fig. 2). At lowest space velocity (v=0,04 $^{-1}$), no tar was detected in gas and full tar conversion occurs.

As in case of dolomite, the influence of temperature is obvious: tar concentration in gas decreases from initial 21.1 g/m3 up to 4.0 g/m3 and 0.6g/m3 at 700°C and at 800°C respectively. Tar was fully decomposed at 900°C (Fig. 3).

Seeking to assess the efficiency of catalysts, tar concentrations are recalculated to decomposition efficiency in percentage:

$$X(\%) = \frac{(C_{in} + C_{out})}{C_{in}} \cdot 100\% \qquad (2)$$

The obtained results of calculations are presented in figure 4. As it may be seen, tyre char catalyst is more effective at all temperatures, when comparing with dolomite catalyst. When using dolomite catalyst, tar conversion at 900 °C temperature was 96.0 %, meanwhile, using tyre char catalyst under the same conditions full conversion was obtained.

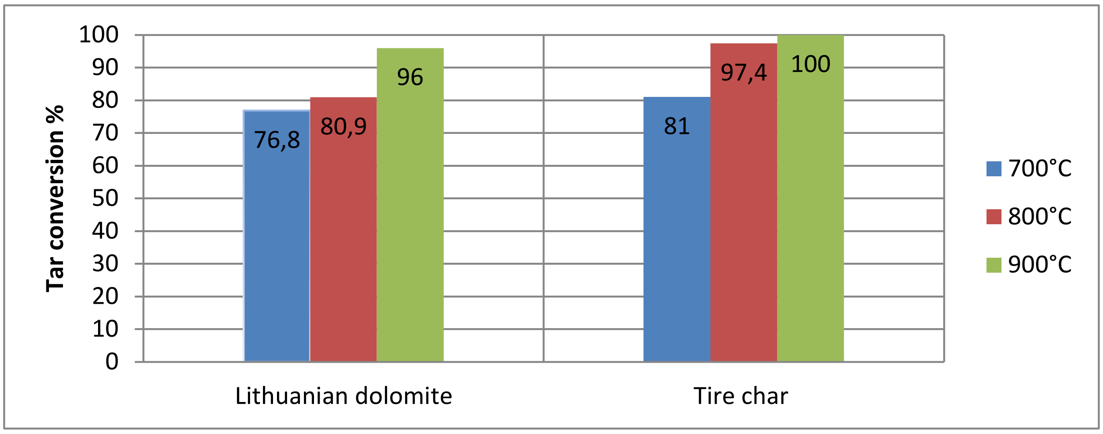

Fig. 4.Tar decomposition efficiency in case of different catalysts at constant space velocities of $v=0.04\ s^{-1}$

In case of dolomite catalyst tar decomposition is effective only at 900°C temperature and is close to full conversion (96.0%), while at lower temperature (700, 800°C) the effectiveness of decomposition was approximately ~80%. Comparing the obtained results with similar studies by other authors, it is determined that at 800°C the effectiveness of tar decomposition varied from 71.4 to 88.6% and at 900°C from 96.8 to 99.7% [5, 6, 7].

In case of tyre char catalyst the effectiveness of decomposition at 800°C was equal to 97.4%, so it is possible to obtain a full tar conversion even at 900°C by increasing the quantity of catalyst. It is observed that at 800°C the effectiveness of tar decomposition varied from 96.7 to 97.0 % and at 900°C from 99.1% to full conversion and are in good agreement with others [8, 9].

4. CONCLUSIONS

Experimental studies demonstrated that by selecting a suitable quantity of catalyst ($v=0.04\ s^{-1}$) and supplying water vapour ($H_2O/C=1$) the full conversion of tar can be achieved.

- Dolomite catalyst is effective only at 900°C temperature and is close to full conversion (96.0%). At this point two residual compounds were detected, i.e., benzene and toluene. The effectiveness of tar decomposition at lower temperature decreases and is equal approximately to ~80%.
- In case of tyre char catalyst the effectiveness of decomposition at 800°C was equal to 97.4%, which allows assuming that it is possible to obtain a full tar conversion even at 900°C by increasing the quantity of catalyst. However, further research is required.

The analysis performed shows that the effectiveness of dolomite, found in Lithuania, and activated tyre char is comparable with the effectiveness of dolomite, found in other countries, as well as char, derived from wood.

REFERENCES

1. DEVI, L., PTASINSKI, J.K., JANSSEN, J.J.G.F., A review of the primary measures for tar elimination in biomass gasification processes. Biomass and Bioenergy, 24 (2003), p. 125–140.
2. ZAKARAUSKAS, K., STRIŪGAS, N., STRAVINSKAS, G. Thermal decomposition of biomass and analysis of tars destruction // 8th international conference of young scientists on energy issues CYSENI 2011, Kaunas, Lithuania, May 26-27, 2011. Kaunas: LEI, 2011. ISSN 1822-7554, p. 1–6.

3. Sampling and analysis of tar and particles in biomass producer gases. Technical report preapared under CEN BT/TF 143 „Organic contaminants („tar“) in biomass producer gases“. July 2005.
4. Standard operating procedure for the analysis of PAHs and atrazine by GC/Ion trap MS / Surratt, Kaye; Peters, Cathy. - Chicago, IL: U.S. Environmental Protection Agency, Great Lakes National Program Office, 1995.
5. DELGADO, J., AZNAR, M.P. Biomass Gasification with Steam in Fluidized Bed: Effectiveness of CaO, MgO, and CaO-MgO for Hot Raw Gas Cleaning, Industrial & Engineering Chemistry Research, 36 (1997), p. 1535–1543.
6. ORIO, A., CORELLA, J., I. NARVAEZ, I. Performance of Different Dolomites on Hot Raw Gas Cleaning from Biomass Gasification with Air, Industrial & Engineering Chemistry Research, 36 (1997)– 3800-3808.
7. GUSTA, E., DALAI, A.K., UDDIN, MD.A., SASAOKA, E. Catalytic decomposition of biomass tars with dolomites, Energy&Fuels, 23 (2009), p. 2264–2272.
8. GILBERT, P., RYU, C., SHARIFI, V., SWITHENBANK, J. Tar Reduction in Pyrolysis Vapours from Biomass over a Hot Char Bed, Bioresource Technology, 100 (2009), p. 6045–6051.
9. MUN, T.Y., SEON, P.G., KIM, J.S. Production of a Producer Gas from Woody Waste via Air Gasification using Activated Carbon and Two-Stage Gasifier and Characterization of Tar, Fuel, 89 (2010), p. 3226–3234.

CYSENI 2012, May 24–25, Kaunas, Lithuania
ISSN 1822-7554, www.cyseni.com

MANAGEMENT OF VEGETABLE AND FOOD WASTE FOR BIOGAS PRODUCTION

M.K. Zalewski, A.G. Chmielewski, J. Palige, O.K. Roubinek
Institute of Nuclear Chemistry and Technology
Dorodna 16, 03-195 Warsaw – Poland
Phone+48225041164
Email: m.zalewski@ichtj.waw.pl

ABSTRACT

At the present, many technological solutions which are applied for biogas production exist all over the world. Biogas, which can be produced in controlled methane fermentation conducted by human in systems designed for this purpose, is an example of alternative energy carrier. The Institute of Nuclear Chemistry and Technology with Uniserv company and in cooperation with researchers (Association of Polish Electrical Engineers SEP) from Zamość created own, Polish solution for biogas production from vegetable waste. Investigations were carried out on experimental installation of 10 kW in Szewnia Dolna (in cooperation with Ekopol company), which is based on two stage system - separate hydrolyser and fermentor. The grass from the Roztoczański National Park was tested as a substrate, however in order to increase biogas efficiency create different mixtures contain the following substrates: maize silage, whey and manure on colza straw The biogas plant working in the optimal operation parameters ensures methane concentration in biogas in the range of 58% - 69% and with concentration of hydrogen sulphide from 540 ppm to 1300 ppm. In the case of using mixtures with manure on colza straw obtained biogas of lower concentration of methane (about 60%) and higher concentration of hydrogen sulphide (about 3000 ppm). The results from experimental installation were obtained using analytical devices such as: portable gas meters, gas chromatography, for suspensions was used spectrophotometer and for dry matter – elementary analyser. The aim of this paper is presentation of results obtained from the experimental biogas plant working on the base of polish technology thought, which will be used in the future to create engineering design assumptions for biogas plant.

Keywords: biogas, anaerobic digestion, two-stage fermentation, food waste, vegetable waste

1. INTRODUCTION

1.1. Anaerobic digestion

Biogas is produced by anaerobic digestion of organic materials, with the participation of a diverse population of microorganisms. During the process, complex organic matter breaks down into the reduced gasous product [1,2,3]. Biogas consists mainly of methane and carbon dioxide and very small amounts of other substances such as sulphur compounds and siloxanes. The biogas production includes four main stages. In the first stage the complex, water-insoluble organic fraction is hydrolysed to water soluble monomers (amino acids, monosaccharides, fatty acids). Then, a group of anaerobic microorganisms degrades the hydrolysis products into volatile fatty acids, alcohols, hydrogen and carbon dioxide (acidogenesis). The next step is acetogenesis – methanogenic substrates such as acetic acid, hydrogen and carbon dioxide are forming from the acidogenesis products. The last stage is methanogenesis, which proceeds two ways: in the first – acetic acid is used as a substrate, in the second – hydrogen and carbon dioxide. The acetogenic bacteria are producers of hydrogen. The methanogens are responsible for the production of methane and during the last phase of anaerobic digestion, require hydrogen to survive. The environmental requirements make that these two groups of microorganisms live together in symbiosis [4, 5, 6].

1.2. Scheme and description of the experimental installation for biogas production in Szewnia Dolna

The experimental installation for biogas production was built in Szewnia Dolna (the small town in Lublin Voivodeship). The process is based on technical solutions of Polish patent [7]. The biogas plant uses anaerobic technology for biomass conversion, which is carrying out in a two-step system (separation of hydrolysis and fermentation).

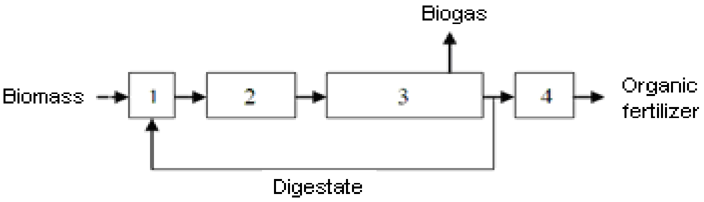

Fig. 1. The block diagram of the installation in Szewnia Dolna, 1 – biomass tank, 2 – hydrolyser, 3 – fermentor, 4 – digestate reservoir

The raw material is fed into the biomass tank (1), where is mixed with processing water and directed through the rotary pump with a shredder to hydrolyser (2). The fermentation effluent with the methane bacteria recycled by pipeline from the fermentor (3) to hydrolyser causes acceleration of the hydrolysis process and allows for adequate amount of dry matter in suspension. The pH and temperature of the fermentation mixture, and the oxygen concentration in the gas were measured. The biomass after hydrolysis is transported by a pump to the fermentor. The slurry in the digester is mixed by a system of pumps. Biogas can be removed from the surface of the fermentation mixture to the biogas reservoir. The digested biomass is directed into the digestate tank (4). The biogas flow rate is determined by the gas meter as well as the gas displacement device.

The greater stability of the process, the shorter residence time, the higher load of digester by dry matter, and the higher efficiency of two-stage process compared to the single stage process are advantages of the system.

The bioreactor for the hydrolysis is a horizontal tank with a volume of V_h= 1.5m^3 and equipped with manhole and viewing window. It was made of polyethylene (PE-HD). The tank is thermally insulated with a layer of glass wool. The mixture of gases (carbon dioxide and removed air by the carbon dioxide from biomass) has the outlet at the top of the tank.

The bioreactor for fermentation is a closed tank with a volume of V_f =8m^3. The tank is equipped with manhole and viewing window. The tank is operating in a horizontal position and is made of polyethylene (PE-HD). The tank is thermally insulated with a layer of glass wool. The biomass after hydrolys is fed into the fermentation tank by the pipeline. The aqueous suspension of biomass, which undergoes fermentation takes about 70% by volume of the tank. Above the surface of the suspension is the gas cushion of biogas with a volume of about 2m^3. The upper part of the reservoir has a biogas outlet from the fermentor.

The content of the digester is not homogeneous. The unmixed volume of the bioreactor is stratified. The surface is covered with a layer of flotated suspension and the bottom contains a concentrated sludge. This is a negative phenomenon, which reduces the rate of biochemical processes, and therefore an important parameter of methane fermentation is the degree of mixing of content of bioreactor. The fermentation sludge takes the form of agglomerates of floc. The outer part of the agglomerate is surrounded by acidogenic bacteria, sulphate-reducing bacteria and the homoacetogenic bacteria binding hydrogen with carbon dioxide and producing acetate. Under the outer layer are the homoacetogenic and methanogenic bacteria, which consume hydrogen and carbon dioxide. In the middle part dominate methanogenic bacteria (decaying acetates). A natural way of mixing in the digester occurs while increase the amount of gas bubbles and their release and the generation of convective heat currents by adding fresh, heated medium. However, natural mixing is not sufficient to achieve optimal performance of biogas production, therefore mechanical stirrers, pneumatic equipment, or hydraulic pumps are assembled in fermentors. Continually adding fresh material is the easiest way to mix the substrate. The hydraulic system (providing simultaneous transport of the slurry from the hydrolyser to the fermentor) is applied in the installation. Additionally, the motion of the suspension is obtained by the action of circulating pumps. The outlet pipes are placed at the bottom of the fermentor. The pumped slurry feeds the fermentor by free falling stream of liquid which breaks the scum formed during methane fermentation. This system worked well in practice. In order to confirm the effectiveness of the hydromixing of suspension in the fermentors were carried out also numerical simulations - Computational Fluid Dynamics (CFD). Currently, almost exclusively a computational simulation of unsteady, three-dimensional fluid flow uses CFD. Visualization of velocity vectors, streamlines and trajectories of particles helps the user understand the mixing process and identify problems (dead spaces, partial mixing, plug flow). With the discretization and numerical solution of partial differential equations describing the flow, it is possible to approximate determination of the velocity distribution, pressure, temperature and other parameters in the flow. The CFD is based on the Navier-Stokes equations. The developed k-ε turbulence model (solving additional transport equations for turbulence kinetic energy (k) and turbulence kinetic energy dissipation (ε)) is one of the models used in CFD. The substrates used in methane fermentation are non-newtonian fluids and their rheological properties significantly affect the nature of the flow, it is therefore necessary to develop a CFD model including information about the rheological properties of the fluid.

The biogas plant started its operation from the inoculation by bacterial flora (taken from the municipal biological wastewater treatment plant in Zamość) mixtures of substrates – maize silage and straw (residue from the corn cobs). Grass and grass silage are used for start of working the installation. Whey is used to pH adjustment. After stabilization of operating parameters, substrates was changed on the maize silage and manure with a high content of colza straw. In the future, will be tested materials, such as brewing, glycerol fraction waste, slurry, lucerne, millet, mangolds, and results will be used to optimize blend compositions.

2. METHOLOGY

The test sample of the feed material was dried in oven at 105 ºC and weighed every hour until a constant weight for determination of dry matter (DM). Subsequently, the sample was burned at 550 °C up to burnout of the organic part (only inorganic part remained) for organic dry matter (ODM). The determination of mass ratio of carbon to nitrogen in the biomass samples was carried out simultaneously. The measurements were performed at the Elementary Analyzer Flash 1112 NCS. The measurement of carbon and nitrogen content in the organic sample was conducted by the separation of nitrogen from organic matter in the gaseous form (N_2) and carbon in the form of CO_2. The preparation and measurements were performed on the elementary analyzer equipped with a chromatographic column separation of the mixture of obtained gases. The first step was to prepare the dry, homogeneous sample. Inside the elemental analyzer are two quartz reactors: the first - oxidation, the working temperature of about 1050 °C, designed for combustion of the sample and the total oxidation of received products and the second – filled with filings of copper at a temperature of 650 ºC, designed to reduce the nitrogen oxides to free atmospheric nitrogen N_2. The combustion gases (nitrogen and carbon dioxide) after adsorption of water in adsorbent are transported by a carrier gas (helium) to column chromatography for their separation, then to the detector in order to determine their concentration in the sample.

While the research on the experimental biogas plant every day were measured concentration of methane, carbon dioxide, hydrogen sulphide and hydrogen in biogas by using two different portable gas meters. Daily, biogas samples were collected in glass vessels and transported into the Institute for chromatography analysis.

Daily, samples of suspensions from biomass tank, hydrolyser, fermentor, and digestate reservoir and were measured by using spectrothotometer.

3. RESULTS OF RESEARCH FROM THE EXPERIMENTAL INSTALLATION FOR BIOGAS PRODUCTION IN SZEWNIA DOLNA

In the course of research in the plant, the optimal parameters of substrates were determined (fragmentation, supply frequency, frequency and intensity of hydromixing. The results for organic and inorganic dry matter and the ratio of carbon to nitrogen (C:N) – using the elemental analyzer were presented below table 1.

Table 1. The results of substrates analyses

Substrate	Dry matter %	Organic dry matter %	C:N
Manure on colza straw	21,7	62,6	23,99
Maize silage	36,6	63,4	38,52
Whey	6	80	-
Fresh grass	18	74	16
Grass silage	20	75	30

Daily samples of the liquid from the tank with biomass, hydrolyser, fermentor and digestate were collected to designate the pH and concentration of the following components: Chemical Oxygen Demand (COD), NH_3, NH_4^+, Cadmium, Iron, Potassium, Manganese, Copper, NO_3^-, NO_2, Volatile Fatty Acids (VFA), Sulphides, Total Nitrogen, and Total Phosphorus (P, PO_4^{3-}). In order to obtain quantitative composition of samples, spectrophotometric analysis were carried out by using spectrophotometer PF-12 and reagents NANOCOLOR. Spectrophotometer also functions as a photometer (making photometric measurements for a specific wavelength of light). The sample of processing water also were collected, in order to determine its chemical composition. The measurement results from spectrophotometric analysis for COD was shown at below Fig. 1.

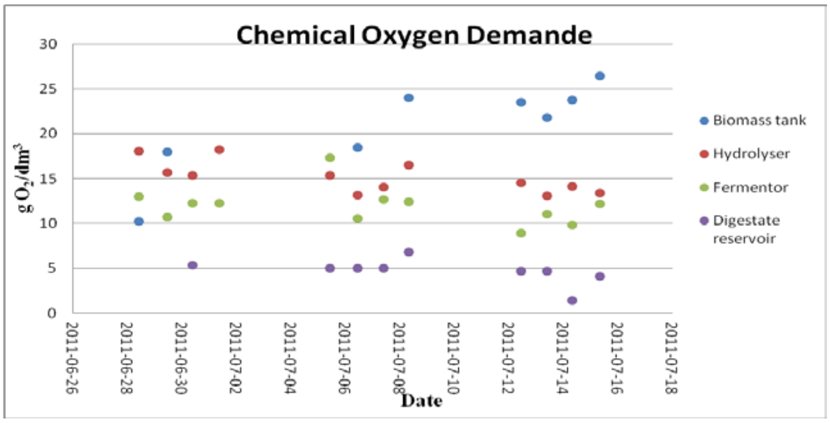

Fig. 1. Graph of change chemical oxygen demand depending on the time

Using the portable gas meters were measured daily concentrations of CH_4, CO_2, O_2, H_2S, H_2 in the received biogas. In the Institute of Nuclear Chemistry and Technology, the composition of biogas samples were also measured using chromatographic analysis. The installation was equipped with temperature gauge (in fermentor and hydrolyser), and pressure gauge (measurement of biogas pressure in the digester). The resulting concentration of CH_4 in the fermentor using by portable gas meters was 58% -69%, it was confirmed by chromatographic analysis. The result is the chromatogram whereby based on the calibration curve, the percentage of carbon and nitrogen in the burned organic sample is determined. The results are slightly better than in the literature data [8, 9].

The biogas contained H_2S (540-1300 ppm). The results suggest that in the industrial installation any increase of hydrogen sulphide can be adjusted by the addition into the fermentor small amounts of iron salts. The amount of hydrogen does not exceed 1.5%.

4. CONCLUSION

The hydromixing of suspension in hydrolyser and fermentor, which was applied and tested in the experimental conditions in the biogas plant in Szewnia Dolna, provides the mixing in the entire volume of the installation.

The analyzes of chemical composition of the substrates show that caution should be exercised when composing the charge of hydrolyser in order to avoid a raw material, which may have elements and chemical compounds that are inhibitors of fermentation. The origin, history and the conditions of substrates storage should be monitored.

According to literature data [8,9], photometric analysis, showed a high decrease of COD in the liquid digestate in comparison with the liquid from hydrolyser, which proves the correct course of the anaerobic digestion.

Photometric analysis revealed the presence of acetic acid in liquid digestate, which has not been sufficiently decomposed in the methanogenesis. It is recommended to extend the residence time by recirculation of the liquid in the fermentor or use the next stage of fermentation in the second fermentor, which will increase the yield of biogas in the process.

The measurements of biogas pressure and volume of biogas space allow to estimate the biogas yield of about 0,35-0,46 m^3/kg of dry matter, although the realization of process at a temperature below 30ºC (36 ºC as recommended in the literature [4,5]). The presented results in this paper will be used in the future to create engineering design assumptions for biogas plant.

The research conducted by the Institute of Nuclear Chemistry and Technology in Warsaw and SEP Zamość will allow for the introduction of Polish technological solutions in the biogas industry. The Institute of Nuclear Chemistry and Technology prepares engineering project, which are part of the research phase – "System requirements of agricultural biogas plants and micro biogas plants" within the framework of the strategic project – "Advanced technologies for energy".

REFERENCES

1. BASTONE D., KARAKSHEV D., Influence of environmental conditions on methanogenic compositions in anaerobic biogas reactor, *Appl. Envir. Microbiology*, 2005, 71, p. 331–338.
2. SZEWCZYK K. *Analysis of processing operation of obtaining biogas from vegetable waste*, Warsaw University of Technology, 2010.
3. WEILAND P., Biogas production: current state and perspectives, *Appl. Microbiol. Biotechnol.*, 2010, 85, p. 849–860.
4. LEVEN I., ERRIKSON A.R.B., Effect of process temperature on bacterial and archael communities in two methanogenic bioreactors treating organic household waste, *FEMS Microbiol. Ecol.*, 2007, 59, p. 683–693.
5. WEILAND P., Biomass digestion in agriculture: a successful pathway for the energy production and waste treatment in Germany, *Eng. Life Sci.*, 2006, 6, p. 302–309.
6. WEILAND P. *Biogas, production, utilization,* Institut fur Energetik und Umwelt, 2005.

7. CHRZANOWSKI K., KRYŁOWICZ A., USIDUS J. *The method and system for producing methane and electricity and heat*, No. 197595.
8. NiZAMI ABDUL-SATTAR, MURPHY, Jerry D. Optimizing the opertaion of a two-stage anaerobic digestion systems digesting grass silage, *Environmental Science & Technology*, 2011, 45, p. 7561–7569.
9. VOGEL, Telse; AHLHAUS, Matthias; BARZ. Mirko; Optimization of biogas production from grass by dry-wet fermentation, *Engineering for rural development*, Jelgava, 28.-29.05.2009

CYSENI 2012, May 24–25, Kaunas, Lithuania
ISSN 1822-7554, www.cyseni.com

INVESTIGATION OF WIND POWER PLANT GENERATION EFFICIENCY

D. Sankauskas, V. Katinas
Lithuanian Energy Institute
Breslaujos str. 3, LT-44403 Kaunas – Lithuania
Phone +370 616 25100
Email: d.sankauskas@mail.lei.lt

ABSTRACT

Analysis of output of wind power plants and stand-alone wind turbines (WT) installed in the coastal region of Lithuania and in continental part was done. It was established that factor Cp of WT was about 0.26, i.e. WT used 26 % of all nominal installed capacity per year. The capacity factor mainly depends on climate conditions of the WT site. Usually small WT are installed near buildings, where wind flow is interrupted by the obstacles and roughness of the terrain. The investigation of climate conditions of WT sites in Lithuania apparently showed that the selection of sites for installation of WT must be done more carefully. According to investigation of climate conditions, it is possible to use about 30 % of nominal capacity of WT per year in the coastal region of Lithuania, but more efforts must be put for the selection of WT installation sites. Also the technical-economical evaluation of wind power plants is performed for different tower heights. Payback period calculations are presented for different wind speeds and discount rates. Feasibility of wind power plant development in Lithuania is analyzed.

Keywords: Wind power plants, wind energy

1. INTRODUCTION

Due to decreasing space for wind power plant (WPP) construction in the seashore region, construction of wind power plants is started in the mainland part of Lithuania. With the increasing number of wind power plants, it is easier to compare them with each other. However, the payback time of a wind power plant must be evaluated before construction of a wind power plant in any place. This depends not just on wind speed in the selected territory, but also, on land rent conditions, distance to the power grid and the need of an additional infrastructure, etc.

In case of economical wind power plant evaluation, it is also very important to consider the fact that an average annual wind speed in different years can vary up to 30 % [4, 5].

2. ROTOR EFFICIENCY

The kinetic energy (E) of air of mass (m) flowing at speed (V) can be expressed as

$$E = \frac{m \cdot V^2}{2} \tag{1}$$

Since the density is the mass of unit volume, i.e. the volume can be defined as the product of the cross-sectional area perpendicular to the wind (A) and the horizontal length of incoming wind (L) which can be expressed as $L = V \cdot t$. Then wind kinetic energy can be described as

$$E = \frac{1}{2}\rho A t V^3. \tag{2}$$

The power is the time rate of energy, therefore the rate of kinetic energy can be expressed as

$$E = \frac{1}{2}\rho A V^3. \tag{3}$$

Note that a mass of air passing through the rotor per unit time is *m* while the rate of momentum change is $\dot{m}(V_1 - V_2)$. This momentum change creates the resulting thrust of the wind turbine. Fig. 1 shows the schematic diagram of the wind turbine stream tube [2]. In this Figure, V_1 and V_2 represent upwind and downwind speeds, respectively at a considerable distance from the rotor.

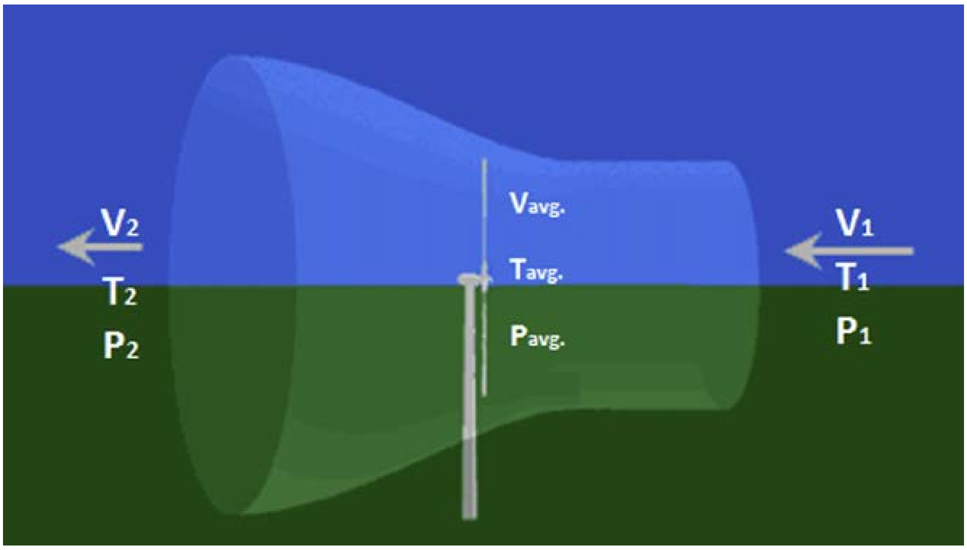

Fig. 1. Diagram of wind turbine stream tube [2]

Therefore, the rate of extracted kinetic energy can be expressed as follows:

$$P = \dot{m}(V_1 - V_2)V_{avg}\,. \tag{4}$$

While the rate of change in kinetic energy is

$$E_p = \frac{1}{2}\dot{m}(V_1^2 - V_2^2) = W_{out}\,. \tag{5}$$

Eqs. (4) and (5) should be equal, so the retardation of the wind before and after the rotor is equal, therefore

$$V_1 - V_{avg} = V_{avg} - V_2\,. \tag{6}$$

Assuming that the direction of the wind across the rotor is axial symmetric and the velocity is uniform throughout the swept area *A*, the power extracted by the rotor is:

$$P = \rho A V_{avg}(V_1 - V_2)V_{avg} = \rho A(V_1 - V_2)V_{avg}^2\,. \tag{7}$$

By simplifying the equation above it becomes:

$$P = \frac{\rho A V_1^3}{4}(\alpha + 1)(1 - \alpha^2)\,, \tag{8}$$

where $\alpha = \frac{V_2}{V_1}$ and $\frac{(\alpha+1)(1-\alpha^2)}{2}$ are called "power coefficient". Differentiating Eq. (8) and equating it to zero, shows that the maximum value of α cannot exceed more than and the power will be maximum at this value of α, i.e. when the downwind speed is one third the upwind speed.

Maximum power coefficient cannot be greater than 0.593. Therefore, maximum obtainable wind power is 59.3% of the total available wind power. The extracted energy may well be put to useful work but, some may be spilled back into the wind as turbulence and thereby dissipated as heat.

Comparison among wind energy and variation of the wind power plant capacity with changing wind speed is presented in the Fig. 2. With wind speed exceeding 11 m/s [3], wind power plant is operating at its nominal capacity, and its capacity is not increasing with the increase of wind speed. When wind speed exceeds 25 m/s wind power plant is stopped in order not to damage its elements.

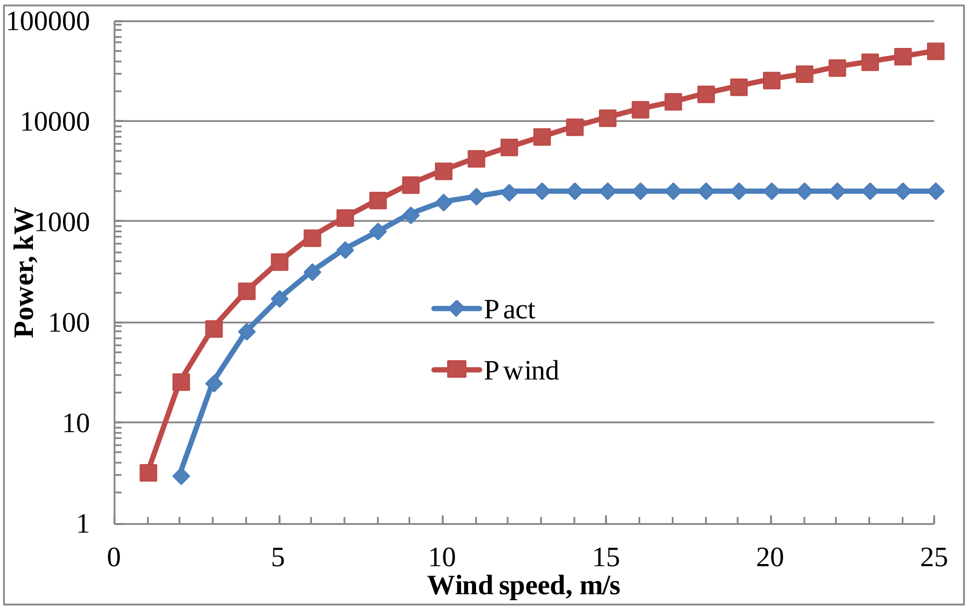

Fig. 2. Comparison between the actual output power of the wind turbine Enercon E-82 (2 MW) and the wind power

3. ECONOMICAL CALCULATIONS OF WIND POWER

Output of wind power plants depends on wind conditions of the territory. As WPP technologies are expensive and investments to WPP constructions are large, economical viability of the project must be estimated before planning starts. For this purpose, precise measurements of wind energetic parameters must be made in the selected territory, wind energy resources must be estimated and WPPs with adequate technical characteristics must be selected. Only when wind speed measurements have been made and it is ensured that wind conditions are good enough, investment requirements and payback time of the project can be evaluated.

WPP price usually constitutes a major part of all required investments (Table 1)

Table 1. Distribution of WPP construction costs [6]

1	Wind power plant	75 %
2	Preparation of the foundation	5 %
3	Grid connection and control costs	15 %
4	Land price	2 %
5	Access roads	1 %
6	Other expenditures (project, investigations and consulting)	2 %
	Total:	**100 %**

Expenditures for wind speed measurements, consulting, geological investigations, WPP planning constitute a small share of the total project. It must be noted that precise wind speed measurements and qualified analysis are one of the most important conditions for successful project implementation, as even small inaccuracies of measurement data can cause large WPP energy generation losses in the future.

It is important to consider project's is technical feasibility, i.e., if grid connection is possible, and soil is suitable for WPP construction, etc. All these factors can be related to additional investments and even project termination.

Most important parameters causing WPP payback time is an average wind speed in the hub-height and feed-in tariff.

Payback time of the wind power plant (Enercon) was calculated using feed-in tariff of 30 LTL ct/kWh and different tower height. The price of the wind power plant increases with the increasing tower height, but wind speed is higher in higher elevations.

Calculations were performed using discount rates DR=5% and DR=7%.

Results show that payback time with tower height of 78 m and average annual wind speed of 7 m/s, reaches 12 and 10 years (DR is equal to, respectively, 7% and 5%). When average wind speed in the height of 78 m is below 6,5 m/s, project payback time exceeds 15 years (Fig. 3, 4).

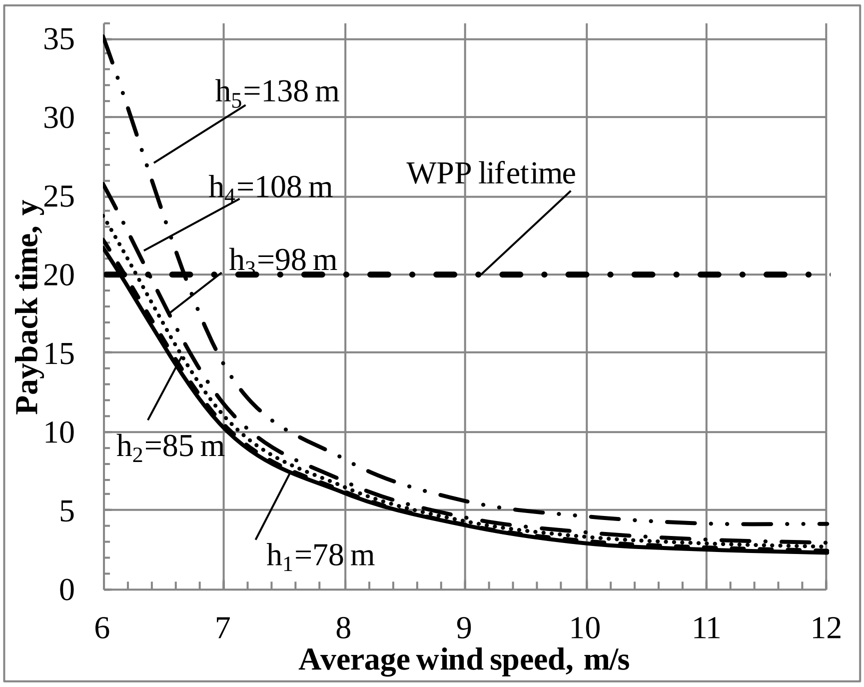

Fig. 3. Wind power plant (Enercon) payback time with DR 5%

Payback time of the 138 m height tower is radically different from others due to much higher construction costs.

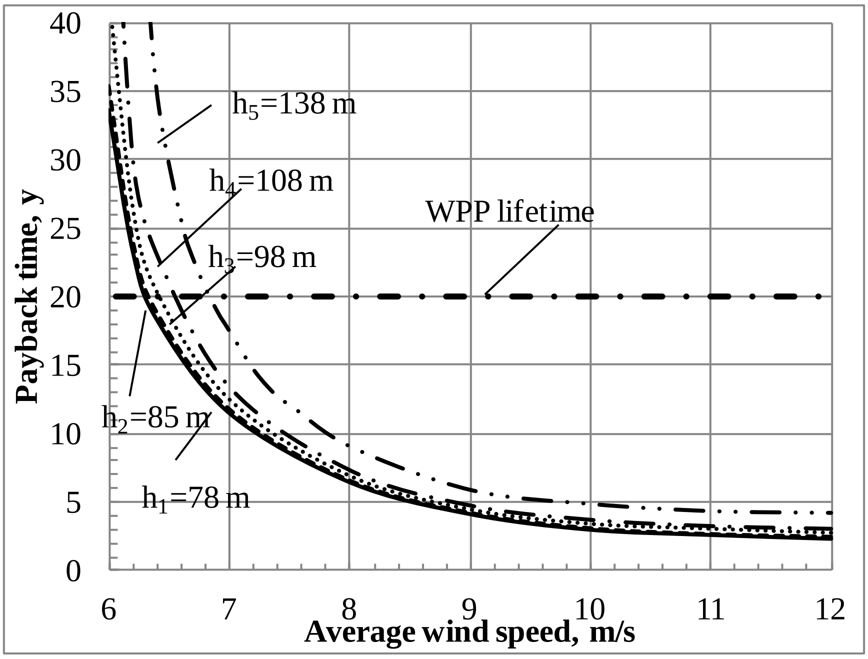

Fig. 4. Wind power plant payback period with DR 7%

4. ANALYSIS OF THE CAPACITY FACTOR

Capacity factor of wind power plants is highest in winter months, and in summer months it is almost 2 times lower than in winter (Fig. 5). Average annual capacity factor in Lithuania varies from 0.23 to 0.36. Litgrid data base [1]. This depends on the place where the wind power plant is constructed. Also, depending on the year, capacity factor of the same wind power plan can vary up 30 % [4, 5].

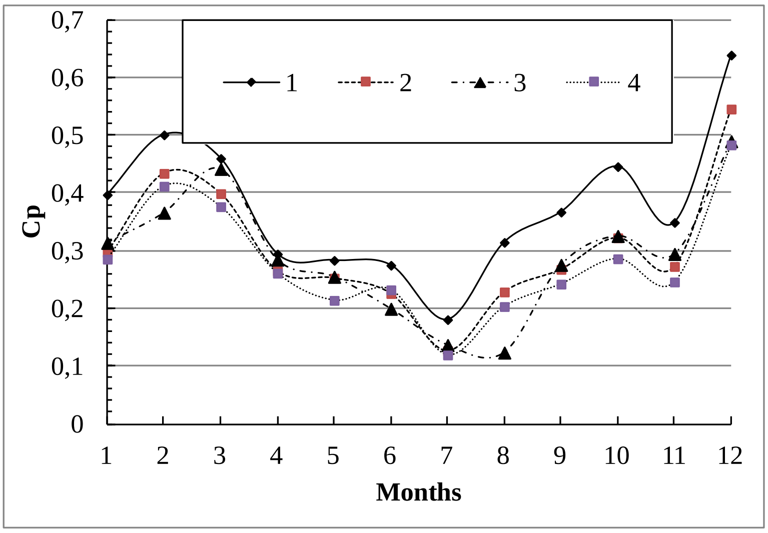

Fig. 5. Variation of wind power plant capacity factor, 2011. 1 – Mockių WPP; 2 – Kreivėnų WPP; 3 – Akmenėlių WPP; 4 – Anužių WPP

Fig. 5 shows some of the best operating wind power plants. We can see that places suitable for wind power plants can be found not only in the seashore region (line 3 – Akmenėlių WPP). Which is about 170 km from the Baltic Sea. The capacity factor of this WPP was 0.29 in 2011.

Annual capacity factor of the most efficient power plant (line 1 – Mockių WPP) in 2011 was 0.38, and it exceeded 0.5 – 0.6 in some months. This WPP is erected on the coast of Kuršių Marių (Curonian Lagoon).

Kreivėnai and Anužiai wind power plants are not far from each other (20 km distance), and this is evident in the capacity factor graph. Capacity factor of both these power plants is approximately 0.28.

5. CONCLUSIONS

With a discount rate of 7%, payback time of a wind power plant (Enercon) exceeds 12 years, when an average wind speed at the hub-height is above 7 m/s, and electricity feed-in tariff is 30 LTL ct/kWh.

If the average wind speed in the selected territory is below 6 m/s, such project does not pay back during its lifetime (20–25 years).

Capacity factor variation shows that there are suitable territories for wind power plant construction out of the seashore zone. More measurements in the mainland part of Lithuania must be made for this purpose.

REFERENCES

1. http://www.litgrid.eu/index.php?1973822023.
2. Redha A. M. et al. Thermodynamic performance assessment of wind energy systems: An application. Energy 36. 2011, p. 4002–4010.
3. Product overview. http://www.enercon.de/p/downloads/EN_Productoverview_0710.pdf.
4. Boccard N. Capacity factor of wind power realized values vs. estimates. Energy policy 37. 2009, p. 2679–2688.
5. Yang M. et. al. Wind power generation in China: Understanding the mismatch between capacity and generation. Renewable Energy 41. 2012. 145-151 p.
6. The economics of wind energy http://www.ewea.org/fileadmin/ewea_documents/documents/00_POLICY_document/Economics_of_Wind_Energy__March_2009_.pdf.

CYSENI 2012, May 24–25, Kaunas, Lithuania
ISSN 1822-7554, www.cyseni.com

MODELING OF LARGE ELECTRICAL POWER SYSTEM DEVELOPMENT UNDER ENERGY MARKET CONDITIONS

O. Kochukov, A. Mutule
Institute of Physical Energetics
LV-1006 – Latvia
Phone +37167558659
Email: olegsk@edi.lv

ABSTRACT

Aim of this paper is to incorporate energy market principles in large power system modeling process. The paper describes application of zonal (regional) energy price formation algorithms and interaction of power systems on energy import/export issues. The developed methodology is implemented in LDM-TG (Latvian Dynamic Model – Transmission and Generation) information technology, which was created and is being improved by the Institute of Physical Energetics, Latvia. The information technology provides the opportunity to perform dynamic optimization of system development together with operational state calculations. The authors discuss the possibilities to optimize long-term sustainable development of large electric power systems under energy market conditions.

Keywords - Large power systems, energy market, sustainable development

1. INTRODUCTION

Over the past two decades a number of countries have decided to take the path of market liberalization. Despite slight differences, the motivation for liberalization of the power sectors world wide has shared common ideological and political reasons. In particular, a strong belief that the success of liberalization in other industries can be duplicated in the power sector and a ‘need’ for splitting the vertically integrated monopoly structures that traditionally have managed generation, transport and distribution. The introduction of competition has been justified by the perceived benefits of introducing market forces in an industry previously viewed as a natural monopoly with substantial vertical economies. The breach of the natural monopoly character has been possible, in turn, due to changes in generation technologies and improvements in transmission. Therefore the motivation behind electricity liberalization is, in the long run, to promote efficiency gains, to stimulate technical innovation and to lead to efficient investment.

Today’s electricity market can be based on two main pricing principles – nodal and zonal pricing [1].

Nodal price is the sum of generation marginal cost, transmission congestion cost and cost of marginal losses, and can be different for different buses (or nodes), even within a local area. Nodal prices are the ideal reference because the electricity value is based on where it is generated and delivered. However, they generally lead to higher transaction costs and greater complexity of the pricing mechanism.

On the other hand, the zonal price may be different for various zones or areas, but is the same within a zone, i.e. a portion of the grid within which congestion is expected to occur infrequently or has relatively low congestion-management costs.

The most effective way of forecasting network’s behavior according to authors opinion is computer modelling. This paper aims to implement zonal pricing principles in modelling of large power system development process.

2. POWER SYSTEM DEVELOPMENT OPTIMIZATION PRINCIPLES

2.1. Criteria for decision making

The long-term economic design of the grid means to balance between investments and the cost of maintenance, operation and supply interruptions, taking into account the environmental criteria and other limitations. Flexible solutions which take into account future uncertainties, e.g. generation limitations, uncertain load development, technical development, etc., should be selected. In this evaluation socioeconomics as well as market functioning shall be included.

In tasks on technical systems development, variables are - development actions, but technical criteria are - limitations, for instance links maximal capacity, etc. Usually, for development optimization tasks following multiple criteria are defined: capital investments on one side of scales required for actions realization, while on the opposite side there are gained benefits (operation and maintenance costs reduction, overload reduction, new consumer’s connection, power supply security improvement etc.).

Part of this gained benefit has monetary value but there are such benefits which can hardly be evaluated monetary. Still to initiate optimization is required. The economic estimation of development actions is a thorny task. The development actions must be estimated applying the method which is named as economic life cycle concept. Capital contribution efficiency is estimated observing operation, maintenance, and technical costs, caused by emergency situations/faults and others. In development action estimation process, calculation of technical economic criterion cannot be based on one-year figures. The criterion must reflect the whole economic life-cycle of the object.

The development optimization is hampered by the fact that it occurs under information uncertainty conditions. It should be taken into consideration in the decision-making process, and the appropriate methods have to be applied [2].

Economical criteria of optimization process includes: incomes for sold energy, investments, maintenance costs, losses costs, energy production costs, unserved energy costs, ecological penalties.

Technical criteria depends on the specific System. In dynamic models for development optimization, limitations by technical parameters are observed not with strict constraint values, but with so-called fuzzy constraint method. Applying fuzzy constraint method the objective function is supplemented by additional criteria (penalty functions). Penalty function value within the limits is not high, but as the distances expand, it increases considerably (Fig. 1).

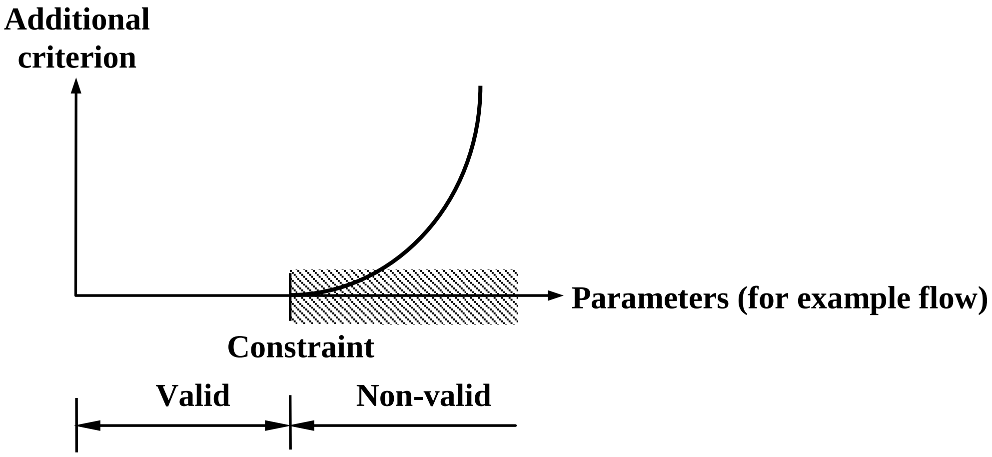

Fig. 1. Fuzzy constraint method

Above mentioned criteria are considered in objective function and used for power system (PS) development plan selection. The major criterion of large technical systems (LTSs) development process is management optimization target function which shall display and integrate technical, economical, power supply reliability, ecological etc. parameters depending on specific technical system. Let us designate this target function as system development process *g* quality criterion and mark with *F(T, g)*. Target function is calculated by formula:

$$F(T,g)=\sum_{t=1}^{T}F(e(t)), \tag{1}$$

where t – development step serial number;
T – number of development steps in estimation period;
$F(e(t))$ – system quality criterion in development step t and state $e(t)$;
g – development plan (process) $e(1), e(2), \dots, e(t), \dots, e(T)$.

For the estimation period of PS sustainable development optimization, T should be assumed longer than the economic life cycle period. The relevant information for this period is uncertain; therefore, the decisions made have to be specified regularly. In Fig. 2 is presented principal scheme of decision making method under uncertainty.

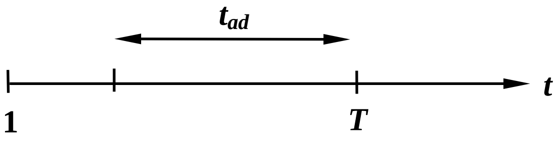

Fig. 2. Estimation (T) and adaptation (t_{ad}) periods

2.2. LDM-TG information technology

LDM-TG software developedment started in last century and still continues. It is being developed by Laboratory of Power System Mathematical Modeling for calculation of optimal sustainable development of power systems [2].

Elaborating given information technology, the key target was to create new transmission network and generation system development management concept and methods to validate the made decisions when simulating situations and their respective probable consequences thus forwarding background for optimal development plan selection. In order to ensure transmission network and generation sustainability, it is necessary to precisely analyze consequences of the made decision while developing project design of electric power system. Therefore, in design of this information technology dynamic methods are utilized, enabling one to observe development process and far perspective, if required, for the period up to 5 development steps – 20-30 years.

Important concept related to system economic analysis complex is possible (alternative) actions. Generally, *development action* (D-action) reflects activity - new system object construction, as well as existing objects extension, reconstruction and modernization. D-action is assigned along with capital investments and relevant network elements (elements which are included or excluded from the estimation calculation scheme as a result of the D-action). The D-actions are assigned by user according to the specific task, experience etc [2].

Technical system *developement state* (D-state) in optimization task is set of D-actions and is specified by system graph, its element parameters and other technical, economic, ecological etc. parameters. D-state in particular moment *t* may be defined as realized D-actions within the period 0..*t*:

$$e(t)=e(0)\cup\{x(1)\}\cup\{x(2)\}\ldots\cup\{x(t)\}, \qquad (2)$$

where $\{x(t)\}$ - all step 0..*t* realized D-action set.

D-state can be classified as technically valid or technically non-valid - if at least one technical limit is not satisfied.

Power system development step (D-step) is time period when none of D-actions is realized - system graph and its parameters are not changed. In D-step period it is assumed that annual consumption of the first year of D-step, twenty four hours, seasonal and monthly consumption is preserved for the period of all further years. Performing mathematical calculations, we assume that all D-step period realized D-actions are realized simultaneously, going on from D-step *t - 1* to D-step *t*.

In estimation period which is divided into T D-steps, may be various D-states *e (t)*. A sequence of D-states *e (t)*, if *t = 1, 2, ..., t, ..., T*, is called large technical system development plan (D-plan), which will be marked with *g (k)*. Graphical model of D-plan is guided path graph (see Fig. 3).

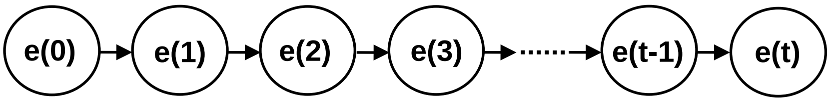

Fig. 3. Large technical system development plan

The detailed description of D-plan calculation algorithm is given in flowchart of Fig. 4.

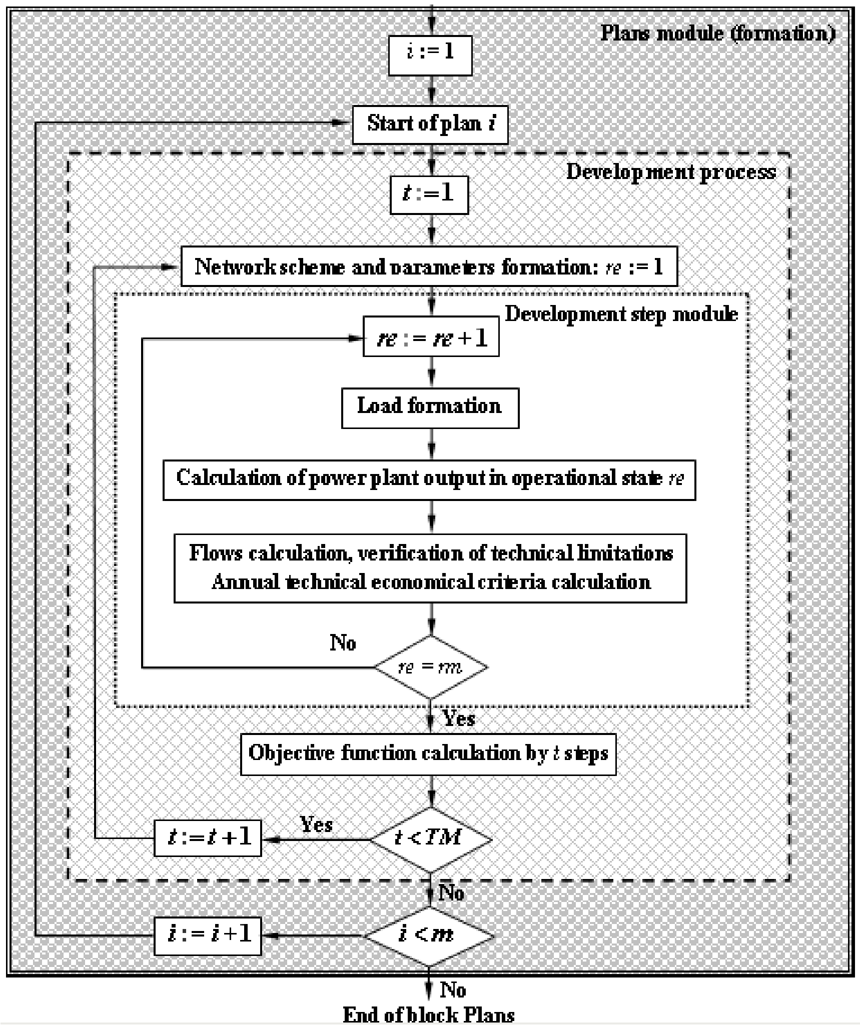

Fig. 4. Flowchart of module *Plan Calculation*

re – Index of current operational state; *rm* - Number of operation states;
t – Index of current development step; *TM* - Number of development steps;
i – Index (ordinal number) of development plan; *m* - Number of development plans

Module *D-Plan Calculation* has tree loops: 1) external on D-plans; 2) D-step, were D-Step $e(t)$ is formed; 3) central on operation state re, consist of calculation of load, power plant output and annual costs.

It is necessery to mention that block *Network scheme and parameter formation* (Fig. 4) includes *generator ranking* block that will be used further in this paper.

3. INCORPORATION OF ENERGY MARKET PRINCIPLES IN LARGE POWER SYSTEM MODELING PROCESS

3.1. Power plant output calculation

Algorithm of power plant output calculation deserves special attention in frame of given topic. Flowchart of Fig. 5 gives an idea of ranking and loading of generators in energy market conditions.

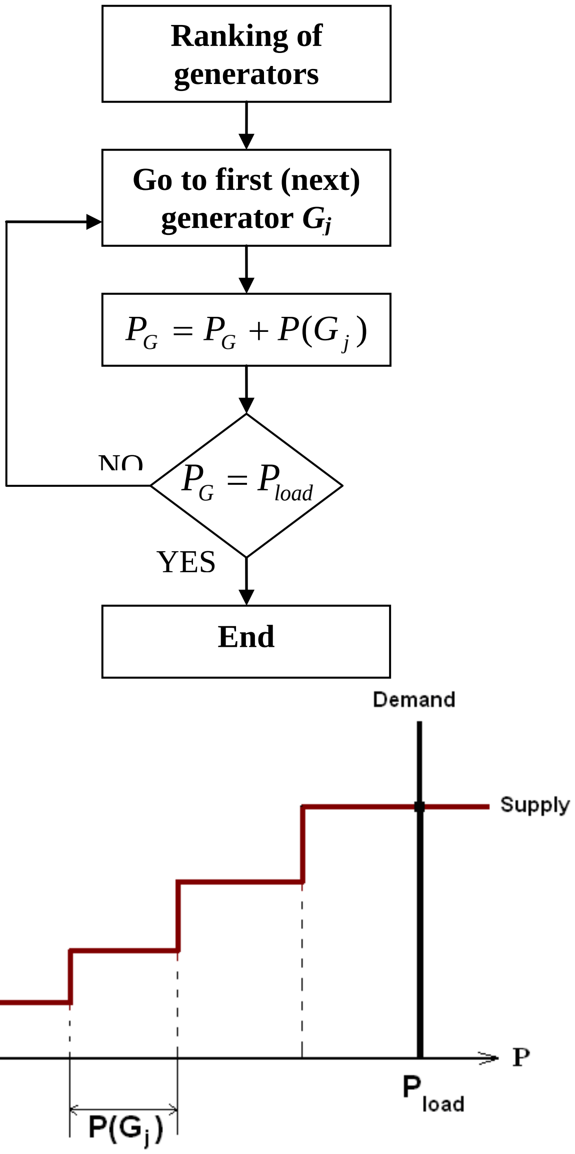

Fig. 5. Algorithm of power plant output calculation and principles of power plant ranking

P_G – generation capacity of whole system; P_{load} – load of whole system;
$P(G_j)$ – capacity of power plant *i*; *C* - Electricity price.

The first step of the algorithm is forming of input data, which include calculated system load and ranking of power plants (or generators). Performing ranking, all generators of the system are sorted by generation price, so that cheapest go first. Usually generation price is generator's variable production costs, however it can include also other components. The second step is generator one by one loading (increasing variable P_G) and checking the power balance of the whole system. If generation capacity is equal to demand capacity, loading process is over, otherwise – the next generator is loaded and process repeats.

Such approach enables to achieve minimal production costs for whole system, loading the cheapest generators. However, there are also disadvantages of the algorithm. For example, distance between generator and consumer is not considered, therefore it can happen that losses costs will exceed difference in generation costs.

3.2. Incorporation of zonal pricing principles in modelling algorithms

Another major point of implementation energy market in power system development modelling is calculation of zonal electricity prices. In earlier versions of LDM-TG there was no option to split model to zones by price, therefore it was impossible to model energy market. The newest test version has possibility to manage up to 10 zones. At data input step the only input parametr for zone is *zone name*. After zones are formed they can be used as one of the network node's parameters (see Fig. 6).

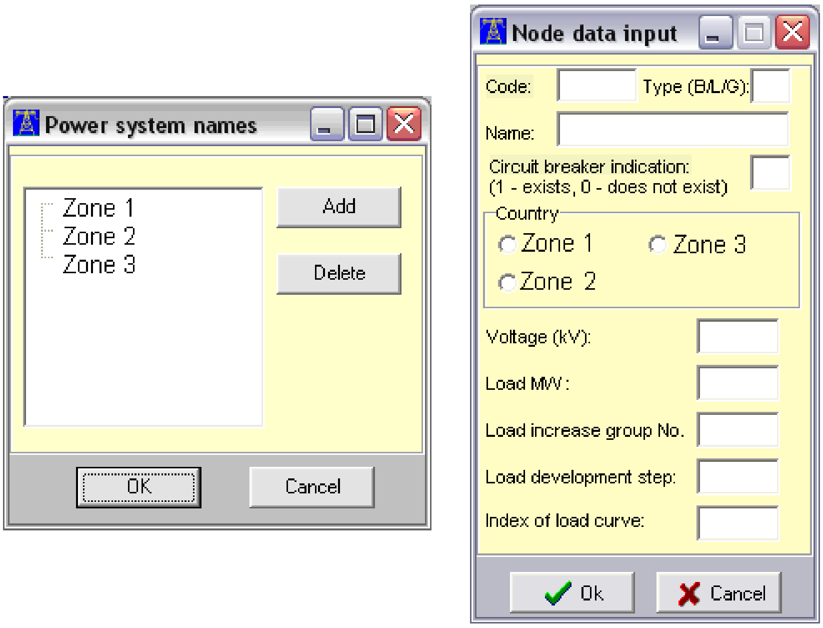

Fig. 6. Zone formation and node data input in LDM-TG environment

In developed algorithm it is assumed that area electricity price is price of the last (most expensive) generator which is needed in order to cover the system load. Therefore, different operational states of the power system (e.g. day, night, spring, summer, winter etc.) can lead to different prices of electricity in the same area due to changing load (Fig. 7).

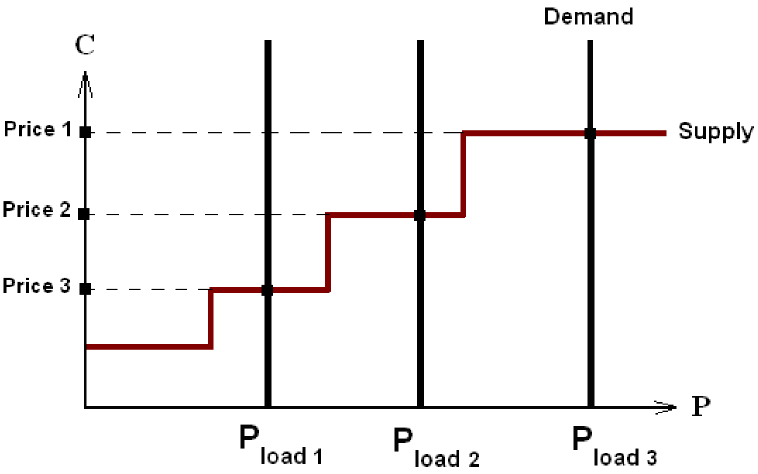

Fig. 7. Relation of zonal electricity price and load

Operational states influence not only load, but also generation of the particular system. For example, hydrological situation in spring is the best in terms of hydro power plant generation capabilities, therefore zonal electricity price in that time would decrease, especially in regions with high level of hydro power plant integration [3]. This is modeled with additional parameter of price for each operational state.

LDM-TG zonal electricity price formation test algorithm itself is illustrated in Fig. 8.

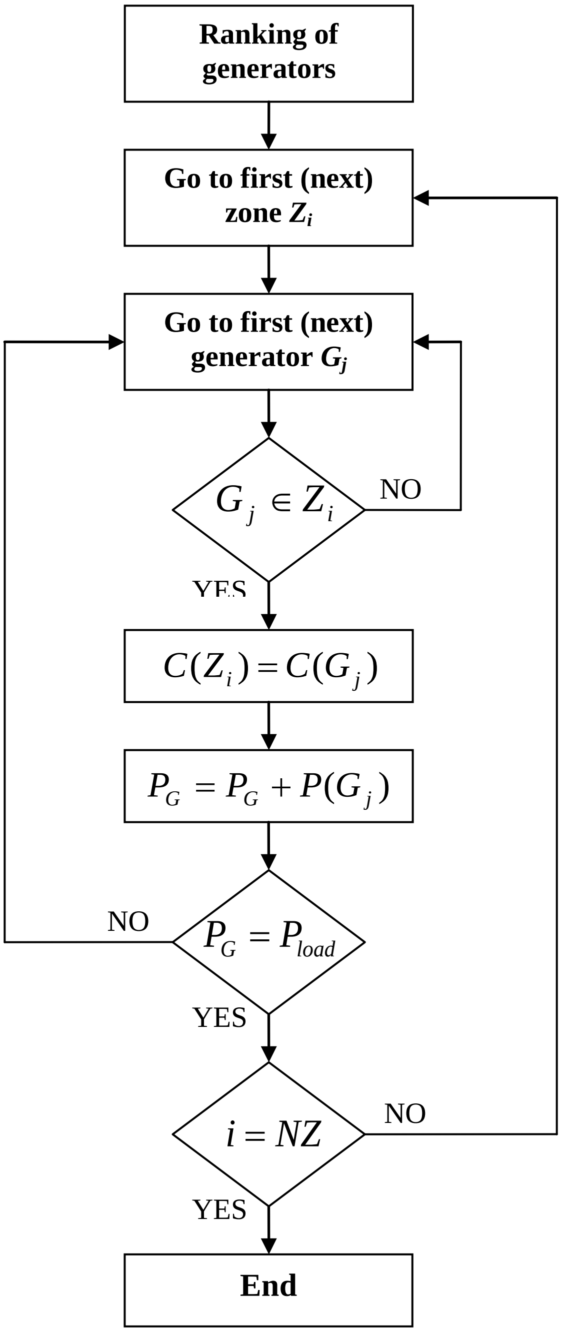

Fig. 8. Test algorithm of zonal electricity prices calculation in LDM-TG information technology Z_i –zone number i; G_j –generator number j; C – electricity price; P_G – generation capacity of whole system; P_{load} – load of whole system; $P(G_j)$ – capacity of generator number j; NZ – total number of zones.

The given algorithm has two loops – on zones and power plants (internal). Similar with algorithm of power plant output calculation, system load and ranking of power plants (or generators) are entered as input data. On the second step algorithm is going to first zone and checks all its power plants one by one. If power plant belongs to the current zone, the price of the power plant becomes price of the current zone. Since power plants are sorted by generation costs, every next generator has higher costs and costs of the last one will be maximal. At the same at every step algorithm is checking if current calculated generation capacity is enough to cover the load of current zone. If no, next generator is checked, otherwise – algorithm goes to next zone or ends process if all zones are checked.

Formation of multiple zones with their generation costs has direct impact on results of network development optimization by changing economic criteria. The main parameter which is changed is electricity price (price what is be paid by consumer). In given information technology it is assumed that electricity price is equal to generation costs of zone. Therefore profit of the power plant is difference between electricity price and generation costs. According to this statement it can be concluded that some power plants working under market conditions can operate with minimal profit or without profit at all, as usually they are bidding only with variable production costs.

4. CONCLUSIONS

Liberalization of energy market in the world is irreversible process. In order to follow the innovations and better understand network current and future behavior it is necessary to have strong instrument for modelling. LDM-TG is developing for more than 20 years and now enters the new step – energy market modelling.

Good decision making policy have to be economically justified and sustainable due to huge investments and plenty of related factors. This paper explains the power system development optimization principles that remain valid also for energy market. However, particular changes in methodology of some block calculation have to be done.

The paper explains the methodology forming electric power system zones, algorithms of power plant output calculation and zonal electricity price formation together with its influence on economic calculations.

These algorithms are in test mode at the moment. It is planned to test them by modelling small imaginary networks, as well as big existing systems, such as ENSTO-E (United power system of Europe, Scandinavia and United Kingdom).

REFERENCES

1. RAFAL WERON. *Modeling and Forecasting, Electricity Loads and Prices*. Chichester: John Wiley & Sons Ltd., 2006, p. 20–27.
2. MUTULE, A., O. KOCHUKOV, KRISHANS, Z.Application of Risk Assessment Method for Power System Interconnection Cost and Benefit Evaluation. Turkey: PMAPS, 2012.
3. KRISHANS, Z.; MUTULE, A.; MERKURIEV, Y.; OLEINIKOVA, I. *Dynamic Management of Sustainable Development: Methods for Large Technical Systems.* London: Springer, 2011. 5-6, 52–60 p.
4. Journal *Enerģija un Pasaule*. Riga: LZA, 2012, Nr. 1 – p. 40–22.

CYSENI 2012, May 24–25, Kaunas, Lithuania
ISSN 1822-7554, www.cyseni.com

FEASIBILITY STUDY OF OVERHEAD LINES REPLACEMENT WITH UNDERGROUND CABLE LINES IN THE MV DISTRIBUTION NETWORK

I. Priedite-Razgale
Institute of Physical Energetics
Aizkraukles 21, Riga, LV-1006 – Latvia
Phone +371 26071681
Email: prieditei@inbox.lv

A. Lvovs, J. Rozenkrons
RTU Faculty of Power and Electrical engineering
Kronvalda 1, Riga, LV-1010 – Latvia
Phone: +371 25970020, +371 29618349
Email: aleksandrs.lvovs@inbox.lv; jroz@eef.rtu.lv

ABSTRACT

In the paper the latest statistics of middle voltage network power line failures and causes of these failures are analyzed. The paper is based on the analysis of the Latvian statistical data, but these statistical data are also compared with other countries' statistics, which is quite similar in most countries. It means that information included in the paper can be widely used in any middle voltage electricity distribution network reliability calculations and analysis all over the world.

In the paper possibilities to reduce number of failures using different methods are presented and also compared quality of energy distributed through the network for two cases – when network is formed by overhead or cable lines is also compared. This paper presents possibility to improve reliability of distribution network using underground cables instead of OHL and also demonstrates that the perception that cable lines are more expensive than overhead lines is wrong. Conclusions made on the basis of OHL and cable line fault statistics analysis are of high importance for planning of reliability centred maintenance.

Keywords: power distribution faults, power system economics, power distribution lines, power system reliability, costs

1. INTRODUCTION

Growing interest to small scale renewable energy sources during recent years increased the role of distribution network as a critical infrastructure for electrical energy usage in long-term perspective. This makes reliability level of distribution network even more important and this promotes bigger money inflow for reliability improvement of distribution system.

Actuality of the performed work is based on the fact that Latvian DSO (Distribution System Operator) “Sadales tikls” is planning to replace 6000km of medium voltage OHL placed in forest territory by underground cable lines in approx.30 years, replacing in average 200km of lines annually. Taking into account the scale of so called “cable implementation program” and tendency to require higher reliability values of power supply, burying cables instead of OHL should be evaluated.

According to statistics [1–3], more than 80% of all power supply interruptions occur because of outages and faults at the level of distribution network. Due to this, bigger attention should be paid to this part of electrical networks.

There is a perception that the overhead power lines are much cheaper than cable lines. However, the feasibility assessment indicates that this perception is wrong because it does not take into account that the cable lines have lower maintenance costs and less frequent failure (in spite of the high construction prices).

Decision of feasibility study performance only for medium voltage distribution network (not including low voltage network) was made because of bigger potential for total economical savings of society (utility costs of reliability and customer costs of reliability). Customer costs of reliability that occur in case of power supply interruption are potentially bigger in case if fault occurs in medium voltage power line comparing to fault in low voltage line.

2. COMPARING QUALITY OF ENERGY

Power quality is becoming increasingly important because of development of renewable energy technology. Power quality affects by many factors, including type of power line. For example, in cable lines there are no temporary interruptions but in OHL temporary interruptions are frequent occurrence. Effects of temporary interruptions are voltage dips. Voltage dip is temporary reduction of the r.m.s. (effective) voltage at a point in the electrical supply system below a specified start threshold. Such voltage dips occur due to falling trees (because of storm or trees age), etc. Voltage dip can be characterized by four parameters- voltage dip start threshold; voltage dip end threshold, voltage dip duration and voltage dip residual voltage.

Voltage dip start threshold is r.m.s. value of the voltage on an electricity supply system specified for the purpose of defining the start of a voltage dip. Voltage dip end threshold is r.m.s. value of the voltage on an electricity supply system specified for the purpose of defining the end of a voltage dip. Voltage dip duration time between the instant at which the r.m.s. voltage at a particular point of an electricity supply system falls below the start threshold and the instant at which it rises to the end threshold. Voltage dip residual voltage is minimum value of r.m.s. voltage recorded during a voltage dip.

Although in cable lines there are no temporary interruptions but there are lot of mechanical cable damage caused by digging. In OHL that type of damage does not exist. That is why from the power quality and power reliability point overhead line and cable lines are comparable. [4]

3. STATISTICS OF MV NETWORK POWER LINE FAILURES

As can be seen from Fig. 1, total number of failure to 100km in Riga (Latvia) in the last 20 years is predictable because of small fluctation between 2.7 and 4.8. Over the past 10 years in Riga (Latvia) average number of failure per 100km has decreased from 4.15 to 3.27 that can be explaned by the fact that preventive measures to prevent damage to cable lines are effectively applied in Latvia. [3]

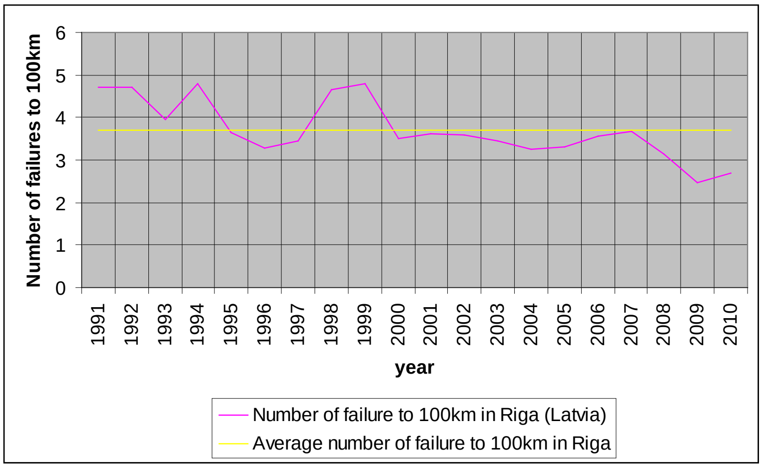

Fig. 1. Total number of failure to 100km in Latvia

The Fig. 2 shows statistical comparison of cable failure in three different regions- NYC and Westchester (USA), Texas and Dallas (USA) and Riga (Latvia). The average number of failure in NYC and Westchester is 3.94, in Texas and Dallas (USA) is 4.38 but in Latvia only 3.60. The Fig. 2 also shows that in USA number of cable failure tends to increase but in Latvia decrease. This fact can be explained by the fact that in Latvia is used more effective preventive measures for decreasing cable failure and also by the fact that network of cable lines in Latvia are significantly smaller than cable lines in USA and that is why in Latvia is possible improve cable lines more quikly than in USA. [1-3]

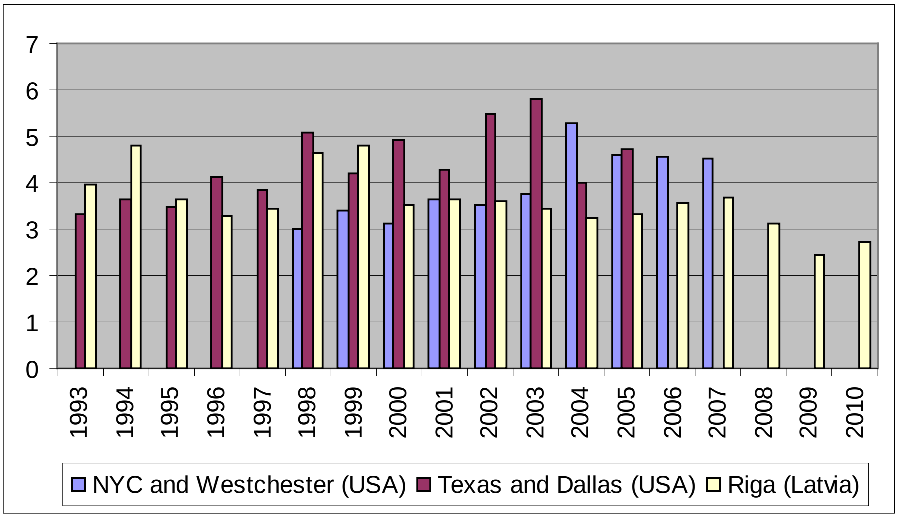

Fig. 2. Comparision of total number of failure to 100km in Latvia and USA

4. ANALYSIS OF MV NETWORK POWER LINE CAUSES OF FAILURE

Failure of power lines may cause due effect of various factors. All these factors can be divided into 4 groups- biological, chemical, physical factors and also weather conditions. These factors are shown in Table 1. Biological and physical factors impact on both type of line (CL and OHL), chemical factors impact on CL and OHL pole but weather conditions impact only on OHL. This explains why failures in overhead lines and cable lines are different.

Table 1. Factors that causes power line failure

Biological factors	Animals
	Vegetation
	Humans
Chemical factors	Contamination
	Moisture
	Ageing
Weather conditions	Storms
	Lightning
	Outdoor temperature
	Air humidity
	Snow
	Ice
Physical factors	Excessive load
	Lack of maintenance
	Wear out
	Design
	Manufacture

In Fig. 3 are shown comparision of cable damage types in Latvia and USA. In Latvia more than two-thirds and in USA less than half of all failure are caused by impact of mechanical factors. This can be explained that biggest problem of cable lines in Latvia is perfunctory and insufficient trained personnel servicing cable lines [1-3].

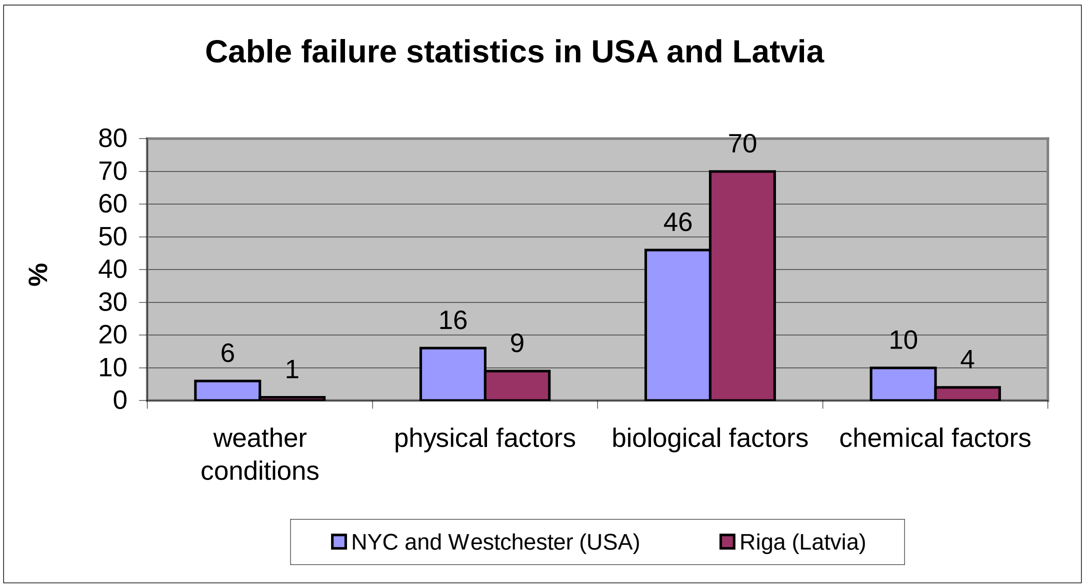

Fig. 3. Comparision of cable damage types in Latvia and USA

5. POSSIBILITIES TO REDUCE NUMBER OF FAILURES

Taking into account the fact that most cable damage are caused by biological factors, attention should be paid to possibilities of implementation and improvement of cable lines installation and exploitation. It would be advisable to revise existing standards with the aim of improving. Also the number of cable damage can be reduced by improving training of network exploiting engineers.

Another possibility to reduce number of failures (especially for overhead lines) is replacement of overhead lines with cable lines.

For comparison of economical performance of the networks, formed by two different types of power lines, from construction, maintenance and fault elimination costs point of view, detailed data about number of maintenance works, failure rates, costs of materials and work, etc. should be known. These data are used in the algorithm of methodology for costs estimation (see Fig. 4.). Brackets used in the algorithm's diagram correspond to equation numeration.

In common situation expenses related with construction and exploitation of the network can be calculated using (1). Equation (1) gives total costs of network for some period of time, e.g. 1 year or life time of power lines, taking into account power lines' life time and different costs for lines of the same type (OHL or cable lines) but different parameters, e.g. cross section.

$$C = \sum_{i=1}^{n} (C_i + C_{mi} + C_{fe.i}) \ , \qquad (1)$$

where C – total costs of network for some period of time [monetary units/time period]; C_i – total construction costs of lines with parameters i [monetary units]; C_{mi} – total preventive repair/maintenance costs of lines with parameters i [monetary units]; $C_{fe.i}$ – total fault elimination costs for lines with parameters i [monetary units]; i – number, corresponding to power line with specific parameters; n – total number of lines with different parameters used for the network.

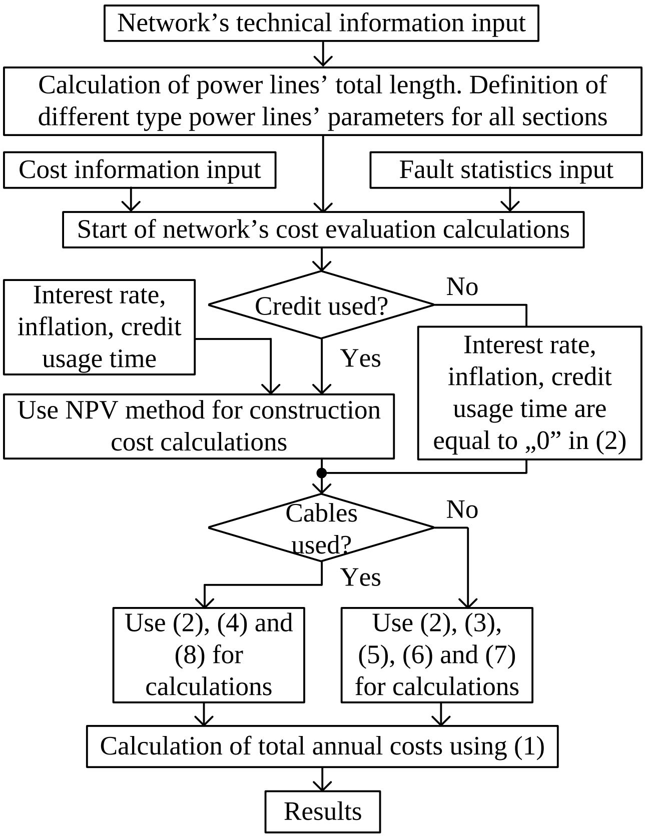

Fig. 4. Algorithm for cost estimation methodology

Total construction costs C_i for one year of line type's exploitation period, in their turn, are calculated using (2). The costs calculated by (2) consider that utility takes credit for constructing the network. NPV method is used to get real costs in present day money value. NPV method includes construction cost increase due to bank interest rate and cost discounting due to inflation. In case if utility doesn't take credit for construction of network, it will make changes in network using available money (from tariff). As soon as construction costs will not stay at the same value and will increase year by year, interest rate in equation (2) should be replaced by inflation value, because costs will increase by value of inflation. In this occasion construction costs also should be discounted with the value of inflation. Total construction costs in (2) are given for 1 year of exploitation.

$$C_i = \frac{C_{1\mathrm{km}i} \cdot l_i \cdot \left(1 + \frac{int_r}{100}\right)^{t_{cr}}}{\left(1 + \frac{inf}{100}\right)^{t_{cr}} \cdot t_{ei}}, \tag{2}$$

where $C_{1\mathrm{km}i}$ – construction costs of lines with parameters i [monetary units / km]; l_i – length of lines2) with parameters i [km]; int_r – interest rate [%]; inf – inflation [%]; t_{ei} – exploitation time of lines (life time) with parameters i [years]; t_{cr} – time of credit [years].

Calculation of preventive repair/ maintenance costs should be calculated separately for overhead and cable lines because of differences in maintenance works performed. Equation (3) is proposed for preventive repair/ maintenance costs evaluation of overhead lines, but (4) – for cable lines.

$$C_{mi} = N_i \cdot (C_{org} + C_{op.s} + C_m) \cdot \frac{l_i}{100} + \\ + l_i \cdot 1000 \cdot l_{pzi} \cdot C_{cpz} \cdot \frac{1}{p_{cp2}}, \qquad (3)$$

where N_i – number of preventive repair works (maintenance works) during 1 year [monetary units/(km*year)]; C_{org} – costs of maintenance works managing [monetary unit/preventive repair work]; $C_{op.s}$ – costs of operative switchings [monetary unit/switching]; C_m – costs of materials used during one maintenance work [monetary units /repair]; $l_{pz.i}$ – total protective zone length (to both sides of line) of lines with parameters i (for OHL up to 20kV is 2x6.5=13m; for cable line 2x1=2m – according to [5]) [m]; C_{cpz} – protective zone maintenance costs (for hew of trees and bushes) [monetary unit/m^2]; p_{cpz} – time interval between maintenance works performed in protective zone [years].

$$C_{mi} = \frac{l_i \cdot 1000 \cdot l_{pz.i} \cdot C_{cpz}}{p_{cpz}} \qquad (4)$$

As in case with preventive repair/ maintenance costs evaluation, fault elimination costs of overhead lines should be evaluated using different formulas, than those used for cable lines. Fault elimination costs take into account costs of physical repair of damaged part of line, fallen trees removal costs, preparation of required documentation and changes in existing documentation, etc. In addition to this, calculations of fault elimination costs should be separated for different types of OHL faults:

- in case of power line fault that has conducting wire interruption in all phases;
- in case of power line fault that has conducting wire interruption in all phases, damage of insulators at closest poles and small damage of 2 closest poles;
- in case of power line fault that has conducting wire interruption in all phases, damage of insulators at closest poles and fully damaged 2 closest poles.

The aim of case study was to estimate costs related to construction and exploitation of network built by OHL or cable lines. To estimate the costs, calculation process was divided into two parts for both types of networks:

- calculation of construction costs;
- calculation of annual costs.

When replacing existing OHL of the network with theoretical cable lines, cross section of respective cables was selected in such way, that it ensures at least the same capacity (maximal allowed current flow through cable) as overhead line.

To evaluate lifetime costs of OHL and cable line network, the part of real Latvian 20kV rural distribution network (further – the network) was used. The network is formed mainly by OHL with cable lines in some sections. It was assumed that the network is placed in 3 different environmental conditions. Part of lines are located in forest, part of lines – along roads, but the third part – in fields. Placement of lines was taken proportionally to placement of whole medium voltage network of Latvia. Information about failure rates of OHL placed in different locations were taken from [9]. Table 2 and Table 3 provide information about type and carrying capacity (maximal allowed current) values for the network's most commonly used OHL and cables. Total length of lines of the network is slightly above 280 km.

Table 2. Types of overhead lines most commonly used in the network

Nr. of element	Type	Carrying capacity [A]
1	AS-25	130
2	AS-35	175
3	AS-50	210
4	AS-70	265
5	SAX-70	310

Table 3. Types of cable lines most commonly used in the network

Nr. of element	Type	Carrying capacity [A]
1	N2SY 3(1*240/25)	320
2	AOSB-20-185	280
3	OSB-50	135

The network in normal operating state is powered from two 110/20kV substations. The network also has some interconnections with other parts of distribution network for the purpose of power supply reservation. In normal condition interconnections are opened and network operates independently from other networks. Fig.5 schematically shows structure of the network. In Fig.5 "DP" corresponds to "Distribution point".

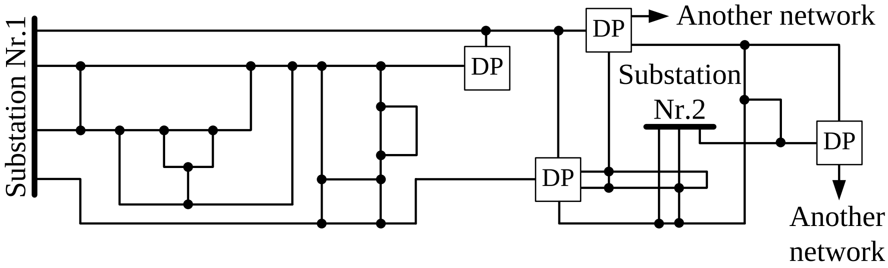

Fig. 5. Schematic scheme of 20kV rural network

In the case study there were studied two possible scenarios for network construction:

- utility takes credit for construction of network and in such case construction costs for cable line and OHL networks are calculated using NPV method. Taking credit for construction of network usually is exceptional case for utilities. Interest rate for materials of both networks was assumed to be 7%, but inflation – 3%. Calculation period was assumed to be equal to 30 years – lifetime of OHL. Lifetime of cable lines was assumed to be 45 years;
- utility makes reconstruction of network step by step (changes OHL to cable lines with small portions). Such scenario is more common practice for utilities, because network construction is closely related with reconstruction of existing network. In this case utility doesn't take credit. For these calculations it was assumed that prices for materials and labour will increase proportionally to inflation and net present value of the costs will stay at the same level.

Actual costs of construction works were taken from Latvian DSO [6] and represent cost level for year 2010. The costs include expenses for all materials, equipment and workers needed for construction OHL or cable line and don't include VAT (a value added tax). Information about costs is given in Table 4.

Table 4. Costs of construction works

Type of line	Costs, EUR/km	Notes
20kV OHL	37766	
20kV cable line	17620	For rural network. Asphalt price not included.

Annual costs consist of maintenance and fault elimination costs. Maintenance costs are the costs needed for annual preventive maintenance performance. Usually only cable lines don't have such type of costs. But exploitation costs, in their turn, are typical for both cable and overhead lines and are related with elimination of outages. Annual costs are more complex comparing to construction costs as they include different positions for different types of power lines.

According to [7, 8], number of maintenance works during one year period for middle voltage OHL vary from 1 maintenance with duration of 40 hours for "35 kV OHL section with standart length" [7] to 30 and 67 maintenance works with durations of 10 and 12 hours for 100 km of 10 and 35 kV OHL respectively [8]. Taking into account voltage level of network used in this study, 45 maintenance works per year per 100 km of line seems to be reasonable number.

Taking into account differences in nature of outages and damage made to OHL and cable line during outage, these types of power lines include different positions of exploitation costs.

6. RESULTS

Results of calculations are showed at Fig.6. Bars represent different types of lines – OHL and cable lines and consist of different types of costs. At the base of bars (in blue) there are construction costs, in the middle (in violet) there are maintenance costs and on the top of bars (in yellow) – fault elimination costs.

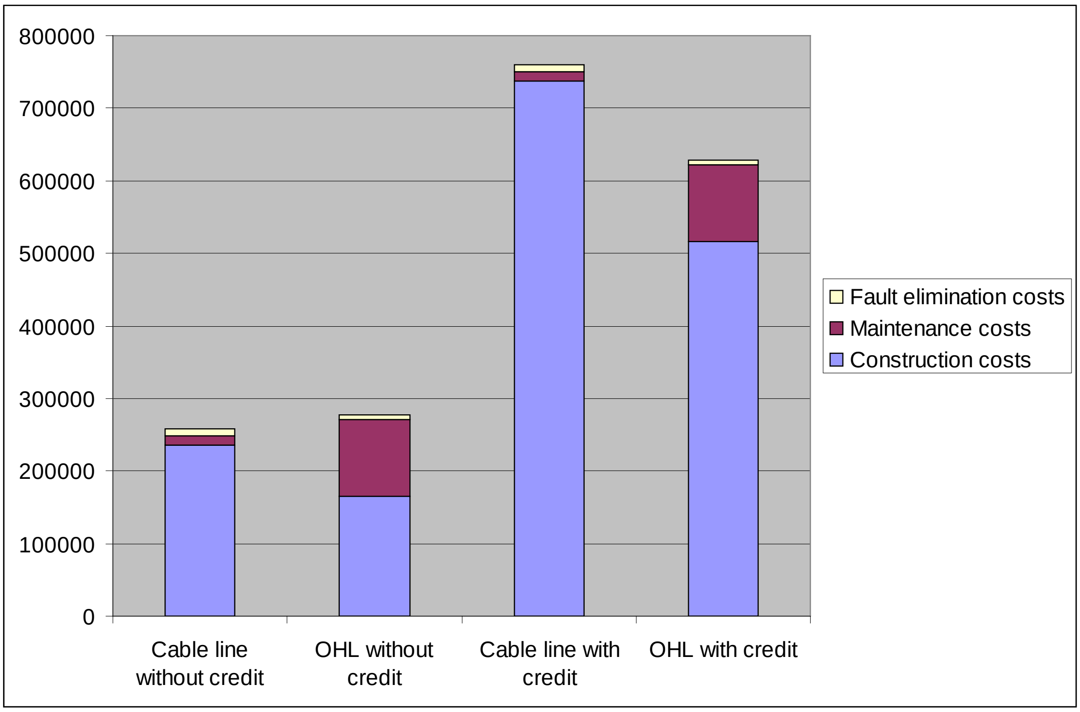

Fig. 6. Annual costs for power lines of the network (with and without credit)

As can be seen from results cable lines have bigger proportion of construction costs, but OHL – vice versa – annual costs. This can be explained by initial costs of lines and their reliability during exploitation. It also can be seen, that if utility takes credit for network construction – costs of cable network increase dramatically. But if utility does not take credit for network construction that is also closer to reality, shows, that construction of cable network can be beneficial for utility from economical point of view – difference between annual costs of the network exploitation is more than 3.4% (difference – 9260 Eur).

Evaluation of the real cable and overhead line formed network's costs was made. Analysis of two possible scenarios of investments in the grid showed, that investments made in network step by step, as it is usually done in practice, give economical advantage to cable line network comparing to overhead line network.

Relatively small difference in annual costs of networks when credit not taken (only 3.4%) in the whole distribution system level grows to big savings. One more aspect that gives advantage to cable line network is almost full absence of transient failures that will reduce customer costs dependant on reliability and will push area of optimal reliability level down – to smaller total costs of reliability.

The results show that placement of underground cable lines instead of overhead power lines for medium voltage distribution network is economically competitive and absolutely feasible because of comparable total costs for utility.

Taking into account that difference in total costs between OHL and underground cable line formed network are not big, usage of cables instead of OHL would be definitely reasonable only for distribution network, as soon as medium voltage lines provide electricity to big consumers or a lot of small consumers. In case of planning low voltage network reconstruction with OHL replacement by underground cable lines, customer costs of reliability and load values should be definitely analysed before making final decision.

7. CONCLUSION

Evaluation of the real cable and overhead line formed network’s costs was made. Analysis of two possible scenarios of investments in the grid showed, that investments made in network step by step, as it is usually done in practice, give economical advantage to cable line network comparing to overhead line network.

Relatively small difference in annual costs of networks in case of not taking credit (only 3.4%) in the whole distribution system level grows to big savings. One more aspect, that gives advantage to cable line network is almost full absence of transient failures, that will reduce customer costs dependant on reliability and will push area of optimal reliability level down – to smaller total costs of reliability.

REFERENCES

1. Smith J. T., Harp R. Cable Failure Statistics and Analysis at TXU Electric Delivery Company: http://www.pesicc.org/iccwebsite/subcommittees/subcom_e/E4/2004/F2004_Harp.pdf (accessed at 01.02.2012.)
2. Campbell, T. Three Decades of Cable Failure Data. Presentation from ICC Meeting-St. Petersburgh Beach, FL. Subcommittee A, March 10, 2008: http://www.pesicc.org/iccwebsite/subcommittees/subcom_a/Presentations/Spring08/A2.Campbell.pdf (accessed at 01.02.2012.)
3. Latvian DSO – JSC “Sadales tikls” documentation
4. European Standard EN50160 Voltage characteristics of electricity supplied by public electricity networks (LVS EN 50160+AC:2011 (LV))
5. Protection zone law (of Latvia). Web page: http://www.likumi.lv/doc.php?id=42348 (accessed at 01.02.2012.)
6. Web page of Latvian DSO – JSC “Sadales tikls”: http://www.latvenergo.lv/pls/portal/docs/PAGE/LATVIAN/FILES/vid_izm_300311.pdf
7. Гук Ю.Б., Лосев Э.А., Мясников А.В. Оценка надёжности электроустановок. Москва: „Энергия”, 1974, 200 с.

8. Балаков Ю.Н., Мисриханов М.Ш., Шунтов А.В. Проектирование схем электроустановок. 2-е изд. Москва: "Издательский дом МЭИ", 2006. 288 с.
9. Antikainen J., Repo S., Verho P., Järventausta P., “Possibilities to Improve Reliability of Distribution Network by Intended Island Operation,” *International Journal of Innovations in Energy Systems and Power*, Vol. 4, no. 1, p. 22–28, Apr. 2009. http://ijesp.com/Vol4No1/IJESP4-1-4Antikainen.pdf (accessed at 01.02.2012.)

CYSENI 2012, May 24–25, Kaunas, Lithuania
ISSN 1822-7554, www.cyseni.com

NEW TRANSMISSION EXPANSION CONCEPT AND ITS FORWARD AND REAL-TIME SMART MANAGEMENT COMPONENTS

N. Radziukynienė, A. Klementavičius
Lithuanian Energy Institute
Breslaujos str. 3, LT-44403 Kaunas – Lithuania
Phone (8-37) 40 19 44
Email: neringa@mail.lei.lt

ABSTRACT

The paper identifies 4 major contemporary challenges of power transmission expansion in modern world as 1) respond to the increasing power demand of customers; 2) replace the worn-out transmission grid equipment by new ones; 3) provide the bulk power transportation for regional and continental electricity markets; 4) ensure reliability and security of transmission grids.

The paper suggests the 3-component transmission expansion concept based on *build-the-grid*, *outside-the-grid* and *inside-the-grid* components where the first component refers to new physical grid capacities while others to the management of grid users and control of grid equipment. The analytical review of new transmission expansion approaches and technologies is provided. It covers the forward and real time management of grid users (within *outside-the-grid* component) and smart control of transmission grid (within *inside-the-grid* component). The scope of forward management includes distributed generation, demand side management and distributed storage while the real-time management – demand response with original classification to 6 product categories, and automated generation control. The concept promotes the “soft” transmission expansion in the *outside-the-grid* and *inside-the-grid* directions and could be useful for transmission system operators, smart grid developers and transmission grid users.

Keywords: electricity transmission, expansion, transmission grid, grid capacity, transfer capability, smart control, grid user, demand-side, forward management, real-time management

1. INTRODUCTION

Conventionally, the power transmission expansion concept is based on building a new infrastructure of transmission grid, i.e. on introducing new physical grid capacities. It corresponds to the simple principle as “A new line gives additional transferred megawatts in the specific direction across the grid”. Actually, a physical capacity has a certain range (or, at least, margin) of transfer capability depending on grid loading, load flow distribution and weather. Nevertheless, as an opportunity to increase the transfer capabilities, the grid operational aspects were underestimated, mainly because the *build-the-grid* approach was sufficient and practically available.

Historically, the power transmission systems were expanded rather freely, without considerable land restraints for new transmission lines, substations and associated equipment. Also the financing issues did not pose significant barriers and complications. Coincidently, with the end of Era of Industrial Growth and transition into Information Era (about 1989)[1], the situation has changed and transmission system operators faced a new reality: how to expand in the environment of constrained investments and missing sites for new routes and substations? As experiences have revealed over the last 2 decades, to permit, site, and construct the new transmission lines has become extremely difficult, costly, time-consuming and controversial. The public pressure against siting (placement) of new grid equipment, often approximate to the standpoint “NOT-IN-MY-

---

[1] according to Robert T. Kiyosaki and Sharon L. Lechter, see their book *Cashflow Quadrant: Rich Dad's Guide to Financial Freedom* (2000)

BACKYARD“, is putting serious barriers for transmission grid expansion. It gives stimulus to revise the conventional concept of transmission grid expansion and look for opportunities as how to extract more transfer capabilities from the existing grid capacities.

2. CHALLENGES FOR TRANSMISSION GRID EXPANSION AND SUGGESTED CONCEPT

The continuous growth of power demand and the ensuing necessity to add new generation (by extension of existing power plants and connection of new ones) raise a continuous challenge against transmission system operators (TSO) or independent system operators (ISO) to expand the transmission capacities in order to match them to the needs of increased energy transfers.

The second challenge arises from the aging and wearing-out of transmission assets. The grids should be retrofitted, reengineered and replaced by new ones. The replacing capacities of transmission lines can be installed with higher load-carrying ratings in the same routes (right-of-ways).

Furthermore, operators also face the third challenge as to provide a technical infrastructure for wide area electricity markets with bulk energy transits over several systems, i.e. to support deregulated market unconstrained by transmission. Regarding the European Union (EU), it concerns the Internal (Single) EU electricity market, a policy target based on consolidated pan-European transmission grid (also called TEN-E, Trans-European network for energy). It gives a strong momentum for transmission expansion in terms of reinforcement and extension of national grids and cross-border interconnections, and enhancement of interoperability of the grids [1].

Finally, the forth challenge refers to operational security of transmission grid. The grid should be expanded in a way ensuring the increasing demands for security and reliability of the interconnected grid. The grid should be robust for the spread of disturbances, and transmission congestions under “the bulk transportation across the Europe“.

To cope with the above-mentioned challenges, we assume that the new approaches to transmission expansion, advanced transmission technologies as well as smart management and control of transmission grids will be the major instruments, besides to the consistent regulatory framework and appropriate investment policy measures, facilitating the TSOs, transmission planners and other power sector stakeholders.

Here we suggest the following definition of transmission expansion: it is activities and efforts to develop and extend the transmission capacities and transfer capabilities of transmission system, by both building of physical grid capacities and optimized, smart management of those capacities combined with interventions into behaviour of grid users. Furthermore, this concept is laid out in 3 components:

1. *Build-the-grid* component: strategic extension of grid, connection of new transmission assets. It is conventional investment-related expansion;
2. *Outside-the-grid* component: smart management of grid users as power producers, consumers and traders. It deals with energy-to-grid inputs (from user) and energy-from-grid outputs (to user) in the transmission and distribution grids (in planning, scheduling and real-time control phases);
3. *Inside-the-grid* component: scheduling and real-time control of grid’s configuration and equipment.

The 1st component rests upon the planning and installing of transmission grid capacities, i.e. equipment and infrastructure, including grid control and automation equipment with embedded information and communications technologies (ICT).

The 2nd component rests upon the management of grid users, i.e. upon the measures applied outside the grid. By means of co-ordination of loads (energy-from-grid outputs/energy-to-user inputs) and generations (energy-from-user outputs/energy-to-grid inputs), the TSO can solve time-specified and location-specified transmission shortages, for instance, by creating counterflows on tie lines congested by the cross-border exchanges.

The 3rd component addresses the elimination of transmission shortages through changes in grid topology (configuration) and equipment set points, e.g. by regulating the VARs injection/absorption of reactive power devices, changing the switch-on/switch-off states of circuit breakers and switches, dynamic setting control for FACTS and smart relays, short-term operation beyond parameter tolerances et al.

The expansion in the 2nd and 3rd directions can be qualified as "soft" approaches with zero investments or, at least, minimal ones. Both components provide possibilities to get more transfer capability from the invariant grid capacities.

The transmission expansion concept could be written by two conceptual expressions, for medium/long term period T and real-time timescale t (moment, e.g. hour, half-hour), respectively:

$$\Delta TC_T = \Delta TC_T^{(1)} + \Delta TC_T^{(2)}, \tag{1}$$

$$MTC_t = MTC_t^{(2)} + MTC_t^{(3)}, \tag{2}$$

where ΔTC_T – transfer increase of transmission grid over period T;

- $\Delta TC_T^{(1)}$ – increase gained by introduction of new grid capacities (expansion in 1st component);
- $\Delta TC_T^{(2)}$ – increase gained by geographic planning of new regional generation, including distributed one with incentive feed-in tariffs, and regional load levels, including various demand side management programs (expansion in the 2nd component);
- MTC_t – marginal increase of transfer capability in timescale t with respect to operation-determined value of grid capacities;
- $MTC_t^{(2)}$ – increase gained by scheduling and real-time control of generators and loads (expansion in 2nd component);
- $MTC_t^{(3)}$ – increase gained by scheduling and real-time control of grid topology and equipment (expansion in 3rd component).

In the following sections 3, 4 and 5, we provide the review of approaches and grid management technologies which enable the increases $MTC_t^{(2)}$ and $MTC_t^{(3)}$.

3. OUTSIDE-THE-GRID COPONENT: FORWARD MANAGEMENT OF GRID USERS

The *forward management* of grid users is classified to the *outside-the-grid* component of transmission expansion concept. Its rationale is to solve or mitigate the future lacks of transmission capacities by strategic management of grid users, i.e. influencing ahead their energy-from-user outputs (generations) and energy-to-user inputs (loads) in the specific zones of transmission grid and in specific timescales. Essentially, the forward management aims at developing the future guidelines for grid users as how to change their behaviour in exchange to some economic benefits.

The forward management is based on programs (plans) from medium-term (say, several months) to long-term (several years) periods) working as strategies whose objective is the modification of future patterns of generations and loads hosted by grid users. The programs will address the grid users, both existing and potential, by sending them economic signals from the transmission planner, TSO, ISO, distribution system operator (DSO) or other stakeholders participating in the program. The signals should encourage the existing grid users to reshape their energy inputs and outputs, and the potential users – to establish themselves and to take the offered energy use patterns for favourable tariffs, bill credits or buy-out services.

Actually, the forward management may incur some administrative and operational cost for TSO/DSO to implement the incentive scheme. Anyway, these costs will be significantly lesser than alternative investments into new physical capacities.

Hereafter the focus on grid users covers distributed generators, demand-side participants and electricity storage units.

3.1. Distributed generation

The distributed generators might be considered all those connected to ("scattered across") the distribution grids. The large-scale deployment of distributed generation may actually change the status of distribution grids from passive to active. It means that a power flow will be reversed; instead of flowing only downstream the grid, from transmission system to customers, the power may also flow upstream the grid, from generators, connected to medium and low voltage level up to transmission grid.

To connect the new generators in area with weak transmission grids may be equivalent to introduction of an additional transmission line. If forward management programs for distributed generation succeed in establishing a lot of new producers, the net loading of distribution grids will decrease or, at least, grow at less rate. Accordingly, some transmission capacities will be unloaded and the construction of new capacities deferred. Thus the deployment of distributed generation can be regarded as indirect transmission expansion.

The following categories of distributed generators seem to have good future prospects:

- *renewables-driven generators*; here the intermittent renewables may cause some grid-integration troubles for TSO/ISO/DSO;
- autoproducers, mainly industrial customers;
- in-house generators (including microturbines and fuel cells) of residential and other small customers;
- microgrids;
- virtual power plants;
- grid-supportive generators owned by external business entities (conceivably energy service companies) and connected to DSO or user's grid.

Specifically, notion of microgrid refers to a low voltage network connecting several customers with distributed generators, local electricity storage devices and some controllable (both dispatchable and undispatchable) loads. A microgrid can work in islanded mode, i.e. as autonomous system. Like a microgrid, a virtual power plant is a self-balancing corporate body consisting of several members – distributed generators, autoproducers, customers and stationary energy storage devices. However, different from a microgrid, these members are connected to the nodes scattered across the grid and therefore build up only a virtual network, which, in fact, cannot function in islanded mode.

In future, deployment scale of distributed generation may depend on the availability of hydrogen grids. Fuel cells equipped with inverters would be connected to those grids and permanently fed with hydrogen. We assume that fuel cells could participate practically in all aforementioned categories of distributed generation.

According to controllability criterion, 2 types of distributed generators could be distinguished: uncontrollable and controllable generators. The latter type will be contracted by TSO, ISO, DSO for the real-time management purposes (see section 4).

3.2. Demand side management

The demand side consists of customers and retail suppliers. The reduction of the demand (i.e. loads) can be viewed as generation of “megawatts“.

Historically, demand side management (DSM) appeared as a planning policy originally pursued at shaving the peak loads in power systems in order to avoid or defer the construction of new generation capacities. It was implemented by incentive long-term tariffs for customers. This policy resulted in the appreciable shifts of loads from peak hours to off-peak periods, mainly in electrical heating, air conditioning and some industrial processes in Germany [2] and United States [3].

The classical definition of DSM determines it as planning and implementation of electric utility’s activities designed to influence customer uses of electricity in ways that will produce desired changes in the utility's load shape [4]. North American Reliability Council (NERC) refers to a broader definition: all activities or programs undertaken to influence the amount and timing of electricity use [5]. Sometimes the energy efficiency aspect is emphasized: DSM aims at improving energy efficiency which is reduction of kilowatt-hours of energy consumption for the same service or activity, reduction of kilowatts of power demand or displacement of demand from peak to off-peak time [6]. The DSM for network purposes is specified by term *network-driven DSM*. International Energy Agency (IEA) defines it as efforts to reduce demand on the electricity network in specific ways that maintain system reliability in the immediate term and defer over the longer term the need for network augmentation [7].

In the forward management of grid user inputs and outputs, the latter DSM notion is quite appropriate. According to it, DSM is structured to load level management and load shaping [7]. Both constituents work as marketing instruments. Load level management mainly deals with strategic electrical energy conservation (energy efficiency). Load shaping addresses the strategic load shifting from peak hours to off-peak hours, load valley filling, identification and contracting the controllable loads for real-time management. Both instruments definitely support the promotion of distributed generation for end users, including micro-generators.

Load shaping programs certainly will be tariff-based. Here two major types of tariffs will be offered: time-of-use and critical peak tariffs. First ones reflect daily and monthly variations in electricity costs [8] or, in rewording, present the rate and price structures with different unit prices for use during different blocks of time [5]. Time-of-use tariffs may also include rates for declared capacity demand. The second ones represent the deterring (very high) peak prices for time blocks with difficulties for TSO/ISO to overcome the expected peak demand.

Contrary to load shaping, the load levelling programs can hardly be based on tariffs, unless the distributed generation (particularly, *renewables-driven*) is incorporated into energy conservation. Being aimed at the end-use efficiency improvements that slow down the load growth, those programs may even conflict to some extent with operator’s goals to transmit the larger transits. On the other hand, the duties, tasks and specificity of TSO/ISO/DSO are not favourable for intervention into customer’s preferences of electrical appliances. Introduction of energy-efficient appliances into customer’s “yard” or his energy-saving behavior are better addressed by other protagonists like energy agencies, municipalities, electrical appliances industry, energy service companies, with some limited participation of operators and power utilities. Ultimate success of those programs will rest with balancing the DSM protagonists' and customers' interests.

Besides to load level and load shaping management, third constituent of DSM concept could be distinguished – demand response management. It deals with drafting and implementation of demand response programs aiming at establishment of grid user subsystems that will participate in real-time management of transmission system. Those grid users will provide various demand response products for TSO/ISO/DSO (see section 4.2).

3.3. Distributed storage

Distributed energy storage could be regarded as “minor” distributed generation. It is bi-directional (load/generation) electrical device with energy-to-user inputs in loading phase and energy-from-user outputs in discharge phase.

Most likely the major application of distributed storage in forward management will be to serve for peak shaving policies. Properly motivated by such programs (plans), end-users provide themselves with storage devices to meet their loads in power system’s peak hours. Accumulated during off-peak hours, the stored energy is converted to peak electricity and discharged respectively in peak hours. The second application may be a higher reliability of supply: to use these devices as back-up sources for autonomous electricity supply during interruptions in delivery from grid. Also the third reason can be outlined – to add storage to own distributed generator, in particular driven by intermittent resources (wind, solar), seeking to compensate frequent unavailability of generator. Specifically, the microstorage for both individual end-users and microgrids seems to become a reality in some 20 years.

Also the forward management of distributed storage may encourage both customers and various business entities to acquire storage devices and become contractual ancillary service providers of

- balancing services needed to keep system load and supply (generation plus imports) in balance;
- congestion mitigation services needed to counteract local transmission congestions.

Battery energy storage seems to be major type of distributed storage. It is a chemical-based energy storage set-up with shunt-connected voltage source converters capable of rapidly adjusting the amount of energy injected to or absorbed from an AC system. It is assigned to the second generation of FACTS controllers.

The modern *superconducting magnetic energy storage* (SMES) system for connection to distribution and industrial grids is already available in a market. It is called D-SMES (distributed SMES) system. Today it is acknowledged as a proven voltage regulation technology. A system stores and instantaneously discharges a large quantity of power. It contains a superconducting electromagnetic energy storage device with electronic converter that injects and absorbs real and reactive power into/from the AC system. The converters predetermine the qualification of SMES systems as FACTS controllers.

Having started with voltage stability and power quality problems for large industrial customers, SMES systems are extending their scope of application into reliability and transfer enhancement in transmission system.

Specifically, a SMES system can be transported on standard truck trailers, with one 250-kW system per trailer. The inverters provide up to 2.3 times nominal instantaneous over-current capability and can also be configured for continuous VAR support. Each 250-kW trailer operates independently, improving reliability. Six SMES systems have been installed for pilot application recently in the Midwestern United States [9].

It can be expected that SMES technology will evolve to considerably bigger unit storage capacities. Consequently, the systems will be connected directly to transmission grid.

Compressed air energy storage (CAES) is a modification of the gas turbine technology, in which low-cost electricity is used for storing the compressed air with subsequent release to drive a turbine in high-cost hours or generation shortage situations. The air can be stored in an underground cavern, but options of underwater storage and on-ground tanks are also considered. Intermittency of wind generation is another factor acting as a driver for CAES. The CAES is increasingly analyzed as a technology supplementing wind power generation and increasing its value.

Recently there have been only 2 operating CAES plants – in Germany (390 MW) and in the USA (110 MW). Plants of such a scale can be market players. According to [10], if CAES plants operate both on the spot market and the regulating power market, they may be feasible, i.e. their operation may be cost-effective. Moreover, small-scale CAES may also have a future. Some authors even consider that micro-CAES with man-made air vessels is a more adaptable solution than large-scale CAES with geology-dependent underground caverns [11].

4. OUTSIDE-THE-GRID COPONENT: REAL-TIME MANAGEMENT OF GRID USERS

Same as the forward management, the real-time management of grid users is also assigned to *outside-the-grid* component of transmission expansion. It covers the load, distributed generation and storage subsystems established (i.e. identified, organized into some groups and even contracted) by forward management programs. This management deals with the energy-to-user inputs (from grid) and energy-from-user outputs (to grid) done intentionally by the users for the grid needs, i.e. to counter both regular and irregular transmission shortages (both scheduled and contingent) in real time. Transmission shortages may be caused by unavailability or loss of transmission equipment due to overloading, congestion, outages, bottleneck on the cross-border interconnections and other triggering events.

This management is based on TSO/ISO/DSO interventions on energy-to-user inputs (loads) and energy-from-user outputs (generations).

Controllable (by the operator) outputs and inputs may be classified to dispatchable and non-dispatchable. As regards dispatchable ones, operator intervenes by switching and changing them directly, i.e. without user involvement. Considering non-dispatchable ones, interventions cover the rescheduling actions (operator changes the load, generation and storage/discharge patterns initially scheduled by their hosts) and the respective notifications (recommendations or instructions) to the grid users (users implement the notified changes in operational hour). To increase the controllability, the operators should contract the hosts of controllable inputs/outputs as ancillary service providers.

Uncontrollable inputs and outputs can be considered as the real-time price pressure on grid users. The users are offered to take the convenient spot prices or to obviate inconvenient ones by changing their energy-from-grid inputs and energy-to-grid outputs within the specific timescales.

4.1. Automatic generation control

As known, the major functionality of automatic generation control (AGC) systems operated by TSO/ISO is to provide the secondary reserve services in individual control areas. AGC systems could be extended by additional generators including tertiary reserve units called on for elimination of irregular transmission shortages in operational hour. Here the inclusion of distributed generation and storage as well as customer loads into AGC system might be an opportunity. As a matter of fact, it will require the high-intelligent ICT to be integrated into power system on a large scale in order to carry out the automated monitoring, decision-making and coordinated control of multiple new reserving subsystems and units.

4.2. Demand response

The demand response and its products is rather a recent concept. In accordance with American viewpoints [13] as well as some international ones [7], demand response is rather a subcategory of DSM, which represents its real-time segment. Nevertheless, European Commission prefers the parallelism of both categories [12]. Anyway, we see the concept presented by North American Reliability Council as the most comprehensive: “Demand response is designed to change on-site demand for energy in intervals from minutes to hours and associated timing of electric demand/energy use (i.e. lowering during peak periods) by transmitting changes in prices, load control signals or other incentives to end-users to reflect existing production and delivery costs" [13]. It could be noted that this concept includes the aspect of *network-driven DSM* (see section 3.2) as it refers to "delivery costs".

We suggest the following categorization of demand response products:

1. *Direct load control*. It deals with dispatchable loads established during implementation of DSM programs. The direct switching of loads is carried out by TSO/ISO/DSO dispatching centres and remote grid controllers. This product provides operator with firm amounts of demand that could be immediately disconnected to mitigate the transmission shortages.

2. *Interruptible loads.* They cover loads under direct control and undispatchable loads, the latter being manually reduced or disconnected by the customers themselves in accordance with contractual provisions, either after a notice from operator or without it.

3. *Load shifting, including peak shaving and valley filling.* Load shifts are scheduled by TSO for the customers who agree to change their load schedules for the next day or intra-day hours in accordance with contractual arrangements. Customers switch their loads manually.

4. *Real-time pricing.* It is based on occasional spot prices for the next day or intra-day hours. The TSO/ISO offers them to customers, individually or via power exchange (electricity auction), with expectations to attain their response in load curtailment, shifting or increase, respectively. Such a response is absolutely subjected to customer's willingness.

5. *Load curtailment bidding.* It is based on customer's downwards-regulation bids for his load submitted to TSO/ISO (balancing auction). The customers offer amounts of load curtailments, timescale (hours) and specific prices for the next day or intra-day. TSO/ISO buys out the appropriate bids on competitive basis and subsequently the selling customers manually perform the curtailments. This product is equivalent to upwards-regulation by tertiary reserves.

6. *Distributed generation control*. TSO schedules the level of customer's generation (or aggregated load, e.g. of virtual power plant or microgrid) for the next day or intra-day hours. The product also may include direct control of customer's generation or operator's call for generation change.

All aforementioned demand response products (with exception of real-time pricing) can be regarded as balancing services provided by the demand-side in the framework of certain balancing mechanism. Here the consolidation of balancing market and intra-day market seems to be a promising cost-effective approach [14].

5. INSIDE-THE GRID COMPONENT: SMART CONTROL OF TRANSMISSION GRID

As said in section 2, the real-time (on-line) control of grid equipment in transmission systems can be viewed as 3rd (*inside-the-grid*) component of transmission expansion. Like a real-time management of energy-from-grid outputs and energy-to-grid inputs, it is a "soft" (operational) expansion and aims at the gain of momentary or short-term transmission margin. It will solve transmission shortages, the dominant proportion of which will be taken by unscheduled (contingent) situations. The control technologies in this area will rely on distributed automation, distributed intelligence and extended communications, all 3 drivers widespread across the transmission and distribution grids.

The real-time control consists of central (remote) and decentralized (distributed, local) segments. Proportion of decentralized segment will progressively extend, with accompanying enhancement of coordination of distributed controllers on "peer-to-peer" basis. Along with it, the hierarchy of control will persist: the central control segment will send permanently schedules, queries, guidelines, notifications, instructions and direct control orders to decentralized one.

With the growth of embedded intelligence, the grid will approximate to the smart grid that monitors, thinks, acts, self-repairs and adjusts to respond quickly to customer needs [20]. Hence, the transmission expansion will be only one of advantages of smart grid, along with the improvements in grid security, reliability, cost-effectiveness, integration of renewables, and market liberalization.

Intelligence into the grids will be embedded through IED (intelligent electronic devices), computers of control centers (masters, hubs), various intelligent controllers (including FACTS as well), smart meters and real-time simulators.

Communications between smart controllers, automation devices, customers and generators will be multi-directional, of “end-to-end” type and based on various physical media. The present and future capability of the internet technology is estimated to be insufficient. The amount of data transfer will bring the communications to the level of intensive data traffic. The digital information will be sent via wired media like twisted pairs (copper cable), telephone line, coaxial cable, fiber-optic cable, power line carrier and broadband over power line. Wireless media will include radio, cellular, wireless fidelity (Wi-Fi), satellite and microwave. Accordingly, the common communication protocols will be developed and adopted [13].

The real-time monitoring technologies will provide dispatchers and smart controllers with information enabling them to make the adequate on-line solutions of transmission control. In addition to conventional SCADA/EMS (supervisory control and data acquisition/energy management system), the new monitoring technologies are on the horizon as Wide Area Monitoring Systems (WAMS), Wide Area Protection Systems (WAPS), advanced metering infrastructures (a new generation of automated meter reading systems), and various telemetering systems including those with temperature sensors on current-carrying transmission elements.

As known, thermal rating of a line corresponds either to conductor’s damage limit or critical line sag, i.e. the minimum conductor clearance to ground or on-ground objects. Usage of the static thermal ratings often accounts for the underutilization of thermal limits of the conductors in overhead lines. The idea to use the line’s actual capacity margins that fluctuate in accordance with air temperatures, solar radiation, precipitations and wind velocities was offered 30 years ago [15]. Based on real-time measurements of conductor temperatures, this idea was named dynamic thermal rating approach. Only nowadays the real spread of this approach is getting to start, mainly because of the developments in smart temperature sensors and transfer technologies of sensed data.

The effectiveness of the dynamic rating approach was recognized by a number of cases. In Buffalo Ridge region (South Dakota, USA), wind power park’s production was frequently curtailed on windy days, because it was assumed that the static thermal rating of nearby transmission line of 115 kV was too low to support the power transfer in case of contingency in the region. The real-time monitoring of this critical line revealed a significantly higher transmission capacity during periods of maximum output of wind power park and justified park’s operation without curtailments [16].

To release the overloading and eliminate risky operation in vicinity of thermal limits, the smart grids are expected to redistribute power flows by moving a portion of flow from overloaded paths onto underloaded ones. Such a redistribution (rerouting) will be based on integrated decision combining the control of grid equipment and energy outputs and inputs. Grid equipment control refers to the control of circuit breakers and other change-over-switches (including feeder reclosers and sectionalizers at distribution level), control of setpoints of FACTS, HDVC links, transformers and conventional reactive power devices.

The automatic grid reconfiguration can be performed as static, with pre-set sequence of switching procedures, or as dynamic, if coordinated by automatic reconfiguration controller [17]. Thus the grid automation will yield a new functionality when the grid itself optimizes its configuration [13]!

The roll-out of smart metering will contribute to on-line control of grid loads [8]. A lot of utilities already benefit the automated meter reading systems, ranging from selected customer groups to entire residential areas. Advanced metering infrastructure as a new development of reading systems is coming with a considerably higher level of automation. Namely, its two-way communication enables advanced applications, like automated demand response and information system to support distribution automation [18]. Here a smart meter functions like a sensor for several distribution applications. The smart metering will be capable to perform connect/disconnect functions and to provide data for direct load control and grid reconfiguration solutions. Furthermore, a smart meter may be envisaged in future to automatically participate in electricity market (day-ahead, intraday) and buy the cheaper energy for customer's certain appliances which are directly controlled by a meter!

Also smart metering is entering the SCADA systems. SCADA started to extend down from transmission to distribution level. The so-called SCADA/DMS (distribution management systems) monitor and control the switches on remote sections of medium voltage feeders. According to some estimations [19], the scale of feeder automation in North America was recently less than 20% only. Meanwhile majority of HV/MV (high/medium voltage) substations, 60-80%, were considered as automated with SCADA/ESM. The further extension of SCADA system will step down up to the customer level (say, SCADA/CUSTOMER systems, the common term is not proposed yet).

Smart grid will enable TSO/ISO/DSO to get more power out of the existing grid infrastructure, to decrease the unscheduled power flows (inter alia, loop flows), to support the scheduled flows and maybe to approach the on-line control of AC power flow magnitudes and directions on the selected transmission lines and corridors!

6. CONCLUSIONS

Nowadays the transmission system operators and planners face, at least, 4 challenges for electricity transmission expansion:

- respond to the increasing power demand of customers;
- replace the worn-out transmission grid equipment by new ones;
- provide the bulk power transportation for regional and continental electricity markets;
- ensure reliability and security of transmission grids.

Conventionally, the grid expansion concept was based on introduction of new transmission equipment, i.e. on *build-the-grid* approach. Nevertheless, in the modern world, the expansion of physical grid is strongly impeded by the land restraints for new transmission lines and their financing problems.

In the suggested 3-component transmission expansion concept, the *build-the-grid* component (strategic expansion) is supplemented by the *outside-the-grid* component (management of grid users) and *inside-the-grid* component (real-time control of grid equipment). The 2nd component (addressing the forward and real-time management of grid users) and 3rd one (control of transmission grid) are aimed at the additional transfer capabilities under the same grid capacities.

The analytical review of the approaches and technologies within the 2nd and 3rd components specifies the measures as how to implement the components.

Smart grid targets and enabling technologies will particularly contribute to the transmission expansion in *outside-the-grid* and *inside-the grid* components. Also smart technologies will reduce difference between the transmission and distribution grids.

The promotion of network-driven demand side management and demand response strengthens the emerging grid-user-centric approach to transmission grid. The categorization of demand response products as suggested in the paper may bring the demand response closer to transmission expansion needs.

The suggested concept may be interesting for transmission grid operators, planners, traders, grid users and other electricity sector stakeholders. It may encourage them to address *outside-the-grid* and *inside-the-grid* components. The stakeholders also may benefit the reduced or avoided investment-to-grid cost.

REFERENCES

1. Directive 2005/89/EC of the European Parliament and of the Council of 18 January 2006 concerning measures to safeguard security of electricity supply and infrastructure investment.
2. BORSTELMANN, P. 1979. Die Entwicklung der elektrischen Raumheizung in der Bundesrepublik Deutschland. In *ETA Elektrowärme*. 1979, No. 6, p.329–334.
3. GORZELNIK, E.F. 1984. Thermal-storage heating fills valleys. In *Electrical world*, No 9, p. 89–90.
4. GELLINGS, C.W. 1985. The concept of demand-side management for electric utilities. In *Proceedings of the IEEE*, Vol. 73, Issue 10, p.1468–1470.
5. North American Energy Reliability Council (NERC), 2007-1. *Demand response discussion for the 2007 long-term reliability assessment.* February 2007. 9 p.
6. GUPTA, K.P. 2006. Energy conservation by demand side management by standardization and energy labelling. Paper presented at the Conference "India Electricity–2006**",** May 11-13 2006, New Delhi. 23 p. Link to the internet <http://www.ficci.com/media-room/speeches-presentations/2006/may/may12-elec/Concurrentiii/GERC.doc.pdf>
7. International Energy Agency (IEA). 2008. *Implementing agreement on demand-side management technologies and programmes.* 2007 Annual Report. International Energy Agency, Stockholm. January 2008. 67 p.
8. CER. 2007. *Demand-side management and smart metering.* Consultation paper prepared by Irish Commission for Energy Regulation. CER 07/038. 13th March, 2007.
9. FERC. 2005. *Principles of effective and reliable reactive power supply and consumption.* Staff Report prepared by Federal Energy Regulatory Commission. Docket No AD05-1-000. February 4, 2005. 175 p.
10. LUND, H., SALGI, G. 2009. The role of compressed air energy storage (CAES) in future sustainable energy systems. In *Energy Management and Conversion*, May 2009, p.1172–1179.
11. KIM, Y.M., FAVRAT. 2010. D. Energy and energy analysis of a micro-compressed air energy storage and air cycle heating and cooling system. In *Energy*, January 2010, p. 213–220.
12. European Commission, Directorate-General for Research. 2006. *European Smart Grids Technology Platform: vision and strategy for Europe's electricity networks of the future.* Luxembourg, 2006. 37 p.
13. North American Energy Reliability Council (NERC), 2007-2. *NERC data collection for demand-side management for quantifying its influence on reliability*. December 2007, 57 p.
14. Frontier Economics. 2005. *Benefits and practical steps towards the integration of intraday electricity markets and balancing mechanisms.* A report prepared Frontier Economics Ltd and Consentec for the European Commission. London. December 2005. 100 p.
15. DAVIS, M.W. 1978. A new thermal rating approach: The real-time thermal rating system for strategic overhead conductor transmission lines. In *IEEE Trans. Power App. Syst.*, Vol. PAS-96, No. 3, March 1978, p. 803–809.
16. ORESCHNICK, P. 2007. Dynamic rating allows more wind generation. In *Transmission and Distribution World*, November 2007, p.p.58-64 (in special supplement *Digital Transmission*).

17. KLEMENTAVIČIUS, A. Future approach to momentary interruptions in distribution networks. Paper presented at XVII International conference "Electromagnetic Disturbances 2007", 19-21 September 2007, Bialystok, Poland, p. 4.2-1 – 4.2-6.
18. BUSH, R. and MUSSER, P. 2005. Focus on efficiency. In *Transmission and Distribution World*, February 2005. p. 44–49.
19. WOLF, G. 2007. The road to assets management. In *Transmission and Distribution World*, April 2007. p. 8–10 (in special supplement *Digital distribution*).
20. National Energy Technology Laboratory. 2007. *A systems view of the modern grid*. Report (white paper) conducted for the U.S. Department of Energy Office of Electricity Delivery and Energy Reliability, January 2007.

CYSENI 2012, May 24–25, Kaunas, Lithuania
ISSN 1822-7554, www.cyseni.com

BANDWIDTH CALCULATION OF SHORT RANGE COMMUNICATION VEHICULAR NETWORK

E. Petersons, N. Bogdanovs
Riga Technical University
Lomonosova iela 1, LV-1019 Riga – Latvia
Phone +37129727288
E-mail: meistars86@inbox.lv

ABSTRACT

As we know, high bandwidth wireless local area networks are gaining popularity. This paper offers a cyclic model of a wireless vehicular network and presents a bandwidth calculation of each network node. When assessing the performance of a wireless LAN, it is especially important to consider how this LAN will be used. When analyzing wireless networks, there arises a need to evaluate the whole network or a part of it. Whole Vehicular network, discussed in this work, consist of three layer networks. When analyzing wireless networks, the theory of queues net is used. During the research involving analytical methods, wireless network performance characteristics of various types were assessed.

In fact, the cyclic model was developed which is applicable to determine data transfer rate depending on the number of moving objects in the area of the wireless base station. In this article it was found that bandwidth of depending on the distance to the base station. Buzen's method was used for the cyclic closed network IEEE 802.11n performance calculation.

Result of experiments, the mathematical models for cyclic Vehicular wireless networks were selected as the ones to be used for choosing an optimal method of performance evaluation for Short range Vehicular communication network.

Keywords: (Cyclic model, Buzen's method, Vehicular network, IEEE 802.11n)

1. INTRODUCTION

Vehicular networks are a novel class of wireless networks that have emerged thanks to advances in wireless technologies and the automotive industry. Vehicular networks are spontaneously formed between moving vehicles equipped with wireless interfaces that could be of homogeneous or heterogeneous technologies [1].

Vehicular network can be deployed by network operators and service providers or through integration between operators, providers, and a governmental authority. Recent advances in wireless technologies and the current and advancing trends in ad hoc network scenarios allow a number of deployment architectures for vehicular networks, in highway, rural, and city environments [3].

The standard IEEE802.11p enables a wireless access to vehicular environment. 802.11p functions in the 5.9 GHz range; this technology permits access to navigational options, multimedia information and also telemetry. For design of a wireless network that would work by 802.11p standard, more expensive equipment is required than for other IEEE wireless network standards like IEEE802.11n. The significant improvement of 802.11n standards comparing to previous standards is the raw data rate of the wireless channel up to 600 Mbps – more than twenty-fold improvement over 27 Mbps of IEEE802.11p maximum data speed.

Goodput is the application level throughput, delivered by the network to a certain destination, per unit of time. The amount of data considered excludes protocol overhead bits as well as retransmitted data packets.

In this article a mass service Markov networks (queue networks) model is researched.

For start, let's define the most important designations for mass service theory [10].

Every system of mass service is defined by three main parameters:

- Distribution of time interval probabilities between two incoming queries.
- Distribution of service time probabilities.
- Control method of each following waiting time.

2. CYCLIC SYSTEM MODEL

An approximation of received experimental data leads to conclude that base station’s packet processing intensity is not a constant value. The base station’s packet processing intensity is a function of [vehicles] distance till base station as it is shown in Fig.1.

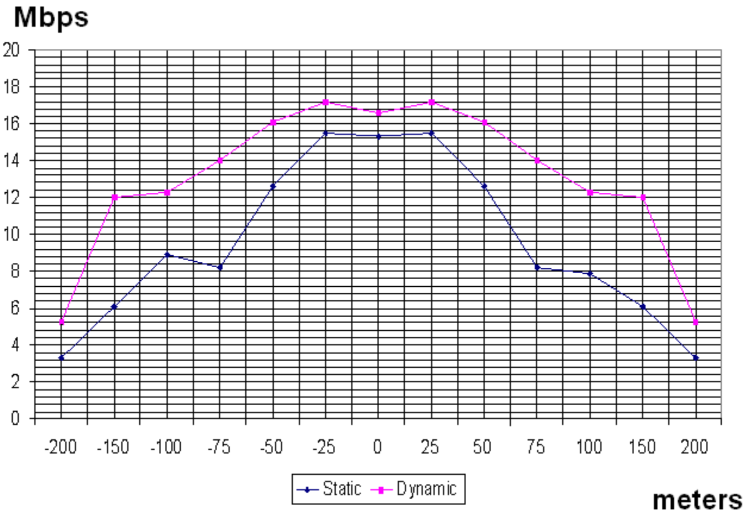

Fig. 1. Experimental goodput in wireless network with one router depending on distance to the mobile client in the stationary and dynamic modes

Let’s investigate a closed network which consists of M independent nodes with N incoming queries. Distribution is exponential with the parameter μ_i According to this research the speed of vehicle movement on highway is characterized by density. The placement of vehicles per meter [1, 2]:

$$\vartheta = \vartheta_0 \left(1 - \frac{k}{k_C} \right) \tag{1}$$

Where, k_c – maximal permissible flow rate, k – flow rate, and ϑ_0 – initial vehicular movement flow rate. Let’s assume that the area of interaction between vehicles and base station can be divided into M intervals. Let’s provide a number of trespassing vehicles per second for each interval according to query intensity and processing. If the interval length equals S_i, and vehicle movement speed equals ϑ_i, then the intensity of vehicle service by road interval equals [6, 7]:

$$\mu_i = \frac{\vartheta_i}{S_i}. \tag{2}$$

Vehicles pass all M intervals successively, and the total number of vehicles in the base station’s range of operation is N [8]. Entering the base station’s range of operation from the zero state (a lack of connection with the station) the vehicle finds itself in the zero state again. Such a system can be described in a form of a closed cyclic mass service system network with M service devices, N queries and exponentially distributed service time. Query service intensity in the i-th interval equals μ_i, as show in Fig. 2.

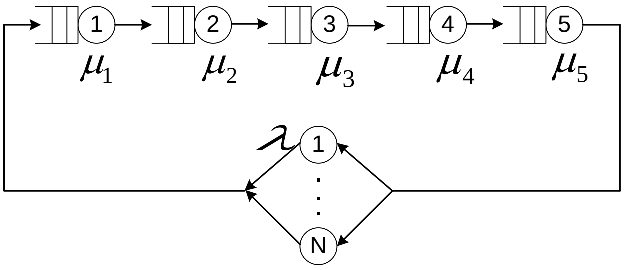

Fig. 2. Closed cyclic system

N vehicles are entering the base stations operating zone, with initial velocity of zero after that velocity grows exponentially [9], as show in Fig. 3 and Table 1.

$$\vartheta_i = \vartheta_o (1 - e^{-\alpha r}) . \tag{3}$$

Where r – distance to base station, ϑ_0 – 60km.h.

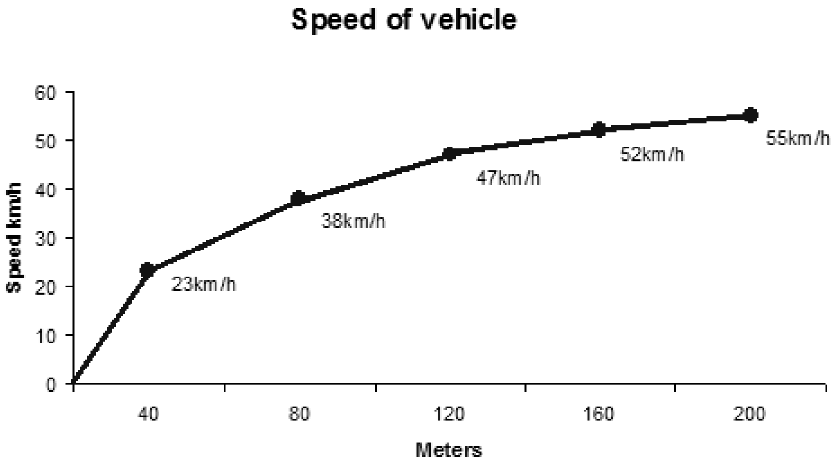

Fig. 3. Speed of vehicle

Table 1. Vehicle speeds

i	Zone 1	Zone 2	Zone 3	Zone 4	Zone 5
m	40	80	120	160	200
ϑ_i	$60\left(1-e^{-0.01275\cdot 40}\right)=23.97$	38.364	47	52.198	55.315
μ_i	$\mu = \frac{\vartheta}{S} = \frac{23970}{3600\cdot 40} = 0.166$	0.266	0.326	0.362	0.384

Due to the periodic nature of this model $x_1 = 1$ and the next step is calculated as following:

$$x_2 = \frac{\mu_1}{\mu_2}, x_3 = \frac{\mu_1}{\mu_3}, \ldots, x_M = \frac{\mu_1}{\mu_M} \tag{4}$$

In closed networks of queues, and provide a technique that can be implemented as a computer program. Then probability of query (vehicle) distribution among service devices (road intervals):

$$P_{n_1,\ldots,n_M} = \frac{1}{G(N)} \cdot \frac{\mu_1^{N-n_1}}{\mu_2^{n_2} \cdot \mu_s^{n_s} \ldots \mu_M^{n_M}} \tag{5}$$

Where G(N) – normalizing constant, μ - intensity of vehicle service, resulted from adding up and equating to one all probabilities or by Buzen's method [3].

Vehicle service intensity will depend as from initial velocity at entering the road segment as from the density of vehicle placement on this segment.

In the practical results we will calculate the base station performance at variable client count. In our case the 200m long base station operational zone is divided to 5 zones, 40 meters each, the third zone being the most adjacent to the base station, as it is show in Fig. 4.

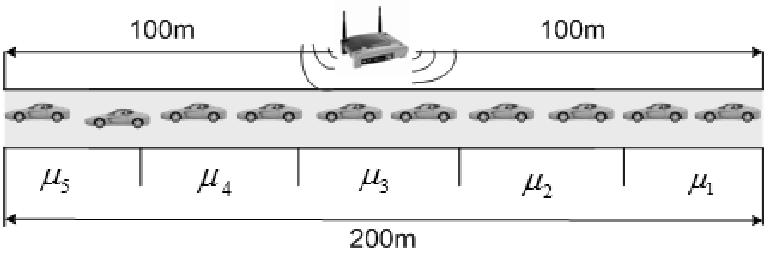

Fig. 4. 200 meter segment consisting of 5 zones

Convolution algorithm (Buzen's algorithm) – one of the most effective methods for closed network analysis, as show in Table. 2. Its name depicts the method of estimating the normalizing constant $G(N)$ from $F_i(k_i)$ that is analogous to convolution of two probability functions[4].

$$G(k,n) = \sum_{j=0}^{k} F(j,n)G(k-j,n-1) \tag{6}$$

$k = 0\ldots K$, $n = 1\ldots N$ then if $n = 1$, $G(k,1) = F(k,1)$.

Estimation of $G(k,n)$ is shown at Fig. 5.

$$\left[\begin{array}{ccc|ccc}
1 & \cdots & G(0,n-1)F(k,n) & 1 & \cdots & 1 = G(1) \\
F(1,1) & \cdots & G(1,n-1)F(k-1,n) & G(1,n) & & \\
\vdots & & \vdots & \vdots & & \vdots \\
F(k-1,1) & \cdots & G(k-1,n-1)F(1,n) & \sum G(k-1,n) & & \\
F(k,1) & \cdots & G(k,n-1)F(0,n) & \rightarrow G(k,n) & \cdots & G(k,N) = G(k) \\
\vdots & & & \vdots & & \\
F(K,1) & \cdots & & G(K,n) & \cdots & G(K,N) = G(K)
\end{array}\right]$$

Fig. 5. Convolution matrix

Algorithm for the Matlab is shower in Fig. 6:

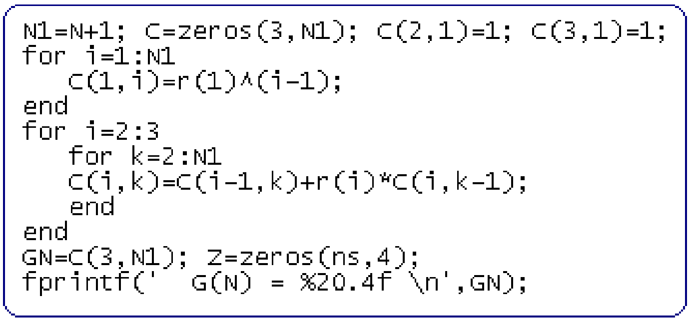

```
N1=N+1; c=zeros(3,N1); c(2,1)=1; c(3,1)=1;
for i=1:N1
   c(1,i)=r(1)^(i-1);
end
for i=2:3
   for k=2:N1
   c(i,k)=c(i-1,k)+r(i)*c(i,k-1);
   end
end
GN=c(3,N1); z=zeros(ns,4);
fprintf('  G(N) = %20.4f \n',GN);
```

Fig. 6. Buzen’s algorithm for Matlab

Table 2. Buzen’s matrix

N	x_1	x_2	x_3	x_4	x_5
0	1	1	1	1	1
1	1	1.624	2.133	2.592	3.025
2	1	2.013376	3.099073	4.288801	5.598626
3	1	2.25634662	3.83377478	5.80233444	8.2265395
4	1	2.407960290	4.35935165	7.022623161	10.584714765
5	1	2.50256722	4.72147721	7.94486124	12.52804273
6	1	2.56160195	4.96483385	8.61152516	14.03616766
7	1	2.62142632	5.125540046	9.078230094	15.155890691
8	1	2.59843961	5.2303262	9.39723381	15.95973448
9	1	2.63577002	5.29800606	9.61133638	16.52190141
10	1	2.644720492	5.341405577	9.753008975	16.906992285

The probability of ith road segment being busy is expressed by equation:

$$P\{n_i \geq 1\} = x_i \frac{G(N-1)}{G(N)}. \tag{7}$$

3. ESTIMATION OF DATA TRANSFER

We will build a network with the first node we represent vehicles generating packets for processing in base station [5].

Average number of moving vehicles, competing for resources of base station is calculated in this manner:

$$E[n_i] = \sum_{K=1}^{M} (x_i)^K \cdot \frac{G(N-k)}{G(N)}. \tag{8}$$

Depending from vehicles distance from base station, packet processing rate and packet processing rate in base station will be different. Each vehicle in sub-zone can exchange packets with base station with intensity λ. The β for ith region is obtained from measurement results as illustrated in Fig. 1, estimated as time spent travelling vehicle’s location to access point. This is packets service intensity in access point, when vehicles are located in ith zone.

Using the $\mathrm{M/M/1//N}^{i}$, model for every sub-zone *i*, we find the probability of base stations idleness [9]:

$$P_0(i) = \left[\sum_{k=0}^{E(n_i)} \left(\frac{\lambda_i}{\beta_i} \right)^k \frac{E(n_i)!}{(E(n_i)-k)!} \right]^{-1} . \tag{9}$$

Goodput of a station providing service for the region i can be obtained from this formula and can be seen in the Fig. 7:

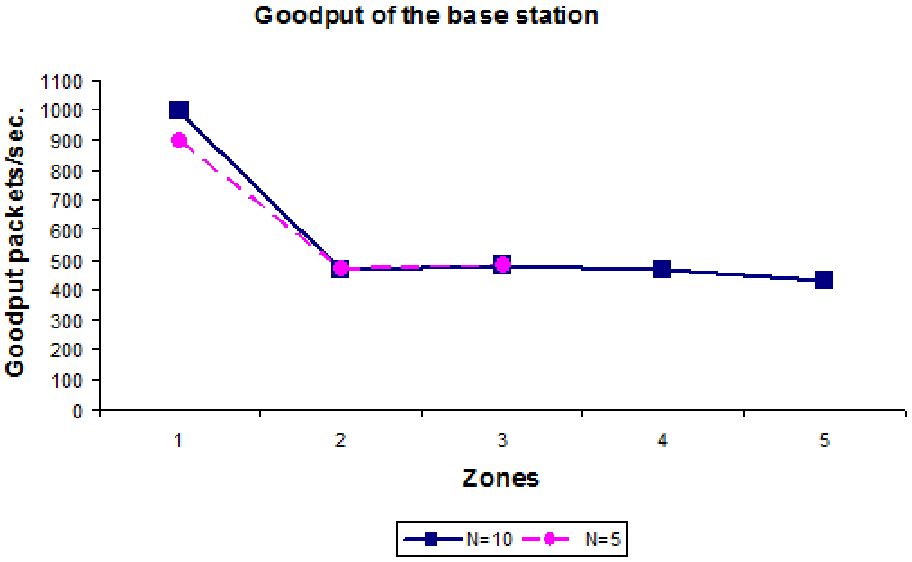

Fig. 7. Goodput for moving vehicles at N=5 and N=10

Goodput for zone *i:*

$$\eta_i = (1 - P_0(i))\beta_i . \tag{10}$$

Summary goodput for 802.11n at N=10 will be:

$$\eta = \sum \eta_i = 3244 \frac{packets}{\text{sec.}}$$

This way the performance of base station is revealed to be connected with traffic parameters as well as with the characteristics of base station to vehicle data transfer system.

CONCLUSION

In this research experimental data is presented, about data transfer rate in wireless networks of IEE802.11.n standard connecting moving objects. Based on the experimental data mathematical patterns were developed binding characteristics of vehicular flow with characteristics of data transfer system. The work presented a simple scheme to compute the maximum goodput of IEEE802.11n for cyclic system network, which the most popular in vehicular network at the moment.

Based on the received data a conclusion can be made that base stations performance appears to be connected as with traffic parameters as with parameters of data transfer system.

In the given research model real data transfer rate estimation was developed, considering the dependence from the number of moving objects located in base stations operational zone. As can be seen in Fig. 7, the data transfer rate on the first road segment with 5 vehicles is 900 packets per second, and 1000 packets per second with 10 vehicles. In the four other road segments data transfer rate is approximately 455 packets per second, this is influenced by vehicle distribution that in turn depends from the vehicle speed. Proceeding from these results, real data transfer rate will depend from the number of objects interacting with base station and their distance from this station.

RFERENCES

1. Gunter Belch, Stefan Greiner, Hermann de Meer, and Kishor S. Trivedi – *Queueing Networks And Markov Chains Modeling and Performance Evaluation with Computer Science Applications*. J. Wiley & Sons. Ltd – 1998.
2. Ipatovs A., Petersons E. *Performance Evaluation Of WLAN Depending On Number Of Workstations And Protocols* // Electronics and Electrical Engineering. – Kaunas: Technologija, 2006. – No. 3(67).
3. D. Gross, J. Shortle, J. Thompson, C. Harris. *Fundamentals of Queuering Theory*. Willy. 2008. 500 p.
4. L. Kleinrock. *Queuing Systems,* John Wiley & Sons Ltd. 1975. 600 p.
5. B.R. Haverkort. Performance of Computer Communication Systems. A Model-Based Approach. John Wiley & Sons Ltd. 1999. 495 p.
6. Jing Zhu, Sumit Roy. "*MAC for Dedicated Short Range Communications in Intelligent Transport System.*" IEEE Communication Magazine, December 2003. p. 60–67.
7. A. Ipatovs, E. Petersons. „*Performance Evaluation of WLAN depending on number of Workstations and Protocols*". Proceedings of International Conference Electrical and Control Techologies,. 2006. 266. – 270 p. ISSN 9955-25054-2.
8. A. Ipatovs, E. Petersons. „*An Experimental Performance Evaluation of the Wireless Network for Mobile Users*". Electronics and electronical engineering, 2009. No. 5(93). p. 21–24. ISSN 1392-1215
9. Х. Иносэ, Т. Хамади. „*Управление дорожным движением*". М. Транспорт 1983 г. 248 с.
10. D. Gross, J. Shortle, J. Thompson, C. Harris. *Fundamentals of Queuering Theory*. Willy. 2008. 500 p.

CYSENI 2012, May 24–25, Kaunas, Lithuania
ISSN 1822-7554, www.cyseni.com

ROOM CLIMATE CONTROL SYSTEMS RESEARCH USING PID CONTROLLER PARAMETERS

A. Klūga, R.Beļinskis, A. Krūmiņš[2]
Riga Technical University
Lomonosova iela 1, LV-1019 Riga – Latvia
Institute of Heat, Gas and water technology [2]
Azenes street 16/20, Riga, Latvia
Phone +37128804978
E-mail: romano1@inbox.lv

ABSTRACT

This paper describes control applications for air handling systems commonly found in rooms climate control. The basic processes such as heating, cooling and ventilation are presented individually then combined into typical air handling systems.

HVAC systems in buildings must be complemented with a good control scheme to maintain comfort under any load conditions. Efficient HVAC control is often the most cost effective option to improve the energy efficiency of a building. However, HVAC processes are nonlinear, and characteristics change on a seasonal basis so the effect of changing the control strategy is usually difficult to predict.

The use of optimization and adaptation principles in regulation systems permits to construct the most modern automatic room climate control systems. However, under different conditions systems can produce different results, so developers face a new challenge – a choice of the most effective adaptation method under certain circumstances. This task of method choice was solved by a dynamic modulation in Simulink MatLab environment that produces many detailed characteristics of algorithm choice, by simulating operating regulators.

Process control is an efficient expression of improving the operation of a process, the productivity of a plant, and the quality of products.

The paper proposes a simple and fast method for calculating the parameters of PID controller, using the results of the calculation, by experience, can quickly and almost certainly set the parameters of PID controller and display system for stable operation and the required level of climate control in the room. It is important for engineers who serve the system is already working HVAC.

Standard PID-regulator was included in the research model.

Keywords: (Room temperature, PID regulator, Simulink MatLab)

1. INTRODUCTION

HVAC systems in buildings must be complemented with a good control scheme to maintain comfort under any load conditions. Efficient HVAC control is often the most cost effective option to improve the energy efficiency of a building. However, HVAC processes are nonlinear, and characteristics change on a seasonal basis so the effect of changing the control strategy is usually difficult to predict.

Process control is an efficient expression of improving the operation of a process, the productivity of a plant, and the quality of products. Nowadays, the demand for accurate temperature control and air ventilation control has conquered many of industrial domains such as process heat, alimentary industry, automotive, industrial spaces or office buildings where the air is cooled in order to maintain a comfortable environment for its occupants. One of the most important problems involved in heat area consist in the desired temperature control and consumption optimization.

A modern process control system is often structured as shown in Fig. 1. As illustrated in this figure, sensors and actuators are connected to controllers via control networks. A sensor provides measurements and status of a physical property, e.g. the flow in a pipe associated with the process. Based on the measurement from sensors, the controller determines any adjustment in the actuators that is needed to maintain the process at a target value [2].

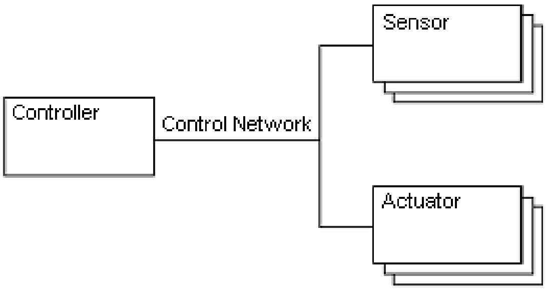

Fig. 1. Control system structure

2. THE STANDART PID ALGORITHM

PID is the most widely used control algorithm in industrial process control. As shown in Fig. 2, the controller compares the process variable (PV) with a reference setpoint (SP). The error is then processed to calculate a new output to bring the PV back to its desired SP. PID stands for “proportional, integral and derivative” components of the algorithm. Each of the three components performs a different task and has a different effect on the functioning of a system. Their outputs are summed up to produce the system output.

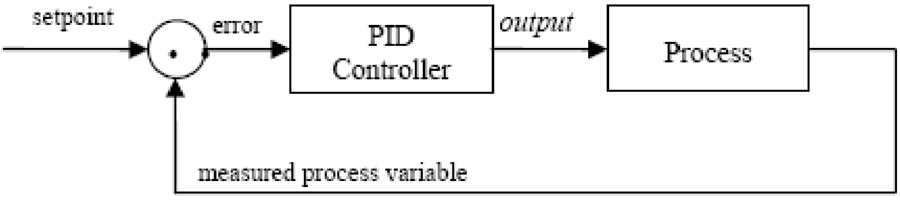

Fig. 2. Control algorithm in industrial process control

It is often advantageous to make a comparison with the open-loop system, since that shows what would happen using the simplest kind of control. Indeed, the open loop requires no sensors (for example temperature, pressure, humidity etc.) and is thus much less costly to build and maintain than the PID system. If the PID system did not perform so much better, it might not be worthwhile [3].

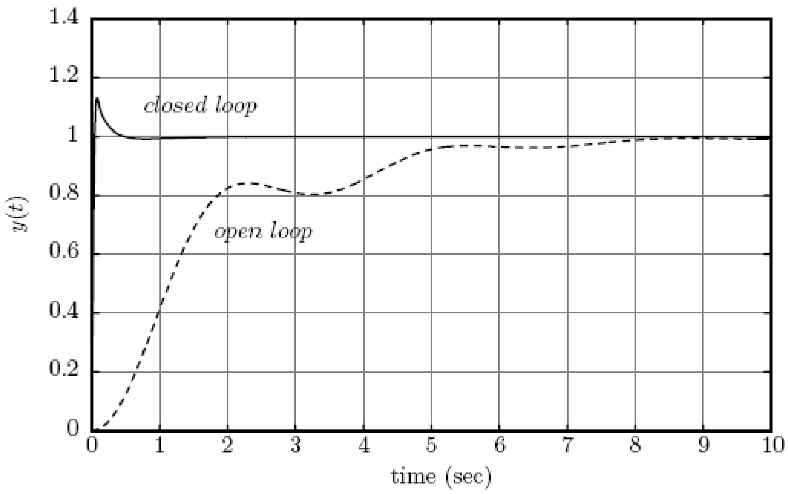

Fig. 3. Step Response for PID and Open-Loop Systems

Though there are many variations of PID algorithms, in its non-interacting form without rate limiting and all actions based on error, the equation for standard PID algorithm is:

$$Output = Kp\left[e(t) + K_I \int e(t)d(t) + K_D \frac{de(t)}{dt}\right] \tag{1}$$

Where KP, KI and KD are the proportional, integral and derivative gains, respectively. E(

In its digital form, the software implementation of the PID algorithm is based on the sampled data for its PV (process variable) being provided on a periodic basis. e(t) in Fig. 3 means number of errors during the reaction system.

3. DYNAMICS OF AIR-HEATING SYSTEM

To explore the application of PID controllers to the room temperature control system, we highlight consider a single-zone heating system, as shown in Fig. 4. In general, since the responses of the AHU (air handling unit) are faster than those of the controlled room, the dynamics of the AHU may be neglected for all practical purposes. Thus, as will be seen later, this rough assumption may be fairly validated. The model, however, possesses the important elements (the controlled room and the AHU) to analyze the air-heating system.

With this system, the room air temperature is measured with temperature sensor. The output signals from the sensors are amplified and then fed back to the PID controllers. Using the errors defined as the differences between the setpoint value (θ_0) and the measured values of the controlled variables (θ), the PID controllers generate the control inputs for the actuators (the supply air damper) so that the errors are reduced. The AHU responds to the control inputs (fs) by providing the appropriate thermal power to the supply airflow it means there are another actuator – i.e. heating coil valve and we have double action. Air enters the AHU at a warm temperature, which increases as air passes the heating coil.

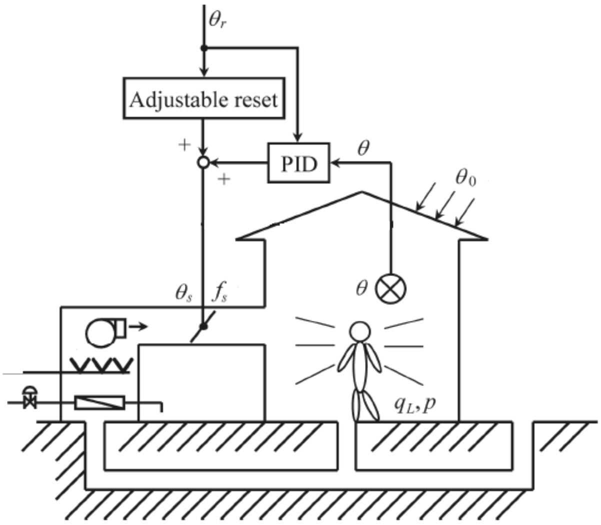

Fig. 4. Overall structure of a single-zone heating system

4. ROOM TEMPERATURE CONTROL MODEL

Simplifying this thermal system to be a single-zone space enclosed by an envelope exposed to certain outdoor conditions is of significant interest to treat the fundamental issues in control system design (Zhang 1992, Matsuba 1998, Yamakawa 2009). This simplified thermal system (the room temperature model) can be obtained by applying the principle of energy balance:

$$C\frac{d\theta}{dt} = w_s(\theta_s - \theta) + \alpha(\theta_0 - \theta) + \mathrm{q}_L \qquad (2)$$

where C – overall heat capacity of air space [kJ/ ºC],
α – overall transmittance room factor [kJ/min ºC],
q_L – thermal load from internal heat generation [kJ/min],
w_s – supply air flowrate [kJ/min K],
ρ – room density of air [kg/m3],
θ – room air temperature [ºC],
θ_0 – outdoor temperature [ºC],
θ_s – supply air temperature [ºC].

The physical model derived in Eqation 2 can be used for numerical simulations. The first term on the right-hand side is the heat gain which is controlled by the supply air flow rate. The second term is the heat gain through the room envelope, including the warm air infiltration due to the indoor-outdoor temperature differential. The third term is the thermal loads from the internal heat generation (people or items having a large specific heat). In this simplified model, any other uncontrolled inputs (e.g., ambient weather conditions, solar radiation and interzonal airflow, etc) are not considered. It should be noted that all variables such as θ, θ_0, θ_s, q_L and w_s in Equation 2 are obviously the function of a time t. For the research simplicity the time t is not presented, the time is constant. When realizing a digital controller, a deadtime exists between the sampling operation and the outputting time of control input, thus w_s, namely supply air flowrate, includes a deadtime.

5. PID TUNING

Ziegler-Nichols method:

Ziegler and Nichols developed technique for controller tuning in the 1940s. In our research we used this method, because it is the most common in HVAC to determine PID controller parameters for system. The idea was to tune the controller based on the following idea: make a simple experiment, extract some features of process dynamics from the experimental data, and determine controller parameters from the features. In this method, the open loop unit step response of the plant (the controller is disconnected from the system) is measured and approximated by small straight lines usually given a form as shown in Fig. 5. In HVAC used also CHR (Chien, Hrones and Reswick) method to determine parameters, but we will use this method to researc our system in featur.

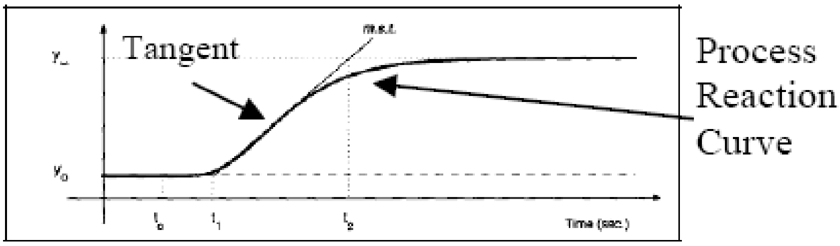

Fig. 5. Plant unit step response

The tangent, in the point of the curve where the first derivative receives its maximum value is drawn (point of inflection). The dτ, T and K parameters are calculated below:

delay time: $td=t_1-t_0$,

response time: $T=t_1-t_0$.

gain
$$K=\frac{y_\infty-y_0}{u_\infty-u_0}$$

where *u* is action time.

The rules of Ziegler- Nichols method for the extraction of PID parameters are as shown in (Table 1).

Table 1. Controller`s parameters by Ziegler- Nichols method

	Parameters		
Controller	K	K_i	K_d
P	$\frac{T}{K\tau_d}$		
PI	$\frac{0.9T}{K\tau_d}$	$\frac{\tau_d}{0.3}$	
PID	$\frac{1.2T}{K\tau_d}$	$2\tau_d$	$0.5\tau_d$

It has to be noted that a major disadvantage of the Ziegler-Nichols method for HVAC systems, is the undesired effect of oscillatory behaviour on a set of systems.

Relay Feedback:

The experiment used in the Ziegler-Nichols frequency response method, where the gain of a proportional controller is increased until the system reaches instability, gives the frequency ω180 where the process has a phase lag of 180° and the process gain K180 at that frequency. Another way to obtain this information is to connect the process in a feedback loop with a relay as shown in Fig. 6. For many systems there will then be an oscillation, as shown in Fig. 7, where the relay output u is a square wave and the process output y is close to a sinusoid. Notice that the process input and output have opposite phase and that an oscillation with constant period is established quickly [1].

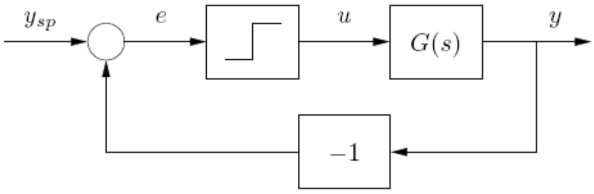

Fig. 6. Process in a feedback loop with a relay

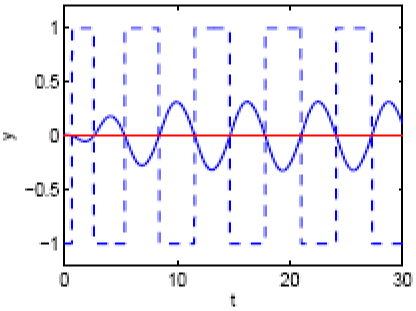

Fig. 7. Many systems oscillation

6. SIMULATION

This article created a simulation in which the input signal is the temperature in the room Fig.8.

As a mean of control, classic PID controller is used. To maintain the desired temperature in the room used actuators which meet the principles of building a system of regulation indoor climate.

System actuators include: the frequency inverter, which regulates the fan speed, the feed air into the room, the air valve to regulate the flow of air into the room and the heating coil, which carries out maintenance of necessary temperature heating of the room upon request.

This system meets the minimum requirements to maintain indoor climate. The transfer functions for actuators were chosen close to real design performances. [4].

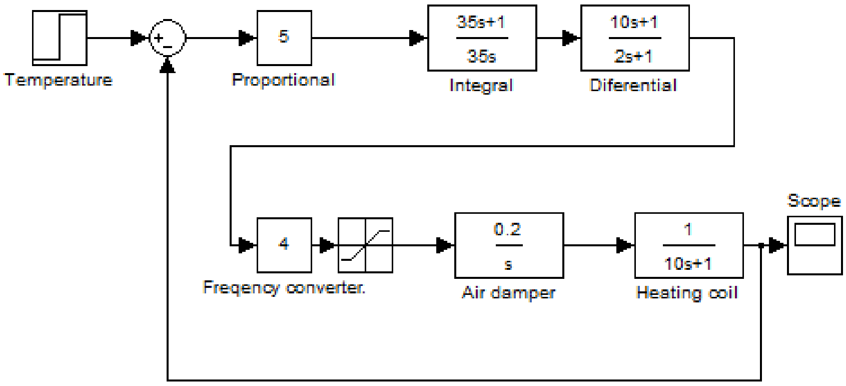

Fig. 8. Room climate simulation model

Changing the input parameters, the temperature of air supplied to the room with the calculation and selection of the coefficients of the PID controller led to a change of air supplied to the premises, as well as thermal energy. These changes, allows to maintain the desired room temperature 22ºC, when the request is for heating the room was administered when the temperature drops below 16ºC in the room. In the simulation carried out shows the reaction time for the stabilization of the system at the required level of temperature in the room, as well as the output of the system on a stable operation at different coefficients of PID. Thermal conductivity rooms and the influence of external factors in the simulation were not considered.

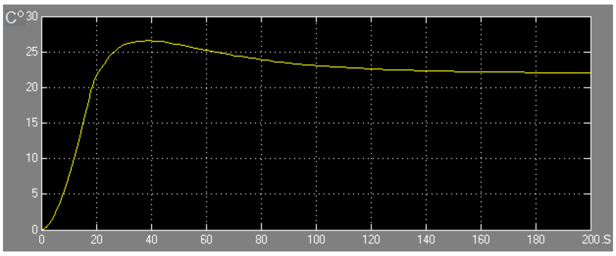

Fig. 9. PID characteristic of the process

As a result, we have simulated the temperature characteristic of the transition process. The graph shows that an arbitrarily chosen coefficients PID roughly similar to the characterization of the transition process, which is calculated by the Ziegler-Nichols method.

7. RESULTS

In the above model of the overshoot is 5%, which is a valid value. An experimental method we have achieved, what would a system without overshoot, this increased the integral coefficient Ti = 700s+1/700 and differential component decreased in 2 times Td = 5s+1/s+1.

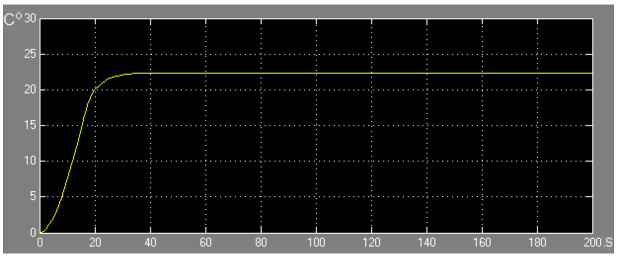

Fig. 10. PID characteristic of the process without overshoot

With an increase of the differential coefficient Td = 700s+1/140s+1, the system becomes less stable, the overshoot of the system increases and is 10%.

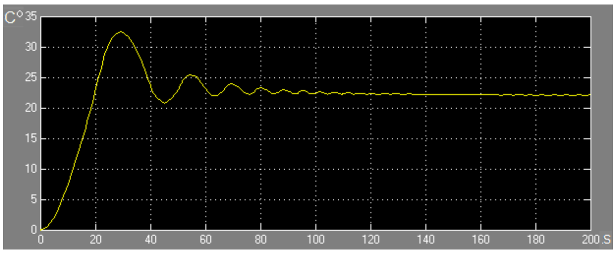

Fig. 11. PID characteristic of the process with overshoot

CONCLUSION

Research show the influence of the parameters of PID controller to work HVAC system as an example of temperature regulation in place, the results give us an idea of the system to maintain the required temperature at various selected parameters of the PID controller. The correct choice of the PID control parameters allows us to effectively manage the executive mechanisms that support the desired room temperature, which leads to a reduction in energy consumption and stable operation of the system as a whole. Was shown the fastest and most common method for tuning the parameters of PID (the Ziegler-Nichols method). There can be vast differences in the results produced by different tuning procedures. The quality of the tuning is very much dependent on the compatibility of the tuning method with the plant behavior and the performance goals (Fig 9 and Fig. 11).

RFERENCES

1. Karl Johan Aström, Richard M. Murray - *Feedback Systems*, Princeton University Press: 2008. – 396 p.
2. Åström. K. & Hägglund. T. “*PID controllers: Theory, design and tuning*”, Instrument Society of America,: 1995. – 164–166 p. and p. 96–198.
3. Raad Z. Homod, Khairul Salleh Mohamed Sahari, Haider A. F. Mohamed, Farrukh Nagi, *“Hybrid PID-Cascade Control for HVAC System”*, International Journal of Systems Control (Vol.1-2010/Iss.4). – Malaysia:, 2010. p. 170–175
4. Борисевич А.В. *“Теория автоматического управления: элементарное введение с применением MATLAB”* – Политехн. ун-та, 2011. – 200 с.

THE CONSTRUCTION OF LITHUANIAN HOURLY METEOROLOGICAL DATA FOR BUILDING ENERGY SIMULATION

P. Bruzgevičius, A. Burlingis, V. Stankevičius
Institute of Architecture and Construction of Kaunas University of Technology
Tunelio str. 60, LT-44405 Kaunas, Lithuania
Phone +37061463313
Email: patrikas.bruzgevicius@yahoo.com
v.stankevicius@ktu.lt., arunas.burlingis@asi.lt

ABSTRACT

In European Union, the energy consumption in buildings accounts for 40% of total energy consumption. This sector is expanding, which is bound to increase its energy consumption. Therefore, the reduction of energy consumption and the use of energy from renewable sources in the building sector constitute important measures required to reduce the Union’s energy dependency and greenhouse gas emissions. In order to construct the energy saving buildings („nearly zero-energy buildings“), it is necessary to evaluate the dynamics of climate impacts. Therefore, one of the goals is to compose the Lithuanian hourly dynamic reference meteorological year. For this reason, we have to analyze the principles of composition of the reference meteorological year and practices of this subject in other countries. According to LST ISO EN 15927-4, the reference (average) meteorological year has to be composed by using the hourly long-term database of essential climate parameters: dry bulb thermometer temperature (ºC), global solar radiation (W/m²), relative humidity of air (%) and wind speed (m/s). After construction the Lithuanian TRY will enhance the accuracy of prediction of thermal-hygric state of building envelopes. Also this model will allow to evaluate the impact of building‘s thermal inertia to average duration of heating season of building, energy use for heating and cooling, prediction of average date for beginning and ending of the heating season. It could be used in building design and modeling, scientific research.

Keywords: reference meteorological year

1. INTRODUCTION

In the countries of the European Union, energy consumption in the building sector accounts for 40 %. As this sector is expanding, the energy consumption increases resulting in the increase of greenhouse gas emissions. The reduction of energy consumption and the use of energy from renewable sources in the building sector are important measures which are necessary to reduce the EU’s energy dependence on the countries exporting energy feedstock and greenhouse gas emissions [1, 2].

When Lithuania joined the EU, according to the provisions of the Directive 2002/91/EC, the country has committed to increase the energy efficiency of buildings taking into account outdoor climatic and local conditions as well as indoor climate requirements and cost-effectiveness. This is being attempted through the implementation of energy-efficient buildings (nearly zero energy buildings) from 2020 [3] which would be designed in accordance with the provisions of the Intelligent Energy-Europe programme (IEE) [4]. Partly this can be done by optimizing the building envelopes. Seeking to achieve this objective, it is necessary to properly assess the dynamics of meteorological conditions that determine the proper selection of the building envelopes in order to ensure, with a certain confidence level, the microclimate categories of the building premises [5].

The design and selection of systems for heating, ventilation and air conditioning in our days are implemented by use of the software that models the microclimate of the building, parallely assessing the energy needs of the building. The dynamics of meteorological conditions affects the results of building modelling and design. But Building Climatology [6] of the Building Code of the

Republic 156-94 provides limited quantities of climatological parameter values. These climatological values are insufficient for accuracy assessment of the dynamics of meteorological conditions in the design and selection of heating and ventilation systems of the building.

Therefore, it is necessary to generate the Lithuanian Test Reference Year TRY. The annual model requires the hourly value of climatological parameters. This set of the basic climatological parameters will consist of the following values: dry-bulb air temperature (DBT), direct normal solar irradiance and diffuse solar irradiance on a horizontal surface (DSR), relative humidity (RH), wind speed (WSP) at a height of 10 m above ground. In some certain cases, such parameter values as the thickness of snow cover, soil temperature, CO and CO_2 concentration, particulate matter content, etc. would be necessary. Ongoing changes in the climatological parameter values have a significant impact on power of the heating and ventilation systems, duration of the heating season and for energy costs.

2. THE EVOLUTION OF DYNAMIC STANDARD CLIMATE

The annual model of the climatological parameter values of the Test Reference Year (TRY) for the calculation of the building energy demand is composed of 365 days that consist 8760 hours. The rates of these parameter values must be close to the multi-annual average values. Over the past 50 years several annual models of this type were proposed throughout the world.

One of the first arrays of climatic parameter values Test Reference Year (TRY) was generated in North America in 1976. It was constructed by the National Climatic Data Center (NCDC) for building simulation and energy calculations, but the source data of this standard model TRY did not contain the climatic parameter values of solar radiation. The selection of method was the main problem for the construction of the standard array TRY. The selected method distinguished the years with the most extreme values of the months which have maximum or minimum average monthly temperature values. The selection principle was based on the rejection of years with the highest and lowest average monthly temperature until the last one year remains. After the selection of months in accordance with the method described above, the array of 12 months is formed which became „Historical Climatology Standard“ for the 1948-1975 period. The data of the standard annual model array (TRY) are published and describe the synoptic situations of 60 areas in the USA [7, 8].

New climatic parameter values were introduced in 1981, the array of Typical Meteorological Year (TMY) was constructed. This array was constructed by the joint forces of laboratories, the National Climatic Data Center (NCDC) and Sandia National Laboratory (SNL). The array of climatic parameter values of TMY consists of 12 typical meteorological months. Typical meteorological months (TMMs) were selected from the multi-year climatic values of the 1952-1975 period [9, 10]. This statistical analysis method is based on four climatic parameters: dry bulb thermometer temperature, dew point temperature, global solar radiation on a horizontal surface, and wind speed values. Actual solar radiation values of the USA are given from only 26 meteorological observation stations, and values of this parameter were recalculated for other 208 meteorological stations by evaluating the type of cloud, and its duration. The months were selected in accordance with the complex Finkelstein-Schafer statistical method [13], by evaluating the coefficients of different weighting factors for the climatic parameter values: total solar radiation of respective month -12/24; dry bulb thermometer temperature of respective month, dew point temperature and wind speed values – 2/24; maximum and minimum daily dry bulb thermometer temperature, dew point temperature value -1/24. The calculated rates of values of selected months with weighting factors were close to the multi-annual observational values. Thus, the TMY array consists of arrays of selected different months. Later, the TMY array was updated with new versions TMY2 [11] of the National Renewable Energy Laboratory (NREL) with new 1961-1990 period characterizing the synoptic situations of 239 areas in the USA. National Solar Radiation Data Base NSRDB developed

TMY3 [12] array with new periods: 1976-2005 30 years, 1991-2005 15 years, 1998-2005 8 years. These versions updated and combined periods of the TMY arrays which characterize the synoptic situations of 1400 areas in the USA.

In 1985 American Society of Heating, Refrigerating and Air-Conditioning Engineers (ASHRAE) approved the research work for development of a set of climatic parameters - Weather Year for Energy Calculations (WYEC), which is intended for building energy calculations. This climate model was designed by using the hourly values of climatic parameters of the 30-year period [14].

The essence of the method is appropriate data selection for WYEC formation. It is necessary to assess each month of the year as the actual month with hourly climatic parameter values, the average dry bulb thermometer temperature value of which would be the closest to the average temperature of that month during the 30-year period. If the average monthly temperature value differs on 0,1 ºC value from the multi-year observational average values, single days of this month of the next year are adopted, so that deviations from the average multi-year temperature value would not exceed the value of 0,1 ºC. (9) The month selected in this way will have the climatic parameter values of the days of that month but of different years. The WYEC data were prepared in 51 North American locations, 46 locations in United States and 5 in Canada. [15] Later, NREL updated the set of data array WYEC of the climatic parameter values by creating a new version of the climatic data model WYEC2 [16].

The array of the climatic parameter values of Canadian weather for energy calculations (CWEC) consists of 12 typical meteorological months. The months were selected in accordance with the complex Finkelstein-Schafer statistical analysis method, as with the TMY method but only evaluating the coefficients of different weighting factors in determining the climatic parameter values. The climatic parameter values measured in 145 meteorology stations were used for the construction of the Typical Meteorological Year TMY model. (17)

The array of the climatic parameter values of the International Weather for Energy Calculations (IWEC) consists of typical meteorological months selected from the 1982–1999 period and characterizes the climatic conditions in 227 locations in the USA and Canada. The months were selected in accordance with the complex Finkelstein-Schafer statistical analysis method and by evaluating the coefficients of different weighting factors in determining the climatic parameter values [18, 19].

In 2005, according to LST EN ISO 15927-4:2005 (Hygrothermal performance of buildings - Calculation and presentation of climatic data - Part 4: Hourly data for assessing the annual energy use for heating and cooling) [20], the Test Reference Year (TRY) model (pattern) is intended for calculating of the annual energy consumption of a building. This TRY model is similar to the TMY model. Climatic, dry bulb thermometer temperature, solar radiation, relative humidity and wind speed parameter values are relevant to the model construction. TRY model includes the months with the least deviations from the average values, the characteristic month is selected according to the statistical rate value FS [13, 20]. International standard recommendations on development of the TRY model in each case are evaluated individually. It depends on climatic conditions, specific terrain defined by geographical latitude, longitude, as well as terrain altitude above sea level, building type, the accuracy of measuring the multi-year climatic parameter values during observations in meteorological stations and the duration of data capture period.

TRY model is developed in Italy, France, United Kingdom, Ireland, Belgium, The Netherlands, Denmark, Portugal, constructed under the rules in force in the European Union. With the small differences for TRY model construction applied in Turkey, Russia, Slovakia, Slovenia [21].

Some countries of the world present their own standard climate construction methods in addition to the above reviewed.

Joseph C. Lam developed the Typical Meteorological Year TMY pattern for Hong Kong. The TMY model is constructed for the 16-year period (1979-1994). The principle of the TMY model construction differs from the original TMY developed by the joint forces of laboratories, the National Climatic Data Center (NCDC), Sandia National Laboratory (SNL), as they have differences in monthly statistical sampling procedures. The TMY model was designed by using the hourly values of climatic parameters and the nonparametric Kolmogorov-Smirnov test, but not the average climatic parameter values and the Finkelstein-Schafer test. [22].

Currently, Lithuania has no standard dynamic climate model for the energy cost prediction, building design by simulation, duration of the heating season, selection of power of the heating and ventilation equipment.

3. CLIMATIC ZONING IN LITHUANIA AND METEOROLOGICAL DATA

The territory of Lithuania is located in the climatic zone of middle latitudes and, according to the B. Alisovas‘ classification of climates, is attributed to the south-western sub-area of the Atlantic continental forest area. Only the Baltic Sea coast climate is closer to the Western Europe climate and could be ascribed to the separate climate sub-area of the Southern Baltic (23). Due to the different distribution of climatic conditions, the territory of Lithuania is classified into four districts and ten sub-districts (Fig. 1). Each of these districts has its own dynamics of meteorological conditions. For this reason we have chosen the fifteen meteorological stations representing these sub-districts. The climate parameters recorded in these stations are going to be used for the construction of the Lithuanian TRY.

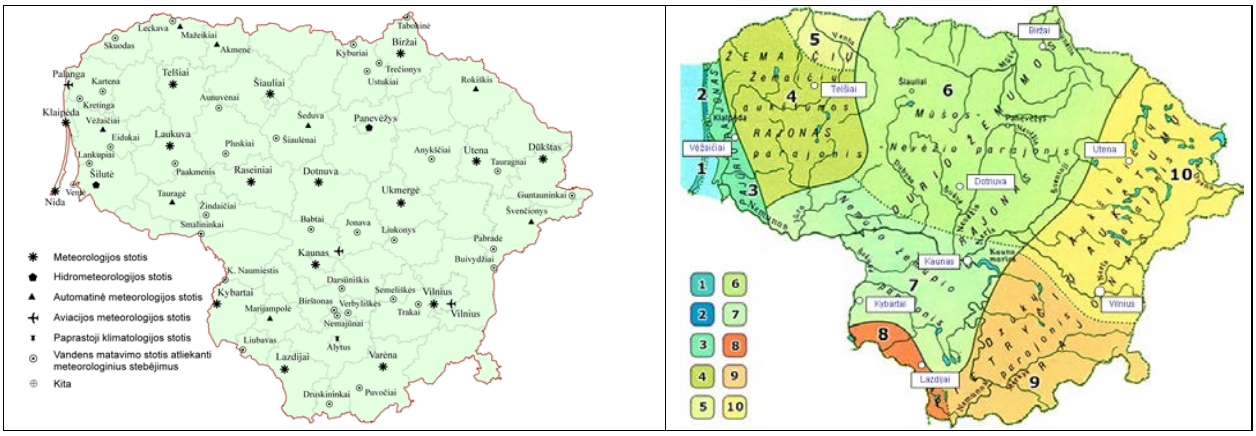

Fig. 1. Meteorological stations and climate zones of the territory of Lithuania

The data of sequences of the meteorological parameter values are statistically interdependent. The main subject of discussion is the period of observation of climatic values which evaluates those factors of statistical effects of recorded values which determine the statistical parameters values. According to the guidelines and recommendations of the technical regulation [24] of the World Meteorological Organization (WMO), the standard climatic norms are created for the 30-year period. Climatological data averages are calculated for the following consecutive periods of 30 years: from 1 January 1901 to 31 December 1930, from 1 January 1931 to 31 December 1960, from 1 January 1961 to 31 December 1990, from 1 January 1991 to 31 December 2020.

For the construction of the Lithuanian TRY, the 1961-1990 period of time equal to 30-year cycle is adopted in accordance with the provisions of the WMO. The construction of the Lithuanian TRY requires the main measured hourly values of climatic parameters: dry bulb thermometer temperature, air relative humidity, solar radiation, wind speed at a height of 10 m above ground (20). All the climatic data is provided by the Lithuanian Hydrometeorological Service.

The climatic parameter values of dry bulb thermometer temperature and air relative humidity, wind speed were recorded four times a day every six hours (01, 07, 13, 19) during the period from 01.01.1961 to 31.12.1965, during the period from 01.01.1966 to 31.12.1990 – eight times a day every three hours (00, 03, 06, 09, 12, 15, 18, 21). Actinometric observations of solar radiation in Lithuania have been performed since 1955 at Šilutė and Kaunas meteorological stations, six times a day every four hours (0.30, 6.30, 9.30, 12:30, 15:30, 18:30), at mean solar time. The hourly values of climatic parameters of direct solar radiation on the surface perpendicular to the direct beam, diffuse solar radiation and total solar radiation are recorded by the self-recording devices.

The construction of the TRY model requires the hourly values of climatic parameters characterizing the local meteorological conditions. In Lithuania, the hourly values of both total and diffuse solar radiation were measured only at Kaunas and Šilutė meteorological stations. Meteorological conditions correlate with each other, and for this reason, the city of Kaunas was selected as representing the average Lithuanian climate.

4. PRINCIPLE OF TEST REFERENCE YEAR

4.1. “Best” months to form the reference year

The test reference year has to be constructed according to the Standard LST EN ISO 15927-4:2005 [20]. The TRY for Kaunas is constructed by using the hourly values of climatic parameters p, where p is the dry-bulb air temperature (DBT), direct normal solar irradiance and diffuse solar irradiance on a horizontal surface (DSR), relative humidity (RH), wind speed (WSP) at a height of 10 m above ground. (20)

For each climatic parameter p, the values of daily average, $\overline{p}$ of are calculated from hourly values of the 30-year period (1961-1990). For each calendar month, the cumulative distribution function $\Phi(p,m,i)$ of the daily average parameter p is calculated by sorting all the values of the data set (total period) in.

For each year, from the data set, the cumulative distribution function $F\left(p,y,m,i\right)$ of daily means within each calendar month is calculated by sorting all the values for that month and that year in ascending order.

For each corresponding calendar month, the Finkelstein-Schafer statistic for parameter p, for each year of the data set is used Eq. (1):

$$F_S\left(p,y,m\right)=\sum_{i=1}^{n}\left|F(p,y,m,i)-\Phi(p,m,i)\right| \tag{1}$$

For each calendar month, the individual months are then ranked from the multi-year record in order to increasing size of $F_S\left(p,y,m\right)$

In the same order, for each calendar month and each year, there are separate categories of climatic parameters – dry bulb thermometer temperature, global solar radiation, relative humidity of air.

For each calendar month and each year, the separate ranks for the three climatic parameters are added.

For each calendar month, out of three months with the lowest overall rating, the wind speed deviation of the monthly average from the corresponding values of wind speed averages of multi-year calendar months is calculated. The month with the lowest wind speed deviation is chosen as the selected month. The month selected in this way is included into the composition of the standard year model of dynamic climate.

The calculation must be performed for each month and for each climatic parameter p, according to the following principle of the processing the stream of statistical data analysis.

4.1. The principle of the processing the stream of statistical analysis data

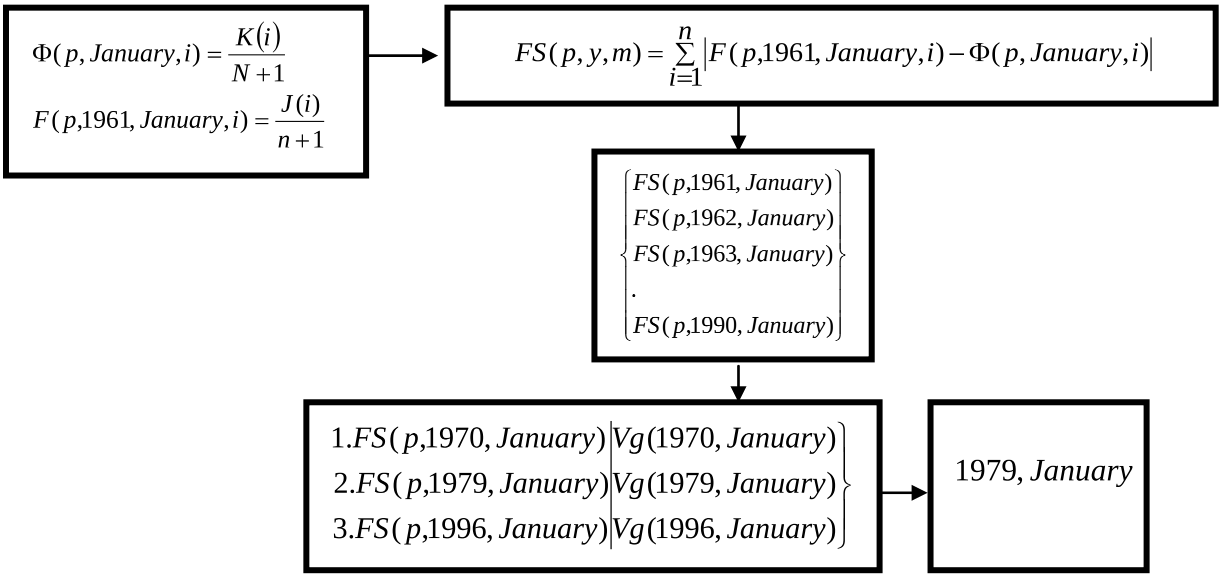

4.2 Smoothing between months

The hourly values of climatic parameters – air temperature and relative humidity – of selected twelve characteristic months must be evenly combined with each other in order to avoid a sudden drop of values between the end of one month and the beginning of another one. The wind speed and direction change during the day, the value of total solar radiation is equal to zero at midnight, therefore, the values of these climatic parameters between months are not being adjusted. The last eight hours of a month and the first eight hours of a day of the subsequent month are adjusted by linear interpolation, through the even distribution of the values between months. The cubic spline method can be applied in order to make the values of the climatic parameters between months more clear.

5. KAUNAS TEST REFERENCE YEAR

The construction of the TRY model requires the hourly values of climatic parameters characterizing the local meteorological conditions. These climatic data are submitted by the Lithuanian Hydrometeorological Service. The TRY model is constructed in accordance with the procedures introduced in Chapter 4.

Fig. 2 shows the DBT and RH values of climatic parameters in Kaunas: the day average values were calculated using the hourly values of the 1961–1990 period of time equal to 30 years.

In order to construct the standard climatic annual model, 12 months were selected in accordance with the Finkelstein-Schafer statistical method [13]. Also the distribution of general set of average cumulative function of parameter values is compared with the partial cumulative distributions, thus the differences in frequency of particular parameter values are determined.

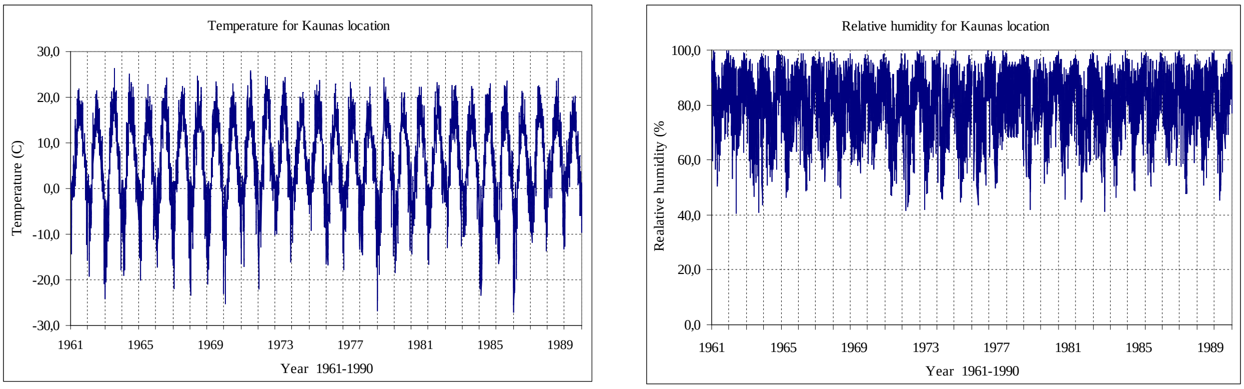

Fig. 2. Annual dry-bulb air temperature and relative humidity for Kaunas. The Figure on the left shows the air temperature and the figure on the right shows the relative humidity

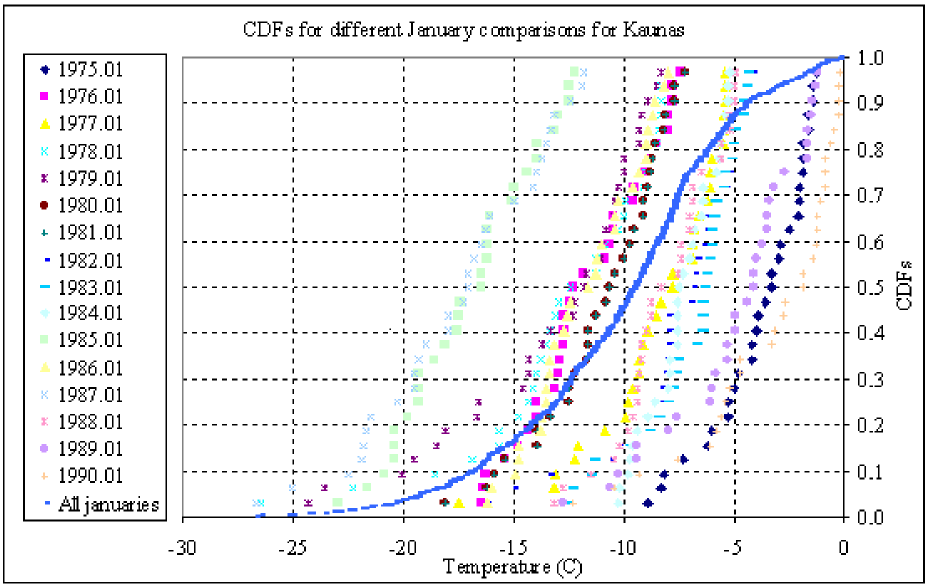

Fig. 3. CDFs for different January comparisons for Kaunas from 1975-1990 year of data set

Fig. 3 shows the principle of the selection process. The blue curve shows the 30 year daily average temperature data obtained from Kaunas Meteorological Station in January. The dotted curves show the variation of months over the cumulative distribution function curve. For each calendar month, out of three months with the lowest overall rating, the wind speed deviation of the monthly average from the corresponding values of wind speed averages of multi-year calendar months. The month with the lowest wind speed deviation is chosen as the selected month. The month selected in this way is included into the composition of the standard year model of dynamic climate.

Upon the selection of DBT and RH climatic parameters of twelve characteristic months, the hourly values must be evenly combined with each other in order to avoid a sudden drop of values between the end of one month and the beginning of another one. The Figures show the smooth consolidation between the months of January and February. The dotted blue line describes the measured values of climatic parameters, and the red one – the smooth consolidation of these values between months.

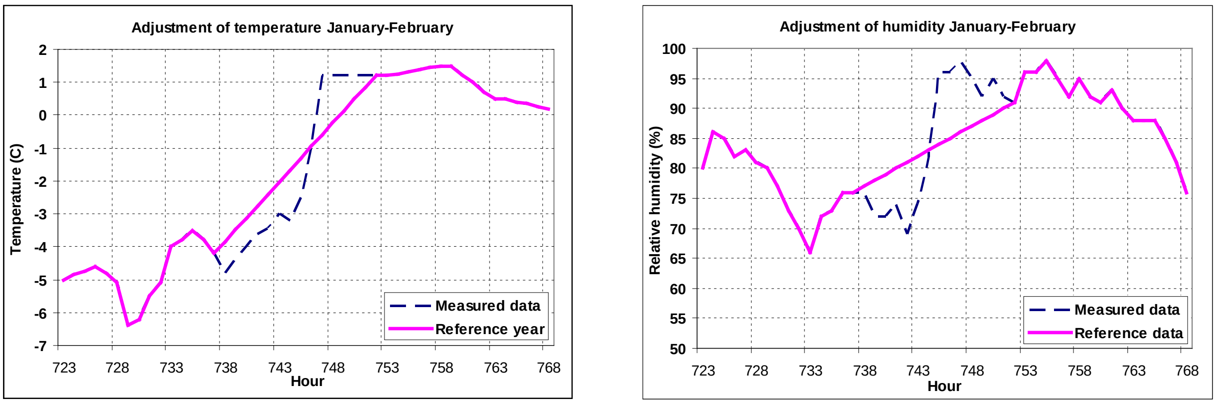

Fig. 4. Example of smoothing between two months of January and February. The figure on the left shows the smoothing of dry-bulb temperature and the figure on the right – of relative humidity

The TRY model for Kaunas will be finished after setting up the data on the hourly parameters of solar radiation and wind speed values from manuscripts to the digital environment. Hourly data for processing of statistical analysis will be prepared in accordance with the procedure described in Chapter 4.

5. CONCLUSIONS

1. The following hourly values of climatic parameters were prepared for the TRY model for Kaunas: outdoor air temperature and relative humidity for the 30-year period.
2. The Lithuanian TRY will enhance the accuracy of prediction of thermal-hygric state of building envelopes. Also this model will allow to evaluate the impact of building‘s thermal inertia to average duration of heating season of building, energy use for heating and cooling, prediction of average date for beginning and ending of the heating season. It could be used in building design and modeling, scientific research.
3. After construction the Lithuanian standard climatic model will complement the database of the IWEC (International weather year for energy calculations) with hourly values of climatic parameters of the 1961–1990 period.

ABBREVIATIONS

DBT-dry-bulb air temperature
DPT-dew-point air temperature
RH- relative humidity
GSR-global solar radiation
WSP-wind speed
ASHRAE-American Society of Heating, Refrigerating and Air-Conditioning Engineers
HVAC - Heating, Ventilation and Air Conditioning
TRY - Test Reference Year
TMY, TMY2, TMY3-Typical Meteorological Year
TMM- Typical Meteorological Months
WYEC-Weather Year for Energy Calculation
IWEC-International Weather for Energy Calculation
CWEC-Canadian Weather for Energy Calculation

NOMENCLATURE

F(p) – cumulative distribution function of p within each individual month.

F_S – Finkelstein-Schafer statistic.
J – rank order of daily means within a calendar month in one year.
K – rank order of daily means within that calendar month in the whole data set.
N – number of days in any calendar month in the whole data set.
m – month of the year.
n – number of days in an individual month.
p – climate parameter (temperature, solar radiation or humidity).
$\bar{p}$ – daily mean of any climate parameter.
y – year.
Φ(p)– cumulative distribution function of p within each calendar month in all the years in a sample.
CDF – cumulative distribution function.

REFERENCES

1. *Directive 2002/91/EC of the European parliament and the Coucil of 16 December 2002 on the energy performance of building*. Official Journal of the European Communities. 2003.4.1.2003, p. 65–71.
2. *Energy Performance of Buildings Directive*. European Commission, 2010. Link to the internet <http://www.euractiv.com/en/energy-efficiency/energy-performance buildings directive/article-187130>.
3. *Directive 2010/31/EC of the European parliament and the Coucil of 19 May 2010 on the energy performance of building*. Official Journal of the European Communities. 2010.18.6.2010, 13-35.
4. *Intelligent Energy Project report.* The beauty of efficiency: European Commission, 2008. Link to the internet <http://ec.europa.eu/energy/intelligent/library/doc/ka_reports/buildings08_en.pdf>.
5. STR 2.09.02:2005 Heating, Refrigerating, and Air-Conditioning.
6. RSN 156-94 Building Climatology.
7. LUND, H. Thermal Insulation Laboratory Technical University of Denmark. September 1975 report No 67.
8. Test Reference Year (TRY) Tape Reference Manual, TD-9706. National Climatic Center, Asheville, North Carolina, 1976.
9. DRURY B. C. Which weather data should you use for energy simulations of comercial buildings. ASHRAE 1998 Transactions 104 Part 2.
10. National Climatic Data Center, U.S. Department of Commerce. Typical meteorological year use's manual. TD-9734, hourly solar radiation-Surfase meteorological observations. Asheville, North Carolina, 1981.
11. NREL/SP-463-7668 (National Renewable Energy Laboratory) Users Manual for TMY2s (Typical Meteorological Year), and TMY2s, Typical Meteorological Year derived from the 1961-1990 national solar radiation database. United States of America, Golden, Colorado. 1995.
12. NREL/TP-581-43156 National Renewable Energy Laboratory) User's Manual for TMY3 Data Sets. Operated for the U.S. Department of Energy Office of Energy Efficiency and Renewable Energy by Midwest Research Institute Battelle. Revised May 2008 Technical Report.
13. FINKELSTEIN, J. M., SCHAFER, R. E. Improved goodness-of-fit tests. Biometrika, 1971, 58, p. 641–645.
14. ASHRAE (American Society of Heating, Refrigerating, and Air-Conditioning Engineers) Weather Year for Energy Calculation. United States of America, Atlanta, 1985.

15. CROW, L.W. Development of Hourly Data for Weather Year for Energy Calculations (WYEC), Including Solar Data, at 29 Stations throughout the United States and 5 ASHRAE Stations in Canada, Research Project RP364 Final Report, November 1983. Atlanta, Georgia: ASHRAE.
16. ASHRAE (American Society of Heating, Refrigerating, and Air-Conditioning Engineers) WYEC2, Weather Year for Energy Calculation 2, toolkit and data. United States of America . Atlanta, 1997.
17. Numerical Logics. Canadian Weather for Energy Calculations (CWEC). User‘s Manual. Canada Waterloo, 1999.
18. THEVENARD, D.J., BRUNGER, A.P., 2002A. The development of typical weather years for international locations. Part I, algorithms. ASHRAE Transactions 108, p. 376–383.
19. THEVENARD, D.J., BRUNGER, A.P., 2002B. The development of typical weather years for international locations. Part II, production. ASHRAE Transactions 108, p. 480–486.
20. LST EN ISO 15927-4:2005 Hygrothermal performance of buildings. Calculation and presentation of climatic data – Part 4: Hourly data for assessing the annual energy use for heating and cooling.
21. LUND, H. Technical University of Denmark Department of Civil Engineering, 2001 Feruary elektronic Cib Publication No. 262.
22. LAM, J.C., HUI, S.C.M. and CHAN, A.L.S. A. Statistical approach to the development of a typical meteorological year for Hong Kong. Architectural Science Review, 1996, Vol. 39, No. 4, p. 201–209.
23. GALVONAITĖ, A. *The climate in Lithuania:* a monograph. Lithuanian Hydrometeorological Service. Vilnius, 2007. 208 p. ISBN 178-9955-9758-2-3.
24. TECHNICAL REGULATIONS VOLUME I. General Meteorological Standards and Recommended Practices 1988 edition. No. 49.

CYSENI 2012, May 24–25, Kaunas, Lithuania
ISSN 1822-7554, www.cyseni.com

SUPPLY AIR TEMPERATURE AND HUMIDITY INTERACTION ON THERMAL PERFORMANCE OF INDIRECT EVAPORATIVE AIR COOLING

G. Frīdenbergs, A. Lešinskis
Institute of Heat, Gas and Water technology,
Riga Technical University
Azenes street -16/2nd floor, LV-1010 – Latvia
Phone +371 26875297
Email: guntars.fridenbergs@rtu.lv

ABSTRACT

In an indirect evaporative air cooling (IEAC) installation air is cooled by means of adiabatic humidification process. By passing over an air/air heat exchanger this air cools the supply or mixed (supply and extracted) air. A clear interaction can be observed between the relative humidity and temperature of the supply air and the thermal comfort implemented in the building. To be able to predict the performances of this technique well, a good knowledge of the supply air relative humidity and temperature are thus important. Paper presents the results of measurements carried out in summers of 2008, 2009 and 2010 in a simulated nonresidential building in 3 cities of Latvia: Riga, Liepaja and Gulbene which makes indirect evaporative cooling usable. An evaluation of the indoor summer comfort is made and the interaction between the thermal performance and outdoor air parameters (humidity and temperature) are investigated.

Work actuality is based on the Latvian Cabinet of Ministers regulation No. 534 Regulations Regarding Latvian Building Code LBN 231-03 "Residential and public buildings heating and ventilation" 118th paragraph, “If the air handling equipment for air cooling assess whether the compression cycle cooling techniques can’t be replaced by a direct or indirect adiabatic cooling techniques to minimize the impact on the environment.” Topic view and updating gives more understandable operating positive and negative aspects, which in turn give engineers new viewpoint to the evaporative cooling as the primary cooling type of application.

1. INTRODUCTION

The usage of mechanical refrigeration units has been increasing and passive cooling techniques have become more and more important over the last years due to the fact that internal loads are growing (due to e.g. computer equipment and lighting). The main shortcommings of active cooling systems are considered the large amount of energy consumption and significant contribution to the emission of greenhouse gases. However, in comparison to air conditioning passive cooling techniques ensure providing cooling with more limited environmental impact. Two types of evaporative cooling systems – direct and indirect evaporative cooling installations - can be distinguished. The supply air to the building is directly humidified in a direct evaporative cooling installation (DEC), but in an indirect evaporative cooling system (IEC) a secondary air flow is cooled by adiabatic humidification using sprayed water. The supply air to the building is cooled down by this in an air to air heat exchanger. As secondary air can be used a fresh outdoor air or return air from the building. In general, the particular system is using a plate heat exchanger and tube heat exchangers as well. The advantage of this approach is that the moisture content of the primary air is not increased as it is for direct evaporative cooling. [21]

This provides and ensures more comfortable indoor climate and less problems (e.g. mould and condensation) can occur. Due to the fact that the return air is humidified in an indirect evaporative cooling installation, there can be observed a clear interaction between the indoor humidity and the thermal performance of the technique. Low energy consumption and easy maintenance are considered the main advantages of indirect evaporative cooling. The particular technique has the highest performance in dry and hot regions, although there is a potential for usage of system in Europe as well due to the moderate humidity during summer. It will be shown as Feasibility index calculations. The buildings with relatively small cooling loads are the most suitable for usage of this technique. A good peak performance is observed for this system, during moderate periods the achieved cooling amount is limited. [1]

The literature survey of existing models is presented in this paper. A fast method of cooling potential is calculated and applied for 3 cities in Latvia: Gulbene, Riga and Liepaja. The time period for calculations and observations were summers of years 2008, 2009 and 2010. The 1D (one dimensional) stationary model of a wet surface heat exchanger was developed for calculation purposes of the outlet conditions of an indirect evaporative cooling installation. For the usage of the model in program MS Excel a validation against experiments in an installation in operation is performed and an explanation for the deviations between the results is given. [2,3] Furthermore, the different parameters that have an influence on the effectiveness of indirect evaporative cooling are evaluated.

2. FEASIBILITY INDEX

A fast method to evaluate approximately the potential of the evaporative cooling is based on the Feasibility Index (FI) [21], defined by:

$$FI = WBT - \Delta T, \tag{1}$$

where ΔT = (DBT – WBT) [31] is the wet bulb depression. DBT and WBT are, respectively the dry bulb temperature and the wet bulb temperature of the outside air. This index decreases as the difference between dry bulb and wet bulb temperature increases, i.e. as air relative humidity decreases. It shows that, the smaller FI is the more efficient the evaporative cooling will be. Thus, this number indicates the evaporative cooling potential to give thermal comfort.

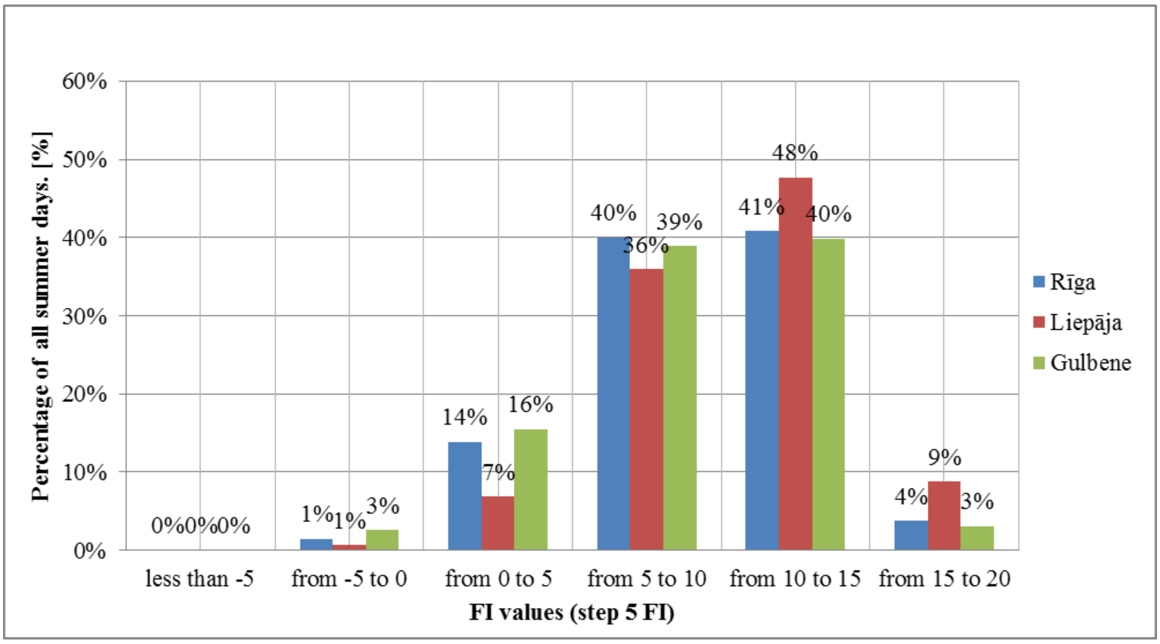

Fig. 1. FI values in summers of 2008, 2009, 2010 in 3 different Latvia cities [6]

Watt [25] recommend that indices that are under or equal to 10 indicate a comfort cooling, indices between 11 and 16 indicate lenitive cooling (relief) and indices above 16 classify the location as not recommended for use evaporative cooling systems. From these limits it is possible to conclude that, to reach a comfort recommended performance index, a wet bulb depression from, at least, 11ºC, is needed. [20,21]

As it is shown in Figure 1 mostly in Latvia all Feasibility index values is between 5-15 (from 79% up to 84%.) It means that evaporative cooling technologies can be implemented in Latvia region.

3. MODELING

Using a control volume method a 1D stationary model was developed for a counter-flow heat exchanger in order to calculate the temperatures in the primary and secondary air channel by solving five partial differential equations. The model does not use the same approximations as the analytical models. For symmetry reasons only half of the path is modeled in a control volume. The airflow paths are discretized exponentially using a grid concentration factor, resulting in smaller control volumes at both path.

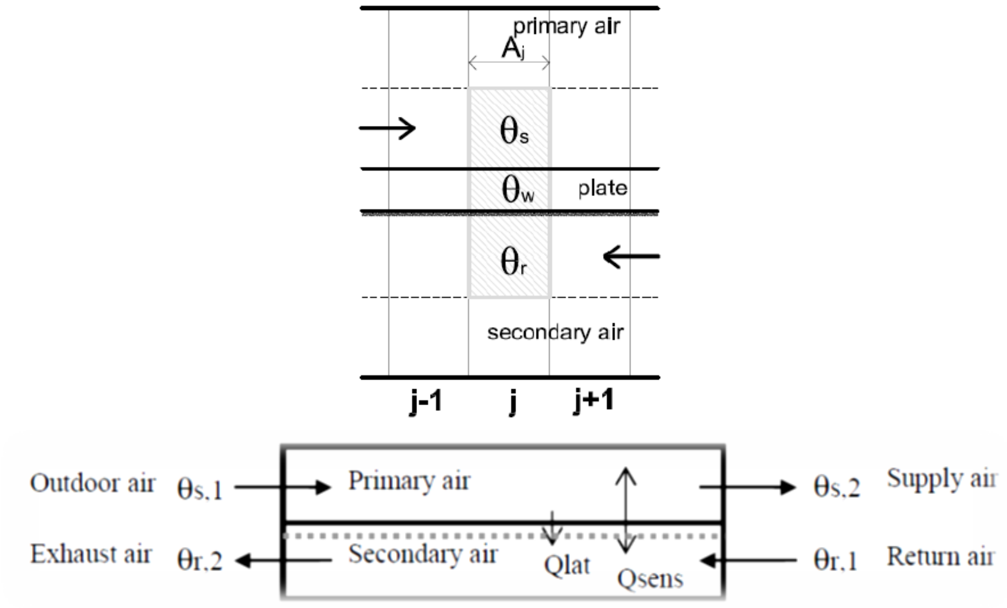

Fig. 2. 1D numerical model for a wet surface heat exchanger [3, 7]

The following assumptions were used [3]:

- 1D stationary heat transfer. Heat transfer to the surroundings is negligible.
- Mass flow rates, heat and mass transfer and specific heat coefficients are constant.
- The heat resistance of the water film and the plate is neglected because the values are small compared to the heat transfer coefficients at the surfaces. [1, 2, 9]
- The water film is stationary. An equilibrium temperature between both airstreams is calculated from the initial water temperature. The model does not take into account the heating of the water by recirculation in the heat exchanger. The plate surface is completely wetted.
- Condensation may occur in the primary air flow [8, 11, 12].

Heat balance secondary air [13,15]:

$$m_r c_r \, (Q_{j-1,r} – Q_{j,r}) = A_j \alpha_r (Q_{j,r} – Q_{j,w}) \qquad (2)$$

Heat balance primary air:

$$m_s c_s(Q_{j+1,s} - Q_{j,s}) = A_j \alpha_s(Q_{j,s} - Q_{j,w}) \tag{3}$$

Heat balance water film:

$$A_j \alpha_r(Q_{j,r} - Q_{j,w}) + A_j \alpha_s(Q_{j,s} - Q_{j,w}) + \beta A_j h_{ev}(p_{j,r} - p_{j,w}) + h_{ev} g_{j,s} = 0 \tag{4}$$

Mass balance secondary air [18,19]:

$$m_r \xi_a(p_{j-1,r} - p_{j,r}) = \beta A_j(p_{j,r} - p_{j,w}) \tag{5}$$

$\mathrm{Max}(p_{j,r}) = p_{sat}(Q_{j,r})$

Mass balance primary air:

$$m_s \xi_a(p_{j+1,s} - p_{j,s}) = g_{j,s} \tag{6}$$

if $p_{j,s} > p_{j,w} : g_{j,s} = \beta A_j(p_{j,s} - p_{j,w})$

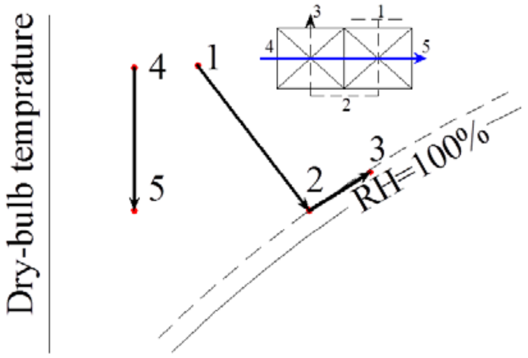

Fig. 3. First type of theoretical model of studied device (Dashed line: return air – Solid line: supply air) [10, 14]

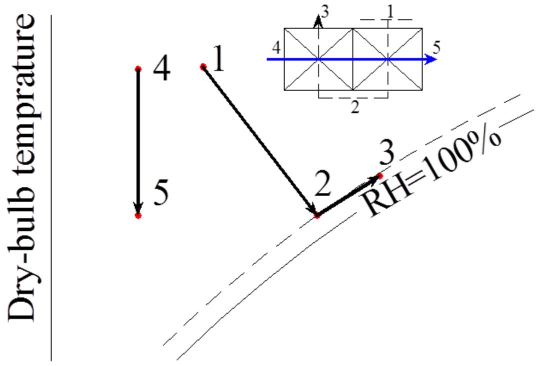

Fig. 4. Second type of theoretical model of studied device (Dashed line: supply air – Solid line: return air) [10, 14]

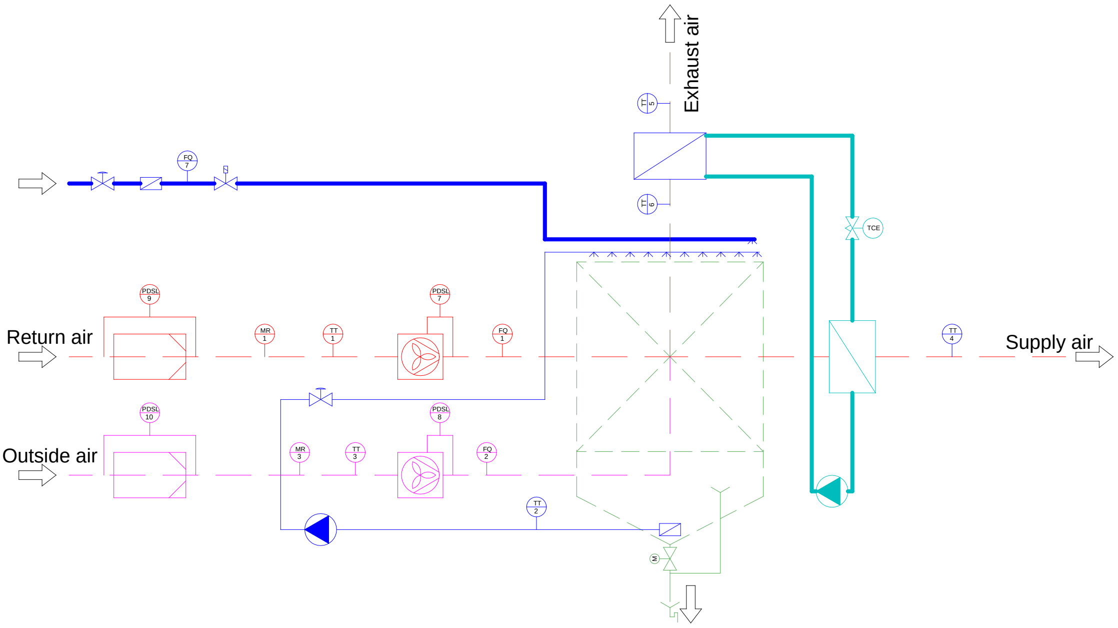

Fig. 5. Practical model of studied device [2, 27]

4. MODEL VALIDATION

To validate the model, experiments were carried out in an air handling unit with indirect evaporative cooling which is installed to provide cool air in non-residential building in Essen, Germany. The installation for building was in operation since September 2011 and was dimensioned to a maximum air flow rate of 6,000m³/h. [2] Indirect evaporative cooling is operating around-the-clock The air handling unit consists of a polypropylene double cross flow heat exchanger with dimensions 1250mm x 1215mm x 997mm. The total heat exchange surface was approximately 300m² which results in an air flow rate of about 20m³/h per m² heat exchange surface. All results are obtained by using measurement devices as shown in Fig. 5 (TT- bulb, MR – relative humidity measurement device, etc). Particular devices are made by Menerga Inc. and they are described in Menerga booklet [2]. At the return air side the air is ventilated between parallel plates while at the supply side distance holders are introduced in order to ensure stability of the parallel plates. The distance between the plates is approximately 5.1mm. [2] Both the supply and return fans are supplied with frequency control and their air flow rates are balanced. Water sprayers are placed at the top of the first part of the heat exchanger (Fig. 6b). The water is collected in a sump below and recirculated. Approximately every hour the system is replenished with fresh water to avoid problems e.g. with bacteria.

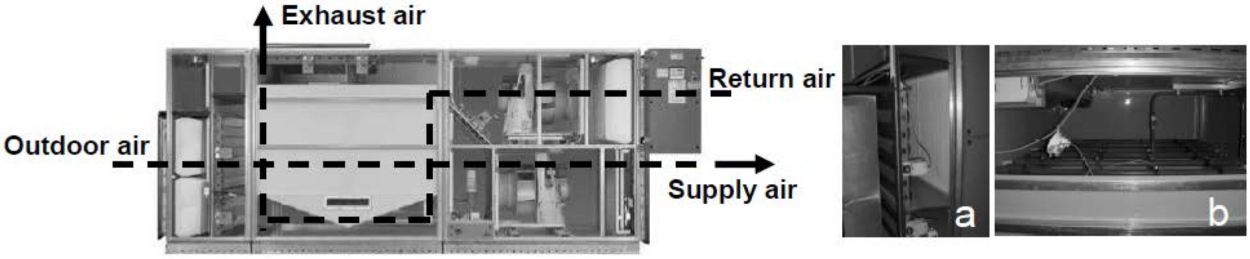

Fig. 6. Operation of the air handling unit with indirect evaporative cooling. (a) Spraying installation in secondary channel and (b) filter, valve and heat exchanger in primary air channel (Menerga, 2007) [2]

To understand what is happening in the heat exchanger the state of the airstreams during two measured periods is schematically shown on a psychometric diagram (Fig. 3, 4). The return air is wetted following lines of constant wet bulb temperature in the first part of the heat exchanger (1–2). At the exit of the first part, the return air is saturated and reaches its wet bulb temperature (2). [21, 23] During the experiments a mist came out of the exhaust air flow which means that the collected water from the sump is carried along the second part of the heat exchanger together with the ventilation air. The sprayed water is heated up by recirculation in the first part of the heat exchanger. To have an indication of the water temperature the water exiting the sprayers was measured and was about 22–23 °C. Due to evaporation effects the water itself will be slightly warmer.

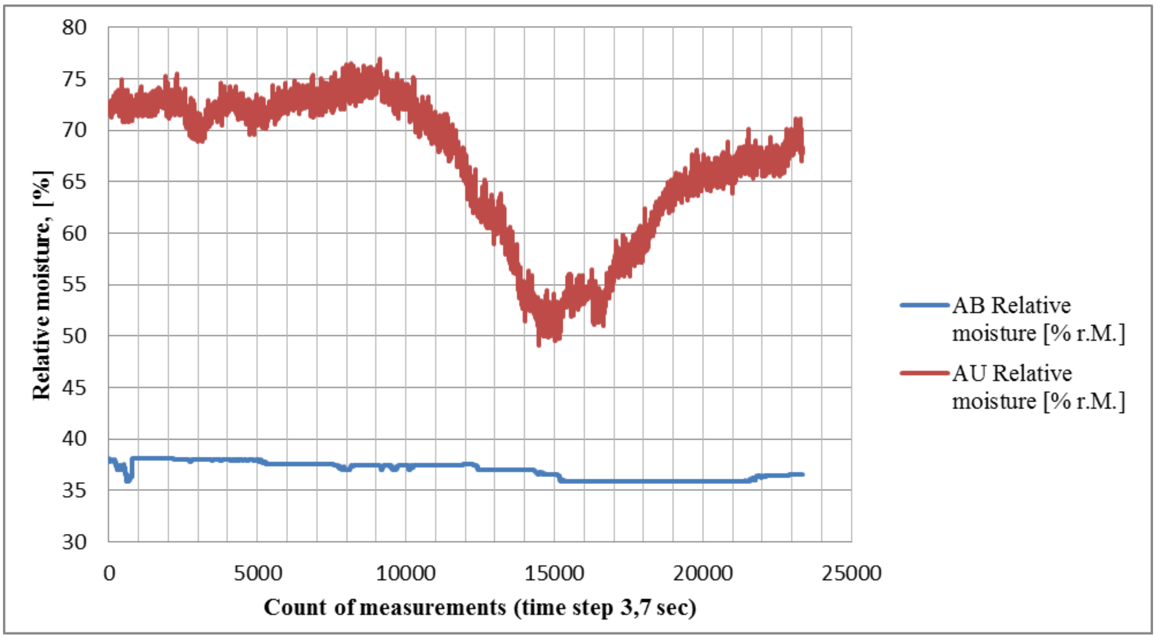

Fig. 7. Measured relative moisture of outside and return air [27]

During measurements (Fig. 8) the outdoor air temperature was variable in range 15–21°C and 50–75% RH and return air was about 27°C and 37% RH. The air flow rate of return air was about 1450 m^3/h and supply air flow rate was about 1240 m^3/h. The outdoor air was now cooled in the heat exchanger to about 16.0°C (4–5). After passing the first part the return air was heated up slightly by flowing over the second part of the heat exchanger due to the warmer outside air in the primary air channel and the water carried along (2-3). The air was further heated in the second part of the heat exchanger and thus it was able to take up more water vapor. As a result the exhaust air stayed saturated (21°C/100% RH).

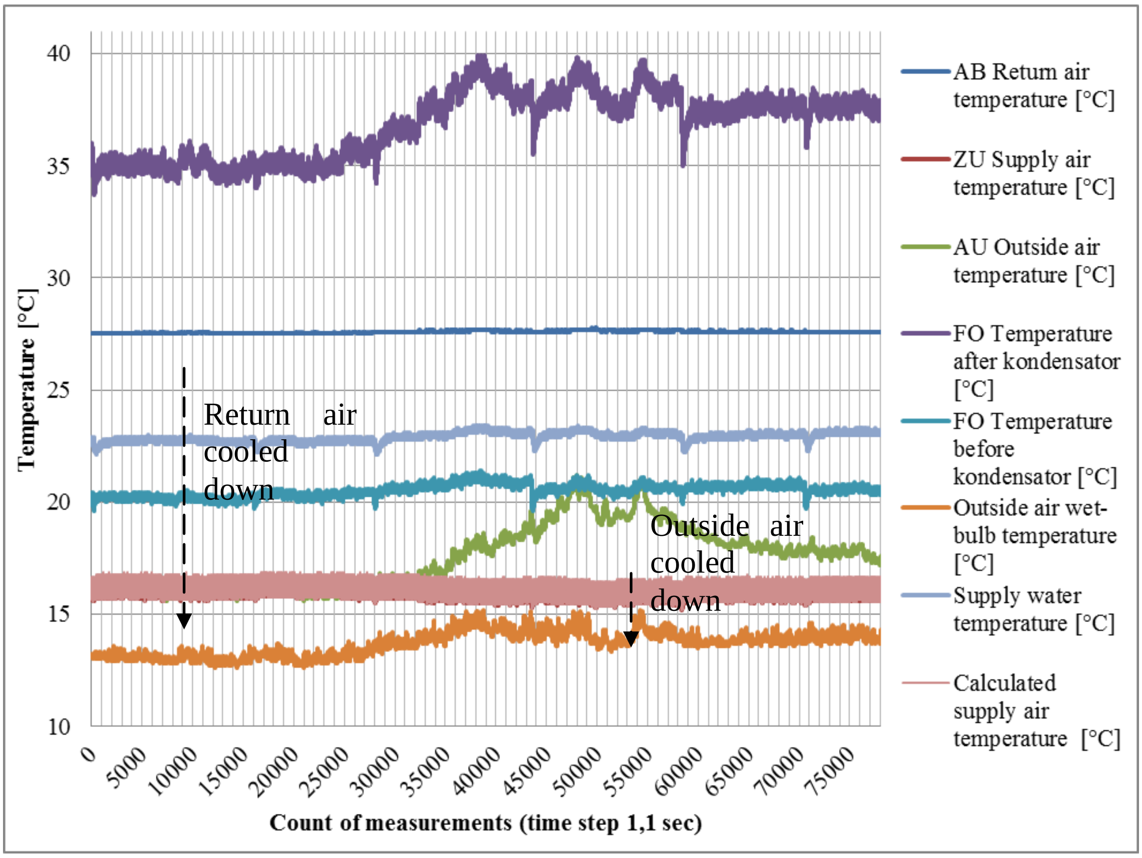

Fig. 8 Measured and calculated air temperatures in device [27]

In order to simulate the double cross flow heat exchanger was modeled as a dry heat exchanger. This is an appropriate approximation because the return air is already saturated when exiting the first part of the heat exchanger. The dry heat exchanger will slightly precool the primary air before entering the wet part of the heat exchanger. At the same time the secondary air is heated up a bit when flowing through the dry part of the heat exchanger. The outlet temperatures of the dry heat exchanger are calculated using ae – NTU (Number of transfer units) correlation for a cross flow heat exchanger with one side mixed and one side unmixed [4]. The combination of both heat exchangers was modeled by using the developed wet surface heat exchanger model and the e – NTU relation for the dry heat exchanger in MS Excel made model [5, 16, 17].

CONLUSIONS

A calculations of feasibility index values in 3 cities of Latvia have been calculated. Data shows that difference 11°C between dry-bulb temperature and wet-bulb temperature is needed.

A 1D numerical model of counter-flow wet surface heat exchanger was developed based on the heat and mass balance of the supply and return air. Using a control volume method the outlet conditions of both supply and exhaust air can be calculated. The model assumes that the heat transfer resistance of both water film and plate are negligible and that the water film is stationary and continuously replenished with water. The model has been validated using measured data in a double cross flow heat exchanger. The installation has been modeled assuming evaporation only takes place in the first part of the heat exchanger. The second and dry part of the heat exchanger was modeled using e – NTU correlation and linked behind the wet surface heat exchanger model in MS Excel. The supply air temperature and the return air temperature just behind the first part of the heat exchanger were in good agreement with the measured data. The model underestimated the temperature of the exhaust air because it does not take into account the fact that the return air is heated by the recirculated water in the second part of the heat exchanger.

NOMENCLATURE

A – heat transfer surface (m²); Q_{lat} – latent heat transfer; Qs_{ens} – sensible heat transfer; c – specific heat of air (J/kg K); α – heat transfer coefficient (W/m²K); P_{air} – air pressure (101325 Pa); β – mass transfer coefficient (kg/Pa/s/m²); D_h – hydraulic diameter (m) (D_h = 2b for plates; Dh=b for channels; b distance between plates); ε – effectiveness (%); g – condensation flow rate (kg/s); θ – dry bulb temperature (°C); h_{ev} – latent heat (J/kg); θ ' – wet bulb temperature (°C); k – conductivity of air (0.025 W/m²K) x; a – specific vapour capacity air (kg/kg/Pa); m – mass flow rate (kg/s); s – supply air; Nu –Nusselt number (-); r – return air; NTU – number of transfer units (-); w – water film interface; p – vapour pressure (Pa); 1 – inlet; 2 – outlet.

REFERENCES

1. STEEMAN M, JANSSENS A, DE PAEPE M. (2007). *Performance evaluation of indirect evaporative cooling by means of measurements and dynamic simulations*, Proceedings of 6th International Conference on Indoor Air Quality, Ventilation & Energy Conservation in Buildings, Oct. 28-31, Sendai, Japan, p. 2–8.
2. Menerga Klimatechnologie. (2007). [Referred on the 3th of January in 2012 y.]. <www.menerga.de>
3. STEEMAN M, JANSSENS A. *A 1D stationary model for assessing the performance of indirect evaporative cooling.* Ghent University, Department of Architecture and Urban Planning, Ghent, p. 2–11.
4. SHAH RK, SEKULIC D.P. *Fundamentals of Heat Exchanger Design*, 2003, p. 482–485.
5. ANDERSON, W.M., 1986, *“Three-stage evaporative air conditioning versus conventional mechanical refrigeration”*, ASHRAE Transactions, Vol. 92, p. 358–370.
6. FRIDENBERGS G., *“Direct and indirect cooler implementing in Latvia region”*, RTU, 2010, 1.-18. lpp.
7. BOURDOUXHE P., GRODENT M., LEBRUN J. *Cooling-tower model developed in a toolkit for primary HVAC system energy calculation—part 1: model description and validation using catalog data*, Proceedings of the fourth international conference on system simulation in buildings – Liege, December 1994. – 1. – 11. 1 p.
8. BRAUN J.E., KLEIN S.A., MITCHELL J.W. *Effectiveness models for cooling towers and cooling coils*, ASHRAE Transactions – 1989. – 2 – 74.
9. CROW, L.W., “*Weather data related to evaporative cooling*”, Research Report n ? 2223. ASHRAE Transactions 78 (1) - 1972 – 153.-164. lpp.
10. ESKRA, N., *“Indirect/direct evaporative cooling systems”*, ASHRAE Journal, may – 1980 - 21.-25. lpp.
11. *Evaporative cooling design guidelines manual for New Mexico schools and commercial buildings* – 2003 – 9.-17. lpp.
12. FACAO J., OLIVEIRA A.C. *Thermal behaviour of closed wet cooling-towers for use with chilled ceilings*, Applied Thermal Engineering 1999. – 48 lpp.;
13. HALASZ, B., *“A general mathematical model of evaporative cooling devices”*, Rev. Gén. Therm., FR, Vol. 37 – 1998. – 245.-255. lpp.
14. HASAN A., SIREN K. *Theoretical and computational analysis of closed wet cooling-towers and its applications in cooling of buildings. Energy and Buildings* - 2002 – 34 lpp.

15. INCROPERA F.P., DEWITT F.P. *Fundamentals of heat and mass transfer*, 4th ed. John Wiley & Sons - 1996. – 298 lpp.
16. KALS WA. *Wet-surfaces air coolers,* Chemical Engineering – 1971. – 68 lpp.
17. Latvijas Metroloģijas centra data base [referred on the 3th of January in 2012 y.]. <www.meteo.lv/pdf_base/meteor_2009.html>
18. LEBRUN J., APARECIDA SILVA C., TREBILCOCK F., WINANDY E. *Simplified models for direct and indirect contact cooling-towers and evaporative condensers,* 6th International conference on System Simulation in Buildings - Liege, December 2002. – 1.-8. lpp.
19. MACLAINE-CROSS, I. L., BANKS, P. J., *"A general theory of wet surface heat exchangers and its application to regenerative evaporative cooling"*, Journal of Heat Transfer, Vol. 103, No. 3, - 1981. – 579.- 585. lpp.
20. NIITSU Y, NAITO K, ANZAI T. *Studies on characteristics and design procedure of evaporative coolers*, Journal of SHASE, Japan – 1969. – No.7 - 12.– 23. lpp.
21. PETERSON J.L. *An effectiveness model for indirect evaporative coolers,* ASHRAE Transactions – 1993. – 99(2) lpp.
22. STABAAT, P., MARCHIO, D, *"Simplified model for indirect-contact evaporative cooling-tower behaviour"*, Applied Energy 78 (2004), - 2003 - 433.-451. lpp.
23. THRELKELD JL. *Thermal environmental engineering,* 2nd ed. Englewood Cliffs: Prentice-Hall, Inc. – 1970. – 342 lpp.
24. TRANE, *"Air conditioning handbook"*. The Trane Company, La Crosse, Wisconsin – 1978. – 281 lpp.
25. WATT, J.R., BROWN, W.K., *"Evaporative air conditioning handbook"*, 3rd Edition, The Fairmont Press, Inc., Lilburn, GA. – 1997. - 184 lpp.
26. WATT J.R. *"Thermodynamic Fundamentals of Indirect-Evaporative air Cooling – part1"*, Thermo-Physical lab, Intexh-Mark – 2010 – 1.-11.l lpp.
27. FRIDENBERGS G., *"Indirect evaporative air cooling modelling under different air flow parameters"*, RTU, 2012, 43.-67.lpp.

CYSENI 2012, May 24–25, Kaunas, Lithuania
ISSN 1822-7554, www.cyseni.com

DESIGNING OF ENERGY EFFICIENT SYSTEM CONSIDERING POWER CONSUMPTION AND RELIABILITY

T. Iešmantas, R. Alzbutas
Lithuanian Energy Institute
Laboratory of Nuclear Installation Safety
Breslaujos str. 3, LT – 44403, Kaunas
Phone +370 37 401945
Email: iesmantas@mail.lei.lt, robertas@mail.lei.lt

ABSTRACT

The topic of this paper is a part of a more broad and complex issue: modelling of physical process and assessment of various variables, such as power consumption, reliability etc., for the purpose of designing a system, which involve network nodes affected by physical processes. First part of this paper is devoted for presentation of tool called Energy Simulator. This tool is intended for the purpose of modelling of network system or processes when power consumption is of interest. Energy Simulator is constructed as a simulation service able to automaticaly construct a model and simulate new/innovative network or system designs and estimate energy use for them. For the optimization of existing systems or for designing the new ones, consumed energy estimate is immensely important part and this new tool could be a handy support for engineers. The usage of this tool is demonstrated for compressed air systems. Implementation of compressed air systems is based on physical network concept when system is represented as consisting of functional elements or subsystems that interact with each other by energy flow and variables of physical processes which impacts the power consumption.

Keywords: Power consumption, compressed air systems, network, designing, simulation and modelling

1. INTRODUCTION

A system is a group of objects, i.e. elements or subsystems whose interaction serves for a common purpose. Many measures are used to evaluate how closely the design of systems and subsystems meets the desired functionality and constraints. Some of the measures include performance, energy and power consumption, reliability, cost of design and manufacturing.

When designing a system, several choices must be made concerning the type of elements to be used and configuration of their assembly. The choice is driven by the objectives with the economic costs, reliability, energy consumption associated to the design implementation, system construction and future operation, etc.

In addition, designing complex engineered artefacts (and collections of them) most likely requires use of simulations coupled with optimization techniques [6]. As complexity increases, ability to employ intuition (even for understanding the computed trade-offs) declines rapidly. Furthermore, a person ability to actually solve these system optimization problems becomes suspect as dimensionality increases.

From all the possible choices of objectives for system design, we confine ourselves to the analysis of power consumption and the analytical modelling with simulation of physical systems in order to estimate such consumption.

The usual practice when estimating power consumption of the new system is to use simplified equations/formulas, e.g. [2]. However, such approach could result in heavily pronounced errors if the system is complex, because processes, that require the usage of energy-consuming equipment, might be very complicated and related constrains might not be satisfied. The tool that would be able to construct complex model, simulate it automatically and at the same time could be used by designer without being exposed to mathematical rigour is of great importance. Such tool would enable designer to create new system or process more efficiently and with more adequacy.

In this paper authors present such a tool – Energy Simulator (ES). General concept is presented in section 2 where architecture and functionalities are described. Further, ES is demonstrated for the case of specific compressed air system in section 3: from model building of such systems and its numerical implementation to the presentation of how general ES functionalities are used in this specific case.

ES can be further processed in other designing task, for example optimization in terms of power consumption. One of possible scenarios is to construct a model for existing system implementation and then, according to some strategy, alter configuration of the system and obtain simulation results of this new system. Processing of these results will lead to another alteration of system configuration. Finally, after some number of steps, new and better system configuration will be found. This new system can then be implemented instead of the old one.

2. ENERGY SIMULATOR TOOL

Energy Simulator is a tool intended for simulation of network system or process, when energy consumption is of interest. ES is constructed as a simulation service able to simulate new/innovative network or system designs and estimate energy use for them. The analytical modelling and simulation is based on “block-based modelling” concept rather than on purely “process-based modelling”. It means that whole physical system or physical process is decomposed into sub-systems or sub-processes represented by independent blocks (one block for one sub-systems or sub-process).

- Sub-system is a specific physical equipment (installation) providing process related output, which depends on process related boundary conditions and sub-system parameters (block parameters). Sub-system may be expressed using differential equations with specific parameters.
- Sub-process is process variable (output of block) related to physical behaviour of other variables (inputs of block) with their weighting coefficients (block parameters). Sub-process may be expressed as a process variable or function dependent on other process variables.

The list and relation of blocks together with blocks’ parameters gives the process configuration, which is the basic information for automatic model generation. The main tasks of ES include the following ES functionalities (for detailed description see table below):

- Get configuration;
- Add blocks;
- Specify configurations;
- Calculate energy use of process configuration.

Table 1. Description of ES functionalities

Functionalities	**Description**
Get configuration	***Purpose:*** to get a process configuration and specify the nodes. The user of this functionality is the internal functionality *Add Blocks.* ***Input:*** configuration ID ***Output:*** configuration ***Comment:*** if data base (knowledge repository - KR) is not used and at the initiation time the configuration is accessible in table form locally, then this functionality is not used.
Add blocks	***Purpose:*** to retrieve the characteristics of relevant blocks from Model Library of the element. The user of this functionality is the internal functionality *Specify Connections* **Input:** the blocks listed in the configuration. The Model Library should be accessible for this functionality. Each model of block shall be represented by mathematical dependencies relating: – relevant physical variables; – energy use and physical variables. ***Output:*** a set of models selected depending on configuration. ***Comment:*** the configuration contains names of blocks. Their characteristics should be identified and included into simulation model. Characteristics are mathematical dependencies of physical variables or dependencies between energy use and physical variables.
Specify connections	***Purpose:*** to specify the connections between blocks. The user of this functionality is the internal functionality *Calculate energy use of process configuration***.** ***Input:*** a set of block models. ***Output:*** the model for specific configuration fully generated for the simulation of process (system) and calculation of energy use. ***Comments:*** Connection might be different in terms of topology (connection points) and characteristics of connecting branches. The connections should be specified in the configuration.
Calculate energy use of process configuration	***Purpose:*** to simulate the process (system) and calculate the energy use. ***Input:*** The input is model for specific configuration fully generated for the simulation of process (system) and calculation of energy use. ***Output:*** The output may be any simulated physical variable and its time series or/and the energy use, which may be calculated depending on the physical variables. ***Comments:*** This functionality uses the simulation model generated using other functionalities.

Interaction of ES functionalities and links to the other database and user (Energy Analyzer - EA) can be graphically represented as in Fig**.** 1. By user or Energy Analyzer we mean other possible software that uses energy consumption estimates as input variables for other type of calculations, e.g. optimization of system configuration.

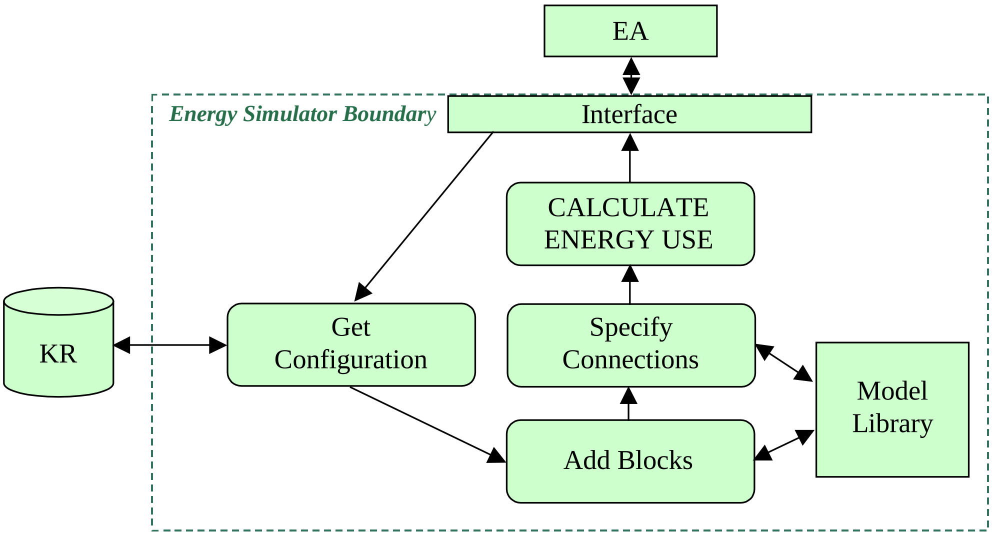

Fig. 1. ES functionalities and links to the database and user

Two functionalities, namely Specify Connections and Add blocks, are related to the application of Model Library, which includes predefined models of possible blocks, i.e. all models of sub-systems or sub-processes. This Model Library contains blocks (together with their models), that are specific for the modelling problem at hand.

In accordance to the predefined configuration, initially, whole system or process is modelled automatically connecting all blocks. This can be visualized drawing the lines between the related blocks. The connected blocks can be mathematically expressed as the system of differential equations or single regression function, which relates all process variables. In addition, for the simulation there is a need to perform the evaluation of unknown relations and values, e.g. numerically solve differential equations or evaluate weighting coefficients for process variables.

The output (response variable) of the whole ES system may be any process variable and the energy use, which is calculated depending on the process variables. This is important in case if the user in the specified timescale seeks to obtain the time series or single estimates (e.g. average) of energy use and at certain sub-systems or sub-processes to perform verification of critical values (e.g. maximum) of process variables, which in turn should confirm that process will be operable and compliant with the pre-defined design constraints. Whole flow of data within ES and between outer users can be summarized as in Fig. 2.

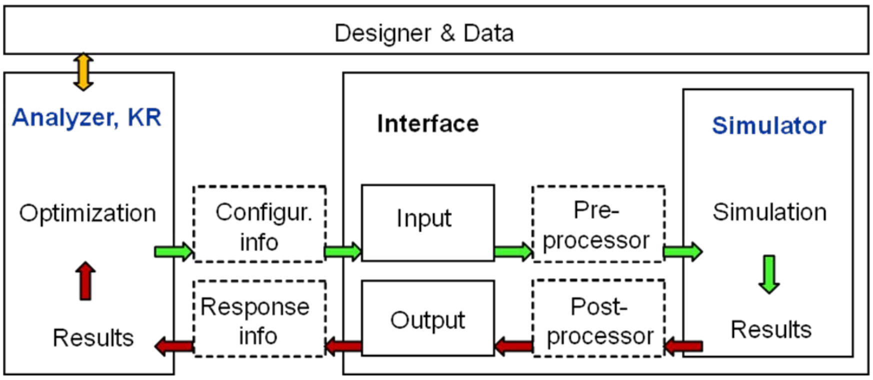

Fig. 2. Interaction between Analyzer (EA), KR and Simulator (ES)

Summarising, the process modelling and energy use simulation includes the following phases:

- Configuration-based model generation.
- Simulation of process (system).

- Calculation of energy use.

The last two phases represent the running of the generated model, i.e. simulating the model and performing the calculations, which results is important for Energy Analyzer. All three phases depends on the modelling approach used for specific system or process. For different cases the configuration, blocks, modelling, simulation and calculation is implemented depending on the used mathematical modelling approach, which itself depends on considered physical phenomena and available information.

As it was mentioned previously, the calculation of response variables can include the calculation of energy use, which depends on the physical process variables. The process variables may be the same as sub-process variables or may be expressed either as variables of functions or variables of equations, which express the relations (e.g. balance of mass and energy).

In case if energy use is directly calculated on the basis of configuration, which represents the process itself, then values of process variables are not simulated, but just expressed as a functions or given as time series. Separate blocks as functions or parts of time series may be related to the sub-processes or even some set points, which define these sub-processes. The modelling representing the whole process then automatically connects all sub-processes and is used for analysis of innovative design and calculation of energy use.

3. ES DEMONSTRATION FOR COMPRESSED AIR SYSTEMS

Compressed air is used widely throughout industry. Almost every industrial plant, from a small machine shop to an immense pulp and paper mill, has some type of compressed air system. In many cases, the compressed air system is so vital that the facility cannot operate without it.

In many industrial facilities, air compressors use more electricity than any other type of equipment. Inefficiencies in compressed air systems can therefore be significant. Energy saving from system improvements can range from 20% to 50% or more of electricity consumption. A properly managed compressed air system can save energy, reduce maintenance, decrease downtime, increase production throughput, and improve product quality. Compressed Air Systems (CAS) consist of a supply side, which includes compressors and air treatment, and a demand side, which includes distribution and storage systems and end-use equipment.

As an important component for power consumption we will use notion of pressure drop – a term used to characterize the reduction in air pressure from the compressor discharge to the actual point-of use. Pressure drop occurs as the compressed air travels through the treatment and distribution system. Excessive pressure drop will result in poor system performance and excessive energy consumption. Overall pressure drop together with produced flow rate will make essential parts in power consumption estimation.

Even though importance of CAS in industrial applications, still not much research has been done about its power consumption or physical process modelling, e.g. Qin and Mckane [1] reported CAS analysis in terms of energy consumption and Kaya *et al.* [2] quantified energy losses in CAS.

Further we will present CAS analysis implementation with ES Tool: definition of used blocks, physical modelling, systems topology introduction into configuration, power consumption estimation, application of ES functionalities.

3.1. Matlab Simscape environment

Energy Simulator concept for compressed air systems was realised under Matlab Simscape™ computational environment. Simscape software is a set of block libraries and special simulation features for modelling of physical systems in the Simulink® environment. It employs the physical network approach, which is particularly suited to simulating systems or processes that consist of real physical elements.

Simscape technology enables to create a network representation of the system under design, based on the physical network approach. According to this approach, each system is represented as consisting of functional elements that interact with each other by variables of physical processes.

These connection ports are bidirectional. They mimic physical connections between elements. User does not have to specify flow directions and information flow when connecting Simscape blocks, just as you do not have to specify this information when you connect real physical elements. The physical network approach, automatically resolves all the traditional issues with types of variables, directionality, and so on.

The number of connection ports for each element is determined by the number of energy flows it exchanges with other elements in the system, and depends on the level of detail. For example, an air compressor in its simplest form can be represented as a two-port element, with energy flow associated with the inlet (suction) and the other with the outlet.

Resulting physical network is described by so called Differential Algebraic Equations (DAE) of the form [7]:

$$\begin{cases} y' = f_1(t,y,x) \\ 0 \ = f_2(t,y,x) \end{cases};$$

where the second is algebraic (i.e. free of derivatives) equation, t denotes time, x and y - time-dependent variables. For example:

$$\begin{cases} y' = tx^2 + y^3 \\ x^2 + y^2 = 1 \end{cases}.$$

3.2. Main CAS elements

The main equipment that is used in compressed air systems is:

- Compressors – machines, that are used to increase the pressure of air;
- Air dryers – when air leaves compressor, it is typically saturated and when it flows through colder parts of system water will condensate. This causes detrimental effects, such as corrosion and contamination of point-of-use processes. This problem can be avoided by proper use of dryers and air filters;
- Air filters – depending on the level of air purity required, different levels of filtration and types of filters are used: to remove solid particles, lubricants, moisture, etc.;
- Receivers are used to provide compressed air storage capacity for a peak demand and to control system pressure by controlling the rate of pressure change in a system;
- Connectors are used for the purpose to connect several elements in order to represent the distribution of the flow.

These four types of CAS elements are implemented in ES as a Simscape based Model library of blocks which are used to simulate physical behaviour of the system. We also implemented a block, called EndUser. This block denotes end point of CAS where compressed air is used for various purposes. We also included a block AirSource intended to represent ambient air conditions.

In addition, to be able to measure and monitor various physical characteristics (pressure, air flow rate, etc.) we created two blocks called FlowSensor and PressureSensor.

3.3. Mathematical modelling of CAS physics

As mention in section 3.1, Simscape provides environment where real physical systems can be modelled by invoking physical network notion. One example of CAS represented by physical network in Simscape environment using created blocks is in Fig. 3.

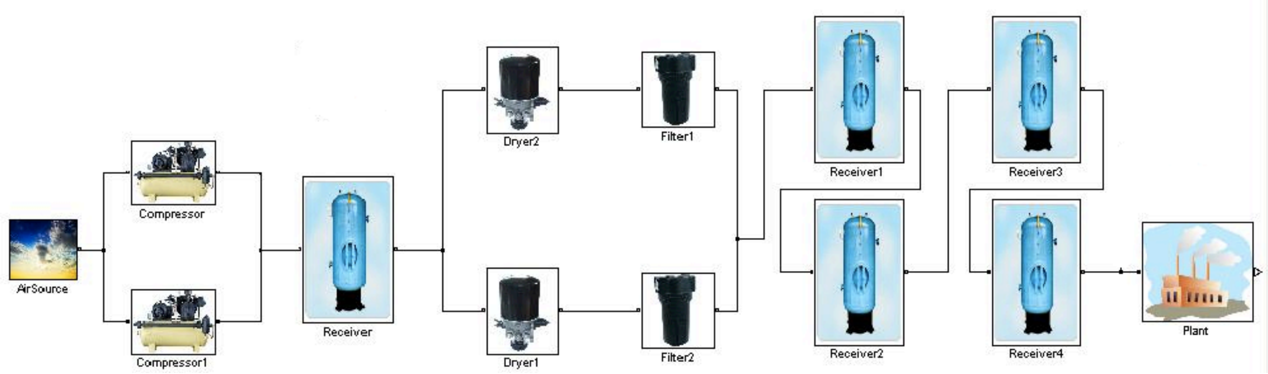

Fig. 3. Example of compressed air system representation by physical network

Each block model is based on such global assumptions:

- Working fluid is an ideal gas satisfying the ideal gas law.
- Specific heats at constant pressure and constant volume (c_p and c_v) are constant.
- Processes are adiabatic, that is, there is no heat transfer between elements and the environment (except for elements with a separate thermal port).
- Gravitational effects can be neglected, that is, underlying equations contain no head pressures due to gravity.

The energy balance for control volume can be expressed as [3]:

$$\frac{dE_{cv}}{dt} = Q_{cv} - W_{cv} + \sum_i \left(m_i \left(h_i + \frac{1}{2} v_i^2 + g z_i \right) \right) + \sum_o \left(m_o \left(h_o + \frac{1}{2} v_o^2 + g z_o \right) \right),$$

where: E_{cv} – control volume total energy; Q_{cv} – heat energy per second added to the gas through the boundary; W_{cv} – mechanical work per second performed by the gas; h_i, h_o – inlet and outlet enthalpies; v_i, v_o – gas inlet and outlet velocities; z_i, z_o – elevations at inlet and outlet ports; m_i, m_o – mass flow rates in and out of the control volume; g – acceleration due to gravity (all units are in SI system).

The ideal gas law relates pressure p, density ρ and temperature T as follows:

$$p = \rho R T,$$

where R is specific gas constant.

Receiver blocks are assembling inlet, outlet and chamber. Inlet and outlet are modelled as a constant area pneumatic orifice. Flow rate through the orifice is proportional to the orifice area and the pressure differential across the orifice [4]:

$$G = C_d A p_i \sqrt{\frac{2\gamma}{\gamma - 1} \frac{1}{RT_i} \left[\left(\frac{p_o}{p_i} \right)^{\frac{2}{\gamma}} - \left(\frac{p_o}{p_i} \right)^{\frac{\gamma+1}{\gamma}} \right]},$$

where G – mass flow rate; C_d – discharge coefficient, to account for effective loss area due to orifice shape; A – orifice cross-sectional area; p_i, p_o – absolute pressures at the orifice inlet and outlet; γ - the ration of specific heat at constant pressure and constant volume.

Constant volume pneumatic chamber model is based on ideal gas law and assuming constant specific heats. The continuity equation for the network representation of the constant chamber is [5]

$$G = \frac{V}{RT} \left(\frac{dp}{dt} - \frac{p}{T} \frac{dT}{dt} \right),$$

where V – chamber volume, t - time.

Filters and dryers are modelled as assembling of inlet, outlet, resistive tube and chamber. Resistive tube modeless pressure drop due to viscous friction along short stretch of pipe with circular cross section and chamber represents the volume of tube. The tube is simulated according to the following equations [4]:

$$p_i - p_o = \begin{cases} \dfrac{RT_i}{p_i}\dfrac{32\mu L}{AD^2}G, \text{ laminar flow} \\ f\dfrac{RT_i}{p_i}\dfrac{L}{D}\dfrac{G^2}{2A^2}, \text{ turbulent flow} \end{cases},$$

where f – friction factor for turbulent flow; D – tube internal diameter; L – tube length; A – cross-sectional area.

Compressors are modelled as perfect flow generators and can be of constant or variable speed and EndUser (or Plant) is just a sink of infinite volume.

3.4. Numerical methods

In order to obtain solution for physical network governed by mathematical laws that were presented in previous section one needs to employ one of Matlab differential equations solvers. However, the choice is not a trivial task, due to resulting complexity of network and the stiffness of the systems of differential algebraic equations. Our search for most efficient solver resulted in the choice of trapezoidal rule using “free” interpolant (in Matlab software it is denoted by ode23t). Since physical network gives rise of previously mentioned DAEs, one needs methods to cope with ordinary differential equations as well as with algebraic equations. Suppose a DAE is like this:

$$\begin{cases} u' = f_1(t,u,v) \\ 0 \ = f_2(t,u,v) \end{cases}.$$

Then these equations are to be numerically solved reaching final time moment t_f on a considered time interval $\left[t_0,t_f\right]$ with initial condition $u\left(t_0\right)=u_0$ and a guess value v_0 for $v\left(t_0\right)$ [8]. Assuming that the algebraic equations $0 \ = f_2\left(t,u_0,v_0\right)$ have a solution V near v_0, the key requirement is that the Jacobian $\partial f_2 / \partial v$ is non-singular in a region containing $\left(t_0,u_0,V\right)$. The implicit function theorem [9] implies the existence of a function $R\left(t,u\right)$ such that $R\left(t_0,u_0\right)=V$ and $0=f_2\left(t,u,R\left(t,u\right)\right)$. The differential equations are then

$$u' = f_1\left(t,u,R\left(t,u\right)\right) = f\left(t,u\right)$$

and the task reduces to solving an initial value problem of an ordinary differential equation. So, each time the integrator needs a value of $f_1\left(t,u,v\right)$ for given $\left(t,u\right)$, the algebraic equations $0=f_2\left(t,u,R\left(t,u\right)\right)$ must be first solved for v. Then any n^{th} step with length h_n of trapezoidal rule is [10]:

$$u_n = u_{n-1} + \frac{1}{2}h_n\left[\,f_1\left(t_n,u_n,v_n\right) - f_1\left(t_{n-1},u_{n-1},v_{n-1}\right)\right].$$

This trapezoidal rule is used together with nonlinear equation solvers step interchangeably.

3.5. Demonstration of ES functionalities

Although graphical representation of each modelled CAS can be represented as in Fig. 3, we emphasise that ES generally operates under virtual Simscape environment, i.e. each CAS that is of interest for designer and being processed by ES, is not represented graphically by default. This rejection of graphical representation is due to necessity to speed up and automatically simulate different configurations. Handling of configurations could even be carried out by supplying each configuration for different processor node in multiprocessor machine case.

3.5.1. Get configuration

ES due to its architecture is able to function in two ways: when all the information about configurations is stored in database (possibly in other country, or other geographical location with internet connection) or when no database is present and information is placed in pre-specified ES location. In first case, when functionality Get configuration is initiated by obtaining just configuration ID, ES connects through web interface to the so called Knowledge Repository and collects data associated with ID. In both cases the result is a table (Table 2) representing the network topology of CAS system.

Table 2 The network topology of CAS system, where NodeName represents physical and measurement equipment; AltBlockNames denotes equipment model – different compressor models, filters, etc.; InputNode and InputNodePort represents the way, that each block is connected with each other (InputNodePort indicates to which inlet of component InputNode is being connected); Arg – measurements that is of importance for user.

NodeName	AltBlockNames	InputNode1	InputNode1 Port	InputNode2	InputNode2 Port	Arg1	Arg2
AirSource1	AirSource		0		0		
Compressor1	IRN160K2S	AirSource1	1		0		
Compressor2	IRN160K2S	AirSource1	1		0		
Receiver1	Receiver5000	Compressor1	1	Compressor2	1		
Dryer1	D600INA	flowSensor1	1		0		
Filter1	IRHE1380	Dryer1	1		0		
Dryer2	D600INA	flowSensor1	1		0		
Filter2	IRHE1380	Dryer2	1		0		
Receiver2	Receiver750	Filter1	1	Filter2	1		
Receiver3	Receiver750	Receiver2	1		0		
Receiver4	Receiver750	Receiver3	1		0		
Receiver5	Receiver750	Receiver4	1		0		
EndUser1	EndUser	Receiver5	1		0		

The obtained configuration includes the physical system topology with links to parameters of blocks and thus it is the input for subsequent functionality *Add Blocks*.

3.5.2. Add Blocks and Specify Connections

Functionality *Add Blocks* is necessary in order to identify and relate each block in configuration to block in Model Library. During this phase, virtual blocks are collected from Model

Library and specific parameters are obtained depending on equipment in a system. For example, compressor model IRN160K2S has the following parameters: $\mathbf{MaxFlow} = \mathit{0.4}\,\mathbf{kg/s}$, $\mathbf{MaxPressure} = \mathit{10\,bars}$, $\mathbf{Power} = \mathit{160\,kW}$.

Such identification and information collection selecting appropriate model is done for each block. After each block has assigned parameters, it is placed in virtual Simscape environment, but does not represent physical network. The topology of CAS is realised with functionality *Specify Connections*. Virtual blocks are connected in accordance to the table, like in Table 2, where *InputNode* and *InputNodePort* carries information which and where each block is connected.

3.5.3. Calculate energy use of process configuration

As already mentioned at the beginning of section 3, in each compressed air system pressure drop occurs as air travels through each equipment block. This implies that, when one system element is replaced by another with different physical characteristics, then overall pressure drop also will be different.

In addition, if some specific installed CAS is taken under consideration and designer wants to build less costly system, then one of criteria is that new system should be able to satisfy plants air demand equally well as the old system. So, in order to compare different alternatives of new system, one way to do this is to check that under the same flow demand resulting pressure drop of new configuration does not lead to inability to supply necessary pressure.

Overall pressure drop together with flow demand is then used to estimate compressor power consumption according to the formula:

$$P = \frac{\dot{m}\Delta p}{\eta},$$

where $\dot{m}$ – volumetric flow rate, Δp - overall pressure drop, η - coefficient of efficiency.

Suppose that flow rate demand over a week of plant is like one showed in Fig. 4. This is flow rate time series that needs to be produced by all compressors. Since the same CAS can have constant and variable speed compressors with different flow capacities some strategy should be used to control them. In real systems it is usual to have constant speed compressors for the purpose to produce general level of demand while variable speed compressors are used to catch the top peaks of flow.

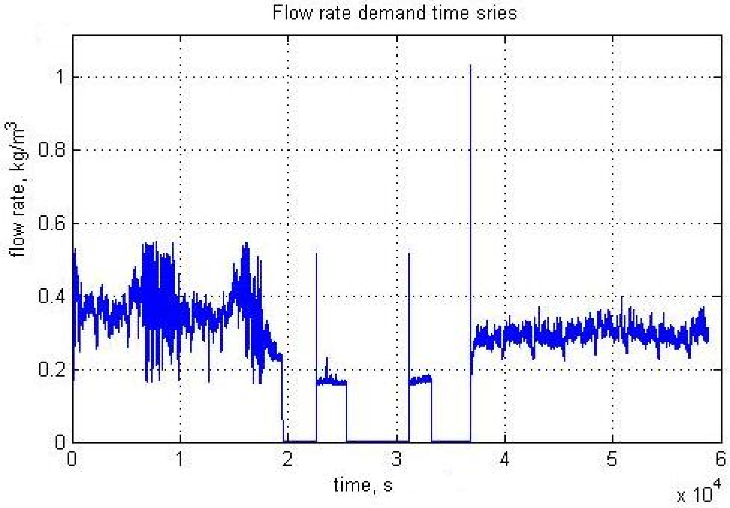

Fig. 4. Flow rate demand of air measure in one week

The provided flow rate demand was satisfied by the newly designed compressed air system, showed above (Fig. 3). Both compressors were identical and of variable speed, but the second was used very shortly at the largest flow peak. Resulted power consumption main characteristics are presented in table below.

Table 3. Main characteristics of power consumption

Maximum (kW)	Minimum (kW)	Average (kW)
202.88	1.35	58.41

Output of this last functionality can also be measurements like pressure, temperature, and flow rate in some specific system places. Places, those are of interest for design purposes. These measurements can be further processed by user or other software, dealing with optimization or can just serve as guidelines for designer.

4. CONCLUSIONS

The presented tool of Energy Simulator proves a valuable framework of modelling for designing of efficient network system considering physical processes and power consumption. Physical network concept and Simscape environment enabled representation of real system as a system of differential algebraic equations. In addition, trapezoidal rule proved to be a way out of the problems caused by stiffness of these equations.

ES functionalities allow this tool to be connected to the external database, in this paper called Knowledge Repository. Such connection can be used for obtaining information about specific system as well as to put results into database from where it can be processed by another software.

ES tool is able to provide power consumption as well as pressure, temperature in various places of virtual model. This flexibility is due to automatic analytical modelling and simulation of physical phenomena. Such measurements in different system locations also enables designer to make place-specific alterations of system configuration.

In addition, due to Simscape richness of various modelling possibilities and due to flexibility of ES tool, other network systems as well as processes could be implemented and analyzed in terms of their power consumption.

ACKNOWLEDGEMENT

This research was done under the project DEMI (Product and Process Design for AmI Supported Energy Efficient Manufacturing Installations) with partial financing from European Commission under the 7th Framework Programme.

REFERENCES

1. QIN, Hongbo Shanghai; MCKANE Aimee, “Improving Energy Efficiency of Compressed Air System Based on System Audit,” 2008.
2. KAYA, Durmus, PHELAN, Patrick, CHAU, SARAC, Ibrahim Energy conservation in compressed-air systems. *International Journal of Energy Research* 26, 837-849 (2002).
3. MORAN, Michael, SHAPIRO, Howard. Fundamentals of Engineering Thermodynamics. Second edition. New York: John Wiley & Sons, 1992.
4. BEATER, Peter Pneumatic Drives. System Design, Modeling and Control. New York: Springer, 2007.
5. SHAPIRO, Howard The Dynamics and Thermodynamics of Compressible Fluid Flow. Vol. 1. New York: John Wiley & Sons, 1953.
6. PAPALAMBROS, Panos, MICHELENA, Nestor. Trends and challenges in system design optimization. *Design* 2154-2159 (2000).

7. KUNKEL, Peter, MEHRMANN, Volker, Differential-Algebraic Equations—Analysis and Numerical Solution, EMS Publishing House, Zurich, Switzerland, 2006.
8. SHAMPINE, Lawrence, REICHELT, Mark, KIERZENKA, Jacek, Solving Index-1 DAEs in MATLAB and Simulink. SIAM Review, Vol. 41, 1999, p 538–552.
9. KUDRYAVTSEV, Dimitrievich (2001), "Implicit function", in Hazewinkel, Michiel, Encyclopedia of Mathematics, Springer.
10. ASCHER, Uri, PETZOLD, Linda. Computer Methods for Ordinary Differential Equations and Differential Algebraic Equations. Philadelphia. 1998.

CYSENI 2012, May 24–25, Kaunas, Lithuania
ISSN 1822-7554, www.cyseni.com

ENERGY CONSUMPTION IN DAY-CARE CENTRE BUILDINGS

Ē. Krūmiņš
Latvia University of Agriculture,
Department of Architecture and Building
Lielā iela. 2, LV-3001, Jelgava, Latvia
Phone +371 29338891
Email: eriks.krumins@inbox.lv

I. Dimdiņa, A. Lešinskis
Riga Technical University, Institute of Heat, Gas and Water Technology
Azenes iela. 16/20, LV-1048, Riga, Latvia
Email: *ilze.dimdina@gmail.com*

ABSTRACT

The aim of the present study was to analyse heat energy consumption in public buildings. Our data contained information about more than 400 public buildings, including data of heat energy consumption depending on the building's use, electric energy consumption and data about the quantity and quality of windows in these buildings in the year 2008. Data was to be analysed dividing all public buildings into twelve groups: schools, special status education schools, day-care centres, hospitals, libraries, cult buildings, recreation centres, local government buildings, museums, sport centres, academy of music, and shelters. The largest groups are schools and day-care centres /kindergartens/. These two groups we were to be analysed particularly.

Our analysis focused on heat energy consumption in buildings with new double-pane windows and frames from polyvinylchloride (PVC) with heat transmittance U≤1.8 W/ (m²•K) and in buildings with simple windows divided into two-panes with two separate wooden frames (heat transmittance U≥2,5W/ (m²•K).

Data analysis showed that partial renovation – change of windows, doors etc. with and without heat insulation of buildings - does not provide the heat energy consumption economy required by the Ministry of Economics by the year 2020, and in the majority of cases made consumption even bigger.

Keywords: heat, energy, day-care centres, renovation, public buildings

1. INTRODUCTION

In the present article, we have reflected and compared the results of our investigations on one of indoor air quality (IAQ) parameters – air temperature, in relationship with heat energy consumption in unrenovated, renovated and newly erected day-care centre buildings. Also have been reflected results of heat loss in current day-care building. Latvian Energy Development Guidelines (EDG) for the years 2007-2016 define that heat energy consumption should decrease by 28%, but by 40% in the time period up the year 2020. Big heat energy demand in buildings is part of Latvia's heritage from the Soviet era. Heat energy consumption in public buildings has been explored very minimally in Latvian scientific research [2], [3], [4]. We did not find similar studies in Latvian scientific publications.

Partially renovated and newly erected buildings do not include the creation of new energy efficiency ventilation systems.

After partial renovation, the IAQ slowly begins to deteriorate because outdoor air infiltration has stopped. Reconstructed, old natural ventilation and mechanical systems do not provide the necessary air exchange and quality. Residential buildings have the same problem.

This unpleasant fact was overlooked for a very long time. Buildings get “sick building syndrome” after some time.

Having clean air indoors is very important for the health of the population as a whole and becomes particularly important for vulnerable groups like babies and children. Various indoor air pollutants (volatile organic compounds, biological pollutants, etc. emitted from furniture, cleaning agents, floor covering materials) are responsible for respiratory diseases and allergies [1].

2. MATERIALS AND METHODS

We have analysed heat energy consumption in unrenovated public buildings and in buildings after partial renovation managed by Riga City Municipality in the year 2008. Our aggregate information contained data on 422 public buildings. We divided all buildings in 12 subgroups: schools, special status educational institutions, music academies, day-care centres, hospitals, libraries, religious buildings, recreation centres, local government buildings, museums, sports centres and shelters. We have analysed energy consumption in 143 day-care centre buildings in Riga and calculated how much heat energy was required for one square metre of floor area in each respective condition of the buildings.

The largest groups are: schools (158 units analysed) and day-care centres (143 units analysed). Our analysis focused on heat energy consumption in buildings that are:

a) unrenovated and with simple windows divided into two panes, with two separate wooden frames with a heat transmittance $U \geq 2.5$ (W/m²·K),
b) partially renovated and newly erected with energy-efficient double-pane windows made and polyvinylchloride (PVC) frames with a heat transmittance $U \leq 1.8$ (W/m²·K).

We obtained our research data after the heating season in the spring and summer of the year 2009. We prepared a special inquiry form and sent it to the chief of every public building managed by Riga City Municipality. After receiving completed forms we sorted them and gathered information. Forms with incomplete information were considered unusable and were discarded. After we finished gathering data we conducted a statistical analysis.

Our data analysis was based on building mathematics, meaning parameters were compared in each of the 12 subgroups separately. We calculated each building group’s floor area and heat consumption for the year. Then we calculated how much heat energy each type of building required per one square metre of floor area. After that we compared findings in unrenovated buildings and in newly erected and partially renovated buildings.

In the 2010/2011 heating season from 10 February to 17 March, we obtained data of IAQ parameter measurements with the data loggers MINILOG (air temperature), EASYLOG (relative humidity of air) and Wöhler CDL 210 (air temperature, relative humidity of air, carbon dioxide concentration). The time gap set for the loggers was 5 minutes. The total data obtained consists of more than 60 000 units. Data was obtained in day-care centre buildings at 1.5-1.7m above the floor. Data was obtained during a cold time of year, as we then have the opportunity to rate the heating systems and the IAQ. We compared the findings of newly erected and unrenovated buildings, and buildings after a partial renovation. The result of the temperature chart of indoor air was compared to the chart of the air temperature outdoors [5].

On 23 January in the 2011/2012 heating season, we implemented a heat losses analysis system throughout the day-care centre building envelope surface. An FLIR P25 thermal camera was set up to do this. An FLIR P25 and a TESTO 845 infrared thermometer with switchable optics were used to obtain temperature difference data.

3. RESULTS AND DISCUSSION

In Table 1 display's information about day-care centre buildings total floor areas, heat consumption in each kind of conditions which was divided in buildings with window covering less than 20% and more than 20% from the building facades.

Table 1. Proportion of total floor areas and total heat consumption per annum in not renovated and in partially renovated and newly erected day-care centre buildings, comparing in per cents

Buildings	Windows covering ≤20% from the building facades		Windows covering >20% from the building facades	
	Total floor areas (8 262m²)	Heat consumption per annum (1 933MWh)	Total floor areas (240 661m²)	Heat consumption per annum (51 169MWh)
Not renovated	64	52	27	23
Partially renovated and newly erected	36	48	73	77

In Table 2 display information about heat and electric energy consumption into 143 units of day-care centre buildings.

Table 2. Heat and electric energy consumption in day-care centre buildings

Total number of units not renovated partially renovated	143 32 111
Total floor areas (m^2)	248 923
Average unit area (m^2)	1 741
Heat energy total consumption (kWh) in this group of buildings per annum	53 102 920
Heat energy average consumption ($kWh\cdot m^{-2}$) in this group of buildings per annum	213
Heat energy average consumption ($kWh\cdot m^{-2}$) in not renovated buildings per annum	184
Heat energy average consumption ($kWh\cdot m^{-2}$) in partially renovated buildings per annum	224
Electric energy total consumption (kWh) in this group of buildings per annum / average - ($kWh\cdot m^{-2}$)	7 010 729 /28
Electric energy total consumption (kWh) in not renovated buildings per annum / average - ($kWh\cdot m^{-2}$)	1 685 457 /25
Electric energy total consumption (kWh) in partially renovated buildings per annum / average - ($kWh\cdot m^{-2}$)	5 325 272 /29
Ventilation with and without air conditioning systems in buildings 1.Total number of units 2.Total power (kW) 3.Total power to building one square metre ($kW\cdot m^{-2}$)	 79 262 $1\cdot 10^{-3}$

We compared total heat consumption in unrenovated buildings, in buildings after a partial renovation and newly erected buildings. Our analysis showed that day-care centre buildings with similar total floor areas have a large heat energy consumption difference. Energy resource consumption does not decrease on the desideratum level determinate in the EDG. The method of analysis was based on Krumins E. et al., [3], [4], [5]. The result of this analysis is reflected in Fig. 1. Normative trend-line for day-care center buildings (y=74,658x+74485) is our finding. Total building heat consumption per annum must be locate on or under the line which equation is y =74,658x+74485.

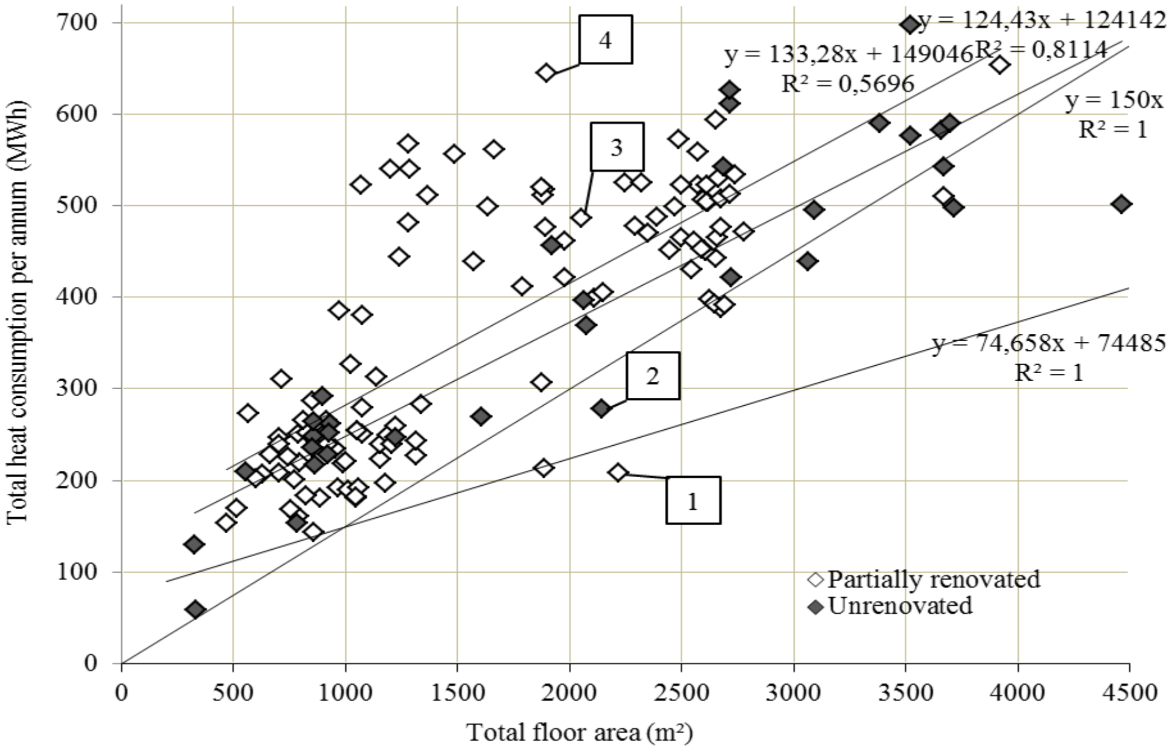

Fig. 1. Unrenovated and partially renovated day-care centre buildings. Total heat energy consumption (MWh) per annum correlation with building floor areas (m^2) with trend-lines: Abstract (y=150x); Unenovated buildings (y=124.43x+124142); Partially renovated buildings (y=133.28x+149046); Normative for day-care center buildings (y=74.658x+74485)

In Fig. 1 we clearly see that in partially renovated day-care centre buildings something was done incorrectly. In day-care centre buildings with similar total floor areas have a big difference in heat consumption per annum. For example, compare building total floor areas (m^2) and heat consumption (MWh) per annum in:

- day-care centre building No.1: 2217m^2 – 208,00MWh (94kWh/m^{2}p.a.);
- day-care centre building No.2: 2142m^2 – 278,02MWh (130kWh/m^{2}p.a.);
- day-care centre building No.3: 2054m^2 – 486,00MWh (237kWh/m^{2}p.a.);
- day-care centre building No.4: 1901m^2 – 645,00MWh (339kWh/m^{2}p.a.).

In Fig. 2 display air temperature indoors in unrenovated, partially renovated and newly erected day-care centre buildings and outdoors. In thermographic lines was fixed correct air temperature indoors, which providing the recommended air temperature indoors +19^{0}C–+25^{0}C as was written in Labour Protection Requirements in Workplaces as prescribed in regulation no. 359 from 28 April, 2009 of The Cabinet of Ministers of the Republic of Latvia and in Regulations No. 596 *Hygiene requirements for educational institutions, implementing preschool program* of the Cabinet of Ministers of the Republic of Latvia.

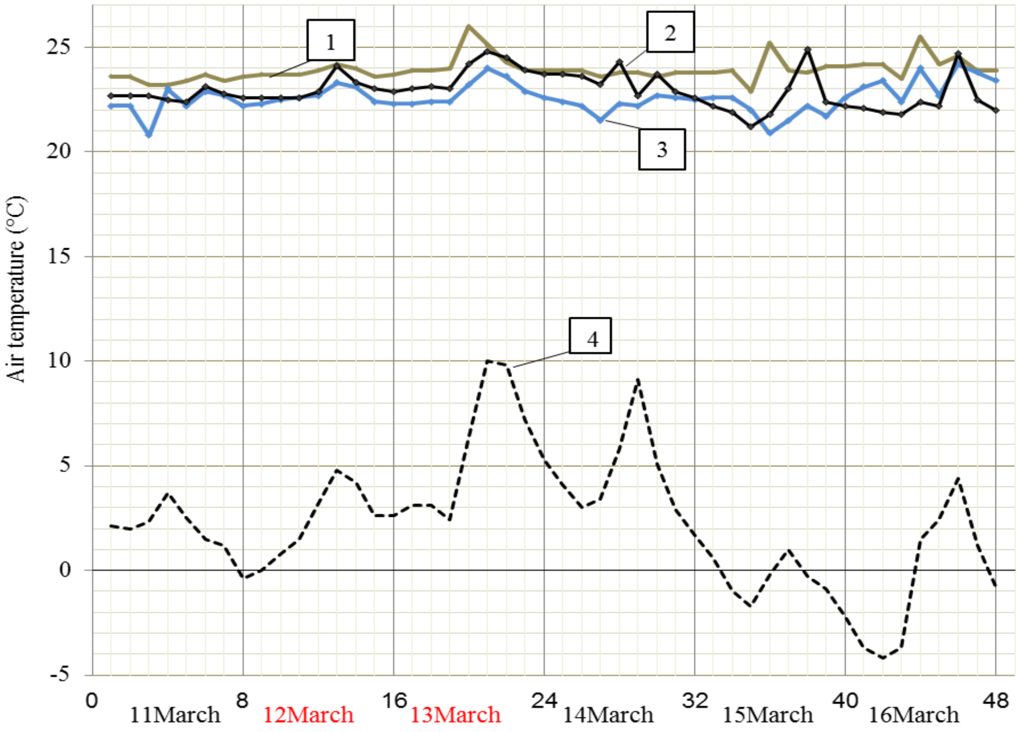

Fig. 2. Air temperature in: 1 – partially renovated building (renovated in 2007, average heat consumption 339kWh/m^2 per annum); 2 – newly erected building (built in 2005, average heat consumption 94kWh/m^2 per annum); 3 – unrenovated building (average heat consumption 130kWh/m^2 per annum); 4 – outdoors

As shown in Fig. 2, in the current case the highest air temperature indoors and largest heat energy consumption in 2008 was in a partially renovated day-care centre building. It was 339kWh/m^2. (In Figure 1 it is day-care centre building No.4: 1901m^2 – 645,00MWh).

It is importantly to use energy economically and effectively. Thus, we attempted to find the causes of such extensive heat energy consumption in partially renovated day-care centre buildings. This was done on 23 January 2012, when we implemented a heat loss analysis throughout the day-care centre building envelope with a thermal camera (FLIR P25), an infrared thermometer with switchable optics (TESTO 845) and a thermo-anemometer with a flexible telescopic probe (AIRFLOW TA-7). The outdoor air temperature was between -3.2^{0}C at 11:00 and -3.6^{0}C at 14:00; the wind direction: E, 4-8m/s in Riga [6].

The following figures will show thermal photos, photos of building cells, thermographic figures – the allocation of temperature degrees in percentages in the local area (Ar1) of the thermal photo, indicators of fixed values and thermographic lines – temperature differences (Li1) in the respective line of the thermal photo (read from left side to right). Current building was partially renovated and partially built in 2007.

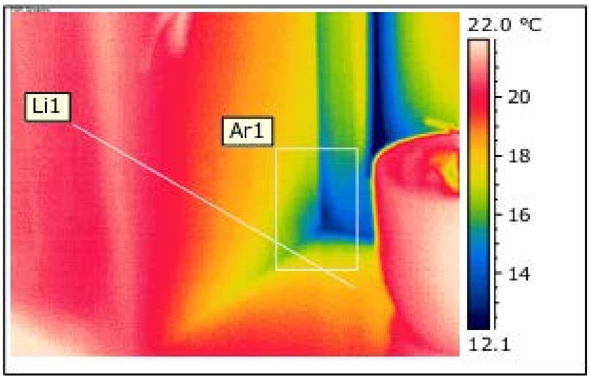

Fig. 3. Thermal photo of the corner

Fig. 4. Photo of the corner

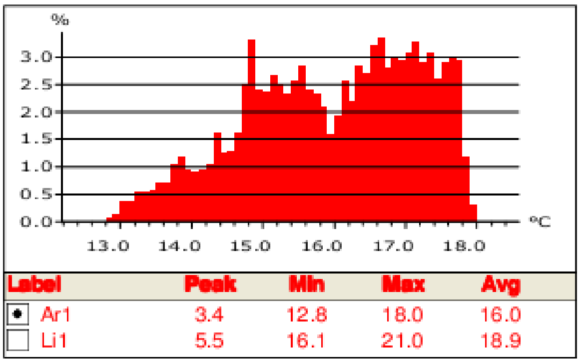

Label	Peak	Min	Max	Avg
● Ar1	3.4	12.8	18.0	16.0
☐ Li1	5.5	16.1	21.0	18.9

Fig. 5. Allocation of temperature degrees in percentages in the local areaAr1

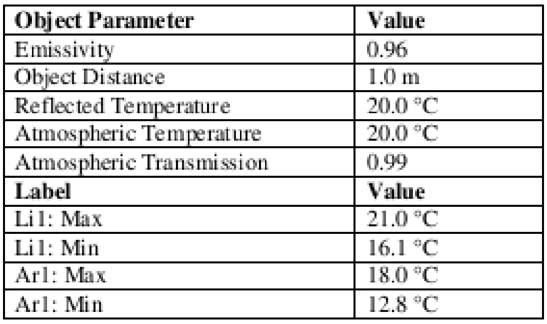

Object Parameter	Value
Emissivity	0.96
Object Distance	1.0 m
Reflected Temperature	20.0 °C
Atmospheric Temperature	20.0 °C
Atmospheric Transmission	0.99
Label	**Value**
Li1: Max	21.0 °C
Li1: Min	16.1 °C
Ar1: Max	18.0 °C
Ar1: Min	12.8 °C

Fig. 6. Indicator of fixed values

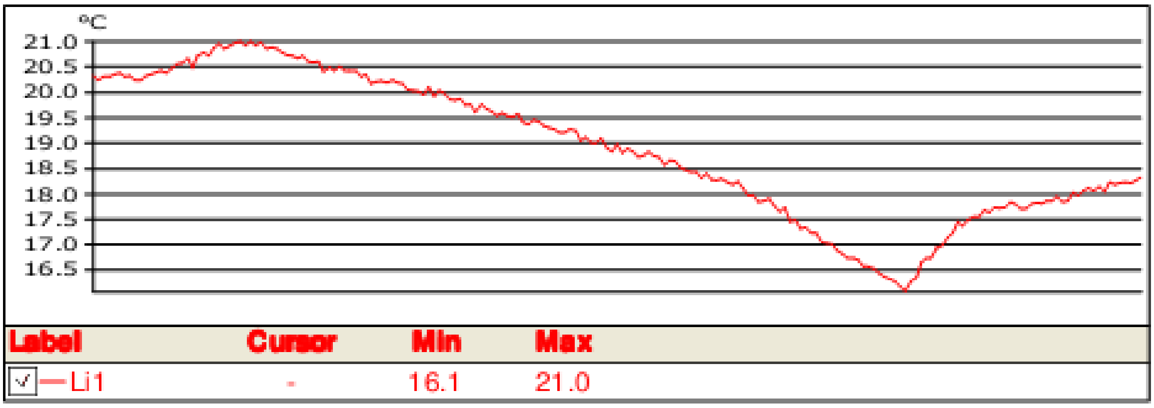

Label	Cursor	Min	Max
☑ Li1	-	16.1	21.0

Fig. 7. Thermographic line Li1 of the thermal photo of the corner

Figs. 3 through 7 display information about heat loss caused in the respective corner. We fixed the improper window compounding with a wall. On the inspection day, the wind speed was low – E, 4-8m/s. Fig. 4 shows the fixed outdoor air infiltration of a windy day's after-effects through the wall via a small gap as a darker shade. The temperature at the top of the corner is very low – only +12.8^{0}C in Ar1. The indoor air temperature was fixed at +21,0^{0}C in Li1.

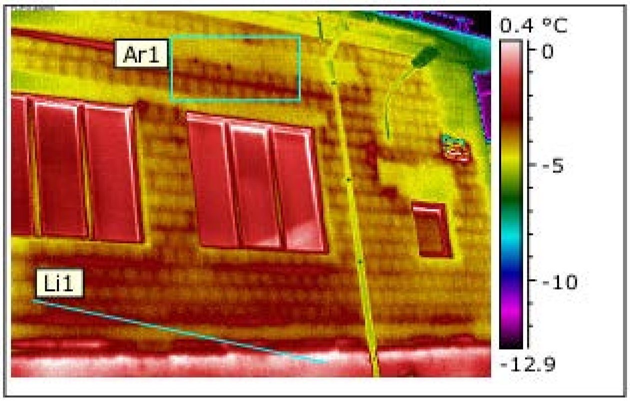

Fig. 8. Thermal photo of the building envelope

Fig. 9. A part of the newly erected building facade's south side without heat insulation

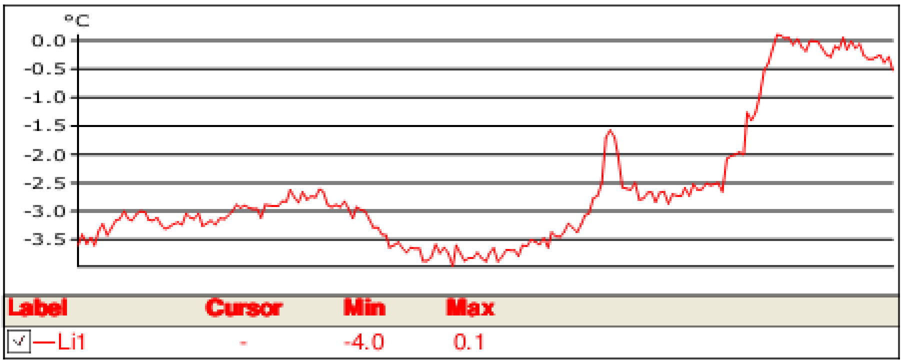

Label	Cursor	Min	Max
☑ —Li1	-	-4.0	0.1

Fig. 10. Thermographic line Li1 of the thermal photo of the building envelope

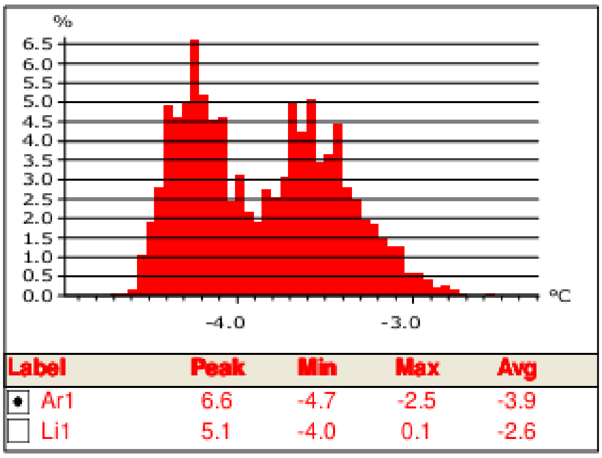

Label	Peak	Min	Max	Avg
● Ar1	6.6	-4.7	-2.5	-3.9
☐ Li1	5.1	-4.0	0.1	-2.6

Fig. 11. Allocation of temperature degrees in percentages in the local area Ar1

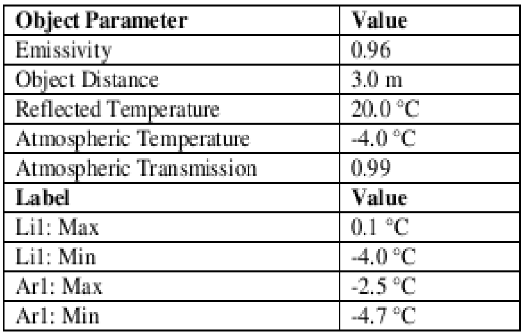

Object Parameter	Value
Emissivity	0.96
Object Distance	3.0 m
Reflected Temperature	20.0 °C
Atmospheric Temperature	-4.0 °C
Atmospheric Transmission	0.99
Label	**Value**
Li1: Max	0.1 °C
Li1: Min	-4.0 °C
Ar1: Max	-2.5 °C
Ar1: Min	-4.7 °C

Fig. 12. Indicator of fixed values

Figs. 8 to 12 display temperature differences on part of the south side of the building envelope surface. The temperature difference of -4.0^{0}C to +0.1^{0}C in Li1 demonstrates that the respective building facade has very large heat losses. The reason for this is the inadequate heat insulation of the building’s current walls. The visible surface of the materials of the inner building wall in Figure 8 confirms this. We can see the same in the following Fig. 13.

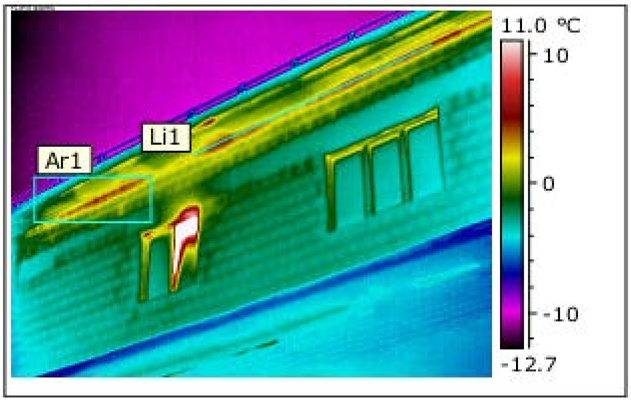

Fig. 13. Thermal photo of part of the building facade

Fig. 14. A part of the newly erected building facade’s west side without heat insulation

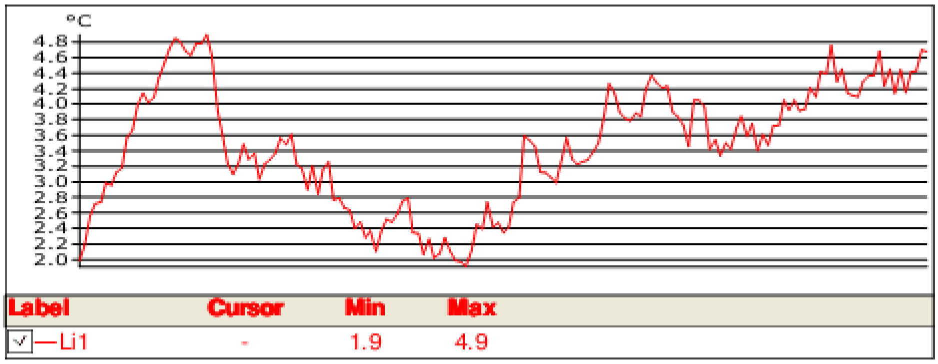

Label	Cursor	Min	Max
☑ —Li1	-	1.9	4.9

Fig. 15. Thermographic line Li1 of the thermal photo of the building façade

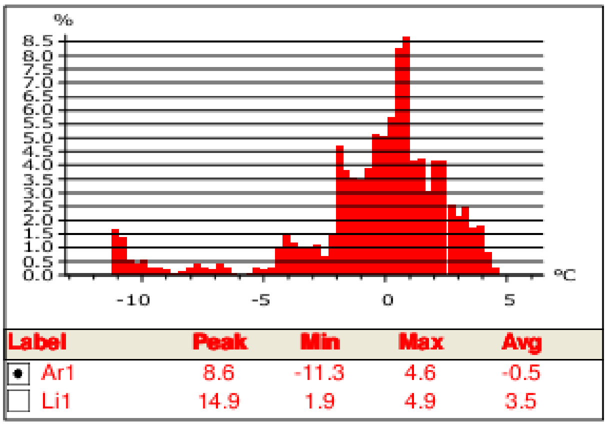

Label	Peak	Min	Max	Avg
● Ar1	8.6	-11.3	4.6	-0.5
☐ Li1	14.9	1.9	4.9	3.5

Fig. 16. Allocation of temperature degrees in percentages in the local area Ar 1

Object Parameter	Value
Emissivity	0.96
Object Distance	3.0 m
Reflected Temperature	20.0 °C
Atmospheric Temperature	-4.0 °C
Atmospheric Transmission	0.99
Label	**Value**
Li1: Max	4.9 °C
Li1: Min	1.9 °C
Ar1: Max	4.6 °C
Ar1: Min	-11.3 °C

Fig. 17. Indicator of fixed values

Figs. 13 through 17 display temperature differences on part of the west side of the building envelope surface. The temperature difference of $+1.9^0$C to $+4.9^0$C in Li1 demonstrates that the roof of the respective building's facade has very large heat losses from rooms via the second floor ceilings to the loft. Eastern winds result in the respective thermal photo in Figure 13. If this building had been built correctly, the thermographic line's minimum and maximum values would not exceed the air temperature outdoors: -4.0^0C.

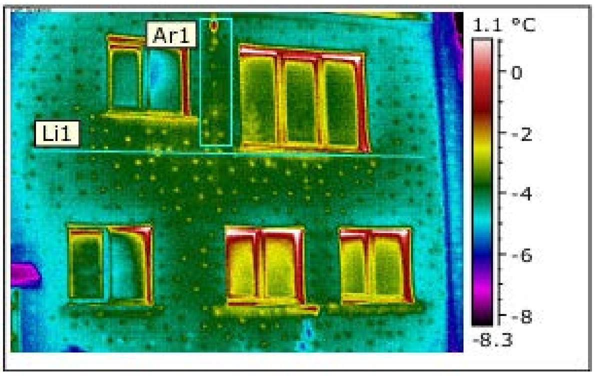

Fig. 18. Thermal photo of part of the building facade

Fig. 19. A part of the renovated building facade's west side with heat insulation

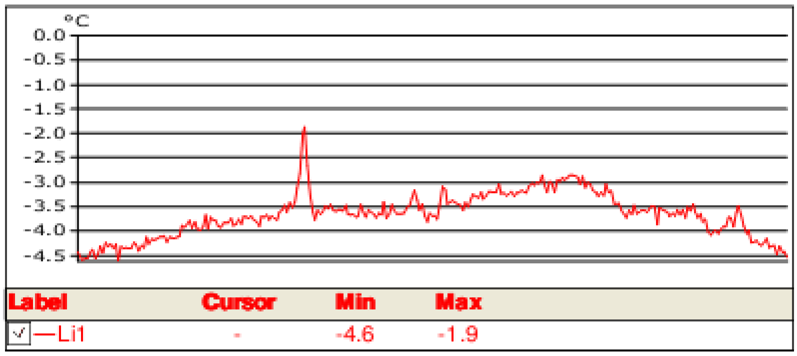

Label	Cursor	Min	Max
☑ —Li1	-	-4.6	-1.9

Fig. 20. Thermographic line Li1 of the thermal photo of the building façade

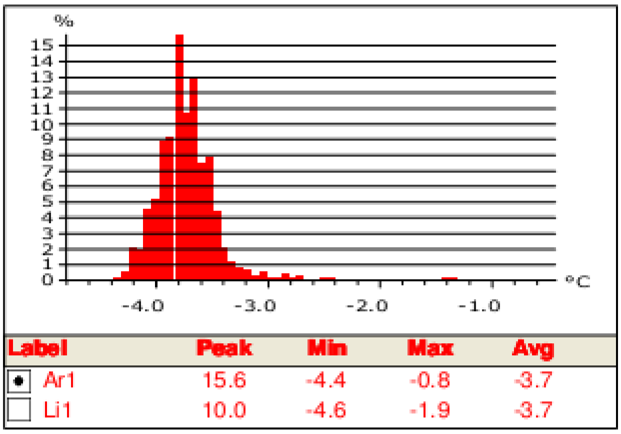

Label	Peak	Min	Max	Avg
● Ar1	15.6	-4.4	-0.8	-3.7
☐ Li1	10.0	-4.6	-1.9	-3.7

Fig. 21. Allocation of temperature degrees in percentages in the local area Ar1

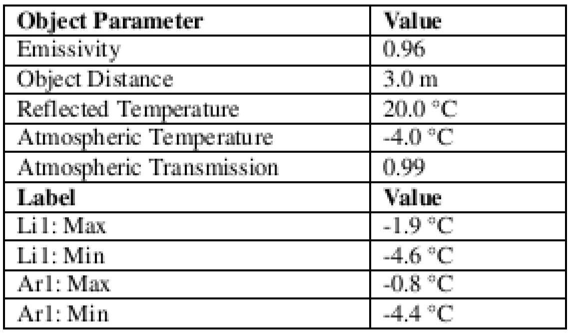

Object Parameter	Value
Emissivity	0.96
Object Distance	3.0 m
Reflected Temperature	20.0 °C
Atmospheric Temperature	-4.0 °C
Atmospheric Transmission	0.99
Label	**Value**
Li1: Max	-1.9 °C
Li1: Min	-4.6 °C
Ar1: Max	-0.8 °C
Ar1: Min	-4.4 °C

Fig. 22. Indicator of fixed values

Figs. 18 to 22 display temperature differences on part of the south side of the building envelope surface. The temperature difference of -0.8^{0}C in Ar1 to -4.6^{0}C in Li1 demonstrates that the respective building facade has large heat losses.

4. CONCLUSIONS

The current study on heat energy consumption has reflected tendencies in day-care centre building and renovation.

Increased heat energy consumption in day-care centre buildings indicates that partial renovation was done with inadequate project solutions.

The main solution to these problems is to take an integrated approach to the IAQ and to establish energy-saving, quality ventilation and air condition systems.

Partial renovation of buildings has not decelerated heat energy consumption.

REFERENCES

1. BERNSTEIN, J A., ALEXIS, N., BACCHUS, H. et al. *The health effects of nonindustrial indoor air pollution // Allergy and Clinical Immunology*. 2007, p. 585–591.
2. KRUMINS, E., DIMDINA., I., LESINSKIS, A. Heat Consumption Analysis In Riga City Public Buildings. Indoor Climate Of Buildings 2010. Proceedings of the SSTP-7th International Conference. High Tatras: Slovak University of Technology, November 28 – December 1, 2010, p.217-223, ISBN 978-80-89216-37-6.
3. KRUMINS, E., DIMDINA., I., LESINSKIS, A. Heat Energy Consumption Analysis in Riga City Not Renovated Public Buildings and in Buildings After Partial Renovation. Enineering for Rural Development 2011. Proceedings of the 10th International Scientific Conference. Jelgava: Latvia University of Agriculture, May 26–27, 2011, p. 348–353, ISSN 1691-3043.
4. KRUMINS, E., DIMDINA., I., LESINSKIS, A. Heat Consumption Analysis in Public Buildings Managed by Riga City Municipality. ROOMVENT 2011. Proceedings of the 12th International Conference on Air Distributing in Rooms, Trondheim: Norwegian University of Science and Technology, June 19–22, 2011, [flash memory] ISBN 978-82-519-2812-0.
5. KRUMINS, E., DIMDINA., I., LESINSKIS, A. Heat Energy Consumption and Indoor Environment in the Three Different Conditions of Day-care Centre Buildings. RURAL DEVELPOMENT 2011. Proceedings 1 of the Fifth International Scientific Conference, Kaunas: Akademija, 24-25 November, 2011, Vol. 5, p. 359–365, ISSN 1822-3230.
6. State Limited Liability Company Latvian Environment, Geology and Meteorology Centre, [Referred on the 23 January in 2012 y.]. Link to the internet <http://www.meteo.lv/public/26902.html>.

ACKNOWLEDGEMENT

Current research has been done with a support of ESF grant.

Contract no. 2009/0180/1DP/1.1.2.1.2/09/IPIA/VIAA/017

ESF
EIROPAS SOCIĀLAIS FONDS

CYSENI 2012, May 24–25, Kaunas, Lithuania
ISSN 1822-7554, www.cyseni.com

HEAT PERMEABILITY MEASUREMENT WITH THERMOGRAPHIC CAMERA

S.Liepiņš
Department of Architecture and Building
Latvia University of Agriculture
Akademijas str. 19, LV-3001, Jelgava – Latvia
Phone +371 29390456
Email: sandris.liepins@inbox.lv

A. Lešinskis
Riga Technical University
Institute of Heat, Gas and Water Technology
Azenes str. 16/20, LV-1048, Riga – Latvia

U.Iljins
Faculty of Information Technologies
Latvia University of Agriculture
Liela str. 2, LV-3001, Jelgava – Latvia

ABSTRACT

Thermographic cameras are widely used for inspecting and analyzing surfaces of building external constructions. The method demonstrates a complete image of thermal spots and is suitable for giving limited conclusions about the whole surface temperature of the construction. The main problem of infrared analysis is exact temperature layout, because different heat transmission areas can be seen on the screen, but heat radiation levels are not so reliable. Such temperature differences can exceed even 50% of the real surface temperature. To explore more accurate surface point temperatures special thermal sensors and devices were applied. By point type infrared and thermo-couple device temperature distribution points on building material surface were gathered, compared and calibrated with the infrared camera output image. Also mathematical temperature curves were calculated to prove the temperature distribution on the surface. Sample for practical research was external wall construction of cold-storage, in Kuiviži, Latvia. Results were compared with manufacturer's technical information. Using thermal imaging cameras with contact measuring devices, and setting the surface temperature proxies in a wide area, heat transfer coefficient of external construction can be calculated by means of a three-temperature method, which includes the point and linear thermal bridges and other places of heat loss in constructions. The method provides an opportunity to expand the experimental use of the thermal image camera for determining heat transfer of external constructions.

Keywords: thermal analysis, heat transfer, infrared method

1. INTRODUCTION

There is a need for thermographic calculations regarding external constructions to design energy saving buildings with good indoor climatic conditions, in combination with efficient and highly durable materials, as well as environmentally friendly technologies. Building external constructions generally consist of foundations, walls and roofs, but this study analyzes only the above-ground parts of those structures. In every type of construction, intra-thermal processes take place. They depend on the properties of the applied materials and exterior environment. Thermal processes in structures can be identified and quantified in cases where one or more structural surfaces are in different heat and moisture (environmental) conditions. The order of thermal designing of bound constructions is regulated by the Latvian building regulation LBN 002-01 ‘Heat transfer in building envelopes’ [1].

The aim of the research was to combine analytical and experimental methods of thermal analysis and carry out experimental thermal analysis of external constructions (composite panels).

Using thermal imaging cameras with contact measuring devices, and setting the surface temperature proxies in a wide area, bound construction heat transfer coefficient can be calculated by means of a three-temperature method, which includes the point and linear thermal bridges and other places of heat loss in constructions. The method provides an opportunity to expand the experimental use of the thermal image camera for determining heat transfer through external constructions.

2. METHODOLOGY

An experimental research for existing building – analysis of wall construction was done. Wall constructions of cold-storage in Kuiviži, Latvia (Fig. 1) are composite sandwich panels, consisting of two metal sheet layers and poly-urethane (PU) thermoisolation filling. Manufacturer ‘ThyssenKrupp Bausysteme GmbH’ gives a heat transfer coefficient of the composite facade panel with PU stuffing: ems-isolier cold storage panel PU 120, thickness 120 mm, heat transfer coefficient $U = 0.190$ W/m^2×K [2].

Fig. 1. Cold-storage, in Kuiviži, Latvia and experimental sample

2.1. Technical devices used in the research

a) Testo 845. A thermometer which operates in the spectrum of infrared waves in a narrow area (points), equipped with a thermocouple probe for contact measuring surface temperature:

- Measurement range: -35˚C to +950˚C;
- Accuracy of the infrared device and thermocouple at room temperature: ±0,75˚C.

b) ThermoPro TP8. Camera of thermal picture, operates in the spectrum of infrared waves (thermographic camera):

- Measurement range: -20˚C to +800˚C;
- Resolution: 384 × 288 thermal pixels (sensors);
- Accuracy: ±1˚C or 1% of the result.

2.2. Description of experimental research method

The experimental research method consists of several parts. Sample was divided into parts over the midfield in the area of 3.0 x 2.4 m, where the step on X-axis was 0,6 m, and the step on Y-axis was 0.5 m.

Measurement points on X-axis were marked from X1 to X5; on Y-axis: from Y1 to Y5. (Fig. 2). According to the matrix principle measurement points XY11 (upper left corner), XY12, XY21 and XY22 (lower right corner) were marked in the corners of the sample.

Surface temperatures were measured in the marked points using the device Testo 845 with a surface thermometer which operates in the spectrum of infrared waves and thermocouple probe. The data gathered is shown in Figure 3. After reading the surface temperature with Testo 845, thermography of the sample was carried out with ThermoPro TP8.

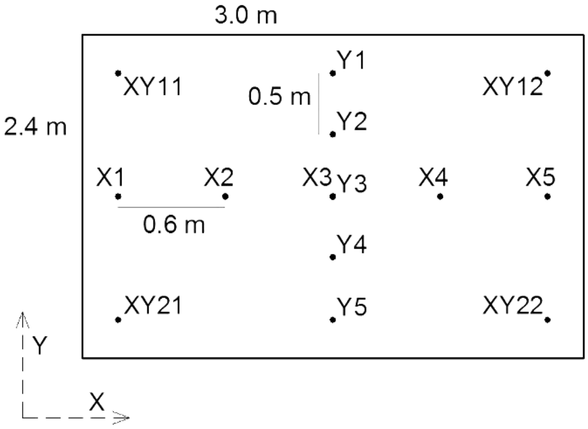

Fig. 2. Scheme of measurement points on the sample surface

Calibrating emission coefficient *ε* of the picture in the infrared spectrum real temperature division on the sample surface was obtained which corresponded to the measurements of thermocouple in characteristic points on X-axis and Y-axis.

Average temperature was chosen; resistance of surface air layers and coefficient of heat transfer coefficient *U* (W/m^2×K) were calculated using the results of civil physics formulas.

3. RESULTS AND DISCUSSIONS

Weather conditions were fixed outside +12.6 ºC, wind speed 0 m/s, but temperature in the cooling chamber changed from -17.4 °C to -20.0 °C (within 15 minutes), in the conditions of fast and turbulent air.

Measurements of experimantal samples (Fig. 3), where:

- Testo 845, T.C. – temperatures at points read from the Testo 845 thermocouples probe,
- TP8, ε=0.99 (ThermoPro) – results from the programme treated pictures in the infrared spectrum where the coefficient of the surface emission is ε=0.99,
- TP8, ε=0.65 (ThermoPro) – results from the programme treated pictures in the infrared spectrum where the coefficient of the surface emission is calibrated by trial and error method ε=0.65 and corresponds to measured average temperature of frame area and average of Testo 845 temperature pickups (Fig. 4).

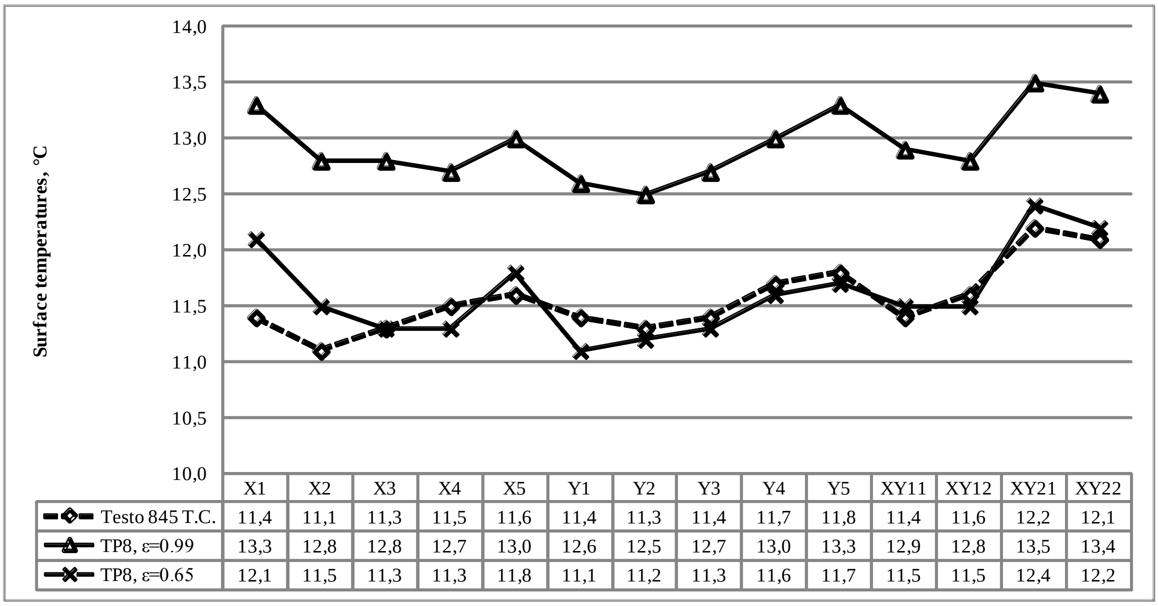

	X1	X2	X3	X4	X5	Y1	Y2	Y3	Y4	Y5	XY11	XY12	XY21	XY22
Testo 845 T.C.	11,4	11,1	11,3	11,5	11,6	11,4	11,3	11,4	11,7	11,8	11,4	11,6	12,2	12,1
TP8, ε=0.99	13,3	12,8	12,8	12,7	13,0	12,6	12,5	12,7	13,0	13,3	12,9	12,8	13,5	13,4
TP8, ε=0.65	12,1	11,5	11,3	11,3	11,8	11,1	11,2	11,3	11,6	11,7	11,5	11,5	12,4	12,2

Fig. 3. Measurement results of the surface temperature on X- and Y-axis

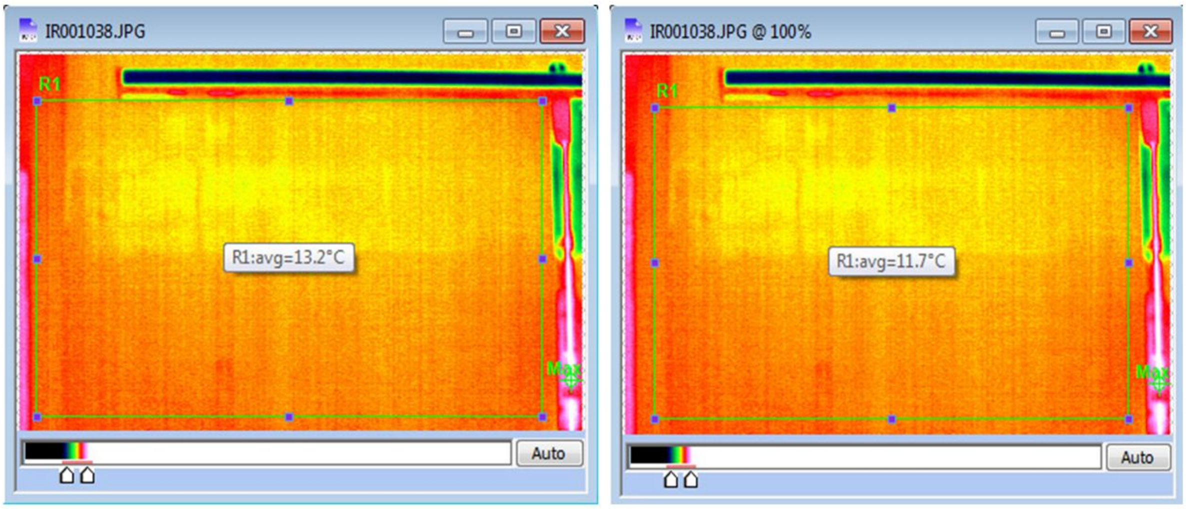

Fig. 4. Measurements of the surface temperature with ThermoPro TP8 (left: with frame T_{avg}=13.2 °C at ε=0.99; right: with frame T_{avg}=11,7 °C at ε=0,65). Analysis made using the programme Guide IrAnalyser

Heat flows *q* and heat transfer coefficient *U* can be defined:

$$q = \propto_1 (T_e - T_1) = U (T_e - T_i) \quad and \tag{1}$$

$$U = \propto_1 \frac{T_e - T_1}{T_e - T_i} \quad , \tag{2}$$

where
α_1 – coefficient of heat transmission on measured surface, W/m^2×K
T_i – temperature inside cold storage, °C
T_e – outer temperature in air, °C
T_1 – temperature on the first surface of the boundary construction, °C [2]

This method is also called ‘method of three temperatures’.

Respectively,

$$q = \propto \Delta T \quad and \quad \propto = \frac{q}{\Delta T} \tag{3}$$

$$\alpha_1 = \alpha_c + \alpha_\lambda \ , \tag{4}$$

where
α_1 – coefficient of heat transmission on measured surface, W/m^2×K
α_c – coefficient of heat transmission by convection, W/m^2×K
α_λ – coefficient of heat transmission by radiation, W/m^2×K [3],

$$\alpha_c = 2 \cdot \Delta T^{1/4} \; and \; \alpha_\lambda = 5{,}67 \frac{\left(\frac{T_e}{100}\right)^4 - \left(\frac{T_1}{100}\right)^4}{T_e - T_1} \quad [3] \, . \tag{5}$$

To calculate heat transfer coefficient *U*, temperatures T_1, T_i and T_e are needed. Temperature on the first surface of the boundary construction T_1 = +11,7 °C, average temperature inside cold storage T_i = -19,9 °C, fixed outer temperature in air T_e = +12,6 °C.

$$\alpha_c = 2 \cdot \Delta T^{1/4} = 2 \cdot (12{,}6 - 11{,}7)^{1/4} = 1{,}948 \frac{W}{m^2 K} \tag{6}$$

$$\alpha_\lambda = 5{,}67 \frac{\left(\frac{273{,}15 + 12{,}6}{100}\right)^4 - \left(\frac{273{,}15 + 11{,}7}{100}\right)^4}{12{,}6 - 11{,}7} = 5{,}267 \frac{W}{m^2 K} \tag{7}$$

$$\alpha_1 = \alpha_c + \alpha_\lambda = 1{,}948 + 5{,}267 = 7{,}215 \frac{W}{m^2 K} \tag{8}$$

$$U_X = \propto_1 \frac{T_e - T_1}{T_e - T_1} = 7{,}215 \frac{12{,}6_{(Te)} - 11{,}7_{(T1)}}{12{,}6_{(Te)} - (-19{,}9_{(Ti)})} = 0{,}1998 \frac{W}{m^2 K} \tag{9}$$

Standardized coefficient of heat transfer given by the manufacturer to the construction U = 0.190 W/m^2×K. After calculations, mismatch U / U_x is Δ = 4.9 %.

4. CONCLUSIONS

Camera of thermal imaging, which shows surface temperatures in the infrared spectrum alone without other devices indicates only the general temperature of the surface, which can differ from actual temperatures >50%, because of an incorrect assumptive coefficient of the surface emission (ε=0,01 to 0,99);

When using the thermographic camera together with other measuring devices and defining surface temperatures in a wide area, it is possible to calculate the heat transfer coefficient of the bound construction, also pointed and linear thermal bridges and other spots of heat losses in the construction. We used the method of three temperatures in the calculations.

REFERENCES

1. Regulations issued by the Cabinet Nr.495, LBN 002-01 Heat engineering of building bound constructions. November 27, 2001 (in Latvian).
2. Ems-isolier cold store panel PU product features. ThyssenKrupp Bausysteme GmbH, 2012 – [referred on the 5th of march in 2012 y.]. Link to the internet http://construction.thyssenkrupp-steel-europe.com/en/produkte/wand/pur_pir/ems_isolier_kuehlhauspaneel.jsp .
3. VALTERS, A., APINIS, A., OGRIŅŠ, M., DANEBERGS, A., LŪSIS, DZ., OKMANIS, A., ČUDARS, J. *Physics*. Riga: Zvaigzne, 1992. 735 p. (in Latvian).

CYSENI 2012, May 24–25, Kaunas, Lithuania
ISSN 1822-7554, www.cyseni.com

CASE STUDY OF ENERGY EFFICIENCY IN AIR HANDLING UNITS IN LATVIA SCHOOLS

G. Plavenieks, A. Lesinskis
Riga Technical University
Institute of Heat, Gas and Water technology
Azenes str. 16-20, LV 1010 Riga – Latvia
Phone +371 29 419967
E-mail: gatis.plavenieks@rtu.lv
E-mail: arturs@lafivents.lv

ABSTRACT

This paper presents a case study of energy efficiency of air handling units for schools in Latvia.

The paper summarizes the possible configurations of air handling units, carried out analytical studies searching for an optimum variant of the energy savings and optimization point of view, taking into account the specifics of learning process in Latvia schools.

Results show the use of air handling units optimization based methods should be encouraged due to the potentials for energy savings combined with improved indoor air quality of learning process in Latvia schools.

Reducing energy consumption, energy efficiency and optimization of air handling units in schools is important to address the global challenges of climate change and natural resources careful use.

Keywords: air handling units, energy efficiency, ventilation in schools

1. INTRODUCTION

Worldwide increase energy consumption. This reflects the economic development and quality of life. This in turn causes increases in energy prices. At the same time it allows develop studies, which may be more economic use of energy resources, as well as invest in systems that use less energy than existing ones [1].

This is one of the main conditions that contribute to research in the field of ventilation. Ventilation system efficiency is important today and will be in the future as well. The opportunities and benefits of more efficient ventilation systems will be important for both indoor comfort and energy-saving point of view.

Great potential for energy conservation is seen in the building sector. If ventilation rates are reduced, energy is saved, but, at the same time, indoor air quality is deteriorated.

Schools is one of building sector with high energy consumption in Latvia, but the same time with great potential to save energy by demand ventilation. The aim of the article is analyze possible scenarios selecting of air handling units (AHU) for schools in Latvia by taking account local specifics. Target is make possible air handling unit selections providing indoor air quality (IAQ) according to Europe normative EN 13779:2007 classification IDA1 to IDA4. Actuality of paper is that it is prepared the same time when reforms where planned in education system by changing period of studies in schools from 2012 in Latvia.

2. MATERIALS AND METHODS

The field surveys were completed as one of the region's schools. This region of the schools built in the last century, hence do not correspond to modern requirements in both quantitative and qualitative terms. Regional management plans renovation an existing schools. The study is divided into several stages-before renovation when the focus is on the analysis of the existing situation, including demographic indicators, indoor air quality solutions and performance, with possible technical-economical solutions, taking into account existing energy prices in the region. Planned after reconstruction of existing schools, to take measurements from the study to assess how the IAQ is EN13779: 2007 requirements and how energy efficient school ventilation system solutions are created and what possible measures to take in order to ensure sustainable solutions.

The study was based on several criteria:

2. Climatic conditions in Latvia (outside temperatures during summer, winter etc.).
3. The Latvian educational system (number of school days, vacations, hours).
4. Air handling equipment and technological parameters (supply temperature etc.).
5. Energy availability and the price of Latvian cities.

It is very important to be aware that a relatively small country like Latvia, climatic conditions may vary from sea side to continental climate. In accordance with the provisions of the Latvian building normative LBN 002-01 Climatology, example, by data shows that during the heating season, the duration of the Aluksne city is 21 days longer than Liepaja city. The energy indicators of AHU's where analyzed - heat efficiency cost of heat consumption supply air heating, in addition to the total electricity consumption, and potential energy savings.

At this moment according to Latvian education ministry information in the school year length is 169 days and summer vacation is 92 days. Latvian schools are held from September to May. Study process does not take place during summer, hence our climatic conditions. There is no need for air cooling system from a technical- economical point of view. It eliminates vital capital formation, as well as operating costs and energy consumption. Latvia has carried out studies and indoor air quality measurement in teaching institutions and kindergartens and schools as well as universities. The main focus of these measurements is focused on the well-being of children and young people, as well as an evaluation of indoor air quality assessment in the classroom. The goal is to find the desired air quality, which stimulate the learning process. As an established research, the common complaint about being sick, such as lethargy, slowness, fatigue, concentration difficulties, eye tiredness etc. It is also observed that a common complaint about indoor air quality is dust, lower or higher temperature, draughts, dry air or the stale air. In addition to measurements of CO2 was found to increase above permissible standards increased the number of students, as well as in the afternoon. [2] This is important from the point of view that in recent years in the implementation of the program " Money follows the student ", which resulted in all the municipalities abolished school with a small number of pupils, adding them to the closest school with a larger number of pupils. Demonstrated that insufficient heating and ventilation is the reason for the correlation between temperature increase and an increase in the number of students [9] demonstrated the direct correlation to yielding to an increase in the amount of fresh air is improving student performance. [3; 8; 9; 10; 11; 12; 17].

To the school ventilation system work in optimal mode, account should be taken of the:

1. The duration of the school year.
2. The maximum number of hours of lessons per day;
3. What is the maximum number of hours of lessons per week.

In Latvia, the duration of the school year:

- 1. class – 34 weeks;
- from 2 class to 8 class- 35 weeks;

- 9 class – 37 weeks;
- 10 and 11 classes – 35 weeks;
- 12 class – 38 weeks.

The maximum number of hours of lessons per day:

- 1 to 3 classes – 5 lessons;
- 4 to 5 classes – 6 lessons;
- 6 to 7 classes – 7 lessons;
- 8 to 12 classes – 8 lessons.

The maximum number of hours of training per week:

- 1 class – 22
- 2 class – 23
- 3 class – 24
- 4 class – 26
- 5 class – 28
- 6 class – 30
- 7 class – 32
- 8 and 9 class – 34
- 10-12 class – 36 [13; 21].

The basic of classification of indoor air is given in EN 13779:2007. This classification applies to the indoor air in the occupied zone. The values for indoor air classes can be given in national regulations. Values presented in EN 15251 may be used as default values. The Latvian building normative LBN 239 ''Ventilation and heating of residential and public buildings'' gives minimal air volume is 15 m^3/h per person. In this case we can modulate basic of classification of indoor air for Latvia base on EN 13779:2007 [5; 6].

Table1. Latvia normative compare to IDA qualification acc. EN 13779:2007

Category	Description of indoor air quality	Rate of outdoor air per person (non smoking area), typical range, m^3h^{-1}.person^{-1}	Rate of outdoor air per person (non smoking area), Default value, m^3h^{-1}.person^{-1}	Modulate air volume per person, m^3/h base on LBN 239
IDA1	High	> 54	72	60
IDA2	Medium	36- 54	45	45
IDA3	Moderate	22- 36	29	30
IDA4	Low	<22	18	15

Indoor air modeling for school buildings from low indoor air quality category IDA4 to IDA2 moderate and medium IAQ, directly connected to investments in air handling units and evaluation of energy consumption [4; 18]. In this case aim is depending of IDA category search of optimal solution for air handling unit configuration.

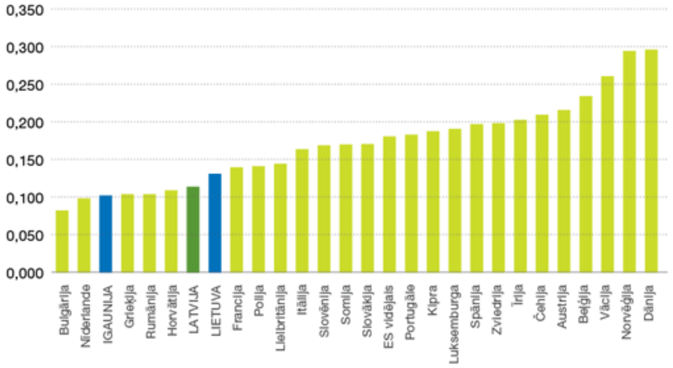

Fig. 1. Electricity price Euro per kW/h (incl. VAT) in Europe union countries

Important factor in school ventilation system is operating costs, including heating of outdoor air. District heating cost where varied different up to 40% in Latvian cities and regions. It is from 32, 21Ls/MWh, excl. VAT in Rujiena city counselling up to 52, 91Ls/MWh in Kegums city[19]. We have found schools where ventilation systems not operated for high operating costs. The main objective is irregular demand for ventilation in the school buildings. Latvian building normative LBN 239 requires minimum 15 m^3/ h fresh air for person that would correspond to the IDA4 level at EN 13779:2007. It is also used for the design of ventilation systems for schools. As a result, in the same cases school's ventilation system does not used due to high operating and maintenance costs. How to find the recommended amount of air for pupils, find an energy saving solutions for Latvia schools ventilation systems optimization [14; 15; 16].

Table 2. Pupils amount data one of the Latvia region's schools

	Secondary school No.1	Primary school No.2	Elementary school No.3	Primary school No.4
Pupils, total	833	24	166	204
Pupils in primary school	350	24	72	131
Pupils in elementary school	358		94	73
Pupils in secondary school	125			
IDA category/ Air volume, m^3/h	IDA4/12500 IDA3/25000 IDA2/37845	IDA4/ 360 IDA3/ 720 IDA2/ 1080	IDA4/ 2490 IDA3/ 4980 IDA2/ 7470	IDA4/ 3060 IDA3/ 6120 IDA2/ 9180

As research object is selected a school No 1, as it learns the greatest number of pupils, as well as the primary school, opens in both elementary and high school. Consequently, classes of loaded are the largest of the region's schools [20].

Study searches for the best possible air handling options in Latvian schools, to ensure maximum IAQ after IDA classification. Were considered 3 possible scenarios on the basis of the Latvian construction regulations laid down the minimum quantity of air to 15 m^3/h to ensure low IAQ IDA4, the next step is 30 m^3/ h for pupils corresponding IDA3, and even increased to 45 m^3/h corresponding IDA2. In addition, air handling is calculated for schools possible configuration with recovery and without from technical-economic point of view. The calculations were made using Microsoft Exel, LCC calculation by ENEU-2000, statistical program SPSS 16.0 and specialized air handling unit's selection program. Air handling unit configurations were analyzed to see connection between components pressure drops in units and their influence to energy consumption.

Table 3. Pressure drops in different air handling unit components with heat recovery

	1 scenario IDA4/ 12500 m3/h			2 scenario IDA3/ 25000m3/h			3 scenario IDA2/ 37845m3/h		
AHU components	DV40	DV50	DV60	DV80	DV100	DV120	DV120	DV150	DV190
Damper, Pa	10	3	3	8	5	3	7	5	4
Filter EU7, Paa	224	161	145	212	184	144	204	171	139
Heat exchanger, Pa	208	157	125	212	173	133	209	177	92
Heater, Pa	23	13	10	47	34	12	23	18	13
Fan, Pa	101	66	42	105	65	40	93	58	37
Damper, Pa	10	3	3	8	5	3	7	5	4
Filtrer EU3, Pa	92	74	63	93	80	67	93	77	64
Heat exchanger, Pa	208	157	125	212	173	133	209	177	92
Fan, Pa	101	66	42	105	65	40	93	58	37
Total pressure drops,Pa	977	700	558	1002	784	575	938	746	482
Difference, %	100%	72%	57%	100%	78%	57%	100%	80%	51%
Investment, Euro	13031	16116	19703	21833	26472	32598	34132	37458	60852

Table 4. Correlation for 1 scenarios air handling units with heat recover

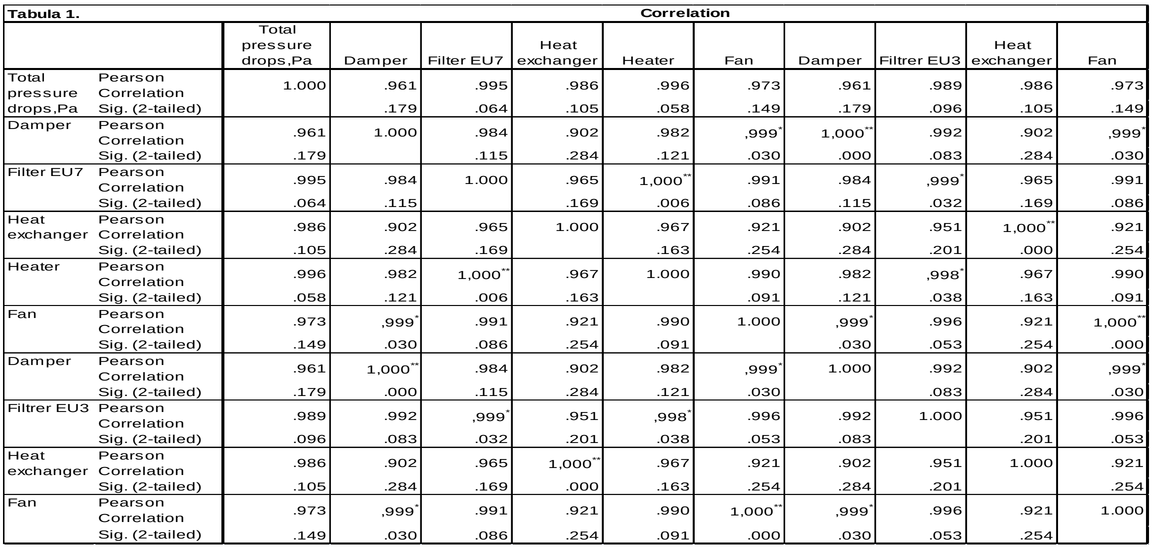

Tabula 1. **Correlation**

		Total pressure drops,Pa	Damper	Filter EU7	Heat exchanger	Heater	Fan	Damper	Filtrer EU3	Heat exchanger	Fan
Total pressure drops,Pa	Pearson Correlation	1.000	.961	.995	.986	.996	.973	.961	.989	.986	.973
	Sig. (2-tailed)		.179	.064	.105	.058	.149	.179	.096	.105	.149
Damper	Pearson Correlation	.961	1.000	.984	.902	.982	,999*	1,000**	.992	.902	,999*
	Sig. (2-tailed)	.179		.115	.284	.121	.030	.000	.083	.284	.030
Filter EU7	Pearson Correlation	.995	.984	1.000	.965	1,000**	.991	.984	,999*	.965	.991
	Sig. (2-tailed)	.064	.115		.169	.006	.086	.115	.032	.169	.086
Heat exchanger	Pearson Correlation	.986	.902	.965	1.000	.967	.921	.902	.951	1,000**	.921
	Sig. (2-tailed)	.105	.284	.169		.163	.254	.284	.201	.000	.254
Heater	Pearson Correlation	.996	.982	1,000**	.967	1.000	.990	.982	,998*	.967	.990
	Sig. (2-tailed)	.058	.121	.006	.163		.091	.121	.038	.163	.091
Fan	Pearson Correlation	.973	,999*	.991	.921	.990	1.000	,999*	.996	.921	1,000**
	Sig. (2-tailed)	.149	.030	.086	.254	.091		.030	.053	.254	.000
Damper	Pearson Correlation	.961	1,000**	.984	.902	.982	,999*	1.000	.992	.902	,999*
	Sig. (2-tailed)	.179	.000	.115	.284	.121	.030		.083	.284	.030
Filtrer EU3	Pearson Correlation	.989	.992	,999*	.951	,998*	.996	.992	1.000	.951	.996
	Sig. (2-tailed)	.096	.083	.032	.201	.038	.053	.083		.201	.053
Heat exchanger	Pearson Correlation	.986	.902	.965	1,000**	.967	.921	.902	.951	1.000	.921
	Sig. (2-tailed)	.105	.284	.169	.000	.163	.254	.284	.201		.254
Fan	Pearson Correlation	.973	,999*	.991	.921	.990	1,000**	,999*	.996	.921	1.000
	Sig. (2-tailed)	.149	.030	.086	.254	.091	.000	.030	.053	.254	

Table 5. Correlation for 2 scenarios air handling units with HR

Tabula 2.		Correlation									
		Total pressure drops,Pa	Damper	Filter EU7	Heat exchanger	Heater	Fan	Damper	Filtrer EU3	Heat exchanger	Fan
Total pressure drops,Pa	Pearson Correlation	1.000	.995	.994	1,000*	.987	.993	.995	1,000**	1,000*	.993
	Sig. (2-tailed)		.065	.072	.012	.102	.077	.065	.008	.012	.077
Damper	Pearson Correlation	.995	1.000	.977	.993	.966	1,000*	1,000**	.993	.993	1,000*
	Sig. (2-tailed)	.065		.138	.078	.167	.011	.000	.073	.078	.011
Filter EU7	Pearson Correlation	.994	.977	1.000	.996	,999*	.973	.977	.995	.996	.973
	Sig. (2-tailed)	.072	.138		.060	.029	.149	.138	.065	.060	.149
Heat exchanger	Pearson Correlation	1,000*	.993	.996	1.000	.990	.990	.993	1,000**	1,000**	.990
	Sig. (2-tailed)	.012	.078	.060		.089	.089	.078	.005	.000	.089
Heater	Pearson Correlation	.987	.966	,999*	.990	1.000	.961	.966	.989	.990	.961
	Sig. (2-tailed)	.102	.167	.029	.089		.178	.167	.094	.089	.178
Fan	Pearson Correlation	.993	1,000*	.973	.990	.961	1.000	1,000*	.991	.990	1,000**
	Sig. (2-tailed)	.077	.011	.149	.089	.178		.011	.084	.089	.000
Damper	Pearson Correlation	.995	1,000**	.977	.993	.966	1,000*	1.000	.993	.993	1,000*
	Sig. (2-tailed)	.065	.000	.138	.078	.167	.011		.073	.078	.011
Filtrer EU3	Pearson Correlation	1,000**	.993	.995	1,000**	.989	.991	.993	1.000	1,000**	.991
	Sig. (2-tailed)	.008	.073	.065	.005	.094	.084	.073		.005	.084
Heat exchanger	Pearson Correlation	1,000*	.993	.996	1,000**	.990	.990	.993	1,000**	1.000	.990
	Sig. (2-tailed)	.012	.078	.060	.000	.089	.089	.078	.005		.089
Fan	Pearson Correlation	.993	1,000*	.973	.990	.961	1,000**	1,000*	.991	.990	1.000
	Sig. (2-tailed)	.077	.011	.149	.089	.178	.000	.011	.084	.089	

Table 6. Correlation for 3 scenarios air handling units with HR

Tabula 3.		Correlation									
		Total pressure drops,Pa	Damper	Filter EU7	Heat exchanger	Heater	Fan	Damper	Filtrer EU3	Heat exchanger	Fan
Total pressure drops,Pa	Pearson Correlation	1.000	.961	.995	.986	.996	.973	.961	.989	.986	.973
	Sig. (2-tailed)		.179	.064	.105	.058	.149	.179	.096	.105	.149
Damper	Pearson Correlation	.961	1.000	.984	.902	.982	,999*	1,000**	.992	.902	,999*
	Sig. (2-tailed)	.179		.115	.284	.121	.030	.000	.083	.284	.030
Filter EU7	Pearson Correlation	.995	.984	1.000	.965	1,000**	.991	.984	,999*	.965	.991
	Sig. (2-tailed)	.064	.115		.169	.006	.086	.115	.032	.169	.086
Heat exchanger	Pearson Correlation	.986	.902	.965	1.000	.967	.921	.902	.951	1,000**	.921
	Sig. (2-tailed)	.105	.284	.169		.163	.254	.284	.201	.000	.254
Heater	Pearson Correlation	.996	.982	1,000**	.967	1.000	.990	.982	,998*	.967	.990
	Sig. (2-tailed)	.058	.121	.006	.163		.091	.121	.038	.163	.091
Fan	Pearson Correlation	.973	,999*	.991	.921	.990	1.000	,999*	.996	.921	1,000**
	Sig. (2-tailed)	.149	.030	.086	.254	.091		.030	.053	.254	.000
Damper	Pearson Correlation	.961	1,000**	.984	.902	.982	,999*	1.000	.992	.902	,999*
	Sig. (2-tailed)	.179	.000	.115	.284	.121	.030		.083	.284	.030
Filtrer EU3	Pearson Correlation	.989	.992	,999*	.951	,998*	.996	.992	1.000	.951	.996
	Sig. (2-tailed)	.096	.083	.032	.201	.038	.053	.083		.201	.053
Heat exchanger	Pearson Correlation	.986	.902	.965	1,000**	.967	.921	.902	.951	1.000	.921
	Sig. (2-tailed)	.105	.284	.169	.000	.163	.254	.284	.201		.254
Fan	Pearson Correlation	.973	,999*	.991	.921	.990	1,000**	,999*	.996	.921	1.000
	Sig. (2-tailed)	.149	.030	.086	.254	.091	.000	.030	.053	.254	

Table 7. Pressure drops of components for AHU without heat recovery

	1 scenario 12 500 m^3/h			2 scenario 25 000m^3/h			3 scenario 37 845m^3/h		
AHU components	DV40	DV50	DV60	DV80	DV100	DV120	DV120	DV150	DV190
Damper, Pa	22	14	8	25	13	10	23	18	10
Filter EU7, Pa	224	161	145	212	184	144	204	171	139
Heater, Pa	46	26	21	48	34	25	46	33	25
Fan, Pa	101	66	42	105	65	40	93	58	37
Total pressure drops,Pa	393	267	216	390	296	219	366	280	211
Investment, Euro	5927	7317	7959	9402	11247	13256	14401	16939	22043

Table 8. Correlation for 1 scenarios air handling units without heat recovery

		Damper	Filter	Heater	Fan	Total,Pa
Damper	Pearson Correlation	1	,969	,969	1,000*	,988
	Sig. (2-tailed)	,000	,158	,160	,016	,100
Filter	Pearson Correlation	,969	1	1,000**	,975	,996
	Sig. (2-tailed)	,158		,002	,142	,058
Heater	Pearson Correlation	,969	1,000**	1	,975	,996
	Sig. (2-tailed)	,160	,002		,144	,060
Fan	Pearson Correlation	1,000*	,975	,975	1	,991
	Sig. (2-tailed)	,016	,142	,144		,084
Total, Pa	Pearson Correlation	,988	,996	,996	,991	1
	Sig. (2-tailed)	,100	,058	,060	,084	

Table 9. Correlation for 2 scenarios air handling units without heat recovery

		Damper	Filter	Heater	Fan	Total, Pa
Damper	Pearson Correlation	1	,907	,978	,980	,962
	Sig. (2-tailed)		,277	,133	,128	,176
Filter	Pearson Correlation	,907	1	,974	,973	,987
	Sig. (2-tailed)	,277		,144	,149	,101
Heater	Pearson Correlation	,978	,974	1	1,000**	,998*
	Sig. (2-tailed)	,133	,144		,005	,043
Fan	Pearson Correlation	,980	,973	1,000**	1	,997*
	Sig. (2-tailed)	,128	,149	,005		,048
Total,Pa	Pearson Correlation	,962	,987	,998*	,997*	1
	Sig. (2-tailed)	,176	,101	,043	,048	

Table 10. Correlation for 3 scenarios air handling units without heat recovery

		Damper	Filter	Heater	Fan	Total, Pa
Damper	Pearson Correlation	1	,990	,964	,962	,981
	Sig. (2-tailed)		,090	,171	,176	,125
Filter	Pearson Correlation	,990	1	,992	,991	,999*
	Sig. (2-tailed)	,090		,081	,086	,035
Heater	Pearson Correlation	,964	,992	1	1,000**	,997*
	Sig. (2-tailed)	,171	,081		,004	,047
Fan	Pearson Correlation	,962	,991	1,000**	1	,997
	Sig. (2-tailed)	,176	,086	,004		,051
Total, Pa	Pearson Correlation	,981	,999*	,997*	,997	1
	Sig. (2-tailed)	,125	,035	,047	,051	

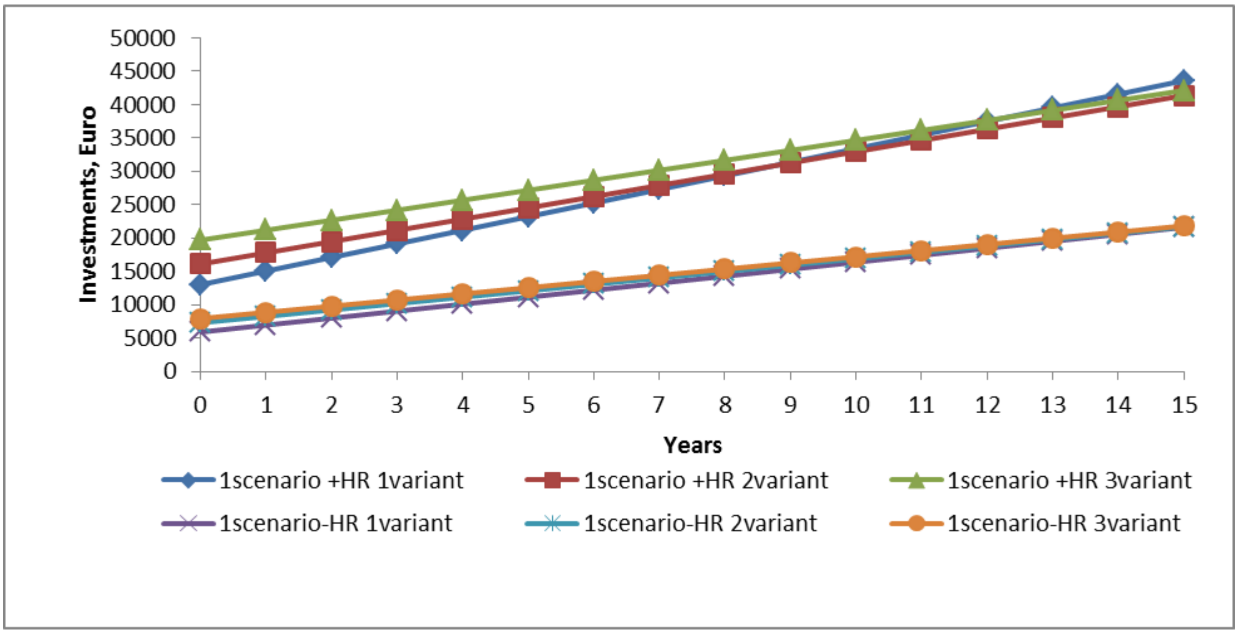

Fig. 2. Life cycle cost calculation for 1 scenario for AHU with and without heat recovery (HR)

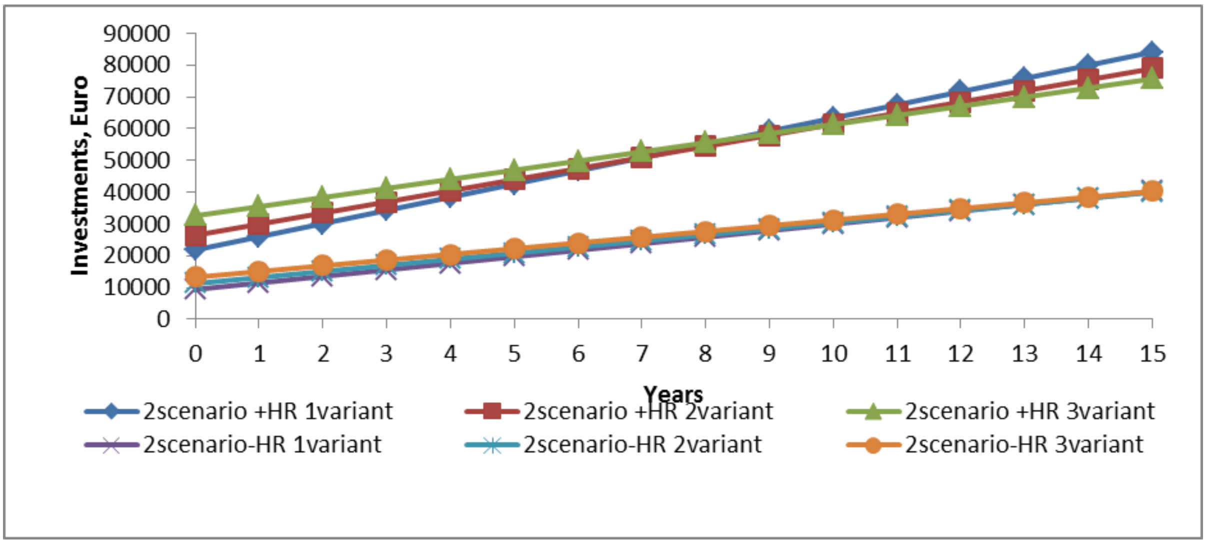

Fig. 3. Life cycle cost calculation for 2 scenario for AHU with and without heat recovery (HR)

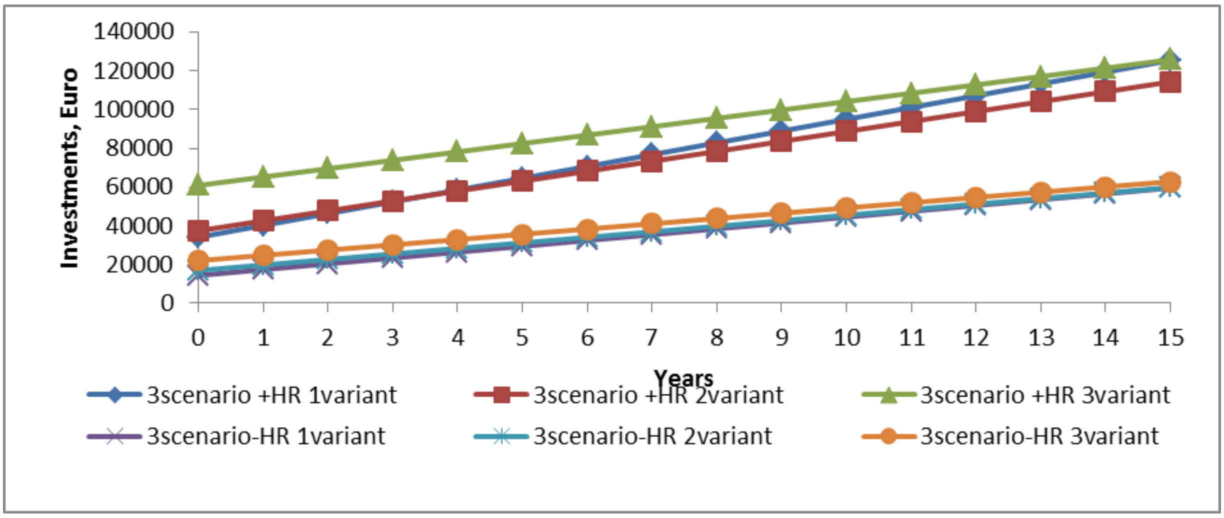

Fig. 4. Life cycle cost calculation for 3 scenario for AHU with and without heat recovery (HR)

Table 11. Investments of AHU per pupil in one of the Latvia region school Nr. 1

	1 scenario (IDA4)					
	AHU with HR			AHU without HR		
AHU size	DV40	DV50	DV60	DV40	DV50	DV60
Investment, Euro	13031	16116	19703	5927	7317	7959
Investment per pupil, Euro	15.6	19.3	23.7	7.1	8.8	9.6
	2 scenario (IDA3)					
	AHU with HR			AHU without HR		
AHU size	DV80	DV100	DV120	DV80	DV100	DV120
Investment, Euro	21833	26472	32598	9402	11247	13256
Investment per pupil, Euro	26.2	31.8	39.1	11.3	13.5	15.9
	3 scenario (IDA2)					
	AHU with HR			AHU without HR		
AHU size	DV120	DV150	DV190	DV120	DV150	DV190
Investment, Euro	34132	37548	60852	14411	16939	22043
Investment per pupil, Euro	41.0	45.1	73.1	17.3	20.3	26.5

3. DISCUSSION

The Education Minister Kilis from 2012 offers to change the layout of the school year, and shorten the school summer vacation. Latvia is one of the shorter school year in the European Union, but vacation is the longest. It was planned with the idea of improving the quality of learning, as well as schoolwork days. The longer winter holidays municipalities are advantageous because dropping school maintenance expenses, but takes into account that the summer time to ensure proper indoor air quality will ensure classroom cooling that is not equipped with a practical one in Latvian school.

Energy cost encourages schools, local municipalities and the Ministry of education (IZM) seek solutions for their reduction. If increase energy prices, if there is a forecast of the growth rate, then it is very important to make the correct today's investment in the future. It is important to analyse not only in Latvia but also in the whole of the EU. Investment for schoolchild helps to analyze local municipality's future investments for improving indoor air quality in schools.

4. CONCLUSIONS

1. Direct correlation was showed between AHU components. When create a correlation table 4 with DV40, DV50 and DV60 system. It showed the correlation table 1 that strikes a balance between total pressure loss and pressure loss of components is significant, since the Pearson product moment correlation coefficient is close to one. By created the correlation table 5 with DV80, DV100 and DV120 systems. We have seen the correlation table that strikes a balance between total pressure loss and pressure loss of components are significant, since the Pearson product moment correlation coefficient is close to one. By created the correlation table 6 with DV120, DV190 DV150 systems. We have seen the correlation table that strikes a balance between total pressure loss and pressure loss of components are significant, since the Pearson product moment correlation coefficient is close to one.
2. Analyzing at the region's schools Nr.1 scenarios to improve indoor air quality in accordance with the IDA qualifications and comparing air handling unit configurations, we can conclude that the system without heat recovery will better contribution as compared to units with heat recovery, initial investment is lower operating costs will be higher, but the recovery will not pay back in 15 years.

REFERENCES

1. Oettinger G. Europeanisation of energy policy. Speech of Commissioner at the European Energy forum. Stasbourg, 19 October 2010. Link to the internet <http://www.energy.eu/DG-TREN-releases/SPEECH-10-573_EN.pdf>.
2. BAKE, M.A.; LAZDINA A. Studentu subjektīvās paššajūtas un veselības traucējumu simptomu saistība ar gaisa kvalitāti auditorijās, *ZRaksti*/ RSU, 2004. p. 194-198.
3. IANNIELLO E. Ventilation systems and IAQ in school buildings. *The REHVA European HVAC Journal*, March 2011, ISSN 1307-3729.
4. Latvijas valsts standarts LVS EN 13779:2007. Nedzīvojamo telpu ventilācija. Ventilācijas un gaisa kondicionēšanas sistēmu veiktspējas prasības.
5. Noteikumi par Latvijas būvnormatīvu LBN 003-01 Būvklimatoloģija, MK noteikumi Nr.376, 2001.
6. Noteikumi par Latvijas būvnormatīvu LBN 231-03 Dzīvojamo un publisko ēku apkure un ventilācija, MK noteikumi nr.534, 2003.
7. KRESLINS A. Gaisa kondicionēšana, Liesma, 1975.
8. WARGOCKI P. Improved indoor air quality improves the performance of office work and schoolwork. Link to the Internet http://www.inive.org/members_area/medias/pdf/Inive/IAQVEC2007/Wargocki_2.pdf.
9. BOERSTA A., KURNITSKI J. Indoor climate and ventilation in schools. *Rehva workshop report CLIMA 2007* Link to the internet < http://www.sisailmayhdistys.fi/attachments/clima07ws/ws_summary_schools.pdf>.
10. MURAKAMI S., KANEKO T., ITO K., FUKAO H. Study on the productivity in classroom. Link to the internet < http://www.phe-kyudai.jp/pdf/pr6_2006.pdf>.

11. BOUSSABAINE H. A., KIRKHAM R. J. Whole life- cycle costing. Blackwell Publishing, 2004.
12. REHVA. 2010. Indoor environment and energy efficiency in schools. REHVA Guidebook No 13 – Part 1 Principles, REHVA.
13. Vispārējās izglītības likums. Link to the internet <http://izm.izm.gov.lv/nozares-politika/izglitiba/vispareja-izglitiba/pamatizglitiba/7043.html>.
14. VALNERIS A. Cilvēka fizioloģija, Zvaigzne ABC, 209.lpp., ISBN 5-405-01529-6.
15. Izglītības sistēmas attīstības projekts- Izglītības un zinātnes ministrija, Rīga, 1999.
16. Ieteikumi Latvijas izglītības iestāžu renovācijai un energoefektivitātes paaugstināšanai- Izglītības un zinātnes ministrija, Rīga, 1999.
17. SEPPANEN O. Scientific basis for design of ventilation for health, productivity and good energy efficiency [*Indoor Air Congress 2008, Copenhagen*], Link to the internet <http://www.buildup.eu/publications/2538>.
18. EN15251. 2007. *European Standard*. Indoor environmental input parameters for design and of energy performance of buildings- addressing indoor air quality, thermal environment, lighting and acoustics.
19. Zemākie apkures tarifi pilsētās ar biokurināmo, Dienas bizness 2011. gada 17.Oktobris.
20. Rīgas apriņķa avīze, Izglītība- prioritāte Nr.1, 5.aprīlis 2011.gada.
21. Higiēnas prasības vispārējās pamatizglītības, vispārējās vidējās izglītības un profesionālās izglītības iestādēm. Link to the internet < http://www.likumi.lv/doc.php?id=69952>

CYSENI 2012, May 24–25, Kaunas, Lithuania
ISSN 1822-7554, www.cyseni.com

MICROCLIMATE PARAMETRES ENSURANCE IN A AIR HEATED BUILDINGS

J. Poderytė, R. Bliūdžius, K. Banionis
Kaunas University of Technology
Studentų str. 48, LT-51367 Kaunas - Lithuania
Phone (+370) 60532017
Email: jurga.poderyte@ktu.lt,
raimondas.bliudzius@ktu.lt, karolis.banionis@ktu.lt

ABSTRACT

The premises in low thermal energy buildings can be heated by air-heating systems. However, the heating system will work effectively only if the building heat losses will be compensated by supplying of not higher than 50 °C air temperature and not more than the minimum amount of required fresh air for building ventilation. The other issue is to maintain the indoor comfort by ensuring the correct air velocity and supplied air temperature differences in operating zone of premises. To assess the effectiveness of air heating system, the research has been made in order to find out the optimal combinations of such parameters as level of thermal insulation, air tightness and ventilation rate. This paper also presents the theoretical studies and experimental results of indoor climate parameters by supplying the heated air in premises.

Keywords: low energy building, air-heating system, indoor comfort, heat losses, air tightness

1. INTRODUCTION

As the amounts of natural resources diminish and the price of energy grows up, the increasing attention is directed towards solving the issues related to energy saving and efficient use in buildings. In order to reduce the consumption of thermal energy the concept of the low energy buildings has spread in the world. During design process the great attention has to be paid to select the optimal shape of the building, the layout of premises, building and living premises orientation in respect of cardinal directions, glazed area and orientation, type of windows, construction of building envelope, ventilation system, degree of insulation, air tightness and thermal inertia in order to get the least amount of heat losses and the greatest amount of solar heat gains during the cold season of the year [1–4].

Ventilation system is the main factor ensuring the microclimate parameters in premises. Natural ventilation system cannot be used in buildings with high level of thermal insulation and air tightness. Thus, the microclimate requirements of the premises are not ensured. Therefore, it is necessary to install a mechanical ventilation system [5] which can be effectively used as air heating system in this way eliminating the need for other sources of heating [6, 7]. When the premises are air-heated, the system will work effectively only if the building heat losses will be compensated by supplying maximum allowable air temperature and not more than the minimum amount of required fresh air for building ventilation. The other issue is to maintain the indoor thermal comfort by ensuring the correct air velocity and supplied air temperature differences in operating zone of premises.

After the literature review was found that in low energy buildings ventilation and air heating system are used to eliminate building heat losses due to ventilation and to ensure good indoor air quality [8-10], but this system is not the main heating system of the building. The thermal properties and indoor climate parameters of the building which can be heated only with air heating systems are analysed in this paper.

2. EFFICIENCY OF AIR HEATING SYSTEM

2.1. Heat demand for heating buildings

The efficiency of air heating depends on the heat demand for heating the building. In order to calculate the demand, heat transfer coefficient of the envelopes, heat losses due to ventilation and solar radiation heat gains into the premises are estimated.

Heat transfer coefficient of the envelopes may be reduced by thickening the thermal insulation layer, diminishing the influence of linear thermal bridges and properly selecting the form of the building. In low energy buildings, linear thermal bridges are allowed only through window and door reveals. As for the form, the area and volume of the premises are selected as similar as possible [5]; the least amount of heat is lost in cube-shaped buildings.

Air, uncontrollably flowing in the building due to natural ventilation and outdoor air infiltration, increases the ventilation heat losses. One of the most important indexes in the reduction of losses caused by exceeding infiltration is air tightness of the building. However, since air exchange is mandatory in buildings, natural ventilation system is replaced with mechanical one. Air exchange should not exceed 0.6 times per hour at the pressure difference of 50 Pa, which corresponds to 0.05 times per hour under natural conditions [7, 11]. Mechanical ventilation system may also be used as air heating system: the pre-heated outdoor air necessary for ventilation is supplied to the premises; to compensate for the most part of heat losses of the building, the temperature of air must be higher than that of the premises. However, the temperature of air cannot exceed 50°C [7], because in such case, dust combustion process begins in the air ducts and the supplied air no longer satisfies the hygiene requirements [2]. To reduce the amount of energy used to heat the supplied air, heat recovery units are installed. Systems with such units pre-heat the fresh air supplied from the outside using thermal energy of the indoor air that is exhausted from the premises [12]. The amount of recovered heat depends on the efficiency of the heat recovery unit: in low energy buildings it should be no less than 80% [12].

Thermal balance of the building is considerably influenced by solar radiation gains through transparent envelopes [13, 14]. Due to the position of the sun with regard to the horizon, the greatest heat gains are measured in the southern and western sides of the building during the heating season; therefore, the living premises should be oriented to these sides by selecting an appropriate area of glazed envelopes. In the northern side of the building, the area of glazed envelopes should be the smallest.

2.2. Research on the efficiency of air heating system

To assess the efficiency of air heating system depending on the energy characteristics of building based on low energy building conception residential building was modelled. The shape of the modelled building is nearly cube. The external dimensions of the building were the following: length – 10.66 m, width – 9.81 m and height – 6.88 m; the total area equalled to 179.90 m² and volume to 719.47 m³. It had two floors: the ground floor included a utility room, toilet, staircase, kitchen, sitting room, workroom, and tambour, while a hallway, two living rooms, bedroom and bathroom were located on the second floor. The plan of the building is shown in Fig. 1. The living rooms, kitchen and sitting room were on the southern and western sides. The total glazed area of the building amounted to 38.03 m²; the area of the glazed envelopes on the southern side was 14.80 m², western – 10.05 m² and eastern – 7.80 m², whereas 5.38 m² glazed area was designed on the northern side following the requirements for natural lighting given in STR 2.02.01:2004 “Residential buildings“ [15].

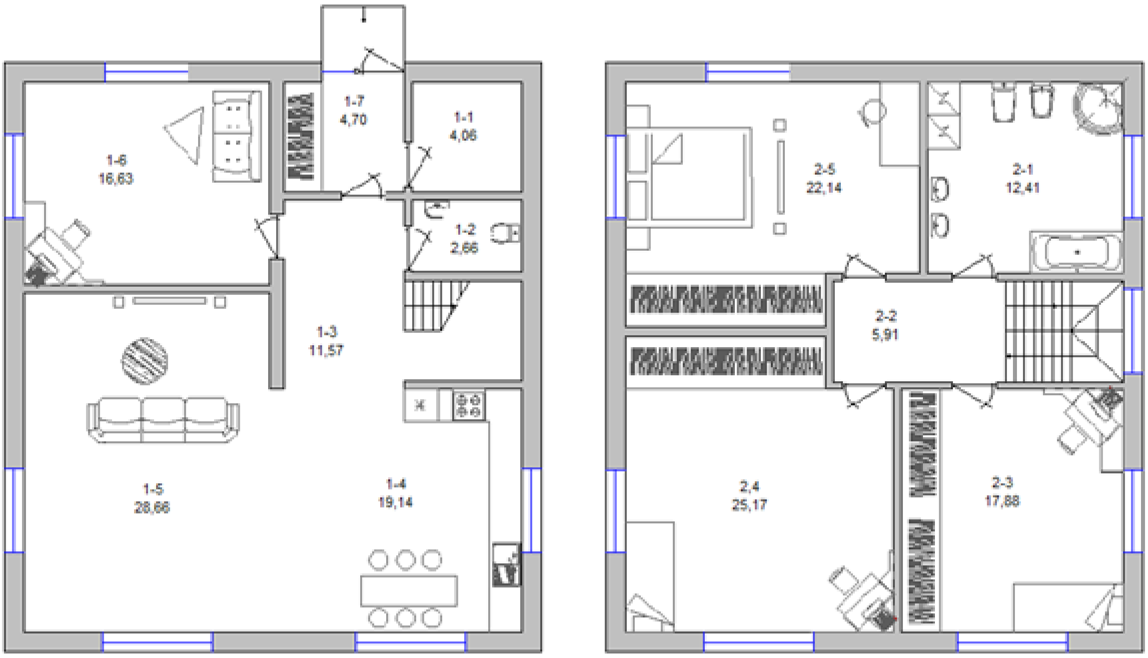

Fig. 1. Plans of the modelled building

Further, 6 calculation variants (Table 1) were modelled by changing the thermal properties of the envelope, air tightness and heat recovery efficiency of the ventilating system

Table 1. Modelled building energy performance

Model No.	Thermal transmittance U_N (W/m^{2}K)					Air tightness n_{in} (ach)	Linear thermal transmittance Ψ (W/mK)				Ventilation system	Heat recovery efficiency
	Walls	Flor	Roof	Windows	Doors		Wall/ ground floor	Wall/roof	Reveal	Wall/wall		
I	0.20	0.25	0.16	1.60	1.60	0.30	0.10	0.00	0.20	-0.10	Nat.[1]	-
II	0.20	0.25	0.16	1.60	1.60	0.05	0.10	0.00	0.20	-0.10	Mech.[2]	-
III	0.20	0.25	0.16	1.60	1.60	0.05	0.10	0.00	0.20	-0.10	Mech.[2]	60%
IV	0.12	0.14	0.10	1.00	1.00	0.05	0.00	0.00	0.05	0.00	Mech.[2]	65%
V	0.11	0.12	0.09	0.85	0.85	0.05	0.00	0.00	0.05	0.00	Mech.[2]	80%
VI	0.10	0.10	0.08	0.70	0.70	0.05	0.00	0.00	0.05	0.00	Mech.[2]	90%

[1]Natural ventilation system; [2]Mechanical ventilation system

Energy characteristics of the first and third models of the building, which satisfy the standard requirements, were taken from STR 2.05.01:2005 “Thermal Technique of the Building Envelope“- [16]. In the second model, the level of tightness was increased and a mechanical ventilation system with heat recovery unit was installed, while the third building model was equipped with a 60% efficient heat recovery unit. In the fourth and sixth building models, the values of heat transmittance coefficients of the envelopes were reduced down to the lowest values currently available in the market. The tightness of the building was preserved constant in all variants, i.e. 0.05 times/h, linear thermal bridges were allowed only through window and door reveals, and finally, the efficiency of heat recovery unit of the mechanical ventilation system was increased from 65% up to 90%.

The heat transfer coefficient was estimated following the characteristics of the building given in Table 1 by STR 2.09.04:2008 “Thermal Output of Building Heating. Heat Demand in Heating” [17]; the calculation results are presented in Fig. 2.

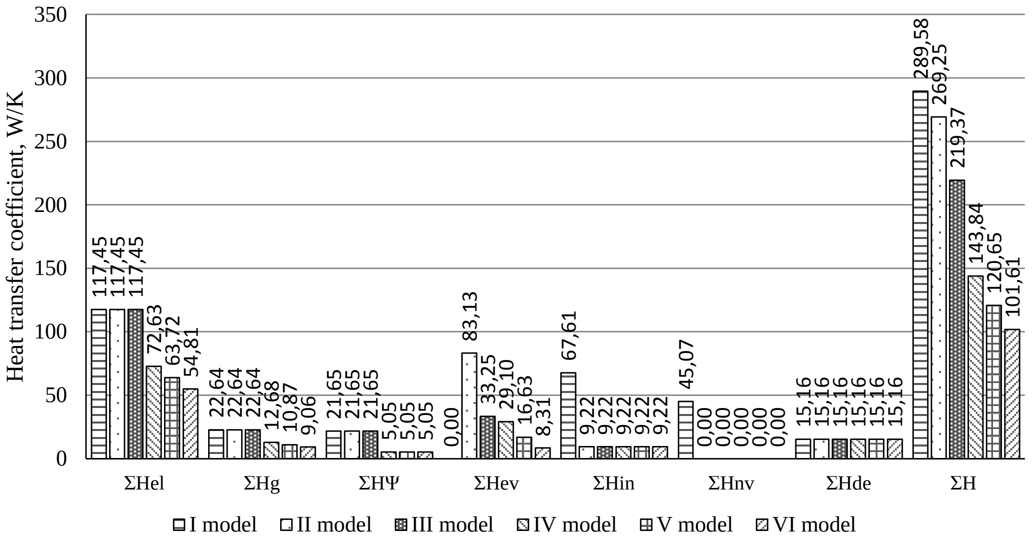

Note: H_{el} – envelope heat transfer coefficient , H_g – steady–state ground heat transfer coefficient, H_Ψ –heat transfer coefficient due to linear thermal transmittance, H_{en} – heat transfer coefficient of premises, H_{ev} –heat transfer coefficient due to mechanical ventilation, H_{in} – heat transfer coefficient due to infiltration, H_{nv} –heat transfer coefficient due to natural ventilation, H_{de} - heat transfer coefficient due to doors opening, H_v –heat transfer coefficient due to ventilation, H – total heat transfer coefficient.

Fig. 2. Modelled building heat transfer coefficient

When the thermal properties of the building and the efficiency of the heat recovery unit were improved, the individual losses of the envelopes (H_{en}) were reduced by 2 times, heat losses of ventilation (H_v) – by 4 times, and individual heat losses of the building – by 3 times, in comparison to the I and VI building models.

Monthly heat demand for heating the building was calculated by assessing the difference between the monthly average outdoor temperature and the temperature of the premises. Heating season data of Kaunas city were used for the calculations: according to the RSN 156-94 “Climatology of Buildings” [18], the heating season lasts for 219 days. Assuming that the building is heated from 29 August till 5 May, two versions of calculations were performed, namely: with and without the impact of solar radiation and internal heat sources (Fig. 3; Fig. 4.).

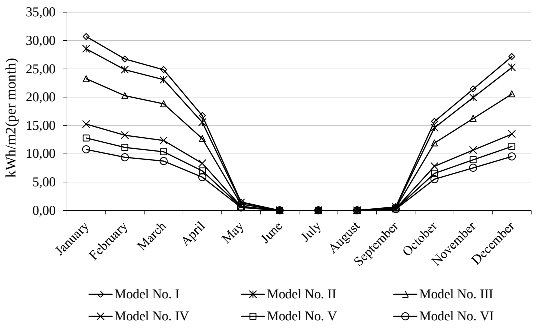

Fig. 3. Building monthly heating demands without an assessment of solar radiation and internal heat sources

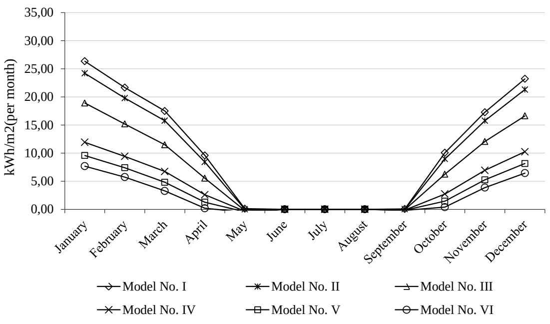

Fig. 4. Building monthly heating demands with an assessment of solar radiation and internal heat sources

In January, additional heat gains due to solar radiation diminish the demand of heat for heating the building by about 4 kWh/m² and 3 kWh/m² in the I and VI building models, respectively. Additional heat gains are the most influential in March and April when the heat demand is reduced to 7 kWh/m². Due to the additional heat gains, the duration of the heating season is reduced, because it is not necessary to heat the building in May and August.

As has been mentioned, an efficient air heating system should cover the heat losses of the building by supplying the premises with the least amount of fresh outdoor air necessary for ventilation. Its temperature must not exceed the limit of 50 °C. Such amount of air was calculated in regard to the III, IV, V and VI building models (Fig. 5.; Fig. 6.).

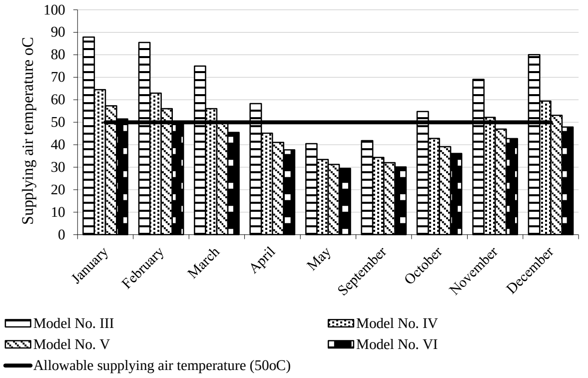

Fig. 5. Supplying air amount to compensate the building heat losses without an assessment of solar radiation and internal heat sources

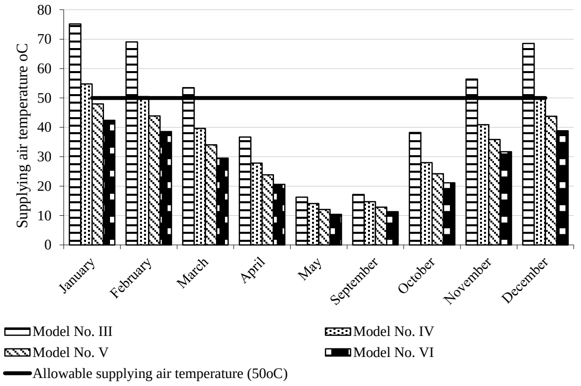

Fig. 6. Supplying air amount to compensate the building heat losses with an assessment of solar radiation and internal heat sources

Fig. 5 shows that when the least amount of air necessary for ventilation is supplied in order to preserve constant temperature of 20 °C during the coldest months of the heating season of the building, meeting the requirements of STR 2.05.01:2005 [16] (Model No. III.), the temperature of the supplied air increases up to 88 °C. In contrast, this temperature amounts to 51.50 °C in the building with the improved thermal properties (Model No. VI). Taking into account the temperature parameters of the supplied air, given in the literary source [7], the air heating system will not operate efficiently in any of the building models since the temperature exceeds the allowed limit of 50 °C. However, after assessing the additional heat gains (Fig. 6.), we observed that the temperature of the air supplied into the premises dropped down. Thus, the air heating system would be efficient in the V and VI building models, and would cover a part of heat losses in the III and IV building models during the heating season.

3. ENSURING MICROCLIMATE CONDITIONS IN THE PREMISES

3.1. Theoretical research on microclimate parameters of the premises

To ensure microclimate parameters by supplying warm air into the premises, it is necessary to consider the hygiene requirements. Following HN 42:2009 [19], during the cold season of the year, the temperature difference between the air in the operating area and the inflowing air must not exceed 3 °C and the speed of air – 0.15 m/s. The microclimate parameters of the modelled building were verified using 1 and 2 formulas [20], [21]:

$$v_x=v_0 \cdot \frac{m_2 \cdot K_v \cdot \sqrt{A_0}}{x_p} \qquad (1);$$

$$\Delta t_x = \Delta t_0 \cdot \frac{n_2 \cdot K_v \cdot \sqrt{A_0}}{x_p} \qquad (2)$$

where: v_x - air flow speed in the operating area [m/s], results in Table 3 ; v_0 – air flow speed near the ventilation grille [m/s]; m_2, n_2 – the damping coefficients of air flow $m_2=m_1 \cdot K_2$, $n_2=n_1 \cdot K_2$, where: $m_1=4.5$, $n_1=3.2$, $K_2=1{,}35$; K_v – correction factor of influence between equal parallel flows $K_v=1$; A_0 – area of ventilation grilles [m^2], meaning in Table 3; x_p – distance from the ventilation grilles to the operating area [m], meaning in Table 3; Δt_x – temperature difference between the operating area and the inflow air in it [°C], results in Table 3; Δt_0 – temperature difference between operating area and the supplying air [°C].

In the modelled building, air is supplied through the ventilation grilles, mounted in the wall above the operating area to the sitting room, living rooms and bedrooms, and is exhausted into the sanitary room and kitchen. The calculations were performed by changing the area of the grilles from 0.01 to 0.035 m². The parameters v_x and Δt_x were estimated assuming that the premises are supplied with the least amount of 50 °C air necessary for ventilation (Table 2, Table 3). According to the STR 2.09.02:2005 [22], the least amount of air supplied to the premises should equal to 4.4 m³/h per person or 1.8-2.5 m³/h per 1 m² of floor area, depending on the purpose of the premises.

Table 2. The parameters of supply air flow in the operating area, if it is supplied across the premise

Premises No. in the plan	Supplying air amount, m³/s	Distance from the ventilation grille to the operating area x_p, m	The area of ventilation grilles A_0, m^2									
			0.010		0.015		0.021		0.022		0.035	
			v_{x1}	Δt_{x1}	v_{x2}	Δt_{x2}	v_{x3}	Δt_{x3}	v_{x4}	Δt_{x4}	v_{x5}	Δt_{x5}
105	0.014	4.90	0.18	3	0.15	3	0.12	4	0.12	4	0.09	5
106	0.008	5.00	0.10	3	0.08	3	0.07	4	0.07	4	0.05	5
203	0.012	4.55	0.17	3	0.14	3	0.11	4	0.11	4	0.09	5
204	0.017	4.90	0.22	3	0.18	3	0.15	4	0.15	4	0.12	5
205	0.015	3.95	0.24	3	0.19	4	0.16	5	0.16	5	0.13	6

Table 3. The parameters of supply air flow in the operating area, if it is supplied along the premise

Premises No. in the plan	Supplying air volume, m³/s	Distance from the ventilation grille to the operating area x_p, m	The area of ventilation grilles A_0, m^2									
			0.010		0.015		0.021		0.022		0.035	
			v_{x1}	Δt_{x1}	v_{x2}	Δt_{x2}	v_{x3}	Δt_{x3}	v_{x4}	Δt_{x4}	v_{x5}	Δt_{x5}
105	0.014	5.10	0.17	3	0.14	3	0.12	4	0.12	4	0.09	5
106	0.008	6.63	0.08	2	0.06	2	0.05	3	0.05	3	0.04	4
203	0.012	4.90	0.15	3	0.13	3	0.11	4	0.11	4	0.08	5
204	0.017	5.40	0.20	2	0.16	3	0.14	3	0.14	4	0.11	4
205	0.015	3.95	0.16	2	0.13	3	0.11	3	0.11	3	0.09	4

The obtained results demonstrated that to ensure microclimate parameters of the premises, it is relevant to select a suitable area of the grilles and the distance from the ventilation grille to the operating area. This is because the increasing area of the grilles reduces the air speed and increases the temperature difference between the ambient air and air flowing into the operating area. However, it is not always possible to combine the parameters of air speed and temperature differences by changing the area of the grilles to meet the hygiene requirements: in such case the shape and dimensions of the premises should be altered.

3.2. Experimental research on microclimate parameters of the premises

Experimental research was carried out in order to verify the accuracy of the methodology presented in Section 3.1. A heating-ventilation system consisting of air heater, ventilator, air duct and air supply grille ((Fig. 7. a), (Fig. 7. b)) was installed in a room which was 2.99 m wide, 5.56 m long and 3.16 m high. The amount of air supplied into the room was regulated using a hand-controlled closing device. The effective area of the grille amounted to 0.01 m² and the distance from it to the operating area was 5.01 m.

Fig. 7. a) The elements of the model of air heating system: 1) ventilator, 2) air heater, 3) smoke machine

Fig. 7. b) The elements of the model of air heating system: 4) ventilation grille, 5) air duct

During the experiment, the speed of the supplied air, its temperature next to the grille and in the operating area, which was raised 2.0 m above the floor, were measured. The results of the experiment are presented in Table 4.

Table 4. Experimental results of indoor climate parameters by supplying the heated air in premises

Exp No.	Air temperature in premises. °C	Supplying air amount, m^3/s	The measured parameters near the ventilation grille		The measured parameters in the operating area		The calculated parameters in the operating area	
			v, m/s	T, °C	v, m/s	T, °C	v, m/s	T, °C
1	17.60	0.011	1.14	43.30	0.01	18.40	0.14	19.82
2	18.10	0.016	1.60	46.78	0.02	19.20	0.19	20.57
3	18.60	0.024	2.36	49.30	0.05	20.50	0.29	21.25
4	19.10	0.028	2.79	50.53	0.01	20.70	0.34	21.81

Note: v – air velocity, m/s; T – air temperature, °C.

The comparison of the estimated values and the results obtained during the experimental research demonstrated that the temperature difference in the operating area did not exceed 1.42 °C, but a considerable difference in air speeds was observed. The air speed measured in the operating area was insignificant, i.e. 0.01 – 0.05 m/s, whereas the estimated values varied within the limit of

0.14–0.34 m/s. To determine the directions of air flow and the limits of coverage, an experiment was carried out by allowing smoke into the room through the ventilation system. We found out that air flow rests at the ceiling and does not go down to the operating area when hot air is supplied to the room (Fig. 8) and for this reason, the air speed in the area was very low or was not detected at all.

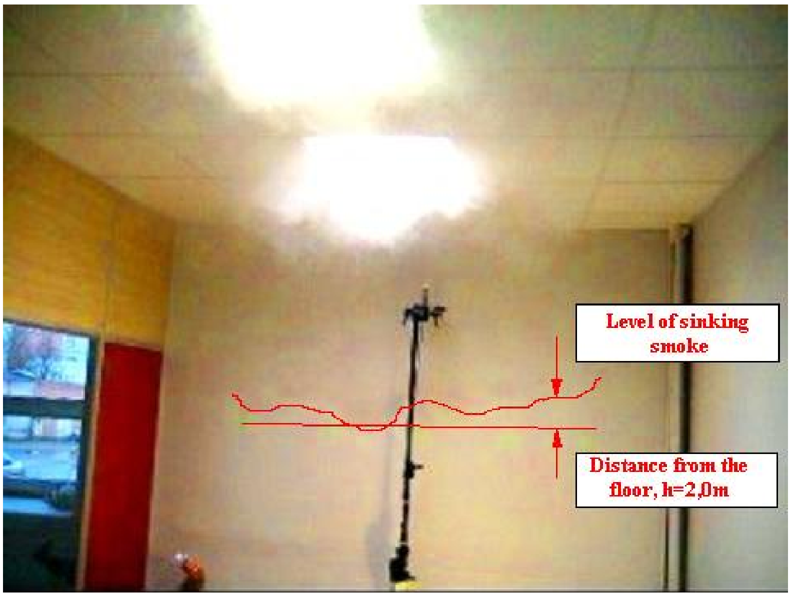

Fig. 8. The experiment with the smoke

4. CONCLUSIONS

1. Following the standard requirements defined in STR 2.05.01:2005 “Thermal Technique of the Building Envelope“, the modelled building requires a considerable amount of heat. This is why the air heating system would not ensure the microclimate parameters of the premises in such building and could not be efficiently used.
2. The efficiency of air heating system depends on the heat demand for heating the building. It may be reduced by improving thermal properties of the building and heat recovery efficiency of the ventilation system as well as by selecting the shape of the building, its orientation regarding the cardinal directions, glazed area, type of windows, and ground plan of premises in order to achieve the greatest solar heat inflows.
3. Under the Lithuanian climatic conditions, the air heating system will operate efficiently if the heat transmission coefficient does not exceed 0.12 W/m²K and 0.85 W/m²K for non-transparent and transparent envelopes respectively, air exchange in the building is within the limit of 0.05 1/h, linear thermal bridges are allowed only through window and door reveals and do not exceed 0.05 W/mK, and finally, the heat recovery efficiency of the mechanical ventilation equipment is no less than 80%.
4. Air supply grilles are installed in the premises of the building with air heating system by selecting the appropriate area of air distributor and the distance from it to the operating area so that the air speed and temperature difference between the surroundings and this area would satisfy the hygiene requirements.
5. Having carried out the experiment by allowing smoke into the room through heating-ventilation system, it was observed that the hot air flow did not move down to the operating area. Therefore, the calculation method of microclimate parameters of the premises used for the theoretical research has to be revised.

REFERENCES

1. CHLELA F.; HUSAUNNDEE A.; INARD C.; RIEDERER P. A new methodology for the design of low energy buildings. *Energy and Buildings*, 2009, Vol. 41, p. 982–990.
2. VENCKUS N.; BLIŪDŽIUS R.; ENDRIUKAITYTĖ A.; PARASONIS J. 2010. Research of low energy house design and construction opportunities in Lithuania, Technological and Economic Development of Economy 16:3, 541–554.
3. SREE D.; PAUL T.; AGLAN H. 2010. Temperature and power consumption measurements as a means for evaluating buildings thermal performance, Applied Energy 87, 2014–2022.
4. FESANGHARY M.; ASADI S.; ZONG WOO GEEM. Design of low – emission and energy - efficient residential buildings using a multi – objective optimization algorithm. *Building and Environment*, 2012, Vol. 49, p. 245–250.
5. SMEDS J.; WALL M. Enhanced energy conservation in houses through high performance design. *Energy and Buildings*, 2007, Vol. 39, p. 273–278.
6. KRAJČIK M.; SIMONE A.; OLESEN B. W.; PETRAŠ D. Experimental evaluation of thermal environment and ventilation effectiveness in a room heated by warm air, Indoor Air 2011, Austin: Austin Convention Center. 2011 June 5–10.
7. FEIST W.; SCHNIEDERS J.; DORER V.; HAAS A. Re – inventing air heating: Convenient and comfortable within the frame of the Passive House concept. *Energy and buildings*, 2005, Vol. 37, p. 1185–1203
8. ATTHAJARIYAKUL S.; LEEPHAKPREEDA T. Real-time determination of optimal indoor-air conditions for thermal comfort, air quality and efficient energy usage. *Energy and Buildings*, 2004, Vol. 36, p. 720–733.
9. FERNANDEZ-SEARA J.; DIZ R.; UHIA F.J.; DOPAZO A.; FERRO J.M. Experimental analysis of an air-to-air heat recovery unit for balanced ventilation systems in residential buildings. *Energy Conversation and Management*, 2011, Vol. 52, p. 635–640.
10. ANDERSEN R.V.; TOFTUM J.; ANDERSEN K.K.; OLESEN B.W. Survey of occupant behaviour and control of indoor environment in Danish dwellings. *Energy and Buildings*, 2009, Vol. 41, p. 11–16.
11. SMEDS J.; WALL M. Enhanced energy conservation in houses through high performance design. *Energy and Buildings*, 2007, Vol. 39, p. 273–278.
12. FERNANDEZ-SEARA J.; DIZ R.; UHIA F.J.; TOPAZO A.; FERRO J.M. Experimental analysis of an air-to-air heat recovery unit for balanced ventilation systems in residential buildings. *Energy Conversion and Management* , 2011, Vol. 52, p. 635–640.
13. OLIVETI G.; ARCURI N.; BRUNO R.; DE SIMONE M. An accurate calculation model of solar heat gain through glazed surfaces. *Energy and Buildings*, 2011, Vol. 43, p. 269–274.
14. OLIVETI G.; DE SIMONE M.; RUFFOLO S. Evaluation of the absorption coefficient for solar radiation in sunspaces and windowed rooms. *Solar Energy*, 2008, Vol. 82, p. 212–219.
15. STR 2.02.01:2004 „Gyvenamieji pastatai“ [Residential buildings]. Vilnius: Ministry of Environment of the Republic of Lithuania.
16. STR 2.05.01:2005 “Pastatų atitvarų šiluminė technika” [Thermal technique of building envelopes]. Vilnius: Ministry of Environment of the Republic of Lithuania.
17. STR 2.09.04:2008 “Pastato šildymo sistemos galia. Šilumos poreikis šildymui” [Power of the building heating system. Energy consumption for the heating]. Vilnius: Ministry of Environment of the Republic of Lithuania.
18. RSN 156-94 RSN 156-94. 1995. “Statybinė klimatologija” [Climatology of buildings]. Vilnius.
19. HN 42:2009 „Gyvenamųjų ir visuomeninių pastatų patalpų mikroklimatas“ [Microclimate in dwellings and public buildings]. Vilnius.

20. В.Н. БОГОСЛОВСКИЙ; И.А. ШЕПЕЛЕВ; В.М. ЗЛЬТЕРМАН. „Справочник проектировщика, Внутренние санитарно – технические устройства, частъ II, Вентиляция и кондиционирование воздуха“. Москва стройизат 1978, 184 p.
21. Juodis E. *Vėdinimas*. Vilnius: „Technika“ 2008, 80 p. ISBN 978-9955-28-370-6.
22. Str 2.09.02:2005 “Šildymas vėdinimas ir oro kondicionavimas” [heating ventilation and air conditioning]. Vilnius: ministry of environment of the republic of Lithuania.

ENERGY AUDIT APPROACH TO A PORTUGUESE UNIVERSITY CAMPUS

E.S. Quintal, H.S. Bernardo
Institute for Systems Engineering and Computers at Coimbra (INESC Coimbra)
Rua Antero de Quental, Nº199, 3000 – 033 Coimbra – Portugal
Phone: (+351) 239 851 040
Email: equintal@inescc.pt
Email: hbernardo@inescc.pt

L.P. Neves
Polytechnic Institute of Leiria, School of Technology and Management
Campus 2,Morro do Lena - Alto do Vieiro
2411-901 Leiria, Apartado 4163
Phone: (+ 351) 239 851 040
Email: lneves@estg.ipleiria.pt
Institute for Systems Engineering and Computers at Coimbra (INESC Coimbra)
Rua Antero de Quental, Nº199, 3000 – 033 Coimbra – Portugal
Phone: (+351) 239 851 040
Email: lneves@inescc.pt

ABSTRACT

This paper proposes to describe the procedure adopted for energy auditing a university campus located in the centre region of Portugal. This energy audit occurred in 2010 and was part of a wider audit process which objective was to prepare the base work for a later building energy efficiency labelling.

The university campus is composed by 9 buildings totalizing a constructed floor area of over 37.400m^2. The buildings were classified in typologies according to the main developed activity. Considering that, there exist 4 academic buildings, 1 research building, 1 library building, 1 administrative building and 2 canteens with food preparation.

This type of building arrangement offers several challenges, especially in what concerns the breakdown of energy consumption per building, since in most cases, the energy supply (electric, thermal, etc.) is shared by different buildings. In this particular case the buildings share the same electrical energy delivery point and several natural gas delivery points. The electrical energy is delivered from the distribution company through two power transformers responsible for its reduction from 15kV to 400V AC from where after is delivered to each building or isolated system. Natural gas is supplied by the utility company in three different delivery points, from where, five different installations are supplied. In 2009 the overall consumption was 1,191 toe which represented a total cost of around 345.000 €.

As stated before, the main goal of this paper is to explore the approach used in this specific case and pinpoint the major challenges and difficulties encountered during field work.

Keywords: Energy audit, energy efficiency in buildings.

1. NOMENCLATURE

DHW – Domestic hot water;
EE – Electrical energy;
ESS – School of Health of Leiria;
ESTG – School of Technology and Management of Leiria;
I – Current;
IPL– Polytechnic Institute of Leiria;
NG – Natural gas;
P – Active power;
PF – Power factor;
Q – Reactive power;
S – Apparent power;
TC– Thermal central;
V – Voltage;
LD – Load diagram.

2. INTRODUCTION

The project and design stage is very important to provide high energy efficiency characteristics to a building. However, the effectiveness of these solutions can only be verified at the operation stage. At this stage, is necessary to adopt energy management methods to reduce the risk of not taking any advantage of the implemented strategies and technologies defined in the project stage. The assurance that a building is energy efficient will only be achieved if the building operation is associated with an effective energy management, as well as, an efficient facilities management.

The implementation of any energy management system should begin with an energy audit. An energy audit is a detailed examination of the energy use conditions in an installation that allows to make recommendations for implementing changes in processes or in energy end use equipment in order to reduce energy bills. The energy audit scope depends of the analysed subject. This means that the audit approach to a services building must be different from the approach to an industrial facility. A building energy audit may emphasize the building envelope, lighting, heating, and ventilation requirements. On the other hand, an energy audit of an industrial facility usually emphasizes the process requirements. [1] [2]

Higher education buildings have specific characteristics that differ from other buildings. They usually are group together in *Campi*, sharing energy supply. Since in most cases, the systems/buildings are not equipped with partial energy meters, the task for determining individual consumption is a true challenge. Besides this, these buildings usually have longer opening hours which results in a longer daily period of occupancy when compared with other services buildings. They can also be equipped with laboratories that sometimes resemble more an industrial facility than a services building, even that those equipments may not operate continuously. In this situation, special attention has to be taken when analysing energy demand in order not to make impossible their operation.

Although electric equipments present high energy efficiency when compared with thermodynamic systems, does not mean that in practise do not exist situations where the process is obtained with huge energy lost. Electric traction and illumination are examples of situation where can occur great energy losses, making electric monitoring and measurement essential to an effective energy management program.

3. CAMPUS DESCRIPTION

The audited university Campus belongs to the Polytechnic Institute of Leiria (IPL) and is located in the centre region of Portugal at Leiria. In Campus currently run the School of Technology and Management of Leiria (ESTG) and the School of Health of Leiria (ESS). Besides these two major schools, other smaller units of education also use the same buildings.

The Campus is composed by nine different buildings, totalizing a constructed floor area of 37.467m^2. Fig. 1 illustrates the current layout of the buildings.

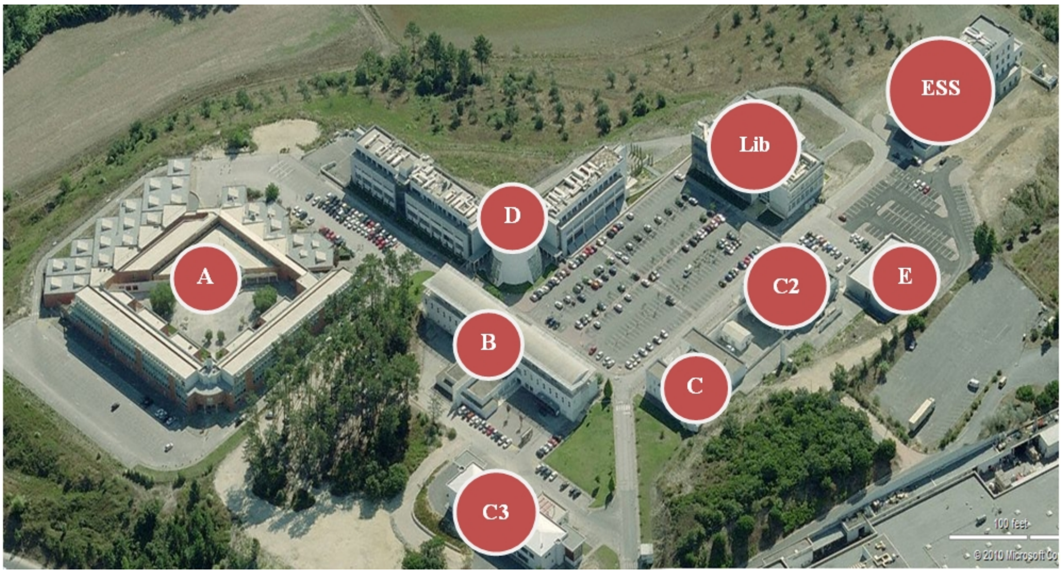

Fig. 1. Campus aerial view *(picture source: Bing Maps)*

Table 1 presents a description of the leading activity developed in the buildings, as well as, their net floor area.

Table 1. Existent buildings

Building	**Activity**	**Net loor area [m^2]**
A	Pedagogic	12.063
B	Administrative	3.135
C	Research	1.320
D	Pedagogic	8.851
E	Pedagogic	507
ESS	Pedagogic	4.438
Lib	Library	3.333
C2	Canteen	2.336
C3	Canteen	1.484
	Total	37.467

3.1. Energy distribution

To better understand the implications of individual building consumption in the overall campus consumption, is fundamental to comprehend how energy is distributed within campus. In this section are described the campus energy reception points, as well as, the internal energy distribution network.

The EE is delivered from the distribution company through two power transformers stations responsible for stepping-down voltage from 15kV to 400VAC, from where after is delivered to each building or isolated system. Table 2 presents the building EE supply.

Table 2. EE distribution

Transformer Station	**Facility**
TS1 (1.250 kVA)	B
	C
	E
	ESS
	Library
	Canteen 2
	Canteen 3
	Chiller
TS2 (630 kVA)	A
	D

In what concerns energy, besides EE is also used NG. NG is used for cooking, for space heating and for DHW production. The supply of NG is done through 3 Reduction and measurement Stations (RS), from which the distribution is made to the various places of consumption in accordance with Table 3.

Table 3. NG distribution

Reception Station	**Facility**	**Purpose**	**Building**
RSA	TC1	Space heating	A
RSB	C2	Space heating, cooking, DHW	C2
	TC2	Space heating, DHW	C2,B,C
	TC3	Space heating	D,LIB
RSC	C3	Space heating, cooking, DHW	C3

The thermal central installed in building C (TC2) is responsible for heating building B and C. The thermal central installed in the library (TC3), is responsible for producing thermal energy for heating and cooling the library and building D.

In 2009, the overall consumption (Fig. 2), considering EE and NG, was 1.191 toe, which represented a total cost of around 345.000 €.

GN consumption analysis is out of the scoop of this paper therefore no separate consumption will be presented.

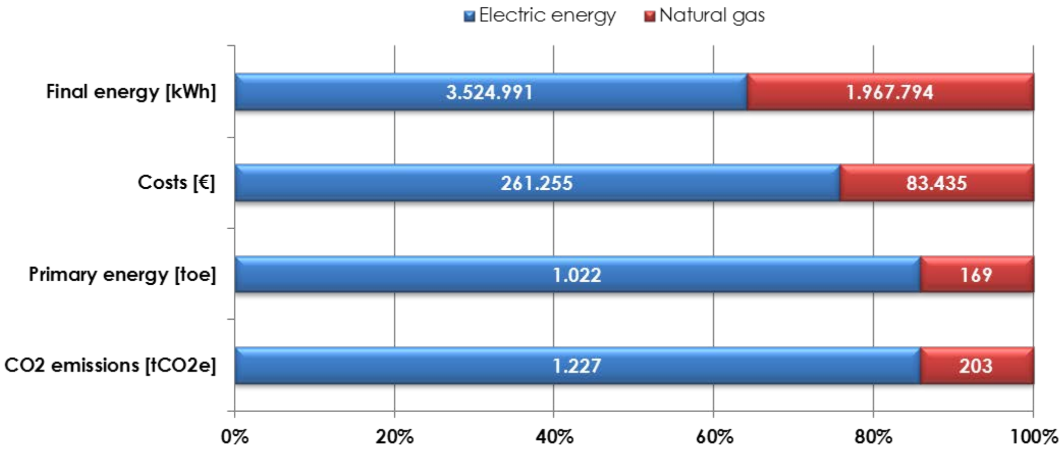

Fig. 2. Synthesis of the energy consumption verified in 2009

4. METHODOLOGY

This paper deals with the methodology adopted for determine and validating the total consumption of electrical power based on data obtained from the monitoring carried out on the internal electrical power distribution network.

In this particular case, the nonexistence of a total energy meter available for accessing and the technical difficulties associated with measuring at 15kV, total consumption had to be obtained by algebraic manipulation of load diagrams of the two existent TS. Fig.3 presents the considered analysis stages from fieldwork preparation to data validation.

Fig. 3. Analysis stages

4.1. Document colection and review

This stage consisted in collection and review of site plans, technical diagrams and utility energy bills. This included EE bills from the previous three years to the audit, electric distribution diagrams and architectural blueprints.

4.2. Site visit

This stage consisted in a site visit to characterize the two TS and determine the type of monitoring equipment to be used, and were to install it.

As consequence of this visit, was decided to install two power analyzers, one at the main switch of each TS, to determine the total consumption of EE on campus.

4.3. Monitoring and data logging

This stage consisted in the installation of the monitoring equipment according to the previous step. For monitoring, were used two Chauvin Arnoux 8334B power and energy quality analysers, equipped with Ampflex current sensors. The monitoring occurred simultaneously at TS1 and TS2.

Table 4 presents a resume of the monitoring performed.

Table 4. Monitoring resume

Equipment	**Quantity**	**Current sensor**	**Installation**	**Measured parameters**	**Integration period**	**Time of monitoring**
CA 8334B	2	Ampflex 6.500A	TS1, TS2	I,V,P,Q,S,PF	15 minutes	7 days

4.4. Data Analysis

This stage consisted in the analysis of the gathered data in the monitoring period. The data analysis consisted in graphing load diagrams and calculating the average daily consumption.

The daily EE average consumption was determined by using equation (1) for both, TS1 and TS2, separately. This equation is based on the demanded active power during the 15 minute integration period.

$$E_{dm} = \frac{1}{n}\sum_{i=1}^{n} P_{n_i} \times 24 \quad [\text{kWh}] \tag{1}$$

In which:

E_{dm} – Daily average consumption of EE based on measurement;

n – Number of integration periods in the monitoring period;

P – Active power recorded at each integration period [W].

The average EE total consumption was determined by using equation (2).

$$E_{dm\ Total} = E_{dm}(\text{TS1}) + E_{dm}(\text{TS2}) \quad [\text{kWh}] \tag{2}$$

As can be seen in equation (2), the EE average total consumption was obtained by adding the daily average consumption of EE based on measurement made at TS1, with the daily average consumption of EE based on measurement made at TS2.

The total load diagram was obtained by adding, period by period, the data from TS1 and TS2 monitoring. This was possible because the monitoring was simultaneous and the internal clocks of the power analysers were set equal.

4.5. Data validation

This stage consisted in the validation of $E_{dm\ Total}$ by comparing it to the average daily consumption obtained from EE bills.

For determine the average daily consumption based on EE bills was used equation (3).

$$E_{db\ Total} = \frac{1}{365}\sum_{i=1}^{m} E_{mb_i} \quad [\text{kWh}] \tag{3}$$

In which:

$E_{db\ total}$ – Daily average consumption based on EE bills;

m – Number of months in one year;

E_{mb} – Monthly electric energy invoice [kWh].

The comparison between $E_{dm\ Total}$ and $E_{db\ Total}$ was performed by using equation (4), which allows determining the accuracy level of the monitoring data.

$$Accuracy = \left(1 - \frac{\left|\left(\frac{1}{365}\sum_{i=1}^{m} E_{mb_i}\right) - \left(\frac{1}{n}\sum_{i=1}^{n} P_{n_i} \times 24\right)\right|}{\frac{1}{365}\sum_{i=1}^{m} E_{mb_i}}\right) \times 100 \quad [\%] \qquad (4)$$

5. DISCUSSION OF RESULTS

The monitoring and the data that allowed to reach the load diagrams (LD) presented in this chapter, took place from 10thto 16th July 2010.

Transformer substation	E_{dm} [kWh]
TS1	6.322
TS2	4.215
Total ($E_{dm\ Total}$)	10.537

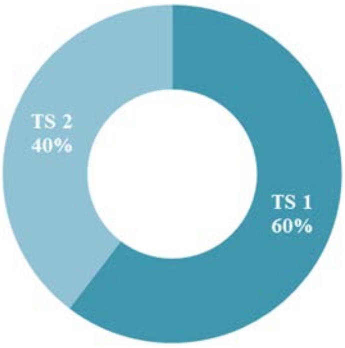

Fig. 4. Breakdown of EE per TS

The data that resulted from the monitoring period allowed to determine the average daily consumption breakdown by TS, as shown in the table and graph of Fig. 4. As consequence, it can be verified that TS1 has an average daily consumption of 5.935 kWh, which represents 60% of total consumption of EE on Campus, being the remaining 40% attributed to TS2, which correspond to an average daily consumption of 3.896 kWh.

Overall, Campus 2 shows a daily average consumption of 10.537 kWh of EE.

5.1. Load profile of Transformer Station 1

In Fig. 5 is shown the LD of TS1, where can be seen the power consumption during the referred week. During the monitoring period, the power required varied from the minimum value of 91 kW recorded at 00h15 on the 11th (Sunday) and the maximum value of 501 kW recorded at 13h15 on the 12th (Monday).

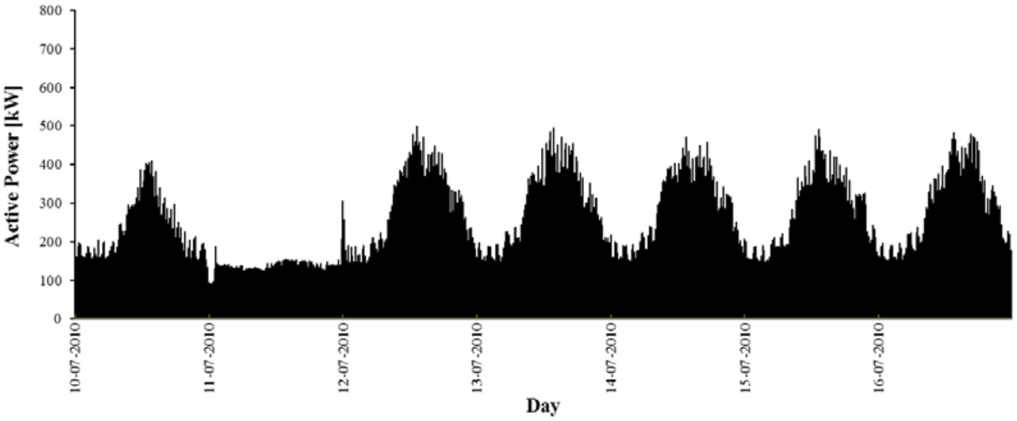

Fig. 5. TS1 - active power from period of 10 to 16 July 2010.

5.2. Load profile of Transformer Station 2

In Fig. 6 is shown the LD of TS2, where can be seen the power consumption during the mentioned week. During the monitoring period, the power required varied from the minimum value of 100 kW recorded at 13h30 on the 11th (Sunday) and the maximum value of 261 kW recorded at 18h30 on the 12th (Monday).

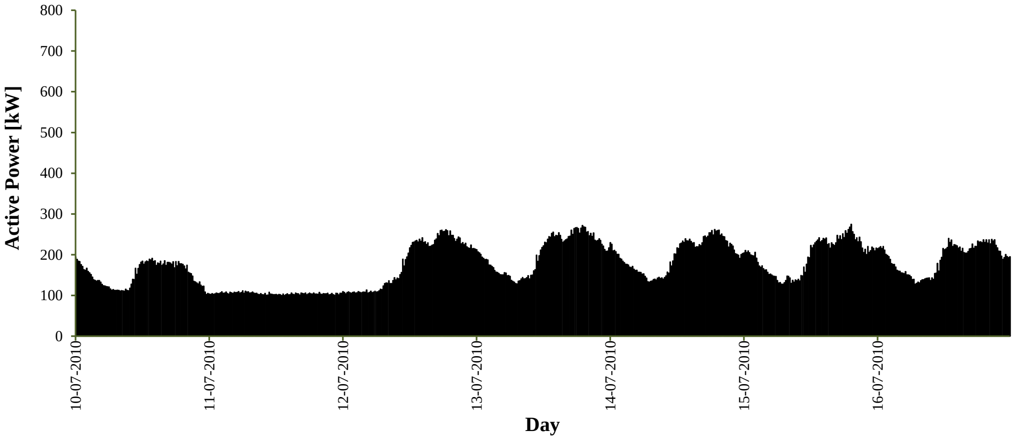

Fig. 6. TS2 - active power from period of 10 to 16 July 2010

5.3. Total load profile

Based on the LD shown in Fig.5 and Fig.6 it was possible to obtain the total LD of Campus 2, shown in Fig. 7.

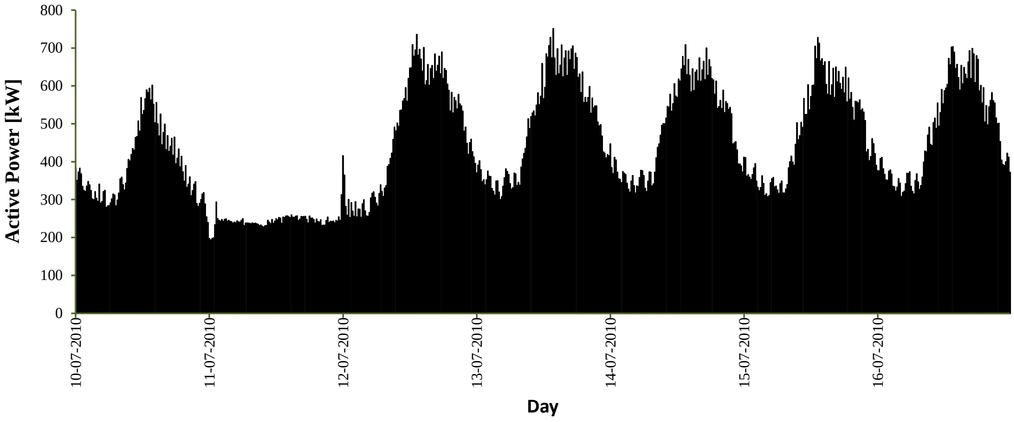

Fig. 7. Total - active power from period of 10 to 16 July 2010

During the monitoring period, the power required varied from the minimum value of 194 kW, registered at 00h15 on the 11th (Sunday) and the maximum value of 752 kW, recorded at 13h45 on the 13th (Tuesday).

Analysing the LD presented in Fig.7 is possible to verify the existence of three different periods during the week where the regime of EE consumption varies significantly. These are: the working days, that present a similar consumption profile among themselves; Saturday, where is registered a decline in the use of EE compared to working days, mainly due to the partial operation of the Campus; Sunday, that arises as the day of the week where is registered the lower EE consumption, since there is no activity on campus.

In Table 5 is presented the average daily values of the EE consumed in the different periods of the week, also determined by using equation (1).

Table 5. Average EE consumption by week period

Week period	**E_{dm} [kWh]**
Workday	11.723
Saturday	9.300
Sunday	5.842

Taking as reference the average daily consumption on workdays, is possible to verify a 21% decrease in consumption on Saturday and 50% on Sunday.

For the reason that workdays represent about 80% of the consumed EE on Campus, is important try to understand how this consumption is distributed throughout the day. For that, was created a typical working day LD (Fig. 8) based on the average of the same 15 minute integration period of each working day.

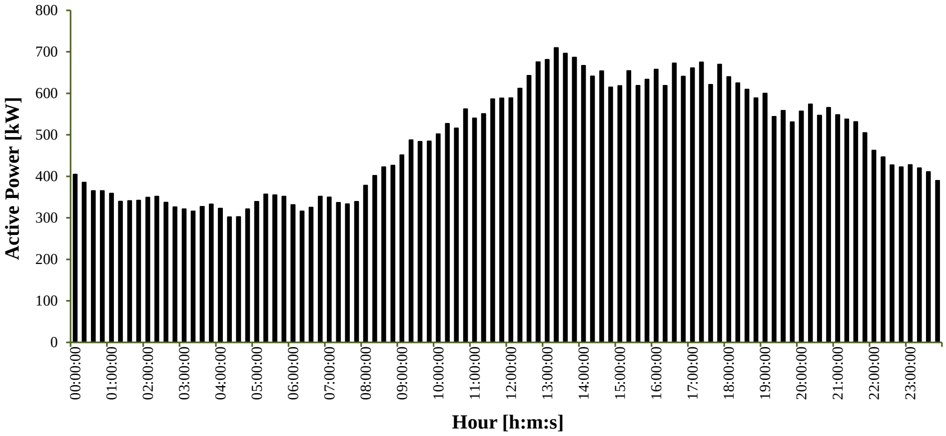

Fig. 8. Typical working day.

Analysing Fig. 8 can be seen that the period with lower consumption of EE occurs between 00h00 and 08h00, however is noted that, even in this period and especially from 04h00, when all buildings are closed, are still required high levels of active power. From 08h00 there is a gradual increase in the request of active power to its maximum value, reached in the period between 13h00 and 14h00. From 14h00 to 18h00, the value of active power presents small oscillations. From 18h00 to 24h00, the value of active power shows a gradual decrease as exception being the period between 20h00 and 21h00, where there is a slight increase that coincides with dinner time.

5.4. Data validation

Table 6 presents the values determined for $E_{dm\ Total}$ and $E_{db\ Total}$.

Table 6. EE total daily consumption comparison

$E_{dm\ Total}$	10.537 kWh
$E_{db\ Total}$	9.660 kWh
Accuracy	92 %

As can be seen in Table 6, the EE consumption value obtained from the 7 days measurement is close from the one that was obtained from the EE bills, being the difference between these two of 8 %. Note that the $E_{db\ Total}$ was obtained from the average of the 3 year period prior to the audit.

The consumption of EE in Campus varies scarcely throughout the year due mainly to the constant daily usage of buildings.

By analyzing the EE bills was also noted that winter consumption does not differ greatly from summer consumption. One aspect to consider for this is that the heating of the most buildings is achieved by the burn of NG, making the consumption of EE being almost taken out of the equation at this time of the year for this matter. Almost, because ESS building recurs to a EE driven heat pump for thermal production. This equipment is responsible for heat production in the winter and cold production in the summer, making its EE consumption fairly even between these two periods.

6. CONCLUSION

Energy audits are a tool to find energy conservation measures, which can lead to significant savings on the customer utility bill.

In most cases, the auditor does not choose the period in which the audit has to be performed, being the timing imposed by the contractor. From the market point of view, is economical unattractive and time-consuming doing several monitoring campaigns covering several different periods of the year, or even, different production periods, in the attempt of tracing the most accurate energy consumption profile possible. As consequence, one of the major challenges encountered in energy audits is determine if the monitoring data gathered in the available time window can be representative of the energy consumption behaviour of the analysed system throughout the year.

In situation like the one presented in this paper, the lack of individualized energy metering per building hinders an effective management of energy consumption, since that energy manager does not have one important tool to full realize the energy profile of a specific building, which could lead to the detection of potential energy waste.

This paper shows that the methodology used for approaching this particular situation, resulted in a 92 % accuracy of the data obtained in the monitoring period. This indicates that this approach is a satisfactory base for a future and more detailed EE consumption breakdown, first per building and then, per system.

It is authors intention to present the results of EE consumption break down per building using the presented methodology, as well as total consumption per building including thermal energy, in future publication.

REFERENCES

1. S. D. Wayne C. Turner, Energy Management Handbook, The Fairmont Press, 2007.
2. W. J. Y. Albert Thumann, Handbook of Energy Audits, The Fairmont Press, 2003.

INFLUENCE OF HEAT MEASUREMENT METHOD ON CONSUMED AMOUNT OF HEAT IN DWELLING HOUSES

R. Savickas
Vilnius Gediminas technical university
Sauletekio av. 9, LT–10223 – Lithuania
Phone +370 652 27 398
Email: romas.savickas@gmail.com

ABSTRACT

As the oil price and related fuel in last decades strictly and constantly rises, the different measures are applied to decrease energy consumption in a buildings. The development of building constructions of a new type and application of better insulation, proper orientation of a building, replacement of natural ventilation system by forced recuperated ventilation system and other means can be described as the main tool to decrease energy consumption. But if we will overheat well insulated building and heat surplus will be thrown away through the open windows, all measures under application will be lost in vain. A lot of studies of the efficient energy consumption recommend organisational measures also. Most popular example for efficient electricity usage is very simple - to turn off the light leaving the premises and only later change bulbs into more efficient. Taking such measures as very important, this article analyses four types of heat measurement methods in a building: then building has only one common heat meter for all entire building, then building has installed heat cost allocator units on every heating device, then every flat in a building has its own heat meter and then every flat in a building is heated by individual gas boiler. All these heat measurement methods influences behaviour of a heat consumer in a different way. Study shows that the total energy consumption in a buildings of the same construction type but with the different heat measurement method differ in a large scale, so due to reconstruction of a heating system and changing the heat measurement method can be achieved an obvious energy consumption and carbon dioxide reduction result.

Keywords: Energy efficiency, Heating energy, Heat energy consumption, Heat meter, Heat cost allocator, Temperature

1. INTRODUCTION

The main purpose of directive 2006/32/EC of the European Parliament and of the Council on energy end-use efficiency and energy services is to make the end use of energy more economic and efficient [1]. European Commission is preparing a new version of this directive (2006/32/EC) for energy efficiency of end-use consumer and energy services. It is planned that this new version will include principles of individual energy metering. After implementation of directive member States shall adopt energy saving obligation schemes and shall require “retail energy sales companies or distribution system operators to achieve annual energy savings among final customers in the Union equal to 1,5% of their market share in the market for final customers in the previous year multiplied by the total volume consumed by final customers in the Member State in the previous year” [2]. It is convenient in energy saving obligation scheme include individual heat metering by heat cost allocators (HCA) or individual heat meters (IHM) in a flats as it makes energy savings comparing to heat consumption in a buildings with common heat meter for whole building, but before applying such measures the final obtained targets, goals and results must be evaluated.

This study analyses and presents a possible energy savings due to application of different heat measurement schemes in a building: by heat cost allocators, individual heat meters in a flats, heat consumption in a buildings with common heat meter for whole building and heat consumption in a building heated by individual gas boilers in a flats. Heat measurement method does not reduces heat consumption in a building, but it changes behaviour of a heat consumer. A lower energy consumption is a consequence of possibility do not overheat corresponding building parts and motivation of every flat to keep desired or even much lower temperature of premises as the neighbors have. Beside installed heat cost allocators or heat metering devices, heating system is reconstructed to be regulated individually also. Practice shows that the reconstruction of a heating system then for whole building is left one common heat meter, does not gives a desirable result in energy consumption decrease as every consumer does not feel direct influence on its bills.

2. METHODOLOGY FOR HEAT MEASUREMENT METHODS EVALUATIONS

For the analysis of energy consumption according to common heat meter for whole building, heat meters in flats, heat cost allocators has been chosen multi-flat dwelling buildings of the same city. The number of buildings, having common heat meter for the whole building is the largest, so as a related consequence the number of such buildings has felt in a larger than four thousands group of analysed buildings. Heat allocator units in buildings mostly appear in two different ways – after a new building was erected and heat allocator units were installed after it or after heating system of an old building was reconstructed to give a possibility to regulate heat consumption of every heat device independently and heat allocator units installed to measure that heat. New buildings has a possibility to measure consumed heat by installed heat cost allocator units on every heating device or to measure heat of whole flat by separate heat meter. As a following consequence the number of analysed buildings with heat cost allocators in an old and new buildings has felt in an approximately the same parts and makes a group of about two hundreds of buildings, the number of analysed buildings with independent heat meters in every flat is slightly more than two hundreds. As the heating in a cities mostly is supplied by a centralised way, the heating of every multi-flat in a building by an individual gas boiler is not as common as other heating methods, for the analysis has been taken a building from a different city.

Every flat in a building, having heat cost allocators, heat meters for every flat or heated by an individual gas boiler, can heat its premises according to its own needs and obtain desired temperature in a premises. So consumed heat amount in every flat will differ and it would be impossible to compare different heat measurement methods according to heat consumption in a flats. Thus for the analysis were taken heat consumption data of common building heat meter showing heat consumption of whole building. As the sum of hot water consumption in a flats may differ from the total consumed hot water amount, for the analysis were taken data of common hot water meter of whole building. Heat amount for heating $Q_{heating}$ is defined from the balance [3]:

$$Q_{\Sigma} = Q_{heating} + Q_{hw},$$

where: Q_{Σ} – total heat consumption in a building, MWh; $Q_{heating}$ - heat amount for premises heating (including heat amount in flats and common areas), MWh; Q_{hw} – heat amount for hot water needs (for hot water preparation and circulation), MWh.

Heat amount for hot water needs Q_{hw} may vary in every building depending on an amount of consumed hot water and hot water circulation type in a building. Heat amount for hot water circulation Q_{hwcirc}, calculated according to heat amount of 160 kWh/flat (circulation in hot water towels and coil-pipes), 80 kWh/flat (circulation in hot water towels) and 10 kWh/flat (circulation in heat substation) [4], would not be precise, so heat amount for hot water circulation Q_{hwcirc} was calculated according to non heating period months, subtracting heat amount for hot water preparation Q_{hwprep} from total heat amount during non-heating season $Q_{\Sigma nh}$:

$$Q_{hwcirc} = Q_{\Sigma nh} - Q_{hwprep}.$$

Heat amount for hot water preparation Q_{hwprep} was defined according to equation:

$$Q_{hwprep} = G \times 0{,}051$$

where: Q_{hwprep} – heat amount for hot water preparation, MWh; G – amount of consumed hot water according to common hot water meter for whole building, m^3; 0.051 – heat amount to prepare 1 m^3 of hot water, MWh/m^3 [4].

Heat amount for heating individually was calculated for every analysed building, later to perform a comparison were defined corresponding heat consumption values of a certain analysed buildings group. To compare heat consumption in all these different buildings the calculations have been performed to eliminate the influence of differences in outside temperatures, number of heating days and heating area in a building. As consequence a non-influential indicator q_n has been got. This indicator q_n defines a heat amount to raise 1 m^2 of a building temperature by 1 ^oC. The indicator q_n has been calculated according to the following equation:

$$q_n = \frac{Q_{heating}}{\left(t_{internal} - t_{external}\right) \times d \times A}$$

where: q_n – non-influential indicator, indicating a heat amount to raise 1 m^2 of a building temperature by 1 ^oC, Wh/DD/m^2; $t_{internal}$ – internal temperature in a premises, usually taken +18^oC, ^oC; $t_{external}$ – external temperature, ^oC; d – number of a days; A – heating area, m^2.

It is important to notice that according to measurement units from the first point of view indicator q_n can look like thermal resistance value, but the main difference between them is that thermal resistance measures power for area unit of partition ($m^2 \cdot K/W$) and indicator q_n describes amount of consumed power for heating area unit of (Wh/K/m^2).

All further analyses and calculations compares different values of indicator q_n for analysed buildings or group of buildings.

3. RESULTS AND DISCUSSIONS

First of all was performed an analysis of all types of buildings to define a total heat consumption tendencies. As Fig. 1 shows heat consumption in all analysed buildings is not constant and decreases every heating season: comparing with 2008/2009 heating season, heat consumption during 2009/2010 heating season has decreased by 3.9 % and during 2010/2011 heating season by 14.4 %.

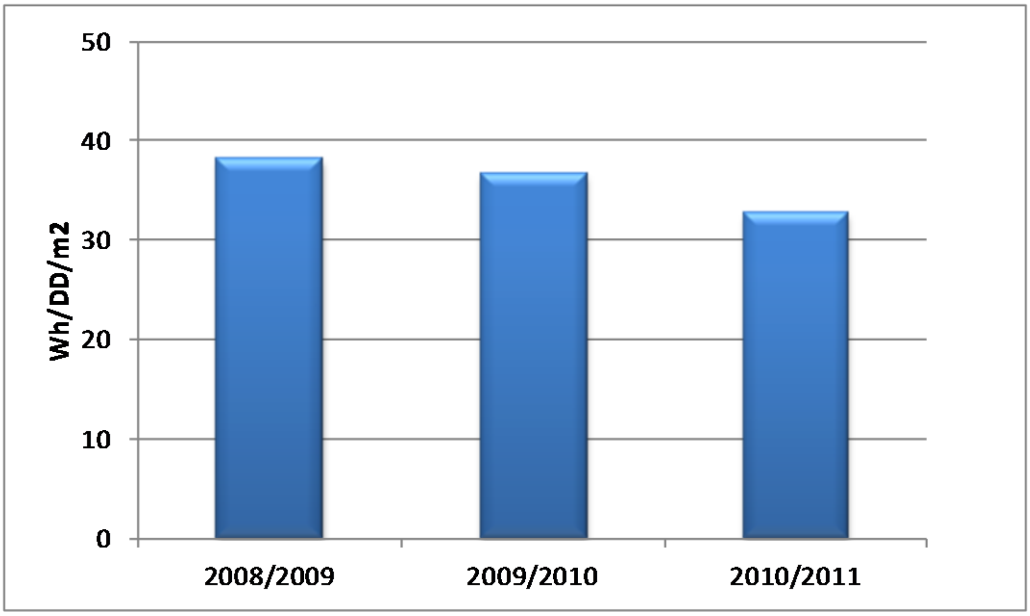

Fig. 1. Heat consumption in all types of buildings

These buildings can be divided in to two groups – new and old construction type. These two groups of buildings have been constructed according to different building norms, partitions have different heat transfer coefficients and consume a different heat amount, so these two groups have to be analysed separately. Heat consumption in new and old buildings during the last three heating seasons is shown below in a Fig. 2.

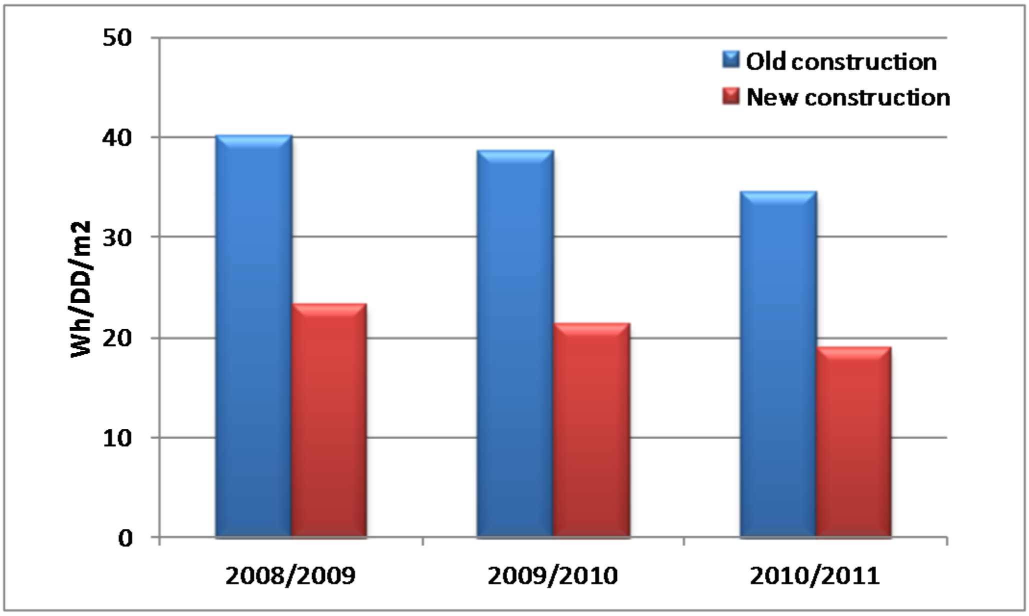

Fig. 2. Heat consumption in new and old buildings

Fig. 2 shows that heat consumption in new and old construction buildings is not constant and decreases every year: in old construction buildings comparing with 2008/2009 heating season, heat consumption during 2009/2010 heating season has decreased by 3.5 % and during 2010/2011 heating season by 14.1 %, in new construction buildings comparing with 2008/2009 heating season, heat consumption during 2009/2010 heating season has decreased by 8.6 % and during 2010/2011 heating season even by 18.6 %. That means that few years ago new construction buildings had a better indoor temperature conditions so heat consumption have decreased in a larger scale.

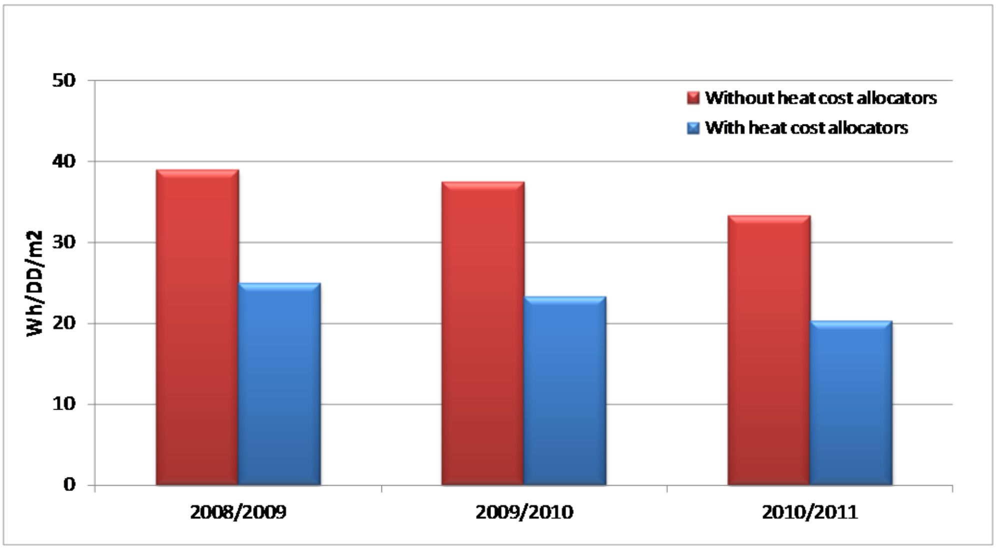

Fig. 3. Heat consumption in buildings with and without heat cost allocators

In a Fig. 3 is presented heat consumption in buildings with and without heat cost allocators. Figure shows that comparing with 2008/2009 heating season, heat consumption during 2009/2010 heating season in buildings without heat cost allocators have decreased by 4.1 % and in buildings with heat cost allocators even by 6.8 %. Heat consumption during 2010/2011 heating season in buildings without heat cost allocators have decreased by 14.7 % and in buildings with heat cost allocators even by 19.3 %. Decrease of energy consumption each year is due to influence of economics (energy price increases), but Fig. 3 shows decrement in every separate group – in buildings without heat cost allocators and with heat cost allocators. That means that buildings with heat cost allocators have a bigger potential to decrease in heat consumption.

After buildings with and without heat cost allocators was divided into a group of old and new buildings, it was determined that the difference between old construction buildings is larger and makes 28.2 %, the difference between new types makes 14.8 %. That means that old construction buildings have a bigger potential to decrease in heat consumption after heat cost allocators installation.

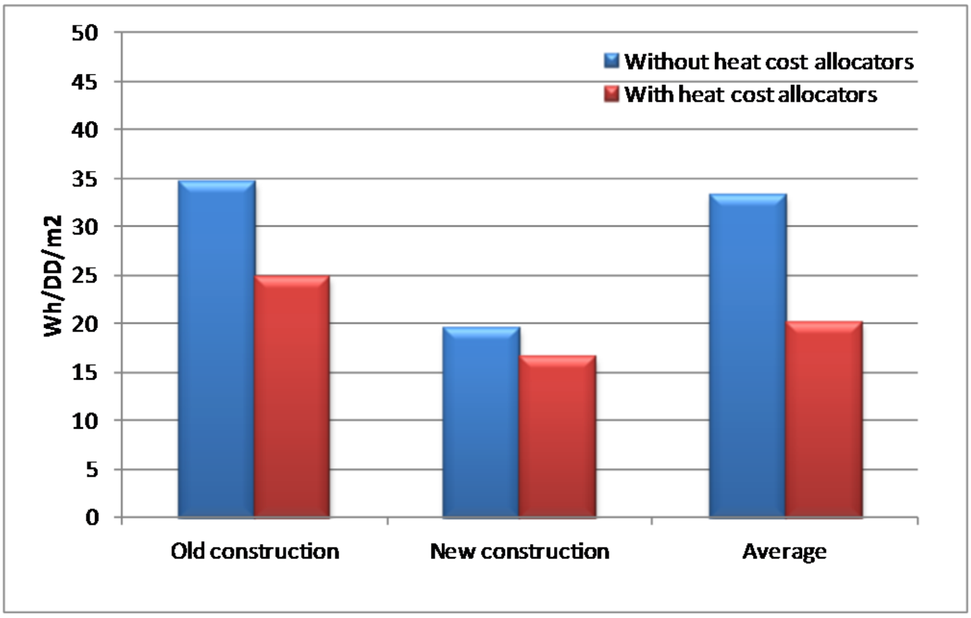

Fig. 4. Heat consumption in old and new buildings with and without heat cost allocators

As the buildings may differ in the height and heating area, further analysis has taken on the scope the number of floors and heating area. Fig. 5 presents that 5 and 9 storey buildings with heat cost allocators on average consumes about 28.4 % less heat energy – 5 storey about 22.9 % and 9 storey about 34.3 %. That means that 9 storey buildings have a bigger potential to reduce heat consumption as heat distribution in 9 floors buildings between different floors may be not as well as at 5 floors buildings. Comparing smaller and larger heating areas buildings after HCA installation, heat consumption in larger 5 storey buildings is about 10.9 % less and in 9 storey buildings about 29.4 % less than in smaller. That means that more is the number of storey and more building has heating area, the larger is potential to reduce heat consumption after HCA installation.

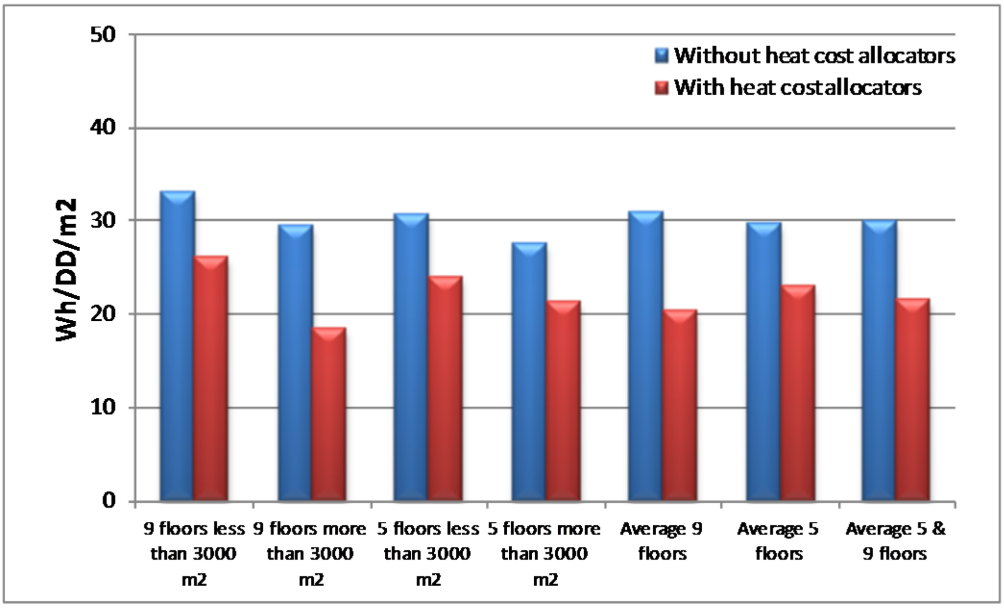

Fig. 5. Heat consumption in 5 and 9 floor buildings with and without heat cost allocators

Heat consumption during 2008/2009, 2009/2010 and 2010/2011 heating seasons in a buildings with individual heat meters (IHM) in a flats is presented in a Fig. 6. Differently from buildings with heat cost allocators, heat consumption in these buildings practically has remained unchanged or just slightly changed. Comparing with 2008/2009 heating season, heat consumption during 2009/2010 heating season has increased by 1.0 % and during 2010/2011 heating season has decreased by 5.6 %. This is because all these buildings with IHM are new construction and newly built.

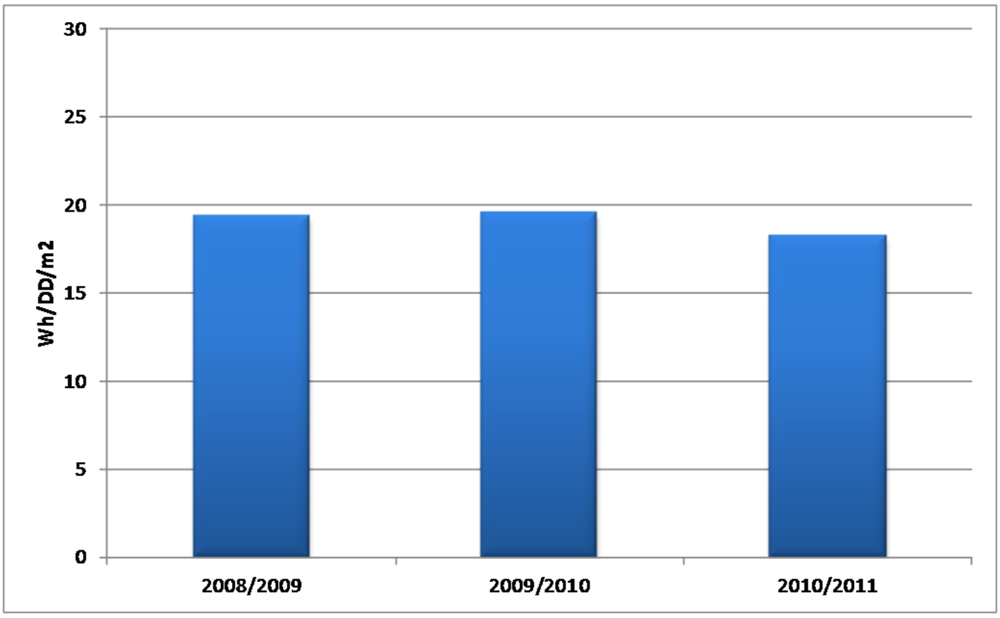

Fig. 6. Heat consumption in buildings with individual heat meters in a flats

Fig. 7 shows heat consumption in buildings with common heat meter for building, heat cost allocators, individual heat meters and gas boilers. Figure shows that individual heat metering in a buildings leads to a huge heat energy consumption decrease so it should be applied as wide as possible. Heat energy consumption in new construction buildings varies not in a large scale comparing with heat cost allocators or individual heat metering in flats, so there is no matter which of them would be applied after a new building will be constructed. Analysis results of heat consumption in building heated by individual gas boilers in flats are not strong due to lack of proper number of buildings and can be taken only as informational. Nevertheless the heat consumption in analysed building is not small.

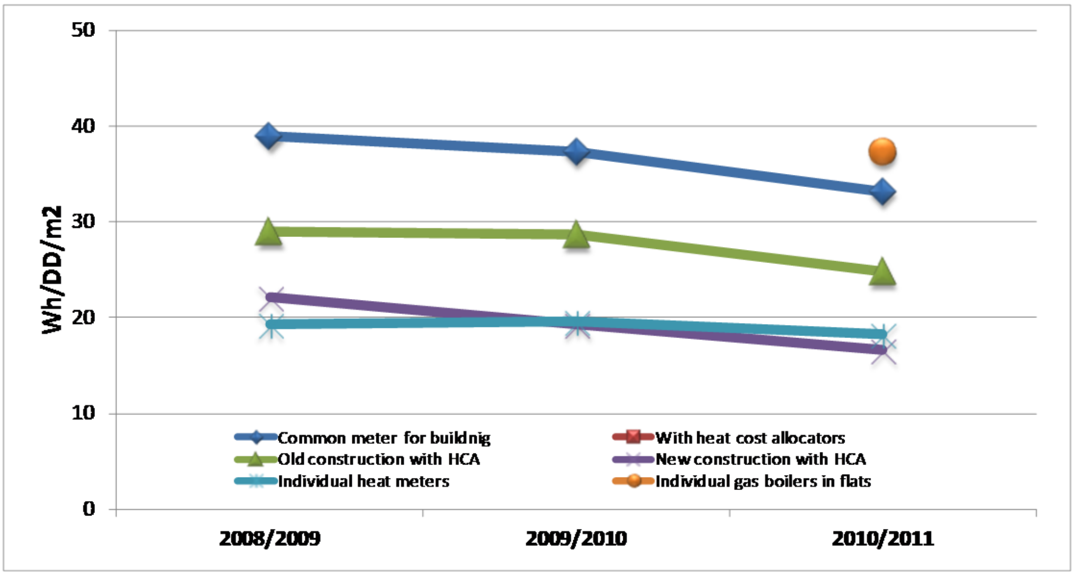

Fig. 7. Heat consumption in buildings with common heat meter for building, heat cost allocators, individual heat meters and gas boilers

4. CONCLUSIONS

Implementation of a new version of directive 2006/32/EC will require for retail energy sales companies or distribution system operators to achieve annual energy savings among final customers in the Union equal to 1.5% for every year. Study shows that due to inceased fuel price final energy consumption during the last years has decreased even in a larger scale, but also other possible means must be taken into consideration, so the obtained results are presented below:

1. An analysis of heat energy for heating shows that heat consumption in a buildings is not constant during the following years and decreases. Comparing with 2008/2009 heating season, heat consumption during 2009/2010 heating season has decreased by 3.9 % and during 2010/2011 heating season by 14.4 %.
2. Heat consumption in a buildings of new construction type has decreased more than in an old construction type. Comparing with 2008/2009 heating season, heat consumption during 2010/2011 heating season has decreased by 14.1 % in an old construction buildings and by 18.6 % in a new construction buildings. Heat consumption in a new construction buildings has decreased in a larger scale so that means that new construction buildings few years ago had a better indoor temperature conditions.
3. Heat consumption in a buildings with heat cost allocators also is not constant and decreases during years. Comparing with 2008/2009 heating season, heat consumption during 2010/2011 heating season in a buildings without heat cost allocators have decreased by 14.7 % and in buildings with heat cost allocators even by 19.3 %. That means that buildings with heat cost allocators have a bigger potential to decrease in heat consumption.
4. Buildings with heat cost allocators consume much less heat energy for heating. Old construction buildings have a bigger potential to decrease in heat consumption after heat cost allocators will be installed. It was determined that the difference between old construction buildings with and without heat cost allocators is larger and makes 28.2 %, the difference between new construction buildings makes 14.8 %.
5. 9 storey buildings have a bigger potential to reduce heat consumption comparing with 5 floors buildings. So more is the number of storey and more building has heating area, the larger is potential to reduce heat consumption after heat cost allocators have been installed.
6. During the last years heat consumption in a buildings with individual heat meters in flats has remained unchanged or just slightly changed. Fig. 7 shows that new type buildings with heat cost allocators consume about the same heat energy amount for heating as buildings with individual heat metering in flats. Old type buildings with heat cost allocators consume about 28.2 % less heat energy for building heating. Such huge heat energy savings also can be achieved after buildings partitions reconstruction (insulation, windows replacement) but it requires a huge amount of investments, so for the heat consumption in a building reduction first of all must be considered reconstruction of heating system and installation of individual heat metering by heat cost allocators or individual heat meters in a flats as it requires much less investment.

REFERENCES

1. THE EUROPEAN PARLIAMENT AND OF THE COUNCIL Directive 2006/32/EC of the European Parliament and of the Council on energy end-use efficiency and energy services, Brussels, 5 April 2006, p. 65–114.
2. THE EUROPEAN PARLIAMENT AND OF THE COUNCIL Proposal for a Directive of the European Parliament and of the Council on energy efficiency and amending and subsequently repealing Directives 2004/8/EC and 2006/32/EC, Brussels, 2011, p. 19–20.
3. GEDGAUDAS M., SLEZAS A., KVEDARAUSKAS J., TUOMAS E. Heat supply. Kaunas: Aušra, 1992, p. 61–87.
4. NATIONAL CONTROL COMMISSION FOR PRICES AND ENERGY For individual types of energy and fuel consumption standards for residential heating and hot water heating, No. O3-116, Vilnius, 2003-12-22, p. 5.

CYSENI 2012, May 24–25, Kaunas, Lithuania
ISSN 1822-7554, www.cyseni.com

PRECISE EVALUATION OF HEAT ENERGY FOR HOT WATER FOR ENERGY EFFICIENCY CALCULATIONS

R. Savickas
Vilnius Gediminas technical university
Sauletekio av. 9, LT–10223 – Lithuania
Phone:+370 652 27 398
Email: romas.savickas@gmail.com

ABSTRACT

Energy efficiency in present days has become a very important subject. While prices of energy resources rise every day, the energy efficiency becomes even more important issue. It is not enough just to reduce energy consumption as much as possible – it is necessary to identify applied measures and to evaluate their impact on energy resources usage. Various measures are applied but it is difficult to separate the individual impact of them on final energy consumption. Without having a precise value of separate applied measure we are blind to apply them further. Since determination of precise values from a final energy consumption balance becomes very important, this article presents how to evaluate the heat energy for hot water circulation system and hot water preparation. Study shows that at present time all most frequently applied calculations can be raised to a new level taking into consideration ground and outside air temperatures as they influences temperature of cold water for hot water preparation and final energy balance. The study analyses more than few thousands of buildings and presents dependence of heat energy for hot water circulation on a ground temperature. The results, conclusions and developed methodologies of this study can be applied for one building or for huge group of buildings as well.

Keywords: Energy efficiency, Hot water, Hot water preparation and circulation, Heat energy consumption

1. INTRODUCTION

Significance of heat consumption for space heating rises adequately with rising fuel costs. But to define the exact value for heating energy, we have to know the part of heat energy for hot water preparation and circulation and to subtract it from the total amount of energy consumed by building services. In most cases heat energy for space heating, hot water preparation and circulation is measured by one common heat meter. There are a lot of different and complex works how to define heat energy for heating purposes, how to get more precise values but it is forgotten that the precision of calculated heat energy for space heating depends on how exactly heat energy for hot water preparation and circulation is defined. About what precision of calculations can be talked simply do not possessing real amount of heat for hot water preparation and circulation. So the main objectives of this research work is to define exact and precise amount of heat energy for hot water preparation and circulation, and to define main factors influencing energy consumption fluctuations.

2. METHODOLOGY FOR EVALUATION OF HEAT ENERGY FOR HOT WATER FOR ENERGY EFFICIENCY CALCULATIONS

The multi-flat dwelling buildings are selected as the main research object as they are the main and socially mostly vulnerable group of buildings in cities. In addition, were selected buildings with centralized district heat supply, having independent heat supply scheme with separate heat exchangers for heating and hot water preparation, having hot water circulation lines. As hot water circulation type can vary depending upon building construction type, all hot water circulation types (hot water circulation only in a heat substation, circulation only in risers, circulation in risers and towel dryers) were analysed separately and later as one group. Mainly five and nine storey buildings were selected for an analysis, as they comprise a major part in a multi-flat dwelling buildings group. Heat energy and hot water consumption data of one year of more than four thousands of buildings were analysed and considered.

Statistical analysis was selected as the main methodology for this research [1]. Statistical analysis is useful while working with large amounts of data to determine general trends, principles and laws. Statistical analysis is also particularly useful when dealing with noisy data as well. It helps to define how much an event is unusual based on analysed historical data. If calculated probability is high and strong – the event approaches to law and can be explained. If probability is low – the way for an explanation would not be found from this method. First of all data checking and summarisation is applied for data analysis. Any outlier's data or doubtful observations after comparing with all data should be identified. Data analysis can be performed by the analysis of variance (ANOVA) and the t-test. The ANOVA and Student's t-test are widely used ways for quantitative (i.e. measurement) data analysis. Also data analysis can be performed by the regression or non-parametric methods. This study is based on linear regression analysis as the relationship between two variables is considered. The coefficient of determination R^2 is used as the main purpose is prediction of future outcomes on the basis of analysed data according to equation:

$$\hat{y} = b_0 + b_1 x , \tag{1}$$

R^2 is calculated as:

$$R^2 = 1 - \frac{SSE}{SS_{yy}} , \tag{2}$$

where:

SS_{yy} – (Sum of Squares), measures the deviations of the observations from their mean:

$$SS_{yy} = \sum_i \left(y_i - \bar{y} \right)^2 . \tag{3}$$

SSE – (Sum of Squares of Error), measures the deviations of observations from their predicted values:

$$SSE = \sum_i \left(y_i - \hat{y}_i \right)^2 . \tag{4}$$

In the case of linear regression coefficient of determination corresponds to correlation coefficient.

3. RESULTS AND DISCUSSIONS

In most cases heat energy in building is measured by one common heat metering device. This heat meter measures all consumed heat energy Q_Σ (Wh) for building's space heating, hot water preparation Q_{hwp} (Wh) and hot water circulation Q_{hwc} (Wh) needs and can be calculated as follows:

$$Q_\Sigma = Q_{heating} + Q_{hwp} + Q_{hwc} . \tag{5}$$

Total heat energy for hot water preparation Q_{hwp} (Wh) can be defined multiplying consumed amount of water G (m^3) by a heat energy to heat it to a defined temperature level:

$$Q_{hwp} = G \times \left(t_{hw} - t_{cw} \right) \times 1{,}159 , \tag{6}$$

where: G – consumed hot water amount, m^3; t_{hw} – temperature of prepared hot water, ^oC; t_{cw} – temperature of cold water for hot water preparation, ^oC; 1.159 – constant, heat energy to heat 1 m^3 of water by 1^oC (calculated from statement that 51 kWh of heat energy is required to heat 1 m^3 of water by 44 ^oC), kWh/m^3, [2].

Consumed amount of hot water G can be defined in two ways: by the sum of all hot water meters in flats or by common inlet hot water meter of a building. Consumed amount of hot water measured by hot water meters in flats is not very precise and comparing it with common inlet meter we will always get that the sum of hot water meters in flats is less than common inlet meter readings. My performed analysis shows that readings in flats usually makes part from 50 to 90% or in some cases even 100% of common inlet meter. Such a big difference mainly appears because of possibility to influence behaviour of hot water meter by applying it to a magnetic field and reducing its rotation speed or by other intervention. Such meters comprise the largest part of all meters in Lithuania. Practice shows that replacement of these meters by antimagnetic meters increases the part of percentage almost to 100% of common inlet building hot water meter readings but the detailed analysis of large number of buildings data must be done and presented separately to use exact numbers. The weight of such study would play an important role and would answer the question if these all hot water meters in flats must be replaced or not. In case they must be replaced because of a need to draw up the readings of hot water meters in flats as close as possible to a common building hot water meter readings, the replacement process would play an undisputed role as the transparency to the consumer would be raised to a new level. Every consumer would know what he pays for and that he does not pay for the hot water (heat for hot water preparation) of his neighbours.

From theoretical point of view the difference in readings between common inlet hot water meter and sum of meters in flats also appears because the common inlet meter measures cold water for hot water preparation, while meters in flats measure almost produced hot water that makes difference between water densities, so the difference of measured water densities makes inaccuracy of measurement. There are also other possible reasons of difference in readings between common inlet hot water meter and sum of meters in flats as nominal flow rate of meter and others, described in literature [3–7].

Due to above described arguments the data from common inlet buildings meters were taken and further analysis will be based on (5) and (6) equations. First of all aheat energy for hot water preparation must be calculated. In most cases for hot water preparation value of 51 kWh/m^3 is used in analysis. But really it is not the exact value and not always this amount of heat is consumed for hot water preparation, because cold water temperature changes during year – in winter time its temperature is lower, in summer time - higher. Considering cold water statistical temperature it is measured at the point it is obtained from, e.g. borehole. After cold water from borehole is supplied to a building, its temperature will change as it is influenced by its ambient conditions - ground temperature. Ground temperature varies depending on outside air temperature. My performed analysis shows that ground air temperature fluctuation period tails away from outside air temperature polynomial trend line (Fig. 1).

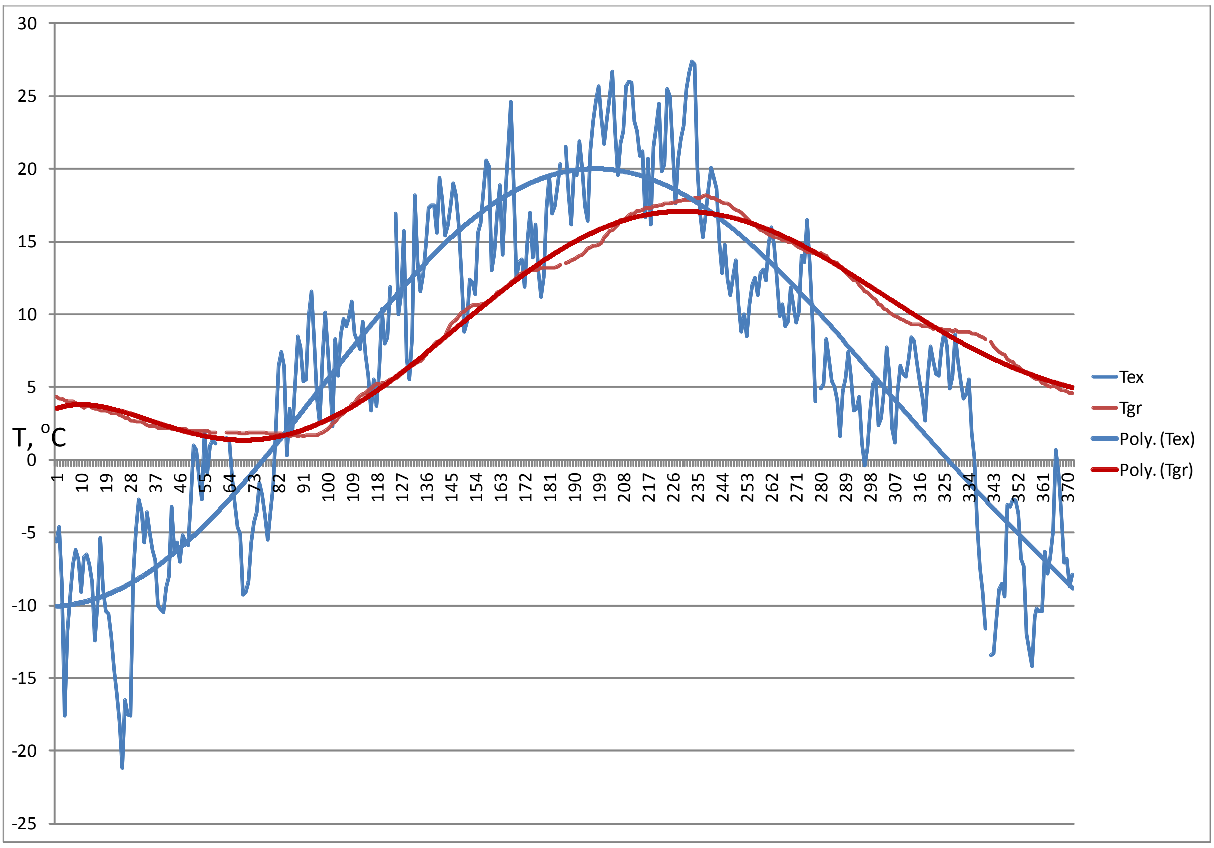

Fig. 1. Outside air and ground temperatures fluctuations during year

Usually heat amount of 51 kWh for production of 1 m^3 of hot water is taken in calculations for all months. But this heat amount is used to heat water by 44°C, so if hot water production temperature is defined as 50°C, cold water temperature for all months will be taken: 50°C – 44°C = 6°C. To increase the calculation accuracy, cold water temperature can be taken equal to ground temperature. Then calculating heat amount for hot water production during certain month average ground temperature must be taken as a cold water temperature during this month and according to (6) equation can be calculated heat amount for hot water preparation of all analyzed buildings. After this procedure according to (5) equation presented balance, can be calculated heat amount for hot water circulation for every specified period of all analyzed buildings. If we take a look at a given data, we will see that the heat amount for hot water circulation for every month is not equal. Fig.1. shows that this heat amount every year constantly fluctuates during season. To explain this dependence we have to define the main factors, influencing heat amount for hot water circulation and as the main factor for a smaller or greater heat losses is an ambient space temperature of hot water circulation pipe. Ambient pipe temperature during heating season varies not in wide range, because premises temperature is practically constant. During non heating season the average monthly ambient pipe temperature depends on average monthly premises temperature and the latter directly depends on the average monthly outside temperature. This study showhs that placed outside air temperature in the same graph with heat amount for hot water circulation, fluctuation line shows us that heat energy for hot water circulation is reverse proportional to outside air temperature – if outside air temperature increases, heat amount for hot water circulation decreases and if outside temperature decreases, the heat amount for hot water circulation increases. This dependence is shown in a Fig. 2.

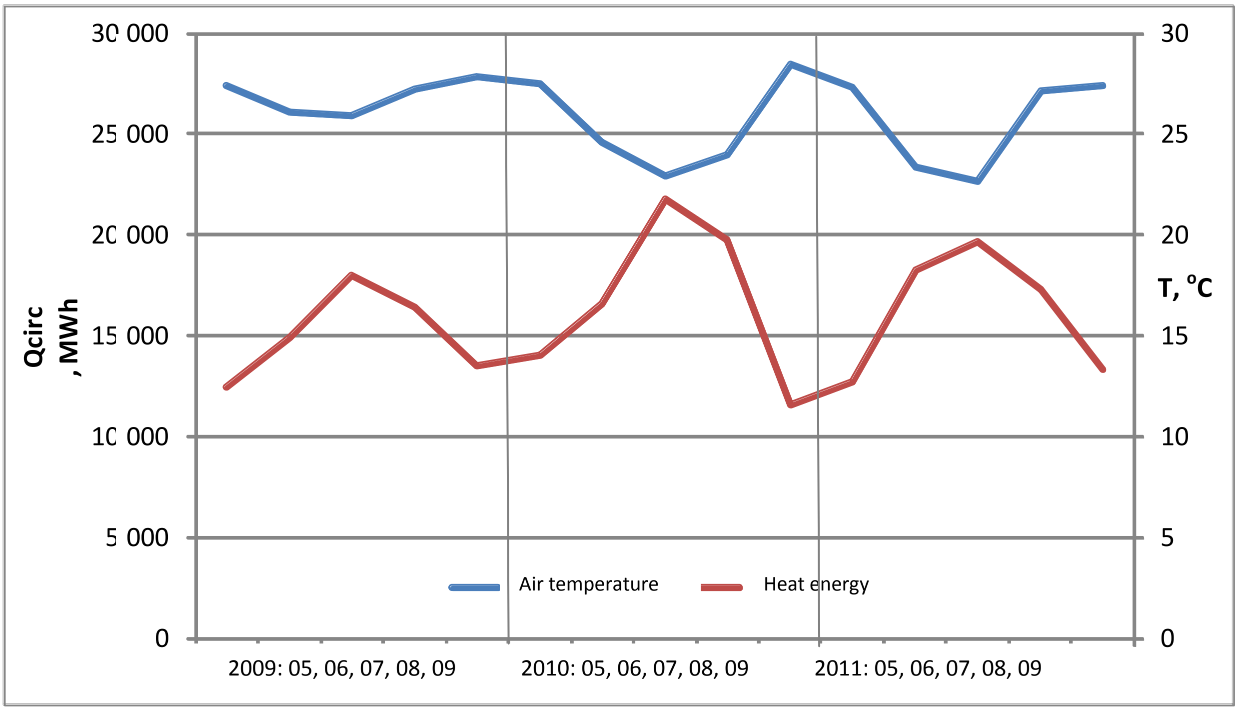

Fig. 2. Calculated heat energy of group of buildings for hot water circulation and outside air temperature

Taking further analysis, the strength of dependence between consumed heat and outside air temperature must be identified. Fig. 3 shows dependence of consumed total heat energy for hot water preparation and circulation on outside air temperature. This dependance is slightly influenced by volume of consumed water too, but not a lot as the volume of consumed hot water in most ways varies during a year, but not a lot between summer months.

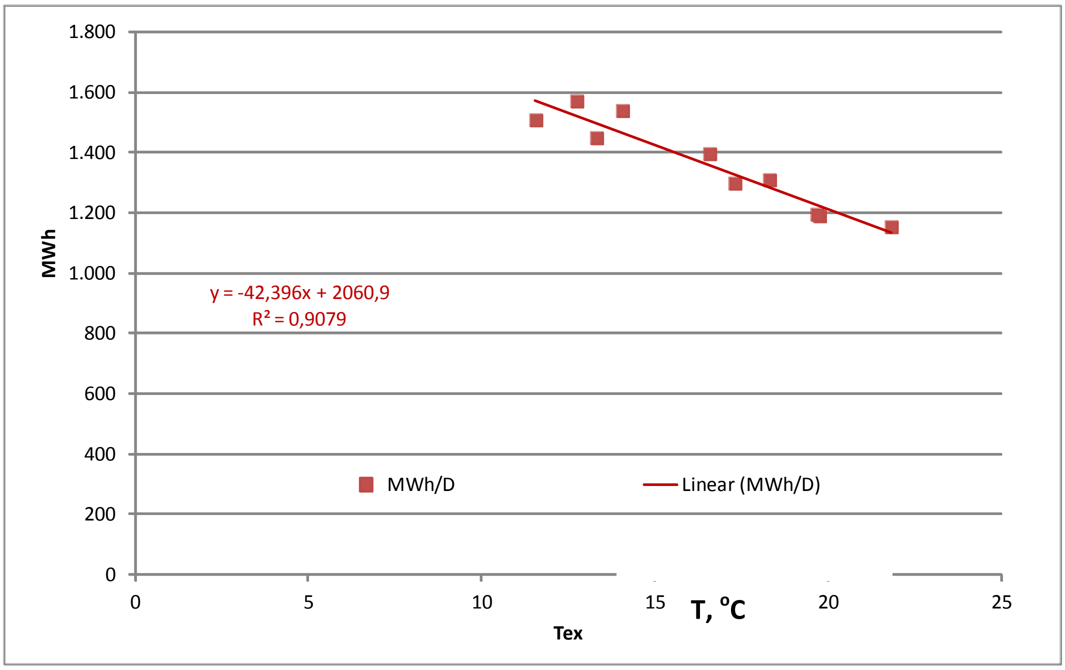

Fig. 3. Dependence of consumed total heat energy (MWh/ day) of group of buildings for hot water preparation and circulation on outside air temperature

The determination coefficient R^2 shows that strength of relation is described by 90,79%. This means that consumed total heat amount for hot water preparation and circulation depends on outside air temperature. As total heat amount for hot water preparation and circulation has dependence, the heat amount for hot water circulation also must have dependence, because heat amount for hot water consumption does not vary to a great extent and may influence the total consumed heat amount as a constant. The question arises: does amount of monthly heat energy for hot water circulation, calculated according to above described methods would be different from heat energy for hot water circulation calculated in a most common way when heat amount for hot water preparation is taken as 51 kWh/m^3. To get the answer Fig. 4 was drawn, which presents two different amounts of monthly heat energy for hot water dependences on outside air temperature.

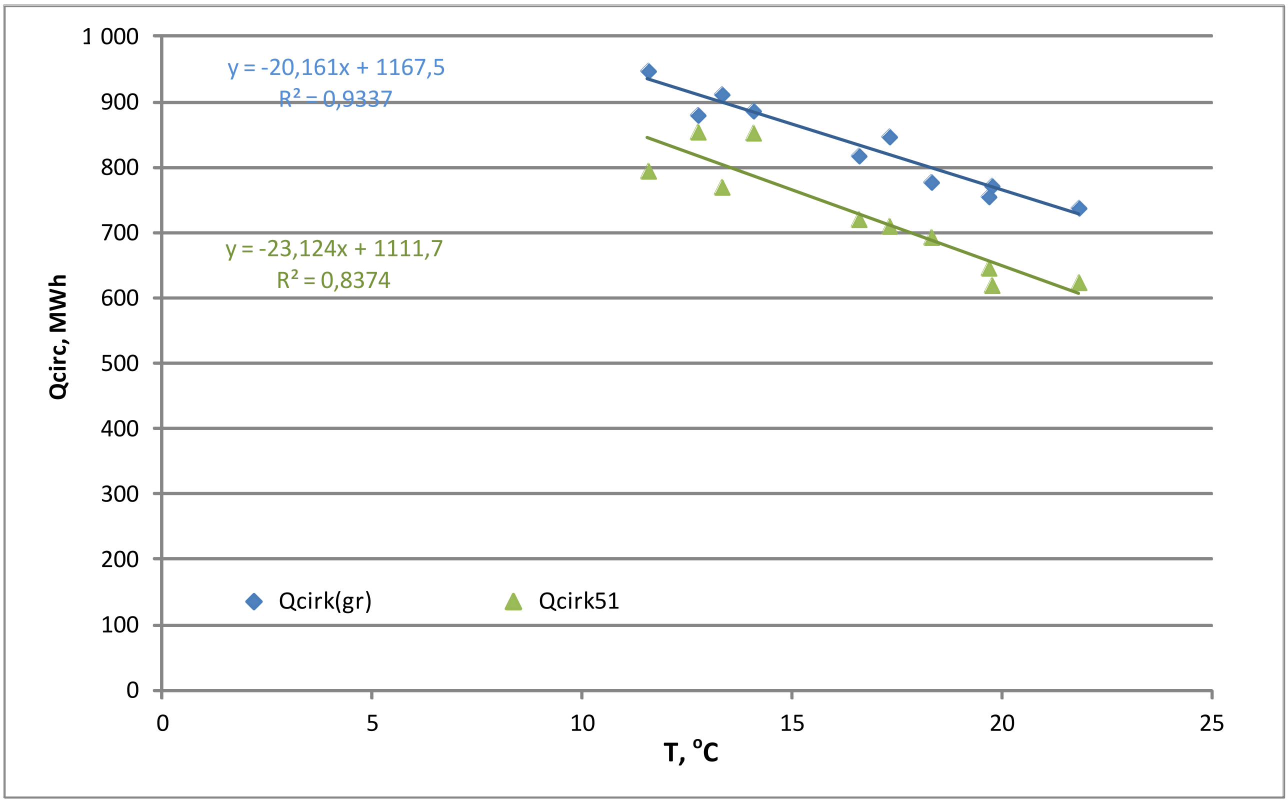

Fig. 4. Dependence of consumed heat amount for hot water circulation on outside air temperature

First part of points and its trend line shows heat energy for hot water circulation, calculated taking into consideration that heat for hot water production depends upon outside air temperature ($Q_{circ(gr)}$) and second part of points and its trend line (Q_{circ51}) is calculated according to heat amount of 51 kWh/m^3. The Fig. 4 shows that given results do not coincide and both trend lines go independently in different directions. Heat amount for hot water circulation $Q_{cirk(gr)}$ is about 13% larger than heat amount Q_{cirk51}. Calculating from total heat energy for hot water preparation and circulation, heat amount $Q_{cirk(gr)}$ makes 61% part from it and heat amount Q_{cirk51} makes 54% part from it (Fig. 5), so heat amount calculated by two different ways differ by about 5 %. This difference is not influenced by volume of consumed hot water as in both cases is calculated for the same volume of hot water.

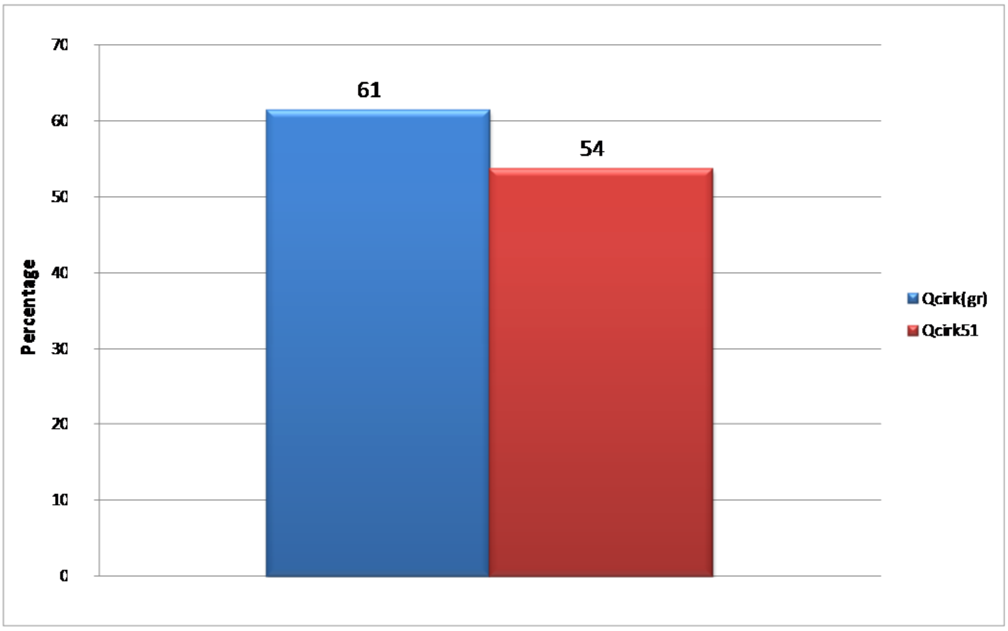

Fig. 5. Heat amounts $Q_{cirk(gr)}$ and Q_{cirk51} as part of total heat amount for hot water preparation and circulation

Calculating heat energy for heating it is necessary to know exact value for hot water. Usually building has only one heat meter for premises heating and hot water needs, so arise the question how to distinguish heat energy for space heating. Heat energy for heating can be calculated according to (5) equation in following ways:

1) according to total consumed heat amount for hot water preparation and circulation;
2) according to consumed heat amount for hot water, calculated taking into consideration outside air and ground temperature;
3) according to heat amount of 51 kWh/m^3 for hot water preparation value;
4) according to National control commission for prices and energy requirements (heat amount of 160 kWh/flat (circulation in hot water towel driers and coil-pipes), 80 kWh/flat (circulation in hot water towel driers) and 10 kWh/flat (circulation in heat substation).

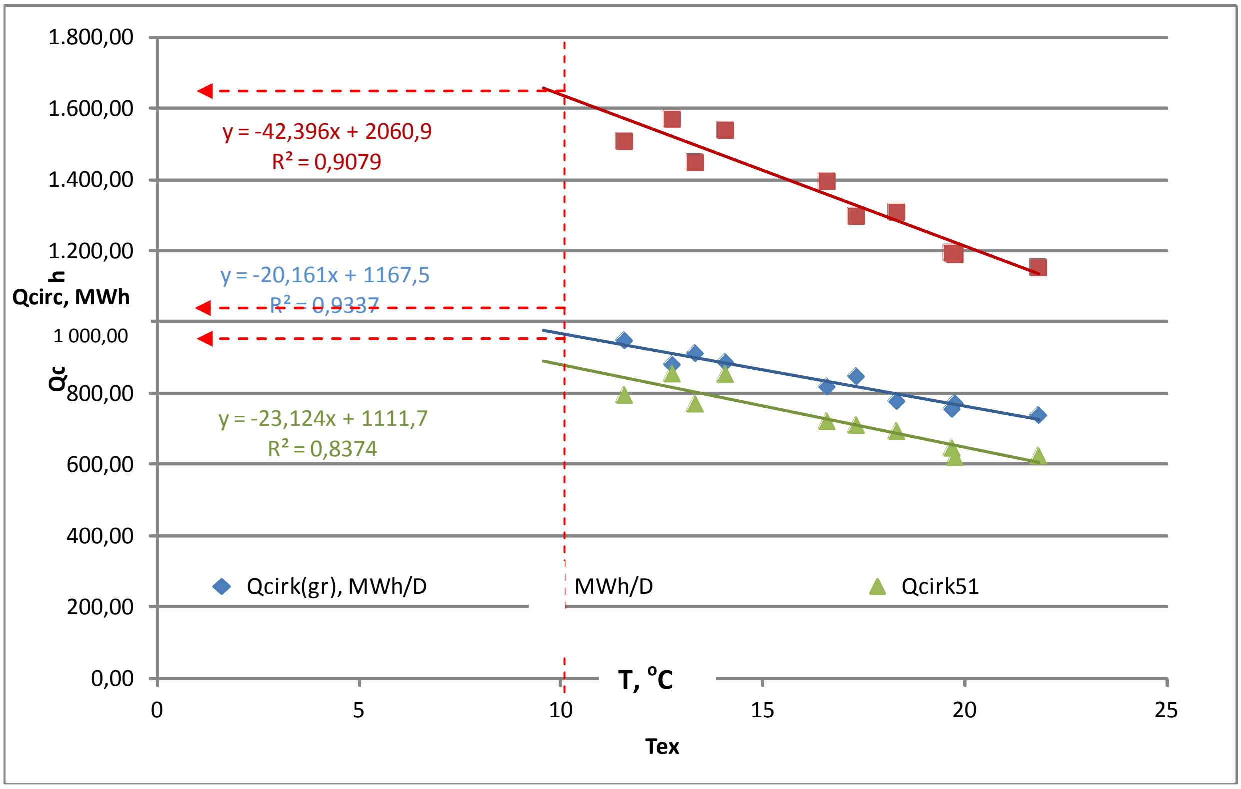

Fig. 6. Heat amount Q_{circ} and temperature, at which must be evaluated heat amount for it

No matter according which way will step out further calculations, arise the question – what heat amount for hot water circulation should be taken as it always varies depending on outside temperature? The answer will be the following - the heat amount should be taken at the temperature, at which ends and begins heating season - at the temperature of +10°C (Fig. 6). Above this temperature circulation heat losses decreases as the building base temperature is reached.

Calculating heat energy for heating during heating season according to the first way, from total heat amount must be subtracted total heat energy for hot water preparation and circulation taken from nearby outside temperature of +10°C. The disadvantage of such calculation is that for every month amount of consumed hot water will be taken the same that is true only approximately. Calculating according to second way must be taken actual amount of consumed hot water and multiplied by a heat for hot water preparation taking into calculations cold water temperature about 5°C. Later heat amount for hot water circulation according to nearby outside temperature of +10°C must be added. The disadvantage of such calculation is that exact cold water temperature is not known. Calculating according to third way must be taken actual amount of consumed hot water and multiplied by 51 kWh/m^3 (a heat for hot water preparation). Later must be added heat amount for hot water circulation according to nearby outside temperature of +10°C.

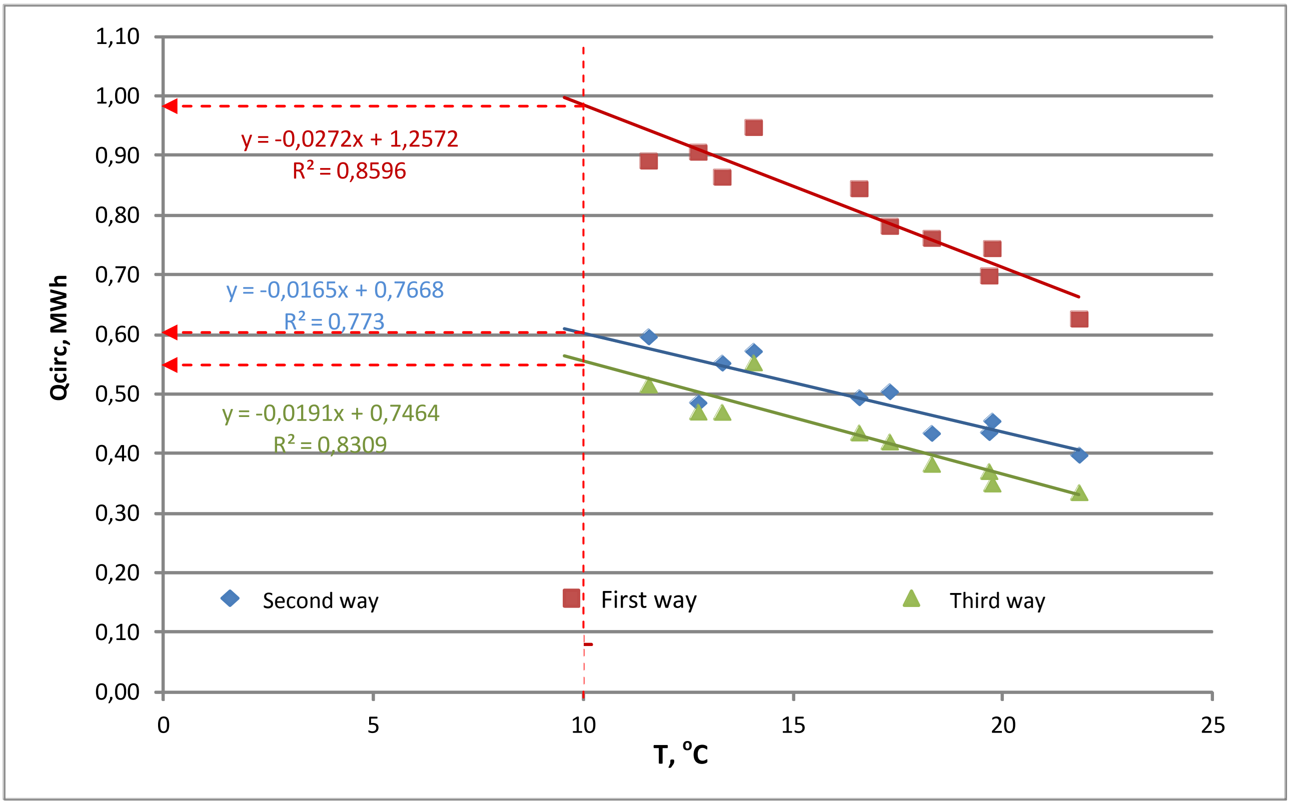

Fig. 7. Heat amount for hot water circulation of 9 storey building

This analysis was performed analysing data of buildings group but in the same successful way it can be applied to analysis of one building. Fig. 7 shows the same analysis data of one 9 storey building of 110 flats, 6200 m^2 and 1983 year of construction. Calculating according to the first way, from total heat amount must be subtracted about 0.98 MWh/d, calculating according to second way must be subtracted 0.60 MWh/d and according to third way must be subtracted 0.55 MWh/d. Second way of calculations gives more exact value. This defined methodology is very important for heat supply companies as they must to predict very precisely fuel amount for the next year/period. For example amount of consumed gas must be predicted as precise as possible, because every additional consumed cubic meter of gas will cost very expensive. For the whole heat supply company it makes a huge amount of money and the investments into calculations becomes not so important.

4. CONCLUSIONS

1. An analysis shows that heat energy consumption for hot water preparation depends on ground temperature and heat amount for hot water circulation depends on outside air temperature.

2. Defined a methodology to evaluate an exact heat amount for hot water circulation and exact heat energy amount for hot water preparation during non heating season.

3. Defined a methodology to evaluate an exact heat energy amount for hot water circulation and exact heat energy amount for hot water preparation for a heating season.

4. An exact values for hot water needs are required to perform calculations of heat energy for space heating. Heat energy amount for heating can be calculated according to (5) equation in the following ways: 1) according to total consumed heat energy amount for hot water; 2) according to consumed heat energy amount for hot water, calculated taking into consideration outside air and ground temperature; 3) according to heat energy amount of 51 kWh/m^3 for hot water preparation value; 4) according to National control commission for prices and energy requirements (heat

amount of 160 kWh/flat (circulation in hot water towels and coil-pipes), 80 kWh/flat (circulation in hot water towels) and 10 kWh/flat (circulation in heat substation)). The second way gives most precise result.

5. Presented methodology can be useful performing energy audits, energy consumption and efficiency analyses, defining an exact budget value for building heating and hot water needs for one separate building or group of buildings.

5. REFERENCES

1. AKSOMAITIS A. Theory of probability and statistics. ISBN 9986-13-893-0. Kaunas: Technologija, 2000, p. 189–195.
2. NATIONAL CONTROL COMMISSION FOR PRICES AND ENERGY For individual types of energy and fuel consumption standards for residential heating and hot water heating, No. O3-116, Vilnius, 2003-12-22, p. 5.
3. SAVICKAS R., SKRINSKA, A. Effectiveness of hot water account in compartment buildings and analysis of consumption uncertainty. Energetika, 2007, Vol. 53, No. 4, p. 76–83.
4. SAVICKAS R. Efficiency of hot water supply systems in buildings, Doctoral Dissertation, Vilnius, 2007, p. 38–42.
5. BALČIKONIS R. Problems of heat and hot water measurement, Thermal technic. 1998. No. 1, p. 5–6.
6. JP BUILDING ENGINEERS, Center for Energy Efficiency in Buildings Heat Metering and Billing: Technical Options, Policines and Regulations. China, Beiyin, 2002. P. xi.
7. INGIMUNDARSON A., WOLLERSTRAND J., ARVASTSON L. On Sizing of Flow Meters Used in Customer Accounting Devices in District Heating Systems. 2005, p. 4.

CYSENI 2012, May 24–25, Kaunas, Lithuania
ISSN 1822-7554, www.cyseni.com

COOLING DEGREE DAYS AND HOURS FOR LATVIA

G. Stankevica
Riga Technical University
1Kalku Street, LV-1658 - Latvia
Phone +371 28324732
Email: galina.stankevica@rtu.lv

ABSTRACT

Calculation of cooling degree days is currently one of the most commonly used methods in heating, ventilation and air conditioning (HVAC) industry to describe the effect of outside air temperature on building cooling energy consumption. This paper presents values of cooling degree days and hours that were calculated using data of outdoor air temperature, measured at meteorological station in Riga (Latvia) during the period of last 10 years. Seven base temperatures were used, i.e. from 19.0°C to 26.0°C with 1°C increment. Fluctuations in a number of cooling degree days were found by comparing them to the values calculated as cooling degree hours. Total cooling degree number was about 50% higher when using degree hour approach, providing more accurate data for future energy consumption estimations. Yearly cooling degree days are given in a tabular form. This data could further complement the local building norms and regulations regarding design of HVAC systems and energy efficiency, filling the gap of missing information for methodology of simplified energy calculations in buildings.

Keywords: Cooling degree days and hours, energy consumption, HVAC systems

1. INTRODUCTION

Nowadays the building sector in member states of European Union accounts for about 40% of final energy consumption and about a third of greenhouse gas emissions, of which about two-thirds are ascribed to residential and one-third to commercial buildings [1]. Even though most of energy in eastern European buildings is used for space heating, e.g. about 70% in Latvian households [2], special attention should be also directed towards space cooling, since the energy consumption it accounts for (mostly electrical energy) is growing rapidly. It is expected that energy demand for cooling will increase even more in the future due to global warming, higher demands for quality of life and comfort, increased use of glazing in architecture, increased number of electric appliances etc., and generally due to economic growth [3].

Several methods are available for energy analysis and estimation of energy demands. These methods differ in complexity, in amount of ambient condition data that needs to be taken into account, time increment used for calculations, detail of description of the building geometry and its characteristics etc. [4]. Degree day method is currently the simplest and well established technique for energy analysis, providing adequate results for simple systems and applications. It is appropriate in cases when the use of building, efficiency of HVAC equipment, indoor temperature and internal gains are relatively constant. Degree day method allows comparison of buildings current and past energy performance, as well as comparison of buildings in different climate zones. In [5] cooling degree day (CDD) data for 171 countries is summarized, where Mali and Nigeria are ranked 1st and 2nd having the highest number of cooling degree days per year, i.e. 4064 and 4033, respectively. This is about 5-7 times higher compared to the warmest EU countries (Greece, Spain and Italy), and almost 70 times higher than in Latvia, were 58 CDD were calculated.

In developed countries advanced building simulation programs are often used by heating, ventilating and air conditioning (HVAC) engineers to determine the cooling demand. These programs provide very accurate results since rather extensive input data on building characteristics and outdoor climatic conditions is used. In many countries, HVAC designers estimate capacities of cooling equipment (e.g. cooling coils at air handling unit), using outdoor design temperature (summer and winter) for the specific location of building. This method provides reasonable results, however often leads to HVAC equipment oversizing, leading to higher capital and running (energy) costs. Degree day method provides adequate results on estimation of cooling requirements for simple cases, e.g. when choosing split type air conditioner for the apartment. This helps to size air conditioning unit more accurately, and therefore avoiding long term problems involving inefficient comfort levels and high energy consumtpion.

The Latvian Cabinet Regulation No. 39 [6] on methodology for building energy performance calculation provides equations for estimation of buildings heating and cooling energy demand. These regulations also state the need to correct heating and cooling energy consumption according to outdoor climatic conditions, based on degree day method. However, all further explanations and calculations on the topic of degree days is provided explicitly for heating period. In addition, Latvian Cabinet Regulation No. 39 [6] refers to Latvian building norms No. 003-01 [7] on climatology, that specifies length of heating period (expressed in days) and no information is provided regarding cooling season. Since very limited data is available regarding cooling energy consumption and degree days and hours in Latvia, the aim of this study is to fill in this gap of information by calculating CDD and CDH numbers for various base temperatures and outdoor air temperature data in Latvia during the last 10 years.

2. METHODOLOGY

2.1. Calculating degree days and hours

Calculation of cooling degree days is currently one of the most commonly used steady-state methods HVAC industry to describe the effect of outside air temperature on building cooling energy consumption. Generally, in the degree day method it is assumed that energy demand for a building is proportional to the difference between the mean daily temperature and a base or reference temperature. The base temperature is usually defined as the temperature below or above which heating or cooling is needed. Cooling degree days can be calculated using equation 1:

$$CDD = \sum_{days} (T_m - T_b)^+ , \tag{1}$$

where: T_b is the base temperature (°C); T_m is the daily mean outdoor temperature (°C) calculated as average between day minimum and maximum values. The plus sign in equation 1 indicates that only positive values are counted.

Traditionally, CDD are determined using 22°C as a base temperature, corresponding to uninsulated building case. However, the base temperature varies from bulding to building due to the differencies in building characteristics (insulation, glazing type etc.), thermostat set-points and other factors. In this study CDD and CDH are calculated for the base temperatures between 19°C and 25°C with 1°C temperature increment.

Total number of cooling degree hours for a month can be expressed as in equation 2:

$$CDH = \sum_{j=1}^{N} (\overline{T_m} - T_b)^+ \tag{2}$$

Where: T_m is the hourly mean outdoor air temperature (°C); N is the number of hours of the month (h). The plus sign indicates that only positive values are summed.

2.2. Ambient data collection

Accurate and reliable ambient data are very important for building energy analysis and simulations, determining accuracy and characteristics of results. The outdoor temperature data for this study was obtained from Latvian Environment, Geology and Meteorology Centre [8] that measured temperature during interval of three hours. The numbers of CDD and CDH in this paper were calculated using outdoor air temperature, measured at meteorological station in Riga (geographic coordinates of 56°57'N latitude and 24°6'E longitude) during the period of last 10 years, i.e. 2001 to 2010.

The mean outdoor temperature during summer months in Riga (Latvia) given as normative values in Latvian building norms No. 003-01 [7] are 15.4°C, 16.9°C and 16.2°C for June, July and August months respectively. The mean outdoor temperature values during the period of recent 10 years (2001 to 2010), calculated in this study are as follows: 15.8°C, 19.3°C and 18.2°C for June, July and August, respectively. Thus, the latest tendencies indicate generally higher mean temperatures in Riga, especially during July and August months. This leads to necessity to reconsider and update the existing climatology norms developed for building engineers.

3. RESULTS AND DISCUSSION

The calculated cooling degree days with base temperatures of 19-25°C are presented in Table 1.

Table 1. Cooling degree days with various base temperatures for Riga, Latvia

Month	**Base temperature [°C]**						
	19	**20**	**21**	**22**	**23**	**24**	**25**
April	0	0	0	0	0	0	0
May	5	2	1	0	0	0	0
June	7	4	2	1	0	0	0
July	43	29	20	13	9	5	2
August	26	17	10	6	4	2	1
September	0	0	0	0	0	0	0
Total	81	53	33	21	13	7	3

According to obtained results, there is no cooling demand during April and September months. The highest energy consumption for cooling is expected during warmest summer months, i.e. July, followed by August and June.

The calculated cooling degree hours with base temperatures of 19-25°C are listed in Table 2.

Table 2. Cooling degree hours with various base temperatures for Riga, Latvia

Month	**Base temperature [°C]**						
	19	**20**	**21**	**22**	**23**	**24**	**25**
April	23	14	8	4	2	1	0
May	204	136	87	52	28	13	5
June	368	251	165	106	66	38	19
July	1361	1040	774	563	399	275	185
August	799	581	409	279	185	120	75
September	70	38	18	7	2	1	0
Total	2825	2060	1461	1012	683	448	284

Calculation of cooling degree hours provides more accurate results. Comparison of CDD and CDH expressed as days is showed in Fig. 1.

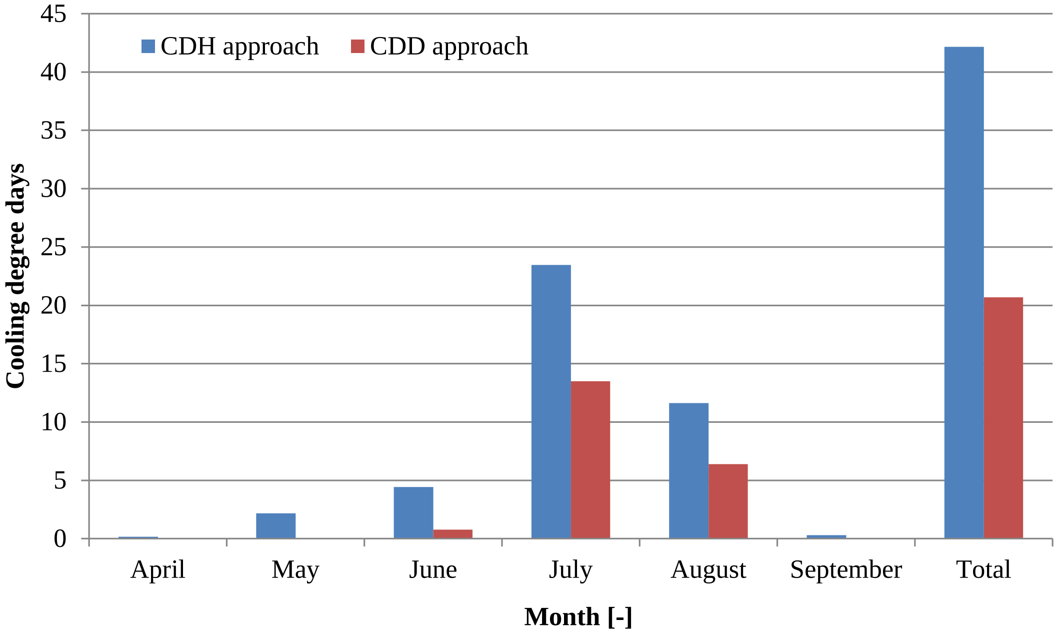

Fig. 1. Calculated cooling degree days and hours expressed as days for the base temperature of 22 °C

When using cooling degree hour method in calculations, some cooling would be required also during April and September months. The total number of cooling degree days is almost 50% higher compared to calculations using cooling degree hours approach. This might lead to significant inaccuracies when estimating energy consumption for cooling.

In addition, it should be also mentioned that data presented in this paper might not be representative for entire city, since temperature varied in some cases for more than 1°C, especially between densely built urban areas and suburbs temperature fluctuations were recorded. The future work should be thus directed towards further examination of outdoor climatic data and energy consumption for HVAC system operation, as well as development of contour map of yearly cooling degree days for entire Latvia’s territory.

Due to confidentiality issues very limited data is available regarding actual energy consumption data in Latvian office buildings. However, some energy consumption data for cooling of air at the air handling unit (AHU) in one office building is presented in Fig. 2.

According to obtained data, the energy for cooling of ventilation air was required only during period May-September, 2010. The energy consumption curve generally follows the calculated cooling degree hours pattern, reaching its maximum in July month. The building examined in this case is very energy efficient one, using both heat and cold recovery at the AHU. Chilled beams are used to provide space cooling, which was actually required almost during the entire year, with exception of January and February months. Further validation of the calculated cooling degree hours and days is required using real object data from numerous office buildings in Riga (Latvia).

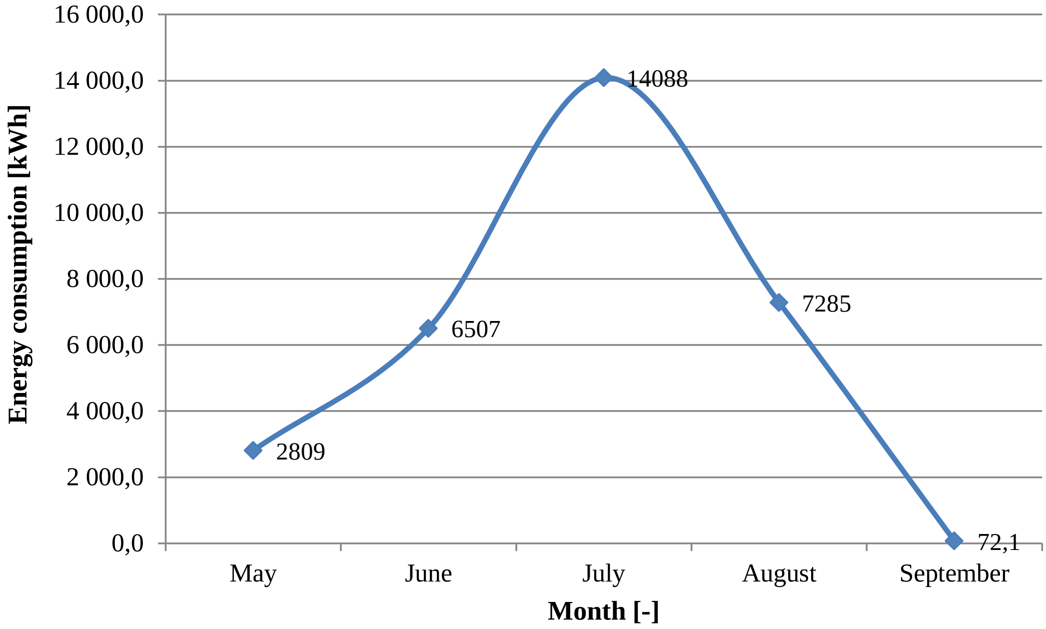

Fig. 2. Energy consumption for cooling of air at the air handling unit

4. CONCLUSIONS

The following paper presents cooling degree day and hour data in tabular format for Riga (Latvia) calculated with various base temperatures and using outdoor air temperature data for the last 10 years. The actual mean outdoor temperature measured during the last 10 years is significantly higher (e.g., about 2°C for July and August months) compared to the normative values given in the local climatology norms, indicating necessity for their update. Total cooling degree number was about 50% higher when using degree hour approach, providing more accurate data for future energy consumption estimations. This data could further complement the local building norms and regulations regarding design of HVAC systems and energy efficiency, filling the gap of missing information for methodology of simplified energy calculations in Latvian buildings. However, further validation of the calculated cooling degree hours and days would be necessary using real object data (cooling energy) from numerous office buildings in Riga.

5. ACKNOWLEDGEMENTS

This work has been supported by the European Social Fund within the project «Support for the implementation of doctoral studies at Riga Technical University».

REFERENCES

1. EC Green-Paper - Towards a European Strategy for the Security of Energy Supply, Commission of the European Communities, 2000 – [referred on the 25th of February in 2012 y.]. <http://aei.pitt.edu/1184/1/enegy_supply_security_gp_COM_2000_769.pdf>
2. KLAVS, G., KUDRENICKIS, I. Energy efficiency policies and measures in Latvia. Institute of Physical Energetics, 2009- [referred on the 15th of February in 2012 y.]. <http://www.odyssee-indicators.org/publications/PDF/latvia_nr.pdf>

3. Greenhouse gas emission trends and projections in Europe 2009. The European Energy Agency, 2009- [referred on the 15th of February in 2012 y.] <http://www.eea.europa.eu/publications/eea_report_2009_9>
4. AYRES, M.J., STAMBER, E. Historical development of building energy calculations. ASHRAE J 1995; 37(2); p. 47–53.
5. BAUMERT, K., SELMAN, M. Heating and Cooling Degree Days, World resources institute, 2003- [referred on the 15th of February in 2012 y.]. <http://cait.wri.org/downloads/DN-HCDD.pdf>
6. MK 39. 2009. Building energy performance calculation method (in Latvian). Cabinet Regulation No. 39. Riga, Latvijas Vēstnesis.
7. LBN 003-01. 2001. Building climatology (in Latvian). Latvian Building norms No. 003-01. Riga, Latvijas Vēstnesis.
8. Latvian Environment, Geology and Meteorology Centre, 2011 Environmental air quality data. [referred on the 13th of January in 2012 y.] <http://www.meteo.lv/public/26902.html>

CYSENI 2012, May 24–25, Kaunas, Lithuania
ISSN 1822-7554, www.cyseni.com

INFLUENCE OF UNSTEADY THERMAL STATE ON ENERGY PERFORMANCE AND PRODUCTIVITY IN OFFICE BUILDINGS

R. Valančius, A. Jurelionis
Kaunas University o Technology,
Faculty of Civil Engineering and Architecture,
Studentų st. 48, LT-51367 Kaunas, Lithuania
Phone 8-37-300492
Email: rokas.valancius@ktu.lt

ABSTRACT

Thermal output of heating and cooling equipment in office buildings is usually controlled according to external air temperature. Yet, due to large outdoor air temperature variations, indoor climate may not always be adjusted to fit into the comfort range. Despite the modern facilities in newly build offices, occupants may be exposed to temporary thermal discomfort that affects their performance. The aim of this study was to outline the influence of variation of indoor air temperature on office work performance and energy consumption. During the experiment in the real office indoor and outdoor climate parameters as well as energy consumption were observed. Employees were asked to fill questionnaires by indicating their thermal sensation, perception of air quality and humidity. The results of the study showed that indoor climate change may cause dissatisfaction of participants, which could lead to lower productivity. The effects of intermittent indoor climate parameters on energy consumption were outlined as well. However, adjusting heating and cooling power according to outdoor air temperature and indoor air temperature reduction during the night and weekends are some of most applied methods for energy saving in buildings. Heating systems operating under the digital weather forecast are still sufficiently expensive and rarely used.

Keywords: energy performance, unsteady air temperature, thermal sensation, human performance.

1. INTRODUCTION

Modern people spend most of their lifetime indoors engaged in all kinds of different activities. Therefore alongside air quality, air temperature is one of the most important parameters of indoor climate. Nevertheless, in many office buildings thermal conditions are not well-controlled due to insufficient heating or cooling capacity, high internal or external loads, large thermal zones, improper control or operation of heating, ventilation and air conditioning (HVAC) equipment as well as other factors.

Building services engineers are interested in improving indoor environments and quantifying the effects. Yet potential health and productivity benefits are not generally considered while expenses for exploitation are usually calculated. Only initial investment, energy and maintenance costs are typically considered.

The comfort air temperature range in Lithuania is regulated by the standards of hygiene [1]. It may vary from +22 °C to +24 °C in case of performing sedentary job in the fixed workstation during the cold season, and from +23 °C to +25 °C during the warm season. Relative humidity should be in the range of 40-60 %, air velocity should not exceed 0.1 m/s – 0.15 m/s accordingly. No probable variations of parameters time-wise are given.

Seppänen et al. [2] outlined a relation between human performance and air temperature based on various productivity studies. It showed that performance increases when air temperature rises up to +21–+22 °C and decreases by approximately 2% per 1 °C increase of air temperature in the range of +23–+35 °C. The maximum performance is achieved at +21.6 °C (Fig. 1).

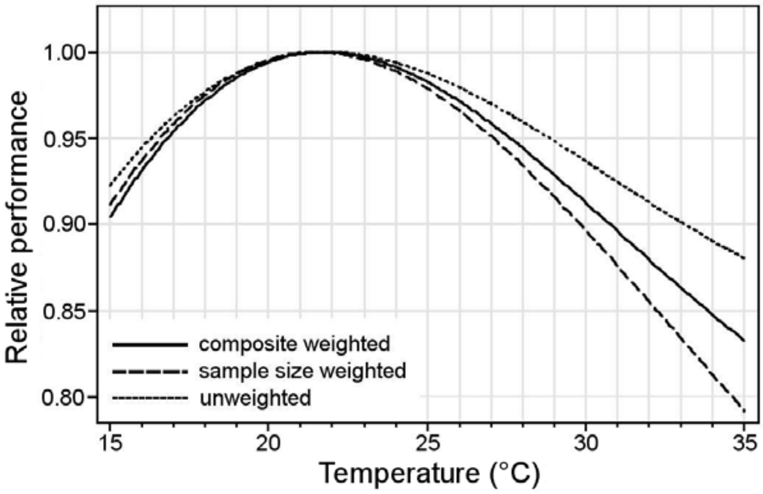

Fig. 1. Normalized relation between performance and air temperature in rooms (Seppänen et al, 2006)

Lan et al. [3] outlined the correlation between indoor temperature, human performance and different clothing insulation (0.86, 1.0 and 1.19 clo) levels during the winter season. It showed that the maximum performance was achieved at 21.9 °C with the clothing insulation equal to 0.86 clo and at 19.7 °C with the clothing insulation equal to 1.19 clo.

The results of the study performed by Valancius and Jurelionis (2011) showed that short-term temperature drop from 22 °C to 18 °C increased general employee productivity by 4.1 %. On the other hand tasks requiring concentration and focus were performed at 10 % higher productivity [4].

Pupeikis at al. [5] defined that in order to increase energy savings in buildings with air temperature reduction function heating power should be enlarged by approximately 50% in most cases. The simulation has showed that for buildings with a medium thermal inertia (time constant τ = 144 h) the expenses by employing the intermittent heating (reduced temperature period: 12 h on working days and 48 h at weekends), pays back after one year. When designing the heating system attention should be paid to thermal inertia of particular building. Research showed that considering various thermal inertias of buildings, the adequate modes of intermittent heating must be chosen.

Rimkus et al. [6] presented climate forecast for Lithuania for XXI century according to which annual air temperature is expected to be higher by 2.3–5.7 ºC till 2080. Extreme alteration is expected on February (mean temperature would rise by 3–9 ºC). According to the forecast, day temperature range splay out, inrush of brief strong winter frosts will be more frequent. In the other study author prognosticated longer duration of the high sun spine during average season [7]. This would be extremely perceptible during May to September. On the other hand, there would be less direct sunlight in the winter. Similar trends are observed in most parts of the world.

The outdoor climate change will undoubtedly have the effect on indoor air temperatures as the heating and cooling power of HVAC systems will not be sufficient to handle the processes.

In this article study of the influence of the temperature swings on building energy consumption and human performance is discussed. The results and conclusions were based on the findings of the experimental research.

2. METHODOLOGY

In order to evaluate the influence of temperature variations to general energy consumption and performance of the employers the real building was selected (Fig. 2). Building was built in 1950 in

Kaunas and was refurbished in 2000. Energy class of the building – E. Evaluated general energy consumption of the building is 240.75 kWh per square meter of net floor area [8] per year.

Fig. 2. The view of the case study building used as an objective of the research

Offices are heated by two natural gas boilers 40 kW of heating power each. Indoor air temperature is controlled according to external air temperature by either compensating heating controller or adjustment of the thermostatic radiator valves.

Indoor air temperature during weekends and after working hours is reduced by 4 degrees. During working days air temperature is decreased in the period from 5.30 pm to 7.00 am, on Saturdays air temperature is set back to optimal from 9 am till 2 pm because some offices in the building are also used in Saturdays.

Natural ventilation is installed in the building. Basic data of the analyzed building is presented in the table 1.

Table 1. Basic data of the case study building used as an objective of the research

Shape, area	Rectangular, 461 m²
Number of floors	2 and garret
Number of employees	34
Construction	Walls: Heavy construction without insulation, U=1.12 W/m²K, Windows (glass, PVC frame) U=1.60 W/m²K
Glazing	13% of the total wall area
Work schedule	8 a.m. – 5 p.m.; no occupancy on Sundays and holidays

The second floor offices “A”, “B”, “C” and “D” were selected for analysis of the air temperature swings and calculation of energy consumption (Fig. 2). Rooms “A”, “B”, “C” are oriented to North-East, there are nine persons performing sedentary work in these rooms. The room “D” is orientated to South-West and it is used as archive and storage room. There are no people working consistently in the room “D”.

Air temperature and relative humidity sensors with data loggers were used (in “A”, “B”, “C” and “D” rooms) to measure external and internal air temperature variation during the observed period. Heat meters (one for “A”, “B”, “C” areas, second for “D” room, the third for the second floor) were installed in order to record energy consumption. The period of the measurement was one month from 7th of January 2012 to 7th February 2012 with values recorded every 30 minutes. At the end of this period the employees were asked to fulfill questionnaires about thermal sensation and indoor climate in the office during this month.

Persons working in the rooms “A”, “B” and “C” were allowed to adjust thermostatic valves on the radiators according to their thermal comfort needs. Supplementary heating device was used in the room “C” on 19th, 20th, 23rd of January ant 7th February. In the room “D” thermostatic valves on the radiators were set to 18 ºC during all investigative period. Blinds were used in rooms “A”, “B”, “C“ in order to avoid direct solar radiation.

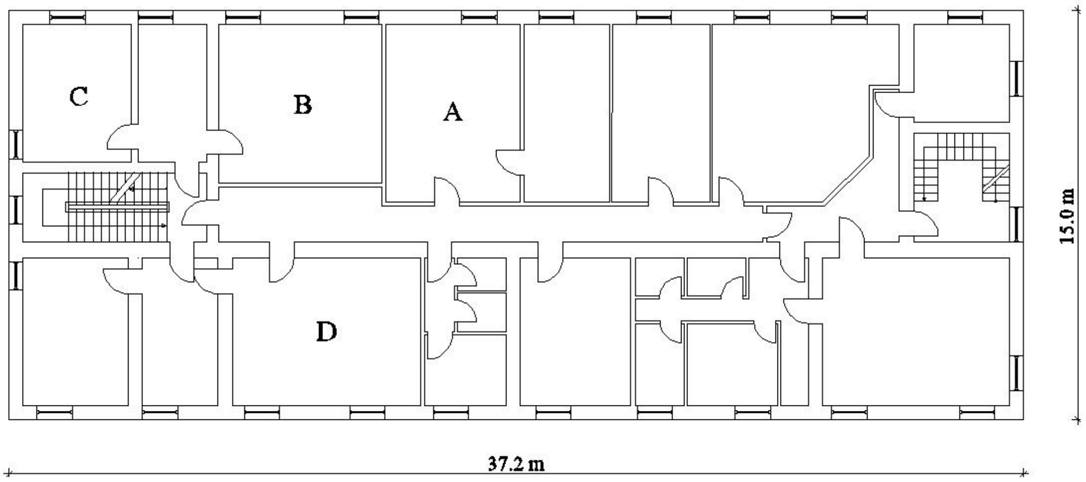

Fig. 2. The view of second floor of the case study building

In the following calculation physical activity level of the occupants was considered equal to 1.2 met (69.6 W/m^2) and average clothing level was considered as invariable – 0.75–1.0 clo (0.116 – 0.160 $m^{2.0}C\cdot W^{-1}$). Relative humidity indoors was 30–50 %, air velocity was lower than 0.10 m/s.

Taking into account that the office building was heated with the gas boilers, energy charges were estimated 0.06 €/kWh. For further calculations assumption on the average employer profit was estimated equal to 20 % of each employee monthly average salary which was approximately equal to 1000 € excluding taxes. It was considered that profit was 9 € per day per person, having in mind that the employees work 8 hours a day, 22 days per month.

3. RESULTS

The results of the questionnaire survey are presented in Table 2.

Table 2. Results of the questionnaire survey performed during the experiment

How often did you felt thermal discomfort because of following reasons last month?				
	Never	Few times	Several times a week	Every day
Draught	53.9	34.6	7.7	3.9
Too high temperature	73.1	23.1	3.9	0.0
Changeable temperature	23.1	42.3	23.1	11.5
Too low temperature	15.4	53.9	19.2	11.5
Stuffy air	23.1	30.8	30.8	15.4
Dry air	42.3	30.8	19.2	7.7

Note: the values in the table are in %, where 0% means the statement is totally untrue, and 100% means the statement is totally true.

Questionnaire survey of the office employees showed that 11 % of the employees evaluated thermal conditions as very good, 54 % as good and 35 % as moderate. There were no respondents who described conditions as bad and very bad. Other results of questionnaires are presented in the table 2. Participants were mostly dissatisfied with intermittent air temperature, too low air temperature as well as stuffy and dry air.

During the analyzed period (01.07.2012 - 02.07.2012) the average day temperature was -6.5 ºC, the lowest observed temperature was -24.7 ºC, the highest recorded temperature 5.4 ºC (Fig. 3). In the rooms “A”, “B” and “C” 4134 kWh or 34 kWh/m² of thermo energy were consumed and in the room “D” respectively 542 kWh or 14.5 kWh/m². Expenses for heating of rooms A”, “B” and “C” were 2.04 €/m² and 0.87 €/m² for the room “D”.

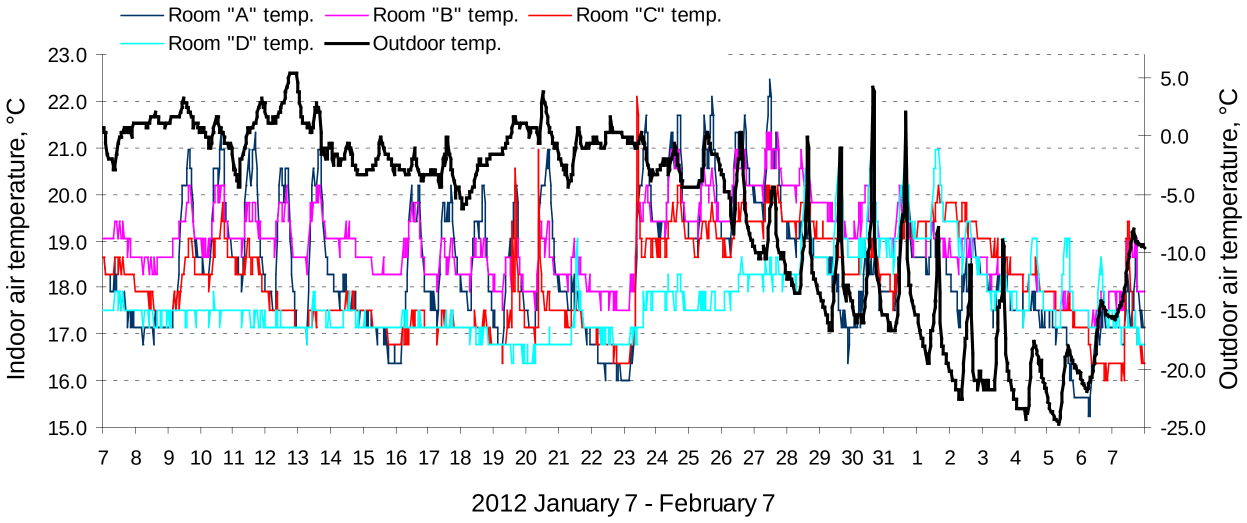

Fig. 3. External and internal air temperature variation during period of the experiment

Figure 3 shows that similar swings of air temperature repeats itself at all selected dates, except the days between 28th of January and 7th of February. At these days temperature changed during the day by 15.6 ºC, the average temperature was -15.4 ºC and the lowest recorded temperature was -24.3 ºC.

Two periods from 9th to 13th of January and from 30th of January to 3rd of February were compared. As the subject for further analysis the exponentials of the room “A” were selected. In the following figures the temperature of the room “A” and the optimal air temperature (Fig. 4), outdoor air temperature (Fig. 5), instantaneous power of heating system (Fig. 6), are presented.

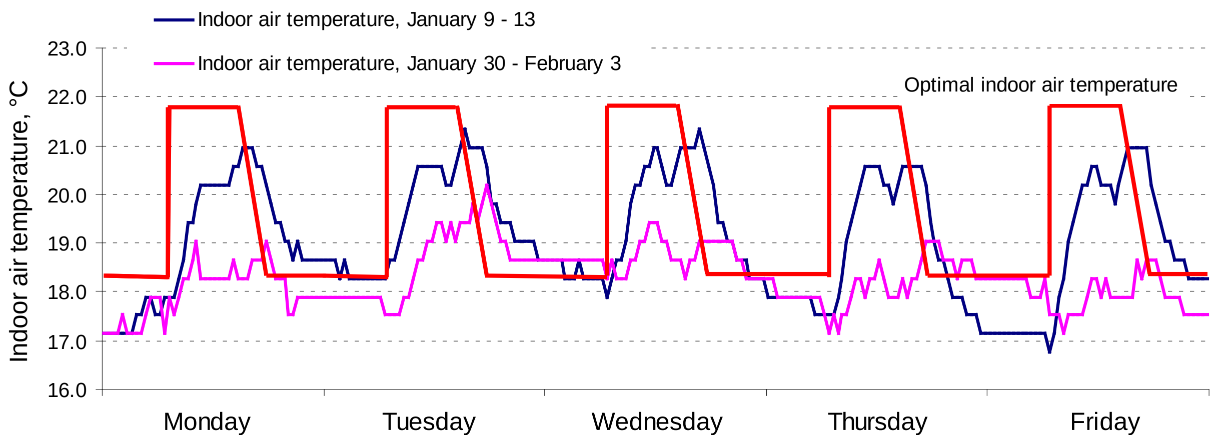

Fig. 4. The optimal air temperature curve and indoor air temperatures in the room “A”

The optimal air temperature curve presented in Figure 4 was established to maximize productivity of the occupants. From the point of view of long term performance, indoor air temperature should be fixed at +21.6 ºC from the moment when the work starts at the office. On the other hand, air temperature should be gradually decreased to +18 ºC one hour before the end of working day in order to use the effect of productivity rise due to temporary lowered air temperature.

It is important to outline, that personal adaptation to thermal conditions of each individual are not taken into account in this study. Results of the research performed with larger groups of individuals were used in order to draw the optimal curve, therefore there is a chance of complaints due to too low temperature in the rooms from certain individuals.

Measurements in the case study building showed that because of imperfection of heating system control as well as thermal inertia of the building, the optimal air temperature drop during off-work time is not possible to achieve. Moreover, the long-term measurements in the offices showed that during working hours the internal air temperature is too low, especially at the morning hours. At the end of the day the rooms are usually overheated (Fig. 4).

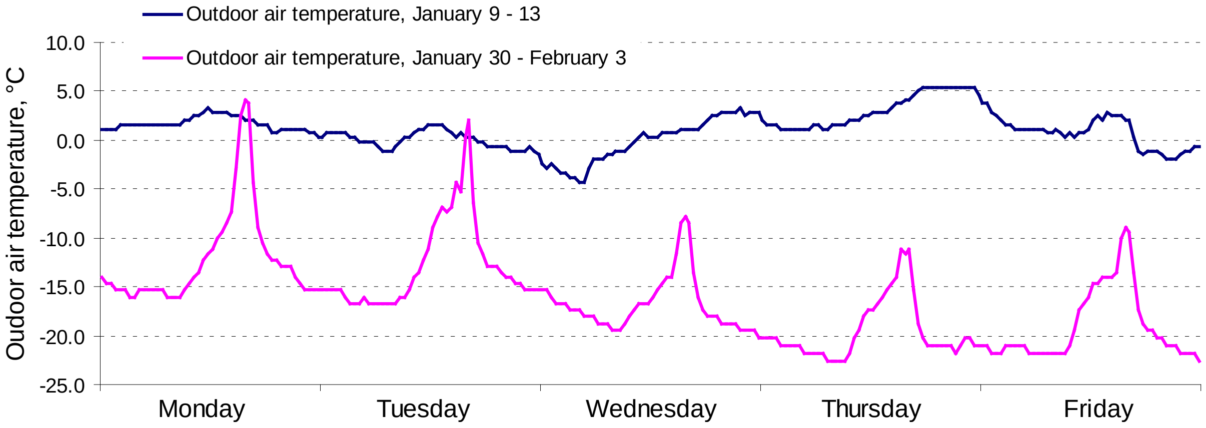

Fig. 5. Outdoor air temperature variations at the period from 9th to 13th of January and at the period from 30th of January to 3rd of February

According to the results of the study reported by Seppänen et al. [2] reliable loss of productivity of the occupants would be approximately 5.2 % in the analyzed building rooms “A”, “B” and “C”. The average value of PMV index [1] would be -0.78 .

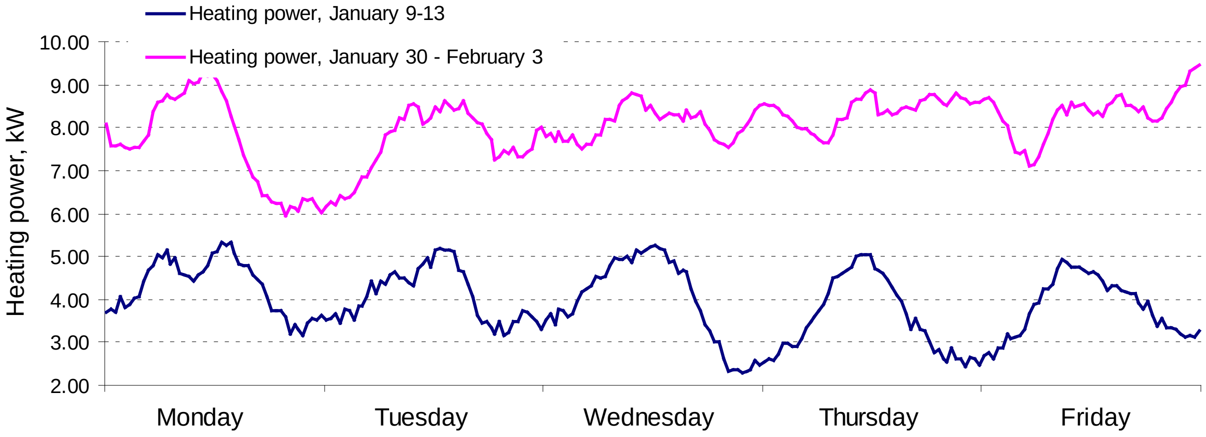

Fig. 6. Heating power (rooms “A”, “B”, “C”) at the period from 9th to 13th of January and the at period from 30th of January to 3rd of February

The loss of productivity of the occupants was calculated and converted to the monetary value. Thermal discomfort of the occupants working in the rooms “A”, “B” and “C” would result in a loss of performance by proximally 93.6 € from 7th of January to 7th of February.

In order to compensate the loss of productivity the rooms “A”, “B” and “C” would need the 212 kWh of additional energy. For that reason in higher heat consumption equal to 12.7 € would be needed at the period from 7th of January to February 7th.

4. CONCLUSIONS

1. The results of the study showed that control of the heating system does not ensure optimal temperature in the analyzed building. According to long-term and short-term productivity studies, air temperature should be fixed to 21.6 ºC and should be reduced to 18 ºC until the end of the work hours.
2. The main complaints received by performing questionnaire survey of the occupants of the case study building were stuffy air, too low air temperature and too high variation of the temperature during the day.
3. In order to ensure optimal air temperature control from the point of view of energy saving as well as maximized productivity of the office work, the power of the heating system should be increased by 18 %. In case the power of the heating system would remain unchanged, temperature control curve should be adjusted to advance the temperature rise in the morning and temperature drop in the afternoon.
4. The financial losses due to decrement of office work performance are 7.4 times higher comparing to additional expenses for increased energy demand evoked by ensuring higher air temperature in rooms.

REFERENCES

1. HN 69:2003 Šiluminis komfortas ir pakankama šiluminė aplinka darbo patalpose. Parametrų norminės vertės ir matavimo reikalavimai, *Valstybės žinios 45-1485, 2003.*
2. SEPPÄNEN O., FISK W.J. AND Q.H.LEI. 2006. Room temperature and productivity in office work, in: *Proceedings of Healthy Buildings Congress 2006.* Vol. 1, p 243–247, LBNL-60952.
3. LAN L., WARGOCKI P., LIAN Z. 2012. Optimal thermal environment improves performance of office work. *The REHVA European HVAC Journal*. 49 (1): 12–17.
4. VALANČIUS R., JURELIONIS A. 2011. Impact of intermittent indoor climate conditions on productivity of the occupants, in: *Proceedings of the 12th International Conference on Indoor Air Quality and Climate – Indoor Air 2011*, Austin, paper ID: 490.
5. PUPEIKIS D., BURLINGIS A., STANKEVIČIUS V. 2010. Required additional heating power of building during intermittent heating, *Journal of Civil Engineering and Management* 16(1): 141–148.
6. RIMKUS E., BUKANTIS A., STANKŪNAVIČIUS G. 2006. Klimato kaita faktai ir prognozes. *Geologijos akiračiai* 1 (61), p. 10–20.
7. RIMKUS E., KAŽYS J., JUNEVIČIŪTĖ J., STONEVIČIUS E. 2007. Lietuvos klimato pokyčių XXI amžiuje prognozė. *Geografija* 43 (2), p. 56–64.
8. STR 2.01.09:2005 Pastatų energetinis naudingumas. Energetinio naudingumo sertifikavimas. Vilnius, 2005.

CYSENI 2012, May 24–25, Kaunas, Lithuania
ISSN 1822-7554, www.cyseni.com

POOL AS A COOLING DEVICE

K. Grinbergs[1]**, P. Shipkovs**[1,2]
1 Riga Technical University
Azenes 16/20, LV-1048 Riga – Latvia
Email: kgrinbergs@inbox.lv

2 Institute of Physical Energetics
Aizkraukles 21, LV-1006 Riga – Latvia
Email: shipkovs@edi.lv

ABSTRACT

Pools are an especially practical and aesthetically appealing execution of a cooling system – provided appropriate temperature modes and external air temperature during the operational season. These temperature modes are observed in trigeneration system cycles, in heat absorption facilities. Heat absorption facilities require a fluid overcooling cycle to store a concentrated fluid. The temperature modes of this cycle (which vary for different producers) produce low-potential heat which cannot be reused for heat energy production, e.g. 35-29°C. To support such a temperature schedule, producers generally recommend installing heat evaporation towers, but those are expensive and will often clash visually with the landscape. A cooling pool may be used instead for both practical and aesthetic reasons, using water sprayers to promote evaporation. Water spraying is necessary to increase the surface area of water-to-air contact: this way, the surface area is equal to the combined areas of all water droplets. The depth of a pool must be no less than 1.5 m, preventing heating by sun rays. Pool cooling properties could be improved with finer droplet size, although this carries higher electricity expenses to produce adequately high pressure before pulverization. Such pools may use fountains which serve both as a cooling facility and an attractive landscaping piece. An evaporation pool is also significantly cheaper to build than an evaporation tower, although water loss may be higher.

In consideration of the facts described above, a pool with a water spraying device was built for this research project. With appropriate air temperature, pressure and relative humidity, heat yield and yield changes were measured.

The goal of this study was to compare the research and experimental parts of the project to similar studies performed previously, in order to determine the practical viability of using heat evaporation pools as well as to develop a complete prototype which may be used as the basis for building similar structures.

Keywords: energy efficiency, cooling systems, heat absorption, heat evaporation pool

1. INTRODUCTION

The world is familiar with various systems of heat carrier cooling systems. For decades, they have developed, the coolants and their chemical composition have changed, but water has always remained an integral part of the technology owing to its unique properties. Water is used as a heat carrier or coolant for cooling spaces and equipment, for accumulating heat, for returning heat to an environment with a lower heat potential, as well as a solvent. This study reviews a number of uses for water, united to create a comparatively simple yet efficient heat carrier cooling facility that can be practically used in the right conditions. This facility is a pool with a cooler and water sprayers to stimulate the cooling process. A pool is an alternative to a heat carrier cooling tower and is suitable for an adequate temperature schedule of a heat absorption equipment cooling cycle. To study the applicability of the system, a pool has been built and connected to a constant heat source (boiler house). The boiler house ensures a constant heat carrier temperature and delivers it to the cooler installed inside the pool, which exchanges its heat with the water in the pool. The pool also has a circulation pump, its suction delivers water from the lower layers of the pool to the sprayers and fountains on the air/water surface of the pool. The installed heat carrier cooling must be maintained regardless of changes in external air parameters. The pool is a closed system; this is its difference form a heat carrier cooling tower, since the temperature of the heat carrier during operation is often close to air temperature.

1.1. Heat Evaporation Pool as an Alternative to a Cooling Tower

The creation of a heat carrier cooling pool (the layout of the test bed is available in Figure 1) is based on the idea of connecting two systems. A cooler (heating element) is placed inside the pool and a circulation pump is installed to deliver water to water sprayers above the pool's surface. Unlike an evaporation tower, which is an open system, a pool is a closed system, so a pool may also be installed inside residential areas such as cities, parks, parking spaces etc.

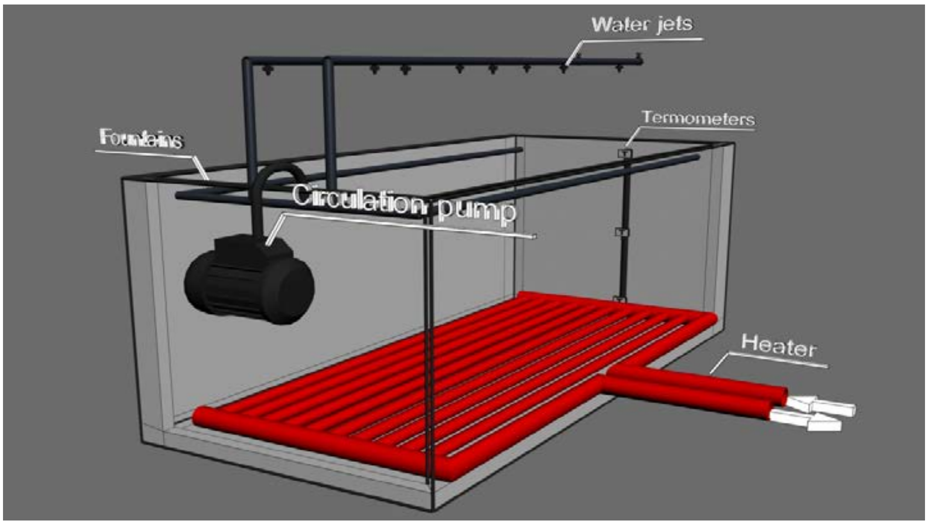

Fig. 1. Principal design of the heat carrier cooling pool

The pool prototype is designed as a test bed equipped with the following devices:

1. Circulation pump – delivers water from the lower levels of the pool to sprayers and fountains. By changing the pump's throughput, the intensity of droplet spraying may be adjusted, affecting the cooling performance.
2. Station for measuring external air parameters: external air temperature, relative humidity, wind speed, wind direction, dew point temperature are measured near the pool.
3. Heat measurement device – measures consumed heat, heat carrier throughput, incoming and outgoing heat carrier temperature, pressure before the throttle valve (which is installed after circulation pump) and sprayers.
4. Cooler – a cooler is installed inside the pool and the heat carrier is fed through it. The cooler is adapted to the size and area of the pool. The flow of heat to be taken out by the system is generated at this level.
5. Sprayers – spraying water is necessary in order to increase the air/water contact area, since the contact area in this case equals the total area of all droplets. The pool's cooling efficiency increases with finer droplets, although this also leads to increased water loss due to evaporation.

Thermometers are installed at three levels inside the pool, measuring temperature changes in various layers. The first thermometer is installed above the cooler, the other is about 0.4 m below the air/water contact plane. The third thermometer is installed above the air/water contact plane. This thermometer reading may be used to forecast changes in heat flow intensity.

The parameters of the experimental heat carrier cooling pool are provided in Table 1:

Table 1. Pool Parameters

Basin surface area S	5 x 2.2 = 11m^2
Basin volume V	11 x 2 = 22 m^3
Basin temperature schedule	34 – 40ºC
Heat-flow cooler Q	3.20 m^3/h
Circulation pump productivity Q	3 – 7 m^3/h
Spray nozzle diameter F	0.01m
Basin heat consumption	59928.80 kJ/h

The heat carrier cooling pool is a heating-related structure. Its advantages compared to a cooling tower are:

- A heat carrier cooling pool is considerably cheaper to construct than a cooling tower;
- A cooling pool is a closed system which can therefore be placed in public spaces;
- A cooling pool is a structure that is considerably smaller than a tower;
- A cooling pool is visually more attractive and fitting for the surrounding landscape compared to a cooling tower.

1.2. Studying the Pool's Cooling Properties

In order to determine the cooling properties of the pool, experimental measurements were performed. Flow to the cooler was supplied at a constant heat carrier temperature (40ºC), studying changes in cooling performance under the influence of changes in air parameters. A temperature difference between incoming and outgoing flow of the heat carrier was specified for the pool to maintain. During the experiment, variable external air parameters and their impact on the cooling properties of the pool were measured.

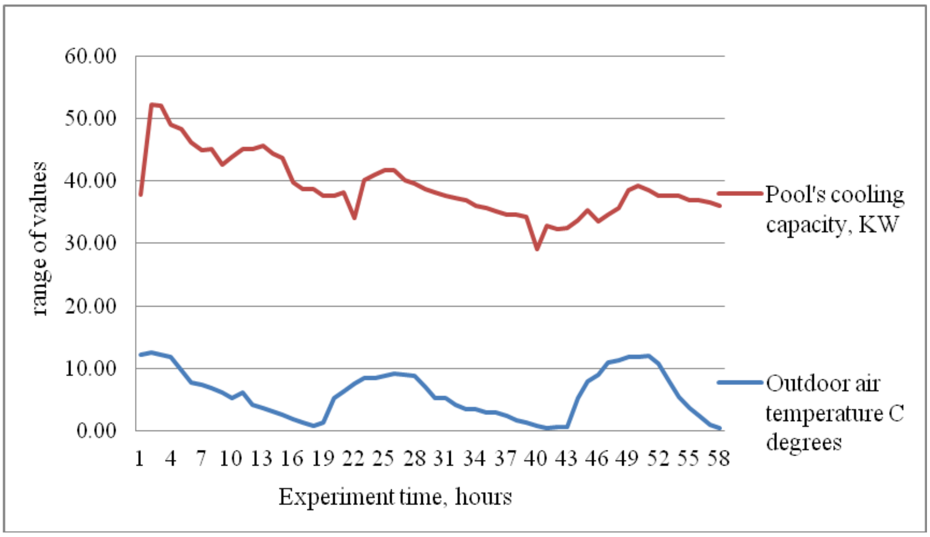

Fig. 2. First stage of measuring heat carrier cooling pool properties

Measurements were performed in two stages. The first stage of measurement took place at low air temperatures, where a direct impact of external temperature on the cooling copy of the pool was observed. The first part of the experiment took place authorising an average external air temperature of + 6.26ºC, lasting 59 hours. The progress of the experiment is reflected in Figure 2. At such a low external air temperature, the cooling performance curve of the pool changes under the influence of external temperatures. At such external air temperatures, cooling is no more necessary.

The second stage of the experiment took place at an average external air temperature of + 21.2ºC. During the day, external air temperature approaches + 30ºC. The progress of the experiment is reflected in Figure 3. At such external air temperatures, the cooling properties of the test bed, i.e. heat carrier cooling pool with sprayers, were studied.

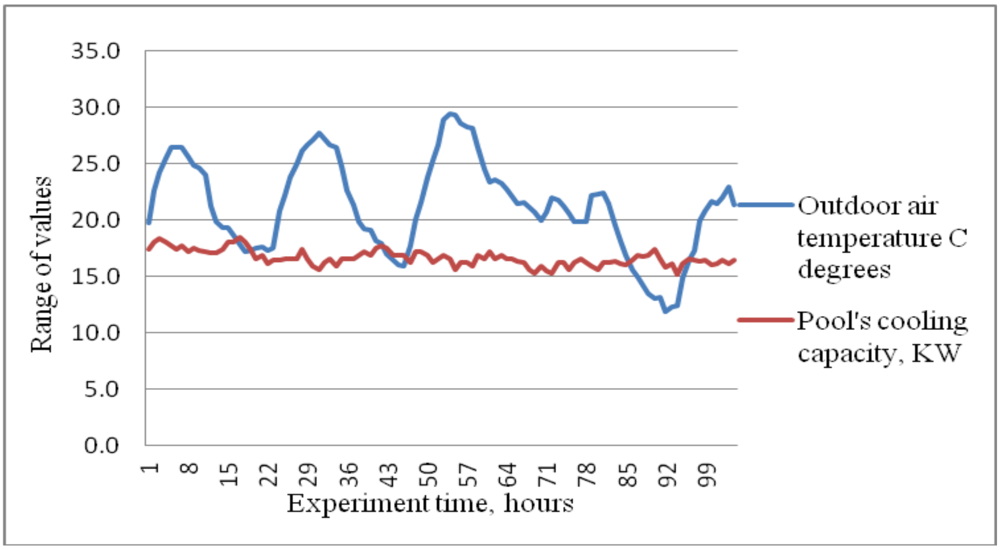

Fig. 3. Second stage of measuring heat carrier cooling pool properties

The experiment took place over the course of 104 hours. Measurements taken during the experiment:

1. Temperature of hot (cooled) water (initial and final) in the heater,
2. Mass, volume, feeding pressure, flow speed, throttle parameters, calculated droplet parameters, droplet area of cooling (sprayed) water,
3. External air temperature, humidity, wind (flow) speed, direction, solar radiation (its characteristics),
4. Distribution of water temperature along the vertical and on the surface of the water.

Experimental and theoretical studies of a spray-based heat carrier cooling:

1. Determining heat balance and capacity in various modes of operation:
   - Varying amounts of removed heat
   - Varying air temperatures, humidity levels, wind speeds and directions
   - Heat flow from the surface plane of the pool
2. Identifying heat transfer ratio expressed in various ways:
   - For droplet surface area W/(m^2·K)
   - For volume sprayed W/(m^3·K)
   - From the surface plane of the pool water KW
   - Spray intensity in kg of water/m^2 of cross-section area
   - For the pool's surface area W/(m^2·K)
3. Calculations of facility capacity, throughput, pool cooling water consumption, application, efficiency.
4. Amount of water evaporating from the surface of the pool and sprayed water droplets

Based on an analysis of data obtained experimentally, the following calculations were performed:

Guided thermal basin volume:

$$Qheat = M \cdot c \cdot (T_1 - T_2), [\mathrm{J}] \tag{1}$$

In which:
M – throughflow [kg/s];
c – specific heat capacity [J/kg·K];
T_1, T_2 - flow, back flow temperature [K].
Heat transition coefficient:

$$Ktr = \frac{Q}{S} \cdot \Delta t, [\mathrm{W/(m^2 \cdot K)}] \tag{2}$$

In which:
Q_{heat} – heat flow [J];
S – basin size [m^2];
Δt - temperature difference [K];
Sprayed water volume:

$$Vspr = \eta \cdot F \cdot \sqrt{2g \cdot \frac{\Delta P}{\alpha_p}}, [\mathrm{m^3}] \tag{3}$$

In which:
η – Yield coefficient (0,6 – 0,75);
F – Spray jet diameter 0.01 [m];
g - Gravitational force 9,8 [m/s];
ΔP - Nozzle pressure drop [kg/m^2];
α_p - Relative water weight 1 [kg/m^3];
Sprayed water amount on cooled heat carrier:

$$Z = \frac{Vspr}{\Delta t}; \; Z = \frac{Vspr \cdot M \cdot c}{Qheat} \tag{4}$$

1.3. Flow of Heat within the Pool, Influencing Factors

Heat flow intensity is a parameter indicating the operational capacity of the pool; the values are reflected in Fig. 4. Changes in heat flow affect the heat transfer ratio and change depending on external air parameters.

During the experiment, heat flow in the cooler layer varied in small range. In turn, the flow of heat above the air/water contact plane is more significant and depends on variations in external air parameters. As the external air temperature increases, the intensity of removal of heat accumulated in the pool decreases (i.e. the water accumulates a higher volume of heat), along with the heat transfer ratio and the pool’s cooling performance. The flow of heat above the air/water contact plane may be both positive and negative; in this case, the deciding factor is water temperature in the upper layer of the pool. Fig. 5 reflects the changes in external air temperature and their impact on the temperature of the cooling water inside the pool along the vertical.

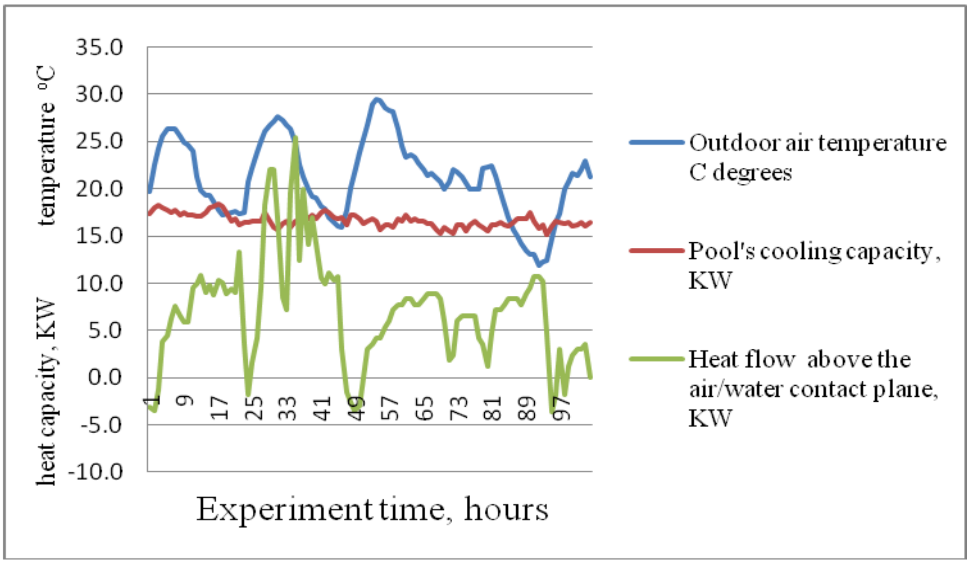

Fig. 4. Flow of heat within the pool, two levels

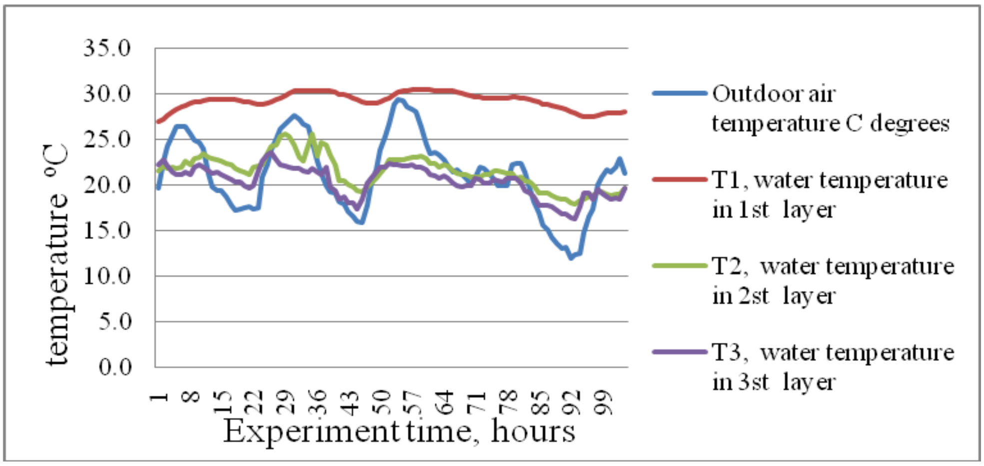

Fig. 5. Impact of external air temperature on the temperature of the cooling water inside the pool, for different layers

The curves show that the temperatures of water inside the pool change depending on external air temperature, although the temperature of cooling water inside the pool changes with a delay, depending on the layer. The temperature changes least in the layer of the cooler. This layer ensures that the heat carrier cools at a constant rate, regardless of changes in temperature in other layers and above the air/water contact plane. This means that, under certain conditions, changes in external air parameters do not impact the pool’s cooling properties. However, the influence of external conditions and the extent of this influence must be determined because these factors will affect operation of the pool.

Extent of external air temperature influence: measurements were taken throughout the experiment because variations in this parameter affect the heat transfer ratio, which is a factor in cooling performance. The impact of external air temperature is reflected in Fig. 6, it shows that when outdoor air temperature is changing, it changes pool’s cooling properties, but although the data displays a statistically significant coincidence this is not a relation, because the sprays positioned above the pool works with constant capacity and do not adjust to the outdoor temperature variations.

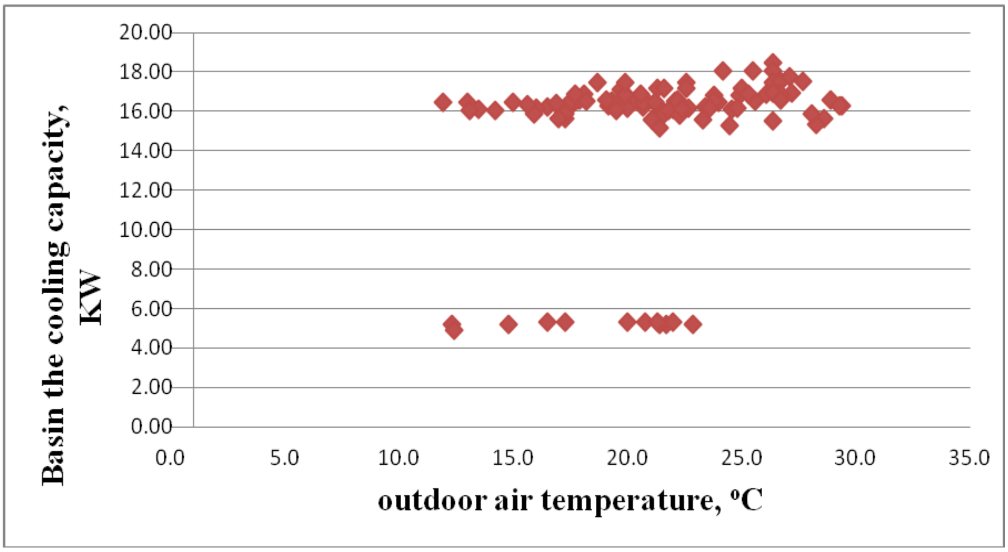

Fig. 6. The pool's cooling capacity changes in outdoor temperature influence

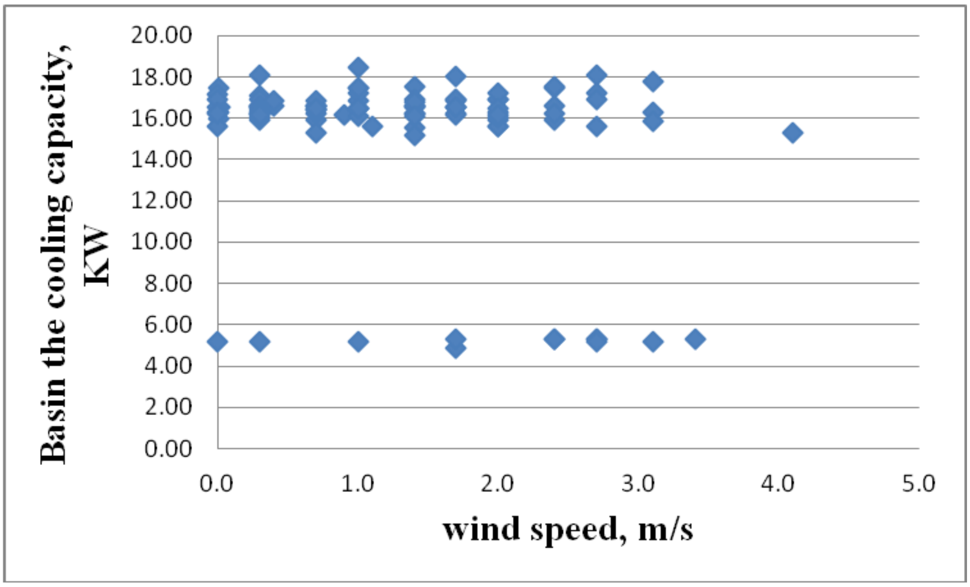

Fig. 7. The pool's cooling capacity changes in outdoor air wind speed influence

External air wind speed – increase in this parameter improves cooling performance. The impact of wind speed on the pool's cooling properties should be considered in the context of cooling water loss. As wind speed increases, the cooling mass of water is lost more rapidly. The pool loses a certain heat potential, facilitating cooling processes. The amount of lost cooling water must be replenished. Fig. 7 shows that when outdoor air wind speed is increasing pools cooling properties are changing, between these data, there is a statistically significant coincidence, but this is not a relation. An analysis of the impact of wind speed indicates that, at a given wind speed, varying results are revealed at a certain point of reading the data. This can be explained by multitude other parameters that affect the pool's cooling performance to a greater or lesser degree. For instance, at a given wind speed, air temperature or air humidity may vary. A parameter must be defined according to which the operation of the pool will be regulated. This is necessary during operation to allow cooling performance to be increased or decreased according to variations in external air parameters, adjusting the operation of the system to changes. The ratio Z has been selected as this parameter: it specifies the amount of water sprayed for the amount of cooled heat carrier in degrees, as the difference between incoming and outgoing temperatures in the cooler. This ratio specifies the range within which the pool should operate at a given heat carrier temperature, meaning that, if the temperature of the heat carrier being cooled rises or falls, the intensity of spraying would change accordingly.

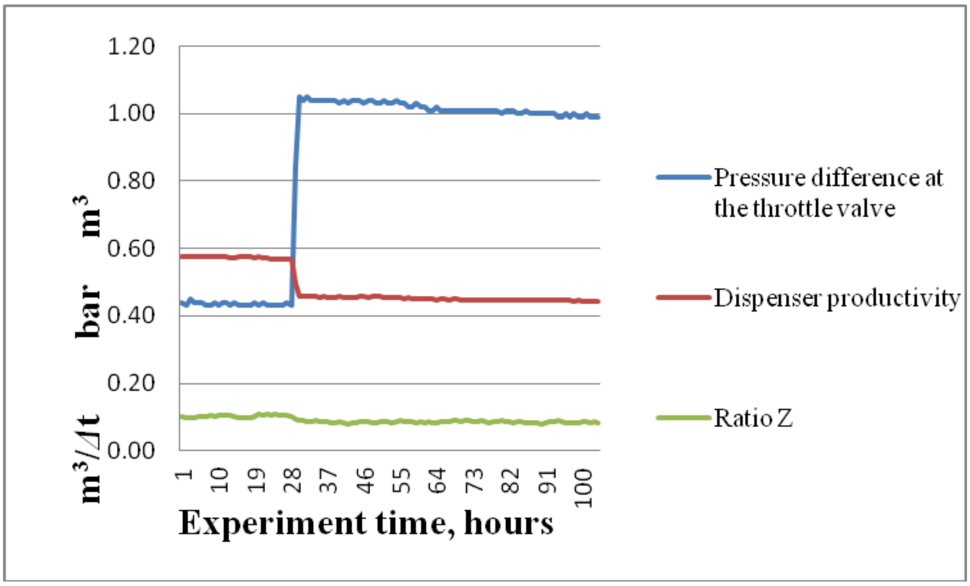

Fig. 8. Impact of change in pressure on sprayer intensity

Fig. 8 shows how the ratio Z changes if, at a constant heat carrier temperature, flow through the throttle valve is reduced, thereby lowering pressure inside the sprayers and changing their performance, which reduces the cooling performance of the pool. By specifying the boundaries of the ratio Z, one may specify under what variations in cooled heat carrier temperature the throughput of sprayers should be changed (and along with it, the cooling performance of the pool). The ratio Z must specify the upper and lower boundary temperature levels, e.g. maximum sprayer intensity given a difference between incoming and outgoing heat carrier temperature readings of 5ºC and minimum intensity for 6ºC. Once these boundaries are specified, the throughput of the sprayers can be altered using the pump or the throttle valve. The temperature of the cooled heat carrier may increase when the water inside the pool cannot discharge the accumulated heat generated by the cooler. Insufficient sprayer performance leads to insufficient water exchange within the pool and insufficient cooling of the water inside it. Thus, the intensity of sprayers must be adapted to the installed Z ratio given the target difference between incoming and outgoing heat carrier temperatures.

2. CONCLUSIONS

The experiment took place at various external air temperatures, the first part of the experiment was conducted at an average external air temperature of 6.26ºC, the second part of the experiment was conducted at an average external air temperature of 21.2ºC. For the first part, the cooling properties of the pool are not important but an analysis of measurements was conducted in order to gain an understanding of changes in external air parameters and their impact on cooling capacity.

Changes in external air parameters – partial air pressure, relative humidity, wind speed, wind direction – affect cooling performance, although their impact is not considered a deciding factor in maintaining the cooling performance of the pool.

Regardless of the drastic changes in heat flow above the air/water contact plane, cooling performance varies within a narrow range. For example heat flow above water/air contact surface varies in 30KW range, meanwhile pool’s cooling properties varies for 3-4KW. The impact of changes in external air temperature is not immediately evident because heat accumulation properties smooth out the resulting changes in heat flow, affected by the heat capacity of pool.

Ratiio Z can be used to regulate the pool's cooling performance if necessary. Ratio specifies the range within which uninterrupted operation of the pool can be ensured, despite the change off external parameters which affect pool's cooling capacity.

The heat accumulation properties of the pool preclude an evaluation of instantaneous changes in the cooling parameters of the pool given the effect of various parameters.

Outdoor air temperature and wind speed measurements show that there is a significant relation between the mentioned parameters and the pool's cooling capacity. To establish the relation there was made regression equation, it was a linear. Found linear function, as shown in the Fig. 6 and Fig. 7 does not fulfils always, as there is a deviation, in which the abnormality arranges very disciplined (at 5 KW). These deviations will be explored in subsequent publications.

The pool may be used as effective cooling facility regardless of the impact of a number of external conditions. The pool can maintain a specific heat carrier temperature schedule given specific parameters. The pool can operate in a stable manner when external air temperature approaches the incoming temperature of the heat carrier cooled by the pool.

3. REFERENCES

1. GEDROVIČS M., *Nekustāmā īpašuma pārvaldnieks,:* Biznesa augstskola Turība, Rīga, 2002, p. 287.
2. DZELZĪTIS E., *Siltuma, gāzes un ūdens inženiersistēmu pamati*, Gandrs, Rīga, 2005, 214 p;
3. NAGLA J., SAVEĻJEVS P., TURLAJS D. *Siltumenerģētikas teorētiskie pamati*, Rīgas Tehniskā universitāte, Rīga, 2008, 98 p.
4. OSIPOVS L., *Ķīmijas tehnoloģijas pamatprocesi un aparāti,: Zvaigzne*, Rīga, 1991, 98 p.
5. ЛЕБЕДЕВ П.Д. *Расчеты и проектирование сушки устройств*, Государственное энергтическое Издательсктво, Москва, 1963, 142 p.

CYSENI 2012, May 24–25, Kaunas, Lithuania
ISSN 1822-7554, www.cyseni.com

ADVANTAGES AND OBSTACLES FOR THE DEVELOPMENT OF INDUSTRIAL SYMBIOSIS IN LATVIA

A. Beloborodko, M. Rosa, L. Ozolina
Institute of Energy Systems and Environment
Riga Technical University
Kronvalda blvd. 1, LV-1010 Riga – Latvia
Phone +371 67089908
Email: anna.beloborodko@rtu.lv

ABSTRACT

Industrial ecology has borrowed its fundamental principles from natural ecosystems, and within this framework, the links between industrial companies are compared to the ecosystems as if information, energy and resource flows between the companies would be organized in an effort to imitate living organisms. If the industry, like an ecosystem, would be organized based on reflexive linkages and cooperation, it would be possible to organize better industrial processes and to ensure efficient and sustainable production. Industrial symbiosis seeks to ensure that the involved companies reach a collective benefit, which is accomplished by finding a suitable use for any waste or process by-product from one company within the manufacturing process of another company. By implementing such resource-saving measures any company can become more environmentally friendly and reduce its impact on the environment. But for the development of industrial symbiosis the involvement of several separate companies to create raw material, resource and energy networks between them is required. This is when the national legislation interferes with the development of industrial symbiosis. It can both enhance such ties, if the country has well-organized and thought-out waste management system and bureaucratic requirements, or limit the formation of industrial symbiosis, if the waste management related regulations incorporated within the legislation create obstacles for the formation of a simple legal relationships between the companies.

The objective of this paper is to determine legislative requirements that promote and limit the development of industrial symbiosis in Latvia. The comparison between Latvia and other European countries is made in order to offer better tools to support industrial symbiosis, more efficient evolvement of waste management system, resource efficiency and sustainable development in Latvia.

Keywords: Industrial ecology, industrial symbiosis, waste management

1. INTRODUCTION

Within the framework of industrial ecology the links between industrial companies are compared to the ecosystems as if information, energy and resource flows between the companies would be organized in an effort to imitate the living organisms. Industrial symbiosis, a sub-field of industrial ecology, seeks to ensure that the involved companies reach a collective benefit, which is accomplished by finding a suitable use for any waste or process by-product from one company within the manufacturing process of another company and therefore using the primary resources more efficiently. If the industry, like an ecosystem, would be organized based on reflexive linkages and cooperation, it would be possible to organize better industrial processes and to ensure energy efficiency and promote sustainable production.

The worldwide research of industrial symbiosis is fairly recent. It has emerged 20 years ago mostly with the exploration of the first fully realized project Kalundborg Industrial symbiosis in Denmark [1]. As the research of industrial symbiosis is a still not a deeply explored area, in Latvia this concept is not widely known. Industrial symbiosis as a term is not defined or used in any Latvian legislation. There are also no governmental incentives or mechanisms developed to introduce this concept. Furthermore until now the research on industrial symbiosis has been weakly conducted in Latvia. There are only few separate studies available regarding the efficient waste management and by-product reuse in the framework of a company or at a country level.

Chertow [2] has studied the process of "uncovering" or discovering already existing material and resource synergies and improving these systems to reach full potential of industrial symbiosis. It has been pointed out that in many cases the "uncovering" of industrial symbiosis has been more productive than creating artificial "eco-industrial parks".

The "uncovering" of industrial symbiosis is a result of serious long-term studies. Complex knowledge about the industrial processes, as well as wide range of information about firms, generated, treated and recycled waste streams and by-product streams is necessary to "uncover" an industrial symbiosis. This is when the national legislation can interfere with the "uncovering" and the development of industrial symbiosis. Legislative requirements can both enhance such ties or limit the formation of industrial symbiosis, dependent on the availability of the information, environmental requirements, tax barriers, waste management system etc. in the country.

Waste is one of the main indicators describing material and resource flows; therefore it is important to gatherer the information about national waste management system. The waste management system of Latvia incorporates two legislative levels. The first one is national, which is represented with the Waste Management Law [3]. The other level is sub-national, which is introduced through Waste management plan 2006-2012 [4] and regulations of local municipalities. The Waste management plan of Latvia 2013-2020 has to be finalized until the end of 2012.

The main aim of this paper is to describe and analyse the existing waste management system in Latvia and to compare it with the other European countries in the context of industrial symbiosis. The main task of the article is to define the requirements that are promoting and limiting the development of industrial symbiosis in Latvia. This will allow offering better tools to be included in the Waste management plan 2013–2020 to promote industrial symbiosis and more efficient evolvement of waste management system, resource and energy efficiency and sustainable development in Latvia.

2. APPROACH

The most common definition of industrial symbiosis is presented by Chertow [2] „engaging traditionally separate industries in a collective approach to competitive advantage involving physical exchange of materials, energy, water and by-products. The keys to industrial symbiosis are collaboration and the synergistic possibilities offered by geographic proximity". According to this definition the most important factors promoting industrial symbiosis are (1) the collaboration of the industries due to the knowledge of shared or potentially usable resources, energy or by-products and (2) the location of the companies.

One of the main policies concerning material and resource flows is waste management policy. In Latvia and European Union (EU) it is based on combination of three principles: waste minimisation and prevention principle, polluter pays principle and proximity principle [3, 5]. The main principles of industrial symbiosis is efficient sharing of resources and using by-products as process resources, geographic proximity of the collaborators and combining economic, environmental and social gains [6]. These sustainable waste management and industrial symbiosis development principles coincide: efficient use of resources will lead to waste minimisation, co-location of the industries fully executes the proximity principle and as the polluter is responsible for his impact on the environment, there is greater motivation to reduce the impact industry creates on the environment as well as to reduce the economic costs. Therefore the implementation of the overall waste management policy is related to setting requisite preconditions for the development of industrial symbiosis and these preconditions should be present in the legislation of Latvia.

However industries are subject to the regulations and requirements of local governments. Costa et.al. [7] have researched the potential influence of governmental policy and legislation in four countries where cases of successive development of industrial symbioses have been identified.

It is concluded that, as the government is the main developer of the states policy, it is capable to influence many factors that are contributing to the development of industrial symbiosis. On the other hand, policies can also create barriers for the development of industrial symbiosis.

In order to understand how the existing policy in Latvia has influenced the development of industrial symbiosis, a set of indicators was adopted from the research of Costa et. al. [7]. Quantitative descriptors as average population, total waste generation and waste treatment data are used to determine total waste generated per capita and the status on waste management performance. Qualitative descriptors are divided in three categories – economic, regulatory and voluntary. A comparison between Latvia and Denmark, Portugal, Switzerland and United Kingdom is presented. In addition waste management situation in Latvia is quantitatively compared with the performance of other Baltic States and EU-27.

3. WASTE MANAGEMENT SYSTEM IN LATVIA

During the last 7 years major changes in Latvian waste management policy have been made. The Latvian Waste Management Law [3] was issued in the end of 2010 and is now the main legislative framework for waste management. The purpose of this Law is to prescribe the necessary procedures for environmentally safe and human life and health preserving waste management system. The main actions include preventing the generation of waste, expanding the separate collection and regeneration network, facilitating efficient use of natural resources and by-products and reducing the amount of waste to be disposed of. It also states the competencies of several institutions and their responsibilities towards developing of the waste management system.

Other crucial document is the Waste management plan 2006–2012 [4]. This plan defines quantitative targets for reduction of specific groups of waste within the planning period and measures that have to be implemented to reach these targets. The Ministry of Environment is responsible for preparation of informative reports about the implementation of the plan [8]. In these reports quantitative results are presented for the overall targets for specific groups of waste. But since the measures stated in the Waste management plan are not defined in quantitative terms, only the status of each measure is presented without the interpretation of concrete results this measure has contributed to.

The most recent report [9] states conformity to the targets for packaging waste and used vehicles. However the target amount for the collected waste electric and electronic appliances was not reached. In 2009 for the packaging waste 45% recycling rate is stated, but more than half of this amount – 24% was exported for recycling. Such export of waste even if it is transported for recycling imposes surplus impact on environment and is not in compliance with industrial symbiosis principles.

At a sub-national level, municipalities develop their own regulations, to provide the necessary framework for implementing the waste management policy. Municipalities are responsible for organising the collection, transportation and disposal of municipal and household hazardous waste in its administrative territory as well as making strategic decisions about the development of new waste management facilities within its territory [3, 4].

To implement the measures stated in the Waste management plan 2006–2012 [4], 12 municipal waste handling regions were initially intended to be created based on the agreements between the local municipalities. After discussions on local level for the most efficient cooperation, 10 regions were formed. In addition the capital city Riga is considered as the 11 region (see Fig. 1).

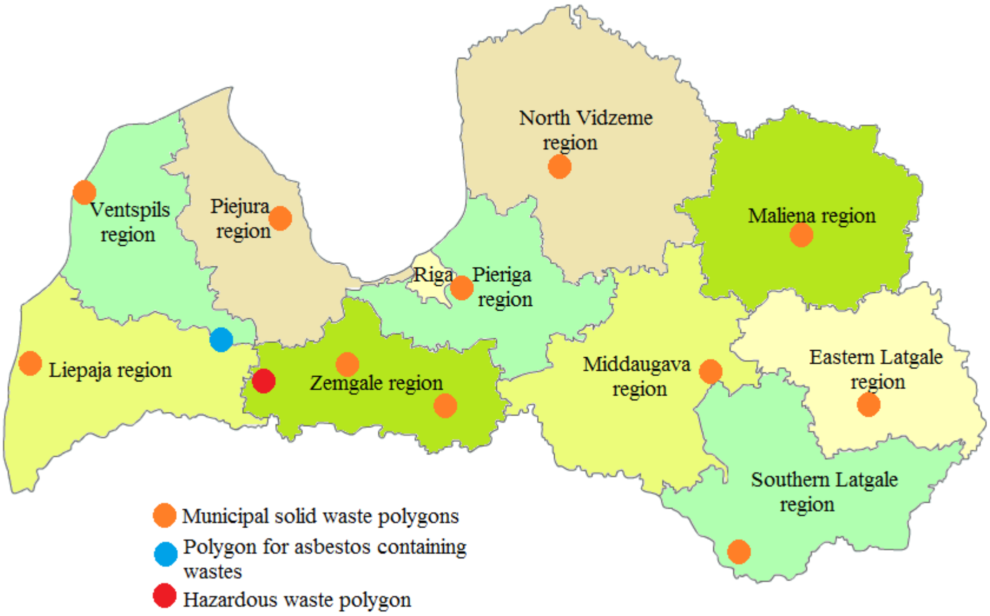

Fig. 1. Municipal waste handling regions and polygons in Latvia [4]

In 1998 there were more than 500 dumpsites in Latvia. Since then new landfills have been developed and the dumpsites have been gradually closed [10]. In each waste handling region there is at least one local landfill – polygon – already built or planned, and waste from all the region has to be landfilled in this polygon (see Fig. 1). Therefore through local management of the waste the proximity is enforced.

Before the introduction of polygons, most of waste was disposed in the unregulated dumpsites therefore the information was not registered properly. In 2002 the waste accounting system was upgraded and data are available from Central Statistical Bureau of Latvia [11]. In Fig. 2 the amounts of collected and treated waste in Latvia since 2002 is presented. In addition the dynamic of Gross Domestic Product (GDP) in this period is shown in Fig. 2.

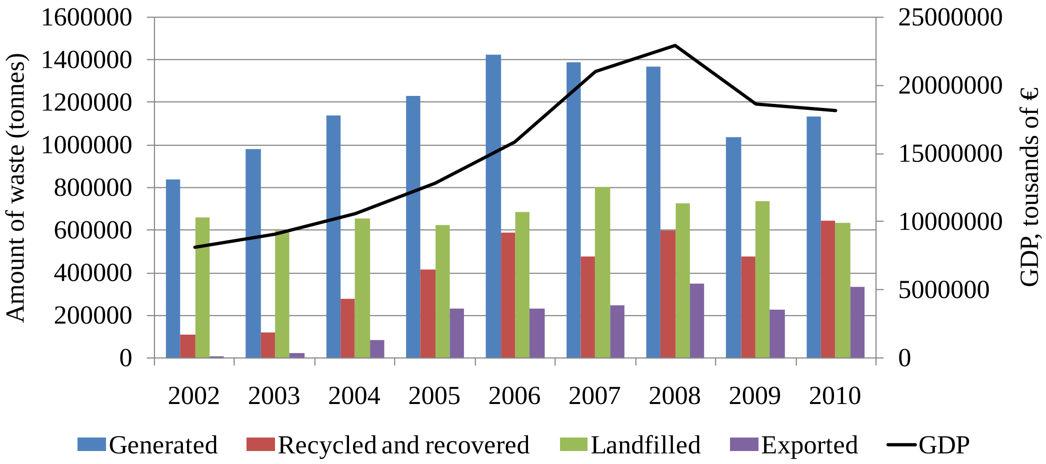

Fig. 2. The amounts of generated, recycled and landfilled waste and the GDP in Latvia [11]

The total amount of generated and collected waste has grown since the beginning of 2002. This could be partly explained with the improvements of the information reporting system. Through the years it can be seen that the increase of the amounts of generated waste is correlating with the wealth level expressed as GDP. The rather steep decrease of GDP in 2009 is followed by the decrease in the amounts of generated as well as the recycled waste, thought the landfilled waste remains constant. It can be seen that in 2010, as Latvia is slowly regaining its economic stability, there is a tendency that the amount of generated waste is increasing again. Therefore there should be a clear policy implemented in the coming years to promote waste prevention, development of separate collection and regeneration system and resource, energy and waste efficiency to create environmentally safe and human life and health preserving waste management system in Latvia.

4. RESULTS

4.1. The comparison of waste management systems in EU

To introduce state waste management policy, different types of tools can be used. These are e.g. economic, regulatory and voluntary instruments. According to study about the waste management policies in three EU member countries and Switzerland by Costa et al. [7], in Denmark the government makes decisions about regulations and taxes. Meanwhile each municipality develops local waste management policy and is responsible for implementing it. This is done also by dialog with the companies and supporting the material exchanges. In United Kingdom economic instruments as Landfill Tax are used. Regulatory instruments are the Waste Protocols Project. Voluntary instrument – the National Industrial Symbiosis Programme – has been introduced particularly to support the development of industrial symbiosis. In Portugal the existing policy instruments as the mandatory electronic information reporting on waste are aimed at promoting industrial symbiosis. In addition economic instruments as landfill and incineration taxes are used and voluntary instruments as Organized Waste Market are supported. In Switzerland an industrial ecology strategy has been established. One of the goals of this strategy is to promote the development of industrial symbiosis by uniting companies, government agencies, universities and local industry.

To implement Latvian waste management policy economic instruments are used e.g. natural resource tax is maintained at national level and is meant to promote efficient use of resources and to limit pollution. The revenues of the tax are partly used to finance the implementation of environment protection projects. Some regulatory instruments as the municipal waste incineration ban and a resultant penalty is introduced at the municipal level. There are no voluntary instruments introduced in Latvia to promote industrial symbiosis.

The collected quantitative data is used for the comparison of waste management systems. Fig. 3 presents waste generation situation in seven countries and the EU-27 level in 2008 [7, 12]. Regarding waste generation, the average level in EU-27 is 5.2 tonnes per year per capita. Two of the addressed countries are producing more than EU-27 level, United Kingdom is lightly over the average with 5.4 tonnes per year per capita and Estonia has generated 14.6 tonnes per capita in 2008. Two other Baltic States Latvia and Lithuania has generated less waste per capita than even the progressive Denmark. This is explained by the lower level of industrial development in Baltic States than in Central Europe. In Estonia the economic development is quite similar to Latvia and Lithuania, the exception is that in Estonian energy and refinery sector a local resource – oil shale is widely used, which mainly contributes to the high 8.2 tonnes per year per capita non-mineral waste generation in Estonia [13].

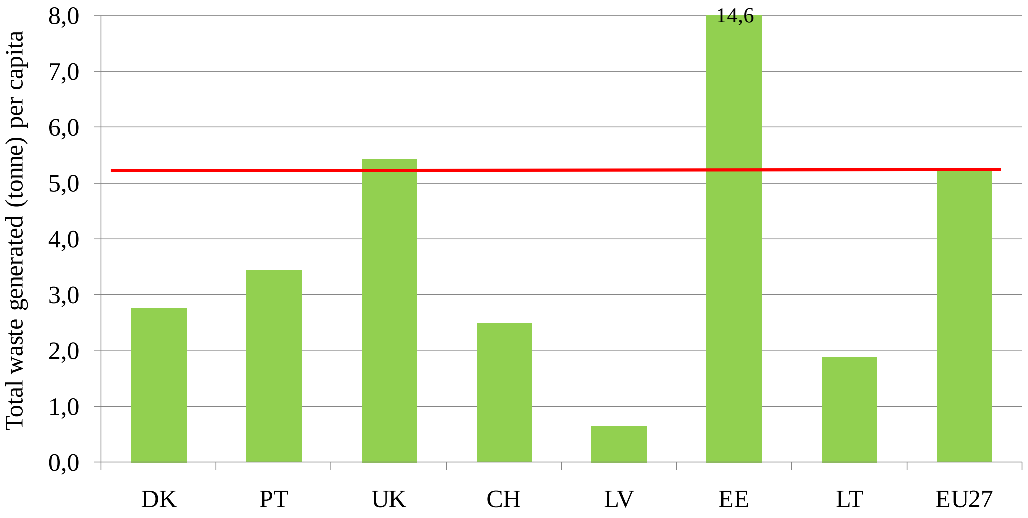

Fig. 3. Total waste generated per capita [7, 12]

To improve the accuracy of this comparison an indicator is introduced. This indicator shows the relationship of the total generated waste per capita and the annual GDP expressed in purchasing power standards (PPS) (see. Fig. 4). Expressing GDP in PPS eliminates differences in price levels between countries [12].

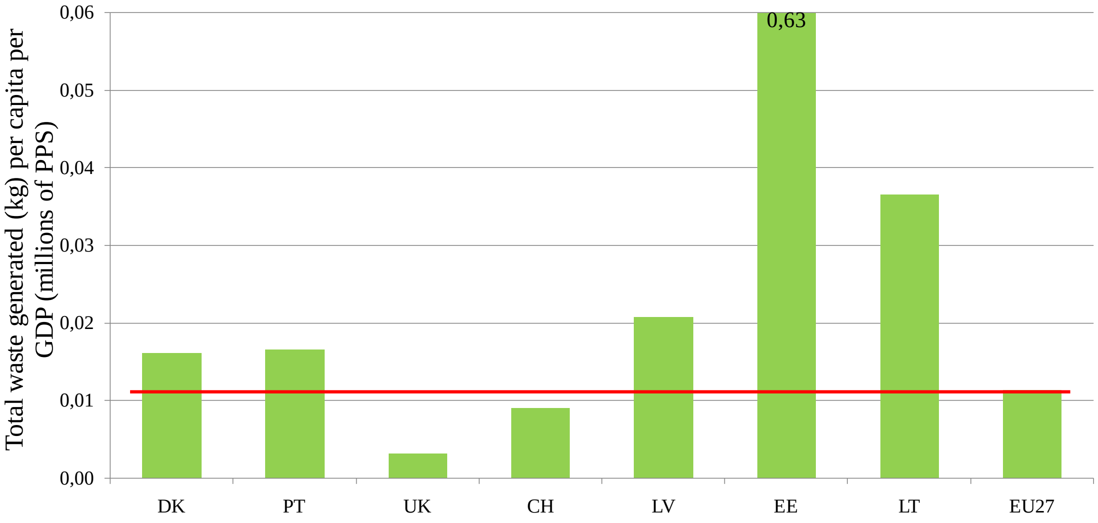

Fig. 4. Total waste generated per capita depending on the GDP [7, 12]

It can be seen from Fig.4, that referring the generated waste to countries industrial development level expressed as GDP has influenced the evaluation of the condition of waste management system. When evaluating countries using the indicator, only two of the addressed countries – United Kingdom and Switzerland – are below the average EU-27 level and only one of these are an EU member. Moreover, according to Fig. 3 United Kingdom is generating more waste than EU-27 average, but it is so due to countries highly developed industry. Therefore United Kingdom has the lowest rating when taking into account the economic perspective.

All other countries are producing more waste per year per capita than the average EU-27 level if addressed to the GDP. It can be seen that the lower industrialization level in all three Baltic States is reflected using this indicator, and thus it is an effective tool for measuring the real development of states waste management system in regard to its economic development.

4.2. Typical barriers for the development and „uncovering” of industrial symbiosis

One of the instruments used for implementing waste management policy in Latvia is the electronic information reporting system. According to the Latvian Waste management Law [3], the Latvian Environment, Geology and Meteorology Centre is the responsible institution for collecting waste handling and landfilling related information and maintaining this electronic information reporting system. The data is publicly accessible in the form of the state statistical survey “3-Wastes” [14]. But in regard to finding potentially symbiotic material and resource flows or even synergies, this database is ineffective due to many limitations for information processing. The main purpose of the database is to provide waste related information for each company itself. Whereas for the “uncovering” and development of industrial symbiosis it is evenly important to be able to see the inter-firm connections, which is not yet possible in this database. For the uncovering of inter-firm resource flows, it would be substantially important to upgrade this information system in a way that the user would be able to access information about the connections between the companies and different waste management actions these firms are performing.

Material reprocessing and regenerating is promoted in various subsections of Latvian legislation and normative documents. One of the downsides for the development of the waste regeneration system as stated in the Waste management state plan [4] is the lack of reprocessing and regeneration firms. Altogether enhancing the amounts of regenerated materials is promoted, but no real further actions are performed. For example, there are no initiatives to promote the development of locally of regionally based reprocessing industries. Moreover, export is promoted as a scenario for handling of the used packaging materials [4].

According to the “3-Wastes” database [14] in 2010 in total 332 763 tons of waste were exported from Latvia which accounts for 40% of total generated waste. This amount included such waste as plastic, glass, paper and cardboard, metal, used tyres and other specific wastes. Some of these wastes, e.g., plastic, paper and cardboard, used tyres, have high potential of energy recovery that could be locally utilized. On the other hand, 27 743 tons of waste were imported in 2010, which also included the same types of waste – plastic, glass, paper and cardboard, metal. In 2010 there were 26 material recycling or recovery companies in Latvia processing the mentioned wastes. The overview of the typical wastes treatment actions for these wastes is depicted in Table 1.

Table 1. The treatment of sorted waste in Latvia in 2010 [14]

	Type of the waste				
	Plastic	Glass	Paper and cardboard	Metals	Used tyres
Total amount of companies	6	1	4	8	7
Energy recovery			+		+
The treatment or recovery of solvents					+
The treatment or recovery of non-solvents	+		+		+
The treatment or recovery of metals				+	
The treatment or recovery of other non-organic materials		+			+

It can be seen from Table 1 that glass recovery and recycling industry is underdeveloped in comparison to other reprocessing. Although the plastic recovery industry is quite developed the waste that could be processed locally is exported to such countries as China, United States and

Panama. The territorial distribution of plastic waste handling and exporting and plastic recycling companies in Latvia is shown in Fig. 3. In 2010 for separately collected municipal plastic waste almost 20 000 tons were recycled in Latvia, nevertheless 175 tons were exported. Latvian Waste management plan states that the largest part of plastic packaging is exported for recycling. Thought in 2010 larger part of plastic packaging was recycled (4 802 tons) than exported (3 201 tons). For used tyres 10 155 tons were reprocessed locally in 2010, still 1 359 tons were exported by Latvian companies. [14]

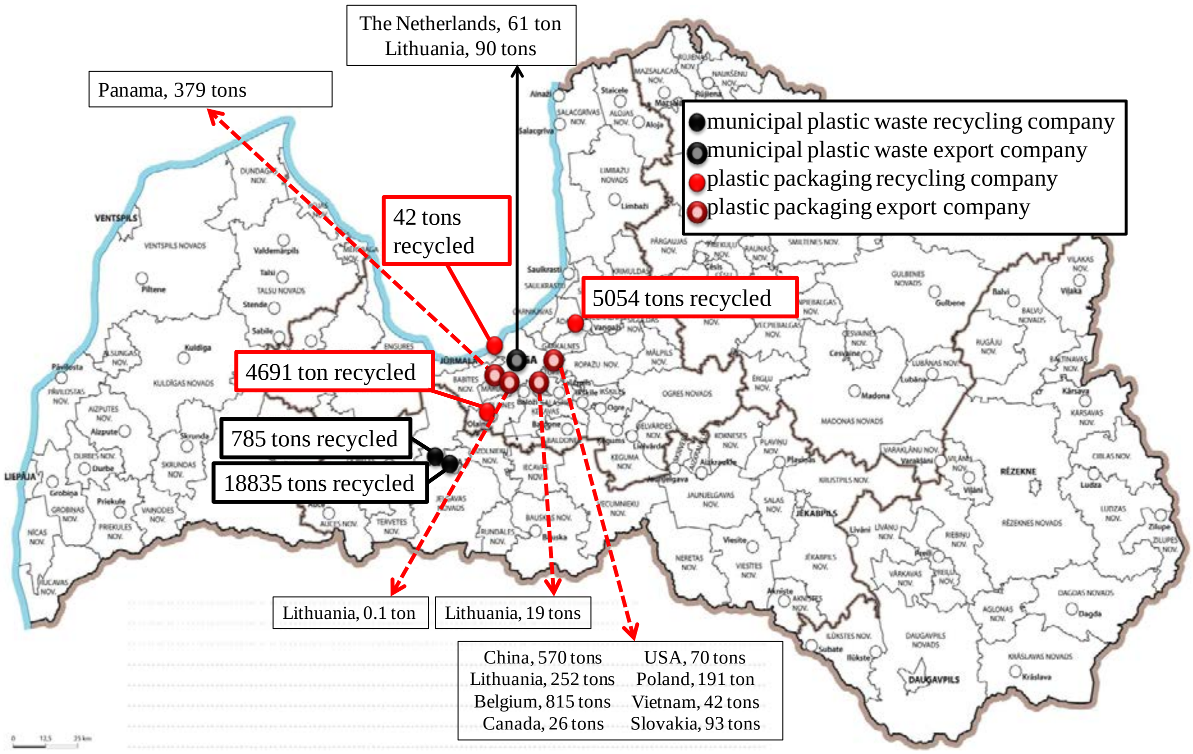

Fig. 3. The recycling and export flows of plastic waste [14]

It is obvious that Latvian companies are exploiting the fact that waste export is promoted to reach out to larger markets and to sell the waste for higher prices. On one side, it is good that export is promoted, as there will always be some materials that will not be recyclable locally in Latvia. But, as a result of this, wastes that could be locally recycled or used for energy recovery are transported in large distances. With this the proximity principle is not abided, because waste is treated further from its origin than it could be. Useless transportation of waste is against the basic principles of industrial symbiosis.

4.3. The positive features in Latvia in regard to implementation of industrial symbiosis

In Latvia several special economic areas (SEA), for example, Liepaja SEA, Rezekne SEA are formed in cooperation of the government and the local municipalities [15, 16]. As well two Freeports are located in Riga and Ventspils [17, 18]. The firms that are located in the SEA or the Freeport area are subject to tax discounts that allow these firms to lower their expenses; therefore they can invest more of their resources into development and manufacturing itself.

The existence of these areas is one of the factors promoting the development of industrial symbiosis in Latvia. A closed area where several manufacturing or processing firms are co-located is a precondition of creating connections and links between these firms. In both SEA the main focus is on manufacturing industry, the main activities in the Freeports are cargo handling and oil pumping. All these industries are related to the use of heavy and dangerous equipment and chemical substances and have high risks of pollution, health requirements and other regulations. Therefore these firms must pass strict criteria of environmental, health and work safety, which are regulated by the government and the presence of such regulations has typically promoted industrial symbiosis.

5. CONCLUSIONS AND DISCUSSION

In absolute numbers Latvia is generating the lowest amount of waste per capita in EU-27. But if an indicator that shows the relationship of the total waste generated per capita and countries wealth level expressed the annual GDP is introduced, the lower level of industrialization in Latvia is reflected. With this indicator it can be seen that in Latvia the total waste generated per capita per GDP is higher than the EU-27 benchmark. To insure that the industrial development in Latvia is reached in a sustainable manner efficient use of resources and energy through the implementation of industrial symbiosis has to be promoted.

The legislative framework can be influential factor in whether industrial symbiosis will develop naturally or not. For example, groundwater scarcity drove the development of Kalundborg industrial symbiosis, but it further developed due to strict policy and requirements from local authorities in Denmark. Some governmental incentives in Latvia do not advantage the local treatment of waste and therefore efficient energy use. No special incentives and motivation are used to develop the by-product processing industry. Sequentially there is great focus is on importing and extracting new resources.

In Latvia there is a state introduced information gathering mechanism and database for the compilation of information about waste streams, waste handling, sorting and landfilling. Unfortunately this database is not highly developed for the purposes of tracking the waste flows from its origins to the recycling or landfilling companies and therefore is not beneficial for industrial symbiosis research. In order to detect the industrial symbiosis and resource sharing the database should be upgraded.

Even though there is some activity in the resource recovery industry, it is underdeveloped and waste that could be locally treated or recovered for energy is being exported to far locations, partly due to states policy. Sequentially, one of the main principles of sustainable waste management system and industrial symbiosis – the proximity principle – is not respected and the current system is disarranged and is not promoting industrial symbiosis through local resource efficiency.

Some positive features in Latvia are observed in relation to government and municipality co-established special economic areas and Freeport's, where due to the specific economic conditions large amount of companies are co-located leading to possibilities of common resource use and by-product exchange while taking into account the proximity principle.

The waste management system in Latvia is mostly based on the European Union requirements, but the implementation as in most of countries is quite peculiar. In contrast to other countries in Latvia industrial symbiosis is not considered at the policy developing level. Therefore there are only few factors benefiting the development of industrial symbiosis, and many obstacles that have to be overcome to introduce this concept.

REFERENCES

1. CHERTOW, M. R. Industrial Symbiosis: Literature and Taxonomy. *Annual Review of Energy & the Environment*, 2000, Vol. 25, No. 1, p. 313–337.
2. CHERTOW, M. R. ‘‘Uncovering’’ industrial symbiosis. *Journal of Industrial Ecology*, 2007, Vol. 11, No. 1, p. 11–30.

3. The Latvian Waste Management Law. 1st of January 2011. Referred on 23.04.12. Link to the internet
< www.vvc.gov.lv/export/sites/default/docs/LRTA/Likumi/Waste_Management_Law.doc>.
4. Waste management state plan 2006-2012. 27th of December 2005. Referred on 23.04.12. Link to the internet < http://polsis.mk.gov.lv/LoadAtt/file45550.zip > In Latvian.
5. Consolidated versions of the Treaty on European Union and the Treaty on the Functioning of the European Union. *Official Journal C 83 of 30.3.2010.*
6. CHERTOW, M. R. Evaluating the success of eco-industrial development. Sheffield: Greenleaf Publishing Limited, 2003. IN AGARWAL A., STRACHAN P. Literature review on eco-industrial development initiatives around the world and the methods employed to evaluate their performance /effectiveness. 2006. Referred on 23.04.12. Link to the internet <http://www2.rgu.ac.uk/abs/National%20Industrial % 20 Symbiosis/ Report%20 for%20 Databuild%20New.pdf >
7. COSTA I., MASSARD G., AGARWAL A. Waste management policies for industrial symbiosis development: case studies in European countries. *Journal of Cleaner Production*, 2010, Vol. 18, No. 8, p. 815-822.
8. Order No.860 29th of December 2005 on Waste management plan 2006-2012. Referred on 23.04.12. Link to the internet < http://polsis.mk.gov.lv/LoadAtt/file45552.doc >. In Latvian.
9. The informative report on Waste management plan 2006-2012 for the fulfilment for the period of 1st January 2009 till 31st December 2010. Referred on 23.04.12. Link to the internet <http://polsis.mk.gov.lv/LoadAtt/file29580.DOC>. In Latvian.
10. The development of national municipal waste management system in Latvia. Referred on 23.04.12. Link to the internet <http://www.varam.gov.lv/files/text/500minuss.pdf>
11. Central Statistical Bureau of Latvia. Referred on 4.03.2012. Link to the internet <www.csb.gov.lv>
12. EUROSTAT database. Referred on 23.04.12. Link to the internet
< http://epp.eurostat.ec.europa.eu/portal/page/portal/eurostat/home/>
13. EUROSTAT News release 136/2011 - 19 September 2011. Referred on 23.04.12. Link to the internet <http://epp.eurostat.ec.europa.eu/cache/ITY_PUBLIC/8-19092011-BP/EN/8-19092011-BP-EN.PDF>
14. State statistical survey “3-Wastes”. Referred on 23.04.12.
15. The Law of Liepaja special economic area. 18th of March 1997. Referred on 23.04.12. Link to the internet
< http://www.likumi.lv/doc.php?id=42426>
The Law of Rezekne special economic area. 4th of November 1997. Referred on 23.04.12. Link to the internet < http://www.likumi.lv/doc.php?mode=DOC&id=45469>
16. The Law of Riga Freeport.11th of April 2000. Referred on 23.04.12. Link to the internet
< http://www.likumi.lv/doc.php?id=3435>
17. The Law of Ventspils Freeport.1st of January 1997. Referred on 23.04.12. Link to the internet
< http://www.likumi.lv/doc.php?id=41737 >

CYSENI 2012, May 24–25, Kaunas, Lithuania
ISSN 1822-7554, www.cyseni.com

REGULATION OF RENEWABLE ENERGY IN EUROPEAN UNION AND PROBLEMS OF IMPLEMENTATION IN LITHUANIA

Karolina Čėsnaitė
Faculty of Law of Vilnius University
P. Vileišio st. 32–34, Vilnius LT-10200 – Lithuania
Phone +37066250883
Email: Karolina.cesnaite@tf.stud.vu.lt

ABSTRACT

Every now and then in Lithuanian media or political discussions questions are raised whether Lithuanian legislation on Renewable energy and governmental acts in this area comply with European Union (herein after - EU) regulation. Considering high expectations for improvement of energy sector in Europe and one of the lead roles of Renewable energy, it is crucially important to impeccably enact every single rule of EU and ensure thorough support for Renewable energy in each Member State.

In this paper author is going to overview regulation of renewable energy in EU and Lithuanian attempts to angle national legislation towards European goals. While analysing national legislation's conformity with EU regulation, questioning National Strategy and action plan, main implementation problems will be disclosed.

Knowledge of the evolution of energy law and objectives of renewable energy in upcoming close future is important not only for lawyers but for engineers, businessman and scientists of this field as well. Information and opinion provided in this paper will enlighten legal aspects of Renewable energy and problems which engineers and businessman may face in energy sector.

Keywords: Renewable energy sources, energy law, implementation, national regulation

1. INTRODUCTION

These days such topics as climate change, pollution, constant growth of energy consumption, lack of clean energy production and others are widely discussed not only in European Union (herein after - EU) but all across the world. Discussions are the inevitable part for realization of such international agreements as United Nations Framework Convention on Climate Change, Kyoto protocol and other particular goals set by EU.

In recent decades EU has been actively participating in international discussions and has already started many initiatives in regulation on renewable energy. EU puts a lot of effort to regulate the production of heat, fuels and electricity from renewable energy sources (herein after - RES). Due to wide range of EU legal rules of energy law and limited paper length, author is not seeking to provide readers with exhaustive overview of legal aspects of the usage of RES. Research of this paper is narrowed to one of the most important and relevant Lithuanian issue – production of electric energy, where it concerns production of electricity from RES.

After entering EU in 2004, Lithuania integrated into the single European market, became an equal member and by signing EU Accession Treaty, took the responsibility to contribute while seeking European goals of energy sector, for example - promotion of usage of energy made of RES. It is not an abstract goal that Member States could try to reach, but actual objectives that States, including Lithuania, have the duty to reach. By this paper, author seeks to pull attention to the importance of national actions and measures that need to be taken in order to realize international legal obligations. Furthermore, author's research is going to cover main problematic aspects of national legislation that interfere with impeccable enactment of EU rules.

While trying to cover national Lithuanian legal actions that are supposed to be a contribution to implementation of EU goals author is going to use comparative method, which will be applied analyzing EU legislation and the conformity of national legal acts. Some other methods such as linguistic and historical may be applied in areas where author is seeking to reveal particular reasoning and connection of corresponding regulations that developed in time.

2. REGULATION OF RENEWABLE ENERGY IN EUROPEAN UNION

While looking through historical aspects and long term discussions held in EU about common plans and united actions of member states which were necessary for evident progress in the use of renewable energy, it is clear that the concept of targets for renewable energy was the first actual step to make plans and discussions into reality. This target concept has been brought up with the common framework of EU energy policy. The formation of this concept is considered to be the fruitful result of EU Commission's 1996 Green Paper [1] and 1997 White Paper on renewable energy [2]. It was widely discussed whether such targets set were only of the informative nature or binding targets that member states had an obligation to follow. These questions were answered by adoption of the renewable electricity Directive [3]. This directive was the first actual leap that made EU obligations taken by signing Kyoto protocol not only linguistic verbalism but a start of particular actions.

Significant results may have been reached if not a long term gap in vain and fruitless discussions. Kyoto protocol came into force only in 2005 and meanwhile EU was dealing with opinion divergence. EU Parliament and Council looked differently into target setting. The before mentioned directives with indicative rather than legally binding targets were seen only of promoting renewable energy, the lack of binding targets were seen by many as the weak point of Community legislation on renewable energy. It was necessary to make those targets legally binding; however Parliament was suggesting legally binding sectoral goals, such as particular targets for different range of energy produced from RES (electricity, transport, heating, cooling) and furthermore even detailed targets for every member state; while EU Council was suggesting targets where member states could specify their targets and decide how to share the main target into sectoral goals.

Significant outcome of this opinion divergence and another step in the development of renewable energy regulation in EU is considered to be the communication from the Commission to the Council and the European Parliament – Renewable Energy Road Map: Renewable energies in the 21st century: building a more sustainable future [4] provided in the beginning of the year 2007. This communication revealed that it is not enough to set sectoral targets, it is necessary to harmonize both methods – set common targets for production of energy of different range and set the shares of targets for member states, leaving them the opportunity to specify measures and tools for individual implementation. This Communication and its connected decisions lead to the so-called '20-20-20 until 2020' agreement. This is one of the most ambitious plans towards control of climate change. It is looking forward to reduce greenhouse emissions by 20%, increase efficiency of energy usage by 20% and seek that at least 20% of used energy would be produced from RES. This agreement was a final breaking-point for the adoption of EU Climate Change Package [5], that EU Parliament finally agreed on the 17th of December, 2008. One of the legally binding acts of this package is the so called Renewable energy directive (herein after – RED) [6] which is furthermost important stage of legal regulation of energy sector in EU. It is a new stage for member states, because RED set binding individual targets for each member.

Countries' energetic interests have become an important part of national security and economical interest, that is the reason why even single acts of particular member state, may have influence not only for neighbouring countries but for all EU as a unity. Due to great influence in independency and countries sovereignty, solidarity in-between member states, and unisonous European decisions in energetic crisis and other unexpected challenges are crucial for integrated and effective energy market of EU. Unanimous EU ambitions in climate change and usage of energy produced from RES is impossible without fluent cooperation, hence the set of goals and targets for particular member states was inevitable.

First of all, the RED specifies the binding targets for each member state so the goals of ’20-20-20 until 2020’ would be reached. National targets varies because of states’ progress in usage or production of energy made from RES, economical and environmental abilities to reach those targets, population, GDP and other reasons that were analysed and calculated always having in mind the main EU principles such as solidarity, proportionality, judiciousness, therefore national target may be higher or lower compared to the overall goal of EU, nevertheless it does not mean that they are inadequate or impossible to reach (see - Table 1).

Secondly, the RED not only sets targets, but lays down main rules and instruments how to reach those targets. Even though there is a lot of area for member states improvisation and ability to specify measures that have to be taken, EU holds control of implementation in its hands. Directive sets a binding obligation for member states to prepare and provide EU Commission with their National plans, that schedule member states legislative actions and other measures that will improve production and usage of energy made from RES inside the country and will promote cooperative instruments and mechanisms in between member states. All the rules and goals set in the RED are inevitable to harmonize national legislations of member states and reach overall EU targets; such obligation to provide National plans is the best option seeking unified and smooth progress in the implementation of EU Climate Change package.

27th article of the RED sets an obligation for member states to ensure that national legal base, necessary for the implementation of this directive, would bring into force not later than 5th December 2010. Looking back historically, it is clear that the Parliament and Council bringing this directive into force, foreseen almost two years term for member states to prepare national plans and transpose EU rules into national legislation. The next part of this paper will reveal how Lithuania managed to prepare for the new stage of implementation.

Table 1. National overall targets

	Share of energy from RES in gross final consumption of energy, 2005	Share of energy from RES in gross final consumption of energy, 2020
Belgium	2.2%	13%
Bulgaria	9.4%	16%
Czech Republic	6.1%	13%
Denmark	17.0%	30%
Germany	5.8%	18%
Estonia	18.0%	25%
Ireland	3.1%	16%
Greece	6.9%	18%
Spain	8.7%	20%
France	10.3%	23%
Italy	5.2%	17%
Cyprus	2.9%	13%
Latvia	32.6%	40%
Lithuania	**15.0%**	**23%**
Luxembourg	0.9%	11%
Hungary	4.3%	13%
Malta	0.0%	10%
Netherlands	2.4%	14%
Austria	23.3%	34%

Poland	7.2%	15%
Portugal	20.5%	31%
Romania	17.8%	24%
Slovenia	16.0%	25%
Slovak Republic	6.7%	14%
Finland	28.5%	38%
Sweden	39.8%	49%
United Kingdom	1.3%	15%

(Source: Directive 2009/28/EC)

3. LITHUANIAN ATTEMPTS TO IMPLEMENT EU LAW ON RENEWABLE ENERGY

Transposition of EU directives is an important condition for validity and effect of such legislation, therefore the set of conditions is important not only for the member states but for whole EU as unified community. Each member state had to prepare amendments and changes of national legal base. These amendments had to be submitted to the Commission of EU. The amounts of prepared amendments may help visualize the in depth change of national legislation. Lithuanian submitted 12 national execution measures- amended legal acts concerning territory planning, levies and charges, natural gas, rules on promotion of production and purchase of electricity produced using renewable and waste energy sources, other administrative measures and the most important, national act on energy produced from RES, which in my opinion almost literally repeats the RED. Other member states put way much more effort in adapting their national legislation, for example Belgium submitted 63 national execution measures, United Kingdom – 35. On the other hand small amount of execution measures may mean that such countries have already progressed in legislation of promoting production and purchase of energy made from RES, for example Austria submitted only 2 execution measures, Germany – 9, but it is quite obvious because these countries are the leaders in implying renewable energy. Analysing national attempts of member states preparation of national execution measures, the first conclusion comes up, that Lithuanian attempts seem like weakly average compared to other member states.

Until the set deadline of RED, Lithuania managed to prepare only the Forecast for the use of renewable energy sources for the years 2010–2020 approved on 14 December 2009 by the Minister of Energy of the Republic of Lithuania. It is a five pages length paper of conceptual nature, which does not provide you with any particular execution or implementation measures. The one most evident reason for such vague execution is the reorganization of national ministries. Newly formed Ministry of Energy of the Republic of Lithuania started its work only in the beginning of the year 2009; therefore it obviously faced some difficulties in the preparation of executive measures and adoption of legal acts and their amendments.

The fact that the main national act on energy produced from RES was adopted only on the 12th of May, 2011, upsets the author of this paper the most. It means that the substantial execution and implementation measures of RED were enacted after almost half of the year after the set deadline of RED. The lack of such legislation complicates chances to imply EU provided rights for the subjects who wish to improve the production of electricity from RES. Furthermore, even if this national act would not have been late, it would not mean that our national subject would not be discriminated compared to subjects of other member states. Every national act has to be followed by acts of the Ministers, administrative rules, substatutory and executive acts. National lateness was noticed by European Commission on the 27 January, 2011 when the first official report on the violation was recorded [7]. On the 29 March and 9 June 2011, Lithuania notified EC with national acts and documents that implement RED. Thus, the response and reparation of situation started during the year 2011. It must be noted that full implementation is still lacking of unprepared orders and acts of different ministries.

Looking into national legal framework dedicated to energy produced from RES it seems that it moves towards the correct direction but the movement is too vague and slow. While ignoring the lateness and lack of substatutory acts, formally national act on energy produced from RES draws comprehensive background for legislation of renewable energy in our legal system. The abundance of newly explained concepts and terms shows how many of them did not even exist or needed adequate assimilation with the terms set in the RED. This act expands and concretizes goals of the RED, as well combines goals of other directives because it sets implementation measures for the directives 2009/72/EC and 2009/73/EC, furthermore this act angles European goals towards Lithuanian particularity. It is necessary to make notice that such comprehensive background is not enough and causes everyday problems for subject which plan to execute their rights in the area of renewable energy.

One of the illustrative examples of Lithuanian vague implementation of the RED could be national executive measures of its 13th article. Part two of this article says that 'Member States shall clearly define any technical specifications which must be met by renewable energy equipment and systems in order to benefit from support schemes.'[6]. Meanwhile, national acts set only an abstract goal to prepare and implement support schemes, which would create favourable conditions to use RES [8]. Without more specified legal framework, Minister of Agriculture on 28th of August 2009 confirmed new activities that could apply for support schemes – production of electricity in rural areas in power plants using energy from wind, solar, hydro and other RES. Some national subjects applied for such support schemes, prepared plans and scheme how to construct and implement such power plants, made calculations and other expensive and necessary preparations, until unexpectedly the Ministry of Agriculture recalled these activities from the list of activities that could apply for support. Only one reason and explanation was provided from the ministry – impossibility to predict prices in 5 years term, due to changes of substatutory legal acts. This example proves the lack of attention given to the implementation of the RED, when national acts and actions of administrative bodies cannot be predicted and by that, makes it impossible to implement vested rights of national subjects. The decisions in cases of Vilnius Regional Administrative Court [9] confirms that such actions of Ministry of Agriculture cannot be tolerated, are illegal because were enacted while breaking main procedures, especially the rules that preserves overall evaluation of circumstances. Such actions violate the principles of objectivity, proportionality and non-abuse of power of law. Obviously, such violations of public body of the Republic of Lithuania cannot conform to the principles of the RED – obligation for the member states to govern on the objective, transparent and non-discriminatory basis. It is only the one example out of many others that can prove the not adequate implementation of the RED. It is crucial to understand that such lateness in the fulfilment of the RED not only makes it hard to implement rights provided in the year 2009 but stops Lithuania from the development and implementation of the goals for the year 2020.

Data set in the National Renewable Energy Plan of Lithuania [10] shows what big challenges still await us in the near future if more aggressive steps and measures would not be taken soon. In the table shown in the 24th part of the national plan, it is clear that compared to total consumption of electricity, there were 4% of electricity produced from RES in the year 2005. Following year it was only 3,7%, 2007 – 4,8% and in the year 2009 – 4,9%. Therefore in the term of four years the growth of consumption of electricity produced from RES was only 0,9%. Taking into account the newest data [11] electricity produced from RES in 2011 reached 10,42%, so comparing with the year 2009 the percentage growth has increased and more than doubled. RED sets the target that average electricity produced from RES consumption in the year 2012 has to be 16,6 % of total electricity consumption, this means that within a one year period the consumption of energy made from RES has to bounce up more than 6 percent. It is obvious that if Lithuanian public bodies wish to have a realistic growth and equal appearance in EU, some determined actions and decisions have to be made in the area of renewable energy. It is crucial to notice that member states prepare their national plans not for predictions or theoretical goals. These documents are the actual steps of implementation of the RED. That means that the Commission of EU would not accept any exceptions, targets had been set and they have to be reached.

4. EXAMPLES OF LEGAL CHALLENGES OF ELECTRICITY PROVIDERS WHO USE RES FOR ENTRANCE TO THE NATIONAL ELECTRICITY MARKET

In this section, author would like to pay attention to some of the problematic aspects of Lithuanian legislation that complicate circumstances and cause actual problems for the new market participants that use RES.

First of all, it would be easier for renewable energy to find a lodgement in energy sector if there were no administrative obstacles. 3rd article of National Law on Public Administration [12] sets grounds for public administrative bodies to follow the principles of institutional assistance, efficiency, “one-desk” and others. While activities of public bodies and entities are based on such principles, decisions should be made and prosecuted faster in a more fluent and effective way, but as current situation and legislation shows new providers of “green” electricity have to face a lot of different public entities and spend a lot of time for gathering all different decisions and exercising many different rules for market entrance. For instance, new electricity suppliers have to prepare plans for infrastructure development including planning the electricity supply networks and these procedures in author’s opinion take inadequate measures and consume too much time. According to the order of Energy and Environment ministries [13] while planning connections of new power plants new potential members of energy market have to face a complicated bureaucratism with participating ministries, municipalities, different entities and departments. The declared objective of National Renewable Energy Act “to ensure the sustainable use of renewable energy development, promote the further development of new technologies and energy use” [14] becomes questionable when new energy producers are forced to face same institutions and their decision-making procedures as well as any other entities planning any other expansion of infrastructure, such as heating or gas supply networks.

Secondly, author would like to pay attention to the lack of legal regulation for the planning and exploitation of wind power plants in territorial waters of Baltic sea. Due to development of modern technologies it is possible to build wind parks further from the shores, diminish difficulties for their exploitation, creating international links (for example NordLink, upcoming NordBalt) it gets easier to provide electricity from such power plants. Main instrumentality for implementation of such wind parks in national territorial waters is legal base that would allow “green” energy developers expand their activities into the Baltic Sea. Possibility to expand the area of renewable energy production is mentioned in national act on Renewable energy [15] but national legal framework which governs legal regime in Baltic Sea does not provide rules for planning, maintaining or operating such power plants or even for preparation of environmental impact assessment.

Thirdly, author discovers the problems that raise from the issues of territory planning and construction law. Due to technical issues and utilized capacity of transmission networks new participants of energy market have to face different regulation. Following the rules of national Electricity Act [16] and Electricity network code [17] one may conclude that the voltage lower than 110kV include low and medium voltage so these lines and equipment by national law are considered as movable objects other than high-voltage lines that should be regarded as immovable objects. The problem arises and situation becomes inadequate when because of different voltage or simply because the capacity of low or medium voltage lines is already utilized new members have to plan the connection to high-voltage lines. Their situation becomes more complicated because high-voltage lines are considered to be immovable objects and by National Construction act [18] they have to be planned, built according to the rules of this law because it is considered to be a structure/building. Furthermore their situations become more complicated not only because of duty to imply the rules of Construction law but they have to prepare different, specialized documents of territory planning [19]. Electricity producers that use RES due to outdated infrastructure and limited capacity of transmission and distribution networks in some regions are still unable to enter the electricity market easily not only because of complicated legal regulations but as well because of physical exploitation of technical possibilities. RED says that “Member States shall take appropriate steps to develop transmission and distribution grid infrastructure, create intelligent networks” [20], national law as well declares the purpose to “ensure sustainable use of renewable sources, allow development of new technologies to promote further development in all possible ways” [21]. This means that to implement both national and international statutory obligations, Lithuania should ensure that new market participants have an opportunity to connect their grid in adequate and proportionate ways or for instance create alternative electricity transmission systems.

These examples of technical, administrative issues or lack of regulation explains how national legal base concerning exploitation of renewable energy is still not fluent enough and impedes the growth of RES usage. It is crucial to understand that it is not enough to have advanced legal acts that provide abstract rights and rules, all the subordinate legislation has to be prepared and harmonized, this would allow the establishment of renewable energy in Lithuania.

5. CONCLUSIONS

Wide range of legal acts and international documents dedicated to energy sector, their complicated nature, hierarchical relationship and mandatory nature draws the attention of lawyers because of its public importance. Initiatives of EU and actions in this important, especially over the past century, sphere is one of the most important step towards the solution of long and fruitless discussions of climate change and the need of clean, green, renewable energy.

Long term relationships of EU members in most important economical and political areas determined the cooperation of member states in the area of renewable energy. The result of the movement towards single goal set in the ’20-20-20 until 2020’ agreement is the RED. The split of the RED targets in between member states raises their obligation to actively participate in its implementation.

Impeccable implementation and transposition of the RED is an inevitable step toward the reach of EU goals. While analysing Lithuanian legislation, the lateness and unconformity has been noticed. Such lacks of national acts and complicated administrative procedures cause lag and ineffective production and consumption of energy from RES.

Lack of substatutory national acts and their narrow nature leads to legal uncertainty, which could easily be removed with bigger involvement of the Ministry of Energy and other relevant authorities. It is necessary to diminish administrative barriers, create regulation for exploitation of wind energy parks in Baltic Sea and harmonize rules for construction and territory planning.

Improvement of national legal framework, development of the existing gaps would mean the creation of suitable environment for renewable energy producers and consumers. More aggressive steps towards impeccable regulation of renewable energy would make Lithuania an equal member state, where national subjects can exercise their equivalent rights and obligations same as other subjects of different EU members.

REFERENCES

1. COM (96) 576.
2. COM (97) 599.
3. Directive 2001/77/EC of the European Parliament and of the Council of 27 September, 2001 on the promotion of electricity produced from renewable energy sources in the internal energy market. Official Journal of the European Communities, 27 October, L 283/33-40.

4. COM(2006) 848.
5. EU Climate Change Package consists of such legislation as Promotion of the use of energy from renewable sources, Greenhouse gas emission allowance trading system, Geological storage of carbon dioxide, and others. For full list, look – http://www.europarl.europa.eu/sides/getDoc.do?pubRef=-//EP//TEXT+TA+20081217+TOC+DOC+XML+V0//EN
6. Directive 2009/28/EC of the European Parliament and of the Council of 23 April 2009 on the promotion of the use of energy from renewable sources and amending and subsequently repealing Directives 2001/77/EC and 2003/30/EC.
7. Official data from National Energy Agency. KLIUKAITĖ, A., RE: del 2009/28/EB pazeidimu, [interactive]. **Programes and Funds Administration Division of Energy Agency** 2012-03-13, 10:24:21 EEST. Internet access: Karolina.cesnaite@tf.stud.vu.lt
8. Order of Minister of Agriculture of the Republic of Lithuania - The order of the Lithuanian rural development programme. Measures for 2007-2013 ‘Support for business creation and development’ Official Gazette, 2009, No. 105-4399.
9. Decisions of Vilnius Regional Administrative Court No. I-1098-815/2011; No. I-1168-365/2011; No. I-1160-244/2011.
10. The Resolution of the Government of the Republic of Lithuania on the national strategy of sustainable development and implementation. 2003 September 11. No. 1160 (Official Gazette, 2003, No. 89-4029).
11. Annual Report from Electricity Division of National Control Commission for Prices and Energy (lit. *Valstybinės kainų ir energetikos kontrolės komisijos Elektros skyriaus „Elektros energijos rinkos stebėsenos ataskaita už 2011 metus“*) [interactive], internet access: <http://www.regula.lt/lt/naujienos/2011/elektros_stebesenos_ats/Elektros_energetikos_rinkos_stebesenos_ataskaita_uz_2011_metus.pdf>, [2012-01-11].
12. Law on Public Administration (with additions and amendments), Official Gazette, 1999, No. 60-1945; 2006, No. 77-2975.
13. Order of Ministers of Energy and Environment for the approval of special rules for plans of development of infrastructure (heating, electricity, gas and oil supply networks) [lit. *Lietuvos Respublikos Energetikos ministro ir Lietuvos Respublikos Aplinkos ministro įsakymas dėl infrastruktūros plėtros (šilumos, elektros, dujų ir naftos tiekimo tinklų) specialiųjų planų rengimo taisyklių patvirtinimo*], Official Gazette, 2011, No. 11-487.
14. Law on Renewable sources energetics (*lit. Lietuvos Respublikos atsinaujinančių išteklių energetikos įstatymas)*. Official Gazette, 2011, No. 62-2936.
15. 22 Artcile of Law on Renewable sources energetics. *Ibid.*
16. 75.2 Article of Electric energy. (*lit. Lietuvos Respublikos elektros energetikos įstatymas*). Official Gazette, 2000, No. 66-1984; 2012, No. 17-752.
17. Order of Minister of Agriculture for the use of Electrical connection code and rules for electricity supply (lit. Lietuvos Respublikos Ūkio ministro įsakymas dėl elektros energijos tiekimo ir naudojimo taisyklių patvirtinimo. Elektros tinklų kodeksas). Official Gazette, 2002, No. 3-88.
18. Law of Constructions *(lit. Lietuvos Respublikos statybų įstatymas)* (with additions and amendments), Official Gazette, 1996, No. 32-788; 2001, No. 101-3597.

CYSENI 2012, May 24–25, Kaunas, Lithuania
ISSN 1822-7554, www.cyseni.com

THE PROFITABILITY OF POWER GENERATING FIRMS AND POLICIES PROMOTING RENEWABLE ENERGY

A. Kažukauskas, J. Jaraitė
Centre for Environmental and Resource Economics (CERE)
Department of Economics
Umeå University
Sweden
Email: andrius.kazukauskas@econ.umu.se.

ABSTRACT

With policies to promote power generation from renewable energy sources (RES) becoming important part of climate and energy policy worldwide, there is now considerable interest in understanding how these different market-based mechanisms affect power generating firms in practice. The existing theory provides conflicting guidance regarding profitability of Tradable Green Certificates (TGC) over Feed-in-Tariff (FIT) based policies. Thus, the main goal of this study is to empirically assess the performance of power generating firms operating in the TGC scheme environment relative to the performance of power generating firms operating under alternatives RES support mechanisms. The main finding of this study is that, in Europe, TGC schemes are associated with higher returns for power generating firms. This supports the hypothesis that higher investment uncertainty induced by the TGC policy nature coupled with some market imperfections lead to higher profits for electricity producers operating in TGC schemes.

Keywords: power generation, European Union, emission trading, feed-in-tariff, renewable energy, tradable green certificates

1. INTRODUCTION AND LITERATURE REVIEW

With policies to promote power generation from renewable energy sources (RES) becoming important part of climate and energy policy worldwide, there is now considerable interest in understanding how these different market-based mechanisms work in practice.

There exist two common policy instruments to promote renewable electricity: Feed-in-Tariff (FIT) and Tradable Green Certificate (TGC) systems. FIT policies are focused on setting the right *price* to drive RES deployment. In contrast, TGC policies set a *quantity* restriction that determines the market price of renewable electricity. In this respect, FIT and TGC policies resemble a pollution tax and a cap-and-trade system, respectively. This fundamental difference between FIT and TGC determines what effects each policy will have on the performance of power generating firms.

FIT policies and TGC systems can be compared in many dimensions, namely cost-efficiency, market distortions and transaction costs. According to the existing literature, one of the main advantages of TGC schemes over FIT systems is cost-efficiency. The EU Commission has favoured TGC schemes over FIT systems on the basis that TGC systems are more market orientated and, therefore, they should create more competitive markets for renewable electricity. [1] The Commission's working paper [1], which is largely based on the theoretical assessment of various RES support mechanisms, suggests TGC as a system which is best suited to achieve the minimum

---

[1] In TGC schemes, power generating firms have to compete in two markets: common electricity markets and green certificate markets. In FIT systems, firms face guaranteed prices and the market demand, thus, firms may directly focus on internal cost minimisation.

cost for electricity generators and electricity consumers. In other words, TGC systems generate the least excess profits for power producing firms.

Markets for electricity might be distorted in many different ways. These distortions might mitigate or even reverse the expected effects of policies promoting renewable energy. The most apparent market distortion is the capital constraint. As TGC schemes imply a much higher risk level for investors in renewable power generation (a price of green certificate is uncertain), the availability of capital and its cost become an issue when compared to FIT systems, where a price for green electricity is fixed and known in advance [2]. Higher capital costs determine higher expected returns for investors in TGC systems. Furthermore, the capital constraint also affects market entry decisions of small RES developers. Contrary, the FIT approach, by guaranteeing a price which is set so that both small and large firms may stay in business, helps firms to access cheaper capital. As a result, the number of firms can be smaller in TGC than in FIT systems. On that account, TGC markets might by characterised by higher market concentration that leads to higher profits.

Additionally, TGC systems are associated with higher transactions costs in the form of fixed administrative costs. This might create additional hurdles for smaller investors to enter the market [3–5]. Again, this limits the potential number of investors and can result in less competitive TGC market.[2]

The main aim of this study is to test the above considerations empirically. The main hypothesis is that TGC systems, due to potentially higher market concentration and higher required capital returns, will be associated with excess profits for renewable energy generating firms. This hypothesis can be rephrased in the words of Nicholas Stern: „(pricing) mechanisms achieve larger deployment at lower costs. Central to this is the assurance of long-term price guarantees. (...) Uncertainty discourages investment and increases the cost of capital as the risks associated with the uncertain rewards require greater rewards ([6], p.366)“.

As RES support mechanisms do not operate in isolation, the secondary aim of this study is to analyse the interactions between RES systems and other policies implemented to reduce greenhouse gas emissions and the resulting effects on power generating firms. In the European Union (EU), the EU-wide emissions trading system (EU ETS) plays a central role in achieving the EU's climate change targets. Hence our focus is on the interaction between the EU ETS and RES systems.

To the best of our knowledge, this study contributes to the existing literature on RES support mechanisms in two ways.[3] First, this is the pioneering *ex post* EU-wide analysis of this kind exploring RES support mechanisms' effects on firm performance, namely profitability. Second, the unique dataset of firms in the European power generating sector with identifications of EU ETS firms allows investigating interactions between RES support policies and the biggest emission trading programme in the world.

The rest of the paper is organised as follows: Section 2 introduces the empirical strategy; Section 3 describes the data; Section 4 presents and discusses the estimation results. A concluding summary is given in Section 5.

2. THE EMPIRICAL STRATEGY

The empirical strategy is designed to analyse the effects of RES support mechanisms on firm performance. In particular, the relationship between Tradable Green Certificates and firms'

---

[2] See Cory, Couture, and Kreycik [15] for more detailed discussion on transaction costs and firm size effects in TGC-based markets.

[3] We refrain from providing a detailed literature review on RES support mechanisms and their interactions with other environmental policies. The comprehensive reviews of relevant literature can be found in Menanteau et al. [16], del Rio and Gual [17], Agnolucci [18] and Bergek and Jacobsson [14].

profitability is investigated. It is assumed that a firm's profitability is a function of the renewable electricity generation support policy choice and other variables:

$$profit_{it} = f(TGC_i, X_{it}), \tag{1}$$

where $profit_{it}$ is the outcome of interest (firm profitability ratio, in particular, EBIT[4] margin over operating revenues); TGC_i is a RES policy dummy (1 is assigned for firms in the EU countries which adapted the TGC support mechanism and 0 is assigned for all other firms)[5]; X_{it} is a vector of firm characteristics (time and country dummy variables, age of the firm, firm category with respect to its size, firm size in terms of its assets etc.). X_{it} vector also contains the annual change in renewable electricity production (in MW).[6] The later variable is used not only to account for potential support level changes for renewable electricity generation but also to control for potential industry lobbying effects. For instance, Marques et al. [7], who analyse the impact of several factors on the use of renewable energy sources in a set of European Union countries, suggest that the lobbying effect of the established industries may be related with the level of renewable energy use.

The analysis is commenced with a simple ordinary least squares (OLS) model. To control for the potentially high level of heterogeneity and possibly outlier-driven results, the iteratively reweighted least squares (IRLS) and random effect models are used as the alternatives to the OLS model.

Initially, the following model is estimated:

$$profit_{it} = \lambda_t + \varrho_c + \beta_1 TGC_i + \beta_2 BROWN_i + x_{it}\delta + \varepsilon_{it}, \tag{2}$$

where λ_t and ϱ_c are the time- and country-specific control variables, respectively; $\boldsymbol{x}_{it}$ is the vector of control variables mentioned earlier; $BROWN_i$ is a dummy variable for firms which were covered by the EU ETS. This dummy variable proxies *conventional* firms using combustible fossil fuels for energy generation.

Further, the panel nature of the dataset is exploited:

$$profit_{it} = \lambda_t + \varrho_c + \beta_1 TGC_i + \beta_2 BROWN_i + x_{it}\delta + \varepsilon_{it} + \eta_i, \tag{3}$$

where η_i are the firm-specific unobserved heterogeneity effects. However, as the policy variable of interest is time-invariant, the fixed effects model prevents identifying the policy effect. The random effects model is used instead.[7]

The random effects model requires the random effects not to be correlated with the explanatory variables. This is a restrictive assumption, particularly in the context of the model we are attempting to estimate, where the firm-specific time varying variables, such as firm total assets and firm age, are likely to be correlated with the unobserved heterogeneity, e.g. managers' abilities.

To control for the potential correlation between the random effects and the other exogenous variables, Mundlak [8] suggested modelling the unobserved heterogeneity (random effects) as a function of the means of the time varying explanatory variables:

---

[4] EBIT stands for Earnings Before net Interest and Tax.

[5] The analysed EU countries have implemented either TGC or FIT policies. The only exception is Finland, which implemented tax reduction incentives for promoting renewable electricity. The inclusion of Finland in the analysis does not affect the main findings of the study in any significant way. Table A 1 in the Appendix provides information on what RES support mechanism each EU country adapted.

[6] Initially, to avoid endogeneity, we lagged this variable, but this did not affect the main results.

[7] In a fixed effects model these variables are "swept away" by the within estimator of the coefficients on the time varying covariates.

$$\eta_i = a_0 + \bar{x}_i\psi + a_i, \tag{4}$$

where $\bar{\mathbf{x}}_i$ is an average of $\mathbf{x}_{it}$ time varying variables over time for each firm and a_0 is a constant term. We assume that time invariant a_i is uncorrelated with $\mathbf{x}_{it}$. Since the Mundlak approach allows taking into account correlation between unobserved firm heterogeneity and firm characteristics, we use it to estimate the effect of TGC systems on firm profitability. The model can now be written as:

$$profit_{it} = \lambda_t + \varrho_c + \beta_1 TGC_i + \beta_2 BROWN_i + x_{it}\delta + \varepsilon_{it} + a_0 + \bar{x}_i\psi + a_i \tag{5}$$

The next step is to explore the interaction between RES support policies and the EU ETS. This is done in two ways. Firstly, to understand whether TGC policies have a different effect on *conventional* fossil fuel power generating firms, we utilise the following model:

$$profit_{it} = \lambda_t + \varrho_c + \beta_1 TGC_i + \beta_2 BROWN_i + \theta_1\,(TGC_i * BROWN_i) + x_{it}\delta + \varepsilon_{it}, \tag{6}$$

where θ_1 is a coefficient of the interaction term between the TGC policy dummy and the dummy identifying conventional energy producers which participate in the EU ETS. It indicates a TGC policy effect for *conventional* energy producers.

Secondly, we extend the last model by controlling for the actual introduction of the EU ETS in 2005:

$$\begin{aligned} profit_{it} = {} & \lambda_t + \varrho_c + \beta_1 TGC_i + \beta_2 BROWN_i + \beta_3 Y05_t + \theta_1\,(TGC_i * BROWN_i) + \\ & \theta_2\,(TGC_i * Y05_t) + \theta_3\,(Y05_t * BROWN_i) + \theta_4(TGC_i * BROWN_i * Y05_t) + x_{it}\delta + \varepsilon_{it} \end{aligned} \tag{7}$$

$Y05_t$ is a dummy variable for the 2005-2007 period corresponding for the first phase of the EU ETS. θ_4 is a coefficient on the triple interaction term and it allows identifying a TGC policy effect for *conventional* firms after 2005, if any.

This model also allows investigating another interesting question. It is widely accepted that *conventional* electricity producers could make windfall profits in the first phase of the EU ETS because of the premium on electricity prices and the free allocation of emission permits [9], [10].[8] There exists a wide literature on how CO_2 price affects electricity prices, but there are very few empirical studies analysing how the EU ETS has affected the actual profitability of *conventional* energy producers. One exception is Yu's [9] study that focuses on this issue using a sample of Swedish energy firms for 2005 and 2006. The study finds that the EU ETS had no or negative effects on the profitability of energy producers. Our cross-country firm level dataset allows us to explore this issue further. θ_3 coefficient in the last model (Equation 7) indicates the effect of the EU ETS on *conventional* energy producers and allows us to test the hypothesis of conventional electricity producers' windfall profits associated with the introduction of the EU ETS in 2005.

It is important to note that even though the policy measures are exogenous for individual firms, the potential country self-selection into implementing TGC or FIT policies might cause bias in the policy effect estimates if the particular countries' decision to adopt FIT or TGC type policies was based on expected firm profitability effects, in particular abnormal profits. To address this issue there is a scope for further research to overcome the strong policy causality assumption of this study.

---

[8] See also Sijm et al. [19]for literature review on how CO_2 price affects electricity price

3. DATA SOURCES AND DESCRIPTION

The Amadeus (Bureau van Dijk) database is a central data source of this study. This database includes firm level accounting and other data in standardised financial format. The general source for the Amadeus is national official public bodies in European countries. The Amadeus database is a very useful information source for cross-country comparisons as it provides harmonised accounts for large fraction of European firms.

Table 1. Descriptive statistics of the variables according to the RES support mechanism (TGC or FIT), full sample, 2002–2007

	FIT			TGC		
Variable	Obs.	Mean	Std.	Obs.	Mean	Std.
EBIT margin	17 817	15.629	31.097	6 460	19.581	30.800
Firm assets, thou EUR	17 771	121 717	2 340 000	6 455	186 698	1 464 705
Size 1	17 817	0.473	0.499	6 460	0.429	0.495
Size 2	17 817	0.299	0.458	6 460	0.287	0.452
Size 3	17 817	0.157	0.364	6 460	0.163	0.369
Size 4	17 817	0.071	0.257	6 460	0.121	0.326
Payroll, thou EUR	9 444	9580	176 444	3 176	9 312	58 050
Added value, thou EUR	6 442	35 981	498 564	2 350	58 639	1 030 887
Return on Assets (ROA)	17 336	4.894	15.079	6 313	5.858	17.437
Return on Equity (ROE)	15 164	16.862	74.777	5 778	19.263	83.657
Return on Employed Capital (ROEC)	12 271	14.656	56.522	4 768	18.453	72.455
Age	17 280	12.113	15.225	6 292	15.102	21.143

Notes: All monetary variables are deflated by their country-specific deflators from Eurostat; Size1 to Size4 indicate the firm size category from the smallest to the largest as defined in the Amadeus database.

Table 2. Descriptive statistics of the variables according to the RES support mechanism (TGC or FIT), restricted sample (without ETS firms), 2002–2007

	FIT			TGC		
Variable	Obs.	Mean	Std.	Obs.	Mean	Std.
EBIT margin	16 296	16.478	32.078	5 977	20.409	31.333
Firm assets, thou EUR	16 257	52 950	657 648	5 973	99 259	757 427
Size 1	16 296	0.516	0.500	5 977	0.460	0.498
Size 2	16 296	0.305	0.460	5 977	0.302	0.459
Size 3	16 296	0.130	0.337	5 977	0.144	0.351
Size 4	16 296	0.049	0.216	5 977	0.094	0.292
Payroll, thou EUR	8 440	3 541	38 088	2 917	5 331	30 007
Added value, thou EUR	5 611	10 772	93 762	2 122	41 460	1 018 728
Return on Assets (ROA)	15 864	5.048	15.499	5 843	6.119	17.862
Return on Equity (ROE)	13 800	17.171	74.929	5 357	19.625	86.204
Return on Employed Capital (ROEC)	10 952	15.352	58.322	4 342	18.677	74.592
Age	15 805	12.006	15.104	5 809	14.684	20.836

Notes: All monetary variables are deflated by their country-specific deflators from Eurostat; Size1 to Size4 indicate the firm size category from the smallest to the largest as defined in the Amadeus database.

Our sample covers EU-27 countries for the period 2002-2007. The data have been cleaned for obvious mistakes (e.g. negative values for assets). The analysis is restricted to the electricity generation sector (NACE 3511). This means that all electricity producers, irrespective of their utilised electricity generating technology, are considered. The Amadeus provides firms with both consolidated and unconsolidated financial accounts. To avoid a double-counting problem, unconsolidated financial accounts are used for the main policy analysis.

Several profitability measures are available and we use the EBIT margin over operating revenues as our main measure for profitability. Other profitability measures are also available such as ROA or ROE. Since in the Amadeus database the EBIT profitability measure is available for more firms than for any other alternative, EBIT margins are used as the main profitability indicator.

The asset-based variable and the categorical size variables are used to control for heterogeneity. There are also other possible proxies available to control for firm size, but as in the case of the profitability measure, the assets size measure is available for more firms. The usage of firm assets as a measure for firm size is a common practice in the empirical industrial organisation literature (see e.g. [11], [12]).

Our dataset also contains information about EU firms in the EU ETS. The EU ETS data, obtained from the European Commission (Community Independent Transaction Log, CITL), were matched with the firm-level data from the Amadeus database. The addresses as well as the names of ETS firms were used as the matching identifiers.

Table 1 summarises the data and separates all variables according to the RES support mechanism (TGC or FIT). All monetary variables are deflated by the country-specific deflators from Eurostat. Of particular note is the fact that firms in the TGC and the FIT type groups are different in terms of size. On average, firms in the TGC group are almost 50 per cent bigger than firms in the FIT group in terms of their assets. As we may expect conventional ETS firms to be relatively bigger than other power generating firms, Table 2 presents the descriptive statistics on the data sample that excludes ETS firms. It is evident, that the same relationship also holds for the reduced sample. This suggests the importance of controlling for firm heterogeneity.

The econometric models specified above also include several country-specific variables: the annual change in electricity price and the annual change in renewable electricity production. These data are available from Eurostat and the International Energy Agency. The former variable controls the dynamics of electricity prices in each country. The latter variable indirectly controls the overall support for renewable energy. We may expect that countries with the higher growth in renewable electricity have more generous support systems for renewable energy.

4. RESULTS

Table 3 summarises the TGC policy effects on the profitability (EBIT margins) of electricity generating firms.[9] In total, three types of models were estimated: the OLS model, the IRLS model, and the random effects model with the Mundlak terms. All models provide consistent evidence that power generating firms operating in EU countries that implemented green certificate trading were more profitable during the period 2002-2007. This finding does not identify the particular sources of this higher profitability, however, it supports our main hypothesis that TGC systems, due to potentially higher market concentration and higher capital returns required by investor, are associated with excess profits for renewable energy generating firms. This result that TGC schemes are linked with higher returns is in line with the earlier country-specific analysis (see e.g. [13], [14]).

---

[9] The use of the other profitability measures (ROA, ROE) produced similar results.

The higher profits due to TGC are not different between conventional electricity producers and other electricity generating firms (*TGC*BROWN*).[10] However, the positive and significant coefficient for the interaction term between the TGC policy dummy and the time dummy representing the first phase of the EU ETS (*TGC*Y05*) suggests that the post-2005 period for electricity generating firms in TGC-based countries was associated with even higher profits. This result might be explained in two ways. First, the EU ETS has decreased the costs disadvantage of renewable electricity and, thus, renewable electricity has become more competitive. Second, the EU ETS has increased the demand for renewable electricity and this has induced the deployment of more and more expensive renewable electricity generating technologies. At each point in time, the certificate price will correspond to the most expensive technology induced in the system, and all power generators with lower costs, thus, receive an extra profit. However, this post-2005 effect is not different between conventional electricity producers and other electricity producers operating in TGC-based countries – the coefficient on the interaction term between the TGC policy dummy, the ETS firm dummy and the ETS period dummy (*TGC*BROWN*Y05*) is not significant.

The latter result provides the answer to the secondary objective of this study – the EU ETS had no effect on conventional power generating firms operating in countries with TGC schemes in place (*TGC*BROWN*Y05*). Also, although one might expect that power generators who must comply with the EU ETS and renewable quota restrictions might benefit from double regulation[11], the coefficient on the interaction term between the ETS period dummy and the conventional firm dummy is insignificant (*Y05*BROWN)*. The descriptive statistics for conventional power producers separated by the pre- and post-ETS period also do confirm this finding (see Table A 2 in the Appendix). This result does not confirm common speculations about windfall profits due to the EU ETS.

Additionally, the estimation results show that power generators with larger assets had higher profitability. Also, the higher growth in renewable energy production (the proxy of the overall support level for renewable energy) led to higher profits (see Table 3, columns 7-9).

---

[10] By inspecting Table 2 and Table A 3 in the Appendix it is obvious that both conventional power generators and other power generating firms operating in TGC-base countries on average had significantly higher profits than firms operating in FIT-based countries.

[11] It has been argued that the coexistence of RES support systems and emission trading may lead to differential treatment of large and small generators. This is so because electricity suppliers owning fossil-fuel-based generation plants can benefit twice if they invest in renewable electricity: they would receive the feed-in tariff/green certificate price and save tradable permits. In contrast, small independent producers would only receive one incentive: the feed-in tariff/green certificate price.

Table 3. The effects of RES support policies on the profitability of power generating firms, full sample

VARIABLES	OLS			IRLS			RE		
	1	2	3	4	5	6	7	8	9
TGC	5.944***	5.886***	3.979***	6.693***	6.470***	5.102***	5.889***	5.794***	4.745***
	(0.812)	(0.854)	(1.128)	(0.723)	(0.754)	(1.027)	(1.461)	(1.511)	(1.610)
BROWN	-12.09***	-12.20***	-11.74***	-12.37***	-12.73***	-11.74***	-11.23***	-11.44***	-10.76***
	(0.593)	(0.626)	(0.850)	(0.776)	(0.878)	(1.382)	(1.658)	(1.868)	(2.037)
TGC* BROWN	-	0.455	0.336	-	1.528	1.874	-	0.903	-0.831
	-	(1.339)	(2.181)	-	(1.683)	(2.751)	-	(3.654)	(4.010)
Y05*BROWN	-	-	-0.820	-	-	-1.659	-	-	-1.092
	-	-	(1.063)	-	-	(1.686)	-	-	(1.247)
TGC*Y05	-	-	2.958**	-	-	2.159**	-	-	1.601*
	-	-	(1.165)	-	-	(1.069)	-	-	(0.822)
Y05	-	-	-1.370	-	-	-0.153	-	-	-0.761
	-	-	(0.877)	-	-	(0.808)	-	-	(1.266)
TGC *BROWN*Y05	-	-	0.395	-	-	-0.363	-	-	2.800
	-	-	(2.621)	-	-	(3.371)	-	-	(2.488)
Renewable electricity (yoy change)	1.133	1.129	0.772	1.634	1.623	1.394	2.643***	2.641***	2.342**
	(1.406)	(1.406)	(1.412)	(1.329)	(1.329)	(1.335)	(0.997)	(0.997)	(1.003)
Firm age	-0.0166	-0.0167	-0.0162	-0.0237*	-0.0242**	-0.0236*	-0.343	-0.339	-0.362
	(0.0116)	(0.0116)	(0.0116)	(0.0122)	(0.0122)	(0.0122)	(0.416)	(0.416)	(0.417)
Lagged assets (log)	1.543***	1.542***	1.533***	2.470***	2.469***	2.456***	0.820***	0.819***	0.810***
	(0.167)	(0.167)	(0.167)	(0.124)	(0.124)	(0.124)	(0.165)	(0.165)	(0.165)
Electricity price (yoy change)	7.247	7.261	4.615	5.962	5.972	4.429	3.628	3.632	1.605
	(4.871)	(4.870)	(4.982)	(4.394)	(4.394)	(4.538)	(3.373)	(3.373)	(3.482)
Other industry dummy	yes	yes	yes	yes	yes	yes	yes	yes	yes
Time dummies	yes	yes	yes	yes	yes	yes	yes	yes	yes
Size dummies	yes	yes	yes	yes	yes	yes	yes	yes	yes
Regional dummies	yes	yes	yes	yes	yes	yes	yes	yes	yes
Mundlak terms	-	-	-	-	-	-	yes	yes	yes
No. of observations	17,045	17,045	17,045	17,045	17,045	17,045	17,045	17,045	17,045
No. of firms	5,704	5,704	5,704	5,704	5,704	5,704	5,704	5,704	5,704
R-squared	0.043	0.043	0.044	0.071	0.071	0.071	0.041	0.041	0.041

Notes: The robust standard errors are in the parentheses. *** $p<0.01$, ** $p<0.05$, * $p<0.1$.

5. CONCLUSIONS

Using the cross-country micro level dataset this study analyses how the choice of renewable energy promotion system affected the electricity production sector in Europe. In particular, we consider more closely Tradable Green Certificates vs. Feed-in Tariffs. The EU Commission has favoured TGC schemes over FIT systems on the basis that TGC systems are more market orientated (in TGC system green power generating plants have to compete not only in common electricity market but also in tradable green certificate markets) and, therefore, they should create more competitive markets for renewable electricity. In other words, TGC systems generate the least excess profits for power producing firms. We test this hypothesis against the alternative suggestion that due to market imperfections, namely because of higher risk, higher capital constraints and higher transactional costs, TGC schemes will be associated with excess profits for renewable energy generating firms.

The main finding of this study is that power generating firms, operating in EU countries that implemented green certificate trading, were more profitable compared to FIT-firms during the period 2002-2007. This result supports our alternative hypothesis of the presence of market imperfection in TGC type systems. However, this analysis is limited in that it cannot identify exact sources of this higher profitability. This aspect needs for further research.

Also we find that the introduction of the EU ETS had no effect on conventional power generating firms operating in countries with TGC schemes in place. The related results also do not confirm common speculations about excess profits in the energy sector due to the EU ETS.

APPENDIX

Table A 1. The distribution of observations by country and RES support policy choice

Country	Freq.	Percent	TGC?
AT	47	0.19	-
BE	303	1.25	yes
BG	310	1.28	-
CZ	150	0.62	-
DE	1,956	8.06	-
DK	275	1.13	-
EE	107	0.44	-
ES	7,302	30.08	-
FI	623	2.57	-
FR	4,877	20.09	-
GB	1,275	5.25	yes
GR	385	1.59	-
HU	315	1.3	-
IE	99	0.41	-
IT	1,915	7.89	yes
LT	25	0.1	-
LU	8	0.03	-
LV	60	0.25	-
NL	107	0.44	-
PL	450	1.85	yes
PT	1,051	4.33	-
RO	603	2.48	yes
SE	1,914	7.88	yes
SI	88	0.36	-
SK	32	0.13	-

Table A 2. Descriptive statistics of conventional firms before (2002-2004) and after (2005-2007) the EU ETS introduction

	2002-2004			2005-2007		
Variable	Obs	Mean	Std.	Obs	Mean	Std.
EBIT margin	924	7.821	15.515	1080	6.681	16.923
Firm assets, thou EUR	919	889232	6932192	1077	1018833	7156975
Size 1	924	0.024	0.153	1080	0.023	0.150
Size 2	924	0.221	0.415	1080	0.185	0.389
Size 3	924	0.419	0.494	1080	0.450	0.498
Size 4	924	0.337	0.473	1080	0.342	0.474
Payroll, thou EUR	569	64102	542511	694	54946	414672
Added value, thou EUR	499	185267	1361842	560	229863	1260849
Return on Assets (ROA)	897	2.637	9.561	1045	3.462	9.498
Return on Equity (ROE)	819	14.632	67.369	966	13.380	66.012
Return on Employed Capital (ROEC)	806	12.268	36.563	939	9.266	42.657
Age	903	14.221	19.264	1055	15.581	18.406

Notes: All monetary variables are deflated by their country-specific deflators from Eurostat; Size1 to Size4 indicate the firm size category from the smallest to the largest as defined in the Amadeus database.

Table A 3. Descriptive statistics of conventional firms by RES policy choice

	FIT			TGC		
Variable	Obs	Mean	Std.	Obs	Mean	Std.
EBIT margin	1521	6.531	14.587	483	9.336	20.649
Firm assets, thou EUR	1514	860122	7685504	482	1270255	4515728
Size 1	1521	0.015	0.122	483	0.050	0.218
Size 2	1521	0.235	0.424	483	0.097	0.297
Size 3	1521	0.446	0.497	483	0.402	0.491
Size 4	1521	0.304	0.460	483	0.451	0.498
Payroll, thou EUR	1004	60341	527270	259	54148	170576
Added value, thou EUR	831	206193	1355069	228	218529	1127751
Return on Assets (ROA)	1472	3.229	9.268	470	2.615	10.318
Return on Equity (ROE)	1364	13.739	73.175	421	14.653	38.418
Return on Employed Capital (ROEC)	1319	8.871	37.969	426	16.169	45.235
Age	1475	13.262	16.431	483	20.122	24.002

Notes: All monetary variables are deflated by their country-specific deflators from Eurostat; Size1 to Size4 indicate the firm size category from the smallest to the largest as defined in the Amadeus database.

REFERENCES

1. EUROPEAN COMMISSION Electricity from renewable energy sources and the internal electricity market. Brussels, 1999.
2. MITCHELL, C.; BAUKNECHT, D.; CONNOR, P. Effectiveness through risk reduction: a comparison of the renewable obligation in England and Wales and the feed-in system in Germany. *Energy Policy* 2006, *34*, p. 297–305.
3. JAGER, D. D.; RATHMANN, M. Policy instrument design to reduce financing costs in renewable energy technology projects. *ECOFYS report* 2008.
4. FOUQUET, D.; JOHANSSON, T. B. European renewable energy policy at crossroads—Focus on electricity support mechanisms. *Energy Policy* 2008, *36*, p. 4079–4092.
5. DINICA, V. Support systems for the diffusion of renewable energy technologies—an investor perspective. *Energy Policy* 2006, *34*, p. 461–480.
6. STERN, N. *Stern Review: The Economics of Climate Change*; Cambridge University Press, 2007.
7. MARQUES, A.C.; FUINHAS, J.A.; MANSO, J.P. A Quantile Approach to Identify Factors Promoting Renewable Energy in European Countries. *Environmental and Resource Economics* 2010, *49*, p. 351–366.
8. MUNDLAK, Y. On the Pooling of Time Series and Cross Section Data. *Econometrica* 1978, *46*, 69-85.
9. YU, H. The EU ETS and Firm Profits: An Ex-post Analysis for Swedish Energy Firms. *Department of Economics, Uppsala University* 2011.
10. SIJM, J.; NEUHOFF, K.; CHEN, Y. CO2 cost pass through and windfall profits in the power sector. *Climate Policy* 2006, *6*, p. 49–72.
11. GEROSKI, P. A.; LAZAROVA, S.; URGA, G.; WALTERS, C. F. Are differences in firm size transitory or permanent? *Journal of Applied Econometrics* 2003, p. 47–59.
12. GODDARD, J.; TAVAKOLI, M.; WILSON, J. O. S. Sources of variation in firm profitability and growth. *Journal of Business Research* 2009, *62*, p. 495–508.
13. VERBRUGGEN, A. Performance evaluation of renewable energy support policies, applied on Flanders' tradable certificates system. *Energy Policy* 2009, *37*, p. 1385–1394.
14. BERGEK, A.; JACOBSSON, S. Are tradable green certificates a cost-efficient policy driving technical change or a rent-generating machine? Lessons from Sweden 2003–2008. *Energy Policy* 2010, *38*, p. 1255–1271.
15. CORY, K.; COUTURE, T.; KREYCIK, C. Feed-in Tariff Policy: Design, Implementation, and RPS Policy Interactions. *National Renewable Energy Laboratory Technical Report NREL/TP-6A2-45549* 2009.
16. MENANTEAU, P.; FINON, D.; LAMY, M.-L. Prices versus quantities: choosing policies for promoting the development of renewable energy. *Energy Policy* 2003, *31*, 799-812.
17. del RÍO, P.; GUAL, M. The promotion of green electricity in Europe: present and future. *European Environment* 2004, *14*, p. 219–234.
18. AGNOLUCCI, P. The effect of financial constraints, technological progress and long-term contracts on tradable green certificates. *Energy Policy* 2007, *35*, 3347-3359.
19. SIJM, J.P.M.; HERS, S.J.; LISE, W.; WETZELAER, B.J.H.W. The impact of the EU ETS on electricity prices. *Energy research Centre of the Netherlands (ECN)* 2008.

CYSENI 2012, May 24–25, Kaunas, Lithuania
ISSN 1822-7554, www.cyseni.com

ESTIMATION OF POWER SUPPLY INTERRUPTION RELATED COSTS. METHODOLOGY, SURVEY QUESTIONNAIRE AND RECEIVED DATA NORMALIZATION

A. Ļvovs, A. Mutule
Riga Technical University, Faculty of Power and Electrical Engineering
Kronvalda blvd. 1, LV-1010 - Latvia
Phone: (+371) 25970020 (A. Ļvovs), (+371) 67558616 (A. Mutule)
Email: aleksandrs.lvovs@inbox.lv (A. Ļvovs), amutule@edi.lv (A. Mutule)

ABSTRACT

This paper deals with problems related to determination of customer costs of reliability – the total amount of costs related with power supply interruptions (loss of production, overtime costs to personnel (stuff), etc.) and expenses related with activities for diminishing negative effect of power supply interruptions (UPS devices, generators, additional insurance, etc.). The paper gives description of different cost estimation methods based on review and analysis of proposals for customer cost estimation and customer cost estimation surveys from different countries. On the basis of analysis of different customer cost estimation surveys and questionnaires, there is proposed new design of questionnaire for surveys with the aim to use it for performing customer cost evaluation study in the frames of "Government action plan" of Latvian government for year 2012. Problem of survey data normalization is discussed and proposal of appropriate normalisation factors, from authors` point of view, is given.

Results of the work presented in the paper could be used when:
- trying to get knowledge of customer valuation of reliability;
- developing financial incentives for performance-based regulation of utilities (system operators);
- developing guaranteed reliability standards;
- etc.

Keywords: customer survey, interruption costs, normalization, reliability improvement worth

1. INTRODUCTION

Nowadays electrical energy is of vital importance to modern society. Power systems that provide electricity to customers have three main tasks – provide electrical energy: 1) in required amounts; 2) in as economical way as possible; 3) with needed quality level. Reliability of power supply has an effect on all the main tasks of power system as soon as power supply interruptions: 1) diminish amount of electrical energy provided to customers; 2) create additional expenses to power supplying companies and customers; 3) worsen quality of power supply.

Taking into account causes of power supply interruptions (nature impact; animals actions that caused fault; equipment faults; etc.) and probabilistic nature of outages, reliability level never can reach absolute value – 100%, and due to that power system will probably never be able to operate without power supply interruptions and provide as much electrical energy as needed. In contradistinction to aforesaid, the last two tasks of power system can be solved from reliability point of view. Reliability level that ensures the best fulfilment of the second and the third tasks of power system is determined by total costs of reliability that, in their turn, are formed by customer costs and utility costs of reliability.

According to [16] there are several terms closely related with reliability:

- Dependability – The collective term used to describe the availability performance and its influencing factors: reliability performance, maintainability performance and maintenance support performance.

- Availability (performance) – The ability of an item to be in a state to perform required function under given conditions at a given instant of time or over a given time interval, assuming that the required external resources are provided. This ability depends on the combined aspects of reliability performance, the maintainability performance and the maintenance support performance.
- Reliability (performance) – The ability of an item to perform a required function under given conditions for a given time interval.

Other term that is used quite frequently is security of power supply. Security of power supply nowadays in some aspects is dependant on political decisions and on diversification of sources of primary energy sources, but not with power system`s ability to perform its functions.

Taking into account that only term “reliability” reflects purely power system`s capabilities under given conditions for a given time interval (without any external activities like maintenance, fuel availability, etc.), it was assumed that usage of reliability of power supply could be the better way to characterize efficiency of power system, comparing to dependability, availability and other terms.

To ensure optimal power supply reliability, that would increase electrical power system’s efficiency, it is important to find optimum between network reliability improvement costs (Reliability improvement costs of utility) and customer costs (expenses) dependant on reliability, that actually represent reliability improvement worth (see Fig. 1).

To ensure optimal reliability level, performance based regulation of network operators is needed. Information of customer power supply interruption costs is essential for performance based regulation, as well as for such activities like [1]:

- Making policies, standards and criteria for quality of supply;
- Monitoring quality of supply;
- Planning of power systems;
- Operation and maintenance.

To evaluate customer costs different methods can be used. Each of the methods has its advantages and disadvantages. The goal of the work described in the paper was to analyse customer costs evaluation methods related to power supply reliability and on the basis of the analysis, propose design of questionnaire for surveys. In the paper, in addition to aforesaid, there are also discussed merits of usage of different data (customer costs of reliability) normalization factors like annual energy consumption, peak load, energy not supplied, etc.

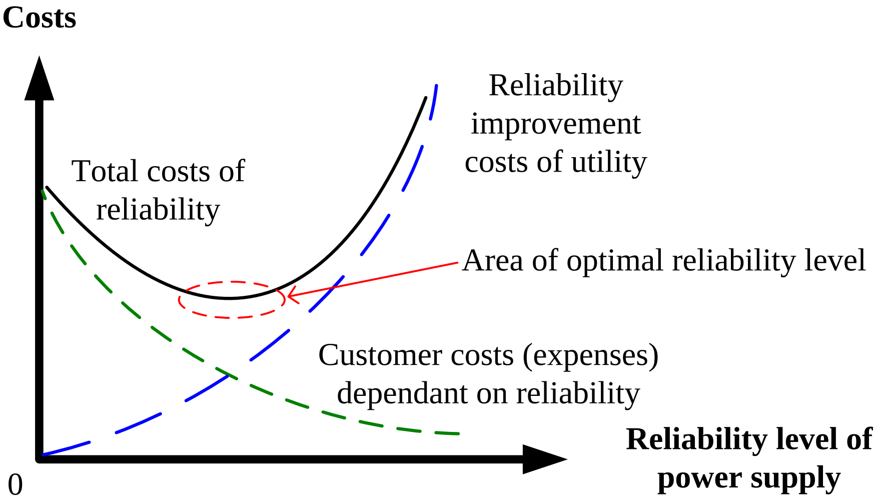

Fig. 1. Utility, customer and total costs depending on reliability level of power supply

2. METHODOLOGIES FOR POWER SUPPLY INTERRUPTION RELATED COSTS ESTIMATION

Definition of customer groups

Performing cost estimation, usually it is need to dealing with different types of customers – different customer sectors, because usually customers from different sectors are influenced in very different way by power supply interruption with the same characteristics. When performing cost evaluation, each sector should be evaluated by adopted approach. Taking into account some practical examples of cost assessment, e.g. [2–4], etc., customers of electrical field can be grouped as follows:

- Residential sector (households);
- Commercial and public services sector;
- Industry sector (excluding „large customers");
- Large customers;
- Infrastructure (transport) sector;
- Agriculture.

For bigger detalisation and more accurate cost assessment, customer sectors can be split in subsectors according to some existing official classification, e.g. the statistical classification of economic activities NACE Revision 2 (applied in EU) [5] or The Standard Industrial Classification Codes (applied in the USA) [6]. Usage of information about subsectors can be useful for evaluation of possible costs of some specific subsector in scale of whole country or region.

2.2. Types of power supply interruption related costs

Power supply interruption related costs in common situation should represent total socio-economic costs of customers. Bigger part of socio-economic costs is formed by individual customer costs. Other (smaller) part is costs of the rest of society. Both types of costs have monetary and non-monetary, as well as direct or indirect costs [2].

Individual customer costs

This type of costs is representing costs of customer that is directly affected by power supply interruption. These costs can be both monetary and non-monetary.

Costs of the rest of society

This type of costs describes costs such costs that occur to other customers that are influenced by interruption through customer that is directly affected by power supply interruption (affected customer). Among these customers there can be suppliers, clients, as well as producers of by-products of affected customer. Also these costs can be both monetary and non-monetary.

Non-monetary costs

Non-monetary costs usually are applicable to household sector. These „costs" (if they can be called so) are related with inconvenience of clients that should change their plans because of inability to perform previously planned works. In some cases power supply interruptions can cause fear and health problems.

Monetary costs

These costs can be evaluated relatively easy (at least in theory). Biggest part of performed researches concentrates at this type of costs. Such costs are more common for sector of services and industry, including transportation and agriculture, but less common for residential sector. Monetary costs consist of costs related to:

- damaged products;
- additional costs for production of products that were not produced due planned time;
- damage of equipment;
- payment of penalties;
- etc.

2.3.Power supply interruption related cost estimation methods

Nowadays there are developed and used a lot of methods for estimation customer cost related to reliability of power supply. Some of them are presented in [2, 4, 7, 10]. All power supply interruption related cost estimation methods can be grouped as shown in figure 2.

All the methods have their own positive and negative sides. Further there is given short description of methods.

2.3.1. Direct worth method

This method is used to evaluate monetary costs of customers that occurred or could occur due to power supply interruption. Usually, using this method, customer is asked to answer questions about different power supply interruption scenarios. Advantage of the method is that direct costs are received exactly from customers that are the best person who knows his costs due to interruption. Disadvantage of the method is that it can evaluate only monetary costs. Also, answering questions used in this method asks high competence of respondent and can take a lot of time. There are also possible so called "strategic responses" that are tended to overestimate costs.

Direct worth method is best suitable for services and industrial sectors.

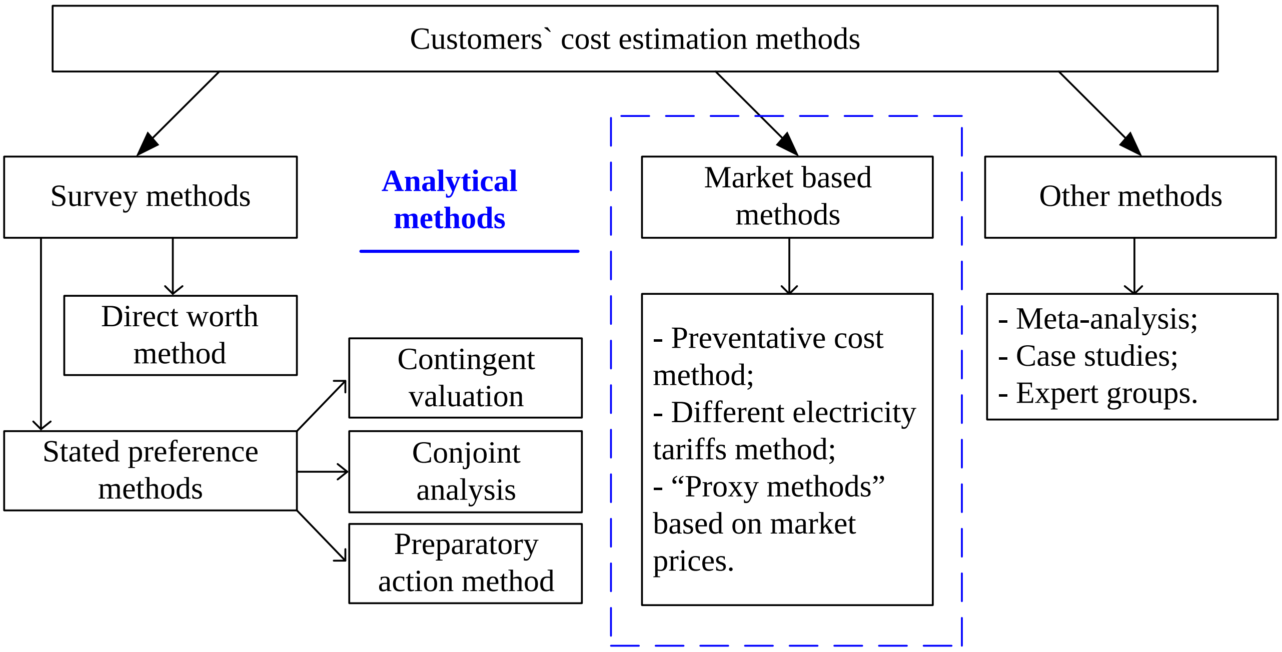

Fig. 2. Classification of customers` costs estimation methods

2.3.2. Contingent valuation method

The method deals with such terms as "willingness to pay" (further in text – WTP) and "willingness to accept" (further in text – WTA). Using the method respondent is asked to answer some questions about the amount of money he would agree to pay for increasing network reliability or how big compensation he would accept in case if reliability of network will worsen. Advantage of the method is that it allows to receive information about both monetary and non-monetary costs, as well the fact that usually questionnaires of the method include only few questions about costs and due to that responding becomes easier comparing to the Direct worth method. As disadvantage there can be mentioned possibility to receive "strategic responses" and "protest responses", when customer indicated high value of willingness to accept and at the same time is has no willingness to pay for reliability improvement. In ideal case WTP and WTA values should be equal.

The method is usually used with the Direct worth method to supplement each other. In such case it is possible to receive more accurate data.

2.3.3. Conjoint analysis method

In case of usage of the method, respondent is receiving a number of possible power supply interruption scenarios that also include some amount of compensation (or increase of electricity bill) in respect of scenario. Task of customer is to rank all scenarios starting with the best scenario for him and ending with the worst scenario. In such case we get information about costs of customer in indirect form. Advantage of the method is in possibility to evaluate non-monetary costs. It is also easier for respondent to rank scenarios rather than indicate monetary costs in WTP/WTA method and this positively affects response rate. In case of the method it is harder to give "strategic response". As disadvantages there should be mentioned complicity of received data processing to monetary values; there also can be problems with creating the right scenarios that correspond to customer. There is also risk that customers will rank proposed scenarios in way that doesn't correlate with real interruption costs.

2.3.4. Preparatory action method

When using the Preparatory action method, respondent is asked to choose from given list some hypothetical preparatory actions that he would choose in case if he would know about power supply interruption. Each of preparatory actions is given costs. As action there could be mentioned purchase of candles or renting diesel generator. Practical examples with real action prices and little amount of time needed for filling questionnaire are advantages of the method. Despite the advantages, the method has one big drawback – preparation of questionnaire could be extremely complex process. Taking into account huge amount of possible preparatory actions it is not possible to include all actions in questionnaire and thus provide all customers with appropriate questionnaires.

This method is rarely used as stand-alone or basic method for cost evaluation, but it could be used as supplementary method to some other methods.

Other methods are not so precise and have bigger drawbacks comparing to previously described methods, mainly because of quite unrealistic assumptions like assumption in "Proxy methods" based on market principles – customer costs of reliability are fully reflected in changes of costs of shares at stock just before and after power supply interruption. Due to the fact and lack of space in the paper, description of the rest methods is not given.

Analysing different questionnaires used in practice, as well as questionnaire proposals, e.g. given in [1], [4] and [7], authors of the paper found out that Direct worth and Contingent valuation methods can be effectively combined to supplement and improve each other. This is the reason of their worldwide popularity among other methods in recent time (see figure 3).

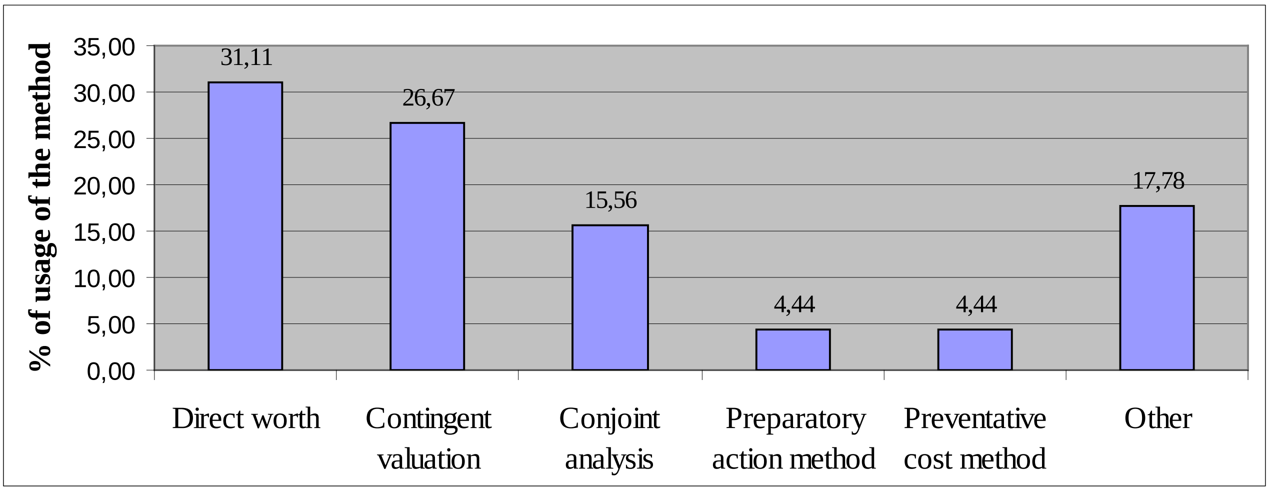

Fig. 3. Percentage of methods used in recent cost estimation studies

Taking into account the fact that Direct worth and Contingent valuation methods, comparing to other methods, could give the most precise data for evaluation of interruption costs, it is reasonable to analyse data needed for cost evaluation and data processing techniques to develop such questionnaire that would be both easily preparable, fillable and at the same time would provide researcher with as much information as possible. Taking into account that among analysed existing and proposed questionnaires, prepared by other researchers, concentrated on some specific topics and in most cases covered only few parameters, authors of the paper decided to develop their own questionnaire to use it in future for customer interruption cost estimation research.

Further is given insight of information needed for power supply interruption cost analysis.

3. COST ESTIMATION USING DIRECT WORTH AND WTP&WTA METHODS

Each of cost estimation should start with definition of targets of estimation. Cost estimation target could be development of reliability standard or just evaluation of interruption cost estimation of some group of customers, e.g. industry sector. Budget of cost estimation undertaking has significant effect on estimation process. After definition of targets and possible scale of survey, normalization factor and other information needed for data processing should be defined before creation of questionnaire.

Normalization factors

Cost estimation survey results are represented by data about costs in monetary units for respective power supply interruption with given duration and occurrence time.

Normalization factors are used to make it possible to use cost estimation data in other researches, as well as for comparison of results received in different countries, regions, or at different years.

Usually normalization data are related with some technical parameters – load and consumed energy. Mostly used normalization factors are [1], [8 – 10]:

- Annual electricity consumption [kWh];
- Average load = annual electricity consumption/8760 [kWh/h = kW];
- Peak load = the average load in the hour of the year with highest consumption [kWh/h = kW];

- Interrupted load at reference time, i.e. the hourly load at the reference time of the survey
- [kWh/h = kW];
- Energy not supplied, i.e. the estimated energy that would have been supplied if the interruption did not occur (kWh).

Cost normalization is performed using equation (1).

$$C_{N,i}(r,t)=\frac{C_i(r,t)}{N_i(r,t)} \tag{1}$$

where

$C_{N,i}(r,t)$ - Normalized (specific) cost for respondent *i* for an interruption of duration *r* or voltage disturbance occurring at time *t* [€/kWh or kW];

$C_i(r,t)$ - Monetary value of respondent *i* (from the survey) for an interruption of duration *r* or voltage disturbance occurring at time *t* [€];

$N_i(r,t)$ - Normalization factor for respondent *i* in [kWh] or [kW].

Annual electricity consumption and peak load are the most popular normalization factors. Their popularity can be explained by advantage - easy availability of data about annual energy consumption and peak load. Results normalised using such two factors are well suitable for results comparison of different researches. But, unfortunately, when using these normalization factors, received results about interruption costs become unusable for real cost estimation if not provided together with respective information about annual electricity consumption and/or peak load as in [8] and [9]. Unusability of results normalised with such factors can be explained by the fact, that data normalised with the annual consumption or peak load can vary in wide borders depending on load curve.

As example, here can be mentioned two metal processing factories – one with two working shifts, but another with only one shift. In principle these two factories could be quite similar and power supply interruption costs theoretically should be approximately the same. But taking into account that the first factory works two times more than the second one (and respectively has 2 times bigger annual energy consumption), its power supply interruption costs after normalisation with annual energy consumption will be 2 times lower.

Numerical example:

Let’s imagine 2 identical metal processing factories. The only difference is in number of working shifts:

1. The 1st metal processing factory works with one shift.
2. The 2nd metal processing factory works with two shifts

Energy consumption of factory during one shift (8 hours) is 200MWh. Taking into account difference in number of shifts, the 1st factory has annual consumption of 73GWh, but the 2nd one – 146GWh.

In case of power supply interruption with duration of 1 hour, e.g. at 10:00AM, both factories could have the same economical losses, e.g. 500 thous. Eur, as their power consumption, as well as energy not supplied at that moment and during the interruption time is the same.

Using annual energy consumption as normalization factor we receive:

– for the 1st factory: $C_{N,1}(1,10^{00})=\frac{500000}{73000}=6.85$ €/MWh;

– for the 2nd factory: $C_{N,2}(1,10^{00})=\frac{500000}{146000}=3.42$ €/MWh.

From results we can see that factories with the same energy not supplied would be characterised by different costs.

To solve the problem either previously mentioned information about value of normalization factor annual energy consumption (or annual peak power consumption, if comparing short interruption costs) should occur simultaneously with normalised results. Another solution is – normalisation made by using interrupted load at reference time (for interruptions with duration < 3 min.) or energy not supplied (for interruptions with duration > 3 min.) as in [10]. Taking into account that consumers may not know their load curve, standard load curves for appropriate loads can be used. Taking into account that in recent times electricity consumers move to free electricity market and number of digital meters expand, realistic information about load curves of bigger consumers already is not or will not be a problem in near future. This makes interrupted load at reference time and energy not supplied the best normalization factors.

Other information includable in questionnaires

Depending on targets of interruption cost estimation, questionnaire could include some additional questions related to:

- customer's sphere of activities;
- region of location;
- changes of power supply interruption costs depending on interruption occurrence;
- number of experienced planned and unplanned interruptions;
- possibilities of power supply reservation;
- etc.

All these information is needed to ensure possibility of precise interruption cost evaluation. When information about cost changes depending on interruption duration and occurrence time is known so called Customer Damage Function (CDF) can be constructed. Individual CDFs are usually combined into Sector Customer Damage Functions (SCDF) that represents costs of customer sectors. SCDF can be calculated using equation (2) [1].

$$c_{SCDF}(r,t) = \frac{1}{m}\sum_{i=1}^{m} c_{N,i}(r,t) \tag{2}$$

where

$c_{SCDF}(r,t)$ - Sector Customer Damage function (SCDF) for averaged respondent in sector *s* for an interruption of duration *r* or voltage disturbance at time *t* [€/kWh or kW];
m – Number of respondents in sector *s*.

For evaluation of costs for large group of customers from different sectors, e.g. customers of 110/20(10; 6) kV substation or region of country, so called Composite Customer Damage Function (CCDF) is used. To create CCDF, SCDF of substation\`s or region\`s of country is needed. As soon as different sectors like Industry, Commercial sector, etc., have different energy and power consumption, they have different impact on total customer costs in case of power supply interruption. Due to the fact, each sector\`s SCDF should be represented in CCDF proportionally to their energy or power consumption [1, 11]. CCDF is calculated according to equation (3):

$$c_{CCDF}(r,t) = \sum_{s=1}^{S} c_{SCDF}(r,t) \cdot W_S \tag{3}$$

where
W_s – proportion of sector in annual energy consumption (at substation, region or country);
S – number of sectors.

4. CREATION OF QUESTIONNAIRE

On the basis of analysis of some cost survey methodologies [2, 4, 7], as well as cost estimation studies [1, 3, 8 – 10, 12-14], etc., authors of the paper found out differences in information asked from respondents of different sectors.

For Industry and Commercial sectors there is tendency of reliability related cost changes depending on season. Taking into account that representatives of the Industry and Commercial sectors are tended to use additional devices for reservation of power supply or some other possibilities to reduce effect of power supply interruptions (e.g. insurance) expenses for these activities also should be evaluated and further included in cost calculations. Questions about these aspects should be included into questionnaires for Industry and Commercial sectors.

For Household sector, on the other side, economical reliability related costs are not as big as for other sectors and expression of satisfaction of dissatisfaction is more common for this sector. According to [13, 14], for households` satisfaction with power supply reliability typically changes because of number of interruptions rather than to interruption time. However, [12] states that customers are not satisfied with power supply reliability level if during a year they experienced at least 1 interruption with exceeding 8 hours.

Aforesaid means that questionnaires for households and other sectors have different target information that should be gathered during surveys. Target of questionnaires for households is to find satisfactory level of reliability for customers and their willingness to pay for reliability level improvement. Target of questionnaires for other sectors is to gather information about customer costs influenced by power supply interruptions.

Taking into account differences between customers of different sectors, authors of the paper developed questionnaire that contains appropriate questions for outage cost estimation in industry and services sectors. The developed questionnaire is based on Direct Worth and Contingent Valuation methods and is proposed for performing customer cost evaluation study in the frames of "Government action plan" of Latvian government for year 2012 [15]. Using information from questionnaire it is possible to normalize costs data using annual energy consumption and peak power consumption. In such case cost data can be compared with majority of foreign survey results. To normalize data with actual energy not supplied or consumed power, load diagrams of corresponding enterprises have to be used.

At the time of writing the paper, the developed questionnaire had been send to number of companies for approbation and authors of the paper already received a couple of fully filled questionnaires. Questionnaire was send to some companies with a small covering letter that was asking to fill questionnaire attached to e-mail. Some of the companies, who had answered questionnaires, had difficulties with filling information about changes of costs in case if power supply interruption occurs in different seasons, days of week or time of a day. Contacting the companies (who had problems) it finally turned out, that their costs don't vary in wide range depending on occurrence time of interruption and they didn't know what answer would be correct in that case. Such misunderstanding can be easily overpassed by giving an example and better explanation of how questionnaire can be filled.

Developed questionnaire (translated from Latvian to English) is given in appendix to the paper.

5. CONCLUSIONS

In order to receive trustworthy data from survey, questionnaires should be short and easy enough in order to not overload respondent. At the same time they should include questions about all topics that are needed for accurate data processing.

Usability of received data – customer interruption costs – is strongly dependant on normalization factors used. The most suitable normalization factors, that allow both different survey's data comparability and allow further data usability for cost evaluation, are Interrupted load at reference time and Energy not supplied. These normalization factors also don't require publishing additional information about annual energy consumption and/or peak load as in case with other factors.

Questionnaire for evaluation of customer costs related to reliability for Industry and Services sectors was developed by authors of the paper taking into account experience of foreign scientifical organisations. The developed questionnaire is based on Direct Worth and Contingent Valuation methods. Approbation of questionnaire showed that it can be used for cost evaluation as companies involved in approbation process gave correct response and had almost no difficulties with answering.

REFERENCES

1. HOFMANN, M.; SELJESETH H.; VOLDEN G.H.; KJOLLE G.H. *Study on Estimation of Costs due to Electricity Interruptions and Voltage Disturbances*. SINTEF Energi AS ; SINTEF Energy Research, 2010. 146 p.
2. *Guidelines of Good Practice on Estimation of Costs due to Electricity Interruptions and Voltage Disturbances*: CEER, 2010 [referred on the 10th of November in 2011 y.]. Link to the internet http://www.energy-regulators.eu/portal/page/portal/EER_HOME/EER_PUBLICATIONS/CEER_PAPERS/Electricity/2010
3. *Understanding the Cost of Power Interruptions to U.S. Electricity Consumers*: Ernest Orlando Lawrence Berkeley National Laboratory; University of California Berkeley, 2004 [referred on the 15th of november in 2011 y.]. Link to the internet http://certs.lbl.gov/pdf/55718.pdf
4. *Assessment of the value of customer reliability*: CRA International, 2008 2004 [referred on the 15th of september in 2011 y.]. Link to the internet http://www.aemo.com.au/planning/0409-0002.pdf
5. REGULATION (EC) No 1893/2006 OF THE EUROPEAN PARLIAMENT AND OF THE COUNCIL of 20 December 2006 establishing the statistical classification of economic activities NACE Revision 2 and amending Council Regulation (EEC) No 3037/90 as well as certain EC Regulations on specific statistical domains. [referred on the 28th of February in 2012 y.]. Link to the internet http://eur-lex.europa.eu/LexUriServ/LexUriServ.do?uri=OJ:L:2006:393:0001:0039:EN:PDF
6. *Standard Industrial Classification (SIC) Code List*: U.S. Securities and Exchange Comission; Division of Corporation Finance. [referred on the 28th of February in 2012 y.]. Link to the internet http://www.sec.gov/info/edgar/siccodes.htm
7. SILVAST A., HEINE P., LEHTONEN M., KIVIKKO K., MÄKINEN A., JÄRVENTAUSTA P. Sähkönjakelun keskeytyksestä aiheutuva haitta (in Finnish language). Finland: Helsinki University of Technology and Tampere University of Technology, 2005. 176 p.
8. CHOWDHURY, A.A., MIELNIK, T.C., LAWION, L.E., SULLIVAN, M.J., KATZ, A. Reliability worth assessment in electric power delivery systems. *Power Engineering Society General Meeting (IEEE)*, 2004, Vol. 1, p. 654–660.

9. WACKER, G., BILLINTON, R. Customer cost of electric service interruptions. *Proceedings of the IEEE*, 1989, Vol. 77, issue: 6. p. 919–930.
10. TIEDEMANN, K.H. Estimating the value of reliability for business customers. PMAPS 2004. Proceedings of the 8th International Conference on Probabilistic Methods Applied to Power Systems. Iowa: Iowa State University. 2004 September 13–16.
11. LVOV, A., MUTULE, A. Estimation of reliability related costs and their affect on choosing substation's high voltage switchgear scheme. IYCE 2011. Proceedings of the 2011 3rd International Youth Conference on Energetics. Leiria: INESC Coimbra and Polytechnic Institute of Leiria. 2011 July 7-9.
12. YANG, Y., BOLLEN, M.H.J. Considering a Customer Dissatisfaction Index in the Reliability of Distribution Networks with Distributed Energy Resources. PMAPS 2008. Proceedings of the 10th International Conference on Probabilistic Methods Applied to Power Systems. Rincon: The Electric Power Engineering Group, University of Puerto Rico – Mayagüez. 2008 May 25-29.
13. DAY, W.R., REESE, A.B. Service interruptions: the customers' views. CIRED. Proceedings of 12th International Conference on Electricity Distribution. Birmingham: International Convention Centre (ICC). 1993 May 17-21.
14. SULLIVAN, M.J., NOLAND SUDDETH, B., VARDELL, T. AND VOJDANI, A. Interruption costs, customer satisfaction and expectations for service reliability. *IEEE Transactions on Power Systems*, 1996, Vol. 11, issue: 2. p. 989–995.
15. Web page of The Cabinet of Ministers of the Republic of Latvia. "Valdības rīcības plāns" (in Latvian. Title in English - "Government action plan"). [referred on the 10th of february in 2012 y.]. Link to the internet: http://www.mk.gov.lv/lv/mk/darbibu-reglamentejosie-dokumenti/ricibas-plans-dv/.
16. LVS IEC 50-191:1990, Starptautiskā elektrotehnikas vārdnīca, 191. nodaļa: Drošums un pakalpojumu kvalitāte (IEC 50-191:1990, *International Electrotechnical Vocabulary, Chapter 191: Dependability and quality of service)*. Rīga: Latvijas Nacionālais standartizācijas un metroloģijas centrs, 1998. 63 p.

APPENDIX

CUSTOMER INTERRUPTION COST ESTIMATION QUESTIONNAIRE

	Region of location	
1	Please, identify in witch region is located your company? (Regions of Latvia are given as example)	
	Vidzeme	☐
	Latgale	☐
	Kurzeme	☐
	Zemgale	☐
2	Please, identify territorial belonging of your company?	
	Rural territory	☐
	Suburban territory	☐
	Urban (city) territory	☐

	Information about company's sphere of activity					
3	Please, provide a code from statistical classification of economic activities „NACE Revision 2" (given in appendix) that corresponds to your company's sphere of activity. In case if you can't identify appropriate code, please choose one of the spheres provided below.					
	Classification code of economical activity:					
	Spheres of activity					
	AGRICULTURE, FORESTRY AND FISHING	☐	TRANSPORTATION AND STORAGE	☐	PUBLIC ADMINISTRATION AND DEFENCE;COMPULSORY SOCIAL SECURITY	☐
	MINING AND QUARRYING	☐	ACCOMMODATION AND FOOD SERVICE ACTIVITIES	☐	EDUCATION	☐
	MANUFACTURING	☐	INFORMATION AND COMMUNICATION	☐	HUMAN HEALTH AND SOCIAL WORK ACTIVITIES	☐
	ELECTRICITY, GAS, STEAM AND AIR CONDITIONING SUPPLY	☐	FINANCIAL AND INSURANCE ACTIVITIES	☐	ARTS, ENTERTAINMENT AND RECREATION	☐
	WATER SUPPLY; SEWERAGE, WASTE MANAGEMENT AND REMEDIATION ACTIVITIES	☐	REAL ESTATE ACTIVITIES	☐	OTHER SERVICE ACTIVITIES	☐
	CONSTRUCTION	☐	PROFESSIONAL, SCIENTIFIC AND TECHNICAL ACTIVITIES	☐	ACTIVITIES OF HOUSEHOLDS AS EMPLOYERS; UNDIFFERENTIATED GOODS- AND SERVICES-PRODUCING ACTIVITIES OF HOUSEHOLDS FOR OWN USE	☐
	WHOLESALE AND RETAIL TRADE; REPAIR OF MOTOR VEHICLES AND MOTORCYCLES	☐	ADMINISTRATIVE AND SUPPORT SERVICE ACTIVITIES	☐	ACTIVITIES OF EXTRATERRITORIAL ORGANISATIONS AND BODIES	☐

	Technical information		
4	Please, specify maximal allowed consumption (kW) allowed for your company, as well as nominal current of fuse/circuit breaker (A) installed at feeding power line, nominal voltage (kV) and number of phases.		
	Maximal allowed consumption (kW)		kW
	Nominal current of fuse/circuit breaker installed at feeding powerline (A)		A
	Nominal voltage (kV)		kV
	Number of phases		

5	Please, specify annual electrical energy consumption (kWh) of your company, e.g. for the last calendar year.	kWh
	Further seven questions are related with sources of reserved power supply (generators, UPS). This equipment is used to serve electricity during outages in power system.	
6	Does your company have any device for reservation of power supply? (In case of negative answer proceed to question Nr.10)	
	Yes	☐
	No	☐
7	What type of reservation device does your company have?	
	Generator	☐
	UPS (Uninterruptible power supply)	☐
	Other. *Please specify*	☐
8	How big power reserve does your device provide?	
	Provides 100% reserve	☐
	Provides 50% reserve	☐
	Provides 25% reserve	☐
	Ensures work of personal computers	☐
	Ensures lighting	☐
9	Please, specify capital costs (price) of device for reservation of power supply.	Eur
10	Have power supply interruptions during last year influenced your decision to buy or to think about buying reserve power supply equipment?	
	Yes	☐
	No	☐
11	Do you use some other possibilities to reduce negative economical effect of power supply interruptions, e.g. insurance?	
	Yes	☐
	No	☐
12	In case if your company uses device for reservation of power supply or some other possibilities to reduce effect of power supply interruptions (e.g. insurance), please specify their annual costs.	Ls
	Electricity consumers experience planned and unplanned power supply interruptions. Unplanned interruptions are related with network faults, but planned interruptions occur due to maintenance of network or other activities, e.g. power meter change. Interruptions have variable durations – from some seconds to several hours.	
13	How much unplanned power supply interruptions has experienced you company during last year?	
	No one	☐
	1	☐
	2-5	☐
	6-10	☐
	>10	☐
	Don’t know	☐
14	How much planned power supply interruptions has experienced you company during last year?	
	No one	☐
	1	☐
	2-4	☐
	>4	☐
	Don’t know	☐
15	Are you satisfied with existing power supply reliability level?	
	Yes	☐
	No	☐

Estimation of approximate power supply interruption cost

Power supply interruptions create extra expenses to electricity users. Additional costs are related with costs of spoiled production; cost of activities (overtime work, etc.) that are tended to provide unserved service to your company's clients what they haven't received due to interruption at your company; damage of equipment and raw materials; penalties for unserved services; etc.

16 **Let's assume** that during one working day in autumn at 10:00AM occurs power supply interruption. In table given below, please specify costs that your company would have in case if interruption has different durations.
If it is possible, please, specify time (in hours) needed for restoration of work process at your company after power supply interruption with respective duration.

	Duration of **unplanned** interruption						
	1 minute	20 minutes	1 hour	4 hours	8 hours	12 hours	24 hours
Costs **[Eur/per interruption]**	▨	▨	▨	▨	▨	▨	▨
Time needed for work restoration **[hours]**	▨	▨	▨	▨	▨	▨	▨

17 **Let's assume** that unplanned power supply with duration of 4 hours will occur in different season, day of week or will starta t different time.
In table that given below, please specify by how much percent (checking only one appropriate box in each row) will change power supply interruption costs in other cases comparing to the case given at question Nr.16.
Filling the information about season assume, that interruption occurs in working day at 10:00AM. Filling information about day of the week assume, that interruption occurs in autumn and at 10:00AM. Filling information about time of the day assume that interruption occurs in autumn in working day.
*** take into account that costs of power supply interruption that occurs in autumns in working day at 10:00 is already checked (in rows with orange) and must not be changed.

		Changes of costs due to unplanned interruption lasting 4 hrs.								
		Costs would decrease by					Costs would increase by			
		-100%	-75%	-50%	-25%	0%	+25%	+50%	+75%	+100%
season	Winter	☐	☐	☐	☐	☐	☐	☐	☐	☐
	Spring	☐	☐	☐	☐	☐	☐	☐	☐	☐
	Summer	☐	☐	☐	☐	☐	☐	☐	☐	☐
	Autums					X				

Day of the week	Working day					X				
	Saturday	☐	☐	☐	☐	☐	☐	☐	☐	☐
	Sunday/other holiday	☐	☐	☐	☐	☐	☐	☐	☐	☐

Time of day	00:00-08:00	☐	☐	☐	☐	☐	☐	☐	☐	☐
	08:00-12:00					X				
	12:00-16:00	☐	☐	☐	☐	☐	☐	☐	☐	☐
	16:00-20:00	☐	☐	☐	☐	☐	☐	☐	☐	☐
	20:00-24:00	☐	☐	☐	☐	☐	☐	☐	☐	☐

18 **Let's assume** that your power supplying company is making some maintenance works that require planned interruption. Assume that your company was informed about interruption well in advance. In table given below, please specify costs that your company would have in case if interruption has different durations.

If it is possible, please, specify time (in hours) needed for restoration of work process at your company after power supply interruption with respective duration.

	Duration of **planned** interruption			
	20 minutes	1 hour	4 hours	8 hours
Costs **[Eur/per interruption]**				
Time needed for work restoration **[hours]**				

19 Imagine that your company normally has one unplanned power supply interruption per year that could occur at any time and lasts for 1 hour.

Let's assume that power supplying company tries to decrease costs of its clients and offers compensation for occurred interruption.

How big amount of money your company would like to receive as compensation for interruption, if unplanned interruption would last one hour longer – for two hours?

Eur

20 Imagine that your power supplying company tries to decrease costs of its clients due to power supply interruptions and wants to increase network reliability by making bigger investments in the existing network

How big amount of money (totally for the whole next year) your company would like to pay as an extra payment for electricity if power supply interruption duration in the next year will decrease by 1 hour?

Eur

Comments, wishes

Thank you for cooperation!

CYSENI 2012, May 24–25, Kaunas, Lithuania
ISSN 1822-7554, www.cyseni.com

OSEMOSYS MODEL APPLICATION FOR DISTURBED ENERGY SYSTEM MODELLING

L. Martišauskas
Lithuanian Energy Institute
Laboratory of Nuclear Installation Safety
Breslaujos str. 3, LT-44403 Kaunas, Lithuania
Phone +370 37 401938
Email: linasm@mail.lei.lt

ABSTRACT

Providing a secure supply of energy comprises two areas: long-term security or resource availability and short-term security – associated with supply disruptions of the primary fuel or the electricity generated. The nation's energy system is a complex, interconnected network in which a disruption in one part of the infrastructure can easily cause disruptions elsewhere in the system. Energy security refers to a resilient energy system. If the energy system is affected with the disturbances, it becomes vulnerable. Analysis of the disturbed energy system helps to identify the weaknesses of the system‘s elements and where it should be strengthened.

The paper presents an open source energy modelling system OSeMOSYS, which is a full-fledged systems optimization model for long-run energy planning, and its application for modelling energy disturbances of the energy system. The model is constructed in terms of sets, parameters, variables, equations, and an objective function. Since model is being developed in a series of component blocks of functionality, author updated and modified model to suit the needs of the particular analysis – disturbed energy system modelling. Application was done by developing new model block designed for the energy disturbances. The paper briefly introduces original OSeMOSYS model but most attention is paid to the new model block and its application to the original model. An example application is made to explain selected functional aspects of the model. The reference energy system is modelled with the set of energy disturbances. The main modelling results of the disturbed reference energy system are presented to highlight the benefits of the developed model.

Keywords: energy security, energy disturbances, energy system modelling

1. INTRODUCTION

Providing a secure supply of energy comprises two areas: long-term security or resource availability and short-term security – associated with supply disruptions of the primary fuel or the electricity generated. Energy security refers to a resilient energy system. This resilient system would be capable of withstanding threats through a combination of active, direct security measures – such as surveillance and guards – and passive or more indirect measures – such as redundancy, duplication of critical equipment, diversity in fuel, other sources of energy, and reliance on less vulnerable infrastructure [1]. If the energy system is affected with the disturbances, it becomes vulnerable. The analysis of the disturbed energy system helps to identify the weaknesses of the system‘s elements and where it should be strengthened.

Modelling of energy disturbances or disturbed energy system is an integral part of energy security analysis. This requires the use of energy system optimization tools. The assessment and pursuit of energy security should be seen in the most optimal variant of the existing energy system infrastructure which can be changed as needed by optimizing energy system (e.g. constructing new power plants). Then comparing energy development scenarios will be determined which is more secure in terms of energy security, but it will not necessarily be with the lowest cost. Most of the energy system optimization tools are designed more for separate scenario analysis. Increasing number of such scenarios makes simulation complicated and time-consuming. Such available tools are not suitable dealing with wide range optimization problems in many model runs, especially stochastic. Mentioned tools are purely deterministic but the energy disturbances have stochastic nature and there is need to use the probabilistic methods. For this goal an open source tools come useful, where the user can change them according to the needs by creating new modules or additional codes. The open source tool BALMOREL [2] is a model for analysing the electricity and combined heat and power sectors in the international perspective, but it is intended for individual scenario analysis modelling scenarios separately and there is no possibility to adapt the model for many random scenario runs. Another known for author an open source tool is OSeMOSYS (Open Source Energy Modeling System) [3, 4]. This model can be freely applied in accordance with user needs – in our case – modelling set of many random disturbance scenarios. The user is able to create individual blocks and add them to a common model. It is one of the advantages of the model, compared to BALMOREL, MESSAGE or other modelling tools. Another advantage is that the model can be modelled as many runs as is needed for the particular analysis. Individual run of each scenario is possible as well. Model developers define such model advantages as **S**imple, powerful and transparent toolkit with **O**pen, well documented code to produce a **F**ree optimization energy model that is **T**ransportable to other platforms [4]. Other advantages of the model are that OSeMOSYS is a fully fledged energy systems optimisation model, with no associated upfront financial requirements to extend the availability of energy modelling further to the communities of students, business analysts, government specialists, and developing country energy researchers [4].

OSeMOSYS model and its application for disturbed energy system modelling are described in the paper further. The paper focuses on the methodology development rather than on the results of calculations.

2. OSEMOSYS MODEL DESCRIPTION

2.1. Linear programming

Linear programming is used for optimized performance modelling of disturbed energy system. Linear programming or optimization in general is a technique used for determining the maximum or minimum of a linear function of non-negative variables subject to constraints expressed as linear equalities or inequalities. Mathematically, this problem in general is formulated as [5]:

Minimize (or maximize) function $z = c_1x_1 + c_2x_2 + \ldots + c_nx_n + c_0$, subject to linear constraints:

$$\begin{aligned} &L_1 \le a_{11}x_1 + a_{12}x_2 + \ldots + a_{1n}x_n \le U_1, \\ &L_2 \le a_{21}x_1 + a_{22}x_2 + \ldots + a_{2n}x_n \le U_2, \\ &\vdots \\ &L_m \le a_{m1}x_1 + a_{m2}x_2 + \ldots + a_{mn}x_n \le U_m, \end{aligned}$$

and bounds of variables:

$$\begin{aligned} &l_1 \le x_1 \le u_1, \\ &l_2 \le x_2 \le u_2, \\ &\vdots \\ &l_n \le x_n \le u_n, \end{aligned}$$

where $x_1,x_2,\ldots,x_n$ are variables; z is the objective function; $c_1,c_2,\ldots,c_n$ are coefficients of the objective function; c_0 is the constant term of the objective function; $a_{11},a_{12},\ldots,a_{mn}$ are constraint coefficients;

$L_1,L_2,\ldots,L_n$ are lower constraint bounds; $U_1,U_2,\ldots,U_n$ are upper constraint bounds; $l_1,l_2,\ldots,l_n$ are lower bounds of variables; $u_1,u_2,\ldots,u_n$ are upper bounds of variables. Bounds of variables and constraint bounds can be finite as well as infinite. Besides, lower bounds can be equal to corresponding upper bounds.

2.2. Concept

The Open Source Energy Modeling System (OSeMOSYS) is a full-fledged systems optimization model for long-run energy planning. At present, OSeMOSYS replicates some of the important functionality in the current system models such as MARKAL, MESSAGE etc. but its structure is open for change by analysts and potentially requires a less significant learning curve and time commitment to prepare and operate the model [3]. OSeMOSYS model is constructed in terms of sets, parameters, variables, equations (some of which are constraints), and an objective function.
OSeMOSYS is designed to be easily updated and modified to suit the needs of a particular analysis. To provide this capability, the model is being developed in a series of component blocks of functionality. Current original OSeMOSYS model scheme with blocks and additional author's developed energy disturbances block is presented in Fig. 1.

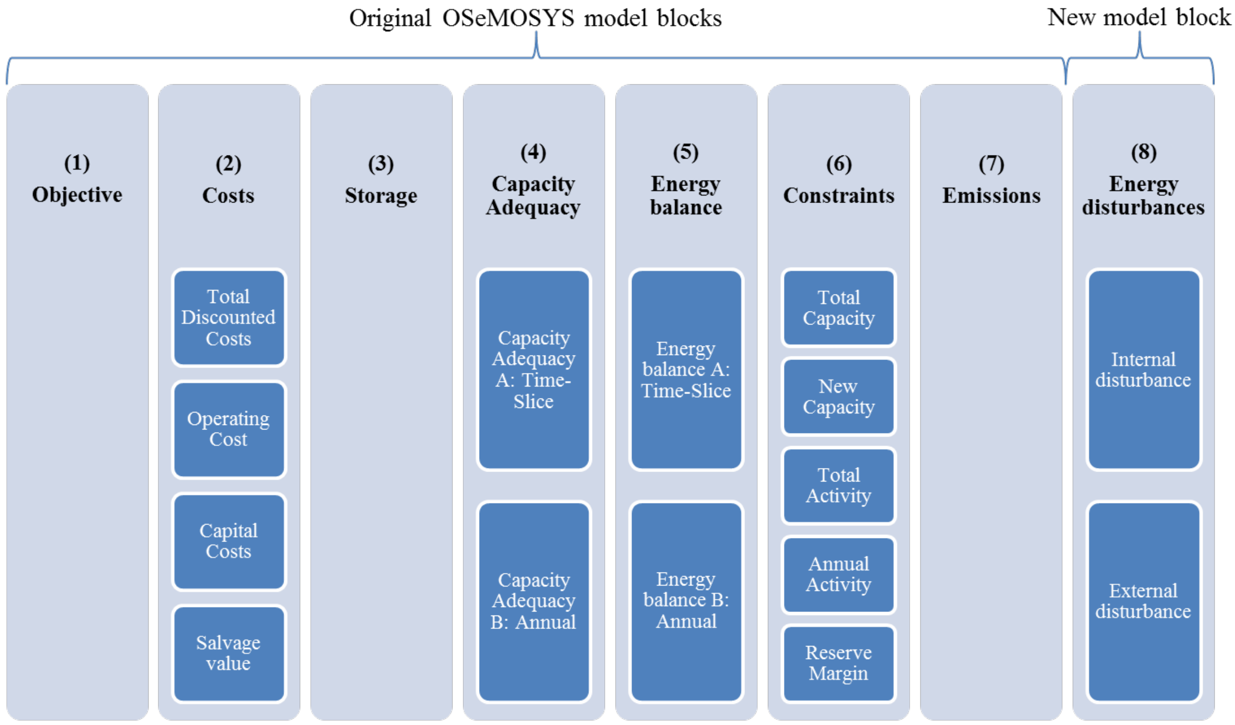

Fig. 1. Original OSeMOSYS model blocks [3] with additional developed block

The collection of the functional component blocks is combined to form a customized model [3]. The objective (block 1 in Fig. 1) in the current version of OSeMOSYS calculates the lowest net present cost of an energy system to meet given demand(s). To meet the objective, there are a number of constraints and specific rules to be followed (blocks 2-7 in Fig. 1). Block of energy disturbances (block 8 in Fig. 1) is developed by the author to analyse disturbed energy system. The main advantage of the model is that it is open source and uses free programming language, solvers, and data interface. The model uses programming language called GNU MathProg (2009) [5]. GNU MathProg is an open source and freely available mathematical programming language intended for describing linear mathematical programming models and represents a subset of the AMPL (2010) language [6]. GNU MathProg is part of the freeware solver called the GNU Linear Programming

Kit (GLPK) [7]. The latest versions of the OSeMOSYS model, GNU MathProg, and GLPK can be freely downloaded from their websites [4-7]. Model validation and verification was performed by other authors [3]. OSeMOSYS model was compared to MARKAL model with the same reference case and obtained results were practically identical.

2.3. Mathematical approach

Only the main aspects of the OSeMOSYS model are described in terms of sets and equations in this section. Model parameters and variables are not described separately but are incorporated into the equations used. All model sets contain entries which are used as indexes to parameters and variables. The sets are summarized in Table 1.

Table 1. Sets of the OSeMOSYS model

Index	***Set***	***Description***
r	*REGION*	Includes the regions modelled.
y	*YEAR*	Contains years over which the model is solved.
t	*TECHNOLOGY*	This is the set of all technologies represented in the application.
l	*TIMESLICE*	Contains the time slices per year. The same number of times slices are carried through for each year.
f	*FUEL*	Contains the fuels used in the model.
m	*MODE_OF_OPERATION*	Contains number of modes in which technologies are operating.
e	*EMISSION*	Includes all pollutant emissions from the operation of a technology.

The model equations are divided into those used to meet capacity and activity constraints, fuel production, capital investment, salvage values, operating costs, and total discounted cost.

The ***objective function*** of the model is to minimize the total discounted cost of an energy system to meet given demand(s) for energy. It is summarized below in equation (1) . $\forall y,t,r$:

$$\text{Minimize } \sum_{y}\sum_{t}\sum_{r} TotalDiscCost(y,t,r), \text{ where} \tag{1}$$

$$\begin{aligned} &TotalDiscCost(y,t,r) = DiscOperatingCost(y,t,r) + DiscCapitalInvestment(y,t,r) + \\ &+ DiscTechnologyEmissionsPenalty(y,t,r) + DiscSalvageValue(y,t,r). \end{aligned} \tag{2}$$

The annual ***operating cost*** of each technology is the sum of a fixed and variable operating cost. The variable cost is a function of the technology's activity level during a time slice. The fixed cost is determined by the total installed capacity of the technology in the system. $\forall y,t,r$:

$$OperatingCost(y,t,r) = FixedOperatingCost(y,t,r) + VariableOperatingCost(y,t,r). \tag{3}$$

Investments are calculated on an annual basis and are assumed to be commissioned and available at the beginning of the year. The capital costs are determined by the level of new capacity invested. $\forall y,t,r$:

$$CapitalInvestment(y,t,r) = CapitalCost(y,t,r) * NewCapacity(y,t,r). \tag{4}$$

A ***salvage value*** is determined, based on the technology’s operational life, its year of investment and discount rate. $\forall\, y,t,r$:

$$SalvageValue(y,t,r) = CapitalCost(y,t,r) * NewCapacity(y,t,r) * \left(1 - \frac{(1+DiscRate(t,r))^{\max(yy)-y+1} - 1}{(1+DiscRate(t,r))^{OperationalLife(t,r)-1}}\right), \qquad (5)$$

where $\max(yy)$ is the last year of modelling period ($yy \in Y$).

The annual ***emissions*** produced for each region are determined by summing the emissions from each technology. If there is a per unit penalty associated with the emission, the penalty per emission for each technology is determined. This is achieved by multiplying the annual emissions from each technology with the per unit emission penalty. $\forall\; y,t,\; r$:

$$\begin{aligned} &AnnualTechnologyEmissionsPenalty(y,t,r) = \sum_e (\sum_m (EmissionActivityRatio(y,t,e,m,r) * \\ &* AverageAnnualTechnologyActivityByMode(y,t,m,r)) * EmissionsPenalty(y,e,r)). \end{aligned} \qquad (6)$$

Then operating cost, capital investment, salvage value, and emissions penalty are discounted to determine a net present value. Discount rate is used for this purpose.

There must be enough ***capacity*** of a particular technology in order to meet its energy use or production requirements. The total capacity of a technology is the sum of new investments made during the modelling period (which have not been retired) plus any residual capacity left over from before the modelling period. The capacity of each technology must be greater than its activity and the activity of each technology is limited by its annual availability. $\forall\, y,t,r$:

$$\begin{aligned} &\sum_l RateOfTotalActivity(y,l,t,r) * YearSplit(y,l) \le TotalCapacityAnnual(y,t,r) * \\ &* CapacityFactor(y,t,r) * AvailabilityFactor(y,t,r) * CapacityToActivityUnit(t,r). \end{aligned} \qquad (7)$$

Fuel ***production*** during each time slice and year must be greater than or equal to its ***use*** (consumption) by technologies plus any exogenous ***demand*** for that fuel. $\forall\, y,\, l,\, f,r$:

$$Production(y,l,f,r) \ge Demand(y,l,f,r) + Use(y,l,f,r). \qquad (8)$$

Summing the production, use, and demand of each fuel for each time-slice during a year gives its annual production, annual use, and annual demand to be met each year. Another energy balance to be satisfied is that the annual production should be larger than or equal to the annual use and annual demand of each fuel.

There can be a maximum or minimum limit on the ***total capacity*** of a particular technology allowed in a particular year and region. $\forall\, y,t,r$:

$$TotalCapacityAnnual(y,t,r) \le TotalAnnualMaxCapacity(y,t,r), \qquad (9)$$

$$TotalCapacityAnnual(y,t,r) \ge TotalAnnualMinCapacity(y,t,r). \qquad (10)$$

Similarly there are constraints for ***new capacity*** investment, ***annual activity*** of a technology, and the ***model period activity*** of a technology or total activity limits.

There should be enough capacity (of specified collection of technologies) to provide a reserve margin (for a specified set of fuels). $\forall\; y,l,r$:

$$\sum_t TotalCapacityAnnual(y,t,r) * ReserveMarginTagTechnology(y,t,r) *$$
$$* CapacityToActivityUnit(t,r) \geq \left(\sum_t RateOfDemand(y,l,f,r) * ReserveMarginTagFuel(y,f,r) \right) * \tag{11}$$
$$* ReserveMargin(y,r).$$

The full OSeMOSYS model mathematical implementation can be found in the paper [3] and website [4].

2.4. The block of energy disturbances

A disturbance to the energy system consists of two parts: the external threats and the weaknesses of the energy supply system. The relevant information about energy supply disturbances can be found in [8, 9]. The disturbances of energy supply that may result from both external and domestic events create a threat for whole energy system. This paper focuses on both types of energy supply disturbances: external and internal. Internal and external disturbances are independent. However, they can occur at the same time.

The OSeMOSYS model consists of a series of functional components or blocks – there is the potential to amend existing ones or create new blocks with added capability. A collection of the functional component blocks combines to form a customized model. Since model is being developed in a series of component blocks of functionality, author updated and modified model to suit the needs of the particular analysis – modelling of the disturbed energy system. This is the author’s contribution to the model. The main objective of the paper is development of new model block designed for the energy disturbances modelling and its methodology application to the original model. The application was done by adding and incorporating this new energy disturbances block to the other blocks in the OSeMOSYS model. To integrate this, new block, new variables, parameters, and sets were added to the code, and all other variable matched existing definitions. The full description of energy disturbances block of the current model is given below.

2.4.1. External disturbance parameters

1) ***Start moment of the external disturbance*** is defined as $EDStart(y,l,r)$. This parameter is a subset of set *YEAR* and $\min(yy) \leq EDStart(y,l,r) \leq \max(yy)$, where $\min(yy)$ and $\max(yy)$ are the first and last year of modelling period respectively ($yy \in Y$). This parameter is important for installation of new technologies.

2) ***Duration of primary energy resources or fuel supply restriction or disruption*** is defined as $EDDuration(y,l,r)$. This parameter has restrictions due to the modelling period:

$$0 < EDDuration(y,l,r) \leq \max(yy) - \min(yy),\ yy \in Y. \tag{12}$$

Duration indicates the continuation of energy supply disturbance. *End moment of the external disturbance* is calculated:

$$EDEnd(y,l,r) = EDStart(y,l,r) + EDDuration(y,l,r),\ EDEnd(y,l,r) \leq \max(yy),\ yy \in Y. \tag{13}$$

3) ***Fuel type or primary energy resource of restricted or disrupted supply*** is defined as $EDFuel(f,r)$. This parameter is a subset of set *FUEL*. If $EDFuel(f,r) = 0$, then external disturbance had not occurred. Primary energy is understandable as energy found in nature that has not been subjected to any conversion or transformation process. It is energy contained in raw fuels as well as other forms of energy received as input to a system.

4) ***Part of primary energy supply deviation from basic supply scenario*** is defined as $EDSupplyChange(y,t,r)$. Potential supply deviation can be from 0 % to 100 % for each type of primary energy compared with the supply amounts of the basic scenario in the appropriate period:

$$0 \le EDSupplyChange(y,t,r) \le 1. \tag{14}$$

This parameter is associated with parameter $TotalTechnologyAnnualActivityUpperLimit(y,t,r)$ and changes its initial value by equation ($\forall\, y, t,\, r$):

$$\begin{aligned} &TotalTechnologyAnnualActivityUpperLimit(y,t,r) = \\ &= TotalTechnologyAnnualActivityUpperLimit(y,t,r) - \\ &- TotalTechnologyAnnualActivityUpperLimit(y,t,r) * EDSupplyChange(y,t,r). \end{aligned} \tag{15}$$

5) ***Fuel or primary energy resources price deviation from projected price in the basic scenario*** is defined as $EDCostChange(y,t,r)$. This parameter is associated with parameter $VariableCost(y,t,m,r)$ and changes the initial value by equation ($\forall\, y, t,\, m,\, r$):

$$VariableCost(y,t,m,r) = VariableCost(y,t,m,r) + VariableCost(y,t,m,r) * EDCostChange(y,t,r). \tag{16}$$

2.4.2. Internal disturbance parameters

1) ***Start moment of the internal disturbance*** is defined as $IDStart(y,l,r)$. This parameter is a subset of set *YEAR* and $\min(yy) \le IDStart(y,l,r) \le \max(yy),\ yy \in Y$.

2) ***Duration of the internal disturbance*** is defined as $IDDuration(y,l,r)$. This parameter has restrictions due to modelling period:

$$0 < IDDuration(y,l,r) \le \max(yy) - \min(yy),\ yy \in Y. \tag{17}$$

End moment of the internal disturbance is calculated:

$$IDEnd(y,l,r) = IDStart(y,l,r) + IDDuration(y,l,r),\ IDEnd(y,l,r) \le \max(yy),\ yy \in Y. \tag{18}$$

3) ***Energy production or transmission technology*** is defined as $IDTechnology(t,r)$. This parameter is a subset of set *TECHNOLOGY*. It includes any element of the energy system which changes energy from one form to another, uses it or produces it. Technology parameter includes energy generation systems (power plants), storages, energy transmission and distribution networks, pipelines, etc.

4) ***Technology availability*** is defined as $IDAvailability(y,t,r)$. Availability parameter shows the maximum share of technology available at the internal disturbance moment. Due to this parameter $IDAvailability(y,t,r)$ has limits: $0 \le IDAvailability(y,t,r) \le 1$. If $IDAvailability(y,t,r) = 0$, then the technology is unavailable at the disturbance moment and if $IDAvailability(y,t,r) = 1$, then technology is operating in the normal conditions without any disruptions or failures. This parameter gives initial values to the parameter $AvailabilityFactor(y,t,r)$ if the internal disturbance has occurred. $\forall\, y, t,\, r$:

$$AvailabilityFactor(y,t,r) = IDAvailability(y,t,r). \tag{19}$$

Annual unsupplied energy amounts in percent are calculated as ($\forall\, y,\, f, r$):

$$UnsuppliedEnergyAnnual(y,f,r)=\frac{ProductionByTechnologyAnnual(y,t,f,r)}{SpecifiedAnnualDemand(y,f,r)}*100. \tag{20}$$

Model period unsupplied energy amounts in percent are calculated as ($\forall\ f,r$):

$$UnsuppliedEnergyModelPeriod(f,r)=\frac{\sum_{y} ProductionByTechnologyAnnual(y,t,f,r)}{\sum_{y} SpecifiedAnnualDemand(y,f,r)}*100. \tag{21}$$

Cost increase of final energy for whole model period is calculated as:

$$CostIncrease=\frac{\sum_{y}\sum_{t}\sum_{r} TotalDiscountedCost(y,t,r)-BasicScenarioCost}{BasicScenarioCost}*100. \tag{22}$$

Basic scenario is modelling energy system without any disturbances. Its cost is defined from the objective function.

3. ENERGY DISTURBANCE SCENARIOS

Both external and internal disturbances are characterized by various parameters. Since values of disturbance parameters are random, it is appropriate to define probability distributions or frequencies of disturbance parameters and to assess distribution parameter values. Available statistical data and expert assessment methods are used to assess statistical frequencies of disturbance parameter values for the case analysed.

Each set of the disturbance parameters corresponds to a different disturbance scenario of the energy system modelling. These disturbance scenarios are modelled with the disturbed energy system. To simulate each scenario, i.e. the impact of disturbance to the energy system, modelling of disturbed energy system functioning and analysis of disturbance impact to the system are needed. For this purpose energy system modelling tools and linear programming method described in the previous sections are used.

Four types of the disturbance scenarios are possible:

1) No disturbances – it is basic scenario, when analysed energy system is modelled without any disturbances and changes.
2) External disturbance has occurred; internal disturbance has not occurred.
3) External disturbance has not occurred; internal disturbance has occurred.
4) Both external and internal disturbance have occurred.

The complete set of disturbances can be generated when probability distributions of disturbance parameters and their characteristics are defined. The set of disturbances is used for the modelling of various disturbed energy system scenarios. External disturbances related to cost increase and supply restriction are analysed in the developed model. We suppose that fuel or energy supply can be restricted to 25%, 50%, 75% and 100% fuel or energy that is needed to provide to consumers. Cost can be increased in the same percent as well:

- Fuel or energy supply restriction (25%, 50%, 75%, 100%);
- Fuel or energy cost increase (25%, 50%, 75%, 100% and more).

Energy system gets in the different states according to the disturbance consequences. These consequences to the energy system are also related to the unsupplied energy and cost increase. The main direct consequences of the energy disturbances are:

- Unsupplied final energy (from 0% to 100%);
- Cost increase of final energy (from 0% to 100% and more).

4. APPLICATION EXAMPLE

4.1. Reference energy system

An example application was made to test selected functional aspects of the model. Kaunas district heating (DH) integrated network is modelled as the reference energy system. The Reference Energy System is a network representation of all technical activities required to supply various forms of energy to end-use activities. Thermal energy to the main Kaunas DH integrated network is supplied from these heating facilities: Kaunas Combined Heat and Power Plant (CHP) (installed capacity 1550 MW and 170 MW for heat and electricity production respectively), Petrasiunai CHP (installed capacity 265.8 MW and 8 MW for heat and electricity production respectively), Pergale boiler house (31.25 MW) and Silkas boiler house (38.3 MW). The modelled Kaunas DH integrated network reference energy system is presented in Fig. 2. Main fuel used is natural gas, reserve fuel – fuel oil. Modelling assumptions are described further.

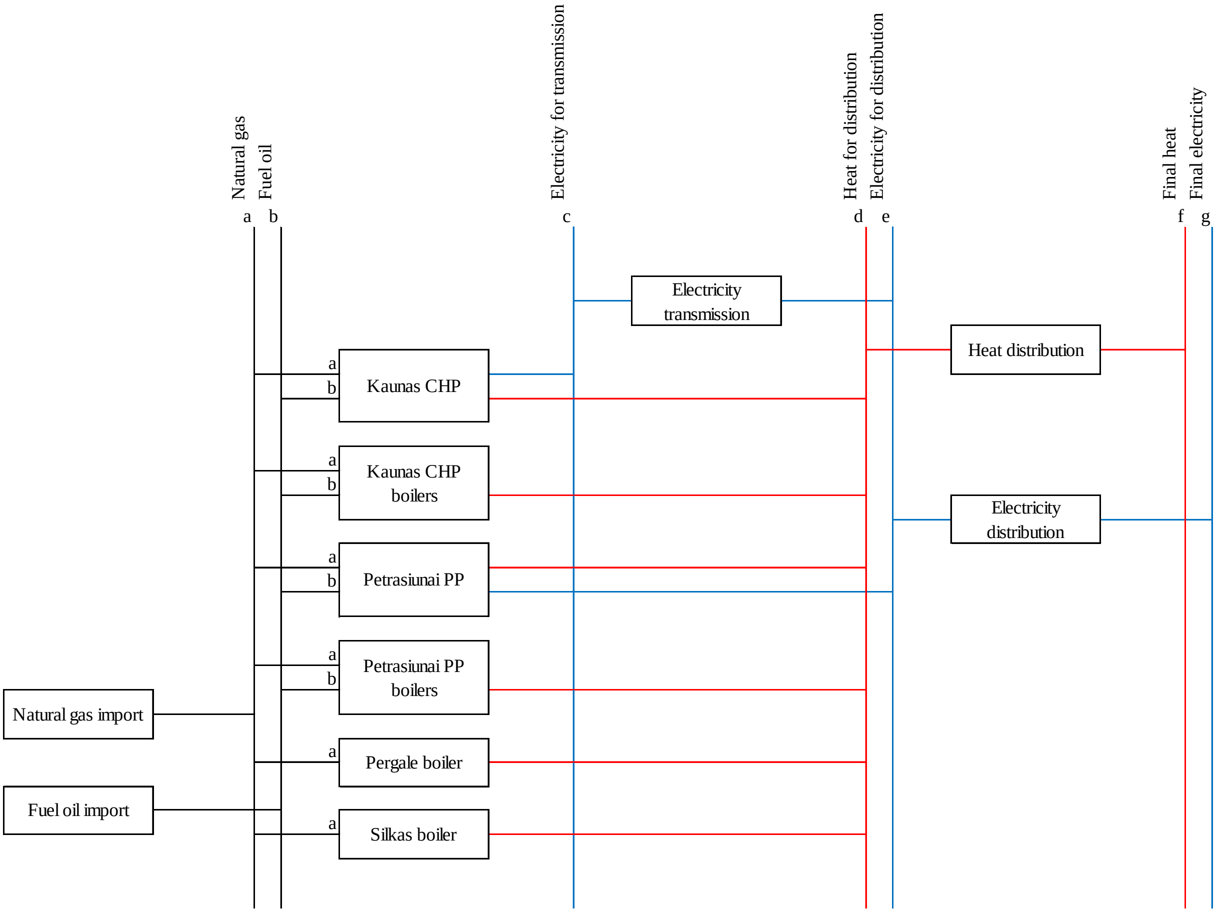

Fig. 2. Reference energy system of Kaunas district heating integrated network

4.2. Modelling assumptions

Modelling assumptions are made using various sources, available statistical data, studies, reports, papers, websites [10-16]. One year period is modelled in analysed case. Average heat demand for Kaunas city is 1559 GWh/year. Maximal and minimal demands are 600 MW and 390 MW respectively for heating season and 132 MW and 80 MW respectively for non-heating season. Fuel oil and natural gas costs used in the modelling are 2011 year average fuel costs (1141 LTL/1000 m^3 of natural gas and 1821 LTL/t.o.e. of fuel oil). Kaunas and Petrasiunai CHP generates not only heat but also electricity according to the electricity and heat ratio. Combined generation units and boilers in these power plants are modelled as separate technologies. Disturbance parameter probability distributions are defined from the available statistical data and expert assessment methods. Probability of reliable heat supply by Kaunas DH network to Kaunas city is 0.9962 [10]. This parameter gives 0.0038 probability of heat supply network failure. Disturbance can occur at any time during the modelling period. Modelling year is divided into the 12 time slices. Each time slice represents a month. Minimal disturbance duration is one month. Supply restriction and cost increase is possible only for imported fuel: natural gas or fuel oil.

4.3. Preliminary results

In order to simulate as many combinations of disturbance parameters as possible and to obtain more accurate results, 1000 model runs were done. Each model run is done with randomly generated scenario according to disturbance parameter probability distributions. The probability, that generated scenario is the basic scenario, is very high. The reason of that is very low probabilities of disturbance occurrence. Preliminary modelling results are presented in Fig. 3, Fig. 4 and Fig. 5.

Unsupplied thermal energy for consumers and cost increase of heat are obtained. Combinations of these two parameters are illustrated in the Fig. 3.

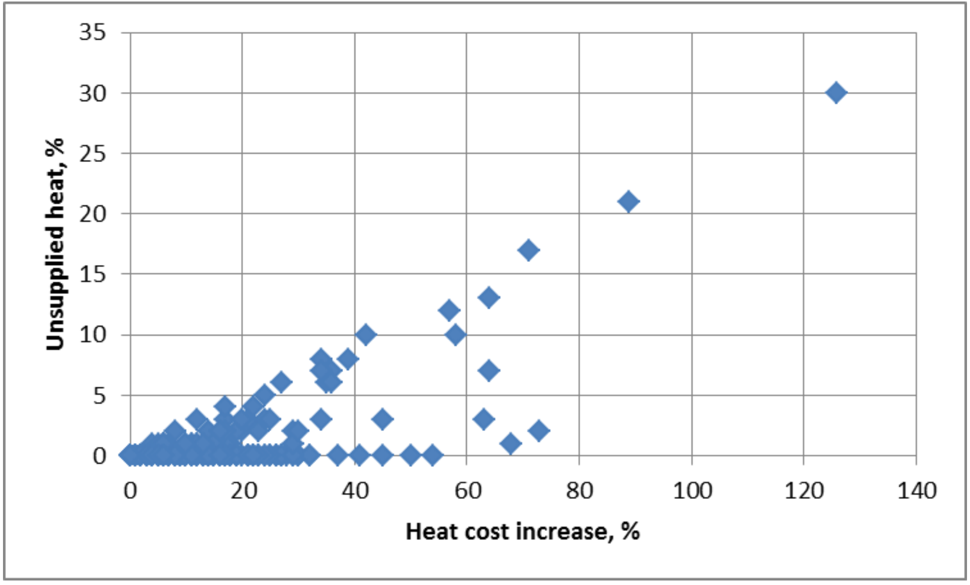

Fig. 3. Scatterplot of unsupplied heat and cost increase of heat in simulated scenarios

Maximal unsupplied heat and cost increase of all simulated scenarios are obtained from the scatterplot. This combination leads to the most severe scenario. According to the results this scenario is characterized by gas supply termination to 100 % and fuel oil supply restriction to 75 % for 5 month period at the same time, i.e. only 25 % of necessary fuel is available to meet the heat demand in Kaunas city for this time period. Fuel oil cost increased 25 % as well. Consequences of this scenario are 30 % of unsupplied heat and 126 % of heat cost increase in the disturbance period if unsupplied heat costs are included.

Cumulative relative frequencies (probabilities) of heat cost increase (Fig. 4) and unsupplied heat (Fig. 5) in Kaunas DH integral network are obtained from the simulated scenarios. For example, probability of 10 % and more heat cost increase is 0.49.

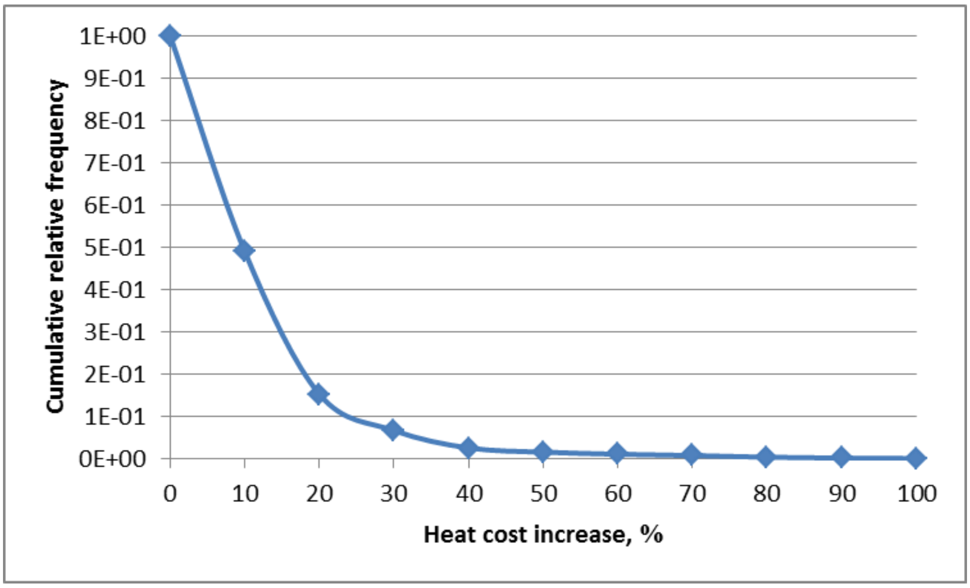

Fig. 4. Cumulative relative frequencies of heat cost increase

For example, probability of 10 % and more unsupplied heat is 0.059. Heat cost increase is due to fuel cost increase in particular scenario.

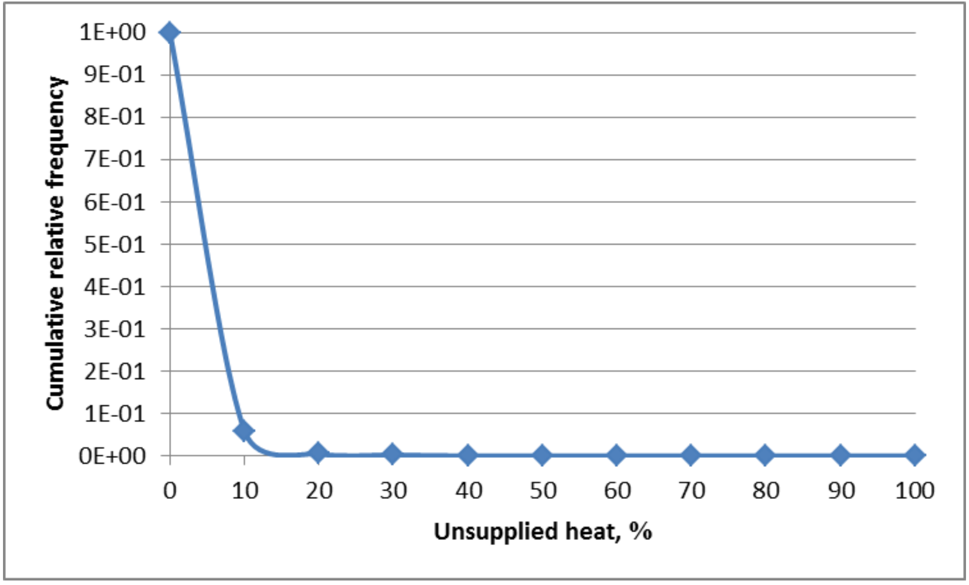

Fig. 5. Relative frequencies of unsupplied heat

Results showed that the most severe scenarios are likely due to fuel supply restriction at the same time period and it leads to unsupplied heat. Fuel cost increase leads to final energy cost increase, but is not as severe as unsupplied energy, but are more probable.

Internal disturbances do not lead to severe consequences of the reliable heat supply network. In addition, Kaunas DH network has significant reserves of heat generation facilities. Therefore severe scenarios are more likely due to external disturbances.

5. SUMMARY AND CONCLUSIONS

The Open Source Energy Modeling System (OSeMOSYS) application for disturbed system modelling is introduced in the paper. Author’s contribution to the model is development of the new model block for energy disturbances modelling and its methodology application. An example application was made to test selected functional aspects of the model. The reference energy system was modelled with the set of energy disturbances. The paper focuses on the methodology development rather than on the results of calculations.

The developed methodology of the disturbed energy system modelling was applied for the calculation of the Kaunas district heating integral network. According to the obtained results taking into account analysed scenarios and developed methodology some conclusions could be drawn:

1. New model block of energy disturbances was successfully integrated to the common OSeMOSYS model.
2. The developed model can be used for any disturbed energy system modelling.
3. Example application showed that most severe scenarios are more likely due to external disturbances, i.e. fuel supply restrictions and cost increases, than internal disturbances.
4. Probability distributions of unsupplied energy amounts and energy cost increase can be defined from the model application for the reference energy system. These results help to identify severity of energy disturbance consequences which reflect energy security issues.

REFERENCES

1. M.H. Brown, C. Rewey, T. Gagliano, *Energy Security*, National Conference of State Legislature. ISBN 1-58024-287-1, 2003.
2. RAVN, H.F., Balmorel: A Model for Analyses of The Electricity and CHP Markets in the Baltic Sea Region, 2001- [referred on the 2nd of March 2011]. Link to the internet <http://www.balmorel.com/>.
3. HOWELLS M., ROGNER H., STRACHAN N., HEAPS C., HUNTINGTON H., SOCRATES K., HUGHES A., SILVEIRA S., DECAROLIS J., BAZILLIAN M., ROEHRL A. OSeMOSYS: The Open Source Energy Modeling System: An introduction to its ethos, structure and development. *Energy Policy*, 39 10 (2011), p. 5850–5870.
4. OSeMOSYS: The Open Source Energy Modeling System, 2011- [referred on the 3rd of March 2012]. Link to the internet <http://osmosys.yolasite.com/>.
5. GNU MathProg programming language, 2009- [referred on the 3rd of March 2012]. Link to the internet <http://lpsolve.sourceforge.net/5.5/MathProg.htm>.
6. AMPL: A Modeling Language for Mathematical Programming, 2011- [referred on the 3rd of March 2012]. Link to the internet <http://www.ampl.com/>.
7. GLPK: GNU Linear Programming Kit, 2008- [referred on the 3rd of March 2012]. Link to the internet <http://www.gnu.org/software/glpk/>.
8. AUGUTIS J., KRIKŠTOLAITIS R., MATUZIENĖ V., PEČIULYTĖ S. Assessment of Lithuanian power supply security depending on nuclear energy. *Safety and Security Engineering III*. Information and Communication Technologies, Vol. 108. WIT Press, Online ISSN 1743-3517, Print ISBN 1-84564-193-1. 2009, p. 235–247.
9. AUGUTIS, A., KRIKŠTOLAITIS, R., ŠIDLAUSKAS, K., MARTIŠAUSKAS, L., MATUZIENĖ, V. Modelling of energy supply disturbances in network systems // Reliability, risk and safety: theory and applications. London: Taylor & Francis Group, 2010. Vol. 3. ISBN 978-0-415-55509-8, p. 1035-1041.
10. KALIATKA, A., VALINČIUS M., AUGUTIS J., KRIKŠTOLAITIS R., RIMKEVIČIUS S., DUNDULIS G., BAKAS R. Reliability assessment method of district heating network (in Lithuanian). *Energetika*. ISSN 0235-7208. 2008. T. 54, Nr. 2, p. 1–9.
11. SC “Kaunas Energy”, 2012 – [referred on the 3rd of March 2012]. Link to the internet <http://www.kaunoenergija.lt/>.
12. JSC “Kaunas CHP”: Kaunas Combined Heat and Power Plant, 2012- [referred on the 3rd of March 2012]. Link to the internet <http://www.kte.lt/en/>.

13. LDHA: Lithuanian District Heating Association, 2012- [referred on the 3rd of March 2012]. Link to the internet <http://www.lsta.lt/>.
14. National Control Commission for Prices and Energy, 2012- [referred on the 3rd of March 2012]. Link to the internet <http://www.regula.lt/en/>.
15. LEI: Lithuanian Energy Institute, 2012 – [referred on the 3rd of March 2012]. Link to the internet <http://www.lei.lt>.
16. Statistics Lithuania, 2012 – [referred on the 3rd of March 2012]. Link to the internet <http://www.stat.gov.lt/en/>.

CYSENI 2012, May 24–25, Kaunas, Lithuania
ISSN 1822-7554, www.cyseni.com

IMPACT OF LEGAL REGULATION TO USE RENEWABLE ENERGY IN DISTRICT HEATING

L. Murauskaitė
Lithuanian Energy Institute
Breslaujos str. 3, 44403 – Lithuania
Phone (+370 37) 401982
Email: lina.m@mail.lei.lt:

ABSTRACT

During heating season district heating became one of the most discussion needed question of energy sector in Lithuania. The main reason of every year increasing district heating price is that more than 70 percent of district heating is produced from natural gas. Compared with the year 2005, natural gas price dramatically increased more than four times. Lithuania receives natural gas from the sole energy supplier - Russia (Gazprom). Lithuania declares the use of energy from renewable energy sources among priorities of energy policy. District heating sector is producing almost 20 percent of heat from renewable energy sources. National and international regulation of renewable energy gains an important role in increasing the use of renewable energy sources in district heating. Also legal regulation became an important tool to diversify energy supply, to reduce air pollution and to meet targets of sustainable development. The main factor limiting further renewable energy growth in district heating is high investment costs and constrains of legal regulation. The aim of this paper is to analyse the impact of legal regulation on the use of renewable energy in district heating from European Union's and national point of view in Lithuania, which is an issue for further investments in growth of renewable energy in district heating sector.

Keywords: renewable energy, district heating, legal regulation

1. INTRODUCTION

In recent years, the consumption of fossil fuel and the mitigation of climate changes have become major challenges for governments all over the world. To engage these challenges, many countries are pursuing the research, development, and demonstration of renewable energy sources (RES) [1]. In the past few years, RES have got rapid development all over the world. RES have become important alternative energy sources to realize energy diversification. During the last few years, political support for renewable energies has been growing continuously both at the national and international level.

Looking at the renewable energy use after 2006, it was a natural gas price boom, increase of social and political pressure for fast developments in clean energy, and financial crisis, which requires adequate government measures to stimulate the economy. The industry of renewables could be important to generate employment and to stimulate growth [2]. Investment in renewable energy sources may bring considerable profits, so more and more enterprises will be involved in this field. The increased use of RES in the heat market can significantly alleviate the negative effects of high-energy costs on the national economy. Successful commercialization of indigenous, non-fossil energy resources is expected to promote regional economical development and employment, help to increase national energy security and to reduce a substantial portion of the increasing trade deficit necessity to import fossil fuels [3].

The main factor limiting further renewable energy growth in district heating is high investment costs and constrains of legal regulation. The aim of this paper is to analyse impact of legal regulation on the use of renewable energy in district heating from European Union's and national point of view in Lithuania, which is an issue for further investments in growth of renewable energy in district heating sector. The paper overviews main EU Directives and

Lithuanian laws and legal documents related to the use of RES in district heating. Also barriers and problems of renewable energy in district heating are noted and options for policy response are given. Last section information is mainly driven by RE-Shaping project that core objective is to assist EU Member State governments in preparing for the implementation of the Renewable Energy Sources Directive and to shape a European policy for RES in the medium to long term.

2. LEGISLATIVE FRAMEWORK OF RENEWABLE ENERGY IN EUROPEAN UNION

In 1997, European Union issued a White paper for development of RES, and formulated the target – renewable energy would account for 12% of total EU energy consumption by 2010 and would account for 50% of energy source composition in EU by 2050. Actually it was only during the beginning of the 21st century that some countries or political blocs (as is the EU case), began to set targets for renewable energy and to define policy measures for the sector [2, 4, 5]. In 2007, EU leaders agreed to an integrated climate and energy policy to combat climate change. The EU's 20-20-20 targets envisage reduces greenhouse gas emissions by 20%, increases in energy efficiency by 20% and makes energy share from renewable source at least 20%.

Main EU Directives, that have an impact on district heating sector, are as follow [6]:

- Directive 2004/8/EC of the European Parliament and of the Council on the *promotion of cogeneration* based on a useful heat demand in the internal energy market and amending Directive 92/42/EEC (11 February 2004) [7];
- Directive 2006/32/EC of the European Parliament and of the Council on energy *end-use efficiency* and energy services and repealing Council Directive 93/76/EEC (5 April 2006) [8];
- Directive 2009/28/EC of the European Parliament and of the Council on *the promotion of the use of energy from renewable sources* and amending and subsequently repealing Directives 2001/77/EC and 2003/30/EC (23 April 2009) [9];
- Directive 2009/29/EC of the European Parliament and of the Council amending Directive 2003/87/EC so as *to improve and extend the greenhouse gas emission allowance trading scheme* of the Community (23 April 2009) [10];
- Directive 2010/31/EU of the European Parliament and of the Council on *the energy performance of buildings* (9 May 2010) [11];
- Directive 2010/75/EU of the European Parliament and of the Council on *industrial emissions* (integrated pollution prevention and control) (24 November 2010) [12].

The Renewable Energy Sources Directive 2009/28/EC which entered into force in June 2009, transforms binding targets into a legislative framework: the European target of 20% RES in the gross final consumption of energy is divided out into binding national targets for the EU-27 member states. No legislative framework at EU level was available in the heating sector before the Directive 2009/28/EC. After one year, by July 2010, member states were required to present National Action Plans of RES (NREAPs) that fixes specific objectives for each member state in the use of RES for each sector, including heating. All 27 NREAPs had been published by January 2011 (which seems quick compared to the implementation of other EU legislations, e.g. Directive 2004/8/EC on cogeneration or Directive 2006/32/EC on energy efficiency) [13]. According to the NREAP, Lithuania has quite ambitious plans to increase RES in heating sector from 27 percent in 2005 to 39 percent in 2020. Taking into account technological possibilities of district heating sector and economic advantage, heat production form RES should be increased by not less than 50 percent. Whether the proposed actions will be sufficient to actually achieve these targets remains to be seen.

Management of energy demand is encouraged in Directive 2010/31/EU. EU members should use the available funds and funding, such as the European Regional Development Fund, for increasing energy efficiency and use of renewable energy in housing sector. According to this

Directive, all new buildings have to be nearly zero-energy buildings by 31 December 2020. New buildings occupied and owned by public authorities have to be nearly zero-energy buildings after the end of 2018. The requirements of this Directive will affect not only construction sector and the price of new houses, but also existing buildings that are subject to major renovation and should therefore meet minimum energy performance requirement. Looking in the long perspective on the influence of Directive 2010/31/EU and Directive 2006/32/EC on energy end-use efficiency, it will be decrease in demand side of district heating. Therefore heating prices should decrease, but the heating losses could become the main factor for inefficient district heating supply.

Later EU Directive 2009/29/EC on improvement of greenhouse gas emmision trading scheme (ETL) pointed out that free allocation shall be given to district heating as well as to high efficiency cogeneration, as defined by Directive 2004/8/EC on cogeneration. From 2013 the basic principle for allocation of ETL should be auctioning. Directive 2010/75/EU on industrial emissions is important for combustion plants, which are in operation after 1 January 2016. These plants should ensuring that emissions into the air from these plants will not exceed the emission limit values. The main threat of this prohibition is for Vilnius, Kaunas and Mazeikiai combined heat and power plants (CHP), which are dependent on combustion of natural gas. Without costly investments in flue-gas cleaning devices mentioned CHP will not be able to be in operation and supply heat for two biggest Lithuania cities. As an alternative could be biomass cogeneration plants. But for instance in Kaunas it is difficult to deal with municipality politicians, who in 2011 summer agreed on detailed plan of new modern CHP, but at the end 2011 changed their minds. Strategic city heating projects should be priority for each city, and the politicians should bring all efforts to make them clear and stable.

As noted by [14], the prices of traditional energy sources do not include the environmental costs. Prices fail to reflect the real costs of their use, when compared to the ones of renewable energy, giving the idea that prices of clean energy are not competitive in the short term. Authors of [15] paper study the interrelationship among prices, income and renewables. The authors conclude that countries with high economic growth deal better with high energy prices (related to the use of renewable energy), because it is easier to support the high costs connected with these technologies [2]. Consequently high investment costs are one of the factors that limit further renewable energy growth, but looking in the long term perspective even in Lithuania it could be beneficial. As recently counted of Lithuanian Energy Consultants Association [16], RES development in district heating in long term period (by 2020) gives over 7 milliard Litas more benefit than costs for the country. On the other hand, it is difficult to create scenarios of RES prices movement in the future, if volume of using RES increases.

The increased spread of anomalous weather in recent times has led to active public discussions about climate protection. The greenhouse gas emissions can be reduced by increasing the share of RES in the heat market - similar to the effect already initiated in the electrical power market. However, a similarly strong impulse in public policy for the heat market is still lacking. Moreover, in the current labour market it should not be forgotten that the increased use of RES creates employment while simultaneously reducing fossil fuel imports. Legislation to promote RES in the heat market thereby creates a fourfold dividend:

(1) contributes to the protection of climate and resources,
(2) reduces the dependence on imports,
(3) strengthens regional value added,
(4) creates future-assured employment [17].

A very large potential in the heat market still remains to be developed. The dividend is therefore correspondingly large. EU Directives that impact on district heating sector have to be the main road for further development on the use of RES. The targets that was set in NREAP have to be followed, but it is necessary to create strong national legislation framework and accessibility to finance RES in district heating.

3. DISTRICT HEATING LEGISLATION IN LITHUANIA

Many states in Eastern and Central Europe, as well as Lithuania, possess extensive district heating networks that were constructed during the days of communist rule in order to provide a universally accessible energy service. But the post-communist transition was marked by the exacerbation of the sector's numerous technical, economic, regulatory and environmental problems, accompanied by its abandonment in favour of alternative methods of heating [18].

Government policy for promoting renewable energy was formulated during 10 years (1990–2000). The policy was revised during 5 year periods for comprehensiveness, coordination and market development. A strategy to promote the use of alternative energy sources such as biomass, small hydro power, biogas, wind energy, etc has been adopted. Promotion of local and renewable energy sources usage and energy efficiency is established in the Law on Energy of the Republic of Lithuania as priority objectives of energy sector regulation [3]. In Lithuania promotion of renewables' use is based on the main legislation acts, which are described in recent study [6]:

- Law on Energy of the Republic of Lithuania [19];
- Law on Electricity of the Republic of Lithuania [20];
- Law on Biofuel of the Republic of Lithuania [21];
- Law on Heat Sector of the Republic of Lithuania [22];
- Law on Renewable Energy of the Republic of Lithuania [23];
- National Energy Strategy [24];
- The National Strategy for the Development of Renewable Energy Sources [25].

The Law on Energy states that energy companies that supply heat to apartment buildings, the heat supply to flats, if users do not wish otherwise. The increasing district heating prices and low income of apartment buildings owners cause discussions about how to become independent from district heating companies. There are several cases, widely announced in media, how people after long bureaucracy procedures were enabled to change type of heating to individual. Results are contradictory, one of them proud to be independent, other honestly say it is costly than district heating. There should not be forgettable that if one of the owners of apartment building disconnects from district heating, others have to pay more for heat loss. The situation may become ridiculous after larger scale of such independency from district heating. Long year created infrastructure and restriction of the pollution would only be just fruitless efforts.

The main legislation act for district heating is Law on Heat Sector. This law provides competition in heating sector, heat buying from independent producers, detailed explanation of heat the contracts cancellation of user initiative, heat supply license, heat pricing etc. Heating prices are regulated by The National Control Commission for Prices and Energy, therefore heating companies profit is limited. This causes inability of investments in new heating devices that uses RES as a fuel. Sources of possible financial support in Lithuania are given at the end of this section.

The Law on Renewable Energy is mainly driven by EU Directive 2009/28/EC. This law repeats goals that were set in mentioned Directive. It aims to ensure sustainable energy supply, promote the further use of renewable energy technologies and their development, especially in regard to the environment (climate change). The Law on Renewable Energy frames an excellent opportunity to significantly reduce costs of producing hot water in apartment buildings using RES technologies, such as solar collectors. However, the pricing of produced heat is unfavourable for independent heat producers, because district heating suppliers have to buy energy made from RES at the lowest price. Consequently hot water that is prepared using solar collectors has to be used by its owners. Finally, the main problem of the Law on Renewable energy is still lacking executive acts that limit further investments in renewable energy.

Lithuanian Energy Agency (LEA) is responsible for the coordination of research, development and implementation of renewable energy projects. Under instructions of the Ministry of Energy, LEA deals with drafting the National Energy Program, other programs regarding the improvement of efficient use of local, renewable and waste energy resources, organization of their implementation, updating and revision, preparation of legal, economic and organizational energy efficiency measures for the enhancement of national energy policy implementation [3].

Situation in the district heating sector in Lithuania is similar to other transition countries:

- Very high consumption of thermal energy – more than 200 kWh/m^2 annually;
- Renovation of building goes very slowly;
- Most heat consumers have no individual regulation, so heating bills do not correspond to their living standard;
- Heat supply volume has been reduced several time from design conditions – many equipment and pipelines are oversized;
- “Old” facilities and schemes are modernized or replaced slowly;
- Low efficiency, poor quality standards, high heat prices;
- Disappointment with such situation forms negative attitude regarding district heating [26].

As the result of such situation, main regulatory problems in Lithuania can be pointed out:

- Destructive competition with gas heating (incorrect pricing policy);
- Planning/zoning of cities still seldom;
- Unregulated disconnections, causing problems of district heating in some cities;
- New obligations to district heating sector are not supported by required financial resources often;
- Approval and financing of investment are unpredictable;
- Lots of speculations and populist decisions in the district heating sector [26].

District heating and cogeneration policy frameworks in Lithuania consist of s*ecure market-oriented energy policies*. Such policies promote liberalisation, competition and customer choice. Therefore it separates monopolistic from competitive activities for privatisation, also harmonises liberalisation of CHP and electricity markets. Moreover policy aimed at d*evelopment of long-term and local energy strategies* and p*romotion of district heating and cogeneration* [27].

District heating and cogeneration regulatory goals in Lithuania are[27]:

1. *Enhance regulatory regimes*: have regulator reporting to President, Parliament and Government; control monopolistic generators; undertake independent audits of regulated companies and regulator.
2. *Foster competition, access to grids*: set regulated prices, price caps, taking into account depreciation; reduce barriers to third-party access to market so as to allow customer choice.
3. *Secure cost-covering, market-oriented prices, tariffs*: reschedule or incorporate old company debt into tariffs or solicit government support.

Consistent policy package is the key to cause a renewable energy in district heating development that is required to meet ambitious targets. Lithuania is promoting the use of indigenous, renewable and waste energy resources by financial measures. However, there is no direct support for RES in district heating. Sources of financial support are [28]:

- Exemption from pollution taxes;
- The Lithuanian Environmental Investment Fund;
- EU structural funds for 2007-2013;
- Lithuanian Rural Development Programme for 2007-2013;
- The Fund of the Special Programme for Climate Change.

However, none of these instruments has been able to sufficiently accelerate the introduction of renewable energies in the heat market. The Law on Renewable Energy gave the beginning for national legislative framework on the use of renewable energy. Main problem of this law is still lacking executive acts that limit further investments in renewable energy.

4. BARRIERS AND PROBLEMS OF RENEWABLE ENERGY IN DISTRICT HEATING

Investments in the energy market have very long-term effects. Therefore the long-term planning is very important. In particular, the task of fulfilling long-term requirements cannot be left to the market forces which are inactive in this regard [4, 17]. RES use will not expand sufficiently on its own accord. For the share of RES to grow within the heat market, the volume of financial aid must also increase until the new technologies can compete in the market without regulatory or financial support [17]. Of course, a new instrument must ensure that the goals defined for expanding RES use in the heat market are achieved in practice. The goals should be achieved at minimum costs. Consequently, there must be minimised not only the direct financial expenditures, but also the administration and inspection efforts.

All of the instruments must be examined with the compatibility with the EU competition regulations. Furthermore, it must be examined the burden imposed on the individual (especially for ordinances) and whether or not an illegitimate extra duty is created (for quantity or price regulations). It is very important to ensure that the financial burden benefits the environment, and that a legally permissible situation exists, that does not convert into an extra duty as a result of extensive state regulation, which is possibly illegitimate because of insufficient benefit to the general public [17].

Table 1 gives an overview of the major RES administrative and legal barriers in EU based on a summary of various studies in [13] research. The second column shows the available policy responses to address these barriers. The implementation of these policy features varies strongly across European member states.

Table 1. Common RES administrative and legal barriers and policy responses [13]

Barrier	Options for policy response
Inefficient administrative procedures (high number of authorities involved, lack of coordination among authorities, lack of transparent procedures, long lead times, high costs for applicants etc.)	Improving and streamlining administrative procedures towards transparent and non-discriminatory processes (“one-stop shop” approach for applications, maximum response periods for authorities, clear guidelines and capacity building for civil servants, limiting administrative requirements to the relevant elements, simplified procedures for small plants, etc.).
RES not or insufficiently considered in spatial planning	Improved spatial planning rules; Definition of RES priority areas; Information and capacity building for local authorities; Participation and/or compensation options for local communities.
No or insufficient standards and codes for RES equipment (specifications not well defined, not expressed in EU/international standards, etc.)	Improvement of technical specifications and codes; Implementation of EU/international standards and certifications.
Tenancy law and ownership law impede the development of building-integrated RES technologies	Implementation of RES-use obligations; Adapt tenancy and ownership law to facilitate RES deployment (facilitating cost sharing, provision of energy services etc.).

The accelerated deployment of RES for heating purposes is too important to allow it to depend on strongly varying public budgets. A subsequent goal is to charge polluters for the necessary additional financing for renewable energy installations. Those groups which bring fossil fuels into circulation or which use them should be burdened [17].

Despite the government policy efforts, accepted legislated base and programs for enhancement of the use of RES, due to expensiveness of alternative energy technologies and various constraints, total contribution to development is not impressive. More effectiveness can be obtained on cooperation with other countries. Also the government must create a special subsidy policy to promote usage of RES [3].

According to authors of [13] paper, “critical success factors include implementing effective and efficient policies that attract sufficient investments, reducing administrative and grid related barriers, especially in currently less advanced countries, dismantling financial barriers in the heat sector, realising sustainability standards for biomass, and lowering energy demand through increased energy efficiency efforts”.

Fig. 1 shows the heterogeneous deployment status of RES in heating (RES-H) technologies in the EU-27 member states in 2009. Lack of statistical data influenced that even in 2011 October, when was presented RE-Shaping project last report [29] about indicators of RES policies in EU, it was impossible to compare the present situation in EU-27. Member states with a very similar deployment status of RES-H are indicated by the placeholder „other MS“. Grid-connected biomass heat installations are very advanced in the Scandinavian countries (Sweden, Denmark and Finland), and to a lesser extent in the Baltic countries and Austria. The other heat technologies, geothermal heat, ground source heat pumps and solar thermal, are still immature in the majority of countries, although the majority of Member States has shown some development and is at the edge to an intermediate deployment status [13, 29, 30]. Comparison with previous report [30] shows that from Baltic countries biggest movement made Estonia (from immature to advanced) in grid-connected biomass heat installations, Lithuania stayed almost in the same place.

Most member states put considerably less effort into supporting RES heating than in the case for RES electricity. This might be partly explained by the lack of a European heating and cooling directive – and therefore the absence of Europe-wide targets and support requirements – until the new RES Directive 2009/28/EC entered into force in 2009 [13].

RES in heating support schemes are almost fully financed by public budgets. The uncertainty of government budgets frequently creates stop–go investment cycles in the RES heating sector. Consequently the scientific policy discussion calls for new, budget-independent RES heating support instruments, such as RES obligations for heat fuel suppliers or building owners, bonus systems comparable to RES electricity feed-in systems, or a combination of these [13, 31]. However, none of member state has introduced such innovative schemes except for building obligations in Germany, Portugal and Spain [13].

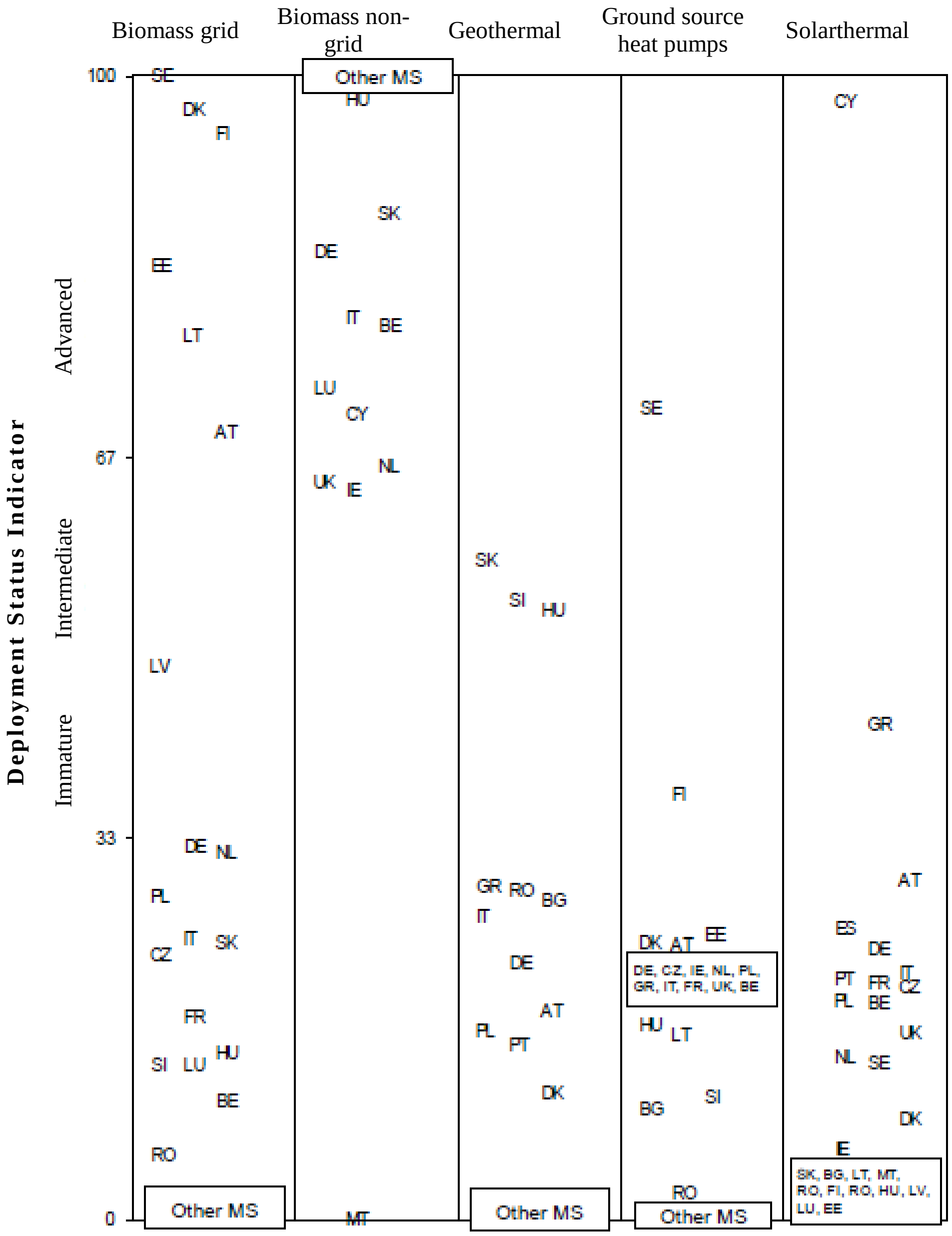

Renewable energy technology market where the share of the potential in sector consumption is <1% are not shown.

Fig. 1. Overview of the deployment status of RES-H technologies [29]

The effectiveness of the policies in increasing the production from renewable energy technologies and the costs are two key aspects for society resulting from the support of renewable energies, expressed by the economic dimension of policy support. These aspects have been represented in the Policy Effectiveness Indicator, which was previously used to evaluate renewable energy technologies exclusively in the electricity sector. RE-Shaping project [30] monitored effectiveness of support policies in the heating and cooling sector. Definition of the Policy Effectiveness Indicator reads as follows:

$$E_n^i = \frac{Q_{n(norm)}^i - Q_{n-1(norm)}^i}{POT_{n-1}}, \tag{1}$$

where: E_n^i - Policy Effectiveness Indicator for renewable energy technologies i in year n; $Q_{n(norm)}^i$ - normalised renewable final energy of renewable energy technologies i in year n; POT_n - additional realisable mid-term potential in year n until 2020.

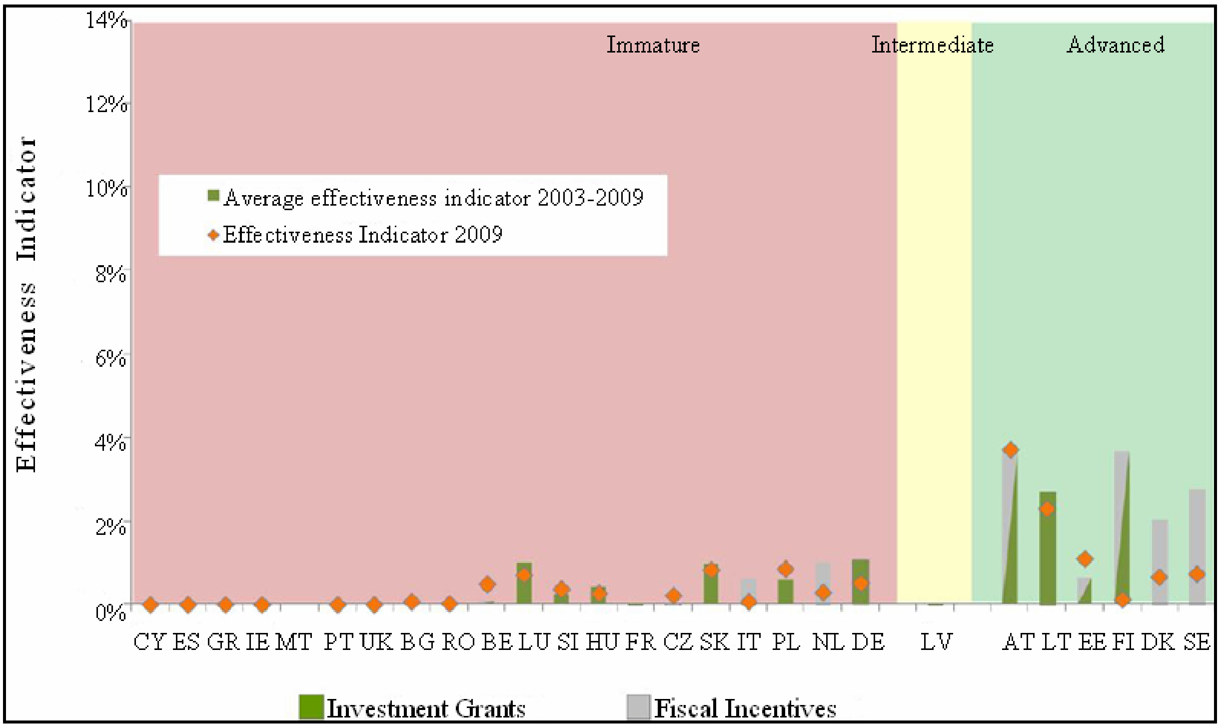

Fig. 2. Policy Effectiveness Indicator for centralised biomass heating plants (District heating plants and CHP-plants) in the period 2003‑2009 [29]

According to the Policy Effectiveness Indicator depicted in Fig. 2, in particular Scandinavian (Finland, Sweden and Denmark) and Baltic countries (Estonia and Lithuania) as well as Austria have supported centralised biomass heating plants effectively between 2003 and 2009. High Policy Effectiveness Indicator values in 2009 for Austria, Lithuania, and Estonia shows a continuation of the effective policy support. Several factors have an effect on the successful support of biomass-derived district heating and CHP-plants. Firstly, the tradition of Northern European countries to use grid-connected heating systems with an existing infrastructure of district-heating networks. Secondly, the biomass availability. Thirdly, sufficiently available heat demand [30]. The present situation of policy effectiveness could be different. The main obstacle is lack of statistical data in 2011 report [29] about indicators of RES policies in EU.

Regulation itself may not represent the main or the only reason why district heating in transition economies is less efficient than, for example, in Western Europe [18]. Despite the government policy efforts, accepted legislated base and programs for enhancement of the use of RES, due to expensiveness of alternative energy technologies and various constraints, total contribution to development is not impressive.

5. CONCLUSIONS

The Renewable Energy Sources Directive 2009/28/EC translates binding targets into a legislative framework. This Directive is only the beginning of renewable energy promotion in district heating.

Lithuania’s situation is very similar to other transition countries. District heating system has many problems not only because of obsolete facilities, political aspects, but also lack of support for renewable energy in the heat market.

Main problems related with the use of renewable energy in heating sector are administrative and legal barriers. The options for policy response could be improving and streamlining administrative procedures towards transparent and non-discriminatory processes (“one-stop shop” approach for applications, maximum response periods for authorities, clear guidelines and capacity building for civil servants, limiting administrative requirements to the relevant elements, simplified procedures for small plants, etc.). Furthermore, there should be information and capacity building for local authorities. Moreover there should be adapted tenancy and ownership law to facilitate RES deployment (facilitating cost sharing, provision of energy services etc.).

REFERENCES

1. SHEN, Y.-C.; LIN, G.T.R.; LI, K.-P.; YUAN, B.J.C. An assessment of exploiting renewable energy sources with concerns of policy and technology. *Energy Policy*, 2010, Vol. 38, No. 8, p. 4604–4616.
2. MARQUES, A.C.; FUINHAS, J.A.; PIRES MANSO, J.R. Motivations driving renewable energy in European countries: A panel data approach. *Energy Policy*, 2010, Vol. 38, No. 11, p. 6877–6885.
3. KATINAS, V.; MARKEVIČIUS, A. Promotional policy and perspectives of usage renewable energy in Lithuania. *Energy Policy*, 2006, Vol. 34, No. 7, p. 771–780.
4. ZHU, B. Further discussion on exploitation of renewable energy sources and its legal regulations. *Energy Procedia*, 2011, Vol. 5, No. 0, p. 2114–2119.
5. ŠTREIMIKIENE, D.; BURNEIKIS, J.; PUNYS, P. Review of renewable energy use in Lithuania. *Renewable and Sustainable Energy Reviews*, 2005, Vol. 9, No. 1, p. 29–49.
6. MURAUSKAITĖ, L. Promotion of renewable energy for district heating in Lithuania as EU member. In Proceedings of the 1st World Sustainability Forum, 2011 November 1-30, Sciforum Electronic Conferences Series.
7. Directive 2004/8/EC of the European Parliament and of the Council on the *promotion of cogeneration* based on a useful heat demand in the internal energy market and amending Directive 92/42/EEC. Official Journal of the European Communities, 21.2.2004, L 52/50.
8. Directive 2006/32/EC of the European Parliament and of the Council on energy *end-use efficiency* and energy services and repealing Council Directive 93/76/EEC. Official Journal of the European Communities, 27.4.2006, L 114/64.
9. Directive 2009/28/EC of the European Parliament and of the Council on *the promotion of the use of energy from renewable sources* and amending and subsequently repealing Directives 2001/77/EC and 2003/30/EC. Official Journal of the European Communities, 5.6.2009, L 140/16.
10. Directive 2009/29/EC of the European Parliament and of the Council amending Directive 2003/87/EC so as *to improve and extend the greenhouse gas emission allowance trading scheme* of the Community. Official Journal of the European Communities, 5.6.2009, L 140/63.
11. Directive 2010/31/EU of the European Parliament and of the Council on *the energy performance of buildings*. Official Journal of the European Communities, 18.6.2010, L 153/13.
12. Directive 2010/75/EU of the European Parliament and of the Council on *industrial emissions* (integrated pollution prevention and control). Official Journal of the European Communities, 17.12.2010, L 334/17.

13. KLESSMANN, C.; HELD, A.; RATHMANN, M.; RAGWITZ, M. Status and perspectives of renewable energy policy and deployment in the European Union—What is needed to reach the 2020 targets? *Energy Policy*, 2011, Vol. 39, No. 12, p. 7637–7657.
14. MENZ, F.C.; VACHON, S. The effectiveness of different policy regimes for promoting wind power: Experiences from the states. *Energy Policy*, 2006, Vol. 34, No. 14, p. 1786–1796.
15. CHANG, T.-H.; HUANG, C.-M.; LEE, M.-C. Threshold effect of the economic growth rate on the renewable energy development from a change in energy price: Evidence from OECD countries. *Energy Policy*, 2009, Vol. 37, No. 12, p. 5796–5802.
16. Lithuanian Energy Consultants Association. Programme of development of renewable energy sources in Lithuanian district heating systems. Vilnius, 2010. .
17. NAST, M.; LANGNIß, O.; LEPRICH, U. Instruments to promote renewable energy in the German heat market - Renewable Heat Sources Act. *Renewable Energy*, 2007, Vol. 32, No. 7, p. 1127–1135.
18. POPUTOAIA, D.; BOUZAROVSKI, S. Regulating district heating in Romania: Legislative challenges and energy efficiency barriers. *Energy Policy*, 2010, Vol. 38, No. 7, p. 3820–3829.
19. Law on Energy of the Republic of Lithuania. Official Gazette, 2002, No. 56-2224.
20. Law on Electricity of the Republic of Lithuania. Official Gazette, 2000, No. 66-1984.
21. Law on Biofuel of the Republic of Lithuania. Official Gazette, 2000, No. 64-1940.
22. Law on Heat Sector of the Republic of Lithuania. Official Gazette, 2003, No. 51-2254.
23. Law on Renewable Energy of the Republic of Lithuania. Official Gazette, 2011, No. 62-2936.
24. National Energy Strategy. Official Gazette, 2007, No. 11-430.
25. The National Strategy for the Development of Renewable Energy Sources. Official Gazette, 2010, No. 73-3725., Vol., No.
26. LUKOŠEVIČIUS, V. Regulatory concepts and issues of district heating. In Technical exchange programme: Sustainable energy regulation. Poland: Warshaw, 2011 March 3-4
27. A REPORT OF THE WORLD ENERGY COUNCIL. Regulating district heating and cogeneration in Central and Eastern Europe, 2004. Link to the internet <http://www.worldenergy.org/documents/dhchp.pdf>.
28. KONSTANTINAVIČIŪTĖ, I. Policy assessment: Case study Lithuania. In RES-H Policy project national dissemination conference. Lithuania: Vilnius, 2011 April 27.
29. STEINHILBER, S.; RAGWITZ, M.; RATHMANN, M.; KLESSMANN, C.; NOOTHOUT, P. RE-Shaping: Shaping an Effective and Efficient European Renewable Energy Market. Indicators Assessing the Performance of Renewable Energy Support Policies in 27 Member States., 2011 October no. EIE/08/517/SI2.529243. Link to the internet <http://www.reshaping-res-policy.eu/downloads/RE-Shaping%20D17_Report_update%202011_final.pdf>
30. HELD, A.; RAGWITZ, M.; MERKET, E.; RATHMANN, M.; KLESSMANN, C. RE-Shaping: Shaping an Effective and Efficient European Renewable Energy Market. Indicators Assessing the Performance of Renewable Energy Support Policies in 27 Member States., 2010 no. EIE/08/517/SI2.529243 Link to the internet <http://www.reshaping-res-policy.eu/downloads/RE-Shaping%20D5D6_Report_final.pdf>.
31. BURGER, V., ET AL. Policies to support renewable energies in the heat market. *Energy Policy*, 2008, Vol. 36, No. 8, p. 3150–3159.

CYSENI 2012, May 24–25, Kaunas, Lithuania
ISSN 1822-7554, www.cyseni.com

MODELING OF ZONAL PRICES WITH APPLICATION IN LONG-TERM DEVELOPMENT PLANNING STRATEGIES

A. Obusevs, I. Oleinikova
Institute of Physical Energetic
Laboratory of Power System Mathematical Modelling
Aizkraukles 21, Riga, LV-1006 Latvia,
Phone +37122120106
Email: A.Obusev@gmail.com

ABSTRACT

Increasing integration in the Baltic electricity market and Europe-wide interconnection establishment makes it necessary to consider markets principals for power system development planning.

In this paper is given a method for modelling of zonal prices with application and long-term development planning strategies. Proposed method of zonal prices is based on Interior Point Method (IPM) for finding maxima of Social Welfare subject to power system constraints. The main parts of this task are improving existing method for criterion calculations in development tasks with market conditions as well as analyze advantages and disadvantages of Method. The results of this research could contribute to development of methods appropriate in sustainable development management of power system.

Keywords: power system, electricity market, power system development

1. INTRODUCTION

Pricing mechanisms for competitive electricity markets determine either a uniform price (UP), a set of nodal or locational marginal prices (LMP), or only a few zonal marginal prices (ZMP). Each of above mentioned mechanisms is characterized by level of complexity, ability for appropriate allocation of investments as well as rightfully allocates costs for final consumers. Defenders of zonal pricing argue that system based on such principles will be well sufficient to achieve economical efficiency goals with lower complexity and therefore higher transparency to market participants. However, in heavy load periods when congestion is expected exists legitimate concern of market power abuse by market participants. Furthermore, arguable is also ability of right allocation and adequacy of incentives for new investments. Also due to that reasons the evolution of market structures worldwide introduces a nodal pricing principle as the proclaimed benchmark of congestion management, effectiveness and conformity with economic theory and physical laws.

According to aforementioned methods of price determination, the optimal prices in a transmission network are the nodal prices resulting from an optimal power flow (OPF) performed by a centralized dispatcher (e.g. an independent system operator - ISO). The OPF model is implemented in parts of the United States (e.g. PJM), and in Australia and New Zealand. However, the Nordic electricity market which running one of the world biggest power exchange Nord Pool Spot is operated on the zonal pricing principles [1].

Entire market is operated by the one market organizer (power exchange) and the 5 TSOs which have to strongly cooperate in order to keep market with electricity working well with minimal constrains as well as maintain security of power system which can not be endanger by market operation. Actual snapshot of Nordic electricity market with depiction of zones and inter-zonal price differentials is shown on Figure 1.

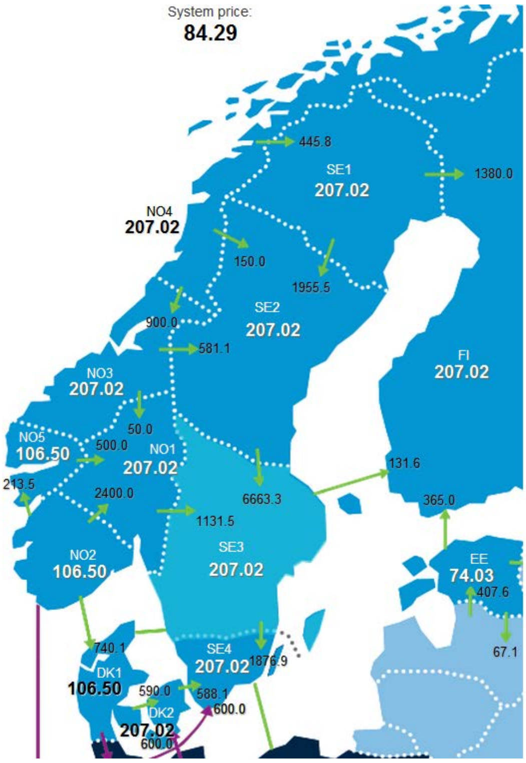

Fig. 1. Nord Pool spot overview on 03.02.2012 08-09

2. OPTIMAL POWER FLOW AND ZONAL PRICES

2.1. Zonal pricing

The zonal pricing method has been introduced as reaction to solve very poor incentive ability of uniform pricing approach. According to the basic principle of zonal pricing, the whole market territory is sub-divided into several zones depending on their respective costs of congestion. Higher prices for electricity are paid in zones where demand exceeds transmission capability (deficit area on Fig. 2) and vice versa. The price is uniform for entire zone. The zones are usually geographically pre-defined according to expected bottlenecks in grid, however, as in case of Nordic market (NPS PX) operation, number of zones can within the year vary according to changes in deployed generating capacities, particularly hydro resources.

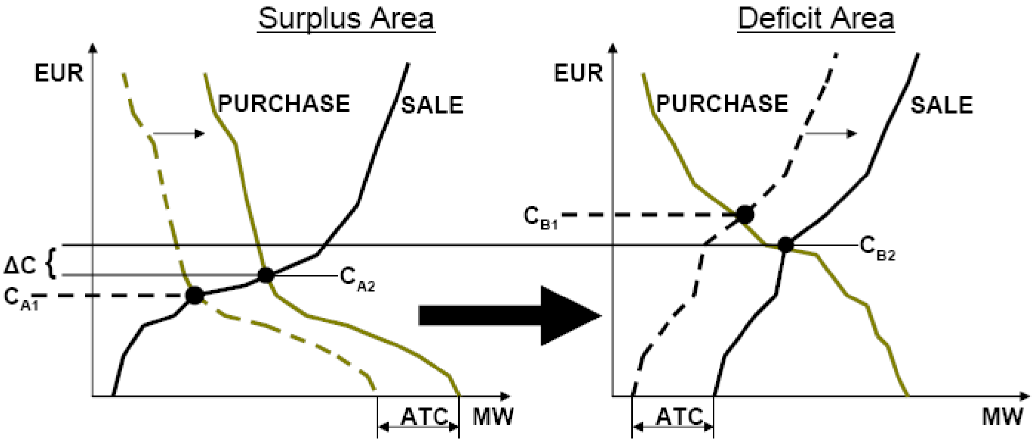

Fig. 2 Zonal price formation

where C_{A1}, C_{B1}- Prices determined as for insulated Areas (without any cross-border interconnection) [m.u./MWh]; C_{A2}, C_{B2} - Prices determined after utilization all available transmission capacity (ATC) of interconnector [m.u./MWh]; ΔC – price difference after utilization ATC (congestion) in [m.u./MWh].

According to Fig. 2, congestion rent between two areas is calculated as:

$$\left(C_{B2} - C_{A2}\right)F_{A\mapsto B} = C_R \, , \tag{1}$$

where $F_{A\mapsto B}$ - planned day-ahead flow in specific hour from surplus area (A) to deficit area (B), [MW]; C_R - Aggregated congestion rent [m.u.].

The optimization task in a case of zonal pricing model is based on so called “social welfare maximization” of consumers’ and producers’ surplus areas. The objective function to be maximized could be expressed:

$$MAX \sum_n \left(\int_0^{d^a} D^a(x)dx - \int_0^{s^a} S^a(y)dy \right), \tag{2}$$

where (a) represents an zone (area), d^a is demand in zone (a) and D^a is the demand function in zone (a), s^a is supply in zone (a) and S^a is the supply function in zone (a) and (n) is the number of zones.

2.2. Formulation of OPF

OPF is a technique that has been used in the electricity industry for several decades. The objective in OPF is to minimize generator operating costs. The objective function is the total cost of generation. The costs may be defined as polynomials or as piecewise-linear functions of generator output. The problem can be formulated schematically as:

$$\min_x f(x), \tag{3}$$

subject to

$$g(x) = 0 \, , \tag{4}$$

$$h(x) \le 0 \, , \tag{5}$$

$$x_{\min} \le x \le x_{\max} , \tag{6}$$

Where $f(x)$ objective function of costs of active and reactive generation; $g(x)$ equaliti constraints of active and reactive power balance; $h(x)$ inequality constraints of power flow limit of line, bus voltage limits; $x_{\min}, x_{\max}$ active and reactive power generation limits.

To guarantee that the OPF can be solved, one of the zones is assigned a zero phase angle by setting its phase angle upper and lower limits to zero (the swing bus).

2.3. Alternating current OPF

The AC version of the standard OPF problem is a general non-linear constrained optimization problem, with both nonlinear costs and constraints. In a system with n_b buses, n_g generators and n_l

branches, the optimization variable x is defined in terms of the $n_b \times 1$ vectors of bus voltage angles Θ and magnitudes V and the $n_g \times 1$ vectors of generator real and reactive power injections P and Q as follows.

$$x = \begin{bmatrix} \Theta \\ V \\ P \\ Q \end{bmatrix}. \tag{7}$$

The objective function (3) is simply a summation of individual polynomial cost functions f_p^i and f_Q^i of real and reactive power injections, respectively, for each generator.

$$\min_{\Theta,V,P,Q} \sum_{i=1}^{n_g} f_p^i(p_i) + f_Q^i(q_i). \tag{8}$$

The equality constraints (4) consist of two sets of n_b nonlinear nodal power balance equations, one for real power and one for reactive power.

$$g_P(\Theta, V, P) = 0, \tag{9}$$

$$g_Q(\Theta, V, Q) = 0. \tag{10}$$

The inequality constraints (5) consist of two sets of n_l branch flow limits as non-linear functions of the bus voltage angles and magnitudes, one for the from end and one for the to end of each branch.

$$h_f(\Theta, V) \le 0, \tag{11}$$

$$h_t(\Theta, V) \le 0. \tag{12}$$

The variable limits (6) include an equality limited reference bus angle and upper and lower limits on all bus voltage magnitudes and real and reactive generator injections.

$$\theta_{ref} \le \theta_i \le \theta_{ref}, \qquad i = i_{ref}, \tag{13}$$

$$v_i^{\min} \le v_i \le v_i^{\max}, \qquad i = 1 \ldots n_b, \tag{14}$$

$$p_i^{\min} \le p_i \le p_i^{\max}, \qquad i = 1 \ldots n_g, \tag{15}$$

$$q_i^{\min} \le q_i \le q_i^{\max}, \qquad i = 1 \ldots n_g. \tag{16}$$

Here i_{ref} denotes the index of the reference bus and θ_{ref} is the reference angle [2].

2.4. Direct current OPF

When using DC network modeling assumptions, the standard OPF problem above can be simplified to a quadratic program, with linear constraints and a quadratic cost function. In this case the dc power flow greatly simplifies the power flow by making a number of approximations including 1) completely ignoring the reactive power balance equations, 2) assuming all voltage magnitudes are identically one per unit, 3) ignoring line losses and 4) ignoring tap dependence in the transformer reactance [3]. The optimization variable is:

$$x = \begin{bmatrix} \Theta \\ P \end{bmatrix} \tag{17}$$

and the overall problem reduces to the following form [2]:

$$\min_{\Theta,P} \sum_{i=1}^{n_g} f_P^i(p_i) \tag{18}$$

subject to

$$g_P(\Theta, P) = 0\,, \tag{19}$$

$$h_f(\Theta) \le 0\,, \tag{20}$$

$$h_t(\Theta) \le 0\,, \tag{21}$$

$$\theta_{ref} \le \theta_i \le \theta_{ref}\,, \qquad i = i_{ref}\,, \tag{22}$$

$$p_i^{\min} \le p_i \le p_i^{\max}, \qquad i = 1 \ldots n_g\,. \tag{23}$$

2.5. Piecewise linear costs

Traditionally, when optimizing the operation of a regulated power system, the objective function in (1) takes a simple smooth quadratic form. The electricity market, however, does not use quadratic cost because it does not cognitively match how market participants want to trade in the real world. The standard OPF formulation in (1)-(4) does not directly handle the non-smooth piecewise linear cost functions that typically arise from discrete bids and offers in electricity markets. When such cost functions are convex, however, they can be modeled using a constrained cost variable (CCV) method. The piecewise linear cost function c(x) is replaced by a helper variable y and a set of linear constraints that form a convex “basin” requiring the cost variable y to lie in the epigraph of the function c(x).

$$c(x) = \begin{Bmatrix} m_1(x - x_1) + c_1, & x \le x_1 \\ m_1(x - x_1) + c_1, & x_1 \le x \le x_2 \\ \ldots\ldots\ldots\ldots\ldots\ldots\ldots & \ldots\ldots. \\ m_n(x - x_n) + c_n, & x_{n-1} \le x \end{Bmatrix}. \tag{24}$$

Fig. 3 illustrates a convex n-segment piecewise linear cost function defined by a sequence of points (x_j, c_j), j=0...n, where m_j denotes the slope of the j-th segment, and $x_0 < x_1 < \cdots < x_n$ and $m_1 < m_2 < \cdots < m_n$.

$$m_j = \frac{c_j - c_{j-1}}{x_j - x_{j-1}}, \qquad \text{j=1...n}\,. \tag{25}$$

The “basin” corresponding to this cost function is formed by the following n constraints on the helper cost variable y.

$$y \geq m_j (x - x_j) + c_j, \quad \text{j=1...n} . \tag{26}$$

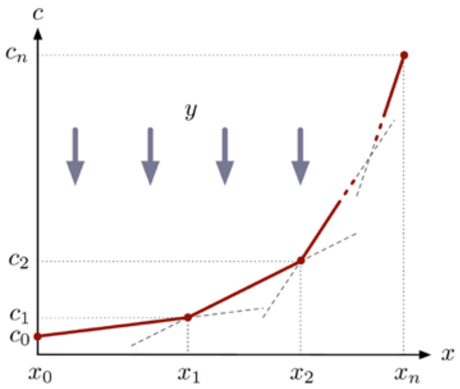

Fig. 3. Constrained Cost Variable

The cost term added to the objective function in place of c(x) is simply the variable y [2].

3. STEP-CONTROLLED PRIMAL-DUAL INTERIOR POINT METHOD

The primal-dual interior point method (PDIPM) and its many variations have become the algorithms of choice for solving OPFs over the past decade [4-7]. Given an optimization problem in the form of (3), PDIPM formulates the Lagrangian with barrier functions as

$$L^{\gamma}(x, z, \lambda, \mu) \equiv f(x) + \lambda^T \cdot g(x) + \mu^T (h(x) + z) - \gamma \sum_{j=1}^{ni} \ln(z_j) \tag{27}$$

Newton’s method to solve the Karush-Kuhn-Tucker conditions

$$\begin{aligned} \nabla_x L^{\gamma}(x, z, \lambda, \mu) = 0; \quad & g(x) = 0; \\ h(x) + z = 0; \quad & [\mu] z \text{ - } \gamma e = 0 \end{aligned} , \tag{28}$$

where z , μ and γ are strictly positive.

Each Newton step involves the solution of a reduced system of (28)

$$\begin{aligned} & M \equiv \nabla^2_{xx} L^{\gamma}(x, z, \lambda, \mu) + \nabla h(x) [\mu] [z]^{-1} \nabla h(x)^T \\ & N \equiv \nabla_x L^{\gamma}(x, z, \lambda, \mu) + \nabla h(x) [z]^{-1} ([\mu] h(x) + \gamma e) \\ & \begin{bmatrix} M & \nabla g(x) \\ \nabla g(x)^T & 0 \end{bmatrix} \begin{bmatrix} \Delta x \\ \Delta \lambda \end{bmatrix} = \begin{bmatrix} -N \\ -g(x) \end{bmatrix} \\ & \Delta z = -h(x) - z - \nabla h(x)^T \Delta x \\ & \Delta \mu = -\mu + [z]^{-1} (\gamma e - [\mu] \Delta z) \end{aligned} \tag{29}$$

The variables are updated according to

$$
\begin{aligned}
&\alpha_p = \min(\xi \min_{\Delta z_j < 0} (-z_j / \Delta z_j), 1) \\
&\alpha_d = \min(\xi \min_{\Delta \mu_j < 0} (-\mu_j / \Delta \mu_j), 1) \\
&x = x + \alpha_p \Delta x; \quad z = z + \alpha_p \Delta z \\
&\lambda = \lambda + \alpha_d \Delta \lambda; \; \mu = \mu + \alpha_d \Delta \mu; \; \gamma = \sigma(\mu^T z) / ni
\end{aligned}
\tag{30}
$$

where ξ and σ are constants.

4. LONG-TERM DEVELOPMENT PLANNING STRATEGIES

A mathematical model of power system (PS) is the system, which makes it possible to calculate and assess criteria of the analysed system with a view to make justified decisions on system sustainable development. To enable computer implementation of the given task, data are required as well as appropriate software providing optimization algorithm and algorithms for calculating generating nodes output and transmission network links load. Active power flow calculation results are used for criterion calculations in development tasks. The major criterion of PS development process is management optimization objective function which shall display and integrate technical, economical, power supply reliability, ecological etc. parameters depending on specific technical system:

$$\max F(T,g) = \sum_{t=1}^{T} F(t, e(t)), \tag{31}$$

where t - development step serial number, T - number of development steps in estimation period, $F(t,e(t))$ - system quality criterion in development step t and state $e(t)$, g - development plan (process) $e(1), e(2), \ldots, e(t), \ldots, e(T)$.

Each plan is characterized by number of realized development actions n and its realization moment t, as well as by each development action realization type. The total number of development plans may be calculated by the following formula:

$$V = \prod_{i=1}^{n} V_i = (T+1)^n \prod_{i=1}^{n} m_i, \tag{32}$$

where n – number of development actions, m_i - development action realization type number, i - development action serial number, T - number of development steps in estimation period.

Obviously, also in real tasks (for example $m = 1, n = 11, T = 15$) the number of comparable development plans attains astronomic quantity (10^{15}). Therefore, it is required to apply specialized dynamic optimization methods in PS sustainable development management process [8].

5. CASE STUDY

5.1. Base case without congestions

For the calculation, consider the example shown in Fig. 4. The model consists three zones with piecewise linear costs for each zone. Transmission lines admittances are assumed to be equal to each other. Results are shown in table 1 and 2.

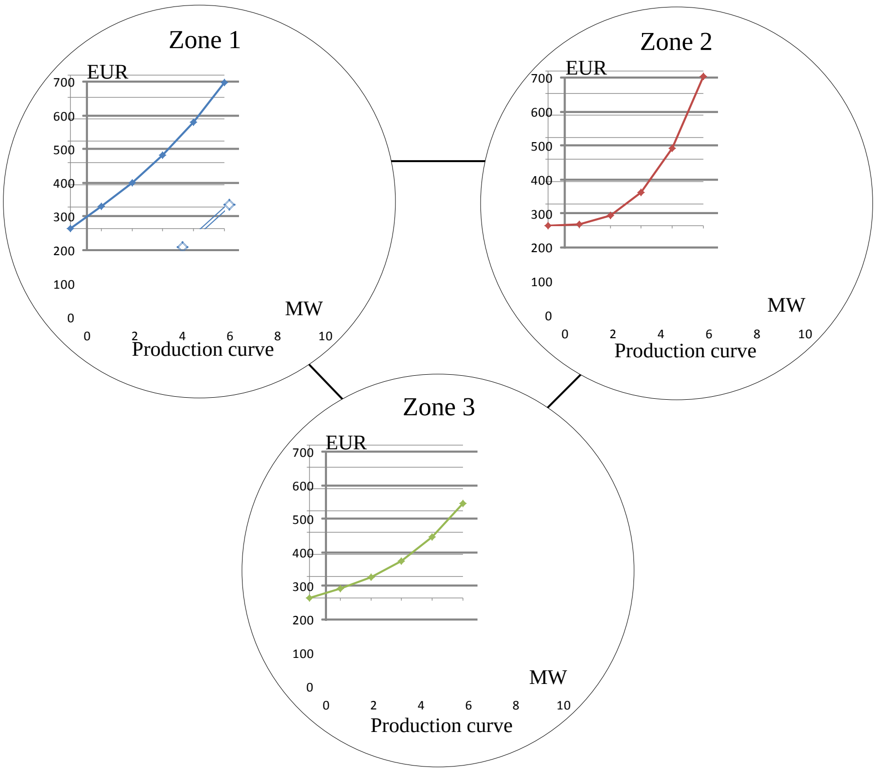

Fig. 4. Three-zone model

Table 1. Base case flows, load, zone prices and export/import (1 example)

Zone number	**Flows**			**Generation, MW**	**Load, MW**	**Zone Price, EUR**	**Total Export or Import, MW**	**Social Welfare, EUR**
	1	2	3					
1	-	1	0	6	5	69.55	1	765,47
2	-1	-	-1	6	8	69.55	-2	
3	0	1	-	8	7	69.55	1	

Table 2. Base case flows, load, zone prices and export/import (2 example)

Zone number	**Flows**			**Generation, MW**	**Load, MW**	**Zone Price, EUR**	**Total Export or Import, MW**	**Social Welfare, EUR**
	1	2	3					
1	-	-0,67	-3,33	6	10	68.09	-4	765,47
2	0,67	-	-2,67	6	8	68.09	-2	
3	3,33	2,67	-	2	7	68.09	6	

5.2. Congested case

In this case we create congestion by changing the transmission line available transmission capacity (ATC). All lines in the model have same transmission capacity and change respectively 0.9MW, 0.5 MW. Results are shown in table 3 and 4.

Table 3. Congested case flows, load, zone prices and export/import (1 example with ATC 0.9 MW)

Zone number	**Flows**			**Generation, MW**	**Load, MW**	**Zone Price, EUR**	**Total Export or Import, MW**	**Social Welfare, EUR**
	1	2	3					
1	-	0.9	0	5.9	5	62.67	0.9	773.68
2	-0.9	-	-0.9	6.2	8	99.67	-1.8	
3	0	0.9	-	7.9	7	54.53	0.9	

Table 4. Congested case flows, load, zone prices and export/import (2 example with ATC 0.5 MW)

Zone number	**Flows**			**Generation, MW**	**Load, MW**	**Zone Price, EUR**	**Total Export or Import, MW**	**Social Welfare, EUR**
	1	2	3					
1	-	0.5	0	5.5	5	62.67	0.5	806.53
2	-0.5	-	-0.5	7	8	99.67	-1	
3	0.5	0	-	7.5	7	54.53	0.5	

Perform the calculation with different ATC. Between: 1 and 2 zone 0.9 MW, 1 and 3 zone 0.7MW, 2 and 3 zone 0.4 MW

Table 5. Congested case flows, load, zone prices and export/import

Zone number	**Flows**			**Generation, MW**	**Load, MW**	**Zone Price, EUR**	**Total Export or Import, MW**	**Social Welfare, EUR**
	1	2	3					
1	-	0.9	0.5	6.4	5	74.67	1.4	805.11
2	-0.9	-	-0,4	6.7	8	99.67	-1.3	
3	-0.5	0.4	-	6.9	7	54.53	-0.1	

Examples show algorithm work based on piecewise linear costs. In connection that piecewise function has 5 parts, some results remain constant with ATC change. In Nord Pool spot each participant can bid 62 positions. In this case calculation results will be more precise and show realistic situation.

6. CONCLUSIONS

The paper describes the course of the research from description of the problem to algorithm development and value calculation. This research reflects one of the many problems, which need to be solved in imminent future and then utilized for power transmission network modeling and development tasks, for example, increasing integration in the Baltic electricity and Europe-wide interconnection establishment.

From the theoretical point of view the nodal pricing principles provides the more efficient system of pricing in comparison zonal prices. On the other hand is large number of nodal prices compared to several zonal prices could be assumed as confusing and with lower transparent.

Discussed pricing principles from the OPF point of view as well as for the sustainable development management applications.

ACKNOWLEDGMENT

The paper is supported by the European Social Fund Project "Scientific Group Supporting Latvian Activities of the European Strategic Energy Technology Plan", No.1DP/1.1.1.2.0/09/APIA/VIAA/027

REFERENCES

1. TARJEI K. “Utilizing Matpower in optimal power flow”. Link to the internet: <http://www.elkraft.ntnu.no/~tarjei/matpower_opf.pdf>
2. RAY D. ZIMMERMAN, CARLOS E. MURILLO-SÁNCHEZ, ROBERT J. THOMAS, “MATPOWER’s Extensible Optimal Power Flow Architecture”. Link to the internet: <http://www.pserc.cornell.edu/matpower/MATPOWER-OPF.pdf>
3. THOMAS J. OVERBYE, XU CHENG, YAN SUN, “A Comparison of the AC and DC Power Flow Models for LMP Calculations”. Proceedings of the 37th Hawaii International Conference on System Sciences – 2004.
4. H. WANG, C. E. MURILLO-S´ANCHEZ, R. D. ZIMMERMAN, AND R. J. THOMAS, “On computational issues of market-based optimal power flow,” Power Systems, IEEE Transactions on, vol. 22, no. 3, pp. 1185–1193, August 2007.
5. KAUSTUV. “IPSOL: An interior point solver for nonconvex optimization problems”. Link to the internet < http://www.stanford.edu/group/SOL/dissertations/kaustuv-thesis.pdf>.
6. RAY D. ZIMMERMAN, CARLOS E. MURILLO-SÁNCHEZ, MATPOWER - A MATLAB Power System Simulation Package, User’s Manual, School of Electrical Engineering, Cornell University, 2011. Link to the internet:: <http://www.pserc.cornell.edu/matpower/manual.pdf >.
7. RAY D. ZIMMERMAN, CARLOS E. MURILLO-SÁNCHEZ & DEQIANG (DAVID) GAN, MATPOWER v4.1 (MATLAB Power System Simulation Package). Link to the internet: <http://www.pserc.cornell.edu/matpower/>.
8. KRISHANS Z., MUTULE A., MERKURYEV Y., OLEINIKOVA I., “Dynamic management of Sustainable Development: Methods for Large Technical Systems”, in Hardcover, 1st ed., Springer, 2010.

CYSENI 2012, May 24–25, Kaunas, Lithuania
ISSN 1822-7554, www.cyseni.com

METHODS USED FOR STIMULATION OF “GREEN” CHP DEVELOPMENT IN LATVIA

T. Odineca
Riga Technical University, Building Faculty, SGUTI
Azenes 16/20, Riga, LV-1048 - Latvia
Phone 371 29597650
Email: tatjana.odineca@gmail.com

ABSTRACT

The paper observes different steps which can be made to stimulate the development of cogeneration using renewable fuels in Latvia.

Latvia, as a European Union Member state, has to increase the share of renewable energy sources (RES) in the final gross energy consumption, to increase energy efficiency and to reduce the greenhouse gas emissions by 2020. The combination of RES and CHP is a key approach to reach the ambitious EU climate protection targets.

The following support schemes are used in Latvia for CHP using RES: feed-in-tariffs, obligate buying of co-generated power, EU earmarked subsidies for the development of RES using CHP plants. The feed-in-tariffs depend on the installed electricity capacity of the CHP units. The main weak point of the policy measures can be identified as discrimination between different cogeneration plants, and particularly of small systems, because at least 75 % of the heat produced has to be supplied to the district heating, hence the policy does not support industrial or auto-use of co-generated heat. It is necessary to simplify technical and administrative procedure for newly constructed CHP plants, especially for the small ones.

The training program “Sustainable heating system with renewable energy resource” has started in Latvia in 2011. The sustainable energy community model (SEC) modified for Latvian conditions is used in the project. While implementing this program it is possible to stimulate the further development of cogeneration, using local RES. Wood is the main local renewable fuel in Latvia. Highly efficient CHP equipment fuelled by RES (like wood gasification) is not yet widely spread and implemented.

Latvia participates in the EU project "CHP goes Green". The target for the selected model cities involved in the project is to promote and install "Green CHP" and the respective technical solutions.

Reaching the 2020 targets set for Latvia will be possible only if sustainable, well-considered long-term energy and environmental policy is implemented, which includes effective support scheme for CHP using renewable energy sources.

Keywords: cogeneration, local level energy policies, main drivers and main barriers for grows of renewable energy

1. INTRODUCTION

To achieve the aims of European Union (EU) energy and climate policy till 2013-2020, the European countries have to concentrate on increasing both energy efficiency and renewable fuels usage. The possible principles of Energy Policy for Europe were elaborated in the Commission's green paper *A European Strategy for Sustainable, Competitive and Secure Energy* in 2006. As a result of the decision to develop a common energy policy, the first proposals, *Energy for a Changing World* were published by the European Comission, following a consultation process in 2007. The European Commission has proposed in its Renewable Energy Roadmap21 a binding target of increasing the level of renewable energy in the EU's overall mix to 20% by 2020. The targets for the member states are calculated using formula: flat rate 5.75% (one for all EU countries) + extra % (according to GDP).

According to the European Climate and Energy package Latvia, as a European Union Member state, has to increase the renewable energy as a part of gross final energy consumption from 35% in 2005 to 42% in 2020 [6], to increase energy efficiency and to reduce the greenhouse gas emissions by 2020. The combination of renewable energy sources (RES) and combined heat and power (CHP) is a key approach to reach the ambitious EU climate protection targets. The aim of the paper is to observe different steps which can be made to stimulate the development of small cogeneration using renewable fuels in Latvia.

2. USAGE OF RES FOR CHP PLANTS IN LATVIA

2.1. Latvian energy policy towards CHP plants

Reaching the long-term goals of Latvia's energy sector is a complex process that involves finalizing a long-term strategy, defining and justifying feasible goals and tasks, as well as establishing specific political, legal and institutional frameworks and tools.

The key strategic document for the energy sector is The Principles of Energy Sector Development 2007-2016, adopted in 2006 [3]. This document defines the fundamental principles of the Latvian government policy, as well as long-term goals and course of action in the energy sector. The importance of the energy sector in the context of overall sustainable development is acknowledged: "The sufficiency of energy supply in the country is the issue of economic development, the quality of life and state security. The goal of the energy sector development is to ensure balanced, safe, sustainable high quality supply of energy for the economy and country's residents." The goals spelled in the document are identical to the "three whales" of the energy sector as defined by the EU, namely: 1) secure supply, 2) encouraged competition and competitiveness, and 3) use of renewable resources.

The following plans of action were mentioned to put the Principles of Energy Sector Development 2007–2016 into practice:

- until 2016 to use the potential of cogeneration with common heating load about 300 MW_{th} in Latvian big cities (including Riga), and 100 MW_{th} in other Latvian cities;
- to stimulate the development of CHP plants and energy producing of renewable sources of energy, using special purpose grants of EU funds for investments;
- to increase the usage of local renewable primary resources from 65 PJ at the moment to 82 PJ in 2016 (36–37% of local resources in Latvian primary energy resources structure);
- until 2016 to increase the energy efficiency of heat production equipments from 68% to 80–90%.

Using of cogeneration technology is considered appropriate to Latvia's situation: Latvia has characteristic centralized power supply system, which means inhabited areas have sufficiently high heat loads to accommodate installation an efficient cogeneration facility. A cogeneration source is close to the heat load, i.e. the energy consumer, who is consuming power at the same time. This means that cogeneration technology has all the advantages of placing an energy source next to the consumer, such as reduced power management and distribution leakage, and increased power supply stability.

A wide variety of fuels can be used in CHP systems, including natural gas, diesel, biofuels, coal, municipal waste. CHP plants operate at total energy efficiencies of 75-95 %, which means that almost all of the fuel is put to productive use. Because less fuel is used, obvious benefits are received:

- reduced fuel costs;
- reduced fuel supply needs, bringing to the reduction in the logistical needs for transportation and storage the fuel;
- reduction in emission levels;
- fewer pollutants passing through the engine or turbine, resulting in a longer life of equipment.

2.2. Review of existing CHP plants in Latvia

Basing on data of the Central Statistical Bureau show that in 2010 in the Republic of Latvia there were 71 active combined heat and power (CHP) plant with total electrical capacity 947.5 megawatts (MW) [6]. These CHP plants produced 3050 gigawatt hours (GWh) of electricity and 4673 GWh of heat, and it is 58.7% of total volume of heat produced.

There are two types of CHP plants:

- public CHP plants primary activity of which is generation of heat energy;
- autoproducer CHP plants are generating heat for their own production and technological use and partly for sale.

Out of 71 CHP plant active in 2010 56 were public cogeneration plants with installed electrical capacity 932.8 MW, it is 98.4% of total installed capacity of CHP plants, and 15 were autoproducer CHP plants with installed electrical capacity 14.7 MW.

In comparison with 2009, electrical power of cogeneration plants has increased by 1.4%.CHP plants of Riga had the highest installed electrical capacity – 876.3 MW.

In 2010 for the production of heat energy and electricity CHP plants mainly used natural gas (98.1%), as well as biogas, fuelwood, coal, residual (heavy) fuel oils and bio-diesel oil.

Out of 71 CHP plant active in 2010 56 plants (both public and autoproducer) with total electric capacity 870 MW were active more than 6 months, of which:

- 3 combined-cycle turbines with electrical capacity 803 MW;
- 1 gas turbine with heat utilisation;
- 48 internal combustion engines with electrical capacity 61 MW;
- 3 steam backpressure turbines with electrical capacity 4 MW;
- 1 condensing steam turbine.

2.3. Usage of renewable energy sources for CHP

Today for the production of energy CHP plants mainly use natural gas (98.1%). It is explained by the fact, that using natural gas as a fuel, it is possible to apply highly effective (with high α-ratio) CHP technologies. One of Latvia's advantages, which also serve as a kind of short-term guarantee of continual supply, is its underground gas storage facilities. The amount of active gas in currently functional Incukalns underground storage may reach 2.3 billion cubic meters, and there are plans to increase this amount to 3.2 billion cubic meters. The expansion of these storage facilities may bring about several significant advantages, such as strategic reserves, economic benefits and improvement of regional energy supply. Nevertheless, it may also boost local energy and production companies' inclination to use imported gas instead of exploring sustainable local options by means of increasing energy efficiency and using renewable energy sources.

Considering the aforementioned local and regional challenges, as well as the EU commitments, it would make sense for Latvia to utilize the potential of local renewable sources, the largest of which is wood. The economic potential of wood is estimated around 45.5 – 82 PJ a year, which constitutes considerable part of the country's total energy consumption.

By now, in Latvia the most common and well known technology where wood biomass is used for cogeneration is steam turbine. There are two CHP plants with steam turbines: AS "Rigas siltums" heat central "Daugavgriva" in Riga (reconstructed in 2004; electrical capacity 0.6 MW and thermal capacity 27,2 MW), and SIA "Kraslavas nami" in Kraslava (works since 2000; electrical capacity 1.25 MW and thermal capacity 34 MW); both are fuelled by woodchips [7].

Wood gasification technology (a thermo dynamical process that converts wood to a gaseous fuel) used in cogeneration process is more effective than common combustion of wood, because generated gas can be a fuel for such effective CHP technologies as gas turbines, gas-steam turbines and internal combustion sets. Wood gasification is less dangerous for enviroment comparing to common combustion, because during gasification process less emissions go to the atmosphere. Usage of wood fuels not only helps to increase the part of renewable energy in gross final energy consumption, but also gives an opportunity to get more independence from importing of fossil fuel resources. Besides, gas distribution system in Latvia does not cover large territories, including the territories with big forest density. The advantage of the use of biomass in cogeneration is self-evident, as it allows high efficiency combined with an increase of renewables' share. While CHP equipment fuelled by RES seems to be first choice from the standpoint of energy efficiency and technical availability, it is not yet widely spread and implemented.

If gas is used in an internal combustion engine for the production of electrical energy, it demands special quality of gasifier and gas. World’s experience of exploitation of this kind of systems shows, that they are sensitive to the changes of fuel parameters, changes of the load of equipment, quality of service, and environmental conditions. Necessity of cleaning, cooling and mixing of gas makes technology rather difficult and expensive.

The idea of wood gasification is becoming rather popular, despite problems related to required high quality of fuel and cleaning of produced gas. Today, there are two CHP plants where wood gasification is applied: SIA „Kņavas granulas” in Vilani (electrical capacity 500 kW and thermal capacity 800 kW) is fuelled by wood granules (the drying of fuel is not necessary), and SIA „Zaļās enerģijas aģentūra“ in Dagda (works since 2010; electrical capacity 500 kW and thermal capacity 800 kW; internal combustion engine installed) is fuelled by dry woodblocks and dried coarse fraction woodchips.

Despite the technology of organic Renkin cycle (ORC) is new for Latvia, the interest for it is increasing. At the moment there are 5 new ORC projects at a construction stage, and there are two CHP plants where ORC is already used: SIA “Osukalns” in Jekabpils (works since 2011; electrical capacity 1.4 MW and thermal capacity 5.3 MW) is fuelled by wood residues, and AS “Satini Energo LM” in Saldus (works since 2011; electrical capacity 0.6 MW and thermal capacity 2.6 MW) is fuelled by woodchips [7].

3. METHODS OF SUPPORT OF „GREEN“ CHP DEVELOPMENT IN LATVIA

3.1. CHP goes „green”

Since 2010 Latvia participates in the EU project "CHP goes Green". The target for the selected model cities (Berlin, Frankfurt/Main, Hannover, Graz, Prague, Riga, Lyon and Paris) involved in the project is to promote and install "Green CHP" and the respective technical solutions.

All players in the decision-making chain are addressed by CHP goes Green: public and private buildings owners, local key politicians, municipalities, planning engineers, installers, energy companies and industry.

The benefits to the target groups are manifold such as:

- solution-oriented contributions to reaching local energy goals;
- information in terms of innovations, competition and best choices;
- the provision of contact with target groups;
- considerations in terms of feasibility of CHP solutions.

The following major outputs related to the goal will be implemented:

- analysis of the regional legal and economical framework and its impact on the regional market exemplarily for the model region;
- derivation of action and implementation plans of good practice specific for the model region;
- the public campaigns addressing policy and decision makers, building owners and young people as future decision makers;

- target-group specific promotion of best practices for RES-fueled CHP approaching different groups of building owners, planners and installers;
- initiating new RES-CHP applications;
- training of above mentioned decision makers with regard to technical, ecological and economical issues to support the practical implementation of RES-fueled CHP.

Access to information is a problem in the public energy supply system of Latvia. The frequently used argument goes that energy consumers do not understand this complex issue and therefore no information needs to be released to the general public, except for the regulated energy tariffs. Yet sustainable development is unfathomable without the awareness and understanding of energy producers' and energy consumers' actions and their mutual interconnectivity. Latvia has not made sure there is a system allowing energy consumers to obtain information about the sources of the energy they consume, about the security of energy supply, price predictability and alternative energy options. The lack of such a system hinders the development of a clear policy of the energy sector and impedes investment.

Within the limits of the project the following public actions are being suggested in Latvia: informative seminars, learning excursions to the CHP plants using renewable fuels, training courses, consultations on making the technically-economic justification for new CHP projects. Unfortunately, the interest for training courses and seminars is not as high as it could be expected. The main reason of it can be the lack of information about the actions of CHP goes Green for the wide circle of people.

3.2. Applying a Sustainable Energy Community model for development of „green“ CHP

A Sustainable Energy Community is the integration and collaborative action in the wider community (e.g. town or region) to expand and replicate ideas tested in the clearly defined geographic area called the Sustainable Energy Zone (SEZ). This is delivered through structured engagement with the wider public, private and community sectors to identify synergies and supporting initiatives to influence positive changes in behavior and policy. An SEC is community in which everyone works together to adopt a more sustainable pattern of energy supply and use. The SEZ establishes sustainable energy targets that are measured and monitored and creates a focal point for partners, projects and proposals to integrate in a structured way. This allows new technologies and techniques to be tried and tested in an incubator or living laboratory environment [8].

Applying the SEC model modified for Latvian circumstances, firstly, it is analyzed the energy efficiency of different Latvian regions, to find out the Sustainable Energy Zone – the most perspective field for using the SEC method.

Then starts the energy development planning process, which includes 8 steps:

- forming the total vision of region (local energy resources, economy, demography, etc);
- defining of motivation power in region;
- defining of base line of development;
- working out the scenarios of development;
- formulating the strategy;
- formulating the plan of actions;
- monitoring and estimating the progress;
- adapting the new information for the planning process.

Table 1. Instruments used for applying of SEC methodology in Latvia

Planning instruments	Institutional instruments	Financial instruments	Communicative instruments
1.Formulating of strategy (for regions and districts) 2. Formulating the plan of actions 3. Energy audit	1. Organising of energy service 2. Cooperation with administration of a district, energy supplying organizations	1. The main instruments: owners, investors, state garanties, budget programms 2. The additional instruments: the RES and ecology funds	1. Meetings with inhabitans of district 2. Informative presentations

In 2011 in Latvia there was started a training program “Sustainable heating system with renewable energy resource”, where the modified SEC model is used. While implementing this kind of programs it is possible to stimulate the farther development of cogeneration in different Latvian regions, using local renewable energy sources.

3.3. Documents regulating producing of energy in CHP plants using RES

The development of cogeneration using renewable energy sources is not possible without support of government. The support schemes in different European countries include feed-in-tariffs, green certificates, obligate buying of co-generated electrical power, tax exemptions or reductions, tax refunds, premium payments. There are also volunteer support actions, which are based mainly on consumers’ wish to pay higher price for renewable energy, but the influence of these actions on development of “green” cogeneration is minimal [1].

The most important energy-related legislative document in Latvia is the Energy Law (2005), which regulates the use of and support for all renewable resources. The government has also adopted a series of regulations for CHP plants; the most notable among them is the Regulation Nr. 221 of the Cabinet of Ministers “The Regulation of electrical energy production and forming of prices while producing electrical energy in CHP” (10 March, 2009), and the Regulation No 198 “The Regulation on Electric Power Production and Pricing Using Renewable Energy Sources”.

Of many possible options of support schemes for CHP using renewable energy sources, in Latvia there are used the following: feed-in-tariffs, obligatory buying of co-generated electrical power, EU earmarked subsidies for the development of CHP plants using RES.

The feed-in-tariffs, defined by Regulation Nr.221, depend on the installed electricity capacity of the CHP units. The main weak point of the policy measures can be identified as discrimination between different cogeneration plants, and particularly of small and micro systems, because at least 75% of the heat produced has to be supplied to the district heating. In the latest edit of the Regulation Nr.221, a few changes referring to small capacity CHP plants were introduced. In period from 2007 to 2010, number of CHP plants with electrical capacity 0.2–5 MW significantly increased.

The policy does not support industrial or individual-use of cogeneration.

The pricing formula for the feed-in tariffs should have economically sound calculations at its base, such as the investment costs into renewable energy technologies, the cost of resources, the differentiation of support level to different power stations. The feed-in tariff pricing for energy produced by biomass and biogas power stations depends on the differential tariff rates for the end users of natural gas. This can seriously complicate cost and income planning for the businesses in question, as well as increase their risks in dealing with lending institutions.

4. CONCLUSIONS

1. Further market penetration of higher share of cogeneration fuelled by renewables requires removing barriers from the legislative and administrative framework, requires planning and cooperation, capacitating of technical decision makers and general awareness-raising and trust-building among potential promoters, multipliers and users. Moreover it is a question of cost if alternatives are considered. It is worth investing in developing the new effective technologies used in cogeneration (wood gasification).
2. Usage of modified for Latvian circumstances SEC methodology is appropriate for development of cogeneration in definite Latvian districts, applying local renewable energy sources (particularly wood).
3. It is necessary to simplify technical and administrative procedure for newly created CHP plants, especially for the ones with small capacity and the ones using renewable fuel. The support mechanisms for using of cogeneration have to apply not only to businesses, but also to individuals. It also can be recommended to abolish the natural gas tariff as an element of the pricing formula for electricity produced at CHP plants using renewables.

REFERENCES

1. Andris Sprūds. Latvian energy policy: towards a sustainable and transparent energy sector. Soros Foundation - Latvia, 2010
2. David Flin. Cogeneration: a user’s guide. 2010 The Institution of Engineering and Technology, London, United Kingdom
3. Enerģētikas attīstības pamatnostādnes 2007. – 2016. gadam: Latvijas Republikas Ekonomikas ministrija, 16.06.2006.
4. Noteikumi par elektroenerģijas ražošanu un cenu noteikšanu, ražojot elektroenerģiju koģenerācijā. Ministru kabineta noteikumi Nr.221. Rīgā 2009.gada 10.martā (prot. Nr.17 56.§)
5. Koģenerācijas stacijās saražotās siltumenerģijas un koģenerācijas stacijās ar jaudu virs 4MW saražotas elektroenerģijas tarifu aprēķināšans metodika: SPRK metodika. 2005.gada 21.decembrī (prot.Nr.54 (263), 6 p.).
6. http://www.csb.gov.lv/en/notikumi/activities-combined-heat-and-power-plants-2010-31985.html
7. http://www.chp-goes-green.info/drupal/sites/default/files/documents/chp-riga/downloads/Nr1_Kogeneracijas_stacijas_prakse.pdf
8. http://www.seai.ie/SEC/SEC_Programme/

CYSENI 2012, May 24–25, Kaunas, Lithuania
ISSN 1822-7554, www.cyseni.com

NUCLEAR WASTE MANAGEMENT PROGRAMMES WITHIN SWEDEN AND IN THE UNITED KINGDOM

U. Roßegger
Technical University of Braunschweig
Section Public Law and Administrative Sciences
Bienroder Weg 87, D-38106 Braunschweig – Germany
Phone +49 (0) 531 391 - 2465
Email: u.rossegger@tu-bs.de

ABSTRACT

In the controversy over a safe and permanent disposal of nuclear waste, numerous solutions have been put forward. While from a scientifical point of view answers are inconclusive, the option of geological disposal seems to be the most common approach in most European countries with regard to high-level nuclear waste.

In view of this discrepancy, the objective of this paper is to analyze the organisation of nuclear waste management (NWM) in Sweden and to a little extent also the United Kingdom. In addition to that, particular focus shall be put on the implementation of the respective national policies. Furthermore it will be shown what kind of responsible agencies were implemented. The paper aims at comparing, contrasting and analysing the various pursued strategies and processes as well as showing the difficulties inherent to finding a site which is both appropriate and meets with political and public acceptance.

After an outline of the historical development of the respective processes, the article attempts to identify special national phases in the development of the nuclear waste management. It then illustrates how national concepts for the direct geological disposal of domestic nuclear fuel have been implemented and which policy regimes have been introduced.

The paper particularly emphasizes the Swedish development which is due to the fact that Sweden can be considered a pioneer in the field of waste storage and its development is therefore debated with special emphasis it iniatiated the process of final high-level waste disposal already in the 1970s.

The following paragraphs will therefore discuss to what extent Sweden' s long experience with the issue of disposal entitles it to the status of a role model for other countries. In addition to that, this question shall also be little contrasted with the national strategy predominant in the UK. As a last point, the paper will question the role which international findings in the field of radioactive waste storage play in influencing the political outcome of countries.

Keywords: Nuclear Waste Management, high level waste, Sweden, United Kingdom

1. INTRODUCTION

Albeit most European countries with nuclear power are favouring the option of geological disposal as the best option to handle spent nuclear fuel (SNF) and high level nuclear waste (HLW), many of them meeting problems when nuclear waste management policies have been implemented. The potential for conflict arises on how to find a site and siting strategies that are politically and publicly acceptable, whereas Sweden seems to implement its policy for nuclear waste management (NWM) successfully. Neither to build the provisions for final storage for low- and intermediate-level waste and the interim storage nor to run these facilities in operation did provoke any strong opposition. Also the process to find a site for the final disposal of HLW has been running without any great obstacles [1].

The approach of the paper is to follow the hypothesis that technical and society conflicts are often settled within the phase of implementation. In Sweden this hypothesis is may be not validate to describe the implementation of nuclear waste management, especially for the final disposal of high level waste. Therefore it is debatable to what extent the principle of countervailing influence – top-down-process versus bottom-up-process – is an explaining factor. An integration of various stages and actors could be understood as a driver and simultaneously as a catalyzer for the whole process. The research of implementation has shifted its contents from the consideration of effectiveness to the importance of implementation for legitimating policy. With regard to NWM the governmental and administrative action has to produce an impact. Nevertheless, functionality resists as a central feature to assure quality management and to supervise the accomplishment of duties and responsibilities. This paper aims to firstly explain the process how to deal with nuclear waste in Sweden. The role of referring to scientific findings, the extent of private action in this process has been to analyze. An adaptation is easier when a formulated policy will put into practice than to handle with negotiations and substantial changes [1]. In general, a strategy has to be consistent to pave the way for locating the final disposal for spent nuclear fuel. Due to this argument some key elements have to take into account: (a) scientific paradigm, (b) environmental and economical cost-benefit-analyses, (c) the political (and) popular dimension of environmental protection, (d) public participation in environmental decision making. An integrated approach considers the technical side of the problem to dispose nuclear waste, the societal and political dimension as well as the legal basis and other framework requirements [2].

2. RESEARCH IMPLEMENTATION AS METHODOLOGICAL APPROACH

The methodology is the approach of research implementation, the question of possible causes for the discrepancy between norm (action program) and reality (impact), when program implementation is forced by orders or other programs. It is important how an operational process is organized, i.e. in the field of high level radioactive waste management. A further side effect is to evaluate success or fail elements in the process. The aim is to come to general evidence on terms and conditions exercised at political stage [8]. When referring to North on the hand and to Scharpf on the other hand, both of them have different approaches. North indicates that institutions shape actors opportunities, mental maps and incentives, while Scharpf points out actors are characterized by capabilities, perceptions and preferences (both together actor orientations). It has to be analyzed about the explaining factor: the transferability to practical issues.

The structure and useful tool of an implementation process can be seen below in Fig. 1. A core element is the tractability of the problem. In this content it derives from the mentioned core element and will be converted into two variables: (1) the ability of statute to structure implementation and (2) nonstatutory variables affecting implementation.

The basic assumption in this paper is the interaction between the technical and the societal context when a nuclear waste management process will be implemented. Whereas the technical system contains geological question, in particular engineered barriers, the societal system comprehends the public and stakeholder processes which are linked to the political system. For this paper the stages in the implementation process are most important.

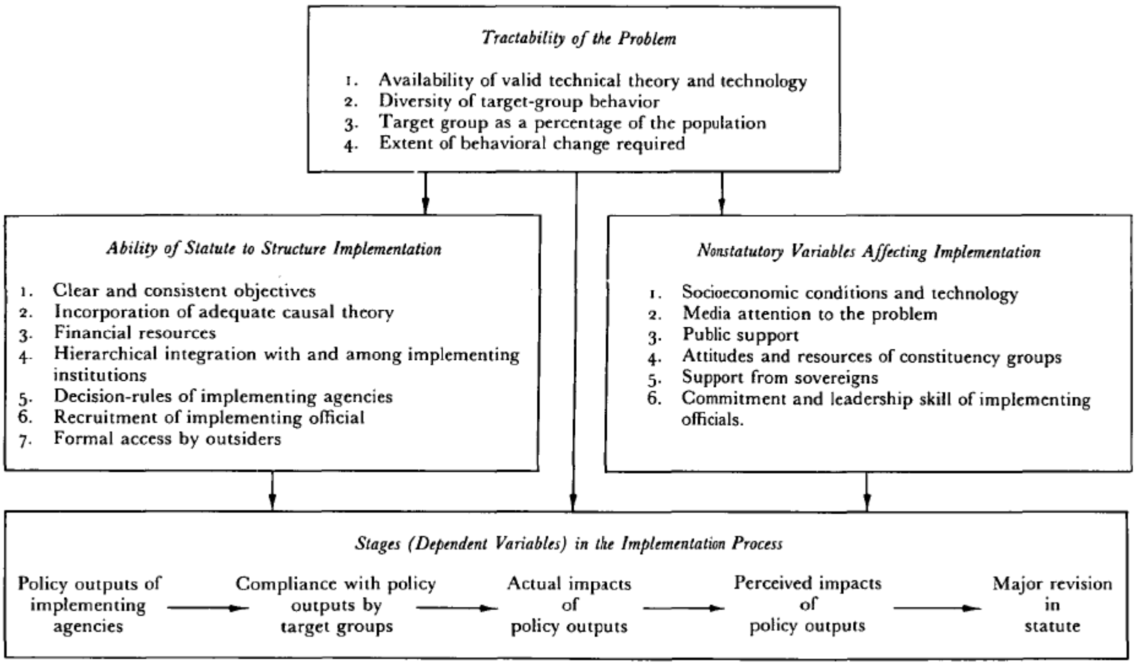

Fig. 1. Skeletal Flow Diagram of the Variables Involved in the Implementation Process [3]

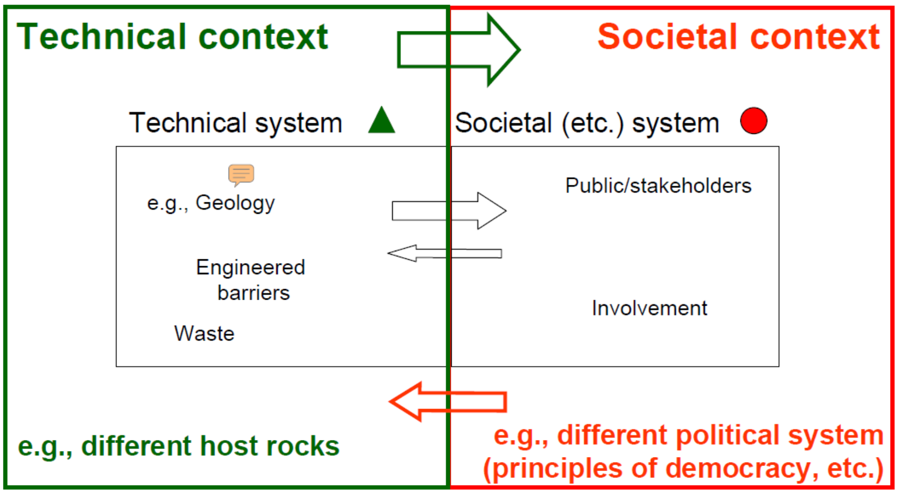

Fig. 2. Radioactive waste governance in the (geo-) technical and socio-cultural context [3]

3. THE SWEDISH SNF DISPOSAL PROGRAM

During the 1970s the process to find a site for final disposal nuclear waste has been started. In Sweden the operators have the responsibility of dispose and final dispose nuclear waste. By following the Swedish parliamentary decision these operators have found a joint associate company named SKB (Svensk Kärnbränslehantering AB) in 1972 Their responsiblity is also about transporting nuclear waste and interim storage. Traditionally there is a long-standing association between the management of spent nuclear fuel in Sweden and the industry-led SKB research, development and demonstration project [3]. For the reason of the success of the KBS project it led to a government affirmation to obsess the KBS concept. The introduction of a new legislation, the Nuclear Power Stipulation Act, has been made in February 1977 and put pressure to the reactor owners. The Act assessed that they must show exactly how and where spent fuel can be disposed in a absolute safety manner. It was linked to the permission can be granted to fuel any other reactor [7, p. 251, 1977 STS – Svensk Författningssamling]. An important change was made when the Stipulation Act had replaced by the Act on Nuclear Activities in 1984. In addition, the wording „absolute“ safety was transfered to the reconfirmation that reactor owners were to be held responsible for a „comprehensive research and development programme“ guaranteeing the safe handling, interim storage and domestic geological disposal [7].

Nearly 30 years the whole process is focused to a stepwise implemenation of the multi-barrier KBS-3 concept for final disposal of nuclear fuel.

Sundqvist [4] says that the Swedish society has a high trust in the nuclear industry because it appears to the public that Swedish nuclear power plants operators have a solution to deal with the nuclear waste disposal problem. In 1977, SKB has installed a labour about reposition technology at the location of the former mine Stripa to start research activities. Already in 1983, the SKB has published a report named „KBS-3“ as a concept of encapsulate the spent fuel, inside of a natural rock formation. Furthermore, it is protected by additional engineering barriers like Bentonite rings.

In the 1990s the laboratory for reposition technology has moved to Oskarshamn at a depth of 460 meters – research work has been set up from 1990 to 1995. In the period from 1993 to 2000 the SKB has made eight feasibility studies. The two local sites Storuman und Malä withdrawal in this process caused by negative municipal referendums. Five out of six local sites - Östhammar, Nyköping, Tierp, Oskarshamn, Hultsfred and Älvkarleby – seemed to be appropriate for a final disposal site. Due to the Swedish Environmental Code, a comprehensive environmental legislation has introduced in 1999 has required an Environmental Impact Assessment process; 20 years after the KBS project was initiated [3] [6].

With regard to sites the SKB has attracted Östhammar (close to Forsmark), Oskarshamn and Tierp as shortlisted. While Tierp has rejected and resigned the two muncipal councils of Östhammar and Oskarhamn have resolved to allow exploration drillings, which began in 2002 [6]. In June 2009, SKB has opted for the location Forsmark. For this reason Oskarshamn Municipality has received a financial compensation. For long-term development projects in the municipality SKB will invest 1.5 billion Swedish kronor [6]. In March 2011, the SKB has submitted an application to the Swedish Radiation Safety Authority to accredit the construction of a repository at Forsmark. According to SKB's view the planning permission for the repository ought to be available in 2015 and site is to be ready in 2025.

Table 1. Timeline of the Swedish Nuclear Waste Management process [4]

Year	Issue
1976	Launch of the ‘KBS’ nuclear fuel safety project
1984	Approval of the industry report about KBS-3 as a basis for the research, development and demonstration programme; reporting on every third year
1990s	The Swedish Nuclear Fuel and Waste Management Company (SKB) conducts geological surveys on regional and local levels in order to select a site for the repository
2002	SKB begins site investigations for a repository at two potential sites: in Forsmark (Östhammar Municipality) and in Simpevarp-Laxemar (Oskarshamn Municipality)
2007	Site investigations are finished
2009	SKB selects Forsmark for the repository. The Swedish Government will nevertheless make the final decision on whether the repository will be constructed on the chosen site
2011	SKB has submitted a licence application again in full on 16 March 2011 to construct the repository in Forsmark

At least, the KBS-3 concept still represents a suitable way how to deal with high-level nuclear waste. The counterpart is that the concept has remained incomplete so long as a local site for final disposal has been undetermined. ELAM/SUNDQVIST [5] conclude that the Swedish nuclear waste management programme has a positive reputation because of the fluidity, heterogeneity and multiple nature of the KBS-3 concept. The question is if KBS Programme has delivered for more than 30 years a practical solution to the Swedish nuclear waste problem or has the KBS Programme just achieved what it initially set out to do. The KBS Programme has always being more concerned with the the production of hard and fast signs of the safe disposability of nuclear waste, rather than with actual disposal itself [7, p. 247]. In general, Sweden has introduced a eleven-part proceeding and its override by five elements: (1) reference design, (2) site description, (3) research and development, (4) results of earlier assessments and (5) databases.

In sum, the Swedish paradigm how to find a national solution to nuclear fuel safety is brought at international level by the reason of recent internationalisation of the Swedish nuclear industry [6]. Therefore, the Swedish underground storage concept is highly interesting for other countries in Europe, e.g. in the United Kingdom [5].

One interpretation of the KBS Programme is that it has labelled as “good nuclear governance” and has established even before the term government was discussed in broader perspective as new forms of “governing without government” [5].

4. THE SWEDISH KBS-3-METHOD

According to the KBS-3-method for the final repository for spent nuclear fuel, SKB’s proposal is to encapsulate the spent nuclear fuel in copper canisters with cast iron inserts and depositing the canisters at a depth of about 500 metres in the bedrocks. Therefore, stable mechanical and chemical conditions are needed. Impermeable copper canisters are embedded in bentonite clay. Additionally SKB points out that the clay constitutes a buffer against minor rock movements and prevents corrosive substances from getting in to the canister. An effective absorption of radionuclides is in place, if the canister is damaged [7].

The idea of the Swedish final repository for spent nuclear fuel is based on the principle of multi barriers. Three barriers, the canister, the buffer and the rock constitute are the repository’ s barriers. In sum, this structure shall prevent radioactive substances from reaching ground level and harming man and the environment. According to SSM regulations (SSMFS 2008:21) [21] the safety assessment has to cover a period for at least 100,000 years after the closure of the repository to contain nuclear waste safe. For this duration the barriers function has to be in place [9].

Regarding the quantitative risk analysis for the first 100,000 years the General Guidance state the following: *“Supplementary indicators of the repository’s protective capability, such as barrier functions, radionuclide fluxes and concentrations in the environment, should be used to strengthen the confidence in the calculated risks.”*

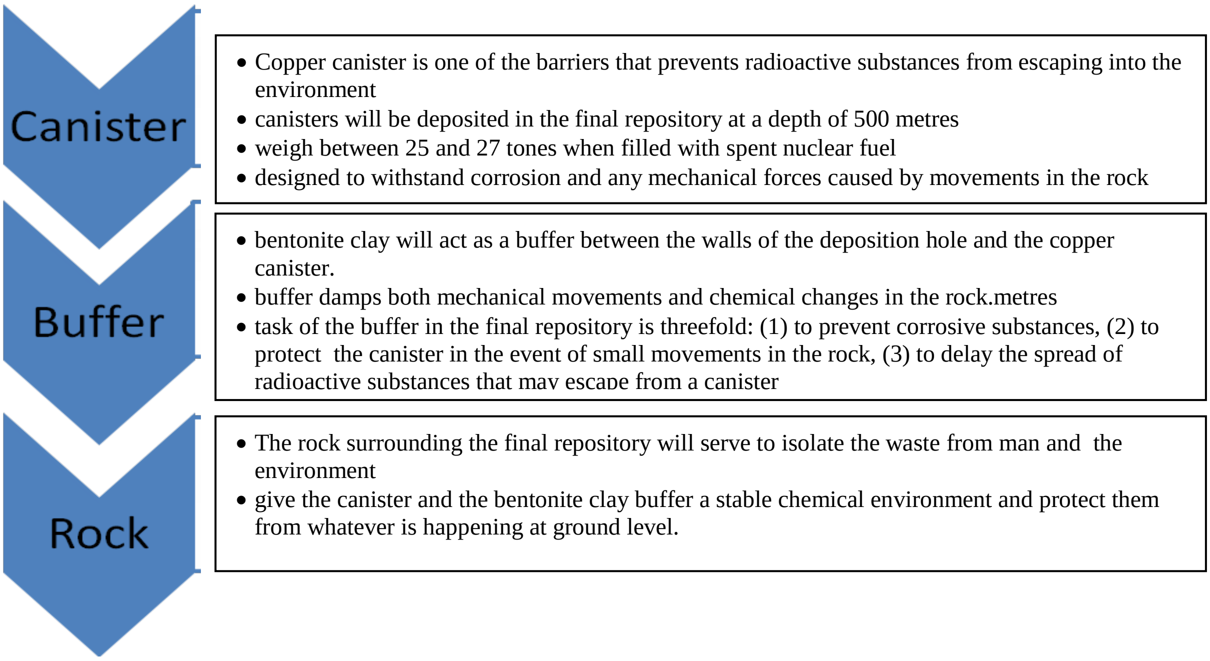

- Copper canister is one of the barriers that prevents radioactive substances from escaping into the environment
- canisters will be deposited in the final repository at a depth of 500 metres
- weigh between 25 and 27 tones when filled with spent nuclear fuel
- designed to withstand corrosion and any mechanical forces caused by movements in the rock

- bentonite clay will act as a buffer between the walls of the deposition hole and the copper canister.
- buffer damps both mechanical movements and chemical changes in the rock.metres
- task of the buffer in the final repository is threefold: (1) to prevent corrosive substances, (2) to protect the canister in the event of small movements in the rock, (3) to delay the spread of radioactive substances that may escape from a canister

- The rock surrounding the final repository will serve to isolate the waste from man and the environment
- give the canister and the bentonite clay buffer a stable chemical environment and protect them from whatever is happening at ground level.

Fig. 3. 3-barrier-system or KBS-3-method

In Sweden the copper canister plays an important role in the design of the repository. Therefore, long-term physical and chemical stability of copper in aqueous environments is required when the safety evolution in a disposal concept is guaranteed. The corrosion resistance of copper is put into question caused by results under anoxic conditions in aqueous solution. The conflict is about the verification of safety of copper in comparison with final disposal while public and political concerns were verbalized. On 16 November 2009, the Swedish National Council for Nuclear Waste has organized a workshop to discuss questions on the issue of“Mechanisms of Copper Corrosion in Aqueous Environments”. The workshop has addressed the fundamental understanding of the corrosion characteristics of copper with regard to oxygen-free environments. There is limited information available about the corrosion mechanism and its implication on the containment of spent nuclear fuel in a copper canister [10]. The following passage at an appropriate seminar report reflects the current status about KBS-3-concept:

The geological environment surrounding the copper canisters will be nearly oxygen-free, and one of the premises on which the KBS-3 rests is the assumption that copper cannot corrode in such an environment. The scientific findings of a small group of researchers at KTH (the Royal Institute of Technology) in Stockholm have therefore been met with widespread interest and debate. Their findings are in short that copper actually can corrode in pure water, free from oxygen as well as from complexing ions. Since the release of the KTH findings, the long-term safety of the KBS-3 method has been questioned. Then the Government will make their own ruling. [10].

5. SWEDISH LEGAL AND REGULATORY FRAMEWORK

With reference to the Swedish law the polluter-pays principle is applied. The owner of a nuclear power plant has the full responsibility for the safe handling and final disposal of spent nuclear fuel and nuclear waste that is produced. The financial aspects are included into the nuclear waste management. In the 1970s Swedish nuclear power plants owners have established the Swedish Nuclear Fuel and Waste Management Company (SKB). The SKB is the implementer of a final disposal programme.

The Government has given the task of Main regulatory body responsible for the supervision of nuclear waste safety and radiation protection is the Swedish Radiation Safety Authority (SSM) – the task has been given to SSM by the Government to review the SKB's application under the Act on Nuclear Activities (ANA). On 1 July 2008, the Swedish Nuclear Power Inspectorate (SKI) and the Swedish Radiation Protection Institute (SSI) were merged to form the joint authority SSM. Another task is the review process of the application according to the Environmental Code, which is done by the Environmental Court who reports the findings to the Government.

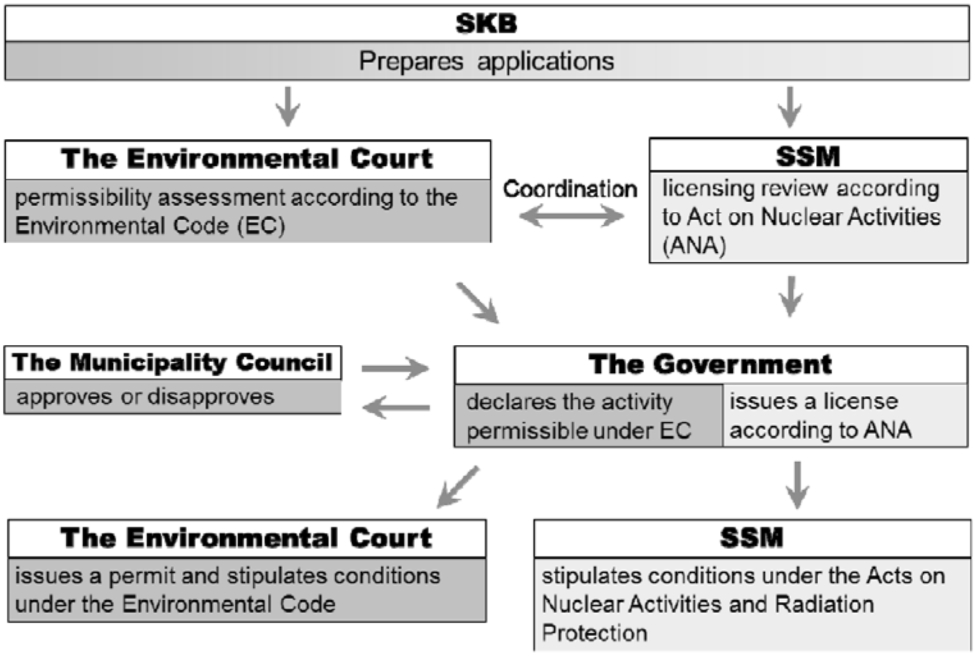

Fig. 4. The licensing review procedure [10]

The SKB is prompted by law to present a nuclear waste handling or rather disposal solution. For the whole process the authorities will review it, based on these results they make their recommendation to the Government. The Government will establish a double structure to receive two proposals. One actor is the Environmental Court which come up with provisions with regard to the Environmental Code. The other player is the SSM who will stipulate conditions under the Acts on Nuclear Activities and Radiation Protection.

In sum, responsibility in the nuclear waste management is divided. The Swedish Nuclear Fuel and Waste Management Company acts as an implementer, regulator function is fulfilled by the Swedish Radiation Safety Authority, its responsibility is for the supervision of nuclear waste safety and radiation-protection. SSM's regulation and guidance on post -closure repository safety has two parts: radiation protection and safety regulation. Another important agency with responsibility is the Swedish National Council for Nuclear Waste [11]. The regulations SSMFS 2008:37 [22] contains some requirements:

- Protection of human health
- General environmental protection goals
- Application of optimization
- Best Available Technique (BAT)

The relevant guidance advises on the reporting of risk, BAT and optimization for different time periods after closure, selection of scenarios, calculation of risk, handling of uncertainty and risk mitigation [12]. According to regulations of safety requirements on the design of the repository, barrier functions and safety reporting as well as regulations to the construction and operational phases of the repository are included.

Another important regulation is the Financing Act. The financing system has been re-organized in 1996 when the Nuclear Waste Fund (NWF) – a government authority – was established to hold the funded assets. The NWF has its own Board of Governors but no working staff, on behalf of them the Financial and Administrative Services Agency controls the administrative and capital management of the Board. Originally the system was invented by the Swedish parliament in 1982; the holder of a license – owner or operator – of a nuclear power plant (NPP) pays a special fee to the state to compensate the costs for safe future management, disposal of the spent nuclear fuel and decommissioning and dismantling of NPP. The fee is determined at a given rate per kWh of electricity produced by a NPP. Nowadays, since 2008, the fee system has reformed to define an amount in kronor, to be paid by a licensee who no longer delivers nuclear energy. Depending on a proposal by the Swedish Radiation Safety Authority the Government decides on the size of the fee. The SSM together with the Government, only for certain cases, approve the pay-off from the NWF [13]. When following the whole Swedish NWM process one can certify a top-down approach and altogether with a commercial organization.

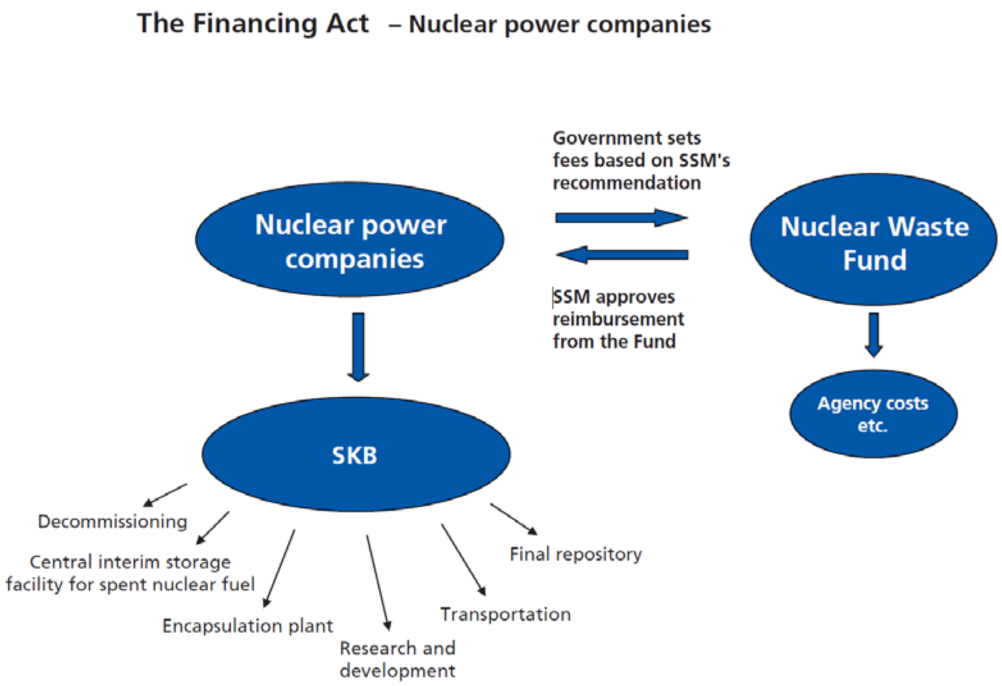

Fig. 5. The financing system for nuclear waste [13]

6. THE SWEDISH REVIEW PROCESS

Due to the implementer function, the Swedish Nuclear Fuel and Waste Management Company has submitted three-part-divided application to deal with nuclear waste [14]:

- *application under the Act on Nuclear Activities for CLAB (an interim storage facility for spent nuclear fuel) and an encapsulation facility in Oskarshamn (1st submission in November 2006, amended in 2009; the application was submitted again completely on 16 March 2011)*
- *an application under the Act on Nuclear Activities for a spent fuel repository, including the site and method (submitted on 16 March 2011)*
- *an application under the Swedish Environmental Code covering the entire repository system (CLAB, encapsulation facility and repository; submitted on 16 March 2011)*

It is expected the review period will take at least two years, the SSM will provide a statement to the Government. Afterwards the Government decides to grant a licence to SKB or rejects the submitted application. For the reason of a step-wise review process, the following steps are compromising five elements regarding licensing issues [14]:

1. to construct, own and operate the facilities;
2. commencement of the construction phase;
3. test operation;
4. regular operation;
5. decommissioning and/or closure.

On 16 March 2011, SKB has submitted its licence applications to the Authority equated with the first step of the review process. Nevertheless, it is a highly important step caused by the final opportunity for broad public involvement through the environmental impact assessment process. The SSM opens the corridor for national consultation whereas special case is a possible municipal veto on the part of the two municipal authorities Oskarshamn and Östhammar. The first step has an enormous significance as several important decisions are to be taken, e.g. selection of method and site. There are difficulties because SKB's application cannot offer all details in terms of construction and operation. Nevertheless, the SKB has to demonstrate its competence to construct and run the facility in fulfilling the compulsory requirements and that the facility can be constructed in an appropriate way: sufficient level of safety and security after the repository has been closed in the future. In particular, the first step contains a strong focus on key assumptions in the analysis of long-term safety. International agencies like the International Atomic Energy Agency (IAEA) have to be involved while it is in compliance with international practice. By designing, constructing and commissioning a nuclear facility such as a repository long-term processes have to take place in steps. The Authority, here SSM, will have an expert circle to review SKB's proposal with regard to construction engineering, plant technology, geology, hydrology, chemistry, materials chemistry, materials engineering, social sciences, technical physics and radioecology. Parallel reviewing will be made by the Environmental Court considering the application under the Swedish Environmental Court [14].

Table 2. Running process of review

Date	Issue
27 May 2011	Swedish Radiation Safety Authority begins its technical review; two phases: (1) initial technical review phase, (2) main review phase. 1st phase involves a broad review of the application documents in order to determine whether the licence applications are sufficiently complete and of sufficient quality to enter the extensive main review phase
November 2012 Phase 1a	Initial technical review phase is anticipated to formally continue until November 2012
November 2012 Phase 1b	When initial acceptance review was completed, the application documents were referred to other bodies for consideration and comments. Over the years the Swedish Radiation Safety Authority have maintained dialogue with the external actors monitoring SKB's work and who have also been interested in the Authority's role in the process. Some of these stakeholders have received funding from the Nuclear Waste Fund for work in this area and have built up their own expertise in the field. The Authority wishes to use this interest and expertise in the area as a platform for requesting the views of national stakeholders on the entire application documents. The consultation (interest and expertise shall be used as a platform to request the view of national stakeholders) responses are to have been received by the Swedish Radiation Safety Authority by 1 June 2012

7. NUCLEAR WASTE MANAGEMENT IN THE UK

It is not a target of this paper to refer every single step of the UK's Nuclear Waste Management process. Therefore, only a short reflection of previous initiatives is necessary. In the 1970s the question has raised, how to handle nuclear waste. The awareness can be seen at the report from the Royal Commission on Environmental Pollution, also known as Flowers Report, when it was stated that:

"… it would be morally wrong to commit future generations to the consequences of fission power on a massive scale unless it has been demonstrated beyond reasonable doubt that at least one method exists for the safe isolation of these wastes for the indefinite future [15].*"*

In 1976, there is the starting point, when the Royal Commission was recommended the formation of a Nuclear Waste Disposal Corporation to propose a solution about nuclear waste management. The period until 2000 can be seen as lost time because no real efforts were made. During a speech of former Environment Minister, Michael Meacher, on 20 July 2000, the need for a new consultation process was highlighted:

"[This would] be the first step of an open and transparent approach that must characterise the radioactive waste management policy debate in the future. The main aim of the consultation paper will be to explore how to involve the public, and groups that represent the public, in that debate" [16].

In the report "Managing Radioactive Waste Safely", a Government´s consultation document, was published in September 2001 [17] to redevelop nuclear waste policy. A consultation process was initiated, e.g. focus groups and dialogues with stakeholders. The result was a governmental announcement in July 2002 to establish a new independent committee (Committeee on Radioactive Waste Management - CoRWM) to review alternatives for managing radioactive waste and to make recommendations. The approach is to carry out an open, transparent and inclusive review to necessarily engage the public and to provide them with the opportunity to express their views. Therefore, the CoRWM is planning an active programme of public and stakeholder debate. In 2006 the Committee has made some recommendations to the Government. Most important one is regarded to site choice: what is known for present knowledge geological disposal is the best method for the long-term management of legacy higher activity waste. The explanatory statement was the fact that geological disposal is internationally recognized as the preferred approach and at end the government has supported this recommendation. A consultation process of the Government has continued, in 2008 the White Paper "Managing Radioactive Waste Safely: A Framework for Implementing Geological Disposal" [18] has offered, with regard to the framework for implementing geological disposal:

- a strong and effective implementing organisation in the Nuclear Decommissioning Authority (NDA);
- strong independent regulation by the statutory regulators;
- independent scrutiny and advice from a reconstituted CoRWM;
- an approach to siting a geological disposal facility based on voluntarism and partnership with local communities.

The guidance line of UK's strategy is to firstly formulate simple questions and answer them:

1. Objective – What is the objective of the strategy?
2. Our Strategy – What is our current strategy, and any associated risks and opportunities?
3. Development – What strategy development do we plan to undertake in the future?
4. Delivery – What have we delivered so far and how do we plan to implement our strategy?

The recent planning assumptions are to propose UK's first waste emplacement in a geological disposal facility by 2040. At the beginning the process is guided by local communities but at a later date more technical stages of MRWS programme will take several decades [19].

As formulated in the White Paper communities are invited to express an interest in taking part in discussions about the siting process for a repository for UK's high level activity radioactive waste. Since 2008, three Councils have expressed their interest: Copeland, Allerdale Borough Councils and Cumbria County Council. These authorities are cooperating with the West Cumbria MRWS Partnership to reflect on whether or whether not to move into the siting process itself. The consultation has started on 21 November 2011 to get statements of people and will run until the 23 March 2012 [20].

The process of finding an appropriate site in the UK comprises six criteria [20]:

1. Safety, security, environment and planning
2. Geology
3. Community benefits and impacts
4. Design, engineering and inventory
5. Siting process
6. Public and stakeholder views

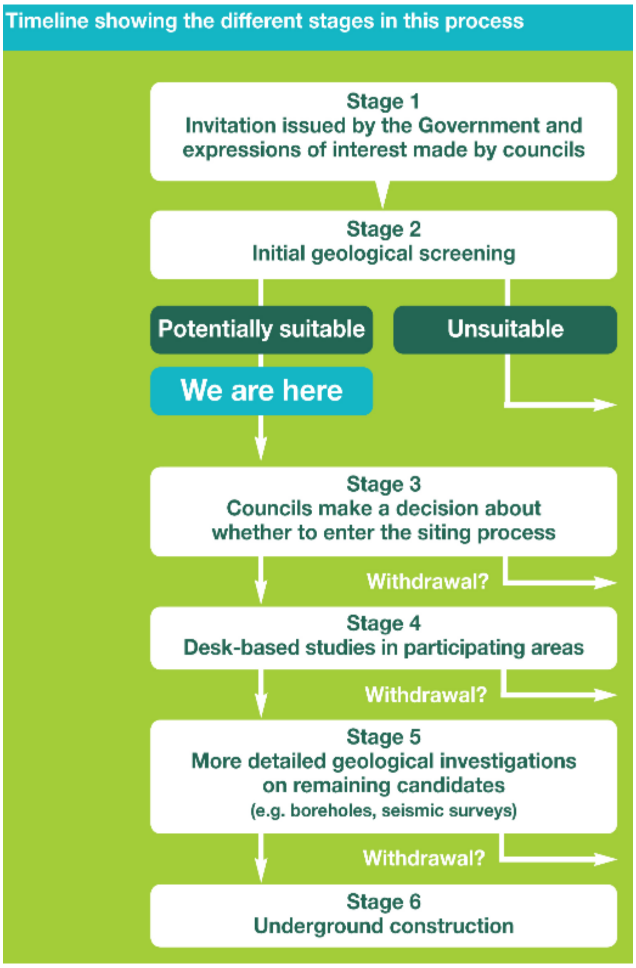

Fig. 6. Criterion 5 UK siting process, the timeline and current status [20]

8. INTERNATIONAL EXPERIENCE OF GEOLOGICAL DISPOSAL

The method of geological disposal has been adopted by a number of countries as a solution for the long-term management of higher activity radioactive waste. The energy sector and with it companies have internationalized especially since the liberalization of the European energy market in the 1990s. Also Swedish companies expanded, but SKB is still communicated as a Swedish company, the involvement of nuclear reactor owners is existent. There is a link between Finnish and Swedish companies, e.g. Fortum holds interests of 50% in two Swedish reactor sites. Fortum also holds a 25% share in SKB. Some joint research projects were started, Posiva Oy the Finnish counterpart of Swedish SKB has adopted the KBS-3 concept as the guiding concept for geological disposal of Finland's nuclear waste [5]. When the European Commission has established a "European Technology Platform for implementing the geological disposal for nuclear waste" on 31 January 2012 some borrowings were made and entanglements of private and state-owned nuclear industries were transferred to the Implementing Geological disposal of Radioactive Waste Technology Platform.

Today, the collaboration between SKB and UK's Nuclear Decommissioning Authority is significantly increasing with the argument that the KBS Programme has shown in past experiences (KBS 1-3) a successful demonstration with regard to a safe repository concept for the final and geological disposal of high activity nuclear waste [5, p. 257]. A new approach was invented in 1992, when SKB has adopted the principle of local acceptability as the main element deciding the site selection of a KBS-3 repository. It can be clearly see that the UK has assumed the same approach for their new final disposal UK concept with the difference that the new approach to find suitable site and process structure is orientated in a bottom-up approach.

9. CONCLUSION

The problem of Nuclear Waste Management has similiarities all over the world. To get rid of nuclear waste depends on countries' respective histories, political cultures and institutional settings. In general, countries have different goals and, hence, processes [13]. The main goal of a waste management concept is to demonstrate safety. For Sweden is a close cooperation between the state and the nuclear industry significant as a result of a strong policy network which was established and persists. An analysis by LIDSKOG has alluded that the policy network has developed both insitutional and interpersonal dimensions. Therefore, it is a structure of inclusion from state and economy, but of exlusion from civil society and environmental organizations [14]. Since the beginning of Swedish nuclear waste management process in the 1970s the responsibility is characterized by a delegation to the nuclear power plant owners themselves. The distance from political institutions decision-making about the issue radioactive waste is a tacit acceptance [14]. Civil society is often tardy involved, a large amount of nuclear waste has already produced, often policy is yet formulated and only the implementation remains. Therefore, the coordination of policy together with parallel policy implementation is a huge restraint to achieve a solution with regard to nuclear waste regulation [15].

In Sweden, a strong connection between nuclear waste management, the licensing of nuclear power plants and the target to achieve the demonstration of a "safe" final storage were fulfilled and presented within KBS-3 method. From the beginning SKB research was more focussed on engineered barriers. The basic strategy has been to demonstrate safe disposal as a question of engineered barriers to prove a principle solution. In 2009, some natural scientists has cast doubt on the KBS-3 method because of copper canister corrosion. Also the process how to make pre-investigations, the selection of the site Forsmark has delivered more questions. A site selection process is presented as a voluntary action of some municipals. Voluntarity is may be helpful for the selection process which additional inspections are necessary and the result were not communicated in an appropriate manner. It is the style of the importance of none-politicizing the issue about a repository – only questions about final disposal: technical and local. To find out the best site is may be not possible when only voluntarity is taking place and decision making leaves open transparent information. One have to think about the fact that a postulate site will not fulfill the final storage concept requirements. Then another solution is needed.

The function of a municipality is crossing three spheres: civil society, state and economy. In the paper it was shown that the UK has oriented oneself at the Swedish KBS-3 concept. Although the KBS programme has promised the safetyness of geological disposal of nuclear waste and includes a belief in the availability of such a long-term solution is one interpretation. Another remark is the question about practical stability, means that the KBS-3 programme was not consistent over time, has resulted in fluidity and still has not proved as appropriate method. A long-term solution for nuclear waste is not closer than before. The Swedish model has widespreaded and a further outcome is that the nuclear industry has a highly control over nuclear waste management and therefore autonomous influence. With regard to learning processes it is necessary to re-integrate processes with regard to checks and balances as a permanent task in nuclear waste management.

Based on the key elements in the beginning the scientific paradigm (a) in Sweden is highly concentrated on the KBS-3-method, while the UK has started all over again and broke with their further NWM concept; the environmental and economical cost-benefit-analyses (b) were not examined in this paper, but the top-down approach in Sweden has shown the confidence in a private organisation of NWM, while the UK broke the strong alliance to the private sector within NWM but today orientates at some extend in the Swedish concept, furthermore the scientic research and questions of process implementation is organised at the University of Sussex; the political and popular dimension of environmental protection (c) is adapted in both countries; public participation in environmental decision making (d) is uneven when comparing both countries, process proceeding elements are focussed on public participation, whereas UK’s transparent site finding process has the potential to become a prototype for other countries. In summary, further research in all directions of nuclear waste management is highly demanded.

REFERENCES

1. LIDSKOG, R. and G. SUNDQVIST, On the right track? Technology, Geology and Society in Swedish nuclear waste management. Journal of Risk Research, Volume 7, Number 2, March 2004, p. 251–268 (18).
2. FLÜELER, T., M. STAUFFACHER, P. KRÜTLI, C. MOSER and R.W. SCHOLZ, Cross-cultural space of radioactive waste governance in a globalizing world, Managing Radioactive Waste Problems and Challenges in a Globalizing World, Gothenburg, 15-17 December 2009, http://e-collection.library.ethz.ch/eserv/eth:1633/eth-1633-01.pdf.
3. SABATIER, P.A. and D. Mazmanian, The Implementation of Public Policy: A Framework of Analysis, Policy Studies Journal 8, 1980, p. 538–60.
4. SWEDISH RADIATION AUTHORITY, “We won’t say ‘yes’ until the safety issue has been solved”, http://www.stralsakerhetsmyndigheten.se/In-English/About-the-Swedish-Radiation-Safety-Authority1/The-site-for-a-spent-nuclear-fuel-repository1/News/We-wont-say-yes-until-the-safety-issue-has-been-solved/.
5. ELAM, M. and G. SUNDQVIST, Meddling in Swedish success in nuclear waste managements. Environmental Politics, 2011, 20:2, p. 246–263.
6. ELAM, M. and G. SUNDQVIST, The Swedish KBS Project: A last word in nuclear fuel safety prepares to conquer the world? Journal of Risk Research, Volume 12, Issue 7-8, 2009, p. 969-988.
7. SKB, Social Science Research 2004–2010 Themes, results and reflections, Boel Berner Linköping University, Britt-Marie Drottz Sjöberg Norwegian University of Science and Technology, Trondheim, Einar Holm Umeå University, April 2011, http://www.skb.se/upload/publications/pdf/SocialScienceResearch2004_2010webb.pdf.
8. SKB, Our method of final disposal, http://www.skb.se/Templates/Standard____24109.aspx.

9. SKB, Long-term safety for the final repository for spent nuclear fuel at Forsmark Main *report of the SR-Site project Volume I,* Technical Report, TR-11-01, Svensk Kärnbränslehantering AB, March 2011.
10. THE SWEDISH NATIONAL COUNCIL FOR NUCLEAR WASTE, *Mechanisms of Copper Corrosion in Aqueous Environments,* A report from the Swedish National Council for Nuclear Waste’s scientific workshop, Report 2009: 4e, on November 16, 2009.
11. OECD, *Radioactive Waste Management Programmes in OECD/NEA Member Countries. Sweden*. 2005, p. 1-9 (2-3).
12. DVERSTORP B., A. WIEBERT and M. JENSEN, *New Guidance for Geoological Disposal of Nuclear Waste in Sweden, 11th IHLRWM conference, 30 April-4 May in Las Vegas, 2006.*
13. KÄRNAVFALLSFONDEN, *Activity Report 2010, http://www.karnavfallsfonden.se/download/18.2595a92612f8a8de34880003547/Verksamhetsber%C3%A4ttelse+2010+engelska.pdf*
14. SWEDISH RADIATION AUTHORITY, *The Review Process,* http://www.stralsakerhetsmyndigheten.se/In-English/About-the-Swedish-Radiation-Safety-Authority1/The-site-for-a-spent-nuclear-fuel-repository1/Review-Process/
15. CONCERNS ABOUT THE "PLUTONIUM ECONOMY", *from "Nuclear Power and the Environment"*, report by Sir Brian Flowers, nuclear physicist - the Sixth Report of the U.K. Royal Commission on the Environment, 1976, http://www.ccnr.org/Flowers_plute.html
16. NO2NUCLEARPOWER, *History of nuclear waste disposal proposals in Britain,* http://www.no2nuclearpower.org.uk/reports/waste_disposal.php
17. DEFRA, *Managing Radioactive Waste Safely. Proposals for developing a policy for managing solid radioactive waste in the UK,* Department for Environment, Food and Rural Affairs, Department of the Environment, National Assembly for Wales, Scottish Executive, September 2001.
18. BERR, DEFRA, *Managing Radioactive Waste Safely, A Framework for Implementing Geological Disposal A White Paper by Defra,BERR and the devolved administrations for Wales and Northern Ireland,* June 2008, http://mrws.decc.gov.uk/assets/decc/mrws/white-paper-final.pdf
19. DECC, *Managing Radioactive Waste Safely: indicative timeline for implementing geological disposal, December 2010,* http://www.decc.gov.uk/assets/decc/What%20we%20do/UK%20energy%20supply/Energy%20mix/Nuclear/geological-disposal-board/982-geological-disposal-timeline.pdf
20. WEST CUMBRIA:MRWS, *Managing Radioactive Waste Safely, March 2012 http://www.westcumbriamrws.org.uk/.* yndigheten.se/Global/Publikationer/Forfattning/Engelska/SSMFS-2008-37E.pdf
21. THE SWEDISH RADIATION SAFETY AUTHORITY’S GENERAL ADVICE ON THE APPLICATION OF THE REGULATIONS, *(SSMFS 2008:21) Concerning safety in connection with the disposal of nuclear material and nuclear waste, 30 January 2009,* http://www.stralsakerhetsmyndigheten.se/Global/Publikationer/Forfattning/Engelska/SSMFS-2008-21E.pdf
22. THE SWEDISH RADIATION SAFETY AUTHORITY’S GENERAL ADVICE ON THE APPLICATION OF THE REGULATIONS, *(SSMFS 2008:37) Concerning the Protection of Human Health and the Environment in Connection with the Final Management of Spent Nuclear Fuel and Nuclear Waste, 30 January 2009,* http://www.stralsakerhetsmyndigheten.se/Global/Publikationer/Forfattning/Engelska/SSMFS-2008-37E.pdf

CYSENI 2012, May 24–25, Kaunas, Lithuania
ISSN 1822-7554, www.cyseni.com

COMPARISON OF FUEL CONSUMPTION, EMISSION, AND ECONOMIC CONSIDERATION IN GOODS DELIVERY PROCESS FROM PORTUGAL TO BRASIL BETWEEN AIRBUS A340 AND CSAV RUNGUE: A CASE STUDY

Adi Saputra
Mechanical Engineering Department, University of Aveiro
Campus Universitário de Santiago, 3810-193-Portugal
Phone +351 966773020
Email: adisaputra@ua.pt

Emiliana Fonseca, Yadira Dias
Management and Industrial Engineering Department, University of Aveiro
Campus Universitário de Santiago, 3810-193-Portugal
Phone +351 910367513
Email: emilianafonseca@ua.pt/ yadira.dias@ua.pt

ABSTRACT

Transportation sector is the largest emissions contributor in the world. Emission generated and uncontrolled can be contributed to increasing of greenhouse gases. Indirectly, it also will be impacted on the increasing of global warming that would affect adversely to the living creatures in the earth. Moreover, fossil energy supplies are depleted increasingly without be offset by the discovery of the new resources. It will increase difficulties to provide the necessities of the life which in the meantime, the source of environmental friendly renewable energy still in the stage of the development process.

According to both conditions, required an act of environmental care and energy efficiency that can be done by people in their life although a small and trivial things. One of the activities that often done by people is delivery of goods either in one island, inter islands and even intercontinental. Various types of delivery have done either by means of sea and air transportations. However, the consumers is rarely knows energy consumption and air pollution generated from each of its delivery types. Now, it is time for consumers to know them because almost all people in the world ever did it. So, this information is important to increase public awareness in support of energy efficiency at least in their life activities.

Therefore, as a first step, this project take a case study to compare fuel consumption, emission, and economic consideration in goods delivery process from Portugal to Brasil between aircraft type of Airbus A340 and marine vessel type of CSAV Rungue. In this case study, can be proved that Airbus A340 is more efficienct than CSAV Rungue according to energy consumption and emission aspects.

Keywords: comparison, fuel consumption, emission, delivery, Portugal to Brasil

1. INTRODUCTION

Freight activity is a common activity which a famous to our ears and difficult to be separated from the public life. This activity has been familiar in our life either is done in the same island and different island or continental. The delivered goods are usual varied from office equipments, foods, clothes, medicines, and even to the correspondences or mailing and packages. Moreover, means of transportation used in this delivery process is also varied from land, sea, and air transportation. Each of this kind of transportation has different characteristic and specification in aspect of energy consumption, emission, and economic consideration among goods delivery process. Not only that even in the same kind of transportation also different in energy consumption, emission, and economic aspects. It dependent on many factors like machine specifications and capacities, maintenances, geographical conditions, etc. Research or more complete case study with very detail characteristics and variables can be conducted deeply in another time.

However, in this paper, will be performed a case study of goods delivery from Portugal to Brasil with compare fuel consumption, emission, and economical aspects between aircraft type of Airbus A340 and marine vessel type of CSAV Rungue. The purpose of this case study is to get comparison data of fuel consumption, emission generated, and economical consideration in goods delivery process from Portugal to Brasil using Airbus A340 and CSAV Rungue. Beside of as an insight, this information is also important to be known by publics in order to increase awareness toward energy efficiency in daily activities. It also can be used in the decision making process by various interested parties however needed further more complex researches in this area.

There are two schemes or options of goods delivery process that will be studied. Delivered goods are from the same location point in Portugal and delivered to same destination point in Brasil. Nevertheless, the first option will use marine vessel of CSAV Rungue while the second option use Airbus A340 plane. Detail scheme of delivery process is described in the table below.

Table 1. Delivery Process Scheme

Option 1	Truck : Company » House1 (Coimbra) House 1 » Port of Lisboa Port Harbour » Company (Coimbra) Ship : Portugal » Brasil (Port of Santos) Truck : Port Harbour » House 2 (Minas Gerais) House 2 » Port of Santos
Option 2	Truck : Company » House 1 (Coimbra) House 1 » Lisboa Airport Airport » Company (Coimbra) Plane : Portugal » Brasil (Confins Airport) Truck : Airport » House 2 (Minas Gerais) House 2 » Confins Airport

Travel distance and time which needed in delivering process of the goods from Portugal to Brasil are described in the following table either use Airbus A340 or CSAV Rungue.

Table 2. Travel Distance and Time

Type of Travel	Distance (km)	Average Time (hours)
House 1 » Port of Lisboa	433.5	5.6
House 1 » Lisboa Airport	420.5	5.2
Port of Lisboa » Port of Santos	8,395	240
Lisboa Airport » Confins Airport	7,437	10
Port of Santos » House 2	1,306	16
Confins Airport » House 2	78.4	2.5

2. METHODOLOGY

The methodology used in determine fuel consumption, emission generated, and economic analysis will be conducted step by step using COPERT IV software analysis, table data, and equations where dependent on to the type of transportation which will be calculated. Calculation of fuel consumption and emission for truck from company location and back to company location again will be conducted by using simulation of COPERT IV software either in Portugal and Brasil. Process of simulation using Copert IV software is based on data from "Emission Inventory Guidebook" which published in 2006, specifications of truck like vehicle classification, type of fuel used, etc. and physical condition of the route like average slope, type of road, distance, and others variabels that available in the COPERT IV software. Value of long distance traveled is obtained with using Google Earth software application where departure and arrival point desired are inserted to the coordinate of Google Earth.

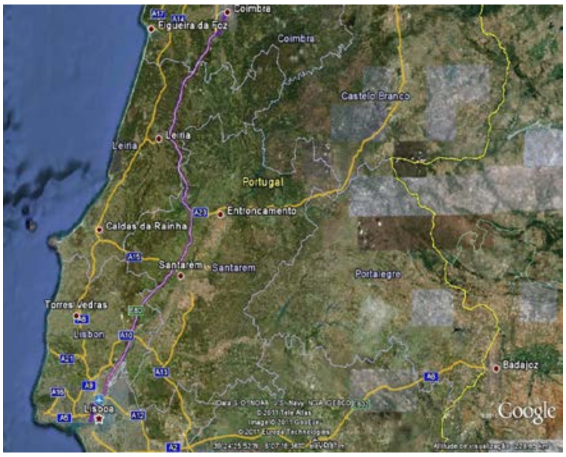

Fig. 1. Using Google Earth Usage To Obtain Long Travel Distance

According to the informations from truck company, the average speed of truck is considered 30 km/h for urban routes and 90 km/h for highway. In this step, also consider to topographic slope of the routes in Portugal and Brasil where we assume the value is 0.

While for sea transportation of CSAV Rungue vessel, fuel consumption and GHG emission are calculated by using two methodologies: “Fuel Consumption” (statistic of fuel) and “Ship Movement” (transport)[1]. However, the most approriate methodology for this case study is “Ship Movement” since calculation of emissions for national and international sea travel is recommended by the report of “Emission Inventory Guidebook”. This methodology is based on the use of data on the ships movement. Overall, information data for this transportation type either fuel consumption, pollutant emissions generated, and travel time is obtained from the company data in the form of equations and table data.

For air transportation, after discuss and research some aviation specifications, finally selected TAP airline as type of air transportation used in this case study. The company has two types of plane that special for long travel distance: Airbus A330 and A340. However, only Airbus A340 which used for travel distances equal to or greater than 7408 km where suitable for this study. There are three types of calculations for pollutant emissions and energy consumption of aircraft: "Very Simple", "Simple" and "Detailed". The first type is not considered because the results are just a estimation of the emissions. While the second type, assumed that the information of aircraft types which used in this country have available. The last type is detailed method where presents and takes into account cruise emissions and LTO times in modes for differents airplanes and flight distances. The latter is divided into "Aircraft Movement Methodology" (transportation) and "Fuel Consumption Methodology" (statistics of fuel)[1].

The most appropriate methodology used for this study is the type of "Detailed", with "Aircraft Movement Methodology" because it is most recommended by "Emission Inventory Guidebook" report for the calculate emissions in IFR (Instrumental Flight Rules) flights. Available information and data related to aircraft movements as the "Take-Off and Landing" and Cruise where was developed based on the reference[1]. A general mathematical equation for calculate the fuel consumption is:

$$Fuel\ Consumption = (D1) + \frac{(D2 - D1) \times (actual\ distance - D1)}{(D2 - D1)} \qquad (1)$$

The corresponding values for these variables were taken from the table of "Fuel Consumption and Emission Factors for Dash 8, Fokker 50 Turboprops and Similar Size" as well as explained in the reference "Emission Inventory Guidebook". Value of D1 and D2 are correspondent to the two values of the distances to interpolate and nm (distance given in nautical miles). The actual distance is intended to calculate the route and climb / cruise / descent must be taken values D1 and D2, for calculating the energy consumption and emissions of NO_x, HC, and CO.

Determine emission pollutant per kilogram of fuel for air pollutants such as $EINO_x$, EICO and EHC, we can use the following equation:

$$Pollutant = \frac{(Pollut.value\ of\ LTO + Tot.value\ of\ pollut.emitt.in\ Kg\ without\ LTO)}{(Fuel\ Value\ of\ LTO + Tot.value\ of\ fuel\ spent\ in\ Kg\ without\ LTO)} \qquad (2)$$

3. RESULT AND DISCUSSION

3.1. Pollutant Emission Analysis

According to the equations and information data given in the reference, total emission which produced by Airbus A340 is described in the following table.

Table 3. Total Emission of Airbus A340 from Portugal to Brasil

Tipe of Plane$^{a)}$	**CO_2**	**CH_4**	**N_2O $^{b)}$**	**NO_X**	**CO**	**NMVOC**	**SO_2 $^{c)}$**	**$PM_{2,5}$ $^{d)}$**	**Combustível Consumido (kg)**
A 340	6363	1.9	0.2	35.4	50.6	16.9	2.0	0.21	2019.9

a) For CH4 and NMVpoOC it is assumed that the emission factors for LTO cycles be 10% and 90% of total VOC (HC), respectively (Olivier, 1991). Studies indicate that during cruise no methane is emitted (Wiesen et al., 1994).
b) Estimates based on IPCC Tier 1 default values.
c) Sulphur content of the fuel is assumed to be 0.05% for both LTO and cruise activities.
d) PM2.5 data (= PM10 emissions) Source: ICAO database (ICAO 2006) and DfT PSDH (UK-DfT 2006)
Source: Derived from ANCAT/EC2 1998, Falk (1999) and MEET 1999 [EIG].

While total emission for truck transportation for option 1 and option 2 of the delivery process scheme is describe in the following table.

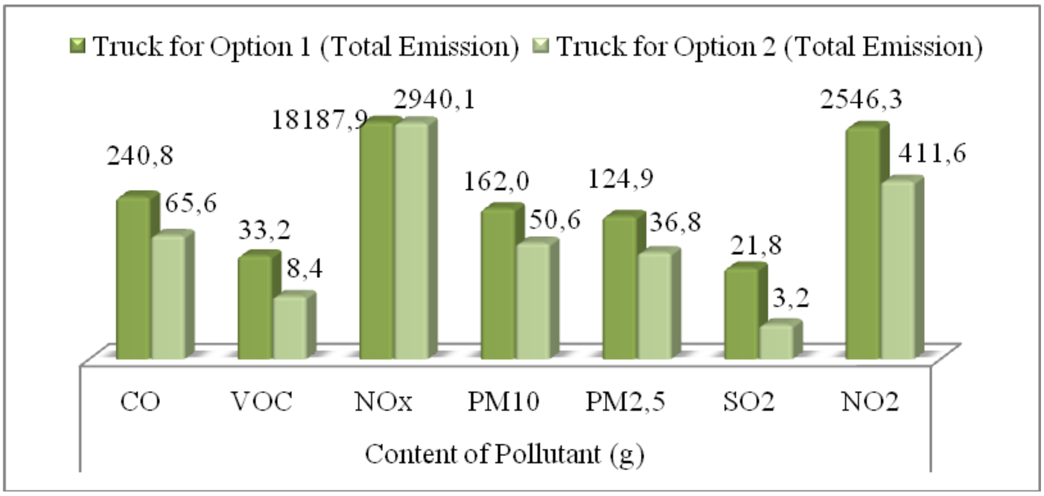

Fig. 2. Total Emission of Truck for Option 1 and Option 2

The total pollutant emission which produced by marine vessel of CSAV Rungue is described by the following table.

Table 4. Total Emission of CSAV Rungue from Portugal to Brasil.

Type of Pollutant	**Calculation Formula**	**Emission (Kg/h)**	**Total Emission (Kg/travel)**
NO_x	17.50E-3 * P * N	6652.1	1.6E6
CO	0.68E-3 * P ^{1,08} *N	722.5	1.7E5
HC	0.28E-3 * P *N	106.4	2.5E4
SO_2 (Potential $\geq$ 2000 kW)	11.34E-3 * P * N	4310.6	1.1E6

Where:
P = Motor Power Vessel (kW)*0,85 MCR (*Motion Comfort Ratio*) [1]
N = Number of Engines of Vessel

[1] MCR= (DISP)/[0.65(0,7DWL + 0,3LOA)* BEAM$^{4/3}$], where:
DISP - *Displacement*: Volume of water displaced by the ship.
DWL - *Distance at Waterline*: Waterline length of the hull.
LOA - *Length Over All*: Total length of the vessel from stem to stern.
BEAM: width of the vessel in the enlarged portion.

So, if it is summarized, will get summarized result for the total emission of goods delivery process from Portugal to Brasil for option 1 and option 2.

Table 5. Summary of Total Emission for Option 1 and Option 2

Tipe of Journey	**Total Emission (kg)**										
	CO	**VOC**	**NO_x**	**PM10**	**PM2,5**	**CO_2**	**HC**	**SO_2**	**CH_4**	**N_2O**	**NMVOC**
Option 1	170,000.24	0.03	1,600,018.2	0.16	0.12	3,427.30	25,000.00	1,100,000	0.0	0.0	0.00
Option 2	104.963.36	0.01	868.20	0.05	0.25	6,868.70	591,39.17	2.00	1.9	0.2	16.90

3.2. Energy Consumption Analysis

This part will present about nominal fuel consumption for all kinds of transportation type in this study. The calculation methodology is the quantification of total fuel mass taken for completion of the trip, according to the mechanical efficiency of each transport study and mathematic correlation with the Lower Heating Value (LHV) of the respective fuels, as described in the following table.

Table 6. Comparison of Energy Consumption per Trip

Kinds of Transport	Tipe of Fuel	PCI of Fuel (MJ/kg)[2]	Mass of Fuel spent/trip (kg)	Energy spent (MJ/trip)
Truck[1]	Diesel	42.3-43.3	Coimbra – Port (PT): 124.97	5,348.7
			Port (BR) – Belo Horizonte: 962.60	41,199.3
			Total: 1,087.57	**Total: 46,547.9**
			Coimbra – Airport (PT): 121.22	5,188.2
			Airport (BR) – Belo Horizonte: 39.24	1,679.5
			Total = 160.46	**Total = 6,867.7**
CSAV Rungue	Heavy fuel	40-40.4	659,000	26.5E6
Airbus A 340	Aviation Kerosene	43.8	52,965.01	23.2E5

[1] Total spending for land transport in both countries.
[2] Source: Ministry of Economy and Innovation, Notice No. 18670/2008

3.3. Time and Cost Analysis

The travel time calculation is carried out from the average distances traveled by land transport (truck), ship, and airplane.

Table 7. Brief Comparison of Time and Cost

Tipe of Journey	Time (hour)	Cost (Euro)
Portugal-Brasil by Airbus A340	17.7	3726.23
Portugal-Brasil by CSAV Rungue	261.6	1791.91

The average travel time information of Airbus A340 from Portugal to Brasil obtained from the company data. While for the ship, the travel time is calculated using the average speed of travel and distance traveled.

Cost analysis in this project is calculated only from the costs associated with the fuel consumption for all three modes of transport studied. Thus were not included other expenses related to transportation, such as wear of equipment and parts, or payment of salaries of employees involved in the transhipment of cargo. In the following table can be verified expenses associated with the inland transport of cargo through the analysis of the total fuel used in every possible travel and the value per unit of fuel, currently practiced in the two countries studied.

Table 8. Cost Analysis Associated With The Land transport

Tipe of Journey	**Price of Gasoline**	**Gasoline Consumption/ Tipe of Journey (kg)**	**Density of Fuel**	**Currency Conversion Factor**	**Total Expenditure (€)**
Port/Portugal	1.33€/L	124.97	0.85kg/L	-	195.54
Airport/Portugal	1.33€/L	121.22	0.85kg/L	-	189.67
Port/Brasil	R$1.98/L	962.60	0.85kg/L	1.00 € = R$2.50[1]	896.91
Airport /Brasil	R$1.98/L	39.24	0.85kg/L	1.00 € = R$2.50[1]	36.56
Airport /Brasil	R$1.98/L	39.24	0.85kg/L	1.00 € = R$2.50[1]	36.56

[1] Source: *Website* Jornal de Negócios

According to the result in the table, can be explained that cost for goods delivery by using airplane in this case Airbus A340 is five times higher than using CSAV Rungue.

4. CONCLUSION

This project is a simple case study that describe comparison of fuel consumption, emission, and economic consideration in goods delivery process from Portugal to Brasil between Airbus A340 and CSAV Rungue. The main objective of this study is to increase the public awareness towards energy efficiency in their daily activities and also can be as a knowledge source and reference for next research which similar and with more various parameter and characteristics.

According to the calculation and analysis have been done, can be conclude that energy consumption of option 1(using CSAV Rungue) is higher than option 2 (using Airbus A340) where option 1 is spent energy 26.5E6 MJ per trip while option 2 is only 2.32E6 MJ per trip.
For emission analysis, can be proved that option 1 produce pollutant of CO, VOC, NO_x, PM10, HC, and SO_2 higher than option 2. However, unexpetedly if option 2 produce contents of PM2.5, CO_2, CH_4, N_2O, and NMVOC higher than option 2.

In the aspect of economic and time analysis, option 2 is more expensive and faster than option 1 where only need 17.7 hours to deliver the goods from Portugal to Brasil while option spent time 261.6 hours to do that. This case study will continue to be developed in the future in order to get the maximum result and performance so in one day could be a reference in the decision and policy making.

REFERENCES

1. European Environment Agency. EMEP / CORINAIR Emission Inventory Guidebook 2006: Group 8: Other mobile sources and machinery. Available in 'http://www.eea.europa.eu/publications/EMEPCORINAIR4 "Accessed November 2, 2011.
2. Google. In 2011. Locations and maps of the routes studied. Google Earth.
3. Information on telephone conversations with company employees TAP Portugal.
4. Information in telephone conversation with employees from APL and CSAV.
5. TheEngineeringToolBox.com. Velocity Units Converting Table. Available in 'http://www.engineeringtoolbox.com/velocity-units-converter-d_1035.html "Accessed November 2, 2011.

6. Petromedia Ltd.2011. Portworld: Distance Calculation. Available in 'http://www.portworld.com/map/ "Accessed November 2, 2011.
7. Grosstonnage.com. Category of Vessel. Available in 'http://www.grosstonnage.com/ "Accessed November 2, 2011.
8. HowManyHours.com.2009.Localizações Cities. Available in 'http://www.howmanyhours.com/pt/index/Lisboa/Belo% 20Horizonte.php "Accessed November 6, 2011.
9. EMISIA. 2011.COPERT IV. Available in 'http://www.emisia.com/copert/ »
10. Christopher, Mr. (2011). Telephonic information about Transportes Pascoal with company employees.

CYSENI 2012, May 24–25, Kaunas, Lithuania
ISSN 1822-7554, www.cyseni.com

ANALYSIS OF ELECTRICITY MARKET PRICE FORMATION FACTORS

M. Turcik, I. Oleinikova
Institute of Physical Energetics-Laboratory of Power Systems Mathematical Modelling
Aizkraukles 21, LV-1006 Riga – Latvia
Phone +37127832726
Emails: turcik.mario@gmail.com, irina@edi.lv

ABSTRACT

This paper is focused on the analysis of spot price formation factors on the organized electricity market operated by Nord Pool Spot power exchange. The target is to identify and rank factors according to price impact as well as analyze their seasonal weight. The results of analysis should contribute to the understanding of price formation, seasonal fluctuations and reasons of unpredictable price spikes which are common feature of the spot markets.

Keywords: electricity market, electricity prices, market analysis, liberalisation

1. INTRODUCTION

Determination of electricity prices whether in rigidly controlled or liberalized electric power industry has been and still is addressed. After liberalisation been introduced, wholesale price for electricity is formed in market environment by demand and supply, likewise on markets with other commodities. However, electricity price is dependent on more factors comparing to other usual commodities. Furthermore, principles of price-based control of electrical power systems as well as proclaimed role of electricity prices as main driver for investments into modernization as well as new projects requires well understanding of price formation factors for short-term as well as long term purposes. The simplified principle of flows in trading with electricity is given in Fig. 1 [1].

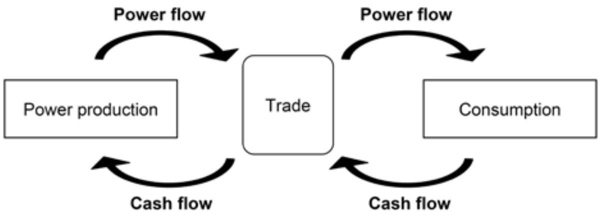

Fig. 1. Principal simplified diagram of trading with electricity

In general, end-user electricity price could be divided into 2 main parts. First, regulated part mainly includes costs of transmission and distribution and other costs, such as subsidy of power production from RES as well as ancillary services (a new trend leads to purchasing of ancillary services based on market principles as well).

Second, deregulated part represents part of end-user electricity price which has been determined by market environment. This part covers mainly costs of production/purchase of electricity, the profit margin of traders and other smaller components. The final share is roughly within 40% to 50% of the end-user electricity price and slightly varies between EU states. Market with electricity means that price is determined by market participants [2]. Electricity price may be formed through organized markets where determination of volume as well as price is performed according to predefined rules of Power Exchange (PX) or through non-organized markets with electricity covered by bilateral trading so called Over the Counter contracts (OTC).

In this article price formation is analyzed and selected factors with expected highest impact to the price on organized power market operated by Nord Pool Spot power exchange (NPS PX) are discussed. Price is always the result of the relationship between supply and demand, affected by many parameters. Therefore, the aim of analysis will be focused on finding *what* and *how* on this market influences the price of electricity. The analysis in detail pointing out on:

- How is supply side correlated with the global fuel markets?
- How sensitive is spot price to the fluctuations on fossil fuel markets?
- What is an impact from introduction of CO_2 emission allowances to the spot price?
- What are the main price drivers on NPS PX?
- How demand side influencing the spot price formation?

Furthermore, in this article presented analysis points to several questions that could be addressed by the future work.

2. SPOT PRICE FORMATION BY ORGANIZED POWER EXCHANGE

Formation of wholesale electricity market price by two-sided auction (PX) is shown in Fig. 2. Market clearing price (MCP) and market clearing volume (MCV) is determined through an two-sided auction from the intersection of the supply curve which is constructed from aggregated supply bids and the demand curve which is constructed from aggregated demand bids [3] [4].

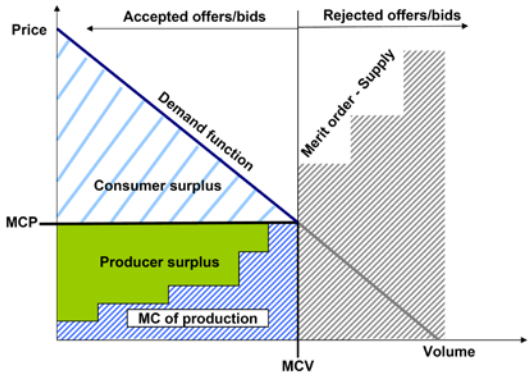

Fig. 2. Spot price formation principle

2.1. Supply curve analysis

Total costs of electricity produced in power plant consist of fixed and variable costs:

$$C_{total} = C_{fix} + C_{var} \tag{1}$$

Fixed costs C_{fix} are related mostly to investment and economic profit to be earned, in short-run its O&M, wages, depreciation, social fund and other obligations which are fixed and independent on level of production. Variable costs C_{var} are all costs which depends on the level of production in particular power plant. Mostly includes costs of fuel and emission allowances. However, once a plant is commissioned, the marginal cost of producing an additional unit of electricity should determine its operation (dispatch). Marginal costs roughly correspond to fuel costs and costs to purchase emission allowances as their volume also depends on the level of production. This fact is an important because determine merit order of power plants in supply curve according to their marginal costs, thereby marginal generator and thus MCP on electricity market. Due to that reason gas and coal-fired power plants are in many cases the marginal plants that set the price in competitive markets [5]. Hence, increases in gas or coal prices are passed on as increases in wholesale electricity prices.

2.2. Demand curve analysis

Demand curve is constructed from aggregated demand bids, thus bidding strategy of customers has significant impact on position of intersection point and therefore final values of MCP as well as MCV on spot market. Natural seasonal load variation of system has of course impact on level of purchased electricity (demand) through spot markets which there causes natural seasonal price variations as well. However, same as for production curve, structure of customers willing to buy electricity have to be investigated in order to obtain comprehensive overview of spot price formation factors.

Aforementioned principles of spot price formation are also applied on Nord Pool Spot PX of which data has been used for analysis. The Nord Pool Spot's algorithm ensures that the lowest-priced source of energy is produced by matching a consumers bid and the last MWh of energy to be produced set the price for all previous production [3].

3. ANALYSIS OF THE SYSTEM PRICE FORMATION FACTORS

Analysis of historical curve of system price of electricity on Nord Pool Spot and analysis of other selected factors such as coal, gas, CO_2 and hydro resources has been performed in order to estimate dependency and behaviour (changes) in system price according to changes is those factors. The first reflection of weight of selected factors could provide proportionality of energy sources in total produced power by production mix of Nordel (DK, SWE, FIN, NOR) on Fig. 3. Considerable long-term hydro production could be a signal of weighty influence of the hydro resources to the system price, however, according to principles of spot price formation (marginal generator), relation of hydro resources and system prices have to be investigated in detail.

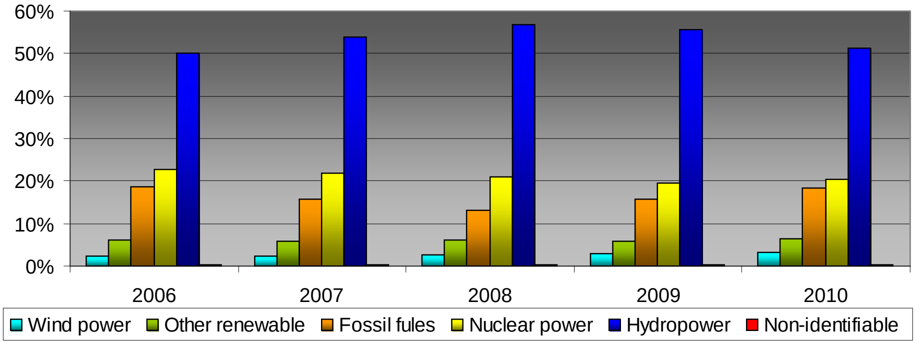

Fig. 3. Nordic area electricity production 2006–2010 by energy source

The nuclear production seems to be a type of production with low historical price volatility, in addition those types of plants traditionally working into base load and on organized spot market usually not playing role of marginal generator, hence, deeper investigation of impacts to the system price is not performed for this type of power plants. However, power plants operated on fossil fuels such as gas or coal has higher marginal costs and often on spot markets playing role of marginal generator (determine market price). Thats why even when production of those power plants is not proportionally highest, significantly influences electricity prices. Tight correlation of plants operated on fossil fuels could be in addition expected with CO_2 emissions as a part of their marginal costs (except fuel costs).

Same as the other commodities, the prices of fossil fuels experiences wide price swings in times of shortage or oversupply. The price cycles may extend over several years responding to the changes in supply and demand [6].

3.1. Past decade development in fossil fuels and emission prices

Gas: The gas spike of last decade occurred in 2008. Regional spot prices and oil-linked gas prices peaked at levels between USD 13 and 15 per MMBtu (1000000 Btu = MMBtu). Oil-linked gas prices in Japan and Continental Europe continued to increase throughout much of 2008 due to the time lag embedded in the contract formulas, but were declining in 2009 to reach USD 7 per MMBtu in the summer of 2009 [7]. However, spot prices started declining in mid-2008 reflecting the impact of the economic crisis on gas demand. Depending on the speed and geographical scope of economic recovery, spot gas prices may well remain weak for some years.

Coal: A coal price has been since 1980 to 2003 relatively stable with general downward tendency and fluctuation due to the natural global economical cycles. Since 2003 the rapid economic growth in China and other developing countries had major impact on world coal production redistribution. To meet rising demand, international coal trade grew by an average of 6.4% per year between 2003 and 2007. Unprecedented spike in coal traded price came up in 2007 and early 2008 due to the sharply increase of demand. Decrease of coal prices has been caused mostly by global recession. Although, most coal is sold under contract and changes in spot markets take time to filter through into prices paid by coal customers, even where contract prices are linked to spot market prices [7].

CO_2 emission allowances: Since introduction of European trading system with emission allowances, those became an important factor which has impact on electricity prices. CO_2 allowances are assumed same as other commodity, thus can be purchased as well as sold according to the best, most profitable actual option for generator [8]. Even when generators received allowances for free, those opportunity costs are more or less reflected to the electricity prices.

4. CORRELATION AND REGRESION ANALYSIS FOR REAL DATA SETS

4.1. Background for correlation and regression in data analysis

Correlation investigating the nature of the relationship between different variables is an important way of numerically quantifying the relationship between them. In other words, correlation is a numerical measure of the degree to which patterns in X and Y corresponds.

In our analysis for quantification of correlation has been used Pearson product-moment correlation coefficient (PPMCC) denoted as „r". PPMCC is a measurement of the linear dependence between two variables X and Y and ranging within -1 to 1. Positive values of „r" indicate a positive correlation between X and Y. Negative values indicate a negative correlation. r = 0 indicates that X and Y are uncorrelated. In principle, correlation between X and Y is equal to correlation between Y and X. The value of „r" is not dependent on units in which analyzed variables are given. Pearson product-moment correlation coefficient is calculated as:

$$r = \frac{\sum_{i=1}^{n}\left(X_i - \bar{X}\right)\left(Y_i - \bar{Y}\right)}{\sqrt{\sum_{i=1}^{n}\left(X_i - \bar{X}\right)^2}\sqrt{\sum_{i=1}^{n}\left(Y_i - \bar{Y}\right)^2}} \qquad (2)$$

However, correlation does not necessarily imply causality. Therefore regression as related concept which is essentially an extension of correlation that introduces an aspect of causality has to be employed in data analysis. Assume that a linear relationship between Y and X exists, and then their relationship is mathematically expressed as:

$$Y = \alpha + \beta X \tag{3}$$

Where, α is the intercept of the line and β is the slope. This equation is referred to as the regression line. In particular, a straight line drawn through the points on the XY-plot provides a convenient summary of the relationship between X and Y. In regression analysis, we formally analyze this relationship. However should be noted that linear regression model will always be only an approximation of the true relationship and it has to be taken into account in conclusions based on results obtained through such technique [9]. Data analysis has been performed in software Statistica and Excel.

4.2. Correlation analysis and estimation of linear trends of variables

According to development tendencies of global fuel prices and emission trading, it could be anticipated that those changes will affect electricity prices by changes in production costs. Measurement of correlation by Pearson product-moment correlation coefficient (r) has been performed between daily average values of Nord Pool Spot system price (NPSsp) and daily average values of 4 factors: Petroleum price denoted as PT Brent, natural gas price index SPCTTTFCALFR1 hereinafter “Gas”, price index All Published Index number 2 (API2) hereinafter “Coal” and CO_2 emmision allowances.

In order to depict seasonal differences within the year and in entire time period under investigation (2006–2011), every year has been divided into 4 equal periods (3 months). Results of correlation analysis are shown in Fig. 4.

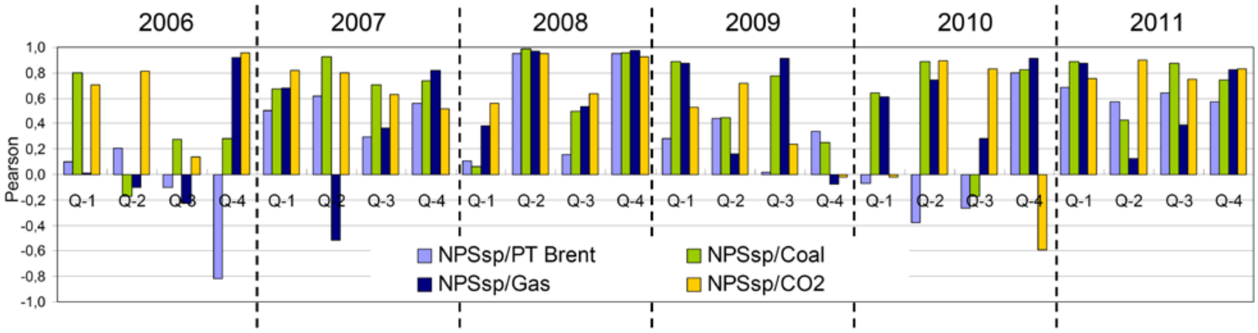

Fig. 4. Correlation of NPS system price with examined factors

From the correlation of NSPsp with other variables on Figure 4 is obvious connection with historical development of fuels and emission, especially in 2 and 4 quarters of 2008 when fossil fuels on world markets reached peak values. Except isolated cases, the vast majority of values demonstrate positive correlation. Significant quarterly observed differences could be explained by fluctuations of fuel and emission prices as well as differences in demand, thus by different marginal generators on spot market.

4.2.1. Estimation of linear trends of variables

In order to compare general tendencies and dynamism in change of variables (NPSsp, PT Brent, Gas, Coal, CO_2) to find out their mutual behaviour, these are modelled using linear regression model. Independent variable is in this case represented by time (X axis), while dependent variable (Y axis) represents values of NPSsp, PT Brent, Gas, Coal and CO_2. Linear regression model is fitted using the least squares method. Input data as well as annual splitting to the quarters is same as for the correlation analysis above.

Obtained results show general linear trend development of particular variable in quarter, to visualise results in the most transparent way, those linear trends are moved to common initial point as is shown on Fig. 5.

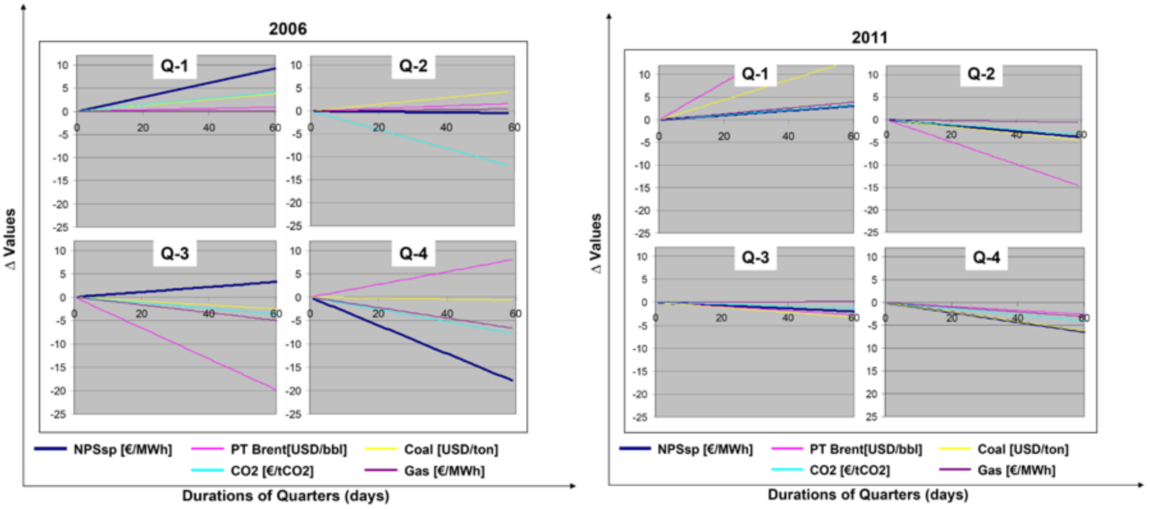

Fig. 5. Quarterly expressed linear trends of NPS system price and examined factors (examples for 2006 & 2011)

Successive scrutiny of all quarters one-by-one from 2006 to 2011 (thus 24 quarters) reveals similarities in general trends and furthermore in dynamics of upward and downward pace between variables as well as their seasonal tendencies. The highest number of identical tendency with NPSsp from all investigated factors has Gas (19 quarters from 24 quarters), the second is Coal (18 from 24), CO_2 (15 from 24) and same PT Brent. This result could be explained by already mentioned fact that marginal generator is often gas or coal-fired power plant.

A linear approximation to estimate tendencies of dependent variables does not need to be in quarters with high volatility (dispersion) of values appropriate one. Hence, to make conclusion about tendencies between depicted trends, fitness of linear regression has to be taken into account by assessment of R-squared values (R^2). The lower value (R^2), the worse demonstration of such trend by linear regression model is. Table 1 gives an overview of R-squared values obtained from linear regression models which should be used in assessment process.

Table 1. Quarterly expressed R-squared values

R^2	**Q-1**						**Q-2**					
	2006	**2007**	**2008**	**2009**	**2010**	**2011**	**2006**	**2007**	**2008**	**2009**	**2010**	**2011**
NPS [€/MWh]	0,891	0,158	0,101	0,308	0,342	0,380	0,001	0,912	0,952	0,185	0,357	0,393
PT Brent [USD/bbl]	0,012	0,785	0,579	0,236	0,076	0,870	0,024	0,441	0,923	0,883	0,484	0,553
Coal [USD/ton]	0,575	0,620	0,732	0,429	0,792	0,639	0,694	0,885	0,945	0,361	0,405	0,353
CO2 [€/tCO2]	0,638	0,005	0,017	0,140	0,093	0,864	0,330	0,700	0,894	0,001	0,306	0,530
Gas [€/MWh]	0,001	0,011	0,389	0,504	0,937	0,722	0,073	0,263	0,955	0,103	0,901	0,079
R^2	**Q-3**						**Q-4**					
	2006	**2007**	**2008**	**2009**	**2010**	**2011**	**2006**	**2007**	**2008**	**2009**	**2010**	**2011**
NPS [€/MWh]	0,166	0,288	0,001	0,802	0,242	0,412	0,916	0,039	0,909	0,400	0,779	0,594
PT Brent [USD/bbl]	0,790	0,000	0,906	0,093	0,054	0,040	0,540	0,567	0,911	0,091	0,736	0,074
Coal [USD/ton]	0,137	0,872	0,677	0,422	0,130	0,313	0,063	0,537	0,802	0,001	0,890	0,673
CO2 [€/tCO2]	0,515	0,026	0,255	0,005	0,404	0,248	0,936	0,144	0,866	0,206	0,654	0,827
Gas [€/MWh]	0,922	0,000	0,396	0,700	0,320	0,020	0,932	0,323	0,949	0,621	0,745	0,895

4.3. Impact of hydro resources to the NPS system price

Considerable proportion of hydro production on overall Nordel electricity production naturally define dependency Nord pool system price on hydro resources, thus higher correlation between them is expected. For the hydrological situation is typical seasonal variation as well as year-to-year differences and those are susceptible to the weather conditions. Deviation of electricity production capacities of hydro power plants from normal average level has impact to the electricity prices. In order to investigate those impacts, find out interdependence and strength of this relation, average weekly potential (TWh) of Norwegian and Swedish power plants and average weekly NPS system price (€/MWh) are input data for the analysis. Employed methodology in regression and correlation analysis in time period under investigation (2001–2011) assume with division of every year to the 3 periods (4 months every) and subsequently rearrangement of data according to particular period into 3 data sets. In such way in first data set are values of first periods (1/3) of all years from 2001 to 2011, second data set contain data of second periods (2/3) from 2001 to 2011 and analogous for third one (3/3). Table 2 shows results of correlation analysis by Pearson product-moment correlation coefficient performed for all three data sets.

Table 2. Correlation level of hydro potential with NPS system price 2001-2011 by period

2001-2011	1/3 of Years	2/3 of Years	3/3 of Years
Hydro/NPSsp	-0.640	-0.453	-0.600

Values in Table 2 shows relatively high level of negative correlation; it could be explained in such way, that negative deviation of hydro resources from normal level causing increase of prices. A result also confirms seasonal differences, thus could be concluded that system price in the first and third periods of years is more “hydro dependent” than in middle parts of the years (second periods). Linear regression analysis of 3 data sets is shown on Figures 6, 7 and 8 respectively. Zero value of X axis represents normal hydro level, positive values (right from 0) level higher than normal and negative value (left from 0) level lower than normal.

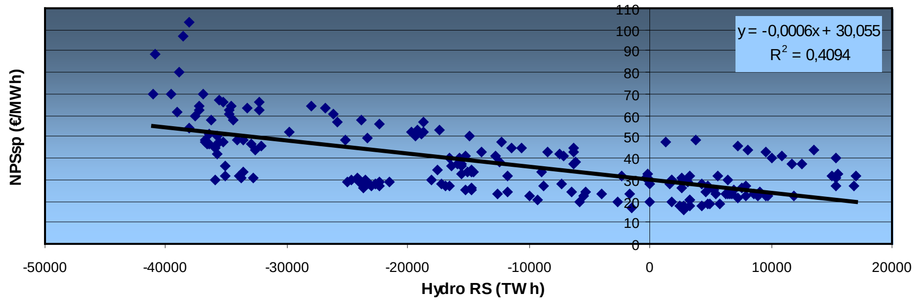

Fig. 6. Linear regression analysis of first periods (1/3) of years 2001–2011

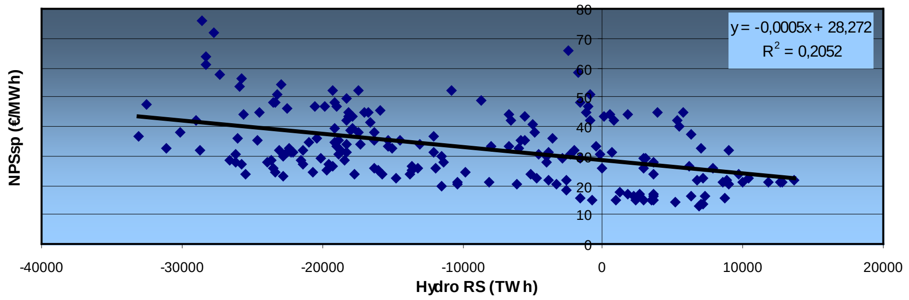

Fig. 7. Linear regression analysis of second periods (2/3) of years 2001–2011

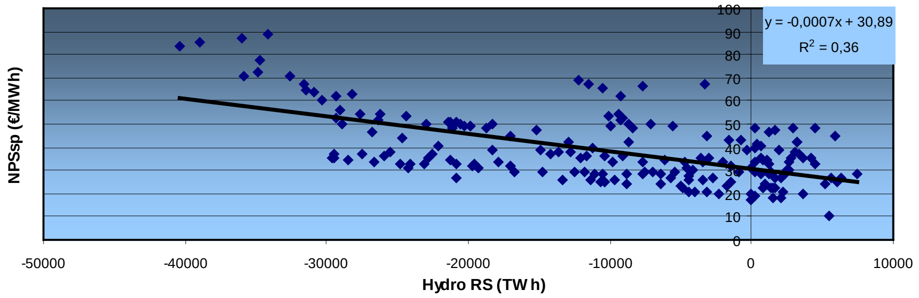

Fig. 8. Linear regression analysis of third periods (3/3) of years 2001–2011

By graphical expression of analyzed data is obvious slightly grouping of values, so that values with higher occurrence could be observed in particular data set. It gives an opportunity to find out range or ranges of characteristic values in linear downward regression models. It is evident that level of hydro reservoirs proves relation with system price and therefore could be concluded that is one of the main factor in system price determination on Nord Pool Spot PX.

5. CONSUMPTION/DEMAND SIDE ANALYSIS

In order to estimate impacts of behaviour of customers who purchase electricity on NPS spot market to the price formation process, strategy of their “buy” bidding has been analyzed. Input data for analysis comprise 6 randomly selected days in different seasons in 2010, 2011 and 2012. Every day consist of 24 hourly results of bidding strategy. Bidding strategy means level of “willing to pay” of customers to purchase electricity on spot market. Two main groups of customers has been recognized, those who are “willing to pay” at 2000 €, what actually represents maximum available bidding value on Nord Pool Spot and second group contains customers with bids within the -200€ to 2000€.

Short term demand flexibility analysis reveals several important facts. Roughly 85% of consumers’ buy bids are placed at the maximal available value of 2000€ per MWh, thus only 15% could be assumed as at least partly flexible price responsive demand of which buy bids are placed within the range -200€ to 2000€. There are no significant distinguishable differences in buy biding behaviour between randomly selected days within the year as well as between examined years as demonstrate results of analysis on Figures below.

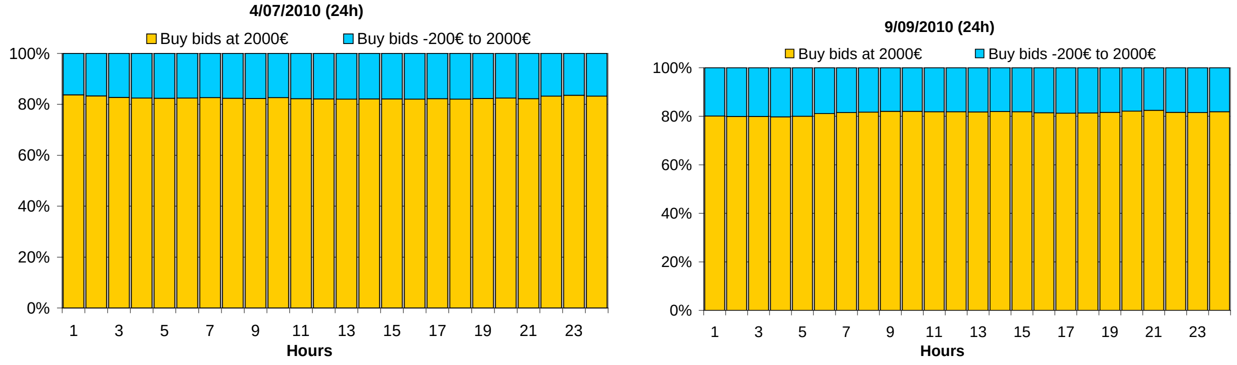

a) b)

Fig. 9. One day buy-bidding analysis of NPS PX: a) 4th July 2010, b) 9th September 2010

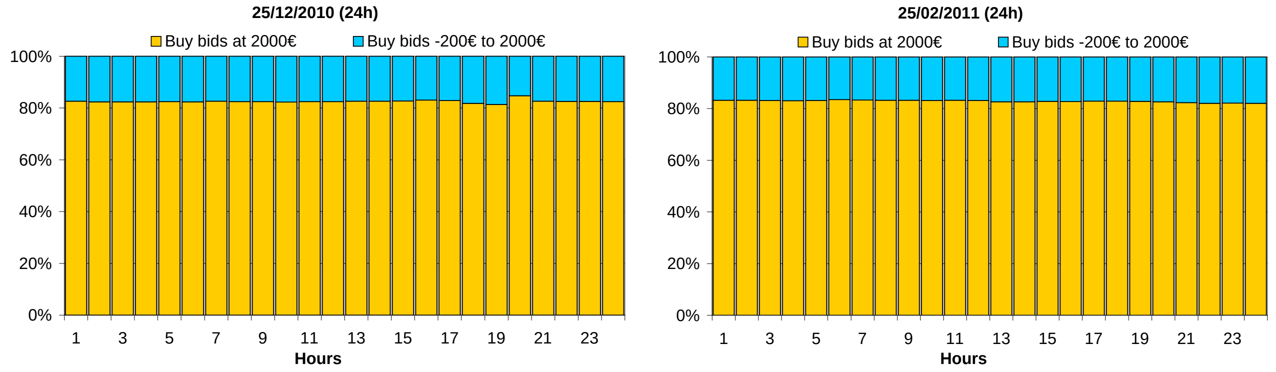

a) b)

Fig. 10. One day buy-bidding analysis of NPS PX: a) 25th December 2010, b) 25th February 2011

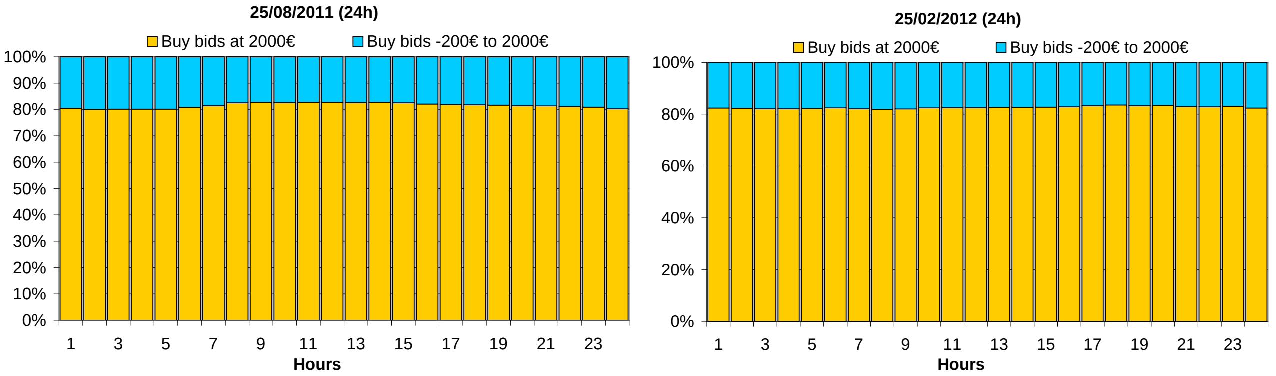

a) b)

Fig. 11. One day buy-bidding analysis of NPS PX: a) 25th September 2011, b) 25th February 2012

Demand curve constructed from aggregated buy bids according to results of analysis may be characterized as very low price responsive demand curve. Such price formation is nearly to markets with pool price determination principle where only supply side has active participation on price formation. This finding has also weighty impact to the understanding of price volatility since could be an answer of unpredictable price spikes as well as high volatility of electricity price on spot market.

6. CONCLUSIONS AND DISCUSSION

The results of analysis of the system price formation factors on Nord Pool gives following assumptions about this market: relatively high level of positive correlation between system price and assumed factors with considerable seasonal and annual differences. From the observation of seasonal linear trends of system price and those factors the highest number of identical tendency with NPSsp from all investigated factors has Gas and then Coal. This could be taken as confirmation of fact that as marginal (price determining) generators on this market are often gas and coal-fired power plants. According to CO_2 emissions, the interesting is their relatively high correlation with NPSsp, even when generators received those allowances for free. This may be explained by the fact that those allowances are now assumed by generators as usual commodity and therefore with trading potential. Furthermore, those allowances are required by fossil fuel fired power plants and those are, as was mentioned above, often marginal generators. The analysis also shows high correlation between hydro situation and NPSsp with high and typical seasonal variations.

From the analysis of demand side is surprising extremely low price responsiveness of consumers, when production side facing almost to the inflexible demand. This bidding strategy may be explained by reliance of consumers in this electricity market, however, such bidding strategy can contribute to occurrence of unpredictable and considerable price spikes during disturbances on supply side.

The target of this article is related to assessment of impacts of fuels and emission allowances to the electricity price. However, it should be noted that correlation between fossil fuel prices as well as vice versa impacts, such as impacts of electricity prices to the fossil fuel prices and prices for emission allowances could be possibly observed, assume the fact that demand for property increasing property prices.

Besides analyzed factors, in liberalised imperfectly competitive environment, the possible price changing factor is represented by abused market power of the one or more involved competitors. This should be taken into account in further investigation as well. Furthermore, it might be expected that increase of power production from intermitted generation sources with low marginal costs of production such as wind or photovoltaic will contribute to the increase of price volatility on spot markets as they provides well appropriate trading option for those hard foreseeable types of power production.

ACKNOWLEDGEMENT

The paper is supported by the European Social Fund Project “Scientific Group Supporting Latvian Activities of the European Strategic Energy Technology Plan”, No.1DP/1.1.1.2.0/09/A-PIA/VIAA/027 and by project VEGA SR No. 1/0414/12.

REFERENCES

1. CHEMISINEC, I.; MARVAN, M.; NECESANY, J.; SYKORA, T.; TUMA, J. *Obchod s elektřinou,* (Market with Electricity), 1st Edition, CONTE spol s r.o., 2010, p. 201, ISBN 978-80-254-6695-7.(in Czech).
2. JUNGHANS, G.; OLEINIKOVA, I.; OBUSHEVS, A.; TURCIK, M. How electricity market price is formed? (Kâ veidojas elektroenerìijas tirgus cena?), From the volume Energija un Pasaule, 2012, Vol. 72, No. 1, p. 42-45 ISSN 1407-5911. (in Latvian).
3. Nord Pool Spot – Power Market Information, [Online]. Available: http://www.nordpoolspot.com/Download-Centre/
4. FROEB, Luke M.; MCCANN, Brian T. *Managerial Economics*, 2nd Edition, South-Western, Cengage Learning, p. 345, ISBN-10: 1-439-07798-3.
5. ROSE, K. The Impact of Fuel Costs on Electric Power Prices, June 2007, p.25 [Online]. Available: http://appanet.cmsplus.com/files/PDFs/ImpactofFuelCostsonElectricPowerPrices.pdf
6. WARON, R. *Modelling and forecasting electricity loads and prices: a statistical approach,* John Wiley & Sons, 2006, p. 192, ISBN 0-470-05753-X,
7. IEA, NEA, OECD: *Projected Costs of Generating Electricity: 2010 Edition.* OECD PUBLICATIONS, 2 rue André-Pascal, 75775 Paris Cedex 16, printed by Actuel Graphic, 218 p. ISBN 978-92-64-08430-8.
8. HARRIS, C. *Electricity Markets: Pricing, Structures and Economics*, John Wiley & Sons, 2006, p. 542, ISBN-10 0-470-01158-0.
9. KNOOP, G. *Analysis of Economic Data*, John Wiley & Sons, Dec 2004, p. 256, ISBN-10: 0470024682.

CYSENI 2012, May 24–25, Kaunas, Lithuania
ISSN 1822-7554, www.cyseni.com

WHY EU ENVIRONMENTAL LAW IS RELEVANT FOR THE ENERGY SPECIALISTS?

J.Urbanavičius
Vilnius University Law Faculty,
International and the EU Law Institute,
Sauletekio al. 9, LT-10222, Vilnius, Lithuania
Phone 0037052366175
Email: jonas@urbanavicius.eu

ABSTRACT

Activities in the energy sector, such as production, transportation, distribution of energy are governed by wide range of legal norms. One of the major groups of such norms belong to the environmental law. This relationship is natural because almost all of the sources of energy are the elements of the natural environment. Moreover, the negative environmental impacts are being observed during the process of production or transportation of energy. After the energy policy was lifted to the level of the EU policies in 2009, the EU legislation in the energy sector became even more relevant.

The EU environmental standards are being constantly revised. There are several reasons for that – first of all, natural and man-made environmental disasters, such as the accident in the Fukushima NPP in 2011; secondly, technical progress in the energy sector. EU environmental legislation is following the innovations and other developments in the energy sector. This leads to the evolution of the environmental law towards the application of the precautionary principle, where scientists play significant role. The paper describes the EU environmental legislation, applicable to the energy sector, and analyzes its perspectives.

Keywords: European Union law, environmental law, energy law, energy regulation

1. INTRODUCTION

It is agreed that many of the environmental issues are caused by our present energy system that is based on fossil fuels and biomass burning. One of the major environmental issues currently is global warming. There are many discussions on the anthropogenic nature of this issue. However, besides global warming, other issues, such as air pollution, acid rain, loss of biodiversity and desertification are undoubtedly caused by human activities. The indicator, showing the relation between human demands and nature's capacity to provide environmental services and regenerate is called the 'ecological footprint'. According to it, human consumption currently is about 25 percent above the capacities of Earth to provide resources and regenerate. Most of this consumption (and, consequently, its impacts on nature) is caused by the activities, related to energy – electricity and heat generation, transport sector, industry (during combustion necessary for its processes as well as using energy sources during the processes, e.g., in steel or fertilizer industry).

Extensive activities in the industrialized countries and various hazardous substances (COx, SOx, NOx, NHx, hydro-carbonates, various metals, particulate matter, nuclear waste, other pollutants) are being emitted to the air, released or spilled to water, landfilled or dumped as waste, incidentally (or accidentally) released to the environment (Although due to the actions taken, actual SO2 emissions were reduced by around 50 percent since 1990 [27]). This causes air, water, soil pollution, loss of biodiversity, and leads to rising number of various diseases, and death (according to World Health Organisation, about 3 million deaths each year might be attributed to the pollution, [26]).

It is understandable that the technical progress cannot be overturn. However, it was agreed (especially in the second half of the 20th century) that this progress may not be reckless and that certain restrictions, especially, as regards the environmental impacts, must be imposed. Since, a variety of environmental legislation is applicable in many areas of economic activities, including energy. The recent tendency of the environmental law is the growing application precautionary approach, where scientists play significant role. Evolution of the EU environmental law towards this approach is overviewed in the article. This is done by giving a general overview of the environmental legislation of the European Union applicable in the energy sector, its evolution and perspectives. More precisely, origins and evolution of the EU environmental law, its sources, integration with other policy areas, as well as main pieces of primary and secondary EU environmental legislation are explained. Finally, new trends and perspectives of the contemporary EU environmental law leading towards the emergence of the new principle of precaution, applicable by the environmental law are overviewed, as well as the role of scientists in this process. The paper is more of a descriptive character, as it is a part of author's wider research on the EU environmental law capacities to ensure high level of the environmental protection in the area of the energy infrastructure. Established methods of the science of law, such as historic, crytical, analytical, dogmatic, are used throughout the paper.

2. EVOLUTION AND STRUCTURE OF THE EU ENVIRONMENTAL LAW

European Union emerged as the economic union. Its core was European Economic Community that was established in 1957 and aimed at creating the customs-free union, and, later – a single market for goods, persons and capital. During the process of integration, new policies were added to the competencies of the EEC. This have lead to the need not only promote, but also restrict economic activities. Thus, environment became the policy area that needed more attention in the supra-national level. The need to ensure better quality of life and protection of the environment were for the first time mentioned only in the declaration of Heads of States in 1972.

2.1. Primary EU Law

Later this need was embedded in the primary law of the European Community ('Primary law' is the funding treaties of the European Union, while the 'secondary law' comprises Regulations, Directives, Decisions). Its role gradually rose, and currently protection of the environment is not only a policy of the European Union, but also a general principle of the EU Law. Sustainable development of Europe, based on, *inter alia*, a high level of protection and improvement of the quality of the environment, is one of the goals of the European Union, entrenched in the Treaty of the European Union [1, Article 3]. The objectives of the Environmental policy itself are: preserving, protecting and improving the quality of the environment, protecting human health, prudent and rational utilisation of natural resources, promoting measures at international level to deal with regional or worldwide environmental problems, and in particular combating climate change [2, Article 191]. The environmental aspects of the EU energy policy lie already in the primary EU legislation as well. In the new TFEU Article 194 (included to the EU law only by the Lisbon Treaty in 2009), dedicated to the EU energy policy, the need to preserve and improve the environment is acknowledged, and promotion of energy efficiency and energy saving and the development of new and renewable forms of energy are set as one of the objectives of the EU energy policy [2].

Before analysing particular legal environmental requirements applicable in the energy sector, one has to bear in mind that legal norms cannot be treated and interpreted separately and in an isolated way. All the norms in the legal system interact with each other, and sometimes between legal systems. Legal system is a way of operation and co-existance of the entirety of legal norms, where all the legal norms are grouped to the legal institutes, sub-branches, branches, are inter-related and operate by guaranteeing each other's interoperability [26, p. 341]. A separate branch of law is one of the elements of the hierarchy of the legal system. Environmental law as a separate branch of law may be described as a set of legal norms regulating social relationships among the interaction of the humanity and the environment. Because they regulate different aspects of the same elements of the environment (environmental law governs protection, while energy law – the use of natural resources), the interaction of the energy and environment is very tense, therefore many legal norms regulating energy may be similarly attributed both to the energy and environmental law [25]. This interaction is reflected not only in theory. In the EU legislation it is implemented through the principle of integration.

2.2. Integration of the EU environmental law and energy sustainability

Article 37 of the Charter of Fundamental Rights of the European Union [3]sets that a high level of environmental protection and the improvement of the quality of the environment must be integrated into the policies of the Union and ensured in accordance with the principle of sustainable development. The principle of environmental integration (if it is not respected by the EU institution, the adopted legal act may be declared void by the Court of Justice of the European Union), among other sectors, is applicable to the energy sector as well. Some scientists [23] even argue that the EU competence in the energy sector finds its roots precisely in the application of this integration principle. Analysis reveals that (before the end of 2010) energy-related EU legislation already consisted of around 80 legal acts in the environmental field adopted from as early as 1992 [24, p. 405].

Practically the contents of the principle of environmental integration was revealed in 1998, in the document of the European Commission on the strengthening environmental integration within Community energy policy [11]. It was acknowledged in this document that energy is essential for achieving economic growth and social welfare, but energy production, transportation and use have impacts on the environment. These impacts may be local, when they concern air quality in towns, waste disposal or noise; they may cover several regions or states and thus have continental dimensions, as with acidification, safe nuclear operation and nuclear waste disposal; climate change has an impact at global level. In order to mitigate negative impacts on the environment, the European Commission proposed several directions (that are being followed since): energy efficiency, co-generation, development if the renewable energies, cleaner use of fossil fuels, reduction of acidification, avoidance of waste disposal at sea, use of waste incineration (although in its position on the forthcoming 7th EU Environmental Action Programme, European Parliament's Committee on the Environment, Public Health and Food Safety has indicated that no waste that is suitable for recycling or composting with respect to the hierarchy of the Waste framework directive must be incinerated [17]. Specific environmental objects of Community Energy Policy were set: to promote energy efficiency and saving; to increase the share of production and use of cleaner energy sources, to reduce the environmental impact of the production and use of energy sources.

The reflection of the environmental integration in the energy sector is its sustainability. In the context of the sustainable development, as described in the Article 3 of the Treaty on European Union [1], sustainability of the energy sector is a balance between the functioning of the common energy market and a high level of protection and improvement of the quality of the environment.

2.3. Secondary EU environmental law

The need to pay more attention to the sustainability of the energy sector was again acknowledged by the European Council in 2007. Heads of States in their conclusions [16] stated that because of the vital importance of achieving the strategic objective of limiting the global average temperature increase to not more than 2°C above pre-industrial levels, one of the objectives of the future EU energy policy must be promoting environmental sustainability and combating climate change. Thus the European Council adopted a so called 20-20-20 plan: to achieve at least a 20% reduction of greenhouse gas emissions by 2020 compared to 1990; to achieve the objective of saving 20% of the EU's energy consumption compared to projections for 2020; and to achieve a binding target of a 20% share of renewable energies in overall EU energy consumption by 2020 (including a 10% binding minimum target to be achieved by all Member States for the share of biofuels in overall EU transport petrol and diesel consumption by 2020).

The EU secondary law implements principles, goals and objectives of the European Union, set both in the founding treaties and in the political statements of the European Council.

Analysing the secondary EU environmental law (adopted by the EU institutions), it may be classified according to various criteria: regulated energy infrastructure objects, protected elements of the environment, various parts of the energy production and realisation chain and so on. However, in the legal literature, the EU environmental law is divided into two parts: general and special part [22]. General part comprises legal norms, governing general environmental issues (horizontal legislation), such as planning process regulation: access to information, public participation, environmental impact assessment; energy efficiency, administrative and financial measures, IPPC, environmental liability.

Special part of the EU environmental law is dedicated to particular legislation governing protection of certain environmental elements and protection against certain pollutants: water quality; air quality; soil protection; protection from noise; nature protection; waste management; radiation security; regulation of chemical substances etc.

2.3.1. General part

Planning process regulation comprises several legal acts. Firstly, Directive on public access to environmental information [4] is aimed at guaranteeing the right of access to environmental information held by or for public authorities and to set out the basic terms and conditions of, and practical arrangements for, its exercise; and to ensure that, as a matter of course, environmental information is progressively made available and disseminated to the public in order to achieve the widest possible systematic availability and dissemination to the public of environmental information. Member states are obliged to make available environmental information held by or for them to any applicant at his request and without his having to state an interest. Environmental information means any information on the state of the elements of the environment, such as air and atmosphere, water, soil, land, landscape and natural sites, biological diversity and its components; and factors, such as substances, energy, noise, radiation or waste, including radioactive waste, emissions, discharges and other releases into the environment, affecting or likely to affect the elements of the environment. Another legal document in the sphere of the access to information is the UN Convention on access to information, public participation in decision making and access to justice in environmental matters (Aarhus Convention), member of which EU is [10]. One more of the human rights entrenched in this Convention is related to the environment is their right to participate in the taking decisions in the area of environment. It is realized through one of the widest applicable EU legal acts in the environmental area: the Directive on the assessment of the effects of certain public and private projects on the environment [9] that obliges Member States to ensure that projects likely to have significant effects on the environment by virtue, *inter alia*, of their nature, size or location are made subject to a requirement for development consent and an assessment with regard to their effects. Secondly, it guarantees that the public is given early and effective opportunities to participate in the preparation and modification or review of the plans or programmes that are necessary to implement (for example, such plans are necessary when planning crude-oil refineries, thermal or nuclear power stations, and similar installations that might have impacts on the environment).

Proper implementation of the EU environmental law is not possible without effective legal remedies. Therefore the Directive on environmental liability with regard to the prevention and remedying of environmental damage [5]. It establishes a framework of environmental liability based on the 'polluter-pays' principle, to prevent and remedy environmental damage.

Among other general EU environmental legal acts applicable in the energy sector, is the Directive, setting a framework for the implementation one of the main goals of the EU energy policy – promotion energy efficiency. Directive on energy end-use efficiency and energy services was adopted in 2006 [6] and is now being reviewed and renewed [13]. In addition, Directive on the promotion of the use of energy from renewable sources must be mentioned as well [7].

Directive on industrial emissions (integrated pollution prevention and control) [8] lays down rules designed to prevent or, where that is not practicable, to reduce emissions into air, water and land and to prevent the generation of waste, in order to achieve a high level of protection of the environment taken as a whole.

This list is only indicative, and much more EU legislation, aimed primarily at ensuring protection of the environment, is applicable in the energy sector (certain administrative, financial measures, emission trading system, system of eco-labelling and others).

2.3.2. Special part

Another part of the EU environmental legislation is dedicated to particular elements of the environment and sets minimal standards of their quality. This is usually done by setting the maximum available levels of certain regulated pollutants, prohibiting certain activities and setting procedures that must be observed. As mentioned above, EU environmental legislation counts around 80 legal acts. The full list of the EU legislation in force and in preparation may be found through the EU law portal eur-lex.eu, thus only sectors regulated by the EU environmental law may be listed:

- air quality
- noise protection
- water quality
- soil protection
- waste prevention
- nature protection and protection of biodiversity
- reaction to the industrial accidents

Some of the legislation from the areas listed above may be applicable in the energy sector as well, depending on the particular energy object.

3. PERSPECTIVES OF THE EU ENVIRONMENTAL LAW

Law is not a stagnant system. It constantly changes and adapts to the changes in the society. Environmental law is not an exception – for example, Directive governing environmental impact assessment procedures, was already changed 34 times, and another review is set for 2012. One can observe a tendency that these amendments and adaptations usually only lead to the environmental standards becoming stricter.

There are two types of catalysts stimulating changes – environmental disasters (both man made and natural), and technical progress. Accidents (wreck of tanker Amoco Cadiz near Bretagne coasts in 1978, resulting in the biggest oil spill near the coasts of Europe, the 'Deepwater Horizon' oil spill in 2010, Accident in Fukushima Nuclear power plant in 2011), and investigation of their causes show that the current system is not sufficient for protection of the environment (both in the terms of applicable environmental quality standards and proper implementation of the environmental requirements). This leads to constant 'upgrade' of the EU environmental law.

For example, at least four major pieces of the environmental legislation, that are relevant to the energy sector, are under revision in the EU institutions: setting new safety standards of offshore oil and gas prospection, exploration and production activities [15], the revision of the Directive on the control of major-accident hazards involving dangerous substances [12]**,** renewal of the Directive on energy efficiency [13], revision of the Directive on Prevention of pollution from ships: sulphur content of marine fuels [14].

On the other hand, not only the constantly deteriorating environmental situation, but new scientific data and technical progress allows to tighten standards of the environmental quality as well (usually resulting in lowering thresholds, as is in the case of the revision of the sulphur content of marine fuel). Moreover, newly discovered technologies (or technologies that just recently became applicable) also trigger changes in the environmental legislation: the constant progress in exploitation of the renewable energy sources foster the progress of the legislation of this sector. Similarly, as the exploitation of the shale gas gains momentum, discussions on the need for new legislation begin. However, another principle of the EU environmental law – sustainable development – must always be born in mind. This remark is especially relevant to the renewable energy, as the data on its negative environmental impacts appear. For example, modern biomass usually is based on the cultivation of mono-cultures. Large land areas are needed in order to fulfil the growing needs. Deforestation of large scale occurs when growing mono-cultures used for biomass. This leads to deforestation (and, accordingly, lesser CO2 capture) and loss of biodiversity. Moreover, fertilizers causing eutrophication of waters, are used to speed up the growth of biomass. Use of wind energy cause nuisance arising out of the equipment noise, aesthetic pollution, and deaths of migratory birds. Hazardous substances used in photovoltaic elements cause accumulation of toxic wastes in the environment. Small hydro plants (below 500MW installed capacity) may interfere with the local fauna and flora [21].

In addition, although renewable energy sources became popular mainly because of their low CO2 impact, even this myth is destroyed. The most recent scientific data leaked, showing that if taking into account 'full cycle', including the manufacturing of installation, transportation, effects of Indirect Land Use Change (ILUC), the biofuels such as palm oil, soybean and rapeseed appear to have much bigger CO2 impact than the fossil fuel [30]. The European Commission seems to recognize some aspects regarding ILUC and is determined to take this into account [31].

As regards production of the so-called unconventional gases (shale gas), it raises a certain legal question: – is the current EU legislation enough to ensure proper environmental protection? Or maybe new legislation must be adopted (or existing adapted). Several environmental accidents related to the extraction of the shale gas in the USA and Great Britain (related to contamination of potable water and mini-earthquakes) lead to the opposition from the society to this type of energy. Some EU member states (France, Bulgaria) even adopted national legislation prohibiting extraction of shale gas in their territories (while others, such as Lithuania and Poland are promoting shale gas as a means to their energy independence). Therefore there is a immense pressure on the EU institutions to have their say on the issue. Both the European Parliament and the European Commission have released studies on the necessity of the new environmental legislation with concurring conclusions [49; 50]. Just recently the European Parliament has issued an official Draft Report on the environmental impacts of shale gas and shale oil extraction activities. In this report, a conclusion is drawn that current legislation is sufficient, however, the constant and effective monitoring of the extraction activities as well as better coordination between the controlling institutions must be ensured. This is essential, as more data from the monitoring of the future mass scale exploitation activities may reveal new threats to the environment. Therefore the legislative bodies have to be ready to react in case it appears that the current legislation does not ensure proper level of protection.

The above mentioned tendencies are related to the emergence of the new concept of the environmental law, that is the precautionary approach or precautionary principle. It is not agreed so far, whether this concept may be called a principle of the environmental law, or it rather remains at the level of the 'approach' [20, p. 76-77]. Under this concept, policy makers should govern the environmental issues as an indispensable basis for the wellbeing of humankind, both now and in the future, and should be prepared to tackle risks about which there is no definitive proof that there is a causal relation between the suspected activity and the harm, or that the suspected damage will occur [19, p. 52; 20, p. 74]. The concept of the precautionary approach thus differs from the well established principle of prevention. Another important aspect of the precautionary approach, as can be seen from the examples above, is the dependence of the environmental legislation on the science in general. There are several reasons for this. Firstly, science indicates and points to the ecological problems to which the law must respond. Secondly, environmental issues are usually analysed through scientific descriptions of the physical world. Still, it is agreed that a long way has to be gone both by the lawyers and the scientists until the precautionary approach becomes fully applicable principle of the environmental law [20, p. 75-76].

4. CONCLUSIONS

As can be seen from the analysis, the EU environmental law is deeply integrated into other areas of EU competence. Energy is no exception. Although became one of the EU policies only several years ago, it was widely regulated by the EU legislation, as regards its environmental implications. Tens of pieces of the EU environmental legislation are applicable in the energy sector. This amount is only increasing, as new legal acts are adopted, and environmental integrations are integrated to other areas of law. In addition, the existing legislation is constantly being revised, thus strengthening environmental regulation. Both newly available technologies and environmental accidents are reasons for these developments. The current trends leads towards the institutionalisation of the precautionary approach as the fully recognized principle of the environmental law. All these developments influence activities performed in the energy sector. Thus scientists should take actively collaborate with lawyers in order the future EU environmental legislation ensures proper protection of the environment for future generations.

REFERENCES

EU legislation

1. Treaty of the European Union, Official Journal L C 83, 2010.03.30.
2. Treaty on the Functioning of the European Union, Official Journal L C 83, 2010.03.30.
3. Charter of Fundamental Rights of the European Union, Official Journal L C 83, 2010.03.30.
4. Directive 2003/4/EC of the European Parliament and of the Council of 28 January 2003 on public access to environmental information, Official Journal L 041 , 14/02/2003 P. 0026 – 0032
5. Directive 2004/35/CE of the European Parliament and of the Council of 21 April 2004 on environmental liability with regard to the prevention and remedying of environmental damage, Official Journal L 143 , 30/04/2004 P. 0056 – 0075.
6. Directive 2006/32/EC of the European Parliament and of the Council of 5 April 2006 on energy end-use efficiency and energy services, Official Journal L 114, 27.4.2006, p. 64–85.
7. Directive 2009/28/EC of the European Parliament and of the Council of 23 April 2009 on the promotion of the use of energy from renewable sources and amending and subsequently repealing Directives 2001/77/EC and 2003/30/EC, Official Journal L 140, 05/06/2009, p. 16-62
8. Directive 2010/75/EU of the European Parliament and of the Council of 24 November 2010 on industrial emissions (integrated pollution prevention and control), Official Journal L 334, 17/12/2010 P. 0017 – 0119.

9. Directive 2011/92/EU of the European Parliament and of the Council of 13 December 2011 on the assessment of the effects of certain public and private projects on the environment (Codified version, Oficial Journal L 26, 28/01/2012, p. 1-21
10. Council Decision 2005/370/EC of 17 February 2005 on the conclusion, on behalf of the European Community, of the Convention on access to information, public participation in decision-making and access to justice in environmental matters, Official Journal L 124 , 17/05/2005 P. 0001 – 0003.

Other documents of the EU institutions

11. Communication from the Commission of 14 October 1998: Strengthening environmental integration within Community energy policy, COM(1998)0571.
12. Proposal for a Directive of the European Parliament and of the Council on control of major-accident hazards involving dangerous substances, 21 December, 2010, COM(2010)0781, not published in the Official Journal.
13. Proposal for a Directive of the European Parliament and of the Council on energy efficiency and repealing Directives 2004/8/EC and 2006/32/EC, 22 June 2011, COM(2011)0370, not published in the Official Journal.
14. Proposal for a Directive of the European Parliament and of the Council amending Directive 1999/32/EC as regards the sulphur content of marine fuels, 15 July 2011, COM(2011)0439, not published in the Official Journal.
15. Proposal for a Regulation of the European Parliament and of the Council oh safety of offshore oil and gas prospection, exploration and production activities, 27 October 2011, COM(2011)0688), not published in the Official Journal.
16. Presidency Conclusions. [referred on 4th March, 2012], Link to the internet <http://register.consilium.europa.eu/pdf/en/07/st07/st07224-re01.en07.pdf>
17. Draft Report on the review of the 6th Environment Action Programme and the setting of priorities for the 7th Environment Action Programme – A better environment for a better life, PE478.523, 15 December 2011, European Parliament Committee on the Environment, Public Health and Food Safety, [referred on 4th March, 2012], Link to the internet <http://www.europarl.europa.eu/meetdocs/2009_2014/documents/envi/pr/887/887278/887278en.pdf>
18. Draft Report on the environmental impacts of shale gas and shale oil extraction activities, PE483.605, 11 April 2012, European Parliament Committee on the Environment, Public Health and Food Safety.

Special literature

19. BEYERLIN U., MARAUHN T., International Environmental Law, Oxford: Hart Publishing, 2011, p. 452, ISBN 978-1-84113-924-1.
20. DE SADELEER N., The Precautionary Principle in International Law, in:Kerbrat Y., Maljean-Dubois S (eds) The Transformation of International Environmental Law, Oxford: Hart Publishing, 2011, p. 338, ISBN 978-1-849-46259-4.
21. GOLDEMBERG J., LUCON O., Energy, Environment and Development, London: Earthscan, 2010, p. 448, ISBN 978-1-84407-748-9.
22. RAGULSKYTĖ-MARKOVIENĖ, R., Europos Sąjungos aplinkos teisė: raida ir perspektyvos [Environmental Law of the Euroean Union: Development and Perspectives], in: Teisė [Law], 2011, Vol. 78, p. 93-103.
23. SCHMITT, S., SCHULZE, K. Choosing environmental policy instruments: An assessment of the ‘environmental dimension’ of EU energy policy, In: Tosun, Jale, and Israel Solorio (eds)

Energy and Environment in Europe: Assessing a Complex Relationship? European Integration online Papers (EIoP), Special Mini-Issue 1, 2011, Vol. 15, Article 9, [referred on 4th March, 2012], link to the internet <http://eiop.or.at/eiop/texte/2011-009a.htm>

24. SOLORIO, I. Bridging the Gap between Environmental Policy Integration and the EU's Energy Policy: Mapping out the 'Green Europeanisation' of Energy Governance, Journal of Contemporary European Research., 2011, Vol. 7, Issue 3, p. 396-415. [referred on 4th March, 2012], Link to the internet <http://www.jcer.net/ojs/index.php/jcer/article/view/284/293>
25. URBANAVIČIUS J., Energetikos teisės vieta teisės sistemoje [Energy Law in A System of Law], in: Teisė [Law], 2011, Vol. 81, p. 158-169.
26. Risk factors estimates for 2004, World Health Organisation, [referred on 4th March, 2012], Link to the internet <http://www.who.int/healthinfo/global_burden_disease/risk_factors/en/index.html>
27. Energy and environment report 2008. Copenhagen: European Environmental Agency, 2008, Vol. 6, p. 99, ISBN 978-92-9167-980-5.
28. Impacts of shale gas and shale oil extraction on the environment and on human health, European Parliament, DG for Internal Policies, Policy Department A, June 2011, PE464.425, [referred on 4th March, 2012], Link to the internet <htttp://www.europarl.europa.eu/committees/en/studiesdownload.html?languageDocument=EN&file=44388>
29. Final Report on Unconventional Gas in Europe, European Commission, Brussels, 8 November, 2011, [referred on 4th March, 2012], Link to the internet <http://ec.europa.eu/energy/studies/doc/2012_unconventional_gas_in_europe.pdf>

Other literature

30. Biodiesels pollute more than crude oil, leaked data show, EurActiv.com, 30 January 2012, [referred on 4th March, 2012], link to the internet <http://www.euractiv.com/climate-environment/biodiesels-pollute-crude-oil-leaked-data-show-news-510437>
31. Biofuels: Commission adopts Report on indirect land use change, European Commission Press Release, 22 December 2010, [referred on 4th March, 2012], link to the internet <http://europa.eu/rapid/pressReleasesAction.do?reference=IP/10/1772&format=HTML&aged=0&language=EN&guiLanguage=en>

CYSENI 2012, May 24–25, Kaunas, Lithuania
ISSN 1822-7554, www.cyseni.com

ENERGY CRITICAL INFRASTRUCTURE ASSESSMENT METHODS

B. Jokšas
Lithuanian Energy Institute
Breslaujos str. 3, LT-44403 Kaunas
Phone +370 (37) 401941
Email: joksas@mail.lei.lt

I. Žutautaitė
Vytautas Magnus University
Vileikos str. 8, LT-44404, Kaunas
Phon: +370 (37) 327898
Email: i.zutautaite@if.vdu.lt

ABSTRACT

More and more often attention is focused on the problems related to protection of state critical infrastructure. The protection of critical infrastructure has become the topical subject of the economy and national security in all countries. Critical infrastructure is defined as any elements or sectors (for instance, electricity, gas/oil, transportation, communication and etc.) or part of thereof in a state. That is considered an important for maintenance of physical integrity, energy security and economic welfare. It is not possible to achieve the acceptability level of political, energy sustainability or economic development if infrastructure network of the country are at risk or vulnerable.

There are some adopted directives of European Commission (EC) 114/08/EC or United State (US) Department of Homeland Security and etc. All these document talk about critical infrastructure identification and designation for assessment of the need to improve their protection.

In this work one of the main issue of critical infrastructure assessment is there is no single measurable unit that can accurately reflect "interdependency" among critical infrastructure sectors. Today there are not so much governing documents of Lithuanian energy critical infrastructure for identification and assessment. Review of basic governing document of Lithuanian energy critical infrastructure and proposed assessment methods based on network system is presented in this work. All these governing documents are compared with EU directives. The main assessment issues for Lithuanian energy critical infrastructure are formulated.

Keywords: Critical infrastructure, energy sector, assessment methods, network system

1. INTRODUCTION

These days' critical infrastructure is an asset, system, part thereof or technical networks. All sectors' activities are included in this network, such as energy supply, transport services, water supply, gas and oil supply, information and communication technology systems. The functioning of these systems is crutial to maintain essential functions of society. Incapacity (disease) of certain infrastructure features can cause harm to population, the country's economy or national security. Critical infrastructure is described like complex network system, where sector's elements are connected in one of level. All these levels of the sectors are connected in one large system Fig. 1.

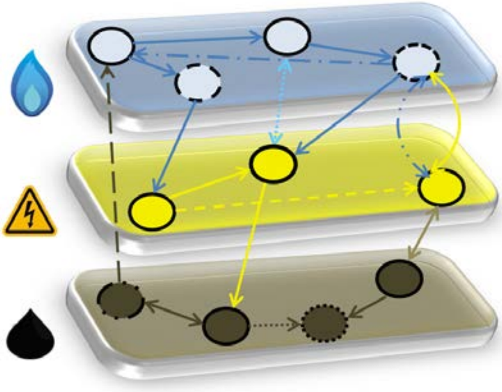

Fig. 1. Critical infrastructure scheme

Critical infrastructure sectors between the EU countries are related in various connections. So it is important to identify and understand global behavior and intrinsic weakness of these systems and their components.

Another relevant area of study is relationships that exist between sectors of infrastructure's and within infrastructure. Each sector has elements which depend on elements in another sector. For example, employ pumps of gas supply systems. These pumps are often driven by electrical motors, which are loads in the electrical system. Disruption caused by one sector of infrastructure could affect other sector's elements. So it is important to describe dependencies between infrastructure sectors. These dependencies are often implicit and poorly understood. Accordingly some disruption in sector could induce cascading failure effect in the infrastructure. One of the task of the research is to understand the cascading failure among infrastructure systems. It is the main point described in the European Union adopted Directive 114/08/EC. There are a certain number of critical infrastructures in the Community, the disruption or destruction of which would have significant cross-border impacts. This may include transboundary cross-sector effects resulting from interdependencies between interconnected infrastructures.

In this paper we survey the methods and tools through a literature review, which are used in critical infrastructure modeling. Also classification of the methods and tools for research modeling of critical infrastructure is presented in this paper. Review of basic governing document of Lithuanian energy critical infrastructure and proposed assessment methods based on network system is presented in this work.

1.1. Description of critical infrastructure

A common understanding of critical infrastructure includes all assets which are essential for any country that their destruction or degradation would have a debilitating effect on public health, national security or national. Disruption in some sector of critical infrastructure (for example, damage caused by human, natural disasters, terrorist attacks) is likely to have cascading effects on other sectors [1].

According to EU Directive 114/08/EC critical infrastructure is defined as means critical infrastructure located in Member States the disruption or destruction of which would have a significant impact on at least two Member States. This includes effects resulting from cross-sector dependencies on other types of infrastructure. Also the primary and ultimate responsibility for protecting ECIs (European critical infrastructures) falls on the Member States and the owners/operators of such infrastructure.

Disruptive events in one part of the infrastructure may spread out through the system. This property is called ‘‘interdependence’’ [2].

Interdependence of critical infrastructure sectors in literature are generally displayed like scheme showed in Fig. 2 [3].

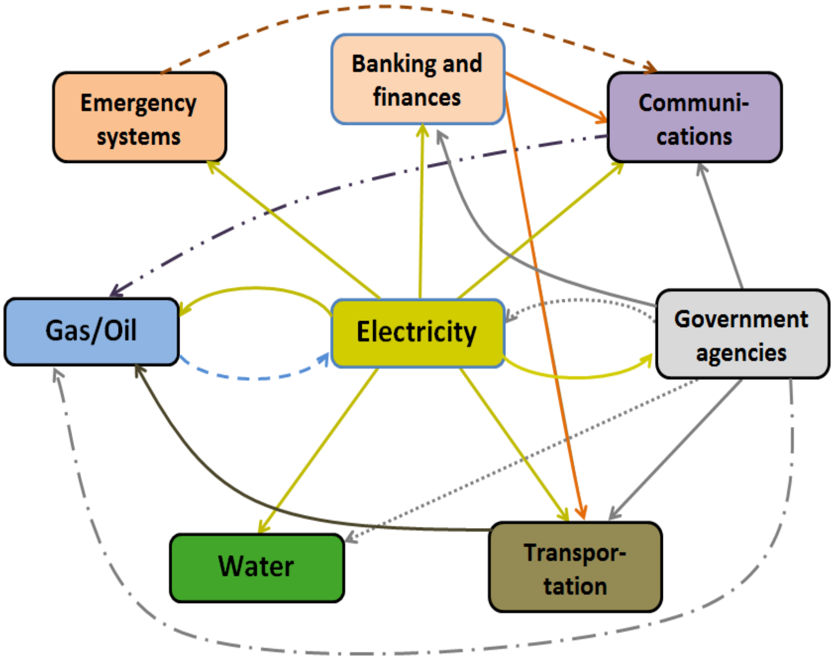

Fig. 2. Example of interdependences within critical infrastructure

Therefore it is very important to focus attention on studying interdependencies of critical infrastructure's sectors to international attacks, accident or natural disasters. One of the most difficult issues of assessment is define consequences induced by disruption of natural events. One of example is nuclear accident at the Fukushima nuclear power plant in Japan. This event caused by an earthquake, pose a danger to human life of country, neighbouring countries and world ecology. This event forced governments to focus attention on critical infrastructure protection and to encourage scientific research in identifying the sectors dependence and modeling critical infrastructure. Whereas there are numbers of different types of threats, so often descriptive methods of critical infrastructure modeling in the literature are turned on the protection of specific threats.

One of the world leading programs is by the Member states of European Union adopted Directive 114/08. This Directive defines critical areas in which efforts must focus on prevention and protection of infrastructure. Table 1 summarizes the list of critical infrastructure defined by EU Directive [4].

Table 1. List of critical infrastructure sectors, in the European Union Directive

SECTORS EU DIRECTIVE 114/08	
Energy	Electricity Oil Natural gas
Transport	Roads and highways Railroads Aviation Inland waterways Shipping and ports

The other world leading program is by United States adopted National Infrastructure Protection Plan (NIPP,2009).

NIPP identifies three specific areas of concern related to interdependencies: cross-sector interdependencies, the cyber dimension, and the international aspect of critical infrastructure. These issues provide more detail about the sub-levels of interdependencies within the national and international network of critical infrastructure [2].

The first issue is cross-sector interdependencies. The NIPP states that the critical infrastructure sectors form a network of critical functions and directs sector-specific agencies to consider relevant interdependencies when developing sector-specific plans.

The second issue of concern in the NIPP is described as cyber dimension of interdependencies. The NIPP identifies the global cyber infrastructure as base of the U.S. economy and a critical element of national security.

The third issue of concern is international critical infrastructure protection. The NIPP suggests that the international nature of threats and the global network of critical infrastructure assets (e.g., energy, transportation, and telecommunications) need special consideration within the risk management and vulnerability analysis framework.

List of critical infrastructure sectors in NIPP is in the following Table2.

Table 2. List of critical infrastructure sectors, in NIPP

SECTORS US NIPP
Agriculture and food
Bank and finances
Communications
Military installations and defence
Energy
Technologies of information
National monuments and icons
Transportation systems
Drinking water treatment plants

The NIPP proposed six steps of risk management framework that contain:

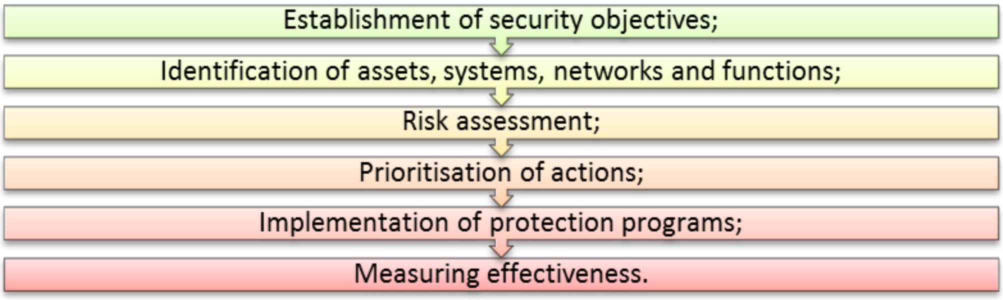

Additionally, NIPP provides a framework for feedback and continuous improvement in a flexible approach.

2. METHODS OF CRITICAL INFRASTRUCTURE PROTECTION AND INTERDEPENDENCIES

Critical infrastructure modeling is consisted of several point of task such as simulation techniques and mathematical models. In modeling of the critical infrastructure is an important to choose the modeling methods which let to take decision-making procedures and provides the visualizations of the critical infrastructure. In this section we looked at most frequently used mathematical methods, which are described in papers related to modeling techniques. Generally these methods are combined with supplementary computation techniques:

- Continuous time-step simulation (CS) [5, 6],
- Discrete time-step simulation (DS) [7, 8],
- Monte Carlo simulation (MC) [9, 10],
- Decision trees (DT) [11, 12],
- Geographic information systems (GIS) [13, 14],
- Risk management techniques (RISK) [15, 16],
- Event monitoring or real time record (RTR) [17].

Classification of the most used methods for performing vulnerability assessments and risk management of critical infrastructure (from 1999 to 2010) [18] is given in Table 3.

2.1. Descriptions of the methods

Rating matrix is a matrix that is used during risk assessment to define the various levels of risk as the product of the harm probability categories and harm severity categories. This is a simple mechanism to increase visibility of risks and assist management decision making. This method is widely popular because it allows combination with every computational technique, so it allow facilitate sensitivity analysis. Rating matrix is a chart that allows systematically identifying, analyzing, and rating the strength of relationships between sets of information. Rating matrix is especially useful for looking at large numbers of decision factors and assessing each factor's relative importance. The procedure has four steps:

1. Firstly, the rating criteria must be determined. According to these criteria the overall performance of equipment as well as the functional performance of its subsystems will be rated. It is then useful to group these rating criteria according to their nature (e.g. economical-technical or mechanical-electrical).

2. Secondly, weights have to be assigned for each criterion, which represent how important the criterion for the overall rating is. In order to assign weights, following method is being used:

Every rating criterion is compared to each other criterion and a "comparison factor" is determined, which shows the relative importance of the examined criterion to each other criterion of the group.

3. In this way, the decision maker has to compare only two criteria at a time. The next step is the design of a scoring system. The scoring range will be here determined (e.g. 0 to 1), and a score will be assigned to every possible condition state of the equipment with regard to each rating criterion.

4. Finally, the score for each rating criterion is multiplied by its weighting factor and the overall condition/degradation state of the equipment under examination is rated.

A relational database is used to maintain data gathered by the master scanner and remote sensors, and to store system status information. It used to establish relationships between the components modeling in critical infrastructure. Relational databases represent the properties of the system in a precise manner. This method let merged with monitoring of events, real time recording, geographical referencing (GIS), error logs, access control, risks components, etc.

Multi-agent systems allow the simulation of complex phenomena that cannot easily be described analytically. Multi-agent approaches are often based on coordinating agents whose actions and interactions are related to the emergence of the phenomenon to be simulated. A multi-agent system is defined as a system constituted of several collaborating agents, with each one responsible for a specific task, such as network communication, data filtering or data analysis.

Multi-agent method is used to define interdependencies between agents taking into account their input, output, mechanism and control parameters.

In some ways, multi –agent system complements traditional analytic methods:

Analytic methods enable to characterize balance of the system, while the multi-agent models are able to generate this balance.

- Multi-agent models can explain the emergence of higher order patterns – network structures of human activities and the Internet, power law distributions in the sizes of traffic jams, wars, stock market crashes, and social segregation that persists despite populations of tolerant people.
- Rather than focusing on stable states, the models consider a system's robustness – the ways that complex systems adapt to internal and external pressures so as to maintain their functionalities.
- Agent-based models consist of dynamically interacting, rule-based agents. An agent-based model can exhibit complex behavior patterns and provide valuable information about the dynamics of the real-system simulated.

However, multi-agent systems allow us to communicate imprecise, approximate knowledge. Knowledge stored in these models can be used as an important heuristic for finding a suboptimal solution in even very complex environments.

Table 3. Classification of the most used methods for conducting vulnerability assessments and risk management of critical infrastructure

APPLICATION/METHODOLOGY	MODELLING TECHNIQUES					STAGE				
	Multi-agent System	System Dynamics	Rating Matrices	Relational DB	Network Theory	Identifica-tion	Risk assessment	Prioritization of actions	Programme Implement-ation	Measuring Effectiveness
Agent-based infrastructure modeling and simulation	•					•	•			
Athena					•		•			
CASCADE			•			•	•			
(CARVER2) Criticality, accessibility, recoverability, vulnerability, espy ability (notoriety), Redundancy			•			•		•		
Centre for energy, environmental, and economic systems analysis			•	•		•	•		•	•
Computer(emergency) security incident response team				•		•		•	•	
Critical infrastructures interdependencies Integrator					•			•		•
Critical infrastructure modeling system	•						•	•	•	•
Critical infrastructure protection decision support system		•				•		•	•	•
Critical infrastructure protection modeling and analysis		•							•	•
Critical infrastructure simulation by interdependent agents	•			•				•	•	
Agent-based simulation model of the U.S. economy	•					•	•			•
Distributed engineering workstation				•	•	•	•	•		
DUTCH APPROACH			•			•	•	•		
EAR-PILAR			•	•		•	•	•	•	
Geographic information systems and risk assessment						•	•			
Electricity market complex adaptive system	•					•	•	•		
Fast analysis infrastructure tool			•	•		•	•			
Financial system infrastructure	•					•	•			
Failure modes and effects analysis			•			•	•	•		
Fort Future	•					•	•	•		•
Fault tree analysis			•			•	•	•		
Enterprise risk administration			•	•		•	•	•	•	
GIS Interoperability								•		•
GoRAF	•			•			•	•	•	
CERT Government Initiatives				•		•		•	•	

HAZard and Operability analysis			•		•	•	•	•		
Interdependent energy infrastructure simulation system	•					•		•	•	
Inoperability input–output model			•		•	•		•	•	
Infrastructure Disruption		•							•	•
Infrastructure risk analysis model			•				•	•	•	
Intepoint vu	•							•	•	
Knowledge management and visualization			•							•
LUND				•	•	•	•			
MARGERIT			•			•	•		•	
Methodology for interdependencies			•	•		•	•			
Multi-layer infrastructure networks	•					•				
Modular dynamic model		•					•		•	•
Multi-network interdependent critical infrastructure program for analysis of lifelines				•		•		•		
National agent-based laboratory for economics	•					•		•	•	•
Net-centric effects based operations model	•			•				•	•	•
Network security risk assessment model				•				•	•	•
NGFAST			•			•	•			•
Critical infrastructure protection initiative			•			•		•		•
Pci information			•						•	
Risk maps						•				
Security of activities of vital Importance										
Threat ensemble vulnerability assessment			•						•	
Transportation routing analysis geographic information system				•		•	•	•		
TRansportation ANalysis SIMulation System	•									•
Urban infrastructure suite	•					•	•	•	•	
UML.CI				•		•				
US ARMY RISK MITIGATION		•					•		•	•
Water infrastructure simulation environment	•					•			•	•
Virtual Interacting Network Community			•				•		•	

The features of the system are precisely described by network theory. It let identification of vulnerable spot in the critical infrastructure. The practical applicability of this method is reduced to specific cases of smaller systems. Markov models can be used to represent internal component failure and repair processes, as well as the influences between components that cause failure propagation. The models can also consider an abstract graph, neglecting power flows. Then critical infrastructure networks can be considered as "small-worlds".

System Dynamics method let studying and understanding the behavior and the underlying structure of a complex system over time. It represents a fundamentally interdisciplinary top-down approach, which is grounded in the theory of nonlinear dynamics and feedback control. All dynamics in a system are assumed to arise from the interaction of two types of feedback loops, positive and negative ones, which are represented in "loop diagrams". Changes in stocks and flows are described with differential equations.

The other main issue of modeling energy critical infrastructure is evaluation of interdependencies between the sectors. How to describe mutual influence of interacting sectors? We reviewed research new papers of modeling critical infrastructure interdependencies from 2011 to 2012. [19–39] The mostly used methods for modeling interdependencies of critical infrastructure are showed in Fig. 3.

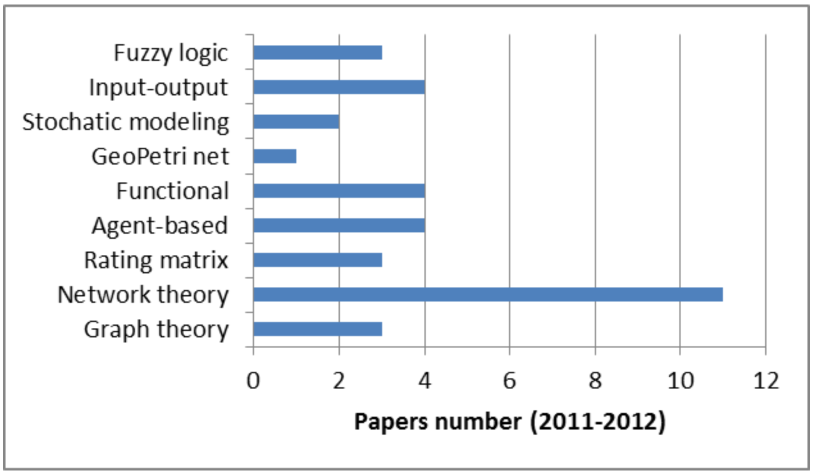

Fig. 3. Methods of critical infrastructure interdependencies modeling

Overview of papers showed, that infrastructure influence of interacting generally were modeled by network theory [22, 26-32,36-38] together with Agent-based [25, 36, 37] and Functional methods [21, 31]. Network theory allows to refer the properties of the system in precise manner. So it is used for modeling infrastructure interdependence.

2.2. Network system modeling method

The functioning of technical system could be described as dynamic network. Objects of energy system such as power generation, power transmission and distribution networks and networks components (transformers, pressure station and etc.), could be nodes of considered network. Physical objects are represented as nodes. Physical and functional communication between objects is defined by links.

An hazard is negative effect, natural physical ageing of the system, influence of external factors to the system vitality and so on affects network system dependability and quality of service.

A number of network nodes. The number of network nodes is marked as *N*.

Additive hazard. It is a sort of hazard, when hazards in the nodes of the network can be added to or a part of hazard moved to the other nodes. The examples of the additive hazard are: collection of hazardous materials, amount of fake money in the supermarkets, transport intensity at the crossroads, etc, marked as H.

Flow intensity. q_{ij}: $q_{ij} \geq 0$ – coefficient of flow intensity in the network lines; it marks the part of hazard in the node i that will be transmitted to the node j.

Hazard transfer cycle. Hazard transfer in the network from one node to the other is regarded as one hazard transfer cycle.

Network node resistance. $R_{(j)}(\cdot)$ is coefficient of the resistance of node. It marks which part of the hazard is stopped, before the getting into the node j ($0 \leq R_{(j)} \leq 1$, i.e., percentage). For instance, $R_{(2)}(\cdot) = 0.7$ means that 70% of hazard is stopped before the getting into the 2nd node. The resistance of node can be created by the security systems, antivirus computer software, etc. “Observed” value of node j resistance $R_{(j)k}$ could be obtained

$$R_{j(k)} = \frac{\breve{q}_{j(k)} - P_{j(k)}}{\breve{q}_{j(k)}}, \quad \breve{q}_j = \sum_{\substack{i=1 \\ i \neq j}}^{N} q_{ij}, \quad \hat{q}_j = \sum_{\substack{k=1 \\ k \neq j}}^{N} q_{jk}. \tag{2.1}$$

$k = 1, 2, \ldots$, here k – number of cycles, $\breve{q}_{j(k)}$ – the flow of hazard to the node j in the k^{th} cycle, $\hat{q}_j$ – the flow of hazard from the node j, $P_{j(k)}$ – amount of hazard that gets into the node j during the k^{th} cycle.

The mathematical model of hazard distribution within the network system with deterministic resistance of nodes was proposed in Augutis & Ušpuras monograph [41]. After the $k+1^{th}$ cycle the hazard in nodes is

$$\vec{H}(k+1) = \vec{H}(k) \cdot \tilde{Q} + \vec{H}(0), \tag{2.2}$$

$\tilde{Q}$ – network flow matrix, with respect of resistances $R_{(j)}$, $j = 1,\ldots, N$, of nodes, is defined as

$$\tilde{Q} = \begin{pmatrix} q_{11} & q_{12}(1-R_{(2)}) & \cdots & q_{1N}(1-R_{(N)}) \\ q_{21}(1-R_{(1)}) & q_{22} & \cdots & q_{2N}(1-R_{(N)}) \\ \vdots & \vdots & & \vdots \\ q_{N1}(1-R_{(1)}) & q_{N2}(1-R_{(2)}) & \cdots & q_{NN} \end{pmatrix}, \tag{2.3}$$

q_{ij}:$\{0 \leq q_{ij} \leq 1, q_{i1} + \ldots + q_{iN} = 1\}$ marks the part of the hazard in the node i that will be transmitted to the node j.

Performing reliability analysis of a real system, the true values of resistances of the system nodes are unknown. In this case the resistance of node is assumed as a random variable. The model of hazard distribution, presented in Augutis & Ušpuras research work [41], is extended by two cases:

- when resistance is assumed as a random variable. In this case it is important to obtain the of node resistance that is necessary for the forecast of the level of hazard in the node (in all the network system as well). For instance, to forecast how long (how many cycles) system can operate normally under the influence of hazard – to make decision in what moment supporting system should be switched on (i.e., alert generation),
- when resistance is assumed as a random process (with known trend of it). For instance, the system with self-learning feature has an increasing resistance. In the period of ageing system has a decreasing resistance.

Research on resistance approximation with probabilistic distribution is presented in research work [40]: beta distribution is suggested as suitable probabilistic distribution to model nodes’ resistance and given some approximations of probabilistic distribution of hazard.

3. LITHUANIAN ENERGY CRITICAL INFRASTRUCTURE

Assessment of situation of critical infrastructure is slightly complicated in Lithuania. Whereas Lithuania is part of the European Union, then by European Union adopted Directive 114/08/EC is binding on for Lithuania. Assessment of critical infrastructure is performed partly in Lithuania. Methods of assessment have been not developed. Risk assessment was performed for separate objects of Lithuania energy sector. For example: risk-based water level control in Kaunas hydropower system [42], risk Analysis of Petrol Transportation [43], the analysis of Kaunas (Lithuania) district heating system [46]. Incomplete list of initiating events was analyzed in these works.

The requirements of EU adopted Directive 114/08/EC are incorporated into Lithuanian laws [47, 48]. Lithuania critical infrastructure is described by the main government document strategic importance to national security companies and facilities law 1998, Nr. 115-3230; 2009, Nr.93-3968. Critical infrastructure is defined as the subject of national significance. The list of critical infrastructure (subject of national significance) of Lithuania energy sector is described by government documents. This critical infrastructure list is energy object of state significant. This list is described by government document (strategic importance to national security companies and facilities law 2002, Nr. 103-4604; 2009, Nr.93-3968):

- “Lietuvos energija” AB – The Company operates three power plants in Lithuania: the Lithuanian Power Plant (the LPP), the Kruonis Pumped Storage Hydroelectric Plant (the KPSHP) and the Kaunas Hydroelectric Power Plant (the KHPP).
- “LITGRID” AB – “LITGRID” is the Lithuanian electricity transmission system operator managing electricity flows in Lithuania and maintaining stable operation of the national electricity system. (330-110 kV).
- “LESTO” AB– “LESTO” distributes and transmits electrical power throughout the entire territory of Lithuania and is a distribution network operator. (35-10-0,4 kV).
- “Lietuvos dujos” AB – “Lietuvos Dujos” AB covers natural gas import and sales to its clients, transmission and distribution services, sustainable development of Lithuania’s natural gas supply infrastructure.
- “ORLEN Lietuva” AB – Public Company “ORLEN Lietuva” is a petroleum refining company operating the only petroleum refinery in the Baltic States as well as crude oil and petroleum product network and marine terminal.
- SE Ignalina Nuclear Power Plant.
- Stock Company Klaipedos Nafta.

The list of objects is quite short in comparison to other countries. It could be possible to use experiences of assessments works, which were done before. For example: Risk Analysis of Petrol Transportation [43], Methodology of the energy supply disturbances affecting energy system [45]. Network theory was one of the main method used in these works. Therefore, creation of the assessment model for energy critical infrastructure of Lithuania using network theory might be suggested. It will let to assess functionality and interaction of energy critical infrastructure.

4. CONCLUSION AND DISCUSSION

Currently, one main universal method of assessment does not developed for Energy critical infrastructure.

Commonly used method of critical infrastructure modeling and assessment is:

- Network theory;
- Rating Matrices;
- Multi-agent System.

Network system modeling method is used for assessment of comparatively small critical infrastructure. For the modeling and assessment of energy critical infrastructure in Lithuania it is necessary:

- to make list of threats and disturbances;
- to make analysis of consequences caused by disturbances;
- to assess dependency between sectors.

Network theory could be suggested creating assessment model for energy critical infrastructure of Lithuania.

REFERENCES

1. A. LÖSCHEL, U. MOSLENER, D. RÜBBELKE, Energysecurity-conceptsand indicators. *EnergyPolicy*, Vol. 38, 2010 – p. 1607–1608.
2. National Infrastructure Protection Plan. US Department of Homeland Security. U.S. Department of Home Security. Washington DC (USA). 2009. referred on the 1th of march in 2012y. Link to the internet <http://www.dhs.gov/files/programs/editorial_0827.shtm.>.
3. L. NESS, *Securing Utility and Energy Infrastrucures*, Wiley Interscience, Cheschester (England), 2006. 340 p. ISBN-13: 978-0471705253
4. Directive 114., On the identification and designation of European critical infrastructures and the assessment of the need to improve their protection. *Official Journal of the European Communities*. Brussels (Belgium), 2008. 75 p.
5. L.R. QUARLES, Y.Y. HAIMES, *IIM: Inoperability Input–Output Model*. [referred on the 3th of march in 2012y.]. Link to the internet: <http://www.thei3p.org/docs/publications/IIM-factsheet-Feb2007.pdf>.
6. F.G Australian, M. CSIRO, CIPMA: Critical Infrastructure Protection Modeling and Analysis. *Informatics and Statistics*, 2009.
7. B. DRABBLE, T. BLACK, C. KINZIG, G. WHITTED. Ontology based dependency analysis: Understanding the impacts of decisions in a collaborative environment. *Collaborative Technologies and Systems*, 2009.
8. H. A. RAHMAN, J. R. MART, K.D. SRIVASTAVA, A hybrid systems model to simulate cyber interdependencies between critical infrastructures, International Journal of Critical Infrastructures, January 25, 2012 – p. 265–288.
9. W. JUNQIANG, L. GENGYIN, Z. MING, K.L. LO. Monte Carlo simulation based assessment of available transfer capability in AC-DC hybrid systems. *Critical Infrastructure (CRIS), 2010 5th International Conference. On Critical Infrastructure*. 2010.
10. P. KARMEN, B. FLAVIO, G. EUGENIO. Seismic risk assessment of interdependent critical infrastructure systems: The case of European gas and electricity networks. Earthquake engineering and structural dynamics. 2012.
11. S. KHALED, Z. TAREK. Integrated Decision-Support Framework for Municipal Infrastructure Asset. *Pipelines 2010: Climbing New Peaks to Infrastructure Reliability—Renew, Rehab, and Reinvest Proceedings of the Pipelines 2010 Conference*. 2010.
12. S.M RINALDI, J.P. PEERENBOOM, T.K. KELLY. Identifying, understanding, and analyzing critical infrastructure interdependencies. *Control Systems, IEEE*. 2002.
13. Critical Infrastructure Activities and Events. Homeland Security NIPP news. 2011. referred on the 1th of march in 2012y. Link to the internet <http://www.fbiic.gov/public/2011/feb/NIPP_News_Dec2010-Jan_2011.pdf>

14. L. CHING-TING; F. CHIN-FENG; A. YIH, A GIS-based simulator for CIIP interdependency analysis. *Computer Symposium (ICS)*, 2010 International. 2011
15. National guidelines for protecting critical infrastructure from terrorism protecting critical infrastructure from terrorism. *National counter-terrorism committee*. 2011. ISBN: 978-1-921725-57-9 referred on the 1th of March in 2012y. Link to the internet < http://www.nationalsecurity.gov.au/agd/WWW/rwpattach.nsf/VAP/(689F2CCBD6DC263C912FB74B15BE8285)~Protecting+Critical+Infrastructure+from+Terrorism+PDF.pdf/$file/Protecting+Critical+Infrastructure+from+Terrorism+PDF.pdf >
16. C. SCARLAT, C. SIMION, E.I. SCARLAT. Managing new technology projects: Some considerations on risk assessment in the case of NPP critical infrastructures. *Emergency Management and Management Sciences (ICEMMS), 2011 2nd IEEE International Conference on*. 2011 ISBN: 978-1-4244-9665-5.
17. V. THANESWARAN, H. AARON, K. SHANIKA Global detection of flooding-based ddos attacks using a cooperative overlay network. *Nss '10 proceedings of the 2010 fourth international conference on network and system security*. 2010. ISBN: 978-0-7695-4159-4.
18. M. JOSE YUSTA, J. GABRIEL CORREA, R. LACAL-ARÁNTEGUI, Methodologies and applications for critical infrastructure protection: State-of-the-art, *Energy Policy*, Vol. 39, 10, October 2011 – p. 6100–6119.
19. I.B. UTNE, P. HOKSTAD, J. VATN. A method for risk modeling of interdependencies in critical infrastructures. *Reliability Engineering & System Safety*, June 2011, Vol. 96, Issue 6 – p. 671–678.
20. G. Oliva, S. Panzieri, R. Setola. Agent-based input–output interdependency model. *International Journal of Critical Infrastructure Protection*, July 2010, Vol. 3, Issue 2 – p. 76–82.
21. J. JOHANSSON, H. HASSEL. An approach for modelling interdependent infrastructures in the context of vulnerability analysis. *Reliability Engineering & System Safety*, December 2010, Vol. 95, Issue 12 – p. 1335–1344.
22. D. KLEPPINGER, R. BROADWATER, C. SCIRBONA. Generic reconfiguration for restoration. *Electric Power Systems Research*, March 2010, Vol. 80, Issue 3 – p. 287–295.
23. K. G. CROWTHER. Risk-informed assessment of regional preparedness: A case study of emergency potable water for hurricane response in Southeast Virginia. *International Journal of Critical Infrastructure Protection*, July 2010, Vol. 3, Issue 2 – p. 83–98.
24. Y. GE, X. XING, Q. CHENG. Simulation and analysis of infrastructure interdependencies using a Petri net simulator in a geographical information system. *International Journal of Applied Earth Observation and Geoinformation*, December 2010, Vol. 12, Issue 6 – p. 419–430.
25. F. HARE, J. GOLDSTEIN. The interdependent security problem in the defense industrial base: An agent-based model on a social network. *International Journal of Critical Infrastructure Protection*, December 2010, Vol. 3, Issues 3–4 – p. 128–139.
26. T. AKAMATSU, T. NAGAE. A network of options: Evaluating complex interdependent decisions under uncertainty. *Journal of Economic Dynamics and Control*, May 2011, Volume 35, Issue 5 – p. 714–729.
27. M. OUYANG, L. DUEÑAS-OSORIO. An approach to design interface topologies across interdependent urban infrastructure systems. *Reliability Engineering & System Safety*, November 2011, Vol. 96, Issue 11 – p. 1462–1473.
28. X. LIU, W. LI, Y.L. TU, W.J. ZHANG. An expert system for an emergency response management in Networked Safe Service Systems. *Expert Systems with Applications*, September 2011, Volume 38, Issue 9, p. 11928–11938.

29. C.-L. CHAI, X. LIU, W.J. ZHANG, Z. BABER. Application of social network theory to prioritizing Oil & Gas industries protection in a networked critical infrastructure system. *Journal of Loss Prevention in the Process Industries*, September 2011, Vol. 24, Issue 5 – p. 688–694.
30. S. CHIARADONNA, F. DI GIANDOMENICO, P. LOLLINI. Definition, implementation and application of a model-based framework for analyzing interdependencies in electric power systems. *International Journal of Critical Infrastructure Protection*, April 2011, Vol. 4, Issue 1 – p. 24–40.
31. P. TRUCCO, E. CAGNO, M. DE AMBROGGI. Dynamic functional modelling of vulnerability and interoperability of Critical Infrastructures. *Reliability Engineering & System Safety*, Available online 9 December 2011.
32. G. OLIVA, S. PANZIERI, R. SETOLA. Fuzzy dynamic input–output inoperability model. *International Journal of Critical Infrastructure Protection*, December 2011, Vol. 4, Issues 3–4 – p. 165–175.
33. R. PANT, K. BARKER, F. H. GRANT, T. L. LANDERS. Interdependent impacts of inoperability at multi-modal transportation container terminals. *Transportation Research Part E: Logistics and Transportation Review*, September 2011, Vol. 47, Issue 5 – p. 722–737.
34. E. CAGNO, M. D. AMBROGGI, O. GRANDE, P. TRUCCO. Risk analysis of underground infrastructures in urban areas. *Reliability Engineering & System Safety*, January 2011, Vol. 96, Issue 1 – p. 139–148.
35. I. EUSGELD, C. NAN, S. DIETZ. “System-of-systems” approach for interdependent critical infrastructures. *Reliability Engineering & System Safety*, June 2011, Vol. 96, Issue 6 – p. 679–686.
36. S. WANG, L. HONG, X. CHEN. Vulnerability analysis of interdependent infrastructure systems: A methodological framework. *Physica A: Statistical Mechanics and its Applications*, December 2011.
37. E. ZIO, L.R. GOLEA. Analyzing the topological, electrical and reliability characteristics of a power transmission system for identifying its critical elements. *Reliability Engineering & System Safety*, Available online 31 January 2012.
38. M. BECCUTI, S. CHIARADONNA, F. D. GIANDOMENICO, S. DONATELLI, G. DONDOSSOLA, G. FRANCESCHINIS. Quantification of dependencies between electrical and information infrastructures. *International Journal of Critical Infrastructure Protection*, Available online 28 January 2012.
39. M. YAZDANI, A. ALIDOOSTI, M. H. BASIRI. Risk Analysis for Critical Infrastructures Using Fuzzy TOPSIS. *Journal of Management Research*, 2012, Vol. 4, No. 1: E6.
40. I. ŽUTAUTAITĖ, Parameters estimation of non-stationary processes models using Bayesian approach. Vytautas Magnus University, Kaunas 2010. (in Lithuanian; doctoral thesis). ISBN 9789955125679
41. J. AUGUTIS, E. UŠPURAS. Monograph: Technology risk. Lithuanian Energy Institute, Vytautas Magnus University, Kaunas. 2006. (in Lithuanian). ISBN 9986492890
42. J. SIMAITYTĖ, J. AUGUTIS, B. GAILIUŠIS. Risk-based water level control in Kaunas hydropower system. *Environmental research, engineering and management*. 2006. ISSN 1392-1649. No. 3, p. 5-12.
43. V. VOLKOVAS, R. KRIKŠTOLAITIS, V. MATUZAS, V. DOROŠEVAS, E. AUGUTIENĖ. Risk Analysis of Petrol Transportation. *Environmental research, engineering and management*. 2005. ISSN 1392−1649. No. 1(31) – p. 45−54.
44. A. KALIATKA, M. VALINČIUS, J. AUGUTIS, R. KRIKŠTOLAITIS, S. RIMKEVIČIUS1, G. DUNDULIS, R. BAKAS. Patikimumo įvertinimo metodikos taikymas Kauno miesto

centralizuotam šilumos tiekimo tinklui. *Lietuvos Šiluminės technikos inžinierių asociacija.* 2009. – p. 4 (in Lithuanian).

45. J. AUGUTIS, R. KRIKSTOLAITIS, L. MARTISAUSKAS Methodology of the energy supply disturbances affecting energy system. WASET org. cop. 2011. p. 7.
46. S. RIMKEVICIUS, A. KALIATKA, M. VALINCIUS, G. DUNDULIS, R. JANULIONIS, A. GRYBENAS, I. ZUTAUTAITE. Development of approach for reliability assessment of pipeline network systems. *Applied Energy*. June 2012. Vol. 94 – p. 22–33.
47. Lietuvos Respublikos strateginę reikšmę nacionaliniam saugumui turinčių įmonių ir įrenginių bei kitų nacionaliniam saugumui užtikrinti svarbių įmonių įstatymas, Nr.: 103-4604 (in Lithuanian).
48. Lietuvos Respublikos civilinės saugos įstatymas (Žin., 1998, Nr. 115-3230; 2009, Nr. 159-7207) (in Lithuanian).

CYSENI 2012, May 24–25, Kaunas, Lithuania
ISSN 1822-7554, www.cyseni.com

ISSUES RELATED TO AN EXTENSIVE USE OF RENEWABLE ENERGY SOURCES IN LITHUANIA

J.L. Konstantinaviciene
Kaunas University of Technology
Laisves av. 55, LT-44309 Kaunas – Lithuania
Phone 865062037
Email: julija.konstant@gmail.com

ABSTRACT

Increasing environment pollution and change in our atmosphere temperature lead to global climate crisis, and in turn energy deficiency as well as decreasing non-renewable energy sources reserves. This leads to the necessity for extensive use of renewable energy sources. Lithuanian energy strategy should be based on use of sources of alternative energy. The strategy of use of alternative energy would be an efficient way to solve major environmental problems and to secure the independence of energy, all the more so, there is a sufficient variety of substituted energy sources in Lithuania. Theoretical and empirical investigations performed by international teams of specialists and scientists have proved that extensive use of renewable energy sources is becoming increasingly important as an economical research object. However, alternate energy sources are not sufficiently used in Lithuania. The article examines and reveals the basic renewable energy sources use problems and their reasons, and points out the future alternative sources expansion trends. There is a review of possibilities of assimilation of modern energy sources in the article. On the basis of the scientific research and assessment of the current status of renewable energy resources in Lithuania, the author of article analyzes possibilities of developing of renewable energy resources in Lithuania.

Keywords: renewable energy sources, alternative energy, energy sector

1. INTRODUCTION

Extensive usage of renewable energy sources (RES) is like an indicator that shows whether a country is able to utilize a workforce suitably, can perform strategic thinking as well as to think ahead and demonstrate the ability of appropriate usage of financial tools. The relevance and significance of the RES uptake in Lithuania clearly shows when considering, how many problems can be resolved by giving priority to ones own resources and their usage, especially given the fact that Lithuania has enough of RES to meet its own needs. Development of renewable energy sources is, in fact, a part of implementation of climate change policies, which are improving energy efficiency and ensuring security of energy supply. [8]. The implementation of extensive use of renewable energy sources may increase security of energy supply for public and private companies, districts or even regions [8]. Projects carried out for RES implementation provide improved comfort and have an impact on both social and economic sphere [8].

Furthermore, Lithuania is highly dependent on energy imports. Our country is oil importer [25] and also is entirely dependent on import of natural gas to meet it’s domestic needs. The oil and natural gas import mostly from Russia. So, the extensive use of RES would enable to seek for energy independence.The requirements [14] of European Union (EU) also encourage the extensive use of renewable energy sources in Lithuania.

Theoretical and empirical investigations performed by international teams of specialists and scientists [4; 6; 8; 9; 14; 25; 26; 27; 28] confirm the fact that extensive use of renewable energy sources is becoming increasingly important as an research object of economics. Identification of this problematic situation gives the opportunity to formulate the scientific problem with the question: what are the main problems of under-use of RES in Lithuania and how deal with these problems?

The object of work – RES and issues related to use of RES in Lithuania.

The aim of work – to analyze the main issues related to use of RES in Lithuania. To achieve the aim, it has been formulated the following **objectives**:

1. To evaluate the use of RES in Lithuania.
2. To identify the main problems of under-use of RES and their causes.
3. To define the possibilities of RES developing in Lithuania.

Research methods: systematic, logical and comparative analysis of scientific literature.

2. THE USE OF RES IN LITHUANIA

Global demand for energy is increasing rapidly. Natural resources are not limitless. The ongoing war shows how delicate economic relations are. Those countries that possess resources make their own term. Therefore it is necessary to find other ways to obtain energy [18; 27; 28]. One way is the use of renewable energy sources: biofuel, geothermal, hydropower, wind and solar energy [18]. While assessing the use of RES in Lithuania, all types of use of RES have to be analyzed.

Lithuania has a relatively high potential to produce biofuel. In order to produce biofuel one can use straw, wood waste and municipal waste [18]. Over the past three years the number of bio-fuel boilers used in Lithuania grew twice: in 2005 there were about 200 bio-fuel boilers (total installed capacity of 420 MW), and in 2010 there were already over 400 bio-fuel boilers in use in Lithuania (total installed capacity of 710 MW) [13; 19]. However, most technology is based on wood and wood waste burning, whereas straw burning is a completely different process and requires special boilers, that are not too many in Lithuania today (20 – 30), because straw-burning technologies in Lithuania are still on an initial stage of development [13]. Lithuania uses only 10 percent of wood cutting waste [10]. The actual reserve of raw material for the production of wood waste is from logging, but it is used only partially because of the collection and processing associated with the additional manpower, machinery and transportation costs, which causes the need for support in order to promote the use of RES and its development [9]. The second major resource in Lithuania is straw; this material when recycled can produce three times cheaper heat [13]. Farms annually produce about 4 million tons of straw, of which about 500 thousand could be able to heat houses, nevertheless there is only 3 percent of straw used for heating purposes so far [10; 13; 26]. Whilst, using only straw, Lithuania will be able to fill the gaps in its thermal energy resource problems for 100 percent [18]. It should be noted, that while burning straw and wood waste, CO2 emission equals zero [18]. Currently, in the country's district heating (DH) supply sector, the heat produced from RES totals only 19 percent [26]. DH production’s transfer from gas to biofuel is a realistic way to reduce costs of heating to the population [10]. Heavy investment flow is devoted to modernization of heating economy every year, namely from 2006 to 2010 there was 1.65 milliard LTL invested [19]. The comparison of gas and biofuel prices shows that biofuel is cheaper and more stable in the economic perspective (table 1).

Table 1.The comparison of heating prices, while using biofuel and gas [19]

Heating price	**2011.06**	**2011.07**	**2011.08**	**2011.09**
Heating price while using biofuel, ct/kWh (Kelmė)	23.7	23.6	23.3	23.2
Heating price while using gas, ct/kWh (Anyksčiai)	29.6	31.5	31.9	32.7

RES share in the total fuel balance of heat production in year 1997 – 2010 gradually has been increasing: in 2008 this share accounted for 17.7 percent, in 2009 and 2010 – 19.3 percent each [10]. Nevertheless the full potential (Table 2) is not exploited, and the objective in the year 2020 is to reach 85 percent [19].

Table 2.The potential and demand for biofuel in Lithuania [19]

Biofuel potential, thousands (toe)	**Lithuanian demand, thousands (toe), 2011**	**Lithuanian demand, thousands (toe), 2020**
1354	520	940

In the electrical power balance in the year 2010, biomass power plants totalled 114 GWh, and biogas plants – 28 GWh [3] as show the different studies about biogas production [8; 17]. The theoretical potential for electricity production from biogas in Lithuania is considerable – 3389 GWh [8; 17]. Electricity produced in biofuel plants in 2020 is projected to increase by 4 percent of the total electricity consumption [11]. Main biofuel used in Lithuania are bio - diesel and bio - ethanol (table 3).

Table 3.The dynamics of development of biofuel in Lithuania [14; 16; 21; 22; 23; 24]

Biofuel	**2007**	**2008**	**2009**	**2010**	**2020**
Bio - ethanol, produced, thousand tons		17.1	24.5	39.3	
Bio - diesel, produced, thousand tons		64.6	104.7	89.2	
Share of biofuel in the fuel for transportation, %	3.8	4.3	5.6	–	15

The analysis of the dynamics of biofuel use in Lithuania shows that production of biofuels and their use is increasing but not fast enough. According to experts [26], unused reserves of biofuels are very large; those are enough to produce the heat necessary for Lithuanian consumers. Total of biomass in Lithuania consists of over 2 million toe: municipal waste – 200 000 toe, straw – 840 000 toe and biomass from wood – 1103 000 toe [10]. The assessment of biofuel usage in Lithuania shows, that biofuel production in Lithuania has received little attention, as well as lack of promotion can be seen, whereas the development of biofuel production can provide benefits to the whole society.

Geothermal energy in Lithuania is used only for the production of heat and represents a small percentage as a resource (table 4), but in the western part of the country geothermal potential is used more actively [2, 18]. In Lithuania for “green” electricity production there is mainly used **hydropower**. This kind of energy amounted 540 GWh [9] generally in total balance in 2010 (Table 4). In 2002 Lithuania had just few hydro capacities – 113 MW [25], and in 2010 – already 1027 MW [4]. The hydropower source is suitable (desirable) because of low operating cost electricity. However in Lithuania technical hydropower’s potential is significantly limited by the environmental conditions [2]. One of the fastest growing and most environmentally friendly RES in Lithuania is **wind power**. Every year more and more electrical energy in Lithuania is produced from wind energy (table 4): in 2005 Lithuania had only 4 small wind power plants with an annual production of 1.8 GWh of electricity [2], in 2006 compared to 2005, 6 times more wind energy was used to produce electricity [20]; in 2007, compared to 2006 – 7.5 times more [21]. In 2007 wind power produced electricity accounted for 0.8 percent of all electricity produced in Lithuania, in 2008 and 2009 – 1 percent in each year; in 2010 – 3.9 percent [2]. In 2010 wind power supplied to the network 224 GWh of electricity [24]. Wind energy potential is good enough, especially on the seaside [18]. Lithuanian climate conditions are favourable for wind power development.

Table 4.The energy balance of geothermal, hydro and wind energy in Lithuania [2; 24]

RES	**2005**	**2006**	**2007**	**2008**	**2009**	**2010**
Geothermal energy, GWh	16.9	9.7	9.0	3.8	29.7	26.4
Hydro energy, GWh	450.7	397.1	420.6	401.9	424.3	540.0
Wind energy, GWh	1.8	13.7	106.1	131.1	157.7	224.0

Solar energy is a very important renewable energy source. In 2010 Lithuania produced and supplied to the electrical grid 2.4 MWh of solar energy [24]. This amount of electricity is commonly consumed by an average of 700 homes per year. There is an opinion, that solar electricity as for Lithuania's economic potential is very limited, due to its expensive technology and unsuitable climatic conditions [2; 9]. On the other hand, this approach is not entirely justified, because in Lithuania, the annual average solar energy is about 1000 kWh/m2, while in southern Germany – 1260 kWh/m2, and the north of Germany – 970 kWh/m2, which means that the climatic conditions for solar energy in Lithuania are only slightly worse than in Germany [15]. Lithuania has possibilities to use solar energy intensively.

The dynamics of electricity produced from RES in Lithuania [2] shows, that from year 2003 to 2005 renewable sources of electricity installed capacity changed very little, higher growth observed in 2006 – 2007, and in 2008 this tendency slightly slowed down. In 2007 production of electricity from RES amounted to 4.6 percent of total electricity production; in 2008 – 4.9 percent. In 2010 in Lithuania from RES was produced and placed on a network 895 GWh of electricity, which accounted for 9.7 percent of all electricity consumed per year in Lithuania and 16 percent of all electricity produced in Lithuania [4]. The analysis showed that the maximum electrical energy from RES in 2010 balance sheet was produced by hydroelectric power (540 GWh), second place – wind energy (224 GWh), followed by – biomass (114 GWh) and biogas (28 GWh) plants. Electricity produced from RES share it is planned to increase to 21 percent, in comparison to total national electricity consumption [16].

Table 5.RES in Lithuania (2009; 2020) [19]

RES	**2009, ktne**	**2009, %**	**2020, ktne**	**2020, %**
Sun	0	0	1	0
Wind	14	2	99	5
Hydro energy	37	4	59	3
Biofuel	53	6	188	9
Geothermic	5	1	20	1
Biomass	763	88	1626	82
Total	872	100	1993	100

An analysis of RES use dynamics in Lithuania has showed that Lithuania has a relatively high RES potential. The main renewable energy source is biomass. However, alternative energy sources are not used sufficiently, because the use of RES is growing very slowly in Lithuania. In order to increase the usage of RES in Lithuania and to pursue the obligations to EU (Table 5), it is essential to determine the causes that influence the slow development of this activity and to identify the main RES uptake problems.

3. THE MAIN PROBLEMS OF UNDER-USE OF RES AND THEIR CAUSES

Based on completed RES situation in Lithuania and the assessment of the scientific literature [1; 6; 8; 11; 13; 25; 27 and 28] there are main causes for the problematic uptake of RES in Lithuania identified. Lithuania has some direct support measures or tax incentives to use renewable energy sources available. There are pollution taxes, fuel taxes, value added tax (VAT) and excise tax allowances for biomass and biofuel, feed-in prices for electricity produced from renewable energy source etc. [8; 25]. But it should be noted, that Lithuania has the weak legal framework, unregulated use of RES technology return, the lack of biomass boilers and equipment necessary, as well as poor logistics to ensure smooth work.

Another important reason is the lobbying pressure of mined fuel corporations because of the representatives of the natural energy resistance; i.e. oil, gas, coal and nuclear energy industries as well as centralized distribution system businesses, that simply do not want to lose investments in their businesses and fight for the market share, and more often – for their monopoly positions. For this reason, various myths are created and artificial barriers are made in order to prevent access to cheaper energy for consumers. One recent example is the company "Vilniaus energija", which cut off the heat purchase contract with the Grigiskes Paper Mill, allegedly because of unreasonable heating requirements set by the state [5]. As a result, heat is directly discharged into the air, although it could meet up to 10 percent of total demand for lower prices in Vilnius [5]. What is more, president of the Republic of Lithuania [5] expressed the suspicion that the Vilnius Energy wants to "seize the biofuel boiler stations business", because it offers to pursue biofuel boiler station construction without any competition what so ever. Therefore, it is essential to attract more players into the RES market in the future in order to prevent monopolies. So, it is clear that the main stakeholders are market forces in this process. However, state, municipalities, nongovernmental organizations may play considerable role as connecting, integrating and promoting chain between the financing organizations and energy consumers [8].

The list of reasons for the slow uptake of RES in Lithuania is continued with traditional thinking, the Lithuanian authorities' decisions inertia and irrationality, as well as the traditional thinking of usage, weak public awareness and lack of understanding of the RES. Customers must have insufficient information to make informed choices. Most public utilities provide little information about their emissions or the fuels they use. Use of RES is relatively new area. Most of customers know about it little and think that alternative energy does not can be highly reliable [8]. These reasons form three main problems for the overall uptake of RES in Lithuania:

- Market barriers;
- Lack of investment capacity and institutional barriers;
- Public authorities' and institutions' infantilism.

The most important thing is to understand that the main essence of all EU directives, policies and measures is to overcome energy market failures as regulation of monopolies in energy sector by dealing with energy externalities, energy affordability, asymmetry of information and energy security [8]. Assessing the use of RES in Lithuania and identifying the key problems for overall use of RES and the causes of the latter ones is an expansion potential of the RES in Lithuania determined.

4. THE POSSIBILITIES OF RES DEVELOPING IN LITHUANIA

In 2009 the European Parliament and Council took on directive 2009/28/EC on promoting the use of renewable energy [14]. Under this directive, Lithuania has committed itself, that in 2020 in the final energy usage balance, the RES will be no less than 23 percent. It is also panned till the year 2020 to transfer heat production sources to biofuel's and municipal waste's usage, which requires about 1.1 milliards LTL of investment [16; 26]. Lithuania is committed to the European Union [10; 13; 14; 18], that in 2020:

- Renewable heat from the CH sector will take 60 percent. (currently – 18 percent), and decentralized heating sector – 80 percent;
- Electricity obtained from RES will reach up to 21 percent (currently – 8 percent.) Including wind turbines could produce up to 10 percent of all electricity consumed in the country (at present – about 2 percent), and biofuel power – up to 4 percent;
- Usage of RES in the transport sector – 15 percent (currently – 5 percent).

Renewable energy accounted for 15.2 percent in total balance in Lithuania in 2010. On the one hand, the target of reaching 23 percent planned for 2020 is not easy (especially given, that over the past ten years, this figure increased by about 3 percent [18]). On the other hand, Lithuania has a great potential. It is stated [12] that Lithuania every year needs about 20 TWh of heat and about 10 TWh of electricity. All Lithuanian RES together make up about 40 TWh [12] of annual energy potential in Lithuania (biofuel, biogas, wind, sun energy, hydro power, geothermic and municipal waste) [12]. Therefore, Lithuania with its potential RES is able not only to meet all the needs of the country, but also could export the excess of clean energy. Therefore, it is necessary to put effort and find ways to use RES widely.

Evaluation of the use of RES in Lithuania showed that the most promising development in Lithuania can be identified, biomass and wind energy. Hydropower potential is severely limited by environmental conditions. The strict environmental requirements have conditioned the development of biogas production in all EU countries. The biogas received during anaerobic decomposition of the organic waste can be utilized as energy source for electricity and heat generation or as gas fuel. The one of the main raw material sources for biogas production in Lithuania may be organic waste in stockbreeding sector. The huge amounts of waste at the stockbreeding farms must be properly handled and usefully utilized. The organic waste can be used for feeding, digesting. Also the waste can be burned or processed into biofuel or biogas [8; 17]. Various forms of support must be employed in order to accelerate the development of RES. Economic tools and other state policies measures should be used to address these issues [8]. Lithuania could pursue its obligations to EU. We also have to stop to pay big money for mined energy. The best solution is to reduce subsidies for fossil fuel based energy sources [25] and redirect it to the use of RES development. It will contribute to saving the financial resources, reducing air pollution, creation of new work places, as well as benefits for Lithuanian economy and the perspective to have enough energy resources, what could ensure true energy independence. It is also very important for public authorities to demonstrate motivated efforts and tangible results. As already noted, Lithuania have some direct support measures or tax incentives to use renewable energy sources available. Lithuania is the only country in Baltic region which apply VAT exemptions from biofuels [3; 25]. This has positive impact for the implementation of EU requirements. Renewable energy sources do not emit such pollutants like SO2, CO2 etc. into atmosphere. Pollution taxes have specifically impact on enhanced use of RES. The high taxes on emissions increase competitiveness of renewable in electricity, heat and transport fuels markets [25]. However, it is not enough. The implementation of EU green certificate system instead of local feed in prices applied for electricity produced from RES would have the positive impact on deployment of renewable energy technologies [25]. It is necessary to develop and implement policies by aiming directly at encouraging the development and diffusion of environmentally friendly technologies. Also it is necessary to inform public about RES technology innovation [8]. It is important to provide the support to renewable energy projects increasing competitiveness of enterprises by implementing new technologies [25]. Structural funds are the European Union’s main instrument for supporting social and economic restructuring across the EU. They account for over a third of the EU total budget [25]. Support from EU funds can be very useful in promoting RES in Lithuania. However their use needs more rationality and more orientation of state policy towards extensive usage of renewable energy sources [7; 8].

It must be remembered that Lithuania has obligations, responsibilities not only for the EU, but for its society and future generations. Therefore each member of society has to contribute to this work. In order to reach the overall aim the society should be united.

5. CONCLUSIONS

After the analysis of usage of RES in Lithuania, identification of key problems of under-use of RES and their causes, and after determining the possibilities of RES expansion in Lithuania, the following conclusions were made:

1. The analysis of RES use dynamics showed that in Lithuania main focus is set on the RES such as water, wind and biomass. One of the most popular and widely used RES in Lithuania is of wood biomass. It is argued that the most promising development in Lithuania can be assigned to biomass and wind energy. Hydropower potential is severely limited by environmental conditions. Solar and geothermal power production is limited by high technology costs. It was also found that in Lithuania renewable energy potential is high enough to meet the needs. Nonetheless, dynamics of RES use are still quite slow. This proves that Lithuania poorly utilizes its assets.
2. According to the literature review, three main problems for poor usage of RES in Lithuania where identified. It are market barriers, lack of investment capacity and institutional barriers, as well as society’s and state institutions’ infantilism.
3. It is necessary to understand that the main essence of all EU directives, policies and measures is to overcome energy market failures as the regulation of monopolies in energy sector and also as energy affordability, asymmetry of information and energy security. Also Lithuania has to stop to pay big money for mined energy. The best solution is to reduce subsidies for fossil fuel based energy sources and redirect it to the use of RES development.
4. The state, municipalities, nongovernmental organizations must play considerable role as connecting, integrating and promoting chain between the financing organizations and energy consumers. It is necessary to develop and implement environmentally friendly technologies and also to inform public about RES technology innovation.
5. EU structural funds can have the huge role in promoting renewable energy sources in Lithuania. Use of EU funds needs more rationality and more orientation of state policy towards extensive usage of RES.
6. Carried out theoretical studies have shown that Lithuania has the possibilities to adapt the existing energy infrastructure for wide usage of RES. In such way it is possible to create benefits for the Lithuanian economy and to find less harming the nature energy sources.

LIST OF LITERATURE

1. BLAŽYS, A., URBONAS, P. Analysis of possibilities of usage geothermal energy. Science – future of Lithuania. 2009, Vol. 1, No. 1.
2. COWI Baltic. Atsinaujinančių energijos išteklių panaudojimo elektros energijos gamyboje apimčių analizė ir rekomendacijų dėl elektros energijos, kuriai gaminti naudojami atsinaujinantys energijos ištekliai, gamybos ir supirkimo skatinimo 2010–2020 m. parengimas. No. 3. 2008 – [referred on the 16th of December in 2011 y.]. Link to the internet <http://www.lsta.lt/files/studijos/2008/AEI_elektra_galutine.pdf>.
3. Danish Energy Authority. Environmental related energy sector programme-Lithuania. Enhancement of the Use of Local and Renewable Energy Sources-Lithuania. Fiscal and

Financial Measures Promoting Use of Renewable Energy Resources in Selected Countries. Elaborated by Danish Energy Authority, October, 2003.

4. GIEDRAITIS, V., RASTENIENĖ, A. Tvarios energijos perspektyvos Lietuvoje. 2011 - [referred on the 5th of December in 2011 y.]. Link to the internet <http://www.technologijos.lt/n/technologijos/energija_ir_energetika/S-22914/straipsnis?name=S-22914&l=2&p=1&utm_source=Susije_po_straipsniu&utm_medium=Vidine_navigacija&utm_campaign=Vidine_navigacija>.
5. GRYBAUSKAITĖ, D. “TV – 3” News, 2012 February 20.
6. HAGEN, A. Pagrindiniai energijos gamybos ir vartojimo, klimato kaitos politikos ir atsinaujinančios energijos gamybos aspektai Norvegijoje. Training materials: Darni energetika. Atsinaujinantys energijos šaltiniai. Efektyvus energijos naudojimas. VŠĮ “DVI Darnaus vystymo iniciatyvos”, 2010.
7. KLEVAS, V., ANTINUCCI, M. Integration of national and regional energy development programs in Baltic States. Energy Policy, 2004.
8. KLEVAS, V., SANKAUSKAITE, V., KLEVIENE, A., BUBELLIENE, J. Economic policies encouraging the development and diffusion of environmentally friendly sustainable energy technologies. LEI, 2010.
9. KLEVAS, V., ŠTREIMIKIENĖ, D. Lietuvos energetikos ekonomikos pagrindai. LEI, 2006. ISBN 9986-492-96-3.
10. LAPINSKAS, R. Biomasės svarba Lietuvos energetiniam sektoriui. Savivaldybės tarnybų, šilumos tiekėjo “Litesko” ir visuomenės atstovų pasitarimas šilumos tiekimo klausimais. Druskininkai, 2012 February 14 - [referred on the 21st of February in 2012 y.]. Link to the internet <http://www.biokuras.lt/uploads/File/2012.02.14_R.Lapinskas_prezentacija.pdf>.
11. Lithuanian Association of bioenergetics and Energy Saving. ES parama uždegė žalią šviesą. 2011 - [referred on the 5th of December in 2011 y.]. Link to the internet <http://www.energijaplius.lt/lt/naujienos/4/es-parama-uzdege-zalia-sviesa>.
12. Lithuanian biomass energy association LITBIOMA. Už tikrą energetinę Lietuvos nepriklausomybę. Press Conference “Kaip panaudoti Lietuvos išteklius nepriklausomos energetikos sukūrimui”. Vilnius: Lithuanian parliament, 2012 January 3 - [referred on the 20th of February in 2012 y.]. Link to the internet <http://www.biokuras.lt/lt/aktualijos/pasirasytas-pareiskimas-uz-tikra-energetine-lietuvos-nepriklausomybe-.html>; <http://www.biokuras.lt/uploads/File/AEI_pareiskimas_2012_01_03.pdf>.
13. Lithuanian biomass energy association LITBIOMA. Visam šildymo sezonui Lietuvoje pakaktų pusės ūkininkų turimų šiaudų, 2011 - [referred on the 19th of February in 2012 y.]. Link to the internet <http://www.biokuras.lt/lt/aktualijos/visam-sildymo-sezonui-lietuvoje-pakaktu-puses-ukininku-turimu-siaudu.html>.
14. Ministry of Energy of the Republic of Lithuania. Atsinaujinančių išteklių energijos naudojimo 2010 – 2020 m. prognozių dokumentas. 2009 - [referred on the 14th of December in 2011 y.]. Link to the internet <http://www.enmin.lt/lt/activity/veiklos_kryptys/atsinaujantys_energijos_saltiniai/Prognoze.pdf>.
15. Ministry of Energy of the Republic of Lithuania. Lietuvos Respublikos energetikos ministerijos 2010 metų ataskaita. 2011 - [referred on the 6th of December in 2011 y.]. Link to the internet <http://www.enmin.lt/lt/activity/ataskaita/2010veiklosAtaskata.pdf>.
16. Nacionalinė atsinaujinančių energijos išteklių plėtros strategija. Nutarimas dėl nacionalinės atsinaujinančių energijos išteklių plėtros strategijos patvirtinimo. No. 789. 2010 - [referred on

the 15th of December in 2011 y.]. Link to the internet <http://www3.lrs.lt/pls/inter3/dokpaieska.showdoc_l?p_id=376097>.

17. NAVICKAS, K. Possibilities and limits of biogas utilization in Lithuania. Leipzig, 2004.
18. ŠIMĖNAS, J. Lietuva žengia tvariosios energijos link. The magazine “Elektros erdvės”, National Association of Electrical Engineering, 2011, No. 1 (26).
19. STASIŪNAS, V. Lietuvos centralizuoto šilumos tiekimo sektorius ir jo vystymosi perspektyvos. Seminar “Biomasės panaudojimas CŠT sektoriuje – esama situacija ir kliūtys jos plėtrai”. Vilnius: Vilnius Gediminas technical university. The Lithuanian District Heating Association, 2011 December 6 - [referred on the 22nd of February in 2012 y.]. Link to the internet <http://www.biokuras.lt/uploads/File/1_V_Stasiunas_LT.pdf>.
20. Statistics Lithuania. Energetikos statistika 2006 m. Kuro ir energijos poreikis 2006 m. didėjo. 2007 – [referred on the 9th of December in 2011 y.]. Link to the internet <http://www.stat.gov.lt/lt/news/view/?id=1923>.
21. Statistics Lithuania. Energetikos statistika 2007 m. 2007 m. didėjo atsinaujinančios energijos naudojimas. 2008 - [referred on the 9th of December in 2011 y.]. Link to the internet <http://www.stat.gov.lt/lt/news/view/?id=2605>.
22. Statistics Lithuania. Energetikos statistika 2008 m. 2008 m. didėjo atsinaujinančios energijos naudojimas. 2009 - [referred on the 9th of December in 2011 y.]. Link to the internet <http://www.stat.gov.lt/lt/news/view/?id=6715>.
23. Statistics Lithuania. Energetikos statistika. 2009 m. mažėjo bendrasis šalies kuro ir energijos sunaudojimas. 2010 - [referred on the 9th of December in 2011 y.]. Link to the internet <http://www.stat.gov.lt/lt/news/view/?id=7843>.
24. Statistics Lithuania. Energetikos statistika. 2010 m. keitėsi šalies kuro ir energijos sąnaudų struktūra. 2011 - [referred on the 9th of December in 2011 y.]. Link to the internet <http://www.stat.gov.lt/lt/news/view/?id=9044>.
25. STREIMIKIENE, D.; KLEVAS, V. Promotion of renewable energy in Baltic States.Renewable and Sustainable Energy Reviews. 2007, No. 11.
26. TAVORIENĖ, V. Biokuro gamyba – vėžlio žingsniais, 2010 - [referred on the 17th of February in 2012 y.]. Link to the internet <http://verslas.delfi.lt/energetics/biokuro-gamyba--vezlio-zingsniais.d?id=38909459>.
27. ŽILINSKAS, E. Ateities iššūkiai pasaulinei energetikai mažinant aplinkos taršą. 2008 - [referred on the 19th of October in 2011 y.]. Link to the internet <http://ekologija.blogas.lt/ateities-issukiai-pasaulinei-energetikai-mazinant-aplinkos-tarsa-29.html/>.
28. ŽILINSKAS, E. Atsinaujinanti energetika. Nuo politinių subtilybių iki realių technologinių galimybių. 2008 – [referred on the 19th of October in 2011 y.]. Link to the internet <http://www.technologijos.lt/n/technologijos/energija_ir_energetika/straipsnis?name=straipsnis5803&l=2&utm_source=Rinktiniai_po_straipsniu&utm_medium=Vidine_navigacija&utm_campaign=Vidine_navigacija>.

CYSENI 2012, May 24–25, Kaunas, Lithuania
ISSN 1822-7554, www.cyseni.com

MODELING THERMAL AND GAS-DYNAMICS PROCESSES IN STEAM TURBINE EXHAUST HOOD

S. Alyokhina
A. N. Podgorny Institute for Mechanical Engineering Problems of the National Academy of Sciences of Ukraine
st. Dm. Pozharsky 2/10, Kharkiv, UA-61046, Ukraine
Phone +380572942794
Email: alyokhina@ipmach.kharkov.ua

ABSTRACT

The operation safety of the any turbo-installations depends from the effectiveness and reliability of working its basic constructs. For that purpose are required to use modern approaches to constructions of turbine equipment of Thermal Power Station (TPS) and Heat Power Plant (HPP). It is impossible without detailed investigation of thermal and gas-dynamic processes.

The investigations of thermal and gas dynamics processes in steam turbine exhaust hood have been carried out. The numerical solving of conjugate heat transfer problem was used. This approach allowed to define thermal field of steam and solid case and velocity field of steam. These results of investigations will be used at solving inverse heat transfer problems for definition of heat transfer coefficients on inner surfaces of exhaust hood.

Keywords: steam turbine exhaust hood, conjugate heat transfer problem, thermal and gas-dynamics processes

1. INTRODUCTION

The operation safety of the any turbo-installations depends from the effectiveness and reliability of working its basic elements. For that purpose are required to use modern approaches to constructions of turbine equipment of TPS and HPP. It is impossible without detailed investigation of thermal and gas-dynamic processes.

The exhaust hoods are very important part of steam turbines. In particular the construction of exhaust hood has big influence to economy and reliability of turbine [6.1, 6.2]. Its aerodynamic performances influence economy of turbine. During the operations the operating environment in exhaust hood of high pressure cylinder (HPC) has the complex structure and the walls of exhaust hood are subjected to the temperature differences at changing of the turbine's operating regime. So it's very important to make thermal and gas-dynamic processes investigations in this turbine element.

2. PROBLEM DEFINITION

Today the turbine K-325-23.5 of joint-stock corporation corporation "Turboatom" is one of perspective project of Ukrainian turbine construction industry [3]. It is necessary to make investigations for its reliability and long operation. The main part of these investigations is identifications of thermal and gas-dynamic processes in construct elements.

The high-pressure cylinder of turbine K-325-23.5 shown on Fig. 1. The exhaust hood has toroidal form with two exhausts in bottom. The exterior casing of HPC covered by isolation. This fact was taken into account in thermal investigation.

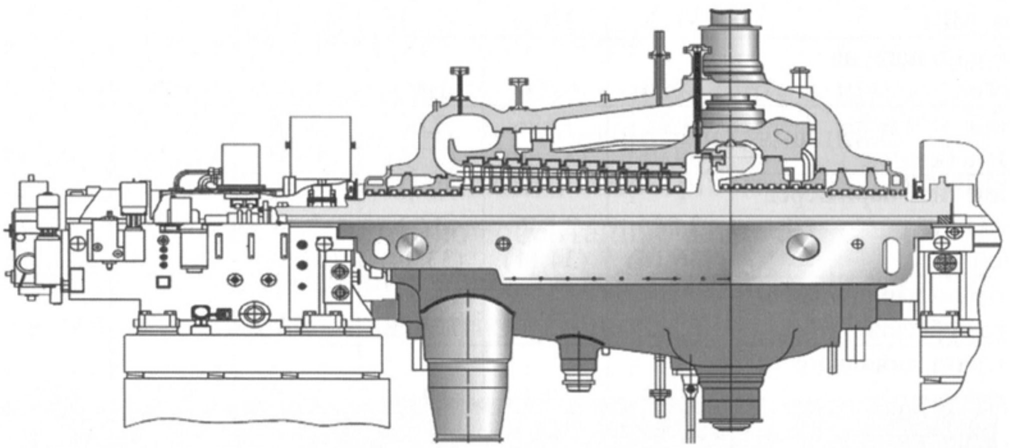

Fig. 1. The high-pressure cylinder of turbine K-325-23.5

Thermal and gas-dynamics processes were investigated on the rated duty of turbine.

3. METHODOLOGY OF SOLVING

The test operation with complex objects like exhaust hood of steam turbine is very difficult problem which associated with risk of equipment damage and the high financial expenditure. The solution of this problem is computational modeling.

One of problem at investigation of thermal and gas-dynamic processes is problem of boundary conditions definition in zones where operation environment has contact with metal casing. The taking into account the cooling of steam near the solid surfaces is problem also. In this case the effective instrument are the conjugate heat transfer problems which taking into account the interference of heat transfer in solid body and gas environment.

The mathematical model of conjugate heat transfer problem consists of following equations:

1) for gas environment:

– continuity equation (mass sources and sinks are absent):

$$\frac{\partial \rho}{\partial \tau} + \mathrm{div}(\rho \mathrm{v}) = 0\,, \tag{1}$$

where ρ – density of gas, kg/m^3; τ – time, s; v – velocity vector, m/s;

– equation of motion of viscous gas:

$$\rho \frac{d\mathbf{v}}{\partial \tau} = -\mathrm{grad}\left(p + \frac{2}{3}\mu_e \,\mathrm{div}\,\mathbf{v} \right) + 2\mathrm{div}\left(\mu_e \dot{\mathbf{S}}\right)\text{б} \tag{2}$$

where p – static pressure, Pa; μ_e – effective coefficient of dynamic viscosity, kg/m·s, $\dot{\mathbf{S}}$ – tensor of strain rates.

– energy equation:

$$\frac{\partial}{\partial \tau}(\rho E) + \mathrm{div}\left(\mathrm{v}(\rho\, E + p)\right) = \mathrm{div}\left(\lambda_e \mathrm{grad} T\right),$$

where E – total energy, carried to mass unit; T – temperature, K; λ_e – heat conductivity coefficient (in consideration of turbulent constituent), W/(m·K). In consequence of small absolute value of dissipative function there are not sources of heat here which were generated of mechanical work of gas flow.

2) for solid medium – the equation of heat conduction (the Fourier equation):

$$\mathrm{div}(\lambda \mathrm{grad} T) = c_p \rho \frac{\partial T}{\partial \tau}, \tag{3}$$

where λ – heat transfer coefficient; T – temperature, K; c_p – heat capacity of material, J/kg·K.

For closure the differential equations system added of the equation of gas environment state is dependence the density of environment from temperature and pressure. For calculation of the turbulent components which were included to equations of moving and energy was used the Menter's model of the shear stresses k-ω [6.4]. The physical characteristics in equations were considered as functions of temperature and pressure in working interval of temperatures.

A control-volume-based technique [5] is used for solving of model's equations.

The calculation area for exhaust hood of HPC was realized in 3D mesh (Fig. 2). On entry of exhaust hood were specified the velocity (54.78 m/s) and pressure of operating environment which calculated for parameters after 12-th turbine stage: the temperature of steam 287.6°C, pressure 41.575 at.

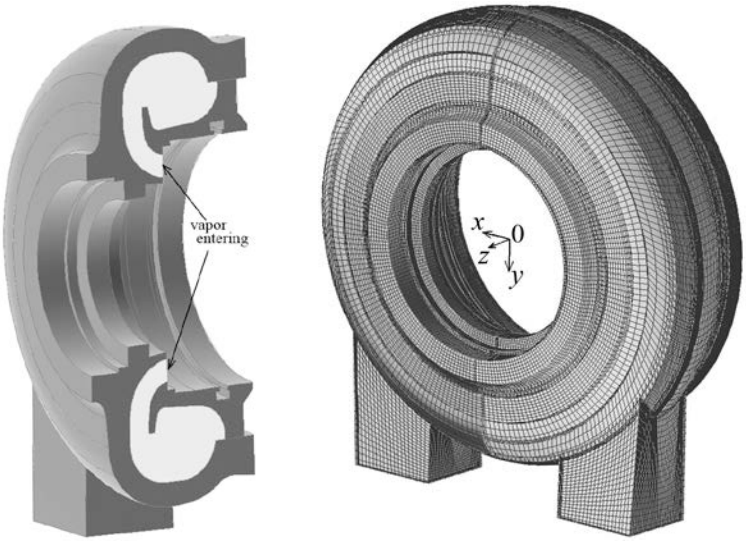

a) b)

Fig. 2. The calculation area: a) the fragment of calculation area; b) the three-dimension mesh of casing elements

The calculating mesh has more than 1.5 million nodes which allows to consider thermal and gas-dynamic processes and take into account flow specifics near the solid body.

4. INVESTIGATION RESULTS

The solution of direct conjugate problem of heat transfer allowed defining the structure of flow in exhaust hood of HPC (Fig. 3). This figure shows that after moving by steam channel of HPC the flow go to cave of exhaust hood where become twisted and after divided go to the bottom exhaust (Fig. 3, a). The structure of flow in section which placed in plane z0y shows the character of the steam moving lengthways of inner surfaces of exhaust hood (Fig. 3, b). The small flow separation occur near the exit of diffuser (point 15) and near the zone where connected the casing and the iron ring (points 9 and 10).

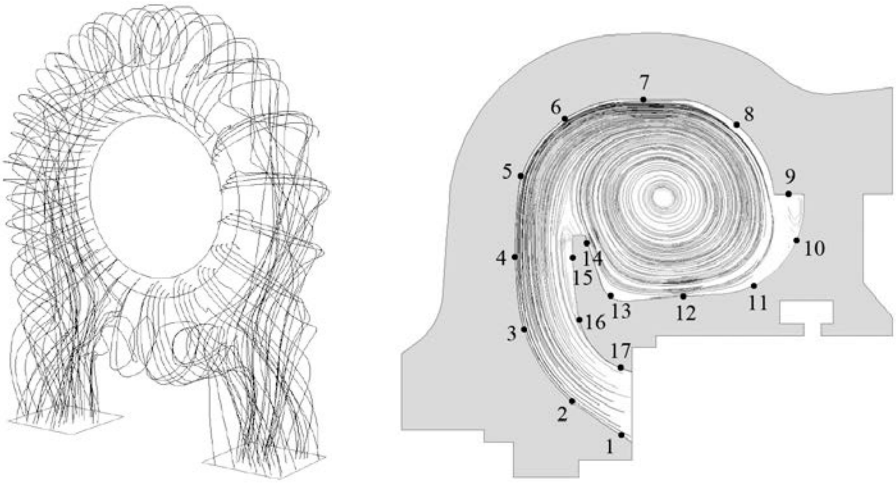

a) b)

Fig. 3. The structure of flow in exhaust hood of HPC: a) current streamlets for all calculation area; b) current streamlets in section which placed in plane z0y

The steam velocity distribution (Fig. 4) in exhaust hood influence on the heat exchange conditions on its surfaces.

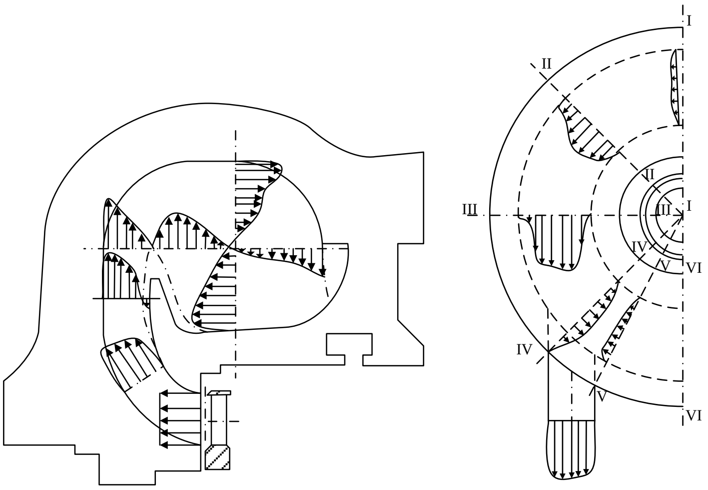

a) b)

Fig. 4. The components of steam flow in exhaust hood: a) circumferential component; b) flow rate component

In toroidal camera the flow rate increases from section I-I to section IV-IV. In the bottom part of exhaust hood the steam moves from section VI-VI to section V-V. Distribution of velocity magnitude in vertical section is shown on Fig. 5.

The solving of conjugate heat transfer problem allows to define thermal field in solid body and gas. The thermal field in vertical section is shown on Fig. 6. The high speed of gas cause the uniform temperature distribution in inner cavity of exhaust hood. Outer case of HPC have warmed up uniformly also, the highest temperature of metal in salient part (deflector).

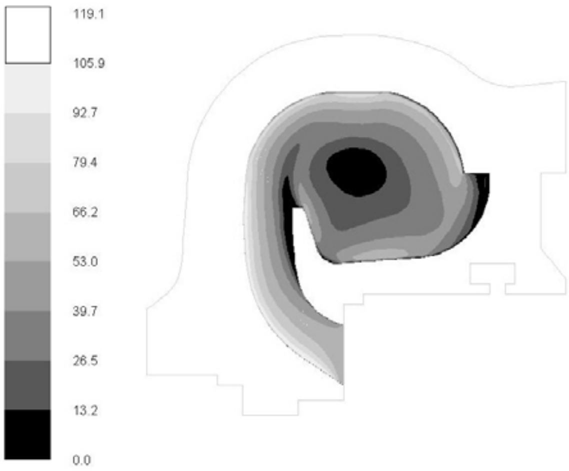

Fig. 5. The velocity magnitude field (m/s) in vertical section of exhaust hood

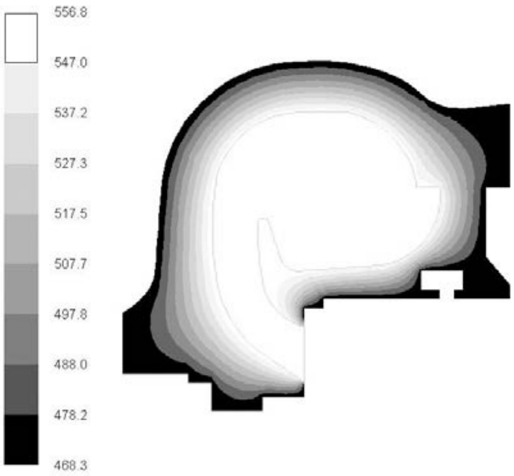

Fig. 6. The thermal field (absolute degree) in vertical section of exhaust hood

5. CONCLUSIONS

The uses of modern modeling methods of thermal and gas-dynamics processes which based on the solving of direct heat transfer problems allows to identify heat transfer conditions in different elements of turbine. These methods have high effectiveness at modeling processes in exhaust hood of high-pressure cylinders of steam turbines.

The uneven distribution of temperature in solid body of exhaust hood requires to make investigations of thermal stress conditions. For this purpose will be solved the inverse heat transfer problem which based on results of presented investigations. After that the heat transfer coefficients on inner surfaces of exhaust hood will be defined which will be used like boundary conditions in thermal stress investigations.

The results of this work have shown that next investigations of thermal and gas-dynamics processes in exhaust hood on varying conditions of operations are necessary.

6. REFERENCES

1. Dejch M. E., Zarjankin A. E. The gas-dynamics of diffusers and exhaust hoods of turbines. M.: Energy, 1970. – 384 c. – in rus.
2. Schegljaev A. V. The steam turbines – M.: Energy, 1976 – 368 c. – in rus.
3. The construction of steam turbine of new generation with power 325 MW / V. G. Subotin, E. V. Levchenko, V. L. Shvetsov, O. L. Shubenko, A. O. Tarelin, V. P. Subotovich – Kharkiv: Folio, 2009. – 256 p. – in ukr.
4. Menter F. R. Two-Equation Eddy-Viscosity Turbulence Models for Engineering Applications // AIAA Journal, 32(8), 1994 – p. 1598–1605.
5. Fletcher K. The computation methods in fluid dynamics – M.: Mir, 1991. – V. 1. – 502 p.; V. 2 – 552 p. – in rus.

CYSENI 2012, May 24–25, Kaunas, Lithuania
ISSN 1822-7554, www.cyseni.com

INFLUENCE OF COOLING TOWER ON THERMAL PARAMETERS OF CIRCULATING WATER SYSTEMS

A.A. Brin, A.I. Petruchik
A. V. Luikov Heat and Mass Transfer Institute
National Academy of Sciences of Belarus
15, P. Brovki St., 220072, Minsk, Belarus
Phone +375 17 2842222
Email: brin@hmti.ac.by

ABSTRACT

The physical criteria of thermal efficiency of evaporative cooling of water in cooling towers are proposed. The thermal efficiency depends on water temperature difference between inlet and outlet of cooling tower, which by-term depends on several parameters, such as flow rate through the cooling tower, air temperature, relative humidity of air, inlet water temperature. The overall performance of circulating water cycle is characterised by ability of cooling tower to take away from cooled equipment the necessary quantity of heat at design value of temperature of chilled water and at minimum power expenses. In a circulating water cycle the electric power is spent for work of engines of pumps and fans of cooling towers. In cooling towers the air intake is defined by aerodynamic resistance of cooling tower and its technical condition. For calculation of efficiency of cooling tower the mathematical model is developed. It takes into account the values of heat and mass transfer coefficients, temperatures, flow rate and pressure of water, meteorological conditions and also electric power expenses.

Keywords: cooling tower, circulating water, optimization, modelling

1. INTRODUCTION

In present work an applied problem of maintenance of demanded parametres of water cooling in circulating water cycles with cooling towers are considered. The first way is extensive since water temperature reduction in a circulating water cycle is reached due to the increase of circulating water flow, frequency rate of circulation or the irrigation area. The choice of the practical realization scheme of the given way depends on cycle characteristics: quantity and productivity of pumps, efficiency and loading of cooling towers etc.

Frequently the demanded water temperature, arriving to the cooled equipment is below the actual water temperature at cooling tower outlet. In this case it is required to raise efficiency of cooling tower. The efficiency of cooling tower is theoretically limited by the temperature of wet bulb thermometer and technologically – by flows of thermal agents.

It is easy to show that technologically the maximum possible temperature drop of water in cooling tower $\Delta T_{\max}$ with given water flow, air flow, water temperature on the cooling tower inlet, temperature and humidity of air on the cooling tower inlet can be found proceeding from balancing correlations as:

$$\Delta T_{\max} = \frac{\left(P_{\mathrm{t}} + P_{\mathrm{e}}\right) \cdot Q_{\mathrm{a}}}{c_{\mathrm{w}} q_{\mathrm{w}}}, \qquad (1)$$

where P_{t} is a maximum quantity of heat which is taken away by one cubic meter of air due to the heat transfer, J/m^3; P_{e} is a maximum quantity of heat which is taken away by one cubic meter of air due to the evaporation, J/m^3; Q_{a} is a volume flow rate of air, m^3/s; c_{w} is a water cpecific heat, J/(kg·°C); q_{w} is a mass flow rate of water, kg/s.

2. MATHEMATICAL MODEL

The developed mathematical model is based on the models of evaporative cooling of water droplets obtained by the authors previously [1, 2]. We describe a field of air velocity by means of average value, which is determined in the approximation of one–dimensional description of cooling tower aerodynamics. The droplets are spherical and there are no interactions between them. The model represents a system of ordinary differential equations:

– equation for variation in the droplet radius $R_{\mathrm{md}}(z)$ as a consequence of its evaporation:

$$\frac{dR_{\mathrm{md}}(z)}{dz} = -\frac{\gamma(\mathrm{Re})\left[\rho_s(T_{\mathrm{md}}(z)) - \rho_v(z)\right]}{\rho_w v_{\mathrm{md}}(z)}, \tag{2}$$

where md = 1 when droplets are moving upward, md = 2 when droplets are moving downward, ρ_v and ρ_s are the water density and the saturated water density in air, respectively, kg/m^3;

– equation for variation in the droplet velocity $v_{\mathrm{md}}(z)$:

$$\frac{dv_{\mathrm{md}}(z)}{dz} = \frac{g}{v_{\mathrm{md}}(z)} - C(\mathrm{Re})\frac{\rho_a[v_{\mathrm{md}}(z) - v_a]^2}{2v_{\mathrm{md}}(z)}\frac{\pi R_{md}(z)^2}{m}, \tag{3}$$

where v_a is an air velocity, m/s; $C(\mathrm{Re})$ is an aerodynamic drag coefficient [1, 2], dimensionless; ρ_a is an air density, kg/m^3; m is a droplet mass, kg;

– equation for variation in the volume-average droplet temperature $T_{\mathrm{md}}(z)$:

$$\frac{dT_{\mathrm{md}}(z)}{dz} = -\frac{3\left\{\alpha(\mathrm{Re})\left[T_{\mathrm{md}}(z) - T_a(z)\right] + \gamma(\mathrm{Re})r\left[\rho_s(T_{\mathrm{md}}(z)) - \rho_v(z)\right]\right\}}{c_w \rho_w R_{\mathrm{md}}(z) v_{\mathrm{md}}(z)}, \tag{4}$$

$$\alpha(\mathrm{Re}) = \frac{\lambda_a(2 + 0.5\mathrm{Re}^{0.5})}{2R_{\mathrm{md}}}, \quad \gamma(\mathrm{Re}) = \frac{D(2 + 0.5\mathrm{Re}^{0.5})}{2R_{\mathrm{md}}}, \quad C(\mathrm{Re}) = \frac{24}{\mathrm{Re}}\left(1 + \frac{1}{6}\mathrm{Re}^{2/3}\right),$$

where $\alpha(\mathrm{Re})$ (W/m^2·°C) and $\gamma(\mathrm{Re})$ (m/s) are the heat and mass transfer coefficients, respectively, depending on the Re number [3]; r is a latent heat of vaporization, J/kg; λ_a is a thermal conductivity of air, W/m·°C; D is a diffusion coefficient for water vapour, m^2/s;

– equation for variation in the temperature of the vapour-air mixture $T_a(z)$ with allowance for heat transfer of droplets moving upward (subscript 1) and downward (subscript 2) alike:

$$\frac{dT_a(z)}{dz} = \frac{4\pi R_1(z)^2 N_d}{\rho_a c_a (v_1(z) - |v_a|)}\alpha(\mathrm{Re})\left[T_a(z) - T_1(z)\right] + \frac{4\pi R_2(z)^2 N_d}{\rho_a c_a (v_2(z) - |v_a|)}\alpha(\mathrm{Re})\left[T_a(z) - T_2(z)\right], \tag{5}$$

where N_d is a number of droplets, m^{-3}; c_a is an air cpecific heat, J/kg·°C;

– equation for variation in the density of water vapour $\rho_v(z)$ in air with allowance for mass transfer of drops moving upward (subscript 1) and downward (subscript 2) alike:

$$\frac{d\rho_v(z)}{dz} = -\frac{4\pi R_1(z)^2 N_d}{v_1(z) - |v_a|}\gamma(\mathrm{Re})\left[\rho_s(T_1(z)) - \rho_v(z)\right] - \frac{4\pi R_2(z)^2 N_d}{v_2(z) - |v_a|}\gamma(\mathrm{Re})\left[\rho_s(T_2(z)) - \rho_v(z)\right], \tag{6}$$

The solution of the system was implemented in the MathCAD 14 environment using the Runge-Kutta method.

3. RESULTS

Numerical calculations were performed using the above mathematical model (2)–(6). The efficiency of the cooling tower is defined by the dimensionless parameter:

$$\eta = \frac{T_{w0} - T_{wf}}{T_{w0} - T_{lim}}, \tag{7}$$

where T_{w0} is the water temperature at the inlet to the cooling tower, °C; T_{wf} is the water temperature at the outlet from the cooling tower, °C; and T_{lim} is the temperature of the wet bulb thermometer, °C.

The dependence of the ratio of temperature of the chilled water T_{wf} calculated according to (1) to the temperature of the wet bulb thermometer T_{lim} versus the ratio of mass flow rates of water q_w and air q_a is shown in Fig. 1.

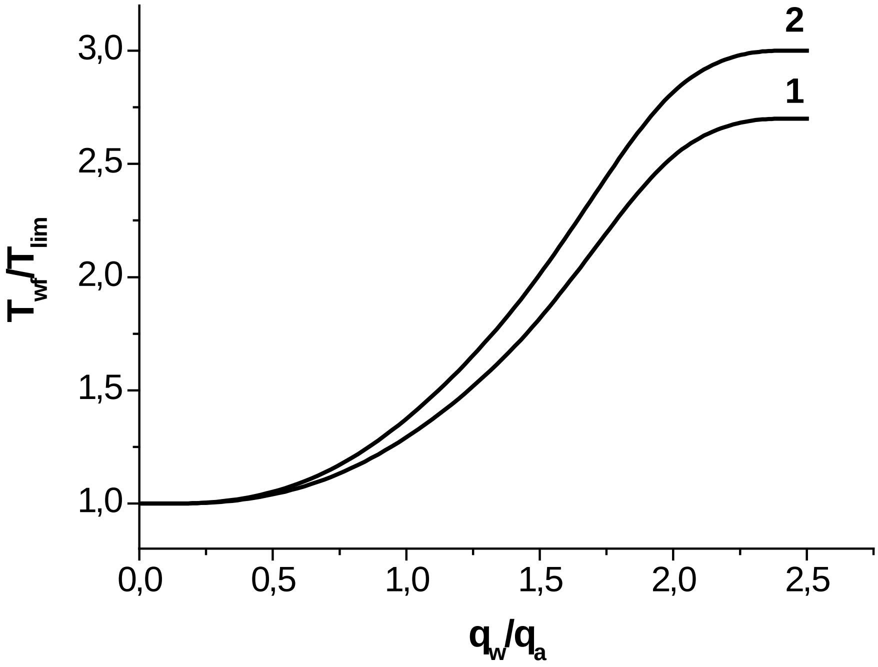

Fig. 1. The dependence of the ratio of temperatures of the chilled water and the temperature of the wet bulb thermometer T_{wf}/T_{lim} versus the ratio of mass flow rates of water and air q_w/q_a: curve 1 is for the T_{w0} = 25 °C, curve 2 – T_{w0} = 35 °C

It is seen from Fig. 1, that by reducing the initial water temperature at the cooling tower inlet it is possible at the same ratio of mass flow rates of water and air to reduce chilled water temperature at the cooling tower outlet T_{wf}.

Technologically, it is possible to reduce the water temperature at the cooling tower inlet increasing the circulating water flow rate in cooling tower more than it is required for the cooled equipment. Besides the use of the additional water pump the air flow rate is proportionally increased due to ejection. Further the demanded volume of chilled water from cooling tower goes to the equipment and the rest of chilled water arrives to the hot water collecting tank. In a tank hot and cold water mixes up and moves to the cooling tower.

For example, the equipment requirs 50 m^3 of waters per hour at a temperature 25 °C. Thus the water on equipment outlet is heated up to 35 °C. Thus, the cooling tower is required, cooling the water from 35 °C to 25 °C. Let, for some reasons, the cooling tower is not effective enough and can cool water from 30 °C to 25 °C. If we will pump the water with temperature 35 °C on such cooling tower, then, taking into account the corrections on initial water temperature with other parameters being equal it will cool the water to 27,5 °C [4, 5] and does not provide the demanded parameters (Fig. 2, *a*). For maintenance of demanded parameters of work of a circulating water cycle it is proposed to increase the water flow rate through the cooling tower up to 100 m^3/h and to reduce the water temperature at cooling tower inlet to 30 °C (Fig. 2, *b*). Further, 50 m^3/h of water at temperature 25 °C pumps to the equipment, and the rest of water mixes up in a tank.

Thus, the cooling tower which is not effective enough allows providing demanded parameters of a circulating water cycle.

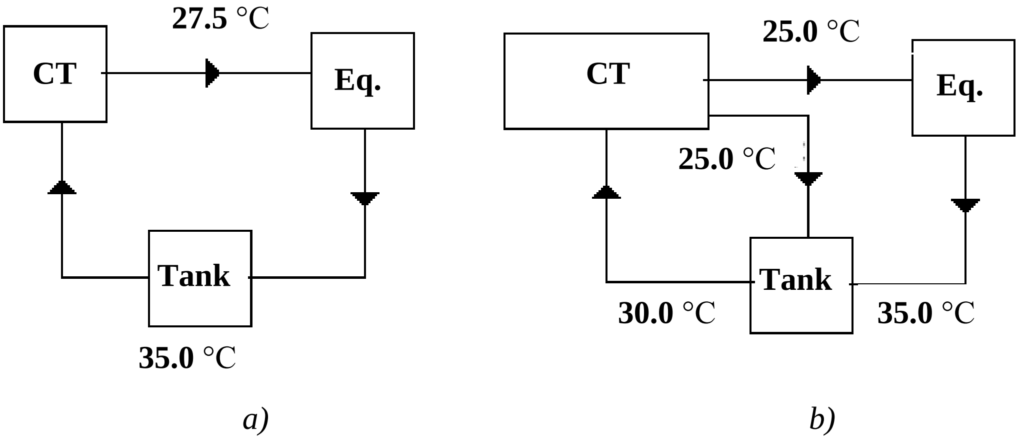

Fig. 2. Circulating water cycle: a – traditional, b – with recirculation line from cooling tower. CT – cooling tower, Eq. – equipment

On the given example (Fig. 2, *b*) the way of achievement of demanded parameters at the expense of parallel work of cooling tower is considered. It is worth to note that for achievement of demanded parameters of cooling also is applied consecutive cooling of water in cooling towers when all chilled water from one cooling tower pumps to the second one. As well as in case of parallel work of cooling towers, consecutive cooling does not allow to reach the temperature of chilled water below the temperature of the wet bulb thermometer. Refrigerators and chillers are applied to cooling of water below the temperature of the wet bulb thermometer. Our theoretical calculations [6] show that the temperature of chilled water below the temperature of the wet bulb thermometer can be reached in vacuum cooling towers.

Numerical calculations were performed using the above mathematical model (2)–(6). The calculated dependence of the cold water temperature leaving the cooling tower T_{wf} versus the wet bulb temperature T_{lim} for two values of air velocities is shown in Fig. 3. The dependence in Fig. 3 was obtained at constant hot water temperature entering the cooling tower T_{w0} = 35 °C, water flow makes 50 m^3/h, curve 1 – is for air velocity v_{a} = 1 m/s, curve 2 – is for air velocity v_{a} = 2 m/s. The air flow makes correspondently 25 000 m^3/h and 50 000 m^3/h.

As it is seen from Fig. 3 the temperature of cold water, leaving the cooling tower T_{wf}, is 4–5 °C above the temperature of the wet bulb thermometer T_{lim} at air velocity v_a = 2 m/s, and T_{wf} is 8–10 °C above T_{lim} at air velocity v_{a} = 1 m/s. Depending on air velocity the water temperature drop in our calculations is 6–10 °C.

Thus we can reach the same results by means of increasing water flow or air flow. The described above cooling tower parameters can be produced by additional air flow created by fan with electrical power 6 kWt or water pump with power 7,5 kWt.

Taking into account mathematical model (2)–(6) and equation (1) effective cooling towers with required parameters at minimal energy consumption can be developed for various hydraulic and thermal loads.

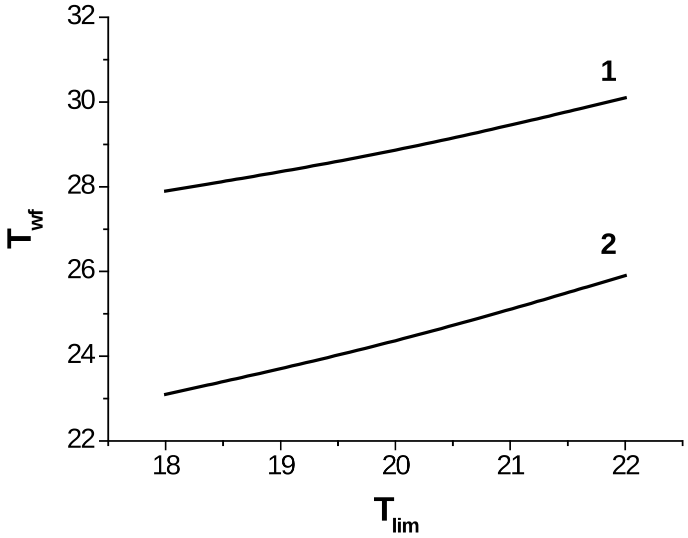

Fig. 3. Calculated dependence of the cold water temperature leaving the cooling tower T_{wf} versus the temperature of the wet bulb thermometer T_{lim} for two values of air velocities: curve 1 – is for air velocity $v_a = 1$ m/s, curve 2 – $v_a = 2$ m/s

4. CONCLUSIONS

The results obtained facilitate the development of a novel method of improving the efficiency of water cooling in circulating water cycles with cooling towers. Cooling tower circuit can be effective if required parameters are produced at minimal energy consumption. It is shown, that the cooling tower which is not effective enough allows to provide demanded parameters of a circulating water cycle, using a new scheme of water cooling (Fig. 2, *a*).

In considered cooling tower circuits required parameters were reached by increasing of water and air flows. Energy consumptions for water and air flow increasing were compared. It was shown that air flow can be increased at lower energy consumption than corresponding water flow. With the increase of air flow in two times the cooling tower efficiency increases by 20–40 % depending on atmospheric conditions. Effective cooling tower should be designed taking into account the hydraulic and thermal loads.

REFERENCES

1. SOLODUKHIN, A.D.; FISENKO, S.P.; PETRUCHIK, A.I. Simulation of cooling of water droplet and film flows in large natural wet cooling towers. *Inzh.-Fiz. Zh.*, 2001, Vol. 74, No. 1, p. 45–49.
2. FISENKO, S.P.; PETRUCHIK, A.I.; SOLODUKHIN, A.D. Evaporative cooling of water in a natural draft cooling tower. *Int. J. Heat Mass Transfer*, 2002, Vol. 45, p. 4683-4694.
3. ЖУКАУСКАС, А.А. Конвективный перенос в теплообменниках. М.: Наука, 1982, c. 472. (in Russian)
4. BRIN, A.A.; PETRUCHIK, A.I.; FISENKO, S.P. Mathematical modeling of evaporative cooling of water in a mechanical-draft tower. *Inzh.-Fiz. Zh.*, 2002, Vol. 75, No. 6, p. 68–73.
5. БРИНЬ, А.А.; ПЕТРУЧИК, А.И. Тепловой расчет эжекционной градирни и способ повышения ее эффективности. *Инж.-физ. Журн.*, 2011. Т. 84, № 2, с. 270-273. (in Russian).
6. PETRUCHIK, A. I.; FISENKO, S. P. Simulation of low air pressure cooling tower. 15th International Association Hydraulic Research Symposium in Cooling Tower and Heat Exchangers, Beijing, China, 23–26 October, 2011, p. 159-161.

CYSENI 2012, May 24–25, Kaunas, Lithuania
ISSN 1822-7554, www.cyseni.com

RESEARCH OF VISCOSITY INFLUENCE TO CORIOLIS MASS FLOWMETERS FLOW RATE MEASUREMENT ACCURACY

E. Maslauskas, M. Kulokas
Lithuanian Energy Institute
Breslaujos str. 3, LT-44403 Kaunas – Lithuania
Phone +370 37 401864
Email: maslauskas.e@mail.lei.lt, kulokas@mail.lei.lt

ABSTRACT

Coriolis mass flow meters used commonly in high-accuracy liquid flow measurement systems. However some issues are raised, which related with different effects to the flow meter measurement accuracy. One of such question: how fluid viscosity affects metrological characteristics of Coriolis flow meters. These and othere tasks carried out by using water and working fluid with reference devices.

Stationary reference flow facilities for testing the flowmeters were developed and also operated at LEI using water or Exxsol. Measurements with other liquids are performed in the places, where liquids accounting systems are installed. It is advisable to use the portable reference facilities (the standard volume) for these measurements. However, the use of standard volume determines requirements of stability environment conditions, liquid and atmosphere temperature equability. For laboratory research of flowmeters with any viscosity fluids was developed flow facility. Only the flowmeters flow resistance is limited using of high viscosity fluids.

The measuring facility and its functioning are described in this paper. Also was calculated experimental measurements spread and uncertainty. Experimental studies of the Coriolis meters are performed using different viscosity liquids. Studies are showed, that the mass flow CMF errors using different viscosity fluids varies quite in narrow range, but it must be taken, that by measuring of the volume flow the viscosity depends on the measurement of density also. Thus, the combined measurement error in some cases may be higher than permissible error.

Keywords: Coriolis flow meter, test facility, viscosity, density measurement, liquids other than water, flow

1. INTRODUCTION

For measurement various fluids flows are used rotary vane, turbine and Coriolis mass flow meters (CMF). The Measuring instruments are selected taking into the type of fluid, its viscosity, the terms and conditions of use and the required measurement accuracy.

Fluid density and viscosity are physical properties, having greatest influence and in practice affecting the measurement accuracy of the fluid and widely considered in the literature. Others source of measurement errors are usually air/gas bubbles, comprised in the fluid metering section (two-phase flow), various pulsations, which generate mainly the vibrations of the measuring device or the line, or environmental factors.

In the long time of measurement devices operation, the increasing of measurement error is the result of aging of electronic components, mechanical wear, fatigue mechanical elements and other causes. To prevent using of non-compliant devices, each of them must be verified in fixed time intervals. Often the verification of measurement system carried out in two steps: the measurement system components verificated individually (partial verification) and afterwards carried out complex verification. In this case, the reference device must be movable. The measure is the most common reference measuring tool, used for measuring reference volume. However, their using is associated with considerable transportation costs, the significant increasing of measurements uncertainty, concerning difference of environment and fluid temperatures and its change. Coriolis mass flow meters (CMF) using as a portable reference device, would solve these problems.

A very important feature of CMF is universality and the ability to measure the liquid and gas flow when the density and viscosity is very different. Stappert [1] and O'Banion in [2] reviewed the performed studies which justify allowing the using of CMF for natural gas accounting, here arisen problems and pointed out the basic requirements for the using of CMF gas accounting. As one of the main advantages of CMF is a relatively small change of the errors between the calibration with gas and with water, but the CMF density measurement accuracy is not enough for accurate measurement of gas volume. Therefore measurement of gas flow with CMF required density measuring devices, providing to the CMF information about gas density.

For low flow measurement with CMF the phase stability is very important when changing external factors. Phase difference can occur in the absence of flow (q = 0). Therefore CMF record flow, which can be described as "zero flow". The source of zero phase shifts are various: from the sensing tube manufacturing tolerances to external influences (temperature changes, mechanical stress, etc.). In [3] it is reviewed the causes of zero phase shift and importance of its removal. Experiments were performed with some "U" type CMF sensors and proved the assumption that in the sensors, influenced with additional mass, temperature and vibration damping, emerges additional phase shift effect, when CMF is registered additional flow rate. This study show, how some imperfections, caused in the production or operation time, can affect to the CMF sensor readings. Performed "zero correction" by stopping the flow of the pipeline partly allows avoiding this zero shift. But, the change of the conditions can occur of the phase difference again.

However CMF is relatively new device and despite of many studies, needed to explore of many factors influence to CMF. One of the questions is: how fluid viscosity influences to fluid volume and mass flow measurement accuracy. At low Reynolds numbers (Re) CMF reading may deviate under the influence of fluid-dynamic forces. In Kumar performed research [4] is showed the relationship between this deviation and Reynolds number by using numerical simulation. He explained this effect by a periodic shear mechanism, which interacts with the oscillatory Coriolis. The assumption, wich identify by using the numerical simulation, where confirmed in experiments with diferent viscous liquids. Nine DN250 size PROMASS meters were used as experiment objects. But in this research the operating of CMF was limited in the lower range of Re > 800 and only partially fills this gap. In this case it is interesting for us the operation of smaller size CMF.

Therefore the aim of this study is fluid viscosity effect to the accuracy of flow measurement with CMF in small Re, and justifying an universal method for calibration and verification of accounting fluid measurement systems.

2. METHODS AND EQUIPMENT OF RESEARCH

For experimental studies is used two curved tube "U" type CMF. It nominal diameter of the inlet is DN15, the sensing tube diameter d_{in} = 8 mm, a working temperature range is -50 to +200 °C and maximum pressure is 4 MPa. It is performed the research of higher nominal flow (DN80 and d_{in} = 40.5 mm) and the same type CMF with ethanol at installation place and with water at stationary laboratory facility. Detailed characteristics of the CMF are in [5]. The maximum permissible error of device:

$$\delta_{\max} = \pm 0.10\% \pm \frac{q_0}{q} 100\%, \tag{1}$$

here q_0 = 0.325 kg/h for DN15 device – zero point stability, q is flow rate.

The investigation was performed in low flow using water ($\nu \approx 1$ mm/s^2) and silicone oil. Experimental liquid viscosity and density was measured using a laboratory viscosity and density meter SVM3000 (density measurement accuracy $\Delta\rho = \pm$ 0.0005 g/cm^3 and viscosity $\delta_\mu = \pm 0.35$ %).

The facility for testing flow meters with viscous liquids has been specially designed and manufactured, because the fluid viscosity varies in a broad range and usually testing facility becomes unsuitable, where the liquid is forced to move with the pump. Therefore it is selected another way to make flow. The compressed air presses experimental liquid from the tank through the metering section. Primary tank is changed together with working fluid to accelerate and simplify change of liquid at facility.

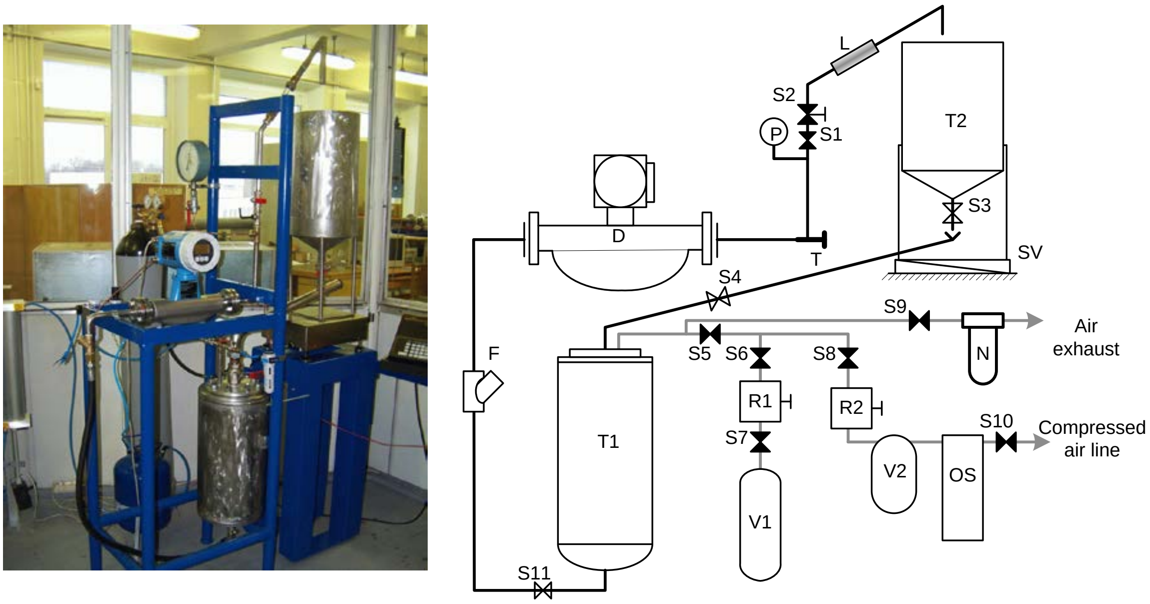

Fig. 1. The research facility of CFM with various viscosity liquids

Compressed air is supplied through a valves S5, S6, S7 from the air cylinder V1 (up to 15 bar) or S5, S8 and S10 (up to 8 bar) from the compressed air line through humidifiers OS and pressure vessel V2. The pressure in the main tank T1 makes the liquid flow through the filter F, CMF D and the temperature and pressure measuring unit T, P to open weighing tank T2. Here the liquid is weighed, recalculated by mass or volume and compared with CMF measured mass or volume. Measurement begins and finished with the opening and closing the valve S1. It is regulates pressure and flow rate with valve S2. The working pressure is determined by R1 reducer, if required pressure above 8 bar, or R2 if less 8 bar. The weighed on the scales liquid is returned to the operating tank T1 through the valves S3 and S4. Theretofore the air is released through the cesspool N and opened valve S9.

Mass flow measurement uncertainty was calculated according to expression:

$$\mathrm{M_e} = k\cdot(M_e\cdot(1+dM_t\cdot(t_o-20+dt_o))+M_d+M_a+M_t+V_{ts}\cdot\rho_s+M_g)\,. \tag{2}$$

Here k is air buoyancy, M_e is reading of the scales, dM_t is the scales correction for zero drift, t_o is the ambient temperature, dt_o is ambient temperature change, M_d. is correction of the balance discretion, M_a is correction of instrument repeatability, M_t is correction for the nonlinearity of the balance, V_{ts} is change in volume of the liquid line after CMF for the thermal expansion, ρ_s is liquid density in scales, M_g is correction for the liquid evaporation and splashing.

Buoyancy coefficient k is given by

$$\mathrm{k} = \frac{1-\dfrac{\rho_o}{\rho_{sv}}}{1-\dfrac{\rho_o}{\rho_s}}\,, \tag{3}$$

here ρ_o is density of air, ρ_{sv} is density of scales weight, ρ_s is density of liquid.

Air density is calculated by the formula:

$$\rho_o = \frac{3.4844 p_o + \varphi_o(-0.00252 t_o + 0.026582)}{t_o + 273.15}, \tag{4}$$

here p_o is atmosphere pressure, φ_o is air humidity, t_o is air temperature.

Table 1. Calibration measuring possibility of test facility.

Parameter	Value	St. Uncertainty X_i	Distri-bution	Weighing coefficient W_i	$W_i^2 \cdot X_i^2$
Reading of the scales M_e, kg	8.0	3.0E-04	Normal	1.001	9.02E-08
Scale discretion M_d, kg	0	5.0E-06	Uniform	1.001	2.51E-11
Linearity M_t, kg	0	6.0E-05	Normal	1.001	3.61E-09
Temperature zero drift dM_t, 1/°C	0	2.0E-06	Normal	20.0	1.60E-09
Repeatability M_a, kg	0	1.0E-05	Normal	1.001	1.00E-10
Environment (air) temperature t_o, °C	20.0	0.1	Normal	-2.89E-05	8.32E-12
Environment (air) temperature change dt_o, °C	0	0.5	Uniform	-2.89E-05	2.08E-10
Air humidity φ, %	45.0	1.0	Normal	-5.70E-09	3.25E-17
Atmosphere pressure P_o, kPa	101.3	1.0	Normal	8.34E-05	6.96E-09
Air density ρ_o, kg/m^3	1.204	0.018	Normal	7.02E-03	1.60E-08
Liquid evaporation and splashing M_q, kg	0	1.0E-04	Normal	1.001	1.00E-08
Pipe thermal expansion, V_{tv}, m^3	0	6.7E-08	Normal	1.001E+03	4.45E-09
Liquid density ρ_s, kg/m^3	999.8	0.25	Normal	-9.66E-06	5.78E-12
M_{water} = 8.009 kg				U_{st}, kg	0.00036
				U_{ex}, kg	0.0007
				U_{ex}, %	0.009
M_{water} = 4.005 kg				U_{st}, kg	0.00034
				U_{ex}, kg	0.0007
				U_{ex}, %	0.017
$M_{silicone\ oil}$ = 8.009 kg				U_{st}, kg	0.00037
				U_{ex}, kg	0.0007
				U_{ex}, %	0.009

In Table 1 presents the calibration measuring possibility of the facility for the water or silicone oil of mass 8 and 4 kg. The calculations are performed for only one type of silicone oil, because their densities are very similar and the evaporation component already becomes negligible to the lowest viscosity oil.

Analogous to [6], using in table 1 presented data, it were performed calculations by Monte-Carlo method, to determine the expanded uncertainty and output distribution. These calculations performed using specialized computing package „MATLAB" and [7]. For this data analysis was selected the number of iterations ($N = 10^6$). In the finally, the output result distribution is similar to normal distribution.

3. EXPERIMENT RESULTS

Investigations were carried out using water, two viscous silicone oils and a mixture of oils in changing the liquid viscosity in increasing and decreasing sequences. After each fluid replacement was performed the zero correction. The results were analyzed considering to the Reynolds number, which calculated in accordance to average speed in tube and its diameter value. At 2300 <*Re* <4000 flow regime was considered to meet the transition from laminar to turbulent regime. However, it remains an open question due to the effects of vibration on the flow regime changes. Therefore it is needs to perform additional resistance regularity analysis, it relating with flow in vibrating tube of CMF. Mass flow measurement errors curves of different viscosity fluids are presented in Fig. 2 and Fig. 3. From Fig. 2 shows that the at low viscosity (water flow) mass flow rate measurement errors is close to 0 and remains a fairly constant regardless of that, the fluid flow profile approaching to laminar according to *Re*.

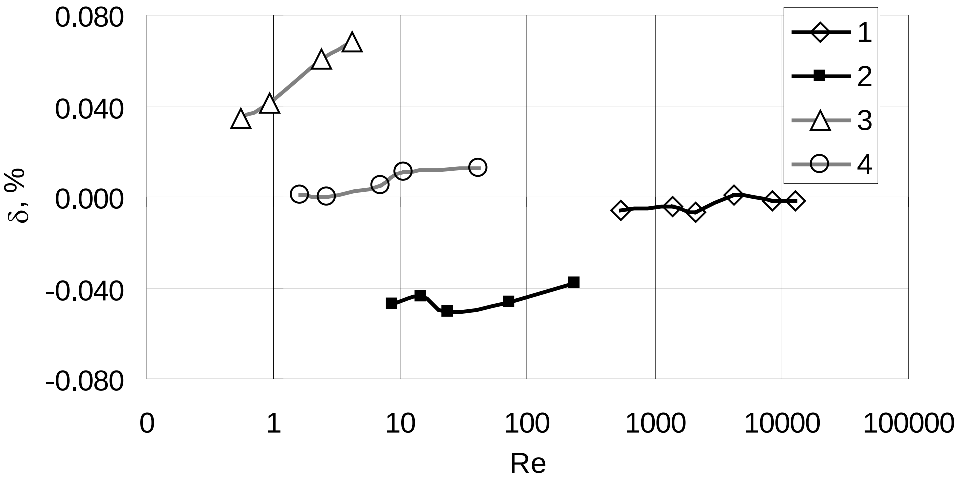

Fig. 2. Change of CMF errors according Re_d (p = 6,5 bar) at 1 – water ($\nu \approx$ 1,0 mm/s^2), 2 – silicone oil DOW CORNING ($\nu \approx$ 60 mm/s^2, $\rho \approx$ 0.97 g/cm^3), 3 – silicone oil MOLYDUVAL SYLO D/500 ($\nu \approx$ 600 mm/s^2, $\rho \approx$ 0.97 g/cm^3), 4 – mixture of oils ($\nu \approx$ 200 mm/s^2, $\rho \approx$ 0.97 g/cm^3)

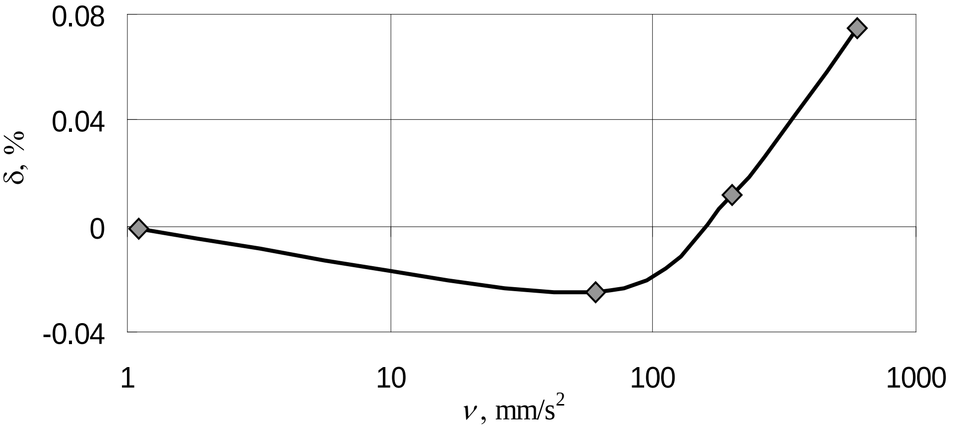

Fig. 3. Errors of CMF mass flow rate readings acording viscosity change, when q_m = 0.2 m^3/h

However, in the beginning at increasing viscosity and decreasing Re_d, the errors comes negative, but further it is observed quickly evolution of positive values. This variation is correlated with the character of the resistance coefficient change in channels. It means this, that at high viscosity and laminar flow, CFM indicates flow rate higher than it is actually. The response of the tube to Coriolis forces changes with approaching to the transition flow regime and with formation of vortex structure. In the fully evolved turbulent flow vibrations do not influences to the flow structure.

In Fig. 3 showed character of change errors in viscosity axis ν, when flow rate is q=0.2 m^3/h. This flow rate is maximal using MOLYDUVAL SYLO D/500 ($\nu \approx$ 600 mm/s^2). Such character of errors change is in others flow rates.

In the experimental facility it was not possible research of high nominal flow CMF. Therefore similar type meters were tested in the laboratory facility and at operating conditions. In the first case, the two CMF was measured with water mass flow in laboratory facility, using weighing method, in the second case, measure was determined with ethanol ($\nu \approx$ 1.5 mm/s^2) at operating conditions in ethanol factory, using direct volume measuring method. Measurement results are presented in Fig. 4. It appears that both meters characteristics are different, which can be explained by the inequality of CMF. However, both characteristic clearly shifted downward at measurements in installation place, compared with measurements, performed in the laboratory with water.

This difference can be explained by the following reasons:

- installation conditions;
- weighing and volume measuring methods differences;
- differences in fluid viscosity.

However, the first two reasons are most likely.

It leads to the conclusion that after installation in the workplace it is needed to verify to understand measurement errors and if necessarily, to introduce correction. It is also necessary to carry out such inspections and monitoring and if needed, to reduce the time between calibration or verifications.

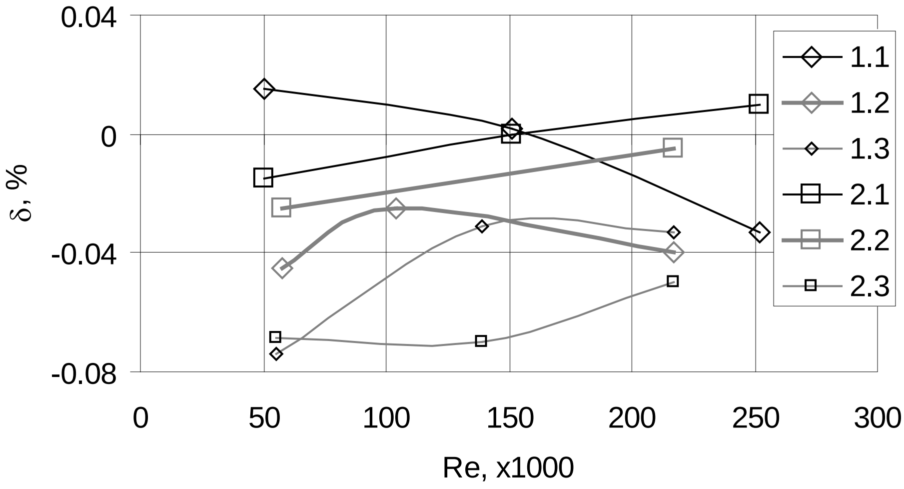

Fig. 4. CMF errors at measuring in laboratory with water and in operating place with ethanol: 1.1 and 2.1 – water flow measuring errors; 1.2 and 2.2 – ethanol flow measuring errors; 1.3 and 2.3 – ethanol flow measuring errors after 6 months.

Also it was carried out measurement with compressed natural gas (CNG) flow at filling automotive cylinders. Compressor was fed compressed gas to 200 bar into the cylinder, which has been weighed before and after the measurement. CMF readings are compared with the reading of scales. The test was performed to filling to the empty cylinder and filled from starting pressure 100 bar. Here we have the influence, which related with high pressure gradients and its quick change.

From authors performed investigation [8] at compressed natural gas filling station, it is proved earlier published [1] and [2] proposition, that it is suitable for CNG flow measurement with CMF, which were calibration with water.

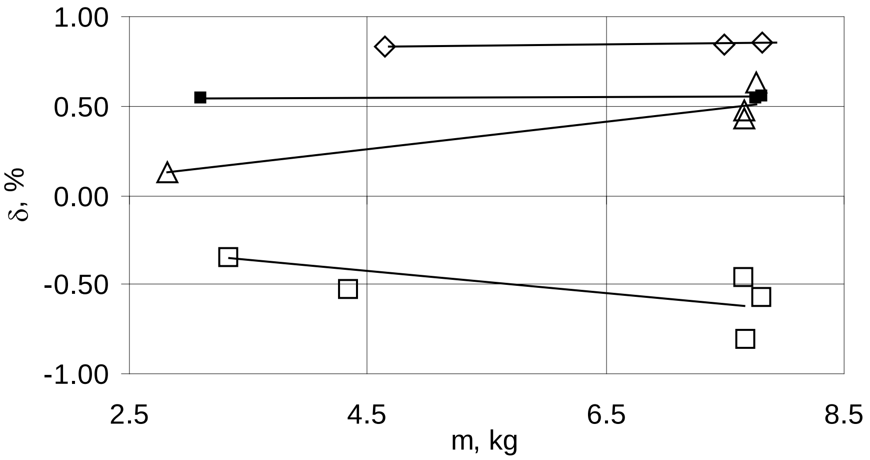

Fig. 5. Errors of compressed natural gas measurements with CMF at gas station. Filled weight $m \approx 4$ kg (equivalent to $p_0 = 100$ bar) and $m \approx 7$ kg (equivalent to $p_0 = 0$ bar)

In Fig. 5 you can see, that with change of pressure and herewith viscosity in large ranges, errors of all measurements not exceed maximal permission error ($\delta_{max} = \pm 1$ %). But it is seen significant approach of errors to decreasing tendency, when pressure drop is smaller, i.e. when flow starts from pressure $p_0 = 100$ bar.

4. CONCLUSIONS

1. CMF mass flow errors of measurement with different viscosity (1 ÷ 600 mm/s^2) liquids, varies quite in the narrow range (for the particular CMF from -0.03 % to +0.07 %), but clearly is visible influence of small Re.
2. Volumetric flow rate is measured with the lower accuracy concerning the density measurement errors variation. Therefore, using CMF for liquid volume accounting systems calibration – verification as the reference device, it is necessary to take attention into the fluid viscosity.
3. For the more significant measuring systems with CMF, is useful monitoring of periodic calibration and if necessary the change of calibration period.

5. REFERENCE

1. Stappert K. Coriolis mass flow meters for natural gas measurement. Link to the internet <http://www.documentation.emersonprocess.com>.
2. O’Banion T., Stappert K. Fundamentals of Coriolis meters (for gas measurement). American school of gas measurement technology. Link to the internet <http://www.asgmt.com/infostore/onlinepapers>.
3. Enz S., Thomsen J.J., Neumeyer S. Experimental investigation of zero phase shift effects for Coriolis flowmeters due to pipe imperfections. Flow Measurement and Instrumentation, 2011, Vol. 22, issue: 1, p. 1–9.
4. Kumar V., Anklin M. Numerical simulations of Coriolis flow meters for low Reynolds number flows. Journal of Metrology Society of India. 2011, Vol. 26, No.3, p. 225–235.

5. Coriolis Flow Measuring System Promass 80/83 F, M. Technical Information TI 053D/24/ae. Endress+Hauser. Link to the internet <http://www.amjequipment.com/eh/Flow/Coriolis%20Mass.htm>.
6. Maslauskas E., Bončkus A. Evaluation of water volume and flow rate measurement capabilities by reference facility. 7th annual conference of young scientists on energy issues CYSENI 2010, Proceedings of annual conference of young scientists on energy issues. [CD]. Kaunas: Lithuanian Energy Institute. 2010 May 27–28.
7. ISO/IEC Guide 98-3/Suppl.1:2008. Propagation of distributions using a Monte Carlo method.
8. Kulokas M., Maslauskas E. Research of viscosity influence on the density measurements 8th annual conference of young scientists on energy issues CYSENI 2011, Proceedings of annual conference of young scientists on energy issues. [CD]. Kaunas: Lithuanian Energy Institute. 2011 May 26–27.

CYSENI 2012, May 24–25, Kaunas, Lithuania
ISSN 1822-7554, www.cyseni.com

THE METHOD OF SYSTEMATICAL EVALUATION OF THERMAL RADIANT INFLUENCE ON THE INTERACTION OF UNSTEADY HEAT AND MASS TRANSFER PROCESSES OF EVAPORATING DROPLET

K. Norvaišienė, G. Miliauskas
Kaunas University of Technology
Department of Thermal and Nuclear Energy
K. Donelaičio str. 20, Kaunas, LT-44239 – Lithuania
Phone +370 37 300437
Email: kristina.tiuksaite@stud.ktu.lt

ABSTRACT

Investigation of unsteady heat and mass transfer processes transition to equilibrium evaporation state which is characteristic under experimental investigation for water droplets heated by conduction and thermal radiation using the hypothetical droplet model was provided. Modeling is performed using the combined analytical – numerical method. The universality of fluxes change on droplet surface which underlies assumption for describing of droplet thermal state and phase change parameters by characteristic curves depending on time expressed by Fourier number. Results of investigation compared with experiment results of other authors.

Keywords: water droplet, thermal radiation, interaction of transfer processes.

Nomenclature: a - thermal diffusivity (m^2/s),
I - index of control time,
L - latent heat of evaporation (J/kg),
m_v - vapour mass flux density ($kg/ m^2\ s$),
n - number of the term in infinite sum,
q - heat flux (W/m^2)
r - coordinate of a droplet (m),
R - radius of a droplet (m),
R_{ii} – dispersity of droplets,
T - temperature (K),
η - non-dimensional droplet coordinate,
λ - thermal conductivity (W/m K),
P- heat and mass transfer parameter of droplet
t - control time (s), τ - time (s),
Subscript
C – droplet centre, c – convective,
co – condensation regime,
e - equilibrium evaporation regime,
g - gas,
vg - vapor-gas mixture,
i - time index in a digital scheme,
I - index of control time,
j - index of droplet cross-section,
J - index of droplet surface,
k – conductive,
R - droplet surface, r – radiative,
m - mass average,
s – saturate,
Σ – total,
f - phase change.
Superscript
+ External side of a surface, - internal side of a surface.

1. INTRODUCTION

Liquid injection is widely applied in modern thermal technologies, the efficiency of which depends on intensive heat and mass transfer processes of dispersed liquid and highly developed contact surface between liquid and gas phase. Liquid hydrocarbons, their mixtures and water are among the most widely used liquids. The evaporation rate of hydrocarbon droplets decides the process of liquid fuel combustion. Water, which is naturally dispersed into droplets, is met in natural phenomena, whilst artificially dispersed water is applied in thermal regulation systems, the processes of air conditioning, mixture evaporation, fuel combustion, gas compression [1], etc. In order to ensure optimal run and further development of energy and industrial technologies under acceptable long-term economical, social and environmental conditions, it is necessary to know and control thermo-hydro-mechanical processes in these technologies.

The interaction of heat and mass transfer processes determines the thermal state of droplets and phase transformations on their surfaces. This interaction is influenced by many factors: unsteadiness of transfer processes; the Stefan's hydrodynamic flow; radiative flow absorbed in semitransparent liquid; temperature and pressure drops in the Knudsen layer; the size of droplets and slipping of droplets in gas; turbulence of a two-phase flow surrounding droplets, etc. In scientific literature these factors are evaluated by researches which are known as the "droplet problem". The history of theoretical and experimental investigations counts more than one hundred years [2], though the "droplet problem" still remains urgent due to the above-mentioned necessity to recognize regularities of combined heat and mass transfer in two phase flows. The experimental and theoretical researches methods of droplet evaporation are studied in detail and systematically in the paper [3].

From all mentioned factors, the thermal radiant flow is the factor whose influence on evaporating droplets to calculate is the most difficult. During the earlier investigations of sprayed liquid systems, the influence of thermal radiation flow on transfer processes was not taking into account. A semitransparent liquid droplet absorbs the radiation energy by its entire volume. This process is very complicated because it is determining by the variable intensity of spectral radiation flow inside the droplet. The thermal radiation affects the process of droplets heating and evaporation and influences the interaction of transfer processes inside and outside the droplet. Modeling the sprayed liquid systems it is not possible to neglect interaction of the transfer processes. In the paper [4] for the first time was presented that radiation absorption can significantly distort temperature field in a semitransparent liquid droplet and even change the direction of temperature field gradient. The spectral radiation field inside semitransparent liquid droplet can be calculated using the geometrical optics or the electromagnetic wave theory and is discussed in [5]. This work have the practical importance, the results of this investigation shows that, the effect of radiation absorption by a droplet is to cool the ambient atmosphere and can control the fire by water sprays. The influence of spectral radiation on heat and mass transfer interaction of semitransparent liquid droplets is not enough investigated, although the optical characteristics of many liquids are known [6, 7]. Detailed combined analytical and numerical research methods for the "droplet" problem are presented in [5, 8]. Comparison of the theoretical and experimental results is urgent for the reliability of the "droplet" models and practical use of their results. But the experimental research of heat and mass transfer of evaporating droplet in radiant medium are complicated and very few. The experiments of V. Ivanov and E. Smirnova [9] can be considered as exclusive ones. The authors investigated the rate of equilibrium evaporation of water droplets heated by air conductivity and radiation from hot wall. The experiments were performed with large water droplets, evaporating in equilibrium conditions in the dry air. The constancy of droplet size was ensured by a special capillary system and the authors stated that maximal error of droplet evaporation rate did not exceed 5%. This work is performed applying a model of a hypothetical droplet, similarly to the mentioned case of experimental research [9] and using the combined analytical and numerical methods [8, 10, 11], when numerical simulation schemes of unsteady evaporating droplets are concluded for algebraic-integral equations of the system. This system is resulting from analytical restructuring of an droplet heat and mass transfer differential equations based on the initial assumption that in translucent droplets takes place the composite heat transfer by conduction and radiation. In this paper is presenting work of the systematic evaluation of the transformation of heat and mass transfer processes from unsteady to equilibrium case, as droplet is heated by radiation and conduction and its diameter remains constant during the evaporation process.

2. ANALYTICAL-NUMERICAL METHOD OF INVESTIGATION

In the models of combined methods for analytical and numerical “droplet problem” research the schemes of non-stationary temperature field are being constructed not for the primary systems of differential and integral equations, but for its solutions – the system of algebraic and integral equations. The main advantages of this method are avoidance of the indeterminacies, related to the selection of time and coordinate steps and reliable control of numerical research convergence. To make a reach for numerically repeat of boundary conditions in work [9] the model of hypothetical droplet was applied using droplet with physical properties of water and with surface source of mass, when the source secures volume stability of heating and evaporating droplet.

The temperature of the interphase contact surface is determined when there is a balance of the energy flux’s taken to the surface and taken from the surface of droplet.

$$\vec{q}_{\Sigma}^{\,+}(\tau)+\vec{q}_{\Sigma}^{\,-}(\tau)+\vec{q}_{f}^{\,+}(\tau)=0 \tag{1}$$

In the case of combined heat transfer in a droplet by conduction and radiation, the unsteady temperature field (2) in a spherically – symmetrical droplet is defined by the method [8] which takes into account influence of radiation absorption peculiarities in a semi-transparent droplet and the rate the droplet’s surface temperature change:

$$T(r,t)=T_R(t)+\frac{2}{r}\sum_{n=1}^{\infty}\sin(n\pi\eta)\int_{0}^{t} f_n(\tau)\exp\left[-a\left(\frac{n\pi}{R}\right)^{2}(t-\tau)\right]d\tau. \tag{2}$$

The function f_n takes into account the influence of the radiant absorption in a droplet and the rate of change of droplet surface temperature on the unsteady temperature field of a droplet. Radiation flux is calculated using the method described in [12].

The conductive component is determined by the gradient of temperature field in the droplet, described by expression (2):

$$q_k^{-}(\tau)=-\lambda(\tau)\left.\frac{\partial T(r,\tau)}{\partial r}\right|_{r\equiv R^{-}} \tag{3}$$

The density of heat flux of phase transformations:

$$q_f^{+}=m_v^{+}\cdot L \tag{4}$$

Is determined by the density of water vapor flow on the droplet surface, which is described by using the Shorin-Kuzikovsky model [12], which evaluates the influence of the Stefan flow on the mass transfer.

As a droplet is carried by gas flow without slipping, the intensity of stagnate water droplet conductive heating is calculated for $Nu\equiv 2$, additionally evaluating the influence of the Stefan’s hydrodynamic flow [13]:

$$q_k^+(\tau)=\frac{\lambda_{vg}(\tau)}{R}\left[T_g-T_R(\tau)\right]\cdot\frac{\ln\left[1+B_T(\tau)\right]}{B_T(\tau)} \tag{5}$$

The function of the Spalding transfer number (B_T) (6) evaluates the influence of hydrodynamic Stefan flow:

$$B_T(\tau)=\frac{c_{p,vg}(\tau)\left[T_g-T_R(\tau)\right]}{L(\tau)}\cdot\left[1+\frac{q_k^-(\tau)}{q_k^+(\tau)}\right] \tag{6}$$

The Nusselt number (*Nu*) for a droplet is described by Abramzon-Sirignano model, as Spalding transfer number is selected using the recommendations presented in [11].

Size of a droplet and temperature of sprayed liquid are predicted for the initial conditions of heat and mass transfer. As temperatures of a radiant source and gas are selected and volumetric part of liquid vapor in gas is predicted, the parameters of the droplet’s surrounding are determined. When modeling evaporation of a single droplet, the parameters of surrounding are set to be constant.

For a “hypothetical” droplet with constant volume is being applied an additional condition:

$$\frac{dR(\tau)}{d\tau}\equiv 0. \tag{7}$$

Equations (1-7) can be solved numerically, by the iteration method. Using this method number *J* of a control droplet cross-section is selected freely; the position of the cross-section is defined by dimensionless droplet coordinate η_j ($\eta_j=0$ when $j\equiv 1$; $\eta_j=1$ when $j\equiv J$). Control time *t* is selected and number *I* of time coordinate change steps is provided ($\tau=0$ when $i\equiv 1$; $\tau=t$ when $i\equiv I$). The thermal state of water droplets, convectively heated by gas and influenced by radiant energy source is calculated numerically, solving the equation (2), as temperature of a warming droplet surface is selected using the method of the fastest descent, requiring accuracy of the balance (1) to be not less than one hundredth percent. Gauss method is used, when expression is integrated according the incidence angle of light beam. The spectrical optical characteristics of the water were taken according [6] recommendations.

3. RESULTS AND DISCUSSION

Warming and phase transformations of water droplets heating are modelled using the numerical method, when neglecting slipping of droplet in the dry air of temperature $T_g(\tau)=const$. Conductive heating is determined by the difference between temperatures of air and droplet’s surface and in the case of combined heating the spherical wall having the air temperature and emissivity equal 0.95 radiates additionally.

Systematic evaluation of the interaction requires researching of heat and mass transfer processes during the cycle of a droplet lifetime: from water injection until the moment when the droplet evaporates out completely. One can predict a number of characteristic time instants, during which essential qualitative changes in the mode of phase transformations and peculiarity of heat exchange occur. Usually they are shown in real time: $0\div\tau_{co}\div\tau_e\div\tau_f$. In such case, as the change of the thermal state of conductively heated droplet is indicated in time scale, we get a number of curves, which show the change of the state of conductively heated droplet in regards to its diameter (Fig. 1 a), when $T_o\,(R_{ii})=const$. In the case, when is seeking the commonality – the characteristic lifetime of heated droplets, expressed by Fourier number - scale time: $0\div Fo_{co}\div Fo_e\div Fo_f$ (Fig. 1 b), we get characteristic curves, which show the change of the thermal state of conductively heated droplet, when $T_o\,(R_{ii})=const$ and not depend on droplet diameter *R*, (Fig. 1 b, curves 4-6).

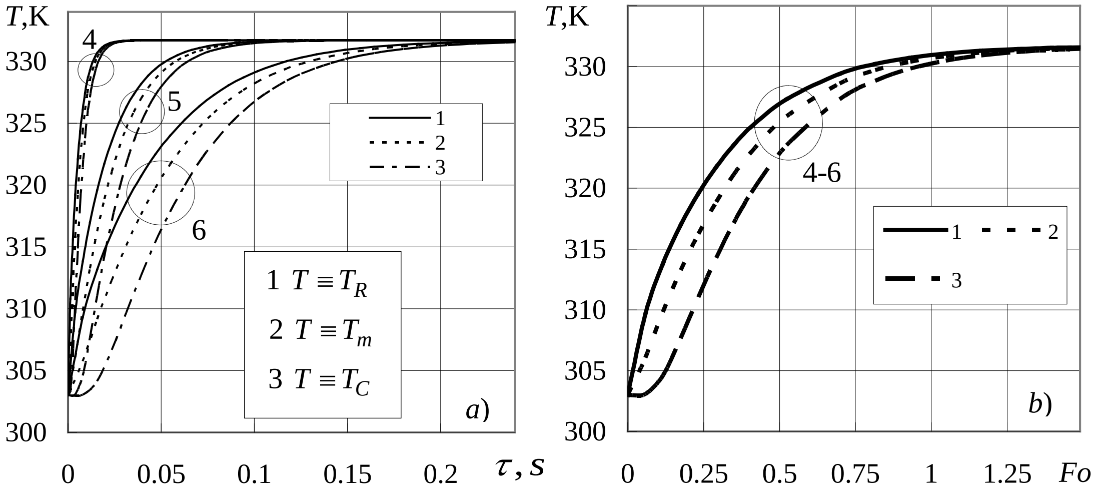

Fig. 1. Variation of conductively heated water droplet thermal state in real time (*a*) and in Fourier number based time duration (*b*). $R \cdot 10^6$, m: (4) 50, (5) 100, (6) 250; T_g=873K; T_0=303K.

In the case, when $T_o\,(R_{ii}) \neq const$, droplets' heating is convenient to analyze in time scale expressed by Fourier number [14]: $0 \div Fo_{co,k} \div Fo_{e,k} \div Fo_{f,k}$, is described by the characteristic curves, which reflect dynamics of the phase transformation and thermal state parameters of water droplets, independent of the sprayed liquid dispersity. This characteristic lifetime of droplets combines the three modes of droplet phase transformations [15]: the first one - condensation mode of phase transformations $0 \div Fo_{co,k}$; the second mode of unsteady evaporation $Fo_{co,k} \div Fo_{e,k}$ and an equilibrium evaporation mode, which actually starts, when entire heat supplied to the droplet is used for evaporation of water. At the time instant $Fo \equiv Fo_{co,e}$ droplets warm up till temperature $T_{e,k}$, which ensures the mode of equilibrium evaporation. In the third mode of phase transformations the temperature $T_{e,k}$ remains constant.

A reference study showed that the widest researches were performed in equilibrium evaporation mode; radiation was neglected when examining the condensing mode. Recently unsteady evaporation is more and more interesting for researchers, though systematic evaluation of unsteady process interaction is still missing.

The influence of heating conditions on the thermal state of droplets and phase transformations can be evaluated using a comparative method, gradually approaching towards more complicated boundary conditions of heat and mass transfer. Therefore, a well-examined case of droplet heat exchange is necessary. Such case can be the following: the droplets are heated by conduction, the influence of radiation and natural as well as forced convection are neglected. Heating and evaporation processes of conductively heated water droplets are thoroughly researched and they distinguish themselves in many properties, which are convenient for comparative analysis. These properties are revealed, as the curves, which show the change of heat and mass transfer parameters, are presented in Fourier number based time scale.

Then, the change of thermal state can be represented by the characteristic curves (Fig. 1 b), which couple warming of all larger droplets heated by conduction (in this case, the influence of the Knudsen layer can be neglected) in the cases defined by water's initial temperature (Fig. 2). In this case, when the duration expressed by Fourier number, the characteristic curves of surface, mass average and centre temperatures of conductively heated droplet can be described by the family of characteristic curves (Fig. 2 a), not depending on droplet diameter, but taking into account the variation of sprayed water temperature, $T_o\,(R_{ii}) \neq const$.

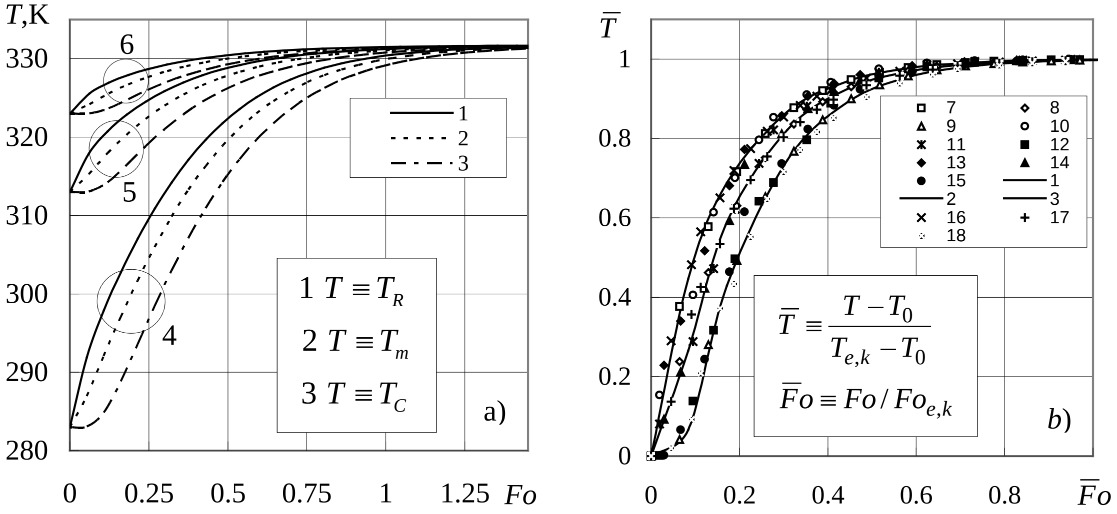

Fig. 2. Influence of initial water temperature on characteristic curves (*a*) and universal curves of water droplets thermal state variation (*b*). T_0 K: (4,7-9) 283, (5,10-12) 313, (6,13-15) 323, (16-18) 303; T_g=873K.

In such a case, was proposed method, when these results expressed in normalized form in respect of a Fourier number, and would be possible the family of characteristic curves (Fig. 2 a) to couple into universal curves (Fig. 2 b).

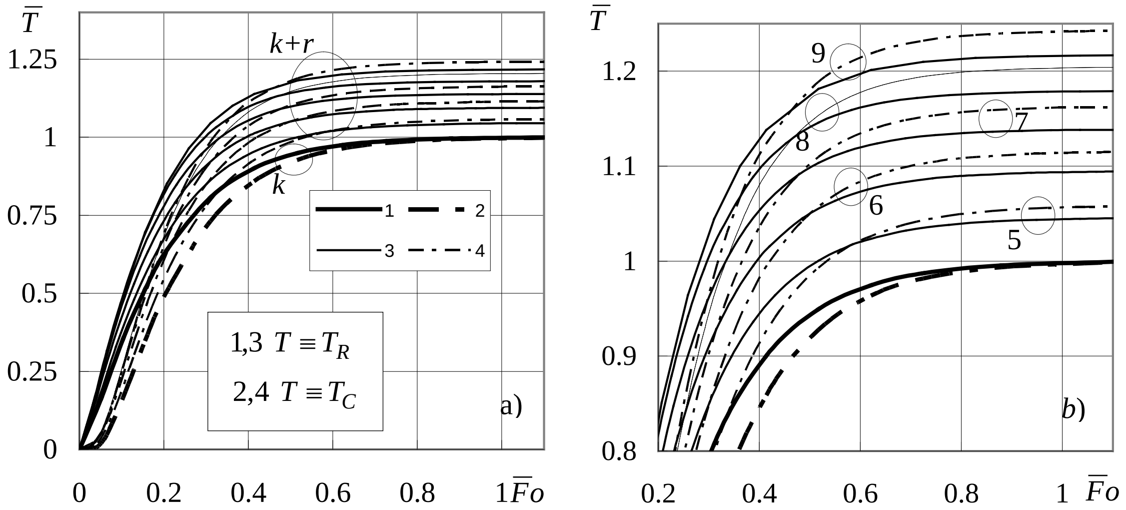

Fig. 3. Influence of the radiant absorption in the droplet on the droplet surface and centre temperature. $R{\cdot}10^6$, m: (5) 50, (6) 100, (7) 150, (8) 200, (9) 250; T_g=873K; T_0=303K; $T_{sr} \equiv T_g$.

The universal curves combined into etalon curve, deviation from etalon curve shows the influence of radiation in the case of combined droplet heating (Fig. 3 a). For larger droplets this influence is more pronounced (Fig. 3 b, curve 9). The thermal radiation makes influence on the thermal state of warming droplet, appreciably evoking the deformations of unsteady temperature field, which reflect the changes of droplet surface and center temperatures dynamics (Fig. 3).

It is very important that the variation of heat and mass transfer parameter of the conductively heated droplet can be described by specific characteristic curves. This requires expressing desired parameter in normalized form in respect of the Fourier number, ensuring the variation of investigational parameter in the universal interval from 0 till 1, and to adjust the universal time variation interval (from 0 till 1), in the case when time is expressed by ratio of Fourier number. The universal duration 0-1 of the unsteady phase transformation mode of conductively heated droplets is shown by time parameter $\overline{Fo}_k \equiv \mathrm{Fo}/\mathrm{Fo}_{e,k}$, normed according to the Fourrier number, representing the beginning of equilibrium evaporation; and the heat and mass transfer parameters P of a droplet are normed according to their initial and equilibrium evaporation values [16]:

$$\overline{P}_{in,k} \equiv \frac{P_{in,k} - P_{in,0}}{P_{in,e,k} - P_{in,0}}. \qquad (8)$$

For the preparation of the specific parameter variation curves for conductively heated droplet is sufficient to model an evaporation process of the freely chosen droplet.

If the characteristics curves [16] of the intensity of evaporation on droplet surface and phase transformation heat flux of conductively heated droplets will presented by expression (8), they will be revealed by the universal curves (Fig. 4).

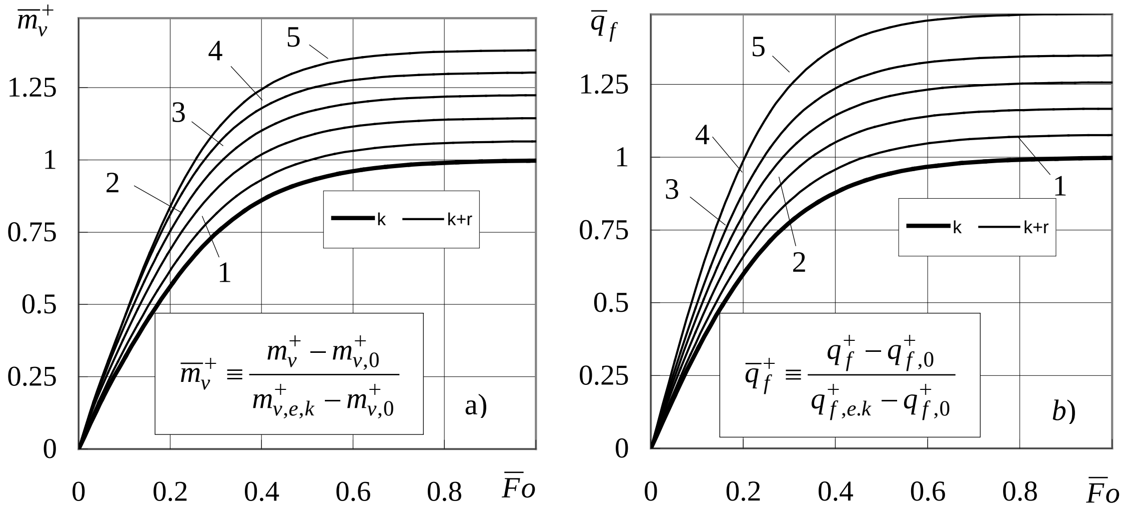

Fig. 4. Influence of the radiant absorption in the droplet on the intensity of evaporation (a) and phase transformation heat flux (*b*). $R \cdot 10^6$, m: (1) 50, (2) 100, (3) 150, (4) 200, (5) 250; $m_{v,0}^+$, kg/m^{2}s: (1) 0.0364, (2) 0.0182, (3) 0.0121, (4) 0.0091, (5) 0.00728; $m_{v,e,k}^+$, kg/m^{2}s: (1) 0.165, (2) 0.0826, (3) 0.055, (4) 0.0413, (5) 0.033; $q_{f,e,k}^+ \equiv q_{k,e}^+$; T_g=873K; T_0=303K; $T_{sr} \equiv T_g$.

In the case of combined droplet heating the deviation from etalon curves shows the influence of radiation (Fig. 4) to intensity of droplet evaporation and phase transformation on droplet surface. As seen in the Fig. 4, for larger droplets this influence is more pronounced, because in larger droplets radiant flow is being absorbed more. The complicated transformations of droplet thermal state going under the influence of radiation shows the variation peculiarities of conductive heat flux in a droplet (Fig. 5 b). When droplets are cooling down, the thermal energy accumulated in a droplet has opportunity to joint into the process of evaporation and make it accelerate. In the case of combined heating the equilibrium evaporation begins when the temperature gradient ensures that the whole radiation absorbed by the droplet will be fully transferred to the droplet surface. The radiation flux absorbed by water makes assumptions for formation of negative gradient temperature field in the droplet and enables the radiant energy to participate in the process of water evaporation. Then, the part of radiation energy absorbed in the droplet (Fig. 5 b), will be transported to the droplet surface by conduction.

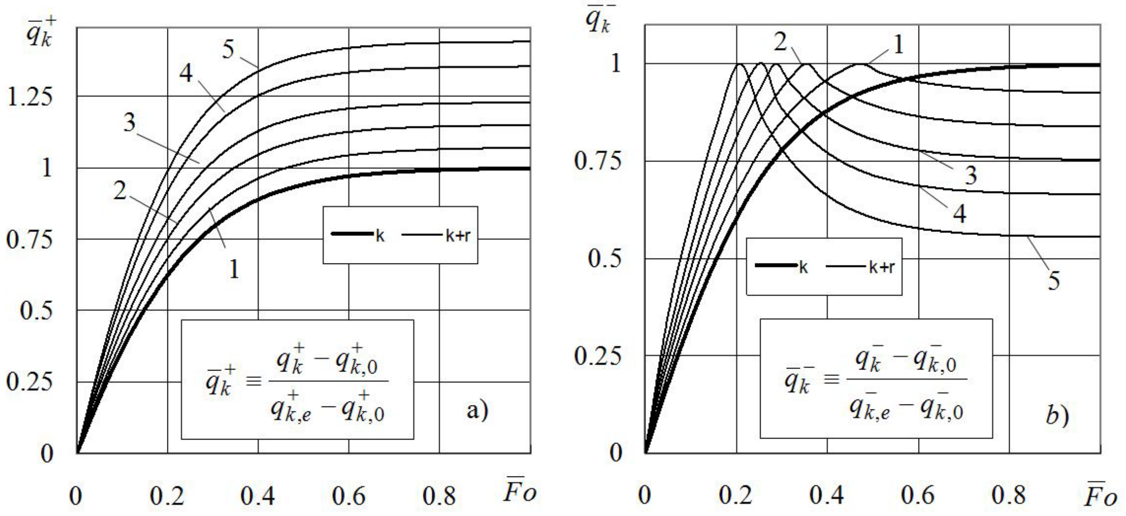

Fig. 5. Influence of the radiant absorption in the droplet on the heat fluxes heating by conduction external side of droplet surface (*a*) and internal side of surface (*b*). $R \cdot 10^6$, m: (1) 50, (2) 100, (3) 150, (4) 200, (5) 250; $q_{k,e}^+$, kW/m^2: (1) 390, (2) 195, (3) 130, (4) 97, (5) 78; $q_{k,e}^- = 0$; T_g=873K; T_0=303K; $T_{sr} \equiv T_g$.

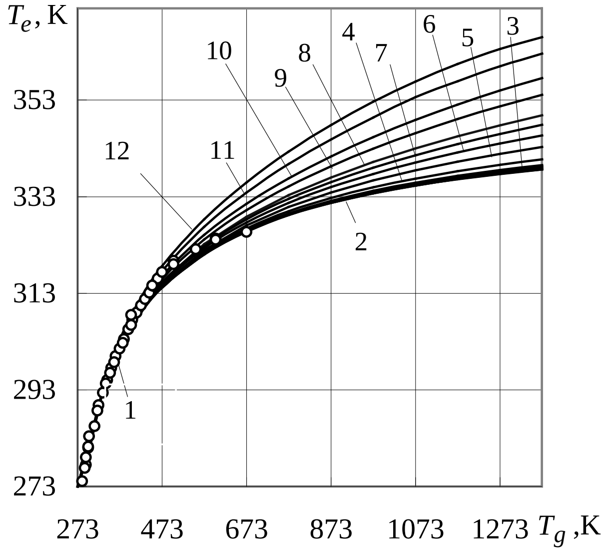

Fig. 6. Dependence of temperature of droplets evaporating in dry air at equilibrium conditions on droplet size, ambient temperature and heating mode: points - experiment [9], lines - present model. (1, 2) conductive heating, (3-12) combined conductive and radiant heating, when $T_{sr} \equiv T_g$ [17]. $R \cdot 10^6$, m: (3) 25, (4) 50, (5) 100, (6) 150, (7) 200, (8) 250, (9) 375, (10) 500, (11) 750, (12) 1000

The heat flux expressed in the Fourier number scale also varies according to the etalon curve, deviation from which shows the influence of radiation on the heat fluxes in the case of combined droplet heating (Fig. 5). Hence, the variation of heat fluxes on the surface and inside of warming droplet is distinctive, and the intensity of variation depends on the size of droplet and heating mode (Fig. 5).

Equilibrium evaporation of a hypothetical droplet with constant diameter can last infinitely; though heat fluxes at its surface do not change. Therefore, as the unsteady evaporation mode comes to an end, the parameters of the thermal state of a droplet settle and their values can be compared with the experiment presented in [9] (Fig. 6). Temperature of conductively heated droplets under the conditions of equilibrium evaporation in dry air is influenced only by temperature of surroundings. That is confirmed by the results of modeling, performed under wide boundary conditions.

These results well correlate with the experimental results of the thermal state of water droplets in air with low and medium temperature air, presented by other authors (Fig. 6).In case of combined heating the equilibrium evaporation mode droplets obtain with higher temperature and the influence of radiation on the state of larger droplets is more significant (Fig. 6).

CONCLUSIONS

1. After composing the variation curves of different parameters *P* and comparing them with universal curves of corresponding parameters of conductively heated droplets, it is possible to present the systematic evaluation of the cases of more complex than conduction case influence on the thermal state and phase transformation of evaporating droplet.

2. The influence of absorbed radiation on droplet heat and mass transfer parameters is more pronounced, when the temperature of radiation source is higher and droplets are larger.

REFERENCES

1. VAN DER BURGT, M. J, Top hat: a smart way to get over 60% efficiency in simple cycle. *Modern Power Systems*, 2004, August, p. 19–25.
2. FUKS, N.A. Evaporation and droplet growth in gaseous media, *Pergamum Press*, 1959, London.
3. SAZHIN, S.S. Advanced models of fuel droplet heating and evaporation. *Progress in Energy and Combustion Science*, 2006, Vol. 32, No. 2, p. 162–214.
4. MILIAUSKAS, G. TAMONIS, M., SVENCHIANAS, P. Radiation and combined heat transfer in spherical volume of selective-radiating and absorbing medium (3. Radiative-conductive heat transfer in the presence of external heating sources). Lietuvos TSR Mokslo Akademijos darbai serija B, 1988, Vol. 3, p. 92–102.
5. TSENG, C.C., VISKANTA. R. Enhancement of water droplet evaporation by radiation absorption. *Fire Safety*, 2006, Vol. 41, p. 236–247.
6. HALE, G.M., QUERRY, M.R. Optical constants of water in the 200-nm to 200-μm wavelength region. *Applied Optics*, 1973, Vol. 12, No.3, p. 555–563.
7. TUNTOMO, A., TIEN, C.L. Optical constant of liquid hydrocarbon fuels. *Combustion Science and Technology*, 1992, Vol. 84, No.1-6, p. 133–140.
8. MILIAUSKAS, G. Regularities of unsteady radiative-conductive heat transfer in evaporating semitransparent liquid droplets. *Int. J. Heat Mass Transfer*, 2001, Vol. 44, No.4, p. 785–798.
9. SHCUKIN, E.P., KRASOVITOV, V.G., JALAMOV, J.I. Evaporation and condensative growth of large and moderately large droplets in gaseous media at any temperature differences, 1991, VINITI 3706-B091, p. 96.
10. MILIAUSKAS, G. Interaction of the transfer processes in semitransparent liquid droplets. *Int. J. Heat Mass Transfer*, 2003, Vol. 46, No.21, p. 4119 - 4138.
11. MILIAUSKAS, G., SABANAS, V. Interaction of transfer processes during unsteady evaporation of water droplets. *Int. J. Heat Mass Transfer*, 2006, Vol. 49, p. 1790–1803.
12. KUZIKOVSKIJ, A.V. Dynamic of spherical particle in powerful optical field. Izv. VUZ Fizika, 1970, No.5, p. 89–94.
13. SIRIGNANO, W.A. Fluid dynamics and transport of droplets and sprays, 1999, Cambridge, Cambridge University Press.

14. MILIAUSKAS, G., SINKUNAS, S., MILIAUSKAS, G. Evaporation and condensing augmentation of water droplets in flue gas. *Int. J. Heat Mass Transfer*, 2010, Vol. 53, p. 1220–1230.
15. MILIAUSKAS, G., NORVAIŠIENĖ, K., MILIAUSKAS, G. Phase transformations of water droplets that slip in flue gas. *Power engineering*, 2010, Vol. 56, No. 2, p. 132–138.
16. MILIAUSKAS, G., NORVAIŠIENĖ, K. Influence of thermal radiation on the energetic state and evaporation of water droplets. *Power engineering*, 2011, Vol. 57, No. 4, p. 241–248.
17. MILIAUSKAS, G., SINKUNAS, S., NORVAISIENE, K., Influence of thermal radiation to the interaction of heat and mass transfer processes under evaporation of water droplets. ICCHMT'2011. 7th Inter-national Conference on Computational Heat and Mass Transfer. 2011, Turkey, Istanbul, 1–8.

CYSENI 2012, May 24–25, Kaunas, Lithuania
ISSN 1822-7554, www.cyseni.com

LOW PRESSURE EVAPORATION OF BINARY PICOLITER DROPLET ON SUBSTRATE

V.I. Saverchenko, J.A. Khodyko
Luikov Heat and Mass Transfer Institute,
Minsk, 220072 – Belarus
Phone 8-029-31-600-31
Email: wellura@gmail.com

ABSTRACT

The evaporation of picoliter droplet in free molecular mode on a substrate has many perspective scientific and industrial applications. Results of our research of the low pressure evaporation of picoliter droplet of water have been recently published. We use the same experimental technique for this work. Low pressure (60 Torr) evaporation of a picoliter water-ethanol droplet had been observed by the optic digital microscope through the glass hood. The evaporation time was determined by means of visualization. It is worthy to note that distinctive pinning effect during fast droplet evaporation was observed. It was also found that when droplet is generated its shape remains constant but when it evaporates diameter remains constant. For further insight the mathematical model of evaporation process was developed. For simulation the trick of time reversal was used. Calculated and measured evaporation times are in good concordance.

Keywords: evaporation time, pinning effect, binary droplet, metal substrate, free molecular regime, simulation, heat of mixing

1. INTRODUCTION

The classical problem of evaporation of liquid on solid substrate is steel actual in spite of long history of investigation. An interest to it is bound with new applications. For example there are a new ways of producing of nanoparticles from colloidal solutions [1] and applications in biophysics and medicine [2, 3].

In this work the process of evaporation of picoliter binary droplet on metallic substrate under low pressure is investigated. The low pressure conditions allow to accelerate the process of droplet evaporation considerably.

2. EXPERIMENTAL SETUP

An experimental investigations were carried out on the original experimental setup shown in Fig. 1.The droplet is pressed through the hole with diameter about 10μm in brass substrate. The setup is developed in such way, that the droplet appears in the same place each time. The observation takes place through the transparent glass cap by an digital optic microscope, produced by QXS Company. The zoom is 60x. The process of evaporation was registered on video (Fig. 2). The binary droplets had a base diameter approximately150 μm.

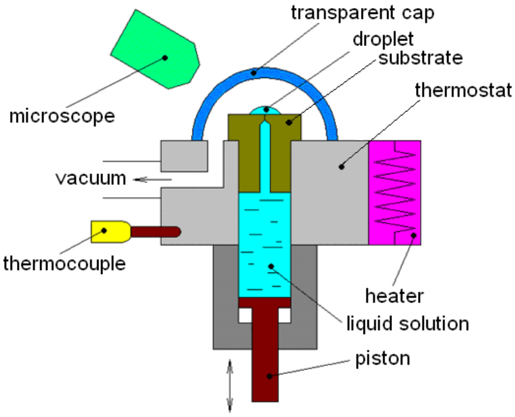

Fig.1. Schematic view of an experimental stand

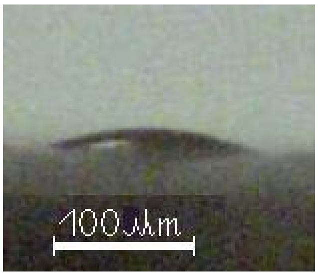

Fig. 2. The aqueous solution of ethanol droplet with height 10μm.

3. RESULTS OF EXPERIMENTS

Experimentally established dependence of the average evaporation rate of picoliter droplet versus the initial concentration of ethanol is shown in Fig. 3. Metal substrate provide high heat supply for the droplet evaporation. The measurements was made at air humidity 55% and pressure 60 torr. The temperature of the substrate was 301K. The process visualization shows that the evaporation rate sharply increases when maximum height of the droplet decrease to few micrometers [3]. The physical sense of such acceleration is that heat conductivity of liquid layer is enough to supply the surface of droplet with heat. During experiments a strong pinning-effect was observed. This means that the diameter of droplet base stay the same during the evaporation process but only height of the droplet decreases. So the shape of fast evaporating droplet looks like a cylinder.

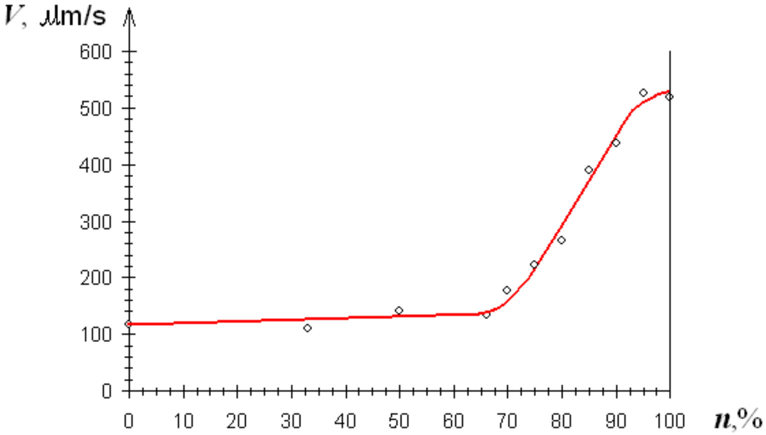

Fig. 3. Dependence of an evaporation rate of the droplet from the concentration of an ethanol

4. CALCULATIONS

The mathematical model of evaporation process of picoliter droplet on substrate, developed in [4], is generalized on the case of binary droplets. Because of high difficulty and volume of this theoretical model we do not describe it in this little paper. For pure water and pure ethanol simulation results are shown in Fig. 4. The calculation was made for the pressure 60 torr and initial droplet height 5 μm. Temperature of surrounding air and substrate was 300K. It is noticeable that the evaporation rate sharply increase when h ~ 2μm.

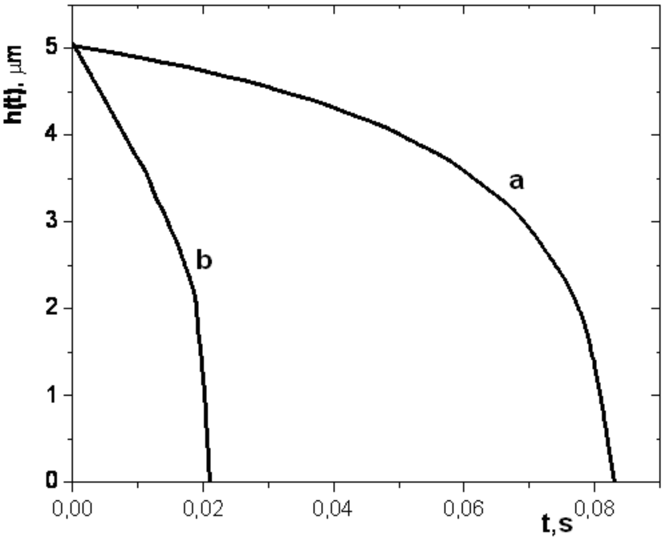

Fig. 4. Illustration of evaporation process through the parameters of droplet (substrate temperature 300 K): a – evaporation of water droplet; b – evaporation of ethanol droplet

The calculations also shows that average evaporation rate of ethanol droplet is 4 times higher than that of water. This is in well correlation with experimental data. It is interesting to note that the surface temperature of pure ethanol falls to 260 K when that of water falls only to 298 K.

ABBREVIATIONS

h – intermediate droplet height, μm; t – time, s; V – evaporation rate (dh/dt), μm/s; n – concentration of an alcohol, %.

5. CONCLUSION

The original experimental setup for evaporation of picoliter droplet on the substrate under low pressure was developed. Evaporation of aqueous solutions of ethanol was measured due to visualization by digital microscope. It is established, that increasing of initial ethanol concentration lead to increasing of average evaporation rate. This conclusion is confirmed by numerical calculation. Pinning-effect is observed in our experiments. Theoretical estimations shows that the main mechanism of heat transfer is thermal conductivity as the convection is diminished by viscosity. One-dimensional mathematical model of ree molecular evaporation of picoliter is developed. The calculation results are in good agrement.

REFERENCES

1. Narayanan S., Wang J., Lin X.-M. Dynamical self-assembly of nanocrystal superlattices during colloidal droplet evaporation by *in situ* small angle X-ray scattering // Phys. Rev. Lett. 2004. Vol. 93, (135503).
2. Yahno T. A., Kozakov V. V., Sanina O. A., Sanin A. G., Yahno V. G., Droplets of biological liquids drying on solid substrate: dynamics of mass morphology, temperature and mechanical properties // Technical Physics. 2010. Vol. 80, Iss. 7, p. 17–23.
3. Tarasevich J. J., Pravoslavnova D. M.. Qualitative analysis of droplet drying of multicomponent solution on solid substrate //Technical Physics. 2007. Vol. 77, Iss.2, p. 17–21.
4. Saverchenko V. I., Fisenko S. P., Hodyko J. A.. Low pressure evaporation of picoliter droplet on solid substrate // J. Eng. Phys. and Thermoph. 2011. Vol. 84, № 4, p. 670–675.

CYSENI 2012, May 24–25, Kaunas, Lithuania
ISSN 1822-7554, www.cyseni.com

OBLIQUE SHOCK WAVE EVOLUTION WITH DISTANCE FROM ENDWALL IN ARGON AND AIR

O.G. Penayzkov, A.V. Skilandz
Physical and Chemical Hydrodynamics Laboratory
Heat and Mass Transfer Institute 220072, Minsk, Belarus
Phone +375172841520
Email: Skilandz.av@gmail.com

ABSTRACT

Characteristic sizes of an oblique shock wave and its influence on the flow dynamics behind a reflected shock wave must be known for exact shock-tube measurement of kinetic parameters. In the present paper, some parameters and common regularities of oblique shock development were defined in argon and air for a cylindrical shock tube 76 mm in diameter. Oblique shock wave characteristics were determined at a location of 50, 150 and 250 mm from the endwall. A moment of passage of the structural elements of the reflected shock wave through measuring sections is determined by measuring the deflection of a plane-parallel light beam. It is found experimentally that the projection length of the oblique shock wave along tube (*l*) in argon is significantly less than that in air. Its size grows with increasing the Mach number and the distance from the endwall. At a distance of 250 mm from the endwall it is 3 mm for argon at M=3.5 and 14 mm for air at M=3.5. The increase in the data scatter with increasing the Mach number and the distance from the endwall may indicate the violation of flow symmetry relative to the central tube axis.

Keywords: shock wave, bifurcation, oblique shock wave

1. INTRODUCTION

The interaction of a shock wave with a boundary layer is a classic phenomenon of high-speed streams, which largely determines the performance of airfoils in the aviation industry. The interaction of a reflected shock wave with a boundary layer (SWBLI) causes the curvature of the shock wave front near the surface, and under certain conditions it can lead to the formation of the bifurcation structure shown in Fig. 1. The process of formation of such structures in the physics of shock waves is called the bifurcation of a reflected shock wave.

As a result of bifurcation of a reflected shock wave, a gas is detached from the wall region with its subsequent accumulation below the triple point (B) at the surface. The gas near the surface moves with the shock front.

The shock waves bifurcation studies are useful for the understanding of the shock wave interaction with aerodynamic surfaces in flows, nozzles and in air intakes [1]. Bifurcations have a strong influence on the flow instability caused by the interactions with the shock wave with the boundary layer. Because of bifurcation, the pressure near the surface differs from that in the flow, which complicates the technique of measuring the flow pressure. In shock tube studies, the bifurcation influence on the kinetics of reactions behind the reflected shock wave is also of great interest [2].

The purpose of this study is to determine the regularities of development of the bifurcation structure in air and argon with increasing Mach number and depending on the distance to the endwall in a cylindrical channel for air and argon.

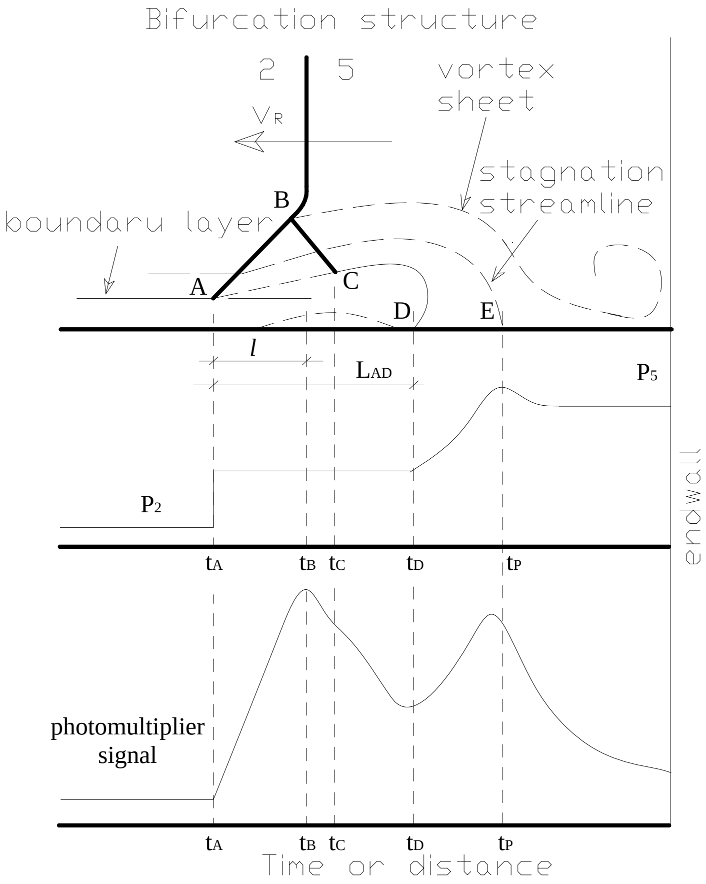

Fig. 1. Bifurcation structure, corresponding pressure at the surface and photomultiplier signals:

AB – oblique shock wave; BC – rear leg; A – flow separation point; B – triple point; arrow at V_R show reflected shock wave spreading direction; numbers 2 and 5 correspond to conditions after incident and reflected shock wave respectively

2. EXPERIMENTAL FACILITY AND MEASUREMENTS

Measurements were performed in a 76 mm dia., helium-driven shock tube at deflection of a plane-parallel beam passing through a small angle to the reflected shock wave plane wave over three shock tube cross-sections (bases) at a location of 50 mm, 150 mm and 250 mm from the endwall. Light passed through the quartz optical windows, built-in at the level of the corresponding measuring cross-sections. The width of light beams was cut to 0.55 mm using a diaphragm. Taking in account the width and slope of the light beam, the method resolution amounted to 0.8 mm. Since the optical system did not allow the simultaneous measurement of more than two bases, it was moved to the third base to make measurement on the third. Thereafter, experiments were repeated under the same conditions. Pressures were measured by PCB Piezotronics pressure sensors mounted flush at a distance of 50 mm, 150 mm, 250 mm from the endwall, and at the endwall of the shock tube. The arrangement of pressure sensors, their designation, as well as the scheme of light beam propagation are seen in Fig. 2. The plane-parallel light beam obtained by the illuminating part of an optical system IAB-451 was used in experiments. The light beams which passed through the test volume were recorded using photomultipliers PMT-119 identified in Fig. 1 as PMT-1 and PMT-2. Photomultipliers were used to obtain signals at a distance of 50 mm and 150 mm and 150 mm 250 mm from the endwall for different measurement series, respectively. Typical observed oscillograms for pressure and PMT are presented in Fig. 1.

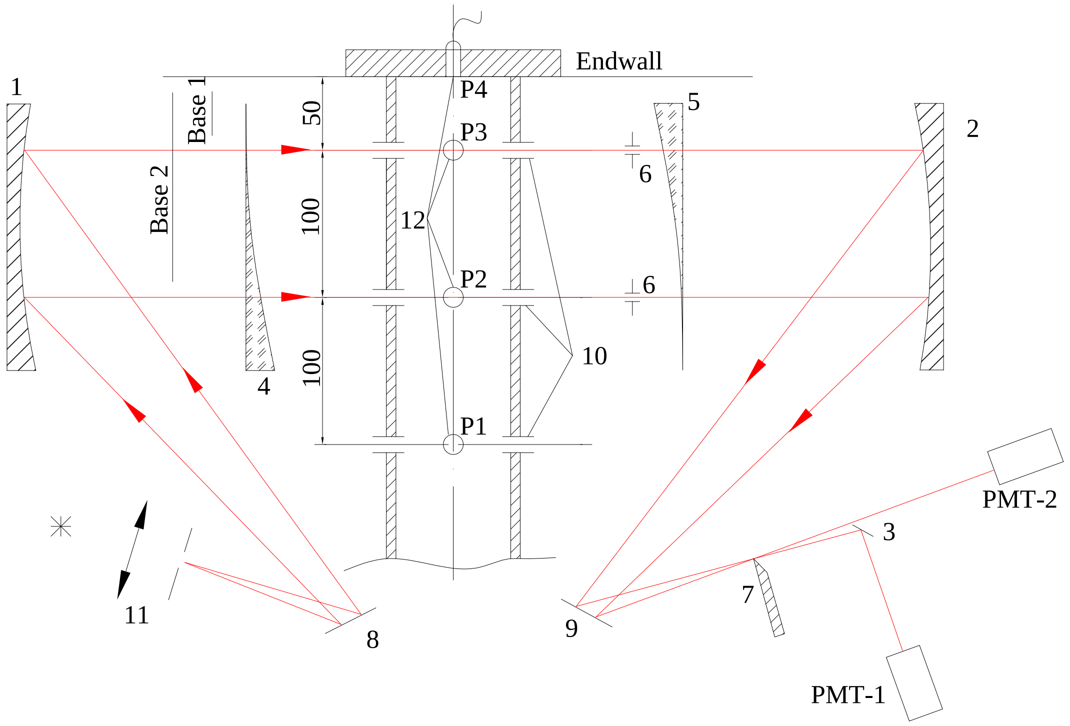

Fig. 2. Optical scheme, the light beams propagations scheme of and location of pressure sensors in the experiments: 1, 2, 3 – mirrors, 4, 5 – meniscus, 6 – vertical diaphragm with the width of 0.5 mm, 7 – knife, 8, 9 – rotary elements of the setup; 10 – optical windows, 11 – vertical slit and the lighting system IAB-451, 12 – pressure transducers

We measured a value of the time difference between flow separation point passage (t_A) and normal reflected shock wave passage (t_B), that is, Δt_{BA}. The corresponding notations are presented in Fig. 1. The length of the projection of an oblique shock wave onto the shock tube surface (*l*) was calculated as the product $\Delta t_{BA} V_R$, where V_R is the velocity of the reflected shock wave. The Mach number values and the conditions behind the reflected shock wave were determined using specialized thermodynamic substances databases CHEMKIN.

Studies were performed in the following conditions:

for argon $T_5 = 670 - 2900$ K, $P_5 = 0.365 - 1.652$ MPa, $\rho_5 = 2.79 \pm 0.14$ kg/m^3, $\gamma_2 = \gamma_5 = 1.667$, M = 1.56 – 3.50;

for air $T_5 = 480 - 1740$ K, $P_5 = 0.395 - 1.419$ MPa, $\rho_5 = 2.80 \pm 0.13$ kg/m^3, $\gamma_2 = 1.334 - 1.394$, $\gamma_5 = 1.303 - 1.386$, M = 1.50 – 3.60.

3. RESULTS AND DISCUSSIONS

3.1. Study of bifurcation in argon

According to Mark‘s theoretical calculations [3], the bifurcation structure in argon can exist within the range M = 1.57 – 2.8. When the bifurcation over a flat surface is shot using the schlieren method, the bifurcation existence limits in pure argon could not be detected. The method we used allows us to analyze more carefully the phenomena occurring near the shock wave front due to the high sensitivity of the method and the possibility of quantitative evaluation of changes in the front structure near the surface as the distance from the endwall is increased.

As the Mach number is increased, from the oscilloscope records of the photomultiplier signals after passing through the shock front, changes in shape and in distance of peak (increase of *l*) from the beginning of the signal growth (Fig. 3) can be seen.

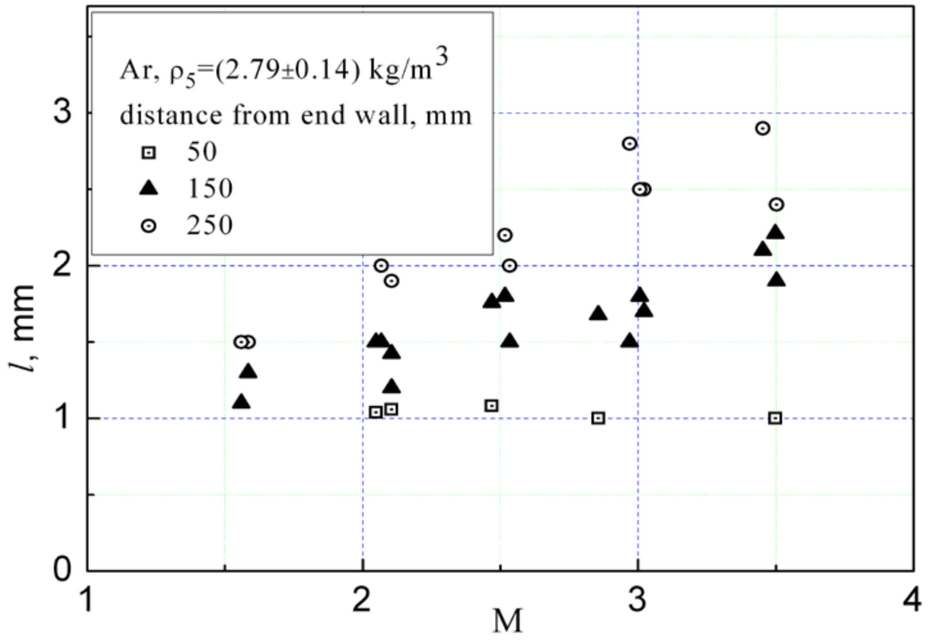

Fig. 3. Length *l* vs. Mach number of an incident shock wave for argon

At a distance of 50 mm, *l* does not grow, but as the distance is increased from the endwall, *l* values grow. This may indicate a transition to the interaction with a turbulent boundary layer developing at a certain distance from the endwall.

During the transition to M > 3, the oscilloscope records show that photomultiplier signals change significantly the shape that manifests itself in broadening the peak and may point to the transformation of the interaction of the reflected shock wave with the boundary layer due to the bifurcation disappearance or also due to the transition to a turbulent boundary layer.

This can be explained as a slight deviation of the shock wave from the axial symmetry. The influence of only deviations from the axial symmetry are not confirmed by the pressure signals that do not reach a plateau immediately behind the shock front for M > 3. This is a manifestation of differences in the region properties behind a normal shock wave and near the surface. These results point to the presence of bifurcation or a slight front curvature at the surface.

At a distance of 250 mm from the endwall the length *l* is 3 mm for argon at M = 3.5. However, for argon with 8% of air mixture, the disappearance of the front curvature is observed with M > 3.6 [3]. The authors marked the low sensitivity of the method and theoretical value of the upper limit of the existence of bifurcation for a mixture with M = 3.27.

From signal studies, we may suggest that there is a systematic error of *l* at a rate of 0.6 mm. Perhaps, *l* values should be reduced by 0.6 mm, although the dependecies presented in the paper do not consider this fact. The error in determining *l* does not exceed 0.7 mm.

3.2. Study of bifurcation in air

For air, *l* values grow with increasing M and distance to the endwall (Fig. 4). The growth of their scatter with increasing distance to the endwall is probably caused by the deviation of the wave front from the axial symmetry. In the investigated M range, one cannot see that the *l* values achieve maximum as the distance is increased, as it is described in [4], for $P_0 = 2.6$ kPa at M = 6.9 for nitrogen, but the growth rate of *l* reduces significantly with increasing distance. The growth of the *l* remains close to a linear pattern for each measuring cross-section. Deviation from this pattern at low M is, possibly, due to the sensitivity and resolution of the method or due to the change in the values of the factors affecting the growth of the bifurcation structure. If the dependence *l*(M) is linear in character, then the approximating dashed lines in Fig.4 can point to the M value, from which the bifurcation structure starts growing depending on the Mach number equal to 1.75. The graphs show that the growth of the bifurcation structure depending on the distance to the endwall is preseved for a wider range of Mach numbers than the growth in dependence on the Mach number, which can also be a manifestation of the deviation of the shock wave front from the axial symmetry. In [3], at a distance of 0.177 feet (54 mm) for M = 2.15, $P_1 = 6.08$ kPa, the height of the triple point was 5.2 mm at an oblique angle wave angle of 48°. Using these parameters, the length of the oblique shock wave projection onto the tube surface is 4.4 mm. That in our case is achieved only for M = 2.6 at a distance of 50 mm.

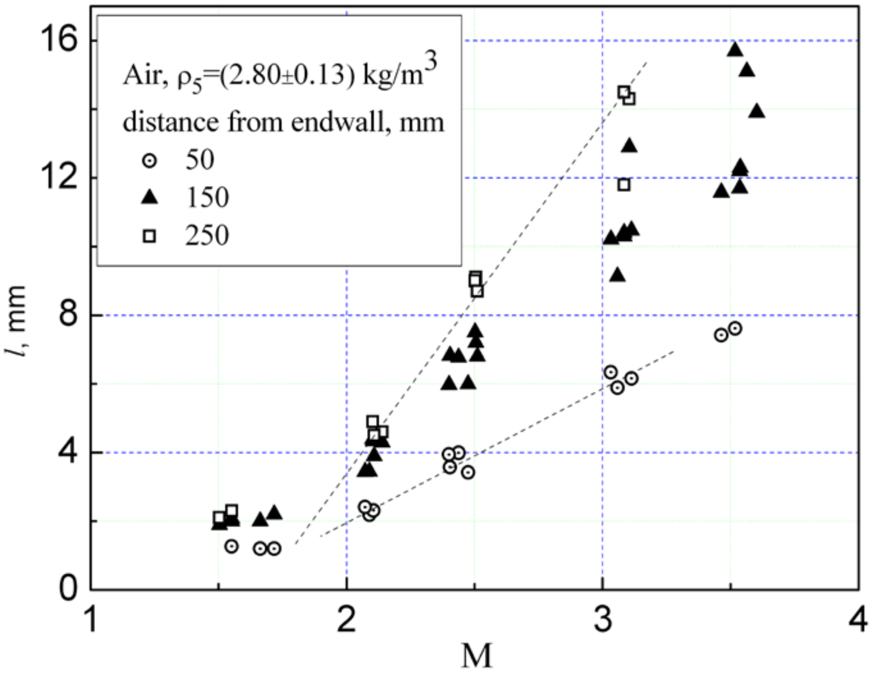

Fig. 4. Dependence of length values *l* on the Mach number of the incident shock wave for air

In air, the slope angle of an oblique shock to the surface for M = 1.8 - 4.3 is in the range of values from 53 ° to 47 °. In view of the tangent value of such angles, the obtained results for *l* can be used as an estimate of the height of the triple point. According to theoretical calculations, the bifurcation existence in air is possible within the range M = 1.33 – 6.45. The presence of the upper limit has not been experimentally found to be associated with the dissociation of oxygen and nitrogen at high Mach numbers. The results [3] shows that the transition from a laminar to a turbulent boundary layer at the flat surface in air occurs at M = 2.15 at a distance of 69 – 107 mm from the endwall when $P_1 \approx 3$kPa. At M = 2.15 the boundary layer Mach number assumes a supersonic value.

In this study, the constant value of the gas density behind the reflected shock wave is maintained rather than the pressure in front of the incident shock wave. Changing P_0 , on the one hand, and M, on the other hand, (for M = 3.5 – $P_0 = 16$ kPa, at M = 1.5 – $P_0 = 70$ kPa) complicates the analysis of pressure wave form signals, since the both parameters affect the dynamics of the boundary layer, which can also lead to a shift of the transition from a laminar to a turbulent boundary layer. In this case, there may be a reduction of the distance to the transition with decreasing Mach number due to a necessary pressure P_0 increase. However, the distance of transition, founded by Mark, is almost the same as the distance to the measuring base of 50 mm, other parameter values being close to ours. From this we can assume that the transition to a turbulent boundary layer is a probable cause of growth of a rate of the bifurcation structure size rise in the close value of the Mach number of 2.15.

4. CONCLUSIONS

1) The bifurcation influence can be considerably reduced by selecting a measuring cross-section near the end surface of the shock tube.

2) There is a slow increase in l at low Mach numbers for air, as well as for argon. That could be explained due to a small pressure difference at the wall and in the central part of the flow behind the reflected shock wave.

3) For argon:

- at a distance of 50 mm in argon, the signs of the l growth are not observed, but as the distance from the endwall is increased, the l value grows;
- the results indicate the presence of bifurcation or a slight front curvature at the surface boundary.

4) For air:

- there is a significant decrease in the rate of the l growth with increasing distance from the endwall;
- the Mach number value for the start of growing the bifurcation structure size as a function of the Mach number is 1.75;
- the growth of the bifurcation structure as a function of distance to the endwall is preserved for a wider range of Mach numbers than the growth as a function of the Mach number;
- the transition to the turbulent boundary layer is a probable cause of the rate growth of the bifurcation size rise at Mach number close to 2.15.

5) The influence of the transition from a laminar to a turbulent boundary layer on the interaction of the reflected shock wave with the boundary layer is of particular interest of further research.

REFERENCES

1. COULDRICK, J.S. A study of swept and unswept normal shock wave/turbulent boundary layer interaction and control by piezoelectric flap actuation. *A thesis submitted for the degree of doctor of philosophy*. Australia, New South Wales, 2006. 268 p.
2. PETERSEN E.L., Hanson R.K. Measurement of reflected-shock bifurcation over a wide range of gas composition and pressure. *Shock Waves*, 2006, Vol. 15, p. 333−340.
3. MARK, H. The interaction of a reflected shock wave with the boundary layer in a shock tube. *NACA TM 1418*, 1958. 127 p.
4. TAYLOR, J., HORNUNG, H. Real gas and wall roughness effects on the bifurcation of the shock reflected from the endwall of a tube. Proceedings of the Thirteenth International Symposium. Niagara Falls, New York: State University of New York. 1981 July 6–9.

CYSENI 2012, May 24–25, Kaunas, Lithuania
ISSN 1822-7554, www.cyseni.com

LIQUID HYDROCARBONS DROPLET HEATING AND EVAPORATING PROCESS NUMERICAL RESEARCH

J. Talubinskas, G. Miliauskas
Kaunas University of technology
K. Donelaičio st. 20, 44239 –Lithuania
Phone: 8 673 43907, 37 300437
Email:Julius.talubinskas@gmail.com

ABSTRACT

In the boiler, internal combustion and rocket engines liquid fuel (generally liquid hydrocarbons or their mixtures) combusted in the sprayed form. Droplets evaporation speed – one of fundamental combustion process efficiency factor. That factor measuring process in the combustion torch is very difficult. So in practice applied theoretical droplets evaporation research methods. Their properly can dispute. The plenty of research methods - heat and mass transfer process in sprayed liquid systems research tasks variety result.

In this paper the results of modeling unsteady temperature field in hydrocarbons evaporated droplets heated by conduction and radiation are presented. The spontaneous circulation simulation results are summarized by Rayleight’s criterion.

Keywords: Hydrocarbons droplets, conductively and combined heating, evaporating, modeling

1. INTRODUCTION

Liquid fuel generally combusted in the sprayed form. Its combustion efficiency determines droplets evaporation speed. Non - stacionarity of the heat and mass transfer processes and their interactions are very important factors in the sprinkle liquid fuel heating and evaporation process. High-temperature two phase flow multiple heat and mass transfer processes additionally affect the interaction of translucent droplets absorbed radiation flux. Experimentally investigate the multiple heat transmission of droplets rather difficult, so widely used theoretical methods [1]. Modeling multiple heat spread of the droplets of liquid existence instability assessment problem in its. Spontaneous circulation of liquid warming droplets can occur when Archimedes forces is on, and they forced circulation can lead to gas sliding friction force acting on the surface. The exposure of the liquid droplets flowing on the surface and formed vortices passes into the interior layers of the droplets. Hydrodynamic mode of the liquid droplets determines the solution methodology of "drop" inner problem. The simplest form of droplets heat transfer models that deny the influence of radiation. Suggesting that the droplets while maintaining a uniform temperature is warming up their volume, they concluded "the infinite heat conductivity", or "infinite fluid mixing" strain. These droplets heat transfer models to define the effective conductivity model [2], which additionally take into account the fluid-flow finite intensity of thermal impact on the spread of the droplets. Translucent droplets radiation absorbed by the flow describing the spectral radiation models [3-5] et al. enables the evaluation of the combination of heat spreading droplets. Recently developed combined analytical and numerical models of droplet non-stationary evaporation [5, 6]. Then the temperature field of droplets of a multiple their heating case describing integral equation the endless lines. Despite their numerical solution schemes, convergence control is convenient, but inconvenience causes the need to know the evaporating droplet surface temperature. Šis metodas taikytas angliavandenilių lašelių šilimui ir garavimui modeliuoti [7, 8] darbuose.

In this paper, the systematically results of modeling of hydrocarbons unsteady temperature evaporated droplets heated by conduction and radiation are presented. Droplets heating and evaporating are analyzed in Fouer number universal time scale. The spontaneous circulation simulation results are summarized by Rayleight's number. The possibility of spontaneous circulation in a non-isothermal hydrocarbon droplet was evaluated by comparing the results of modelling with experimental data of symmetrical heating of spherical water volume [9].

2. PROBLEM FORMULATION

Droplet surface temperature is reduced by iterative methods for solving energy flows balance at the droplet surface describing equation:

$$\vec{q}_{\Sigma}^{\,+}(\tau)+\vec{q}_{\Sigma}^{\,-}(\tau)+\vec{q}_{v}^{\,+}(\tau)=0, \tag{1}$$

requiring to the droplet surface inflow and outfall energy flow matching in (1) expression marks "+" and "-" parameter indicates the droplet surface internal and external side parameters respectively. Total heat flux surface structure of both sides of the droplet determines radiation and convection heat flow sands: $\vec{q}_{\Sigma} \equiv \vec{q}_r + \vec{q}_c$. Translucent liquid light spectral absorption coefficients are a finite size, so the radiation absorption in the liquid surface can be disproved. Then $q_r^- \equiv q_r^+$ the vectors will be directed to the drop when radiate higher temperature than the liquid radiation source. Heat convection flow of a droplet outside surface will be determined according to Nusselt criteria articulated in the intensity of droplet heating and droplet surface and surround the temperature difference, and this determines the direction of the flow vector:

$$q_c^+ = Nu\frac{\lambda_{vg}}{2R}\left(T_g - T_R\right)\cdot \ln\frac{1+B_T}{B_T}. \tag{2}$$

Spalding heat transfer parameter function in (2) expression takes into account the vaporized droplet convective heating intensity of Stefan hydrodynamic flow effect. Spalding heat transfer parameter for non-stationary evaporation of droplet is defined as [5]:

$$B_T \equiv \frac{c_{p,vg}\left(T_g - T_R\right)}{L}\left(1+\frac{q_c^-}{q_c^+}\right). \tag{3}$$

Heat convection flow of a droplet surface internal side will lead temperature field on the droplet gradient and liquid circulation intensity:

$$q_c^- = -\lambda_{ef}\left.\frac{\partial T(r,\tau)}{\partial r}\right|_{r\equiv R^-} \tag{4}$$

Unsteady temperature field in the droplet is calculated according to integral type equation [5]:

$$T(r,\tau)=T_R(\tau)+\frac{2}{r}\sum_{n=1}^{\infty}\sin\frac{n\pi r}{R}\int_0^{\tau} f_n(\tau_*)\exp\left[-a\left(\frac{n\pi}{R}\right)^2(\tau-\tau_*)\right]d\tau_*. \tag{5}$$

The f_n function account radiantive heat flux in the semi-transparent droplet and the dynamics of its surface temperature:

$$f_n = (-1)^n \frac{R}{n\pi}\frac{dT_R}{d\tau} + \frac{1}{\rho c_p R}\int_0^R \left(\sin\frac{n\pi r}{R} - \frac{n\pi r}{R}\cos\frac{n\pi r}{R} \right) dr \,. \tag{6}$$

Temperature gradient in (4) expression [5]:

$$\left.\frac{\partial T(r,\tau)}{\partial r}\right|_{r\equiv R^-} = \frac{2\pi}{R^2}\sum_{n=1}^{\infty} n(-1)^n \int_0^{\tau} f_n(\tau_*) \exp\left[-a\left(\frac{n\pi}{R}\right)^2 (\tau-\tau_*) \right] d\tau_* \,. \tag{7}$$

In the initial droplet evaporation stage observed a positive temperature gradient field and convection heat flow comes to a drop and with a liquid absorbed radiation intense heats droplet. When internal droplet layers heats more, in the droplets are formed negative temperature gradient field and the convection heat flow changes direction. This includes the assumption of radiation energy absorbed by the droplets integrate in the evaporation process. When the temperature gradient ensures absorbed radiation flux from the droplet-conducting surfaces – starting equilibrium evaporation mode.

Evaporation leads to the flow of steam heat flux density: $q_v^+(\tau) \equiv m_v^+(\tau)\cdot L(\tau)$. Vapor mass flux density is calculated based on the Shorin-Kuzikovskij model [10, 11]:

$$m_v = \frac{D_{vg}}{T_R}\frac{\mu_g}{R\cdot R_\mu} p \ln\frac{p - p_{v,\infty}}{p - p_{v,R}} \,. \tag{8}$$

Natural circulation of fluid within a droplet is induced by non-uniformity of temperature field, which has been expressed by difference of temperatures at droplet surface and in the center of it: $\Delta T_l \equiv T_R - T_C$. The intensity of natural circulation in the droplet is described by Rayleigh number:

$$Ra = \frac{\beta_l g R^3}{\nu_l a_l}\Delta T_l \,. \tag{9}$$

The circulation of liquid is said to onset when Rayleigh number exceeds the critical value i.e. $Ra > Ra_{cr}$. Otherwise the processes in the droplet are dominated by diffusion. Research of fluid behavior in spherical volume with non-uniform temperature field [9] demonstrates that critical values of Rayleigh number are strongly dependent on the method of volume heating. For asymmetric heating the critical value is in the range of 200 to 300, and for symmetric heating it can reach few thousands.

The model of the droplet does not consider the slippage between two phases i.e. droplet and its environment. In this scenario the effect of gaseous phase to fluid circulation in the droplet are not considered as the forces inducing such circulation are absent. The droplet is heated by conductivity: $Nu = 2$ and $q_c^+ \equiv q_k^+$. The surface temperature of the evaporating droplet is calculated using energy conservation principle and has been implemented using the method of the steepest descend:

$$\lambda_{vg}\frac{T_g-T_R}{R}\ln\frac{1+B_T}{B_T}-\lambda_l\frac{\partial T(r,\tau)}{\partial r}\bigg|_{r\equiv R^-}-m_v^+L\equiv 0\,. \qquad (10)$$

System of equations (2)–(10) can be solved numerically. Using iterative method number J of the control droplet cross-section is selected arbitrary. The position of the cross-section is defined by the dimensionless droplet coordinate η_j (η_j=0, when j≡1 and η_j=1, when j≡J). Time τ is selected and number I of time coordinate steps is provided ($\tau_i=0$, when $i\equiv 1$ and $\tau_i\equiv\tau$, when $i\equiv I$). Temperature field in the droplet is determined from eq. (5) iteratively varying droplet surface temperature on the basis of energy conservation principle at the surface and using the method of the steepest descent. The final result is achieved when the energy balance (10) error from the previous iteration is no greater than 0.01 percent. The local radiation flux density in a semi-transparent droplet is calculated using the technique described in ref. [5]. Its numerical solution algorithm requires the function $T(r,\tau)$ to be predefined to be able to calculate the spectral radiation intensity in the droplet and take into account the peculiarities of the complex refractive index of a semi transparent liquid. The value of the complex refractive index for n-decane and n-heptane is known [12].

3. RESULT AND DISCUSSION

The heating and evaporation of n-decane, n-heptane and n-hexane hydrocarbon droplets in dry air with temperature T_g and pressure of 0.1 MPa was modeled. The impact of the Knudsen layer on the evaporation of the droplets was ignored. In the case of conductive heating it was assumed that the droplets do not move relative to the air around them. In the case of combined heating, the outside air temperature $T_{sr}\equiv T_g$ black radiation source was assumed.

The heating and evaporation processes of droplets highly depend of liquid nature, droplets disparity and air temperature (Fig. 1-5).

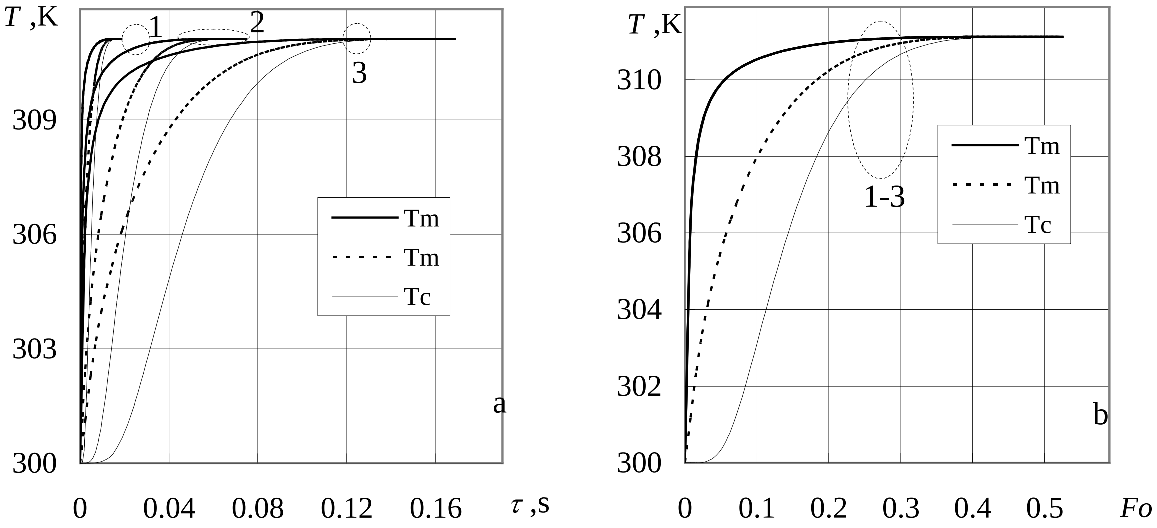

Fig. 1: n-hexane (C_6H_{14}) droplets conductively heating in high temperature air. Real times scale (a), Fourier number scale (b). $R\cdot 10^6$, m: 1 – 50, 2 – 100, 3 – 150; T_g=1200K; T_0=300 K

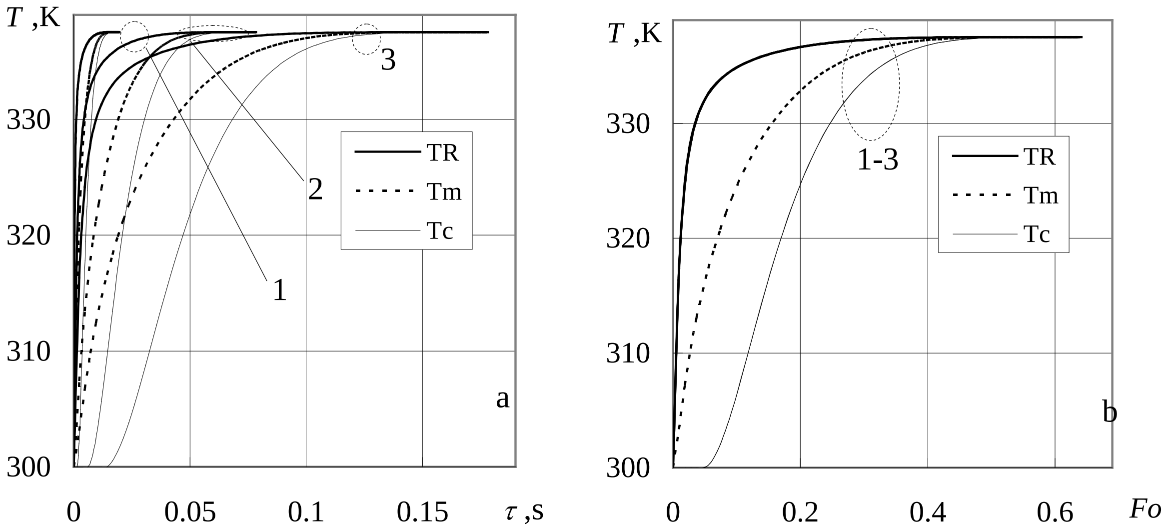

Fig. 2: n– heptane (C_7H_{16}) droplets conductively heating in high temperature air. Real times scale (a), Fourier number scale (b). $R\cdot10^6$, m: 1 – 50, 2 – 100, 3 – 150; T_g=1200K; T_0=300 K

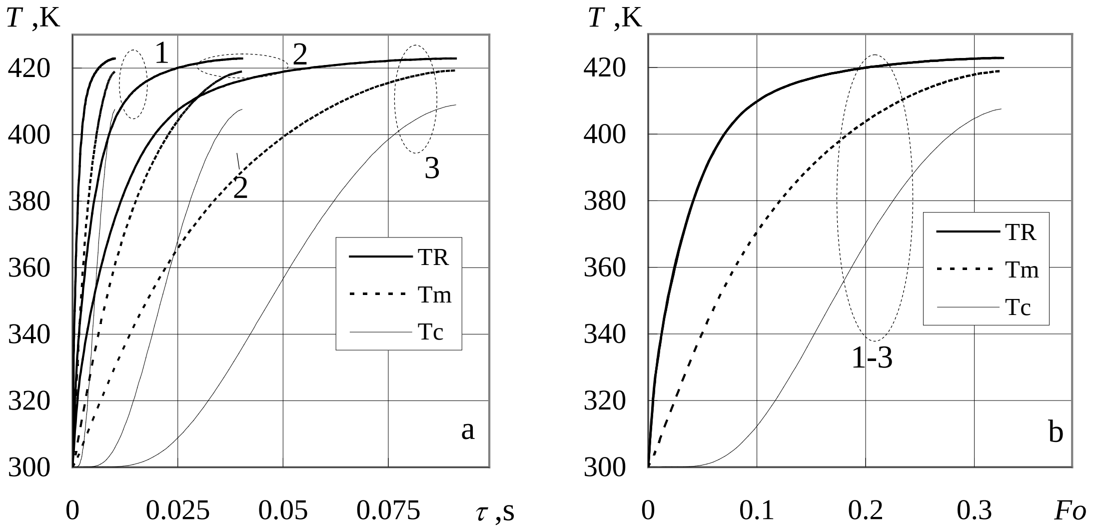

Fig. 3: n – decane ($C_{10}H_{22}$) droplets conductively heating in high temperature air. Real times scale (a), Fourier number scale (b). $R\cdot10^6$, m: 1 – 50, 2 – 100, 3 – 150; T_g=1200K; T_0=300 K

Dynamics of conductively heated hydrocarbon droplets thermal state for the analyzed liquid droplets depends on size droplet in real time scale (fig. 1-4 a), but is invariant of droplet size in the domain of Fourier number (fig. 1-4 b). The evaporation of conductively heated hydrocarbon droplets in low temperature air warms to the temperature $T_{e,k}$ of equilibrium evaporation, which does not alter during such evaporation mode (fig. 5). Droplets of n-decane in the high temperature air evaporate in the unsteady regime of evaporation not reaching an equilibrium state (fig. 3).

For each type of liquid the characteristic curves of droplet surface temperature $T_R(Fo)$, center temperature $T_c(Fo)$ and droplet mass mean temperature $T_m(Fo)$ dynamics can be established. It allowed optimization of the numerical model for droplet heating and evaporation processes. The characteristic droplet temperature non-uniformity curves are established based on the droplet surface temperature and droplet center temperature dynamics. They clearly depict that liquid properties have influence to temperature non-uniformity (Fig. 6).

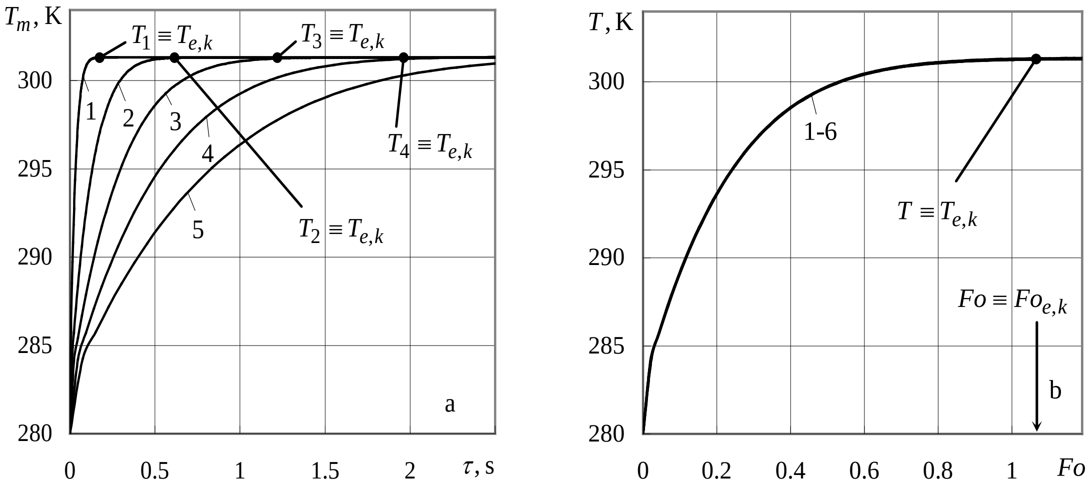

Fig. 4: n – hexane droplets conductively heating in low temperature air. Real times scale (a), Fourier number scale (b). R·10^6, m: 1 – 50, 2 – 100, 3 – 200, 4 – 300, 5 – 400, 1 – 600; $T_g = 473$ K

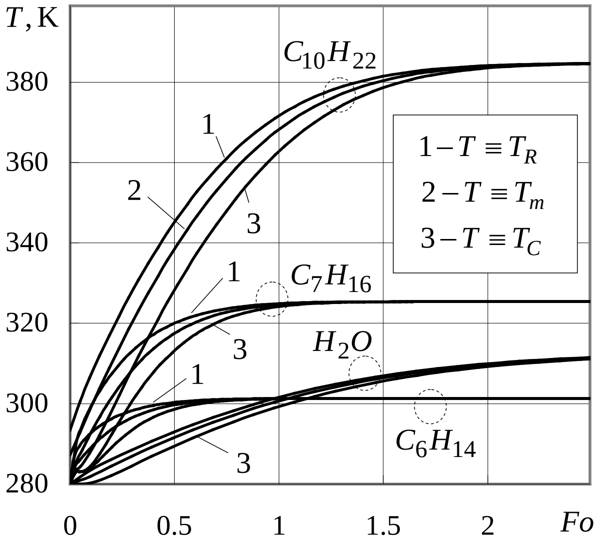

Fig. 5: Hydrocarbons n-hexane, n-heptane, n-decane and water (H_2O) droplets conductively heating in 473K air temperature [7]

The intensive temperature increase of droplet external fluid layers during the initial droplet heating stage causes rapid rise of the droplet temperature non-uniformity. Later the temperature non-uniformity reduces and eventually vanishes when droplet equilibrium evaporation mode is entered. The results show that water droplets establish equilibrium evaporation earlier than hydrocarbon droplets. Therefore, non-uniformity in water droplets vanishes earlier, as well. In the modeled cases (Fig. 6, 7) non-stationary evaporation of hydrocarbon droplets lasts up to 80% of phase transformation duration, but for water droplets it is just 20%.

Droplet temperature non-uniformity is significantly influenced by gas phase temperature, which has effect on droplet equilibrium evaporation temperature. For air temperature of 473K droplet equilibrium evaporation temperature is 301.3K for n-hexane, 325.4K for n-heptane, 384.8K for n-dekane and 313K for water. Droplet equilibrium evaporation temperature increases to 311.3K, 337.8K, 406.4K and 332.1K correspondingly when air temperature is increased by 1000K to 1473K [8].

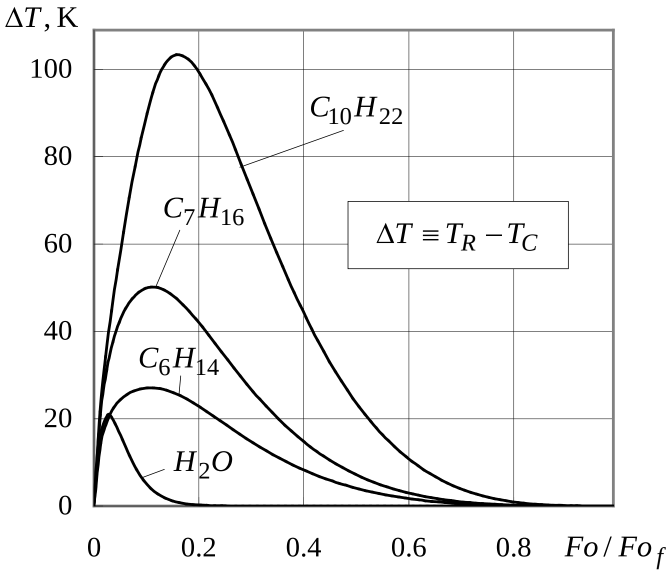

Fig. 6: The dynamics of non-uniformity of temperature field for conductively heated droplets in 1073K air. Fo_f is universal evaporation process time [7]

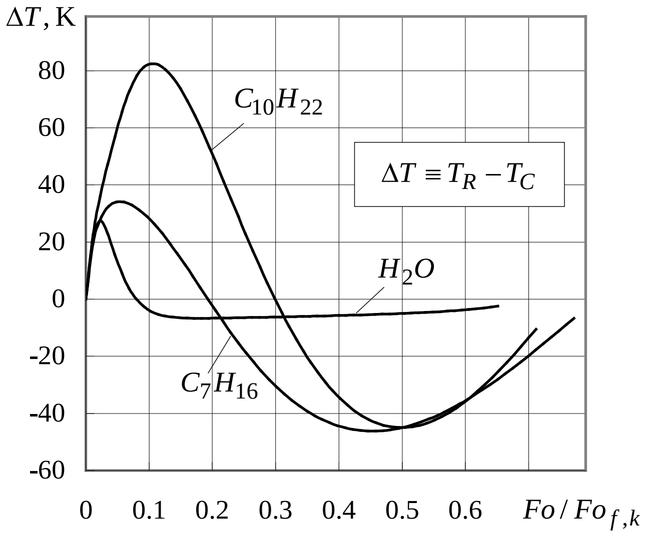

Fig. 7: The effect of fluid radiation absorption property to non-uniformity of droplet combines heating. $R_0 = 500 \cdot 10^{-6}$ m; $T_{l,0} = 283$ K; $T_g = 1073$ K

For hydrocarbons with higher saturation temperature (in this instance it was n-dekane) droplet equilibrium evaporation temperature is higher and the spike of temperature non-uniformity is more pronounced. Therefore, conditions for fluid natural circulation are favorable. For sprinkled of liquid temperatures close to droplet equilibrium evaporation temperature droplet temperature non-uniformity will be smaller and will last shorter compared to sprinkled of liquid with temperatures significantly below it. Substantial influence has a warming effect on droplet semi-transparent fluid absorbed radiation flux (Fig. 7). Combined heating case, compared with droplet heating by conductivity, droplet thaw process altered not only quantitatively but also qualitatively, and change its image non-isothermal. Combined heating non-isothermal droplets observed two peaks. First, the heat conductivity and the cause a rapid drop warming surface layers. He gradually intensifying suffocate central droplet layers thaw. Subsequently, the radiation effects to the central layers of the droplet surface warms more and begin to form a second peak non-isothermal droplets. At its peak, it reaches a balanced formation of the evaporation conditions changed when the temperature drops a field gradient of droplets absorbed radiation provides a full output of the flow conductivity (if liquid droplets do not circulate), the droplet surface. Non-isothermal second peak is weaker than the first. Therefore, the conditions for self-circulating the liquid droplets is determined by the first rise (Fig. 8).

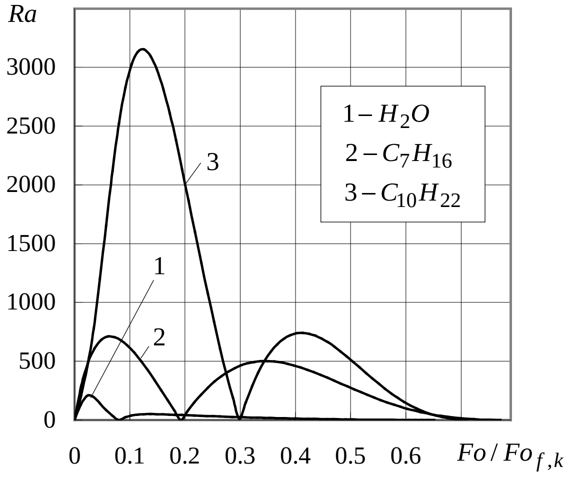

Fig. 8: The effect of liquid properties and radiation to droplet internal natural fluid circulation.
$R_0 = 500 \cdot 10^{-6}$ m; $T_{l,0} = 283$ K; $T_g = 1073$ K

4. CONCLUSION

1. The thermal state of the liquid hydrocarbon droplet changes during evaporation. The peculiarities of this change are influenced by the method of droplet heating, droplet diameter and liquid fuel molecular weight.
2. A numerical study of the *n*-decane droplet heating and evaporation showed that in the case of heating the droplet conductively, the thermal state change expressed using Fourier's criterion is universal and can be stated with typical droplet surface, centre and average mass temperature describing curves.
3. When time is expressed by Fourier's criterion, other conductively heated droplet heat and mass transfer parameters can be described and presented in a non-dimensional form. In the case of combined droplet heating, a deviation in the heat and mass transfer parameters regarding universal curves obtained from conductive heating helps evaluate how the radiation affects them.
4. According to the results of the provided numerical investigation of evaporating pure hydrocarbon *n*-decane droplet thermal conditions, it is clear that Archimedes forces in high molecular weight hydrocarbon droplets caused by internal temperature gradient are insufficient to cause spontaneous fluid circulation in the common for thermal technologies range of droplet size.
5. The temperature difference between the surroundings of the droplet and the droplet itself affects the thermal and hydrodynamic state of the evaporating hydrocarbon droplet. Therefore it is important to investigate the process of droplet evaporation in different initial temperature conditions of the droplet and its surroundings.

5. NOMENCLATURE

a – thermal diffusivity, m^2/s; B – Spalding transfer number; c_p – specific heat, $J/(kg\ K)$; D – mass diffusivity, m^2/s; Fo – Fourier number; L – latent heat of evaporation, J/kg; m_v – vapor mass flux, $kg/(s{\cdot}m^2)$; n – number of the term in infinite sum; p – pressure, Pa; q – heat flux density, W/m^2; R – radius of a droplet, m; r – radial coordinate, m; Ra – Rayleigh number; Nu – Nusselt number; T – temperature, K; η – non-dimensional coordinate; λ – thermal conductivity, $W/(m\ K)$; μ – molecular mass, $kg/kmol$; ρ– density, kg/m^3; τ – time, s; m_g -
Subscripts: C – droplet centre; e – equilibrium evaporation; g – gas; i – time index in a digital scheme; I – index of control time; j – index of droplet cross-section; J – index of droplet surface; k – conductive; l – liquid; m – mass average; r – coordinate of a droplet; R – droplet surface; v – vapour; vg – vapour-gas mixture; 0 – initial state; ∞ – far from a droplet.

REFERENCES

1. SAZHIN S.S., Advanced models of fuel droplet heating and evaporation. Progress in Energy and Combustion Science, 32, 2006, p. 162–214.
2. ABRAMZON B., SIRIGNANO W.A., Droplet vaporization model for spray combustion calculations. Int. J. Heat Mass Transfer, 32, 1989, p.1605–1618.
3. LAGE P.L.C., RANGEL R.H., Single droplet vaporization including thermal radiation absorption. J. of Thermophysics and Heat Transfer, 7, 1993, p. 502–509
4. DOMBROVSKY L.A., Thermal radiation forms no isothermal spherical particles of a semitransparent material. Int. J. Heat Mass Transfer, 43, 2000, p. 1661-1672.
5. MILIAUSKAS G., Regularities of unsteady radiative-conductive heat transfer in evaporating semitransparent liquid droplet. Int. J. Heat Mass Transfer, 44, 2001, p. 785–798.
6. SAZHIN S., Modelling of heating, evaporation and ignition of fuel droplets: combined analytical, asymptotic and numerical analysis. J. of Physics: Conference Series, 22, 2005, p. 174–193.
7. MILIAUSKAS G., SINKUNAS S., TALUBINSKAS J., SINKUNAS K., Peculiarities of hydrodynamics in the evaporation of hydrocarbon droplets, Advances in Fluid Mechanics VIII: WIT Transactions on Engineering Sciences 69, Boston, 2010, p. 283–292.
8. MILIAUSKAS G., TALUBINSKAS J., ADOMAVICIUS A, PUIDA E., Thermal state and hydrodynamics of evaporating hydrocarbon droplets. 1. A possibility of natural circulation of the liquid in the droplet, Mechanika 18(2), 2012, p. 170–176.
9. GERSHUNI G.Z., ZHUKOVICKIY E.M., Konvektivnaja ustoicivost neszimaemoi zidkosti, Nauka, Moskva, 1972.
10. KUZIKOVSKIJ A.V., Dynamic of spherical particle in powerful optical field, Izv. VUZ Fizika, 5, 1970, p. 89–94.
11. SHORIN S.N. Teploperedacha, Vishaja Shkola, Maskva, 1964.
12. TUNTOMO A., TIEN C.L., Optical constant of liquid hydrocarbon fuels, Combust. Sci. and Tech., 84, 1992, p. 133–140.

CYSENI 2012, May 24–25, Kaunas, Lithuania
ISSN 1822-7554, www.cyseni.com

A NEW APPROACH TO EVALUATING RESPONSE OF THE TURBINE GAS METERS

A. Tonkonogovas, A. Stankevičius
Lithuanian Energy Institute
Breslaujos 3, 44403 – Lithuania
Phone +370 37 401-832
Email: andriust@mail.lei.lt

ABSTRACT

Turbine gas meters are widely used for natural gas accounting. When operating in pulsing flows, the essential so called the meters' dynamic error has appeared. This error is determined by meters rotation inertia. Earlier we experimentaly investigated the meters' inertia main characteristic - inertia time constant. According to this study the time constant is inversely proportional to the finite fluid flow rate. However our last investigations have shown that besides flow rate one more factor effects on the time constant, namely current rotation frequency.

The both factors influence has been evaluated by the new processing of the previous experimental data. The numerical differentiation of rotation frequency curve in dimensionless exponent form has been applied. The essential difference in comparison with previous study has been found. Obtained results will be used for numerical simulation of the meters' response and dynamic error in pulsing flows under different conditions.

Keywords: turbine gas meter, response, inertia time constant

1. INTRODUCTION

Problem of influence of flow pulsations on metrological characteristics on turbine gas meters (TGM) has been studied during last 80 years. In pulsing flow TGM rotor‘s rotation frequency (meter‘s reading) pulses too, however, because of inertia of rotation with lag of phase and reduction of pulsation amplitude. The second effect, following from the first one is overregistration of the passed gas volume, or so called dynamic error. The main frequency of rotation exceeds frequency of the appropriated average flow rate.

One of the first to evaluate and predicate the dynamic error was W. F. Z. Lee et al. [1]. His studies were developed by N. Lehmann [2], K. N. Atkinson [3], R. J. McKee [4] and B. Lee et al. [5]. N. Lehmann got analytical solution for turbine gas meters dynamic error at flow pulsations of rectangular form, which are not occur in practice. The most known are the results of the K. N. Atkinson. They are obtained for sine flow pulsations and are included into ISO document [6]. Analogical results were presented by R. J. McKee [4]. All obtained results are based on solution of differential equation of turbine meter rotation in the transitional flow, which contains a certain number of hard-to-evaluate parameters. This is the main reason that different investigators results are fragmentary and often disagreed. According to investigations, for example, B. Lee et al. [5] in practice the flow pulsation occurs by complex law, for which the results were absent until recently.

Recently J. Tonkonogij et al. proposed and implemented the new method of simulating the turbine gas meter behavior in pulsing flow of arbitrary pulsation law [7]. The combined calculating-experimental method has been developed. The method stimulates the meter inertia time constant as the principal and the only characteristic of the meter for the simulation of the meter behavior in transitional flow. The dependence for inertia time constant should be experimentally evaluated by measuring of meter response to the sharp flow rate changing from one value to another. This dependence can be used for calculating the meter response to flow changing by any law.

Regardless to the method of solving the problem determining the main characterizing parameter is the inertia time constant of the turbine gas meter's rotor. Following [7] we mean by time constant the factor *T* in the exponent on right side of the equation

$$\Omega = \frac{\omega - \omega_{\mathrm{fin}}}{\omega_{\mathrm{in}} - \omega_{\mathrm{fin}}} = e^{-\frac{t}{T}}; \qquad (1)$$

where Ω - dimensionless excessive rotation frequency, ω_{in}, ω_{fin} – initial and finite TGM rotation frequency respectively, [Hz]; *t* – time, [s].

Equation (1) is analogical to some other processes in which the principal parameter varies in time exponentially. In particular, similarly described changing of solid body temperature in a liquid with constant temperature (the regular thermal regime of the type.Time constant sometimes is called index of inertia.

K.N. Atkinson [3] have proposed for evaluation of time constant expression of such a type:

$$T = \frac{C}{Q}; \qquad (2)$$

where *C* – constant, depending on the parameters of inertia of rotor [m^3], *Q* – actual flow rate value, [m^3/h].

Constant C is evaluated from this expression:

$$C = \frac{(1+\eta)J}{\rho r^2}; \qquad (3)$$

where ρ – fluid density [kg/m^3]; *r* – mean radius [m]; *J* – mean moment inertia of the rotor, [kg·m^2]; η – dimensionless flow deviation factor.

Analogical dependence has been suggested in [7]. However, direct experimental results in [7] shows that the time constant depends also on the initial or current TGM rotation frequency (initial or current its meter' reading). This is illustrated, for example, by the plot in Fig. 1.

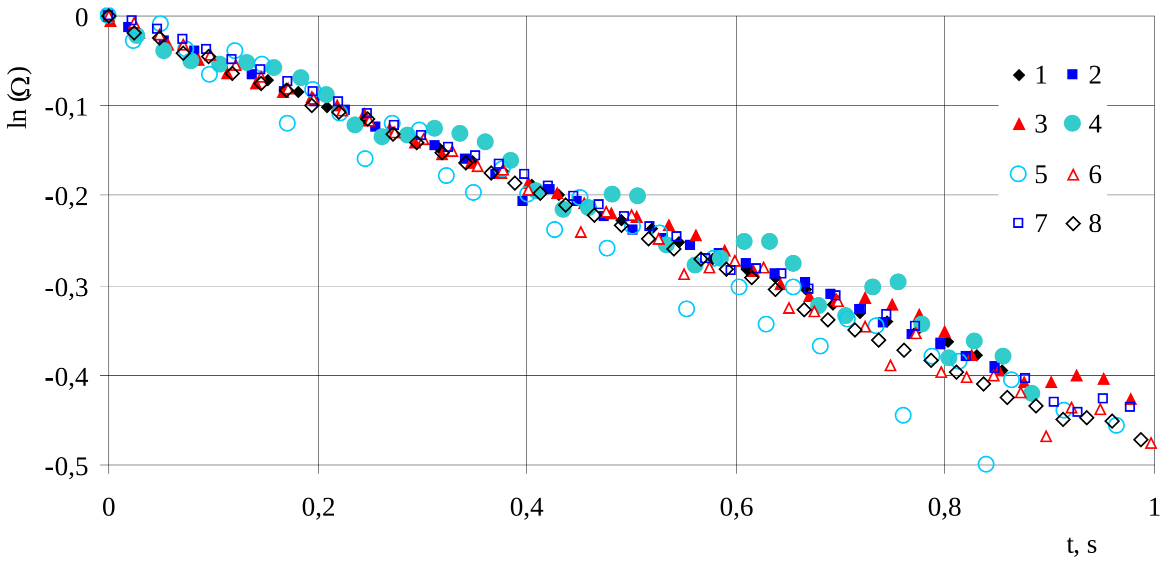

Fig. 1. Dependence of dimensionless rotation frequency on time, Q_{fin} = 200 m^3/h. 1 – 8 – Q_{in} = 0; 50; 100; 150; 250; 300; 350; 400 m^3/h

At observance in general linear character of changing of the logarithm of the dimensionless excessive rotation frequency in time there is stratification depending on the initial (current) rotation frequency.

In [7], this stratification was not taken into consideration and the dependence of the type (2) was recommended. Due to the importance of constant time for calculate the dynamic error, it was decided to clarify the dependence of time constant, not only from the finite flow rate, but also on the initial or the current value of the meter readings.

2. EXPERIMENTAL METHODOLOGY AND RESULTS

Facility, that has been previously developed and dedscribed in [7], have been used for the experiments. This facility allows to measure response of TGM under test on sharp (step) flow change. Simplified scheme of this facility is presented on Fig. 2.

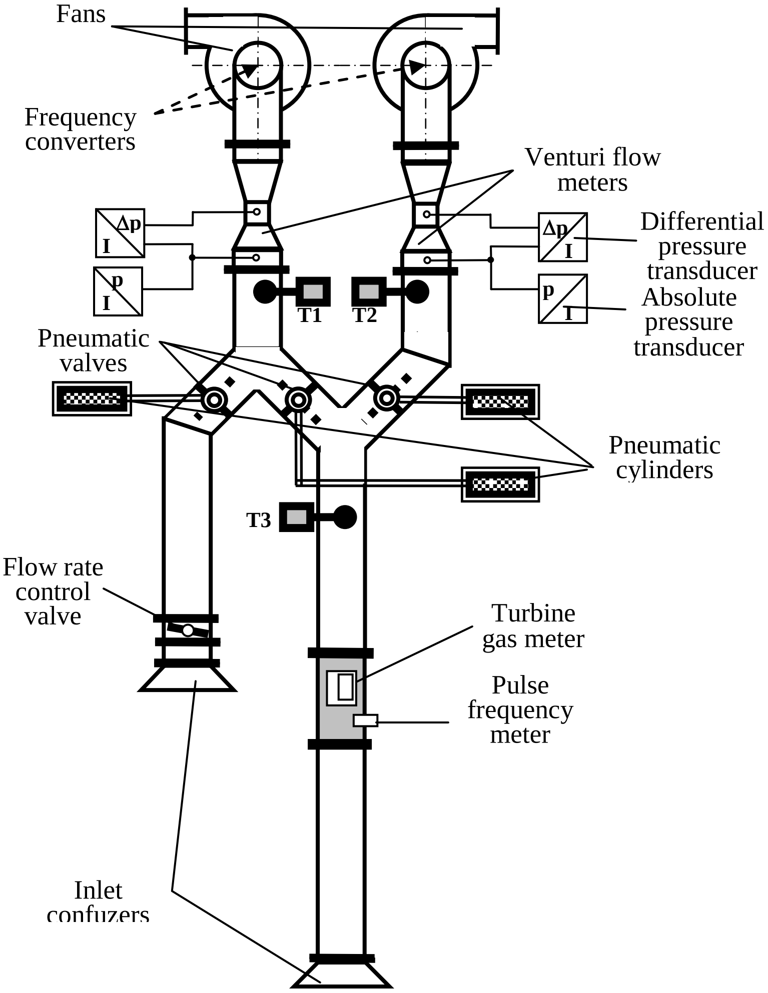

Fig. 2. The simplified scheme of the facility for investigation of tachometric flow meters response to sharp flow change

Air flows in every measurement line are provided independently by two fans. Instant switch of the meter under test from one measurement line to another one is ensured by the system of three valves with pneumatic actuators. For air flow rates measurement in each line by flow rate meters of Venturi type have been used. To control the transition process at rapid change of the flow rate pressure drop across the Venturi flow meter in the line of finite flow rate was measured by low-inertia diaphragm pressure transducer with a differential transformer.

Change in time of the tested meter rotation frequency has been evaluated from measuring time of receipt pulses from the meter. The pulses have been received and time of each was measured by high accuracy analog-digital converter of ACP 16/16 type which ensures data registration with frequency up to 500 000 records per second.

With the initial flow rate value of 700 m^3/h it has been measured the TGM response to the sudden step change in flow rates to values in the range from 0 up to 600 m^3/h. The results are provided in Fig.3.

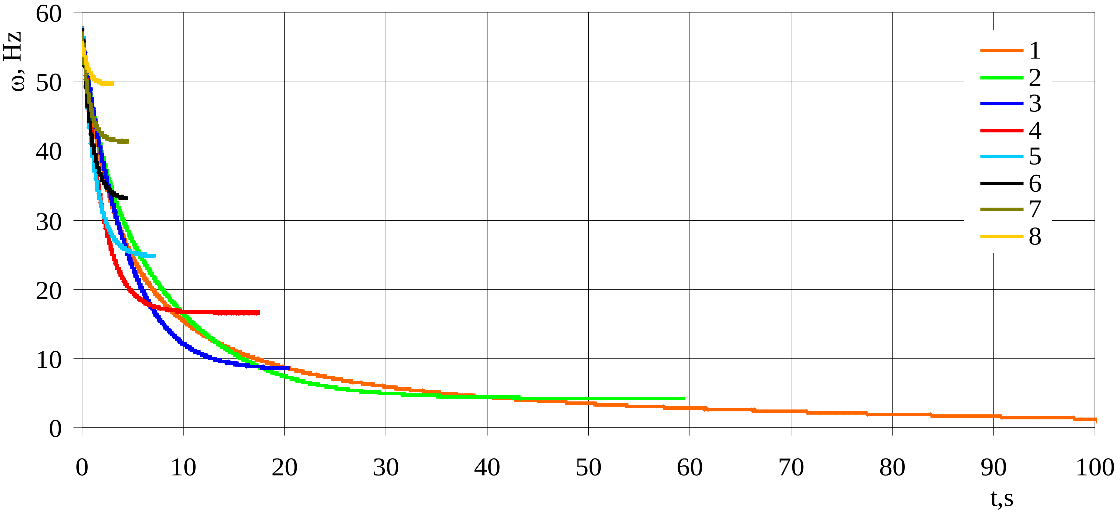

Fig. 3. TGM response on sharp change of flow rate. Q_{in} = 700 m^3/h.
1 – 8 – Q_{fin}= 0; 50; 100; 200; 300; 400; 500; 600 m^3/h.

3. PROCESSING AND ANALYSIS OF RESULTS

The results have been processed in the following order:

1. For each test dependence of logarithm of dimentionless exceeded rotation frequency on time have been plotted;
2. Each dependence has been approximated by power polynomial of the n-th degree (depending on the plot charater n was in the range from 2 up to 6);

$$\ln\Omega = a_1 t + a_2 t^2 + \ldots + a_n t^n \tag{4}$$

3. Presenting (1) in logarithmic form

$$\ln(\Omega) = -\frac{t}{T} \tag{5}$$

and using (3), it has been obtained the expression for evaluation of *T* value

$$T = -\frac{1}{a_1 + a_2 t + \ldots + a_n t^{n-1}} \tag{6}$$

The results of processing are presented in Fig. 4 as dependence of a time constant on the difference between the current and finite rotation frequencies (meter readings).

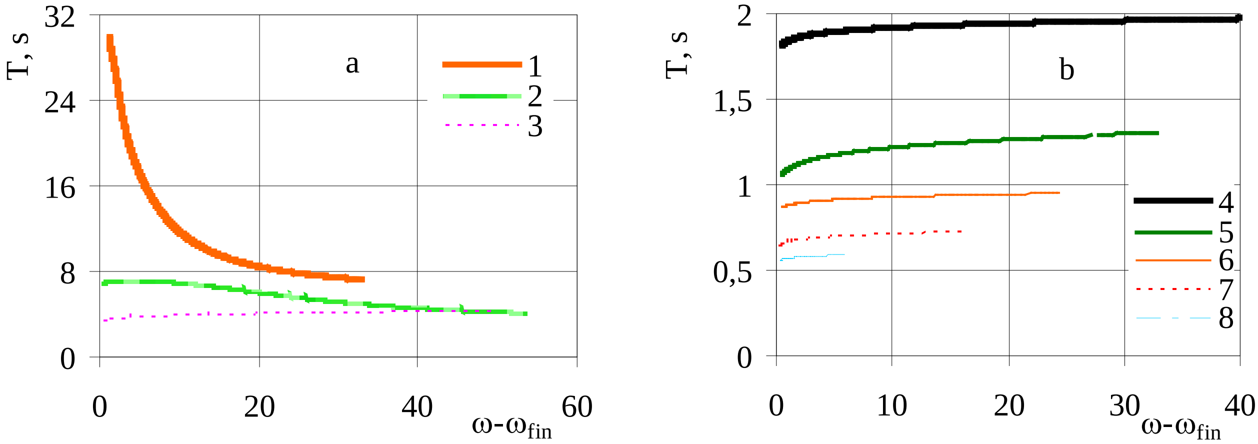

Fig. 4. Dependence of inertia time constant on the difference between the current and finite rotation frequency. Q_{in} = 700 m^3/h. 1 – 8 the same as in Fig. 3

The character of the influence of the difference of current and finite rotation frequencies on inertia time constant is explained by controversial affecting on factors of inertia time constant. The first factor is positive and this is hydrodynamic forces aspiring to accelerate the transition process.

The second factor is the braking one - this is discrepancy of current rotation frequency to common hydrodynamic picture.

Analysis of graphs, presented in Fig. 4 suggests the following conclusions. Initial rotation frequency of velocity meter does not affect inertia time constant. The last depends on the difference between the current and finite rotation frequencies. Results for different values of the initial frequency coincide at the same current frequency.

4. CONCLUSIONS

1. Previously made assumption about independence of time constant on the initial (current) rotation frequency is not confirmed.
2. The most important affecting factor, besides finite flow rate value, is the current value of rotation frequency (meter reading), or more precisely the difference between the current rotation frequency and frequency, corresponding finite value of flow rate.
3. Especially significant influence of difference of rotation frequencies in the region of small values of this difference.
4. Previously generally accepted expression (2) is valid only for sufficiently small values of the frequency difference.
5. The results obtained for the time constant should be used to calculate the meter’response and dynamic error using the method develop by us previously. We shall expect a essential change in results.

REFERENCES

1. LEE W.F.Z., KIRIK M.J., MILLINGTON B. Gas turbine flow meter measurement in pulsating flow. *Journal of engineering for gas turbines and power.* 1975, Vol. 97, p. 531–539.
2. LEHMANN N. Dynamisches Verhalten von Turbinenradgaszahlern. DAS GAS UND WASSERFACH -GWF- 131 1990, Nr.4, Gas Erdgas, p. 160–167.
3. ATKINSON K. N. A software tool to calculate the overregistration error of a turbine meter in pulsating flow. *Flow measurement and instrumentation,* 1992 Vol. 3 No 3, p. 167–172.

4. MCKEE R. J. Pulsation effects on single- and two rotor turbine meters. *Flow measurement and instrumentation*, 1992, Vol. 3 No 3, p 151–166.
5. LEE B. CHEESEWRIGHT R., CLARK C. The dynamic response of small turbine flow meters in liquid flows. *Flow measurement and instrumentation*, 2004, Vol. 15 No 5–6, p 239–248.
6. *LST ISO/TR 3313:1998*. Measurement of fluid flow in closed conduits – Guidelines on the effects of flow pulsations on flow-measurement instruments.
7. TONKONOGIJ J., PEDIŠIUS A., STANKEVIČIUS A. The new semi-experimental method for simulation of turbine flow meters rotation in the transitional flow. World Congress of Science, Engineering and Technology (WCSET 2008), Paris, France. 2008 July 4-6. ISSN 1307-6884, p. 208–212.

RESEARCH OF DOL EFFECTS IN TIMBER ELEMENTS IN BENDING

A. Brokāns
Latvia University of Agriculture
Faculty of Rural Engineering
Akademijas str. 19, LV-3001 Jelgava-Latvia
Phone: +371 29122859, +371 28608255
Email: coldzero@inbox.lv

ABSTRACT

Creep in timber structures is a phenomenon that importantly affects functional compliance of building structures in extended years of exploitation. Creep phenomena is affected by surrounding temperature (T, °C), relative humidity (RH, %), and timber moisture content (MC, %), volume of constructive element, width of annual rings, amount of latewood and other factors.

In order to adequately predict influence and development intensity of creep during building construction lifetime it is important to determine proper creep coefficient c_r values that are adequate for wood and environmental conditions in region of Latvia.

Paper presents study of creep behaviour in variable enviromental conditions – temperature, relative humidity and moisture content, that are characteristic for region of Latvia. These conditions are very important for timber constructions that are subjected to long-term load. Appropriate creep coefficient c_r values are required to predict behaviour and deformations of timber constructions. Experimental research represents timber beam four point long-term loading in bending with variable cross section height-span length ratio under uncontrolled climatic conditions. There were used 12 timber beams with two different span lengths – 1.32 m and 1.50 m. Timber beam cross section dimensions – 60 mm x 30 mm. Timber beams were not dried and moisture content at the start of experiment varied from 19% to 33%. Applied load was theoretically calculated so that instantaneous deflection u_{inst} do not exceed 150 part of span length. Applied load values – 0.40 kN (kilo Newton) and 0.31 kN.

The conclusions were made that moisture content fluctuations and negative air temperature accelerate creep development and intensity. Estimated creep coefficient should rate not only type of timber material and service class but strength class too.

Keywords: Creep phenomenon, creep coefficient, long-term loading, height-span length ratio, instantaneous deflection

1. INTRODUCTION

Molecular structure of wood is a very complex system with uneven distribution of molecules. Bodig and Jayne [1] found that wood has very manifold physical and mechanical properties because of its anisotropy and fibrous structure which needs to be taken into consideration when using wood in construction. Wood structure is the reason why mechanical and physical properties of wood are significantly affected by the surrounding environment. Wood adapts to the environment in which it is located. This process is called hygroscopicity – material ability to absorb moisture from the surrounding environment. During this process, the water molecules penetrate into the wooden cells that physically alter the material. Heterogeneous structure of wood with a high level of hygroscopicity causes swelling and cracking of the material. Climatic variability and, in particular, a large amount of moisture content changes has a very negative impact on the wooden constructions in long term loading.

For the first time the idea of different short-term and long-term timber loading behavior was expressed by the French naval architect George Louis Le Buffon [2].

When loading timber structures with long-term constant load deflection increases over time. This process is called creep. Creep is a deformation increase at constant load (Schniewind [3]).

Thelandersson [4] and Hunt [5] proved that work in linearly elastic phase and creep phenomena are the most basic wood mechanical properties. Serviceability (deflection) requirements are often the main, to determine the size of the beam cross section dimensions, if they are subject to long-term and permanent load.

Over time, as a result of creep development, wooden structures does not longer fulfils serviceability requirements, deflections become unacceptably large and, in the worst case, the construction even loses its load-bearing capacity and collapses. Creep is a “time-dependent” deformation. Under long-term load, at low stress levels and under normal moisture and temperature conditions wood behaves in linear manner. Whale [6] and Morlier [7] stated that at a higher level of stress and/or under changing environmental conditions, wood shows non-linear correlation between stresses and deformations.

To ensure the safe operation of the wooden structures throughout the expected construction lifetime (50 and even more years), it is necessary to accurately predict timber construction element behavior under long-term load at the design stage. Necessary for this purpose, as far as possible, objective design parameters can only be obtained on a pilot study database. Therefore I decided to contribute to solving this problem and to examine how creep develops in timber construction elements (beams) in bending and which are determinative factors and how they influence creep development.

2. MATERIAL AND METHODS

The experimental creep test was started in December 2011 and carried out in a newly constructed house which is not currently populated at this moment. This house was not heated in the winter period; therefore, the climatic conditions were not controlled in any way that allowed checking the timber beam creep operation and development in variable climatic conditions of ambient humidity and temperature.

Experimental creep test at this moment represents twelve (free of knots) pinewood (*Pinus sylvestris* L.) beam long-term loading in four point bending. Test model is given in Fig. 1. Timber beam cross section nominal dimensions - 60x30 mm. At this stage of research two types of span length (*L*) - 1.32 m (group of beams KS-3) and 1.50 m (group of beams KS-4) are loaded with long-term load. It is designed to load two more types of span length *L* – 1.08 m and 1.20 m in continuation of research.

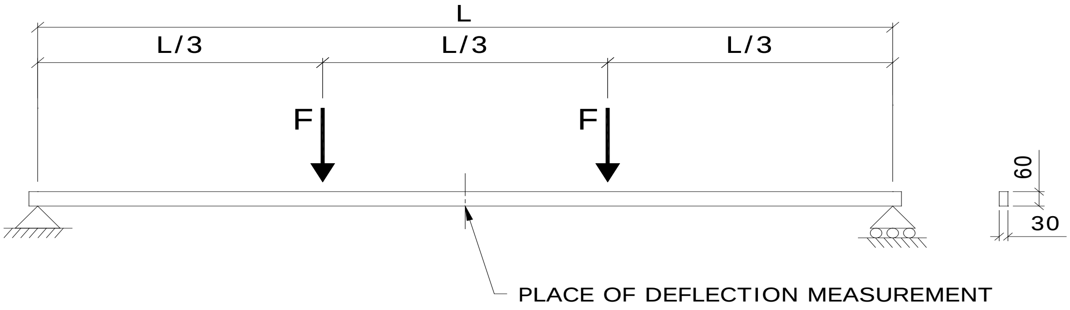

Fig. 1. Test model; *F* – concentrated force

Timber beams were loaded in four point bending with two concentrated forces (*F*) that each force were calculated so as instantaneous deflection u_{inst} at the middle of span do not exceed 150 part of timber beam span length – $u_{inst} \leq \frac{L}{150}$. Timber beam theoretical calculations are given in Table 1. Four different timber beam span lengths were chosen to examine how span to depth ratio (18, 20, 22, 25) influence creep development. For lumber and glued laminated beams the European static standard ratio is 18:1 [7].

Table 1. Timber beam theoretical calculation

No	**Load**	**Span length**	**Design moment**	**Span-heigth ratio L/h**	**Cross section width**	**Cross section heigth**	**Second moment of area about the strong axis**	**Bending stress** $\sigma<1.4$ kN/cm^2	**Inst. defl.** u<L/150	**Allowed inst. defl. L/150**
	F, kN	L, m	M_d, kNm		b, cm	h, cm	I_y, cm^4	σ, kN/cm^2	U_{inst}, cm	cm
1	0.6	1.08	0.216	18	3	6	54.00	1.200	0.71	0.72
2	0.31	1.50	0.155	25	3	6	54.00	0.861	0.98	1.00
3	0.49	1.20	0.196	20	3	6	54.00	1.089	0.80	0.80
4	0.4	1.32	0.176	22	3	6	54.00	0.978	0.86	0.88

Concentrated forces were represented by clay and silicate bricks which were suspended on timber beams (Fig. 2). The deflection measurements were made with dial indicators. Measuring precision of indicators – 0.01 mm. Measuring diapason of indicators – 50 mm. The dial indicators were placed in the middle of the span on the compressed side of the beam. The environmental climatic condition parameters were recorded once in the day. Temperature (T, ° C) in the room and outdoor was fixed with mercury-in-glass (Hg) type thermometers.

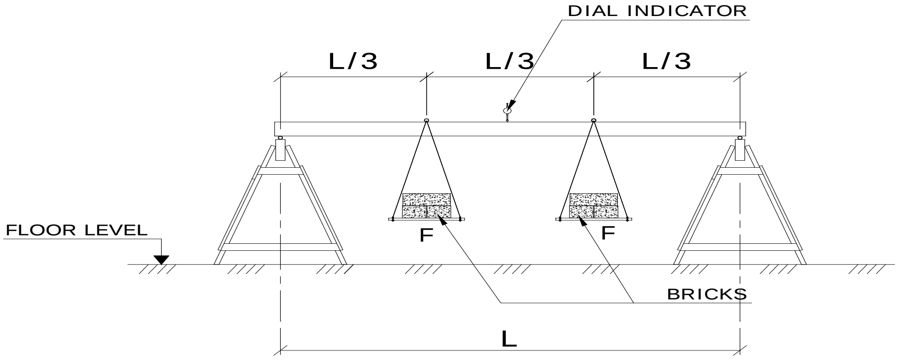

Fig. 2. Timber beam loading

Parallel to the environmental climatic condition parameter recording, timber beam moisture content (MC, %) and relative humidity (RH, %) recordings were made daily.

Moisture content of timber beams were measured with moisture content meter “MD-2G” (measuring diapason – 5%...40%, precision – 1%). Relative humidity was measured with hygrothermometer “Testo 605-H1” (measuring diapason – 5%...95%, precision - ± 3%).

In order to judge about the timber beam strength properties, theoretical modulus of elasticity (MoE) was calculated after registering instantaneous elastic deflection u_{inst} immediately (1 minute) after loading. Theoretical MoE (E_{app}) of rectangular cross-section elements, which are loaded in bending with two symmetrical concentrated forces, was calculated using equation 1:

$$E_{app,inst} = \frac{F \cdot a}{4 \cdot b \cdot h^3 \cdot u_{inst}} (3 \cdot L^2 - 4 \cdot a^2), \tag{1}$$

where F – sum of two concentrated forces, kN;
a – distance from support to concentrated force, cm;
L – timber beam span, cm;
b – width of cross section, cm;
h – height of cross section, cm;
u_{inst} – instantaneous deflection, cm.

As the time-depencent parameter the relative creep (known also as the creep coefficient) was quantified and relationships examined. Creep coefficient in this study is expressed in terms of the initial elastic deflection (u_0):

$$c_r(t,T,MC) = \frac{u_t - u_0}{u_0}, \tag{2}$$

where u_t is the deflection at time (t) in step with the moisture content of wood (MC) and temperature of air (T).

Prior to testing approximately 2 cm length samples were cut of from the end of all beams across the wood fibers in radial direction. Using loupe with precision of 0.1 mm annual ring quantity in 1 cm of wood and amount of latewood in one annual ring were determined.

3. RESSULTS ANS DISCUSSION

The values of moisture content for the twelve loaded beams at the start of the test were variable from 19% to 33% with the mean value of moisture 25.25% with a coefficient of variation (COV) of 19%. After 64 days of test, moisture content exhibited a mean value of 12.17% with a COV of 11%.The monthly average for outdoor temperature were 3.5 ºC (December), -1.1 ºC (January) and -10.2 ºC (first 17 days of February). The monthly average for indoor temperature ranged form 3.9 ºC to -4.9 ºC with a mean value of 0.2 ºC.

Monthly average for indoor relative humidity ranged from 55.8% to 76.4% with a mean value of 68.2%.

The sizes of the beam cross-section presented mean values of 30.68 mm in width and 58.36 mm in height. Span to depth ratio for loaded beams were 22 for group KS-3 and 25 for group. KS-4.

Immediately (1 minute) after loading, instantaneous deflection u_{inst} of timber beams were registered. Theoretical MoE was calculated using equation 1. Summary of those results are given in Table 2.

Table 2. Modulus of elasticity of timber beams

Marking	**Instantaneous deflection**	**Modulus of elasticity (MoE)**
	U_{inst}, cm	$E_{app.inst}$, kN cm^{-1}
KS-4.10	0.80	859.62
KS-4.9	1.30	528.99
KS-4.8	1.20	573.08
KS-4.7	0.50	1375.39
KS-3.10	0.60	1007.84
KS-3.9	0.70	863.86
KS-3.8	1.20	503.92
KS-3.7	0.90	671.89
KS-3.3	0.79	767.39
KS-3.5	0.77	784.31
KS-3.2	0.48	1251.97
KS-3.1	0.48	1251.97
	Mean value of MOE	**870.02**

MoE represents high distribution of the results – from 503.92 kNcm^{-1} (timber beam KS-3.8) to 1375.39 kNcm^{-1} (KS-4.7) with a mean value of 870.02 kNcm^{-1} and with COV of 34%. High distribution of these results can be explained by that fact part of beams - KS-4.8, KS-4.9, KS-3.3, KS-3.5, KS-3.7, and KS-3.8 were cut out of sapwood, remaining 6 specimens from heartwood. Density and moisture content of timber beams were very different at the start of test when theoretical calculation were provided. Sapwood is actively conducting portion of the stem in which parenchyma cells are still alive and metabolically active [10]. The sapwood is the active, "living" wood that transports the water (or sap) from the roots to the leaves. Heartwood (or duramen) is wood that as a result of a naturally occurring chemical transformation has become more resistant to decay. Heartwood is dead wood. That is the reason why weigth of timber beams at the start of test were so different.

Table 3 summarizes the main results for the instantaneous deflections u_{inst} and creep deflections $u_{creep,64}$ after 64 days of test. In addition, relative creep deflections after 7 days ($u_{creep,7}$) and 64 days ($u_{creep,64}$) of test are given. Values of instantaneous and creep deflections are divided in 3 groups which correspond to accurate loading duration and span length of timber beams. According to Eurocode 5, 1 week is the limit between short-term and medium-term load duration classes, 6 months is the limit between medium-term and long-term load duration classes and 10 years is the limit between long-term and permanent load duration classes.

Relative deflection values after 64 days of test showed that loaded beam behavior under long-term load is very different. A detailed analysis shows that four beams - KS-3.1, KS-3.3, KS-3.10 and KS-4.7 exhibited a very high value of 1.91; 1.96; 1.84 and 1.99) for relative deflection u/u_{inst} with a mean value of 1.93. Creep deflection for these four timber beams presented 4.40 mm, 7.60 mm, 5.03 mm and 4.94 mm. The remaining 8 specimens presented relative creep values ranging between 1.35 and 1.60. The relative deflection mean value for all timber beams after 64 days of test presented the value of 1.63 with COV of 14%.

Table 3. Results of instantaneous and creep deflections

Marking	**Instantaneous deflection**	**Creep deflection**	**Relative deflection after 64 days**	**Relative deflection after 7 days**	**Mean value of inst. deflection**	**Mean value of creep deflection**
	U_{inst}, mm	$U_{creep,64}$, mm	$U_{creep,64}/U_{inst}$	$U_{creep,7}/U_{inst}$	$U_{inst,mean}$, mm	$U_{creep,64,mean}$, mm
KS-4.10	8.00	4.28	1.54	1.03	9.50	5.04
KS-4.9	13.00	6.71	1.52	1.05		
KS-4.8	12.00	4.22	1.35	1.11		
KS-4.7	5.00	4.94	1.99	1.14		
KS-3.10	6.00	5.03	1.84	1.16	8.50	5.09
KS-3.9	7.00	4.08	1.58	1.06		
KS-3.8	12.00	5.89	1.49	1.08		
KS-3.7	9.00	5.36	1.60	1.13		
KS-3.3	7.90	7.60	1.96	1.18	6.30	4.24
KS-3.5	7.70	3.01	1.39	1.06		
KS-3.2	4.80	1.95	1.44	0.98		
KS-3.1	4.80	4.40	1.91	1.06		

The established relative creep ratio values after 7 days of test ranged between 0.98 (KS-3.2) and 1.18 (KS-3.3) with a mean value of 1.09 with a COV of 5%. The value of the coefficient of variation (COV=5%) testifies that dispersion of the results is small and they are credible.

Analysis of relative creep relationships versus time during 64 days is analyzed in Fig. 3. Curves of timber beams summarize the relative creep histories for the test beams under long standing (64 days) load. This diagram shows that test period of 64 days can be divided in two periods: period A) from the start of the test to forty second day (1.-42.); period B) from forty second day to sixty fourth day (42.-64.). These two periods – A and B are marked in Fig. 3. Creep development speeds of 10 specimens in period A were very similar, with an exception of two timber beams – KS-4.9 and KS-3.3. Creep developments for these two beams were 0.11 mm/day and 0.17 mm/day correspondingly. Nine specimens presented creep development speed values from 0.03 mm/day to 0.07 mm/day. Timber beam KS-3.2 showed negative (-0.02 mm/day) creep development during period A – that means, deflection of this beam after loading decreased. Mean value of creep development speed during period A showed value of 0.057 mm/day.

Start of the period B, when rise of creep development speed was registered, represents perfect compatibility with rapid decrease of surrounding air temperature and relative humidity. Fast decrease of indoor relative humidity in this cold period caused subsequent fall of the moisture content of timber beams.

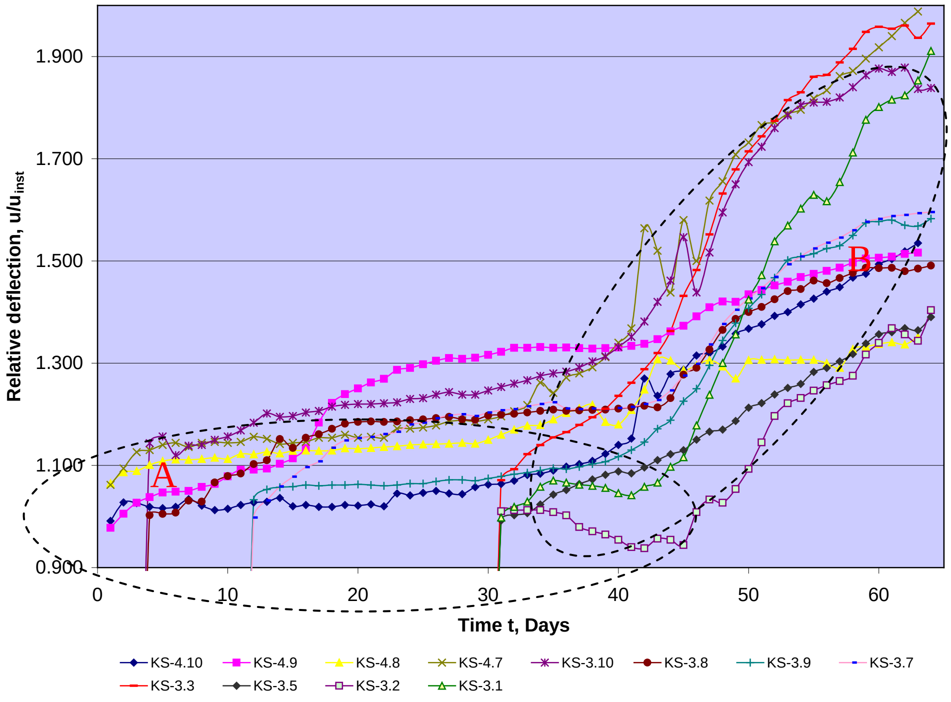

Fig. 3. Development of bending creep during 64 days

Creep development speed values of all timber beams during period B were much higher than in period A. Two timber beams - KS-3.1 and KS-3.3 represented creep development speed values of 0.17 and 0.23 mm/day, other 10 specimens recorded speed values ranged between 0.08 mm/day and 0.14 mm/day with a mean value of 0.115 mm/day.

In this case we can conclude that, registered decreasing period of air temperature (starting in 42nd day of test) initiated fast fall of indoor RH and MC of timber beams which lead up to much faster creep development which continued till 64th day of test. Relative humidity and moisture content depleted together with air temperature which is demonstrated in Fig. 4. Period of negative indoor air temperature continued for 23 days (starting from 43rd day of test).

Fig. 4 represents hygroscopic behavior of wood – moisture content of timber beams during air temperature decrease experienced faster drying than it was before this mentioned cycle. Decrease of moisture content continued even when the rise of air temperature started. Timber beam moisture content at the start of test ranged from 19% to 33% with a mean value of 28%. Moisture content mean values of all beams after 64 days were 12.17%.

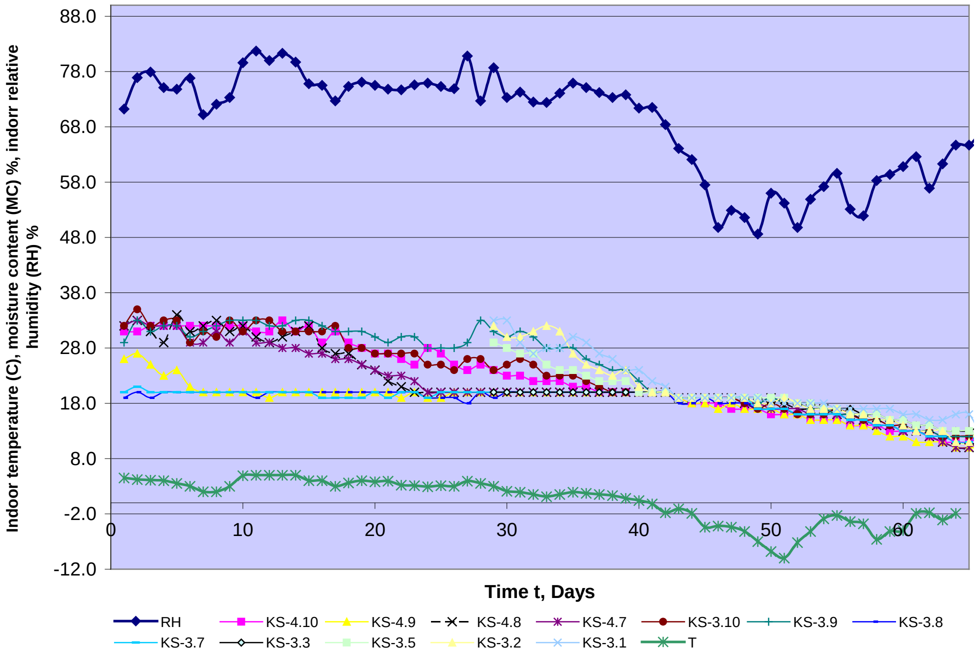

Fig. 4. Temperature, moisture content and relative humidity during 64 days

Summarize of creep coefficient c_r of all timber beams during period A and B is given in Table 4. Creep coefficient was calculated using equation 2. Analysis of creep coefficients shows that period A represent values ranging from -0.05 to 0.33 with a mean value of 0.18.

Table 4. Relative creep coefficients of timber beams

Period	**Timber beam**											
	KS-4.10	**KS-4.9**	**KS-4.8**	**KS-4.7**	**KS-3.10**	**KS-3.9**	**KS-3.8**	**KS-3.7**	**KS-3.3**	**KS-3.5**	**KS-3.2**	**KS-3.1**
A	0.12	0.33	0.19	0.31	0.33	0.12	0.21	0.21	0.24	0.09	-0.05	0.05
A+B	0.54	0.52	0.35	0.99	0.84	0.58	0.49	0.60	0.96	0.39	0.40	0.91

Creep coefficient values during 64 days of test varied from 0.35 to 0.99. Four timber beams (KS-4.7, KS-3.10, KS-3.3 and KS-3.1) represent creep coefficient values from 0.84 to 0.99, other 8 specimens shows values from 0.35 to 0.60. Mean value of creep coefficient c_r during 64 days – 0.63. Distribution of these results is high with a COV of 37%. High distribution of these results can be explained by that same fact like it was with MoE of timber beams - part of beams were cut out of sapwood, part from heartwood, density and moisture content of timber beams were different at the start of test.

Results of annual ring quantity in 1 cm of wood of wood and amount of latewood in one annual ring are given in Table 4.

Table 4. Annual ring quantity in 1 cm of wood and amount of latewood in one annual ring

Marking	Number of annual rings N	Distance between end annual rings *l*, cm	Sum of latewood Σσ, cm	Annual rings in 1 cm, *n*	Amount of latewood %, *m*
KS-3.1	15	1.87	0.85	8.0	45
KS-3.2	17	2.36	1.03	7.2	44
KS-3.3	9	2.10	0.93	4.3	44
KS-3.5	6	2.23	0.93	2.7	42
KS-3.7	12	2.35	1.17	5.1	50
KS-3.8	9	2.60	1.17	3.5	45
KS-3.9	16	2.15	1.12	7.4	52
KS-3.10	11	2.45	0.69	4.5	28
KS-4.7	12	2.00	0.99	6.0	50
KS-4.8	13	2.70	1.11	4.8	41
KS-4.9	10	2.90	1.64	3.4	57
KS-4.10	16	2.70	1.30	5.9	48

Six timber beams – KS-4.8, KS-4.9, KS-3.3, KS-3.5, KS-3.7, and KS-3.8 are cut out from the heartwood of stem, other 6 beams are cut of from sapwood. Table 4 represents that number of annual rings in 1 cm of wood for these beams vary from 2.7 to 5.1 with average of 3.97. An average number of annual rings in 1 cm of wood for remaining 6 timber beams – 6.5.

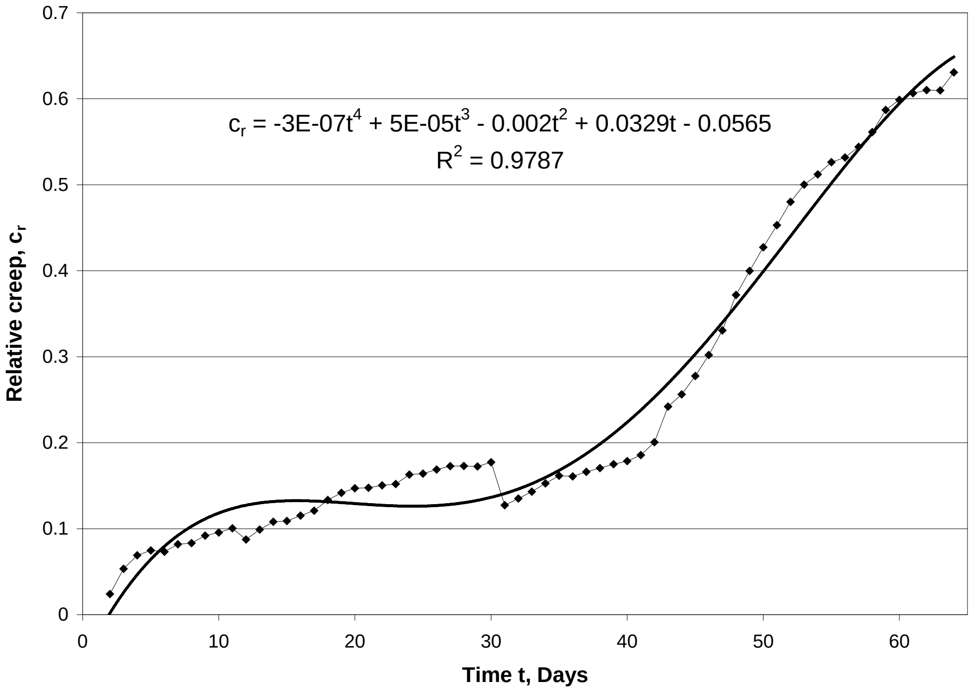

Fig. 5a. Polynomial approximation of average relative creep values versus time under load

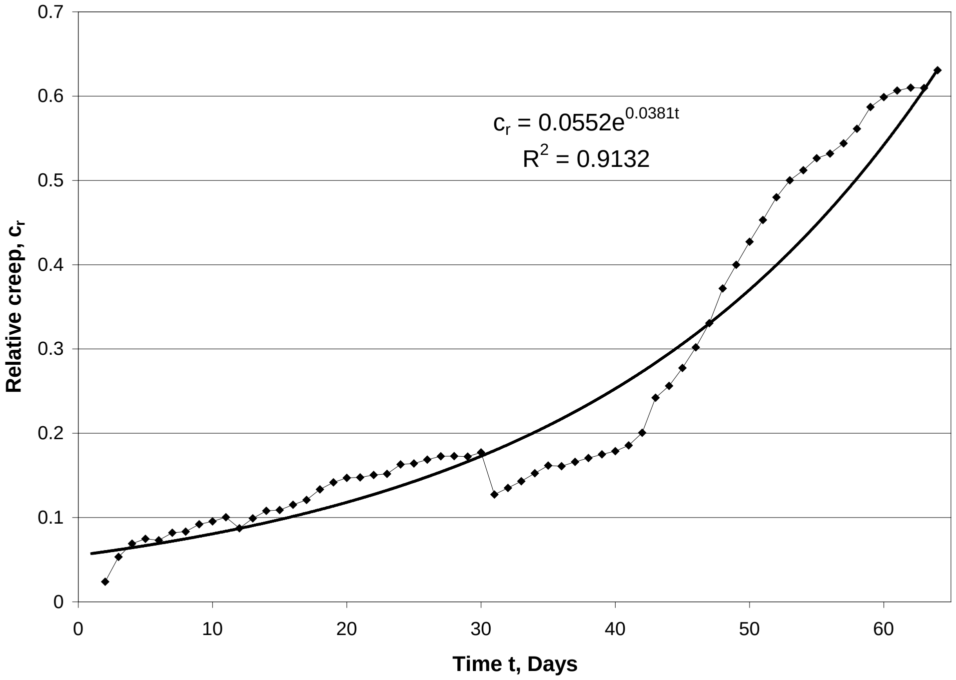

Fig. 5b. Exponential approximation of average relative creep values versus time under load

Different mathematical models were examined to describe the creep relationships according to the test data. Best fitting between test curve and regression model may be obtained by exponential and polynomial curves. In this study the linear relationships were found as sufficiently good approximations testified by the coefficient of determination R^2 values close to unity (Fig. 5a and 5b).

4. CONCLUSIONS

This provisional study provides background for future experiments in order to establish accurate factor system for prediction of final deformations in timber structures.

Creep of wood is dependent on season – moisture variation causes fluctuation in creep curves. Relative humidity fluctuations and radical decrease of air temperature (indoor temperature receded to minus 10° C), accelerated creep development speed that continued even when constant increase of air temperature was observed. Small cross-section beams are especially influenced by humidity cycling. Small sample size and variability in MoE make it difficult to make more detailed conclusions at this stage of test.

The estimated creep coefficient c_r during 64 days of test presented the mean value of 0.63 with a COV of 37%. Such a high distribution of results can be explained by that fact part of beams was cut out of sapwood, part from heartwood. Width of annual rings for wood that is cut out of heartwood is much bigger than it is for sapwood. Strength properties (MoE) for timber beams which are cut out of mature wood is much more worse that it is for timber beams that are cut out from sapwood. This coherence is illustrative in Table 2. Further studies are needed to estimate influence of this factor on creep development.

It is possible that precision of results were affected by the deformation of supports but that is only assumption. It is planned to measure deformation of supports in prolongation of test.

Further studies on wood structure and creep behavior under variable climatic conditions are necessary to adequately judge about all influencing factors. These studies are necessary to define appropriate creep coefficient values corresponding to climatic conditions and growing conditions of Latvian forests.

5. REFERENCES

1. Bodig, J.; Jayne, B.A. *Mechanics of wood and wood composites*, Van Nostrand Reinhold, New York, 1982, 712 p.
2. Buffon, G.L. *Experiences sur la Force du Bois*, (Experiments on the strength of wood), Paris L` Academie Royale des Sciences. Histoire et Memoires, 1740, p. 453–467 (in French).
3. Hunt, D.G. *A unified approach to creep of wood*, The Royal Society, 455, 199, p. 4077–4095.
4. Morlier P. *Creep in timber structures*, In: Report of RILEM Technical Committee 112-TSC. London, 1994, 149 p.
5. Schniewind, A. P. Recent progress in the study of the rheology of wood, *Wood Science and Technology*, 2, 1968, p. 188–206.
6. Thelandersson, S. *Serviceability limit states - Deformations*. In: Timber Engineering STEP 1, Centrum Hout, The Netherlands, 1995, p. A17/1-A17/8.
7. Whale, L.R.J. *Deformation characteristics of nailed or bolted timber joints subjected to irregular short or medium term lateral loading*. Ph. D. Dissertation. South Bank Polytechnic, London, U.K, 1988, 260 p.
8. LVS EN 408. *Timber structures – Structural timber and glued laminated timber – Determination of some physical and mechanical properties*, 2003, 30 p.
9. EUROCODE 5 – *Design of timber structures – Part 1-1: General – Common rules and rules for buildings*, 2004, 123 p.
10. Forest Products Laboratory. *Wood handbook—Wood as an engineering material*. General Technical Report FPL-GTR-190. Madison, WI: U.S. Department of Agriculture, Forest Service, Forest Products Laboratory, 2010, 508 p.

CYSENI 2012, May 24–25, Kaunas, Lithuania
ISSN 1822-7554, www.cyseni.com

INVESTIGATION OF COMPOSITE THERMAL INSULATING MATERIALS LIKE “MICROSPHERES – BINDING COMPONENT”

S.M. Danilova-Tretiak, V.L. Dragun, L.E. Evseeva, V.G. Leschenko
A.V. Luikov Heat&Mass Transfer Institute of NAS of Belarus
Brovki str., 15, Minsk 220072 –Belarus
Phone (+375)172842135
Email: dts@hmti.ac.by

ABSTRACT

At present, the wide range of thermal insulating materials are used including composite coating which consists of hollow ceramic (or glass) microspheres with characteristic size of 10-50 µm. The spheres are mixed in binding material. After drying the coating has thickness of about 0.3 mm and represents several layers of microspheres, which are bound in thin film of acrylic binder, for example. Such coating is characterized by simple technology of application and, as it is mentioned by manufacturer advertisement, allows reduction of heat losses, has high enough vapor permeability and low wettability. But mechanisms and real effect of such coatings on thermal insulation of enclosing structures are not explored completely.

The results of complex (thermo-visional, thermal gravimetric, microscopic) investigation of the composite material like “microspheres-binding material” are presented in this paper. The experiments are carried out in laboratory conditions and on real objects in use. Dependence of material’s thermal conductivity on temperature and microspheres content is analyzed. It is shown that new generation materials with microspheres filler influence on energy saving ability of enclosing structures, but advertising calculated parameters are not confirmed by experiments. Recommendations for using composite materials like “microspheres-binding material” as thermal insulation are also presented here.

Keywords: composite material, thermal insulating, microspheres, binding component, temperature

1. INTRODUCTION

At present, composite coating which consists of hollow ceramic (or glass) microspheres with characteristic size of 10–50 µm thermal material is used for different purposes [1, 2]. The spheres are mixed in binding material which is a mixture of latex and acrilic polymers components. Such composition allows the material to be light, flexible, with good adhesion to metals, wood, plastic, glass, concrete after drying. After drying the coating has thickness of about 0.3 mm and represents several layers of microspheres, which are bound in thin film of binder. Such coating is characterized by simple technology of application and, as it is mentioned by manufacturer advertisement, allows reduction of heat losses not less then 30%, has enough high vapor permeability and low wettability. But mechanisms and real effect of such coatings on energy efficiency of enclosing structures are not explored completely.

Hollow glass microspheres (HGM) are fine-disperse easily-friable powders consisting of thin-walled glass spherical particles. The particles have low packed density of about 0.2 g/cm^3. Unique properties of microspheres (and consequently of composites like “microspheres – binding component”) such as low density, small size, spherical form, high hardness and melting temperature, chemical inactivity define a wide range of microspheres applications in modern industry – for enhancing thermal characteristics of polymers, particularly in producing of heating pipeline insulation, light pliant thermal insulating sealants, anticorrosive coatings for inner surface protection of water-supply and drain tubes, fillers for fire-protecting ceramics, cement, stucco gypsum and so on.

Special binding material which is the base of coatings under investigation must satisfy the definite requirements depending on composite application. In the case of thermal insulating coatings of building walls the composite can consist of acrylic resins with modifing additives and the requirements are:

- the coating must stay flexible both at high and low temperatures;
- the coating must cover the surface completely making seamless membrane which is permeable for water vapour diffusion;
- the coating must stand up actively to the effects of environment.

Though different modifications of such coatings are used in practice already the properties of such composites are not explaned completely. There are papers devoted to coatings investigation from optical point of view [3, 4], but regarding the influence of thermophysical behavior of coating and its components on efficiency of thermal insulation does not considered precisly. The results of complex (thermo-visional, thermal gravimetric, microscopic) investigation of the composite material like “microspheres-binding material” are presented in this paper.

2. METHODOLOGY

To be successful in usage of composite materials like “microspheres – binding component” as thermal insulating ones it is necessary to know about their properties particularly thermophysical behavior because it defines the quality of thermal insulating materials.

Thermal conductivity of composites filled with glass microspheres was investigated. The device which realizes the method of monotonic heating of samples by one-directional heat flow was used [5]. The error of measurements was not higher than 6-8 %. For temperature measurements in this stage of investigation the chromel-alumel thermocouples with diameter of 0.2 mm were used.

The samples were prepared in the following manner: the coating was applied on the copper foil base of 50 µm thickness. Total thickness of the sample was 0.6–1.0 mm. Because copper thermal conductivity is much higher than one of coating, we can neglect thermal resistance of the base.

Thermographic investigation of coating with microspheres was carried out using thermal camera “IRTIS-200” (Russia) in spectral band of 3-5 µm. For temperature control by contact method the electronic thermometer TC-5 (Russia) was used. The experimental stand has looked like stainless steel leaf with thickness of 0,5 mm. The metal was coated with thermal insulating composite material. In laboratory experiments the heater was placed behind the sample on distance of 20-50 mm from leaf surface. Additionally, thermografic observation of heat pipelines in working conditions which were protected with the investigated materials was carried out.

Thermal camera indication depends not only on the temperature itself but also on emissivity of the object. Radiation from surrounding objects is reflected by the sample and also come into camera. Besides, air absorbance of infrared spectrum has influence on the signal as well. Modern thermal cameras allow compensation of two last factors automatically in time. But if camera is one-band, as it was in our case, then it is necessary to prescribe emissivity value separately. Scanning of the object by thermal camera was used to define coating emissivity. Then control temperature measurement was carried out by contact thermometer. Emissivity value was set at coincidence of contact thermometer and thermal camera readings [6]. Emissivity of the investigated coating was 0.82 in average.

3. THE RESULTS AND DISCUSSION

Thermal insulating materials are characterized by low thermal conductivity due to air between fibers (for fiber materials) or in pores (for porous materials).

First, thermal insulating materials (as they are declared in advertising) like “full microspheres – binding component” were investigated. The influence of spheres loading (in volume percent) on thermal conductivity is presented in Fig. 1.

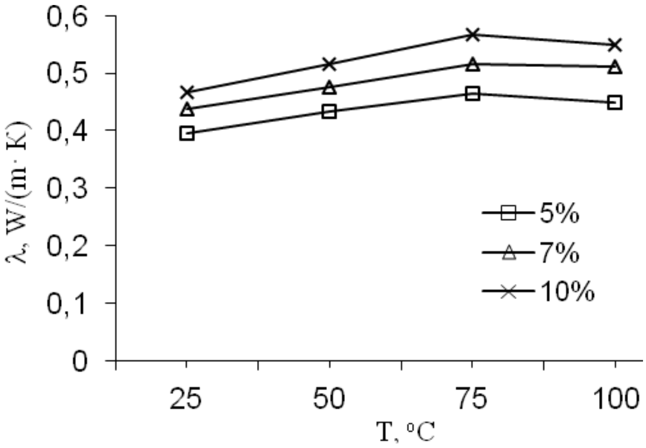

Fig. 1. Thermal conductivity vs temperature
for composites with different microspheres loading

Reduction of thermal conductivity at 100 ^{o}C is explained by water evaporation from the sample. As a result porousity arise and thermal conductivity decrease.

The higher glass microspheres loading is, the thermal conductivity of material become higher. It is because glass microspheres in this case are full and thermal conductivity of glass is higher than one for binding material. The density also shows an increase (ρ=1120, 1260, 1307 kg/m^3 at spheres loading of 5, 7 and 10% respectively).

If HGM are used as filler of composite then the above dependence is reversed. Because in this case the filler has own porosity, higher microspheres loading causes lower density and thermal conductivity of the material. So, when filler loading is 3%, the composite density was 1540 kg/m^3 and thermal conductivity was 0.55 W/m·K at temperature of 25-50 ^{0}C. Increasing the filler loading twice leads to density reduction up to 1160 kg/m^3 and thermal conductivity to 0.33 W/m·K. So, adding of HGM to binding component allows reduction of composite thermal conductivity but the value stays quite high in comparison with advertised one by some producers (0.01 and less [7, 8], for example).

The results of thermal gravimetric analysis of HGM are shown in Fig. 2. Thermogravimetric curve represents uniform mass reduction of pure filler (microspheres) while heating. Hard rest mass after heating up to 900 ^{o}C was equal to 73% from the initial mass value. The value dT in figure is a difference between temperature of our and reference samples. Reference sample (usually it is Al_2O_3) is not transmuted under reached temperature. Minimums of the curve (2) correspond to endothermal processes while maximums do to exothermal ones. These peaks reflects phase transitions or chemical reactions in substances.

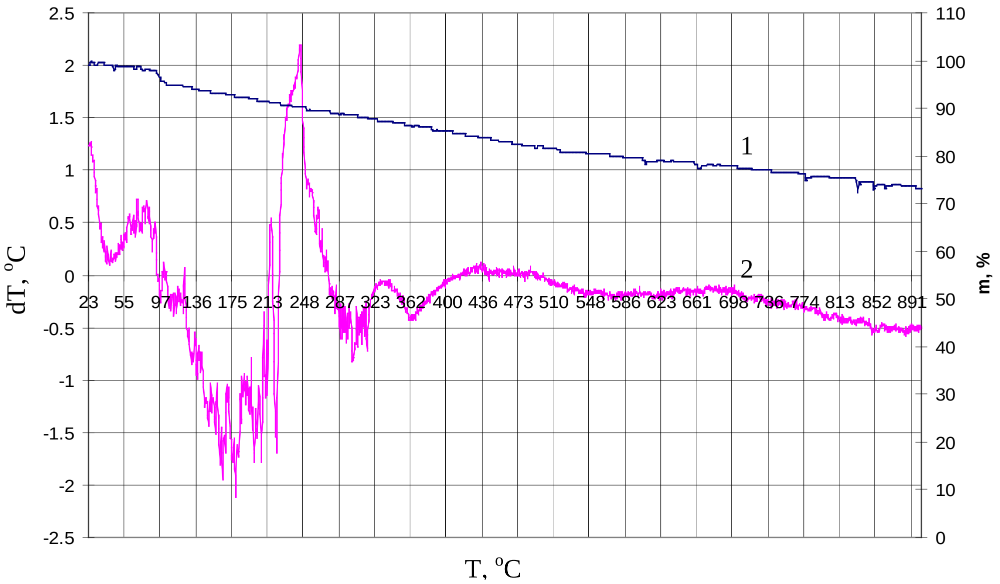

Fig. 2. Thermogravimetric (1) and differential thermal analysis (2) curves for HGM

The results of thermal gravimetric analysis of composite like “microspheres – binding component” (loading is 50 weight percent) are shown in Fig. 3. The curve (1) has several steps which correspond to intensive mass losses. The first stage of mass loss begins at 35 °C and ends at 110 °C. On this stage approximately 40% of mass has been lost without damaging of the material itself. It deals mainly with dehydration of the composite. The next sharp mass reduction is observed in temperature interval of 275-340 °C. It is determined by some organic components of composite evaporating at high temperature.

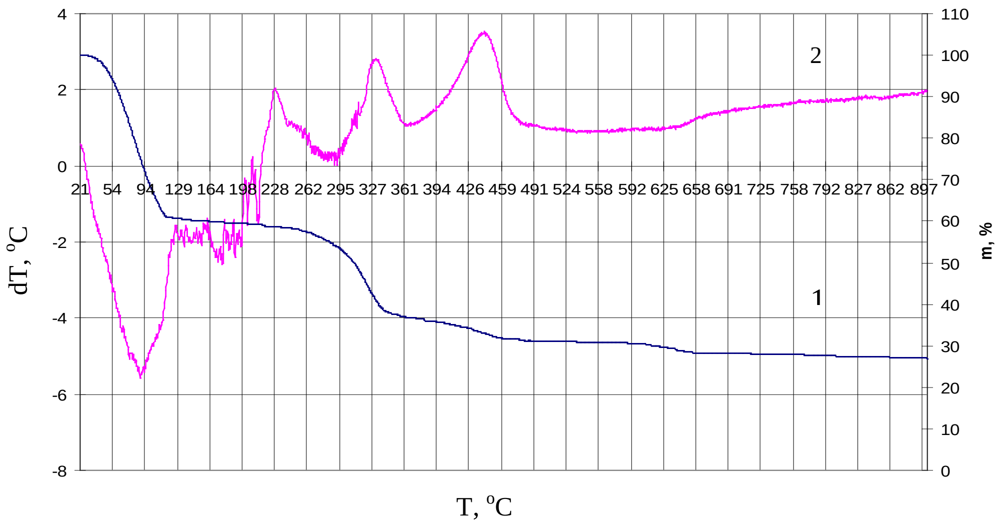

Fig. 3. Thermogravimetric (1) and differential thermal analysis (2) curves for composite like “microspheres – binding material”

Total mass losses of the sample were equal to 72%. In this experiment hard rest of the sample looks like damaged due to high thermal tension glass microspheres that is clear from analysis of thermogravimetric curves for composite and pure filler and is proved by microscopic investigation (Fig. 4).

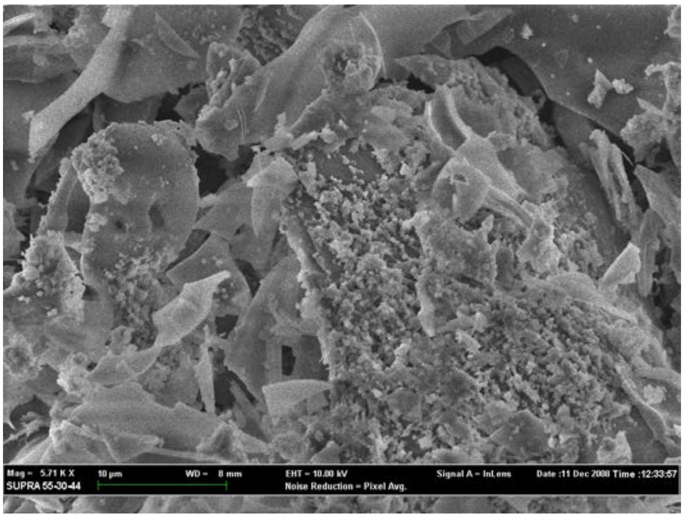

Fig. 4. Hard rest of the composite after heating up to 900 °C
(electronic scanning microscope)

The stainless steel leaf and a part of heat pipeline were coated with composite like “microspheres – binding components” to check it`s applicability for thermal insulation by thermographic investigation (Fig. 5). In laboratory experiments the heater was placed behind the sample on distance of 20-50 mm from leaf surface. It was placed behind the edge of the leaf for simultaneous registration of infrared radiation of both heater and coated leaf. In 50 min after heating started, the temperature of protecting plate (stainless steel leaf coated with HGM composite) reached just 77 °C while heater temperature to that moment was stable and equal to 500 °C.

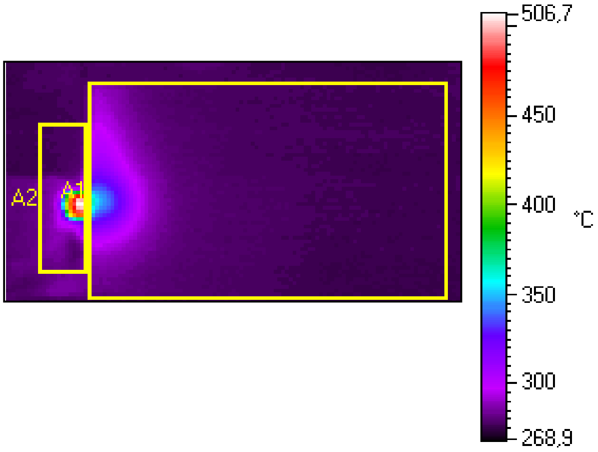

Fig. 5. Thermogram of heater part (A2) and protecting plate (A1)
which partially blanks out the heater

Thermogram of heat pipeline coated with composite like “microspheres – binding component” is shown in Fig. 6. The temperature of uncoated tube is 54,2 °C in average. Coating with composite causes reduction of pipe surface temperature approximately by 20% and reduces heat losses from hot pipe. Estimation of temperature distribution of real object was carried out in consideration of different parts emissivity updating.

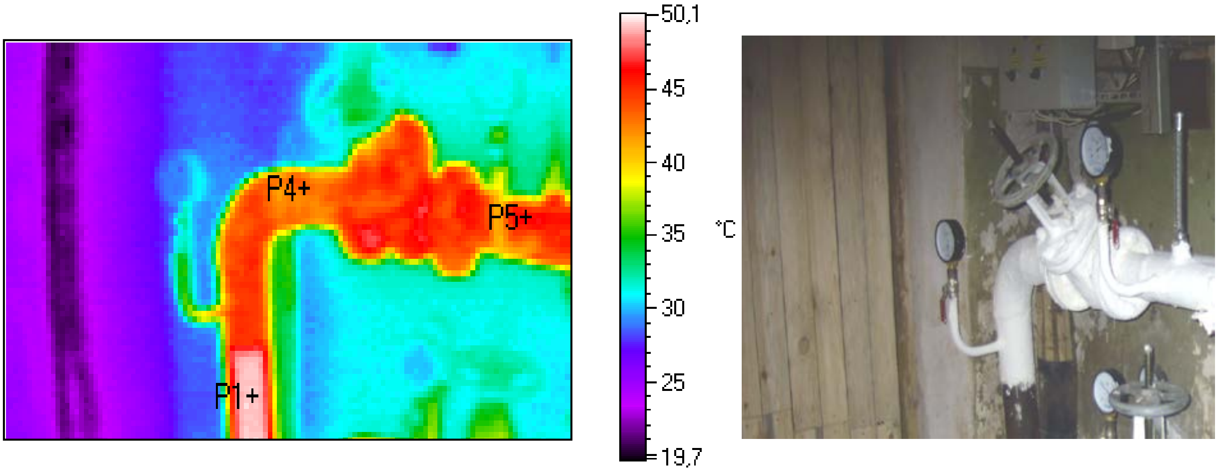

Fig. 6. Image of a part of heat pipeline in infrared (thermogram) and visual spectrum bands

4. CONCLUSIONS

It is observed that adding of full or porous glass microspheres into bounding component has different influence on thermal conductivity of the compound. Thus, full microspheres cause thermal conductivity and density increase due to high thermal conductivity and density of glass itself. Adding of porous filler shows reverse effect – increase of its loading and compound porosity leads to density and thermal conductivity reduction.

Despite reduction of thermal conductivity due to adding of glass microspheres the values of this parameter stay still high in comparison with advertisement (measured thermal conductivity of the composite material is 0.3–0.5 W/m·K).

During heating the composite material is transmuted due to dehydration (at 35–110 ^{o}C) and evaporation of some organic components (at 275–340 ^{o}C).

Complex investigation showed that usage of hollow glass microspheres in mixture with binding component allows their application as thermal insulation in some cases such as heat pipelines, for example. It is especially actual for insulation of heated equipment elements which could not be insulated with traditional heat protecting materials. It should be noted that the temperature of such coating should not exceed 200 ^{o}C as a result of thermal gravimetric analysis. Using of the coatings for heat losses reduction from building walls, as it is advertised by producers, requires more accurate and longer time investigation.

REFERENCES

1. Patent Ru 2374281, 2008. Anticorrosion and thermal insulating coating on the base of porous microspheres.
2. Patent Ru 2310670, 2006. Paint-coating thermo- and moisture insulating.
3. GERMAN, M., GRINCHUK, P. Mathematical model for calculation of thermal insulating properties “ceramic microspheres – binding component”. *JEPTER*, 2002, V. 75, № 6, p. 43–53.
4. KOZLOV, A., GRITZKOVA, I., GUSEV, S. Photon crystalls on the base of polymeric microspheres. Scientific-technical journal *Photonic*s, 2009, № 6, p. 8–11.
5. PLATUNOV, E. *Thermophysical measurements in monotone regime*. Moscow: Energy, 1973.144 p. (in Russian).
6. ***GOSSORG***, Zh., **Infrared** *Thermography: Principles, Technique, Application*. Mir, Moscow: Mir, 1988, 416 p. (in Russian, translated from French).
7. http://www.assystem.lv/ru/?s=1297804910
8. http://www.rostovstroi.ru/mat/gker.php

CYSENI 2012, May 24–25, Kaunas, Lithuania
ISSN 1822-7554, www.cyseni.com

ENTIRELY HYPERELASTIC PRESSURE SENSOR SYSTEM

A. Linarts, J. Zavickis, M. Knite
Institute of Technical Physics
Azenes street 14/24 – 322, LV-1007 Riga – Latvia
Phone +37126400209
Email: artis.linarts@rtu.lv

ABSTRACT

Our recent research approved polyisoprene nanostructured carbon black composite (PNCBC) as a promising material for soft - hyperelastic piezoresistive pressure sensor application. Compared to other materials that are used for pressure sensors the PNCBC is relatively cheap, hyperelastic and is easily produced in various shapes and sizes.

In the current article we present an original attempt to develop a completely hyperelastic pressure sensor system using layered composite approach. The composite layers are made only from PNCBC elements each with various concentrations of carbon black. They have been semi-vulcanised separately so that they could maintain their shape during the final vulcanization when all elements are cured together to form a uniform sensor system. Raw rubber compositions with necessary vulcanization ingredients and variable concentrations of electro conductive carbon black were made in Baltic Rubber factory. Electrical percolation shift as well as piezoresistive effect under 1 and 10 atmospheres of pressure was determined to evaluate most suitable PNCBC for each element. These properties are known to be crucially dependent on the geometry and structure of the conductive filler as well as mixing methods. To improve sensors sensitivity we used 6 piezoresistive elements that where connected in series connection. It is also possible to monitor each element response if we use a different electrode placement in composite layers. The dimensions of developed sensor system are 100x70x5mm but they can be easily adjusted for specific application requirements.

The elaborated sensor system is capable to detect graduate pressure changes, vibration or sharp impacts. We believe that it is a good competitor in field of tactile sensors or artificial skins.

Keywords: Hyper-elastic, polyisoprene, carbon black, piezoresistive, pressure sensor

1. INTRODUCTION

Most of the pressure sensors are rigid systems made from brittle materials therefore their usage is limited due to vulnerability to withstand impact, vibrations or large deformations. However industries like automotive, civil and medical engineering and robotics are interested in cheap, reliable, various shape and elastic pressure sensors. Our previous research approved polyisoprene nanostructured carbon composites to be a prospective materials for nowadays demands [1]. However the sensing properties of this material are extremely dependant on fabrication conditions, filler type and concentration [2-3]. External force changes the resistivity of this composite due to deformation caused particle movement that leads to destruction and construction of conductive networks, this effect is also know as piezoresistivity. It has been known that various conductive fillers like carbon nanotubes [4], graphite [5] and metallic powders [6] can be used to manufacture piezoresistive polymer composites. In this research we propose PNCBC to be used as a prospective material for elaboration of large scale entirely hyperelastic pressure sensor (EHPS) and determine EHPS response under external 0,1 and 1 MPa of pressure in cyclic loading conditions as well as we determine the processing pressure influence on the piezoresistive sensitivity and behavior of EHPS under 0,1 MPa of pressure.

2. METHODOLOGY

2.1. Evaluation of raw materials

Natural polymer - polyisoprene was mixed with necessary curing ingredients (sulphur, zinc oxide, stearic acid and N – Cyclohexyl – 2 - Benzothiazole Sulfenamide) and various high structure carbon black (Degussa Printex Xe2 with specific surface area of 950m^2/g, DBP absorption 380ml/100g, average primary particle diameter 30nm) concentrations using roll mixing in Baltic Rubber factory (BRF). The optimal vulcanization conditions of polyisoprene nanostructured carbon black composites were determined at BRF using Monsanto 100 dynamic rheometer. To determine electrical as well as piezoresistive properties of each PNCBC composition flat, round shaped samples (diameter of 18mm and average thickness of 1mm) with brass foil electrodes were made by curing the raw rubber in stainless steel mould using Rondol thermostated press for 15 minutes under 3 MPa of pressure at 150 °C. After moulding the samples were shelf aged at room temperature for at least 24 hours before any measurements were made. Afterwards the electrical conductivity of each PNCBC sample was measured using Keithley 6487 Picoammeter/Voltage source and piezoresistive behaviour was determined using Zwick/Roell Z2.5 universial material testing machine coupled with Agilent 34970A data acquisition/switch unit. Due to technical limitation of measuring equipment PNCBC samples with conductivity lower than 10^{-8} S/m were not tested for piezoresistivity. Obtained results determined the selection of materials for elaboration of entirely hyperelastic pressure sensor (EHPS). The EHPS were made in various processing pressures (0,5MPa; 1MPa; 2MPa; 3MPa) to determine the most suitable conditions. The specific electrical conductivity versus carbon black (CB) concentration (expressed in mass parts per hundred rubber (p.h.r.)) in PNCBC composites is shown in Fig. 1.

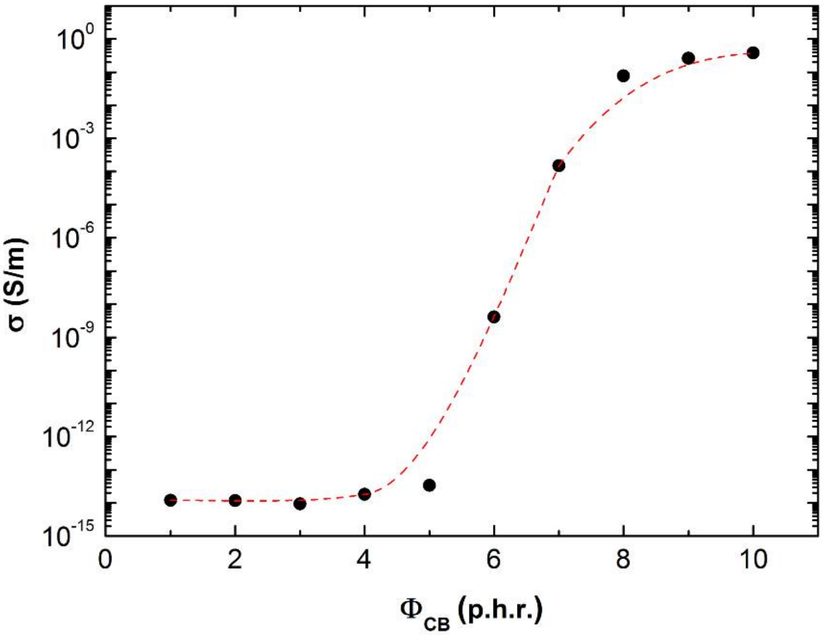

Fig. 1. The electrical percolation transition of PNCBC

As can be seen from Figure 1 the percolation shift is found to be in the region from 5 to 8 p.h.r. CB - according to the concept of piezoresistivity, the PNCBC should be the most sensitive if the conductive filler concentration is within the range of percolation shift. The piezoresistive properties of PNCBC samples with concentration from 7 to 9 p.h.r. CB was determined under external pressure for up to 1 MPa – the loading and unloading speed was kept constant at 10 kPa/s (Fig. 2). The highest piezoresistive sensitivity was observed for PNCBC samples with 8 p.h.r. CB, PNCBC samples with lower CB concentrations were not tested for piezoresistivity because the initial conductivity was too low to successfully perform these tests.

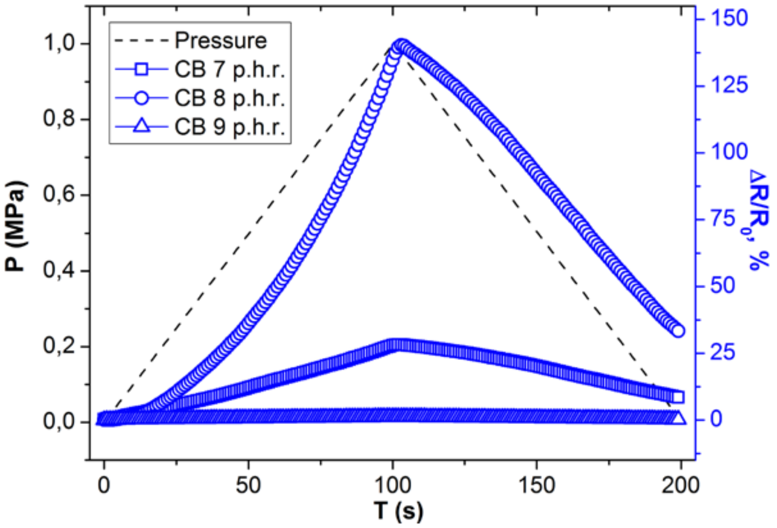

Fig. 2. Piezoresisitive behaviour of PNCBC with 7, 8, and 9 p.h.r. CB under 1MPa of pressure

2.2. Elaboration of entirely hyperelastic pressure sensor (EHPS)

The EHPS archetype was made using layered composite design were pressure sensitive elements were joint with electrode elements and incorporated into protective non-conductive natural rubber shell without CB filler. As a pressure sensitive elements PNCBC with 8 p.h.r. CB was used - the piezoresistive sensitivity of this composition under 1 MPa of pressure was previously found to be 140%. PNCBC with 10 p.h.r. CB was used in hyperelastic electrode elements on both sides of sensitive elements since the specific electrical conductivity for this composition was the highest. The placement of electrode layers in EHPS was designed to insure that the sensitive elements were connected in series connection to provide better piezoresistive sensitivity under external pressure. All EHPS elements initially were semivulcanized separatelly for 11 minutes under 3 MPa of pressure at 140 °C to insure that they could maintain their shape during final vulcanization when all elements where assembled in designate positions and cured together under 3 MPa of pressure at 150 °C for 20 minutes. To determine the influence of the vulcanization pressure on the piezoresistive behavior of sensor the EHPS elements was semi-vulcanized and final product was vulcanized into one solid block under 0,5; 1 and 2 MPa of pressure (EHPS 0,5; EHPS 1; EHPS 2). To connect EHPS to measuring equipment two small wires with soldered brass foil extensions were added to the side electrode layers. Fig. 3 shows schematic placement of electrode and sensing elements in protective rubber shell. Fig. 4e shows AA cross section view of Fig. 3.

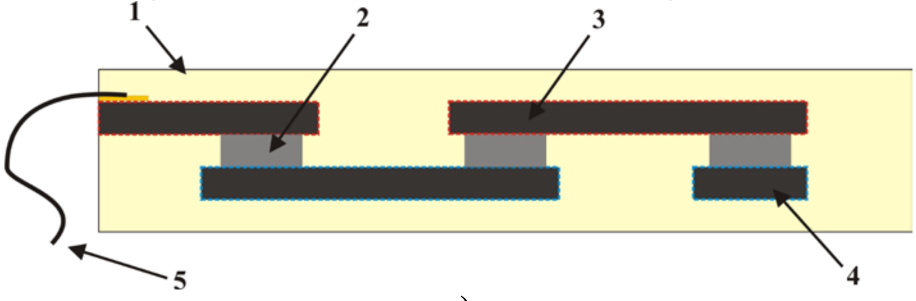

a)

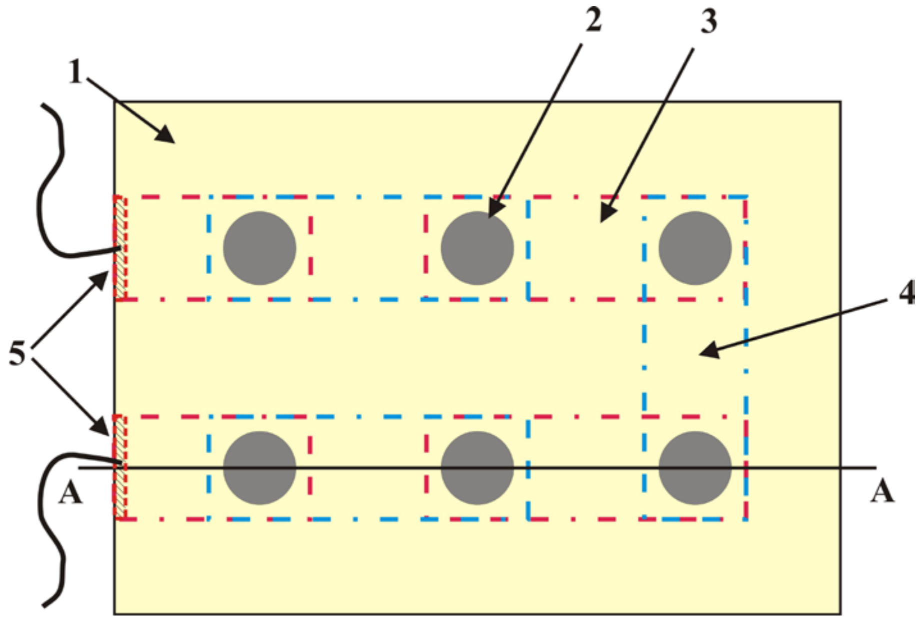

b)

Fig. 3. a) . Planar schematic view of EHPS and b)Schematic AA cross section of EHPS, consisting of : 1 - non conductive outer shell, 2 – piezoresistive PNCBC, 3 – upper layer of conductive PNCBC, 4 – lower layer of conductive PNCBC, 5 – wires with soldered small brass foil plates

3. RESULTS AND DISCUSSION

The piezoresistive behavior of EHPS under 0,1 MPa and 1 MPa operational pressures was determined (Fig. 4.). As can be seen in Fig. 4 the piezoresistive behavior is very similar under 0,1 and 1 MPa of cyclic operational pressure, however the piezoresistive sensitivity under 0,1 MPa of pressure is extremely low (less than 2 %) as well as the piezoresistive behavior under repeated cyclic loading tends to decrease gradually. This can be explained with different speed of electrical relaxation for separate structural PNCBC elements of EHPS. This leads to the decrease of total piezoresistive efect in both ranges of operational pressure.

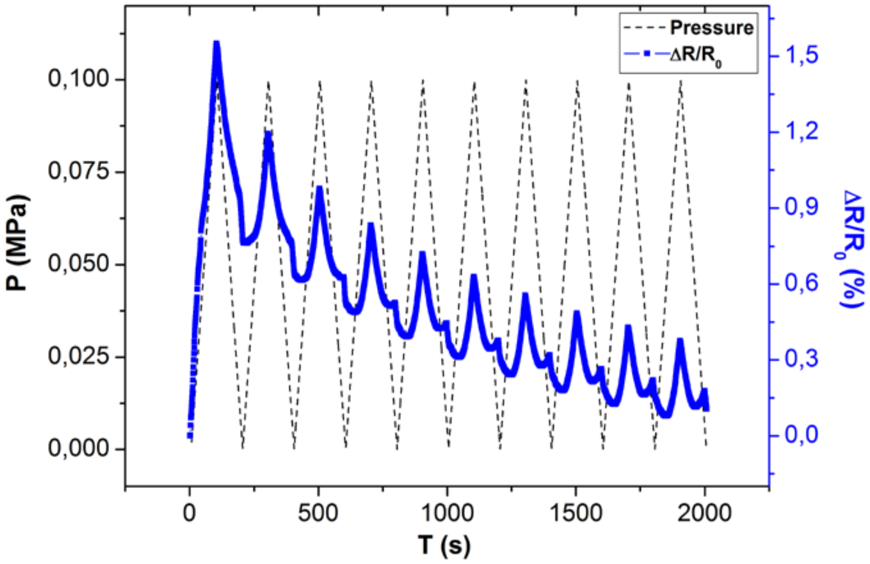

a)

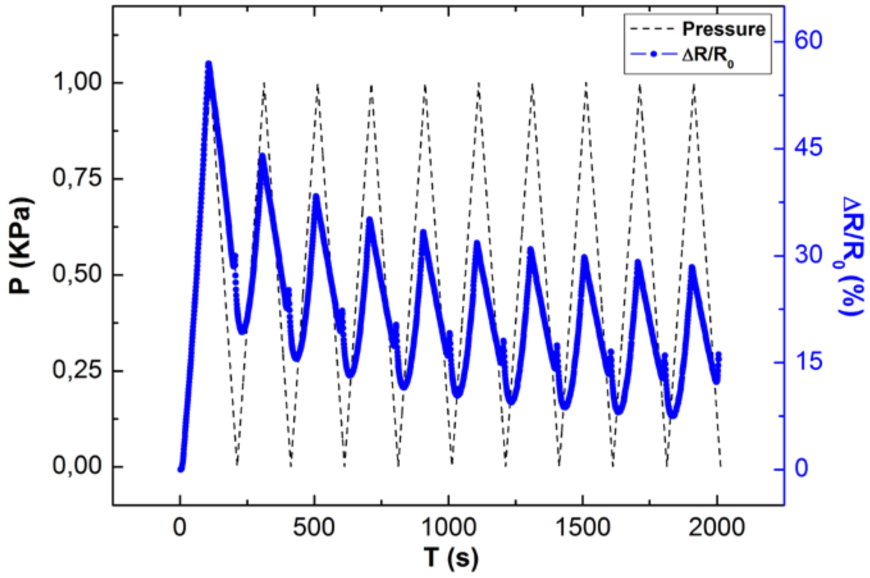

b)

Fig. 4. Piezoresistive behaviour of EHPS under operational pressure up to: a) 0,1 MPa and b) 1 MPa

Fig. 5. show piezoresistive behaviour of EHPS made using different proccesing pressures under 0,1 MPa operational pressure. We can see that EHPS, which was made using highest proccesing pressure – 3 MPa, appears to be the most piezo-sensitive. As we can see for small operational pressures (0,1 MPa), the sensitivity of EHPS drops considerably when proccesing pressure is reduced – this can be explained by increase of the free volume in PNCBC therefore reducing the overall contribution of tunneling currents between CB particles on the electrical conductivity of the composite. The high piezoresistivity of PNCBC therefore is ensured by the increase in distance between closely situated particles and following decrease of tunnelling currents under external pressure.

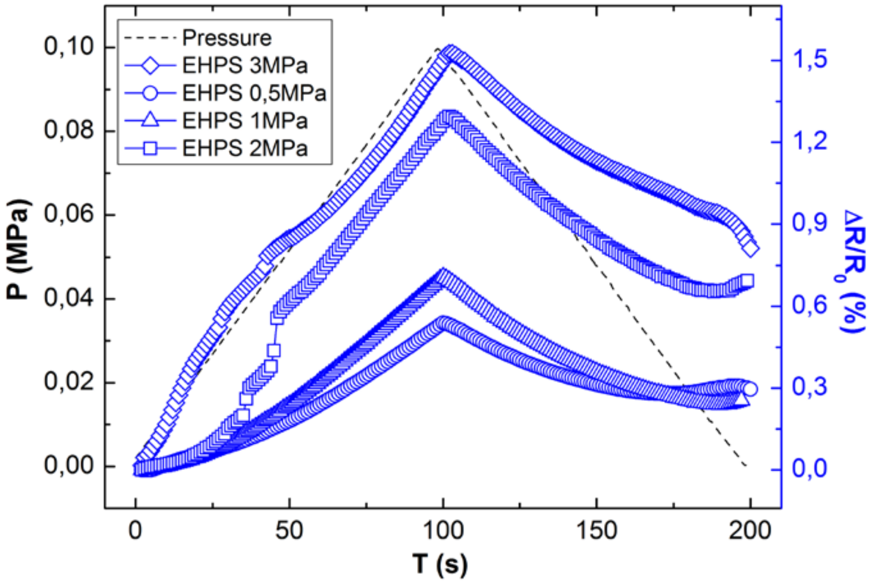

Fig. 5. Piezoresistive behaviour of EHPS with different proccesing pressures under operational pressure up to 0.1 MPa

4. CONCLUSIONS

The entirely hyperelastic pressure sensor prototype has been succesfully elaborated by using functional element approach. The raw materials for EHPS was chosen from PNCBC with various CB concentrations after careful examining of their piezoresitive properties.

The design of EHPS needs to be improved because the piezo-sensitivity under 0.1 MPa operational pressure is very low (up to 1.5%) as well as the piezoresisitive behaviour under cyclic operational pressures tends to decrease gradually.

The optimal proccesing pressure of EHPS was found to be 3 MPa.

5. ACKNOWLEDGEMENTS

This work has been supported by the European Social Fund within the project „Support for the implementation of master studies at Riga Technical University“.

REFERENCES

1. KNITE, M., TETERIS, V., KIPLOKA, A., KLEMENOKS, I., Reversible tenso-resistance and piezo-rezistance effects in conductive polymer-carbon nanocomposites. *Advanced Engineering Materials*, 2004, Vol. 6, p. 742–746.
2. KNITE, M., ZAVICKIS, J., TETERIS, V., LINARTS, A., Polyisoprene–multi wall carbon nanotube composite structure for flexible pressure sensor application. *Journal of Nanoscience and nanotechnology*, 2011, Vol. 11, p. 8677–8681.
3. ZAVICKIS, J., LINARTS, A., KNITE, M., The downshift of the electrical percolation threshold in polyisoprene–nanostructured carbon composites. *Energetika*, Vol. 8, p. 44–49.
4. SOLTANI, R., KATBAB, A., The role of interfacial compatibilizer in controlling the electrical conductivity and piezoresistive behavior of the nanocomposites based on RTV silicone rubber/graphite nanosheets. *Sensors and Actuators A*, Vol. 163, p. 213–219.
5. BAUTISTA-QUIJANO, J.R., AVILES. F., AGUILAR, J.O., TAPIA, A., Strain sensing capabilities of a piezoresistive MWCNT-polysulfone film. *Sensors and Actuators A*, Vol. 159, p. 135–140.
6. JOHNSON, O., KASCHNER, G., MASON, T., FULLWOOD, D., Optimization of nickel nanocomposites for large strain sensing applications. *and Actuators A*, Vol. 166, p. 40–47.

CYSENI 2012, May 24–25, Kaunas, Lithuania
ISSN 1822-7554, www.cyseni.com

BROADBAND IMPEDANCE SPECTROSCOPY OF $Li_{2.2}Ti_{1.7}(PO_4)_3$ Li^+ ION CONDUCTING CERAMIC

D. Petrulionis, **T. Žukauskas**
Faculty of Physics, Vilnius University
Saulėtekio ave. 9/3, LT-10222 Vilnius, Lithuania
Phone +37052366064
Email: dalius.petrulionis@ff.stud.vu.lt

ABSTRACT

A solid electrolyte material $Li_{2.2}Ti_{1.7}(PO_4)_3$ was synthesized by a solid state reaction and studied by X-ray powder diffraction, the results of which were consistent with the material having a NASICON type framework structure. A ceramic for the electrical and surface investigation of the material was sintered. The material surface was subsequently investigated by X-ray photoelectron spectroscopy. Li 1s, Ti 2p, P 2p and O 1s spectra were fitted and the empirical chemical formula of the material surface was determined. The electrical characterization was performed by means of two impedance spectrometers, working in the frequency ranges of 10 Hz to 3 GHz, using the two probe method, and 10 Hz to 100 kHz, using the four probe method. All of the electrical measurements were carried out in the temperature range of 300 K to 700 K. Two distinct dispersions of the electrical parameters were observed, which were attributed to Li^+ ion relaxation in the grain and grain boundary regions of the ceramic. Bulk, grain boundary and total conductivities of the ceramic were determined form their respective complex plane plots. High operating frequency of the impedance spectrometer enabled determination of the high frequency limit of dielectric permittivity from its complex plane plot.

Keywords: Li ion solid electrolytes, Fast ion transport, Ionic conductivity, Impedance spectroscopy, NASICON, Superionic conductor

1. INTRODUCTION

Current generation of high energy density batteries based on Li^+ ion chemistry are seeing widespread use as a superior replacement for other battery technologies, such as Ni-Cd and lead-acid, in existing applications and as a novel technology, used in practical implementation of previously unfeasible products like the electric vehicle [1]. Present state of the art Li^+ ion batteries use a polymer based electrolyte coupled with a plasticizing organic solvent. This often brings the usual disadvantages related to the presence of a liquid in the battery, namely the risk of leakage and pollution, corrosion, temperature instability and other safety concerns, along with a limited potential for miniaturization [2]. Conversely, a solid electrolyte material would present none of the aforementioned disadvantages along with a high resistance to shocks and vibrations, while ideally retaining a high, exclusively ionic conductivity at the working (usually room) temperature. Solid electrolyte based batteries also possess a high potential for miniaturization using conventional thin-film techniques [2]. Many of the same characteristics are also important for the application of solid Li^+ ion conductors in high sensitivity CO_2 gas sensors, where they have also seen recent research [3] and [4].

The NASICON type framework structure $LiTi_2(PO_4)_3$ material is a pure Li^+ ion conductor, exhibiting a high ionic conductivity at room temperature [5]. The ionic conductivity of this material can be enhanced by substituting $Ti^{4+} \rightarrow M^{3+} + Li^+$ in the system $Li_{1+x}M_xTi_{2-x}(PO_4)_3$ (where M = Fe, Sc, Al, Y, B, In, Ga and La) [5], [6], [7] and [8], thereby increasing the concentration and the migration rate of Li^+ ions [9]. Similar effects are also observed for the substitution $Ti^{4+} \rightarrow Mg^{2+} + 2Li^+$ in the system $Li_{1+2x}Mg_xTi_{2-x}(PO_3)_4$, as reported in [10].

It was noted, that an increase in Li^+ ion concentration in the above mentioned class of compounds might be achieved by methods other than aliovalent metal doping, with the material still retaining NASICON type framework structure. In this work we present an investigation of $Li_{2.2}Ti_{1.7}(PO_4)_3$ fast Li^+ ion conductor electrical parameters and its relevant physical characteristics.

2. METHODOLOGY

2.1. Sample preparation and physical characterization

The $Li_{2.2}Ti_{1.7}(PO_4)_3$ powder was prepared by a solid state reaction from Li_2CO_3 (99.999 %), TiO_2 (extra pure) and $NH_4H_2PO_4$ (extra pure) precursors according to the diagram in Fig. 1a and the X-ray powder diffraction (XRD) patterns of the resultant compound were recorded at room temperature using Brucker D8 Advance equipment. The equipment used CuKα_1 ($\lambda = 1.540$ Å) radiation and 0.02 degree step, with time per step varying from 1 s to 8 s. Lattice parameters were deduced by fitting the XRD patterns with TOPAS software. In order to investigate the surface and electrical parameters of the compound, the raw powder was uniaxially cold-pressed at 130 MPa and the resultant pellets were sintered in air, according to the diagram in Fig. 1b.

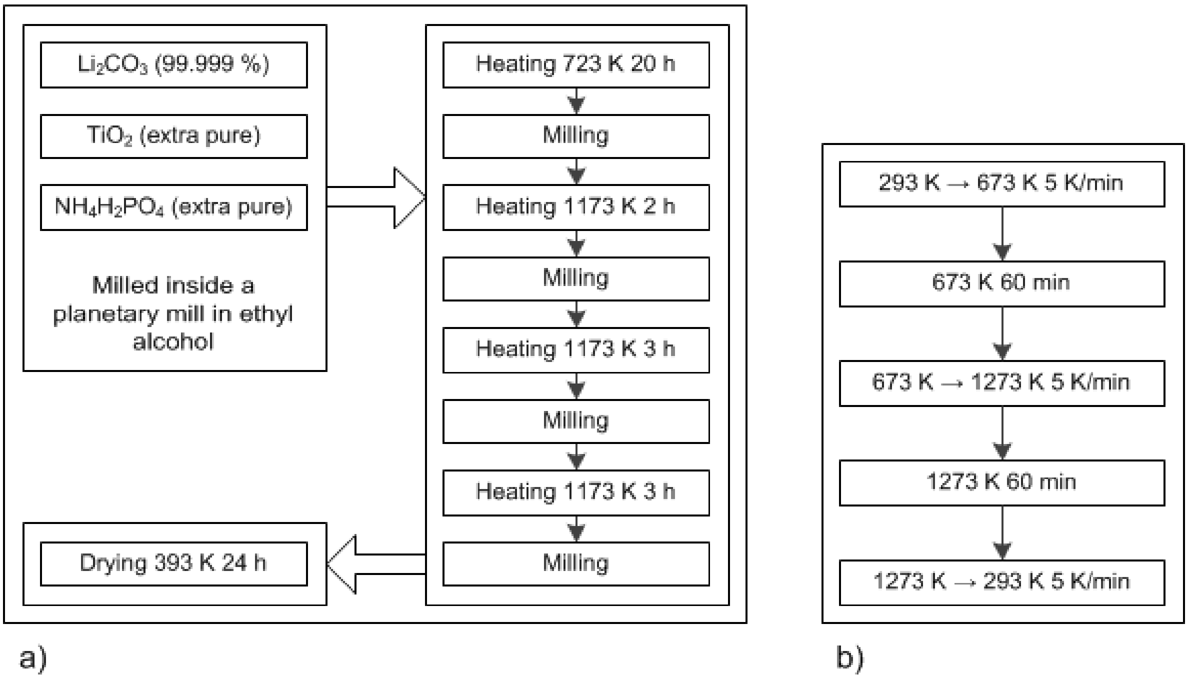

Fig. 1. a) Powder preparation by solid state reaction steps, b) Ceramic pellet sintering steps

The chemical bonding states and elemental composition of the unpolished ceramic surface were determined by X-Ray photoelectron spectroscopy (XPS). The spectra were recorded using LAS-3000 (ISA-Riber) surface analysis apparatus, equipped with a double-pass cylindrical mirror analyzer MAC2. The XPS were obtained using Mg-Kα ($h\nu = 1253.6$ eV) radiation at an average of 10 scans with a step size of 0.05 eV. Before the measurement, the samples were kept in a preparation chamber (residual pressure 1.6×10^{-8} Pa) for 1 day. The residual pressure in the analyzer chamber was 1.3×10^{-8} Pa. In order to extract the core level shifts and relative intensities of the components, a curve-fitting procedure was used. Fitting of the core-level data was performed using a nonlinear fitting procedure, using XPSPEAK 41 software. Li 1s, Ti 2p, P 2p and O 1s spectra were fitted.

Cylindrical (Fig. 2a) and cuboid (Fig. 2b) samples were prepared from the sintered pellet for the two and four electrode measurements, respectively. Porous Pt electrodes were deposited on the contact surfaces by applying Pt paste (GVENT Electronic Materials LTD) and firing the samples at 973 K.

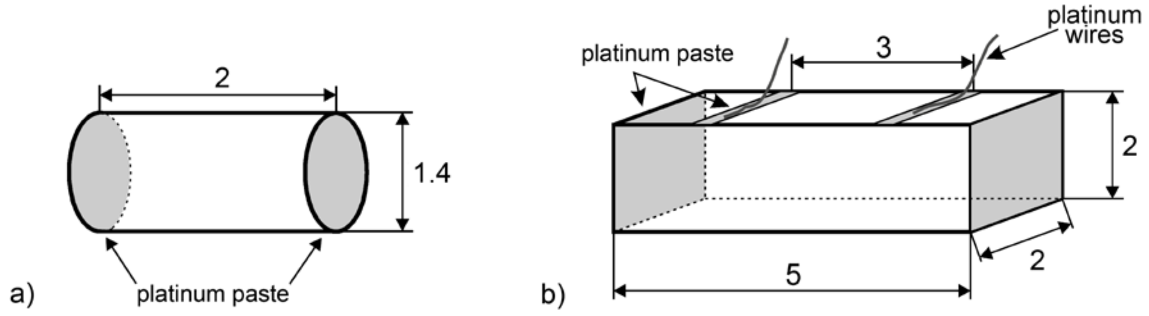

Fig. 2. Sample geometry for a) two and b) four electrode measurements. All dimensions are in mm

2.2. Electrical characterization

The electrical behavior of the ceramic was characterized by means of two impedance spectrometers working in the frequency ranges of 10 Hz to 1 MHz and 300 kHz to 3 GHz, when using the two probe method, and 10 Hz to 100 kHz, when using the four probe method. All of the measurements were carried out in the temperature range of 300 K to 700 K.

Two electrode measurements in the frequency range of 10 Hz to 1 MHz were carried out using the vector voltmeter–amperemeter method while the system was swept in the frequency domain by means of fixed frequency sine signals. The voltage and current through the system were measured by a two channel TiePie HS3 computer oscilloscope. A custom current to voltage converter, allowing accurate vector current measurement, was used. The complex impedance ($\tilde{\rho} = \rho' - i\rho''$), admittance ($\tilde{\sigma} = \sigma' + i\sigma''$), permittivity ($\tilde{\varepsilon} = \varepsilon' - i\varepsilon''$) and dielectric losses ($\tan(\delta)$) of the sample were calculated. The four electrode vector voltmeter–amperemeter measurements were carried out employing the same spectrometer, using voltage measurement points on the sample itself, formed by the previously deposited Pt electrodes.

Two electrode measurements in the frequency range of 300 kHz to 3 GHz were carried out using an Agilent E5062A network analyzer, connected to a heated coaxial line and sample system, with the sample forming a part of the line's inner conductor. The electrical parameters of the sample were calculated from the transmission and reflection coefficients of the system as in [11]. The temperature control loop for both spectrometers was comprised of an Amprobe TMD90 digital thermometer and a Mastech HY 3005 power supply, both of which were connected to a computer.

The bulk (σ_b), grain boundary (σ_{gb}) and total (σ_{tot}) conductivities of the ceramic were calculated from the complex plane plots as in [12]. The Maxwell relaxation frequency (f_M) was calculated by finding the zero-crossing points of the second derivative of the imaginary impedance dependence on the excitation field frequency. The values for the activation energies of σ_b, σ_{tot} and f_M were calculated from the slopes of their respective linear fits [12].

3. RESULTS AND DISCUSSION

3.1. Physical characterization

The results of XRD investigation are presented in Fig. 3. The spectrum consists primarily of $Li_{2.2}Ti_{1.7}(PO_4)_3$ peaks, characteristic of the rhombohedral NASICON type framework structure. A small amount of impurities is observed as secondary and tertiary peaks, which correspond to $Li_4P_2O_7$ and $LiTiPO_5$ phases, marked with asterisks and circles, respectively.

The primary phase was determined to belong to the $R\bar{3}c$ space group and the lattice parameters were calculated to be $a = 8.5148$ Å and $c = 20.8718$ Å, with $Z = 6$ formula units making up the unit cell, having a volume of $V = 1310.52$ Å^3. Bulk density of the material, calculated from the diffraction results, is $d = 2.86$ g/cm^3, while the relative density of the ceramic after sintering was found to be 83.9 %.

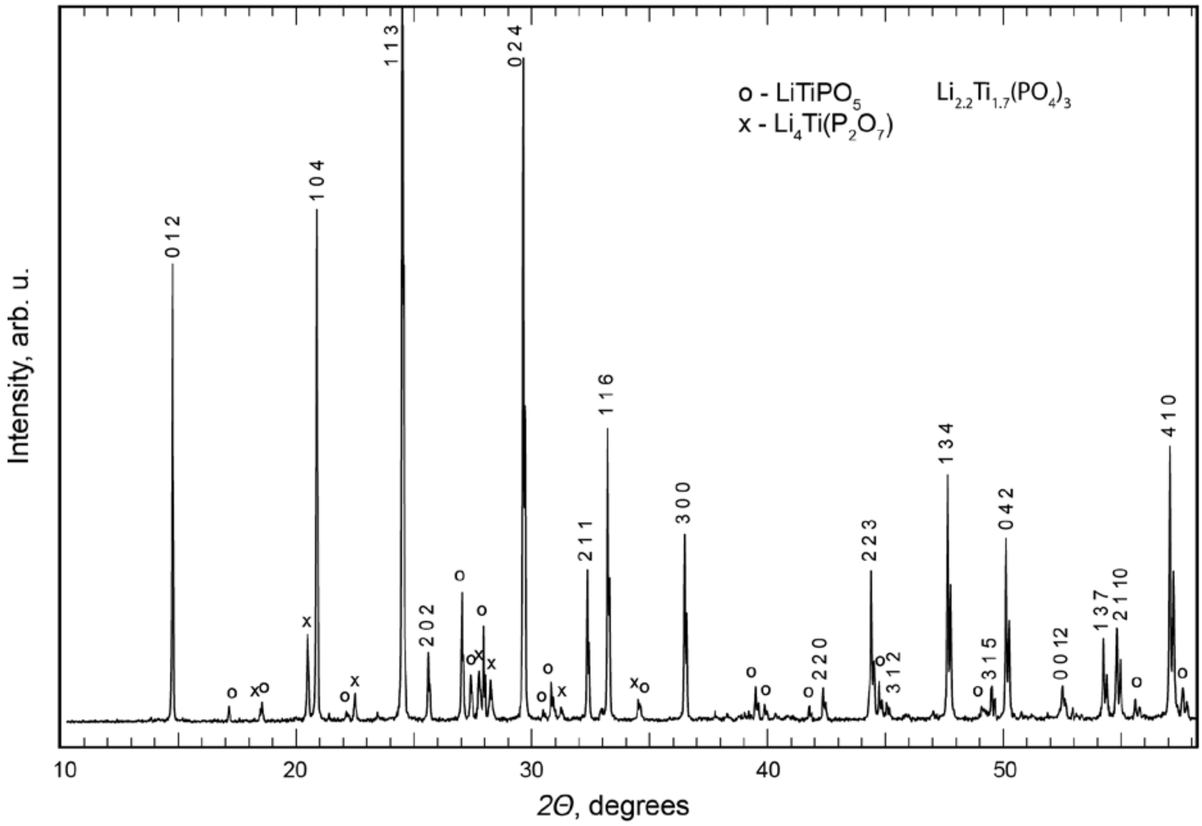

Fig. 3. $Li_{2.2}Ti_{1.7}(PO_4)_3$ X-Ray powder diffraction pattern

XPS spectra of the sintered ceramic samples are given in Fig. 4. Noise in the Li 1s photoelectron spectrum is due to the inherent limitations of the XPS technique for atoms with small atomic number. Due to the low quality of Li 1s spectrum attempts at deconvolution to multiple peaks were not made. In order to exclude sample charging effects, all data were corrected by a linear shift, such that the maximum of the C 1s peak of adventitious carbon corresponded to the binding energy of 284.6 eV.

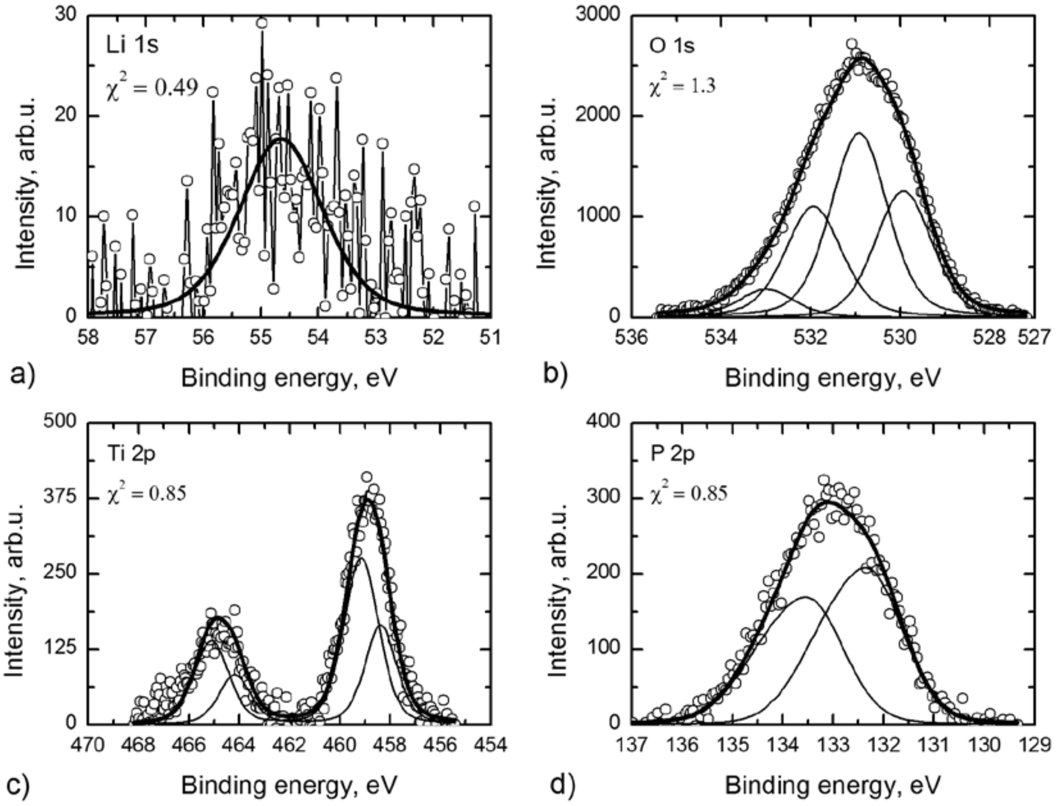

Fig. 4. X-ray photoelectron spectra of the sintered ceramic samples, showing a) Li 1s, b) O 1s, c) Ti 2p and d) P 2p photoelectron spectra

Results of the XPS investigation are given in Table 1. The empirical chemical formula of the ceramic surface, calculated from the XPS spectra, is $Li_{2,8}Ti_{1,8}(PO_4)_3$.

Table 1. Surface analysis results of the sintered ceramic samples

Spectra	Bindig energy, eV	Splitting energy, eV	Amount, at.%	χ^2
Ti $2p_{3/2}$	458.4	5.8	36.4	0.85
	459.1	5.95	63.6	
P $2p_{3/2}$	132.2	1.0	54.5	0.85
	133.35	1.0	45.5	
O 1s	529.9		27.0	1.3
	530.9		41.2	
	531.9		25.3	
	533.0		6.5	
Li 1s	55.0		100	0.49

3.2. Electrical characterization

Frequency dependencies of the electrical conductivity of the ceramic are presented in Fig. 5a. The low frequency and high temperature components of the two electrode measurement have been truncated at low frequencies and omitted at high temperatures, as the effects introduced by the blocking Pt electrodes start to dominate the graph under those conditions, obscuring any useful information.

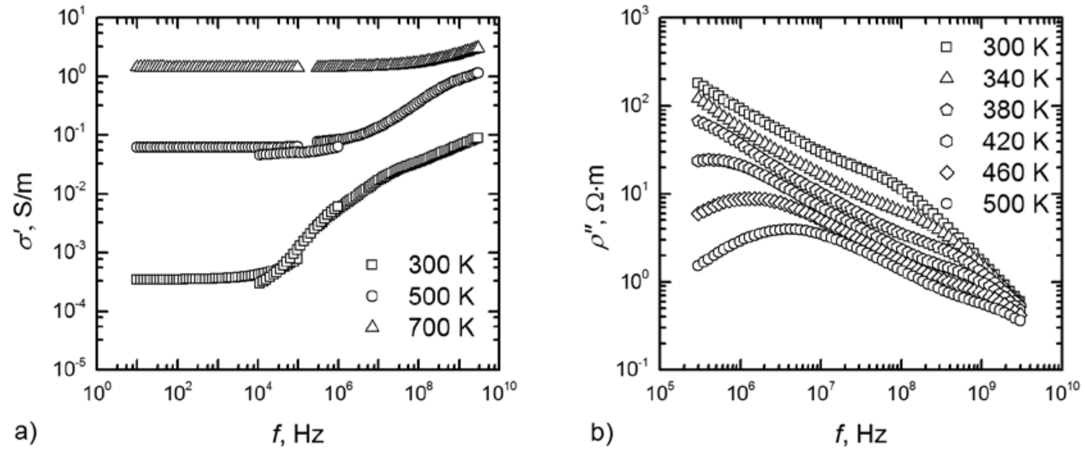

Fig. 5. Frequency dependencies of a) total conductivity and b) imaginary part of the impedance. Data truncated where appropriate

Two relaxation processes were identified, which were attributed to fast Li$^+$ ion transport in the grain and grain boundary regions of the ceramic samples. Both of the relaxation processes are thermally activated, shifting upwards in frequency with an increase in temperature in accordance with Arrhenius law, as depicted in Fig. 6a. The activation energies of σ_b and σ_{tot} are $\Delta E_b = 0.20\,\mathrm{eV}$ and $\Delta E_{tot} = 0.35\,\mathrm{eV}$, respectively.

In Fig. 5b two sets of thermally activated peaks of the imaginary part of the impedance are clearly visible. The set of low frequency peaks corresponds to Li$^+$ ion relaxation in grain boundaries, while the less prominent high frequency peaks are associated with Li$^+$ ion relaxation in the ceramic grains.

Maxwell’s relaxation frequency (Fig. 6b) was calculated from the zero crossings of the second derivative of the imaginary part of complex impedance dependence on frequency (shown in Fig. 5b). It varies from 51 MHz at 300 K to 1.14 GHz at 500 K and is thermally activated, having an activation energy of $\Delta E_f = 0.20\,\mathrm{eV}$.

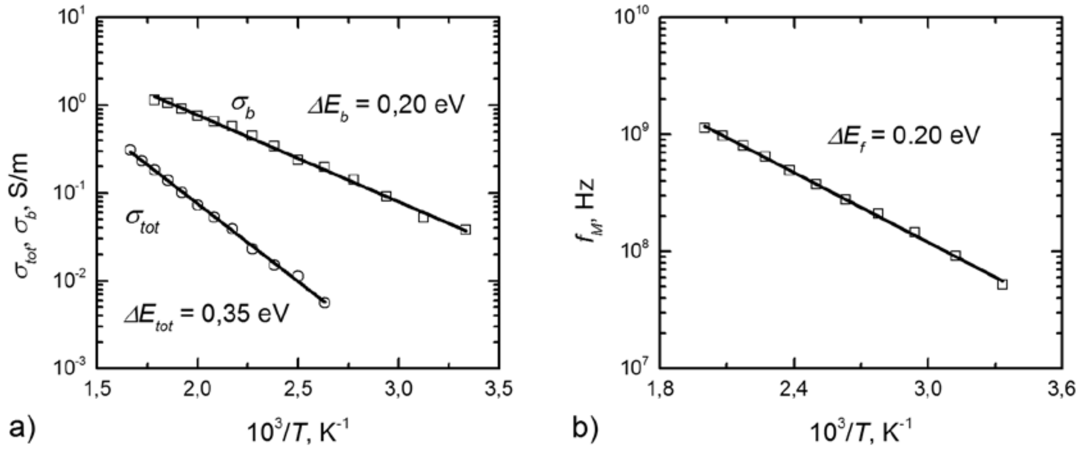

Fig. 6. Arrhenius plots of a) total and bulk admittances and b) Maxwell resonant frequency for ion migration in the ceramic grains, as calculated from the imaginary part of complex impedance dependence on frequency

Complex plane plots of the impedance and admittance at the temperature of 300K are presented in Fig. 7. Any discontinuities in the graphs are due to the electrode induced ion blocking effects in the two electrode sample.

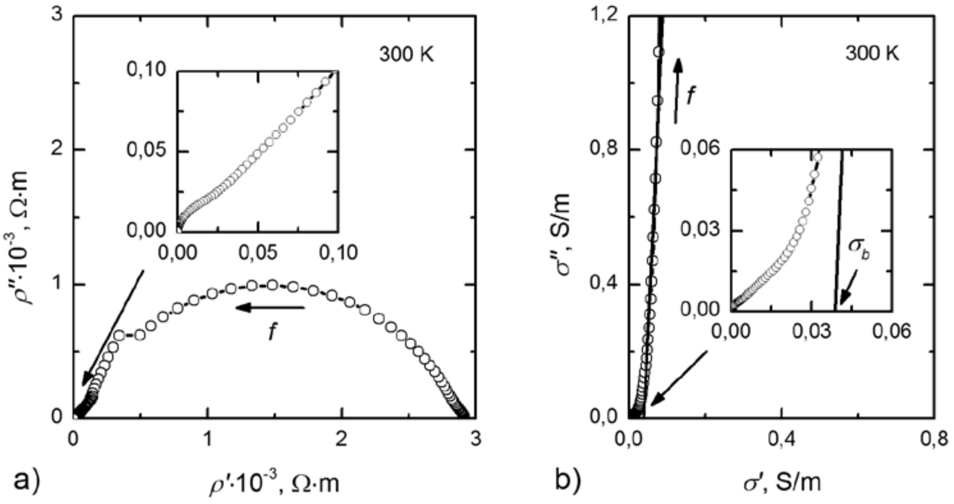

Fig. 7. Complex plane plots of a) impedance at 300 K, with inset showing the high frequency arc, and b) admittance at 300 K, with inset showing the σ_b

The complex impedance plot in Fig. 7a exhibits two highly overlapping semicircles, corresponding to the grain boundary impedance in the low frequency region and bulk impedance in the high frequency region, which is shown in the inset. Fitting of the larger semicircle resulted in a grain boundary admittance value of $\sigma_{gb} = 0.35\,\mathrm{mS/m}$. The high frequency behavior, corresponding to the dispersion region associated with the bulk conductivity can be more easily ascertained from the complex admittance plot in Fig. 7b. Fitting the linear high frequency portion of the plot yields $\sigma_b = 38\,\mathrm{mS/m}$, as can be seen in the inset. The grain boundary impedance dominates the total impedance of the sample by two orders of magnitude.

Dielectric permittivity and dielectric losses in $Li_{2.2}Ti_{1.7}(PO_4)_3$ increase with temperature, as shown in Fig. 8.

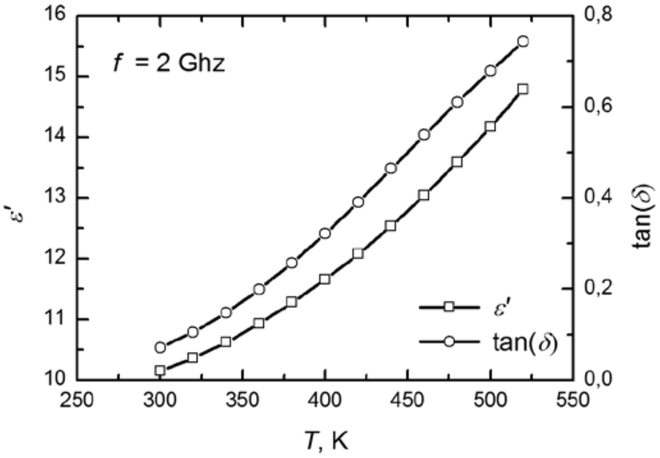

Fig. 8. Dielectric permittivity of the ceramic in electric fields oscillating at 2 GHz

The increase in the real part of dielectric permittivity is caused by a combination of Li^+ ion migration polarization, lattice vibration polarization and electronic polarization, while the increase in $\tan(\delta)$ is due to the conductivity contribution to the imaginary part of complex permittivity. All of the measurements were recorded at the frequency of 2 GHz, which is above the Maxwell's relaxation frequency in the temperature range given.

Complex plane plots of the dielectric permittivity are given in Fig. 9.

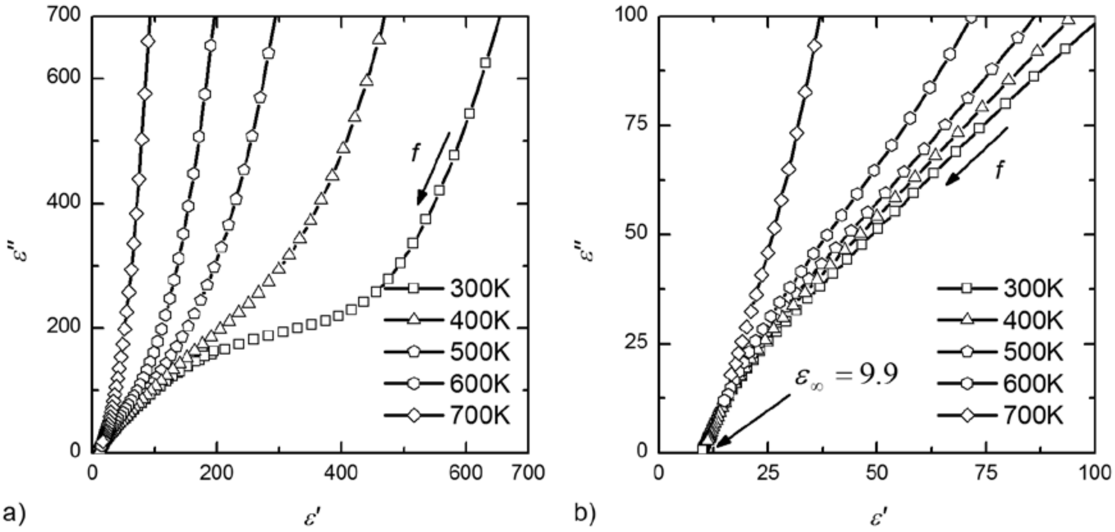

Fig. 9. Complex plane plots of dielectric permittivity at various temperatures, showing a) overall and b) high frequency behavior

The 300 K graph in Fig. 9a exhibits a partially obscured semicircle, formed by the dielectric permittivity response in the ceramic grains. The grain boundary effects partially overlap with those in the ceramic bulk, dominating the total permittivity response with increasing temperature due to the thermally activated nature of the grain and grain boundary relaxation processes.

High frequency portion of the permittivity graph, shown in Fig. 9b can be seen to converge to a single point on the ε' axis for all temperatures. This allows for the determination of a temperature invariant high frequency limit for the permitivity, which was found to be $\varepsilon_\infty = 9.9$.

4. CONCLUSIONS

Solid electrolyte $Li_{2.2}Ti_{1.7}(PO_4)_3$ powder was synthesized by a solid state reaction and studied by XRD. The primary phase of the synthesized material was found to have a NASICON type framework structure and belong to the rhombohedral symmetry (space group $R\bar{3}c$) with 6 formula units in the lattice. This result is consistent with the substitution $Ti^{4+} \rightarrow 4Li^+$ in the system $Li_{1+4x}Ti_{2-x}(PO_4)_3$.

A ceramic of the compound was sintered. XPS investigation of the ceramic surface yielded the empirical formula $Li_{2,8}Ti_{1,8}(PO_4)_3$.

The material was investigated by impedance spectroscopic techniques in the frequency range of 10 Hz to 3 GHz and temperature range of 300 K to 700 K. Two thermally activated dispersion regions of the conductivity were observed, correspondig to Li^+ ion relaxation in the ceramic grains and grain boundaries, with the latter dominating the total impedance of the sample by two orders of magnitude.

Measurements in fields oscillating above the Maxwell relaxation frequency allowed the determination of the high frequency limit of dielectric permittivity, which was found to be $\varepsilon_\infty = 9.9$. The permitivity values of the investigated compound are caused by varying contributions of Li^+ ion migration, lattice vibration and electronic modes of polarization. Dielectric losses in the material increase with temperature due to the ionic conductivity contribution to the imaginary part of complex permittivity.

The high steady state Li^+ ion conductivity of $\sigma_{tot} = 0.35\,\text{mS/m}$ at 300 K suggests possible applications in high energy density solid state batteries.

ACKNOWLEDGEMENT

This work was partly supported by the Lithuanian Science Council Student Research Fellowship Award (D. P.).

REFERENCES

1. MASQUELIER, C. Solid electrolytes: Lithium ions on the fast track. *Nature Materials*, 2011, Vol. 10, No. 9, p. 649–650.
2. KNAUTH, P. Inorganic solid Li ion conductors: An overview. *Solid State Ionics*, 2009, Vol. 180, No. 14-16, p. 911–916.
3. FERGUS Jeffrey W. A review of electrolyte and electrode materials for high temperature electrochemical CO2 and SO2 gas sensors. *Sensors and Actuators B: Chemical*, 2008, Vol. 134, No. 2, p. 1034–1041.
4. INHEE, L.; AKBAR Sheikh A.; DUTTA Prabir K. High temperature potentiometric carbon dioxide sensor with minimal interference to humidity. *Sensors and Actuators B: Chemical*, 2009, Vol. 142, No. 1, p. 337-341.
5. AONO, H.; SUGIMOTO, E.; et al. Ionic Conductivity of Solid Electrolytes Based on Lithium Titanium Phosphate. *Journal of the Electrochemical Society*, 1990, Vol. 137, No. 4, p. 1023–1027.
6. XU, X.; WEN, Z.; WU, J.; YANG, X. Preparation and electrical properties of NASICON-type structured $Li_{1.4}Al_{0.4}Ti_{1.6}(PO_4)_3$ glass-ceramics by the citric acid-assisted sol–gel method. *Solid State Ionics*, 2007, Vol. 178, No. 1-2, p. 29–34.
7. ORLIUKAS A. F.; KEŽIONIS A.; KAZAKEVIČIUS E. Impedance spectroscopy of solid electrolytes in the radio frequency range. *Solid State Ionics*, 2005, Vol. 176, No. 25-28, p. 2037–2043.
8. CRETIN, M.; FABRY P. Comparative study of lithium ion conductors in the system $Li_{1+x}Al_xA_{2-x}^{IV}(PO_4)_3$ with A^{IV}=Ti or Ge and $0 \leq x \leq 0{\cdot}7$ for use as Li+ sensitive membranes. *Journal of the European Ceramic Society*, 1999, Vol. 19, No. 16, p. 2931–2940.
9. NUSPL, G.; TAKEUCHI, T.; et al. Lithium ion migration pathways in $LiTi_2(PO_4)_3$ and related materials. *Journal of Applied Physics*, 1999, Vol. 86, No. 10, p. 5484–5492.
10. ORLIUKAS, A.; DINDUNE, A.; et al. Synthesis, structure and peculiarities of ionic transport of $Li_{1.6}Mg_{0.3}Ti_{1.7}(PO_4)_3$ ceramics. *Solid State Ionics*, 2007, Vol. 157, No. 1-4, p. 177–181.
11. KEŽIONIS A.; KAZAKEVIČIUS E.; ŠALKUS T.; ORLIUKAS A. Broadband high frequency impedance spectrometer with working temperatures up to 1200 K. *Solid State Ionics*, 2011, Vol. 188, No. 1, p. 110–113.
12. BARSOUKOV, E.; MACDONALD, Ross J. Impedance Spectroscopy: Theory, Experiment and Applications. John Wiley and Sons, Hoboken, New Jersey, 2005.

CYSENI 2012, May 24–25, Kaunas, Lithuania
ISSN 1822-7554, www.cyseni.com

MORPHOLOGICAL AND STRUCTURAL CHARACTERIZATION OF STEAM-EXPLODTED HEMP FIBRES

A. Putnina, S. Kukle
Riga Technical University, Institute of Textile Technology and Design
Azenes 14/24, LV-1048 – Latvia
Phone 0037128899974
Email: anna.putnina@rtu.lv

J. Gravitis
Latvian State Institute of Wood Chemistry,
Laboratory of Biomass Eco-Efficient Conversation, Riga
Dzerbenes Str. 27, Riga LV-1006, Latvia,
Phone 0037122544448
Email: jgravit@edi.lv

ABSTRACT

Cellulosic materials have a great potential for multifunctional nanomaterial formation. They are abundant, renewable, have a self-assembled well-defined nanofibrillar structure. Hemp fibre (cannabis sativa) is one of the plant-based bast fibres and has diverse reinforcing applications in different industry areas. Cellulose was extracted from drew-retted hemp fibres of variety Bialobrzeckie grown in Agricultural Science Centre of Latgale using adopted steam explosion technique (STEX) together with mild alkali treatment. It is possible to decompose natural fibre hierarchical structure down to microfibrilles by using STEX. Also, lignine and pectine, sugars and other components are removed by this method. The alkali treatment removes a certain amount of lignin, hemicellulose, wax and oils covering the external surface of the fibre cell wall and depolymerises the native cellulose structure.

Influence of pre-treatment intensity, temperature and pressure of steam explosion process on hemp cellulose acquisition are investigated and discussed. Scaning electron microscopy (SEM) and Fourier transform infrared spectroscopy (FTIR) were used to observe structural changes of fibres after alkali treatment.
Results show that STEX treatment conditions at 220 ^{o}C and pressure 23 bars leads to partial disintegration of hemp fibre bundles. Combination of hydrothermal and alkali treatments allow to remove approximately 26 % constituents including hemicelluloses, pectins/waxes and water.

Keywords: steam explosion, hemp fibre, cellulose, alkali treatments

1. INTRODUCTION

As hemp is a renewable resource with the high biomass yield it could be considered as potential abundant local source of biomass for a range of applications. Some newer industrial uses of plant cellulose have been developed and are found to be promising. One of them is to use cellulose nanoparticles as fillers in biocomposites and to improve their mechanical and barrier properties [1]. Therefore it is of interest to determine the hemp fibers potential, find appropriate solutions and sustainable systems.

The aim of the study was to examine the effect of alkali treatment and thermal treatment (steam explosion (STEX) auto-hydrolysis on the dew-retting hemp fibre microstructure. STEX ezperimental setup used for this study are described in detail elsewhere [18]. The biomass (wood or non-wood forest material, agricultural waste and fibre materials, waste from forestry, municipal and plantation management) for sustainable use has been treated with saturated steam, usually at pressures up to 40 atmospheres. The treatment time varies from some seconds to some minutes.

Disintegration of technical hemp fibres to elementary fibres with the aim to find out the best technologies without usage to environment harmful chemical pre-treatments is important milestone.

Each lignocellulosic fiber is a composite where rigid cellulose microfibrils are embedded in a soft matrix of lignin and hemicellulose [2]. Technical fiber consists of elementary fibres glued together by an interphase consisting of hemicellulose and pectins[3]. The degree of polymerization in hemicelluloses is much lower than in cellulose and is in a range from 20 to 300. Hemicellulose can form covalent bonds to lignins by attached ferulic acid and p-coumaric residues [4]. Hydrogen bonds are formed between xylan and cellulose. Due to this linking effect of hemicelluloses, hemicelluloses degradation leads to disintegration of the fibers into cellulose microfibrils resulting in lower fibers bundle strength [5]. It has been found that thermal degradation of hemicellulose occures at a lower temperature (150-180°C) than cellulose (200-230°C) by during wet oxidation [6] and composite manufacturing [7]. The amorphous regions of fibers are susceptible to acid attack and, under controlled conditions, could be removed leaving crystalline regions intact.

Different technologies could be used to prepare harvested hemp for further processing. The hemp bast is separated into large fibers bundles during water retting or dew-retting, then additional treatment is required to defibrillate these bundles into single fibers and/or small fiber bundles. In the middle lamellae between the single fibres pectin and lignin can be degraded using chemical Enzyme [8–10], wet oxidation [11, 22] and NaOH treatment [12, 13] as well as physical defibrillation methods like steam explosion [14, 15] or ultrasound treatment [16].

Sodium hydroxide (NaOH) is the most commonly used chemical for bleaching and/or cleaning the surface of plant fibers. It is reported that alkali treatment removes lignins, pectins, hemicelluloses, ash, and resulted in some extraction during the process [19]. Investigations show when the NaOH concentration was increased, the density of the alkali-treated hemp fibers decreased from 1.249 g/cm^3 to 1.127 g/cm^3 after alkali treatment (6 wt.% NaOH), corresponding weight loss 13.6 % [20]. At the same time range of investigations witness that rather severe pre-treatment regimes could change the fine structure of the cristallic cellulose I to amorphous cellulose II [21].

As reported in [17] after steam explosion in retted hemp fibres the content of cellulose increased from 73% to 85–90%, but in raw hemp fibres from 60–64% to 73–75%. The results of other investigation [18] show that most lignins from lignocellulosic fibers were removed when oxidative conditions were applied since it is decomposed to low molecular phenolic compounds and oxidized to carboxylic acids.

2. METHODOLOGY

Hemp fibres used for the research are Bialobrzeeskie type grown in the Agricultural Science Centre of Latgale Two methods of fibre desintegration were used. As first, fibres were alkali treated with 3 wt. % and 4 wt. % NaOH at 80°C for 1 h.

The second applied method of steam explosion auto-hydrolysis. The number of chemical and physical processes occur during the STEX treatment, but two of them are the most important. 1) The functional groups are removed and thereby acid molecules are formed in the system (for example, acetic groups in hemicellululoses provide formation of the acetic acid) during the process. These newly formed acids act as catalysts of hydrolysis of the treated material (auto-hydrolysis); 2) At the end of the STEX process abrupt release of the pressure occur. The difference of pressure in the tissues of the material and surroundings blasts provides an effective defibration of wood or other plant biomass.

The lignocellulosic material, can provide “self-sufficient” chemical and physical transformation under conditions of steam explosion, both the processes, hydrolysis and defibrilation, can be achieved just by the “tools” inherent in the system itself, without any additional reagents except steam [2].

Hemicellulose recovery in acid hydrolysates can only be maximized at lower treatment severities, whereas the development of substrate accessibility requires more drastic conditions in which sugar losses are inevitable [43]. To account for this heterogeneity, such STEX treatment parameters as temperature, residence time into the steam reactor, steam preasure are considered as experiment variables (Table 2).

After treatment, within a split second, the biomass is decompressed (exploded) to one atmosphere. Empirically, the so-called severity parameter or the reaction ordinate R_0 can be expressed as [18]:

$$R_0 = t * \exp\,[(T- 100)/ 14.75], \qquad (1)$$

where: duration of treatment (t, minutes) and temperature (T, ^{o}C) express the STEX severity against the base temperature T_{base} or reference = 100 0C. R_0 dimension is minutes but in practice log R_0 is used.

The following ratio has therefore been used as a measure for the degree of esterification [32, 37]:

$$DM = a1749/(a1630+a1749). \qquad (2)$$

Crystality index (CrI) supposed to be the measure of cellulose crystallinity level [38, 29]:

$$CrI = a1372/a2900. \qquad (3)$$

LOI describes the order of crystallinity rather than the amount of crystalline cellulose relative to the amorphous components:

$$LOI = a1429/a893. \qquad (4)$$

Extraction treatment with distillate water at T 100 ^{o}C during 3 h with following alkali treatment with 0,4 wt.% NaOH and washing to remove released components after STEX were done (Table 3).

NaOH solulable components and residue after NaOH treatment were determined by weight changes (Table 3).

Morphological and structural analysis of both sample groups were performed using SEM (VEGA Tescan 5136M) and FTIR technique.

As micrographs are qualitative sources to follow transformations which happen during treatments fourier-transform infrared spectroscopy (FTIR) were used to characterize influence of alkali treatment parameters more detailed on such hemp fibers constituents as lignins, hemicelluloses and extractives.

3. RESULTS AND DISCUSSIONS

As seen from micrographs of Fig. 1(A) shows untreated elementary hemp fibers are joint in bundles, at a higher magnification the void regions present on the bundle become visible; some surface and structure defects seen on micrograph could arose during hemp stalk primary processing or combing (Fig. 1, C). After alkali treatment (4 wt.% NaOH, 1 h, T 800 ^{o}C) part of fiber bundles are separated to a smaller bundles or elementary fibers (Fig. 1, B); surface of elementary fibers with diameter of (1÷2) μm are quite clean, only a few non soluble plasters, probably lignins, are seen on the surface (Fig. 1, D).

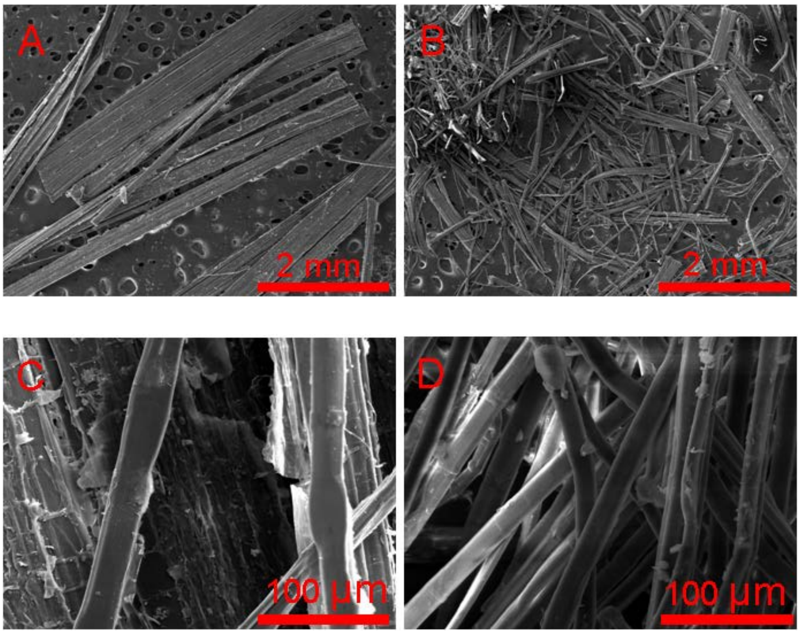

Fig. 1. A – untreated hemp fibres; B – alkali (4 wt.% NaOH) treated hemp fibers; C – untreated hemp fibres SEM micrographs; D - alkali (4 wt.% NaOH) treated hemp fibers SEM micrographs

Like a fingerprint no two unique molecular structures produce the same infrared spectrum. This makes infrared spectroscopy useful for several types of analysis, but at the same time arouse range of interpretation problems becoming apparent sometimes in diametrically opposite explanations of FTIR graphs absorption bands.

Together with hemicellulose, lignins form a matrix for cellulose fibres [38]. Lignins in fibres are complex hydrocarbon polymers with aliphatic and aromatic constituents, forming a three dimensional network. Apart from forming the matrix in the secondary cell walls of plant fibres, lignins also decrease the permeation of water through the cell walls [20]. As mechanical properties of lignin (E = 4 GPa) compared to cellulose (E = 70–135 GPa) are low [23] and water through the cell walls of technical fibres has to be removed for futher applications, the removal of lignin from technical fibres is more than desirable.

Hemp fibers hardwood lignins contain residues derived from both coniferyl and sinapyl alcohols (lignin type GS, S/G ratio 0,8)[26].

Absorbace peak at the frequency 1618 cm^{-1} was found as more intensive and broad (1605 to 1639 cm^{-1}) for hemp lignins [26]. Unfortunately lignins content of hemp fibers depends upon hemp variety and could be in a range from 3 % (Uso) till 13 % (Futura 77) [27] and supposedly family of lignins differ too.

Investigations [28] of hemp fibers structural morphology changes subjected to bleaching show that lignin contents of untreated fibres under investigation are 6.61% (4.89% non solulable, 1.72% solulable), after bleaching become 3.18 % (3.18 % non solulable, 0.35% solulable); hemicellulose content at the same time decrease from 10.66 % (untreated fibres) to 1.85 % after treatment.

FTIR graphs (Fig. 4) for hemp fibres show disapearing of absorption band corresponding to frequency range 1700–1750 cm^{-1} with the peak at 1732 cm^{-1}. Such absorption band adressed to functional groups C=O or COOH- [29], where 1738 cm^{-1} corespond to hemicellulose, 1736 cm^{-1} to pectins and waxes. Absorbance at frequency ranges 1722–1732 cm^{-1} decreases if hydrolized hemicellulose is removed from fibers surface as seen from graphs of Fig. 4. As a result of 4 wt.% NaOH treatment pectins and waxes (freaquency?) are removed as well (Fig. 3).

The (methyl-esterified) carboxyl groups absorb in the region of 1749 cm^{-1} and the absorbance at 1605-1630 cm^{-1} is caused by the ionized COO - groups [30–36].

DM values calculated by equation (2) decrease from 0.21 (non treated) up to 0,16 for 4 wt.% NaOH treated fibers. Actual values of this factor are impossible calculate precisely after treatment because absorbance peak (Fig. 3., frequency 1749 cm^{-1}) has removed at all.

Absorption intensity of bands at frequency range 1300–1450 cm^{-1} are higher for alcali treated hemp fibres (Fig. 3).

Calculations of CrI after baseline corrections shows increse of crystallinity after 4 wt.% NaOH alkali treatment from 0,17 up to 0.21 (23.5 %). According to the calculated CrI values, alkaline-treated fibre exhibits a substantial increase in crystallinity. It corresponds to statement that alkalization depolymerizes the native cellulose I molecular structure producing short length crystallites [22].

The baseline-corrected absorption peaks at 1430 and 897 cm^{-1} correspond to the sensitive absorption frequencies of crystalline and amorphous cellulose structures, respectively [39, 40, 29].

LOI values decrease approximatley 7 % for alcali treated fibres from 2,43 up to 2.25. As LOI describes the order of crystallinity rather than the amount of crystalline cellulose relative to the amorphous components it is small difference. This observation is in accordance with results reported in the literature, where no significant change or an increase in LOI is published for similar treatment conditions [41, 42, 22].

The disappearance of the peak (1245–1259 cm^{-1}) after alkalization (Fig. 3) indicates the removal of hemicellulose materials rather than lignins [22].

Table 2. Steam explosion treatment parameters

Variants	**STEX parameters**				**Moisture, %**		**Evaporable fractions, %**
	Temperature, 0C	**Pressure, bar**	**Time, s**	**logR$_0$**	**Before STEX**	**After STEX**	
A	**180**	**10**	**60**	**2.36**	**6.51**	**~ 75**	**7.0**
B	**200**	**16**	**60**	**2.94**	**6.51**	**~ 75**	**7.0**
C	**220**	**23**	**60**	**3.42**	**6.51**	**~ 75**	**8.4**

Micrograph (Fig. 2, D, G) shows after mild STEX treatment (logR0 = 2.36) only part of fiber bundles are half separated to a smaller ones or elementary fibres. Loose amorphous matrix clusters cover bundles/fibers surfaces.

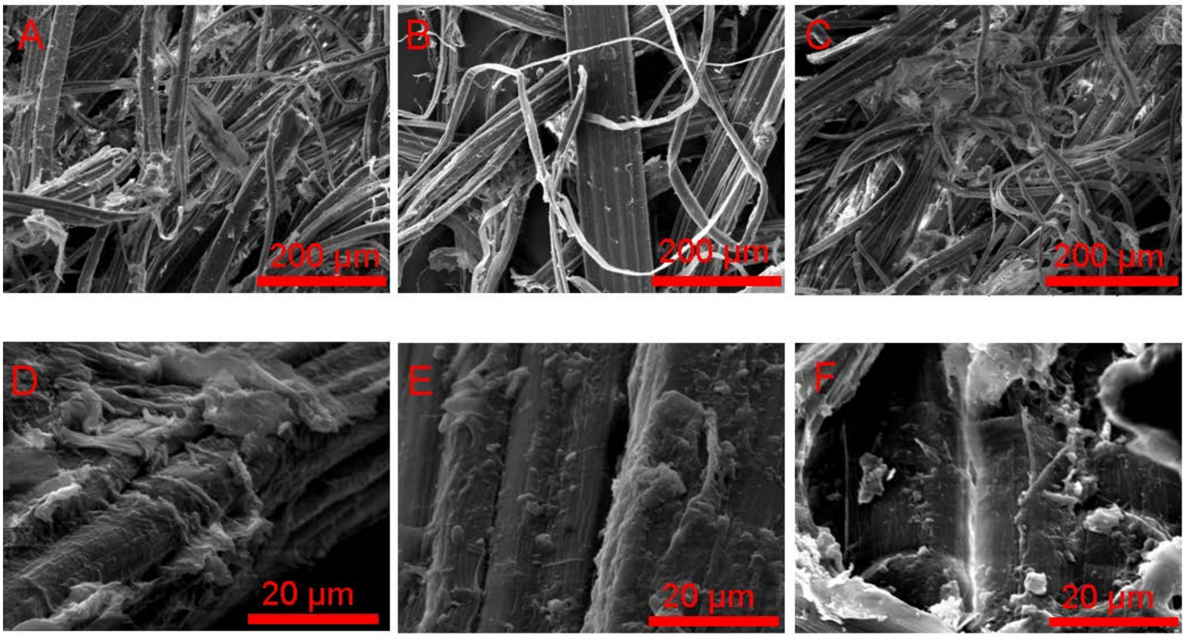

Fig. 2. A, D – hemp fibres SEM micrographs after STEX (10 bar, T 180 ^{0}C); B, E – hemp fibers SEM micrographs after STEX (16 bar, T 200 ^{0}C); C, F – hemp fibers SEM micrographs after STEX (23 bar, T 220 ^{o}C)

The micrographs of Fig. 2 (B, E) reveal that increase of logR_0 = 2.94 (pressure 16 bar, T 200 ^{0}C) doesn’t improve separation of fibers as hemp fibers are exclusive nature composite and STEX treatment is still classified as medium mild.

Hemp fibers subjected to more severe STEX treatment (logR_0 = 3.42) seen in micrograps of Fig. 2 (C, F). Fibers bundles are separated to 10–20 μm diameter components and extracted clusters of matrix seen as separate units or loose appliques on fiber surfaces.

Part of non-cellulosic substances are evaporated (loss 8.4 % of weight) during STEX treatment (Table 2). Disintegration and/or weakening of the binding of fibres in the bundles is decisive important for further separation of the hemp fibres in subsequent operations

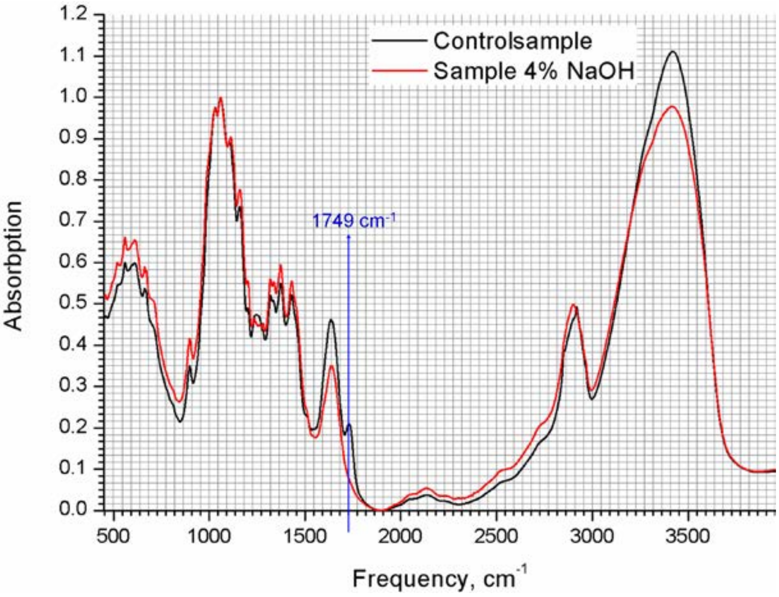

Fig. 3. FTIR spectrograms of untreated and alcali treated (4 wt.% NaOH) hemp fibers

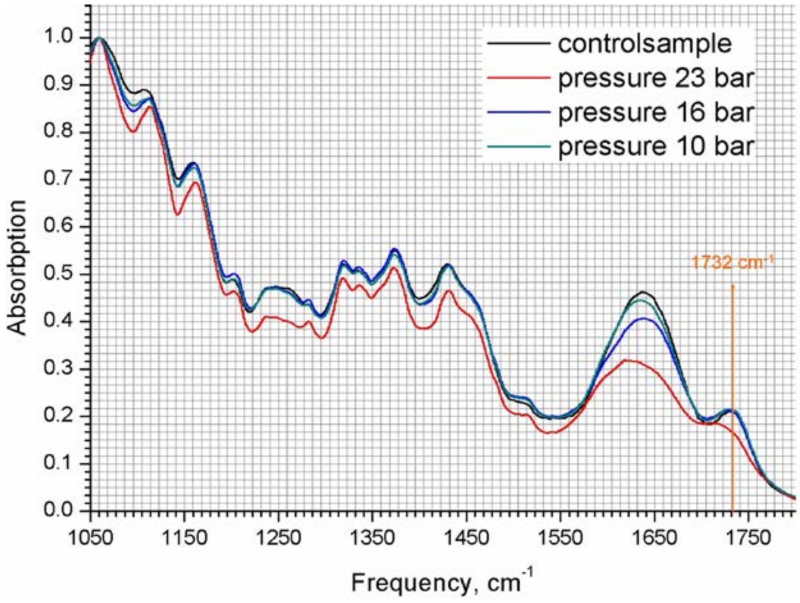

Fig. 4. FTIR spectrograms of hemp fibers subjected to steam explosion treatment corresponding to frequency range 1050-1800 cm^{-1}

One of the most noticeable modification of FTIR graphs (Fig. 4) before and after STEX treatment is the disappearance of the absorbance peak centered at 1732 cm^{-1} at a pressure 23 bar, characteristic of hemicelluloses.

Substantial decrease of absorbance intensity at the frequency range 1580–1680 cm^{-1} allow to suppose that lignin content in the dry residue after STEX treatment C (Table 2) decrease substantially as investigations of [26] reported hemp lignins most powerful absorption band at the frequency range 1605–1639 cm^{-1}. Besides absorbance peak corresponding to the mentioned above frequency range has moved from 1638 to 1620 cm^{-1} witnessed that lignins are still present in dry residue.

Crystallinity index has increased by 47 % (from 0,29 to 0,43) after STEX treatment with preasure 23 bar at temperature 220 ^{o}C. Lateral order index LOI increases from 2.4 up to 3 after treatment.

Previous studies [29] have shown that the band at 1335 cm^{-1} is composed of a broad, poorly defined main band with an accompanying shoulder. When the crystallised cellulose I and/or II content are increased, this band is gradually converted into a perfectly defined doublet. From this doublet the ratio 1335/1316 can be used to monitor the conversion process. Reduction of this ratio can be interpreted as an increase in the crystallised cellulose I content [25]. In our experiment decrease of value of calculated ratio 1335/1316 from 2 up to 0,4 (80 %) witnessed about substantial growth of cellulose I content in hemp fibres after STEX treatment (Table 2, C). It could be explained as growths of crystallic cellulose I content in relation to amorphous celluloses as in result of treatment main part of amorphous cellulose are removed.

Table 3. Modes of hemp fiber samples STEX treatment and after-treatment

Sample label	Pressure, bar	log R_0	Residue after STEX, %	Water solulable components, %	Residue after water treatm. %	NaOH solulable components, %	Residue after NaOH treatm. %
0	**0**	**0**	**100**	**4.4**	**95.6**	**13.4**	**82.2**
1	**10**	**2.36**	**93**	**6.4**	**86.5**	**10.9**	**75.7**
2	**16**	**2.94**	**93**	**9.1**	**83.9**	**8.8**	**75.1**
3	**23**	**3.42**	**91.6**	**10.6**	**81**	**7.6**	**73.4**

Evaporation intensities corresponding to presure range 10-16 bar is stable (7 %)(Table 3) and increase with the presure 23 bar. After STEX treatment at presure 23 bars and following water treatment all water solulable components are removed living dry residue 81 %. Drying was carried out at room temperature, while there is no change in mass. During the last treatment with 0,4 wt.% NaOH and subsequent washing content of extracted components decrease with increasing pressure. It shows that part of NaOH solulable components have been converted in evaporable and water solulable substances during STEX treatment and removed during first water treatment (Table 3).

4. CONCLUSIONS

Content of water solulable components increase 2,4 times With growing STEX intensity from log R_0= 0 to log R_0 = 3.42 .

Examination of FTIR spectrograms of untreated and treated hemp fibers allow to evaluate effectiveness of alcali and steam explosion treatment to remove hemicelluloses and pectins.

Growth of crystalinity index of cellulose treated at 4%NaOH and STEX was 28 % and 47 % respectively. Both treatments lead to depolymerization of the native cellulose I molecular structure producing short length crystallites. A high crystallinity index results in stiff, strong fibers.

Medium severe STEX treatment combined with following hydrothermal and alkali treatments allow to remove approximately 26 % constituents from hemp fibers including hemicelluloses, pectins/waxes, water.

STEX treatment (log R_0 = 3.42) leads to partial disintegration of hemp fiber bundles. and reduction of 1335/1316 ratio from 2 up to 0.4 (80 %) indicates substantial growth of cellulose I content in hemp fibres after treatment. More severe STEX intensity (higher log R_0 value) can increase level of disintegration. Usage of mechanical/physical treatment just after STEX treatment could separate fiber bundles to the microlevel diameter fibers.

ACKNOWLEDGEMENTS

This research has been supported by the European Social Fund within the project «Support for the Implementation of Doctoral Studies at Riga Technical University».

REFERENCES

1. FAN, M. *Elementary hemp fibres and strength*. BioResources 5(4), 2010, 2307-2322.
2. GRAVITIS J. *Nano level structures in wood cell wall composites.* Cellulose Chemistry and Technology, 2006, 40(5), p. 291–298.
3. SZALKOWSKI, Z. *Podstawy chemicznej technologii surowcov I wlokeien lykowych,.* Warszawa, 1967.
4. BJERRE, A.B.; SCHMIDT, A.S. *Development of chemical and biological processes for production of bioethanol: Optimization of the wet oxidation process and characterization of products.* 1997, Riso-R-967(EN), Riso National Laboratory: p 5–9.
5. MORVAN, C, JAUNEAU A, FLAMAN A, MILLET J, DEMARTY M. *Degradation of flax polysaccharides with purified endo-polygalacturonase*. Carbohydrate Polymers, 1990,13, p. 149–163.
6. BJERRE AB, OLESEN AB, FERNQVISt T, PLÖGER A, SCHMIDt AS. *Pretreatment of wheat straw using combined wet oxidation and alkaline hydrolysis resulting in convertible cellulose and hemicellulose.* Biotechnol Bioeng, 1996, 49, p. 568–577.
7. MADSEN, B., 2004. *Properties of plant fibre yarn polymer composites – An experimental study*. Ph.D. thesis, BYG-DTU, Technical University of Denmark, ISBN 87-7877-145-5
8. THYGESEN A., THOMSEN A.B., SKAMMELSEN SCHMIDT A., JORGENSEN H., AHRING B.K., OLSSON L. Production of cellulose and hemicellulose-degrading enzymes by filamentous fungi cultivated on wet-oxidised wheat straw. Enzyme Microbial Technology, 2003, 32 (5), p. 606–615.
9. MADSEN, F.T.; BURGERT, I.; JUNGNIKL K.; FELBY, C.; THOMSEN, A.B. *Effect of enzyme treatment and steam explosion on tensile properties of single hemp fiber*. 12th International Symposium on Wood and Pulping Chemistry (ISWPC), 2003, Madison, 80 p.
10. BRÜHLMANN, F.; LEUPIN, M.; ERISMANN, K.H.; FIECHTER, *A. Enzymatic degumming of ramie bast fibers.* Journal of Biotechnology, 2000,76, p. 43–50.
11. THOMSEN, A.B.; RASMUSSEN, S.; BOHN, V.; NIELSEN, K.V.; THYGESEN, A.. *Hemp raw materials: The effect of cultivar, growth conditions and pretreatment on the chemical composition of the fibres.* Riso National Laboratory. Report No.: R-1507.
12. WANG, H.M.; POSTLE, R.; KESSLER, R.W.; KESSLER, W. *Removing pectin and lignin during chemical processing of hemp for textile applications*. Textile Research Journal, , 2003, 73, p. 664–669.
13. GARCIA-JALDON, C.; DUPEYRE, D.; VIGNON, M.R. *Fibres from semi-retted hemp bundles by steam explosion treatment.* Biomass & Bioenergy, , 1998, 14, p. 251–260.

14. MADSEN ET, AL.; VIGNON, M.R.; GARCIA-JALDON, C.; DUPEYRE, D. *Steam explosion of the woody hemp chénevotte*. International Journal of Biological Macromolecules, 1995, 17, p. 395–404.
15. ZIMMER, H.; KLOSS, D. *Ultraschallaufschluss von Hanf. Ziele-Technologie-Anwendung-Resultate-Qualitätsmanagement.* Proceedings of the Bioresource Hemp '95 Symposium; Frankfurt, Germany. Nova-Institute.
16. KLINKE, H.B.; AHRING, B.K.; SCHMIDT, A.S.; THOMSEN, A.B. *Characterization of degradation products from alkaline wet oxidation of wheat straw.* Bioresour Technol, 2002, 82. p. 15–26.
17. THYGESEN, A. *Properties of hemp fibre polymer composites -An optimisation of fibre properties using novel defibration methods and fibres characterisation*, PhD thesis, The Royal Agricultural and Veterinary University of Denmark, ISBN 87-550-3440-3.
18. GRAVITIS, J.; DOBELE, G.; ABOLINS, J.; TUPCIAUSKAS, R.; VEVERIS, *A. Non-sulphur lignin studies under biorefinery concept and evaluation of energy consumption by steam explosion.* Paris, January, 2011.
19. SGRICCIA, N.; HAWLEY, M.; MISRA, C. M. Characterization of natural fibre surfaces and natural fibre composites. *Composites Part A Applied Science and Manufacturing* (2008)
Vol. 39, No.: 10, p.: 1632-1637, ISSN: 1359835X.
20. MWAIKAMBO, L.J.; ANSELL, M.P. *Chemical Modification of Hemp, Sisal, Jute, and Kapok Fibres by Alkalization.* Journal of Applied Polymer Science, 2002. 84: p. 2222–2234.
21. BLEDZKI, A.K.; GASSAN, J. *Composites reinforced with cellulose based fibres.* Progress in Polymer Science, 1999. 24(2): p. 221–274.
22. THYSINGEN, A. Hemp fiber microstructure and use of fungal defibration to obtain fibers for composite materials. Journal of Natural Fibres, 2006, p. 19–37.
23. COLOM, X.; CARRILLO, F. *Crystallinity changes in lyocell and viscose-type fibres by caustic treatment.* European Polymer Journal, 2002. 38(11): p. 2225–2230.
24. RIO, J., GUTIERREZ, A.; RODRIGUEZ, I.M. *Composition of non-woody plant lignins and cinnamic acids by Py-GC/MS, Py/TMAH and FT-IR*. Journal of Analytical and Applied Pyrolysis, 1-2, 2007, Vol. 79, p. 39–46.
25. THYGESEN, A. *Properties of Hemp Fibre Polimer Composites*. PhD Thesis. ISSBN 87-550-3440-3. Denmark. 2006.
26. WANG, B.; SAIN, M.; OKSMAN, K. Study of structural morphology of hemp fiber from the micro to the nanoscale. *Applied Composite Materials*, vol. 14, no. 2, p. 89–103, 2007.
27. KORTE, S. *Processing-Property Relationships of Hemp Fibre*. Canterbury: University of Canterbury, 2006.
28. SYNYTSYA, A..; COPIKOVA, J.; MATEJKA, P.; MACHOVIC, V. Fourier transform Raman and infrared spectroscopy of pectins. *Carbohydrate Polymers*, 2003. 54(1): p. 97–106.
29. SENE, C.; MCCANN, M.C.; WILSON, R.H.; GRINTER, R. *Fourier-Transform Raman and Fourier-Transform Infrared Spectroscopy (An Investigation of Five Higher Plant Cell Walls and Their Components).* Plant Physiology, 1994. 106: p. 1623–1631.
30. CHATJIGAKIS, A.K.; PAPPAS, C.; PROXENIA, N.; KALANTZI, O.; RODIS, P.; POLISSIOU, M. FT-IR spectroscopic determination of the degree of esterification of cell wall pectins from stored peaches and correlation to textural changes. *Carbohydrate Polymers,* 1998. 37(4): p. 395–408.
31. MANRIQUE, G.D.; LAJOLO, F.M. *FT-IR spectroscopy as a tool for measuring degree of methyl esterification in pectins isolated from ripening papaya fruit*. Postharvest Biology and Technology, 2002. 25(1): p. 99–107.

32. KACURAKOVA, M.; WILSON, R.H. Developments in mid-infrared FT-IR spectroscopy of selected carbohydrates. *Carbohydrate Polymers*, 2001. 44(4): p. 291–303.
33. KAMNEV, A.A.; COLINA, M.; RODRIGUEZ, J.N.M.; PTITCHKIN, A.; IGNATOV, V.V. *Comparative spectroscopic characterization of different pectins and their sources*. Food Hydrocolloids, 1998. 12(3): p. 263–271.
34. FILIPPOV, M.P., *Practical infrared spectroscopy of pectic substances*. Food Hydrocolloids, 1992. 6(1): p. 115–142.
35. BARROS, A.S.; MAFRA, I. D; FERREIRA, S.; CARDOSO, A.; REIS, J.A..; LOPES DA SILVA, DELGADILLO, I.; RUTLEDGE, D.N.; COIMBRA, M.A. *Determination of the degree of methylesterification of pectic polysaccharides by FT-IR using an outer product PLS1 regression*. Carbohydrate Polymers, 2002. 50(1): p. 85–94.
36. NELSON, M.L.; O'CONNOR, R.T. *Relation of Certain Infrared Bands to Cellulose Crystallinity and Crystal Lattice Type. Part II. A New Infrared Ratio for Estimation of Crystallinity in Celluloses I and II*. Journal of Applied Polymer Science, 1964. 8: p. 1325–1341.
37. OH, S.Y.; YOO, D.I.; SHIN, Y.; SEO, G. *FTIR analysis of cellulose treated with sodium hydroxide and carbon dioxide*. Carbohydrate Research, 2005. 340 (3): p. 417–428.
38. SHANKs, R.A.; S. OUAJAI, *Morphology and Structure of Hemp Fibre after Bioscouring*. Macromolecular Bioscience, 2005. 5: p. 124–134.
39. GASSAN, J.; A.K. BLEDZKI, *Alkali Treatment of Jute Fibers: Relationship Between Structure and Mechanical Properties*. Journal of Applied Polymer Science, 1999. 71: p. 623–629.
40. OUAJAI, S.; SHANKS, R.A., *Composition, structure and thermal degradation of hemp cellulose after chemical treatments. Polymer Degradation and Stability*, 2005. 89(2): p. 327–335.
41. RAMOS, L.P. *The Chemistry involved in the steam treatment of lignocellulosic materials.* Quim. Nova, Vol. 26, No. 6, 863-871, 2003.

CYSENI 2012, May 24–25, Kaunas, Lithuania
ISSN 1822-7554, www.cyseni.com

GAS SENSITIVITY OF EXCESS-IRON NI-ZN FERRITE

A. Sutka, G. Mezinskis
Riga Technical University, Institute of Silicate Materials
Azenes 14/24, LV-1048, Riga - Latvia
Phone 0037126138155
Email:andris.sutka@rtu.lv

ABSTRACT

Application of new materials allows to offer more sensitive, selective and long term stable sensors, as well as to employ its modification possibilities for gas sensor efficiency improvement. The aim of the present work is to compare gas response to acetone of nanostructured sol-gel auto-combustion synthesis derived stoichiometric and excess-iron cubic spinel type nickel zinc ferrite with formula $Ni_{0.3}Zn_{0.7}Fe_{2+z}O_4$ (where $z = 0$ and 0,1) is compared. Detailed synthesis steps and gas sensing measurement methodology were described. The sensor material was characterized by x-ray diffraction, scanning electron microscopy and direct current resistance measurements. X-ray diffraction analysis confirms that samples formed the single phased cubic spinel structure and no peaks from impurity phases were detected. The scanning electron microscopy reveals nanosized grains less than 100 nm in diameter. Plots of resistance versus temperature show adsorbed water contribution to the conductance. Overall, sensors were tested at temperature interval from 150 ^{o}C to 325 ^{o}C in order to identify operating temperature of the material. The response-recovery characteristics also were performed. It was found, that with excess-iron in the Ni-Zn ferrite, changes its DC electrical resistivity, type of conductivity, as well as response to reducing gas (more than 2 times) and operating temperature. Obtained relationships can be explained with Fe^{2+} formation in the material, thus increasing charge carrier (electron) concentration. This leads down to higher oxygen adsorption ability which can act with test gas. Overall performed study reveals alternative way how to enhance sensitivity of spinel type ferrite gas sensor materials avoiding synthesis of complicated nanostructures or precious metal doping.

Keywords: Nickel-zinc ferrite, non-stoichiometry, gas sensor, combustion synthesis

1. INTRODUCTION

Spinel ferrites are important technological materials due to its semiconducting and ferrimagnetic properties [1]. Recently as semiconductors ferrites also provides chance to use them as gas sensitive material. A large number of stoichiometric spinel ferrites for example $ZnFe_2O_4$, $NiFe_2O_4$, $CdFe_2O_4$, $MgFe_2O_4$, $CuFe_2O_4$, $CoFe_2O_4$, $NiZnFe_2O_4$, $MnZnFe_2O_4$, $MgZnFe_2O_4$, etc. have shown sensitivity to certain gases [2-7]. At the same time information about ferrite gas sensors in comparison with single metal gas sensors is still limited and do not contain information about gas sensing properties of complex or non-stoichiometric iron deficient or excess-iron spinel ferrite compounds. Depending on dopant type and concentration in complex or non-stoichiometric spinel ferrites varies its electrical resistivity.

The conductivity in spinel ferrites is due to hopping of charge carriers (electrons or holes) between cations presented by more than one valence state occupying the octahedral sites [8]. Zinc or cadmium ions shows strong affinity to tetrahedral site, but iron, nickel, manganese, and cobalt ions, for example, show tendency to occupy octahedral sites. Electron hopping between Fe^{3+} and Fe^{2+} provides n-type, but hole hopping between $Ni^{3+}\leftrightarrow Ni^{2+}$, $Mn^{3+}\leftrightarrow Mn^{2+}$, $Co^{3+}\leftrightarrow Co^{2+}$ provides p-type conductivity.

The gas sensitivity of metal oxide semiconductor sensors is highly affected from electric resistivity [9]. In our previous works influence of zinc ion concentration on sensitivity of p-type nickel ferrite [10], as well as iron ion non-stoichiometry effect on sensitivity of n-type zinc ferrite [11] were investigated. It was found that with zinc addition to nickel ferrite, response to different VOC's decreases, attributed to extinguishing p-type charge carriers (holes) and carrying small amount of dopants in the semiconductor structure. This was confirmed with change of conductivity type by increasing temperature. In case of zinc ferrite response increased by going from iron deficiency to excess due to increase of Fe^{2+} concentration, thus increasing charge carrier (electron) concentration, leading down to increase adsorbed oxygen species on grain surface. It is known, that n-type materials surface coverage with oxygen ions at elevated temperature is limited by the supply of electrons. Higher charge carrier concentration leads to increase of adsorbed oxygen species on surface, thus larger change of the resistance with reactive gas, such as acetone, interaction could be expected. Adsorbed oxygen (O^{-}_{ads}) reaction with the reducing gas (R) can be represented by simple irreversible reaction [12]:

$$O^{-}_{ads} + R \rightarrow RO + e^{-} \qquad (1)$$

The aim of the present work is to compare gas sensitivity of stoichiometric and excess-iron Ni-Zn ferrite. It is interesting if iron-excess Ni-Zn ferrite will show higher response towards volatile organic compounds (VOC's) in comparison with stoichiometric Ni-Zn ferrite, as it was observed for $ZnFe_2O_4$ in our previous work, because from one side Ni ion restricts, but excess-iron enhances Fe^{2+} formation, thus increasing charge carrier (electron) concentration in the Ni-Zn ferrite material.

2. METHODOLOGY

2.1. Synthesis

The ferrite samples with chemical formula $Ni_{0.3}Zn_{0.7}Fe_{2+z}O_4$ (z = 0 and 0,1) was prepared with sol-gel auto combustion technique [13]. Analytical grade of desired metal nitrates according to the molar proportions were dissolved in distilled water (Table 1). Then 1 mole citric acid monohydrate ($C_6H_8O_7{\cdot}H_2O$) was added to nitrate solution. Metal nitrates acts as an oxidizing agent and citric acid carboxylate groups act as a reducing agent for combustion reaction. To increase metal cation chelating with citrates, nitrate/citric acid mixture was neutralized (pH=7) by using ammonium hydroxide (NH_4OH) 26% solution in water. Obtained solution were mixed in 100 cm^3 chamotte crucible and evaporated at 80 ^{o}C temperature on magnetic stirrer until viscous gel was formed. By cooling down to room temperature gel should become solid. Additionally the gel was dried for 24 hours to remove water residues. Gel was heated up to 250 ºC to initiate combustion reaction, and the as-burnt product was obtained. The processing steps employed for the synthesis of ferrite samples are shown in Fig. 1.

Table 1. Molar proportions of raw materials for ferrite synthesis

Chemical formula	Solution components	Molar ratios of metal nitrates	Metal nitrate and citric acid molar ratios
$Ni_{0.3}Zn_{0.7}Fe_2O_4$	A: $Ni(NO_3)_2{\cdot}6H_2O$ B: $Zn(NO_3)_2{\cdot}6H_2O$ C: $Fe(NO_3)_3{\cdot}9H_2O$ D: $C_6H_8O_7{\cdot}H_2O$	A:B:C = 0.3:0.7:2	(A+B+C):D = 1:1
$Ni_{0.3}Zn_{0.7}Fe_{2.1}O_4$	A: $Ni(NO_3)_2{\cdot}6H_2O$ B: $Zn(NO_3)_2{\cdot}6H_2O$ C: $Fe(NO_3)_3{\cdot}9H_2O$ D: $C_6H_8O_7{\cdot}H_2O$	A:B:C = 0.3:0.7:2.1	(A+B+C):D = 1:1

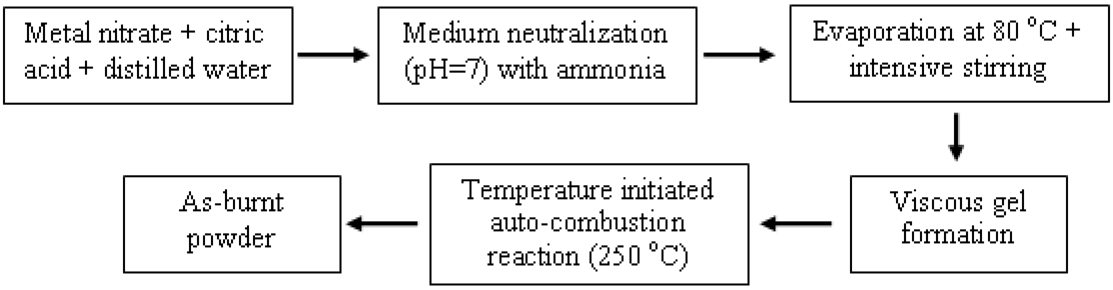

Fig. 1. Processing steps of ferrite powders

2.2. Sample preparation

Ferrite samples in form of pellet for electric and gas sensing measurements with 10 mm diameter and 1 mm thickness were prepared from as-burnt powders in a uniaxial press at 5 MPa and sintered at 800 °C for 1 hour. As a binder solution of polyvinyl-alcohol with a concentration 10 wt% was used.

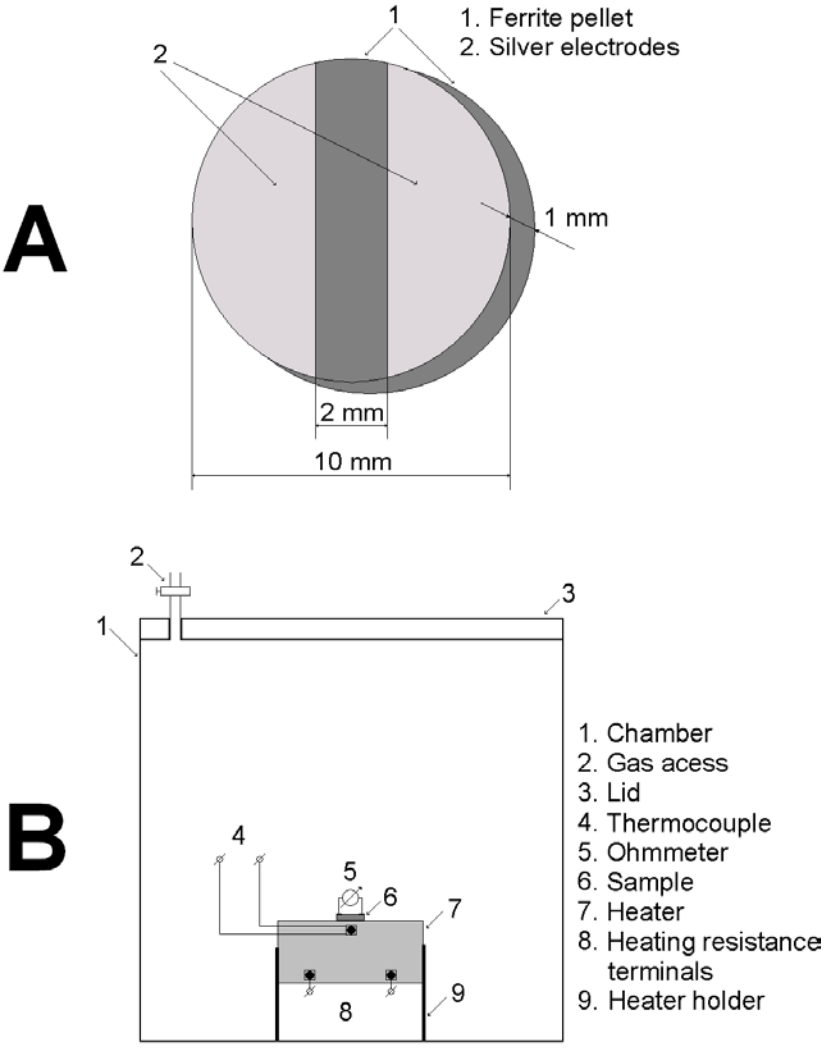

Fig. 2. Gas sensor element (A) and schematic representation of experimental array (B)

2.3. X-Ray studies

For crystalline structure analysis X-Ray powder diffraction (XRD) were used. XRD was recorded for 2θ from 10° to 60° at a scan rate of 1° min^{-1} using an Ultima+ X-ray diffractometer (Rigaku, Japan) with CuKα radiation. Sample crystallite size was calculated by using Debye-Scherrer equation:

$$D = \frac{k\lambda}{B \cdot \cos\theta}, \tag{2}$$

where D – crystallite size (nm), k – Scherrer constant (for cubic crustalline structures as spinels and spherical particles k is equal to 0,94), λ – wavelength of the X-Ray radiation (0,154178 nm), B – width at half maximum intensity in radians.

2.4. Microstructural studies

Microstructural studies were carried out with a Quanta 200 scanning electron microscope (FEI, Netherlands). For grain size and microstructure determination scanning electron microscopy (SEM) was performed on fracture surfaces of sintered pellets.

2.5. Direct current (DC) measurements

The DC electrical resistance was measured using the two probe constant current method. In this method current from the constant current source, flows through the unknown resistance, and the voltage drop is measured by the electrometer voltmeter. Using this method, resistances up to about 10^{14} Ω can be measured. For temperature variation of electrical resistivity, the sample was kept in the closed chamber and maintained from 20 to 400 ^{o}C. Samples for electrical measurements from both sides were coated with high purity silver paint.

2.6. Gas sensing measurements

For sensing measurements the disks about 1 mm thickness and 10 mm in diameter were silvered on a face, as shown in Fig. 2A.

In order to improve their stability, the sensing elements before testing were heated at desired temperature longer than 12 hours as recommended other authors [14]. Then sensor element was introduced in Teflon chamber and placed on chamotte heater. Since the sensitivity of gas sensors is greatly influenced by operating temperature, the sensor was used to detect acetone vapours at various temperatures between 150 ^{o}C to 325 ^{o}C at ambient atmosphere pressure. At temperatures below 150 ^{o}C the sensor surface is believed to be coverage with inactive –OH groups [15]. Gas response dependence from concentration do not display in which conditions material possess highest sensitivity. More sensitive gas sensor materials will detect lower gas concentrations.

The test gas was injected into chamber with micropipette through the inlet. Schematic representation of experimental arrangement is shown in Fig. 2B.

Required gas concentration was calculated using Eq. (3):

$$V = \frac{C_{ppm} V_a M}{24.5 \times 10^9 D}, \tag{3}$$

where V is required liquid volume (cm^3), D is the density of the liquid (g/cm^3), V_a is the volume of test chamber (cm^3), M is the molecular weight of the liquid (g/mol) [16]. The response S was determined with Eq. (4):

$$\begin{cases} S = \dfrac{R_a}{R_g} & if \quad R_g < R_a \\ S = \dfrac{R_g}{R_a} & if \quad R_g > R_a \end{cases}, \tag{4}$$

where R_a is the clean air resistance but R_g is the resistance in the presence of test gas at the given temperature [2].

3. RESULTS AND DISCUSSIONS

3.1. Characteristics of sensor material

The diffraction pattern of the ferrite samples sintered at 800 ^{o}C is shown in Fig. 3. Sintering forms pure cubic spinel type structure and no additional peaks are observed ensuring the phase purity. Crystallite size (Table 2) for material was calculated by means of line broadening of the most intense (311) diffraction peak and are located about 35 deg for both compositions. The pore fraction calculated by considering experimental density and the theoretical density (observed from X-Ray data) of the sintered pellets was above 60 %, thus satisfying requirements for materials used as gas sensors [17].

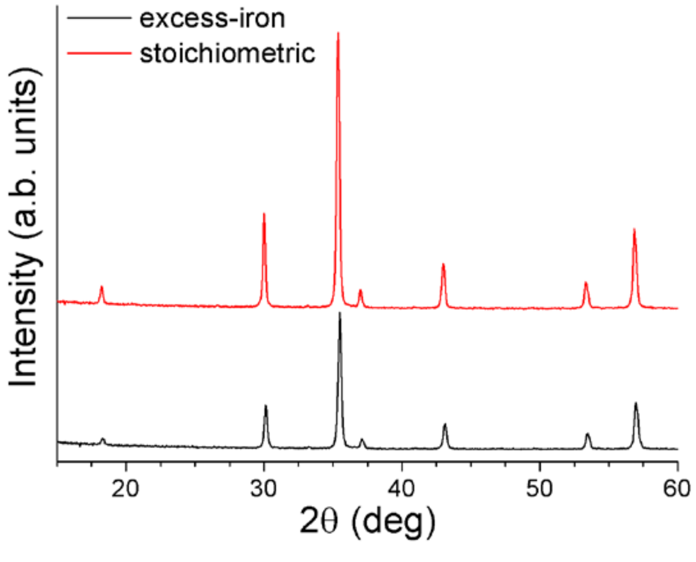

Fig. 3. XRD pattern of Ni-Zn ferrite samples sintered at 800 ^{o}C. All unmarked peaks correspond to spinel lattice different refalcting planes. Other peaks for impurity phases were not detected

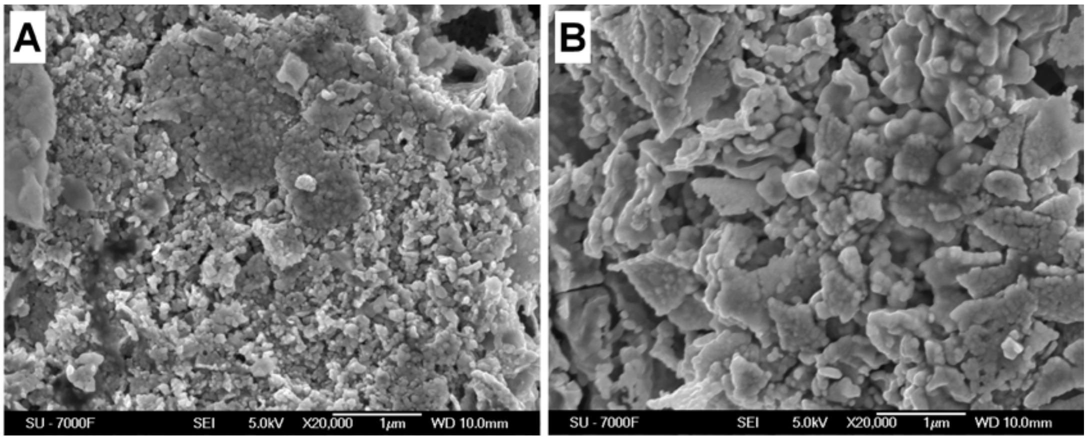

Fig. 4. SEM micrographs of stoichiometric (A) and iron-excess (B) Ni-Zn ferrite gas sensor sample fractured surfaces

Fig. 4. shows typical SEM image of the sintered ferrite sample fractured surfaces. Micrograph of the samples shows microstructure with nanosized grains. Presented structure is suitable for gas sensing applications, because nanosized grains possess high specific surface area for gas/solid interaction thus increasing response to analytical gases [18]. Generally no morphological differences were apparent between samples with differing iron content.

Table 2. Some properties of gas sensor elements

Parameter	Value
Crystallite size, nm	35±2
Grain size, nm	<100
Porosity, %	65±2

3.2. Resistance and its dependence from temperature

Room temperature DC electrical resistivity for stoichiometric and excess-iron samples was $3.9\cdot10^8$ and $1.4\cdot10^7$ Ω·m, respectively. Decrease of the resistance for excess-iron Ni-Zn ferrites in comparison with stoichiometric Ni-Zn ferrites is attributed to increase of Fe^{2+} concentration, thus addition of extra electrons [18].

The resistivity dependence from temperature is shown in Fig. 5. The resistance decreases by increasing operating temperature showing semiconductor behaviour. In the same time the plot log ρ versus operating temperature produces anomalous change of resistance. Increase (for p-type) or decrease (for n-type) of the resistance is attributed to desorption of chemisorbed water [19]. Adsorption of water traps e^- from metal oxide semiconductor conduction or valence band in case of n-type or p-type semiconductor according to equation $H_2O + e^- \leftrightarrow OH^-$ [20]. Desorption at higher temperatures returns e^- and hence increases (p-type) or decrease (n-type) resistance of the material $OH^- - e^- \leftrightarrow H_2O$ [20]. Desorption of chemisorbed water will promote oxygen adsorption and could enhance sensitivity, thus it is important to determinate resistance dependence from temperature to find out optimal stabilization, as well as operating temperature of sensor element [21].

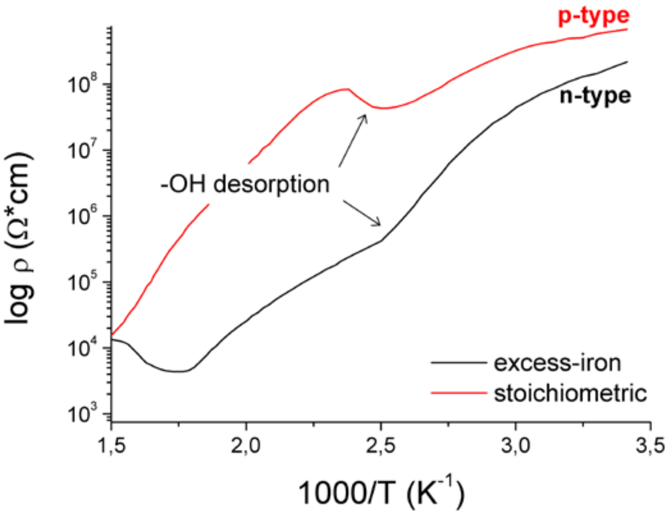

Fig. 5. DC resistivity as a function of temperature in stoichiometric and excess-iron ferrite samples

3.3. Gas sensing properties

The gas sensing response of stoichiometric and excess-iron Ni-Zn ferrites to acetone at concentration 500 ppm as a function of operating temperature in the range from 150 ^{o}C to 325 ^{o}C is shown in Fig. 6. Excess-iron Ni-Zn ferrite ($Ni_{0.3}Zn_{0.7}Fe_{2.1}O_{4-}$) exhibits higher response at all tested temperatures. Observed relationship is attributed to high Fe^{2+} concentration in the non-stoichimetric Ni-Zn ferrite, thus increasing charge carrier (electron) concentration and leading to higher oxygen adsorption in turn to oxidize test gas [11]. In comparison with single metal oxide gas sensors obtained material in some cases characterizes with higher response [22], but in some cases with lower response where SnO_2 nanowires were used [23].

With increasing operating temperature response increases to maximum and then decreases (Fig. 6). The maximum response of sensor element could be attributed to three reasons: (i) increase of concentration of oxygen species on the surface by replacing adsorbed hydroxyl groups; (ii) conversion of adsorbed oxygen species by following reactions: $O_{2(gas)} \rightarrow O_{2(ads)} \rightarrow O_2^{-}{}_{(ads)} \rightarrow 2O^{-}{}_{(ads)} \rightarrow 2O^{2-}{}_{(ads)}$, thus attracting more electrons from semiconductor and enhancing change in resistivity during the reaction between oxygen and test gas [24]; (iii) increase of thermal energy of gas molecules to overcome the activation energy barrier of the surface reaction with adsorbed oxygen species [6]; Decrease of sensitivity after maximum can be attributed to reduction of gas adsorption ability at higher temperatures [6]. Overall maximum response temperature corresponds to operating sensor temperature and for excess-iron ferrite is situated at 300 ^{o}C, but for stoichiometric sample at 275 ^{o}C.

Change of the conductivity by gas exposure is shown in Fig. 7. Conductivity changes in a moment when gas is introduced into testing atmosphere. In the same time obtained response and recovery time is longer than that of the literature values [18] due to bulk nature of the sensor element. As we can see conductivity for stoichiometric Ni-Zn ferrite decreases, but for excess-iron Ni-Zn ferrite increases, attributed to different type of charge carriers.

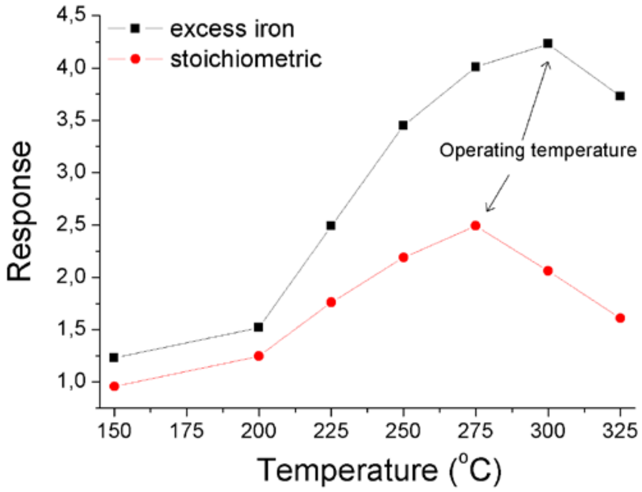

Fig. 6. Response dependence from temperature for stoichiometric and excess-iron Ni-Zn ferrites for the 500 ppm acetone gas

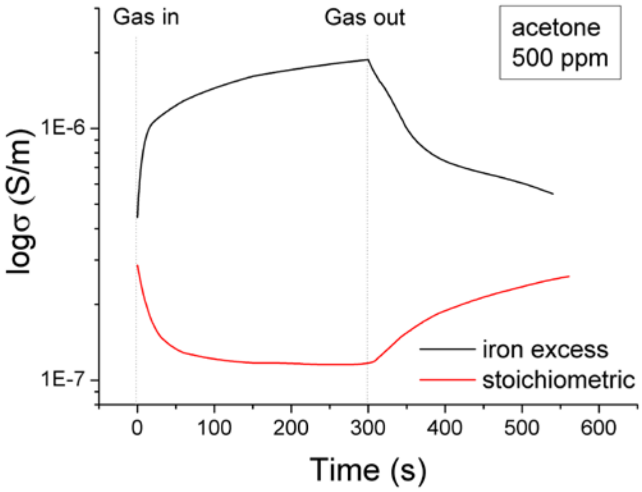

Fig. 7. Conductivity variation with time for stoichiometric and excess-iron Ni-Zn ferrites

It is known, that electrical conductivity for n-type semiconductors decreases (or increases) when oxidizing (or reducing) gases react with oxygen species absorbed on the grain surface [25]. By interaction with reducing gas, oxygen concentration on solid surface decreases thus releasing trapped electrons and introducing them back to the sensor material and increasing conductance [24]. Oxygen reaction with acetone can be shown with following equation:

$$CH_3COCH_3 + O^- \rightarrow CH_3CO^+ + CH_3O^- + e^- \qquad (4)$$

From observed relationships depicted in Fig. 7. we can conclude, that stoichiometric Ni-Zn ferrites possess p-type conductivity, but excess-iron Ni-Zn ferrites - n-type. This is attributed to hole transfer between nickel ions in case of $Ni_{0.3}Zn_{0.7}Fe_2O_4$ and electron transfer between $Ni_{0.3}Zn_{0.7}Fe_{2.1}O_{4-}$ as pointed out in the introduction of the paper. In non-stoichiometric excess-iron ferrites Fe easily dissolves in the spinel phase by partial reduction of Fe from $3Fe_2^{3+}O_3$ to $2Fe^{2+}Fe_2^{3+}O_4$ thus increasing Fe^{2+} concentration and enhancing electron hopping [16].

The stability of the sensors was confirmed to reverse showing good response even after 3-4 months.

4. CONCLUSIONS

As confirmed by XRD and SEM microanalysis the sol-gel auto-combustion method can be applied for synthesis of the nanometric single phase spinel type Ni-Zn ferrite gas sensor materials with different iron stoichiometry. Stoichiometric Ni-Zn ferrite possess p-type, but excess-iron ferrite n-type conductivity, giving evidence for Fe^{3+} reduction to Fe^{2+}. Excess-iron Ni-Zn ferrite in comparison with stoichiometric, exhibits higher response to acetone at all tested temperatures, what could be attributed to higher oxygen adsorption ability for interaction with test gas. Overall performed study reveals alternative way how to enhance sensitivity of spinel type ferrite gas sensor materials avoiding synthesis of complicated nanostructures or precious metal doping.

ACKNOWLEDGEMENT

This work has been supported by the European Social Fund within the project «Support for the implementation of doctoral studies at Riga Technical University».

REFERENCES

1. SUGIMOTO, M. The past, present, and future of ferrites. *Journal of American Ceramic Society*, 1999, Vol. 82, No. 2, p. 269–280.
2. SUTKA, A., STINGACIU, M., MEZINSKIS, G., LUSIS, A. An alternative method to modify the sensitivity of p-type $NiFe_2O_4$ gas sensor. *Journal of Materials Science*, 2012, Vol. 47, No. 6, p. 2856–2863.
3. CHEN, N., S., YANG, X., J., LIU, E., S., HUANG, J., L. Reducing gas-sensing properties of ferrite compounds MFe_2O_4 (M=Cu, Zn, Cd and Mg). *Sensors and Actuators B:Chemical*, 2000, Vol. 12, No. 1, p. 178–180.
4. GOPAL, REDDY, C., V., MANORAMA, S., V., RAO, V., J. Preparation and characterization of ferrites as gas sensor materials. *Journal of Materials Science Letters*, 2000, Vol. 19, No. 9, p. 775–778.
5. KAPSE, V., D., GHOSH, S., A., RAGHUWANSHIB, F., C., KAPSE, S., D., KHANDEKAR, U. Nanocrystalline $Ni_{0.6}Zn_{0.4}Fe_2O_4$: A novel semiconductor material for ethanol detection. *Talanta*, 2009, Vol. 78, No. 1, p. 19–25.
6. KADU, A., V., JAGTAP, S., V., CHAUDHARI, G., N. Studies on the preparation and ethanol gas sensing properties of spinel $Zn_{0.6}Mn_{0.4}Fe_2O_4$ nanomaterials. *Current Applied Physics*, 2009, Vol. 9, No. 6, p. 1246–1251.
7. MUKHERJEE, K., MAJUMDER, S., B. Reducing gas sensing behavior of nano-crystalline magnesium–zinc ferrite powders. *Talanta*, 2010, Vol. 81, No. 4-5, p. 1826–1832.
8. GUL, I., H., AHMED, W., MAQSOOD, A. Electrical and magnetic characterization of nanocrystalline Ni-Zn ferrite synthesis by co-precipitation route. *Journal of Magnetism and Magnetic Materials*, 2008, Vol. 320, No. 3-4, p. 270–275.
9. KOROTCENKOV, G. The role of morphology and crystallographic structure of metal oxides in response of conductometric-type gas sensors. *Materials Sience and Engineering R: Reports*, 2008, Vol. 61, No. 1-6, p. 1–39.
10. SUTKA, A., MEZINSKIS, G., LUSIS, A., STINGACIU, M. Gas sensing properties of Zn-doped p-type nickel ferrite. *Sensors and Actuators B:Chemical*, 2012, doi: 10.1016/j.snb.2012.04.059.
11. SUTKA, A., MEZINSKIS, G., LUSIS, A., JAKOVLEVS, D. Influence of iron non-stoichiometry on spinel zinc ferrite gas sensing properties. *Sensors and Actuators B:Chemical*, 2012, doi:10.1016/j.snb.2012.03.012

12. VARPULA, A., NOVIKOV, S., HAARAHILTUNEN, A., KUIVALAINEN, P. Transient characterization techniques for resistive metal oxide gas sensors. *Sensors and Actuators B:Chemical*, 2011, Vol. 159, No. 1, p. 12–26.
13. SHOBANA, M., K., RAJENDRAN, V., JEYASUBRAMANIAN, K., KUMAR, N., S. Preparation and characterisation of NiCo ferrite nanoparticles. *Materials Letters*, 2007, Vol. 61, No. 13, p. 2616–2619.
14. TIANSHU, Z., HING, P., JIANCHENG Z., LINGBING, K. Ethanol-sensing characteristics of cadmium ferrite prepared by chemical coprecipitation. *Materials Chemistry and Physics*, 1999, Vol. 61, No. 3, p. 192–198.
15. McCAFFERTY, E., ZETTLEMOYER, A. C. Adsorption of water vapour on α-Fe_2O_3. *Discussions on Faraday Society*, 1971, Vol. 52, p. 239–254.
16. ARSHAK, K., GAIDAN, I. NiO/Fe_2O_3 polymer thick films as room temperature gas sensors. *Thin Solid Films*, 2006, Vol. 495, No. 1-2, p. 286–291.
17. KOROTCENKOV, G. Metal oxides for solid-state gas sensors: What determines our choice? *Material Science and Engineering B*, 2007, Vol. 139, No. 1, p. 1–23.
18. TIEMANN, M. Porous metal oxides as gas sensors. *Chemistry - A European Journal*, 2007, Vol. 13, No. 30, p. 8376–8388.
19. VALENZUELA, R. *Magnetic ceramics*. Melbourne: Cambridge University Press, 1994. 181 p. ISBN 0-521-36485-X.
20. KOTNALA, R., K., SHAH, J., SINGH, B., KISHAN, H., SINGH, S., DHAWAN, S., K., SENGUPTA, A. Humidity response of Li-substituted magnesium ferrite. *Sensors and Actuators B:Chemical*, 2008, Vol. 129, No. 2, p. 909–914.
21. CALDARARU, M., SPRINCEANA, D., POPA V., T., IONESCU, N., I. Surface dynamics in tin dioxide-containing catalysts II. Competition between water and oxygen adsorption on polycrystalline tin dioxide sensor. *Sensors and Actuators B:Chemical*, 1996, Vol. 30, No. 1, p. 35–41.
22. Li, X., Chang, Y., Long, Y. Influence of Sn doping on ZnO sensing properties for ethanol and acetone. *Material Science and Engineering C.* 2012, Vol. 32, No. 4, p. 817–821.
23. QIN, L., XU, J., DONG, X., PAN, Q., CHENG, Z., XIANG, Q., LI, F. The template-free synthesis of square-shaped SnO_2 nanowires: the temperature effect and acetone gas sensors. *Nanotechnology*, 2008, Vol. 19, No. 18, 185705 (8 pages).
24. MOSELEY, P., T. New trends and future prospects of thick- and thin-film gas sensors. *Sensors and Actuators B:Chemical*, 1991, Vol. 3, No. 3, p. 164–174.
25. ARSHAK, K., GAIDAN, I. Development of a novel gas sensor based on oxide thick films. *Materials Science and Engineering B*, 2005, Vol. 118, No. 1-3, p. 44–49.

CYSENI 2012, May 24–25, Kaunas, Lithuania
ISSN 1822-7554, www.cyseni.com

ANALYSIS OF THERMAL DESTRUCTION OF CHARCOAL BY CO_2 GAS

V. Gurskienė, A. Šlančiauskas
Lithuanian Energy Institute
Laboratory of Combustion Processes
Breslaujos str. 3, LT-44403 Kaunas – Lithuania
Phone 837401 877
Email: gurskiene@mail.lei.lt

ABSTRACT

During the biomass gasification, common problems are the tar formation and incomplete conversion of carbon into CO. The literature review specifies the best ways for tar decomposition by the increasing the temperature and the introduction of steam. As the air oxygen is used as an oxidizer, an increased amount of ballast N_2 is obtained in the generated gas. It is known that at high temperature a reversible reaction $C+CO_2 <–> 2CO$ occurs when the carbon can be thereby combusted and the yield of combustible CO gas can be increased. During the experiment, a pulverized carbon from wood pyrolysis was placed into a hot quartz tube, which was used as a micro reactor, where the temperature of 1000–1100°C was maintained. The rate of carbon gasification on the basis of Arrhenius formula was determined.

Keywords: tar destruction, biomass gasification, carbon, combustion with CO_2

1. INTRODUCTION

Recently, biomass gasification are widely studied. Many attentions gives to development of gasification systems to utilize biomass residues and other organic wastes. The main product obtained in gasification of biomass is synthetic gas mainly composed from H_2 and CO. The resulting syngas may be used as a fuel for internal combustion engines, gas turbines, hydrogen production industry, and synthetic diesel production.

The main problems in gasification system are: formation of tars which tend to deposit on surfaces of turbine blades, moving parts of internal combustion engines or hydrogen separation membranes, condensates, burns-in and other ways influences long-term exploitation of the equipment [1]; and incomplete conversion of carbon into CO. Tars and remaining carbon (charcoal) could be reduced using CO_2 reforming. This process consumes CO_2 from combustion equipment's and reduces environmental pollution with CO_2. The proper gasification process can significantly reduce the CO, CH_4, NOx emissions [2].

In one of the papers, Lopamudra Devi et al. [3] present a model developed at the University of Oklahoma where the tar decomposition temperature reached 1100 ^{0}C, using a downdraft gasifier. The gasification experiment indicated the tar decomposition temperature and the efficiency of hot and cold CO and H_2 gas, respectively 73% and 63%, and accordingly the specific air supply rate was 542 kg_{air} /mm^2 and the maximum tar destruction temperature was 1100 ^{0}C.

The other works report, that the main problem in biomass gasification is tar production at low temperature. Therefore, it is proposed to treat the gas after gasification or to gasify in a manner minimizing the tar production. This means that a high temperature of 1100 ^{0}C and higher should be achieved. Besides, active additives are introduced, such as catalysts: dolomite, olivine, carbon, etc.

2. BACKGROUND

Downdraft gasifier

By “Eureka” project VP1-3.1-ŠMM-06-V-003 in Lithuanian Energy Institute, Laboratory of Combustion Processes the downdraft gasifier for biomass ant other wastes is designed and tested. The aim of the research is the production of qualitive and clean gasified gas. For this reason, the air and steam are supplying into the gasifier, which scheme is shown in Fig. 1.

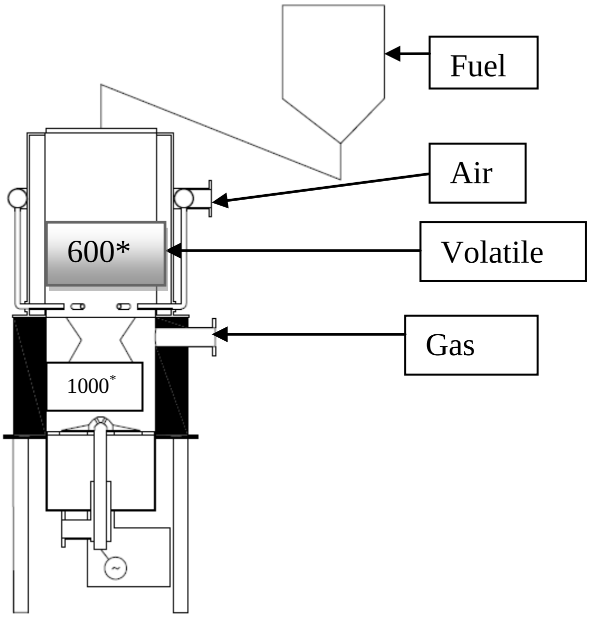

Fig. 1. Scheme of the downdraft gasifier used in research

It can be seen from Fig. 1, that the fuel in this downdraft gasifier is provided from upstairs, the air and gas from side flanks. In a combustion zone at between 500–600^{0}C temperatures the volatiles are generated. The amount of volatiles in the combustion zone can be reduced by raising the temperature up to 1000^{0}C and conversion into non-condensable gas occurs. For this reason, a downdraft gasifier is desirable, because of low amount of tars.

Tar formation

Tar – is viscous liquid mixture of hydrocarbons, which can plug up and damage the burning equipment and the repair, can be very expensive. For that reason, the amount of tar must be significantly reduced to avoid breakdowns [1–3].

From the scientific literature it is known, that the tar formation depends on temperature. Firstly, the biomass is supplied into the reactor, where the temperature is approximately 500–600^{0}C and the emission of volatiles is observed. At the temperature of 500–600^{0}C the formation of non-condensable gas begins, such as H_2, CH_4, CO, CO_2 and H_2O. Increasing the heating temperature, tar is destroyed and then gained incondensable liquid mixture.

The main methods for tars reduction are: primary and secondary [4]. Primary tars reduction method includes the reforming by thermal and steam cracking. The secondary method includes the cleaning of tars into barrier filters after the gasification.

3. CARBON GASIFICATION BY BOUDUARD REACTION MODEL

A reversible reaction of carbon with carbon dioxide is known as a Boudouard reaction [5]:

$$C + CO_2 \rightarrow 2CO \tag{1}$$

The Boudouard reaction has the following steps. Firstly, combustion first layer of carbon, then flows CO_2 gas and carbon becomes free site (C_{fas}), and forming a carbon-oxygen surface complex, C(o) and CO. Secondly, forming a carbon active site and CO_2. Thirdly, the carbon-oxygen complex produces a molecule of CO.

$$C_{fas} + CO_2 \rightarrow C(o) + CO\,, \tag{2}$$

$$C(o) + CO \rightarrow C_{fas} + CO_2\,, \tag{3}$$

$$C(o) \rightarrow CO\,, \tag{4}$$

$$CO + H_2O \leftrightarrow CO_2 + H_2\,. \tag{5}$$

All reactions from (2-5) occur under environmental conditions and depend on:

- oxygen concentration, expressed by partial pressure P_{O_2},
- H_2O concentration, expressed by partial pressure P_{H_2O},
- CO_2 concentration, expressed by partial pressure P_{CO_2},
- direct activation of carbon surface,
- activation propability of carbon surface (quick, slow reaction).

The reaction rate according to the temperature could be calculated by Arrhenius equation:

$$r = k \cdot \exp\left[-\frac{E}{RT}\right], \tag{6}$$

where r is the reaction rate , E – the activation energy, k constant represents the molecular rate.

4. MATERIALS AND EXPERIMENTAL SET-UP

Two types of carbon were used in experiment: A type carbon, which was gasified at about 900°C and B type carbon, which was pyrolysed from the waste tire. The pulverized A type carbon using a crucible, which weight was 2.134 g, was placed into a hot quartz tube; the weight of B type carbon was 0.354 g. With a help of insulated thermocouple measured and maintained the temperature in the range of 1000-1020°C . The wall of hot quartz tube was insulated on both sides.

In the first experiment pure CO_2 gas was used, while in the second and third ones mixture of CO_2 + N_2. The gas flow rates were accordingly: 0.0006 l/s and 0.0003+0.0003 l/s. All the experimental set-up system was insulated and the pressure was created by connected gauge meter.

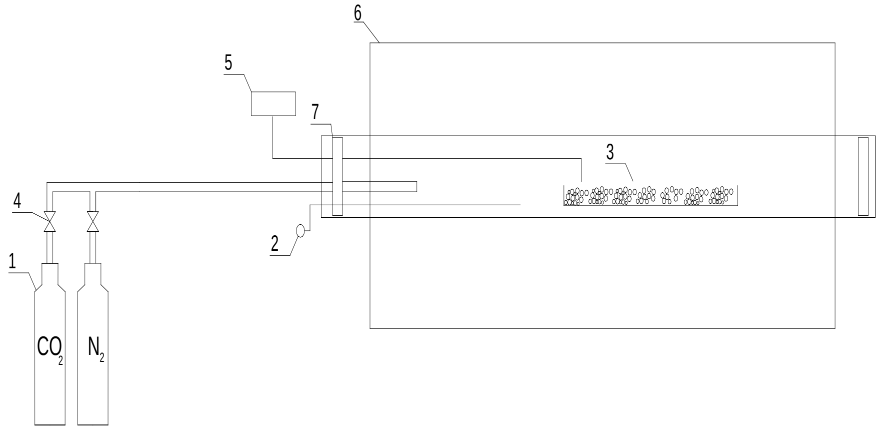

Fig. 2. The scheme of experimental set-up for carbon destruction. 1 – CO_2, N_2 gas cylinders; 2 – gauge meter; 3 – pulverized pyrolysis carbon; 4 – valve; 5 – temperature indicator; 6 – furnace; 7 – quartz tube

5. RESULTS AND DISCUSSION

Measurement results are presented in Fig. 3.

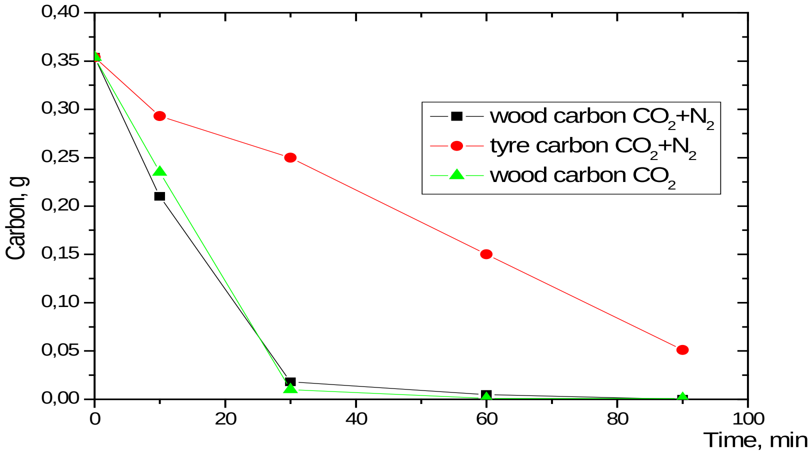

Fig.3. Wood and tire pyrolysis residue carbon combustion in CO_2 and CO_2+N_2 environment

The obtained results showed, that tested carbon species has different gasification time. As can be seen from the Fig. 3. the longer time for fully gasification of tire carbon is needed, comparing with biomass charcoal. The main reason of longer gasification time was remaining tar in the coal. Wood carbon was gasified in 30 minutes, while the full gasification of tire carbon requires three times longer residence time - 90 minutes.

The wood carbon curve falls sharply and it shows that carbon gasification process occurs at first thirty minutes, differently than tire carbon. As mentioned before, it is under the influence of the carbon type.

There was found:

- Carbon gasification is linearly dependent on time;
- Carbon type influence the reaction velocity;
- Nitrogen gas (50% addition) has no effect on reaction rate.

Carbon reduction goes linearly over the time and shows that the carbon conversion into CO gas occurs when carbon layer by layer is burned from the surface. How many carbon is burned and CO gas formed we can calculate by the number of moles, so: C- 12 kmol, CO – 28 kmol.

5.1 Chemical kinetics of homogeneous reaction

In evaluation how quickly or slowly chemical reaction occurs in the reactor, it is needed to know reaction velocity constant [6]. For that purpose a homogenous reaction was used. It depends on the initial chemical material and the concentration of the product respectively.

Chemical reaction velocity is calculated by the formula:

$$-\frac{d(c_0 - c_x)}{dt} = k_1(c_0 - c_x)\,, \tag{7}$$

where c_o – initial concentration, c_x – obtained product, k_1 – reaction constant. The integration constant is known, when t=0, c_x=c_o:

$$-\ln(c_0 - c_x) = k \cdot t - \ln c_0\,. \tag{8}$$

According the experimental data, the reaction constant value k was calculated using this equation:

$$-\frac{d(c_0 - c_x)}{dt} = k_1(c_0 - c_x)\,. \tag{9}$$

Then the reaction constant is found from graphs (Fig. 3.) as a line slope:

$$-\frac{dc_x}{dt} = \frac{\Delta c_x}{\Delta t} = k\,. \tag{10}$$

The experiment data is showing a straight line, (g/s):

$$k_1 = \frac{\Delta c_x}{\Delta t} = \frac{0.31 - 0.12}{1800 - 600} = 1.6 \cdot 10^{-4}\,. \tag{11}$$

The reaction occurred on a carbon surface, which area is, (m^2):

$$F = 0.025 \cdot 0.015 = 3 \cdot 10^{-4}\,. \tag{12}$$

The reaction velocity for pulverized wood carbon provided by CO_2 gas, (g/m^2s):

$$v_1 = \frac{k_1}{F} = \frac{1.6 - 10^{-4}}{3.75 \cdot 10^{-4}} = 0.43\,. \tag{13}$$

Reaction velocity for pulverized waste tire carbon, (g/m^2s):

$$v_1 = \frac{k_2}{F} = \frac{3.83 - 10^{-5}}{3.75 \cdot 10^{-4}} = 0.01\,. \tag{14}$$

The Arrhenius equation is quite simple, but remarkably useful formula to describe the constant of reaction rate. The activation energy E, a frequency factor A and temperature dependence on the reaction are included there. On our experimental basis for founded reaction constant and Boudouard reaction application for carbon gasification [5] we can propose the empirical Arrhenius relations for investigated carbon.

$$k = A \cdot \exp\left[-\frac{E}{RT} \right] \tag{15}$$

Table 2. Values of the carbon reaction constants at 1020^{o}C

Type of carbon	Activation energy E, (J/kmol)	Pre-exponential factor, A
Wood carbon	$1.98 \cdot 10^{8}$	$4.2 \cdot 10^{4}$
Tire carbon	$2.12 \cdot 10^{8}$	$3.5 \cdot 10^{4}$

6. CONLUSIONS

Lower-quality organic fuel usually is used for heat production, but gasification is another possibility for waste conversion. The produced gas could be a fuel of high quality and more widely used in the industry. Under the Eureka program in LEI, Laboratory of Combustion a gasification facility is produced and this article discusses the ways how to improve the calorific value of the producer gas.

From a literature review and our experimental data the reduction of tar is roughly known. It was ascertained that the most effective way is to use higher temperatures (900-1100°C) and steam injection in the reactor. Tars are generating during the volatiles evaporation at temperatures from 500 to 700 °C. Using higher temperatures and steam yields to more stable gases H_2, CO, CH_4.

A lot of carbon at the bottom part of the gasification reactor is left. This carbon can be oxidized into CO gas. This gasification process is slow at 1000 °C and getting higher temperatures is needed more oxygen or air . In this article the oxidation reaction is analyzed using the CO_2 effect.

After the experiments with wood and tires carbon, the reduction of CO_2 into CO gas was performed. The reaction speed and constants of Arrhenius law were established.

REFERENCES

1. Basu P. Biomass Gasification and Pyrolysis Practical Design, tar production and destruction, 2010, p. 365.
2. Heidi C. Buttermann and Marco J. Castadi, Influence of CO_2 injection on biomass gasification, 2007, p. 8875–8886.
3. Lapamudra Devi, K.J.Ptasinski, Frans J.J.G. Janssen, A review of the primary measures fo tar elimination in biomass gasification, Enviromental Technology Group, 2002.
4. T. Yamazaki, H. Koru, S. Yamagata, N. Murao, S. Ohta, S.Shiya, T. Ohba, Effect of superficial velocity on tar from downdraft gasification of biomass, 2005.
5. K. Svoboda, M. Hartman, J.Cermak, Combustion Mechanisms – Solid Phase, in: Pollutants from Combustion, Kluwer Academic Publishers, Dordrecht 2000, p. 35–50.
6. J. Janickis, „Fizikinė chemija“, Vilnius, Mokslas, 1997.

ACKNOWLEDGEMENT

This work is related with activities of project “Eureka” VP1-3.1-ŠMM-06-V-003.

CYSENI 2012, May 24–25, Kaunas, Lithuania
ISSN 1822-7554, www.cyseni.com

DEVELOPMENT OF ALGORITHMS FOR SIMULATION OF DIFFUSION COMBUSTION OF STEEL, AND RECOVERY OF THE DIFFUSION COEFFICIENT OF OXYGEN IN THE IRON OXIDE LAYER

V.I. Ignatenko, S.I. Shabunja, V.V. Martynenko
A.V. Luikov Heat and Mass Transfer Institute
P. Brovka str. 15, 2000072 Minsk – Belarus
Phone +37517-2842110
Email: v.i.ignatenko@gmail.com

ABSTRACT

The present work is part of a research program to study the combustion of steel in oxygen at high pressure. The purpose of the simulation was melting and burning of iron, as well as the restoration of the diffusion coefficient of oxygen through the oxide layer on the basis of experiments.

In the paper provides an overview of experiments and research in the field of combustion of metals. Also presents a model of melting iron cylindrical rod in an argon environment. It was obtained by melting fronts at different values of laser power. In modeling these facilities were given parametrically as effective. On the basis of experiments comparing the obtained melting fronts with those calculated in the model, it is planed to find the coefficient of laser radiation absorption core. This parameter is poorly studied in the literature there is very limited information on this parameter.

Further simulated heterogeneous combustion process of the rod in an oxygen environment, the diffusion coefficient of oxygen included in the review of the model parametrically. On the basis of future experiments, changing the value of laser power and its impact on the time bar based on the thickness of the oxide layer and the melting front, it will be possible to restore the diffusion coefficient.

Keywords**:** metal combustion, heat conduction, burn criteria, flammability, diffusion coefficient of oxygen

1. INTRODUCTION

The topic of iron and steel combustion in oxygen continues to occupy attention for several reasons. First, steel is the most widely used material for storage and conveyance of gaseous oxygen. Most of its use occurs in conditions under which combustion is possible. Fires are rare, however, owing to strict adherence to practices and guidelines which reduce the possibility of ignition to near zero. Nevertheless, a fundamental understanding of iron and steel combustion mechanisms is desired for predicting the speed of burning, the thresholds of propagation, and the extent of damage should such fires be initiated.

Another reason for developing greater understanding into the mechanisms is to explain differences among different types of steels. Once insights are gained, it might be possible to safely extend the range of use in oxygen for some types of steels, with accompanying economic advantage. For example, it may be possible to safely substitute less expensive steel materials into valve bodies instead of more expensive materials that would be chosen with today's level of understanding for use in certain size and pressure applications. Despite the fact that the problems of ignition and combustion of solid metals are engaged in more than half a century, most of the research was to carry out standard tests aimed to determine whether the combustion process to occur under certain conditions. But we are also interested in the process, answer questions exactly how it proceeds and what the parameters affecting it. Unfortunately this information is not so much.

One of the most important and still poorly studied aspects in the combustion of metals is the question of oxygen transport. In particular, the coefficient of oxygen diffusion through the iron oxide to the surface reaction isn’t clearly known. Presented in the literature are limited in the temperature range 1840-1940 K and have a large scatter [1].

This paper presents the modeling of the melting and combustion of metal rods and determination of the diffusion coefficient of oxygen, iron and iron alloys were selected for the investigation and they are consistently reported to burn heterogeneously. The Wolfram Mathematica 7 program was utilized to solve the developed model that predicts temperatures within the test samples.

2. BACKGROUND

It is generally understood that the behavior of a fire spreading along a metal piece in oxygen atmosphere depends on the metal properties, spread direction, dimension of the sample, the oxygen pressure and temperature. Typical combustion experiments in the field of steel are mainly carried out for two configurations of sample ignition: the burning region spreads upward (the ignition of the bottom surface of the rod) and the burning region spreads downward (the ignition of the upper surface). In the first configuration a molten iron oxide mass, wich is the luminous spherical part at the bottom end of the test piece, is formed (Fig. 1). As the burning region spreads, the molten mass becomes too large to be supported, it drops. Just after the greater part of the molten mass drops, the remaining molten mass starts to increase again. This behaviour is repeated at regular intervals [2].

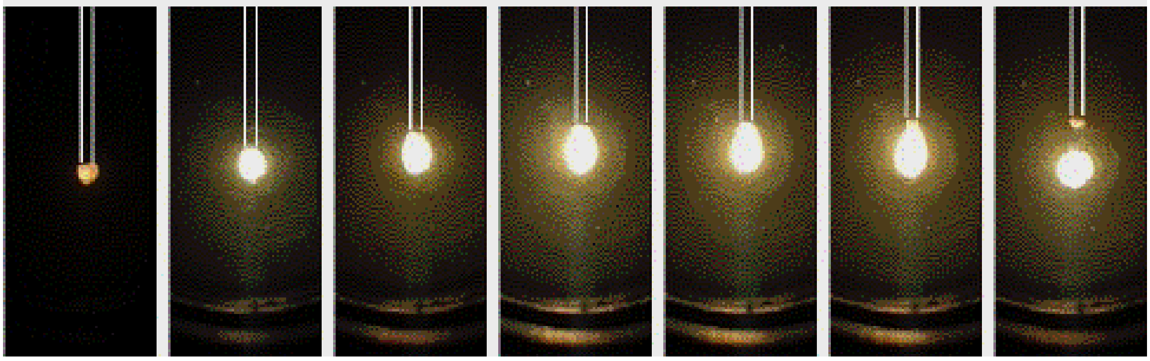

Fig. 1. Typical aspects of fire spread along iron rods, upwards spread

At a higher oxygen pressure the molten iron oxide flows downward along the rod and comes into contact with the unburned region surface (Fig. 2.). The unburned region surface, where a sufficient amount of the molten iron oxide remains, starts burning. Thus, the spread in this case is usually an intermittent discontinuous one.

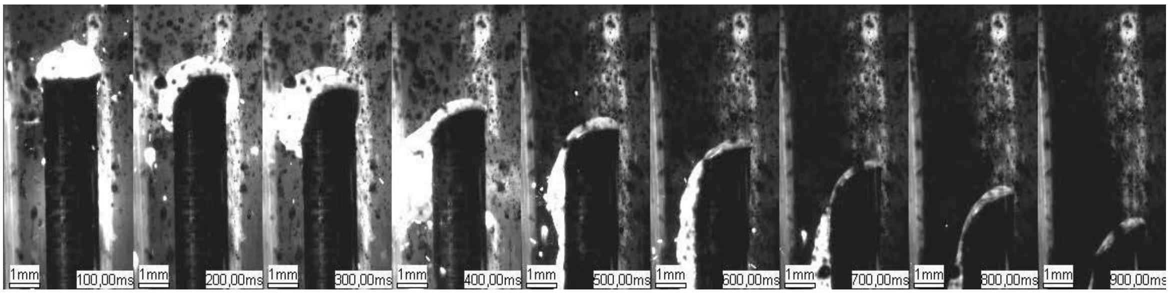

Fig. 2. Typical aspects of fire spread along iron rods, downwards spread

Despite the variety of tests, the vast majority of them performed without the preliminary model, but it’s based on existing guidelines so-called standard tests, including those developed by the National Aeronautics and Space Administration (NASA), ASTM, International Organization for Standardization (ISO) [3]. The usual results are obtained in the form of qualitative findings, characterizing the process in whole, but do not explain the reasons for the phenomena.

As a result, there is a considerable amount of experimental data of the iron and steel combustion, but it's usually are the results of standardized tests, which are fixed in terms of ignition, the diameter of the rod and its attachment, the method of oxygen supply, etc. Publications reflecting the consistent study of the combustion process by varying the parameters, measurements of various characteristics, the statement and testing hypotheses are also some very small [2, 4-5]. The main parameter is the variation of oxygen pressure, and the observed result is expressed in terms of: the rod went out immediately after ignition; the rod is partially burned down; burned down the rod completely. Such information is not enough.

3. MODELING OF MELTING AND BURNING OF CYLINDRICAL RODS

3.1. Statement of the Problem

Most of the tests presented in the literature deal with the upwards combustion, that is, the lower surface of the sample was ignited. This configuration is justified if the purpose is to create conditions for sustainable long-term process of combustion. The drop is formed at the lower end of the rod, and it separated from the sample under the influence of gravity, providing a better supply of oxygen to the interface reaction. However, in this case it is impossible to say with certainty about the structure of the separated droplets. Therefore, in our problem, we use the inverse configuration.

Fig. 3. shows a schematic of the experiment. Investigated sample is a thin iron (the main component of steel) cylindrical rod, its diameter is 3.2 mm.

However, there is a problem in tests with the downwards combustion of the rods, too: the melt flows down the sides of the rod, asymmetrically, while causing additional heating of the lower layers of the rod (which cannot be accurately taken into account in the modeling). To avoid these errors, put the rod in a tight-fitting an insulating shell. The entire system is placed in an airtight chamber. In the case of pure melting it is filled with argon, in the experiments of burning chamber filled with oxygen, respectively. Laser was chosen as an igniter. In addition, the laser power is chosen so that the maximum temperature of the rod lying in the region below the boiling point of iron, as the vapor will contribute an additional scattering of the laser power, which extremely problematic take into account.

Thus, there are following configurations during the combustion in this system: lower layer of the rod is solid iron (steel), then a layer of liquid iron thickness of l_L, and then the oxide layer thickness of l_{FeO} and the oxygen gas cloud of a known concentration near the top surface of the rod. By varying the parameters of laser power and heating time, we'll obtain different values of thickness and that will depend on the reaction rate. The rate of reaction depends on the oxygen transport to the surface reaction. That is, analyzing the thickness and based on a constructed model the conclusions about the diffusion coefficient can be made.

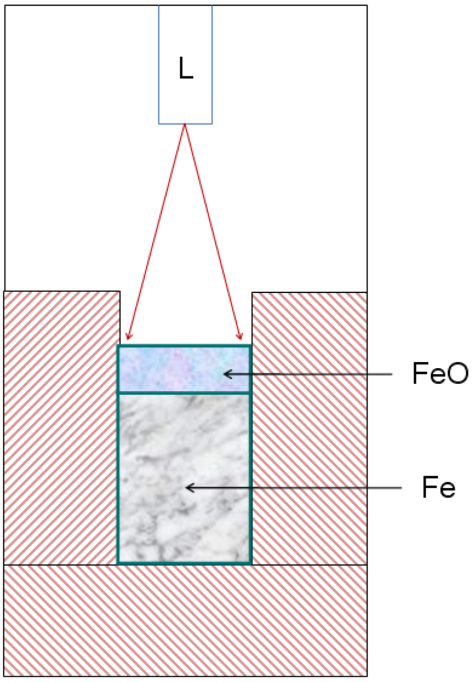

Fig. 3. Schematic of the experiment

3.2. Modeling of the melting process

In this section present the simpler problem of melting a rod of finite length. The chamber of the experimental apparatus is filled with argon. The combustion will not occur since there is no oxidizing environment. There is need to modeling the temperature profile along the entire length of the rod. Using this model the values of the coefficient of absorption for different laser powers can be obtained by analyzing the thickness of the melt. This model will be applied to describe the temperature profile along the metal rod in the simulation of the combustion process, too.

The distribution of heat in the rod is described by the heat equation:

$$C_P \rho \frac{\partial T}{\partial t} = \frac{\partial}{\partial z}\left(\lambda \frac{\partial T}{\partial z}\right), \tag{1}$$

where, C_P is the heat capacity of the environment, ρ is the density of the material, λ is the coefficient of thermal conductivity.

Since the density is a function of temperature $T(t)$, as well as taking into account that

$$C_P = \left(\frac{\partial H}{\partial T}\right)_P, \tag{2}$$

rewrite (1) as:

$$\frac{\partial(\rho H)}{\partial t} = \frac{\partial}{\partial z}\left(\lambda \frac{\partial T}{\partial z}\right), \tag{3}$$

where, H is a specific enthalpy of the material.

The transition from heat capacities to enthalpy due to the type of temperature dependence. For enthalpy this dependence is a smooth s-shaped relationship (Fig. 4.), the graph of the heat capacity has a pronounced peak in the phase transition region (Fig. 5.). It is likely that by operating the heat capacity, our next step will not be small enough to account for this peak. Should always take into account this fact and carefully select the intervals. It is therefore advisable to use enthalpies. The result will not change, but we can avoid unnecessary errors.

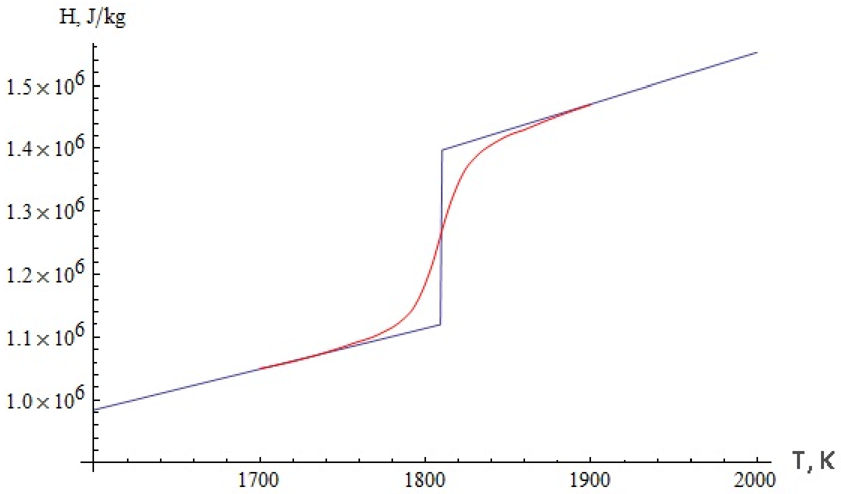

Fig. 4. The enthalpy near phase transition

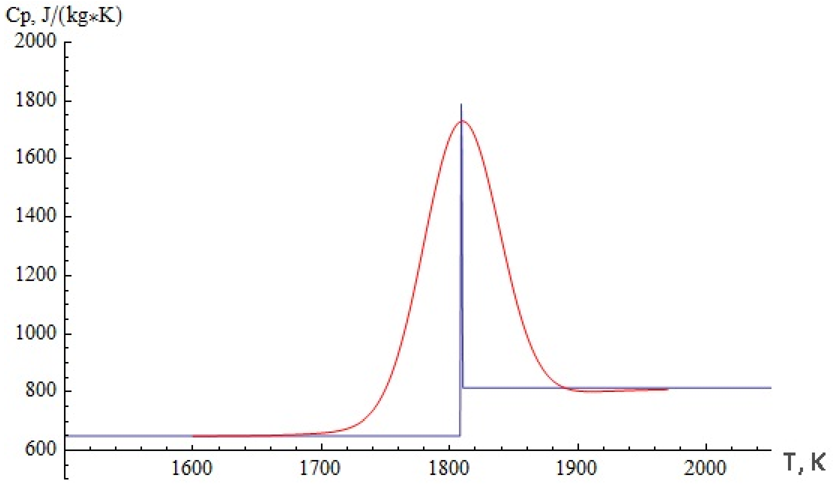

Fig. 5. The heat capacity near phase transition

The energy absorbed by the surface of the rod is defined as heat that absorbed due to the interaction of laser radiation with matter, per unit area:

$$J_L = A_0 \frac{P}{S}, \tag{4}$$

where, P is a power of laser radiation in Wt, S is an area of the irradiated surface in m², A_0 is an absorption coefficient for rod.

Attempts to determine the absorption coefficient for the A_0 have been taken by Müller [6], but its meaning is not clear. Therefore, let's now just assume that P is the effective power P_{eff}.

In our case we are dealing with a one-dimensional problem with one parameter - the distance from the upper surface of the heated rod. We consider the dynamics of the temperature profile in the core over time.

The difference scheme is:

$$H_i^{n+1} = H_i^n + \tau\lambda \left\{ \frac{T_{i+1}^n - 2T_i^n + T_{i-1}^n}{h^2} \right\}. \tag{5}$$

In (5), i-components are characterized by the distance from the surface of the rod along its axis, n is the time parameter.

Boundary conditions:

$$\begin{aligned} -\lambda \frac{\partial T}{\partial z}\bigg|_{z=0} &= J_{La} - \varepsilon\sigma T^4 \\ -\lambda \frac{\partial T}{\partial z}\bigg|_{z=L} &= 0 \end{aligned} \tag{6}$$

In addition, the solution converges to the time interval must satisfy the condition:

$$\tau \le \frac{h^2 C_P \rho}{2\lambda} \tag{7}$$

Modeling was carried out in Wolfram Mathematica 7. The full program code can be found in Appendix 1.

In model an adjustment for laser power was carried out to limit temperatures to the boiling point of the iron (Fig. 6).

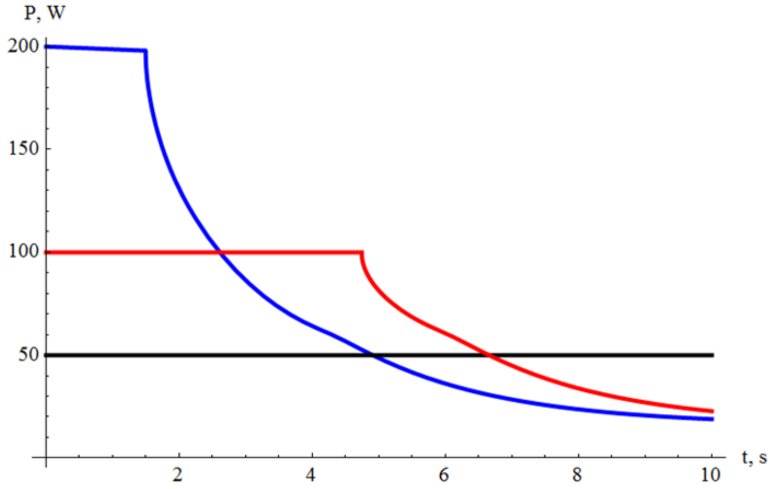

Fig. 6. An adjustment for laser power

Fig. 7 and Fig. 8 are presented for comparison of the temperature distribution with no amendments and with the amendments to the laser power, respectively.

Fig. 9 show the values of the thickness of the melt mass after a certain period of time. As the laser power in the model adopted for the effective power P_{eff}, on the basis of the experiment, setting the real power P_{La} and comparing the thickness of the melt in the experiment and used in the simulation, they can get the value of absorption coefficient A_0 rod. That is, using the value obtained in the experiment, we find from the model corresponding P_{eff} and then evaluate the desired ratio by the formula:

$$A_0 = \frac{P_{eff}}{P_{La}} \tag{8}$$

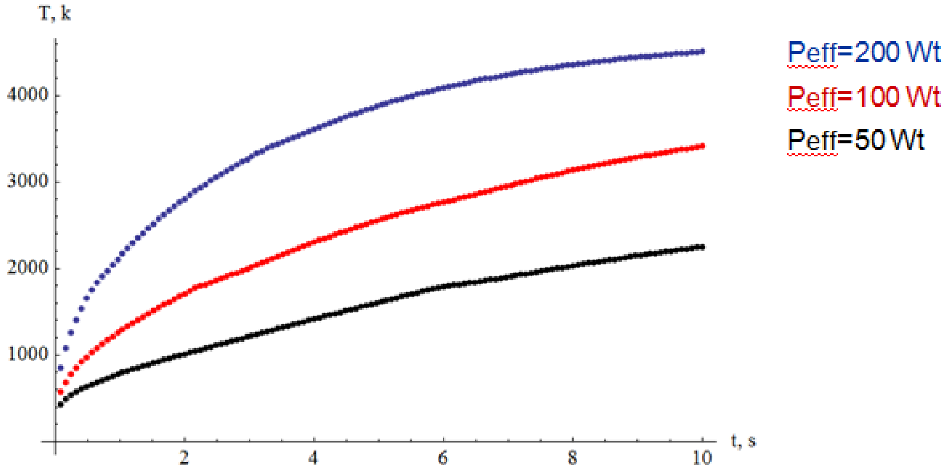

Fig. 7. Temperature distribution in the iron rod, without adjustment

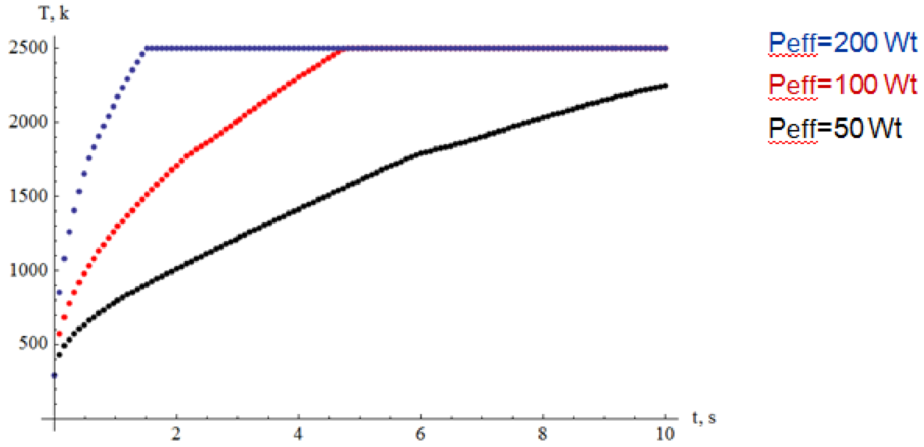

Fig. 8. Temperature distribution in the iron rod, with adjustment

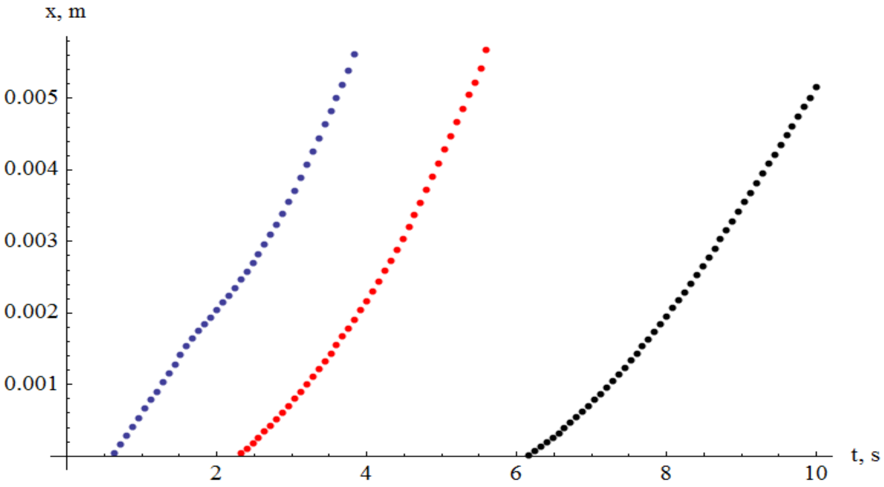

Fig. 9. Melting front

Generally speaking, this ratio will vary for models of melting and burning, as the absorbing surface of the different (Fe and FeO, respectively). However, this will be the same order. The coefficient A_0 gives characteristic of our particular experiment, so we'll use it for burning experiments.

3.2. Modeling of the combustion process

On the basis of the thermodynamic law of mass action is calculated equilibrium composition of mixtures of iron and oxide 0.5:0.5, corresponding to the stoichiometric ratios for the oxidation of iron. Thus, the combustion reaction of iron for oxygen is written as:

$$\mathrm{Fe}+\frac{1}{2}\mathrm{O}_2\rightarrow\mathrm{FeO} \qquad (9)$$

In these processes, possibly incomplete oxidation of metals. The reason for this is the dissociation of oxides at a fixed stoichiometric ratio. The degree of dissociation decreases with increasing pressure. For iron in the range of interest pressures dissociation is practically nonexistent and is the only product.

It is assumed that the oxidation of the metal occurs on the surface of its liquid phase, in accordance with reaction (9). It is further assumed that the composition of the reaction products of combustion is thermodynamic equilibrium. In the present modeling, we remove the product from the surface occurs. Oxygen is supplied to the boundary of the metal only through diffusion. Since the length of the oxide layer l_{FeO} is a small quantity (on the order of a millimeter), it is assumed that the temperature in the entire volume of the oxide is the same at a given time and is equal to T (t).

The equation of conservation of energy in the coordinate system associated with the surface of the burning metal looks the same as for the melt (see Eq. 3).

The energy balance for the oxide layer:

$$\frac{\partial}{\partial t}\left[m_{FeO}H_{FeO}(T_{\mathrm{cov}})\right]=G_{O_2}\cdot H_{O_2}(T_{\mathrm{cov}})+G_{Fe}\cdot H_{Fe}(T_{\mathrm{cov}})- \qquad (10)$$

$$-\lambda\frac{T_{\mathrm{cov}}-T_0}{h}-\varepsilon\,\sigma T_{\mathrm{cov}}^4+J_{La}$$

At our current level of understanding the physics of burning iron in oxygen limiting process (i.e. determining the rate of combustion) is the transfer of oxygen from the gaseous medium to the area (surface) burning. As noted in the previous section, a variant of the model with evaporation and combustion of iron vapor cannot be realized, and the most likely mechanism is a surface burning.

Accepted that the oxidation of iron with oxygen occurs instantaneously at the point where they meet the relevant atoms. In this model the process on the surface of the iron to grow the oxide layer through which oxygen diffuses to the metal, where a chemical reaction and heat release. The density of the flow of oxygen through the oxide film thickness will be determined by the membrane and the diffusion coefficient, which in turn is strongly dependent on temperature.

If you do not remove the oxide membrane, the diffusion flux of oxygen will decrease, the amount of burning iron will decrease and the temperature is lowered, i.e., extinction should occur. If we wanted to modeling a stable combustion (as in the standard tests with burning rods), it would be necessary to introduce a model of the mechanism of removal of the oxide film. However, in view of the problem, this issue does not matter. Moreover, it is recorded the exact values of the volume of molten iron (refrigerated) and oxide that formed during the reaction.

In the model, oxygen gas is in contact with the liquid oxide membrane and, of course, is dissolved in it, i.e., membrane is the solution of "free" oxygen in the oxide of iron. "Free" oxygen is a set of oxygen atoms and ions that contain chemically bound oxygen is weakly [7]. Limit of free oxygen in this solution - the value is called solubility. Its value is determined by the pressure of gaseous oxygen on the surface of the solution and the temperature of the solution. It is the oxygen that was taken as a boundary condition on the surface of the membrane. The dissolved oxygen diffuses into the depths of the melt from the outer surface of the membrane. First, it is in the form of free oxygen, and then there is transport of oxygen in the bound form due to mutual diffusion of

FeO and Fe. Thus, the melt consists of two areas in the first two components - O and FeO, in the second, too, two - FeO and Fe. Also it is taken solid iron, but it is only calculated the heat transfer. The density of the mass flux of oxygen expression:

$$G(O_2) = D_O \frac{C_O^0}{l_{FeO}}, \tag{11}$$

where, D_O is coefficient of diffusion of oxygen through a layer of iron oxide thickness l_{FeO}, C_o^0 is the concentration of oxygen near the surface of the rod.

The diffusion coefficient is a function of the temperature:

$$D_O = A_D \exp\left[-\frac{U_D}{T}\right], \tag{12}$$

where, the parameters A_D and U_D are unknown constants, which are to be determined.

The full program code can be found in Appendix 2. Fig. 10–12. presents the resultant of modeling.

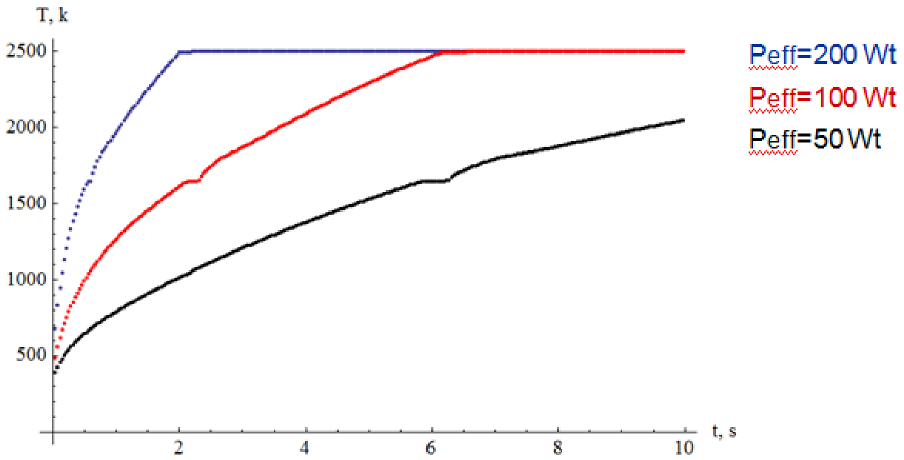

Fig. 10. Temperature distribution in the iron rod, burning case

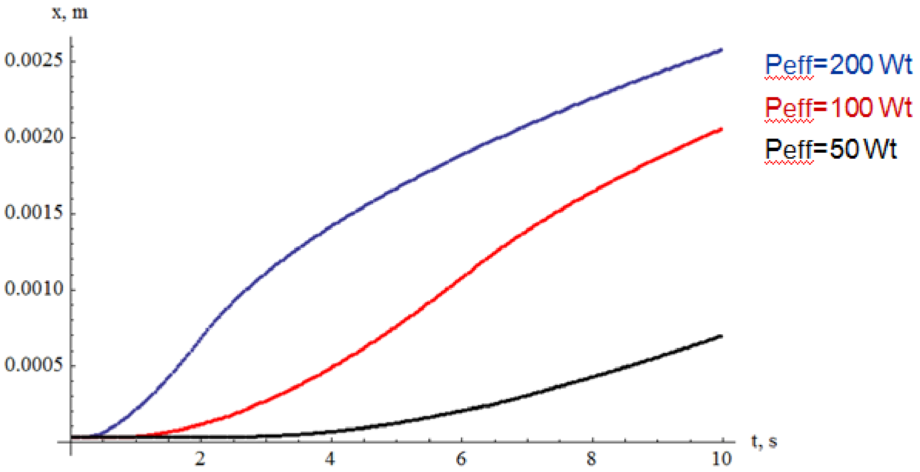

Fig. 11. Thickness of the oxide layer

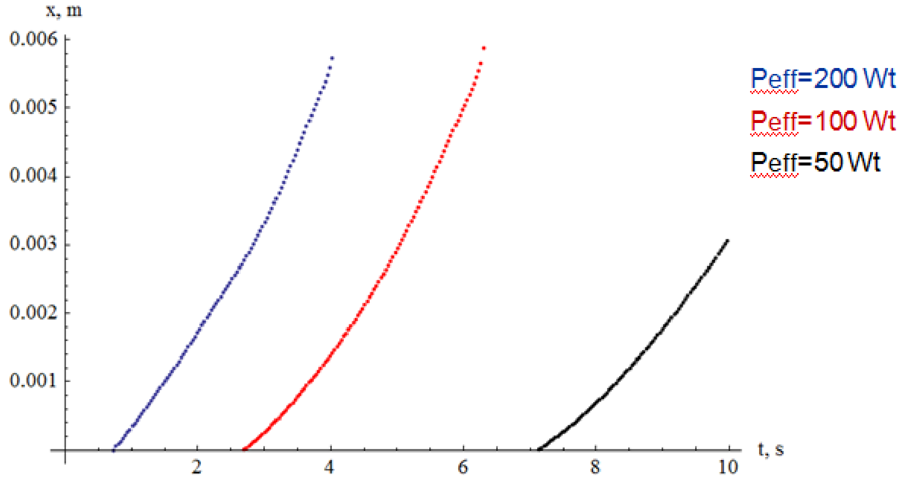

Fig. 12. The melting front, burning case

Taking off the melting front and the thickness of FeO in the experiment, and comparing them with the model, they could be obtained the values of the diff usion coefficient A_D and U_D . By varying the parameters of laser power and time of its impact on the rod, they can get the temperature dependence of the diffusion coefficient $D_O(T)$ for different capacities.

CONCLUSION

This work is part of a research program to study the combustion of steel in oxygen at high pressure. To date, despite the fact that research in this area has been going on for a long time, there is a lot of surface information gaps and uncertainties.

This paper presents a model of melting iron cylindrical rod in an argon environment to estimate the coefficients of laser radiation absorption core. Also there were simulated heterogeneous combustion process of the rod in an oxygen environment. On the basis of future experiments, changing the value of laser power and its impact on the time bar based on the thickness of the oxide layer and the melting front, it will be possible to restore the diffusion coefficient.

Since during the simulation there were specified parametrically a large number of variables, in amount they will give some average error that can be implemented only after the experiments. This summer is expected to complete the experimental part of the program. After processing the experimental data, among other things, we will identify errors and improve the developed model.

The aims of this work were:

1. Evaluation of the absorption coefficient of laser radiation rod;
2. Laser power control for the implementation of treatment regimes with controlled temperature of the surface;
3. Determination of the diffusion model of oxygen transport in the melt of the oxide;
4. Creating and testing a model for the combustion of classic experiments on combustion of rods (experiments NASA) and the combustion plate (experiments Air Liquide).

REFERENCES

1. V.N. Andronov, B.V. Chekin, S.V. Nesterenko. Zhidkie metally I shlaki. Moskow, Metalurgiya, 1977.
2. J. Sato and T. Hirano. Fire Spread Mechanisms Along Steel Cylinders in High Pressure Oxygen // Combustion and Flame. – 1989 – p. 279–287.
3. Defining the flammability of cylindrical metal rods through characterization of the thermal effects of the ignition promoter/ T. Steinberg [et al.] // Flammability and Sensitivity of Materials in Oxygen-Enriched Atmospheres. – 2010. – Vol. 12. – p. 21–34.
4. Multiphase Oxidation of Metals / T. Steinberg [et al.] // Metallurgical and Materials Transactions B, 28B. – 1997. p. 1–6.
5. The combustion of iron in high-pressure oxygen/ T. Steinberg [et al.] // Combustion and Flame. – Vol. 89. –1992 – p. 221–228.
6. M. Muller. Etude du processus d'initiations par laser de la combustion d'un alliage metallique sous atmosphere d'oxygene/ Rapport d'avancement de thèse au 15.06.2010.
7. The Solubility of Oxygen in Liquid Iron Oxide During the Combustion of Iron Rods in High-Pressure Oxygen / T. Steinberg [et al.] // Combustion and Flame. – 1998. – Vol. 113 – p. 27–37.

CYSENI 2012, May 24–25, Kaunas, Lithuania
ISSN 1822-7554, www.cyseni.com

SWIRL BURNER FOR CRUDE AND TECHNICAL GLYCERINS AND OTHER UNCONVENTIONAL FUELS

A.Y. Maturana, J.D. Pagliuso
Sao Carlos School of Engineering, University of Sao Paulo
Avenida do Trabalhador São Carlense 400, São Carlos (SP), CEP: 13566-582-Brazil
Phone: +55 16 81686321, +55 16 33738306, +55 16 33739389
Email: aymermaturana@usp.br, josmar@sc.usp.br

ABSTRACT

This study investigated the direct combustion of crude and technical glycerins, by-product and derivative, respectively of Brazilian biodiesel manufacture process as an alternative of sustainable energy use and develop an efficient swirl burner for glycerins and other raw materials. It aims to increase the knowledge on the matter and contribute to the improvement of the economic and environmental perspective of biodiesel industry and isolated populations. It was evaluated the combustion of crude glycerin from bovine tallow biodiesel and technical glycerin from soy biodiesel process. Due to commercial unavailability of a capable burner for burning glycerin, a swirl burner was developed for crude and technical glycerin combustion, but it was also used successfully in other alternative and conventional fuels: Beef tallow and Diesel, respectively. The procedures for evaluating the burner was main based in the quantification of emissions of SO_2, NO_x, CO, CO_2, particles, formaldehyde, acetaldehyde and acrolein. Similarly, were quantified fundamentals operational parameters for combustion process. The tests on developed swirl burner were carrying out using a full-instrumented calorimetric flame tube furnace, continuous gas analyzers, automatic data acquisition systems and other auxiliary equipment. The results were compared with the performance of Brazilian Diesel at similar conditions and finding that the emissions of CO, NO_x, SO_2 and THC were 44%, 95%, 58% and 51% correspondingly smaller than those of Diesel. The particulate matter emitted by crude glycerin combustion and even more, by technical glycerin, was several times higher than those emitted by the Diesel. Also, the emission of acrolein detected in flue gas from crude glycerin (214 ppbv), apparently have not represents danger to the population.

Keywords: Glycerol, emissions, acrolein, biofuels, bioenergy, biodiesel, alternative energy

1. INTRODUCTION

For the last decade, the growth of biodiesel production is occurring exponentially [1]. During the year 2011 global production of biodiesel was around 30 million tons [2, 3] and in Brazil 2.8 million tons, equivalent to 9% of total production in the world [4] that represents 300,000 tons of crude glycerin per year. According to [5], the conventional market in Brazil uses approximately 40,000 tons per year of crude glycerin, which represents only a 13.3% of total production in the country. Thus, thanks to the biodiesel industry, this market is saturated and more than half of the glycerol-producing companies in the world were closed due to low prices [6]. In 1992, 29.5% of glycerol was produced by the soap industry, 56% for the oil chemical industry, 9.8% by synthetic process and 4.6% derived from biodiesel and it was only from the year 2007 that approximately 72% of world production of glycerin has been origin in the biodiesel industry [7]. So because of that refining capacity and consumption of glycerin are limited, low prices discourage the construction of new refining plants, generating an over supply crisis. A projection made based on information presented by [8 - 12] allows estimating a total global market of glycerin in one million tons per year, valued at one billion of American dollars. The same projection showed that the production of biodiesel since 1995 has increased more than 55 times. In the same period, glycerin reduced by more than 4 times, their market price and the biodiesel production was more than three times higher that necessary to meet global demand. The main strategy to solve the problem of oversupply has been the search for alternatives uses of glycerin, such as feeding animals, additives for oil drilling, materials engineering in medicine or as fuel [13–16].

One might think that the most obvious option, considering the large number of applications that can generate high added value, would refine crude glycerin and try to produce one or more higher value products, or sell it without any treatment. However, the crude glycerin contains a large amount of impurities such as alcohol, salts, metals, soap, fatty acids and water, among others. Consequently, the cost associated to refining of crude glycerin is high. According to [17], this cost is approximately US $ 0.33/kg. Considering these situations, the right question would be: What is being done with the crude glycerin that cannot be sold on the market? The answer is, still not enough. Therefore, the possibility of using glycerin as fuel to generate power by direct combustion or gasification becomes a real option, which depends of the development of appropriate technology to succeed. But it is important to explain that the process of direct combustion of glycerin, when compared with conventional fuels, is more complex and difficult. Some of its physical and chemical properties, such as solid state at room temperature, high viscosity, high flash point and high activation energy make this process difficult [18].

Probably as a result of this difficulty there is still a small number of relevant works on this subject. Since Martin Mittelbach in 1979 studied the removal of free fatty acids of residual glycerin, to produce a liquid fuel for using in a conventional diesel engine, without generating any potentially aggressive deposit for the machine [19], this study identified only four formal studies. The work make for [20] estimates the combustion of mixtures of "yellow grease" (frying fats and oils previously used, among others) with crude glycerin derived from soybean oil using a conventional combustion system. [20] Reported initially have been tested using 100% of crude glycerin as fuel, but the results have shown little success, due to turbulence in the boiler, complicated physico-chemical characteristics and impossibility for setting certain parameters, resulting in that the system could not maintain a stable flame. The failure reported by [20] in their experiments with crude glycerin, is probably linked to the fact that they use a conventional combustion system for an unconventional fuel. Similarly, [21] examined the possibility of using the technical glycerin (80% glycerol) and stable emulsion of glycerol and heavy oils such as a liquid fuel for combustion systems. As [20], [21] also described to have had major difficulties in the direct use of crude glycerin as a fuel, attributed to high viscosity, density, and high ignition temperature compared to other conventional liquid fuels. But they report having had satisfactory results using the emulsions; thanks his experiments were conducted using a combustion system with important modifications over a conventional system. Similarly, [22] reports not to be used conventional equipment for direct combustion of glycerin. They use a swirl burner with an “adiabatic” combustion chamber to improve flame stability and efficiency of combustion. This work focused on the development of a refractory burner based on other previously designed for different fuels. The tests conducted by [22] was carry on using United States Pharmacopeia (USP) glycerol, a mixture of 80% of glycerol and 20% of water, crude glycerin derived from soybean oil, from used frying oil and from chicken fat as fuels. [22] Reported success in his experiments, but the information provided was limited. More recently, [23] continue the work of [22], focusing on the redesign of the burner previously used and conducting and conducting a more extensive study of emissions and using glycerol USP, demetilated and metilated glycerins derived from chicken fat, Diesel and propane as fuels. [23] Stated, that a flame of glycerin is not able to sustain itself and spread itself in a quiet and open environment, because it can not generate sufficient heat to support the combustion. Apparently the greatest difficulty for large-scale combustion of glycerin is based on the unavailability of commercial burners with the ability to efficiently burn the most common types of glycerins derived from biodiesel industry. This condition requires the development of a specific burner for this application, but with the ability to work with conventional or other unconventional fuels. This is precisely the goal assumed for this study. With respect to the above, this study aimed to develop a swirl burner for the combustion of crude and technical glycerins to contribute to the viability of this material as an energy alternative. One of the main objectives of the study was to make a significant contribution to the limited knowledge in this area, especially regarding the environmental performance of crude glycerin combustion. It is expected to improve profitability and sustainability of the biodiesel industry, as well as the conditions of life and socio-economic development of populations located in remote areas, where communication and transportation are still precarious and there is a limited access to energy derived from fossil sources, prioritizing wood as a primary source. Thus, in remote areas, the local production of energy from renewable and cheap sources can be a viable alternative to reduce deforestation.

2. METHODOLOGY

In this study, the glycerin is defined as a raw or crude mixture of glycerol, alcohol, salt, water, mono, di or triglycerides, fatty acids, free esters, organic matter and non-glycerol (MONG) co-product of the biodiesel process. The technical glycerin is considered the product obtained by after the first flash distillation of the crude glycerin, allowing removing most of the alcohol, water, MONG and other impurities. The crude glycerin used is derived from bovine tallow biodiesel and the technical glycerin from soybean oil biodiesel. The two glycerins were provided, respectively, for a biodiesel fuel manufacturing plants in the states of Sao Paulo and Rio Grande do Sul in Brazil. The crude glycerine is originally solid, dark brown, with strong and penetrating odor, but with a similar consistency to the beef tallow solidified. The technical glycerin is a viscous liquid, yellow and practically odorless. In addition, for comparative purposes, was also evaluated the combustion of Brazilian common Diesel (approximately equivalent to the fuel oil No.2) and industrial bovine tallow.

An instrumented calorimetric flame tube furnace built with 304 stainless steel in four modules each one with three calorimeters was used for combustion tests. Because the crude glycerin from beef tallow is solid at room temperature, the system integrated an adjustable instant electric heating unit and filtering which supplied the material to the burner in liquid state above 70°C and below 30 cSt. The supply of crude glycerin to the heater was performed manually. Diesel was pumped from a storage tank located 1.5 m above the floor. Then it passed through a filter and finally through a burette coupled to an electronic balance before entering the burner. The fuel consumption was determined gravimetrically. The consumption of crude and technical glycerins was measured in the same way as that of Diesel, starting from different storage tanks. The flow of air entering the burner, was measured with previously calibrated orifice plates.

The combustion gases were collected in each calorimeter using refractory probes connected to a Teflon tube, which carried the samples to a selector valve responsible for selecting the desired sampling point. From this point a pistons vacuum pump sucked the gas and forced it to pass through a 2μm-particle filter and a condenser before entering the Horiba Enda 1400 (MPA-510, VIA-510 and FIA-510) gas analyzers. O_2, CO_2, CO, SO_2, total hydrocarbons (THC) and NO_x from gases were continuously measured using analyzers with error/precision ±0.05% calibrates with standard gases before each test. The acquisition of all data was performed by an acquisition system composed of a microcomputer with an acquisition board, coupled to a chassis module with a multiplier equipped with 32 channels connected to a terminal block. The signals transferred by the data acquisition board were processed in LabView 7.1 software. The data acquisition time was set at 1 s and 30 s for automatic and manual acquisition, respectively. The total duration of each test was 60 min or more. The content of acrolein in the combustion gases was determined according to the Brazilian standard ABNT NBR 12026, which describes the analytical method for the determination of aldehydes and ketones in exhaust gas motor by liquid chromatography, and using 2,4 dinitrophenyl hydrazine (DNPH) [24]. Thermogravimetric analyses were carried out in triplicate utilizing a Shimadzu TDA-50H thermogravimetric analyzer. In each case the temperature raised from room temperature to 900 °C with heating rate of 15°C min^{-1}. 10 mg of the sample were placed in an aluminum crucible using an allowance of ± 0.5 mg. The reacting atmosphere was synthetic air at a constant flow rate of 100 ml min^{-1} over the sample. Additionally, to minimize factors that might generate errors in the TG curves, a "white" was performed under the same experimental conditions.

Assuming a homogeneous mixture of combustion gases within the furnace, the gas samples for determining the concentration of particles were collected by a probe located in the last sampling point of the furnace using a vacuum pump operated with an average flow of 8.5 lmin^{-1}. The particles were retained during testing on standard cellulose filters for quantitative analysis with ultra low ash content (<0.01%) and particle retention <2μm which had previously been weighed. Thereafter the particulate matter (PM) was determined according to the Brazilian standard ABNT NBR 12019:1990 using an analytical balance with precision ± 0.0001 g. Similarly, the higher heating value (HHV) and the rheological properties of the fuels tested were determined using a bomb calorimeter and a rotational rheometer coupled to a thermostatic bath, respectively. The elementary and especific chemical analisys (metals, salts, glycerol, alcohol, water and (MONG)) of the fuels were conducted in the Analytical Center of the University of Sao Paulo.

It was determined that it would be advantageous to use a swirl burner for the combustion of crude glycerin, because this type of burner can increase by a factor of five or more times the flame stability and improve the heat transfer compared to a simple conventional burner [25 – 27]. Increasing the intensity of the swirl, the rate of fuel-air mixture is also increased [25]. Since the number of swirl (S) is defined as in equation (1) [28].

$$S = \frac{G}{r_e x G_x} \tag{1}$$

where G is the angular momentum of the flow (tangential), G_x the axial flow and r_e the radius of the output of the turbulent flame as indicate by [29] and [30] for a swirl burner. Because the measurement of S is often difficult, requiring the use of special equipment and procedures, not available in this case, considering thoroughly mixed flow and conservation of the momentum ($v_o r_o = v_e r_e$) the number of swirl S is defined in terms of the geometry of the burner as in equation (2).

$$S_g = \frac{r_o \pi r_e}{A_t}\left[\frac{F_t}{F_a}\right]^2 \tag{2}$$

where S_g is the geometrical swirl number; r_o the radius of the tangential inlet of air measured from the center of the burner; A_t the area of the tangential entry of air; F_t the tangential flow and F_a the total flow. But, remembering that due to the losses in the system, the geometrical swirl number (Sg) is always greater than S [25].

For comparative purposes, the first tests were performed using Diesel and glycerin as fuel for a conventional monobloc burner for oil and gas, with a 0.55 kW motor, 3430 rpm sirocco fan type and an oil pump commercially available in Brazil. The initial testing started with the fuel entering at various temperatures (60, 80, 100, 110, 130, 150 and 160 °C) and viscosities. All the theoretical parameters of combustion, including the excess of air coefficient, were evaluated from the balanced combustion equations and the physico-chemical characteristics of fuel, using the principles of mass and energy balance and the classical thermodynamics.

3. Results and discussions

The results for physicochemical characteristics of crude glycerin from bovine tallow biodiesel and technical glycerin from soy biodiesel are listed in Table.1.

Table 1. Physicochemical characteristics of crude and technical glycerins

Parameters	Units	Crude glycerin	Technical glycerin
Density (20°C)	kg m^{-3}	1061	1290
Sodium Chloride	mg kg^{-1}	190	10000
pH	-	7.9	-
Sulfate	mg kg^{-1}	7200	-
Sulfur	mg kg^{-1}	2403	-
Acidity	mg KOH/g^{-1}	0.86	-
Citrate	mg kg^{-1}	11	-
Silver Chloride	mg kg^{-1}	115	-
Phosphorus	mg kg^{-1}	395	-
Methanol	% mass	7.6	0,20
Ash	% mass	4.0	10
Water	% mass	1.5	7,0
Glycerol	% mass	48.5	80,0
MONG (1)	% mass	46.4	3,0
HHV	MJ kg^{-1}	25.52	14.75

(1): Matter Organic Non Glycerol (MONG) represented by convention; difference obtained by subtracting the sum of the percentages of glycerol, water and ash from 100.

As its show in Table.1 it can be said that of the two types of glycerin studied, the technical glycerin have a significant corrosive, abrasive and electrically conductive potential due to their high concentration of sodium chloride and other salts. This high concentration of salts is considered negative for the combustion process, because this salts are converted in particle material that can generate dangerous emissions and solid deposits wich have the potencial of causing corrosion and obstruction of the surfaces of burner and furnace. The high content of MONG in the crude glycerin reveal the cause of its original solid state at room temperature, since the MONG is mainly composed of soaps (ester) and residues of carboxylic acids, and magnesium stearate. Relevantly, Table.1 shows that the high heating value (HHV)) of the crude glycerin is comparable to that of ethanol (≈ 27 MJ kg^{-1}) and higher than that of methanol (≈ 23 MJ kg^{-1}).

The preliminary tests conducted with a Diesel performed in the conventional burner, had the expected success, but using glycerin (crude or technical) the results were completely unsatisfactory and in no case was possible to produce fuel atomization even if it was placed a permanent source of ignition. The problems encountered were mainly the following: inability to control the process and flow of the glycerin by high viscosity produced when the hot fuel losses heat by passing throug the cold metal and the fan of the conventional burner, overheating of some structures and parts of the burner, the impossibility of atomization and ignition, fuel pumping difficult. Thus, for the developed swirl burner, left to consider the crude glycerol as the most extreme case, due to physico-chemical characteristics, and additional studies were performed, including the differential thermal analysis (DTA), and rheology. The DTA of crude glycerine (Fig. 1) confirmed that the substance is physicochemically complex and revealed that below 300 °C, it is necessary to provide external energy support, probably in radiative-convective form to the combustion process, which in practical terms resulted in pre-heat the combustion chamber of the burner developed (burning liquefied petroleum gas (LPG) or Diesel) before the entry of glycerol and until that the external surface of the combustion chamber to become red. The pre-heating of burner’s chamber resulting in a key factor for the ignition, flame stability and maintenance of the combustion. Because this, it was adopted as standard procedure, but involved the use of external thermal insulation on the burner to minimize heat loss from the system. The overall effect of the pre-heating is to provide an important part of the activation energy that glycerin need to ignite and maintain this state until its own energy, released during the oxidation reaction (Fig. 1).

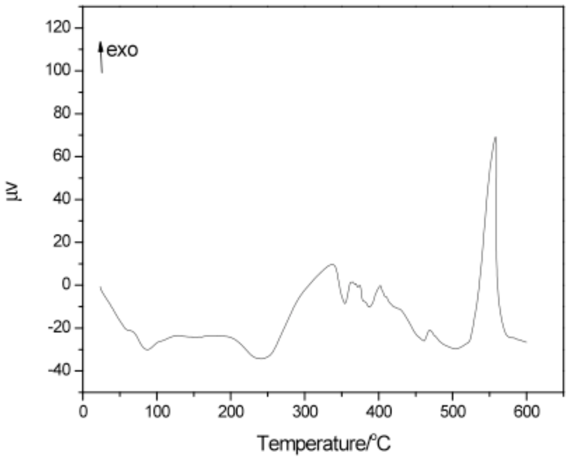

Fig. 1. Results of differential thermal analysis (DTA) for crude glycerin

According to Fig. 2, the inlet temperature of the crude glycerine to the burner must be greater than 90 °C, to ensure a viscosity lower than 30 mPa.s. This is the point at which the atomizing nozzle and the pump used to provide glycerin are within their respective working ranges. In Fig. 2, it is noted that at 70 °C the viscosity of the crude glycerol is about 20 times greater than the technical glycerin and 500 times that of Diesel.

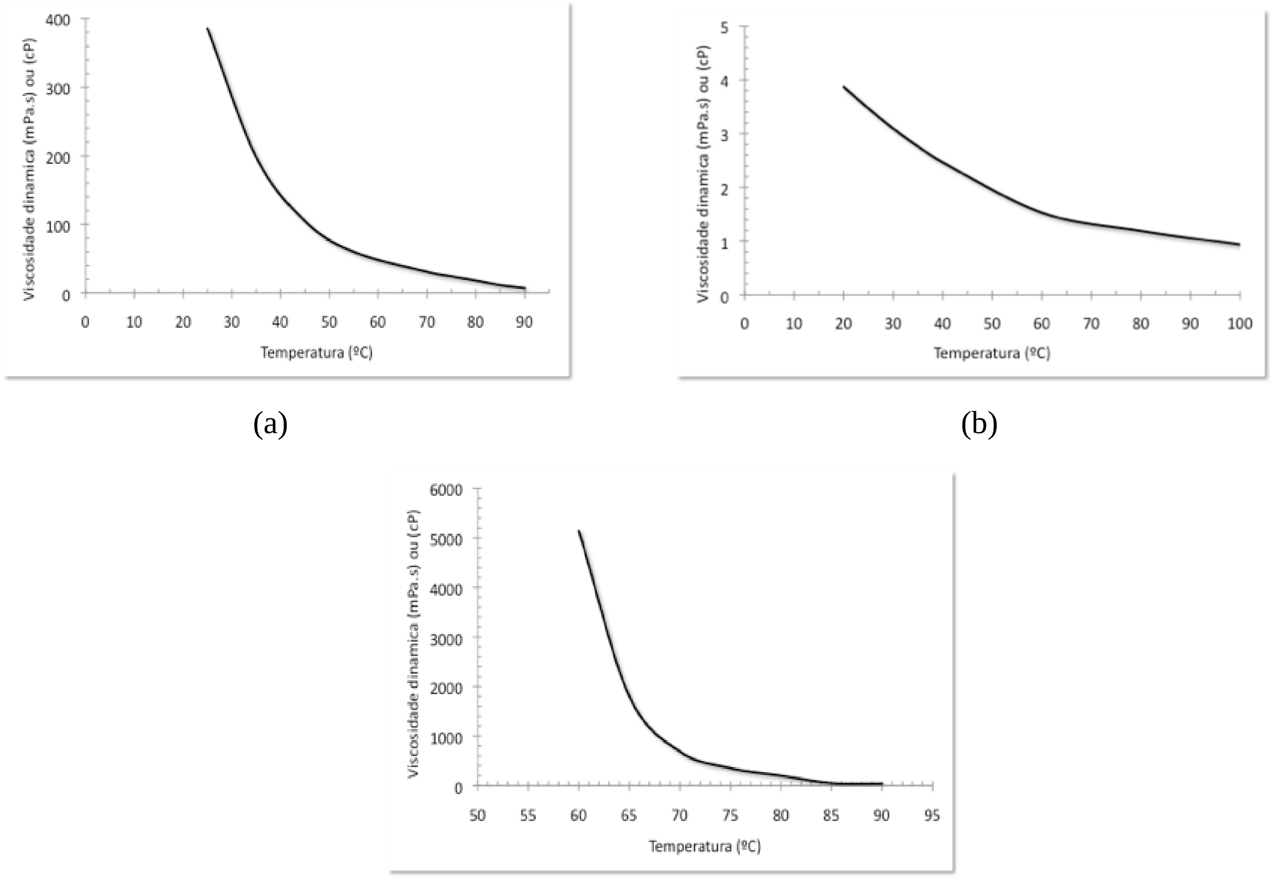

(a) (b)

(c)

Fig. 2. Variation of dynamic viscosity for (a) Technical glycerin (b) Diesel and (c) crude glycerin

The collected experiences with tests using Diesel and glycerin in conventional burner, the information from the physico-chemical analysis, rheology and thermal analysis, and other relevant concepts about burners and combustion under swirls conditions presented in [31 - 36] allowed to establish a minimum criteria, requirements and basic needs to be considered in the design of the burner.Thus, the protype was built with the characteristics showed on Table.2. The configuration that allows swirl effect, generate outer recirculation zones designed to increase the residence time, provide more stability to the flame and reduce emissions.

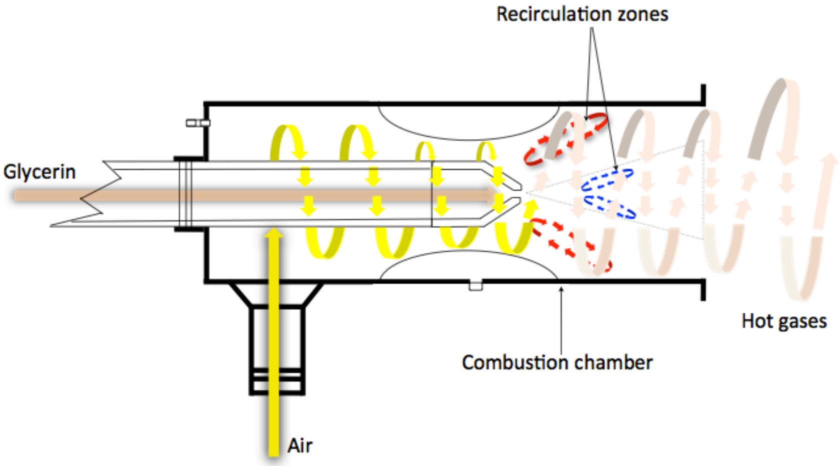

Fig. 3. Standar internal circulation of the prototype of the swirl burner developed

Table 2. Characteristics of the prototype burner developed

Weight	9.3 kg
Power	52 kW
Ignition	Electric
Material	Stainless steel and aluminum
Security system	Auto-off for optical flame detection
Glycerin heating system	Electrical spiral resistance
Air inlet	Tangential/axial
Atomizing nozzle	Danfoss for fuel oil
Fuel input	Axial

Consequently, the geometrical swirl number (S_g) for the developed burner is constant and equal to 3.34 because the tangential flow is equal to the total flow. This amount ensures an appropriate level of turbulence, since a swirl number zero its equivalent to a conventional burner without any swirl, and an S_g exceeding 1.1 correspond to a flame with high intensity turbulence, as deduced from information reported by[37].

The prototype was tested successively for about 45 times, including security aspects, electrical, mechanical and operational functioning. All results were satisfactory, but also showed some improvement opportunities, including the need to replace the heating internal burner, initially wire spirals, which proved to be slow, with low mechanical strength and susceptible to corrosion by another of cartridge type that provided instant warm-up and maximum corrosion resistance caused by the passage of glycerin, especially the technical, resulting in the final prototype shown in Fig. 4.

This final prototype produced stable flames with all the fuels tested. Flames from the technical glycerin shown to be the less stable and more difficult, apparently by the lower calorific value and higher content of water and salts.

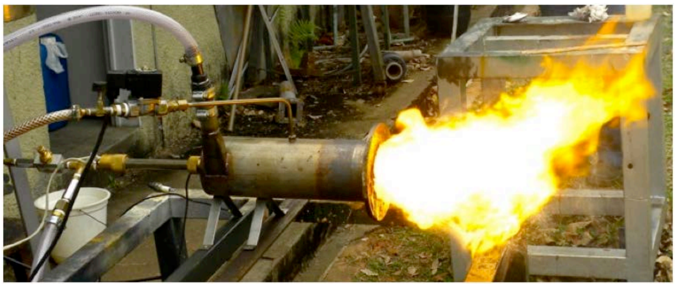

Fig. 4. Final prototype burner operating outdoors with crude glycerin

Table 3. Emissions from the final prototype burner coupled to the flame tube furnace

Parameters	Bovine tallow	Diesel	Crude glycerin	Technical glycerin
Coefficient of air excess	1.25	1.26	1.26	1.23
O_2 (% v/v)	4.169	4.335	4.408	3.890
CO_2 (% v/v)	10.274	10.992	11.301	11.643
CO (ppm)	103	149	83	111
HCT (ppm)	18	59	29	41
SO_2 (ppm)	0	77	32	18
NOx (ppm)	8	105	5	6
Particulate matter (mg/Nm^3)	-	126	1650	10541
Acrolein (ppbv)	-	0	214	-

In the final prototype, the crude glycerin burned with intense yellow flame with high volume and good stability, low smoke under suitable conditions of air and expressed little or no tendency to rise. The intense yellow color of the flame was due to the presence of high sodium content in the glycerin, as reported in Table.1. A flame with intense yellow, theoretically improve the heat transfer, providing good radiant capacity due the presence of incandescent particles of salts [27]. As shown in Table. 3, overall emissions from the combustion of crude glycerin are compare favorably with those of Diesel, except in the case of particulate matter, whose emission to the crude glycerin exceeded by several times the amount emitted by Diesel. In the case of emissions produced by combustion of technical glycerin, there was a high emission of particles greater than five times of the crude glycerin, associated with a high salt content contains this substance (Table.1). However, the same results show that the emissions of CO, NO_x, SO_2 and THC of the crude glycerol were on average 44%, 95%, 58% and 51% respectively smaller than the Diesel. The emissions produced by the combustion of the technical glycerin, with the exception of particulate matter, were even lower. Moreover, for acrolein, the result clearly differentiate allow the chemical nature of diesel oil and crude glycerin, mainly constituted by a tri-alcohol. [22] Report that they found 17.5 ppbv of acrolein in the combustion gas of glycerol (USP 99.9%), however, [20] reported an emission rate <0.004 kg m^{-1} for acrolein and <0.004 kg h^{-1} for acetaldehyde in the combustion of a mixture of 10% of glycerol and 90% of residual oil named "yellow grease."

4. CONCLUSIONS

Of the two types of glycerin studied, the technical glycerin have a significant and greater corrosive, abrasive and electrically conductive potential due to their high concentration of sodium chloride and other salts that can generate particles causing dangerous emissions and solid deposits wich have the potencial of causing corrosion and obstruction of the surfaces of burner and furnace.

The high content of MONG in the crude glycerin reveal the cause of its original solid state at room temperature, since the MONG is mainly composed of soaps (ester) and residues of carboxylic acids, and magnesium stearate.

The high heating value (HHV)) of the crude glycerin is comparable to that of ethanol (≈ 27 MJ kg^{-1}) and higher than that of methanol (≈ 23 MJ kg^{-1}).
Below 300 °C, it is necessary to provide external energy support in radiative-convective form to the combustion process of glycerin.

Probably the most important aspect in the combustion of crude glycerol is the pre-heating of the combustion chamber due to it provides an important part of the activation energy necessary for the combustion process.

The inlet temperature of the crude glycerine to the swirl burner must be greater than 90 °C, to ensure a viscosity lower than 30 mPa.s. This is the point at which the atomizing nozzle and the pump used to supply glycerin are within their respective working ranges.

The emissions of CO, NO_x, SO_2 and THC of the crude glycerol were on average 44%, 95%, 58% and 51% respectively smaller than the Diesel. The swirl burner developed also proved to be efficient for direct combustion of bovine tallow, wich is another unconventional fuel.

The combustion of crude and technical glycerin would be recommended technically and environmentally, if they are adopted the necessary controls to prevent or reduce to acceptable limits particulate emissions. At the same time, it was observed that the developed swirl burner fulfill the stated purpose and overcoming the initial expectations.

REFERENCES

1. THOMPSON, J, HE, B. (2006). Characterization of crude glycerol from biodiesel production from multiple feedstocks. Applied Engineering in Agriculture, V. 22, p. 261–265.
2. MME (2010). Boletim Mensal de Energia: Dezembro de 2010 Ministerio de Minas e Energia do Brasil, Departamento de Planejamento Energetico, v. 1, N. 12/2010, p. 1–2.
3. ENERS (2010). Production of Biodiesel in the world: 2007, 2008, 2009. Biofuels Plataform, Energy Concept, Lausane-Switzerland 2010, V. 1, p. 1–3.
4. MME (2010). Boletim Mensal de Energia: Dezembro de 2010 Ministerio de Minas e Energia do Brasil, Departamento de Planejamento Energetico, V.1, N. 12/2010, p.1–2.
5. MANTOVANI, H.C. (2006). Aproveitamento da Glicerina no Agronegócio. IV Seminário Internacional do Agronegócio Bioenergia e Mercado de Carbono, p. 1–27.
6. BONET, J. et al. (2009). Revalorization of glycerol: Comestible oil from biodiesel synthesis. Food and Bioproducts Processing.
7. HENARD, M.C. (2007). Impacts on Oilseed Industry Following Biofuel Boom. Available in: <http://www.theinnovationgroup.com/chemprofiles/glycerin.htm>. Accessed in: 24 Mar. 2011.
8. BONDIOLI, P. (2003). From Oilseeds to Industrial Products: Present and near future of oleochemistry. Italian Journal of Agronomy, V. 7, N. 7, p. 129–135.
9. FONSECA, P. et al. (2009). Glycerol Valorization: New biotechnological routes. Food and Bioproducts Processing, V. 87, N. 87, p. 179–186.

10. OLEOLINE (2010). Glycerine Market Prices: 16 August 2010. Oleoline: The Independent Oleo Reporter, p. 1-1.
11. USSEC (2007). Glycerin Market Analysis. U.S. Soybean Export Council Report, V. 1, N. 1, p. 1–35.
12. MANEELY, T. (2006). Glycerin Production and Utilization. Biodiesel one-day course: From field to fuel V. 1, p. 1–17.
13. O'DRISCOLL, C. (2007). Seeking a new role for glycerol. Biofuels Bioproducts and Biorefining, V. 1, N. 1, p. 7.
14. SLINN, M. et al. (2008). Steam reforming of biodiesel by-product to make renewable hydrogen. Bioresource Technology, V. 99, N. 13, p. 5851–5858.
15. ADHIKARI, S.; FERNANDO, S.D.; HARYANTO, A. (2008). Hydrogen production from glycerin by steam reforming over nickel catalysts. Renewable Energy v.33, p.1097-1100.
16. BATISTA, F. (2007). Brasil não tem destino certo para glicerina gerada por biodiesel. Gazeta Mercantil.
17. WERPY, T. et al. (2004). Top Value Added Chemicals from Biomass. Report of the United States Deparment of Energy, V. 1.
18. MATURANA, A.Y.; PAGLIUSO, J.D. (2011). Thermal decomposition behavior of gross glycerin. In: Proceedings of the 21st International Congress of Mechanical Engineering, 2011, Natal, Brazil. Natal, Brazil: ABCM.
19. PAHL, G. (2008). Biodiesel: Growing A New Energy Economy. Second Edition. White River Junction, Vermont (USA): Chelsea Green Publishing Company.
20. PATZER, R. et al. (2007). Stack emissions evaluation: Combustion of crude glycerin and yellow grease in an industrial fire tube boiler. Agricultural Utilization Research Institute, V. 1, N. 1, p. 1–10. Available in: <http://www.auri.org/research/Glycerin%20Report%20Final.pdf > Accessed in: 14 Mai. 2011.
21. STRIŪGAS, N. et al. (2008). Processing of the glycerol fraction from biodiesel production plants to provide new fuels for heat generation. Energetika, V. 54, N. 3, p. 5–12.
22. METZGER, B. (2007). Glycerol Combustion. 1-53 pp. Dissertation (Master of Science) - North Carolina State University, Raleigh, 2007.
23. BOHON, M.D. et al. (2010). Glycerol combustion and emissions. Proceedings of the Combustion Institute, V. 33, N. 2, p. 2717–2724.
24. ABNT (2002). Associação Brasileira de Normas Técnicas (ABNT). NBR 12026: Veículos rodoviários automotores leves: determinac□ão da emissão de aldeídos e cetonas contidas no gás de escapamento, por cromatografia líquida – Método DNPH. Rio de Janeiro.
25. MULLINGER, P.; JENKINS, B. (2008). Industrial and Process Furnaces: Principles, design and operation. Firts Edition. Oxford: Butterworth-Heinemann.
26. CHEN, R. (1989). The role of the recirculation vortex in improving fuel-air mixing within swirling flames. Symposium (International) on Combustion, 22 nd, Seattle, WA, p. 1989.
27. CHANDER, S.; RAY, A. (2005). Flame impingement heat transfer: A review. Energy Conversion and Management, V.46, p.2 803-2837.
28. CLAYPOLE, T.; SYRED, N. (1981). The effect of swirl burner aerodynamics on NOx formation. Symposium (International) on Combustion, V. 18, N. 1, p. 81–89.
29. CHERVINSKY, A.; TIMNAT, Y.M. (1967). Effect of swirl on flame stabilization. Haifa: Technion-Israel Institute of Technology, Department of Aeronautical Engineering.
30. SALVI, G. (1975). La Combustion. Segunda Edicion. Madrid: Editorial Dossat S.A.
31. CHEN, R. et al. (1990). A comparison of bluff-body and swirl-stabilized flames. Combustion Science and Technology, V. 71, p. 197–217.

32. SYRED, N.; BEER, J. (1974). Combustion in swirling flows: a review. Combustion and Flame, V. 23, N. 2, p. 143–201.
33. FEIKEMA, D.; CHEN, R.; DRISCOLL, J. (1990a). Enhancement of flame blowout limits by the use of swirl. Combustion and Flame, V. 80, N. 2, p. 183–195.
34. TANGIRALA, V.; CHEN, R.H.; DRISCOLL, J.F. (1987). Effects of heat release and swirl on the recirculation within swirl-stabilized flames. Combustion Science and Technology, V. 51, p. 75–95.
35. TANGIRALA, V.; DRISCOLL, J. (1988). Temperatures within non-premixed flames: effects of rapid mixing due to swirl. Combustion Science and Technology, V. 60, N. 1, p. 143–162.
36. TANGIRALA, V., R.H.C.J.F.D. (1987). Effects of heat release and swirl on the recirculation within swirl-stabilized flames. Combustion Science and Technology, V. 51, p. 75–95.
37. HUANG, Y.; YANG, V. (2005). Effect of swirl on combustion dynamics in a lean-premixed swirl-stabilized combustor. Proceedings of the Combustion Institute, V. 30, N. 2, p. 1775-1782.

HEAT TRANSFER IN THE PLASMA-CHEMICAL REACTOR DESIGNED FOR CERAMIC MATERIALS CONVERSION INTO FIBRE

M. Milieška, R. Kėželis, V. Valinčius
Lithuanian Energy Institute
Breslaujos str. 3, LT-44403, Kaunas – Lithuania
Phone +370 37 401 895
Email: milieska@mail.lei.lt

ABSTRACT

Heat transfer in the plasma chemical reactor designed for ceramic materials melting and conversion into fibre is analysed in this paper. Two plasma-chemical reactor work regimes, when reactor is working without and with dispersed particle injection into its channel, are discussed. The heat transfer in the plasma-chemical reactor takes place between plasma flow, reactor walls and dispersed particles. For the first reactor work regime the heat transfer dependence on additional air flow is explained. It was noted that heat transfer between plasma flow and reactor walls is smaller in the beginning of the reactor, the relative distance x/d≤5,6, because plasma flow enters the reactor through the narrowing confuser and the flow breaks away from the reactor walls. The generalized heat transfer results have a good agreement with classical case. For the second reactor work regime the injected dispersed ceramic particle size, kind and flow rate influence on the heat transfer without particle melting in the channel is analysed. It is observed that only dispersed particle mass concentration in the plasma flow has significant influence on the decrease of heat transfer to the reactor walls.

Keywords: plasma-chemical reactor, heat transfer, two-phase flow

1. INTRODUCTION

The one of most important processes taking place during ceramic material fibrillation in plasma-chemical reactor is the heat transfer. The intensive heat transfer between plasma flow and dispersed particles is the main thing which makes the fibre production successful. However, not all plasma heat quantity is transferred to the dispersive particles. As the melting of dispersive particles takes place in the channel of plasma-chemical reactor, the heat loss to the reactor walls occurs. The melted material flows on the walls of the reactor channel so it losses the heat to the reactor walls, too. In order to ensure the success of optimal fibrillation process with the lowest energy consumption, the heat transfer to the dispersive particles and reactor walls must be controlled.

As the plasma-chemical reactors designed for melting and fibrillation of ceramic materials are not commercial devices but rather made experimentally by scientists for their research works their principles of operation are usually comparatively very different. The gas and particle behaviour, the physical and chemical processes, and etc. are different in various plasma-chemical reactors, so the overall generalization of the processes during the fibre production is impossible. Consequently, every plasma-chemical reactor is studied individually [1-2].

So, this work is appointed to determine the dependence of heat losses to the reactor walls on plasma flow parameters and to evaluate the influence of dispersive particle addition on the heat transfer in plasma-chemical reactor applied for melting and fibrillation of raw ceramic materials and developed in Plasma Processing Laboratory of Lithuanian Energy Institute.

2. METHODOLOGY

The plasma-chemical reactor (Fig. 1) consists of plasma torch (PT) and 0.24 m length channel made of stainless steel. The precise description of plasma torch and additional equipment of experimental set-up has been depicted in detail elsewhere [3].

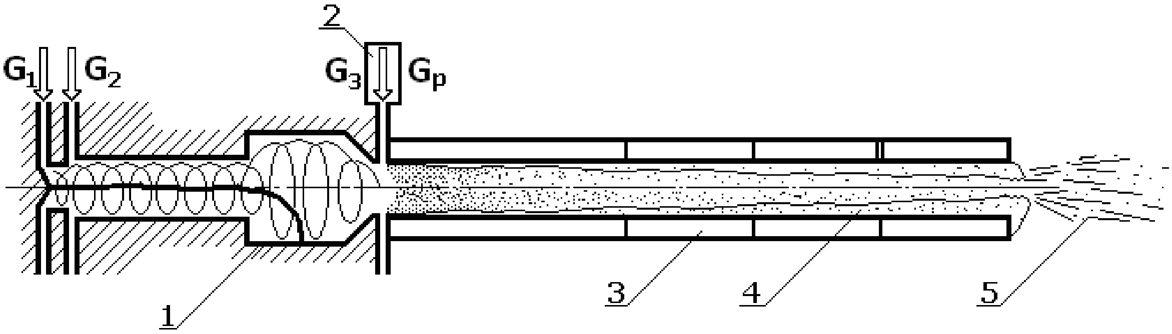

Fig. 1. The plasma-chemical reactor: 1 – plasma torch, 2 – air and dispersed particles, 3 – cooled walls, 4 – melt flow, 5 – fibre and granules; G_1, G_2 and G_3 – air flows, G_p – dispersive particle flow

The channel of the plasma-chemical reactor is divided in four sections with 0.016 m inner diameter. The length of first section which is connected to plasma torch is 0.09 m, and other three sections are 0.05 m in length. All sections are cooled by water and insulated from each other, so no heat transfer between each section takes place.

During the experiments the plasma torch arc current and voltage, plasma forming ($G_1+G_2=G_{1,2}$) air flows and dispersive particle carrying (G_3) air flow, plasma torch and reactor walls cooling water flows (G_w) and their temperature changes (ΔT_w) are measured. The raw dispersed particles flow (G_p) is estimated by weighting the particles initially and after the experiment. The duration of particle feeding to the reactor is measured, too.

The plasma flow temperature (T_f) in the plasma torch and each section is estimated from heat balance as described in [4]. The heat flux to the reactor walls is calculated from:

$$q = cG_w \Delta T_w \, , \tag{1}$$

where c is the specific heat capacity of water.

Heat transfer coefficient between a fluid and a solid:

$$\alpha = \frac{q}{S\left(T_f - T_{wall}\right)}, \tag{2}$$

where S is the inner surface area of reactor walls and T_{wall} is the reactor wall temperature. The initial wall temperature measurements showed that wall temperature slightly varies around 550 K for wide range of plasma flow temperatures.

The heat transfer in the plasma-chemical reactor is generalized using similarity theory as described in [5], using Nusselt and Reynolds number's coherence. The Nusselt number is:

$$Nu_x = \frac{\alpha x}{\lambda_f}\left(\frac{T_f}{T_D}\right)^{0.9} . \tag{3}$$

The Reynolds number is:

$$\mathrm{Re}_x = \frac{4Gx}{\pi d^2 \mu_f}; \tag{4}$$

where x is the distance in the channel, λ_f is the thermal conductivity of the plasma flow, d is the inner diameter of the reactor channel, μ_f is the kinematic viscosity of the plasma flow, G is the sum ($G=G_1+G_2+G_3$) of all air flows in the reactor channel.

As the air plasma flow temperature exceeds 2500 K, the component of air O_2 starts dissociating [6]. Because of the dissociation the dependence on temperature curve of enthalpy deviates from a logarithmic straight. So, in our calculations of Nusselt number for temperatures above 2500 K the multiplier $\left(\frac{T_f}{T_D}\right)^{0.9}$ is added, where T_D is the dissociation temperature.

3. RESULTS AND DISCUSSIONS

The majority of theoretical and experimental studies of plasma flow heat transfer in the channel of the reactor are performed for steady stabilized flows at channel relative distances *x/d* higher than 15-20. These experiments were performed for the analysis and generalization of these theoretical and experimental results of heat transfer for steady flow. However, the greatest interest should be represented for the unsteady flow at the beginning of the reactor in the ranges of *x/d* between 0-10, where the greatest temperature gradients occurs [7].

The temperature instabilities are caused by the design of plasma-chemical reactor, because the reactor inner diameter is smaller than the diameter of anode of plasma torch, so the plasma flow enters the reactor through the confuser. The velocity and temperature of the plasma flow depends on plasma torch parameters and decreases along the length of the reactor [4]. However, Fig. 2 shows that the heat transfer coefficient (α) between plasma flow and reactor walls has a peak when the relative distance x/d is about 8 and depends on plasma torch parameters.

As the heat flux to the reactor walls was calculated by measuring the cooling water temperature changes in each individual section, the obtained α values can be considered as an average values in the section length, rather than as a value in a specific reactor relative distance x/d, so they were shown in all figures as in the centre of each section.

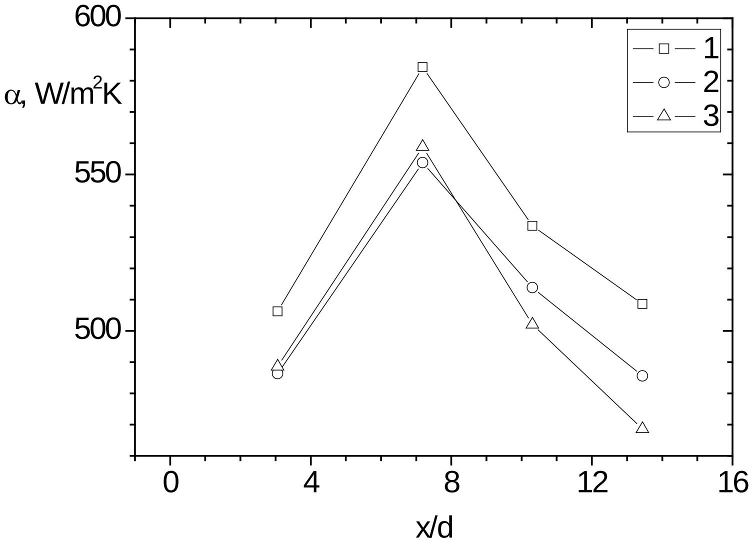

Fig. 2. Heat transfer coefficient dependence on PT parameters in the reactor channel: 1 – power 81 kW, air flow – $20\cdot10^{-3}$ kg/s; 2 – power 66 kW, air flow – $20\cdot10^{-3}$ kg/s; 3 – power 81 kW, air flow – $16\cdot10^{-3}$ kg/s

The heat transfer coefficient peaks appears because of the formation of plasma flow boundary layer on the reactor walls. As the mixed plasma flow enters the reactor from the confuser its velocity across the diameter is uniform. The drag force between plasma flow and reactor walls decreases the plasma flow velocity. Because of increasing friction the heat transfer between plasma flow and reactor walls increases and heat transfer coefficient reaches the maximum. As the plasma flow heat losses increases, the plasma flow temperature decreases, so the heat transfer to the reactor walls decreases despite the increasing friction.

The Fig. 2 shows the dependence of heat transfer coefficient on PT parameters: PT power and plasma forming air flow. The increasing PT power (1st and 2nd regimes) increases the heat transfer between plasma flow and reactor walls, because the plasma flow temperature increases. The decrease of plasma forming air flow (1st and 3rd regimes) as the PT power is constant causes the decrease of heat losses to the reactor walls too, as the plasma flow temperature decreases. On the other hand, the comparison of the 2nd and 3rd regimes in the Fig. 2 shows that as the plasma flow velocity is bigger (when the plasma forming air rate is higher) the plasma losses to the reactor walls in the beginning of the channel is smaller. As the plasma flow velocity is higher it’s interaction with surface of the reactor walls is shorter. As the plasma flow loses its velocity in further reactor channel distances the heat flux to the reactor walls increases compared with lower velocity plasma flow regime.

Because of the technical restrictions dispersed particles can be introduced into plasma flow with the use of gas flow only. The dispersive particle carrying air flow influence on heat losses to the reactor walls was examined without addition of dispersive particles. The PT parameters in further experiments were constant (power - 66 kW, plasma forming air flow rate - $20 \cdot 10^{-3}$ kg/s). The dispersive particles carrying room temperature air flow decreases the plasma flow temperature and increases its velocity [4]. For this reason in Fig. 3 it can be seen, that additional air flow rate decreases the heat transfer significantly in the beginning of the reactor. The higher additional air flow rate – the bigger decrease of α.

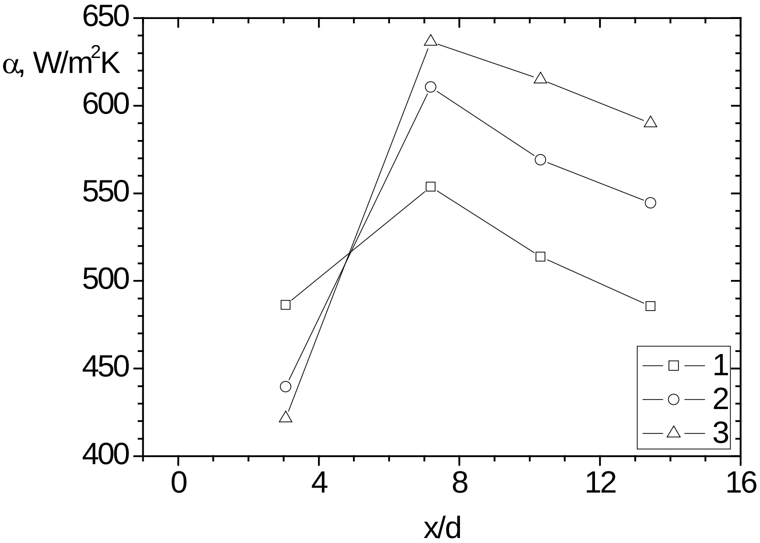

Fig. 3. Heat transfer coefficient dependence on additional air flow rate.
1 – without; 2 – $3 \cdot 10^{-3}$ kg/s; 3 – $6 \cdot 10^{-3}$ kg/s

As the decrease of α in the beginning of the reactor is higher, the increase in further distances is higher. It means, that the high temperature plasma flow breaks away from reactor walls in the beginning of the reactor and is surrounded by low temperature air flow near the walls. The friction to the reactor walls, the heat transfer and turbulence mixes the plasma flow in the reactor and the heat losses to the reactor walls increases as higher temperature flow interacts with reactor walls. As the plasma flow temperature decreases in the reactor relative distances $x/d>8$, the heat flux to the reactor wall decreases too.

While analyzing and summarizing the heat transfer experimental data, the channel diameter usually is the determination size. However, the channel diameter is convenient only for steady flows heat transfer analysis. When examining the flow behaviour at the beginning of the channel where the flow is turbulent, it is convenient to summarize the results by distance x from the beginning of the channel. Such generalization of experimental data is applied when studying the heat transfer of plasma flow on a flat plate case [7].

With the use of similarity theory the heat transfer in plasma-chemical reactor were generalized. The generalized results were obtained for plasma flow Reynolds numbers in the range of (0.5-5) $\cdot 10^5$ (see Fig. 4).

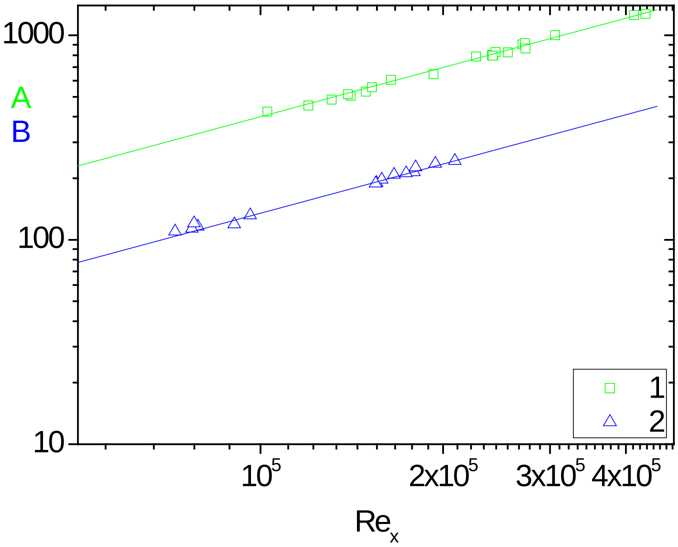

Fig. 4. Generalised heat transfer in plasma-chemical reactor. 1 – *x/d*>5,6; 2 – *x/d*≤5,6. Where A – $\frac{Nu_x}{(G_{1,2}/G_3)^{0,27}(T_f/T_D)^{0,9}}$; B – $\frac{Nu_x}{(G_{1,2}/G_3)^{-0,1}(T_f/T_D)^{0,9}}$

From Fig. 4 it can be seen, that generalized heat transfer for the beginning of the reactor is lower than in further distances *x/d*>5.6.

Generalized equation for distance *x/d*≤5.6:

$$Nu_x = 13{,}5 \cdot 10^{-3}\,\mathrm{Re}_x^{0,8}\left(\frac{G_{1,2}}{G_3}\right)^{0,27}\left(\frac{T_f}{T_D}\right)^{0,9} \qquad (5)$$

and *x/d*>5,6

$$Nu_x = 40 \cdot 10^{-3}\,\mathrm{Re}_x^{0,8}\left(\frac{G_{1,2}}{G_3}\right)^{-0,1}\left(\frac{T_f}{T_D}\right)^{0,9} \qquad (6)$$

The plasma flow in the channel is described using turbulent flow equations as the indicator above Re_x is equal to 0.8. Classical curve of heat transfer for turbulent flows in the tubes is described as:

$$Nu_x = 25.5 \cdot 10^{-3}\,\mathrm{Re}_x^{0,8}\left(\frac{T_f}{T_D}\right)^{0,9} \qquad (7)$$

The values of results obtained in this work for the whole reactor length is around 7% higher compared to the classical case. It can be explained with the fact that up to 10% error can be obtained because of bigger reactor channel surface roughness [8].

The factor above the ratio ($G_{1,2}/G_3$) in equations (5) and (6) which describes the influence of additional air to the heat transfer is bigger in (5) which means that in the reactor relative distances $x/d \leq 5$ the additional air influence is bigger. It also confirms our theory that additional air decreases the heat transfer to reactor walls before it mixes and increases its temperature in further reactor distances.

For optimization of fibrillation process using plasma technology it is very important to examine what is the heat flux from the plasma flow to the dispersive particles because it would be possible to control the particle melting without high energy losses to the reactor walls. It is very hard to estimate the heat flux to the dispersive particles without their and plasma flow temperature measurements in the reactor channel. These measurements are complicated because optical plasma diagnostics methods can not be applied for flows in the tubes and probe techniques usually are limited by the processes of condensation from the gas phase taking place in the channel of the probe [9].

In this work the heat flux to the dispersive particles was determined by measuring the decrease of heat flux to the reactor walls comparing the regimes when the reactor is working without and with the particles. Four different ceramic particle species (Al_2O_3, $Al(OH)_3$, SiO_2 and zeolites) of different size (0.04-0.06 mm, 0.06-0.16 mm, 0.16-0.2 mm and 0.2-0.25 mm) were injected to plasma flow. The plasma flow parameters (PT power – 65 kW, plasma forming air flow – $16 \cdot 10^{-3}$ kg/s, dispersive particle carrying air rate – $1.6 \cdot 10^{-3}$ kg/s) were constant during all experiments. At such plasma flow parameters the average plasma flow temperature (2400 K) in the reactor is a little bit higher than the particle melting temperature (1900-2070 K), therefore the particles even though they get the maximum heat flux, but does not start to melt because of short-term interaction. If the particles were melting during the experiments they would stick to the inner reactor walls and distorted the measurements. The decrease of heat flux to the reactor walls is shown in Fig. 5.

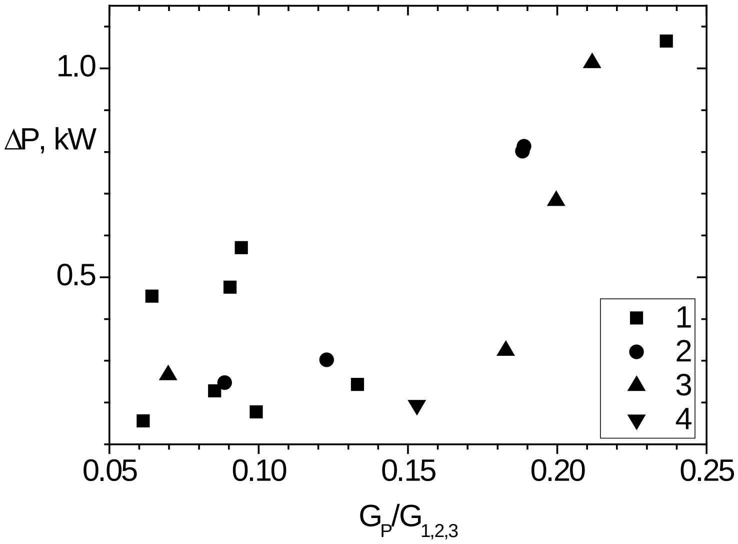

Fig. 5. Dispersive particle diameter influence on decrease of heat losses to the reactor walls where the diameter of particles: 1 – 0.04-0.06 mm, 2 – 0.06-0.16 mm, 3 – 0.16-0.2 mm, 4 – 0.2-0.25 mm

The theoretic calculations shows that the temperature of smaller particles increases faster than larger particles in the same plasma flow [10]. Our experiments show (Fig. 5) that smaller particles obtain more heat from plasma flow and the heat losses to the reactor walls decreases. It can be seen for low and high particle mass concentration in plasma flow. So, the deciding factor in heat transfer between plasma flow and dispersive particles is their size or surface area.

The heat flux to the reactor walls decreases with the increase of mass concentration of dispersed particles in plasma flow. For given experiments, the heat flux to the reactor walls is about 12 kW in the whole reactor length while working without particles. The maximal dispersive particle mass concentration in plasma flow lowers the heat losses up to 10%. If the plasma flow temperature could be measured in the reactor, the general heat flux to the dispersed particles could be calculated.

4. CONCLUSIONS

1. The formation of plasma flow boundary layer on the reactor walls results on the decrease of heat transfer in the beginning of the reactor. The plasma flow friction to the reactor walls decreases the plasma flow velocity and increases the heat transfer to the reactor walls. The heat transfer to the reactor walls decreases in further distances because of the heat loss of plasma flow.
2. As the addition of dispersed particle carrying air increases the heat transfer in the beginning of the reactor decreases and increases in further distances. The generalized heat transfer in the reactor working with dispersive particle carrying air can be described with turbulent flow equations. The heat transfer in the first section of the reactor is about 66% lower than in further distances.
3. The addition of dispersive particles decreases the heat losses to the reactor walls. The increase of mass concentration of dispersive particles from 0.06 to 0.25 decreases the heat losses to the reactor walls from 0.2 kW up to 1.1 kW in the whole length of the reactor.

ACKNOWLEDGEMENT

Part-financed by the European Union (European Regional Development Fund) PlasTEP | # 033 | KST 770123.

REFERENCES

1. ВОЛОКИТИН, Г.Г.; СКРИПНИКОВА, Н.К.; ПОЗДНЯКОВА, Н.А.; ВОЛОКИТИН, О.Г.; ЛУЦЕНКО, А.В. Высокотемпературные Способы Производства Цементного Клинкера с Использованием Низкотемпературной Плазмы и Электродугового Прогрева (Джоулев Нагрев). *Вестник ТГАСУ,* 2008, Vol. 4, p. 106–112.
2. LAKTYUSHIN, A.N.; SERGEEV, V.L.; KHVEDCHIN, I.V. Influence of Plasma-flux Parameters on Raw-material Melting in the Production of Mineral Microfibers. *Journal of Engineering Physics and Thermophysics,* 1997, Vol. 70, No. 2, p. 237–243.
3. VALINČIUS, V., KRUŠINSKAITĖ, V., VALATKEVIČIUS, P.,VALINČIŪTĖ, V., MARCINAUSKAS, L. Electric and thermal characteristics of the linear, sectional dc plasma generator. *Plasma sources science and technology,* 2004, Vol. 13, p. 199–206.
4. MILIEŠKA, M., KĖŽELIS, R., MĖČIUS, V. Influence of gas flow rate on the thermal characteristics of plasma-chemical reactor. CYSENI 2010. Proceedings of annual conference of young scientists on energy issues. [CD]. Kaunas: Lithuanian Energy Instityte. 2010 May 27-28.
5. AMBRAZEVIČIUS, A. *Теплообмен при закалке газов*. 1983, 192 p.
6. WARNATZ, J.; RIEDEL, U.; SCHMIDT, R. Different Levels of Air Dissociaton Chemistry and Its Coupling with Flow Models. *Advances in hypersonics. Modelling hypersonic flows,* 1992, Vol. 2. p. 66–103.

7. Моссэ, А.Л.; Буров, И.С. *Обработка дисперсных материалов в плазменных реакторах*. Минск: Наука и техника, 1980, 208 p.
8. ECKERT, E.R.G., DRAKE, R.M.. *Heat and mass transfer*. R.E. Krieger Pub. Co. (Malabar, Fla.). 1981.
9. OVSYANNIKOV, A. A., ZHUKOV, M.F. *Plasma diagnostics*. Cambridge International Science Publishing, 2000, 571 p. ISBN 1 898326231.
10. ZHANG, T.; GAWNE, D.T.; LIU, B. Computer Modelling of the Influence of Process Parameters on the Heating and Acceleration of Particles During Plasma Spraying. *Surf Coat Technol*, 2000, Vol. 132, No. 2–3, p. 233–243.

CYSENI 2012, May 24–25, Kaunas, Lithuania
ISSN 1822-7554, www.cyseni.com

REVIEW OF CURRENT TECHNOLOGIES AND ACHIEVEMENTS IN INDUSTRIAL GASIFICATION FIELD

A. Saliamonas, N. Striūgas
Lithuanian Energy Institute,
Laboratory of Combustion Processes
Breslaujos str. 3, LT-44403 Kaunas – Lithuania
Phone +370 (37) 401830
Email: saliamonas@mail.lei.lt

ABSTRACT

In today's industry, much attention is given to renewable energy. Changing perceptions of how to effectively use natural resources, forgotten technologies are being re-discovered. Recently, one of such re- discovered technology is gasification. This technology has been rapidly developed in the Second World War. Back then it was focused on the transport, where volatiles extracted from coal were used for the supply in to the internal combustion engines. Today, when the European Union's goal for 2020 is to reduce greenhouse gas emissions by 20% (compared with 1990 levels), gasification technology as a cleaner alternative to traditional combustion, is being adapted for the extraction of volatiles from biomass and waste. This way the increasing problem of industrial, agricultural and domestic waste utilization is being reduced and also, agricultural development is being promoted by introducing the cultivation of energy crops.

In this paper, recent achievements in the development of gasification technologies are overviewed, different types of gasification techniques and devices are compared, and the current pressures, and further development of this technology is discussed. One of the main tasks for Lithuania in achieving energy independence is to increase the use of own available resources and also to increase the efficiency of the use of resources. Gasification technology in that case enables to integrate the low-calorific value waste, energy crops and other biomass types, as a fuel in existing energy systems, thus creating an opportunity to improve their efficiency or to reduce fuel costs, partly by replacing the recovered producer gas obtained from gasification process.

Gasification technology includes the use of carbon, waste and biomass for the generation of the syngas. Since coal gasification is an old and fairly well researched technology, and household or industrial waste gasification is also a very broad topic, so the focus of this work is given to the examination of achievements in the gasification reactor, designed to work with wood pellets and sawdust.

Keywords: gasification, biomass, downdraft reactor, syngas

1. INTRODUCTION

During the past decade, gasification of biomass in various ways has an increased interest worldwide. This is not a new technology. It was developed in the Second World War in Europe and used mainly in transport area [1]. Back then taking care of world's climate and environmental problems wasn't the most important area for science. Today, when the European Union's goal for 2020 is to reduce greenhouse gases emissions by 20% (compared with 1990 levels), gasification technology has a renaissance period because nowadays it has a chance to become a cleaner alternative to traditional combustion by being adapted for the extraction of volatiles from biomass and waste. In this context research that was done mostly for coal gasification can be used and further developed for renewable fuel sources.

Currently gasification is very attractive method for developing countries like Lithuania. To increase the energy services, developing countries are growing rural electrification programs with small and large scale gasification technology [1-8]. Different kind of agricultural (Fig. 1) and domestic waste including sugar cane bagasse, empty fruit bunch (EFB), pine bark, sewage sludge are being used for biogas production [1].

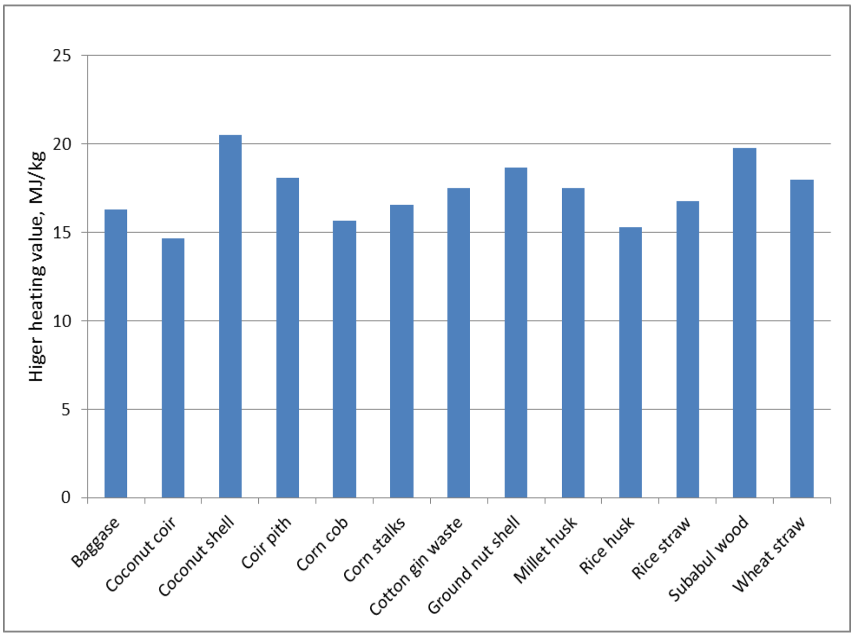

Fig. 1. Average higher heating values (HHV) of various kinds of biomass [4]

There are various modifications of gasification reactors and every type has its advantages and disadvantages. The type of reactor is chosen by the field where it will be used, because the design of gasification is based on the power and tar yield – some types of gasifiers have size limit. The basic types of reactors that can be found in literature are downdraft and updraft gasifiers. They can be used to produce power up to 10 MW,. The fluidized bed and entrained flow reactors that can be used in 10 – 1000 MW range [5] and plasma and free radical gasifiers that have a good potential, but at the moment they are at development stage.

Large scale gasification is mainly used for waste treatment (fluidized bed, entrained flow gasification) [6]. Energy production in not the main goal of technology, but is safely removal of various kind of waste with no pollution. Contrary, small scale gasification technology was developed to produce fuel for internal combustion engines. At first it was used mainly in transport, but nowadays the technology is adapted for electricity production.

The difficulties of small scale gasification are related to tar yield and produced gas with low calorific value.

2. TYPES OF GASIFICATION REACTORS

2.1. Updraft gasifier

More accurately it is called a counter-current fixed bed gasifier. This type of reactor has a fixed bed of fuel through which air or steam and oxygen or other gases such as carbon dioxide flows in counter-current configuration (Fig. 2). The ash is either removed dry or as a slag. It has been reported that the slagging gasifiers have a lower ratio of steam to carbon [6], achieving temperatures higher than the ash fusion temperature. It is required the fuel in such type of reactor must have high mechanical strength and must ideally be non-caking so that it will form a good quality moving bed [3, 7].

Updraft gasifier advantages are:

- Suitability for high-ash (up to 25%) and high-moisture (up to 60%) biomass
- Suitability for low-volatile fuels such as charcoal.
- Ability to utilize combustion heat very effectively and achieve high cold-gas efficiency
- Suitability for direct firing, where the gas produced is burnt in a furnace or boiler with no requirements of cleaning or cooling

The biggest reported disadvantage is very high tar production (30–150 g/nm^3) in an updraft gasifier, which makes it unsuitable for high-volatility fuels. [5, 8].

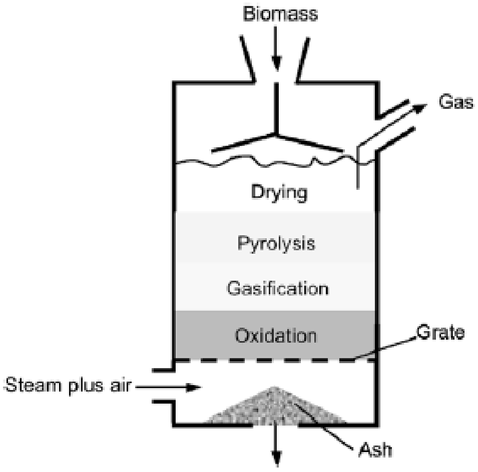

Fig. 2. Schematic of an updraft gasifier with typical reaction zones [5]

2.2. Fluidized bed reactor

This type of reactor is used in large scale industrial applications mainly for waste treatment [5, 6]. The fuel is fluidized in oxygen and steam or air or other gases such as carbon dioxide. Fuels that form highly corrosive ash can be used with Fluidized bed gasifiers. Biomass fuels generally contain high levels of corrosive ash [7]. The ash is removed dry or as heavy agglomerates that defluidize. The fuel must be highly reactive because the temperatures are relatively low in dry ash gasifiers, so low-grade coals are particularly suitable. According to [5], in a typical fluidized bed air enters from the bottom and the fuel is immediately mixed throughout the bed owing to its exceptionally high degree of mixing. Thus, the fresh oxygen entering the grid comes into immediate contact with fresh biomass particles undergoing pyrolysis as well as with spent char particles from the biomass, which has been in the bed for some time. The released tar burns due to oxygen's contact with the fresh biomass, plus oxygen's contact with the spent char particles causes the char burning. The gases flow upward and the solids are back-mixed. Any tar released moves up in the bed and leaves along with the product gas. Tar generation in a fluidized-bed gasifier is averaging about 10 mg/Nm^3. [9] The main advantages of fluidized bed gasifiers:

- Good mixing;
- Possibility of being built in sizes above of fixed-bed gasifiers.

One of disadvantages resulting higher energy costs of the fluidized bed reactor is the requirement for more pumping power to run whole process.

2.3. Entrained flow gasifier

Entrained-flow gasifiers are preferred for the integrated gasification combined cycle (IGCC) plants. Typical operation parameters of such kind of reactor are: 1400 °C temperature and 20 to 70 bar pressure, where powdered fuel is entrained in the gasifying medium. Entrained flow gasifier can have some modifications. In some of them oxygen, the most common gasifying medium, and the powdered fuel enter from the side; in others they enter from the top [5]. The gasification reactions take place in a dense cloud of very fine particles. Most coals are suitable for this type of gasifier due to high operating temperatures and good separation of coal particles [7]. According to [5, 7] the entrained flow gasifiers have high temperatures and pressures that leads to a higher throughput. Tar and methane are not present in the product gas, however thermal efficiency reduces, because gas must be cooled before cleaned. Another disadvantage is high oxygen requirement and fuel particles pulverization because entrained flow reactors require much smaller fuel particles than for other types of gasifiers.

2.4. Plasma and free radical gasifier

Plasma gasifier and free radical gasifier are unusual gasification reactors and very little information can be found about this type of reactor. In plasma type of gasifier a high-voltage current is fed to a torch, which creates a high-temperature electric arc. The inorganic residue is retrieved as a glass-like substance [7]. Free radical gasifier is a single stage reactor, where heat and light energy conversion is employed in a low oxygen environment. It uses electrical input energy to cause thermal breakdown and ultraviolet light based degradation of material, along with harnessing free radical reactions to further convert carbon-based materials into syngas [7].

2.5. Downdraft reactor

Also known as co-current fixed bed gasifier. It is the most attractive configuration of gasification reactor for small scale applications because of simple construction and relatively low tar production. It is similar to the counter-current type, but the gasification agent gas flows in co-current configuration with the fuel [5, 7].

In down draft gasifier (Fig.3) heat needs to be added to the upper part of the bed, either by combusting small amounts of the fuel or from external heat sources to make the reaction front of the gasification process go down the gasifier from top to bottom [10]. The hot produced gas leaves the gasifier, and most of this heat is often transferred to the gasification agent added in the top of the bed, resulting in energy efficiency increase. Since all tars must pass through a hot bed of char in this configuration, tar levels are much lower than in the counter-current (updraft) type.

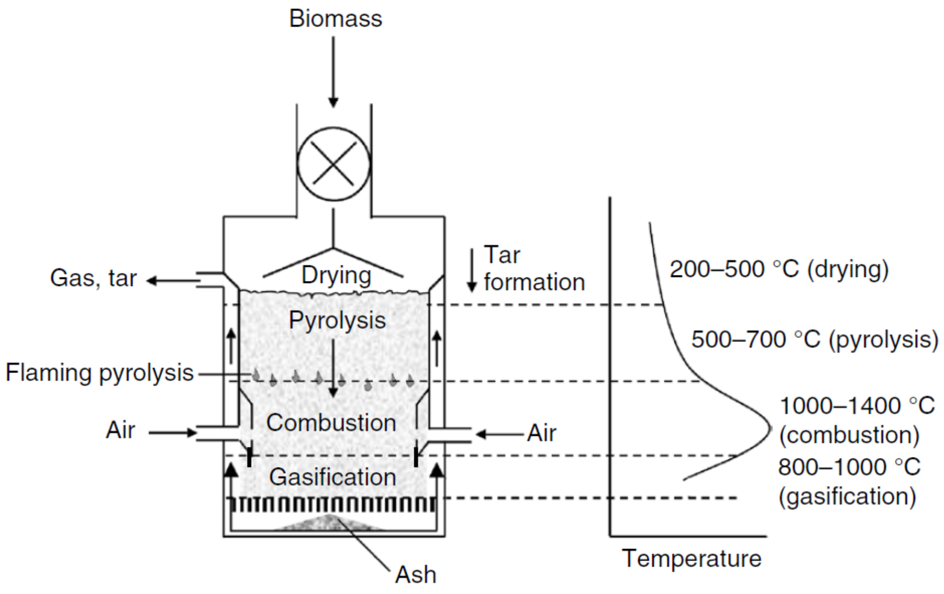

Fig. 3. Schematic of a downdraft gasifier with typical reaction zones [5]

For developing countries, downdraft gasification gives opportunity to develop a decentralised network [1] of small power plants and effectively use renewable energy sources from agriculture. In small countries waste treatment network is developed in other directions (for example waste are used as secondary fuel in combined heat and power plants), the investment for large scale gasification plants would be too big and efficiency of such plant is questionable. On the other hand small scale gasification systems have some disadvantages like low calorie gas, high tar yield and difficulties to adapt different kinds of biofuel for the same reactor. These disadvantages are the challenge for researchers to develop small scale gasification.

3. CURRENT ACHIEVEMENTS IN DOWNDRAFT GASIFICATION

The restrictions for NO_x emission increases rapidly. Finally, downdraft gasification reached a level where it can start to compete with conventional technologies of energy production. The characteristics of syngas production from biomass gasification were investigated in a downdraft gasifier that was combined with a small gas engine system for power generation [11]. It was found, that NO_x emission decreased considerably to the level about 30–40 ppm. In their experiment with only liquid phase gas (LPG) fuel, the NO_x emission upon no load was about 250 ppm. So it seems that environmental effect can be achieved when using syngas from biomass.

To achieve even higher effect an energetic alternative to adapt a fixed bed gasifier with a compact cogeneration system was presented in [12]. The main idea was to cover electrical and thermal demands in a rural area and show an energy solution for small social communities using renewable fuels. The project aimed at an energetic analysis of wood gasifier with capacity of processing between 20 - 30 kg/h of lignocellulosic biomass coupled to a compact cogeneration system. The system is able to produce electricity power of about 15 kW and hot and cold water. The purpose of the system is to assess the viability of this alternative way of generating energy to places where the electricity and the public services (hot water and cold water) are not accessible. The global efficiency of the gasifier coupled to the cogeneration system was 51.42% and it shows that a fixed bed gasifier with a compact cogeneration system is able to cover electrical and thermal demand in a rural area where the shortage of fuel derived from petroleum and the abundance of the residual biomass prevails. In [13] it is also claimed that biomass gasification has good perspective in small-scale plants with power output up to 10 MW and with the combination of a gas engine for combined heat and power production the efficiency potential of 35–40% can be achieved.

One of big advantages of downdraft gasification is the ability to achieve nearly same results with quite wide variety of different bio fuel. The gasification tests to further contribute in the field by studying the impact of the char bed properties such as char bed porosity and pressure drop on the gasification performance as well as the impact of fuel particle when using biomass was presented in [1]. It was found that one reactor can be utilized not only with wood or coal but for a variety of fuels in pellet form, with various air–fuel ratios and temperature levels.

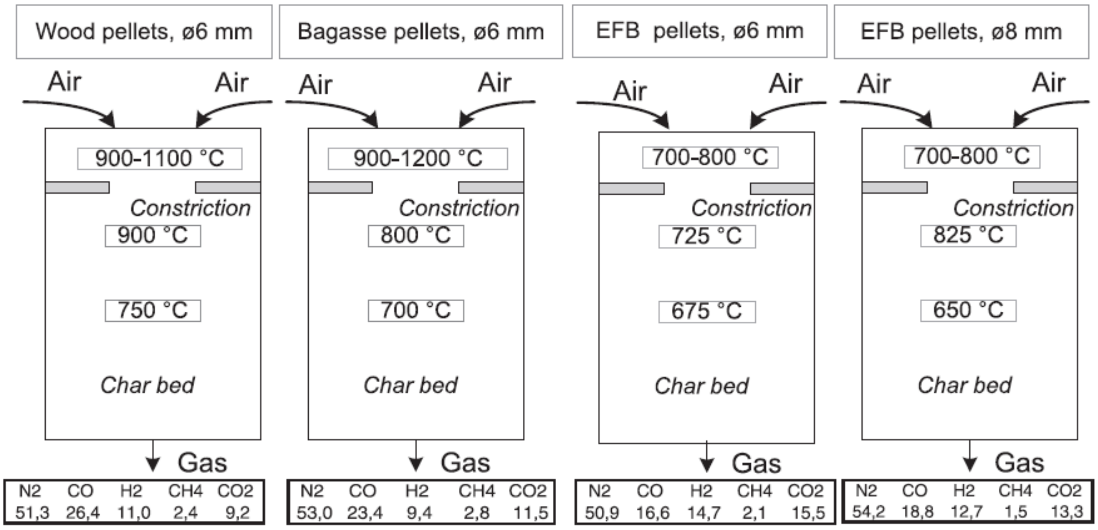

Fig. 4. Downdraft gasifier temperature profiles for different kind of fuel and typical gas composition [1]

The gas compositions, heating values and the equivalence ratio are the same order of magnitude for the same size pellets in the same reactor geometry. And also, the mass consumption rate in a gasifier with certain geometry is a function of pellet geometry but not of the chemical composition (Fig. 4). All the pellets, which were used in the investigation, showed similar shrinking characteristics but different bed dynamics.

In a review [4] it was mentioned that there are ranges of particle sizes when chemical reaction or heat transfer processes control gasification. When particle size is less than 2 mm, chemical reactions control the gasification. Between 2 and 60 mm both – chemical reactions and heat transfer control the process and when particle size is over 60 mm the heat transfer takes the biggest part in control process of the gasification.

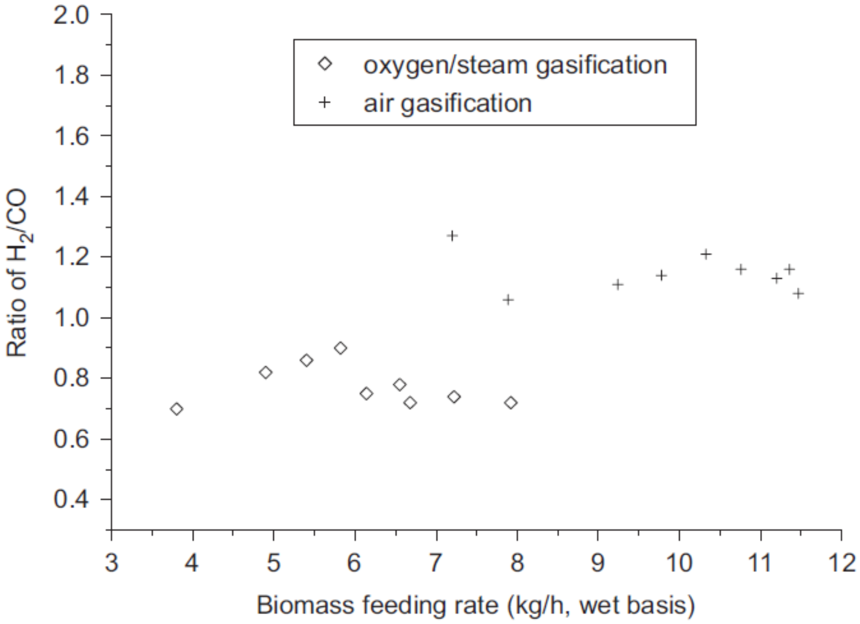

Fig. 5. H_2/CO ratio of oxygen/steam gasification and air gasification [2]

It is possible to achieve a hydrogen rich gas with higher calorie content using oxygen/steam instead of air in downdraft reactor With wide range of biofuel available for the and by . According to [2] biomass oxygen/steam gasification (in comparison with biomass air gasification) improves hydrogen yield depending on the volume of downdraft gasifier. It is also possible to achieve nearly double heating value of fuel gas. During the tests [2] in biomass oxygen/steam gasification, the content of H_2 and CO was 63.27–72.56% and the H_2/CO ratio was 0.70–0.90, while for biomass air gasification it was 52.19–63.31% and 1.06–1.27 respectively (Fig. 5).

Authors of reviewed literature investigated gasification with their own built reactors. Although they used quite different types of fuel and the power of reactors was varying, gas composition and calorific content was approximately the same (Table 1, 2).

Table 1. A summary of results [1-4]

Literature	1	2	3	4
Syngas fed to	Internal combustion engine (ICE)	ICE+ heat exchangers for cogeneration	Flare	Exhaust burner
Gas cleaning	Cyclone, scruber, dust filter	-	One cyclone, two packed bed filters	Triple stage spray shower
Fuel type	Wood pellets (3-5 mm)	Eucalyptus wood	Various types of pelets. 6 - 8 mm diameter , 36 - 50 mm long : (wood, sugar cane baggase, palm oil residue)	pine wood blocks 3x3x3 cm
Fuel parameters, %				
Moisture	21.7	-	7.5-1.3	8
Volatiles	60.9	-	-	82.29
Ash	3.9	-	0.3 - 7.9	0.55
Fixed carbon	14.3	-	-	17.16
C	46.5	-	47.2 - 50.4	50.54
H	5.8	-	5.9 - 6.1	7.08
O	43.5	-	38.2 - 44.3	41.11
N	0.2	-	0.1 - 0.6	0.15
S	0.1	-	0.01 - 0.03	0.57
Cl	-	-	0.01 - 0.46	-
HHV, MJ/kg	17.2	-	19.26-20.27	20.54
Fuel flow, kg/h	45	25	2 - 3.5	3.80-11.4
Working temperature, °C	800 -1000	-	700-1200	798-1108
Exces ratio	0.3 - 0.35	-	0.23 - 0.43	0.27
Producer gas flow, Nm^3/h	80 - 100	50	1.6 - 2.5	0.91-1.62
Producer gas composition, %				
H_2	16.5	16	9.9 - 1.5	26.42-35.39
CO	15.9	20	17 - 25.7	24.59-42.65
CO_2	15.3	13	9.9 - 14.5	2.29-36.41
CH_4	2.1	2	1.5 - 2.8	3.29-8.21
O_2	-	0.6	-	0.89-1.61
N_2	-	48	50.04 - 55	-
C_2H_4	-	0.19	-	0.22-2.07
C_2H_6	-	0.15	-	0.05-0.39
C_2H_2	-	0.01	-	-
Producer gas lover heating value (LHV) MJ/Nm^3	4.6-5	5	4.1-5.4	4.76

4. CONCLUSIONS

Since the environmental regulations for pollution are getting stricter, old technologies like gasification has a new potential for further development.

At the present time biggest interest in gasification is seen in developing countries, especially it has a potential in rural areas where small and medium scale reactors can be used for electricity and power supply.

Gasifiers come in wide range of configurations, depending on output power, fuel type and geometry (size). Most common are downdraft and updraft gasifiers for small scale applications, and fluidized bed or entrained flow for large scale applications. Also there are plasma and free radical gasifiers.

Downdraft gasifier has limitations in size, but its advantages over other types of reactors are small amount of tar, applicable to various fuel types and make similar quality producer gas, simple construction

The efficiency of the gasifier can be increased if reactor is being used not only for electric power generation but also for heat generation. Cogeneration is useful.

The air replaced with steam/oxygen flow increases quality of downdraft reactor. Although to use air is more economically efficient.

The control of gasification process partly depends on fuel particle size. If it is very small, then process is controlled by chemical reactions but if particles are big then heat transfer takes biggest part.

The quality of Produced gas is almost the same for various biofuels. The future development should be pointed at tar removal technologies.

REFERENCES

1. A.A.C.M. BEENACKERS, Biomass gasification in moving beds, a review of European technologies. *Renewable Energy*, 1999, Vol. 16, p. 1180–1186.
2. PENGMEI LV, ZHENHONG YUAN, Hydrogen-rich gas production from biomass air and oxygen/steam gasification in a downdraft gasifier. *Renewable Energy*, 2007, Vol. 32, p. 2173–2185.
3. BULJIT BURAGOHAIN, PINAKESWAR MAHANTA, Biomass gasification for decentralized power generation: The Indian perspective. *Renewable and Sustainable Energy Reviews*, 2010, Vol. 14, p. 73–92.
4. V. KIRUBAKARAN, V. SIVARAMAKRISHNAN, A review on gasification of biomass. *Renewable and Sustainable Energy Reviews*, 2009, Vol. 13, p. 179–186.
5. BASU, Prabir. *Biomass Gasification and Pyrolysis. Practical Design and Theory*. Academic Press, 2010. 365 p. ISBN 978-0-12-374988-8
6. FRANK KAMKA, Andreas Jochmann, Development Status of BGL-Gasification. International Freiberg Conference on IGCC & XtL Technologies. Germany: SVZ Schwarze Pumpe. 2005 June 16–18.
7. *Gasification*. Wikipedia, the free encyclopedia, . [Referred on the 28th of February in 2012 y.] link to the internet <http://en.wikipedia.org/wiki/Gasification>
8. CATHARINA ERLICH, TORSTEN H. FRANSSON, Downdraft gasification of pellets made of wood, palm-oil residues respective bagasse: Experimental study. *Applied Energy*, 2011, Vol. 88, p. 899–90.

9. A. GOMEZ-BAREA , B. LECKNER, Modeling of biomass gasification in fluidized bed. *Progress in Energy and Combustion Science*, 2010, Vol. 36, p. 444–509.
10. JUAN F. PÉREZ , ANDRÉS MELGAR, Effect of operating and design parameters on the gasification/combustion process of waste biomass in fixed bed downdraft reactors: An experimental study. *Fuel*, 2012.
11. YOUNG-IL SON, SANG JUN YOON, Gasification and power generation characteristics of woody biomass utilizing a downdraft gasifier. *biomass and bioenergy*, 2011, Vol. 35, p. 4215–4220.
12. CHRISTIAN RODRIGUEZ CORONADO, JULIANA TIYOKO YOSHIOKA, Electricity, hot water and cold water production from biomass. Energetic and economical analyses of the compact system of cogeneration run with woodgas from a small downdraft gasifier. *Renewable Energy*, 2011, Vol. 36, p. 1861–1868.
13. JESPER AHRENFELDT, TOBIAS P. THOMSEN, Biomass gasification cogeneration – A review of state of the art technology and near future perspectives. *Applied Thermal Engineering*, 2012, p. 1–11.

CYSENI 2012, May 24–25, Kaunas, Lithuania
ISSN 1822-7554, www.cyseni.com

CONVERSION OF PROPANE USING ATMOSPHERIC THERMAL WATER VAPOUR PLASMA

A. Tamošiūnas, P. Valatkevičius, V. Grigaitienė, V. Valinčius
Lithuanian Energy Institute
Plasma Processing Laboratory
Breslaujos str. 3, LT-44403 Kaunas – Lithuania
Phone+37062373965
Email:tamosiunas@mail.lei.lt

ABSTRACT

Propane conversion using atmospheric pressure linear DC (direct current) plasma torch was investigated. The torch is stabilized with water vapour vortex overheated up to 450 K. Argon was used as shielding gas to protect a tungsten cathode from erosion. In the paper the effects of different factors, such as temperature, total flow rate of feed-in gas, H_2O/C_3H_8 ratio, as well as power of the plasma torch on the composition of reaction products is studied. The results obtained with analytical gas chromatography showed the main products H_2 (up to 60 %) and CO (up to 22 %) with relatively high concentrations of CO_2 (higher than 10 %). A gas mixture containing hydrogen and carbon monoxide is known as synthetic gas or syngas. High levels of hydrogen formed after conversion of propane in the plasma-chemical reactor suggests that produced syngas could be of a high calorific value. By improving the plasma-chemical reactor design, thermal water vapour plasma has a potential for being the effective way for the gasification of solid organic materials, such as biomass, municipal solid waste and etc.

Keywords: thermal plasma, water vapour, propane, hydrogen, plasma torch, synthetic gas, reforming

1. INTRODUCTION

Special emphasis on the environment pollution is becoming a serious problem due to the increased use of fossil fuels. Therefore, it implied a large amount of effort in the scientific area for the development of the alternative clean energy. From such a perspective, syngas, a mixture of hydrogen and carbon monoxide, or pure hydrogen is coming to the forefront as the environmental friendly alternative source of the energy. An increasing interest, both from environmental and industrial perspectives, has attracted the use of several syngas production methods, such as steam reforming, partial oxidation, CO_2 reforming, autothermal reforming [1–7].

However, due to the endothermic nature of the reaction, it requires special conditions, such as catalytic and plasma means. Conventional reforming methods have technological and economic limitations, i.e. large size of equipment, high investment and exploitation costs, and limitations on rapid response, extreme operating conditions limiting the reactor lifetime, catalyst sensitivity (coking and deactivation), safety and operability [8-10]. Contrary to the conventional reforming technologies, plasma (both thermal plasma and non-thermal plasma) assisted reforming may offer an alternative for the synthetic gas production and overcome such limitations concerning conventional catalytic methods. Plasma assisted reforming is usually combined with catalysts [11, 12], or without a catalyst [13, 14]. Plasma itself could be considered as a state of medium which helps to induce a specific homogeneous chemical processes.

Thermal plasma with features of relatively high enthalpy to enhance reaction kinetics, high chemical reactivity and high electron density (about 10^{19}–10^{20} m^3) as well as rapid quench rate, high temperature (several thousand K) and better control of the process, provide the possibility of its adjustment in the effective production of hydrogen-rich gas [15].

Despite the mentioned advantages, thermal plasma reforming is distinguished by several disadvantages, such as dependence on electrical energy and electrode erosion due to arc shunting in the discharge chamber thus limiting the lifetime of the equipment.

In this work, thermal plasma reforming of propane for syngas production by atmospheric pressure DC (direct current) electric arc discharge was investigated. Propane was chosen due to relatively low cost and as oxygen acceptor, affecting the specific conditions, to reduce the amount of oxygen molecules in the exhaust fluid gas.

2. EXPERIMENTAL SETUP AND METHODOLOGY

2.1. Water vapor plasma torch with chemical reactor

Fig. 1 presents the configuration of the water vapor plasma torch with chemical reactor used for propane reforming. The water vapor plasma torch stabilized by water vapor vortex is a linear DC thermal plasma generator with a cathode of tungsten, with 2.5 mm diameter embedded into a copper rod, and stair-step anode for suppression of the electric arc shunting in the discharge chamber. The 49-69 kW DC water vapor plasma torch operates at atmospheric pressure with the intensity of the arc current ranging from 120 to 200 A, and voltage 220 to 380 V, respectively. Overheated water vapor (up to 450 K) was used as plasma forming gas, whereas argon as shield gas, screening cathode from the erosion. Water vapor and argon were tangentially injected through the insulating rings into the discharge chamber, where they were heated up to tens of thousands of Kelvin's by means of the electric arc. Thus, the outflow of plasma jet through the exhaust nozzle of the torch is formed with the average velocity of 300 m · s^{-1} and jet temperature of several thousand of Kelvin's. The flow rates of water vapor and argon is controlled by the mass flow controllers and may vary from (1.48–4.48) · 10^{-3} kg · s^{-1}, whereas argon flow rate is fixed, 0.52· 10^{-3} kg · s^{-1}, throughout the experiments.

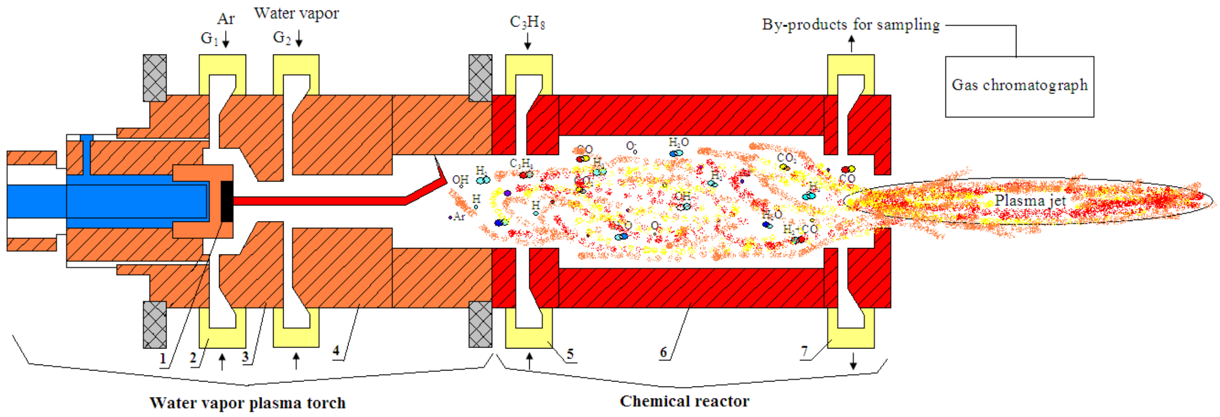

Fig. 1. Schematic diagram of the water vapor plasma torch reformer system. Plasma torch:
1 – tungsten cathode, 2 – insulating rings, 3 – neutral section, 4 – stair-step anode.
Chemical reactor: 5 – gas inlet section, 6 – reaction chamber,
7 – reaction products sampling section

The chemical reactor for reforming consists of three sections. The first section is divided for the inlet of hydrocarbons; the second is a reaction chamber, where the chemical reactions proceeded, such as steam reforming, cracking etc. The last section of the chemical reactor was set up for the analyses of the formed reaction products.

2.2. Reaction products analysis

Reaction products were sampled by the sampling port installed at the very top of the by-products sampling section. Before sampling, the outlet gas passed through the condenser to eliminate moisture and water. After, the gas was collected in the special gas sampling vessels for the analyses. Gas analyses were carried out by a gas chromatograph (GC) (Agylent 7890A) with dual channel thermal conductivity detectors (TCDs). The front channel with nitrogen carrying gas (10 ml min^{-1}) was used for separating O_2, CO_2, CH_4, CO and light hydrocarbons. Meanwhile hydrogen was separated through the molecular sieve packed column of the back channel which operated on helium carrier (30 ml min^{-1}).

2.3. Relevant reactions

To evaluate the reaction performance of the system, water conversion, propane conversion and selectivity were calculated in this work. The conversion rate of water vapor and propane as well as selectivity is defined as follows [13]:

$$Conv(H_2O) = \frac{M_{H_2O,IN} - M_{H_2O,OUT}}{M_{H_2O,IN}} \tag{1}$$

$$Conv(C_3H_8) = \frac{M_{C_3H_8,IN} - M_{C_3H_8,OUT}}{M_{C_3H_8,IN}} \times 100\% \tag{2}$$

$$S(H_2) = \frac{M_{H_2,OUT}}{2 \times (M_{C_3H_{8},IN} - M_{C_3H_8,OUT}) + H_2O_{consume}} \tag{3}$$

$$S(CO) = \frac{M_{CO,OUT}}{(M_{C_3H_8,IN} - M_{C_3H_8}) + (M_{H_2O,IN} - M_{H_2O,OUT})} \times 100\%, \tag{4}$$

where $M_{C_3H_8,IN}, M_{H_2O,IN}, M_{C_3H_8,OUT}, M_{H_2O,OUT}, H_2O_{consume}$ are the moles of the input C_3H_8, H_2O and the output C_3H_8, H_2O and the mole of water input as plasma forming gas, respectively.

3. RESULTS AND DISCUSSION

The operating parameters of the DC water vapor plasma torch during the performed experiments at atmospheric pressure were maintained as follow: arc current intensity varied from 120 to 200 A, voltage range 220–380 V, power available for plasma jet 43–58 kW, flow rate of water vapor varied within the limits of (3.51–4.48) · 10^{-3} kg · s^{-1}, while that of propane from (0.34–0.66) · 10^{-3} kg · s^{-1}.

3.1. Water decomposition

Firstly, in order to investigate the extent of water vapor decomposition the experiments were carried out without the injection of propane. The calculations (Eq. 1) and the results obtained by means of gas chromatography showed (Fig. 2) that approximately 5.5 ± 1% of water vapor was decomposed into pure hydrogen and oxygen. The average amount of hydrogen produced from water vapor decomposition exceeded 9.8 ± 2%.

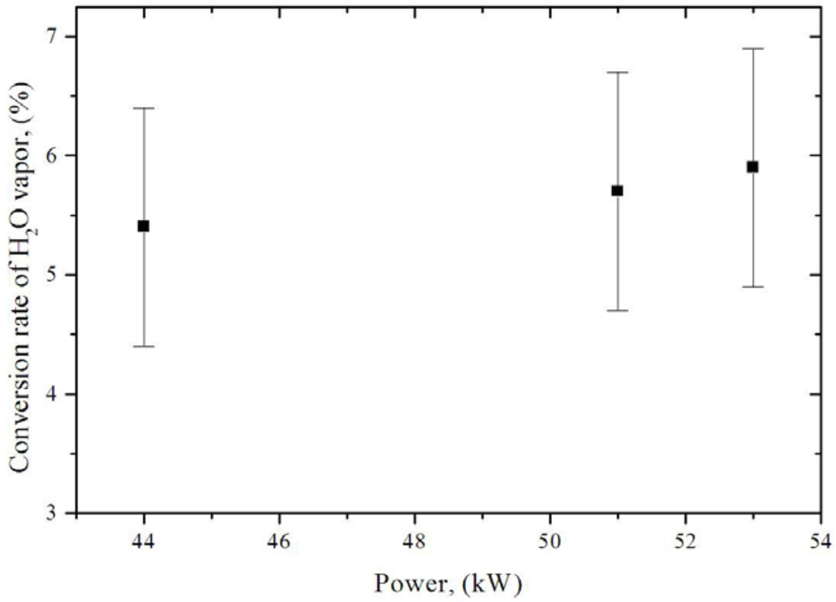

Fig. 2. Conversion rate of water vapor as a function of power available for plasma jet.
Flow rates of water vapor varied from 3.51 · 10^{-3} kg · s^{-1} to 4.48 · 10^{-3} kg · s^{-1}, respectively

3.2. Propane conversion

Propane conversion by steam phase is strongly endothermic (ΔH^0 = 498 kJ mol^{-1}). According to [16] propane steam reforming reaction is described by the equation (5):

$$C_3H_8 + 3H_2O \rightarrow 7H_2 + 3CO \tag{5}$$

Also, steam reforming reaction suffers from competiveness with cracking. Plasma cracking reaction is described by the following equation (6):

$$C_3H_8 \rightarrow C_3H_6 + H_2 \tag{6}$$

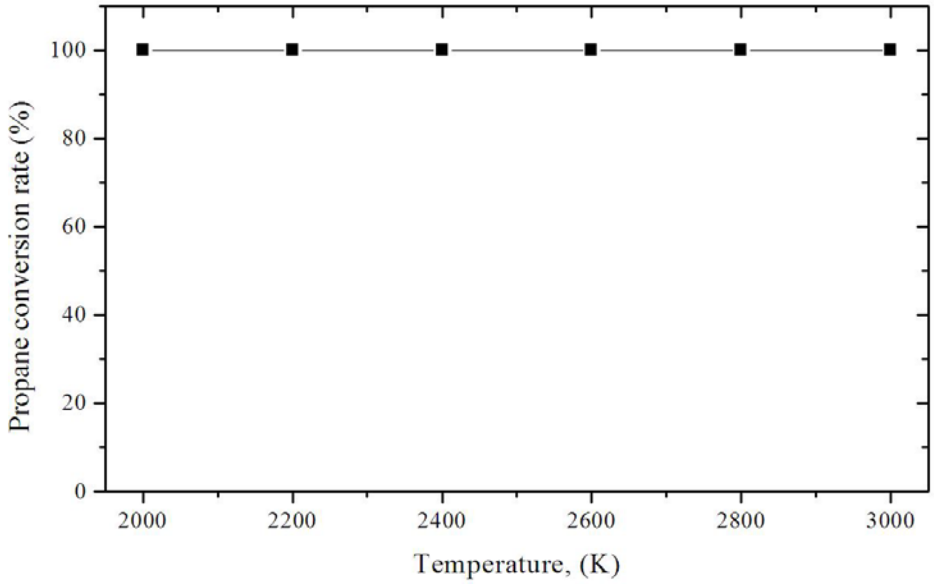

Fig. 2. Propane conversion rate as a temperature function

Fig. 2 shows propane conversion rate calculated according to Eq. 2. It could be seen that conversion of C_3H_8 is 100%. It is possible that total propane conversion is reached due to the high plasma temperatures (2000–3000K) in the plasma-chemical reactor. Such high temperature is an important parameter for plasma reforming. Moreover, another important parameter is a residence time of treated materials inside the plasma-chemical reactor, 280 mm of length and 40 mm in diameter. The residence time varied from 6.4 ms to 8.5 ms and depended on the total flow rate.

The selectivity of H_2 and CO is shown in Fig. 3. With the H_2O/C_3H_8 ratio increased from 5.3 to 13.2, the selectivity of H_2 decreased from 82.2% to 77.7%, while that of CO also decreased from 50% to 23.4%, respectively. The decrease of selectivity could be explained by the fact that O atom in H_2O vapor plasma contributed to $CO + O \rightarrow CO_2$ or $H_2 + O \rightarrow H_2O$ instead of $C + O \rightarrow CO$, which determined lower CO and H_2 selectivity. Low selectivity of CO implies carbon deposition in the reforming process. Carbon depostion on the walls of the plasma-chemical reactor was observed during the experiments.

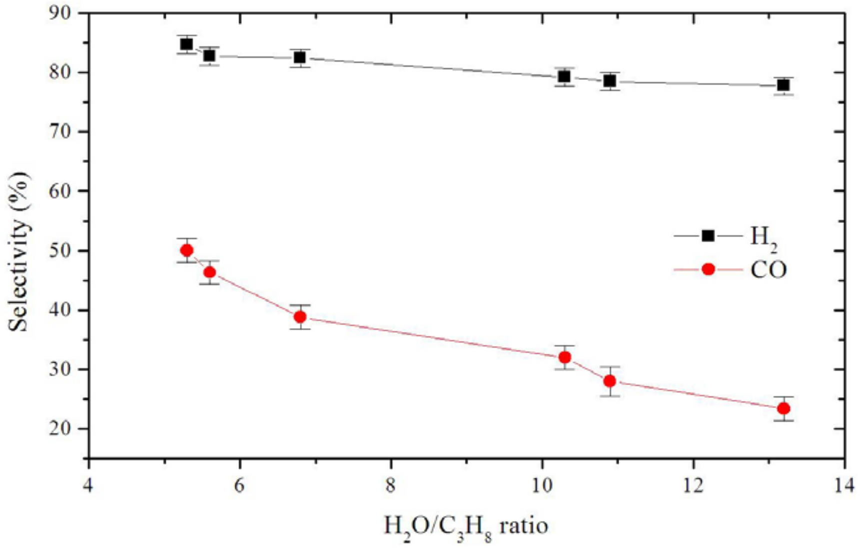

Fig. 3. Selectivity of H_2 and CO as a function of the inlet water vapor to propane ratio

3.3. Composition of reaction products

The analysis of reaction products by gas chromatography showed that the produced gas contains predominantly H_2, CO and CO_2. Moreover, H_2O and O_2 with relatively small concentrations 3–5% and 1–4%, respectively, were found. Table 1 and Table 2 show the results of gas chromatography analyses. The lower part of the Tables point equilibrium concentrations of the reaction products, calculated for the experimental flow rates of input substances under the assumption of complete decomposition of propane, water vapor and CO_2 into hydrogen and carbon monoxide.

Table 1. Composition of gases at the output of the plasma-chemical reactor (in vol%).
H_2O vapor flow rate 3.51–4.48· 10^{-3} kg · s^{-1}, propane 0.34 · 10^{-3} kg · s^{-1}

H_2O/C_3H_8 ratio	H_2	CO	CO_2
5.3	67.78	22.96	7.74
5.6	68.28	21.9	8.13
6.8	67.63	19.37	9.2
1.2 (Equilibrium)	70	30	0

Table 2. Composition of gases at the output of the plasma-chemical reactor (in vol%). H_2O vapor flow rate 3.51–4.48 · 10^{-3} kg · s^{-1}, propane 0.66 · 10^{-3} kg · s^{-1}

H_2O/C_3H_8 ratio	H_2	CO	CO_2
10.3	64.26	17.9	9.11
10.9	65.26	16.76	10.54
13.2	65.37	14.6	11.27
1.2 (Equilibrium)	70	30	0

According to the given data in tables, the concentrations of hydrogen exceeded over 60% in volume. It was observed that it slightly depended on the H_2O/C_3H_8 ratio. The increased content of propane from 0.34 to 0.66 · (10^{-3} kg · s^{-1}), at a fixed water vapor flow rate, showed that the level of hydrogen concentration slightly increased. The same tendency was observed increased the content of water vapor from 3.51 to 4.48 · (10^{-3} kg · s^{-1}), at a fixed propane rate. As mentioned previously in (3.1. section), around 10% of hydrogen came from water vapor decomposition. High levels of pure hydrogen concentration could be explained by the high conversion rate of propane and high H_2 selectivity.

The results in Tables demonstrates that changing H_2O/C_3H_8 ratio from 5.3 to 13.2, the concentrations of CO decreased from 22.96% to 14.6%, while that of CO_2 increased from 7.74% to 11.27%, respectively. This could be explained that the combination mechanism between C atom and O atom decreased, and the selectivity of CO decreased, too. It implies that during the oxidation O atom contributed to $CO + O \rightarrow CO_2$ instead of $C + O \rightarrow CO$, thus, selectivity of CO_2 increased.

The obtained O_2 by GC suggest that there is a further growth potential in propane flow rate, enabling higher levels of CO and/or CO_2 during the oxidation process.

4. CONCLUSIONS

The experimental investigations confirmed that propane conversion into syngas by the atmospheric pressure DC water vapor plasma torch proceed efficiently. The conversion rate of propane was observed to be 100%. Propane conversion depended on the temperature of exhausted plasma jet. Gas mixing and residence time inside the plasma-chemical reactor was sufficient for total propane decomposition. The conversion rate of water vapor without propane flux exceeded 5.5 ± 1% in any studied case. The selectivity of H_2 and CO decreased from 84% to 77.7% and 50% to 28%, respectively.

The main products of thermal plasma reforming observed by gas chromatography were hydrogen (max value 68.28%), carbon monoxide (max value 22.96%) and carbon dioxide (max value 11.27%). Approximately 10% of H_2 came from water vapor decomposition without C_3H_8 flux. The concentrations of condensed H_2O and O_2 varied from 3% to 5% and 1% to 4%, respectively, in the total mass balance.

The concentration of H_2 slightly depended on the H_2O/C_3H_8 ratio. The concentrations of CO decreased from 22.96% to 14.6%, while that of CO_2 increased from 7.74% to 11.27%, respectively, changing the ratio of H_2O/C_3H_8 from 5.3 to 13.2.

ACKNOWLEDGEMENTS

This research was funded by a grant (No. ATE-10/2012) from the Research Council of Lithuania.

REFERENCES

2. KARAKAYA, M., KESKIN, S., AVCI, A.K. Parametric study of methane steam reforming to syngas in a catalytic microchannel reactor. *Applied Catalysis A: General*, 2012, Vol. 411–412, p. 114–122.
3. RABIK, M.A., GRACE, J.R., LIM, C.J., ELNASHAIE, S. S. E. H., GHIASI, B. Steam reforming of propane in a fluidized bed membrane reactor for hydrogen production. *International Journal of Hydrogen Energy*, 2010, Vol. 35, Issue 12, p. 6276–6290.
4. LIU, SH., XU, L., XIE, S., WANG, Q., XIONG, G. Partial oxidation of propane to syngas over nickel supported catalysts modified by alkali metal oxides and rare-earth metal oxides. *Applied Catalysis A: General*, 2001, Vol. 211, Issue 2, p. 145–152.
5. LI, D., SHIRAGA, M., ATAKE, I., SHISHIDO, T., OUMI, Y., SANO, T., TAKEHIRA, K. Partial oxidation of propane over Ru promoted Ni/Mg(Al)O catalysts: Self-activation and prominent effect of reduction-oxidation treatment of the catalyst. *Applied Catalysis A: General*, 2007, Vol. 321, Issue 2, p. 155–164.
6. SUTTON, D., PARLE, S.M., ROSS, J.R.H. The CO_2 reforming of the hydrocarbons present in a model gas stream over selected catalysts. *Fuel Processing Technology*, 2002, Vol. 75, Issue 1, p. 45–53.
7. GUO, J., HOU, Z., ZHENG, X. Autothermal reforming of CH_4 and C_3H_8 to syngas in a fluidized-bed reactor. *Chinese Journal of Catalysis*, 2010, Vol. 31, Issues 9-10, p. 1115–1121.
8. GOKALILER, F., ONSAN, I., AKSOYLU, E. Power-law type rate equation for propane ATR over Pt-Ni/Al_2O_3 catalyst. *International Journal of Hydrogen Energy*, 2012, doi: 10.1016/j.ijhydene.2012.01.114.
9. OUNI, F., KHACEF, A., CORMIER, J.M. Syngas production from propane using atmospheric non-thermal plasma. *Plasma Chemistry and Plasma Processing*, 2009, Vol. 29, p. 119–130.
10. CHEN, Z., YAN, Y., ELNASHAE, S. S. E. H. Catalyst deactivation and engineering control for steam reforming of higher hydrocarbons in a novel membrane reformer. *Chemical Engineering Science*, 2004, Vol. 59, Issue 10, p. 1965–1978.
11. HARDIMAN, K. M., TRUJILLO, F. J., ADESINA, A. A. Deactivation-influenced propane steam reforming: reactor analyses and parameter estimation. Chemical Engineering and Processing: Process Intensification, 2005, Vol. 44, Issue 9, p. 987–992.
12. HORNG, R.F., LAI, M.P., CHANG, Y P., YUR, J.P., HSIEH, S. F. Plasma-assisted catalytic reforming of propane and an assessment of its applicability on vehicles. *International Journal of Hydrogen Energy*, 2009, Vol. 34, Issue 15, p. 6280–6289.
13. YU, Q., KONG, M., LIU, T., FEI, J., ZHENG, X. Non-thermal plasma assisted CO_2 reforming of propane over Ni/Y-Al_2O_3 catalyst. Catalysis Communications, 2011, Vol. 12, Issue 14, p. 1318–1322.
14. NI, G., LAN, Y., CHENG, CH., MENG, Y. WANG, X. Reforming of methane and carbon dioxide by DC water plasma at atmospheric pressure. *International Journal of Hydrogen Energy*, 2011, Vol. 36, p. 12869-12876.
15. TAO, X., BAI, M., WU, Q., HUANG, Z., YIN, Y., DAI, X.CO_2 reforming of CH_4 by binode thermal plasma. *International Journal of Hydrogen Energy*, 2009, Vol. 34, p. 9373–9378.
16. TAO, X., BAI, M., LI, X., LONG, H., SHANG, SH., YIN, Y., DAI, X. CH_4-CO_2 reforming by plasma: challenges and opportunities. *Progress in Energy and Combustion Science*, 2011, Vol. 37, p. 113–124.
17. CHUN, Y.N., SONG, H.O. Syngas production using gliding arc plasma. Energy Sources, Part A, 2008, Vol. 30, p. 1202–1212.

CYSENI 2012, May 24–25, Kaunas, Lithuania
ISSN 1822-7554, www.cyseni.com

PROXIMATE AND ELEMENTAL ANALYSIS OF SOLID BIOFUEL AND THEIR INFLUENCE TO COMBUSTION PROCESS

M. Valantinavičius, **T. Vonžodas**
Lithuanian Energy Institute
Breslaujos str. 3, LT-44403 Kaunas – Lithuania
Phone +370 618 23681
Email: valantinavicius@mail.lei.lt

ABSTRACT

Environmental and economic concerns of reducing CO_2 emissions and of increasing fuel flexibility have been motivating using biomass fuels to substitute fossil fuels for heat and electricity generation. Biomass is composed of three major components: cellulose, hemicellulose and lignin. C, H and O are the main components of solid biofuels and are of special relevance for the gross calorific value, H in addition also for the net calorific value. The fuel N content is responsible for NO_x formation. NO_x emissions belong to the main environmental impact factors of solid biofuel combustion. Cl and S are responsible for a deposit formation and corrosion therefore relevant for high plant availability. Furthermore Cl causes HCl as well as PCDD/F (polychlorinated dibenzodioxin/furan) and S – SO_x emissions and both elements are involved in the formation of aerosols (submicron particle emissions). The ash content influences the choice of appropriate combustion technology and deposit formation, fly ash emissions and the logistics concerning ash storage and utilization. Major ash forming elements (Al, Ca, Fe, K, Mg, Na, P, Si, Ti) are of relevance for the ash melting behavior and deposit formation and corrosion. In addition, volatile elements such Na and K are the main constituents of aerosols. Volatile minor elements (As, Cd, Hg, Pb, Zn) play a major role in gaseous and especially aerosol emissions as well as in deposit formation and corrosion of heating devices and ash utilization. Either partly or non-volatile minor elements (Ba, Co, Cr, Cu, Mo, Mn, V) are of special relevance for ash utilization. Elemental and proximate analysis where performed of different biomass samples and their mixtures.

Keywords: Biomass, Solid Biofuels, Elements, Chemical analyses, Chemical properties

1. INTRODUCTION

The primary production of renewable energy within the EU-27 in 2010 was 166.6 million tons of oil equivalent (Mtoe) – 20% share of total primary energy production. The volume of renewable energy produced within the EU-27 increased overall by nearly 58% between 2000 and 2010, equivalent to an average increase of 5.2 % per annum. But this increase was 10.7% from 2009 to 2010 [1].

About 112.7 Mtoe of primary energy of biomass was produced in the EU-27 in 2010. Biomass provided nearly 70% of all renewable energy, or 6.4% of the total gross inland energy consumption in that year. However, most biomass resources currently consumed in Europe consist of raw timber and wastes from the agro-industries and timber processing. Small amounts of field residues are still nevertheless consumed in most countries [1].

The use of biomass fuels provides substantial benefits as far as the environment is concerned. Biomass absorbs carbon dioxide during the growth, and emits it during combustion. Therefore, biomass helps the atmospheric carbon dioxide recycling and does not contribute to the greenhouse effect. Biomass consumes the same amount of CO_2 from the atmosphere during growth as is released during combustion [2].

Biomass fuels potential includes wood, short-rotation woody crops, some agricultural wastes, short-rotation herbaceous species, wood wastes, waste paper, sawdust, grass, waste from food processing, aquatic plants and algae, animal wastes, and a host of other materials. Biomass is the only organic petroleum substitute which is renewable [2].

Therefore this investigation was especially focused on chemical properties of biomass fuel. The work package concerned aims to analyse high heating value (HHV), ash content, (total) carbon (C) and hydrogen (H), nitrogen (N) and sulphur (S) as well as major (calcium (Ca), iron (Fe), magnesium (Mg), potassium (K), sodium (Na), titanium (Ti)) and minor elements (arsenic(As), barium (Ba), cadmium (Cd), cobalt (Co), chromium (Cr), copper (Cu), manganese (Mn), molybdenum (Mo), nickel (Ni), lead (Pb), antimony (Sb), vanadium (V), zinc (Zn), lithium (Li), selenium (Se)) in solid biofuels. The present paper gives an overview of the influence and impact of these elements on combustion. The fuels considered in this investigation were natural solid biofuels (as defined solid biofuels in [3]) that was forest wood, quick rotation plants and agricultural waste.

1.1 Principles of solid biofuel combustion and technologies

In the ideal case, combustion represents the complete oxidation of the solid organic part of the fuel into the CO_2 gas and H_2O. This conversion occurs in three steps: drying of the fuel (vaporising of water), pyrolysis/gasification (thermal degradation (devolatilisation) in the absence or presence of externally supplied oxygen (air), respectively) and the final oxidation of the charcoal and the flue gases (see Fig. 1.). After drying, the main controlling parameter of the combustion process is the ratio between the amount of air added and the amount of air (oxygen) necessary for a complete combustion of the combustible parts of the fuel, the lambda (λ, excess air) factor [4].

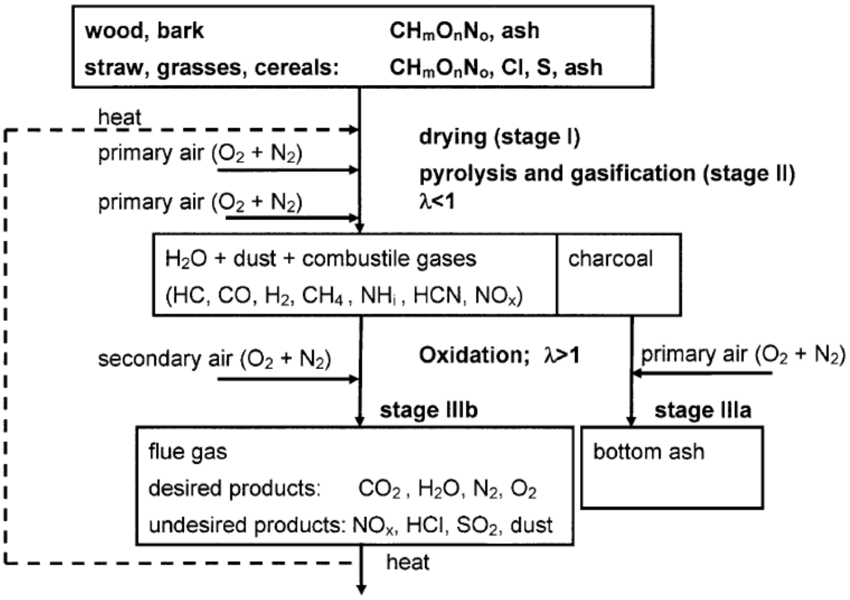

Fig. 1. The principle of biomass combustion process [4]

At λ below 1, incomplete oxidation of the fuel (gasification) takes place and only a part of the fuel energy is converted into the thermal energy. Adding too much air (λ >>1) will cool down the process, leading to the incomplete combustion and thermal losses. Thus, the theoretical optimum of the combustion process is at λ =l. In reality however, this point is difficult to obtain due to mixing constraints between the fuel, flue gas and the air added. Thus, depending on the combustion technology applied, a total λ between 1.1 and 1.8 in large-scale and 1.5 and 2.0 in small-scale applications is common in order to achieve the complete combustion.

In order to achieve a combustion that is as efficient as possible and produces only low amounts of undesired products, each combustion step must be optimised taking into consideration the combustion technology applied and the kind of solid biofuel used.

The application of solid biofuel combustion comprises small-scale (domestic) application for domestic heating (with a nominal boiler capacity (NBC) up to around l00kWth) as well as an industrial application with NBCs in the MWth range for district heating, process heating, electricity production as well as combined heat and power (CHP) production. The technologies used for small-scale applications include wood-stoves, fire place inserts, heat-storing stoves as well as boilers for wood logs, wood pellets and wood chips [4].

2. MATERIALS AND METHODS

2.1 Samples

Three groups of solid biofuel were chosen for this investigation. First group was comprised of traditional forestry biomass fuel. It consisted of different type of wood that was oak, ash, birch, alder and black alder. The second group was comprised of different type herbaceous biomass (straw of wheat, barley, rape and quick rotation plants (reed and miscanthus). The third group was constituted of other biomass residues (shells of coconuts and walnuts). Raw material (wood log) as well as prepared for combustion material (pellets and briquettes) was chosen in this investigation.

2.2 Sample homogenisation and moisture content determination

The moisture content in biomass as measured (at different basis, but normally as received, air-dried and oven-dried basis) varies in the interval of 3-63% and it can reach even 80% for raw wood species [5].

About 1–3 kilograms of each kind of solid biofuel were collected for this investigation. The samples were pulverized until 30 mm size and dried in the oven for 14 hours at 105 °C. Determination of moisture content was conducted after that. Then the samples were pulverized until 0.5 mm size with the mill which had no heavy metals. The samples were put into the hermetic vessels before the investigation in order to prevent them from saturation of the moisture from the ambient.

2.3 Calorific values

In order to determine the higher calorific values of the woods, straws and other solid biofuels, they were burned in a calorimeter bomb of IKA C5000 bench. The lower calorific values were calculated considering humidity and hydrogen contents in the solid biofuel. The basic characteristics of the investigated biofuels are presented in Table 1.

2.4 Determination of ash content

Besides the ash forming minerals the main components of wood are the extractives and insoluble fibres namely lignin, hemicellulose and cellulose [6].

Ash content of the fuel was determined by using thermogravimetric method (TGA) of Perkin Elmer bench. Taken sample of biofuel was heated to 105 °C and this temperature was maintained for a while. After that the reading of balance was recorded. Then the sample was heated again at 550 °C for two hours. Consequently, the residual weight is ash content.

2.5. C, H, N, S, O contents determination

The elemental composition (C, H, N, S, O) analysis of the samples was carried out in the laboratory. Elemental concentrations of those samples were determined using organic elemental analysers (OEA) FLASH 2000.

2.6. Major and minor elements determination

To determine levels of the major and minor elements in woods and other materials, samples of 0.3–0.5 g were wet-digested with 8 ml trace analysis grade nitric acid in a microwave reactor. The exact element concentrations of samples were determined by using inductively coupled plasma-optical emission spectroscopy (ICP-OES) method of Perkin Elmer Optima™ 8000 bench. Control samples were also prepared with the same demineralisation process.

3. CHEMICAL COMPOSITION OF SOLID BIOFUELS INFLUENCE ON THERMAL UTILISATION

3.1 Carbon (C), hydrogen (H), nitrogen (N), sulphur (S), oxygen (O) in biomass

C, H and O are the main components of solid biofuels (Table 1). C and H are oxidised during combustion by exothermic reactions (formation of CO_2 and H_2O). The content of C and H contributes positively to the higher heating value (HHV). CO_2 is formed and emitted as a major product of complete combustion. However, CO_2 emissions from biomass combustion are regarded as being CO_2 - neutral with respect to the greenhouse gas effect if a sustainable utilisation is assumed [7]. In modern furnaces with effective process control systems the concentrations of unburned pollutants can be reduced to levels close to zero [8].

During combustion, the fuel N is almost entirely converted in to gaseous N_2 and nitric oxides (NO_x, [NO, NO_2]). The amount of nitrogen dioxide (NO_2) is very low in modern solid biofuel furnaces. Only an insignificant amount of N is incorporated in the ash. Resent investigation has shown that one of the main environmental impacts of solid biofuel combustion is caused by NO_x emissions. NO_x can be formed via three different reactions pathways. The amount of NO_x increases with increasing temperature. Prompt NO_x is formed from airborne N at temperatures above ~1300°C under low oxygen conditions in the presence of hydrocarbons. Due to the comparatively low furnace temperatures in solid biofuel combustion plants (around 800–l200°C), thermal and prompt NO_x formation is only of minor importance. NO_x formation from the oxidation of fuel N (during a series of elementary reaction steps) is the most important mechanism in biomass combustion units. The NO_x emissions thus increase with increasing fuel N content. Furthermore, the air supply, the geometry of the furnace, the combustion temperature and the type of combustion technology applied are major influencing variables for NO_x formation [4].

Sulphur contained in the solid biofuel (see in Table 1.) forms mainly gaseous SO_2 (to a certain extent also SO_3) and alkali as well as earth-alkali sulphates. Due to the subsequent cooling of the flue gas in the boiler section of the combustion plant, SO_x forms sulphates and condenses on the heat exchanger surfaces or forms fine fly ash particles, or reacts directly with fly ash particles deposited on heat exchanger surfaces (sulphation). Investigations have shown that 40–70% or 60–90% of the fuels S was integrated in the ash in the case of wood chip or bark combustion. In the case of (wheat) straw or cereal combustion (plants equipped with baghouse filters) only 40–55% was integrated in the ash. The efficiency of S fixation in the ash depends on the concentration of alkali and earth-alkali metals (especially Ca) in the fuel (fuels like wood chips and bark can contain high Ca contents and therefore cause a high S fixation). The residual S remains in the flue gas as aerosols and in gaseous form as SO_2 (in minor quantities as SO_3). Emissions of SO_2 are usually not significant for wood combustion due to the typically low concentrations of S in the fuel, and, especially in the case of wood chips and bark utilisation, because of the relatively high embedment in the ash [4].

3.2 Ash content, minor and major elements in biomass

The ash content of the fuel is essential for the choice of the appropriate combustion and gas-cleaning technologies. Furthermore, fly ash formation, ash deposit formation as well as logistics concerning ash storage and ash utilization/disposal depend on the ash content of the fuel. Fuels with low ash content are therefore preferable. Wood usually contains relatively low amounts of ash, while significantly higher values are typically found in herbaceous biomass. Grate or fluidized bed combustion are suitable technologies for ash-rich fuels. Underfeed stokers are not suitable for ash-rich fuels due to the formation of ash layers on the surface of the fuel bed which can cause irregular breakthroughs of the gas and combustion air resulting in increased emissions. The composition, density, size and amount of the fly ash emissions are influenced by the amount of ash forming elements in the fuel as well as by the combustion technology and process control applied [4].

Major (Al, Ca, Fe, K, Mg, Na, Ti) and minor (As, Ba, Cd, Co, Cr, Cu, Mn, Mo, Ni, Pb, Sb, V, Zn) with Cl and S elements, form the ash components. These elements are of relevance for ash melting, deposit formation, fly ash and aerosol emissions as well as corrosion (together with S and Cl) and the utilisation/ disposal of the ashes. Typical concentrations and their ranges of major and minor elements in different solid biofuels are given in Table 2. Major and minor elements influence the ash melting behaviour. Ca and Mg usually increase the ash melting point, while K decreases it [8]. Chlorides and low melting alkali and alumosilicates may also significantly decrease the ash melting point [10]. This can cause sintering or slag formation in the combustion chamber (reduced plant availability and lifetime). In addition, melts occurring in fly ash particles may cause hard deposit formation on cooled furnace walls or heat exchanger tubes. Hard deposit formation due to sticky fly ash particles can be accelerated by alkali and heavy metal salt mixtures (mixtures of alkali chlorides and sulphates with Zn and Pb chlorides) [4].

Herbaceous biomass which contain low concentrations of Ca, Mg and high concentrations of Na and K (Table 2.), start to sinter and melt at significantly lower temperatures than wood fuels. This fact must be considered when selecting the appropriate combustion and temperature control technology [8]. Together with Cl and S, K and Na play a major role in corrosion mechanisms. Moreover, low melting mixtures of alkali and heavy metal chlorides can also cause corrosion by sulphation reactions. During combustion, a fraction of the ash-forming compounds in the fuel is volatilised (especially K, Na, S, Cl, Zn, Pb, Cd, to some degree also refractory species like Ca, Mg and Si) and released to the gas phase. The volatilised fraction depends on the chemical composition of the fuel, the surrounding gas atmosphere, the local temperature and the combustion technology in use. For instance, high combustion temperatures and a reducing atmosphere enhance the volatilisation of the environmentally relevant heavy metals Zn, Pb and Cd. By subsequent nucleation or condensation, these volatiles, together with a solid phase sub-micron particles released from the fuel bed, form fine fly ash particles (aerosols) with sizes between 1 nm and 1 mm. They mainly consist of K, Na, S and Cl. Due to the high volatility of Cd, Zn and Pb amounts of these heavy metals can also be present in the aerosol fraction depending on the heavy metal concentration in the fuel [4].

4. RESULTS

Higher heating value (HHV) is one of the main biomass indicators as it refers to the heat released from the fuel during combustion. In Fig. 2. and Fig. 3. by comparing carbon (C%) and hydrogen (H%) content in different types of solid biofuel to higher heating value, it is seen that by increasing H or C content (%) in biofuel, higher heating value increases. This is because C and H are oxidised during combustion by exothermic reactions (formation of CO_2 and H_2O) and content of C and H contributes positively to the HHV.

Table 1. Ultimate analysis of woods, herbaceous and agriculture waste

Parameter	*HHV*	*Ash*	*C*	*H*	*N*	*S*	*O*
Units	*kJ/kg*	%					
Woody biomass							
Alder (wood+bark)	19658	0.84	49.08	5.94	0.34	0.00	43.20
Ashwood (wood+bark)	19433	1.35	49.00	5.84	0.27	0.00	42.81
Oak (wood+bark)	19550	0.56	48.28	5.93	0.21	0.00	44.28
Birch (wood+bark)	19930	0.86	49.55	6.06	0.30	0.00	42.78
Oak (briquettes)	19915	0.32	49.72	6.04	0.29	0.00	44.12
Black Alder (briquettes)	20200	1.49	50.08	6.29	0.35	0.02	43.85
Herbaceous biomass							
Miscanthus giganteus	18747	4.85	46.82	5.83	0.84	0.08	42.34
Reed (pellets)	19014	5.03	47.26	5.83	0.42	0.06	42.36
Rape straw (pellets)	18756	5.80	46.90	5.88	1.08	0.10	40.82
Wheat straw (pellets)	18727	8.86	46.75	5.94	0.59	0.07	42.18
Barley straw (pellets)	17814	5.91	44.99	5.68	0.90	0.10	40.81
Wheat straw	18417	7.00	45.06	5.77	0.60	0.05	41.66
Other residues of biomass							
Walnut shell (briquettes)	20870	1.87	51.23	6.03	0.77	0.04	40.53
Coconut shells	20652	8.45	50.48	6.75	1.04	0.12	38.14

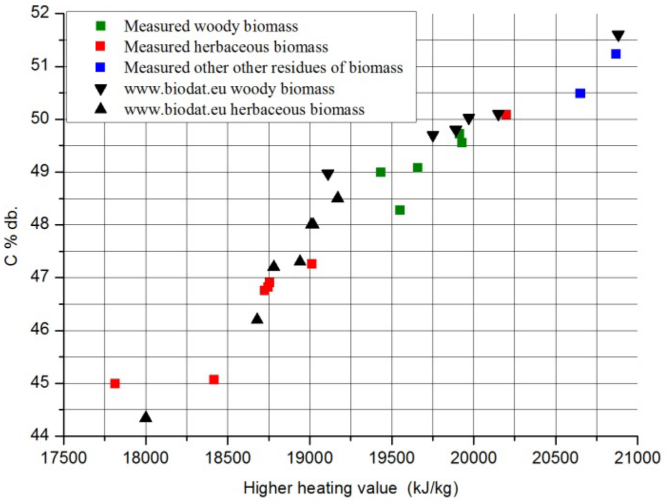

Fig. 2. Carbon content (% db.) and HHV (kJ/kg) in different solid biomass

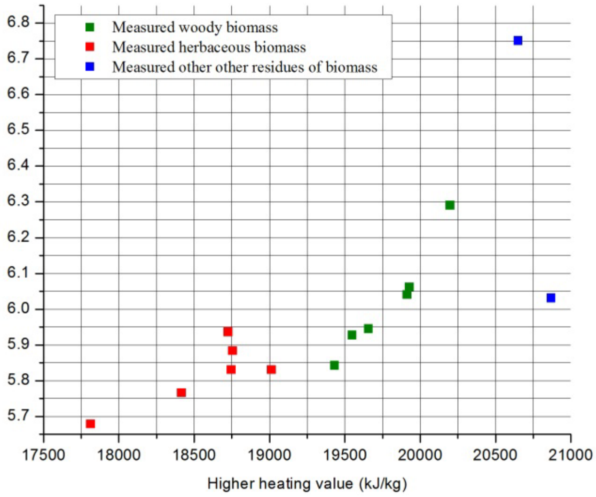

Fig. 3. Hydrogen content (% db.) and HHV (kJ/kg) in different solid biomass

Higher heating value is higher in woody biomass than in herbaceous biomass Fig. 4., because of higher carbon and hydrogen content (Fig. 5. and Fig. 6). It is seen in Fig. 4. that the lowest heating value is in the herbaceous biomass. Woody biomass has a higher heating value and the highest heating value is found in other residues of biomass (walnut and coconut shells).

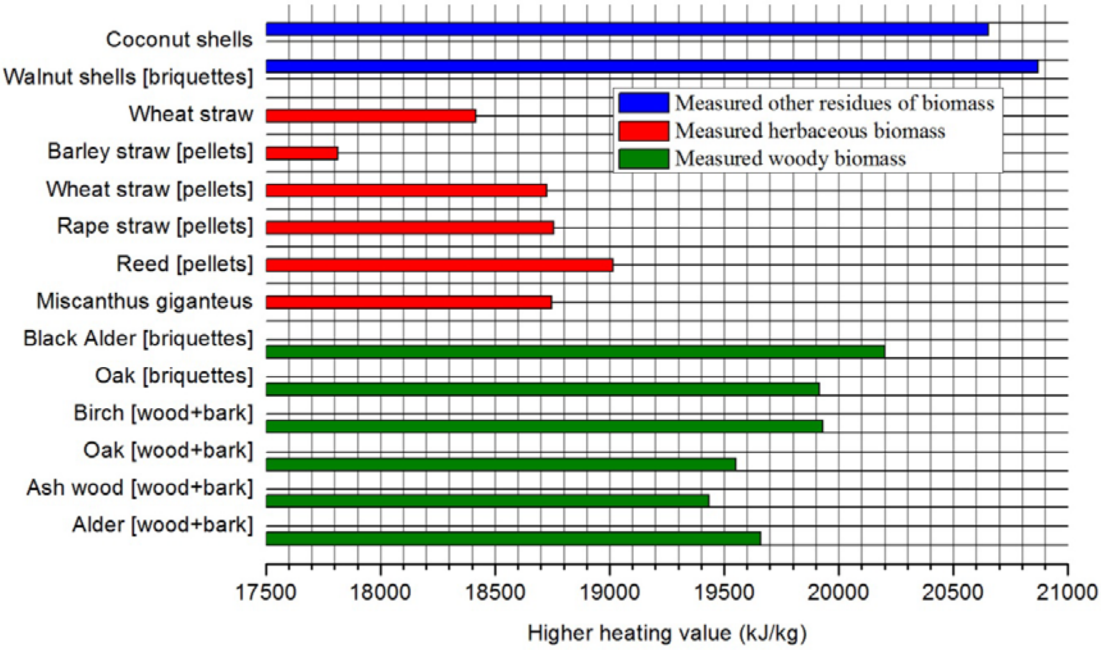

Fig. 4. HHV (kJ/kg) in different solid biomass

The main material properties of interest of biomass as an energy resource are also taken in to the investigation. Fig. 5-10 shows the main characteristics of reference fuels. In these figures the element analysis C, H, N, S, O and ash content of different type of biomass are presented. It is seen that woody biomass has a noticeably higher carbon, hydrogen and oxygen content than herbaceous biomass. In other hand, herbaceous biomass has a higher content of nitrogen and sulphur.

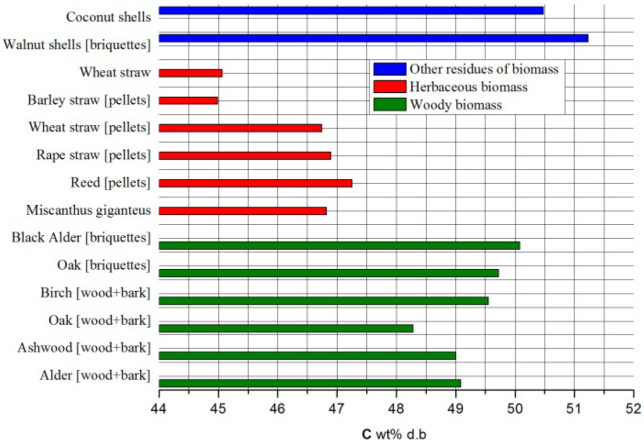

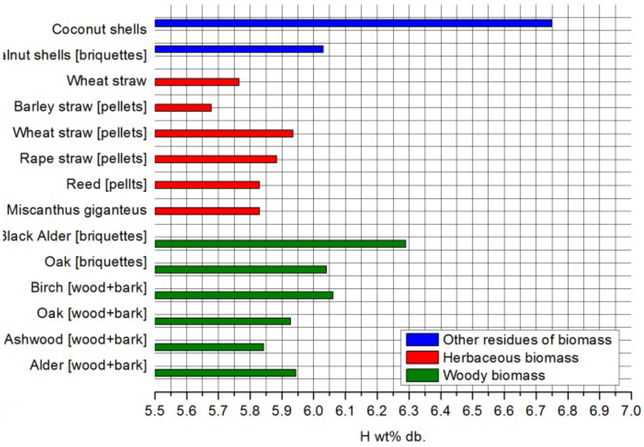

Fig. 5. Carbon content (% db.) in different solid biomass

Fig. 6. Hydrogen content (% db.) in different solid biomass

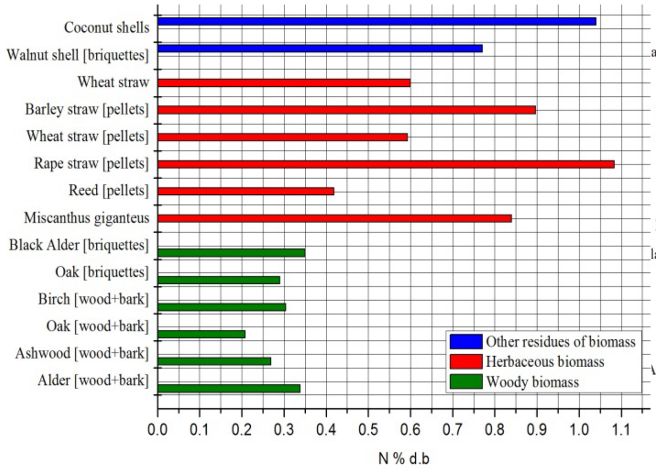

Fig. 7. Nitrogen content (% db.) in different solid biomass

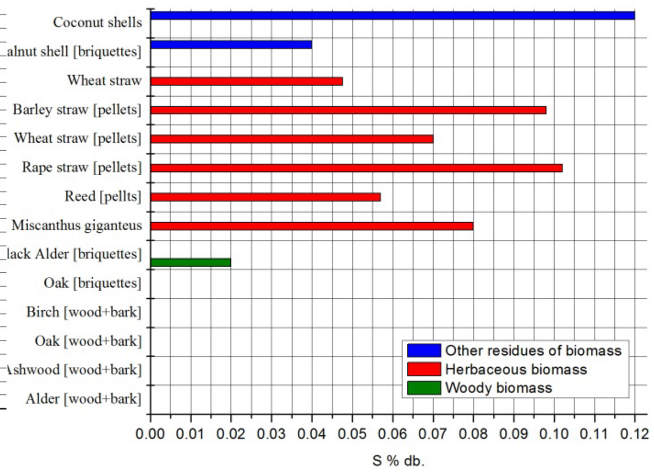

Fig. 8. Sulphur content (% db.) in different solid biomass

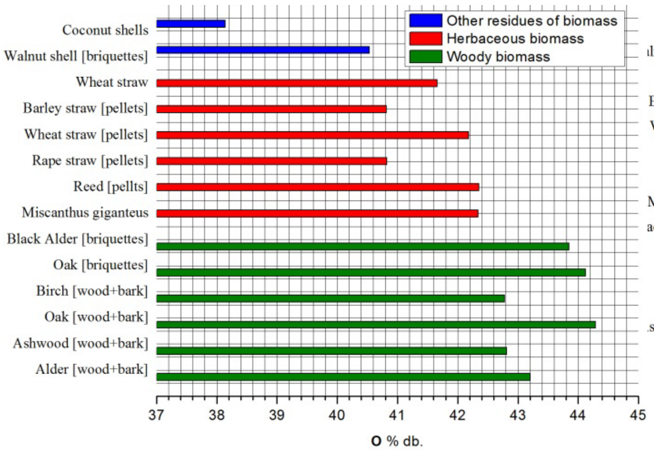

Fig. 9. Oxygen content (% db.) in different solid biomass.

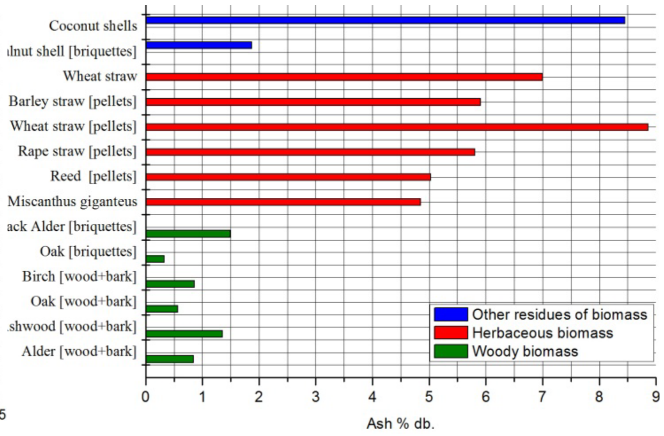

Fig. 10. Ash content (% db.) in different solid biomass

Fig. 11–14 show some of the most important trace elements in the reference fuels. Table 2 shows the major and minor elements (ash-forming elements) characteristics of the reference fuels. The data are presented as average values. The ash-forming elements such as Ca, Fe, K, Mg, Na and Ti in biomass are especially important for any thermochemical conversion process. Major elements content is significantly lower in woody biomass compared to herbaceous and other residues of biomass. This is because woody biomass accumulates major and minor elements in roots and leafs, while herbaceous biomass accumulates in whole plant. Because main ash forming elements are found in herbaceous biomass

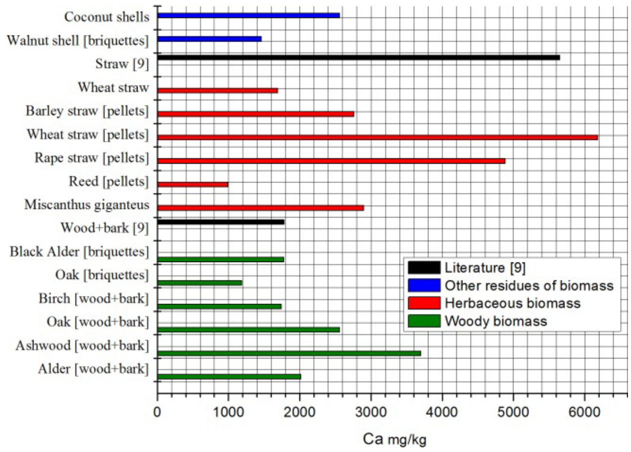

Fig. 11. Ca content (mg/kg) in different solid biomass

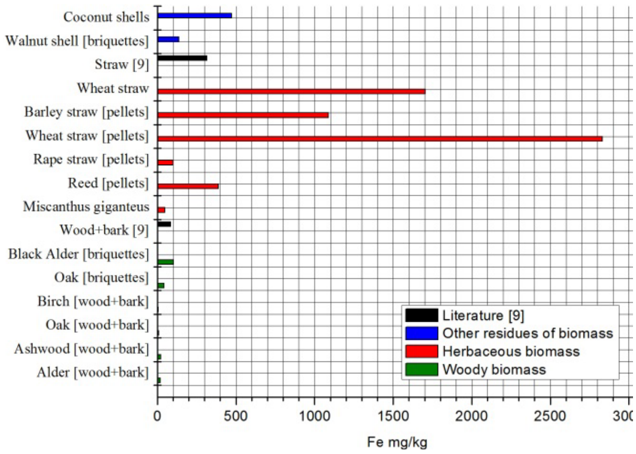

Fig. 12. Fe content (mg/kg) in different solid biomass

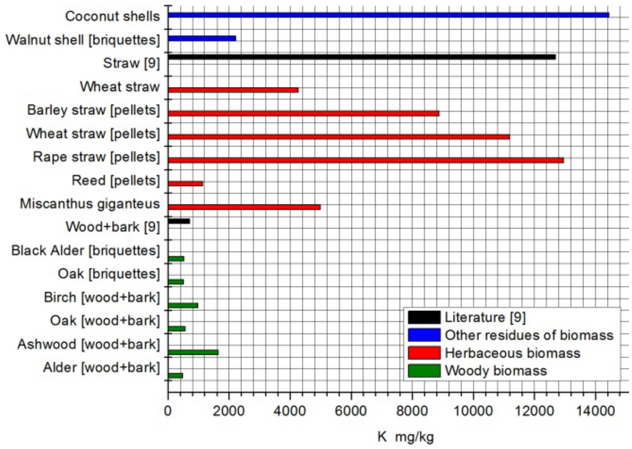

Fig. 13. K content (mg/kg) in different solid biomass

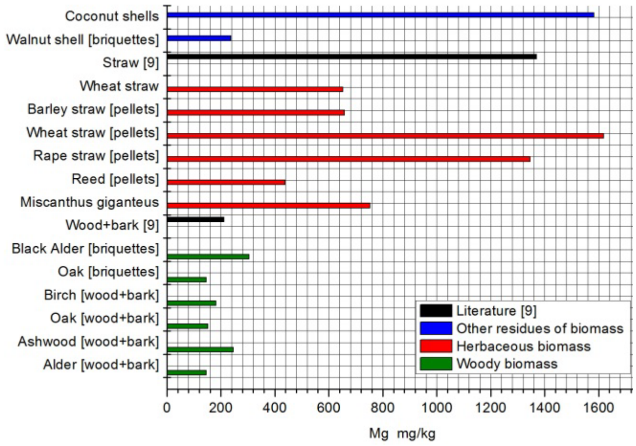

Fig. 14. Mg content (mg/kg) in different solid biomass

Table 2. Major and minor elements in different biomass

Element content (mg/kg)	Ca	Fe	K	Mg	Na	Ti	As	Ba	Cd	Co	Cr	Cu	Li	Mn	Mo	Ni	Pb	Sb	Se	V	Zn
Alder [wood+bark]	2018	17.99	490	145	6.4	0.763	0	5.201	0.22	0.073	0.00	0.953	0.468	10.63	0.394	0.735	3.074	1.105	2.699	0.806	6.92
Ashwood [wood+bark]	3697	22.37	1647	246	75.0	1.175	0	11.24	0.496	0.243	0.00	1.659	5.217	6.415	0.828	2.352	7.405	4.48	11.04	0.927	5.344
Oak [wood+bark]	2556	9.494	562	151	14.5	0.413	0	20.67	0.259	0.077	0.00	1.118	0.62	86.71	0.418	1.096	2.34	1.45	2.464	0.554	1.002
Birch [wood+bark]	1739	6.749	985	182	5.4	0.194	0	4.71	0.251	0.074	0.00	1.739	0.953	7.089	0.525	0.917	1.868	1.623	3.15	0.515	74.46
Oak [briquettes]	1187	41.52	515	146	61.0	5.003	0	0.605	0.483	0.336	0.00	0.605	4.167	29.98	0.8	2.093	5.731	4.22	12	1.215	4.671
Black Alder [briquettes]	1776	103.3	519	304	11.7	6.865	0	4.706	0.315	0.205	0.00	5.989	3.881	26.78	0.976	1.612	1.798	1.799	4.253	1	8.732
Miscanthus giganteus	2897	47.58	4990	752	111.0	2.386	0	12.46	0.55	0.156	0.41	9.624	2.932	73.61	1.567	2.932	4.533	4.177	10.48	1.42	14.41
Reed [pellets]	991	388.35	1140	437	428.5	12.690	0	11.4	0.324	0.167	16.64	1.206	3.474	37.87	1.139	3.09	12.28	4.308	10.18	1.773	22.42
Rape straw [pellets]	4885	99.73	12960	1346	0.7	4.837	0	24.97	0,0	0,0	4.92	1.112	1.347	14.62	0.981	2.412	0.812	1.242	2.783	1.823	17.92
Wheat straw [pellets]	6180	2830	11190	1618	270.7	49.320	0	42.54	0,0	0.368	5.95	3.435	2.095	37.97	6.885	4.108	10.98	4.115	9.33	3.45	21.46
Barley straw [pellets]	2760	1089	8882	658	47.2	21.760	0	27.1	0.07	0.37	1.76	21.8	2.132	28.69	2.046	4.922	10.18	2.651	6.618	1.563	19.88
Wheat straw	1689	1703	4273	652	0.7	4.106	0	31.62	0.389	0.101	0.00	8.062	14.26	11.96	1.8	1.477	3.255	1.892	7.208	1.108	14.37
Walnut shell [briquettes]	1461	136.9	2221	237	4.5	2.533	0	3.025	0.105	0.113	0.00	1.759	0.852	11.87	0.493	1.297	2.295	2.124	4.77	0.835	4.228
Coconut shells	2558	473.1	14440	1583	91.3	31.480	0	6.357	0.437	0.258	0.00	14.42	2.397	33.88	0.311	3.857	3.125	10.65	39.8	3.286	38.81

CONCLUSIONS

The chemical properties of different kinds of solid biofuels effect their thermal utilization therefore characterization of these fuels is important step in solid biofuel research and development in new thermochemical conversion technologies.

By comparing major elements in different types of solid biofuels, it is seen that woody biomass have higher carbon (C) and hydrogen (H) concentration compared to herbaceous biomass, therefore woody biomass has higher heating value which positively correlates with C and H content in fuel.

The ash content influences the choice of appropriate combustion technology and deposit formation, fly ash emissions and the logistics concerning ash storage and utilization therefore determination of major elements which are responsible for ash formation have significant role in solid biofuel research. Sulphur (S), calcium (Ca), iron (Fe), magnesium (Mg), potassium (K), sodium (Na), concentrations are higher in herbaceous biomass, therefore ash content in these biofuels are higher compared to woody biomass.

Experimental results well corresponds to those found in literature, therefore further research in solid biofuel and their influence to combustion process have to be done.

Further research

- Determination of ash melting point of different solid biofuels has to be made, in order to determine the main elements which are responsible for ash melting point.
- Determination of combustion products of different sold biofuel using TGA-GC/MS.
- Experimental combustion chamber development for solid biofuel combustion research.

REFERENCES

1. http://epp.eurostat.ec.europa.eu/portal/page/portal/statistics/search_database [accessed 2012.02.20].
2. A. Demirbas. Combustion characteristics of different biomass fuels. Progress in Energy and Combustion Science 30 (2004), p. 219–230.
3. E. Alakangas., J. Valtanen., J.E. Levlin. CEN technical specification for solid biofuels—Fuel specification and classes. Biomass and Bioenergy 30 (2006), p. 908–914.
4. I. Obernberger., T. Brunner., G. Barnthaler. Chemical properties of solid biofuels—significance and impact. Biomass and Bioenergy 30 (2006), p. 973–982.
5. S.V. Vassilev, D. Baxter, L.K. Andersen, C.G. Vassileva. An overview of the chemical composition of biomass. Fuel 89 (2010), p. 913–933.
6. Z.A. Mayer., A. Apfelbacher., A. Hornung. Effect of sample preparation on the thermal degradation of metal-added biomass. Journal of Analytical and Applied Pyrolysis. Article in press.
7. Van Loo S, Koppejan J, editors. Handbook of biomass combustion and co-firing. IEA BIOENERG Y TASK 32; 2002, p. 171–213 (ISBN 9036517737).
8. Nussbaumer T. Combustion and co-combustion of biomass. In: Proceedings of the 12th European biomass conference, Vol. I; 2002, p. 31–7 (ISBN 88-900442-5-X).
9. G. Baernthalera., M. Zischkab., C. Haraldssonc, I. Obernberger. Determination of major and minor ash-forming elements in solid biofuels. Biomass and Bioenergy 30 (2006), p. 983–997.
10. J. Miles, T.R. Alkali. Deposits found in biomass power plants. Research report NRE1/TP-443-8142 SAND96-8225, Vols. 1 and 2. Oakridge, USA: National Renewable Energy Laboratory; 1996.

CYSENI 2012, May 24–25, Kaunas, Lithuania
ISSN 1822-7554, www.cyseni.com

RADIATION INDUCED PLASMA TECHNOLOGY IN ENVIRONMENT PROTECTION

A.G. Chmielewski, A. Pawelec, S. Witman
Institute of Nuclear Chemistry and Technology
16 Dorodna Street, 03-195 Warsaw, Poland
Phone +48 225041164
Email:s.witman@ichtj.waw.pl

ABSTRACT

Various types of pollutants are emitted into the atmosphere in result of combustion processes. Sulphur and nitrogen oxides which are emitted during the combustion of fossil fuels in energy generation and metallurgy are the most important pollutant. Although the methods for purification of exhaust gases with use of cold plasma are still at an early stage of development, they seem to be very competitive comparing to conventional methods. They are among of the most promising next-generation technologies. The purification methods can be divided into technologies using electrical discharges or electron beam. Flue gas treatment by radiation method, that uses an electron beam, is one of the leading plasma technologies. Radiation technology allows for simultaneous removal of SOx, NOx, HCl, dioxins, furans, mercury and decomposition of volatile organic compounds (VOCs). Removal of pollutants in the same process can reduce investment and operating costs and because of the agricultural use of by-product (as a fertilizer) the process becomes a waste-free process. The paper covers an introduction to plasma technologies and description of selected technologies to be applied in environmental processes. On this background the experience gained during the construction and operation of the demonstrative industrial installation of flue gases treatment by electron beam in Pomorzany Power Station (Poland) as well as future perspective of environmental plasma technologies will be presented.

Keywords: Plasma technology, exhaust gas purification

1. BASIC INFORMATION ABOUT PLASMA

Plasma is often called the fourth state of matter and it is a term assigned to gas, which is ionized. However, due to the fact that over 99.9% of matter in the universe is in plasma state, can be concluded that we should call it the first state of matter. Actually, the plasma is an ionized gas in which atoms have lost one or more electrons, and thus acquired an electric charge. [1]

Plasma occurs in a very wide range of average particle kinetic energy – from 0.2 eV to 2MeV. Therefore, the fundamental classification of plasma is a division on:

- low-temperature plasma, non-thermal, known colloquially as "cold" or electric discharge plasma,
- high temperature, "hot". [2]

Low-temperature plasma is a gas with a relatively small contribution of ionized particles and high content of neutral particles. Another feature is the different temperature of components, ie the lack of thermal equilibrium.

It is assumed that non-thermal plasma occurs in the temperature range from 300 K to 4000 K, but the electrons temeprature can reach up to 30 000 – 50 000 K and few times exceed another particles temperatures. It also called nonequilibrium plasma or cold plasma, because plasma temperature is quite low and electron temperature is high. Most of the energy supplied to the system is used to heat the electrons but not the entire volume of gas. In the non-thermal plasma, the plasma energy is directed to dissociation caused by collisions with electrons and ionization of the gas in order to produce radicals that break down toxic gas molecules.

All methods of producing free radicals, electrons, ions, and all extremely reactive particles can be divided into two basic methods:

- an electrical discharge – this method involves ionization of the gas directly in the area between electrodes above a certain critical potential of ionization.
- electron beam – a method based on the introduction of high-energy electron beam into the reaction medium. [3, 4]

1.1. The ways of plasma generation.

Non-thermal plasma in the gas stream at atmospheric pressure can be generated in several ways:

- with high-energy electron beam (EBFGT – electron beam flue gas treatment),
- generation of discharge through appropriate high voltage applied to two electrodes (gas discharge),
- generation of plasma by using microwaves. [3, 4]

The process of plasma generation by use of electron beam is based on ionization.

Depending on the applied voltage, we can get different types of discharges (such as a corona discharge, glow discharge, arc discharge).

Dielectric barrier discharge (DBD) is one of the most commonly used in cold plasma technology, which is often carried out at atmospheric pressure. In order to occurrence of a barrier discharge, the presence of the dielectric barrier placed on a high-voltage electrode, rarely on both electrodes, or between them, thus forming one or more discharge space, is necessary [5].

2. COLD PLASMA APPLICATIONS IN THE ENVIRONMENT PROTECTION

Non-thermal plasma, generated in barrier discharges, is used in the processes of sterilization and disinfection of solid, liquid and gas media. It also has numerous advantages and the most important are: the lack of harmful to the environment waste products, and the ability of plasma treatment at atmospheric pressure and at ambient temperature.

Among the environmental applications, the most technologically advanced and applied in practice is the potable water treatment technology. Other environmental applications of ozone generated in the barrier discharges in air or oxygen include:

- sterilization of air, water, soil, surface and packages,
- removal of nitrogen oxides (NO_x), sulphur dioxide (SO_2) and volatile organic compounds (VOCs) in the broad sense of combustion processes,
- removal of volatile organic compounds (VOCs) generated in the process of painting, varnishing, hospital waste incineration and other chemical processes,
- recycling and disposal of pollutants - decomposition and combustion of organic waste, volatile and solid exhaust from the engines.

Conventional methods of limiting the amount of pollutants emitted into the atmosphere had already exhausted its maximum potential. Further improvement does not imply the cost reduction of a flue gas treatment. The sharpening legislation on limits for concentrations of pollutants in the gas stream released into the atmosphere is another factor accelerating the development of gas cleaning technologies. Next-generation technologies are different from the traditional because of effective removal of contaminants from transforming them into economically useful products while maintaining favorable economic conditions. [6]

During the combustion processes, all kinds of pollutants are emitted into the atmosphere. Among the most important are sulphur and nitrogen oxides, emitted especially during the combustion of fossil fuels in power and metallurgy sector. The removal of these impurities by conventional methods require complicated installations combining various methods of removing impurities. All these technologies are complex chemical processes related with the formation of waste (gypsum, wastewater, spent catalyst) as well as costly (the cost of raw materials, energy, service and location). [6]

Later of this chapter will be given the key parameters of the industrial plant of flue gas treatment by electron beam located in the “Pomorzany” Power Plant in Poland (established in 1999).

2.1. The “Pomorzany” Power Plant, EBFGT description

The idea of using radiation system for exhaust gases purification was established in Japan in the 60s. Further work, besides Japan, were conducted at leading research centers in the world, including in Germany, USA and of course in Poland, where the Institute of Nuclear Chemistry and Technology in Warsaw participated in developing of this technology. After a series of laboratory and pilot research, the technology was implemented on an industrial scale in the “Pomorzany” Power Plant in Szczecin, belonging to the Dolna Odra Power Plant Group. It was the first in the world this kind of building (plants built in China was developed with marginal removal of NO_x), which is particular importance because of operational experience in the industry.

Fig. 1. View of the “Pomorzany” Power Plant

The essence of the purification of exhaust gases from sulphur and nitrogen oxides is the oxidation of SO_2 and NO to SO_3 and NO_2 respectively, and then in the reaction with steam and ammonia – production of aerosol of ammonium sulphate and ammonium nitrate. Organic compounds are broken down into simpler, less toxic substances, which can be isolated in a traditional precipitator and used as a fertilizer, so this process becomes a waste-free.

Accelerators installed in the reaction chambers are designed to provide the energy necessary for the process. The process consists of four main steps realized in the following nodes installation:

1. Flue gas conditioning.
2. Storage and dosage of reagent – ammonia.
3. Reaction system.
4. Collection and storage of by-product.

Fig. 2. Accelerator applied in the “Pomorzany” EBFGT Plant

Exhaust gas stream before entering the system is initially removed solid impurities, which could be deposited in the system and cause deterioration of the product. Then the gas is sending to the gas humidification tower, where by the heat and mass transfer of drops of water sprays followed by its cooling below 80° C and moisture to more than 12% vol. Media flow is co-current. In the case of too low humidity of inlet gases, adjustment of the humidity at the outlet of the humidification tower by the addition of steam is possible. Ammonia, which is the main reactant of the process, is stored in the form of ammonia water, and is injected into the flue gas humidification column.

Fig. 3. Reaction chamber used in the installation EBFGT in “Pomorzany”

After the addition of ammonia, exhaust gases are entered into the reaction chamber, where they are irradiated by electron beam. In the reaction chamber, inorganic pollutants are oxidising and forming ammonium salts and decomposing volatile organic contaminants. The by-product is received and stored in the electrostatic precipitator in order to transfer to recipient. The product can be used as a fertilizer alone or in the form of mixtures (NPK – fertilizers containing nitrogen (N), phosphorus (P) and potassium (K)). The resulting product as a mixture of sulphate and ammonium nitrate meets all the standards required for this type of fertilizer.

A very important feature of the installation of flue gas treatment by radiation is its very high flexibility. The previous operation was conducted in the flow from 100 000 to 270 000 Nm^3/h. This range is unparalleled in conventional systems. [7]

The maximum efficiency of the system may reach 95% for SO_2 and 70% for NO_x. Under ideal conditions, was observed even higher pollutant removal efficiency (corresponding to 98 and 78%), but generally the operation of the system is optimized to current needs resulting from the emission standards and lower values are maintained. [8] It should be noted that the degree of desulfurization in “wet” installations is in the range 95 to 98%, and the degree of removal of NO_x in the SCR systems reaches 70 - 80%. In turn, if we use other methods of removing nitrogen oxides - the methods of non-catalytic reduction (SNCR) - its efficiency is only about 50%. By-product formed in the flue gas cleaning process is a valuable fertilizer containing two major components of plant nutrients - nitrogen and sulphur. The presence of easily available sulphur in the fertilizer increases its value (recent deficit of sulphur is observed in soil). The product contains total nitrogen in the amount of 24 - 27%, including about 20% of ammonia nitrogen. These are the parameters in accordance with the standard for this type of fertilizer. It follows that the by-product can be used for fertilizer alone, or as a substrate for formation of compound fertilizer.

The main advantages of the installation are:

1. High pollutant removal efficiencies comparable with that of the conventional system. Maximum efficiency is at least 95% removal of SO_2 and 70% removal of NO_x.
2. Simultaneous removal of sulphur and nitrogen oxides from flue gases. In addition, it is proved that this process can also remove other pollutants (volatile organic compounds VOCs, acidic pollutants HCl, HF, dioxins), which allows its application also in other industries that use combustion processes.
3. The high flexibility of the installation operation in relation to changes in process conditions, and especially the intensity of the exhaust stream. The installation can be operated in the range from 100 000 to 270 000 Nm^3/h
4. The simplicity of construction, which together with the relatively small demand of space, facilitates the construction of modernized objects and simplified handling and automation of system.
5. No waste. With the agricultural use of by-product during operation does not produce any solid or liquid waste requiring disposal. Do not form additional costs, and even by selling by-product – the total cost of operation of the installation is reduced.
6. The costs of both capital and operating costs are competitive with conventional flue gas desulfurization and denitrification. Prominent reduction of costs associated with further development of the technology is excepted. [9-12].

Fig. 4. By-product, fertilizer from “Pomorzany” Power Plant

3. SUMMARY

The technology advantages make the method of radiation gas treatment system a competitive solution for the conventional methods in terms of both technological and economic development. Conducted surveys show the applicability for the purification of exhaust gases from combustion processes (broadly defined). Experience gained during the construction and operation of industrial-demonstrative installation of flue gas cleaning in the "Pomorzany" Power Plant will improve further facilities of this type. [6]

Further work on another implementation of this technology, is planned. The Institute of Nuclear Chemistry and Technology in Warsaw cooperate with national and international units in order to promote the use of innovative plasma technologies for environment protection of the Baltic Sea region. The PlasTEP project, headed by the Institute for Plasma Science and Technology in Greifswald, joined 15 partners from 8 countries such as Germany, Denmark, Poland, Lithuania, Latvia, Estonia, Finland, Sweden. By sharing and comparing experiences, the centres participating in the project will form the backbone of a future European centre of environmental friendly plasma technologies (creation of this centre is far-reachning goal of the project). The project participants are working on the development of flue gas cleaning techniques and other greenhouse gases from harmful impurities such as nitrogen oxides, NO_x, SO_x sulfur oxides, volatile organic compounds VOCs, and oil stain removal from seawater.

PlasTEP project is co-funded by the European Regional Development Fund under the Baltic Sea Region program.

PlasTEP

Baltic Sea Region
Programme 2007-2013
Part-financed by the European Union
(European Regional Development Fund)

3.1. Abbreviations

NO_x – nitrogen oxides,
SO_x – sulphur oxides,
SO_2 – sulphur dioxide,
DBD – dielectric barrier discharge
VOCs – volatile organic compounds
SCR – selective catalytic reduction
SNCR – selective non-catalytic reduction
PlasTEP – Plasma of environmental protection project
EBFGT – Electron beam flue gas treatment
INCT – Institute of Nuclear Chemistry and Technology

REFERENCES

1. WARYCH J., Oczyszczanie gazów. Procesy i aparatura, WNT Warszawa.
2. KOGELSCHATZ U., Dielectric-barrier Discharges: Their History, Discharge Physics, and Industrial Application, Plasma Chemistry and Plasma Processing, 2003, Vol. 23, No. 1
3. JAWOREK A., CZECH T., KRUPA A. i in., Kierunki rozwoju elektrostatycznych urządzeń do oczyszczania gazów odlotowych, V Konferencja Naukowo-Techniczna, 2000.

4. MULLER S., ZAHN R., Air Pollution Control by Non-Thermal Plasma, Contributed Plasma Physics, 2007, Vol. 47, No. 7.
5. DORS M., Oczyszczanie gazów odlotowych z tlenku azotu za pomocą plazmy nietermicznej z reakcjami heterogenicznymi, Wydawnictwo IMP PAN, 2008.
6. CHMIELEWSKI A.G., PAWELEC A., WITMAN S., Plasma for environment, Guideline on plasma technologies in environmental protection, 2011.
7. JOSHI S.S., The decomposition of Nitrous Oxide in the Silent Electric Discharge, Transactions of the Faraday Society, 1927, Vol. 23.
8. CHMIELEWSKI A.G., et al., Operational experience of the industrial plant for electron beam flue gas treatment, Radiation Physics and Chemistry, 2004, Vol. 71, p. 439–442.
9. IAEA in collaboration with CHMIELEWSKI A.G., HAN B., SABHARWAL S., Radiation Processing: Environmental Application, *International Atomic Energy Agency*, Vienna, 2007, p. 65–67.
10. CHMIELEWSKI A.G., LICKI J., Application of electron beam from accelerator to purification of exhaust gases from combustion of high-sulphur fossil fuel, Environment Protection Engineering, 2008, Vol. 34, No. 4.
11. CHANG J.-S., *Physics and chemistry of plasma pollution control technology*, Plasma Sources Science Technology, 2008, Vol. 17.
12. KIM S.J., CHANG J.-S., SUENTP code simulations of scale-up and economic evaluation of non-thermal plasma technology for exhaust gas emission control of coal fired plants, Proceedings, 1998, ICESP VII.

CYSENI 2012, May 24–25, Kaunas, Lithuania
ISSN 1822-7554, www.cyseni.com

THE EFFECT OF CROSSED ELECTRIC AND MAGNETIC FIELDS ON ION NITRIDING IN A GLOW DISCHARGE

R.K. Vafin, K.N. Ramazanov
Ufa State Aircraft Engineering University
K. Marx 12, 450008 Ufa – Russia
Phone +73472730763
Email: vafinrk@mail.ru

ABSTRACT

The method of nitriding tool steels in a glow discharge with a magnetic field is considered. The influence of the magnetic field and spatial arrangement of samples of tool steels on the structural-phase composition and surface microhardness is evaluated. The properties of glow discharge in the magnetic field are studied. Volt-ampere and probe characteristics of the glow discharge in crossed electric and magnetic fields have been investigated and the modes of ion nitriding have been established.

Keywords: Crossed electric and magnetic fields, ion nitriding, glow discharge, magnetic field, plasma, intensification of ion-plasma nitriding

1. INTRODUCTION

In order to raise the endurance of tools their surface is modified by various methods, including ion-plasma nitriding characterized by such features as controllability and ecological safety [1, 2].

In ion nitriding the parts are heated to the nitriding temperature due to the energy of gas ions bombarding the surface at simultaneous diffusion of nitrogen ions into the treated surface. The processes in the plasma of glow discharge (dissociation, excitation, ionization, etc.) occur in what is known as the region of cathode drop [3]. One of the factors capable to activate these processes may be superposition of the magnetic field on the glow discharge, which is used successfully in various gas discharge systems [4, 5].

The aim of the present work was to investigate the effect of the magnetic field on the ion nitriding process, on the microstructure, on the phase composition, and on the microhardness of the surface layer of tool steels R6M5 and Kh12.

2. METHODOLOGY

In order to study the process of ion nitriding and the characteristics of glow discharge in magnetic field we used an experimental installation created on the base of a commercial ELU – 5 facility. The facility was equipped with a pulse energy source of type ApEl-M-5PDC, which allowed us to lower the heat load on the electrodes and provided effective arc extinction in a mode of anomalous glow discharge. We placed a standard magnetron (450 x 50 x 100 mm) with magnetic field induction B = 0.03 T in a vacuum chamber of an installation (Fig. 1). The parameters of the discharge were obtained from the readings of the switching power supply display.

We subjected test pieces of tool steels R6M5 and Kh12 after hardening and tempering at 600°C to nitriding.

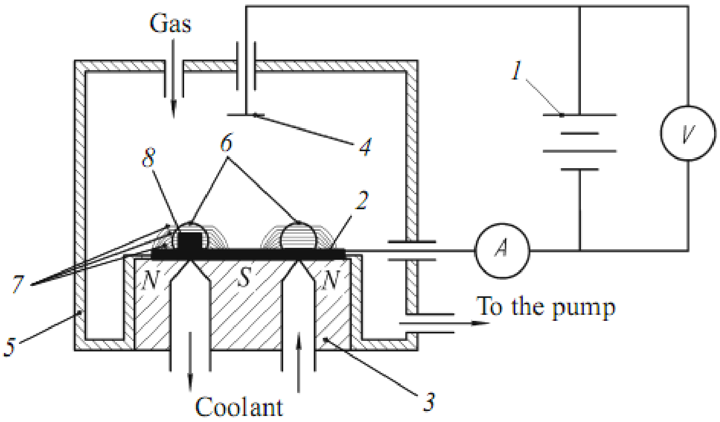

Fig. 1. The Scheme of performance of tests in ELU-5 facility: 1) supply of glow discharge; 2) cathode; 3) magnetron; 4) anode; 5) vacuum chamber; 6) toroidal domain of bright glow; 7) magnetic field lines; 8) test piece

The working gas was a mixture of nitrogen, argon, and acetylene (75% N_2 + 20% Ar + 5% C_2H_2). The acetylene was used for deactivating the retained oxygen and preventing formation of an oxide film on the surface of the steel, which hinders formation of nitrided layer.

The pressure of the working gas was varied in the range of 5–200 Pa and controlled with the help of a VIT-3 vacuum gage. The working temperature (490–510°C) was attained in 2–3 min. The temperature of the test pieces was measured using a Termiks optical pyrometer.

The microhardness of the surface of the test pieces was measured using a Micromet 5101 microhardness meter at a load of 0.49 N. The x-ray diffraction studies were performed with the help of a Shimadzu XRD-6000 diffractometer. The microstructure of the hardened layer was studied under a GSM 6390 (JEOL) scanning electron microscope after etching the laps in a 4% solution of nitric acid in ethyl alcohol.

3. RESULTS AND DISCUSSIONS

The presence of magnetic field at a specific proportion of the discharge voltage to the pressure of the plasma forming gas causes growth in the discharge current and some decrease in the voltage (Fig. 2).

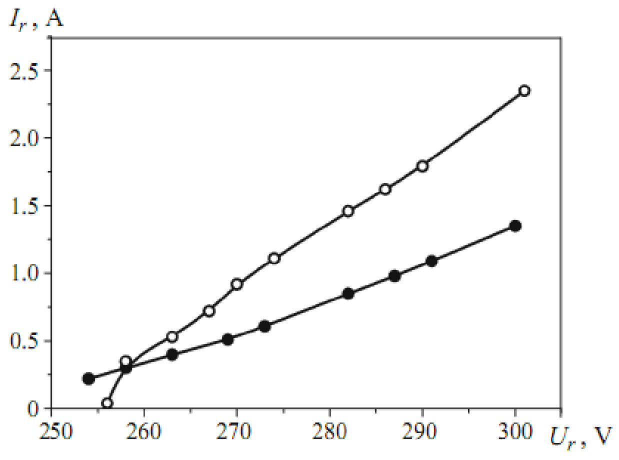

Fig. 2. Volt-ampere characteristics of glow discharge at pressure 200 Pa in the chamber for steels R6M5 and Kh12: o) with the magnetic field;●) without the magnetic field

The growth in the discharge current is stimulated by intensification of the generation of charged particles by the oscillating electrons in the cathode region; the number of ions bombarding the surface increases and so does the number of electrons emitted by the cathode [6].

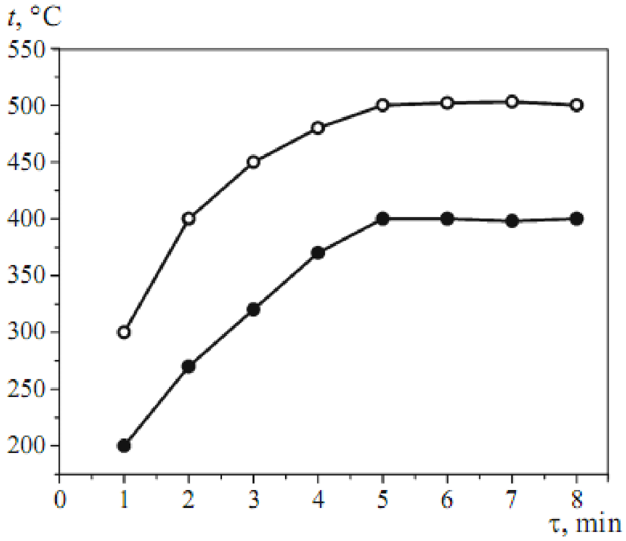

Fig. 3. The temperature of the surface of test pieces of steels R6M5 and Kh12 as a function of heating time in ion nitriding (discharge voltage 550 V; pressure in the chamber 50 Pa): o) with the magnetic field; ●) without the magnetic field

Analyzing the dependence of the temperature of the surface on the heating time we established that the use of magnetic field makes it possible to raise the temperature and the rate of heating. The maximum temperature in glow discharge treatment without the magnetic field at a pressure of 50 Pa and a voltage of 550 V amounts to 400°C (Fig. 3). The magnetic field increases the discharge current and thus promotes growth in the maximum surface temperature to 500°C.

The measurement results of of the microhardness of the studied steels show that after ion nitriding with the application of magnetic field the microhardness on the surface of steel Kh12 amounts to 2100 HV; that on the surface of steel R6M5 is 1950 HV. High level of hardness is a result of formation of fine dispersed nitride particles of alloying elements (Cr, Mo, W, V) on the surface of steels. It is known [1] that the nitride forming elements increasing the microhardness of the surface hinder the diffusion of nitrogen and decrease the thickness of the nitrided layer.

The application of magnetic field accelerates noticeably the formation of nitrided layer.

According to the data of [2], 3-h gas nitriding of steel R6M5 yields a hardened layer with a thickness of at most 25 μm. After nitriding in glow discharge with the application of the magnetic field for 4 h the thickness of the layer is 200 μm (Fig. 4a), which means that the process is quite efficient.

We understood the total thickness of the nitrided layer as that of the layers visible under the microscope, i.e. the nitride and diffusion ones. The nitride layer is formed by nitrides of the alloying elements and looks like a virtually structureless one. The diffusion sublayer is represented by nitrogen ferrite with carbide and fine nitride inclusions. According the data of an x-ray diffraction analysis the surface of steel R6M5 gives reflections of a Fe_3N ε-phase and of CrN nitride (Fig. 5b).

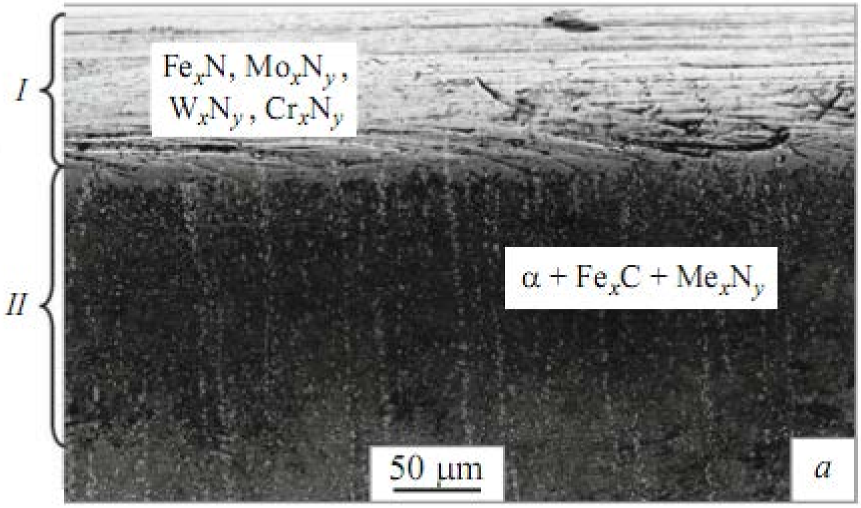

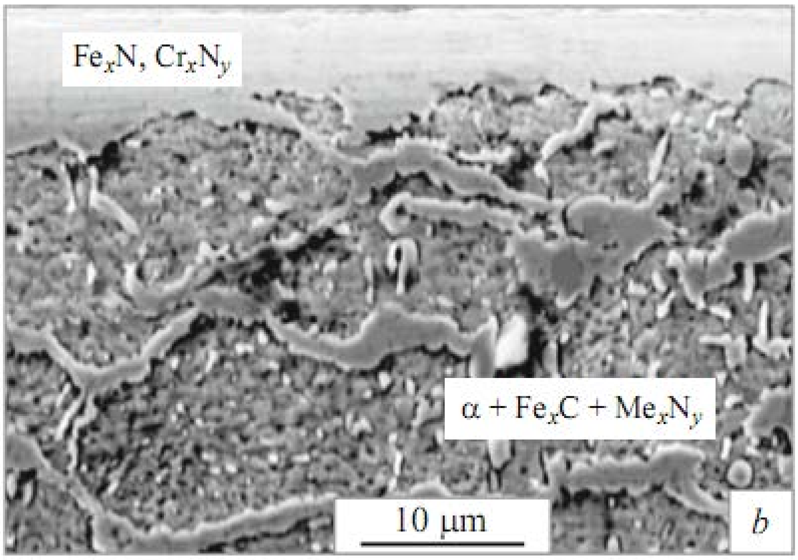

Fig. 4. The microstructure of the nitrided layer of steels R6M5 (a) and Kh12 (b): a) x 270; b) x 2000

On steel Kh12 treated in the same mode the formed nitrided layer is thinner (10 - 15 µm, Fig. 4b), which may be explained by high content of chromium and carbon in it. It is possible that the formation of a dense layer of chromium nitrides hinders the diffusion of nitrogen and the growth of the diffusion sublayer.

The thickness of the nitride layer on steel Kh12 after nitriding with the application of magnetic field for 4 h is 10 µm; that for steel R6M5 is 80 µm. Diffraction analysis shows (Fig. 5d) that the thin nitride zone of the nitrided layer on steel Kh12 consists of the particles of Fe_3N ε-phase and of chromium nitride (CrN). Due to the presence of acetylene in the gas atmosphere we observed the reflections of iron carbides (Fe_3C) on the surface of the test pieces. The peaks of the a iron broaden and become less intense after nitriding, which implies the presence of retained compressive stresses in the nitrided layer.

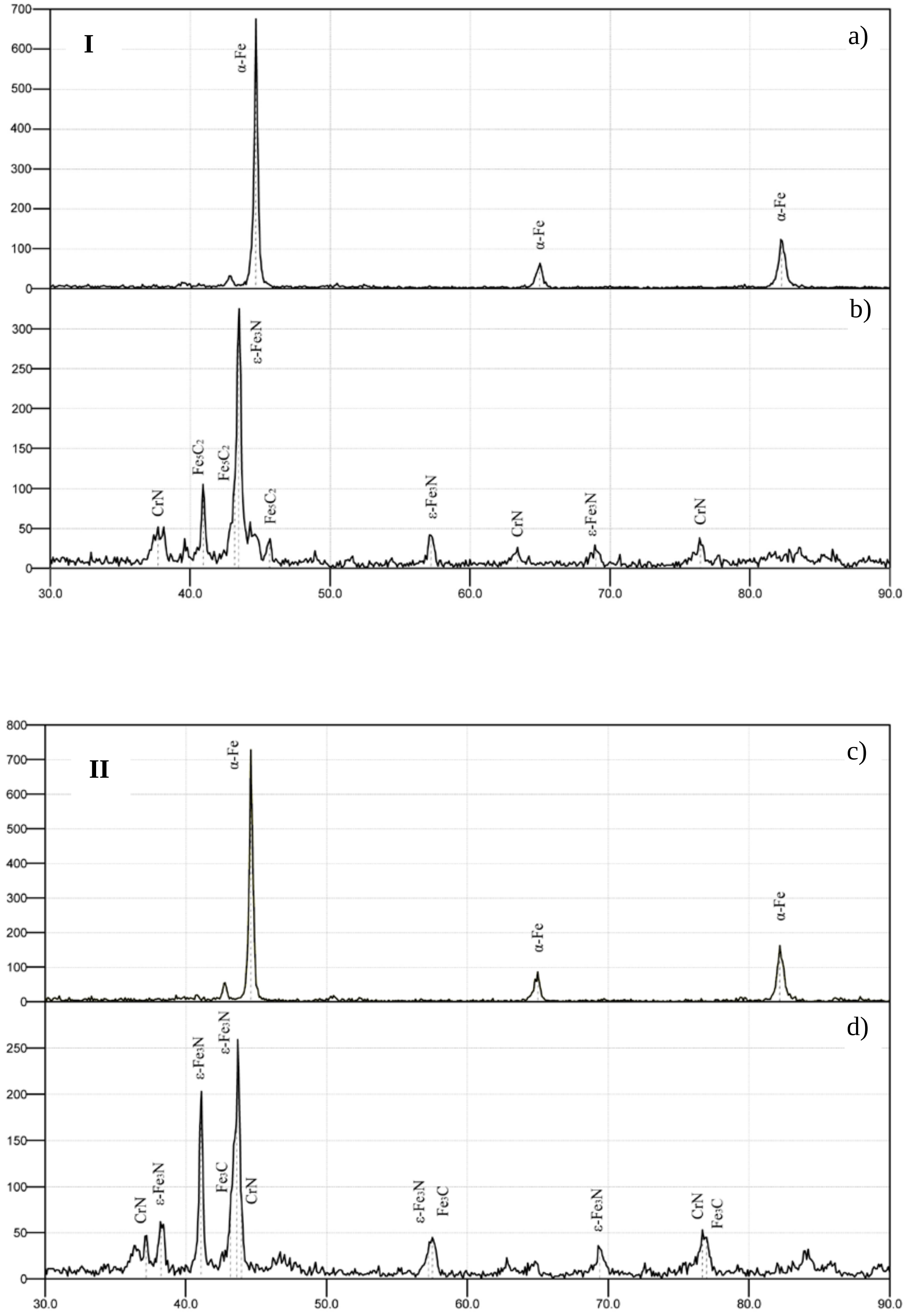

Fig. 5. Diffractograms from the surface of test pieces of steels:
I - R6M5, II - Kh12
(a) before and (b) after ion nitriding with the application of magnetic field

The diffusion zone of the nitrided layer on steel Kh12 (see Fig. 4b) is represented by nitrogen ferrite with carbide and fine dispersed nitride inclusions 1-2 μm in size. There is no defined boundary between the nitride layer and the diffusion sublayer. The transition from the nitrided layer to the lowerlying layers is smooth, which meets one of the requirements on nitrided layers [7, 8].

4. CONCLUSIONS

1. The application of magnetic field during ion nitriding of steels R6M5 and Kh12 causes intensification of diffusion saturation as a result of growth in discharge current at the same discharge voltage and pressure in the chamber.
2. The efficiency of nitriding high speed steel in glow discharge with the application of magnetic field is confirmed by the possibility of forming a nitrided layer with high hardness and thickness of 200 μm in 4 h.

REFERENCES

1. Arzamasov, B., Bratukhin, A., Eliseev, Yu., and Panayoti, T., *Ion Thermochemical Treatment of Alloys.* MGTU Im. Baumana, Moscow, 1999б 400 p.
2. Lakhtin, Yu., Kogan, Ya., Spies, H., Boemer, Z., *The Theory and Technology of Nitriding.* Metallurgiya, Moscow, 1991б 320 p.
3. Budilov, V., Agzamov, R., Ramazanov, K., Ion nitriding in glow discharge with hollow cathode effect. *Metallo ved. Term. Obrab. Met.*, 2007, Vol. 2, No. 7, p. 33–36.
4. Budilov, V., Kireev, R., Ramazanov, K., Vafin, R., *Method for Nitriding in Glow Discharge Plasma*, Pos. Decision on RF Patent No. 2009125030, MPK C23C 8/36, C21D 9/30.
5. Kireev, R., Budilov, V., Ramazanov, K., Vafin, R., *Method for Ion Nitriding of Steel*, Pos. Decision on Patent No. 2009125018RF, MPKC23C8/36, C21D 9/30.
6. Pletnev, S. *Magnetic Field, Properties, Application*, Gumanistika, St. Petersburg, 2004, p. 624.
7. Krukovich, M. Simulation of nitriding process. *Metalloved. Term. Obrab. Met.*, 2004, No. 1, p. 24–31.
8. Kuksenova, L., Lapteva, V., Berezina, E., Structure and wear resistance of nitrided steel, *Metalloved. Term. Obrab. Met.*, 2004, No. 1, p. 31–35.

DISTRIBUTION OF BENZENE CONCENTRATION IN KAUNAS CITY

A. Dėdelė, D. Laurinavičienė, K. Dėdelienė
Vytautas Magnus University
Vileikos str. 8, 44404, Lithuania
Phone +37037 327904
Email: a.dedele@gmf.vdu.lt; dovile@gmf.vdu.lt; k.dedeliene@gmf.vdu.lt

ABSTRACT

Benzene is considered as an indicator of others volatile organic compounds. The aim of this study was to assess distribution of benzene concentration in Kaunas. A passive sampling method was used. The diffusion tube comprises a glass sampling tube open at both ends and filled with activated charcoal. Sampling was carried out in 15 points of Kaunas city. The study was begun in November 2010. Study results present distribution of benzene concentration in autumn, winter, spring, summer seasons. In future the study will be extended. According to measured concentration average concentration in the whole Kaunas city was calculated. The study results showed that mean of benzene concentration in Kaunas city was 1.9 µg m^{-3} and ranged between 1.5 and 2.6 µg m^{-3}. The highest benzene concentrations at sites Kaunas27 (Petrašiūnų district), Kaunas02 (Šilainių district) and Kaunas15 (Vilijampolės district) did not exceed the annual limit value for the protection of human health (5.0 µg m^{-3}), but were higher than the lower assessment threshold value of 2.0 µg m^{-3}. The results of the study were introduced in the ESRI Geographic Information System software ArcGIS, and the extension Geostatistical Analyst was used to obtain map of distribution of benzene concentration.
To get a better view of the distribution of pollutant concentration, the obtained values were spatially interpolated using the IDW (Inverse Distance Weighted) method.

Keywords: air pollution, distribution of benzene concentration, map of benzene distribution, interpolation method

1. INTRODUCTION

Benzene is a Volatile Organic Compound (VOC). It is found in fossil fuels and is produced by the burning of organic material and, as such, occurs in fires, petrol refining, fumes from cooking oils, tobacco smoke, and waste incineration. Benzene is also formed, even during the combustion of lead free petrol, in car engines. Historically, benzene was widely used as a solvent, and is still used in the manufacture of plastics, synthetic fibres, detergents, pharmaceuticals, pesticides, and rubber. Low-level benzene exposure is ubiquitous, and the main route of exposure is through inhalation. Emissions from traffic are the largest source. A disproportionate amount of on-road emissions come from high emitting, older vehicles. Benzene pollution is highest in densely populated areas characterised by high traffic density. Industrial activity can contribute to ambient benzene levels, but its contribution to the total exposure is very low [1, 2, 3].

In European cities, outdoor benzene concentrations ranged from 0.4 to 15.2 µg m^{-3}. In indoor environments, these values were from 0.7 to 63.7 µg m^{-3} [4].

Exposure to benzene is associated with increases in numerous adverse effects including bone marrow damage, changes in circulating blood cells, developmental and reproductive effects, alterations of the immune system, and cancer. A substantial number of epidemiologic studies have provided estimates of the relation between exposure to benzene and the risk of leukemia [5, 6, 7].

The aim of this study was to assess distribution of benzene concentration in Kaunas.

2. MEASUREMENTS METHODS

For determination of benzene concentration a passive sampling method was used. The diffusion tube comprises a glass sampling tube open at both ends and filled with activated charcoal. Each opening in the sampling tube is filled with a cellulose acetate diffusion barrier. Ambient air diffuses into the sampling tube in a controlled manner. Benzene is absorbed on the activated charcoal and desorbed by carbon disulphide in the laboratory and analysed by gas chromatography (Fig. 1).

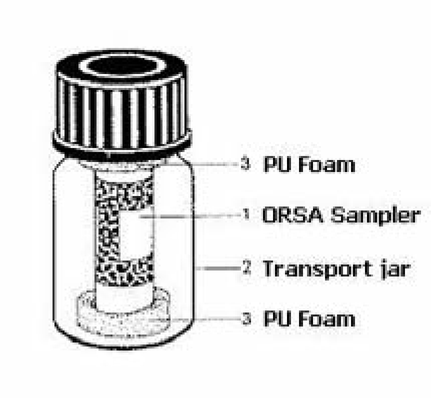

Fig. 1. Passive sampler for determination of benzene concentration [8]

Eight sampling campaigns of 14 days were carried out from November 2010 to July 2011 in Kaunas. Sampling was carried out in 15 points of Kaunas city (Fig. 2). This study is the part of project of “Modernization of Lithuanian air quality monitoring system using diffusive samplers”. This project covers the whole territory of Lithuania [9].

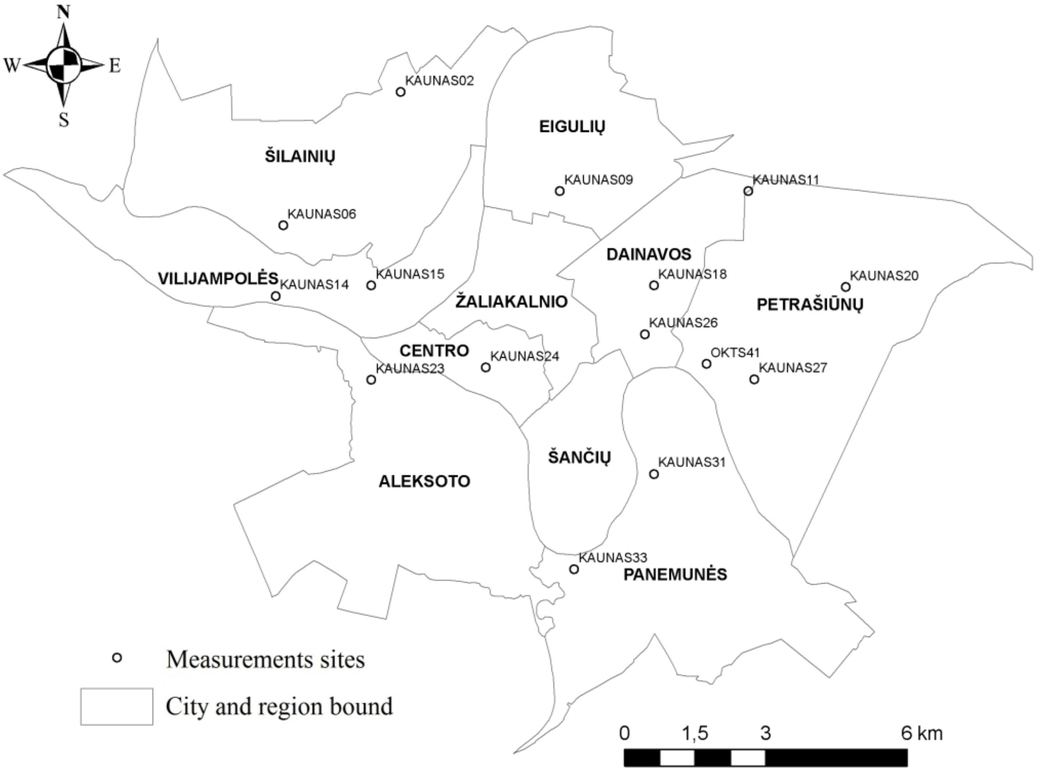

Fig. 2. Benzene sampling points in Kaunas city

The results of the study were introduced in the ESRI Geographic Information System software ArcGIS and the extension Geostatistical Analyst was used to create maps of dispersion of benzene concentration in Kaunas city. To get a better view of the distribution of pollutant concentration, the obtained values were spatially interpolated using the IDW (Inverse Distance Weighted) method.

3. RESULTS AND DISCUSSION

At 15 sites concentrations of benzene in ambient air were measured with passive samplers. The study shows that the mean concentration of benzene for the entire study period (from November 2010 to July 2011) was 1.9 µg m^{-3} with the range of 1.5 and 2.6 µg m^{-3} (Fig. 3). The highest benzene concentrations at sites Kaunas27, Kaunas02 and Kaunas15 did not exceed the annual limit value for the protection for human health (5.0 µg/m^{3}), but were higher than the lower assessment threshold value of 2.0 µg m^{-3} and ranged between 2.3 and 2.6 µg m^{-3}. Low volatile organic compound (VOC) concentrations were observed in Kaunas city by other researchers as well [10].

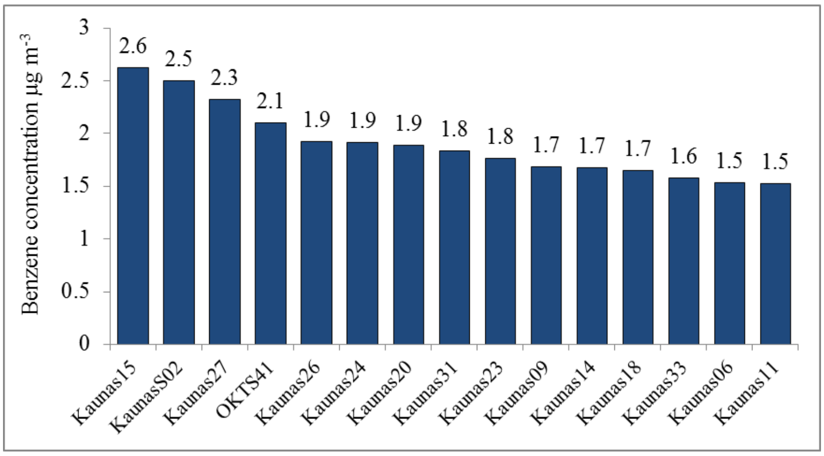

Fig. 3. The mean concentrations of benzene in Kaunas city

Seasonal variations in concentrations of benzene are shown in Fig. 4 and 5. The highest concentrations of benzene (3.2 µg m^{-3}) in Kaunas city were observed during the winter campaign, possibly due to slower dispersion, slower chemical transformations and/or the lengthy "cold start" period required by vehicles in the wintertime. The mean concentrations of benzene were lower than the reported as the higher assessment threshold value of 3.5 µg m^{-3}.

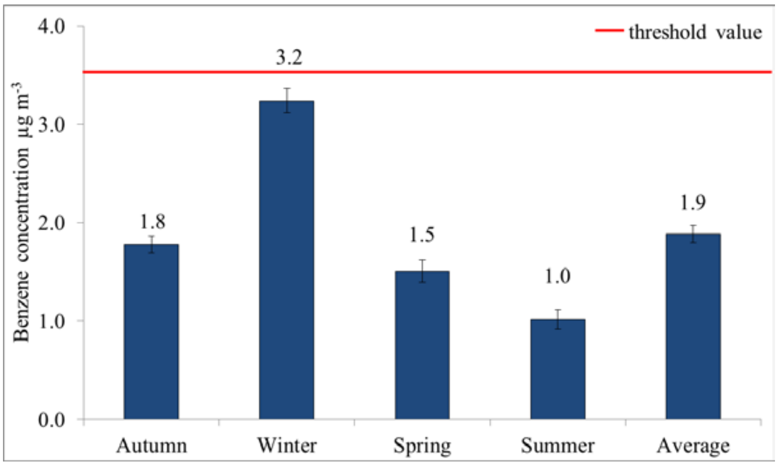

Fig. 4. Seasonal variation of the mean concentrations of benzene in Kaunas city

Seasonal variation of the mean concentrations of benzene in different sampling points is presented in Fig. 5. Higher concentrations of benzene were observed during the winter campaign in all sampling points. In the other study performed in Kaunas higher concentrations of VOCs were also found in the wintertime [10].

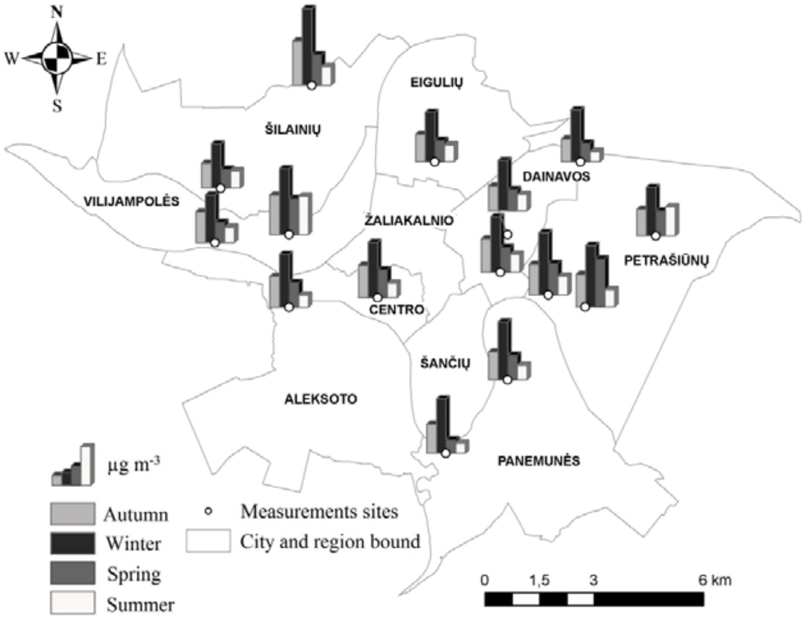

Fig. 5. Seasonal variation of the mean concentrations of benzene in different sampling points

Using Arc GIS software the maps of benzene dispersion in Kaunas city were plotted (Fig. 6). The whole studied area was divided to three classes of: low, medium and relatively high exposure to benzene, according to the annual limit value (5.0 µg m^{-3}).

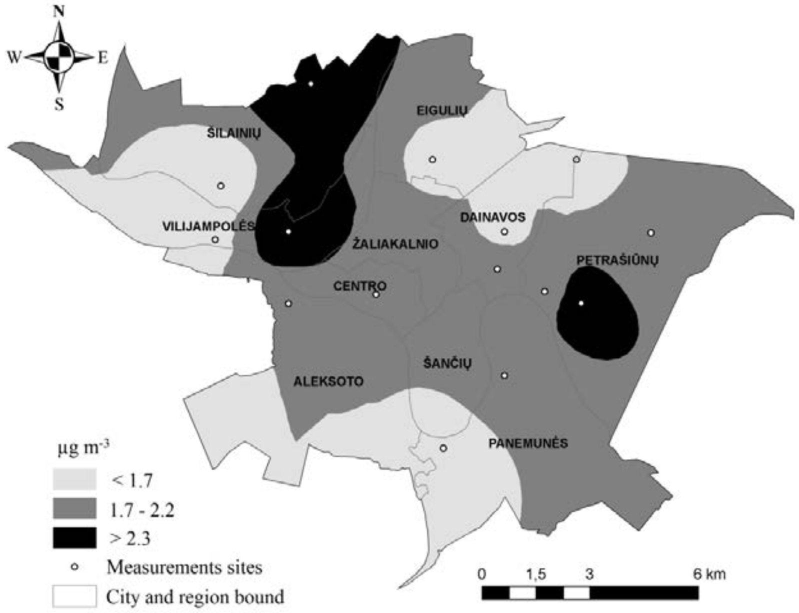

Fig. 6. Dispersion of benzene pollution in Kaunas city The lowest benzene concentration was in districts which are located in the periphery of the city (Fig. 6). The highest concentration of benzene was in part of Petrašiūnai, Šilainiai and Vilijampolė districts

4. CONCLUSIONS

1. The mean concentrations of benzene in Kaunas agglomeration during the study period was 1.9 µg m^{-3} and did not exceed the annual limit value of 5.0 µg m^{-3} for the protection of human health.
2. The highest concentrations of benzene (3.2 µg m^{-3}) in Kaunas city were observed during the winter campaign.
3. The lowest benzene concentration was in districts which are located in the periphery of the city. The highest concentration of benzene was in part of Petrašiūnai, Šilainiai and Vilijampolė districts.

REFERENCES

1. PARRA M.A., ELUSTONDO D., BERMEJO R., SANTAMARÍA J.M. Ambient air levels of volatile organic compounds (VOC) and nitrogen dioxide (NO_2) in a medium size city in Northern Spain. *Science of the Total Environment*, 407, 2009, p. 999–1009.

2. TSAI W.Y., CHAN L.Y., BLAKE D.R., CHU K.W. Vehicular fuel composition and atmospheric emissions in South China: Hong Kong, Macau, Guangzhou, and Zuhai. *Atmospheric Chemistry and Physics*, 2006, 6, p. 3281–8.

3. Brotherton J. Benzene: a case study of the control of a carcinogen in NSW. *NSW Public Health Bulletin*, 2002, vol. 13, p. 209–211.

4. KOTZIAS, D., GEISS, O., TIRENDI, S., BARRERO-MORENO, J., REINA, V., GOTTI, A., CIMINO-REALE, G., CASATI, B., MARAFANTE, E., SARIGIANNIS, D., 2009. Exposure to multiple air contaminants in public buildings, schools and kindergartens – the European indoor air monitoring and exposure assessment (AIRMEX) study. *Fresenius Environmental Bulletin*. 18, p. 670–681.

5. CIARROCCA M., TOMEI G., FIASCHETTI M., CACIARI T., CETICA C., ANDREOZZI G., CAPOZZELLA A., SCHIFANO M.P., ANDRE J.C., TOMEI F., SANCINI A. Assessment of occupational exposure to benzene, toluene and xylenes in urban and rural female workers. *Chemosphere*, 2012, 1, p. 1–7.

6. KHALADE A., JAAKKOLA M.S., PUKKALA E., JAAKKOLA J.J.K. Exposure to benzene at work and the risk of leukemia: a systematic review and meta-analysis. *Environmental Health*. 2010, 9:31.

7. WHO. Air quality guidelines for Europe. European Series, 2nd ed. Copenhagen: WHO Regional Publications; 2000.

8. Passam ag. Laboratory for Environmental Analysis. Link to the internet http://www.passam.ch/benzene.htm

9. *Lithuanian Air Monitoring System Modernization Using Diffusive Samplers*. Final Report, 2010, 194 p.

10. KLIUCININKAS L., MARTUZEVICIUS D., KRUGLY E., PRASAUSKAS T, KAUNELIENE V, MOLNAR P, STRANDBERG B. Indoor and outdoor concentrations of fine particles, particle-bound PAHs and volatile organic compounds in Kaunas, Lithuania. *Journal of Environmental Monitoring*. 2011, 13(1), p. 182–91.

CYSENI 2012, May 24–25, Kaunas, Lithuania
ISSN 1822-7554, www.cyseni.com

GLOBAL CLIMATE CHANGE SCENARIOS ADAPTATION FOR THE PREDICTION OF THE NEMUNAS RUN-OFF

D. Jakimavičius
Lithuanian Energy Institute
Laboratory of Hydrology
Breslaujos str. 3, LT-44403 Kaunas –Lithuania
Phone +370 37 401 965
Email: darius.j@mail.lei.lt

ABSTRACT

The natural and anthropogenic factors have influence on the climate change. In order to assess climate change impact on the surrounding environment, we should be aware of potential climate change scenarios for future. The Intergovernmental Panel on Climate Change scientists have made a lot of climate change scenarios for different climate models and emissions scenarios. Climate change has impact on the hydrological regime of rivers. According to the climate change scenarios, air temperature will rise and precipitation amount will change in XXI century. Changes of meteorological parameters will have influence on the snow cover thickness and duration. For this reason, the river floods will shift from the spring season to the winter season. The maximal discharges of floods could decrease significantly. In the warm period the increasing of air temperature could cause a decrease of the river run-off during the dry period because of additional evaporation. Climate change impact on river run-off could be evaluated by the hydrological modelling in the river catchments. The input data for this modelling are time series of air temperature and precipitation according to different climate change scenarios. The aim of this research is the adaptation of the global climate change scenario data (air temperature and precipitation) for the Nemunas River catchment, which area covers 75% of Lithuanian territory. In this research we used climate change scenarios, prepared by two global climate models (Echam5, HadCM3) and three emission scenarios (A2, A1B, B1). Monthly climate scenarios data (air temperature and precipitation) were recalculated into daily data for the period of 2011–2100. For this purpose, the Delta method was used.

Keywords: Climate change, emission scenarios, Echam5, HadCM3, Delta method

1. INTRODUCTION

Global climate is changing due to the natural and anthropogenic factors [1]. The increase of air temperature is observed: global about 0.8 °C [2], in Lithuania about 0.5 °C [3]. As a result, snow cover forms later, it lasts shorter and water reserves in snow decline [4]. The earlier snow melt causes the earlier spring floods. In this way a distribution of run-off between the seasons is changed. Run-off and spring flood prediction is relevant in many areas such as energy production planning in water–power plants, preparing for floods in emergency management agencies, etc. In order to foresee floods, river discharges have to be forecasted not only for seasons but also for decades. For this purpose hydrologic modeling based on the global climate model (GCM) output data according to different greenhouse gas emission scenarios can be used. Many of the GCM output data, including air temperature and precipitation, have monthly step [5]. In this research HBV (Hydrologiska Byråns Vattenbalansavdelning) model developed by Swedish Meteorological and Hydrological Institute in 1970 was used. This model requires air temperature and precipitation data to have daily step. Hydrological modeling based on two global climate models (HadCM3 and Echam5) under three emission scenarios (A2, A1B and B1) was selected. Climate models can be classified into energy balance, radiation–convection, statistical–dynamic and general atmospheric circulation models. Energy balance and radiation–convection models are primitive and can be used to investigate temperature (energy balance) and convective processes in various layers of the atmosphere (radiation convection) [6]. Statistical–dynamic models are more complex and informative. They are based on the thermodynamics and mixing of air in the vertical layers of the atmosphere [7]. General atmospheric circulation models are the most complex and most commonly used. They are three-dimensional models, which connect processes that take place in atmosphere, ocean and land surface into the one system. Before the beginning of discharge simulation, conversion of air temperature and precipitation data to daily step has to be performed. For such calculations Delta method is widely used [8–11]. Previuos studies show, that this method is appropriate for Lithuanian conditions as well [12]. With the help of this method the future values of monthly meteorological data are compared with the observed ones.

The aim of this study is to prepare the output data of climate change models for the Nemunas run-off calculation using Delta method.

2. METHODOLOGY

2.1. Climate models

A river discharge is changing together with climate. In 1988 World Meteorological Organization (WMO) and United Nations Environment Programme (UNEP) established the Intergovernmental Panel on Climate Change (IPCC). The main activity of the IPCC is publishing of special reports related to the United Nations Framework Convention on Climate Change (UNFCCC). The IPCC report data are widely used in many climate studies and are considered as reliable sources. The IPCC has developed four reports [5] (Fig. 1). Currently mostly prognostic information about climate change from Fourth Assessment Report is used [13].

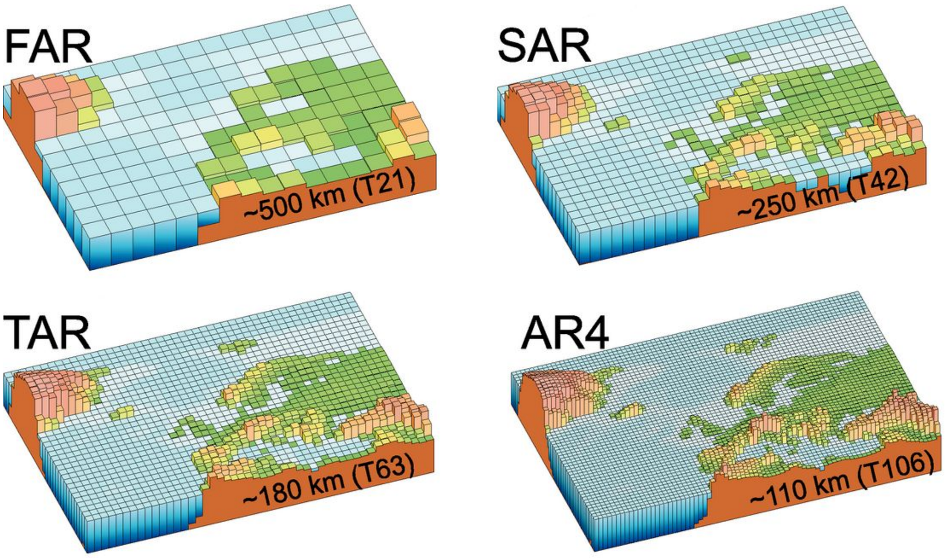

Fig. 1. Geographic resolution characteristic of the generations of climate models used in the IPCC Assessment Reports [5]

In future climate changes will be mostly affected by changes of the greenhouse gas concentration. The Intergovernmental Panel on Climate Change has released a special report about the potential chances of the greenhouse gas concentrations in future. These changes are related to the use of fossil fuel [14]. In Europe three emission scenarios: the most pessimistic (A2), the average and most probable (A1B), and the mildest (B1) are commonly used for simulations.

The A2 storyline and scenario family describes a very heterogeneous world. The underlying theme is self reliance and preservation of local identities. Fertility patterns across regions converge very slowly, which results in continuously increasing population. Economic development is primarily regionally oriented and per capita economic growth and technological change more fragmented and slower than other storylines [5].

The B1 storyline and scenario family describes a convergent world with the same global population, that peaks in mid-century and declines thereafter, as in the A1 storyline, but with rapid change in economic structures toward a service and information economy, with reductions in material intensity and the introduction of clean and resource efficient technologies. The emphasis is on global solutions to economic, social and environmental sustainability, including improved equity, but without additional climate initiatives [5].

The Climate Challenge game is based on the A1B scenario as it provides a good mid-line scenario for carbon dioxide output and economic growth, which leaves scope for the player to either improve or worsen emissions levels [5].

The largest climate research centers are modeling climate in XXI century based on the greenhouse gas emission scenarios. In the European region ECHAM5 and HadCM3 are the most popular. ECHAM5 is atmosphere–ocean general circulation model developed by the Max Planck Institute for Meteorology and German Climate Computing Centre [15]. HadCM3 (abbreviation for *Hadley Centre Coupled Model, version 3*) is a coupled atmosphere-ocean general circulation model (AOGCM) developed at the Hadley Centre in the United Kingdom [16].

2.2. Data preparation for simulation

Lithuanian climate change data in XXI century are given in monthly step. For the modelling of the Nemunas run-off, precipitation and temperature information of Lazdijai, Varėna, Vilnius, Kaunas, Ukmergė, Utena, Panevėžys, Dotnuva, Šiauliai, Laukuva, Tauragė, Raseiniai, Šilutė and Klaipėda meteorological stations (MS) was used. A network of meteorological stations is shown in figure 2. Hydrological modeling using the code HBV requires data in daily step. Delta method was used for conversion from monthly to daily step [17]. This method is based on comparison of monthly values with actually measured ones of the climate normal period [8]. A period of 1961–1990 was selected as a background for calibration and validation of the Nemunas River hydrological model. This period is used as climate norm by WMO [18, 19]. The daily precipitation and temperature data for different scenarios are calculated according to:

$$P_{d.s} = P_{o.d}\frac{P_{m.s}}{P_{o.m}} \tag{1}$$

$$T_{d.s} = T_{o.d} + (T_{m.s} - T_{o.m})\,. \tag{2}$$

Where: $P_{d.s}$, $T_{d.s}$ – predicted daily data of precipitation and temperature according to climate scenarios, $P_{o.d}$, $T_{o.d}$ – observed daily data of precipitation and temperature in the climate normal period, $P_{m.s}$, $T_{m.s}$ – predicted monthly data of precipitation and temperature according to climate scenarios, $P_{o.m}$, $T_{o.m}$ – observed monthly data of precipitation and temperature in the climate normal period.

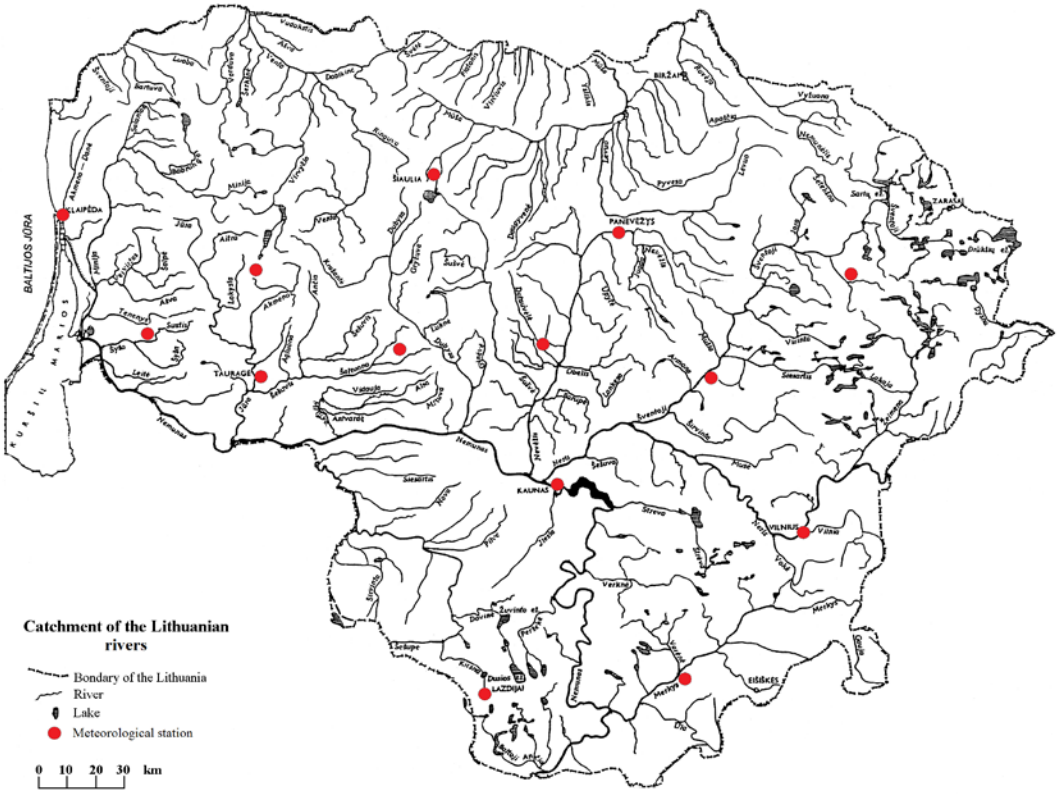

Fig. 2. Distribution of meteorological station in the Lithuania. Compiled by D. Jakimavičius

3. RESULTS

The data of precipitation and air temperature are based on the output data of two climate change models (ECHAM5, HadCM3) and three emission scenarios (A2, A1B, B1). Using Delta method the data conversion was performed and daily step of the meteorological data of 14 MS for the period of 2011–2100 was obtained. Seasonal values of precipitation and air temperature of 2011–2040, 2041–2071 and 2071–2100 under to six climate change scenarios (Echam5 A2, Echam5 A1B, Echam5 B1, HadCM3 A2, HadCM3 A1B and HacCM3 B1) were compared with the values of climate norm (Fig. 3).

According to the data of 14 MS in the climate norm period (CNP, 1961–1990) 128 mm of precipitation fell during winter, 140 mm – during spring, 239 mm – during summer and 185 mm – during autumn. Total annual precipitation was 692 mm. Predicted average (six scenarios) amount of the winter season precipitation will exceed this amount of CNP by 14% in 2011–2040, by 19% in 2041–2070 and by 29% in 2071–2100. All analysed scenarios predict higher amounts of winter precipitation than in CNP (Fig. 3a). An average (six scenarios) amount of spring precipitation will increase by 3 % in 2011–2040, by 9% in 2041–2070 and by 14% in 2071–2100. Smaller, than in climate norm period, amounts of precipitation are expected only under HadCM3 A1 scenario in 2011–2040, whereas the opposite forecast is made under the rest scenarios (Fig. 3b). During the summer season predicted average (six scenarios) amount of precipitation is going to decrease by 3 % in 2011–2040, by 4% in 2041–2070 and by 6% in 2071–2100 comparing with CNP. In autumn forecasted average (six scenarios) amount of precipitation will decrease by 6 % in 2011–2040, by 4 % in 2041–2070 and by 3 % in 2071–2100 comparing with CNP. According to different climate change scenarios predicted amounts of precipitation in the summer and autumn seasons will distribute unevenly (Fig. 3c, 3d). Analysis of the calculated data shows that an average annual amount of precipitation will increase by 1 % in 2011–2040, by 3% in 2041–2070 and by 6% in 2071–2100 comparing with CNP.

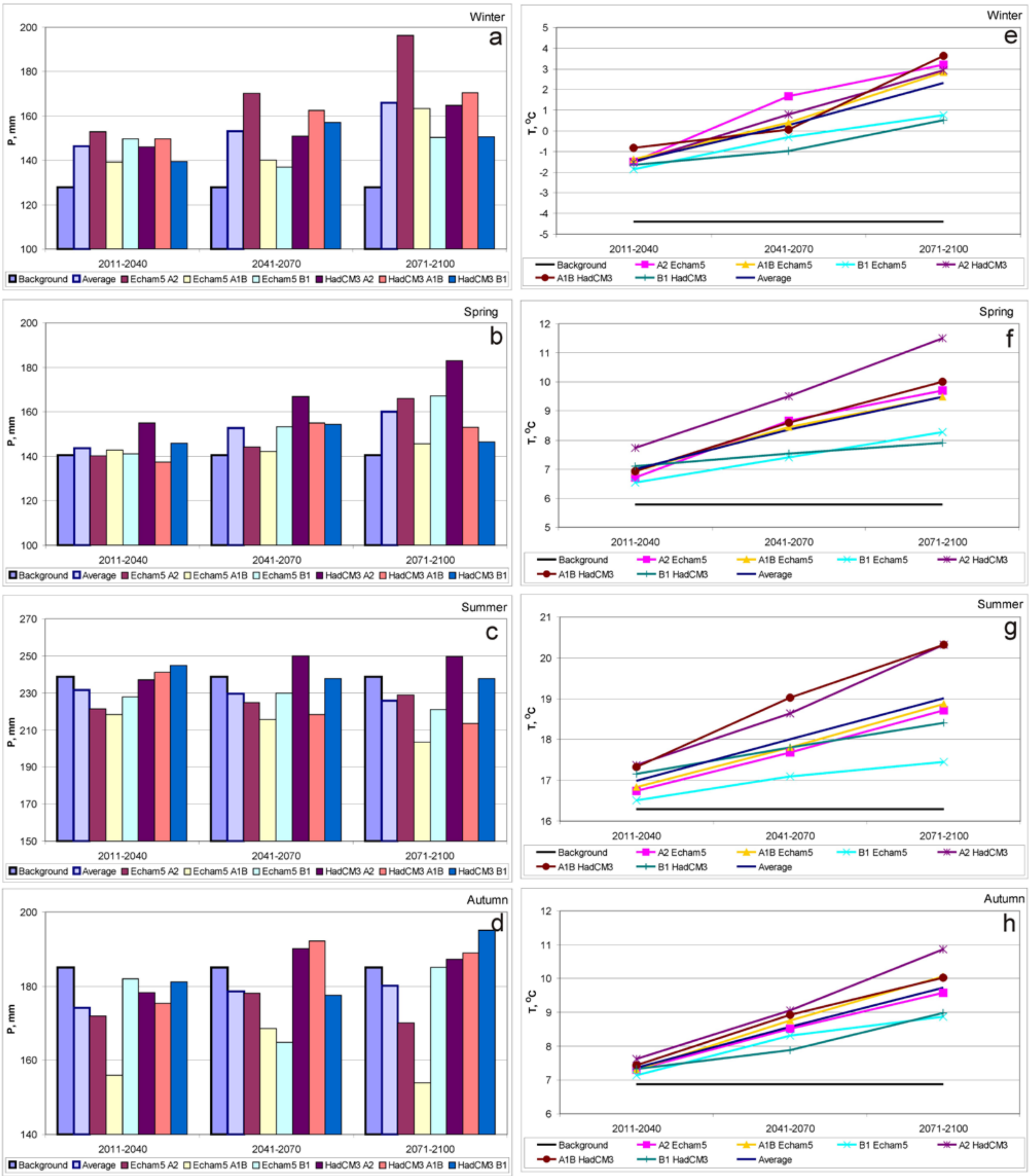

Fig. 3. Distribution of forecasted average seasonal amount of precipitation (a, b, c, d) and temperature (e, f, g, h) according to different climate scenarios in the periods of 2011–2041, 2041–2070 and 2071–2100 in Lithuania

In climate normal period air temperature was -4.4 °C in winter, 5.8 °C in spring, 16.3 °C in summer and 3.9 °C in autumn. According to the data of the selected meteorological stations, an average annual air temperature of CNP was 6.1 °C. The results indicate that in Lithuania air temperature is going to rise. Temperatures are expected to increase mostly in winter. An average temperature of the winter season will be -1.5 °C in 2011–2040, 0.3 °C in 2041–2070 and 2.3 °C in

2071–2100 (Fig. 3e). An average temperature of the spring season is expected to be 7 °C in 2011–2040, 8.4 °C in 2041–2070 and 9.5 °C in 2071–2100 (Fig. 3f). In summer time air temperature is going to increase the least, an average values will reach 17.0 °C in 2011–2040, 18.0 °C in 2041–2070 and 19.0 °C in 2071–2100 (Fig. 3g). Air temperature in autumn is forecasted to rise more quickly than in summer, but slower than in winter. An average temperature in autumn will increase up to 7.4 °C in 2011–2040, 8.6 °C in 2041–2070 and 9.5 °C in 2071–2100 (Fig. 3h). According to different climate change scenarios predicted values of air temperature in all seasons will be higher than in CNP (Fig. 3b-3h). An average air temperature is expected to be 7.5 °C in 2011–2040, 8.8 °C in 2041–2070 and 10.1 °C in 2071–2100, while its value in CNP period equals 6.1 °C.

4. CONCLUSIONS

- The output results of the used climate change models ECHAM5 and HadCM3 according to A2, A1B and B1 emission scenarios are appropriate to predict consistent patterns of air temperature and precipitation in the period of 2011–2100.
- The employed Delta method and the daily air data of temperature and precipitation of climate norm period (CNP) enabled to properly adapt data of climate change models for the territory of Lithuania.
- Consistent patterns of air temperature and precipitation for the period of 2011–2100 were defined. In XXI century annual amount of precipitation will increase by 6%, in winter and spring – by 29 % and 14 %, if compared to CNP. Whereas in the summer and autumn seasons amount of precipitation will decrease by 9 % and 3 %.
- An average annual air temperature is going to increase; in 2100 it is supposed to be 10.1 °C, i.e. 4 °C higher than in CNP. Seasonal analysis revealed, that air temperature would increase the most in winter and spring (by 6.7 °C and 3.7 °C higher than in CNP), and less in the summer and in the autumn (2.7 °C and 2.8 °C higher than in CNP).
- Analysed data of 2011–2100 shov, that the highest amount of precipitation and air temperature are the most often forecasted according to A2 emmision scenario. The least amount of precipitation is expected according to A1B, and the lowest temperature – according to A2 scenarios. Climate change models are less important than emmision scenarios, when the studied meteorological parameters are being forecasted.

REFERENCES

1. Andréasson, J., Bergström, S., Carlsson, B., Graham, L.P., Lindström G. 2004. Hydrological Change – Climate Change Impact Simulations for Sweden. *AMBIO: A Journal of the Human Environment.* Vol. 33(4), p. 228–234.
2. Trenberth K. E., Jones P. D., Ambenje P., Bojarinu R., Easterling D. Observations: surface and atmospferic climate change // In Climate Change 2007: The Physical Science Basis. Contribution of Working Group I to the Fourth Assessment Report of the Intergovernmental Panel on Climate Change (eds. S. Sodomon, D. Qin, M. Manding, Z. Chen, M. Marquis, K. B. Averyt, M. Tignor and H. L. Miller) Cambrige University Press, Cambrige, United Kingdom and New York, NY, USA. 2007, p. 235–335.
3. Bukantis, A. 2007. Indications and causes of climate change. *Global environmental change,* p. 77–106, Vilnius.
4. Bukantis A., Gulbinas Z., Kazakevičius S., Kilkus K., Mikelinskienė A., Morkūnaitė R., Rimkus E., Samuila M., Stankūnavičius G., Valiukevičius G., Žeromskis R. Klimato svyravimų poveikis fiziniams geografiniams procesams Lietuvoje. 2001. Vilnius.
5. Solomon S., Qin D., Manning M., Chen Z., Marquis M., Averyt K.B., Tignor M. Miller H.L. (eds.). 2007. IPCC, 2007: Climate Change. The Physical Science Basis. Contribution of

Working Group I to the Fourth Assessment Report of the Intergovernmental Panel on Climate Change. Cambridge: Cambridge University Press.

6. Wei J., Dickinson R., E., Zeng N. 2006. Climate variability in a simple model of warm climate land-atmosphere interaction. *Journal of Geophysical Research*, Vol. 111, G03009, doi: 10.1029/2005JG000096.
7. Bertrand C, Ypersele J., P., Berger A. 2002. Are Natural Climate Forcings Able to Counteract the Projected Anthropogenic Global Warming? *Climatic Change*, Vol. 55, No. 4, p. 413–427(15).
8. Hay, L.,E., Wilby, R.,L., Leavesley, G.,H. 2000. A comparison of delta change and downscaled GCM scenarios for three mountainous basins in the United States. *Journal of American Water Resources*. Vol. 36, No. 2, p. 387–397.
9. Prudhomme, C., Reynard, N., Crooks, S. 2002. Downscaling of global climate models for flood frequency analysis: Where are we now?. Hydrological Processes 16: 1137–1150.
10. Andreasson, J., Rosberg, J. 2006. Moving on from Delta change towards direct use of RCM output by scaling – A method for transient impact simulations. *Geophysical Research Abstracts*, Vol. 8.
11. Akhtar, M., Ahmad, N., Booij, M. J. (2008) The impact of climate change on the water resources of Hindukush-Karakorum-Himalaya region under different glacier coverage scenarios. *Journal of Hydrology*, 355 (1-4). p. 148–163. DOI:10.1016/j.jhydrol.2008.03.015
12. Kriaučiūnienė J., Meilutytė-Barauskienė D., Rimkus E., Kažys J., Vincevičius A. 2008. Climate change impact on hydrological processes in Lithuanian Nemunas river basin // Baltica. ISSN 0067-3064. Vol. 21, No. 1–2, p. 51–61.
13. Pachauri, R., K., Reisinger, A. (Eds.). (2008). Climate Change 2007 – Synthesis Report. A Report of the Intergovernmental Panel on Climate Change. IPCC, Geneva, Switzerland. pp 104.
14. Nakicenovic, N., Swart, R. (Eds.) 2000. *IPCC Special Report on Emissions Scenarios*. Cambridge University Press, UK. p. 570
15. Roeckner, E., Bäuml, G., Bonaventura. L., Brokopf, R., Esch, M., Giorgetta, M., Hagemann, S., Kirchner, I., Kornblueh, L., Manzini, E., Rhodin, A., Schlese, U., Schulzweida, U., Tompkins, A. 2003: The atmospheric general circulation model ECHAM5, Part 1, MPI Report, No. 349, ISSN 0937-1060. p 140.
16. Pope, V. D., Gallani, M. L., Rowntree, P. R. & Stratton, R. A. 2000. The impact of new physical parametrizations in the Hadley Centre climate model - HadAM3. *Climate Dynamics*, Vol. 16, p. 123–146.
17. Beldring S., Engen-Skaugen T., Forland E. J. (2008). Climate change impacts on hydrological processes in Norway based on two methods for transferring regional climate model results to meteorological station sites. *Tellus 60A*,439–450.
18. World Meteorological Organization. 2007. *The Role of Climatological Normals in a Changing Climate*. WCDMP-No. 61, WMO-TD/No. 1377, p. 46. Geneva.
19. Arguez A., Vose S., R. 2010. The Definition of the Standard WMO Climate Normal: The Key to Deriving Alternative Climate Normals. *Bulletin of the American Meteorological Society 2010*. pp. 18. NOAA’s National Climatic Data Center Asheville, NC.

CYSENI 2012, May 24–25, Kaunas, Lithuania
ISSN 1822-7554, www.cyseni.com

INTRA-ANNUAL THERMAL VARIABILITY OF LITHUANIAN RIVERS

A. Jurgelėnaitė
Lithuanian Energy Institute
Breslaujos str. 3, LT-44403 Kaunas – Lithuania
Phone +370(37)401964
Email: alda@mail.lei.lt

ABSTRACT

A river annual thermal regime is one of its most important water quality parameters, being a key component in determining a distribution of aquatic communities. Most aquatic organisms have a specific range of temperature that they can tolerate. Water temperature change may have effect on abundance, diversity, distribution, growth rate, tolerance to diseases of aquatic organisms.

There is currently renewed interest in understanding the thermal regime of rivers and streams, due to anticipated alterations to the natural thermal regimes of many rivers. This may be a consequence of impoundments, thermal discharges or climate changes.

In Lithuania early studies of river thermal regime focused mainly on ice cover and on the water temperature of the River Nemunas. However water temperature distribution and factors responsible for river thermal processes are not investigated.

The aim of this work is the review and analysis of intra-annual and diurnal water temperature dynamics of Lithuanian rivers. A comparison of multi annual cycles for the rivers of different size and water temperature (warm, cool and cold) highlights that large warm water rivers have identical thermal cycles, whereas the cold water rivers varies more, but the contrasts in the annual temperature regime between the cold rivers are mainly a function of water temperature during the summer months. A comparison of long-term annual water temperature cycles and air temperature cycles using the mean monthly data of the same period shows that river water temperature follows air temperature of neighbouring meteorological stations. Statistical relationships between the average long-term monthly water and air temperatures show high correlation coefficients (0.97-1.00).

Very significant negative trend in the period of 1931-2010 has been identified for ice cover duration in the River Nemunas at Smalininkai and significant positive trend for average winter season air temperature of Vilnius MS. The analysis revealed that warming winters cause shorter ice cover duration or absence of ice cover in the River Nemunas at Smalininkai over the last 30-years.

Keywords: river, water temperature, air temperature, water gauging station

1. INTRODUCTION

River water temperature influences physical, chemical and biological characteristics of water. Temperature is the most significant single determinant of water quality [1]. River water temperature is one of the most important parameters which determine life of the aquatic ecosystem. Most aquatic organisms have a specific range of temperature that they can tolerate [2]. Water temperature change may have effect on the abundance, diversity, distribution, growth rate, tolerance to diseases of aquatic organisms.

Changes in water temperature influence oxidation rate and the solubility of gases and minerals. Chemical and biological reaction rates increase with increased water temperature. The toxicity of contaminants and the efficacy of water treatment, as well as taste and odour, are also affected by water temperature [3].

Despite the importance of river water temperature and abundance of data, the thermal regime of Lithuanian rivers is not sufficiently investigated. A limited understanding exists of intra-annual water temperature dynamics. Most early studies of thermal regime have been restricted to ice cover since knowledge about ice cover is necessary in hydro-technical construction and water economy [4]. Some studies have investigated water temperature of the River Nemunas [5, 6] and thermal regime of the rivers below dams [7, 8]. Assessment of river water temperature in compliance with ecological requirements was made and the classification of river reches according two criterions was made in [9]. River reaches were divided into three groups according to the data of the period 2003–2007.

However the water temperature distribution and factors responsible for the river thermal processes was not investigated. The last time the annual cycle of river water temperature has been analysed only in 1969 [10].

In recent years, there is a growing interest in potential impacts of global warming on thermal structure of water systems. In the future, climate warming effect can have far-reaching implications for use, development, and management of water resources. Many scientific reports examine the potential impacts of climate change over the next century on aquatic ecosystems. Global climate change poses a serious threat to lakes, streams, rivers and other water bodies. The temperature increases and variations in weather patterns projected for the next 100 years will result in changes of the geographic distribution of freshwater fish, interfere with the reproduction of many aquatic species, reduce water quality, and impose added stresses on sensitive aquatic ecosystems [11].

Natural thermal regimes of rivers display diurnal and intra-annual variability. The aim of this work was to characterise and understand temporal variation in water temperature of Lithuanian rivers following both an intra-annual and diurnal cycles.

Analysis was performed using the most recent water temperature data available up to 2010.

2. DATA AND METHODS

In Lithuania the systematic observations of river water temperature were started in 15 sites of 10 rivers in 1945. Since then the number of recording sites has increased considerably, but at the beginning of this century (in 2000) many sites were closed. Till now water temperature in Lithuania was measured at 141 water gauging stations (WGS) in 84 rivers (Figure 1). The data sets are from different periods and have different length (from 30 to 66 years). Majority of sites produce a continuous record. At present water temperature is measured at 64 WGS in 44 rivers.

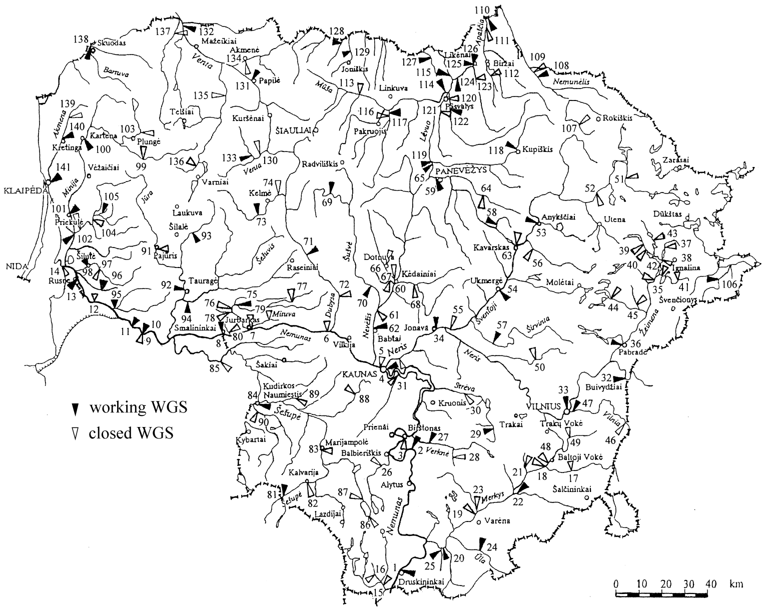

Fig. 1. Water temperature monitoring sites (WGS)

Water temperature observations in WGS have comprised a two-daily measurements (at 08:00 and 20:00), but in annual hydrological yearbooks of Lithuanian Hydrometeorological Service (LHMS) only the averaged decadal and monthly data are presented.

This work analyses the intra-annual thermal cycles of Lithuanian rivers using long-term data series. For the analysis of annual thermal cycles the mean monthly water temperature was calculated for entire period of the observation (data of the water and air temperature from 1945-2010 periods were used). Taking the long-term average values of mean monthly water temperature, curves were fitted for individual rivers. A comparison of long-term annual cycles for the rivers of different size and water temperature (warm, cool and cold) was made to determine the differences in intra-annual thermal behaviour of rivers. Also, a comparison of long-term annual thermal cycles of different rivers and air temperature of geographically closest meteorological stations (MS) was performed. Using the long-term mean monthly data of air and water temperature curves were fitted. Long-term average monthly air temperature data of 14 meteorological stations presented in annual meteorological bulletins of LHMS were used for this analysis. A comparison of annual cycles of water and air temperature was made for the periods of the same duration. The dependence between the long-year annual average monthly river water temperature and atmospheric temperature was explored and coefficients of correlation were calculated.

Selecting the rivers for analysis it was considered important to cover a wide range of size, feeding, latitude. The record continuity was important as well.

For the evaluation of winter freezing period of annual cycle the ice cover duration of the River Nemunas at Smalininkai was analyzed for the period of 200 years. The unique data series of ice cover duration were devided into three periods (1812–70, 1871–1930 and 1931–2010) to search the possible trends. The correlation coefficients between ice cover duration and winter season (December-February) average air temperature in Vilnius MS were calculated for these periods.

On the temporal scale water temperature varies following both a daily and annual cycle [12]. As the water temperature in WGS is measured only twice a day (at 8 a.m. and at 8 p.m.), to understand the river water temperature behavior during the day (over a 24 hour period) hourly water temperature measurements were performed on August 4, 2011 in the River Šventoji at Anykščiai WGS. The thermometer of Anykščiai WGS was used for the measurements.

3. RESULTS

3.1. Annual cycle of water temperature

Water temperature of rivers varies on the basis of spatial and temporal scales. On the temporal scale water temperature varies, following both a daily and annual cycle.

The annual thermal regime of rivers due to intense turbulent mixing and the absence of convection is not very complicated. In the practice the annual thermal cycle of the watercourse can be divided into two periods: ice-free and winter freeze [13].

3.1.1. Ice free period

The studied rivers exhibit strong seasonal changes in water temperature. Analysis of annual cycle of water temperature of different rivers performed using long-term data revealed that the water temperature of Lithuanian rivers is generally close to freezing during the winter, with a sinusoidal annual temperature cycle from spring to autumn (Fig. 2).

The form of the annual water temperature regime is similar for the different rivers. Water temperature is low and changes little during the first three months of a year and usually reaches the minimum in January or February. A steep rise in water temperature begins in April and continuous to increase until the maximum is reached during July. In August water temperature gradually declines and reaches low values in December.

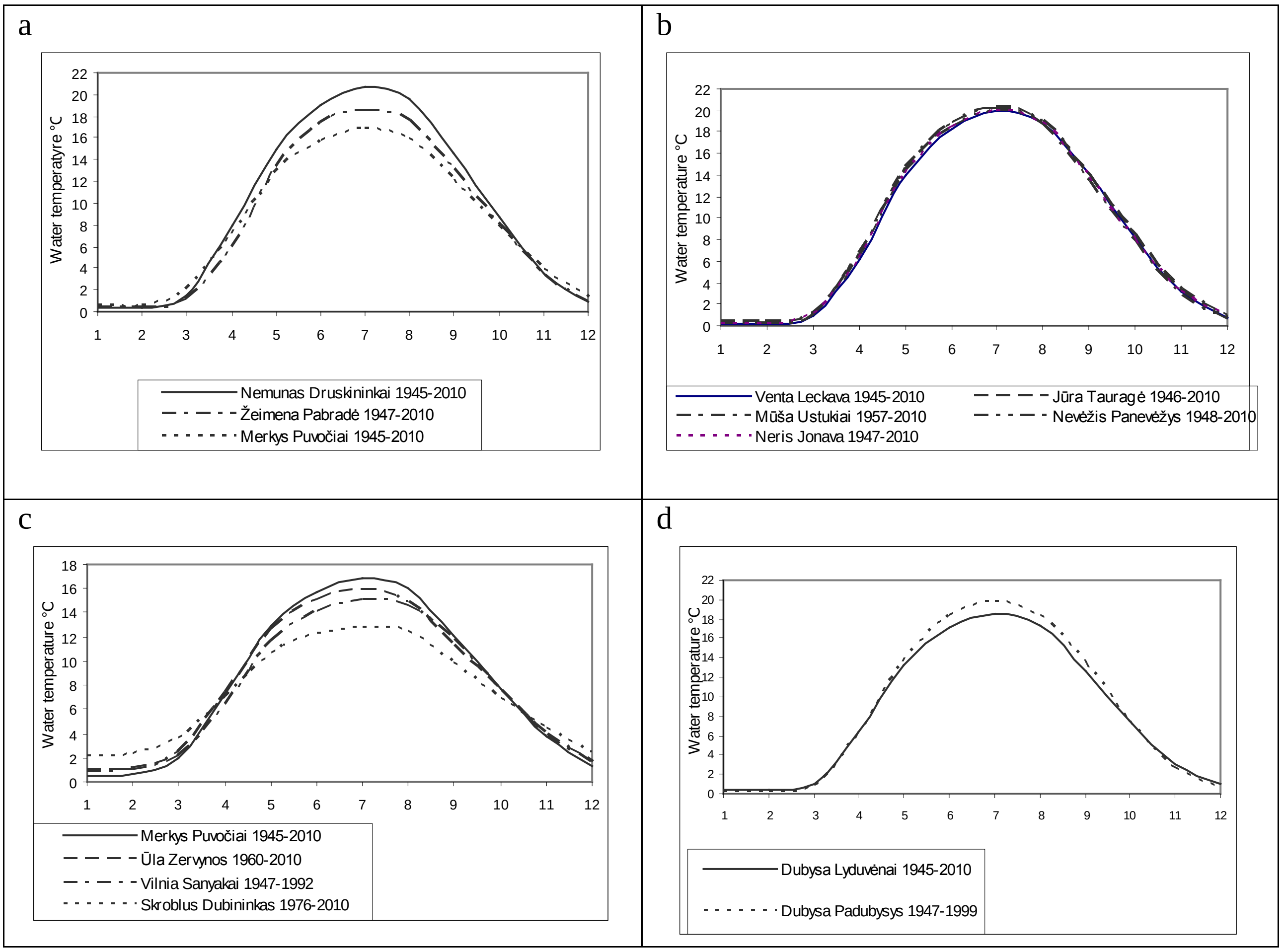

Fig. 2. Long-term annual component (annual cycle) in water temperatures at the warm, cool and cold rivers

However, there are some differences in the nature of annual cycle between the rivers. In [14] the rivers were grouped into three groups according to average water temperature of the warm season (May-October): the warm, cool and cold water rivers. The water temperature averages of the warm season (May-October) were calculated for 41 WGS that have data series covering the 1961–1990 standard normal period. The overall average water temperature of standard normal period (t = 14.9°C) was accepted as the main point for classification of the rivers. The temperature step for this classification was Δt = 0.5°C, because it was ascertained that in the same river and between separate rivers water temperature is statistically ($\alpha = 0.05$) different, when $\Delta t \geq 0.5$°C. The rivers or river reaches, that have water temperature data covering the period of 1961-1990 were divided into the three groups: the warm water ($t \geq 14.9$°C), the cool water (13.4°C<t<14.9°C) and the cold water ($t \leq 13.4$°) rivers or river reaches.

Fig. 2a illustrates the annual cycles of the warm water (Nemunas at Druskininkai), cool water (Žeimena at Pabradė) and cold water (Merkys at Puvočiai) large rivers. It can be seen that these rivers have different thermal regime.

Statistical evaluation was performed to determine whether water temperature differences of these rivers are statistically significant. The null hypothesis H_0 was formulated; it claims that there is no difference between the two rivers data sets of water temperature of the warm season (May-October) on average $H_0 : \bar{x}_1 = \bar{x}_2$. The values of Student's test ($\hat{t}$) were calculated according [15]

$$\hat{t} = \frac{\bar{x}_1 - \bar{x}_2}{\sqrt{S_1^2 + S_2^2}}\sqrt{n}\,.$$

Where: S-standard deviation; $\bar{x}_1$ and $\bar{x}_2$ - averages of all data points; *n*–– number of data points in the set.

Then the Student's T values (theorized values $t_{\alpha;m}$) were established. The significance level α = 0.05 was chosen (hydrology science tends to accept the 95% benchmark) and a total number of degrees of freedom ($m=n_1+n_2-2$) for both data sets was determined. According to the chosen significance level and the number of degrees of freedom a Student's T values ($t_{\alpha;m}$) were found in the statistical table. Calculated values of $\hat{t}$ were compared to the Student's T values $t_{\alpha;m}$ and then $\hat{t} > t_{\alpha;m}$ null hypothesis was rejected and considered that $H_0 : \bar{x}_1 \neq \bar{x}_2$ and averages $\bar{x}_1$ and $\bar{x}_2$ differ from each other in a significant 95% accuracy. Results are presented in Table 1.

Table 1. Parameters of statistical evaluation of warm water (Nemunas at Druskininkai), cool water (Žeimena at Pabradė) and cold water (Merkys at Puvočiai) large rivers

River-water gauging station	Period of measure-ments	Multi-annual mean $\bar{x}$	Standard deviation δ	Calculated value of t-test $\hat{t}$	Degrees of freedom, *m*	Theorised value $t_{\alpha;m}$
Nemunas-Druskininkai	1947–2010	19.7	1.06	11.2	128	1.98
Žeimena-Pabradė	1947–2010	17.8	0.910			
Žeimena-Pabradė	1947–2010	17.8	0.909	10.3	128	1.98
Merkys-Puvočiai	1947–2010	16.2	0.832			

The greatest thermal difference in rivers occurs at maximum summer water temperatures (in July). At peak summer temperature, the cold water River Merkys is 3.7°C colder than the warm River Nemunas. Water temperature of the warm River Nemunas is highest only in the warm season, but in winter water temperature of this river is equal to the water temperature of the cool River Žeimena and slightly lower than the cold River Merkys.

The vast majority of large rivers are the warm water rivers and their annual water temperature cycles are very similar, although they run in different regions of country (Fig. 2b.)

Almost all cold rivers are the small rivers, with the exception of the River Merkys. The annual cycles of cold rivers are more different than those of large rivers; and the smaller the river, the colder its water (Fig. 2c). Also it can be concluded that contrasts in the annual temperature regime between cold rivers are mainly a function of water temperature during the summer months**,** since significant differences between rivers do not become established until April and then increase to the maximum in July and August.

Fig. 2d shows differences of water temperature in annual cycle between two WGS on the same river. Figure shows that the River Dubysa water temperature is higher at the downstream WGS of Padubysys than at headwater WGS of Lyduvėnai. The curves of annual cycles of headwater and downstream WGS of the Šušvė, Šešupė, Jūra and other rivers show the same situation. It may be probably related to the smaller flow volume and lower thermal capacity in headwater WGS. The reverse situation is observed in the River Žeimena. The temperature curve of headwater WGS at Kaltanėnai shows the higher temperature than downstream WGS at Pabradė. The reason is that the river outflows from the lake which waters have the large thermal capacity.

3.1.2. *Winter freezing period*

Observation data for the period of 1945-2010 show that in the first half of this period the most of Lithuanian rivers froze in winter. However**,** the vast majority of rivers do not freeze every year or freeze rarely during the last 30-year period. Rivers were covered with ice only during very cold winters of 1985, 1986, 1996, 2010 and had shorter duration of ice cover.

According to unique, almost 200 year data series of the River Nemunas at Smalininkai WGS the multi-annual ice cover data were graphed and a 5-year and 10-year moving average trend lines were plotted (Fig. 3).

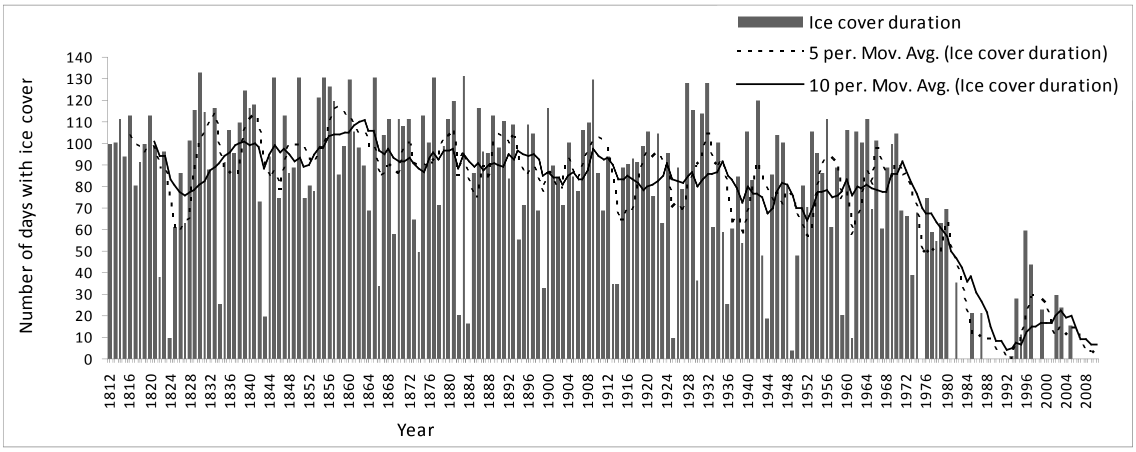

Fig. 3. Duration of ice cover in the River Nemunas at Smalininkai (1811–2010)

The Figure shows a significant reduction in the duration of ice cover in recent years. An average duration of ice cover during the period of 1812-2010 was 75 days. According to Fig. 3 this 200 year period could be divided into 2 periods: 1811-1980 and 1981-2010. During the first period the River Nemunas at Smalininkai froze every year (with the exception of 1975). Duration of ice cover period extended from 4 to 133 days and average ice cover duration of this period was 87 days. In the most recent 30 - year period (1981-2010) average ice cover duration was only 11 days, it extended from 2 to 60 days. The ice cover was even absented 19 years from 1980 to the present date. Moving average analysis revealed decrease in ice cover duration over the last 30 years too.

Mann-Kendall test was used to detect trends in the ice cover duration data time series of the River Nemunas at Smalininkai WGS and air temperature of Vilnius WGS. The presence of trends is evaluated using Z value. A positive (negative) value of Z indicates an upward (downward) trend. A test was applied to evaluate changes of ice cover duration data in 1812-70, 1871-1930 and 1931-2010 periods. In the data of the first and second periods no significant trends was found, whereas in the data of the third period significant trends were identified. Very significant (significance level α=0.001) negative trend in last period was identified for ice cover duration and significant (significance level α=0.01) – for air temperature. A statistically significant correlation was found between the ice cover duration and average winter (December-February) air temperature. Correlation coefficients are presented in Table 2.

The analysis of ice cover duration in the River Nemunas at Smalininkai has revealed that warming winters cause shorter ice cover duration or absence of ice cover. So, it can be maintained that the river ice regime reflects global climate warming trends.

Table 2. Trends of ice cover duration in the River Nemunas at Smalininkai WGS and winter season average air temperature in Vilnius MS

Period	Ice cover duration		Winter season (December-February) air temperature		R
	Z	Trend	Z	Trend	
1812–1870	0.68	Insignificant trend	0.85	Insignificant trend	0.65
1871–1930	-1.41	Insignificant trend	1.03	Insignificant trend	0.74
1931–2010	-6.32	Very significant negative trend	2.85	Significant positive trend	0.63

3.1.3. Comparison of annual cycles of air and water temperatures

The majority of the total energy exchange within a river is thought to occur at the air-water interface. Therefore, the river water mass relatively quickly reacts to changes in meteorological conditions. Water temperature regime in rivers is influenced basically by changes in air temperature [16, 17].

The comparison of annual cycles of river water temperature and air temperatures of geographically closest meteorological stations revealed that river annual thermal cycles follow atmospheric temperature. (Fig. 4). However, the water and air temperatures vary with the lag in time.

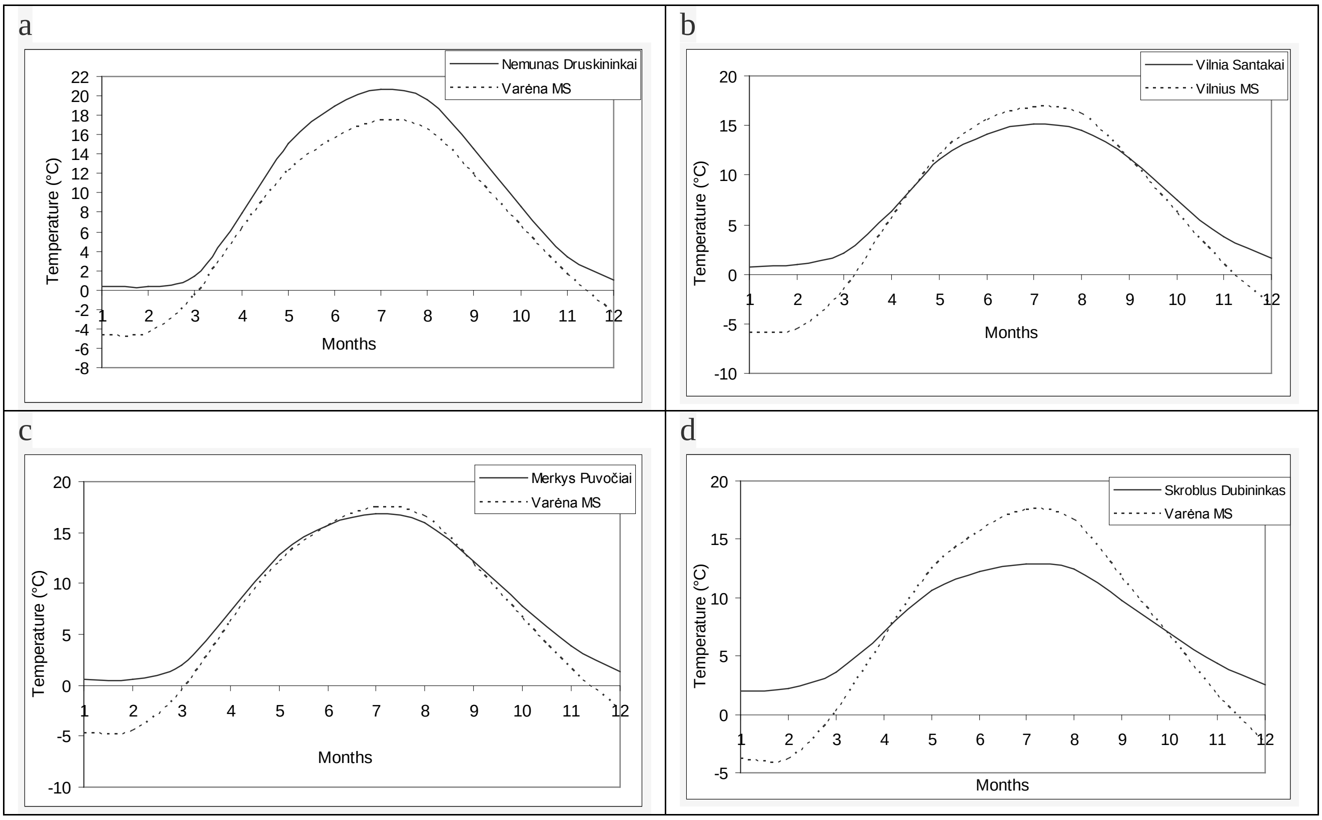

Fig. 4. Long-term annual cycles of river water temperature and air temperature

A comparison of annual cycles highlights that water temperature of large warm rivers is higher than air temperature of neighbouring MS in all seasons of annual cycle (Fig. 4a). The greatest thermal differences occur at summer temperatures (from July to August). At summer the warm rivers are 3–4°C warmer than air temperature.

Water temperature of cold rivers is lower than atmospheric temperature in the warm season, and it is higher - from late autumn to early spring (Fig. 4b). An exception is the River Merkys. The warm season water temperature of this relatively large cold river and air temperature of geographically closest Varėna MS are similar (Fig. 4c). Thus, it can be concluded that the warm season water temperature of small cold rivers is lower than the air temperature of the closest MS; and the smaller and colder the river, the greater the difference **(**Fig. 4b-4d). Small, cold rivers do not freeze in winter.

The relationships between the long-term average monthly river water and air temperatures were established and presented in Table 3.

Table 3. Correlation coefficients between the long-term average monthly river water and air temperatures

River-WGS	MS	Period	n	R
Nemunas-Druskininkai	Lazdijai MS	1945-2010	66	0.99
Merkys-Puvočiai	Varėna MS	1945-2010	66	1.0
Skroblus-Dubininkai	Varėna MS	1976-2010	35	1.0
Verknė-Verbyliškės	Varėna MS	1947-2010	64	0.99
Neris-Jonava	Kaunas MS	1947-2010	64	0.99
Vilnia-Santakai	Vilnius MS	1947-1992	46	0.99
Žeimena-Kaltanėnai	Utena MS	1961-2000	40	0.97
Žeimena-Pabradė	Vilnius MS	1947-2010	64	0.99
Šventoji-Anykščiai	Utena MS	1945-2010	66	0.99
Minija-Kartena	Klaipėda MS	1948-2010	63	0.98
Upita-Eidukai	Šilutė MS	1980-2010	31	1.0
Venta-Papilė	Telšiai MS	1947-2010	64	0.99
Rešketa-Gudeliai	Laukuva MS	1946-1999	54	0.99
Mūša-Ustukiai	Biržai MS	1957-2010	54	0.99

Air temperature is predicted to increase over the coming years as a result of global warming, and this is likely to result in a corresponding increase in water temperature. Water temperature can be identified as being an important climate change indicator.

3.2. Daily cycle of water temperature

As river water temperature varies temporally on a daily cycle, the point in the cycle at which a measurement is taken may affect monthly temperature means calculated from the daily average data. The daily cycle of river water temperature was analysed in order to check whether the mean water temperature of two measurements (8 a.m. and at 8 p.m.) represents the average daily temperature.

The diurnal variation of river water temperature is characterized by amplitude and time of occurrence of the highest and lowest water temperatures. The amplitude of the diurnal cycle of temperature is very variable, its value is related to the height and duration of the sun above the horizon, the source of feeding of the river and the nature of the atmospheric conditions [10].

For the analysis of the diurnal thermal cycle the data of hourly water temperature measurements in the River Šventoji over a 24-hour period were used. The curve of diurnal water temperature variation was plotted (Fig. 5).

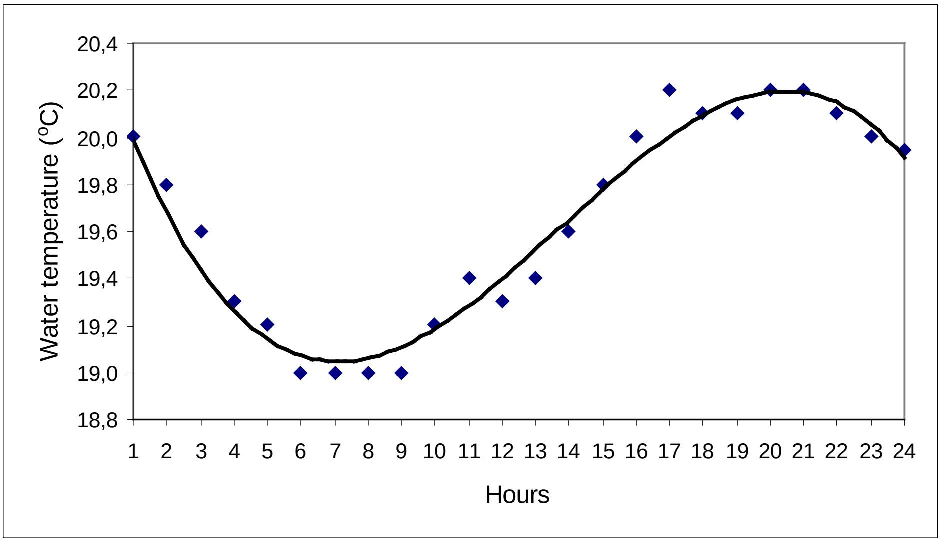

Fig. 5. Daily water temperature variation on the River Šventoji at Anykščiai in August 4, 2011

The curve of diurnal water temperature variation shows that water temperature in a daily course varies from 19.0°C to 20.2°C, therefore daily amplitude of water temperature is 1.2°C. Over a 24-hour period, water temperature was at a maximum in the evening (from 17:00 to 21:00) and at a minimum in the morning (from 06:00 to 09:00). The average temperature of 24–hour period was 19.7°C. It may be noted that the value equivalent to the daily mean water temperature was at the night (between the 02:00 and 03.00) and in the afternoon (between 14:00 and 15:00). Also, it can be seen that average water temperature from 2 measurements of 08:00 and 20:00 is 19.6°C and almost equal to the daily mean water temperature (19.7°C). This pattern justifies the daily measurements (08:00 and 20:00) in WGS of Hydrometeorological Service.

4. CONCLUSIONS

The water temperature of Lithuanian rivers has a sinusoidal annual temperature cycle from spring to autumn. The form of the annual thermal regime is similar for the rivers of different size and water temperature (warm, cool and cold water). The large warm water rivers have identical thermal cycles, whereas the cold water rivers are more various, but the contrasts in the annual temperature regime between the cold rivers are mainly a function of water temperature during the summer months.

Very significant negative trend in the period of 1931-2010 have been identified for ice cover duration in the River Nemunas at Smalininkai and significant positive trend for air temperature of Vilnius MS. The analysis has revealed that warming winters cause shorter ice cover duration in the River Nemunas at Smalininkai over the late part of the record, from 1980 to the present date. The ice cover even often absent over this period.

A comparison of long-term annual thermal cycles of water and air temperatures shows that river water temperature follows air temperature of neighbouring MS. The correlation coefficients between the average long-term monthly water and air temperatures are high (0.97-1.00). Water temperature of the large warm rivers is higher than air temperature in all seasons of annual cycle**,** whereas the warm season water temperature of small cold rivers is lower than the air temperature.

ACKNOWLEDGMENTS

Author would like to express deep gratitude to the reviewers for their helpful comments that allowed to improve the quality of manuscript.

REFERENCES

1. SMITH, K. The prediction of river water temperatures. *Hydrological Sciences-Bulletin-des Sciences Hydrologicue*, 26**,** 1, 1981. No 3 – p. 19–31.
2. Wichert, G.A., Lin, P. A species tolerance index of maximum water temperature. *Water Quality Research Journal of Canada*, 1996. No 31 (4) – p. 875–893.
3. Deas, M.L., Lowney, L.L. Water temperature modelling review: Central Valley. *California Water Modeling Forum*. 2000 – 117 p.
4. Kolupaila, S. Nemuno užšalimai per 120 metų (1811-1930). *Kosmos*. 10-12. 1930 – p. 299–305.
5. Basalykas, A., Darškus, R. Kudaba, Č. at al. Nemunas 1, 1977 – p. 40–43.
6. Grižienė, G.J., Čelkis, R.I., Jablonskis, J.S. Характеристики температуры воды реки Нямунас по данным наблюдений 1945–1980 г. *Труды Академии наук Литовской СССР.* С. Б, 1983 – p. 43–52.
7. Rimavičiūtė, E. Tvenkinių poveikis Lietuvos upių žemutinio bjefo terminiam režimui. [The Impact of Reservoir on Thermal Regime of Lithuanian River Tailwaters]. *Environmental research, engineering and management*. 2000, No 2 (12) – p. 3–12.
8. Meilutytė-Barauskienė, D., Kovalenkovienė, M., Šarauskienė, D. The impact of runoff regulation on the thermal regime of the Nemunas. *Environmental research engineering and management*. 2005. No 4 (34) – p. 43–50.
9. Vanagaitė, J., Valiuškevičius, G. Assessment of river water temperature compliance with ecological requirements in Lithuania. *Geografija* No 47(2) – p. 62–70.
10. Ресурсы повехностных вод СССР, Т. 4, Ч. 1. 1969 – 508 p.
11. Poff, L.N., Brinson, M.M., Day, J.W.J. Aquatic ecosystems and global climate change. *Report of Pew Centre of Global Climate Change*. 2002 – 45 p.
12. Caissie, D. The thermal regime of rivers: a review. *Freshwater Biology*, 51, 2006. – p. 1389–1406.
13. Козлов, Д.В. Основы гидрофизики. 2004. 246 p.
14. Jablonskis, J., Jurgelėnaitė, A. Vandens temperatūros įvairovės savitumai Lietuvos upėse. *Energetika* 2010. No 2(56) – p.163–171.
15. Шторм, Р. Теория вероятностей математическая статистика статистическийконтроль качества. 1970 – 368 с.
16. Одрова, Т.В. Гидрофизика иодоемов суши. 1979 – 311 p.
17. Hammond, D., Pryse, A.R. Climate change impacts and water temperature. *Science Report UK Environment Agency*. 2007 – 101 p.

CYSENI 2012, May 24–25, Kaunas, Lithuania
ISSN 1822-7554, www.cyseni.com

PECULIARITY OF RADIOCESIUM BEHAVIOUR IN LAKES TAPELIAI, JUODIS AND RAUDONASIS

A. Moisejenkova, A. Girgždys
Vilnius Gediminas Technical University
Saulėtekio ave. 11, LT –10223Vilnius – Lithuania
Phone+37067700345
Email: driumas@gmail.com

N. Tarasiuk
Center for Physical Sciences and Technology
The Institute of Physics,
Savanoriu ave. 231, LT – 02300 Vilnius – Lithuania
Phone 852644858
Email: kolia@ar.fi.lt

ABSTRACT

Results of integrated studies of radiocesium behaviour in Lake Tapeliai, Lake Juodis and Lake Red using not only common data of radiocesium activity concentration in lakes water and sediments, but also a complex data set of seasonal variations and vertical profiles of standard water variables are presented. Radiocesium activity concentrations in lake water as well as a vertical structure of the water column considerably depend on the inflows of the colored waters from the lake swampy watershed, which are enriched in radiocesium. It was revealed that under conditions of a super warm regime, radiocesium elevated concentrations in the near-bottom waters may be partially due to the thermodynamic mechanism of its release from the bottom sediments. Concerning extreme radiological situations in closed humic lakes related to their specific vertical structure, they may be treated as critical objects in assessing the risk to humans after radionuclide deposition events. In our study we have attempted to elaborate causes and principles of thermodynamic processes related to radiocesium behavior during seasons.

Also there are compared radiocesium activities concentrations in all three lakes. The radiocesium behaviour dependence on standard lake water variables and lake structure was assessed.

Keywords: radiocesium, bottom sediments, “super-warm” lake, water standard variables

1. INTRODUCTION

A study of the radiocesium behavior in lakes is tightly related to the knowledge of their thermal regime. It implies that an annual course of the lake temperature stratification responsible for mixing conditions of the water column affects radiocesium fluxes and processes providing lake self-cleaning. It is believed [1-3] that elevated radiocesium activity concentrations in hypolimnetic waters are induced by its partial remobilization from lake bottom sediments under anoxic conditions. From time of the first announcement of this effect, many studies were designated to reveal possible mechanisms and an extent of radiocesium release from upper layer of the bottom sediments [4–7]. Radiocesium concentrations in water averaged over the entire volume of the lake are further used in modeling of its migration processes in lake sediments [8-10]. Already earlier Santschi et al. [11, 12] evidenced that after the Chernobyl fallouts in deep thermally stratified lakes, processes of radiocesium direct sorption onto upper layer of the bottom sediments in shallow epilimnetic parts of lakes could significantly eliminate its flux to hypolimnion. It implied the necessity of knowledge of the lake thermal structure variations in evaluating the peculiarities of radiocesium loads in bottom sediments.

The aim of the present work is an integrated study of the radiocesium behavior using comprehensive information on the variations of the standard water parameters Lake Tapeliai, Lake Juodis and Red Lake.

2. METHODOLOGY

2.1. Object of study

Lake Tapeliai (54°46'28"N, 25°26'45"E) is located 17 km to the northeast from Vilnius city in a wooded region at 136.1 m above sea level (a.s.l.) (Fig. 1). It is a first water body in the lake chain connected by a brook. The lake is eutrophic. It consists of four sections: a) a southern shallow terrace (depths ~4−5 m); b) a central deepest part of the lake (depths ~ 7-9 m); c) a northern terrace with a gradual bottom deepening from ~1.5 down to ~6 m depths; d) a small bottom terrace in the western side of the lake (depths ~5-6 m).

Lake Juodis (54°46'49" N, 25°26'29"E*)* is located 16 km to the northeast from Vilnius city in a wooded region (Fig. 1). It is a small (~0.1 km^2) running shallow lake in the lake chain connected by a brook. Its banks are rush-grown, with large marshy zones formed at the brook inflow and outflow areas. The Lake Juodis basin is of the glacier origin (groove type) and consists of two parts. The southern part of the lake is wider and deeper (up to 3.5-m deep). The northern one is a shallow bottom terrace (depth ~1.0−1.7 m).

A small (2.3 ha) humic lake (Fig. 1) belongs to the catchment area of the Varžuva River (41.2 km^2) [13] as part of a source impoundment (6.9 km^2) (Fig. 1). Water of the lake is highly coloured. We denominated it further as Red Lake due to the distinct reddish colour of its sand bottom in the shallow area. It is located 19 km to the northeast of Vilnius in a small depression (~137.4 m above sea level) surrounded by a pine forest. From the north, west and south its open water basin (~1 ha) is separated from the banks by marshy zones. The lake mean and maximum depth amounts to ~1.6 and 4.5 m, respectively.

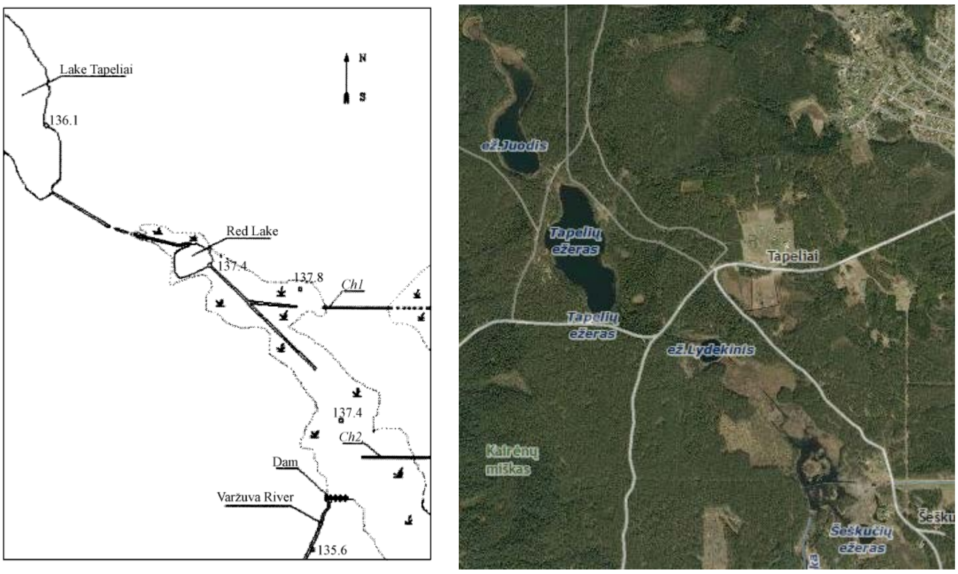

Fig. 1. Location places of lakes

A foretime, it was an ordinary eutrophic lake with transparent water and bottom feeding sources. It was connected by outflowing ditches with Lake Tapeliai (136.1 m a.s.l.) and the catchment of the Varžuva River (Fig. 1). The main sources of the Varžuva River impoundment are a small brook from the swamp (*Ch1*) and the outflow of the drainage ditch (*Ch2*) from a large meadow. Water of both sources is also highly coloured. Some thirty-five years ago, a source zone of the Varžuva River was dammed and an outflowing ditch connecting Red Lake and Lake Tapeliai was blocked by a sand buffer. During the filling of the depression, a thick layer of some 70 cm of humic water covered the surface of Red Lake. Consequences of this event were dramatic. Apparently, bottom-feeding sources of the lake were blocked and the regime of vertical mixing changed. Finally, Red Lake turned into the repository of humic water.

2.2. Parameterization

Vertical profiles of standard water parameters (pH, temperature, oxygen concentration) were episodically measured in the lakes water column. The aim of the study was to estimate lake mixing conditions and seasonal variations of the lake vertical structure. A portable device ProfiLine Multi 197i (WTW) with 10-m cables allowed carrying out these measurements down to the lake bottom. During a warm period, measurements were conducted from an inflatable boat, stabilized by an anchor. In winter, holes were drilled in ice. As a rule, measurements were carried out in the deepest site of the central part of the lake.

2.3. Water and sediments sampling

The Molchanov type bathometer was used for water samples. In this case, parameters of water samples were averaged over the 40-cm depth interval of the sampler. After delivery to the laboratory, only the aerobic water samples were passed through the Filtrak 391 type filters using a vacuum pump system. Hypolimnetic water samples, where on exposure to air an iron oxide floc was created, were not filtered. Further, surface water aliquots and hypolimnetic water samples were evaporated on a water bath to get dry deposits (further cited as total dissolved solids), which were analyzed for the radiocesium content. Radiocesium activity concentrations associated with the suspended particles in water samples from the central part of the lake area were always below the detection limit (~0.010 Bq) and were not considered. Sediment cores were taken in 2003–2009 using the Ekman–Birge type sampler. It was a steel tubing with a square cross-section, and had a manually operated spring bottom shutter. Two versions of this sampler were used: an ordinary one of the 20-cm height (2 sediment cores) and the improved version of the ~40-cm height (17 sediment cores) with cross-sections of 15 × 15 cm and 14 × 14 cm, respectively. The sampling was carried out with the weight compensation, where an additional float controlled the depth the sampler sank into the sediments. Sediment samples without the water layer above the sediment surface were discarded. Sediment cores were sliced into layers of about 2–2.5 cm thickness. Considering that the sampler was not waterproof, the slicing was conducted in shallow waters near the bank using a special spoon to fill the plastic bottles of standard volume and gradually moving the sampler up to the bank. Bottles were held for some time to settle the sediments, and real sediment volumes were determined. Sediment samples were air-dried at room temperature. Their weights as well as weights of dry deposits of water samples were determined using scales VLV-100 (former SU device) where samples were held under thermostatic conditions (in the 40–50°C temperature interval) up to constant weight. Measurements showed that dry deposits of water samples were hygroscopic and could change their weight in ambient air in the range ±5%.

2.4. Radiocesium measurements in sediments and water samples

Sediment samples were analyzed for ^{137}Cs using a SILENA γ-spectrometric system with a HPGe detector (42% relative efficiency, resolution – 1.8 keV/1.33 MeV) according to the gamma line at 661.62 keV of ^{137m}Ba (a daughter product of ^{137}Cs). Measurements were carried out in standard geometry and known efficiencies according to densities of samples. Measurement errors of the radiocesium activity concentrations in samples were evaluated by the GAMMAPLUS software program. They were less than 5% (standard deviation) for active samples and were not larger than 15% for the deepest less active layers of sediment cores. Activity corrections to the sampling date were not made because measurements were carried out shortly after sampling.

Dry deposits of water samples were analyzed for ^{137}Cs using an ORTEC γ-spectrometric system with a HPGe well-type detector (a sensitive volume of 170 cm^3, a relative efficiency of 38%, resolution – 2.05 keV/1.33 MeV). Density corrected calibration was made using four standards prepared in non-liquid matrices in the density range 0.4–1.7 kg·L^{-1} on the basis of Amersham standard solution [14]. Measurement errors of radiocesium activity concentrations in samples were evaluated by the GAMMAVISION software program and they did not exceed 15%.

3. RESULTS AND DISCUSSION

3.1. Measurements results of Red Lake

Measurements of the vertical profiles of standard water parameters carried out in Red Lake during 2002–2008 showed the lake to be meromictic. Only the upper basin of Red Lake water became oxygenated in spring at water temperatures near 4 ^{o}C. Near-bottom waters of the lake are anaerobic (Fig.2).

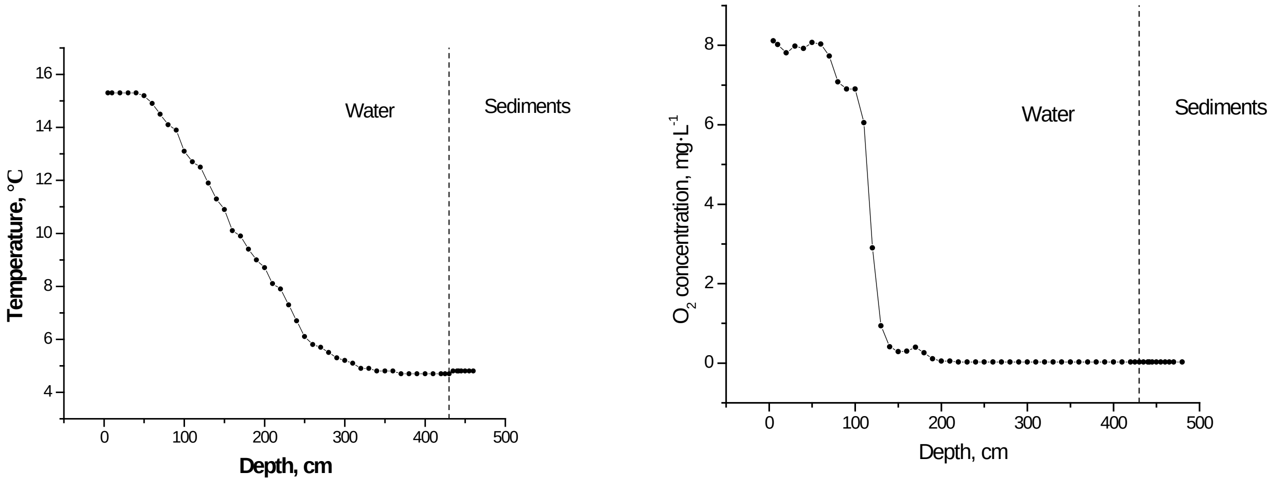

Fig. 2. Vertical profiles of temperature and oxygen concentration in Red Lake, measured on May 14th, 2008

During warm seasons, these oxygen concentrations are typical of the thin surface water layer of 50–70 cm thickness. At the beginning of winter, vertical profiles of oxygen concentrations peak often at the 1–2-m depth and indicate their minimum values in the surface water layer in the immediate vicinity to ice.

Vertical profiles of radiocesium activity concentrations (Bq·kg^{-1}, Bq·l^{-1}) in sediment cores taken at some distances from the deepest site of Red Lake are different. Elevated sedimentation rates and the deepening of radiocesium peak activities to the 3.5–8.5 cm depth interval are characteristic of them. These vertical profiles in one of the cores taken at the 4.1 m depth of water on 24 July 2007 are shown in Fig. 3.

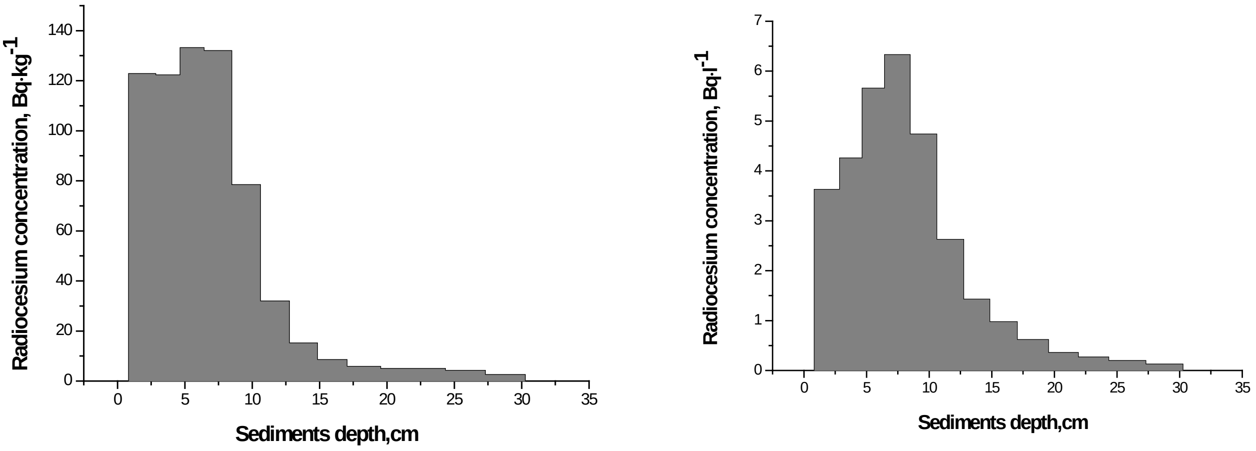

Fig. 3. Radiocesium activity concentration in bottom sediments core of Red Lake, measured on July 24th, 2007

In the case of a normal hydraulic regime of the impoundment when melt-water is partially flushed before the beginning of spring vertical mixing, Red Lake may be treated as a “conservative” system for radiocesium activity concentrations in the upper layer of the bottom sediment and as an analogous model of closed humic lakes. Apparently, as in the case of Red Lake, the vertical structure of closed humic lakes after severe accidents may induce the formation of the extreme radiological situations in limited layers of the water column. As a result, closed lakes with humic water turn into the repository of highly mobile radiocesium in the ionic form and associated with humic substances. Measurements showed (Fig. 4) that radiocesium water-soluble concentrations in Red Lake were the highest among the neighbouring Tapeliai and Juodis Lakes.

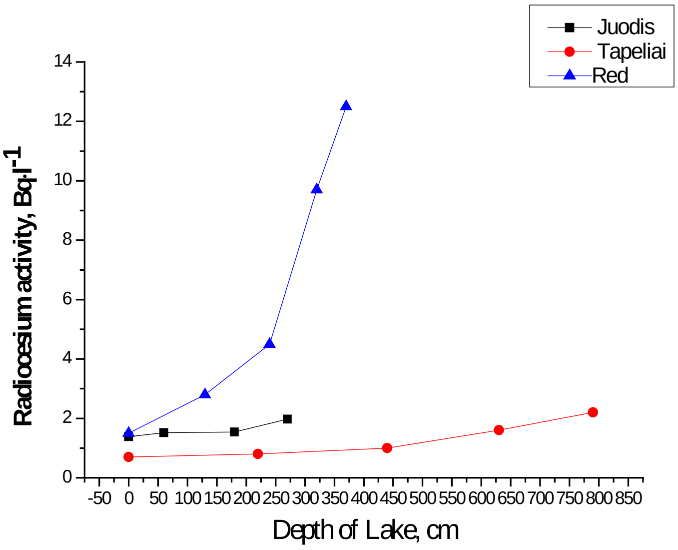

Fig. 4. Radiocesium activity concentration in Lake water

Resuspension of sediments due to the tench activity at the bottom of the upper water layer in the late autumn and spring led to their redistribution distorting originally formed vertical profiles of radiocesium in sediments. These disturbances in the formation of radiocesium vertical profiles in sediments distort assessments of its migration, diffusion coefficients and estimates of sedimentation rates.

3.2. Measurements results of Lake Tapeliai

Measurements of the vertical profiles of standard water parameters (pH, temperature, oxygen concentrations and conductivity) carried out in Lake Tapeliai during 2006 – 2009 showed the lake is dimictic. The water column of the lake becomes totally oxygenated for a very short period in spring at water temperatures near 4 ^{o}C and for a long-term period in autumn due to cooling processes inducing intense gravitational mixing. During other periods, near-bottom waters of the lake are anaerobic. Fig. 5 shows that in summer 2008, a zone of anaerobic waters began at the depth of 5.1 m, sediments heat up 5 ^{o}C.

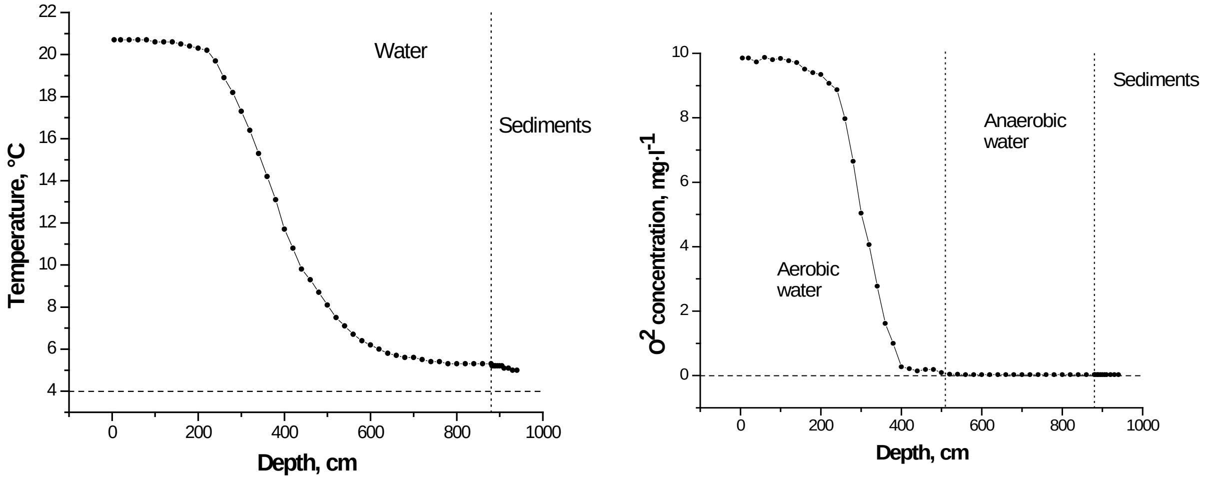

Fig. 5. Vertical profiles of temperature and oxygen concentration in Lake Tapeliai, measured on July 6th, 2008

Vertical profiles of radiocesium activity concentrations in bottom sediments were distinguished for their elevated deepening and did not fit even to the ~40 cm height of our improved sampler. However, estimations of the radiocesium load losses due to the "tails" of its vertical profiles, which did not fit to the sampler height, showed them to be small (≤10%) [15].

Typical forms of the vertical profiles of radiocesium activity concentrations (Bq·kg^{-1}, Bq·l^{-1}) in the sediments as well as those of density of sediment solids in the cores taken in the centre of lake Tapeliai are presented in Fig. 6. Maximum values of radiocesium activity concentrations (Bq·kg^{-1}, Bq·l^{-1}) in the vertical profiles measured in sediment cores all-over the lake varied in the range 160-180 Bq·kg^{-1} and 5.5-7.8 Bq·l^{-1}.

In deep wind-sheltered lakes additional heating of sediments of the deep bottom areas becomes problematic. In such lakes, processes of additional heating take place at lower temperatures and for a shorter period in summer seasons. Ultimately, at some lake depth, processes of the gravitational mixing of the water column can reach the deepest bottom areas at temperatures related to the maximum water density (~4 ^{o}C). In that case, a short-term oxygenation of the whole water column is not related to any additional heating of sediments of deep bottom areas of the lake. A mechanism of heating of the sediments in the deepest bottom areas of the lake is related, apparently, to internal oscillations of the water column (seiches) incited by wind during processes of the gravitation mixing in autumn [16]. Significant overcooling of the water column induces the respective heat losses in the sediments. In turn, buoyancy of interstitial liquids enriched in radiocesium is followed by its release into the completely mixed water column. Therefore, it means that radiocesium will be partially removed with the flushing waters.

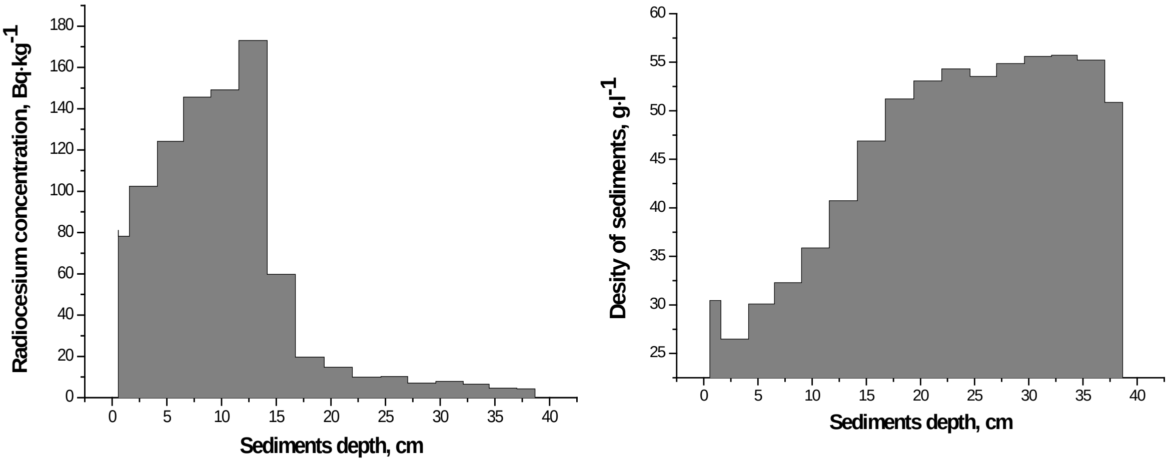

Fig. 6. Radiocesium activity concentration in bottom sediments of Lake Tapeliai, measured on July 6th, 2008

3.3. Measurements results of Lake Juodis

Data on temperature vertical profiles in Lake Juodis show that from the beginning of spring until August sediments act as a heat accumulator. In autumn a decrease in the heat transfer through the water column is followed by its accumulation in the sediment surface layer. At first, it looks like a small temperature rise in the sediment surface layer and later, it may be traced by the formation of a steep temperature gradient (Fig. 6) in the sediment-bottom water interface.

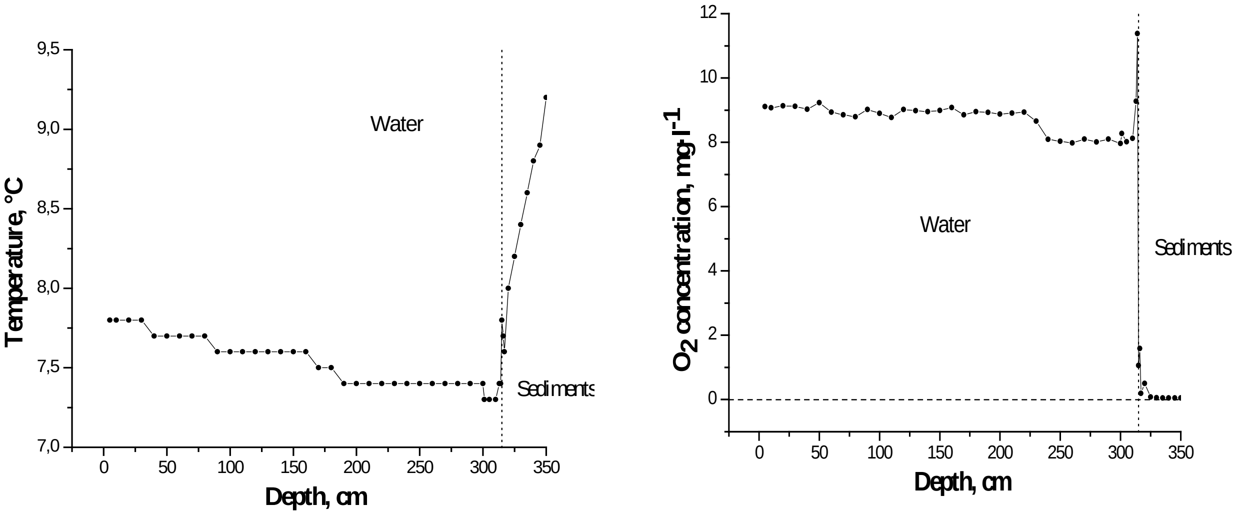

Fig. 6. Vertical profiles of temperature and oxygen concentration in Lake Juodis, measured on November 11th, 2008

The formation of the stagnant water column in deeper lakes with the sediments rich in organics is often followed by the development of the anaerobic zone in the near-bottom waters. It is due to oxygen consumption by decomposition processes of sediment organics and due to the decrease in the downward oxygen flux from the euphotic layer. The intrusion itself of the interstitial liquid with high concentrations of reduced ions induces elevated rates of oxygen consumption in the near-bottom waters as well. Considering that both processes lead to the formation of the anaerobic zone, radiocesium enrichment effects were always meant to be related to that zone formation.

However, the resulting oxidation regime of the near-bottom water layer depends on the spatial distribution of oxygen sources in the lake.

Sediments samples were taken on 11 November 2008 in the temperature stratified water column. Data of the measurements of the vertical profiles of ^{137}Cs activity concentrations are presented in Fig. 7.

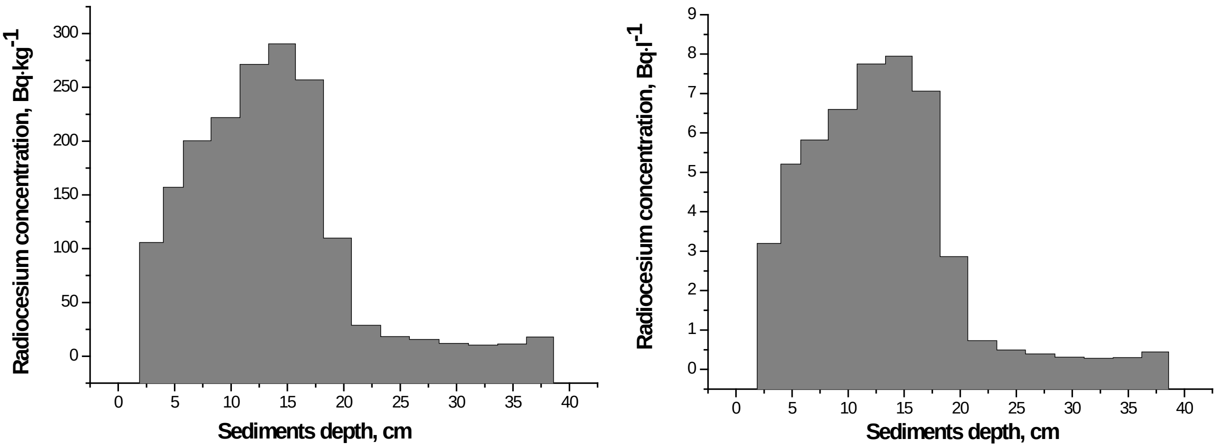

Fig. 7. Radiocesium activity concentration in bottom sediments of Lake Juodis, measured on November 11th, 2008

The vertical profile of ^{137}Cs activity concentrations (Fig. 7) shows that maximum values of radiocesium activity concentration in the vertical profiles measured in sediment cores approximately are 290 Bq·kg^{-1} and 8.1 Bq·l^{-1}, respectively.

Measurement data on temperature and radiocesium vertical profiles in the oxygenated water column showed that an increase in near-bottom water temperatures above 4 ^{o}C related to its larger mineralization due to the interstitial water buoyancy effects was followed by the respective increase in the radiocesium concentration. These data evidenced that formation of the layered structure of the water column due to buoyancy effects and the radiocesium enrichment in the near-bottom water in Lake Juodis in winter did not depend on the formation of the anaerobic zone and were its precursor

4. CONCLUSIONS

Thermodynamic processes of heat redistribution between sediments and the water column are very important for the lake self-cleaning from radiocesium. In lakes such as Lake Juodis or Red Lake where temperatures of the near-bottom water in winter are higher than 4 °C, its primary radiocesium enrichment is mainly due to the specific thermodynamic (buoyancy) mechanism of the sediment interstitial water transfer through the sediment - bottom water interface. In autumn, this mechanism reveals itself under aerobic conditions in cases of the formation of steep temperature gradients in the sediment surface layer due to intense cooling processes as well as due to cooling interruptions on the arrival of warm air masses and the successive thermal stratification of the water column, sharply decreasing a heat flux from sediments.

Present investigations of the radiocesium behavior in Lake Tapeliai showed an advantage of an integrated approach using not only conventional data on radiocesium activity concentrations in lake water and sediments but also a complex data set on seasonal variations and vertical profiles of standard water variables. These complex data show that radiocesium activity concentrations in lake water as well as a vertical structure of the water column considerably depend on the inflows of the colored water enriched in radiocesium from the lake swampy watershed.

REFERENCES

1. ALBERTS, J.J., TILLY, L.J., VIGERSTAD, T.J. Seasonal cycling of cesium-137 in a reservoir, *Science*, 1979, Vol. 203, p. 649–651.
2. DAVISON, W., SPEZZANO, P., HILTON, J. Remobilization of cesium from freshwater sediments, *Journal of Environmental Radioactivity*, 1993a, Vol.19, No. 2, p. 109-124.
3. AVERY, S.V. Fate of cesium in the environment: distribution between the abiotic and biotic components of aquatic and terrestrial ecosystems, *Journal of Environmental Radioactivity*, 1999, Vol. 30, No. 2, p. 139–171.
4. EVANS, D.W., ALBERTS, J.J., CLARK, R.A. Reversible ion-exchange fixation of cesium-137 leading to mobilization from reservoir sediments, *Geochimica et Cosmochimica Acta*, 1983, Vol. 47, p. 1041–1049.
5. COMANS, R.N.J., MIDDELBURG, J.J., ZONDERHUIS, J., WOITTIEZ, R.W., DE LANGE, G.J., DAS, H.A. and VAN DER WEIJDEN, C.H. Mobilization of radiocesium in pore water of lake sediments, Nature, 1989, Vol. 339, p. 367–369.
6. DAVISON, W., SPEZZANO, P., HILTON, J. Remobilization of cesium from freshwater sediments, *Journal of Environmental Radioactivity*, 1993b, Vol. 19, No. 2, p. 109–124.
7. LIU, C., ZACHARA, J.M., SMITH, S.C., MCKINLEY, J.P., and AINSWORTH, C.C. Desorption kinetics of radiocesium from subsurface sediments at Hanford Site, USA, *Geochimica et Cosmochimica Acta*, 2003, Vol. 67, p. 2893–2912.
8. BULGAKOV, A.A., KONOPLEV, A.V., SMITH, J.T., HILTON, J., COMANS, R.N.J., LAPTEV, G.V., CHRISTYUK, B. F. Modelling the long-term dynamics of radiocaesium in closed lakes, *Journal of Environmental Radioactivity*, 2002, Vol. 61, No. 1, p. 41–53.
9. MONTE, L., GRIMANI, C., DESIDERI, D., ANGELI, G. Modelling the long-term behaviour of radiocesium and radiostrontium in two Italian lakes, *Journal of Environmental Radioactivity*, 2005, Vol. 80, p. 105–123.
10. PUTYRSKAYA, V., KLEMT, E. Modelling ^{137}Cs migration processes in lake sediments, *Journal of Environmental Radioactivity*, 2007, Vol. 96, No. 1/3, p. 54–62.
11. SANTSCHI, P.H., BOLLHALDER, S., FARRENKOTHEN, K., LUECK, A., ZINGG, S., STURM, M. Chernobyl radionuclides in the environment: Tracers for the tight coupling of atmosphere, terrestrial, and aquatic geochemical processes, *Environ. Sci. Technol.*, 1988, Vol. 22, p. 510–516.
12. SANTSCHI, P.H., BOLLHALDER, S., ZINGG, S., LÜCK, S, FARRENKOTHEN, K. The self-cleaning capacity of surface waters after radioactive fallout. Evidence from European waters after Chernobyl, 1986–1988, *Environ. Sci. Technol.*, 1990, Vol. 24, p. 519–527.
13. GRIŽIENĖ, G., JABLONSKIS, J., JANUŠEVIČIUS, S., JURGELEVIČIENĖ, I., JURGELIENAITĖ, A., JUŠKIENĖ, A., KRIAUČIŪNAS, R. Hydrography of the Neris river, *Energetika*, 1993, Vol. 1, p. 20–41.
14. GUDELIS, A., REMEIKIS, V., PLUKIS, A., LUKAUSKAS, D. Efficiency calibration of HPGe detectors for measuring environmental samples, *Environmental and chemical physics*, 2000, Vol. 22, No. 3,4, p. 117–125.
15. TARASIUK, N., MOISEJENKOVA, A., KOVIAZINA, E., KARPICZ, R., ASTRAUSKIENĖ, N. On the radiocesium behaviour in a small humic lake (Lithuania), *Nukleonika*, 2009, Vol. 54, No. 3, p. 211–220.
16. ARSENEVA, N.M.; DAVYDOV, L.K.; DUBROVINA, L.N.; KONKINA, N.G. *Seiches in lakes in the USSR.* Leningrad, Leningrad University press, 1963, 276 p. (in Russian).

CYSENI 2012, May 24–25, Kaunas, Lithuania
ISSN 1822-7554, www.cyseni.com

ASSESSMENT OF SOLID WASTE LANDFILL LEACHATE TOXICITY USING AQUATIC MICROINVERTEBRATES AND PLANTS

J. Žaltauskaitė
Vytautas Magnus University
Vileikos str. 8-223, LT-44404 Kaunas, Lithuania
Phone +370 37 327920
Email: j.zaltauskaite@gmf.vdu.lt

ABSTRACT

The large number of municipal solid waste landfills in Lithuania poses a serious environmental threat to our surface and groundwater reserves. The toxicity of Kairiai municipal solid waste landfill was evaluated using bioassays with aquatic organisms. Landfill leachate is complex mixture of various inorganic and organic compounds. Three tests were conducted with several dilutions of untreated and treated leachate samples. Leachate toxicity was assessed using the acute microcrustaceans (*Thamnocephalus platyurus* (24 h) and *Daphnia magna* (48 h)) assays and growth inhibition test of *Spirodela polyrhiza*. Untreated Kairiai solid waste landfill leachate was shown to be severely toxic to *D. magna*, and *T. platyurus* with LC_{50} 3.23% and 3.51% respectively. Treatment of leachate has resulted only in slight reduction in toxicity to microinvertebrates with LC_{50} 5.53% and 3.97 % for D. magna and T. platyurus, respectively. Landfill leachate significantly inhibited the growth of *S. polyrhiza* and EC_{50} for growth rate was 50.1%. The applied bioassays were ranked according to their sensitivity to the landfill leachate as follows: *D. magna* > *T. platyurus* > *S. polyrhiza.*

Keywords: bioassays, landfill leachate, acute toxicity, toxicity testing

1. INTRODUCTION

The large number of municipal solid waste landfills in Lithuania poses a serious environmental threat to our surface and groundwater reserves. Leachate is generated by the percolation of rainwater and moisture through the layers of waste in landfills. Leachate from municipal landfills contains a complex variety of organic and inorganic compounds [1]. Composition of leachate depends of the age of the landfill, the degree of solid waste stabilization, waste characteristics and composition, size of hill, the moisture and degree of rainwater infiltration, temperature and landfill geometry. Leachate can be a major source of contamination to soil, surface waters and groundwater. The major potential effects of a leachate release to surface water are related to oxygen depletion, changes in water body fauna and flora and ammonia toxicity [2]. The exposure of landfill leachate to environment and biota may occur in different ways, such as uncontrolled overflow, rainfall runoff and infiltration.

In Lithuania hazard assessment of landfill leachate is based on the physicochemical parameters (e.g. biological oxygen demand (BOD), pH, chemical oxygen demand (COD), total dissolved solids). However, these parameters do not give an indication on the toxic potential of the leachate. Toxicity bioassays, in contrast to physicochemical analysis, integrate the biological effects of all compounds present and other factors such as bioavailability, toxicants interaction and others. Toxicity bioassay, using species that represent the different trophic levels, is the best approach to evaluate the toxicity of leachate.

The impact of the leachate on living organisms is very high and governed by several factors, such as high load of organic matter, heavy metals, high content of nitrogen. Several landfill leachate toxicity assessment studies have showed the leachate as mutatoxic and genotoxic [3-6]; as endocrine disrupter it may cause various other reproductive effects [7–8].

The main aim of this paper was to determine Kairiai landfill leachate toxicity to aquatic microcrustaceans (*Thamnocephalus platyurus* and *Daphnia magna*) and higher plant *Spirodela polyrhiza*.

2. MATERIAL AND METHODS

The sampling was performed in a landfill leachate storage reservoir of municipal solid waste landfill in Kairiai. The samples of untreated and treated leachate were collected in April of 2009. The sample of pond water in the vicinity of the landfill was also taken for analysis.. Samples were filtered (0.45 μm) and stored in darkness and in refrigerator prior to performance of the biosassays.

Chemical characteristics, determined using Visocolor colorimetric tests (Macherey-Nagel), of sampled leachate are presented in Table 1.

Table 1. Chemical characteristics of untreated, treated landfill leachate and the pond water (mg/l)

	NO_3^-	NO_2^-	NH_4^+	PO_4^{3-}
Untreated leachate	8	0.08	400	8
Treated leachate	12	0.08	100	4.8
Pond water	20	0.5	10	0.2

Such leachate chemistry parameters are typical for the leachate of municipal landfills [2]. Elevated concentrations of pollutants were also observed in the surface and ground water in the vicinity of Kairiai landfill [9].

Toxicity assessment was performed with three different tests: two bioassays with microcrustaceans (Daphtoxkit FTM magna, a 24-48 h mortality (immobilization) test with the *Daphnia magna* [10] and Thamnotoxkit FTM, a 24 h mortality test with *Thamnocephalus platyurus* [11]) and one bioassay with aquatic higher plant *Spirodela polyrhiza*, growth inhibition test.

For toxicity tests a dilution series of five leachate concentrations (i.e., 100, 50, 25, 12.5 and 6.25% leachate) and a control was made. The assays were performed in 3 replicates per treatment. The control for microcrustaceans was growth medium for aquatic invertebrates, made from concentrated salt solutions. The control for plants was modified Steinberg medium (KNO_3 3.46 mM, $Ca(NO_3)_2 \times 4H_2O$ 1.25 mM, KH_2PO_4 0.66 mM, K_2HPO_4 0.072 mM, $MgSO_4 \times 7H_2O$ 0.41 mM, H_3BO_3 1.94 μM, $ZnSO_4 \times 7H_2O$ 0.63 μM, $Na_2MoO_4 \times 2H_2O$ 0.18 μM, $MnCl_2 \times 4H_2O$ 0.91 μM, $FeCl_3 \times 6H_2O$ 2.81 μM, EDTA-$Na_2 \times 2H_2O$ 4.03 μM) [12].

Microbiotests with invertebrates were performed according to the Toxkit Standart Operational Procedures [10]. The crustacean toxicity test to assess the immobilization of *Daphnia magna* was conducted by hatching neonates from ephippia after 72–80 h of incubation at 20–22 °C in standard growth medium of *D. magna* under continuous illumination (6000 lux). 5 organisms were exposed to each dilution sample in 3 replicates. After 24 h and 48 h incubation in dark conditions at 20 °C, the number of dead and immobilized neonates was recorded.

The crustacean toxicity test to assess the mortality of fairy shrimps *Thamnocephalus platyurus* was conducted by hatching them from cysts after 20-22 h of incubation at 25 °C standard growth medium of *T. platyurus* under continuous illumination (3000-4000 lux) [11]. 10 organisms were exposed to each dilution sample in 3 replicates. After 24 h incubation in dark conditions at 25 °C, the number of dead larvae was recorded.

The tests were considered valid if the mortality in control did not exceeded 10 %. Results for the toxicity tests were expressed as the concentration of the sample that produced a 50% effect (mortality) (LC_{50}). LC_{50} values were expressed as a percentage of leachate tested.

The standardised growth inhibition test with *Spirodela polyrhiza* was performed according to OECD Guideline 221 [13]. The stock culture of *S. polyrhiza* was grown in modified Steinberg medium in growth chambers at 24 °C ± 2°C with a light/dark cycle of 16/8 h. 10 double-fronded healthy *S.*

polyrhiza colonies were transferred to Petri dishes containing different concentrations of leachate. Experiment has lasted 7 days and has been conducted in 3 replicates. Toxicity was recorded as percent inhibition of growth (fronds number) (relative to control) of *S. polyrhiza* as a result of 7-day exposure to the toxicant in its growth medium. Specific growth rate was calculated from the following equation with measured fronds number (N) at the end (t_1) and the start of the test (t_0):

$$r = \frac{\ln(N_{t_1}) - \ln(N_{t_0})}{t_1 - t_0} \tag{1}$$

Toxicity values (LC_{50} and EC_{50}) were converted to Toxic Units (TU), i.e. inverse of LC_{50} (EC_{50}) expressed in %: TU = [1/LC50] × 100.

The toxicity classification is reported as follows [14]:

not toxic	TU < 0.4
slightly toxic	0.4<TU< 1
toxic	1 ≤ TU< 10
very toxic	10 ≤ TU< 100
extremely toxic	≥ TU100

Each species endpoint per leachate solution sample was compared to the corresponding reference sample mean using a Students' t test. The difference was significant at $p < 0.05$.

3. RESULTS AND DISCUSSION

Untreated and treated leachate showed very high lethal toxicity to *T. platyurus* (Fig. 1). The mortality of fairy shrimps was higher than 80% in the lowest concentration of untreated leachate and 75% in in the lowest concentration of treated leachate. The results of logistic regression show that the risk of death of tests organisms increases with the concentration of leachate in test solution (untreated leachate: $\chi 2 = 57.75$, treated leachate: $\chi 2 = 50.39$; $p < 0.05$). Calculated LC_{50} values were 3.51% for untreated leachate and 3.97% for treated leachate.

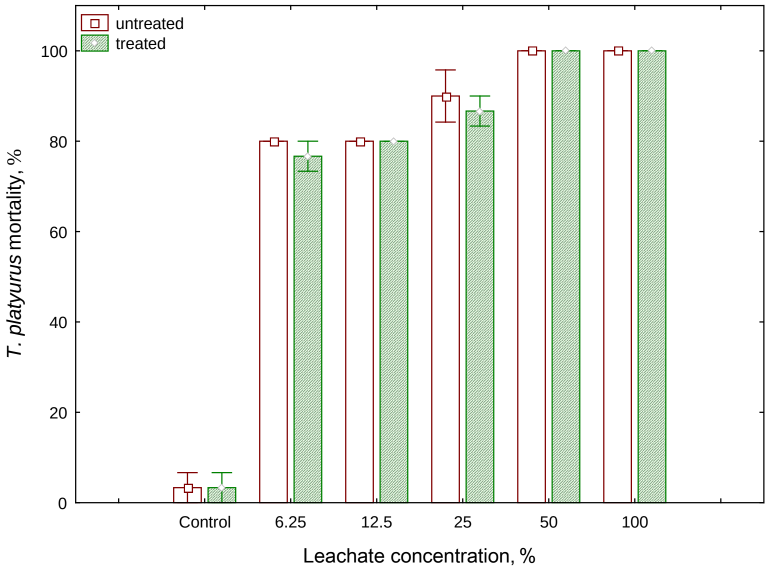

Fig. 1. Mortality of *T. platyurus* exposed to different concentration of untreated and treated leachate

The mortality of *D. magna* (after 24 and 48 h) exposed to different concentrations of untreated and treated leachate was statistically significantly higher of that in control ($p< 0.05$) (Fig. 2A and 2B). The lowest tested concentration of untreated leachate (6.25%) led to the death of 40% of *D. magna* after 24 h of exposure and the toxicity had increased after one more day of exposure, i.e. the mortality reached 70%. Increase in leachate concentration from 6.25 to 12.5% in solution resulted in sharply increase in mortality and it reached 100%.

The toxicity of treated leachate to *D. magna* was slightly lower than that of untreated leachate (Fig. 2B). Only after exposure to undiluted and twice diluted treated leachate died all exposed crustaceans. The solutions containing 6.25-25% of treated leachate caused 20–60% mortality of *D. magna* after 24 h of exposure and the mortality increased to 50–80% after 48 h of exposure

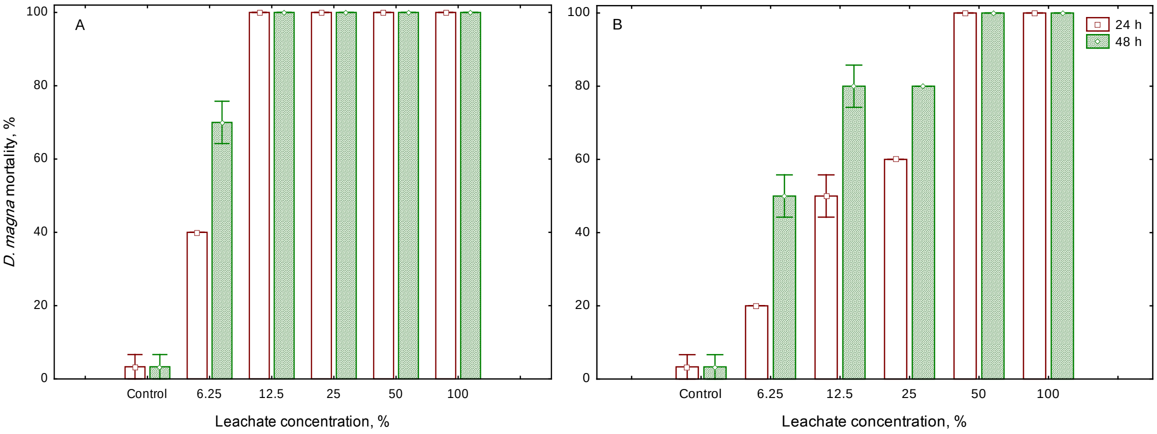

Fig. 2. Mortality of *D. magna* exposed 24 and 48 h to different concentration of untreated (A) and treated (B) leachate

The results of logistic regression show that the risk of death of *D. magna* increases with the concentration of leachate in test solution and the risk is higher in case of untreated leachate (untreated leachate: $\chi 2 = 84.80$, treated leachate: $\chi 2 = 58.97$; $p < 0.0001$). Calculated 24 h LC_{50} values were 4.63% for untreated leachate and 10.80 % for treated leachate.48 h LC_{50} were lower and they reached 3.23% for untreated leachate and 5.53% for treated leachate.

The leachate exhibited high phytotoxicity to the growth of *Spirodela polyrhiza*, representative of *Lemna* spp. (Fig. 3). *Lemna* species is extensively used in ecotoxicological studies and in several studies it was used for landfill leachate toxicity assessment [15–17]. The solutions containing 25-100% of untreated leachate and 50-100% of treated leachate led to breakdown of all *S. polyrhiza* colonies. Exposure to the solutions containing 6.25–12.5% of untreated leachate increased the growth of *S. polyrhiza* by 6–29% and no adverse impact on growth rate was detected. The stimulation of growth may be due to relatively high concentrations of nutrients (nitrogen) in samples. Although the same concentrations of the treated leachate in the solutions inhibited the growth of *S. polyrhiza*.

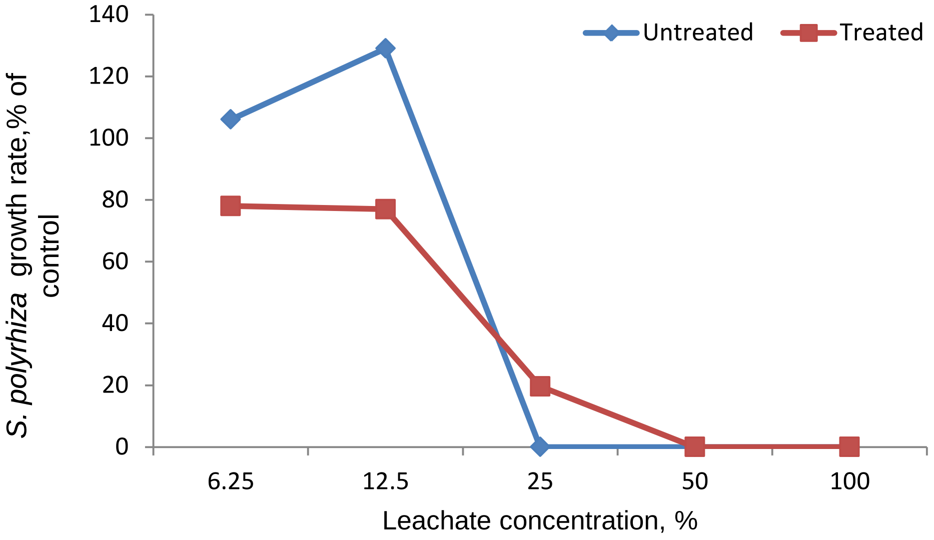

Fig. 3. Growth rate of *S. polyrhiza* exposed for 7 days to untreated and treated leachate

In the growth inhibition tests with *Lemna spp.* any new visible daughter frond is count. As under stress conditions very small fronds may be protruded, so frond number may underestimate the toxic effect to duckweeds. Due to this disadvantage, the other endpoints may be more suitable for toxicity assessment [18].

Based on calculated LC_{50} values for microinvertebrates the toxicity of Kairiai landfill leachate was evaluated (Table 2). Results indicate that untreated Kairiai landfill leachate can be classified as very toxic for aquatic invertebrates. Treatment was found to slightly reduce the toxicity of leachate.

Acute toxicity of municipal landfills leachates was shown during other toxicity studies [19–22] as well. In a study of domestic and industrial waste leachates in France was found that leachate from domestic or industrial landfills had similar toxicity or even leachate of municipal landfill was more toxic [23–24]. During the comparative study of treated and raw landfill leachates toxicity in Chile it was observed that toxicity of treated leachates was 36 times lower than that of raw leachates [25].

Table 2. Toxicity of Kairiai landfill leachate assessed by *T. platyurus* and *D. magna* tests

Test	Toxicity, TU	
	Untreated leachate	Treated leachate
T. platyurus	28.5	25.2
D. magna, 24 h	21.6	9.3
D. magna, 48 h	31.0	18.1

The applied bioassays were ranked according to their sensitivity to the landfill leachate: *T. platyurus*> *D. magna* 24 h> *D. magna* 48 h >*S. polyrhiza*. Despite the fact that applied whole leachate toxicity tests account well for the uncharacterized sources of toxicity and their toxic interactions, but they cannot explain the origin or identity of chemicals affecting toxicity. The other studies showed that total ammonia (un-ionized and ionized) is identified as the prime contributor to acute leachate toxicity to living organisms [23, 26-28]. It is in agreement with the chemical characteristics of leachate (Table 1) as the concentrations of ammonium were very high in the tested leachate.

4. CONCLUSIONS

The results of the acute microinvertebrates D. magna and T. platyurus tests show that untreated Kairiai solid waste landfill leachate is very toxic to aquatic organisms and may pose serious hazards to soil, groundwater and terrestrial waters. The treatment of leachate has slightly reduced the toxicity, though it remains in the same class of toxicity.

The leachate exhibited high phytotoxicity to the growth of *Spirodela polyrhiza*, though in the low concentrations due to relatively high level of nutrients, it exhibited the stimulation for plant growth.

The applied bioassays were ranked according to their sensitivity to the landfill leachate: *T. platyurus*> *D. magna* 24 h> *D. magna* 48 h >*S. polyrhiza*.

REFERENCES

1. ÖMAN, C.B., JUNESTEDT C. Chemical characterization of landfill leachates – 400 parameters and compounds. Waste management, 2008, Vol. 28, p. 1876–1891.
2. KJELDSEN, P., BARLAZ, M.A., ROOKER, A.P., BAUN, A., LEDIN, A., CHRISTENSEN, T.H. Present and long-term composition of MSW landfill leachate: e review. *Critical Reviews in Environmental Science and Technology*, 2002, Vol. 34, Iss. 4, p. 297–336.
3. BEG, M.U., AL-MUZAINI, S. Genotoxicity assay of landfill leachates. *Environmental Toxicology and Water Quality*, 1998, Vol. 13, Iss. 2, p. 127–131.
4. SANG, N., Li, G. Chromosomal aberrations induced in mouse bone marrow cells by municipal landfill leachate. *Environmental Toxicology and Pharmacology*, 2005, Vol. 20, Iss. 1, p. 219–224.
5. BAKARE, A.A., PANDEY, A.K., BAJPAYEE, M., BHARGAV, D., CHAWDHURI, D.K., SINGH, K.P., MURTHY, R.C., DHAWAN, A. DNA damage induced in human peripheral blood lymphocytes by industrial solid waste and municipal sludge leachates. *Environmental and Molecular Mutagenesis*, 2007, Vol 48, p. 30–37.
6. KOSHY, L., PARIS, E., LING, S., JONES, T., BÉRUBÉ, K. Bioreactivity of leachate from municipal solid waste landfills – assessment of toxicity. *Science of the Total Environment*, 2007, Vol. 384, p. 171–181.
7. LAMBOLEZ, L., VASSEUR, P., FERARD, J.F., GISBERT, T. The environmental risks of industrial waste disposal: an experimental approach including acute and chronic toxicity studies. *Ecotoxicology and Environmental Safety*, 1994, Vol. 28, p. 317–328.
8. BLOOR, M.C., BANKS, C.J., KRIVTSOV, V. Acute and sublethal toxicity tests to monitor the impact of leachate on an aquatic environment. *Environment International*, 2005, Vol. 31, p. 269–273.
9. TRIČYS, V. Research of leachate, surface, and ground water pollution near Šiauliai landfill. *Environmental research, engineering and management*, 2002, Vol. 1 (19), p. 30–33.
10. DAPHTOXKIT F^{TM} MAGNA. Crustacean toxicity screening test for freshwater. Standard operational procedure. Gent, Belgium, 2008, 28 p.
11. THAMNOTOXKIT F^{TM} Crustacean toxicity screening test for freshwater. Standard operational procedure. Gent, Belgium, 2008, 28 p.
12. ISO/DIS 20079. Water quality -- Determination of the toxic effect of water constituents and waste water on duckweed (Lemna minor) -- Duckweed growth inhibition test
13. OECD 221, Guideline for the testing of chemicals. Lemna sp. Growth inhibition test, 2004.

14. PERSOONE, G., MARSALEK, B., BLINOVA, I., TÖRÖKNE, A., ZARINA, D., MANUSADŽIANAS, L., NALECZ-JAWECKI, G., TOFAN, L., STEPANOVA, N., TOTHOVA, L., KOLAR, B. A practical and user-friendly toxicity classification system with Microbiotests for natural waters and wastewaters. *Environmental Toxicology*, 2003, Vol. 18, Iss. 6, p. 395–402.
15. CLÉMENT, B., BOUVET, Y. Assessment of landfill leachate toxicity using the duckweed *Lemna minor*. *The Science of the Total Environment*, 1993, Vol. 134, S2. p. 1179–1190.
16. DEVARE, M., BAHADIR, M. Biological monitoring of landfill leachate using plants and luminescent bacteria. *Chemosphere*, 1994, Vol. 28, p. 261–271.
17. MACKENZIE, S.M., WAITE, S., METCALFE, D.J., JOYCE, C.B. Landfill leachate ecotoxicity experiments using *Lemna minor*. *Water, Air, and Soil Pollution*, 2003, Focus 3, p. 171–179.
18. MOHAN, B.S., HOSETTI, B.B. Aquatic plants for toxicity assessment. *Environmental research*, 1999, Vol. 81, p. 259–274.
19. JURKONIENĖ, S., MAKSIMOV, G., DARGINAVIČIENĖ, J., SADAUSKAS, K., VITKUS, R., MANUSADŽIANAS, L. Leachate toxicity assessment by responses of algae *Nitellopsis obtusa* membrane ATPase and cell resting potential, and with Daphtoxkit F^{TM} magna test. *Environmental Toxicology*, 2004, Vol. 19, Iss. 4, p. 403–408.
20. FERRARI, B., RADETSKI, C.M., VEBER, A.-M., FERARD, J.-F. Ecotoxicological assessment of solid wastes: a combined liquid- and solid-phase testing approach using a battery of bioassays and biomarkers. *Environmental Toxicology and Chemistry*, 1999, Vol. 18, No. 6, p. 1195–1202.
21. ŽALTAUSKAITĖ, J. Acute toxicity of municipal waste landfill leachate to aquatic invertebrates. Human and nature safety 2010. Proceedings of 16th international conference. Kaunas: 2010 May 12-14, June 17-19, p. 193–196.
22. ŽALTAUSKAITĖ, J., ČYPAITĖ, A. Assessment of landfill leachate toxicity using higher plants. *Environmental research, engineering and management*, 2008, Vol. 4(46), p. 42–47.
23. CLÉMENT, B., COLIN, J.R., LE DÛ-DELEPIERRE, A. Estimation of the hazard of landfills through toxicity testing of leachates. 2. Comparison of physic-chemical characteristics of landfill leachates with their toxicity determined with a battery of tests. *Chemosphere*, 1997, Vol. 35, No. 11, p. 2783–2796.
24. CLÉMENT, B., PERSOONE, G., JANSSEN, C., LE DÛ-DELEPIERRE, A. Estimation of the hazard of landfills through toxicity testing of leachates. I. Determination of leachate toxicity with a battery of tests. *Chemosphere*, 1996, Vol. 33, No. 11, p. 2303–2320.
25. RONCO, A.E., CASTILLO, G., DÍAZ-BAEZ, M.C. Development and application of microbioassays for routine testing and biomonitoring in Argentina, Chile and Colombia. In: Persoone, G., Janssen, C., &De Coen, W. (eds.) et al., New Microbiotests for routine toxicity screening and biomonitoring 2000. Kluwer Academic/Plenum Publishers, New York. p. 49–61.
26. SVENSSON, B.-M., MATHIASSON, L., MÅRTENSSON, L., BERGSTRÖM, S. *Artemia salina* as test organism for assessment of acute toxicity of leachate water from landfills. *Environmental Monitoring and Assessment*, 2005, Vol. 102, p. 309–321.
27. THOMAS, D.J.L., TYRREL, S.F., SMITH, R., FARROW, S. Bioassays for the evaluation of landfill leachate toxicity. *Journal of Toxicology and Environmental Health. Part B: Critical Reviews*, 2009. Vol. 12, No. 1, p. 83–105.
28. WARD, M.L., BITTON, G., TOWNSEND, T., BOOTH, M. Determining toxicity of leachates from Florida municipal solid waste landfills using a battery-of-tests approach. *Environmental Toxicology*, 2002, Vol. 17, Iss. 3, p. 258–266.

CYSENI 2012, May 24–25, Kaunas, Lithuania
ISSN 1822-7554, www.cyseni.com

MODELLING OF RBMK-1500 SPENT NUCLEAR FUEL AXIAL BURNUP

V. Barkauskas, A. Plukis
Center for Physical Sciences and Technology
Savanorių ave. 231, Vilnius, LT-02300 – Lithuania
Email: vytenis.barkauskas@gmail.com

ABSTRACT

RBMK-1500 spent nuclear fuel (SNF) composition and axial burnup distribution modelling is performed in order to create RBMK-1500 reactor fuel ARP cross-section library that could be used for criticality safety calculations in SNF storage systems taking into account burnup credit. SNF composition modelling is performed using T6-DEPL code sequence from SCALE 6.0 code package with 238-group multigroup energy library and 3D geometry. Fuel depletion is calculated separately for both fuel rod "rings" of RBMK-1500 fuel bundle with ten equal length axial zones for each "ring", to have optimal calculation time and obtain sufficiently detailed information of axial burnup distribution. Fuel depletion conditions are modelled realistically (fuel and graphite temperature), taking into account axial changes of temperature and water-steam mixture density. Concentration of actinides important for burnup credit calculations as well as for non-proliferation issues is evaluated for different fuel enrichment and burnup. Inclusion of actinides in burnup credit application can significantly reduce too conservative assumption of fresh fuel, and still provide adequate and safe reactivity margin for SNF storage systems. As two different materials are used for neutron moderation in RBMK reactors, and in SCALE 6.0 lattice cell pitch composition only one moderator can be selected, further sensitivity investigation and comparison with experimental results is needed.

Keywords: burnup credit, nuclear fuel, axial burnup, RBMK-1500, SCALE 6

1. INTRODUCTION

As both RBMK-1500 type units of Ignalina NPP are permanently shutdown, one of the most important issue regarding nuclear safety is spent nuclear fuel (SNF) storage. After 25 years of Ignalina NPP operation, there are about 22000 SNF assemblies left. At present most of the SNF is stored in SNF pools at the units, and part of assemblies (only 2 % enriched uranium) are stored at dry type SNF storage facility. Issues of nuclear safety of SNF pools and storage facilities are ones of the most challenging for Ignalina NPP in decommissioning stage.

New regulations regarding SNF storage allows possibility of burnup credit (BUC) implementation in safety justifications of SNF storage facilities [1]. BUC application primarily is related with positive economical effect, e.g. possible increment of number of SNF assemblies kept in wet storage facility or increment of number of SNF bundles allowed to store in the same SNF storage cask. BUC application is encouraged by International Atomic Energy Agency (IAEA) and industry [2, 3]. RBMK-1500 type reactor SNF depletion calculations and SNF storage cask criticality calculations were performed by A. Šmaižys et al. [4, 5]. However some general BUC issues were not solved, e.g. axial burnup profile calculations were not performed. New computational codes, improved computational speed and improved capabilities (e.g. 3D modelling geometry) for burnup analysis allow to evaluate fuel depletion more precisely and to extend the understanding of fuel burnup in the reactor. MCNP with ORIGEN were used for depletion calculations for RBMK-1000 fuel and comparison with experimental data were performed by A. Plukis et al [6]. Unlike in previously published calculations, we use the TRITON calculation sequence with Monte Carlo transport simulator code KENO-VI to determine neutron flux for complicated RBMK-1500 reactor channel 3D geometry was used in this study. Axial burnup calculations for ^{235}U depletion and build-up of major actinides important for SNF criticality (^{239}Pu, ^{240}Pu and ^{241}Pu) are presented in this paper. Data obtained during calculations will also allow creating RBMK-1500 reactor fuel ARP cross-section library that could be used for criticality safety calculations in SNF storage systems taking into account burnup credit.

2. MODELLING TOOLS AND PROCEDURE

2.1. Calculations code

SCALE 6.0 code package was used for RBMK-1500 fuel bundle depletion calculations. SCALE codes package is widely used for criticallity and burnup calculations to justify safety of various activities in nuclear field. However no calculations for RBMK-1500 fuel burnup were performed using this code with 3D geometry modelling possibility. We used T6-DEPL code sequence of TRITON control module was used to perform depletion calculation in this study. In this calculation sequence, Monte Carlo transport simulator code KENO-VI is used to determine neutron flux, spectra, and macroscopic cross sections generation. TRITON also provides ability to independently deplete multiple materials within a given system [7].

As several cycle axial multi-region depletion calculations were performed, this feature reduced number of separate calculations needed. Calculations were performed using ENDF/B-VII (V7-238) multigroup energy library.

When TRITON control module runs cross-sections used by ORIGEN-S for each cycle time point are saved as a library that is read by ORIGEN-S for calculations of the next cycle. Each time a new library is produced, the updated cross-section data are appended to the end of the existing library, resulting in a set of time-dependent cross-section libraries in a single file for each mixture being depleted [7].

2.2. Fuel assembly

RBMK-1500 fuel assembly consists of 18 fuel rods arranged in two cocentrical rings with central carrier rod at the centre (see Fig. 1). Two interconnected fuel bundles are used in fuel channel. Fuel rods are filled with sintered uranium dioxide pellets with 2 mm diameter hole at the centre. To simplify calculations, fuel rod was treated as zirconium alloy tube homogeneously filled with uranium dioxide with burnable erbium absorber. Mass of uranium was kept original. Pellet density was reduced to keep proper geometry of the tube. Central carried rod was defined as hollow tube made from zirconium alloy.

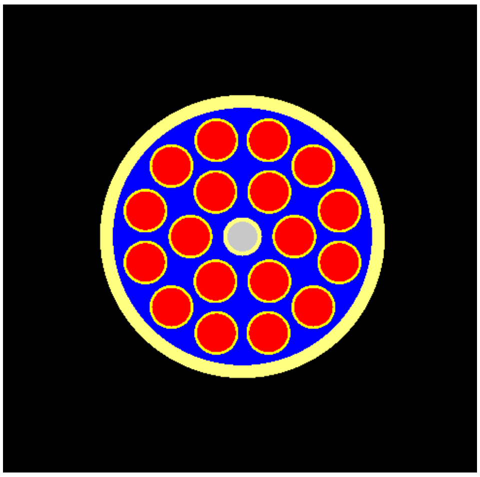

Fig. 1. Cross section of RBMK-1500 reactor type fuel assembly

Depletion was modelled for one 3.41 meter active length fuel bundle, using twenty fuel zones as depletion mixtures – ten equal length axial zones for each – inner and outer – rod ring. Triangular pitch with h=0.802 cm was chosen for lattice cell parameters to assist self-shielding calculations [8]. For self shielding calculations water as a moderator was selected. It was chosen because it was assumed that fuel depletion along fuel channel and axial burnup are mostly determined by neutron spectral distribution change caused by changes of water temperature and density. Selection of water as a moderator allows to evaluate this effect. However this approximation is not fully precise.

Depletion conditions were modelled realistically (normal operation parameters were used). Operational data was taken from Ignalina RBMK-1500 Source book [9]. Main parameters used in the calculations are listed in Table 1. Temperature and water density were approximated as linear functions of height along the channel (Fig. 2).

Table 1. Model parameters

Parameter	**Value**		**Parameter**	**Value**
Fuel enrichment	2.6 %, 2.8 %		Range of water temperature along the channel (upper half)	567–558 K
Fuel pellet density	9370 kg/m^3		Length of fuel element	3.41 m
Average fuel temperature	1273 K		Number of fuel axial zones in inner ring	10
Average graphite temperature	873 K		Number of fuel axial zones in outer ring	10
Average cladding temperature	575 K		Burnup range	0–27 MW·days/kgU
Range of water density along the channel (upper half)	430–220 kg/m^3			

Periodic boundary conditions were used for side boundaries and mirror boundary conditions for top and bottom of one fuel channel. The number of particles per batch and number of batches used for KENO-VI calculations were set to 30000 and 30 respectively. For very beginning of the fuel irradiation we used a very short time interval (10^{-15} days) to produce cross-sections set corresponding to zero burnup. Then irradiation period was divided into equal length (120 days) steps with constant power (25 MW per tonne fuel uranium) applied on fuel bundle. Element concentrations for different values of fuel burnup were taken from the same calculation, as they are saved for each timestep and are available in the output files. Nuclear fuel bundles of two enrichment values (2.6% and 2.8%) with erbium burnable absorber of natural isotope composition were chosen for modelling.

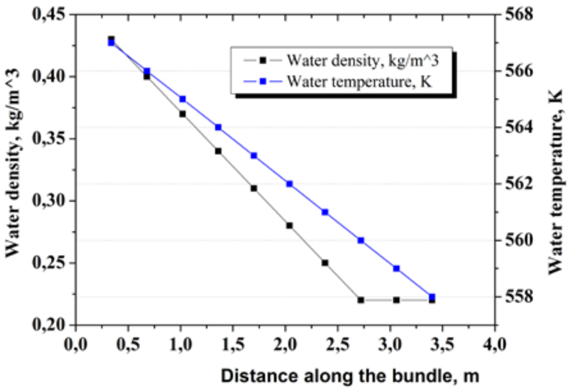

Fig. 2. Water density and temperature axial profiles used in calculations (upper half of the channel)

3. RESULTS AND DISCUSSION

Modelling of RBMK-1500 type reactor nuclear fuel depletion was performed. Concentrations of main actinides important to burnup credit were calculated. Detailed analysis of ^{235}U, ^{239}Pu, ^{240}Pu and ^{241}Pu axial distribution inside SNF bundle was performed.

Distribution of ^{235}U is given in Fig. 3 and Fig. 4. All concentration values are normalized to maximal obtained separate zone concentration value for a given burnup. In Fig. 3 a) for inner ring and Fig. 3 c) for outer ring ^{235}U distribution changes at the beginning of irradiation of fuel in the reactor (up to 3 MW·days/kgU) are given. The difference between concentrations increases between fuel bundle ends at the start of fuel irradiation. However this difference does not grow after certain burnup is achieved (Fig. 3 b) and d)). After long term operation in the reactor core, depletion caused axial distribution becomes more flat and when burnup of 15 MW·days/kg U is achieved, the axial distribution of ^{235}U does not vary essentially along channel axis. In case of 2.8 % enrichment, the differences between depletion of fuel bundle ends are smaller. Outer and inner rings have the same tendency, but inner ring is depleted more homogeneously.

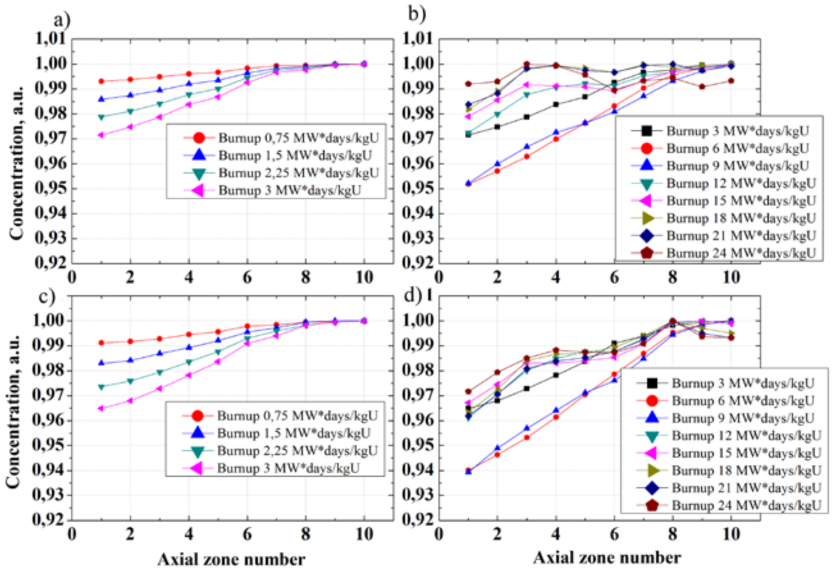

Fig. 3. ^{235}U concentration distribution in case of 2.8 % enrichment uranium fuel for different burnup (Inner ring a) 0–3 MW·days/kgU, b) 3–24 MW·days/kgU; for outer ring c) 0–3 MW·days/kgU, d) 3–24 MW·days/kgU. All values are normalized to maximual concentration zone value for a given burnup)

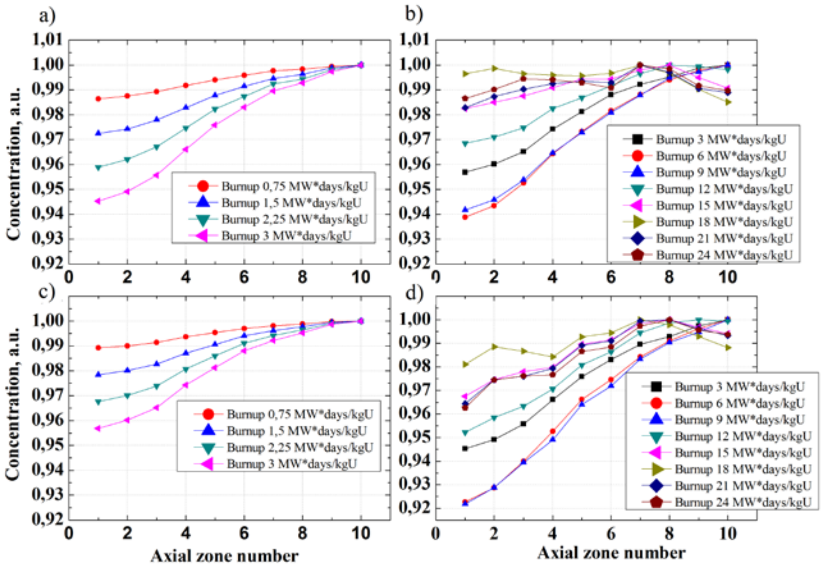

Fig. 4. ^{235}U concentration distribution in case of 2.6 % enrichment uranium fuel for different burnup (Inner ring a) 0–3 MW·days/kgU, b) 3–24 MW·days/kgU; for outer ring c) 0–3 MW·days/kgU, d) 3–24 MW·days/kgU. All values are normalized to maximal concentration zone value for a given burnup)

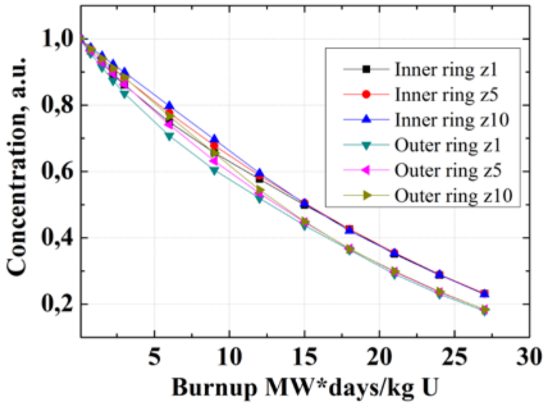

Fig. 5. ^{235}U concentration dependence on burnup for different ring positions (2.6 % enrichment fuel)

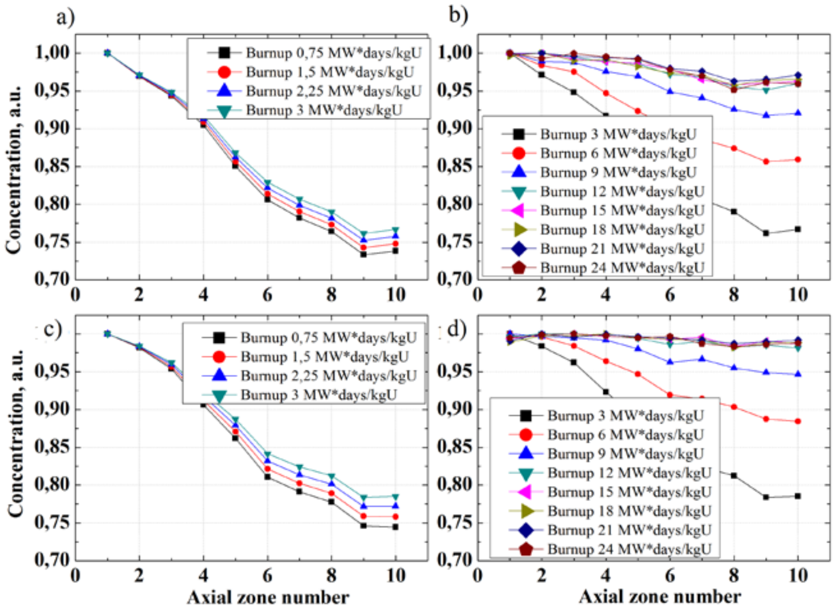

Fig. 6. ^{239}Pu concentration distribution in case of 2.6 % enrichment uranium fuel for different burnup (Inner ring a) 0–3 MW·days/kgU, b) 3–24 MW·days/kgU; for outer ring c) 0–3 MW·days/kgU, d) 3–24 MW·days/kgU. All values are normalized to maximal concentration zone value for a given burnup)

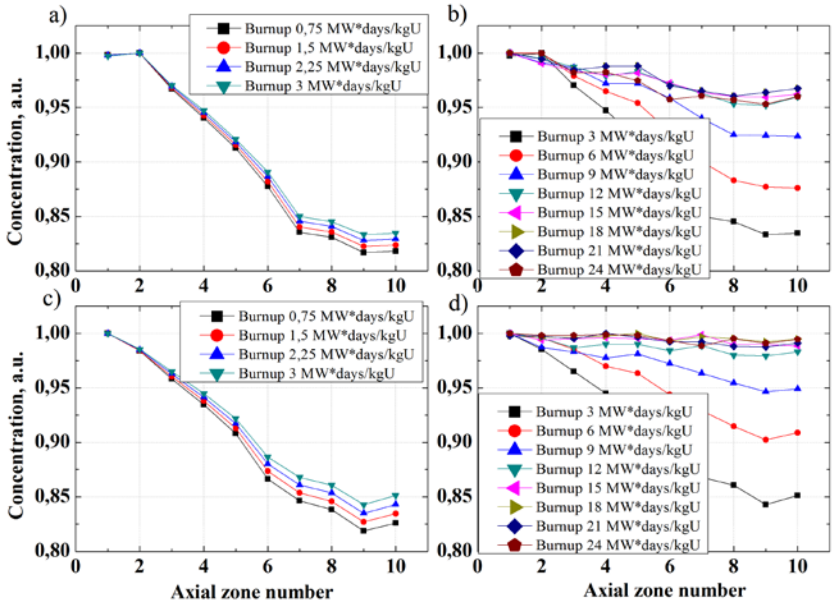

Fig. 7. ^{239}Pu concentration distribution in case of 2.8 % enrichment uranium fuel for different burnup (Inner ring a) 0–3 MW·days/kgU, b) 3–24 MW·days/kgU; for outer ring c) 0–3 MW·days/kgU, d) 3–24 MW·days/kgU. All values are normalized to maximal concentration zone value for a given burnup)

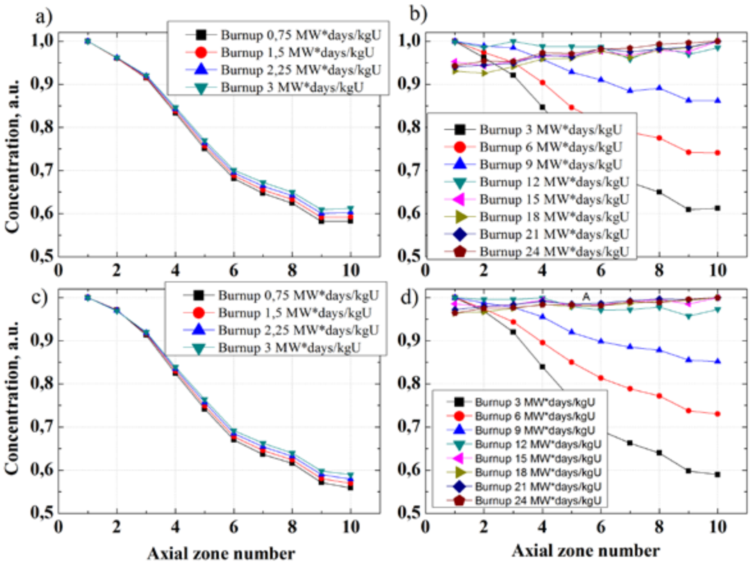

Fig. 8. ^{240}Pu concentration distribution in case of 2.6 % enrichment uranium fuel for different burnup (Inner ring a) 0–3 MW·days/kgU, b) 3–24 MW·days/kgU; for outer ring c) 0–3 MW·days/kgU, d) 3–24 MW·days/kgU. All values are normalized to maximal concentration zone value for a given burnup)

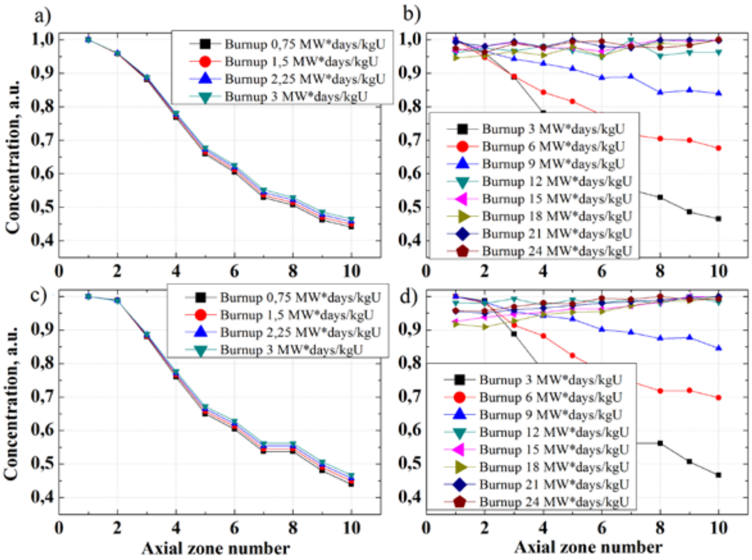

Fig. 9. ^{241}Pu concentration distribution in case of 2.6 % enrichment uranium fuel for different burnup (Inner ring a) 0–3 MW·days/kgU, b) 3–24 MW·days/kgU; for outer ring c) 0–3 MW·days/kgU, d) 3–24 MW·days/kgU. All values are normalized to maximum concentration zone value for a given burnup)

^{235}U concentration dependence on burnup is given in Fig. 5. It is clearly seen, that outer ring is depleted faster, and in the long run (from 15 MW·days/kg U) two different concentration values for both is observable. These values are almost independent from axial position of depleted fuel. Two different values of concentration could be explained by small radial neutron spectrum change inside the channel, which forms two different values observable only after quite long irradiation time.

Formation of all analysed isotopes of plutonium (^{239}Pu, ^{240}Pu and ^{241}Pu) shows the same trend – very fast formation of plutonium at the centre of the reactor core (difference between concentrations at fuel bundle ends reaches 25% for ^{239}Pu, 40 % for ^{240}Pu and 50% for ^{241}Pu), and then flattening of the axial distribution curve when burnup gets higher (Fig. 6–9). Once again, in case of 2.8% enrichment fuel, distribution of plutonium is more homogeneous. Scattering of concentration values along the channel is related to stochastic nature of Monte Carlo calculation and resulting uncertainty.

Several other aspects important to burnup and axial distribution were not addressed in these calculations: neutron leakage, possible influence of control rod in the vicinity of the fuel rod, also uncertainties were not evaluated at this stage of calculations.

4. CONCLUSIONS

Axial burnup distribution of RBMK-1500 type reactor fuel was calculated, using Monte Carlo transport simulation method, taking into account most important actinides. It was found, that axial distribution of uranium and plutonium isotopes is different at different burnup. However the trend was observed, that distribution flattens when burnup value of around 15 MW·days/kg U is achieved. Also distribution changes are smaller in case of higher enrichment fuel. Results show that end-effect may be not important in case of high burnup RBMK-1500 reactor type fuel. However this hypothesis should be evaluated for the bottom-half of reactor channel and 2.4 % enrichment fuel. Also comparison with available experimental data (validation) should be made, neutron leakage effects, uncertainties as well as sensitivity analysis should be performed in further calculations.

REFERENCES

1. Republic of Lithuania Nuclear safety requirements, *General requirements for spent nuclear fuel dry-type storage facility*, BSR-3.1.1-2010.
2. *Practices and developments in spent fuel burnup credit applications*: Proceedings of a Technical Committee meeting held in Madrid, 22–26 April 2002, IAEA Tecdoc-1378.
3. *Advances in Applications of Burnup Credit to Enhance Spent Fuel Transportation, Storage, Reprocessing and Disposition*: Proceedings of a Technical Meeting held in London, 29 August – 2 September 2005, IAEA Tecdoc-1547.
4. ŠMAIŽYS, A., POŠKAS, P. Possibility for BUC implementation in RBMK-1500 fuel dual purpose storage casks, *Practices and developments in spent fuel burnup credit applications*: Proceedings of a Technical Committee meeting held in Madrid, 22–26 April 2002, IAEA Tecdoc-1378.
5. ŠMAIŽYS, A. Analysis of nuclear and radiation characteristics of RBMK-1500 spent nuclear fuel casks and storage facilities, *PhD thesis*, Kaunas 2004.
6. PLUKIS, A., PLUKIENĖ, R., REMEIKIS, V., RIDIKAS, D., MCNP and ORIGEN codes validation by calculating RBMK spent nuclear fuel isotopic composition, *Lithuanian Journal of Physics*, Vol. 45, No. 4, p. 281–287 (2005).
7. DEHART, M., D. *Triton: a two-dimensional transport and depletion module for characterization of spent nuclear fuel*, January 2009, Prepared by the Oak Ridge National Laboratory.
8. PLUKIENĖ, R., PLUKIS, A., GERMANAS, D., REMEIKIS, V., Numerical sensitivity study of irradiated nuclear fuel evolution in the RBMK reactor, *Lithuanian Journal of Physics*, Vol. 49, No. 4, p. 461–469 (2009).
9. ALMENAS, K., KALIATKA, A., UŠPURAS, E. *Ignalina RBMK-1500. A source book*, Lithuanian Energy Institute, 1998.

CYSENI 2012, May 24–25, Kaunas, Lithuania
ISSN 1822-7554, www.cyseni.com

MODELLING OF TWO-PHASE FLOW OF HYDROGEN GAS IN THE DISPOSAL CELL OF REPOSITORY FOR HIGH LEVEL RADIOACTIVE WASTE

D. Justinavičius
Lithuanian Energy Institute
Nuclear Engineering Laboratory
Breslaujos str. 3, LT-44403 Kaunas – Lithuania
Phone +370 37 401 886
Email: justinavicius@mail.lei.lt

ABSTRACT

Spent nuclear fuel and other long-lived high level radioactive waste are best disposed of in geological repositories using a system of engineered and natural barriers. Due to the danger of exposure arising from long-lived radionuclides to humans and the environment, this waste is not allowed to be disposed of in near-surface repositories.

Radioactive wastes conditioned for geological disposal in deep formations will produce a significant amount of gas due to corrosion of steel radioactive waste packages (containers) and the elements of metal constructions. Gas generation will continue for a long period after the repository closure. The accumulation of the gases may lead to a significant desaturation and unacceptable build-up of gas pressure in the disposal tunnels if the gas cannot escape through the low-permeability host rock. For a comprehensive understanding of the long-term hydraulic evolution of the repository, numerical simulations of two-phase flow are compulsory.

In this paper the results of numerical investigation performed using computer code PETRASIM (USA) are presented. The objective was to investigate the transport of generated hydrogen gas in a single disposal cell of repository situated in the clay rock. The analysis was focused on the evaluation of hydrogen release forms (free gas/dissolved gas), peculiarities of gas pressure build-up, desaturation of engineered barrier system, identification of main gas pathways and mass transfer between the disposal cell and the access drift.

Keywords: Gas transport, geological repository, disposal, numerical modelling

1. INTRODUCTION

Gas and its influence on the long-term safety of geological repositories have been investigated for almost two decades. Belgium, Canada, Germany, Finland, France, Sweden, Switzerland, United Kingdom and USA are the countries that have been doing the most of researches as they have more advanced program on radioactive waste disposal. Scientists from each country perform its own investigations and also participate in international collaborative research projects within these experimental and numerical analyses are being performed, obtained results are compared and new theories are formulated. GASNET [1] and PAMINA [2] are the international projects which were held to discuss the gas problem in the perspective of geological repository safety. During these investigations the gas sources, possible transport mechanism and potential risk for geological repository long-term safety were identified.

At present no facts of existence of the potential risks or their possible rejection have been found, hence international investigations are going on. Investigations carried out within EU-FP7 project FORGE (Fate Of Repository Gas) are concentrated on the analysis of the generated gas behaviour in the geological repositories. Researchers of nuclear engineering laboratory of Lithuanian energy institute also participate in the numerical investigations section, which is coordinated by the French national radioactive waste management agency ANDRA. The results of the 1st task of benchmark studies are presented in this paper.

2. THEORETICAL FORMULATIONS

2.1. Gas source term

Radioactive wastes and their disposal packages (canisters), as well as reinforcement steel used in the construction of the repository, are the principal sources of gas generation. Among four possible ways of gas generation (corrosion of metal components, microbial degradation, radiolysis and radioactive decay), anaerobic corrosion of the steel components in the engineered barrier system (EBS) is a dominant source of hydrogen gas [3]:

$$3Fe + 4H_2O \rightarrow Fe_3O_4 + 4H_2. \qquad (1)$$

At present the experimental and numerical investigations are performed to define the corrosion based hydrogen generation rates in the future repositories. The investigations are complex as the generation rates depend on several aspects: chemical conditions of geological environment (potential of hydrogen pH, redox potential Eh), temperature conditions, radiation level, amount of available water in the local environment and the surface area of the corrosion process. The summarized results show [3] that the corrosion rates may vary between 0.1 μm/year ÷ 10 μm/year. Experimental investigations show that the rate of corrosion is unstable, i.e., it could be high at the beginning but then decrease progressively with time due to depletion of reactants or formation and growth of a protective corrosion product film.

2.2. Gas transport

The current phenomenological understanding of the liquid-gas interaction in the porous medium can be subdivided to the following distinct periods:

1. Gas generation rate is small and all the gas generated dissolves in the groundwater existing in the porous materials. Diffusive transport of such dissolved gas is the only mechanism by which the gas is transported in the surrounding EBS and the host formation;
2. When the gas production rate surpasses the diffusive transport capacity of dissolved gas, an immobile gas phase composed of isolated gas bubbles is formed. Gas pressure starts to build up resulting in a gradual desaturation of the EBS and possibly the host rock;
3. Gas generation proceeds till the isolated gas bubbles ultimately form a continuous gas phase (reaching gas entry pressure P_o). As of this stage, two-phase flow starts in the EBS and possibly in the surrounding host rock. Gas is now transported mainly through advective flow, and water is being further expelled;
4. Up to now, there is no definite conclusion about what will happen if the gas pressure keeps increasing. Two hypothesis exist:
    4.1. Some kind of cyclic behaviour of opening and closing of the preferential flow paths is expected [4]. Once the gas pressure locally exceeds the minimal component of the principal tensor of total stresses (equal to the lithostatic pressure), a preferential pathway will be created. Continuous fluid flow models such as PETRASIM will then no longer be applicable to such kind of discrete flow paths. After the formation of open preferential pathways, gas pressure will reduce significantly. Due to the self-sealing capacity of the clays, cracks tend to be closed after gas pressure drops down. This cyclic behaviour of opening and closing of the preferential flow paths goes on until the gas production rate

becomes small enough to allow dissolved gas to be transported via the pore-water in the pore system.

4.2. Dilatancy-controlled gas flow is expected to take place [5]. The process of gas-driven microfracturing leads to an increase of the pore space, which is accompanied by a detectable increase in intrinsic permeability. Because the dilatation does not create a discontinuous pore network, gas flow is still controlled by a continuous two-phase flow model applicable to a porous medium. The main difference with respect to the conventional two-phase flow is that the transport properties of the porous media depend on mechanical deformation.

2.3. Impacts of gas

Impacts to the geological repository long-term safety can be grouped into categories [1] according to the type of effect caused by the generation of gas:

1. The mechanical effect on repository and rock structures caused by the pressure build-up that may follow due to gas generation (disruption of the EBS, fracturing of the host rock);
2. The direct effect of gas on groundwater flow around the repository (induced groundwater flow, forcing of contaminated water from the repository or canisters, transport associated with bubbles);
3. The release of volatile radionuclides and toxic gas up to the biosphere.

3. TASK DEFINITION

The numerical investigation of the 1st test task of FORGE benchmark studies here is presented. In the suggested concept of a geological repository [6], the high-level radioactive waste (HLW) canisters are transported by shafts down to the main tunnel at the 500 m depth, from which they are transported by access drifts to the disposal cell situated in the clay rock. The HLW canisters are placed in these cells one after another and finally they are sealed with bentonite plug (Fig. 1). As the diameter of disposal cell will be slightly more than diameter of HLW canisters, there will be thin engineered gaps between the HLW and engineered disturbed zone (EDZ) and between the bentonite seal and EDZ after the placement of the canisters. After the emplacement of the HLW canisters the access drift, main tunnel and shafts is backfilled with the mixture of crushed rock and compacted bentonite.

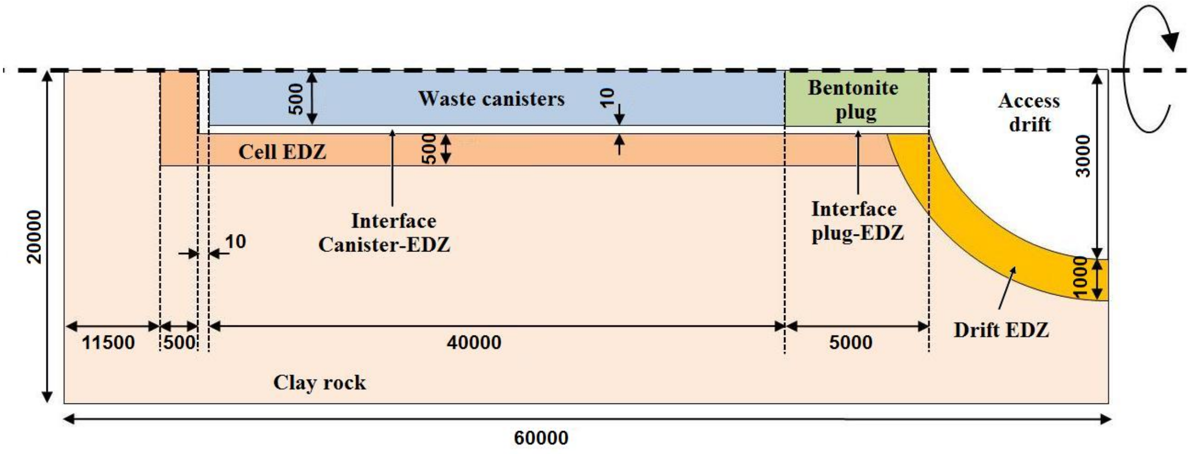

Fig. 1. Representation of the modelling domain [6]

The objective of this test case is to simulate the gas transport in single disposal cell and a part of a drift using a full physical model described in task specification [6]. Important, that the engineered gaps between the HLW canister and EDZ and between the bentonite plug and EDZ should be represented.

4. METHODOLOGY

The gas transport modelling was performed with the original version of TOUGH2 [7] code using PETRASIM [8] as the graphical interface. TOUGH2 is a numerical simulator for nonisothermal flows of multicomponent, multiphase fluids in one, two and three-dimensional porous and fractured media. The EOS5 fluid property module was selected for the description of the thermodynamics of hydrogen gas.

Fluid flow in the repository involves multiphase transient flow processes. For gas flow, a mixture of gases is evolved, with hydrogen being the main constituent. In this study all the gases are treated as hydrogen. Hydrogen dissolution in the pore water follows Henry's law. Gas and water flow are governed by a multiphase extension of Darcy's law:

$$V_\beta = -\frac{kk_r^\beta(S_\beta)}{\mu_\beta}(\nabla P_\beta + \rho_\beta g \nabla z), \tag{2}$$

where β denotes the phase of the fluid (aqueous or gaseous), k is the intrinsic permeability [m^2], k_r^β is relative permeability for phase β, S_β is saturation level for phase β, μ_β is dynamic viscosity of the fluid [kg·m^{-1}·s^{-1})], P_β is the phase pressure [Pa], ρ_β is the fluid density [kg·m^{-3}], g is acceleration of gravity [m·s^{-2}], z is the altitude [m], and V_β is Darcy's velocity for phase β [m·s^{-1}].

Diffusion processes in the gas and water phases are described by Fick's Law. The diffusive flux for the binary mixture of hydrogen and water vapour f^g [kg·m^{-2}·s^{-1}] can be written as:

$$f^g = \rho_g D_{H_2}^g \nabla X_{H_2}^g, \tag{3}$$

where g represents the gas phase, $D_{H_2}^g$ is the diffusion coefficient of hydrogen in the water vapour [m^2·s^{-1}], and $\nabla X_{H_2}^g$ is the gradient of mass fraction of hydrogen gas [m^{-1}].

The diffusive flux for the dissolved hydrogen f^w [kg·m^{-2}·s^{-1}] is written as:

$$f^w = \rho_w D_{H_2}^w \nabla X_{H_2}^w, \tag{4}$$

where w represents the liquid water phase, $D_{H_2}^w$ is the diffusion coefficient of hydrogen in the water [m^2·s^{-1}], and $\nabla X_{H_2}^w$ is the gradient of mass fraction of dissolved hydrogen [m^{-1}].

The TOUGH2 solves mass-balance equations by the integrated finite difference method. The equations are set up by combining mass balance, advection flux and diffusion flux, and solved by supplementing with a number of constitutive equations. The *van Genuchten* [7] model has been selected to express capillary pressure in relation to the saturation of the porous medium. Relative permeability depends on effective saturation and is expressed by *van Genuchten – Mualem* [7] model.

4.1. Numerical model

The numerical model representing the system being analyzed (Fig. 2) was developed according to the given task specification [6], that defines model geometry, description of physical processes and their mathematical expression, characteristic of materials, the initial and boundary conditions.

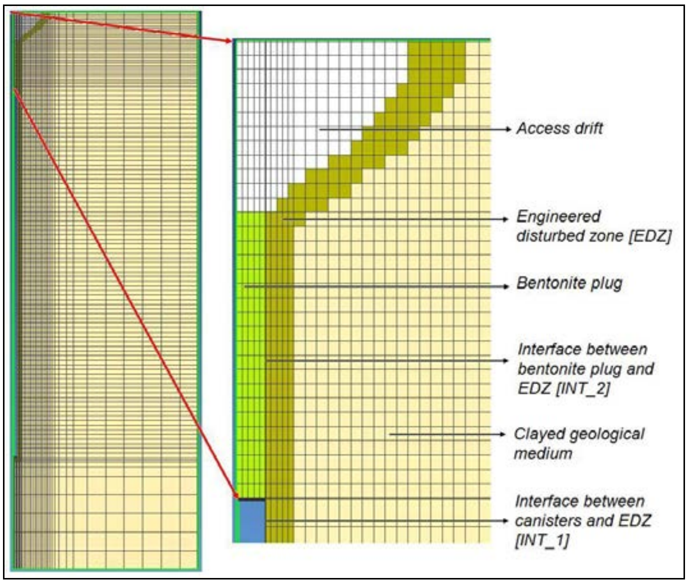

Fig. 2. Computational domain coloured by material type

As most of the materials are assigned to very low permeability, capillary process will be dominant over gravity. Therefore the mesh can be built as axisymetric without losing any important phenomenology. As the scale is quite small (few tens of meters) it is possible to represent fine geometric features and especially the interfaces. Both interfaces considered as centimetre-thick regions and are represented with one layer of grid elements. The grid consists of ~5000 rectangular elements and is refined in EBS due to higher gradients of the physical variables and a finer result resolution required.

4.2. Physical parameters

The materials to be taken into account include the EDZ of the cell and the access drift, the cell plug, the backfill of the access drift, clay rock and the engineered gaps – interface between the cell and the cell EDZ (INT_1] and interface between plug and the EDZ (INT_2). It is considered to represent the gaps as porous medium. The hydraulic characteristics of the first gap are similar to sand (that of very permeable material) while the characteristics of the second one are intermediate between sand and bentonite because of the presumable swell of the bentonite.

The canisters are constituted of a material impermeable to both water and gas flow and is not explicitly represented in the model. Table 1 provides the summary of physical characteristics of materials used in the modelling. The large range of permeability values of the different materials indicates some convergence problems of the numerical schemes.

Table 1. Physical parameters of the materials

Material / **Parameter**	**Interface INT_1**	**Interface INT_2**	**Bentonite plug**	**Backfill**	**EDZ**	**Clay rock**
Porosity (%)	100	30	35	40	15	15
Intrinsic permeability k (m^2)	$1 \cdot 10^{-12}$	$8 \cdot 10^{-18}$	$1 \cdot 10^{-20}$	$5 \cdot 10^{-17}$	$8 \cdot 10^{-18}$	$8 \cdot 10^{-21}$

The molecular diffusion coefficients of H_2 in water and gas phase are $4.59 \cdot 10^{-9}$ $m^2 \cdot s^{-1}$ and $9.5 \cdot 10^{-5}$ $m^2 \cdot s^{-1}$ respectively. Solubility limit of hydrogen in water is $7.6 \cdot 10^{-6}$ $mol \cdot Pa^{-1} \cdot m^{-3}$.

4.3. Initial and boundary conditions

Gas transport analysis is considered to be isothermal with a constant temperature of 20 °C, i.e. residual heat removal from canisters is neglected. It is assumed that the only source of H_2 gas generation is the corrosion of radioactive waste canisters. A gas-production term ($Q_g^{H_2}$ = 100 mol/year/disposal cell) is represented by a simple step function lasting 10.000 years. It is imposed on the external surface of the cylinder that represents disposed canisters. In the numerical model the hydrogen was injected into the interface between the canisters and EDZ (Fig. 3.).

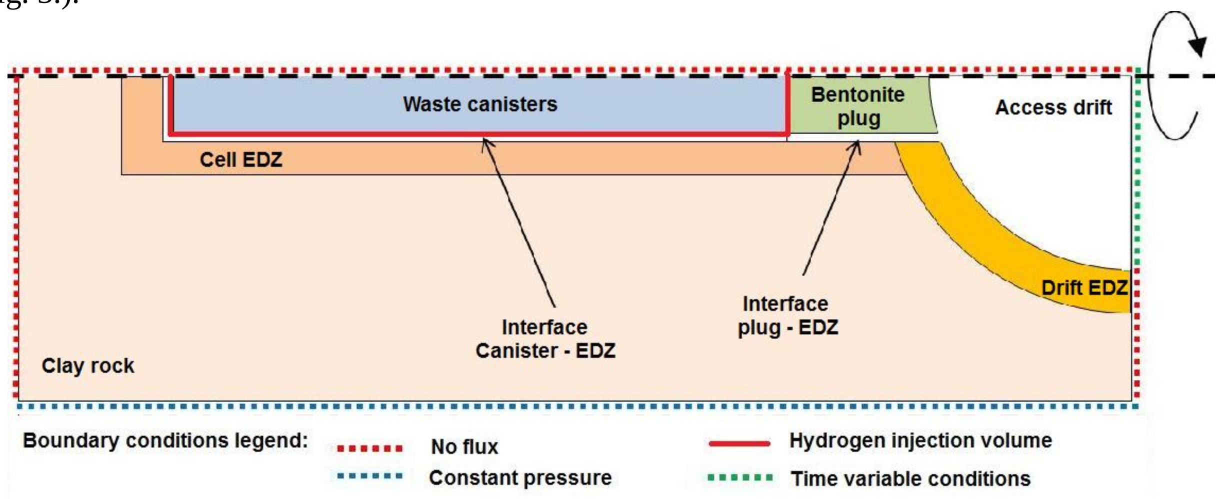

Fig. 3. Schematic representation of the boundary conditions [6]

After the closure of the repository, the gas (mainly air) saturation is 30% in the bentonite plug and access drift and 95 % in the interfaces. The remaining part of computational domain is fully water saturated.

Initial groundwater pressures set to be 5 MPa in all water saturated parts of the model (according to a continuous formulation, the gas and water pressures are the same if there is only dissolved gas). In other parts of the model that are not initially fully saturated with water, gas pressures set to be 0.1 MPa. Water pressure then is in capillary equilibrium with the gas pressure and is deduced from the gas pressure and the saturation by applying *Van Genuchten* model associated with each material.

The outer radial boundary conditions (constant water pressure P_w = 5 MPa) and the conditions on the boundary of the access drift (time varying gas pressure and gas saturation) were implemented precisely as described in specification. All other boundary conditions were designated as no-flow consistent with the specification.

5. RESULTS AND DISCUSSION

The simulation time is limited up to 100,000 years after repository closure. The results of the simulation were depicted as the liquid/gas pressure and the gas saturation profiles at 12 observation locations (Fig. 4) and spatial distribution contours of simulated gas saturation. In addition hydrogen flow rates through different surfaces were analyzed.

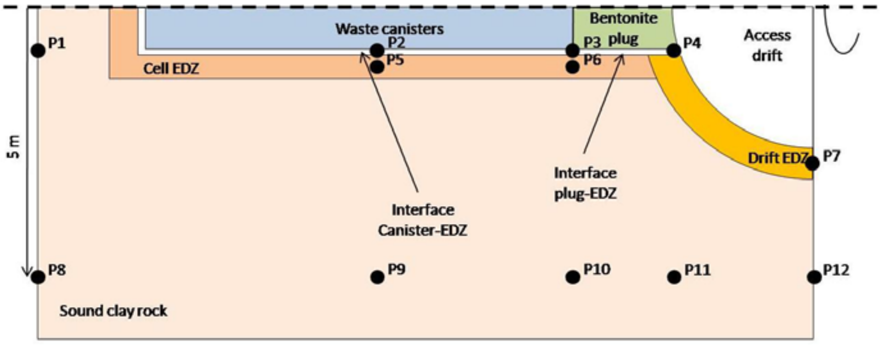

Fig. 4. Schematic representation of the observation points where results are given [6]

Fig. 5 represents gas saturation change over time at observation points where free gas phase being. In addition gas saturation history on outer boundary of access drift is presented. Significant levels of gas saturation are reached within the interfaces (P2, P3, P4) and access drift (P7). The interface is initially well desaturated, but its evolution with time depends on the position of particular observation point. Near the waste canisters (P2), the interface is resaturated up to 16 % from ~10 up to ~1.000 years due to water inflow from the clay rock. No-flow boundary condition between interface and canister in this case is also important. Later, gas builds-up and pushes water away from this interface. The evolution at P3 and P4 is similar to each other: after ~1 year the interface becomes fully gas saturated till the end of gas generation. Full resaturation in both interfaces is reached after ~10.750 years past repository closure. In the EDZ free gas exist only for particular time periods: in the cell EDZ (P5) from ~2,700 up to ~10.200 years, in the bentonite plug EDZ (P6) from ~3 up to ~9 and from ~2,000 up to ~10.200 years and in the drift EDZ (P7) gas saturation history is very closely related to saturation history at drift boundary. No free gas was observed in the undisturbed clay rock.

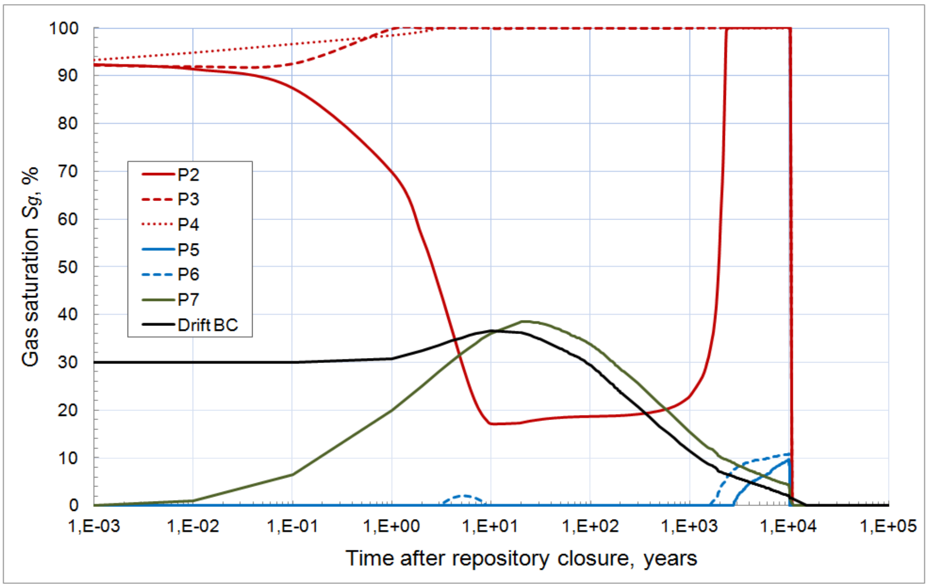

Fig. 5. Evolution with time of gas saturation

Spatial distribution contours of free and dissolved hydrogen (Fig. 6) shows that dissolved hydrogen dissipates more widely than free gas. This is associated with a diffusion of dissolved hydrogen away from the disposal cell to the clay rocks.

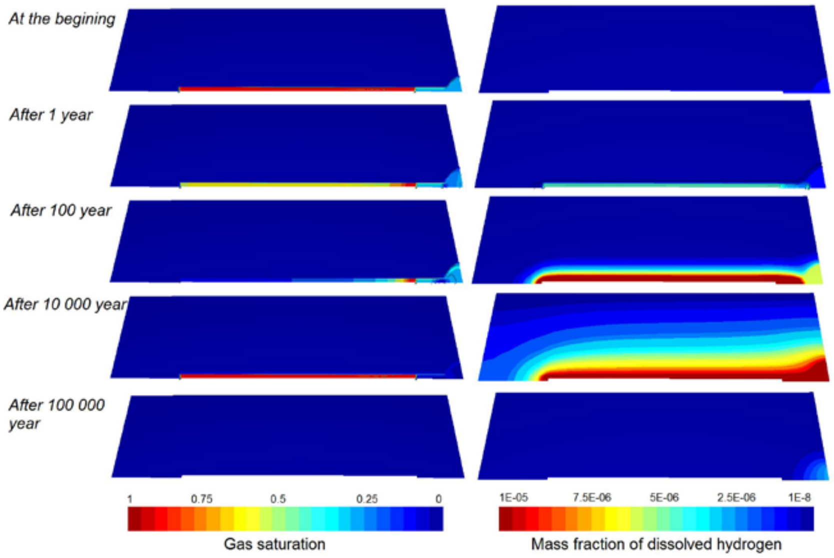

Fig. 6. Spatial distribution contours of free (left) and dissolved (right) hydrogen

Evolution of gas and liquid pressures is presented in Fig. 7. The peak pressure does not exceed 6 MPa and is much lower than lithostatic pressure (~10 MPa) in whole computational domain. These results show that first three mechanisms (see section 2.2) are sufficient to describe gas behaviour in single disposal cell and continuous fluid flow approach realized in PETRASIM code could be used. There will be no mechanical effect on repository and rock structures caused by the pressure build-up that may follow from gas generation.

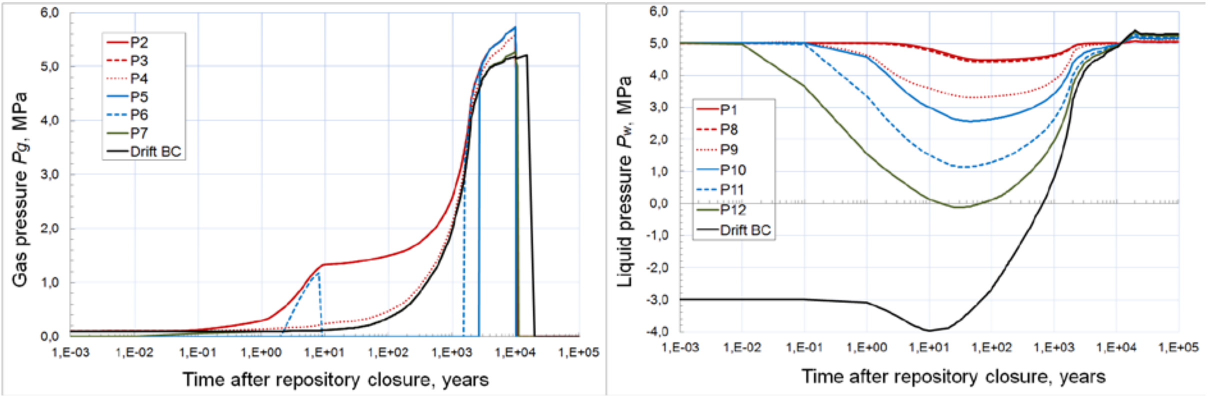

Fig. 7. Evolution with time of gas (left) and liquid (right) pressure

The results of gas flow rates (Fig. 8) show that the loss of gas from the disposal cell is dominated by the transport of free gas into the access drift (positive flow rate imply flow toward the drift) during the period of gas generation (up until 10,000 years). The large negative flow rate at early time is result of the gas movement from the drift toward the EDZ as the water flows towards the access drift boundary and displaces gas in the access tunnel.

Main gaseous hydrogen transport pathway was observed. It comes along the interface toward the drift. After ~5 years, the most part of generated gases moves through surface *S_int1* (Fig. 8). As the gas access to relatively impermeable plug interface, only a quarter of these gases moves through surface *S_int2*. However, the most part of these gases still moves to the access drift over EDZ. The results show that ~90 % of generated hydrogen is transferred from disposal cell toward the access drift in gaseous form while remaining ~10 % dissolved in pore-water.

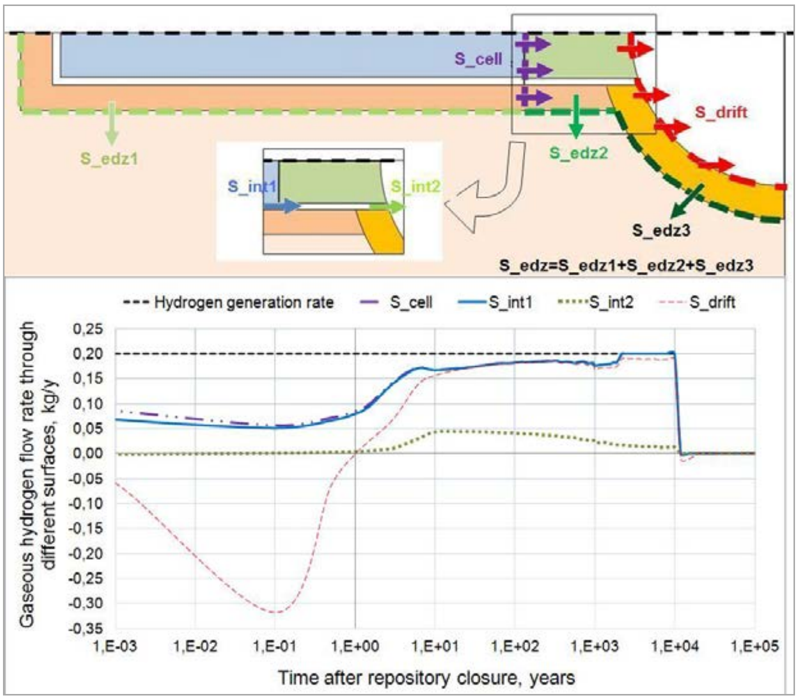

Fig. 8. Comparison of gaseous hydrogen flow rate through 4 different surfaces

Advective flow is the primary transport mechanism of gaseous hydrogen during gas generation period (Fig. 9). The diffusion process has a significant impact on gaseous hydrogen transport only during the first hundred years. Diffusive flow is the primary transport mechanism of dissolved hydrogen into the clay rock.

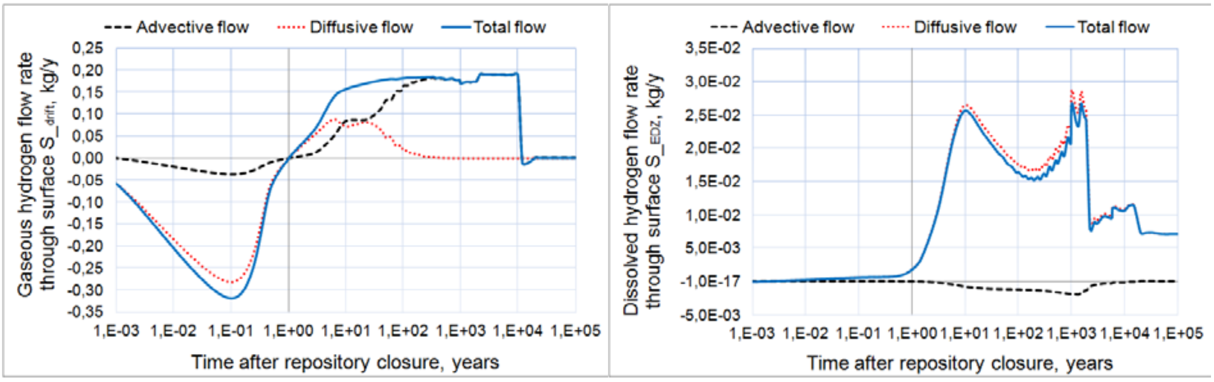

Fig. 9. Flow rates of gaseous H_2 through *S_drift* (left) and dissolved H_2 through *S_EDZ* (right)

6. SUMMARY AND CONCLUSIONS

A numerical model was developed to simulate the gas transport in a single disposal cell of repository for high level radioactive waste situated in the clay rock. The results proved that numerical tool based on two-phase flow theory is capable for modelling the gas transport in a geological repository system. The obtained results allow concluding:

1) Observed peak gas build-up pressure (~5.8 MPa) within modelled domain does not cause mechanical effect on repository and rock structures.
2) Significant levels of gas saturation are reached in the interfaces and access drift; minor amount of gas concentrates in some parts of engineered disturbed zone. During all

simulation period geological media remain hydraulically undisturbed (fully water saturated).

3) Most of generated gas (~90 %) is transported in gas phase by advective flow while remaining part (~10 %) is dissolved and is transported by diffusion into the clay rock.
4) The interface plays an important role for gaseous hydrogen movement from the cell toward the drift.

REFERENCES

1. RODWELL, W. et all. A thematic network on gas issues in safety assessment of deep repositories for radioactive waste (GASNET). Final Report. Luxembourg: European Commission, 2003. 49 p.
2. DYMITROVSKA, M., GENTY, A., LUKIN, D., NAVARO, M., WEETJENS, E. PA approach to gas migration. PAMINA (Performance Assessment Methodologies IN Application to Guide the Development of the Safety Case) deliverable report D3.2.1. Luxembourg: European Commission, 2009. 74 p.
3. LEMY, F. et all. Summary of gas generation and migration. Current state-of-the-art. FORGE (Fate Of repository Gases) milestone M15. Luxembourg: European Commission, 2010. 183 p.
4. MALLANTS, D., JACQUES, D. Performance assessment for deep disposal of low and intermediate level short-lived radioactive waste in Boom Clay. SCK•CEN report R-3793. Mol, Belgium: SCK•CEN, 2004.
5. Effects of post-disposal gas generation in a repository for low- and intermediate-level waste sited in the Opalinus Clay of Northern Switzerland. NAGRA technical report NTB-08-07. Wettingen, Switzerland: NAGRA, 2008. 138 p.
6. WENDING. J. Draft report on definition of benchmark studies on repository-scale numerical simulations of gas. FORGE deliverable report D1.1. Luxembourg: European Commission, 2009. 19 p.
7. PRUESS, K., OLDENBURG, C., MORIDIS, G. TOUGH2 Users’s guide, Version 2.0. Berkeley, California: Lawrence Berkeley National Laboratory, 1999. 198 p.
8. Thunderhead engineering. PETRASIM user manual. Version 5.0, 2010. 112 p.

CYSENI 2012, May 24–25, Kaunas, Lithuania
ISSN 1822-7554, www.cyseni.com

MODELLING OF QUENCH EXPERIMENT USING RELAP/SCDAPSIM CODE

T. Kaliatka
Lithuanian Energy Institute
Laboratory of Nuclear Installation Safety
Breslaujos str. 3, LT-44403 Kaunas – Lithuania
Phone +37037401911
Email: tadas@mail.lei.lt

ABSTRACT

Within the frame of the QUENCH test-program realised by Forschungszentrum Karlsruhe the loss of coolant accidents in Light Water Reactors is analysed using an experimental reactor core. Main issue of this test series is the qualitative and quantitative determination of the hydrogen source term. Another issue is to ascertain the behaviour of the bundle with different absorber rod and cladding materials. The QUENCH-03 test was performed January 21, 1999 with the objective to investigate the behaviour on reflood of PWR fuel rods with little oxidation. The simulation of the high hydrogen production rate due to a partly molten shroud like in QUENCH-03 is a challenge for all Severe Accident codes. This article presents the description of developed model of Quench facility using RELAP/SCDAPSIM code. Calculation results are compared to the results of a representative bundle heating and quenching experiment performed at the German Research Center in Karlsruhe. The results of comparisons show what developed model and RELAP/SCDAPSIM code are acceptable for the modelling of severe accident phenomena. However in order to have better agreement with experimental data there is a need to improve the model according the results of sensitivity and uncertainty analysis.

Keywords: Quench experiment, RELAP/SCDAPSIM, severe accident

1. INTRODUCTION

The most important accident management measure to terminate a severe accident transient in a Light Water Reactor is the injection of water to cool the uncovered degraded core. For instance failure of the main and emergency cooling-systems can lead to an accident with severe core degradation even with core meltdown. To prevent total meltdown of the uncovered and overheated core the reflooding with water is an unavoidable accident management measure. Analysis of the TMI-2 [1] accident and the results of integral out-of-pile (CORA [2]) and in-pile experiments (LOFT [3], PHEBUS, PBF) have shown that before the water succeeds in cooling the fuel pins there will be an enhanced oxidation of the Zircaloy cladding that in turn causes a sharp increase in temperature, hydrogen (exothermal zirconium-steam-oxidation reaction) production and fission product release. Within the frame of the QUENCH test-program realised by FZK the loss of coolant accidents in LWR (Light Water Reactor) is analysed using an experimental reactor core to determine the produced amount of hydrogen, the so-called hydrogen source term.

QUENCH experimental program started in the year of 1996 in the FZK Karlsruhe research centre (Karlsruhe Institute of Technology – KIT since 2009). Up to now in total 15 QUENCH tests were performed. A review of objectives and boundary conditions is given in [1]. Two tests were performed with B4C control rods (CR), one with a AgInCd CR, all the others used an unheated but instrumented fuel rod simulator. The latest QUENCH tests deal with the behaviour of different cladding materials. Based on the post-test calculations of the QUENCH the capability of the best estimate codes (RELAP/SCDAPSIM, ASTEC, ATHLET-CD, etc.) can be established and evaluated. In the following the post-test calculations of the QUENCH-03 test with RELAP/SCDAPSIM are discussed.

2. QUENCH TEST

The QUENCH program was initiated at FZK, as a follow-up program of the former CORA test series, which investigated the interactions of the materials in case of hypothetical severe accidents. The main focus of the QUENCH tests lies on the analyses of the hydrogen generation especially during the reflood, because in the CORA tests temperature escalations together with a high hydrogen production were detected, but the mechanisms therefore were not fully understood at that time [5]. The following chapter deals in general with the QUENCH facility at FZK and especially with the test conduct of test QUENCH-03.

The QUENCH facility essentially consists of the out-of-pile bundle (Figs. 1 and 2). This bundle includes 20 heated rods, one unheated central rod, which can be used for measurement devices or as a control rod, as well as four corner rods. The 21 simulator rods have a length of about 2.5 m, while approximately 1 m of the heated rods is electrically heated. For the experiment as well as for the calculations the beginning of the heated length is defined as height 0 m.

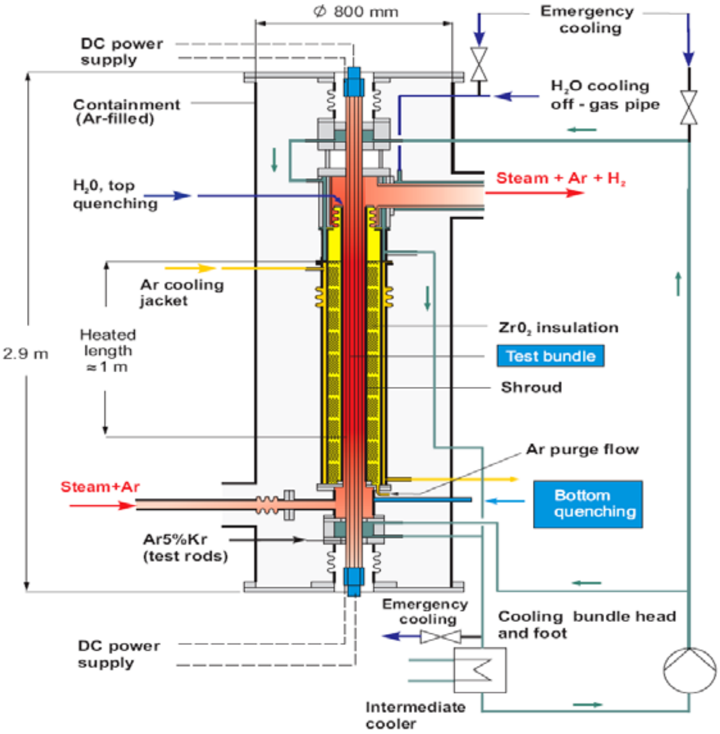

Fig. 1. Test section of the QUENCH bundle [6]

The tungsten heaters (outer diameter: 6 mm) are surrounded by annular pellets made of ZrO2 simulating the fuel pellets, which are bordered by Zircaloy-4 claddings (outer diameter: ~ 11 mm). The 21 rods and the 4 corner rods are arranged in a 5x5 matrix (Figure 2). To be able to detect fuel rod failure, the heated rods are filled with argon-krypton or helium, which can be detected by a mass spectrometer in the off-gas pipe. The 4 corner rods made of Zircaloy are implemented for additional thermocouple instrumentation as well as to enable the measurement of the axial oxide layer profile by withdrawal the corner rods at different times during the test progress [1].

The bundle is surrounded by a shroud of three layers. The first one is made of Zircaloy at the inner side (outer diameter: ~ 85 mm), followed by a central ZrO2 insulation layer and a double-walled cooling jacket made of steel at the outer side, to provide the encasement of the bundle and to simulate surrounding fuel rods in a real fuel element. The whole test section with the shroud is encapsulated by a steel containment (Fig. 1).

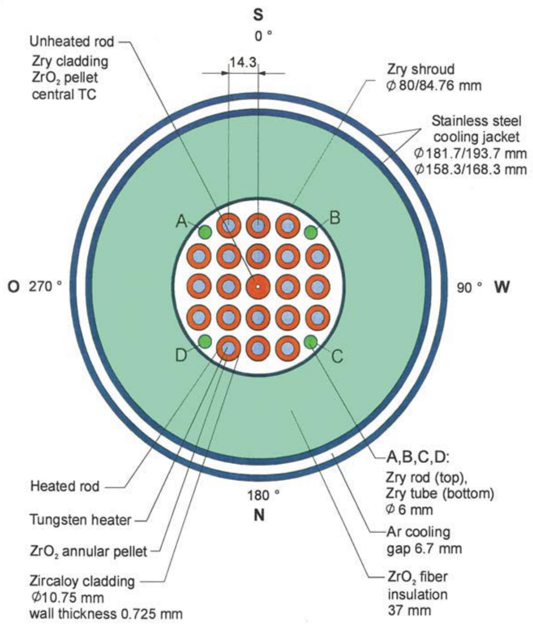

Fig. 2. Test section and bundle cross section of the QUENCH bundle [6]

Generally each QUENCH test consists of different phases: Heat-up, pre-oxidation, which is optional and not used in QUENCH-03, transient and a quenching phase, which means that the bundle is quenched by water or cooled by saturated steam. Before the quench phase superheated steam and argon are injected at the bottom of the facility as carrier gas to be able to transport and measure the reaction products from the test section.

Feature of the Quench-03 experiment is by the fact that super-heated core is cooled with water, the water supply starts in the late phase (after 200 s), when the fuel temperature starts to increase sharply. In the fuel bundle the 2100 °C temperature is reached in this experiment. Due to the high temperature partially melts and violates cladding made of the three layers. In the QUENCH-03 test, the pre-oxidation phase can be neglected because at the beginning of the transient phase the claddings should only be lightly oxidized with an oxide layer of approximately 30 μm as it is in the normal operation state of a pressurized water reactor (PWR). The progression of the QUENCH-03 test can be seen in Fig. 3:

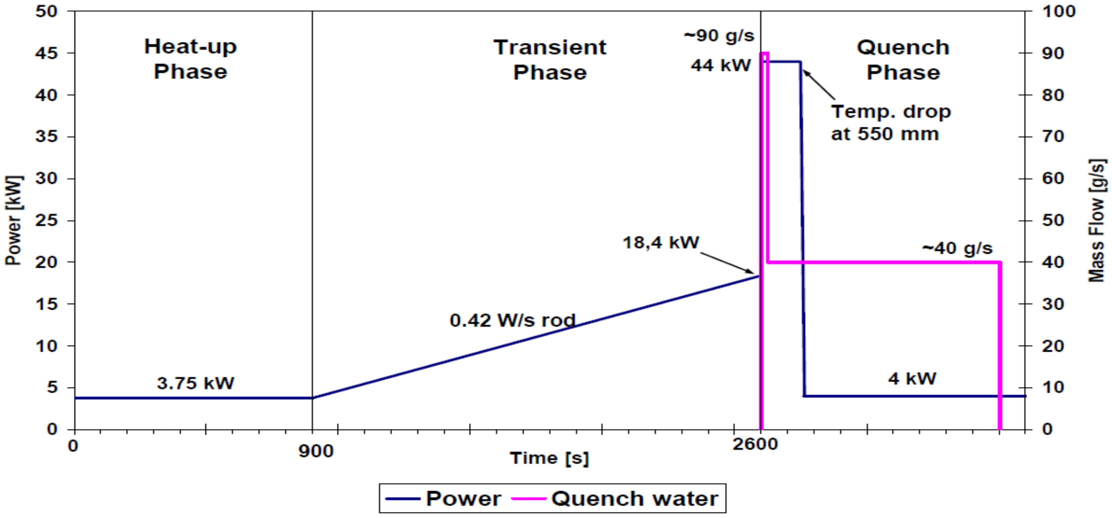

Fig. 3. Progression of the QUENCH-03 test

The first phase of QUENCH-03 is the heat-up phase, where the bundle was heated by a series of stepwise increases of electrical power from room temperature to approximately 900 K in an atmosphere of flowing argon (3 g/s) and steam (3 g/s). In order to stabilize the test set-up the reached temperature was hold for about 9000 s with an electrical power input of 3.75 kW. During this stabilization phase, shortly before the end, the data logging was switched on.

The transient phase follows and started at about 900 s and lasted roughly 2600 s. The bundle was ramped from 3.75 kW at 0.42 W/s per rod to 18.4 kW giving an average temperature increase of about 0.4 K/s between 900 K and 1400 K and about 1.6 K/s between 1400 K and 2070 K. At the end of the transient phase the electrical power reached a value of about 18.4 kW and 30.1 MJ of electrical energy in total was put into the system. Afterwards the thermocouples in the upper area of the shroud and upper bundle elevations show the same behaviour, due to the exothermal zircon-steam-reaction that runs faster at higher temperature levels. This reaction gave an additional energy input of 18.4 MJ into the system from which 16.3 MJ was released during quenching. The thermocouples at 750 mm bundle elevation detected a maximum temperature of over 2400 K causing a thermocouple failure at that elevation and higher.

Reaching the defined temperature of 2400 K inside the bundle at 2600 s led to the initiation of the final quench phase, in which the reflood water was injected firstly at a high rate of 90 g/s for 25 s to fill the lower plenum. With the initiation of reflooding the electrical power was increased from 18.4 kW to 44 kW to compensate the convective heat losses occurring due to the boiling of the inserted water at the hot structure material. At 2625 s the water injection rate was reduced to 40 g/s. The water mass flow resulted in a local flooding rate at the bottom of 1.3 cm/s. After reaching the maximum at 2627 s the electric power was reduced to 37.5 kW until 2747 s. During this period substantial temperature escalations occurred in the upper bundle area so that the claddings and the shroud collapsed at about 2627 s. Due to this collapse it came to melt formation and relocation which results in an increase of the surface available for oxidation and subsequently resulted in an additional massive hydrogen production. In the period from 2747 to 2762 s the electrical power was reduced from 37.5 to 4 kW to simulate the typical decay heat of a LWR [6].

3. RELAP/SCDAPSIM MODEL OF THE QUENCH-03 TEST

RELAP/SCDAPSIM is designed to describe the overall reactor coolant system (RCS) thermal hydraulic response and core behaviour under normal operating conditions or under design basis or severe accident conditions. The RELAP5 model calculates the overall RCS thermal hydraulic response (temperature, pressure distribution, etc.), control system behaviour (changing operating power settings, etc.), reactor kinetics, and the behaviour of special reactor system components such as valves and pumps. The SCDAP model calculates the behaviour of the core and vessel structures under normal and accident conditions. The SCDAP also includes models to treat the later stages of a severe accident including debris and molten pool formation, debris/vessel interactions, and the structural failure (creep rupture) of vessel structures. The latter models are automatically invoked by the code as the damage in the core and vessel progresses.

Test Quench-03 was modelled using RELAP/SCDAPSIM code [7]. The reference input deck, developed by SDTP [8] was used for the benchmarking. Quench nodalization scheme is presented in Figure 4. Space between heated rods and the outer cooling loop of the Quench facility was modelled using RELAP5 components: pipe, time-dependent volumes and junctions, single junctions, and others.

Imitators of fuel rods and surrounding shroud are modelled using the components of the SCDAP package: "fuel", "Cora" and "Shroud". In total 5 components are described using SCDAP package:

- component 1 - one central rod (not heated), modelled as a "fuel" element is composed of ZrO_2 pellets in the centre, a gas-filled gap and cladding of Zircaloy;

- component 2 – 8 heated rods (around the central rod) which simulates heated fuel rods, modelled using "Cora" component which is composed of tungsten heating elements in the centre, ZrO_2 pellets, gas-filled gap and cladding of Zircaloy;
- component 3 – 12 heated rods, modelled using "Cora" component;
- component 4 – the four rods in the corners, modelled as "fuel" component;
- component 5 – shroud of the bundle, modelled as "shroud" component, which consists of the inner Zircaloy layer, an insulating layer of ZrO_2 and Inconel layer (using properties of stainless steel).

The first four components are connected to the RELAP5 structure, which describes space between heated rods - pipe element "010" (Fig. 4). Element “010” is divided in axial direction in 18 nods with $3.009*10^{-3}$ m length of each. The fifth component (shroud of the bundle), in order to have heat exchange in the wall, is connected to hydrodynamic structures of RELAP5. This structure – pipe elements "013" and “018" is modelling the outer cooling circuit of the shroud. Layer thickness of shroud component heat structures is $1.2*10^{-3}$ m and has 5 radial mesh points. Element “013” in axial direction is divided in 13 nods and element “018” is divided in 5 nods with $3.684*10^{-3}$ m length of each.

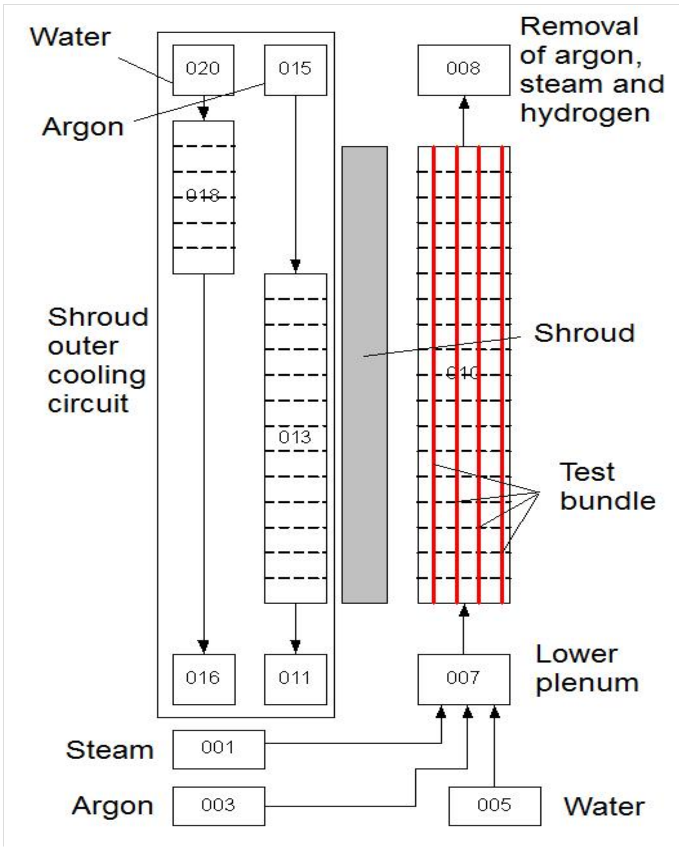

Fig. 4. Nodalization scheme of QUENCH test

3.1. Model assumptions

For the modelling of Quench-03 experiment three sets of parameters were applied: 1) used in Reference input deck, 2) “MAX” and 3) “MIN”. In those three sets the electric heating power, cooling water intake and thermal properties of Inconel and ZrO_2 were varied. This was done in order to evaluate the calculation uncertainties. According to the previous experience of the modelling of PHEBUS FPT-1 experiment [9] – two sets of parameters were prepared: it is expected that the set marked as “MAX” case will give the maximal temperatures of the fuel rods, cladding and etc; the set of “MIN” case is prepared for the opposite reason to receive the minimal temperatures of the fuel rods, cladding and etc.

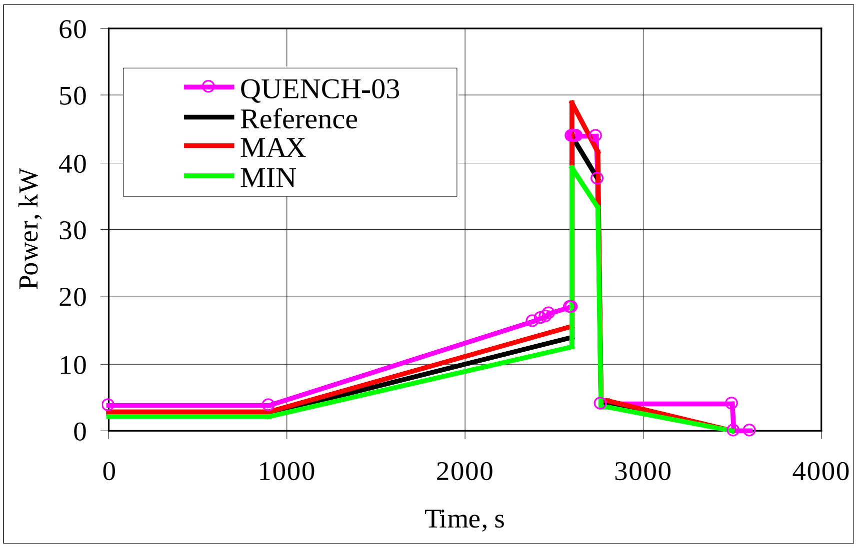

Fig. 5. The comparison of the electric heating power used in experiment and in the model (three sets)

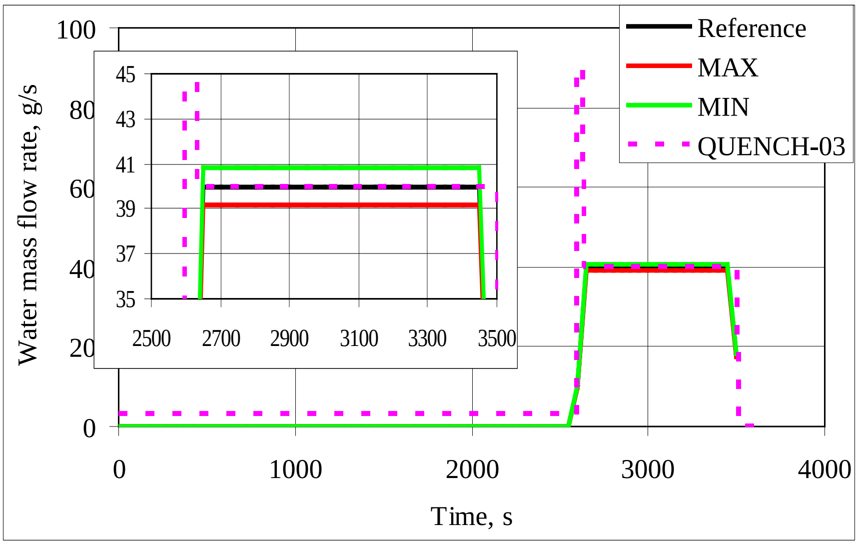

Fig. 6. The comparison of steam and water mass flow rate in the model (three sets) and in the experiment

The behaviour of electric heating power and cooling water intake which are used in the experiment and in the three sets of the models of RELAP/SCDAPSIM code are presented in Fig. 5 and Fig. 6. As it can be seen from Figure 5, the reference power in the model was chosen lower than described in the experimental measurements. This was done in order to assess the potential loses to the environment. The max and min sets are made according to the reference case multiplied by 1.11 and 0.89 respectively assuming that maximal power is 111%, minimal – 89% from the reference power. The intake of cooling water is the same in the model of the reference case and in the experiment (Fig. 6), except for the water supply of 90 g/s mass flow (water flow starts at 2600 s and is continues during 25 s). In the experiment for the short term, water was supplied at high flow rates up to fill the lower collector of existing pipelines. In the model water is filled directly into the lower collector, so the short term high flow rate of water was not modelled. The MAX and MIN sets are made according the reference case multiplying the water mass flow rate by 0.98 and 1.02 respectively. The reference thermal properties of shroud layers (ZrO^2 and Inconel) were also varied in the model. The variation of the ZrO^2 and Inconel thermal properties shown in Fig. 7 and Fig. 8. By increasing the thermal conductivity of shroud layers we are removing the larger part of heat from the fuel rods imitators to the shroud cooling circuit. That leads to the decrease of fuel and cladding temperatures. The same situation could be applied for the specific heat and the density of the shroud layers. That is why the lower values of shroud layer thermal properties (in “MAX” case) comparing to reference values was used in order to receive maximal calculation results value of fuel or cladding temperature. This approach was tested in the PHEBUS experiment benchmark, presented in paper [9].

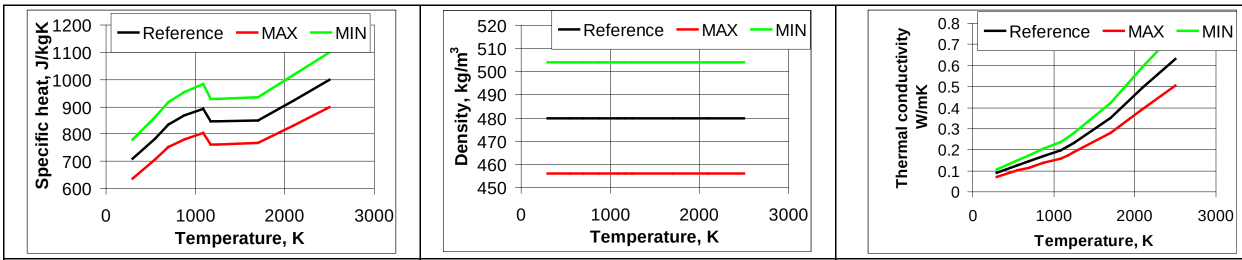

a) b) c)

Fig. 7. The thermal properties of ZrO^2. a) specific heat, b) density, c) thermal conductivity

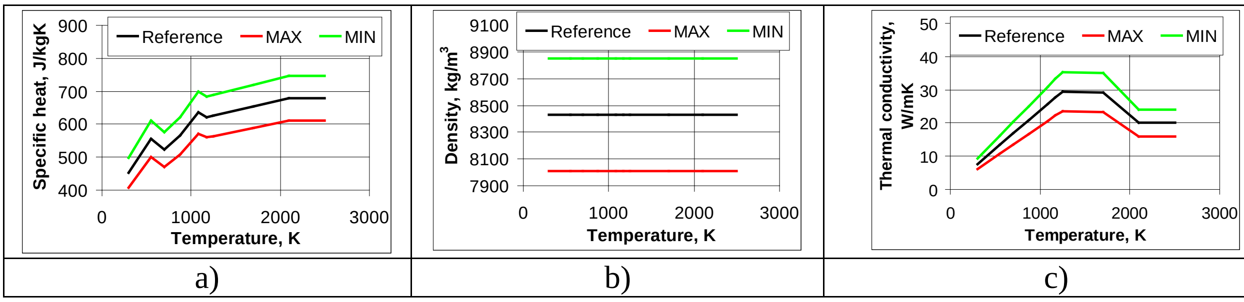

a) b) c)

Fig. 8. The thermal properties of Inconel. a) specific heat, b) density, c) thermal conductivity

4. CALCULATION RESULTS

In the Fig. 9 the temperature deviations in the central not heated rod (which is modeled as the fuel rod, but without heat generation) is presented. Curve named QUENCH-03 presents the experimental data. Curves named ”Reference”, “MAX” and “MIN” are the calculation results of RELAP/SCDAPSIM code for the three sets of parameters. In the Fig. 9 a) the calculated temperature of central rod in 350 mm height is compared with experimental data, in the Fig. 9 b) the calculated temperature of central rod in 950 mm height is compared with experimental data. These two calculation points (in height 350 mm and 950 mm) were presented in order to have feeling of temperature variation in central rod in axial direction. Summarizing received calculation results, it could be said that they are in reasonable agreement with experimental data.

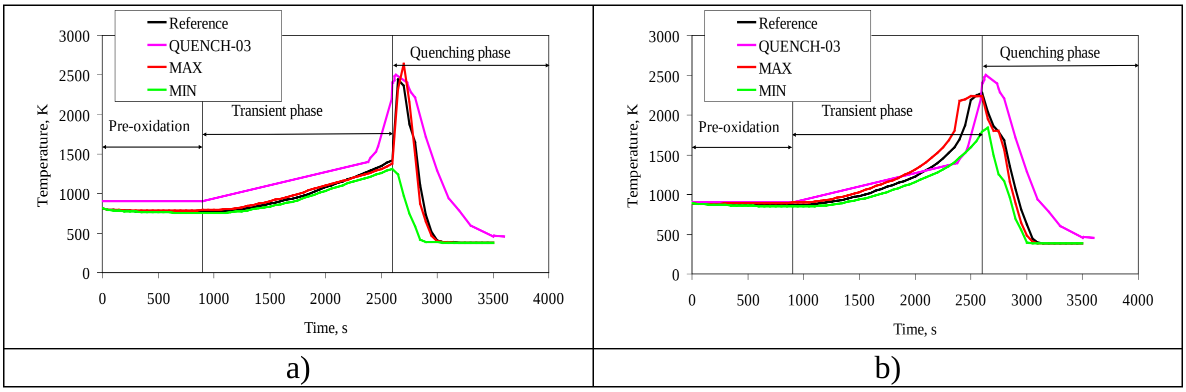

a) | b)

Fig. 9. Temperature variation in not heated central rod. Comparisons of experimental data and calculation results received using RELAP5/SCDAPSIM: a) temperature in the central rod in 350 mm height, b) temperature in the central rod in 950 mm height

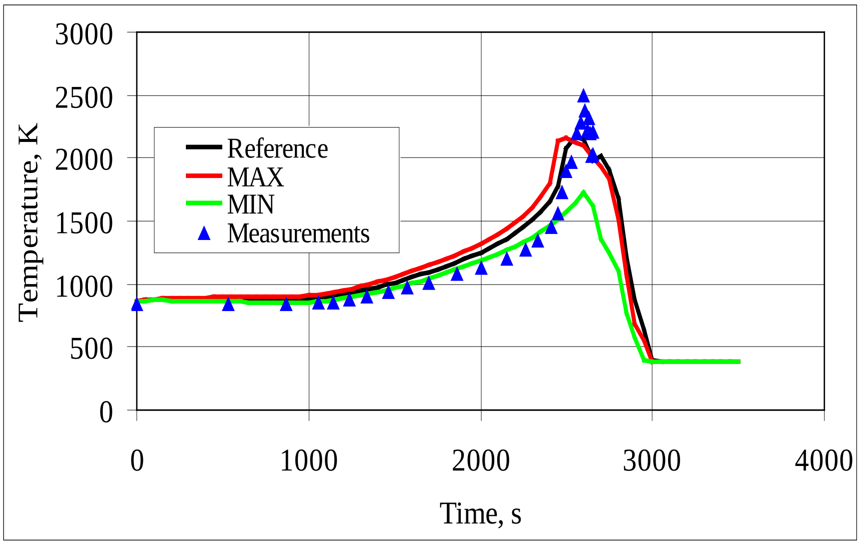

Fig. 10. Temperature deviation of outer cladding of fuel bundle placed near the central rod at 750 mm height

The temperature of outer cladding of fuel bundle placed near the central rod in 750 mm height is presented in Fig. 10. In this figure curves named “MAX”, “MIN” and “Reference” is the calculation results of three sets of model parameters; “Measurements” – with thermocouple measured data during the experiment in the fuel bundles in 750 mm height and 45° angle of fuel bundle [6]. The maximal value of cladding temperature (“MAX”) is similar to reference, but minimal value (“MIN”) is significantly lower. This is because the varied parameters have different impact on the calculation results. In order to clarify it is necessary to provide sensitivity analysis, which is planed to perform in the future.

The temperatures in shroud inner face are presented in Fig. 11. The time moment of shroud failure observed during the experiment is presented in this figure. Measurements of shroud inner face temperature received form thermocouple placed in 750 mm height and 180° angle of the shroud [6] are presented and compared with RELAP/SCDAPSIM code calculations in Fig. 11. Temperature calculated using RELAP/SCDAPSIM code, “Reference” and “MAX” sets of parameters have similar configuration of the curve deviation. The calculation results of “MIN” set of parameters is in good agreement with measured shroud inner face temperatures, when the shroud is intact. After the shroud failure experimental measurement data of shroud inner face temperature is in better agreement with calculation results of “MAX” set of parameters. This shows that model of QUENCH test should be improved. The sensitivity and uncertainty analysis of calculation results will indentify what parameters have the biggest influence to calculation results and it will help to improve the model.

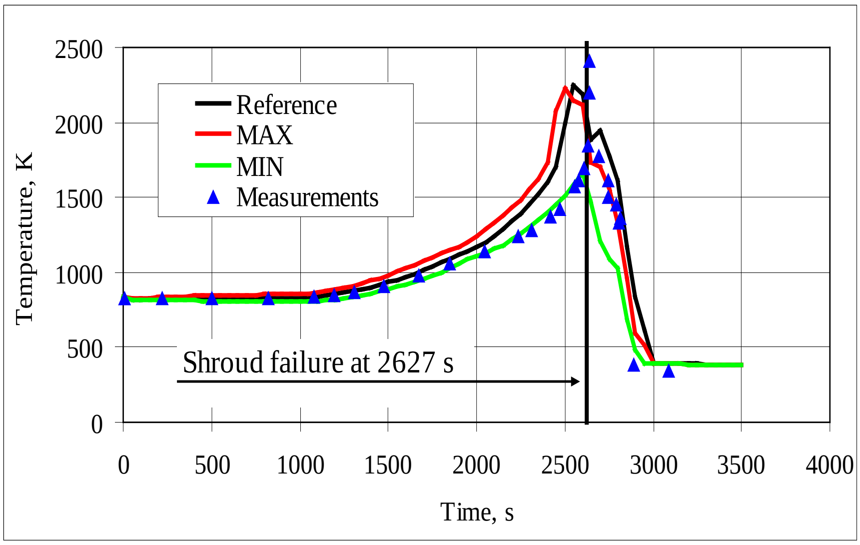

Fig. 11. Shroud inner face temperature in the height of 750 mm

The integral mass of the hydrogen produced due to reaction of steam and zirconium is presented in Fig. 12. The calculation results of produced hydrogen mass in reference and max cases are higher than it has been measured during QUENCH-03 experiment. Different situation is observed in case of parameter set leading to minimal calculated temperatures. In this case the mass of hydrogen is the same in the point of between transient and quenching phases, but later calculated mass is much lower then measured point. From Fig. 12 it is clear that the calculation of integral hydrogen mass is very sensitive to fuel cladding temperature (our varied physical parameters).

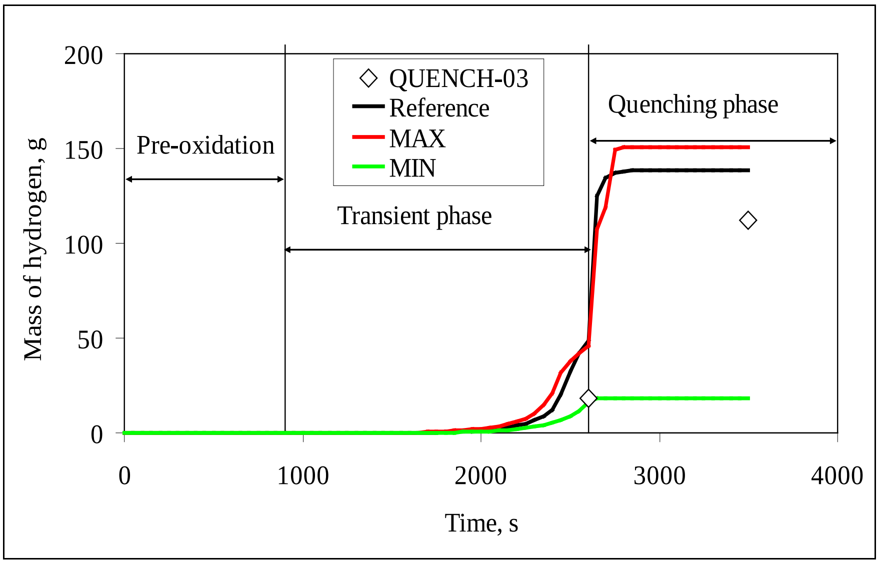

Fig. 12 QUENCH-03 experimental measurements [10] and the calculation results of integral mass of hydrogen production

5. CONCLUSIONS AND SUMMARY

The model of QUENCH-03 experiment for the RELAP/SCDAPSIM code was created. The QUENCH-03 experiment was modelled using RELAP/SCDAPSIM code and the processes in the fuel bundle were analyzed. In order to assess the uncertainties of calculation results, it was made three sets (MIN, Reference and MAX) of parameters and calculations of these sets were provided. Calculation results were compared with experimental data. After the analysis of received results of benchmark, it could be concluded that RELAP/SCDAPSIM code and developed input deck are suitable for the analysis of processes in fuel bundles of QUENCH experiments. In the future the sensitivity and uncertainty analysis will be performed in order to clarify parameters which are most important to calculation results and the QUENCH model will be improved.

ACKNOWLEDGMENTS

This paper was prepared on the basis of work, which was carried out within the framework of the Severe Accident Research Network of Excellence 2. This work is also supported by the Agency for Science, Innovation and Technology (MITA) in Lithuania.

REFERENCES

1. BROUGHTON, M.J., KUAN, P., PETTI, D.A., A Scenario of the Three Mile Island Unit 2 Accident, *Nuclear Technology,* 87, 34, 1989.
2. HOFMANN, P., HAGEN, S., NOACK, V., SCHANZ, G., SEPOLD, L., Chemical-Physical behaviour of Light Water Reactor core components tested under severe reactor accident conditions in the CORA facility, *Nuclear Technology,* Vol. 118, 1997, p. 200.
3. HOBBINS, P.R., McPHERSON, G.D., *Summary of results from the LOFT LP-FP-2 test and their relationship to other studies at the power burst facility and of the Three Mile Island Unit 2 accident*, OECD/LOFT final Event, ISBN 92-64-03339-4, 1991.
4. Forschungszentrum Karlsruhe: QUENCH Programme at FZK – QUENCH Test Matrix, http://hikwww2.fzk.de/quench/, 01. July 2009.
5. STEINBRÜCK, M.; et al. Core reflooding: Synthesis of the QUENCH program and its impact on code modelling, Proceedings of the 1st European Review Meeting on Severe Accident Research (ERMSAR-2005), Aix-en-Provence, France, 14-16 November 2005.
6. HOFMANN, P., et al. *Experimental and Calculational Results of the Experiments QUENCH-02 and QUENCH-03*, Wissenschaftliche Berichte, FZKA 6295, Institut für Materialforschung, Institut für Reaktorsicherheit, Projekt Nukleare Sicherheitsforschung, Forschungszentrum Karlsruhe, July 2000.
7. ALLISON, M., WAGNER, R. J. *RELAP5/SCDAPSIM/MOD3.2 (am+) Input Manual Supplemental*, Innovative Systems Software, LLC (2001). Link to the internet <www.relap.com>
8. SCDAP Development & Training Program. Link to the internet <http://www.sdtp.org>
9. VILEINISKIS V., KALIATKA A., Best estimate analysis of PHEBUS FPT1 experiment bundle phase using ASTEC code ICARE module, *Nuclear Engineering and Design*. In press.
10. STEINBRÜCK, M. Analysis of Hydrogen Production in QUENCH Bundle Tests, Wissenschaftliche Berichte, FZKA 6968, Institut für Materialforschung, Programm Nukleare Sicherheitsforschung, Forschungszentrum Karlsruhe, May 2004.

CYSENI 2012, May 24–25, Kaunas, Lithuania
ISSN 1822-7554, www.cyseni.com

ANALYSIS OF AEROSOL, FISSION PRODUCT AND IODINE BEHAVIOUR IN PHEBUS CONTAINMENT

A. Kontautas, E. Urbonavičius
Lithuanian Energy Institute
Breslaujos str. 3, LT-44403 Lithuania
Phone+370 37 401983
Email: aurkon@mail.lei.lt, egis@mail.lei.lt

G. Weber
Gesellschaft für Anlagen-und Reaktorsicherheit (GRS) mbH
Garching b., D-85748 Germany
Phone +49 (89) 32004-506
Email: gunter.weber@grs.de

ABSTRACT

The aim of the present work is to demonstrate the applicability of the created model using lumped parameter code COCOSYS (Containment Code System) for integral analysis of thermal-hydraulic proceses, aerosol transport and deposition, fission product behaviour and iodine chemistry during severe accident conditions in the containment of nuclear power plant. Analysis of PHEBUS containment under FPT2 experiment conditions was performed. Model with nodalization of 16 nodes was created in cooperation with experts of GRS mbH (Germany), where GRS was responsible for the iodine part. The performed analysis showed that thermal-hydraulic parameters are in good agreement with the measured results and gives good basis for further analysis of aerosol and fission product deposition analysis as well as for iodine chemistry analysis. The performed analysis showed that all the processes are represented adequatelly exept for diffusive particles' deposition on the vertical surfaces of external structures. Further investigation of diffusive deposition of particles is required. The analysis of the iodine behaviour shows that I_2 injection from the circuit is the most important source of gaseous iodine in the containment. Only little I_2 is produced in the sump, because of the high pH and the iodine-silver reaction. The measured I_2 concentration in the gas phase is somewhat underestimated and the measured organic iodide concentration is well matched. Summing up, the containment behaviour of aerosols, fission products and iodine analysis in FPT2 are fairly well simulated by COCOSYS code.

Keywords**:** containment, COCOSYS, PHEBUS

1. INTRODUCTION

The lumped-parameter codes are the main tool to investigate the complex response of the containment of Nuclear Power Plant in case of an accident. Continuous development and validation of the codes is required to perform realistic investigation of the processes that determine the possible source term of radioactive products to the environment. Validation of the codes is based on the comparison of the calculated results with the measurements performed in experimental facilities. Integral investigation is very important for comprehensive validation of computer codes. Together with the experts from GRS mbH the performance of integral analysis of aerosol, fission products and iodine behaviour using COCOSYS code in PHEBUS containment was agreed. LEI was responsible for the numerical simulation of aerosol and fission product behaviour. The analysis of iodine behaviour part was contributed by GRS mbH.

The PHEBUS containment analysis for different FPT tests is performed at Lithuanian Energy Institute for several years using COCOSYS lumped parameter code [1]. Initially, the attention was concentrated on the development of the nodalisation and the investigation of thermal hydraulic phenomena [2]. The performed analysis showed that adequate radial nodalisation is essential to model correct flow pattern in the containment. Further the investigation of aerosol deposition and distribution for FPT-1 test was performed [3]. Received results showed a good agreement with experimental data for aerosol total deposition, which is the sum of all deposition processes in containment atmosphere. Nevertheless, calculated aerosol mass deposition on the external containment walls was too small and the percentage deposition distribution evaluation did not agree with experiment. After that, the parametric analysis of aerosol density, solubility, boundary layer thickness was performed and it also shows only minor influence on the aerosol behaviour [4]. With every step of the analysis the nodalization was improved to better representation of the processes in the containment.

This paper presents the results of integral analysis of thermal-hydraulic processes, aerosol, fission products and iodine behaviour in PHEBUS containment under FPT-2 test conditions. System was represented by the numerical model of 16 nodes. For the analysis nodalisation was recomposed from 16 to 6 nodes by combining two or more zones to one iodine zone. The reduction of spatial resolution is due to experience gained in the similar test FPT-1, in which the iodine was well mixed distribution in the whole containment [5].

2. DESCRIPTION OF EXPERIMENT FPT-2

2.1. Geometric conditions

The PHEBUS containment vessel is a 10 m^3 tank (see Fig. 1), made of electro-polished stainless steel (AISI 316L), in which aerosols and gases conveyed through the experimental circuit during the test are collected. Height of containment is 5 m with an inner diameter of 1.8 m. The altitude of containment vessel is shown in Fig. 1. The containment wall represents a surface of about 25 m^2. The containment has cylindrical form with rounded bottom and top. The outer vessel walls were heated to avoid steam condensation and subsequent aerosol deposition on the containment top vault and vertical walls during the test. The top vault is equipped with a group of three condensers, which are designed to control heat transfer, steam condensation and thus simulate the cold structures of a reactor building. Total surface area of condensers is 3.333 m^2. The condenser surface is divided into two parts: the cooled condensing or “wet” condenser surface (area: 0.775 m^2 per condenser) and the non-condensing or “dry” condenser surface (area: 0.336 m^2 per condenser). The lower part of each condenser is kept dry by heaters and contains the equipment to collect condensate from the upper cooled part. When the collection device is full, the condensate is automatically drained into the sump. The cooled surfaces of condensers are covered with epoxy paint as a source for organic iodine formation. The sump is a lower vessel part closed by a curved bottom structure with a volume of 0.1 m^3. The sump has a diameter of 0.584 m and height is 0.6 m in order to reproduce a representative atmosphere-water exchange surface. The sump was initially filled with 120 l water. The injection pipe tag to the containment of steam, hydrogen and aerosols is located at the level of -2.86 m. Pipe tag is in the centre of containment and is pointed to the condensers.

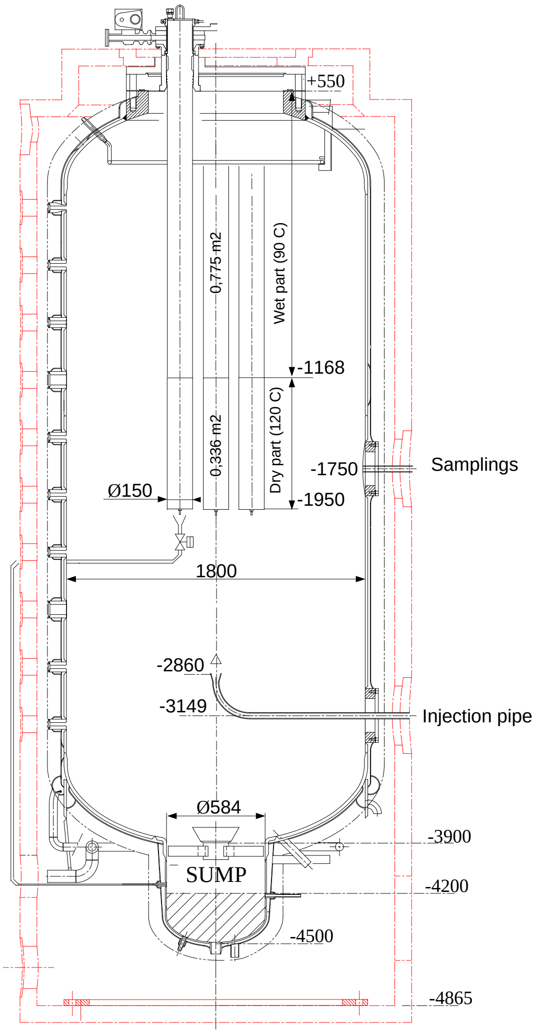

Fig. 1. Schematic view of PHEBUS containment

2.2. Initial and boundary conditions

The composition of the containment atmosphere consists of condensable gases (i.e., steam) and non-condensable gases (i.e., H_2, O_2, N_2 and He). During the test preparation phase the nitrogen is injected into containment to avoid any explosion hazards with the possible hydrogen injection during experiment. As a result the initial pressure in containment increases up to 1.95 bar, the average atmosphere temperature is 108 ^{o}C and the average relative humidity – 51.48 %. The sump initially buffered at pH = 8.7 and alkaline throughout the whole test.

Measured steam and hydrogen flow rates into the containment are shown in Fig. 2. Steam injection into the containment started after -3180 s. The steam flow rate to containment is 0.47 g/s and corresponds to the coolant flow rate through the reactor core. In the course of performed test the core temperature increases and the fuel cladding starts oxidising due to zirconium and steam interaction. In this chemical reaction the hydrogen is generated and together with the steam is released to the containment. Therefore during the course of test the steam flow rate decreases when the hydrogen flow rate increases. The first fuel-clad failure in the experimental reactor, with real irradiated fuel, was recorded at about 5630 s and ~3000 s later (8730 s) the control rod failed [6]. As a consequence, aerosols arrived to containment after ~9000 s and finished after ~19500 s (see Fig. 3**) [6]**. The total injected mass of aerosols is 44.69 g. As could be seen from Fig. 3 aerosol flow rate is not stale and it is consequence of unstable processes in reactor during fuel degradation. The total mass of iodine injected was 0.89 g and the most of which was injected as CsI (caesium iodide) and other part react with Ag, In, Cd and etc. The I_2 injection rate was taken from data given in the final FPT-2 report [6]. The mass fraction of gaseous iodine was measured in the circuit cold leg and in the containment during the injection period.

Sequential samplings devoted to the analysis of gases and aerosols characterisation are implemented in the containment and detailed description of sampled volumes with thermal hydraulic conditions is given in PHEBUS FPT-2 test Final report [6].

During the whole test period the temperature of containment walls in contact with the gas phase was 110 °C, temperature of the “wet” condensers 90 °C, temperature of the “dry” condensers 120 °C, and temperature of walls in contact with the sump 90 °C. The containment vessel boundary conditions are chosen to limit the relative humidity to from about 50 up to 70 % during the transient, in order to prevent steam condensation on the external containment walls. Steam condensation in the containment was controlled by the cooled condensing surfaces of the condensers. More detailed description of thermo-hydraulic conditions is given in paper [3].

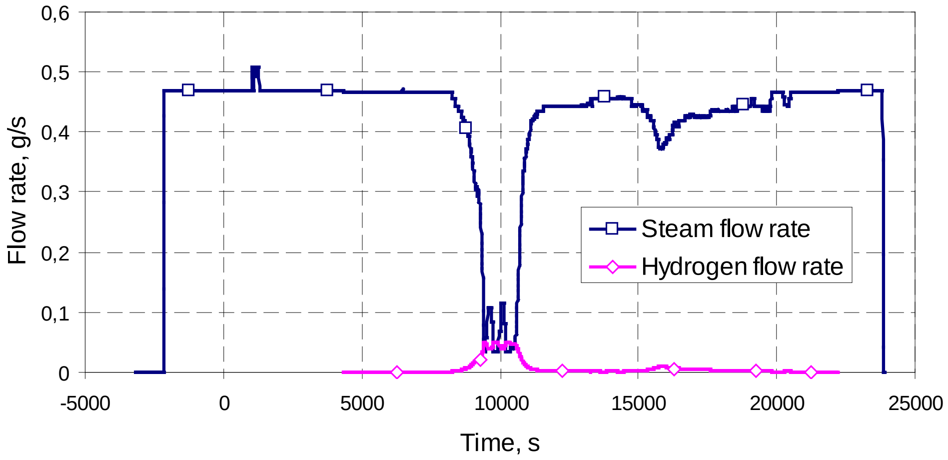

Fig. 2. Steam and hydrogen flow rates to containment during FPT-2

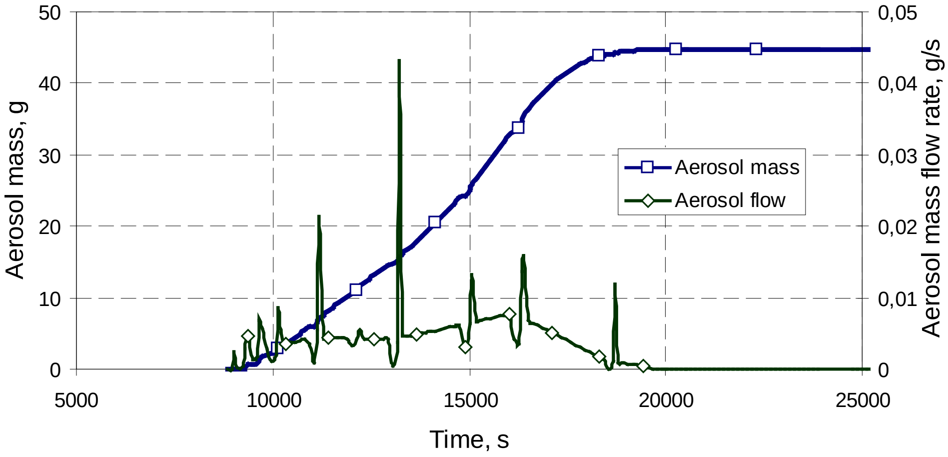

Fig. 3. Injected aerosol mass and flow rate to containment during FPT-2

3. MODELS OF PHEBUS CONTAINMENT

For simulation of the aerosol and fission product transport in the PHEBUS containment a model of 16 nodes for COCOSYS code was developed. The nodalization scheme of the model is shown in Fig. 4 (a)**.** In the model the radial subdivision of the containment consists of two rings in close level above the sump. There is a centre node R1H1 and node R2H1 that represent the bottom part of the vessel. Above -3350 mm and below 0 mm levels there are three rings of almost equal areas. The diameter of the radial subdivision was defined in such way that the flow areas are similar. Such approach to nodalization gives similar flow velocities. A ring close to the external containment walls is 175 mm width. At the top vault of the vessel there is one additional node. Simulation at the top vault by single node gives the well-mixed conditions at the top of facility. Similar approach is used at the bottom of facility. Above the SUMP nodes are defined in such way that there are two junctions to the SUMP. Such approach ensures better mixing and allows avoiding dead-end node, which is not recommended for lumped parameter codes [1].

For the iodine calculation a coarser nodalisation was used as it is shown in Fig. 4 (b). The 16-zone nodalisation was reduced to 6 zones by combining two or more zones to one zone for iodine calculation. The reduction of spatial resolution is due to experience gained in the similar test FPT1 [5], in which the iodine mass was well mixed throughout the whole containment. Only near the condenser and the sump the resolution was chosen to be higher in order to model local deposition and mass transfer effects.

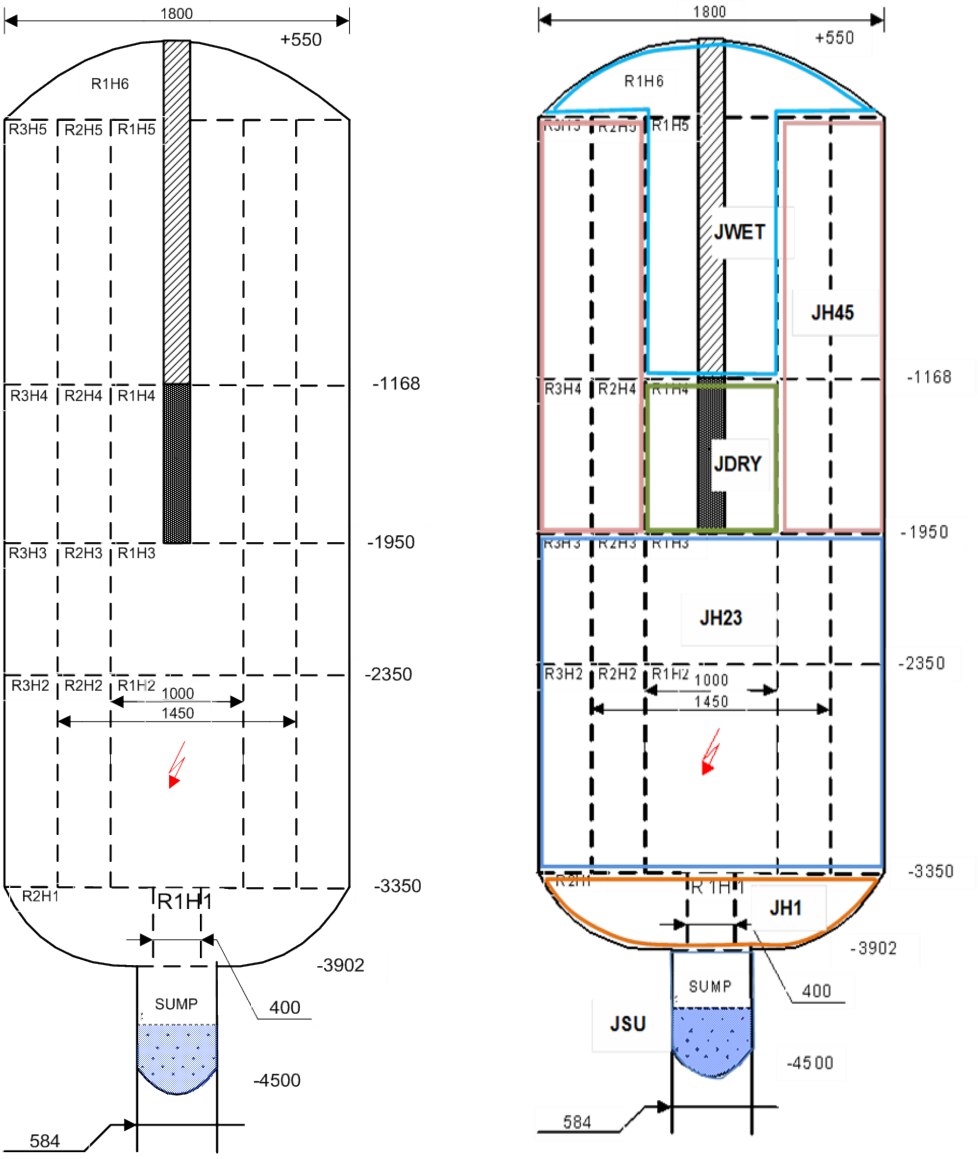

(a) (b)

Fig. 4. Nodalization scheme of PHEBUS containment. (a) – aerosol and fission product analysis nodalization; (b) – iodine analysis nodalization

In the model 11 structures for the simulation of heat transfer through the containment walls to the outer atmosphere are defined. Structures represent the thermodynamic parameters of walls inside the containment. Two more structures are defined for the simulation of heat transfer between condensers and the inner atmosphere. All PHEBUS containment surfaces and condensers are made of stainless steel. Only the surface of the condensers is covered with epoxy paint to investigate chemical interactions of iodine with the paint.

For the simulation of the gas flows between the nodes there are defined atmospheric junctions with real geometric areas. Also, there are defined junctions for simulation of the water drainage from the "wet" condenser to the sump.

In the developed model the initial and boundary conditions (e.g. initial pressure, temperature, humidity, etc.) are defined according to FPT-2 test specification and described in Section 2.2 [6].

The aerosols diameter range is assumed 10^{-8} – 10^{-4} m. Assumption is made according to experimental results [6] and COCOSYS recommendations [1]. The models of gravitational, diffusive and diffusiophoretic deposition mechanisms are considered in the model. It is assumed that aerosols could be washed down from the vertical walls by condensate flow and slip through the vertical junctions. Aerosol particles are assumed to be spherical. The soluble (Cs, Rb and I) and non-soluble (Ce, Te, Zr, Ru, Sn, In, Ag, W, U, Ba, Mo, Cd, Re and Tc) aerosols are defined in the model. The composition of elements detected in containment is given in Final test report [6]. It was supposed, that the solubility factor for soluble elements is 1.73 and for non-soluble is 1.0. Solubility factor is equivalent to the number of ions into which a salt dissociates in a solvent, which is in the reactor case water.

4. RESULTS OF ANALYSIS

4.1. Results of aerosol deposition

The calculated mass of aerosols suspended in the containment atmosphere is shown together with the corresponding measured data in Fig. 5. Aerosol injection into the containment started after 9100 s and after ~17600 s a maximum of the suspended airborne aerosol mass was observed. In general the calculated airborne aerosol mass is overestimated during the whole of the analysed period, but the difference is less than 2 g. The maximal airborne mass measured is ~19 g, while the calculated one is ~21 g in the whole containment. The difference between the calculated and measured mass does not change significantly, which shows that total deposition rates are rather well calculated by COCOSYS.

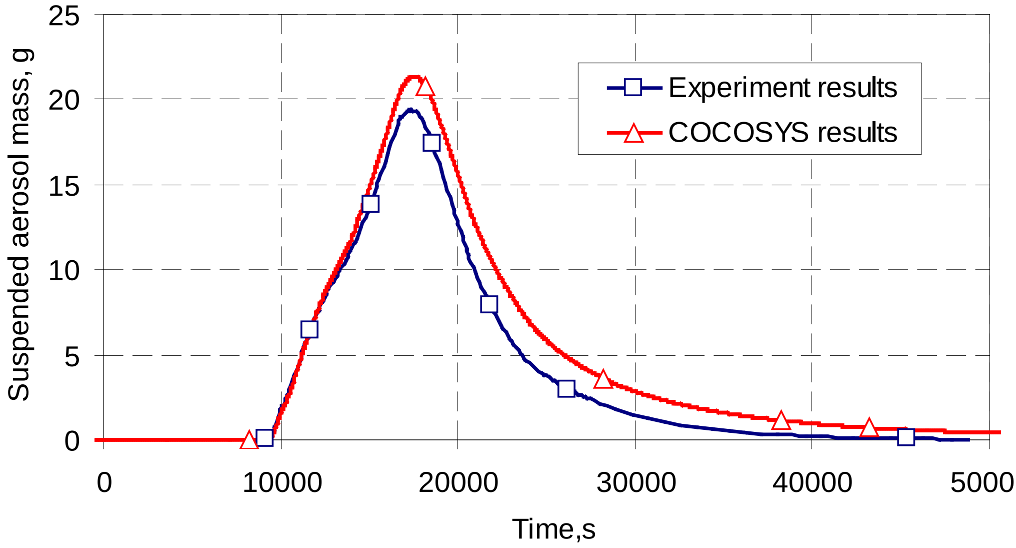

Fig. 5. Suspended aerosol mass in PHEBUS containment

Distribution of aerosol deposition on different surfaces in the containment is shown in Table 1. The largest aerosol deposition is on the containment floor around the sump, where 74% of total injected to containment aerosol mass (44.69 g) is deposited. On the condensers and in the sump there are deposited 14% of aerosol mass, while on the vertical containment walls and removed by the sampling 12%. The results received with COCOSYS shows good agreement for the particles deposition on the condensers surfaces and in SUMP, but the mass deposited on the containment walls and removed by the sampling is significantly lower (1% instead of measured 12%) while deposition on the containment floor is overestimated. The deposition on the external vertical walls is determined by the Brownian diffusive deposition, which is weak, except for very small particles.

The diffusive deposition of aerosol is larger than the gravitational only for particles smaller than 0.1 μm [7].

Table 1. Distribution of aerosol deposition

	Floor of containment	Condenser surfaces and sump	Containment walls + samplings
Experiment results	74.0%	14.0%	12.0%
COCOSYS results	86.0%	13.28%	0.72%

4.2. Results of fission products deposition

The fission products are treated as the radioactive part of the aerosol particles. Fig. 6 presents the comparison between the measured and calculated tellurium mass suspended in the containment atmosphere. The calculated tellurium mass is in good agreement with measured results, and the difference is less than 0.02 g. The maximal measured mass is 0.52 g, while calculated is 0.51 g. The difference between the calculated and measured mass does not change significantly, which shows that total deposition rate are rather well calculated by COCOSYS. It should be noted that the performed analysis does not include chemical reactions of tellurium with steel, paints and other materials. In this part of analysis the tellurium is treated as aerosol.

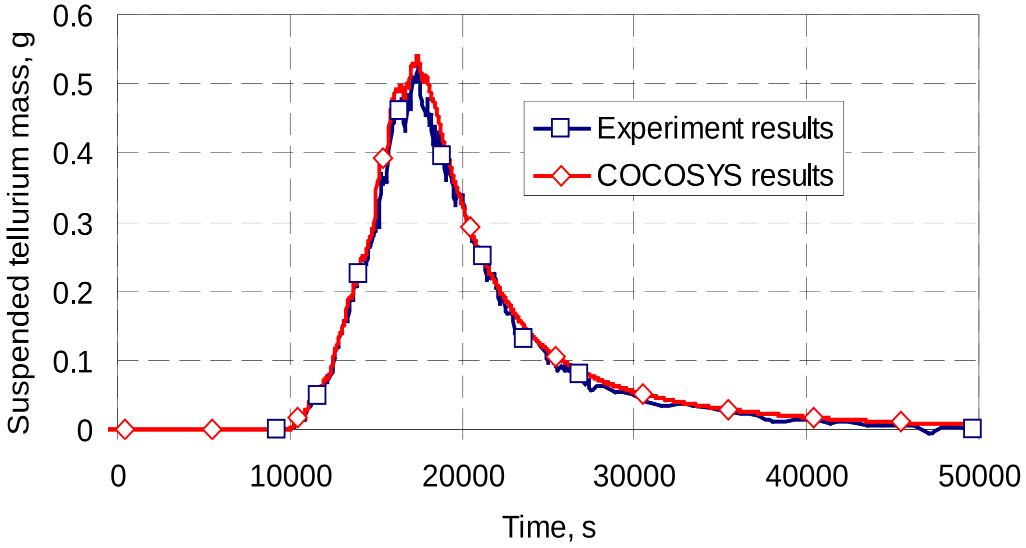

Fig. 6. Suspended tellurium mass in PHEBUS containment

The distribution of fission product deposition is related to aerosol deposition. The distribution of tellurium deposition is shown in Table 2. The most part of tellurium injected is deposited on the containment floor around the sump, where 75.69% of tellurium mass is deposited. On the condensers and in the sump there are deposited 13.58% of tellurium mass, while on the vertical containment walls and removed by the sampling 10.73%. The results received with COCOSYS code shows quite good agreement for the particles deposition on the condensers 14.38%, but the deposition on the containment walls is only 2.49%. Therefore deposition on the floor of containment is overestimated 83.13%.

Table 2. Distribution of tellurium deposition

	Floor of containment	Condenser surfaces and sump	Containment walls + samplings
Experiment results	75.69%	13.58%	10.73%
COCOSYS results	83.13%	14.38%	2.49%

4.3. Results of iodine behaviour

Fig. 7 shows the calculated concentration of gaseous I_2 in the containment and the comparison with experimental values derived from online and sequential Maypack measurements. The calculated values are somewhat underestimated. In addition, the calculated peak at the beginning, which results from the injection, is confirmed by one measured value. Unfortunately, no measurement points are available in the chemistry phase after 205000 s, but the measured total gaseous iodine (I_2 + organic (R) I) concentration indicates also a good evolution for this second part of the test Fig. 8.

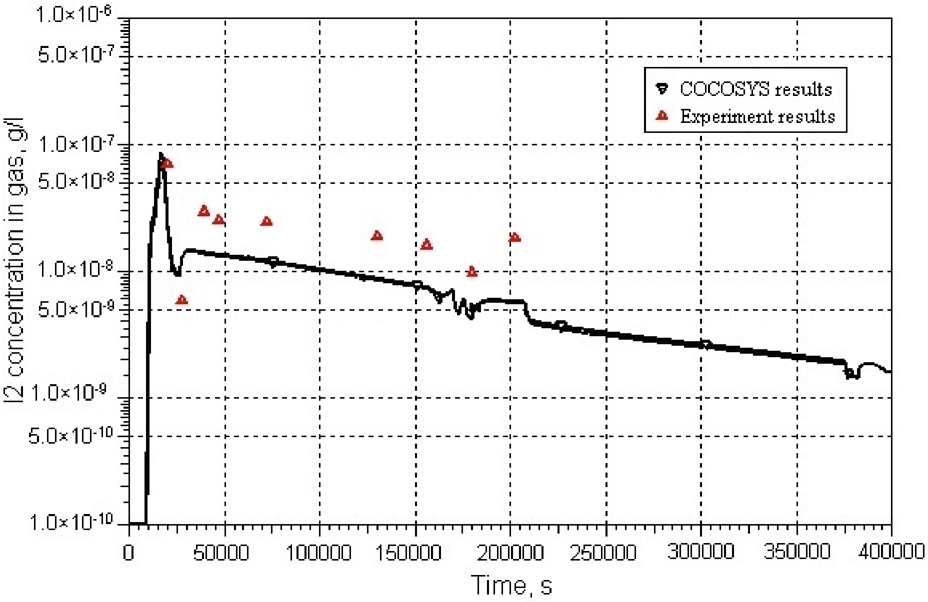

Fig. 7. Gaseous I_2 concentration in PHEBUS containment

Fig. 8 shows the total gaseous iodine concentration, i.e. essentially I_2 and RI. Calculated results with COCOSYS are shown in black thick line with small circuits. Measured results from different sampling techniques (SM, OLGA, ZGC, TGC) are shown with green markers. The maximal measured concentration is ~$2.5 \cdot 10^{-7}$ g/l, while the calculated concentration is ~$1.0 \cdot 10^{-7}$ g/l. Nevertheless, calculated concentration shows a good agreement with the measured values from five different sampling devices.

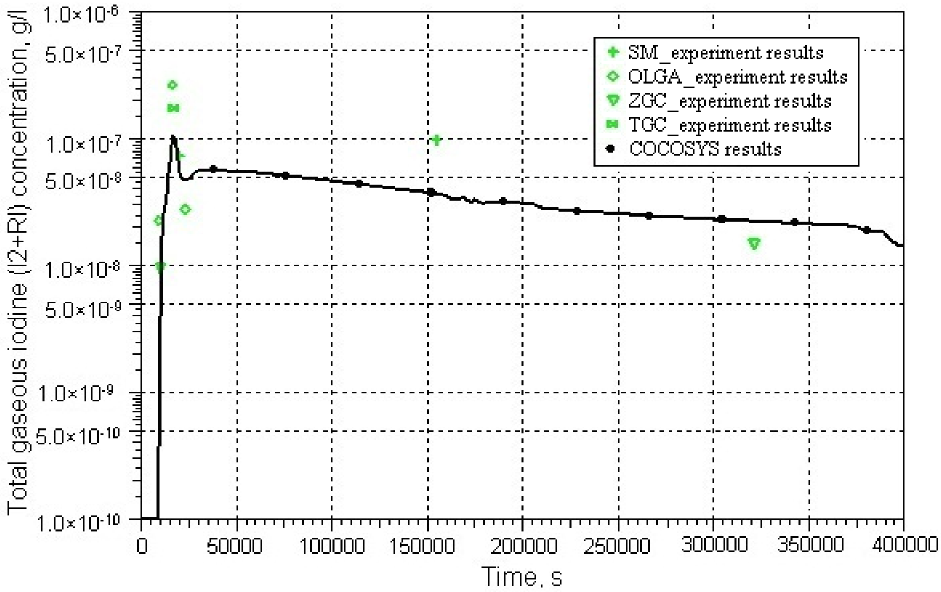

Fig. 8. Total gaseous iodine (I2 + RI) concentration in PHEBUS containment

Fig. 9 shows iodine (I^-) concentraton in SUMP. Calculated results with COCOSYS are shown in black thick line with small triangles. Measured results by gamma station 12 are shown with red markers. The comparison between measured and calculated results shows a good agreement until washing phase (177060 s). During washing phase iodine concentration is clearly overestimated. It could be explained, that washing of CsI from the elliptic bottom was not as efficient as modelled or insoluble iodine species (e.g. AgI) are formed on the elliptic bottom before washing as indicated by the rise of the measured iodine concentration at the sump bottom during washing. Green line shows calculated I_2 concentration. As it could be seen in Fig. 9, due to the relatively high pH of 8.7 only little I_2 was formed by radiolysis and hydrolysis reactions.

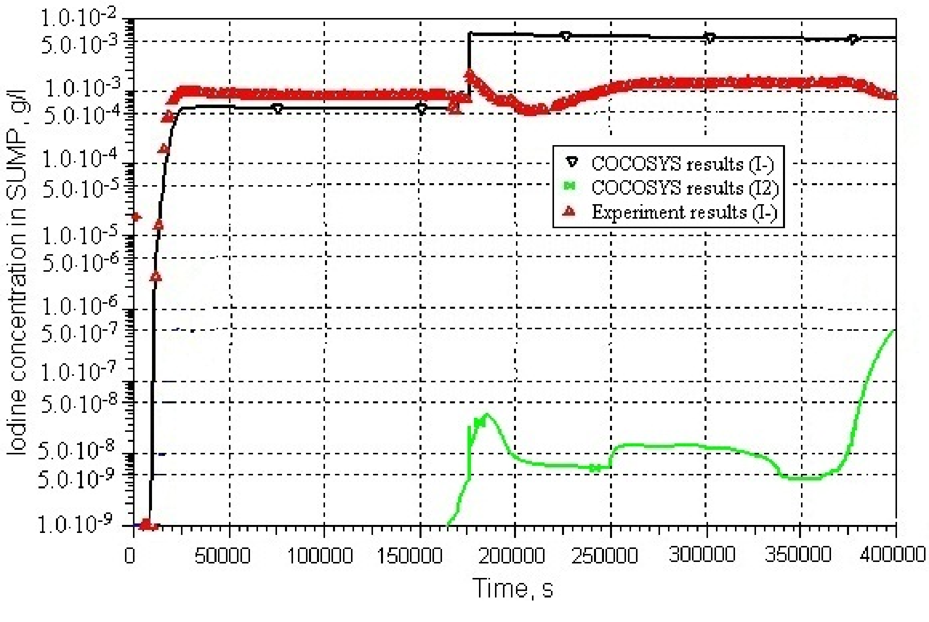

Fig. 9. Iodine concentration in SUMP

An integrated analysis of PHEBUS FPT-2 test comprising aerosol, fission products and iodine behaviour using was performed with COCOSYS. Simulation results shows, that integral analysis using COCOSYS code could be performed.

5. CONCLUSIONS

Integral analysis of thermal-hydraulic processes, aerosol, fission products and iodine behaviour using lumped parameter code COCOSYS was performed in PHEBUS containment under FPT-2 test conditions.

The deposition rate of the aerosols and fission product (tellurium) is calculated well, which shows that the aerosol and fission product deposition model, which is implemented in COCOSYS is suitable for such analysis.

Deposition of aerosols and fission products on the containment walls is significantly smaller than measured and could not be explained by the diffusive deposition model available in COCOSYS. Diffusive deposition has to be further investigated.

The measured I_2 concentration in the gas phase is somewhat underestimated while the measured organic iodide concentration is well matched. Only little I_2 is produced in the sump, because of the high pH and the iodine-silver reaction.

REFERENCES

1. ALLELEIN, H.-J., ARNDT, S., KLEIN-HEẞLING, W., SCHWARZ, S., SPENGLER, C., WEBER, G. COCOSYS: Status of development and validation of the German containment code system. Nuclear Engineering and Design, Vol. 238, Issue 4, p. 872–889, 2008.
2. KONTAUTAS A., URBONAVIČIUS E. Vidinių srautų modeliavimo įtaka aerozolių nusėdimo skaičiavimams PHEBUS FPT-1 eksperimente. Šilumos energetika ir technologijos-2007: konferencijos pranešimų medžiaga, Kauno technologijos universitetas, 2007 vasario 1–2. Kaunas: Technologija, 2007. ISBN 978-9955-25-338-9, p. 93–96.
3. KONTAUTAS, A., URBONAVIČIUS, E., RIMKEVIČIUS, S. Influence of the nodalisation and modelling parameters on the results calculation of aerosols deposition in PHEBUS experimental facility. Energetika, 2007, ISSN 0235-7208. T. 53, Nr. 4, p. 16–27.
4. KONTAUTAS A., URBONAVIČIUS E., Analysis of aerosol deposition in PHEBUS containment during FPT-1 experiment, Nuclear Engineering and Design, Vol. 239, p. 1267–1274, 2009.
5. BOSLAND L., WEBER G., KLEIN HESSLING W., GIRAULT N., CLEMENT B.. Modelling and Interpretation of Iodine Behaviour in PHEBUS FPT-1 Containment with ASTEC and COCOSYS codes. Nuclear Technology, Vol.177, No.1, p. 36–62, 2012.
6. GREGOIRE, A.C.; MARCH, P.; PAYOT, F.; RITTER, G.; ZABIEGO, M.; BRENAECKER, A.; BIARD, B.; GREGOIRE, G.; SCHLUTIG, S. Final report FPT2. IRSN and Commission of the European Union Institute for Energy, 1968 psl. Batiment $N^0$250-P 111-BP N03, 2008.
7. ALLELEIN H.J., AUVINEN A., BALL J., GÜNTAY S., HERRANZ L. E., HIDAKA A., JONES A. V., KISSANE M., POWERS D., WEBER G., 2009. State of the art report on nuclear aerosols. Nuclear Energy Agency/Committee on the safety of nuclear installations, 2009.

General sponsor:

LITHUANIAN
ENERGY
INSTITUTE

Sponsors:

A Member of The Linde Group AGA

VAE
Visagino atominė elektrinė

REO Investment

PlasTEP

BEA
Lithuanian Nuclear Energy Association

The Lithuanian District Heating Association

Baltic Sea Region
Programme 2007-2013
Part-financed by the European Union
(European Regional Development Fund)

AB KAUNO ENERGIJA

HIA

EUROPEAN NUCLEAR SOCIETY

CALL FOR PAPERS:
www.cyseni.com

Lithuanian Energy Institute
Young Scientists Association
Breslaujos str. 3, LT—44403 Kaunas, Lithuania
www.lei.lt jms.lei.lt